

INDIAN JOURNAL OF PHYSICS

VOL. 41

AND

PROCEEDINGS

OF THE

Indian Association for the Cultivation of Science, Vol. 50

(Edited in Collaboration with the Indian Physical Society)

(With Six Plates)

Published by the Registrar, Indian Association for the Cultivation of Science,
Jadavpur, Calcutta-32 and printed by Prakesh Chandra Chakrobertty,
Eka Press, 204/1, B. T. Road, Calcutta-35

1967

BOARD OF EDITORS

K. BANERJEE	S. R. KHASTGIR
G. N. BHATTACHARYA	D. S. KOTHARI
D. M. BOSE	B. D. NAG CHOUDHURI
S. N. BOSE	K. R. RAO
S. D. CHATTERJEE	R. RAMANNA
P. S. GILL	D. B. SINHA
B. N. SRIVASTAVA	S. C. SIRKAR
A. BOSE (<i>Secretary</i>)	

EDITORIAL COLLABORATORS

R. K. ASUNDI
D. BASU
J. N. BHAR
V. G. BHIDE
H. N. BOSE
S. K. CHAKRABORTY
J. S. CHATTERJEE
K. DAS GUPTA
N. N. DAS GUPTA
J. DHAR
A. K. DUTTA
S. DUTTA MAZUMDAR
C. S. GHOSH
S. GHOSH
S. N. GHOSH
S. GUPTA
D. N. KUNDU
R. C. MAZUMDAR
A. MOOKHERJI
Y. G. NAIK
S. R. PALIT
H. RAKSHIT
B. RAMCHANDRA RAO
A. SAHA
N. K. SAHA, N. N. SAHA, D. SHARMA
VIKRAM A. SARABHAI
A. K. SENGUPTA
NAND LAL SINGH
M. S. SINHA
N. R. TAWDE
P. VENKATESWARLU.

AUTHOR INDEX

AUTHOR	SUBJECT	PAGE
Agarwal, V. D.	See Gupta, H. C.	
Agrawal, V. D. and Gupta, R. C.	Nuclear magnetic relaxations and molecular reorientation fre- quencies of α hydroquinone and hydroquinone	241
Bagchi, R. N.	See Pal, A. K.	
" "	See Ghosh, U.S.	
Banerji, S.	See Neogy, D.	
Banerjee, S. B. and Mukherjee, D. K.	Study of hydrogen bonding in 2, 4-and 3, 5-xlenol (L)	230
Banerjee, S. B.	See Mukherjee, D. K.	
Banerjee, Sunil Kumar	See Ghosh, S. K.	
Banerjee, S. N.	See Jha, R.	
Banerjee, S. N. and Sil, N. C.	Effect of higher order partial wave phase shifts in elastic electron scattering by helium atom	358
Banerjee, S. N.	Excitation of 1'S state to 2'S state of helium atom by electron impact in Ockkur approxima- tion	266
Banerjee, S. N., Jha, R. and Sil, N. C.	Elastic resonance in electron hydrogen scattering	482
Barua, A. K.	See Deb, S. K.	
" "	See Singh, Yashwant	
" "	See Ghosh, A. K.	
" "	See Pal, Arun K.	
Basu, R. N. and Dutta, S. N.	On the performance calculations of three phase transmission lines by relaxation method	382
Basu, S. P. and Sinha, D. B.	On heat transfer in nucleate boiling-(2)	516
Bapat, R. N.	The near ultraviolet absorption spectrum of cyclohexyl benzene	587
Bhadra, T. C.	On the acoustic of shocks gene- rated by the rupture of dia- phragms in a tube	486
Bhattacharya, D. M.	See Chatterjee, G.	

AUTHOR	SUBJECT	PAGE
Bhattacharya, H.	Isospheric absorption in the VLF band	701
Bhattacharyya, J.	See Kastha, G. S.	
Bhattacharyya, S. C., Mazumdar, S. K. and Saha, N. N.	The crystal structure of sercosine hydrochloride	850
Bhattacharyya, S. N.	Structural effects in non-electrolyte solutions	579
Bhattacharya, Tapan	A simple analysis of the non-uniform field effects on the Gunn devices	498
Bhutra, M. P.	See Tandon, S. P.	
Bishui, P. K., Mukherjee, D. K. and Sirkar, S. C.	Raman spectra of CH_2Cl_2 , CHCl_3 and CCl_4 at 64°K	553
Biswas B. N.	An improvement in the technique of time measurement (L)	545
Bose, R. K.	Interrupted wave-synchronisation Note on torsional vibrations of non-homogeneous spherical and cylindrical shells	209 533
Bose, D. N.	Field effect measurements on GaAs	695
Bose, R. K.	Note on forced vibration of a thin non-homogeneous circular plate with a central hole	886
Chakravarty, A. S.	On the electric-quadrupole transitions of the octahedral complexes of the transition metal ions	602
Chakraborty, D. K.	See Chatterjee, S.	
Chakraborty, J. N.	Light scattering behaviour of acacia catechuic acid in course of its neutralisation with sodium hydroxide (L)	463
Chakrabarti, N. B. and Datta, A. K.	Diversity combining using carrier lock and sideband lock techniques (Part II)	87
Chakravorty, S. C.	See Chatterjee, S.	
" "	See Kundu, M. L.	
Chatterjee, A.	See Ghosh, D. K.	
Chatterjee, G., Bhattacharya, D. M. and Sil, N. C.	Matrix elements incorporating momentum transfer (L)	934

AUTHOR	SUBJECT	PAGE
Chatterjee, Gurudas, and Sil, N. C.	Differential capture probability of electron in proton-hydrogen collision at low energies	246
Chatterjee, S. and Chakravorty, S. C.	An x-ray study of the condensation product of diamino succinic acid and pyrrotic acid $C_{10}H_{12}N_2O_8$ (I.)	627
Chatterjee, S. and Chakraborty, D. K.	Band energy of Gold	134
Chatterjee, S. D.	See Sastri, R. C.	
" "	See Ganguly, S. R.	
Chattopadhyay, S.	On the assignments of the vibrational frequencies of some benzyl compounds	759
Chivate, (Miss) Pushpa	See Mande, Chintamani	
Choonkar, N. S.	On the absorption spectra of Ni^{++} ion in aqueous solution	21
Chorghade, S. L.	Crystallographic studies on hydrazobenzene $C_6H_5NH.NH.C_6H_5$	336
Das, (Miss). D.	Magnetic studies on α -silicon carbide (SiC) crystal	525
Das, J. N.	Electron impact on hydrogenic bound electron	332
Das, N. C.	Note on electrical response in a piezo-electric plate transducer with a prescribed input	611
Das Gupta, A.	Thermal conductivity of sulphur dioxide and diethyl ether at different temperatures	419
Datta, A. K.	See Chakrabarti, N. B.	
Datt, S. G., Verma, J. K. D. and Nag, B. D.	On the growth of single crystals of naphthalene	139
Datta, Sunil K.	See Mazumdar, Manju	
De, M.	On the thermal expansion of γ -phase Cu-Mn alloys at high temperatures	79
Deb, S. K.	Thermal diffusion in monatomic polytomic gas mixtures	718
Deb, S. K. and Barua, A. K.	Thermal diffusion and intermolecular forces in binary inert gas mixture	646

AUTHOR	SUBJECT	PAGE
Deka, G. C.	A note on "hammer" tracks having no associated beta-particle (L)	615
Dube, S. N.	On the temperature distribution of a viscous in-compressible fluid in a circular pipe under unsteady rate of heat addition	433
Dutta, A. K.	Nuclear radius, proten content, electron scattering, charge density, magic number and born-approximation modification	538
Dutta, B. (nee Sinha)	See Kastha, G. S.	
Dutta, M.	Symmetries of higher order and their invariance	347
Dutta, S. N.	See Basu, R. N.	
	D. C. three wire electrical power transmission network as solved by relaxation method	352
Dutta Gupta, R. R.	Pulse, width, frequency and height control in a transistor blocking oscillator	1
Dutta Roy, S. K., Ghosh, B. and Sahoo, B.	Magnetic susceptibility of some U^{+4} compounds at low temperature	362
Ganguly, S. R., Mondal, S. K., and Chatterjee, S. D.	Cosmic ray stars in photographic emulsion at high altitude	471
Ganguly, Suman and Samanta, Sishutosh	Studies on the fading of the radio waves returned from the sporadic E-region of the ionosphere	908
Ganguly, Chhaya and Sil, N. C.	S-wave neutron strength function, potential scattering radius and the optical model	816
Ghosh, A. K.	The lifetime of metastably bound polar molecules	663
Ghosh, Samir and Sengupta, Sima	Cosmic ray fluxes at different zenith angles (L)	788
Ghosh, S. K.	See Dutta Roy, S. K.	
Ghosh, A. K. and Barua, A. K.	Stretching and the difference in the intermolecular potentials of H_2 and D_2 from low temperature data	341
Ghosh, D. K., Chatterjee, A. and	Microwave spectra of ethyla-	

AUTHOR	SUBJECT	PAGE
Saha, A. K.	mine molecule (L)	467
Ghosh, U. S., Bagchi, R. N., Pal, A. K. and Mistra, S. N.	Orthorhombic ligand field theory of the magnetic behaviours of $\text{Cu}(\text{NH}_4\text{SeO}_4) \cdot 6\text{H}_2\text{O}$	286
Ghosh, N. N.	A note on induced 4-dimensional Lorentz transformation	570
Ghosh, S. K., and Banerjee, Sunil Kumar.	Study of the transverse vibration of the elastic-plastic string under different plasticity conditions	677
Ghumman, B. S., and Sood, B. S.	Inelastic interactions of gamma rays with K-shell electrons	737
Gupta, M. P. and Roy, P. K.	The crystal structure of potassium hydrogen fumarate, $\text{KC}_4\text{H}_3\text{O}_4$ (L)	787
Guha, S. S., Mazumdar, S. K. and Saha, N. N.	The crystal and molecular structure of L-ornithine-hydrochloride (L)	624
Guha Thakurta, S. R.	Termoelectric power of tungstenite (WS_2) single crystal (L)	940
„ „ „	Electrical properties of single crystal tungstenite (WS_2)	99
„ „ „	Certain thermistor characteristic of single crystals of tungstenite (WS_1) (L)	618
Gohel, V. B.	See Patel, M. M.	
Gujrathi, S. C. and Mukherjee, S. K.	Decay of Tm^{176} and levels of Yb^{176}	633
„ „ „	Decay of Tm^{174}	667
Gupta, R. C. and Agrawa, V. D.	Study of intra-molecular motion of hydroxyl group by proton resonance method	559
Gupta, R. C.	See Agrawal, V. D.	
Gupta, S. B. and Sil, N. C.	Elastic scattering of electrons by hydrogen atom	163
Gupta, S. L. and Saha, N. K.	Gamma-gamma directional correlations in Pr^{144}	48
Gupta, R. N. and Mondal, S. K.	Radio-frequency conductivity of ionized gases in magnetic field	153
Hiranandani, M. R.	See Rangarajan, R.,	
Iyengar, K. N.	See Rangarajau, R.	
Jha, R., Banerjee, S. N. and Sil, N. C.	Elastic scattering of electrons by helium atom	891

AUTHOR	SUBJECT	PAGE
Jha, R.	See Banerjee, S. N.	
Jha, R.	Elastron scattering by atomic hydrogen in Oohkur approximation	373
Jha, R. and Sil, N. C.	Elastic scattering of electrons by atomic hydrogen	875
Joshi, M. M. and Yamdagni, R.	Flame emmission spectrum of SnO molecule in the visible region	275
Joshi, R. V. and Menon, A. K.	Luminescent decay of variously pretreated KCL : TI phosphors	115
Kar, A. K.	See Pahari, S.	
" "	See Sannigrahi, A. B.	
Kastha, G. S., Bhattacharyya, J. and Roy, S. B.	Eyring's equation of relaxation time and dielectric absorption of 3.14 cm microwaves in polar liquids. Part III. Substituted toleunes and α -bromonaphthalene	313
Khastha, G. S.	See Sinha, (Miss) B.	
Kachhva, C. M. and Saxena, S. C.	Classical theories of dielectric constants	440
Khastha, G. S., Dutta, B. (nee Sinha), and Roy, S. B.	Dielectric absorption of and internal rotation in anisoles and substituted anisoles in solutions in non polar solvents	725
Khan, R. M.	Cherenkov radiation in a semi infinite dielectric medium with a conducting boundary	270
	Cherenkov radiation by line charge (L)	226
Khan, M. Y.	Renninger effect in quinaldic acid (L)	549
Khan, R. M.	Cherenkov radiation in a medium of variable dielectric constant	171
Khan, T. P.	On the classical radiation by an electron in uniform circular motion in the form of multipoles (L)	305
Khan, R. M.	Cherenkov radiation in dielectric medium with conductivity	260

AUTHOR	SUBJECT	PAGE
Khawas, B.	X-ray study of the monoclinic modification of para acetotoluidide crystals (L)	777
Krishna Murty V. G.	See Kr ; Rao, K. V.	
Krishna Rao, K. V. and Krishna Murty, V. G.	Temperature variation of the photoelectric constants of ammonium chloride- (L)	150
Krishnaswamy, (Mrs.) M.	See Ratho,	
Kumar, P.	See Neogy,	
Kumar, S.	See Srivastava, S. P.	
Kundu, M. L. and Chakravorty, S. C.	Space group of O-benzoyl benzoic acid (L)	
Kundu, S. K.	Amplitude perity and X ^o -meson	882
Lal, A.	An isotope effect in the collection of recoiled products of C ₂ H ₅ Br, and CH ₂ Br ₂	39
Madan, M. P.	See Srivastava, S. P.	
Mahalanobis, A.	See Neogi, D.	
Mangal, P. C. and Trehan, P. N.	A note on 222 Kev gamma-ray transition in the decay of Ba ¹³³ (L)	938
Mandal, S. K.	See Gupta, R. N.	
Mande, Chintamani, Nagavekar, A. S.	Effect of chemical combination on the symmetry of the K _a lines of cobalt	897
A. S. and Chivate, (Miss) Pushpa		
Majumdar, S. K.	See Roy, P. N.	
" "	See Bhattacharyya, S. C.	
Mazumdar, Manju, and Dutta, Sunil K.	Magnetic susceptibility and ligand field behaviour of pure and diluted crystal of FeSiF ₆ . 6H ₂ O	590
Mazumdar, Saroj K.	A note on the dispersion relation for very high temperature plasma	507
Mazumdar, S. K.	See Guha, S. S.	
Menon, A. K.	See Joshi, R. V.	
Misra, S. C.	A theory of classical liquids (L)	864
Mitra, B.	The (n, 2n) reaction cross section of p ³¹ , Zn ⁶⁴ , Ga ⁶⁹ and Ag ¹⁰⁷ for 14.6 Mev neutrons	752
Mitra, S. C. and Okonji, B. U.	Pressure dependence of the electrical conductance of pressed classiterite powders.	919

AUTHOR	SUBJECT	PAGE
Mitra, S. C.	Electrical conductivity of natural stannic oxide	448
Mitra, S. N.	See Ghosh, U. S.	
Mohanty, B. K.	Second harmonic generation in two level systems.	655
„ „	Generation of non linear dipole moment in a two level system	60
Mondal, S. K.	See Ganguly, S. R.	
Mukherjee, A. K.	The magnetic properties of specular hematite (L)	781
„ „	Magnetic properties of natural crystal of hematite (L)	465
Mukherjee, D. K. and Banerjee, S. B.	Infrared study of effect of environments on hydrogen bonding in catechol, resorcinol, and quinol	108
Mukherjee, D. K.	See Banerjee, S. B.	
„ „	See Bishui, P. K.	
Mukherjee, (nee Dasgupta) Indrani	Space group and unit cell dimensions of copper monochloroacetate, 2.5 hydrate (L)	776
Mukherjee, S. K.	See Gujrathi, S. C.	
„ „	A note on the relaxation times of the proton in cane sugar solution and glycerine with added paramagnetic Cu^{++} ions	16
Nag, B. D.	See Datt, S. C.	
Nain, V. P. S.	See Saksena, M. P.	
Nain, V. P. S. and Saxena, S. C.	Second virial coefficient of non-polar gases and gas mixture and Buckingham-Garra-konovalow potential	199
Narasimhan, K. S. V. L. and Sinha, K. P.	Electrical and thermal properties of PbTe doped with magnetic impurities	803
Neogy, D., Banerji, S., Kumar, P. and Mahalanobis, A.	A convenient and sensitive balance for measuring magnetic anisotropies of single crystals.	744
Nigavekar, A. S.	Mande, Chintamani	
Okonji, B. U.	See Mitra, S. C.	

AUTHOR	SUBJECT	PAGE
Pahari, S. and Kar, A. K.	Semiempirical one centre and two centre electron repulsion integrals	704
Pahari, S.	See Sannigrahi, A. B.	
Pal, Arun K. and Barua, A. K.	Effect of cluster formation on the viscosity of dense gases	323
„ „ „ „	Viscosity of polar nonpolar gas mixture	713
Pal, Arun K.	Intermolecular forces and viscosity some polar organic vapours	823
Pal, A. K.	See Ghosh, U. S.	
Pal, A. K., Bagchi, R. N., Saha, P. R. and Saha, R. K.	E.P.R. investigation on orthorhombic g tensors in copper rubidium sulphate hexahydrate, copper cesium sulphate hexahydrate and copper thallium sulphate hexahydrate	856
Palit, S. R.	Possibility of a real deviation from Faraday's law of electrolysis (I)	309
„ „	Electrode glow during electrolysis (I)	622
„ „	A simple experimental demonstration of the breakdown of Faraday's law of electrolysis (I)	782
„ „	Electrode glow during electrolysis and liberation of hydrogen and oxygen together on the electrodes (I)	860
„ „	See Sarkar, D. K.	
Panda, B. C.	See Ratho, T.	
Patel, M. M. and Patel, S. P.	The emission spectrum of the CdBr molecule (The visible system)	155
Patel, M. M., Gohel, V. B., Trivedi, M. D.	Modified Varshni Shukla potential function for diatomic alkali halide molecules	235
Patel, S. P.	See Patel, M. M.	

AUTHOR	SUBJECT	PAGE
Paul, (nee Das), D.	Temperature variation of magnetic susceptibility of molybdenite single crystal (L)	943
Rajput, M. S. and Sehgal, M. L.	Radioactive decay of Nd ¹⁴⁷	176
Raju, B. B. Venkata Pathi	See Rama Mohan, R. V.	
Rama Mohan, R. V., Reddy, K.	γ - γ —directional correlation studies and level scheme of Ba-134	30
Venkata, Raju, B. B. Venkata Pathi, and Swami Janananda		
Ramamohan, R. V.	Excitation spectra of even-even nuclei of non-deformed region (L)	779
Ranjarajan, R., Iyengar, K. N. and Hiranandani, M. R.	Mass distribution studies in nuclear fissions using lexen detector	902
Rao, M. Raja and Swami Janananda	The measurement of the Icc of the 192 kev transition in In-114m	55
Rao, K. Suryanarayana	See Shashidhar, M. A.	
Rao, Monoranjan	Attenuation characteristic of VLF waves from the waveform of atmospherics	844
Ratho T. and Krishnaswamy (Mrs), M.	On the structure of complex silver lutidine perchlorate	327
„ „ „ „	On the structure of complex silver quinoline perchlorate	511
„ „ „ „	Space group and unit cell dimensions of complex lutidine nitrate (L)	871
„ „ „ „	On the determination of unit cell dimensions from powder diffraction data of complex silver lutidine nitrate	864
Ratho, T. and Panda, B. C.	Low-angle x-ray measurements on air-dried and alkali-treated macromolecular systems-wool (L)	932
Redey, K. Venkata	See Rama Mohan, R. V.	
Roy, P. K.	See Gupta, M. P.	
Roy, P. N., Majumdar, S. K. and Saha, N. N.	The crystal structure of glycocyamine hydrobromide	771
Roy, S. B.	See Sinha, (Miss) B.	
„ „	See Kastha, G. S.	
Saha, A. K.	See Ghosh, D. K.	
Saha, N. K.	See Gupta, S. L.	

AUTHOR	SUBJECT	PAGE
Saha, N. N.	See Roy, P. N.	
" "	See Bhattacharyya, S. C.	
" "	See Guha, S. S.	
Saha, Pada Renu	An anomalous magnetic behaviour of $KCr_3(C_2O_4)_3 \cdot 3H_2O$ studies between room temperature and liquid oxygen temperature (L)	628
Saha, P. R.	See Pal, A. K.	
Sahoo, B.	See Dutta Roy, S. K.	
Saksena, M. P., Nain, V. P. S. and Saxena, S. C.	Second virial and zero-pressure Joule-Thomson coefficients of polar and nonpolar gases and gas mixtures	123
Samanta, Sishutosh	See Ganguly, Suman	
Sannigrahi, A. B., Kar, A. K. and Pahari, S.	H.M.O. calculations on tetrabenzonaphthalene (L)	708
Saran, Anil	See Singh, Yashwant	
Sarkar, D. K. and Palit, S. R.	Test of viscosity theories of Flory, Kurata, Ptitsyn and Palit for dilute polymer solutions	389
Sastri, R. C. and Chatterjee, S. D.	Investigation of thermionic emission at low intensity with a Geiger counter	
Sastri, R. C. and Chatterjee, S. D.	On the emission of exo electrons in a Geiger counter (L)	617
" " " "	Image inversion of Geiger pulse(L)	147
Saxena, S. C.	See Kachhva, C. M.	
" "	See Nain, V.P.S.	
" "	See Saksena, M.P.	
Sehgal, M. L.	See Rajput, M. S.	
Seike, Shinichi	Tri-harmonic stress function	121
Sen Gupta, N. D.	On a representation of the dirac matrices	378
" "	On the frequency shift in Thomson scattering (L)	631
Shaha, R. K.	See Pal, A. K.	
Sengupta, Sima	See Ghosh, Samir	
Shashidhar, M. A. and Rao, K. Suryanarayana	Electronic absorption spectra of 2-, 4-6-and 7-methyl quino-line vapours	299

AUTHOR	SUBJECT	PAGE
Sil, N. C.	See Jha, R.	
" "	See Chatterjee, G.	
" "	See Ganguly, Chhaya	
" "	See Chatterjee, Gurudas	
" "	See Gupta, S. B.	
" "	See Banerjee, S. N.	
Singh, Yashwant and Barua, A. K.	Effects of anharmonicity on the intermolecular potentials derived from crystal properties	685
Singh, Yashwant, Saran, Anil and Barua, A. K.	On the representation of three-body nonadditive interactions in solids	413
" " "	Contribution of bound double molecules to the second virial coefficient	426
Singh, Kartar and Singh, Santokh	N ¹⁴ quadrupole resonance in benzene sulphonamide (L)	862
Singh, Sanktokh	See Singh, Kartar	
Sinha, K. P.	See Narasimhan, K.S.V.L.	
Sinha, (Miss) B., Roy, S. B. and Kastha, G. S.	On the relation between the energy of activation for dielectric relaxation and the interaction energy of polar organic molecules in dilute solutions in non polar solvents	183
Sinha, D. K.	A note on longitudinal disturbances in a semi infinite piezoelectric rod in a magnetic field (L)	784
" "	A note on mechanical response in a piezoelectric ceramic transducer under the influence of a body-force	925
Sinha, D. B.	See Basu, S. P.	
Sinha, S. K.	Acoustical free induction in a quadrupolar spin system in a cubic crystal	453
Sirkar, S. C.	See Bishui, P.K.	
Sood, B. S.	See Ghumman, B.S.	
Srivastava, S. P., Kumar, S. and Madan, M. P.	Infrared absorption frequency of ionic crystal	833
" "	Debye Temperature of Ionic Crystals	828

Author Index

xiii

AUTHOR	SUBJECT	PAGE
Swami Jnanananda	See Rama Mohan, R.V.	
„ „	See Rao, M. Raja	
Tandon, K.	See Tandon, S. P.	
Tandon, S. P., Bhutra, M. P. and Tandon, K.	Electron affinity of halogen atoms	70
Trehan, P. N.	See Mangal, P.C.	
Trivedi, M. D.	See Patel, M.M.	
Verma, J. K. D.	See Datt, S.C.	
Yamdagni, R.	See Josh, M.M.	

SUBJECT INDEX

SUBJECT	AUTHOR	PAGE
Acoustic free induction in a quadrupolar spin system in a cubic crystal	S. K. Sinha	453
Acoustic of shocks generated by the rupture of diaphragms in a tube.—On the	T. C. Bhadra	486
Amplitude parity and X^0 -meson	S. K. Kundu	882
Anharmonicity on the intermolecular potentials derived from crystal properties.—Effects of	Yashwant Singh and A. K. Barua	685
Band energy of gold	S. Chatterjee and D. K. Chakraborty	134
Chemical combination on the asymmetry of the $K\alpha$ lines of cobalt.—Effect of	Chintamani Mande, A. S. Nigavekar and Miss Pushpa Chivate	897
Cherenkov radiation by line charge	R. M. Khan	226
Cherenkov radiation in dielectric medium with conductivity	„ „ „	260
Cherenkov radiation in a medium of variable dielectric constant	„ „ „	171
Cherenkov radiation in a semi-infinite dielectric medium with a conducting boundary	„ „ „	270
Classical liquid.—A theory of (L)	S. C. Misra	864
Conductivity of ionized gases in magnetic field.—Radio-frequency	R. N. Gupta and S. K. Mandal	153
Cosmic ray fluxes at different zenith angles	Samir Ghosh and Sima Sengupta	788
Cosmic ray stars in photographic emulsion at high altitude	S. R. Ganguly, S. K. Mondal and S. D. Chatterjee	471
Crystals of naphthalene- On the growth of single	S. C. Datt, J. K. D. Verma and Nag, B. D.	139
Crystallographic studies on hydrazobenzene	S. L. Chorghade	336
Crystal and molecular structure of L-ornithine-hydrochloride. The	S. S. Guha, S. K. Mazumdar and N. N. Saha	624
Crystal structure of clycocyamine hydrobromide.—The	P. N. Roy, S. K. Mazumdar and N. N. Saha	771

SUBJECT	AUTHOR	PAGE
Crystal structure of potassium hydrogen fumarate, $\text{KC}_4\text{H}_3\text{O}_4$.—The (L)	M. P. Gupta, and P. K. Roy	787
Crystal structure of sarcosine hydrochloride.—The	S. C. Bhattacharyya, S. K. Mazumdar and N. N. Saha	850
Debye temperature of ionic crystal	S. P. Srivastava, S. Kumar and M. P. M	828
Decay of Tm^{176} and levels of Yb^{176}	S. C. Gujrati and S. K. Mukherjee	633
Decay of Tm^{174}	"	667
Dielectric constants.—Classical theories of	C. M. Kachhava and S. C. Saxena	440
Dielectric absorption of and internal rotation in anisoles and substituted anisoles in solutions in non-polar solvents	G. S. Kastha, B. Dutta (nee' Sinha) and S. B. Roy	725
Differential capture probability of electron in proton-hydrogen collision at low energies	Gurudas Chatterjee and N. C. Sil	246
Dipole moment in a two level system. —Generation of non-linear	B. K. Mohanty	60
Directional correlation studies and level scheme of Ba-134.	R. V. Rama Mohan, K. Venkata Reddy, B. B. Venkata Pathi Raju and Swami Jnanananda	30
Dirac matrices.—On a representation of the	N. D. Sen Gupta	378
Directional correlations in Pr^{144} . —Gamma-gamma	S. L. Gupta and N. K. Saha	48
Dispersion relation for very high temperature plasma.—A note on the	Saroj K. Majumdar	507
Diversity combining using carrier lock and sideband lock techniques (Part II)	N. B. Chakrabarti and A. K. Datta	87
Elastic scattering of electrons by hydrogen atoms	S. B. Gupta, N. C. Sil	163
Electrical and thermal properties of PbTe doped with magnetic impurities	K. S. V. L. Narasimhan and K. P. Sinha	803
Electrical conductance of pressed classiterite powders.—Pressure dependence of the	S. C. Mitra and B. U. Okonji	919
Electrical conductivity of natural stannic oxide	S. C. Mitra	448

SUBJECT	AUTHOR	PAGE
Electric-quadrupole transitions of the octahedral complexes of the transition metal ions—On the	A. S. Chakravarty	602
Electrical power transmission network as solved by relaxation method.—D.C. three wire	S. N. Dutta	352
Electrical properties of single crystal of tungstenite (WS_2)	S. R. Guhathakurta	99
Electrical response in a piezo-electric plate transducer with a prescribed input.—Note on	N. C. Das	611
Electrode glow during electrolysis (L)	Santi R. Palit	622
Electrode glow during electrolysis and liberation of hydrogen and oxygen together on the electrodes (L)	" "	860
Electron affinity of halogen atoms	S. P. Tandon, M. P. Bhutra and K. Tandon	70
Electron hydrogen scattering.—Elastic resonance in	S. N. Banerjee, R. Jha and N. C. Sil	482
Electron impact on hydrogenic bound electron	J. N. Das	332
Electron repulsion integrals.—Semiempirical one centre and two centre	S. Pahari and A. K. Kar	704
Electron scattering by helium atom.—Effect of higher order partial wave phase shifts in	S. N. Banerjee and N. C. Sil	358
Electron scatterin by atomic hydrogen in Ochkur approximation	R. Jha	373
Emission spectrum of the CdBr molecule (the visible system).—The	M. M. Patel and S. P. Patel	155
E.P.R. investigation on orthorhombic g-tensors in copper rubidium sulphate hexahydrate, copper cesium sulphate hexahydrate and copper thallium sulphate hexahydrate	A. K. Pal, R. N. Bagchi, P. R. Saha and R. K. Saha	856
Excitation of $1'S$ state to $2'S$ state of helium atom by electron impact in Ochkur approximation	S. N. Banerjee	266

SUBJECT	AUTHOR	PAGE
Exo electrons in a Geiger counter.—On the emission of	R. C. Sastri and S. D. Chatterjee	617
Faraday's law of electrolysis, —A simple experimental demonstration of the breakdown of (L)	Santi R. Palit	782
Field effect measurements on GaAs	D. N. Bose	695
Faraday's law of electrolysis.—Possibility of a real deviation from (L)	S. R. Palit	309
Forced vibration of a thin non-homogeneous circular plate with a central hole.—Note on	R. K. Bose	686
Field effects on the gun devices.—A simple analysis of the non-uniform	Tapan Bhattacharya	498
Gamma-ray transition in the decay of Ba ³³ —A note on 222 Kev (I.)	P. C. Mangal and P. N. Trehan	938
Hammer tracks having no associated beta-particle.—A note on (L)	G. C. Deka	615
Heat transfer in nucleate boiling-(2).—On the	S. P. Basu and D. B. Sinha	516
H.M.O. calculations on tetrabenzonaphthalene (L)	A. B. Sannigrahi, A. K. Kar and S. Pahari	708
Hydrogen bonding in 2, 4 and 3, 5-Xylenol—Study of	S. B. Banerjee and D. K. Mukherjee	230
Image inversion of Geiger pulse (L)	R. C. Sastri and S. D. Chatterjee	147
Inelastic interactions of gamma rays with K-shell electrons	B. S. Ghumman and B. S. Sood	737
Isos of the 192 keV transitions in In-114m.—The measurement of the	M. Raja Rao and Swami Jnanananda	55
Induced 4-dimensional Lorentz transformations—A note on	N. N. Ghosh	570
Infrared absorption frequency of ionic crystals	S. P. Srivastava, S. Kumar and M. P. Madan	833
Infrared study of effect of environments on hydrogen bonding in catechol, resorcinol and quinol	D. K. Mukherjee and S. B. Banerjee	108
Ionospheric absorption in the Vlf band	H. Bhattacharya	701

SUBJECT	AUTHOR	PAGE
Intermolecular potentials of H_2 and D_2 from low temperature data.—Stretching and the difference in the	A. K. Ghosh and A. K. Barua	341
Intermolecular forces and viscosity of some polar organic vapours	Arun K. Pal	823
Interrupted wave synchronisation	B. N. Biswas	209
Intra-molecular motion of hydroxyl group by proton resonance method.—Study of	R. C. Gupta and V. D. Agrawal	559
Interactions in solids.—On the representation of three-body nonadditive	Yashwant Singh, Anil Saran and A. K. Barua	413
Joule-Thomson coefficients of polar and nonpolar gases and gas mixture.—Second virial and Zero-pressure	M. P. Saksena, V. P. S. Nain and S. C. Saxena	123
Lifetime of metastably bound polar molecules. The	A. K. Ghosh	663
Ligand field theory of the magnetic behaviours of $Cu(NH_4SeO_4)_2 \cdot 6H_2O$.—Orthorhombic	U. S. Ghosh, R. N. Bagchi, A. K. Pal, and S. N. Mitra	286
Light scattering behaviour of acacia catechuic acid in course of its neutralisation with sodium hydroxide (L)	J. N. Chakraborty	463
Longitudinal disturbances in a semi-infinite piezoelectric rod in a magnetic field.—A note on (L)	D. K. Sinha	784
Luminescent decay of variously pretreated KCl. TI phosphors	R. V. Joshi and A. K. Menon	115
Magnetic anisotropies of single crystal.—A convenient and sensitive balance for measuring	D. Neogy, S. Benerji, P. Kumar and A. K. Mahalanobis	744
Magnetic behaviour of $KCr_3(C_2O_4)_3 \cdot 3H_2O$, studied between room temperature and liquid oxygen temperature.—An anomalous (L)	Pada Renu Saha	628
Magnetic properties of natural crystals of hematite (L)	A. K. Mukherjee	465
Magnetic properties of specular hematite.—The (L)	A. K. Mukherjee	781

SUBJECT	AUTHOR	PAGE
Magnetic studies on α -silicon carbide (SiC) crystals	Miss D. Das	525
Magnetic susceptibility of some U ⁴ compounds at low temperatures	S. K. Dutta Roy, B. Ghosh and B. Sahoo	362
Magnetic susceptibility and ligand field behaviour of pure and diluted crystal of FeSiF ₆ .6H ₂ O	Manju Majumdar and Sunil K. Datta	590
Magnetic susceptibility of molybdenite single crystal.—Temperature variation of (L)	D. Paul (nee Das)	943
Matrix elements incorporating momentum transfer (I.)	G. Chatterjee, D. M. Bhattacharya, and N. C. Sil	934
Neutron strength function, potential scattering radius and the optical model.—S-wave	Chhaya Ganguly and N. C. Sil	816
Nuclear fission using Lexan detector.—Mass distribution studies in	R. Rangarajan, K. N. Iyengar and M. R. Hiranandani	902
Nuclear magnetic relaxations and molecular reorientation frequencies of α -hydroquinone and γ -hydroquinone	V. D. Agrawal and R. C. Gupta	241
Nuclear radius, proton content, electron scattering, charge density, magic numbers and born-approximations modifications	A. K. Dutta	538
Photoelastic constants of ammonium chloride.—Temperature variation of the (L)	K. V. Krishna Rao and V. G. Krishna Murty	150
Piezoelectric ceramic transducer under the influence of a body-force.—A note on mechanical response in a	D. K. Sinha	925
N ¹⁴ quadrupole resonance in benzene sulphonamide (L)	Karter Singh and Santokh Singh	862
Radiation by an electron in uniform circular motion in the form of multipoles.—On the classical (L)	T. P. Khan	305
Radioactive decay of Nd ¹⁴⁷	M. S. Rajput and M. L. Sehgal	176

SUBJECT	AUTHOR	PAGE
Radio waves returned from the sporadic e-region of the inosphere. -Studies on the fading of the	Suman Ganguly and Sishutosh Samanta	908
Reaction cross-section of P^{31} , Zn^{64} , Ga^{69} and Ag^{107} for 14.6 MeV neutrons. —The (n, 2n)	B. Mitra	752
Recoiled products of C_2H_5Br , $C_2H_4Br_2$ and CH_2Br_2 .—An isotope effect in the collection of	A. Lal	39
Relation between the energy of activation for dielectric relaxation and the interaction energy of polar organic molecules in dilute solution in non-polar solvents.—On the	(Miss) B. Sinha, S. B. Roy and G. S. Kastha	183
Relaxation times of the proton in cane sugar solution and glycerine with paramagnetic Cu^{++} ions.—A note on the	S. K. Mukherjee	16
Relaxation time and dielectric absorption of 3.14 cm microwaves in polar liquids-part III. substituted toluenes and -bromonaphthalene.—Eyring's equation of	G. S. Kastha, J. Bhattacharyya and S. B. Roy	313
Renninger effect in quinaldic acid (L)	M. Y. Khan	549
Scattering of electrons by atomic hydrogen.—Elastic	R. Jha and N. C. Sil	875
Scattering of electrons by helium atoms.—Elastic	R. Jha., S. N. Banerjee and N. C. Sil	891
Second harmonic generation in two level systems	B. K. Mohanty	655
Second virial coefficient.—Contribution of bound double molecule to the	Yashwant Singh, Anil Saran and A. K. Barua	426
Second virial coefficient of non-polar gases and gas mixtures and Buckingham-Varre Knowalov potential	V. P. S. Nain and S. C. Saxena	199
Space group of O-benzoyl benzoic acid (L)	M. L. Kundu and S. C. Chakravorty	547

SUBJECT	AUTHOR	PAGE
Space ground and unit cell dimensions of copper monochloroacetate 2.5 hydrate (L)	Indrani Mukherjee (nee Dasgupta)	776
Space group and unit cell dimensions of complex silver lutidine nitrate.-(L)	T. Ratho and Mrs. M. Krishnaswamy	864
Spectra of ethylamine molecule. -Microwave	D. K. Ghosh, A. Chatterjee and A. K. Saha	467
Spectra of even-even nuclei of non-deformed region.-Excitation (L)	R. V. Ramamohan	779
Spectra of Ni ⁺⁺ ion in aqueous solution —On the absorption	N. S. Chhonkar	21
Spectra of 2-.4-6- and 7-methyl quino-line vapours—Electronic absorption	M. A. Shashidhar and K. Suryanarayana Rao	299
Spectra of CH ₂ Cl ₂ , CHCl ₃ and CCl ₄ at 64°K.—Raman	P. K. Bishuni, D. K. Mukherjee and S. C. Sirkar	553
Spectrum of cyclohexyl benzene.—The near ultraviolet absorption	R. N. Rapat	587
Spectrum of SnO molecule in the visible region.—Flame emission	M. M. Joshi and R. Yamdagni	275
Structural effects in non-electrolyte solutions	S. N. Bhattacharyya	579
Structure of complex silver quinnoline perchlorate.—On the	T. Ratho and Mrs. M. Krishnaswamy	511
Structure of complex silverlutidine per chlorate.—On the	T. Ratho and Mr. M. Krishnaswamy	327
Symmetries of higher order and their invariance	M. Dutta	347
Temperature distribution of a viscous in-compressible fluid in a circular pipe under unsteady rate of heat addition.—On the	S. N. Dube	433
Technique of time measurement.—An improvement in the (L)	B. N. Biswas and G. Dutta	545
Thermal conductivity of sulphurdioxide and diethyl ether at different temperatures	A. Das Gupta	419

SUBJECT	AUTHOR	PAGE
Thermal diffusion and intermolecular forces in binary inert gas mixtures	S. K. Deb and A. K. Barua	646
Thermal diffusion in monatomic polyatomic gas mixtures	S. K. Deb	719
Thermal expansion of γ -phase Cu-Mn alloys at high temperatures.—On the	M. De	79
Thermionic emission at low intensity with a Geiger counter.—Investigation of	R. C. Sastri and S. D. Chatterjee	793
Thermistor characteristics of single crystals of Tungstenite (WS_2).—Certain(L)	S. R. Guha Thakurta	618
Thermoelectric power of tungstenite (WS_2) single crystal (L)	S. R. Guha Thakurta	940
Thomson scattering.—On the frequency shift in (L)	N. D. Sen Gupta	631
Torsional vibrations of non-homogeneous spherical and cylindrical shells	R. K. Bose	533
Transistor blocking oscillator.—Pulse width, frequency and height control in a	R. R. Dutta Gupta	1
Transmission lines by relaxation method.—On the performance calculations of three phase	R. N. Basu and S. N. Dutta	382
Transverse vibration of the elastic-plastic string under different plasticity conditions.—Study of the	S. K. Ghosh and Sunil Kumar Banerjee	677
Tri-harmonic stress function	Shinichi Seike	121
Unit cell dimensions from powder diffraction data of complex silver lutidine nitrate.—On the determination of	T. Ratho and Mrs. M. Krishnaswamy	871
Varshni-Shukla potential function for diatomic alkali halide molecules.—Modified	M. M. Patel, V. B. Gohel and M. D. Trivedi	235
Vibrational frequencies of some benzyl compoundd.—On the assignments of the	S. Chattopadhyay	759
Viscosity of dense gases.—Effect of cluster formation on the	A. K. Pal and A. K. Barua	323

Subject Index

xxiii

SUBJECT	AUTHOR	PAGE
Viscosity of polar-nonpolar gas mixtures	Arun K. Pal and A. K. Barua	713
Viscosity theories of Flory, Kurate, Ptitsyn and Palit for dilute polymer solutions.—Test of	D. K. Sarkar and S. R. Palit	389
VLF waves from the waveforms of atmospherics.—Attenuation characteristic of	Monoranjan Rao	844
X-ray measurements on air-dried and alkali-treated macromolecular system-wool.—Low angle (L)	T. Ratho and B. C. Panda	932
X-ray study of the condensation product of diamino succinic acid and pyruvic acid $C_{10}H_{12}N_2O_8$.—An (L)	S. Chatterjee and S. C. Chakravorty	627
X-ray study of the monoclinic modification of para acetotoluidine crystals (L)	B. Khawas	777
BOOK REVIEWS	76, 152, 232, 312, 470, 712, 790, 867	

INDIAN JOURNAL OF PHYSICS

VOL. 41

No. 1

AND

VOL. 50

PROCEEDING

No. 1

OF THE

INDIAN ASSOCIATION FOR THE CULTIVATION OF SCIENCE

(Edited in collaboration with the Indian Physical Society).

JANUARY 1967

PUBLISHED BY THE
INDIAN ASSOCIATION FOR THE CULTIVATION OF SCIENCE
JADAVPUR, CALCUTTA-33

INSTRUCTIONS TO AUTHORS FOR PREPARATION OF MANUSCRIPTS

Original scientific papers on all branches of Physics and allied subjects such as Chemical Physics, Mathematical Physics, Applied Physics, Geophysics, Biophysics, Crystallography and Mineralogy etc.; are accepted for publication in Indian Journal of Physics provided these are not merely records of routine laboratory tests and contain original contributions to the knowledge of these Sciences. Normally, the author or at least one of the joint authors should be a member of the Indian Association for the Cultivation of Science or of the Indian Physical Society. Papers from authors other than members will be also accepted under special circumstances. Mss. for publication, in duplicate should be sent to the Assistant Secretary, Indian Journal of Physics, Indian Association for the Cultivation of Science, Jadavpur, Calcutta-32. Mss. submitted should be typewritten with double space, on one side of good quality paper, with sufficient margin on the left and at the top. Each paper should begin with an abstract just after the title of the paper and the name and full address of the author or authors. References in the text should be given either by quoting the year of publication within parantheses, if the surname of the author occurs in the text, or by quoting the surname of the author followed by the year within parantheses at the proper place. In case the reference has more than one name, all names other than the first should be replaced by *et al* in the text as shown. For example, "Thermal transformation..... was studied by Bernal *et al* (1959) and Das Gupta (1960)". Or "Thermal decomposition ... studied by different workers (Cuthbert, 1947 ; Weiden, 1954)". The full references should be given at the end of the paper, under head *References*, arranged alphabetically by surname, followed by initials, year of publication, standard abbreviated name of journal with single underline, volume with double underline, and the page *e.g.* : Perkins, H.D., 1950, *Proc. Royal Soc.* **A203**, 309. If more than one paper by the same authors occur in the same year, in the same journal or not, both in the text and in the *References* these should be chronologically signified by adding *a, b, c*, etc., to the year. Names of same author or authors successively coming in *References* may be replaced by a long 'dash'. Name of same journal coming in *References* successively may be also replaced by long dashes similarly. Positions for text figures and diagrams should be indicated in margin. Line diagrams should be drawn on white Bristol board or tracing paper with black Indian Ink and interior of the diagrams should contain the minimum number of index letters (preferably of simple Gothic style) or numerals (preferably Roman type). Where possible different graphs in the same diagram should only be differentiated by, full line, dotted line, dashed line, crosses, circles, squares etc. Full captions of all figures with serial numbers should be given in a separate sheet. Numerals for scales and description of coordi-

(Contd. to 3rd cover)

PULSE WIDTH, FREQUENCY AND HEIGHT CONTROL IN A TRANSISTOR BLOCKING OSCILLATOR

R. R. DUTTA GUPTA

INSTITUTE OF RADIOPHYSICS AND ELECTRONICS,
UNIVERSITY COLLEGE OF TECHNOLOGY,
CALCUTTA-9

(Received December 9, 1964)

ABSTRACT. A transistor blocking oscillator gives a sequence of rectangular pulses of identical height, width and spacing. Modified forms of such transistor blocking oscillators are described with a view to control pulse width, frequency and height thereby increasing the versatility of the circuit. Expressions for these quantities have been derived and confirmed by experimental results.

INTRODUCTION

A free-running transistor blocking oscillator gives a sequence of rectangular pulses of identical height, width and spacing. Its versatility is greatly increased if these parameters can be controlled in a smooth and continuous fashion. The present paper considers some modifications of the basic transistor blocking oscillator circuit to meet these requirements.

The modification described to control the pulse width includes an emitter follower in the feedback loop of the blocking oscillator. The technique permits the production of relatively longer pulses, the width of which can be controlled by means of an external resistance in the emitter circuit of the oscillator. A theoretical relation giving the pulse width as a function of this resistance and other related parameters has been derived and found to be reasonably reliable as revealed by experimental results. An experimental circuit designed on the above ideas permitted a 6 : 1 variation in pulse width as against a 2 : 1 variation obtained with a simple blocking oscillator without the emitter follower.

Methods devised to enable control of amplitude and frequency of the generated pulses independent of each other consisted in introducing in the basic blocking oscillator circuit a biased diode and a linearising arrangement permitting a constant current discharge of the condenser. The height and frequency were found to have linear dependences upon the appropriate control voltage. Since the variations were linear and independent of each other, these could be used to obtain a faithful modulation of either amplitude or frequency. It has also been pointed out that the arrangement offers the possibility of analogue multiplication of two independent parameters x and y used as the two control voltages.

Present Address : Electronics and Radar Development Establishment, Bangalore-1.

Linvill and Mattson (1955) were the first to give a comprehensive picture of the operation of a transistor blocking oscillator and the analysis given by them still remains outstanding because of its simplicity and directness of approach. Since the present paper follows closely the treatment given by these authors, it is desirable to restate first the relevant portion of the analysis in some detail.

ANALYSIS OF TRANSISTOR BLOCKING OSCILLATOR BY LINVILL AND MATTSON

For convenience in analysis, the operation of a transistor blocking oscillator is divided into two parts viz, (1) the regenerative period and (2) the ON period of the oscillator. We shall consider only the ON period in the following and introduce the expression for the pulse width of the basic blocking oscillator as given by Linvill and Mattson

The transistor blocking oscillator is shown in Fig. 1 and its equivalent circuit during the ON period in Fig. 2. During this period, the current gain of the tran-

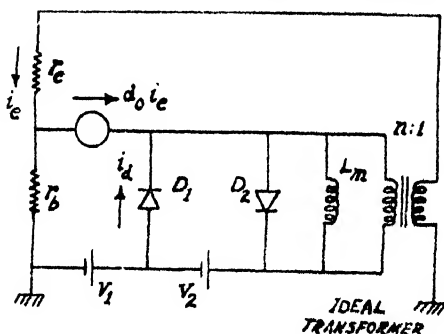
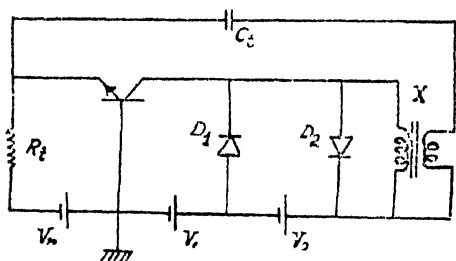


Fig. 1. The Transistor Blocking Oscillator. Fig. 2. Circuit Approximant of the Transistor Blocking Oscillator during the ON Period

sistor can be approximately treated as a constant and the effect of the leakage inductance of the transformer and the collector capacitance of the blocking oscillator transistor may be neglected. The diode D_1 represents a short circuit and D_2 an open circuit. Referring to Fig. 2, it can be seen that at the termination of the switching period, the magnetising inductance L_m does not carry appreciable current, though the voltage V_2 is applied directly across it through the diode D_1 . The emitter current i_e is obtained by considering a voltage V_2/n (where n is the transformer turns ratio) on the secondary side driving the current through the effective resistance at the emitter point, which is $r_e + r_b(1 - \alpha_0)$, where r_e : emitter resistance, r_b : base resistance and α_0 : grounded base current gain of the transistor. Thus we get,

$$i_e = \frac{V_2}{n[r_e + r_b(1 - \alpha_0)]} \quad (1)$$

The current entering the transformer primary is of course i_e/n . The diode current

Pulse Width Frequency and Height Control, etc.

through D_1 at the outset is given by the difference between the collector current (obtained as $\alpha_0 i$) and the current entering the transformer and is obtained as

$$i_d = \frac{V_2}{n[r_e + r_b(1 - \alpha_0)]} \left[\alpha_0 - \frac{1}{n} \right]. \quad (2)$$

The pulse width τ_L is the time required for this amount of current to build up in the magnetising inductance L_m . The build up of current in the inductance L_m due to the constant voltage source V_2 , effectively connected across it through D_1 , is obviously linear with time. Thus, denoting this current by $i(t)$, we get,

$$i(t) = \frac{V_2}{n} t. \quad (3)$$

Equating (2) and (3), the pulse width is obtained as,

$$\tau_L = \frac{(\alpha_0 n - 1)L_m}{n^2[r_e + r_b(1 - \alpha_0)]}. \quad (4)$$

It may appear from eqn. (4) that pulse width variation could be effected by controlling r with the help of emitter current. However, since the emitter (or collector) current in a switching circuit is practically controlled by the external load on the collector an attempt at effecting such a variation proves to be futile. The only way to vary effective r_e would be to introduce additional feature in the basic blocking oscillator circuit shown in Fig. 1.

MODIFIED TRANSISTOR BLOCKING OSCILLATOR CIRCUIT FOR PULSE WIDTH CONTROL

The circuit consists essentially of a transistor blocking oscillator, the feedback path of which includes a transistor S_2 preceding the transformer X (Fig. 3). The primary function of S_2 , arranged in the form of an emitter follower, is to decrease the instantaneous balancing current $i(t)$ flowing through the diode D_1 and the base of transistor S_2 . The diode current i_d is the initial switching current flowing through D_1 and the transistor S_1 —the process being the same as in the conventional Linvill and Mattson oscillator as described earlier. Since, however, the current $i(t)$ is less and hence the time taken for balancing longer, the pulse duration also is much longer. In the following, we deduce an expression for the duration of the pulse thus lengthened.

The modified blocking oscillator circuit as shown in Fig. 3 is arranged to work from external trigger pulses—a triggered configuration being found necessary for accurate measurement of pulse width. When a trigger pulse of right polarity arrives at the input (i.e. the cathode of the diode D_3), the regenerative feedback, via the transistor S_2 and the transformer X , switches the oscillator transistor S_1 to the ON state. At this point the diode D_1 conducts and clamps the collector S_1 to the voltage E_3 . Also since the diode D_1 is short, the constant voltage source

E_1 is effectively connected at the input of the emitter follower S_2 . Taking the voltage gain of the emitter follower to be unity, it is easy to see that the input

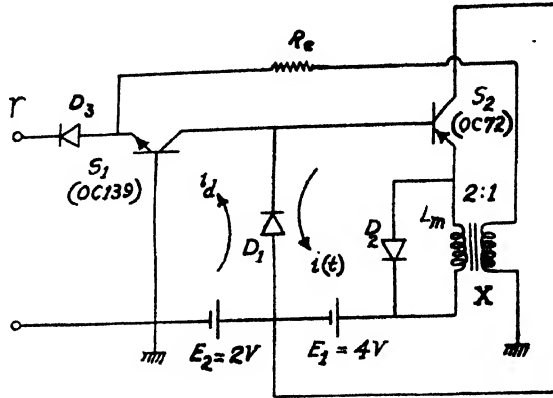


Fig. 3. Modified Transistor Blocking Oscillator Circuit for Pulse Width Control.

voltage E_1 appears undiminished at the output, i.e., across the primary terminals of the transformer X .

Following Linvill and Mattson 1955, it is easy to show that

$$i_e = \frac{E_1}{n} \cdot \frac{1}{[R_e + r_e + r_b(1 - \alpha_1)]}, \quad \dots (5)$$

$$i_c = \frac{\alpha_1 E_1}{n[R_e + r_e + r_b(1 - \alpha_1)]}, \quad \dots (6)$$

- where i_e : current flowing through the emitter of S_1 ,
 i_c : current flowing through the collector of S_1 ,
 R_e : external resistance in series with the emitter of S_1 ,
 r_e : emitter resistance of S_1 ,
 r_b : base resistance of S_1 ,
 and α_1 : low frequency grounded base current gain of S_1 .

Denoting the current flowing through the secondary of the transformer by i_e , that entering the primary is obviously i_e/n , n being the transformer turns ratio. If the grounded emitter current gain of the transistor S_2 be denoted by β_2 , the base current i_b required to maintain the emitter current will be given by

$$i_b = \frac{i_e}{\beta_2 n}$$

or,
$$i_b = \frac{E_1}{\beta_2 n^2 [R_e + r_e + r_b(1 - \alpha_1)]}. \quad \dots (7)$$

Thus the diode current is given by

$$i_d = (i_c - i_b) = \frac{E_1}{n[R_e + r_e + r_b(1 - \alpha_1)]} \left(\alpha_1 - \frac{1}{\beta_2 n} \right). \quad \dots (8)$$

Again, since the voltage across the primary of the transformer is E_1 , the current through the magnetising inductance L_m of the primary will rise linearly with time giving

$$i_L = \frac{E_1}{L_m} t, \quad \dots (9)$$

where i_L : current through L_m .

and t : time.

The current flowing through the base of S_2 , due to the magnetising current i_L at the emitter, is obviously $\frac{i_L}{\beta_2}$. Denoting this current by $i(t)$ we may write from eqn. (9)

$$i(t) = \frac{E_1}{\beta_2 L_m} t. \quad \dots (10)$$

Proceeding after Linvill and Mattson (1955) one gets from eqns. (8) and (10),

$$\tau = \frac{\beta_2 L_m}{n[R_e + r_e + r_b(1 - \alpha_1)]} \left(\alpha_1 - \frac{1}{\beta_2 n} \right), \quad \dots (11)$$

where τ : pulse duration.

Since for a junction transistor $\alpha_1 \simeq 1$, $\frac{1}{\beta_2 n} \ll \alpha_1$ and $r_b(1 - \alpha_1) \simeq 0$, eqns. (11) may be re-written as

$$\tau = \frac{\beta_2 L_m}{n(R_e + r_e)} \quad \dots (12)$$

Eqn. (12) is more convenient than (4) in so far as it involves a new parameter R_e which can be used for controlling the duration τ in a simple manner.

MODIFIED CIRCUIT FOR PULSE REPETITION FREQUENCY AND HEIGHT VARIATION

The modification of the original Linvill and Mattson transistor blocking oscillator for independent control of pulse repetition frequency and height is shown in Fig. 4. In this, the transistor S_1 , together with the feedback transformer X , constitutes the usual transistor blocking oscillator. The new feature introduced is a second transistor S_2 (of the $n-p-n$ type) acting as a constant current device. Also, experience had shown that the hole storage effect due to saturation is

negligible for low power transistors and hence the clamping diode used for eliminating saturation in the collector-base region of the transistor is not included in the present circuit.

During the time when the blocking oscillator is ON, condenser C charges to a positive value as usual. The discharge of this condenser determines the time after which the transistor S_1 again becomes forward-biased and gives a second pulse. Usually, this discharge time or the quiescent period of the blocking oscillator is determined by the leakage resistance and the bias voltage in series with it—the combination being shunted across C . In the present system, however, instead of this combination, the second transistor S_2 , as mentioned above, is so arranged that a constant current discharge of C takes place.

In order to analyse the performance of the present circuit, we shall consider separately the aspects involving pulse frequency and pulse amplitude variation.

(a) *Pulse frequency variation* : It has been pointed out that the transistor S_2 allows a constant current discharge of C . This arises out of the fact that the collector current of a transistor is independent of collector voltage, base bias being kept constant. If now the working of the combination of the blocking oscillator and the constant current discharge device be so arranged that the quiescent period of the oscillator becomes much larger than the width of the generated pulse, then as will be presently shown, the repetition frequency of the pulses may be made to vary linearly with the variation of the voltage V_E (Fig. 4).

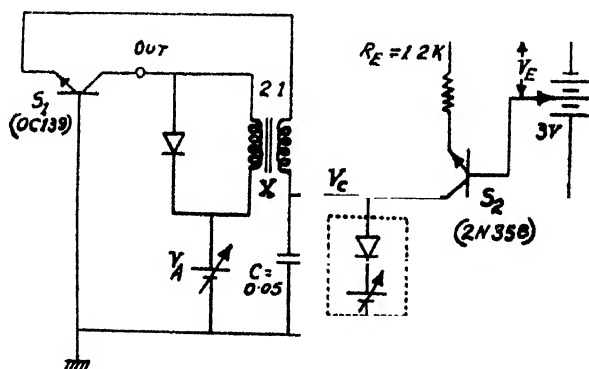


Fig. 4. Modified Transistor Blocking Oscillator Circuit for Pulse Frequency and Amplitude Control.

Referring to Fig. 4, if the voltage to which the condenser charges during the ON period of the blocking oscillator be denoted by V_c , then the time taken for the condenser to return to zero, i.e., the point where the oscillator is again turned

on (actually the oscillator is turned on at a slightly negative potential) is obviously given by

$$\frac{i_c T}{C} = V_c,$$

$$\text{or,} \quad T = CV_c \quad \dots (13)$$

where i_c : collector current of S_2

and T : quiescent period of the oscillator.

Again, considering the transistor S_2 , the voltage across the emitter resistance R_E is given by,

$$v_e = V_E - V_{be}, \quad \dots (14)$$

where V_{be} : voltage drop across the base-emitter junction.

Therefore the current i_e in the emitter circuit is found as

$$i_e = \frac{v_e}{R_E} = \frac{V_E - V_{be}}{R_E} \quad \dots (15)$$

Eqn. (15) ignores the effect of the emitter resistance of the transistor which is made much smaller than the external resistance R_E . Also, denoting the grounded-emitter current gain of S_2 by β , the portion of i_e flowing through the base is given by

$$i_b = \frac{i_e}{\beta}$$

which in the light of eqn. (15), becomes,

$$i_b = \frac{V_E - V_{be}}{\beta R_E}, \quad \dots (16)$$

where i_b : current flowing through the base of S_2 .

Collector current i_c is given by the difference between the emitter and the base currents, i.e.,

$$i_c = i_e - i_b. \quad \dots (17)$$

Combining eqns. (15), (16) and (17),

$$i_c = \frac{\beta - 1}{\beta} \cdot \frac{V_E - V_{be}}{R_E}. \quad \dots (18)$$

Substituting eqn. (18) in (13), we get,

$$T = \frac{CV_c \beta R_E}{(\beta - 1)(V_E - V_{be})}. \quad \dots (19)$$

As has been mentioned earlier, for small pulse widths as compared with the quiescent period, the frequency will be determined by T alone. Thus taking the inverse of eqn. (19), we get,

$$f = \frac{1}{T} = \frac{(\beta-1)(V_E - V_{be})}{CV_c\beta R_E}, \quad \dots (20)$$

where f : pulse repetition frequency.

It is seen from eqn. (20) that, other parameters remaining constant, the pulse repetition frequency becomes linearly related with V_E , the base voltage of the discharging transistor S_2 .

Incidentally, it may be recalled that according to eqn. (19), a linear variation of T is possible through variation in V_c . This may have use in certain special fields of application.

(b) *Pulse amplitude variation*: Considering the transistor blocking oscillator in Fig. 4 (shown inside the dashed enclosure), it may be seen that the amplitude of the generated pulse at the collector is equal to the supply voltage of the oscillator transistor S_1 . Therefore, by injecting the control signal in series with the supply voltage, linear pulse amplitude variation could be directly obtained. The straightforward method has one drawback however. Since the voltage to which the condenser C charges depends upon the height of the generated pulse, the quiescent period and hence the repetition frequency of the oscillator also changes with change in supply voltage (eqns. 19 and 20). However, if an arrangement is made for holding the condenser voltage constant, the simultaneous change in frequency with amplitude variation may be avoided. This may be achieved by using a reference diode across the condenser, or, alternatively a biased diode may be used (shown within the dotted lines in Fig. 4). Since the cathode of the diode is biased positive, the diode remains open circuit as long as the voltage across the condenser remains smaller than the bias voltage. However, as soon as the voltage across the condenser rises above the bias voltage, the diode within the dotted lines becomes short circuit and clamps the condenser to the bias supply voltage. Thus V_c in eqn. (19) becomes equal to the bias supply voltage, thereby ensuring a fixed p.r.f.

RESULTS

(i). *Variation of Pulse Width*: The experimental circuit for the study of variation of pulse width is shown in Fig. 3 where the following values were used.

$$n = 2, \quad L_m = 150\mu\text{H}, \quad r_e = 30 \text{ ohms} \quad \text{and} \quad \beta_s = 27.$$

(a) *Pulse width without emitter follower*: Pulse width as observed without the emitter follower S_2 was $\tau_L = 1\mu\text{sec}$, the calculated value from eqn. (4) being $1.25\mu\text{ sec.}$ (taking $\alpha_0 \approx 1$).

(b) *Pulse width with emitter follower* : The experimental values of τ when the emitter follower is included are shown in Table I. It may be seen that columns (3) and (4), giving the observed and calculated values as based on eqn. (12) lend sufficient support to the relevant theoretical deduction.

TABLE I

R_e (ohms)	$(R_e + r_e)$ (ohms)	Pulse Duration τ (μsec)	
		Observed	Calculated
35	65	31	32.4
45	75	26	27
55	85	24	23.8
70	100	19	20.3
100	130	17	15.5
150	180	11	11.3

(ii) *Variation of frequency* : The experimental circuit arrangement is shown in Fig. 4. The values of the various circuit parameters used are the following :

$$\beta = 30, C = 0.05\mu F, R_E = 1.2K \Omega \text{ and } V_{be} = 0.1 \text{ volt.}$$

Table II gives the results of experimental measurements of pulse frequency for the given circuit, in which the respective pulse periods are also included. The

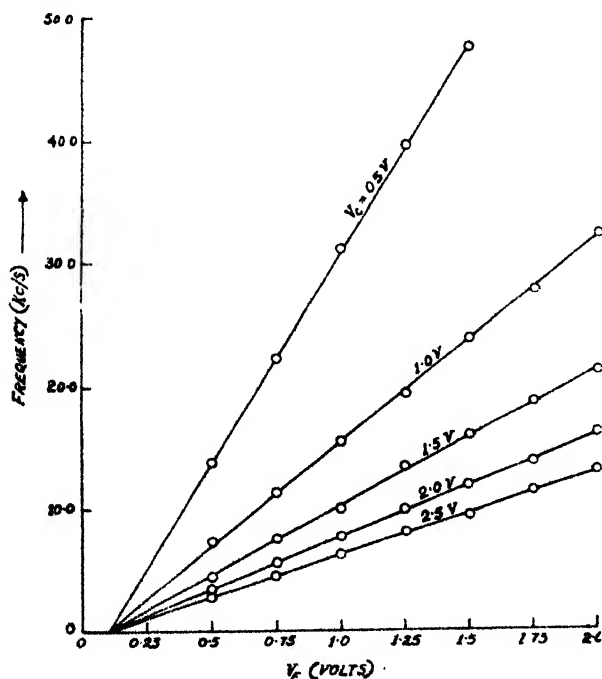


Fig. 5. Variation of Pulse Frequency.

nature of variation is shown graphically in Fig. 5 where the solid lines represent the theoretical curves with V_c as parameter and the small circles, the experimental results. It may be seen both from the table and the graphs that the agreement

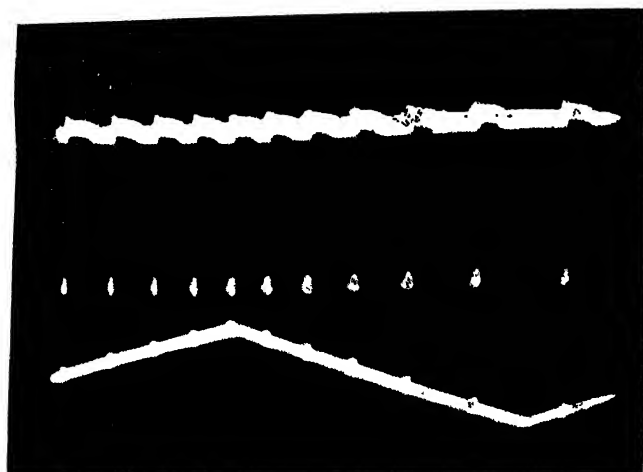


Fig. 6. Linear Frequency Modulation.

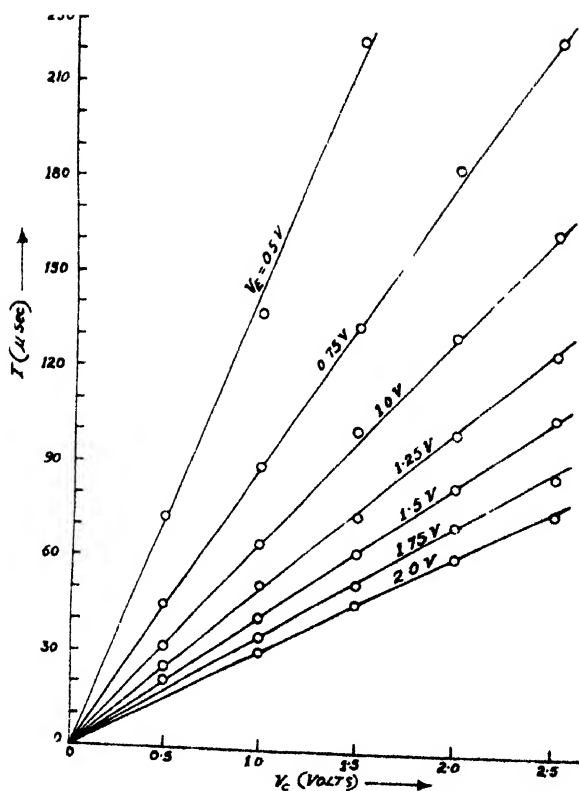


Fig. 7. Variation of Pulse Time Period.

between the observed and the calculated values as based on eqn. (20) is very good. This suggests the possibility of faithful pulse frequency modulation using the arrangement. The expected linear frequency modulation is illustrated by the oscillographic records shown in Fig. 6. It is seen that the amplitude remains a constant during the modulation cycle thereby implying independent variation of both the parameters.

In Fig. 7 are given the theoretical lines depicting the variation of T with V_c with V_E as a parameter. The corresponding experimental results are also given by small circles. Here again the experimental results appear to support the theoretical deduction.

TABLE II

V_o (Volts)	V_E (Volts)	Frequency f (kc/s)		Pulse Time Period $T(\mu \text{ sec})$	
		Theoretical	Experimental	Theoretical	Experimental
0.5	0.50	13.75	33.8	72.0	72.5
	0.75	22.25	22.3	44.5	45.0
	1.00	31.25	31.2	32.0	32.0
	1.25	39.64	39.8	25.0	25.2
	1.50	48.25	48.0	20.5	20.8
1.0	0.50	7.00	7.3	145	137
	0.75	11.25	11.3	89	88.5
	1.00	15.50	15.5	64.5	64.5
	1.25	19.75	19.5	50.5	51.3
	1.50	24.10	24.0	41.3	41.6
	1.75	28.35	28.0	35.5	35.8
1.5	2.00	32.70	32.7	30.5	30.6
	0.50	4.6	4.5	213	222
	0.75	7.5	7.5	133.5	133
	1.00	10.35	10.0	96	100
	1.25	13.2	13.5	75.5	74
	1.50	16.0	16.0	62.5	62.5
2.0	1.75	18.9	19.0	52.5	52.6
	2.00	21.75	21.5	45.9	46.5
	0.50	3.5	3.5	286	286
	0.75	5.6	5.5	178	182
	1.00	7.7	7.7	129	130
	1.25	9.8	10.0	100.5	100
2.5	1.50	12.0	12.0	83.5	83.5
	1.75	14.1	14.0	71.5	71.5
	2.00	16.25	16.2	61.5	61.7
	0.50	2.75	2.7	364	370
	0.75	4.5	4.5	223	222
	1.00	6.25	6.2	162	162
3.0	1.25	7.9	8.0	125.5	125
	1.50	9.6	9.5	104	105
	1.75	11.5	11.5	88	87
	2.00	13.25	13.2	76.2	75.7

(iii) *Variation of Amplitude* : As has been mentioned in the previous section, the amplitude V_A of the generated pulse should be equal to the supply voltage

(Fig. 4). The results of experimental measurement of pulse amplitude as given in Table III confirm the expectation. This is shown graphically in Fig. 8. It was

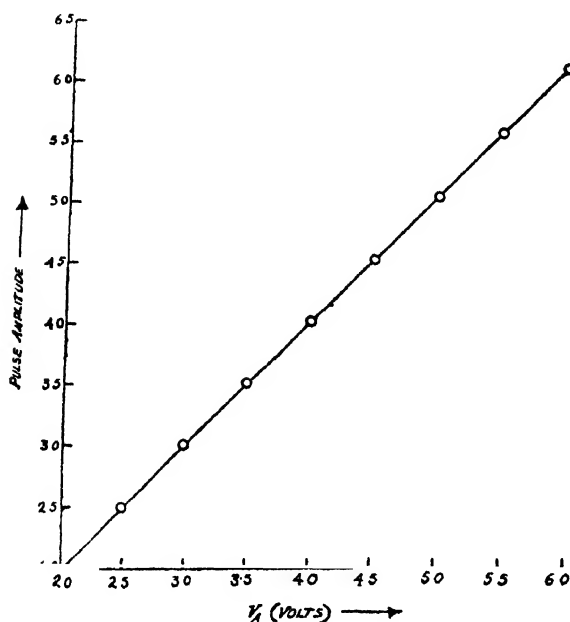


Fig. 8. Variation of Amplitude.

also found in this connection that the pulse repetition frequency remained unaffected with the variation of V_A —thereby enabling amplitude control independent of frequency. This is also demonstrated in Fig. 9 where the oscillographic record

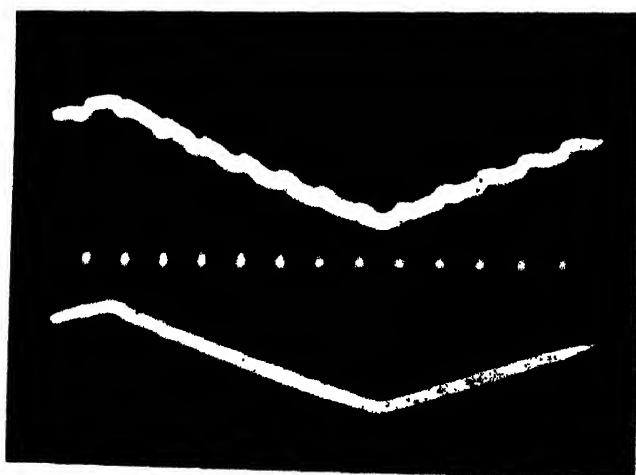


Fig. 9. Linear Pulse Amplitude Modulation.

reveals that the frequency remains unaltered (equal spacing of the pulses) while amplitude varies linearly with supply voltage.

TABLE III

V_A (Volts)	Pulse Amplitude	
	Theoretical	Experimental
2.0	2.0	2.0
2.5	2.5	2.5
3.0	3.0	3.0
3.5	3.5	3.5
4.0	4.0	4.0
4.5	4.5	4.5
5.0	5.0	5.0
5.5	5.5	5.5
6.0	6.0	6.0

DISCUSSIONS

Eqn. (12) shows that width of the generated pulse in a blocking oscillator with an emitter follower in the feedback loop is directly proportional to β_2 . Hence, it was thought that pulse width modulation might be achieved by working the emitter follower at low collector voltages, the variation of which, in turn, might vary β_2 . By actual measurement, however, no significant variation of β_2 could be obtained. The scheme for pulse width modulation was, therefore, abandoned. However, in the production of long pulses, the circuit appeared to have more flexibility than that of the Linvill and Mattson type. For the latter circuit eqn. (4) gives

$$\tau_L \approx \frac{L_m}{nr_a} \quad (21)$$

for $\alpha_0 \approx 1$ and $n \gg 1$.

Comparing eqn. (21) with (12), which gives expression for pulse width with an emitter follower, it is seen that for a given total of the emitter resistance ($R_e + r_e$), the pulse duration with an emitter follower in the feedback loop is β_2 times longer than τ_L , the duration in the Linvill and Mattson circuit. It is also easy to see that for the same pulse duration, the feedback transformer in the modified circuit has a much lower value of magnetising inductance than that which would be necessary in order to avoid pulse droop that would arise in the straightforward blocking oscillator circuits handling pulses of comparable width.

A second desirable feature, obtained through the introduction of the emitter follower, arises out of the fact that the circuit provides a low impedance output point. This also results in its capability of handling a greater load.

Coming to the consideration of manual control of pulse width by the variation of R_e in the emitter circuit of the blocking oscillator (as may be useful in laboratory

equipments), it is easy to see that increasing R_e reduces regeneration of the blocking oscillator. This sets an upper limit of R_e , beyond which the blocking oscillator would not function. Since pulse width varies inversely with the resistance in the emitter circuit, the highest possible value of R_e corresponds to the minimum pulse width. Introducing a resistance R_e at the emitter end in the Linvill and Mattson oscillator too one could achieve width variation. For such an arrangement the highest value of R_e was found to be about 37 ohms giving a pulse width of 0.6μ sec (theoretical value as based on eqn. (4) with r_e replaced by $r_e + R_e$ is 0.56μ sec, the r_e value under operating condition being about 30 ohms. Referring to 1(a) of the Results, the maximum limit of the generated pulse width is found to be 1μ sec (corresponding to $R_e = 0$). Thus the pulse width variation, obtainable in the Linvill and Mattson oscillator, lies in the range of 0.6μ sec to 1μ sec.

Now, referring to the blocking oscillator with the emitter follower, it is seen that the loss of regeneration due to R_e is compensated for by the extra current gain provided by the emitter follower. It is, therefore, permissible to increase R_e to a much higher value corresponding to a much greater reduction of pulse width. However, introduction of the factor β_2 in the expression for pulse width increases the overall length of the pulse.

Taking a typical example, as given in Table I, the range of pulse width variation is seen to be from 11.3μ sec. to 32.4μ sec. It may be mentioned that the upper limit for $R_e = 0$ corresponds to 67.5μ sec. Thus, it is seen by comparing the two blocking oscillator circuits that, so far as the percentage variation of pulse width is concerned, the modified circuit with the emitter follower in the feedback loop is distinctly superior to an ordinary Linvill and Mattson arrangement.

As has been seen in the preceding section, linear variation of pulse frequency and amplitude with independent voltages is possible. Figs. 6 and 9 suggest that the circuit as shown in Fig. 4 should be very suitable for effecting both pulse frequency and amplitude modulation.

Another possible application of the modified blocking oscillator circuit is in the field of analogue multiplication. This results from that fact that both frequency and the amplitude of the train of generated pulses may be varied independently of each other. For, recalling that the output of an integrating circuit is proportional to the instantaneous amplitude v of each one of the individual pulses, the total output due to n pulses will be given by

$$Q = K n v, \quad \dots (22)$$

where Q : total output of the integrating circuit
and K : factor of proportionality.

If the time integral corresponding to 1 second be considered, n becomes identical with frequency. Thus writing,

$$\text{and } v = V(1 + K_1 x) \quad \dots (23)$$

$$f = F(1 + K_2 y) \quad \dots (24)$$

where V : pulse height in the absence of any external voltage.
 x : external voltage expressed as a fraction of V and injected in series with V_A . This is one component of multiplication.
 K_1 : constant of proportionality,
 f : instantaneous pulse repetition frequency of the blocking oscillator,
 F : pulse repetition frequency of the blocking oscillator in the absence of external voltage,
 and K_2y : frequency change expressed as a fraction of F corresponding to second component of multiplication y in series with V_E .
 one gets from eqns. (22), (23) and (24),

$$Q = KVF(1 + K_1x)(1 + K_2y).$$

or,
$$Q = KVF(1 + K_1x + K_2y + K_1K_2xy). \quad \dots (25)$$

Eqn. (25) shows that the integrator output consists of a steady term, two linear terms—one proportional to the first component of multiplication and the other to the second component—and finally the required product term. It is therefore clear that by balancing out the steady and the linear terms at the output of the integrator, one is left only with the desired product term proportional to xy .

ACKNOWLEDGMENT

The author takes this opportunity of expressing his sincere thanks to Prof. J. N. Bhar for his kind interest in the work. He is particularly grateful to Prof. S. Deb for first suggesting the work and taking active interest in it by way of constant helpful discussions.

REFERENCE

Linville, J. G. and Mattson, R. H., 1955 *Proc. I.R.E.*, **43**, 1632.

A NOTE ON THE RELAXATION TIMES OF THE PROTON IN CANE SUGAR SOLUTION AND GLYCERINE WITH ADDED PARAMAGNETIC Cu^{++} IONS(*)

S. K. MUKHERJEE

DEPARTMENT OF PHYSICS, DALHOUSIE UNIVERSITY,
HALIFAX, NOVA SCOTIA, CANADA

(Received July 15, 1965)

ABSTRACT. The spin-lattice relaxation time of the proton has been determined from Bloembergen's formula, in which the numerical factor has been modified to take into account the interactions arising in the case of cane sugar solution and glycerine with added Cu^{++} ions. The spin-spin relaxation time could be estimated from measurements of n.m.r. signal strength. It has been shown that in both of these liquids, T_1 and T_2 are of the order of 10^{-4} sec.

Bloembergen,¹ Purcell and Pound (1948) have propounded a theory of nuclear magnetic relaxation, which was successfully applied by them to pure liquids including, among others, water, glycerine, ethyl alcohol etc. These authors have also extended their theory to the case of dilute aqueous solutions of paramagnetic ions like Cu^{++} , Fe^{++} etc., and have been successful in explaining the reduction in the spin-lattice relaxation time T_1 of protons in these media, which was first observed by Bloch, Hansen and Packard (1946). The magnetic moment of a paramagnetic ion is of the order of one Bohr magneton, which is about 1840 times bigger than the nuclear magneton. Therefore, on addition of these ions to a liquid like H_2O , the intermolecular magnetic interaction between a liquid molecule and a neighbouring ion largely predominates over the intramolecular interaction between the two protons in the same molecule.

In a previous work Mukherjee, (1964) we have reported measurements of nuclear magnetic resonance signals in aqueous cane sugar solution and glycerine, both containing very small quantities of dissolved paramagnetic Cu^{++} ions. Our sample of glycerine ($\text{C}_3\text{H}_8\text{O}_3$) was 97.5% pure by weight (density at room temperature = 1.251g. cm^{-3}) and contained about 2.2×10^{18} Cu^{++} ions dissolved per cm^3 of the medium. From tables (4), the value of its viscosity was found to be $\eta = 6.6$ Poise at 23°C , so that $\eta/T = 2.2 \times 10^{-2} \text{P}^\circ\text{K}$, where T denotes the temperature in degrees Kelvin. The n.m.r. frequency was 15.5 Mcs./sec. If our glycerine sample did not contain Cu^{++} ions, its spin-lattice relaxation time T_1 and spin-spin relaxation time T_2 should very closely follow the same dependence on η/T respectively as the T_1 and T_2 of the 98% pure glycerine (5) investigated by Bloembergen *et al*(*). Using Bloembergen's data we find,

(*) the attention of the reader is drawn to Fig. 13 on page 705 of the article by Bloembergen *et al* (1948).

that in our case, T_1 and T_2 are both independent of the n.m.r. frequency and $T_1 \approx T_2 \approx 2 \times 10^{-2}$ sec.

However, due to the presence of Cu^{++} ions, the relaxation times will be reduced. To account for the reduction in the value of T_1 , we propose the following formula :

$$1/T_1 = 9.6\pi^2\gamma_p^2\eta N_i\mu_i^2/kT \quad \dots (1)$$

where γ_p is the gyromagnetic ratio of the proton, η is the viscosity of the medium, N_i is the number of ions per cm^3 of the medium, μ_i is the magnetic moment of the paramagnetic ion, k is the Boltzmann's constant and T , the absolute temperature. This equation differs by a numerical factor only from a similar equation given by Bloembergen *et al* (1948) for the T_1 of protons in H_2O . In modifying his equation, we have assumed that 8 protons are available for interaction with one Cu^{++} ion, i.e., one ion interacts magnetically with one molecule of glycerine and, as usual, the diffusion constant D is the same for the glycerine molecules and the divalent Cu^{++} ions. Assuming $\mu_i = 1.9$ Bohr magnetons (6) and putting numerical values in equation (1), we get $T_1 = 1.3 \times 10^{-4}$ sec. The order of magnitude of T_1 thus calculated, seems to be reasonable and our calculation shows that T_1 has been reduced by a factor of the order of 100 due to the influence of Cu^{++} ions. It must be mentioned, however, that the modification as represented by equation (1) is based purely on phenomenological considerations. However, the use of this equation appears to be justified by the fact that it apparently gives results of the correct order of magnitude.

According to Bloembergen's theory of the relaxation times of the proton in a liquid medium under conditions of resonance absorption,

$$T_2 \approx T_1 \quad \dots (2)$$

if

$$(2\pi\nu_0\tau_c)^2 < < 1 \quad \dots (3)$$

Here ν_0 is the n.m.r. frequency and τ_c , the so-called "correlation time" given by

$$\tau_c = 4\pi\eta\alpha^3/3kT \quad \dots (4)$$

In this equation, α is the radius of the molecule containing the protons and all other symbols have been explained previously. Solomon (1955) has deduced on theoretical grounds that in a similar system of two nuclear spins, containing paramagnetic ions in solution, T_2 and T_1 are approximately equal if the same condition (3) holds good. It has also been shown experimentally by various workers including Bloembergen *et al*, (1948) Gabillard (1952) and Chiarotti and Giulotto (1953), that such an ionic concentration as used by us, T_2 is approximately equal to T_1 in aqueous paramagnetic solutions. Some of these authors used Cu^{++} ions, but many preferred Fe^{+++} ions.

In a medium like glycerine, when free from paramagnetic ions, the spinspin relaxation time T_2 which is a measure of the reciprocal of the resonance

line-width, arises from (i) a contribution due to the local magnetic fields of the nuclei (ii) a second contribution due to the mutual energy exchange in a spin-spin interaction process between the eight protons in the molecule and (iii) a third contribution given by $2T_1$, which measures the life-time of a nucleus in a particular excited state. (iv) There may be a fourth contribution to T_2 arising from a linebroadening due to the inhomogeneity of the magnetic field over the bulk of the sample. However, due to the presence of Cu^{++} ions in glycerine at the level indicated and the consequent reduction in the value of T_1 , it is reasonable to assume that the contributions (i) and (ii), which are roughly equal, are of the same order of magnitude as the contribution (iii).

In our previous work (Mukherjee 1964), the n.m.r. coil was small (about 1.9 cm long compared to the pole-face diameter of 20.2 cm) and placed at the centre of the field. An accuracy of a few parts in 10^4 was obtained there in the determination of the ratio of the Larmor frequencies of the 1_H and 19_F nuclei. An estimation of the variation of the magnetic field in the medial plane of the air-gap, as one moves away from the centre along a radius, had been made by Guptill *et al* (1950). All these data lead us to believe that the magnetic field is homogeneous to within $\pm 0.03\%$. This value of field inhomogeneity allows us to calculate a line broadening, whose contribution to T_2 is 1.2×10^{-4} sec. (contribution iv). This figure is almost equal to the value of T_1 calculated from relation (1). Thus, although the glycerine molecule is a system of 8 "effective" nuclear spins, complicated by the presence of Cu^{++} ions, it is justified to assume that the total absorption line width is given by the reciprocal of T_1 , at least, as far as the order of magnitude is concerned. Therefore, we can put, $T_2 \approx T_1 \approx 1.3 \times 10^{-4}$ sec. and $T_2/T_1 \approx 1$.

The cane sugar sample used by us had 53.5% by weight of $\text{C}_{12}\text{H}_{22}\text{O}_{11}$ dissolved in water and contained about 2.23×10^{18} Cu^{++} ions per cm^3 of the solution. This number is almost the same as that in the case of glycerine. Measurements were made of the density and viscosity of this solution at room temperature and gave following values: $\rho = 1.254 \text{ g. cm}^{-3}$ and $\eta_s = 20.3 \text{ cP}$ (at 23°C). Cane sugar molecules containing 22 protons are bigger than glycerine molecules. The system contains, in addition, the cupric ions and a relatively large amount of water. Roughly speaking, 1 cm^3 of cane sugar solution contains, beside the cupric ions, about 1.95×10^{22} molecules of H_2O and 1.18×10^{21} molecules of $\text{C}_{12}\text{H}_{22}\text{O}_{11}$. Therefore, on the average, one Cu^{++} ion can be considered to be in the neighbourhood of 1 molecule of $\text{C}_{12}\text{H}_{22}\text{O}_{11}$ and 16 to 17 molecules of H_2O . Hence, effectively the magnetic interaction takes place between one Cu^{++} ion and about 55 protons. Keeping this simplified picture in mind and assuming, as before, the thermal diffusion coefficients of the ion and the two different types of molecules are approximately the same, we can modify the numerical factor in Bloembergen's formula for T_1 . The modified formula now reads:

$$1/T_1 = 66\pi^2 \gamma_p^2 \eta_s N_i \mu_i^2 / kT \quad (5)$$

In this modification of Bloembergen's formula, the same phenomenological arguments have been followed as in the previous case.

In the cane sugar system $\eta_s/T = 6.9 \times 10^{-4} P/^{\circ}K$. Substituting numerical values in equation (5), we get $T_1 = 6.2 \times 10^{-4}$ sec. The radius α of the cane sugar molecule can be estimated from its molar volume, namely, $\alpha = 4.4 \times 10^{-8}$ cm. Substituting in relation (4), we get $\tau_c \approx 1.8 \times 10^{-9}$ sec. (†). With the value of $\nu_0 = 15.4 \times 10^6$ c.p.s., the frequency used in this experiment, we get

$$(2\pi\nu_0\tau_c)^2 \approx 2.9 \times 10^{-2}, \text{ i.e. } \ll 1$$

Hence, from relation (2), we get, for protons in cane sugar solution, $T_2 \approx T_1$ ($\approx 6.2 \times 10^{-4}$ sec.).

The n.m.r. signal to noise voltage ratio is given by the following expression (1.11) :

$$\frac{V_s}{V_n} = \frac{y\zeta N\gamma_p I(1+1)h^2}{48kT} \times \left(\frac{V_c Q \nu_0^3}{kTB F} \right)^{\frac{1}{2}} \times \left(\frac{T_2}{T_1} \right)^{\frac{1}{2}} \quad \dots (6)$$

In this expression γ_p , k , T , ν_0 , T_1 and T_2 have the previous significance, y depends on the law of signal detection and ≈ 1 , ζ is the "filling factor" of our coil (≈ 0.503) N is the number of protons per cm^3 ($N = 6.58 \times 10^{22}$ for glycerine; $N = 6.5 \times 10^{22}$ for cane sugar solution); I is the proton spin ($= 1/2$); h is the Planck's constant. V_c is approximately equal to the volume of the sample coil ($\approx 3.32 \text{ cm}^3$), Q is the quality factor of this coil (≈ 253 at 15 Mcs./sec.) ν_0 is 15.5 Mcs./sec. for glycerine and 15.4 Mcs./sec. for cane sugar solution. B is the band width of the indicating instrument, namely, the level recorder used in our experiment (3) and $B \approx 6.1$ c.p.s. (measured value). F is the effective noise figure of the amplifier system. It has not been possible to measure F and we have eliminated this factor by making comparative measurements under almost identical adjustments of all parts of the apparatus.

As mentioned in the previous report (3), we get, at 23°C , $20 \lg (V_s/V_n)$ equal to 14.0 db. for glycerine and 12.2db. for cane sugar solution, both containing almost equal amount of Cu^{++} ions, as aforesaid. On substitution of numerical values in relation (6) we now get, (T_2/T_1) in glycerine $= 1.43 \times (T_2/T_1)$ in cane sugar solution. However, it has been shown above that (T_2/T_1) in cane sugar solution is ≈ 1 and T_1 in glycerine $\approx 1.3 \times 10^{-4}$ sec. It follows that T_2 in glycerine is 1.9×10^{-4} sec. This value of T_2 in glycerine has the same order of magnitude as that assigned to it in the same liquid, namely $T_2 = 1.3 \times 10^{-4}$ sec., elsewhere in this paper. This fact supports our assumption about the near equality of T_2 and T_1 in glycerine and cane sugar solution in the presence of paramagnetic ions.

(†) For water molecules in the same system, we get $\tau_c \approx 5.7 \times 10^{-11}$ sec.

ACKNOWLEDGMENT

The author is indebted to Professor E. W. Guptill, Head, Department of Physics, Dalhousie University for providing all necessary laboratory facilities. He is grateful to Professor W. J. Archibald for a very stimulating discussion. It is also a pleasure to thank the National Research Council of Canada, Ottawa for the award of an overseas postdoctoral fellowship.

REFERENCES

- Andrew, E. R. 1958. *Nuclear Magnetic Resonance*, Cambridge University Press, London, 1st edition.
- Bloch, F., Hansen, W. W. and Packard, M. E. 1946. *Physical Review*, **70**, 474.
- Bloembergen, N., Purcell, E. M. and Pound, R. V. 1948. *Physical Review*, **73**, 679-712.
- Bloembergen, N. 1961. *Nuclear Magnetic Relaxation*, W. A. Benjamin, Inc., New York.
- Chiarotti, G., and Giulotto, L. 1953. *Nuovo Cimento*, **10**, 54-71.
- D'Ans, J., and Lax, E. 1949. *Taschenbuch fuer Chemiker und Physiker*, **2**. Auflage, Springer-Verlag, Berlin.
- Gabillard, R. 1952. *La Revue Scientifique, Paris*, **90**, 307.
- Gorter, C. J. 1947, *Paramagnetic Relaxation*, Amsterdam New York.
- Guptill, E. W., Archibald, W. J., and Warren, E. S. 1950. *Canadian Journal of Research, Sect. A.*, **28**, 359-66.
- Mukherjee, S. K. 1964. *Report dated May 30*, (forwarded to the National Research Council, Ottawa, Canada).
- Solomon, I. 1955. *Physical Review*, **99**, p. 559.

ON THE ABSORPTION SPECTRA OF Ni^{++} ION IN AQUEOUS SOLUTION

N. S. CHHONKAR*

PHYSICS LABORATORIES, BURDWAN UNIVERSITY, BURDWAN, INDIA

(Received July 23, 1965; Resubmitted June 15, 1966)

ABSTRACT. Oscillator strength of a dozen of nickel salts in aqueous solution were calculated following Van Vleck, Tanabe and Sugano, and Jørgensen from the absorption density measurements. It was observed that stronger the cubic portions of the crystal field the greater were the oscillator strength. The effect of the crystal field on oscillator strength provides a basis to say that the red band splitting is not due to first order L-S coupling or due to second order intermixing in agreement with the findings of Mookherji and Chhonkar that the splitting is due to tetragonal field.

INTRODUCTION

Considerable amount of experimental (Mookherji and Chhonkar 1959, 1960, Chhonkar 1964) and theoretical (Holmes and McClure 1957, Liehr and Ballhausen 1959, Englman 1961) work on the absorption spectra of Ni^{++} ions in state of solution and in crystalline state has been carried out. The characteristics of absorption bands are position, band width and intensity. The positions of absorption bands of Ni^{++} ions in aqueous solution and in different organic solvents have been correlated to some details by the assumption of a crystalline electric field predominantly cubic in nature on which is superimposed a small tetragonal component. It was Mookherji and Chhonkar (1960) who first showed that the splitting of the red band into bands II and III was due to tetragonal field. Later on Bose and Chatterji (1963) applied a rhombic component instead of tetragonal in case of Ni^{++} ions in crystals and got a good agreement with the observed values of Hartmann *et al* (1958.)

The intensity which is proportional to the area of the absorption curve and consequently proportional to the oscillator strength contains information as to the nature of the transition. The line shape gives us information about the environments of the absorbing ion. Our work (1964) on Ni^{++} ions in organic solvents definitely establishes that the cluster about Ni^{++} is more anisotropic than that in aqueous solution and hence the influence of environments. All the previous works were concerned with correlating the oscillator strength of these absorption bands as spin-forbidden spectral transitions taking the field as cubic in symmetry. Experimental findings of Krishnan and Mookherji (1938) do not support a cubic field. In order to understand the behaviour of variation of cubic

*Now at the University of Cape Coast, Ghana.

field on the oscillator strength we have calculated the oscillator strength from the observed absorption density in a number of Nickel salts in aqueous solution in which the strength of cubic field coefficients varied considerably.

The present communication gives an account of the above studies.

EXPERIMENTAL

The experimental details have been discussed by Mookherji and Chhonkar (1959, 1960). For the study in the ultra-violet region the glass prism was replaced by a quartz prism. The measurements were carried out by using stoppered fused silica cells. The variations of absorption in different salt solution are shown graphically in fig 1 to 20. (Mookherji and Chhonkar 1960).

RESULTS

The results of measurements are collected in Table I. The oscillator strength P is given approximately by the relation (Jørgensen 1962)

$$P = 4.60 \times 10^{-9} E_n [\delta(-) + \delta(+)],$$

where E_n is the molar extinction coefficient, n is the band number and $\delta(-)$, $\delta(+)$ are half widths towards smaller and larger wave-lengths. E_n is given by $E_n CX = -\log(I/I_0) =$ absorption density. (C is the concentration per mol per

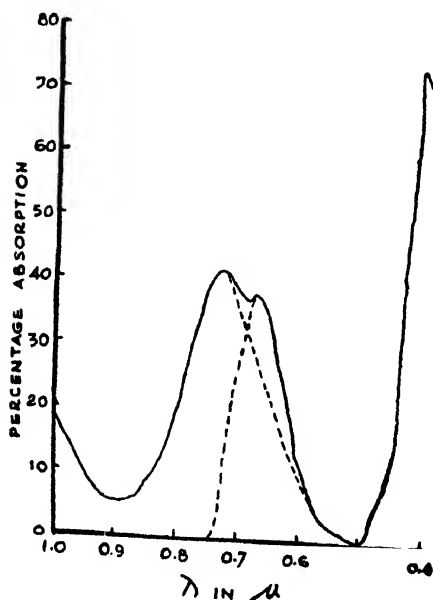


Fig. 1. Absorption curve of NiSO_4 solution (0.1068M).

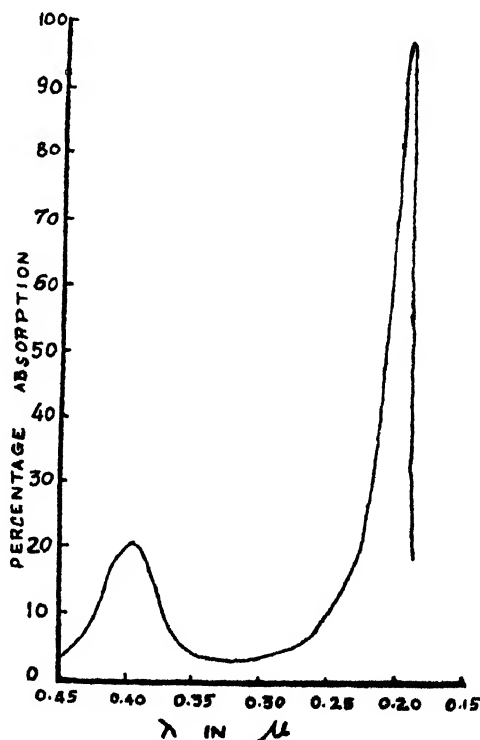


Fig. 2. Absorption curve of NiSO_4 solution (0.0178M).

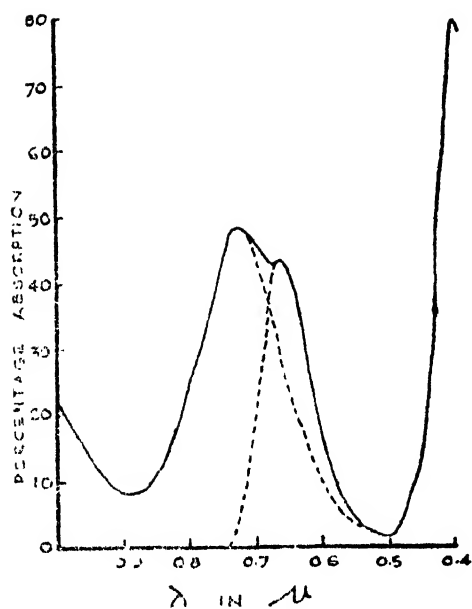


Fig. 3. Absorption curve of $NiSeO_4$ solution (0.129M).

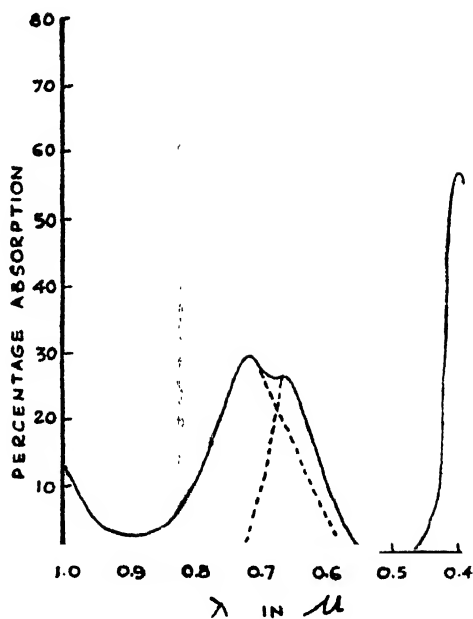


Fig. 4. Absorption curve of $Ni(NH_4SO_4)_2$ solution (0.076M).

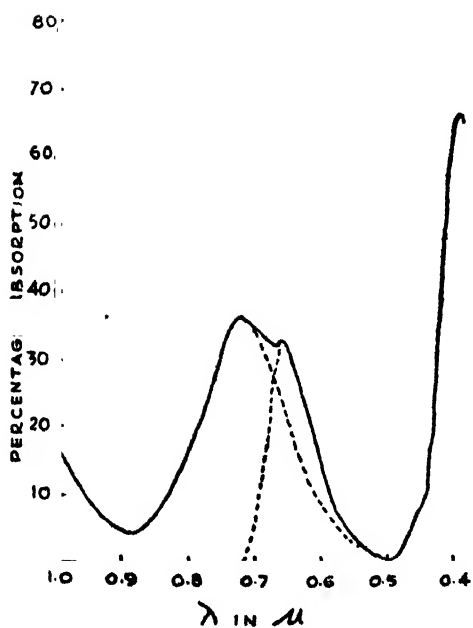


Fig. 5. Absorption curve of $Ni(K_2SO_4)_2$ solution (0.0913M).

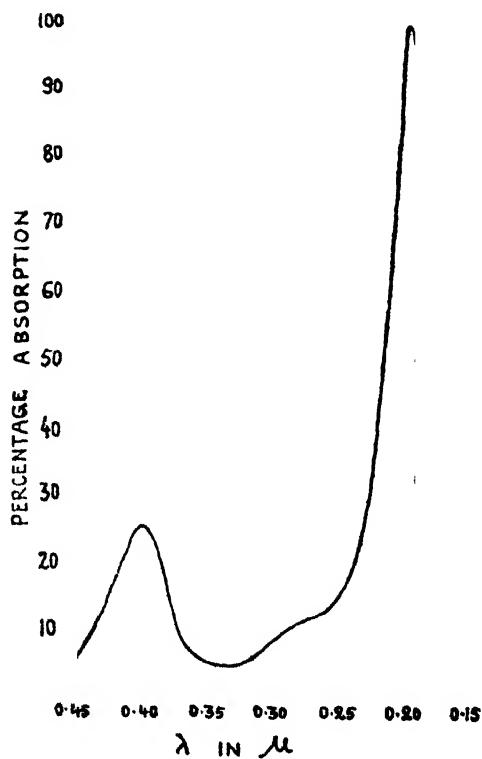


Fig. 6. Absorption curve of $Ni(K_2SO_4)_2$ solution (0.0229M).

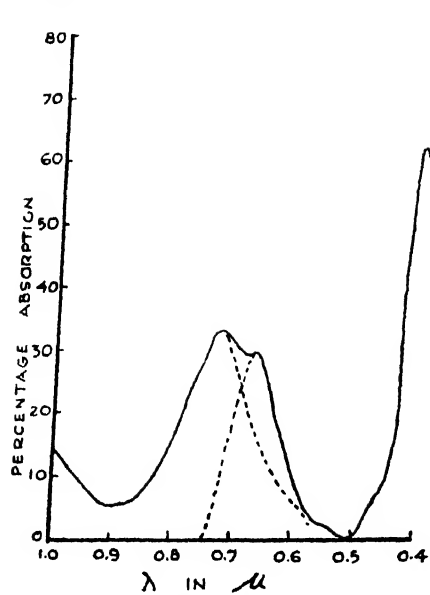


Fig. 7. Absorption curve of $\text{Ni(Rh}_2\text{SO}_4)_2$ solution (0.0727M).

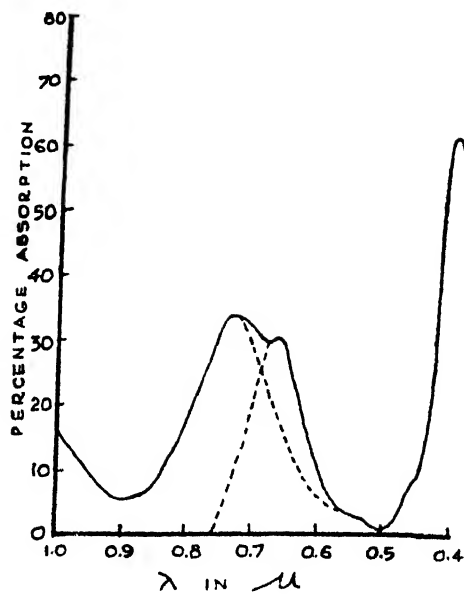


Fig. 8. Absorption curve of $\text{Ni(NH}_4\text{SeO}_4)_2$ solution (0.0818M).

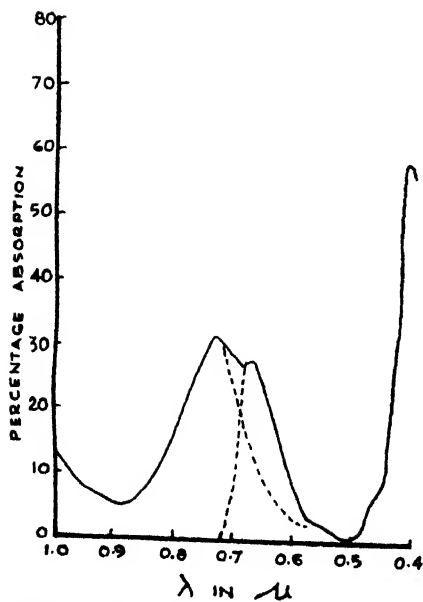


Fig. 9. Absorption curve of $\text{Ni(K}_2\text{SeO}_4)_2$ solution (0.0753M).

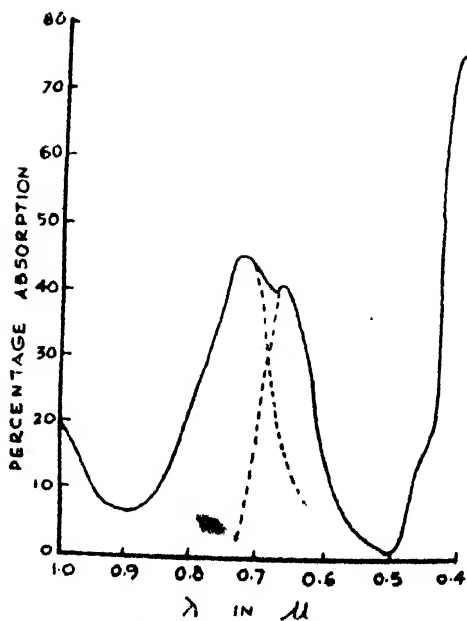


Fig. 10. Absorption curve of NiCl_2 solution (0.1252M).

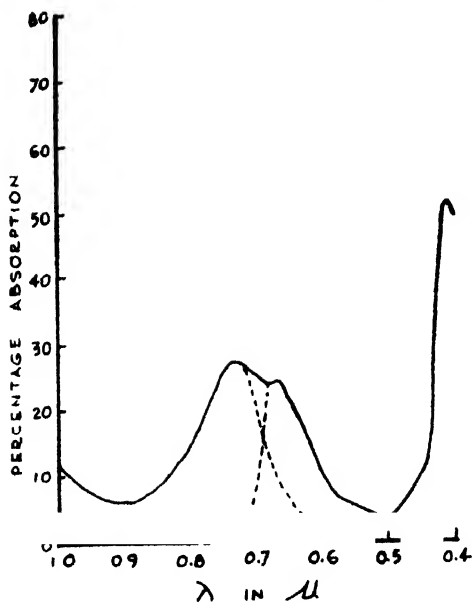


Fig. 11. Absorption curve of NiBr_2 solution (0.0613M).

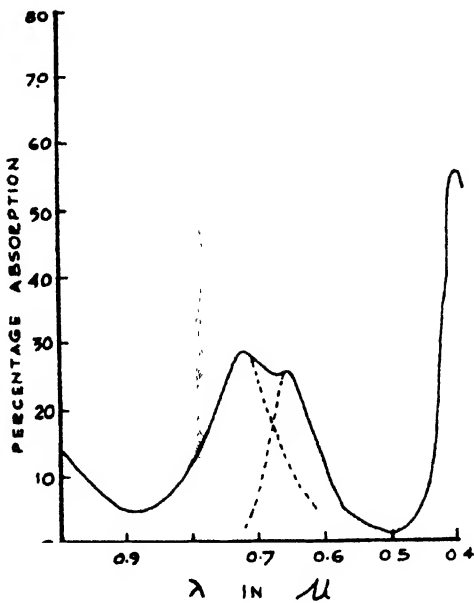


Fig. 12. Absorption curve of $\text{Ni}(\text{NO}_3)_2$ solution (0.0688M).

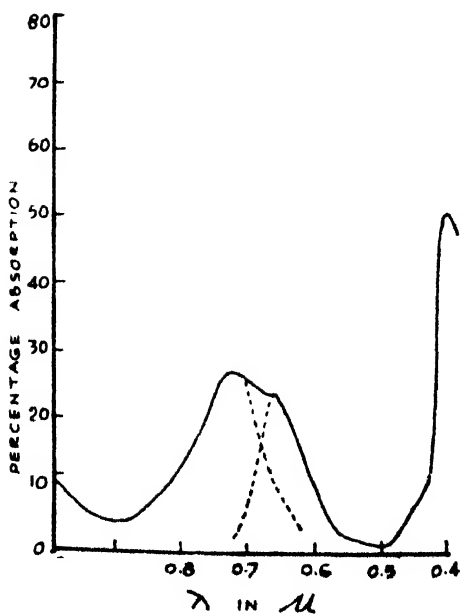


Fig. 13. Absorption curve of $\text{Ni}_3 \text{Bi}_2 (\text{NO}_3)_{12}$ solution (0.0348M)

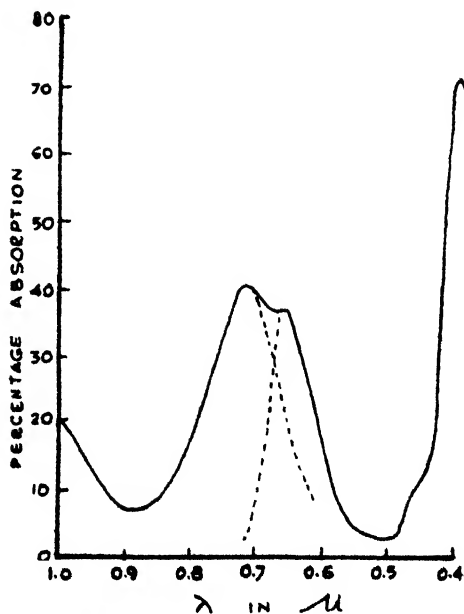


Fig. 14. Absorption curve of $\text{Ni}(\text{HCOO})_2$ solution (0.0906M)

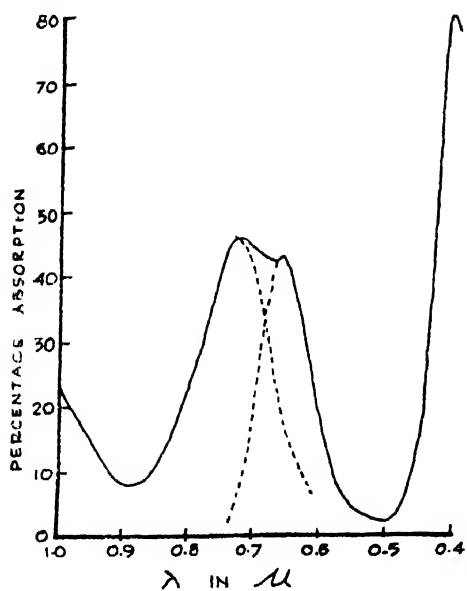


Fig. 15. Absorption curve of $\text{Ni}(\text{CH}_3\text{COO})_2$ solution (0.154M)

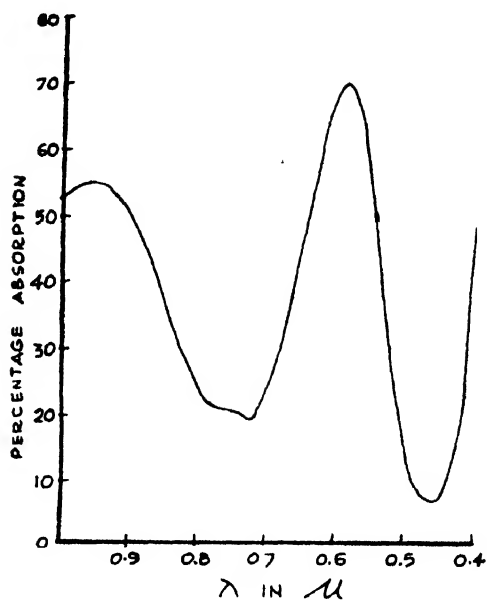


Fig. 16. Absorption curve of $[\text{Ni}(\text{NH}_3)_4](\text{SO}_4)$ (0.08M)

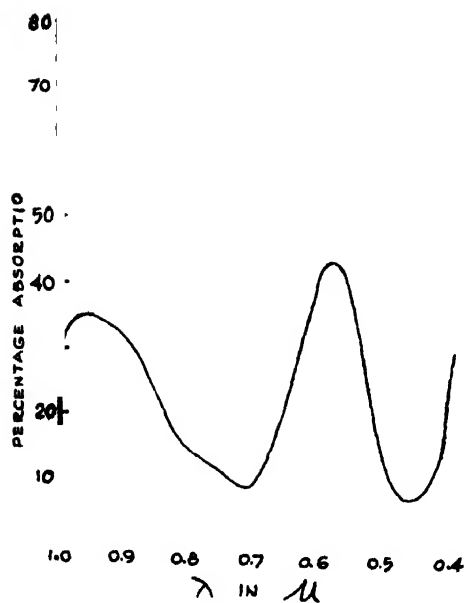


Fig. 17. Absorption curve of $[\text{Ni}(\text{NH}_3)_4](\text{OH})$ (0.162M)

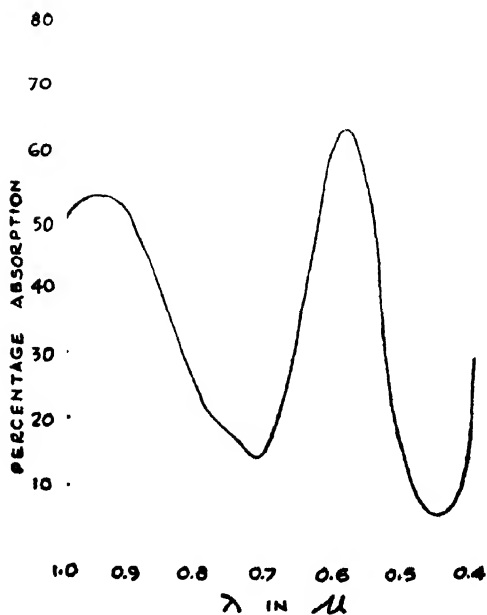


Fig. 18. Absorption curve of $[\text{Ni}(\text{NH}_3)_4](\text{Cl})$ (0.084M)

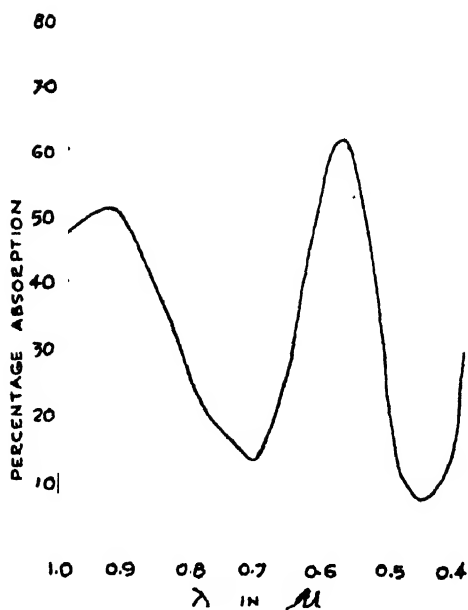


Fig. 19. Absorption curve of $[\text{Ni}(\text{NH}_3)_4](\text{CH}_3\text{COO})_2$ (0.103M)

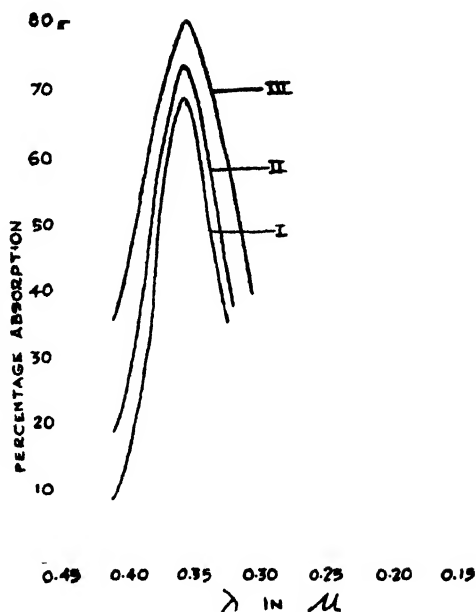


Fig. 20. Absorption curves of
 (I) $[\text{Ni}(\text{NH}_3)_4](\text{SO}_4)$ (0.0712M)
 (II) $[\text{Ni}(\text{NH}_3)_4](\text{Cl})$ (0.084M)
 (III) $[\text{Ni}(\text{NH}_3)_4](\text{CH}_3\text{COO})_2$ (0.077M)

litre per cm. thickness of the solution. The values of $\delta(-)$ and $\delta(+)$ were obtained by a Gaussian analysis and hence P -values could be calculated. These are given in Table I. K , the cubic field coefficient, are taken from Mookherji and Chhonkar (1960).

DISCUSSION

For all the salts studied the absorption spectra are characterised by three band maxima II, III and IV.

An estimation of the P -values following Van Vleck (1937) and Chhonkar (1964) for the bands II, III and IV are given in Table I.

Most of the theoretical workers subjected Ni^{++} ion to a crystal field of cubic symmetry. Under such a field the ground state $^3\text{F}_4$ splits into three levels. Consequently there should be only two absorption band heads. But experimentally three bands were observed. This made these workers to attribute the splitting of the red band due to first order $L-S$ coupling or due to second order intermixing effect.

If this splittings was due to $L-S$ coupling it would have been observed for all the twelve salts of Ni^{++} ion studied by us. But no such splitting could be observed in Nickel amino salts. According to Jörgensen (1958) first order $L-S$ coupling is not capable of accounting for this splitting.

TABLE I

Salt	Band Head	Absorption density	<i>C</i>	$\delta(-)$	$\delta(+)$	$P \times 10^5$	K^*
NiSO ₄	II	.240	.1068	1250	1720	3.07	17,725
	III	.210		1120	1200	2.10	
	IV	.575		1780	1780	8.82	
Ni(K ₂ SO ₄) ₂	II	.195	.0913	1250	1720	2.91	17,745
	III	.172		720	1200	1.67	
	IV	.523		1780	1780	9.60	
Ni(NH ₄ SO ₄) ₂	II	.152	.0760	1150	1740	2.66	17,745
	III	.132		740	1100	1.51	
	IV	.366		1540	1540	6.82	
Ni(RbSO ₄) ₂	II	.171	.0727	1350	1420	3.00	17,725
	III	.150		860	1110	1.87	
	IV	.406		1790	1790	9.20	
NiSeO ₄	II	.285	.1290	1350	1530	2.91	17,725
	III	.244		930	1180	1.84	
	IV	.674		1510	1510	7.26	
Ni(KSeO ₄) ₂	II	.162	.0753	1330	1330	2.65	17,725
	III	.140		600	1200	1.54	
	IV	.377		1516	1570	6.96	
Ni(NH ₄ SeO ₄) ₂	II	.177	.0818	1330	1330	2.65	17,725
	III	.154		1120	1200	1.99	
	IV	.409		1510	1510	6.95	
NiCl ₂	II	.263	.1252	1480	830	2.23	17,725
	III	.229		1040	1130	1.83	
	IV	.640		2060	2060	9.69	
NiBr ₂	II	.137	.0613	1350	830	2.17	17,725
	III	.120		700	1200	1.71	
	IV	.312		1510	1510	7.07	
Ni(NO ₃) ₂	II	.149	.0688	1250	1250	2.49	17,725
	III	.130		620	1440	1.79	
	IV	.347		1510	1510	7.01	
Ni ₃ Bi ₂ (NO ₃) ₁₂	II	.134	.0348	1250	1000	3.99	17,745
	III	.114		650	1250	2.87	
	IV	.307		1300	1300	10.55	
Ni(HCOO) ₂	II	.227	.0906	1190	1530	3.13	17,725
	III	.200		440	1510	1.98	
	IV	.544		1510	1510	8.38	
Ni(CH ₃ COO) ₂	II	.269	.1540	1390	1270	2.14	17,725
	III	.241		810	1460	1.62	
	IV	.664		1510	1510	5.99	
Ni(NH ₃) ₄ SO ₄	II & III	.495	.0800	2120	1950	11.60	22,115
	IV	.509	.0712	1810	2530	14.20	
Ni(NH ₃) ₄ Cl ₂	II & III	.440	.0840	1760	1480	7.75	22,470
	IV	.582		2140	2990	16.30	
Ni(NH ₃) ₄ (CH ₃ COO)	II & III	.431	.1030	2010	2220	8.17	22,512
	IV	.710		3090	3970	29.90	

If the splitting is attributed to second order intermixing, then greater the cubic field splitting the greater would have been this splitting. But our experimental finding is that in the Nickel amino salts where K , the cubic field coefficient is $\sim 22,000 \text{ cm}^{-1}$ this splitting is absent, whereas in Tutton salts where $K \sim 17,000 \text{ cm}^{-1}$ this splitting has been observed and is $\sim 1300 \text{ cm}^{-1}$.

Now coming to the question of oscillator strength of these bands we find that the group of salts having K values $\sim 22,000 \text{ cm}^{-1}$ have greater P -values than those having K -values $\sim 17,000 \text{ cm}^{-1}$ (Table I). Table I further shows that in Nickel Tutton salts P -values are different from those of nitrate and formate of Nickel and Amino salts. This clearly indicates that though the salts are in state of aqueous solution yet the environments about the absorbing Ni^{++} ion are not the same.

REFERENCES

- Bose A. and Chatterjee R. 1963. *Proc. Phys. Soc. (London)* **82**, 23.
Chhonkar N. S. 1964. *J. Chem. Soc.* **41**, 3683.
Englman, R. 1961. *Trans. Farad. Soc.* **57**, 236.
Hartman, H. and Muller, H. 1958. *Disc. Farad. Soc.* **26**, 49.
Holmes, O. G. and McClure, D. S. 1957. *J. Chem. Phys.* **26**, 1686.
Jørgensen, C. K., 1962. *Absorption spectra and Chemical bonding in complex*, Pergamon Press N. Y.
———, 1955. *Acta. Chem. Scand* **9**, 1362.
———, 1958. *Discussion Farad Soc.* **26**, 90.
Krishnan K. S., and Mookherji A., 1938. *Philos. Trans. A* **237**, 135.
Liehr, A. D. and Ballhausen, C. J., 1959. *Ann. Phys.* **2**, 133.
Mookherji A. and Chhonkar N. S. 1959. *Indian J. Phys.* **33**, 74.
———, 1960. *Indian J. Phys.* **34**, 363.
Tanabe, Y. and Sugano, S., 1954. *J. Phys. Soc. (Japan)*, **9**, 766.
Van Vleck, J. H., 1937. *J. Phys. Chem.* **41**, 67.

γ - γ DIRECTIONAL CORRELATION STUDIES AND LEVEL SCHEME OF Ba-134

R. V. RAMA MOHAN, K. VENKATA REDDY, B. B. VENKATA-
PATHI RAJU AND SWAMI JNANANANDA

THE LABORATORIES FOR NUCLEAR RESEARCH, ANDHRA UNIVERSITY,
WALTAIR. (A.P)

(Received December 10, 1965)

ABSTRACT. The decay scheme of Cs-134 is studied and the γ - γ angular correlation measurements are carried out for the cascades 605-797 keV (separated), 1368-605 keV, 963-605 keV, 565-605 keV 800-1168 keV and 432-797 keV. On the basis of experimental data on directional correlations, spin assignments are made for 605, 1168, 1402, 1568, 1645, 1834 and 1973 keV excited levels. Multipole assignments are also made for the 1368, 1040 and 963 keV transitions.

INTRODUCTION

The decay of Cs-134 with a half life of 2.2 years is highly complex. There are several excited levels in Ba-134 with an energy below 2 Mev which give rise to gamma components of different energies, leading to a complex gamma spectrum. The angular correlation study of Ba-134 is obviously complicated because of the different cascades with nearly the same energy components. A number of investigators (Coleman *et al.* 1963; Klema, 1955; Munnich *et al.* 1963; Seagart *et al.* 1963; Schrubur *et al.* 1963, and Stewart *et al.* 1955) studied the decay scheme of this nucleus and proposed different schemes which are not in agreement with one another. The levels at 1568, 1645 and 1770 keV are observed by a few investigators. These workers, however have not made any spin assignments to levels for which there are discrepancies. Hence it is essential not only to find the verity of the assignments in which there have been discrepancies but also assignments are to be made to the latter levels. Therefore a systematic study of decay scheme of Cs-134 is undertaken with a view to verify the spin assignments for the levels already studied and to assign the spin values for the levels which have not been studied so far, employing the directional correlation method.

EXPERIMENTAL DETAILS

A slow-fast triple coincidence scintillation spectrometer having a time resolution of 60 nanoseconds is designed and constructed. The head assembly consists of $1\frac{1}{2}$ " diameter and 1" thick NaI(Tl) scintillators coupled to Dumont 6292 photomultipliers, a fast amplifier and an emitter follower. The power to the photomultiplier is supplied from a well regulated negative high tension unit.

This arrangement permits direct coupling of the photomultiplier anode to the input of the EFP60 fast transient amplifier which has a band width of over 60 mega cycles per second. The output pulses from the cathode follower type of limiter has a fast rise (better than 0.01 microsecond) a flat top and a long trailing edge suitable for clipping by the shorted delay technique. There is no inversion of the pulse while passing through the fast amplifier and cathode follower type of limiter. The standard Bell *et al*, (1952) coincidence unit is used with the reversal of diode connections since the pulses encountered are negative. An integrating circuit is incorporated in the fast coincidence linear amplifier to stretch the pulses and as well as to delay it so that the delays introduced in other single channels are compensated. The triple coincidence unit is additive type cathode follower having a resolving time of 2 microseconds. Compton graded inverted cone type of shields are used around the scintillators to eliminate crystal-to-crystal scattering effects. The energy resolution of each spectrometer is found to be as 8.4% for the 662 keV gamma rays of Cs^{134} .

A cylindrical perspex container having a cavity of 4 mm diameter and 10 mm depth with a wall thickness of 0.25 mm is used as source holder. The container with source is mounted vertically at the intersection of the axes of the cylindrical crystals and is about 5 cm from each crystal. The spectrometer is initially tested for angular correlation measurements using the standard cascade of Ni^{60} and found to be quite satisfactory for the correlation measurements.

RESULTS

Initially the spectrometers are calibrated using the standard sources namely Co^{57} , Ba^{133} , Na^{22} , Cs^{137} , Mn^{56} , and Co^{60} . A good linearity is observed over the desired energy region.

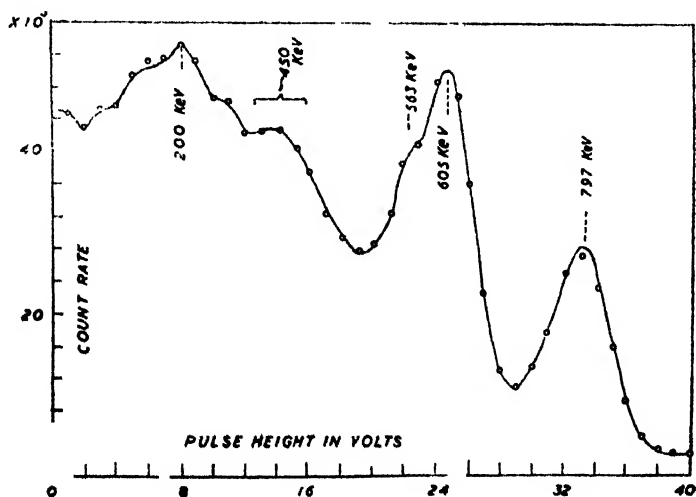


Fig. 1. Singles spectrum of Cs^{134} —lower energy side.

Employing a weak source of Cs^{134} , the singles spectrum of gamma rays is measured in 2π geometry. The count rate vs. pulse height is plotted to obtain its singles spectra as shown in figs. 1 and 2 for the regions of lower and higher

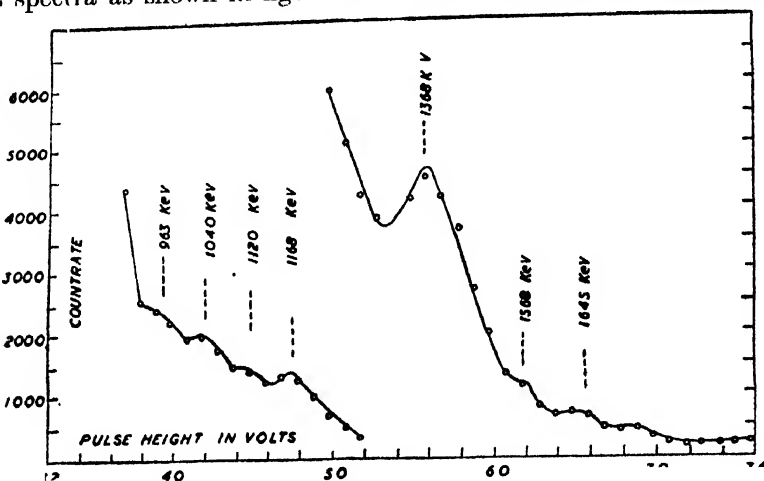


Fig. 2. Singles spectrum of Cs^{134} —higher energy side.

energies respectively. An analysis of these spectra show the presence of gamma 1370, components with energies 200, 432, 563, 605, 797, 963, 1040, 1170, 1568, 1645 and 1726 keV. The energy components 563, 605, 797, 963, 1040, 1170, 1370 and 1568 keV observed in the present investigation are in agreement with those of the results of the recent investigators. In the present analysis, the singles spectra shows two gamma components with energies 1645 keV and 1568 keV which have not been reported by others. The 1120 and 1726 keV gamma components observed in this present case are of very low intensity. It is found to be difficult to accommodate these gamma components in the present decay scheme since these are not in coincidence with any other prominent gamma component. The peak observed at 200 keV can be ascribed to the backscattering contribution.

A broad peak noticed at ~ 450 keV is certainly a gamma component with energy 432 keV which fits the transition between 1834 keV and 1402 keV excited levels. A beta component with end point energy 215 keV give rise to a level at 1834 keV. This beta component had originally been reported by Cork *et al*⁷ (1953) using a double focussing magnetic spectrograph.

Coincidence experiments are carried out employing the slow-fast type of coincidence scintillation spectrometer, in order to find out the decay scheme of Cs^{134} . The two detecting assemblies of these spectrometers are so arranged to subtend an angle of 90° between them in order to minimize the errors arising out of chance coincidences due to the crystal-to-crystal scattering. With this set up coincidence spectra are drawn by selecting the following energies 563, 605, 797, 1040 and 1368 keV in one channel for each run and scanning the other channel over the entire energy region. There is every possibility of interference between

the strong and the adjacent weak components while observing the coincidences with energies 563, 605 and 1040 keV. In order to surmount this difficulty a reasonably small gate (0.5 volt) is employed while taking the coincidence readings.

It is found that the gamma component with an energy 563 keV is in coincidence with the gamma components of energies 605 and 802 keV. The 605 keV component is in coincidence with all gamma components in the lower and higher energy regions. From the 797 keV coincidence curve it is seen that 432 keV gamma component is in coincidence with 797 keV component. From the survey of 1040 and 1368 keV coincidence spectra it can be pointed out that they are in coincidence only with the 605 keV energy gamma component. The channel width at 1368 and 1040 keV is kept 2 volts so as to receive the total radiation from the two peaks at 1368 and 1040 keV. The coincidences observed between these radiations and 605 keV gamma ray are pure and there is no need to consider the interference effects from other cascade. By observing all these coincidence spectra a level scheme for Ba^{134} is drawn as shown in the final diagram.

From the coincidence spectra it is found that there are reasonable coincidences between 1040 keV and 605 keV as well as between 963 keV and 605 keV which suggest the existence of levels at 1645 and 1568 keV excited levels which are populated by beta groups with energies 410 and 490 keV in the decay of Cs^{134} . The 797 keV gamma component is observed to be obviously coinciding with 432 keV, which predicts a level at 1834 keV. A beta feed with an end point energy 210 keV would give rise to this excited level.

The observations of angular correlation are carried out by setting the two channels to two different gamma components which are in cascade. In these observations care is taken to see that the source is intense and is veritically fixed.

TABLE I

Cascade	Present experimental results		Previous investigators results		Authors
	a_2	a_4	a_2	a_4	
605-797keV (separated)	0.098 ± 0.006	0.011 ± 0.006	0.0968 ± 0.0043 0.092 ± 0.004	0.0142 ± 0.0086 0.012 ± 0.004	Coleman Segaert et al
1368-605keV	0.011 ± 0.015	-0.0006 ± 0.001	0.09 ± 0.0086 0.107 ± 0.02	-0.004 ± 0.013 -0.006 ± 0.02	Klema Segaert et al
800-1168keV	-0.1235 ± 0.0015	0.0009 ± 0.001	0.15 ± 0.01	-0.019 ± 0.001	Segart et al.
1040-605keV	0.104 ± 0.021	-0.019 ± 0.008	0.097 ± 0.009 0.102 ± 0.024	0.023 ± 0.011 -0.037 ± 0.03	Munnich et al. Segaert et al.
565-605keV	0.021 ± 0.008	0.099 ± 0.025	0.019 ± 0.019	0.092 ± 0.029	Stewart et al.
432-797keV	-0.1119 ± 0.0042	0.1382 ± 0.0061	—	—	—
963-605keV	0.4952 ± 0.025	0.1203 ± 0.0185	—	—	—

It should be centered within 0.5% variation of the count rate. Coincidences are observed at angles 90° , $112^\circ.30'$, 135° , $157^\circ.30'$ and 180° in each run. Large number of coincidences are observed at each position in order to minimize errors arising out of statistical fluctuations. About 1000 to 2000 coincidence counts are collected at each time and the random coincidences are subtracted each time. The random coincidences are calculated using the formula $2\pi N_1 N_2$ where N_1 and N_2 are the counts from two channels and ' π ' is the resolving time of the coincidence unit. Using the true coincidence number other correlation coefficients are evaluated by the analytical method suggested by White (1963). These values are further corrected for angular resolution. The correction fraction to be applied to coefficient a_2 (measured) varies from 0.947 to 0.959 for the energy region 0 to 2 MeV and the value to be applied to a_4 (measured) varies from 0.908 to 0.921 for the same energy region.

TABLE II

Cascade in keV	proposed spin sequence	Excited level in keV	Spin value
605-797	4(Q)2(Q)0	0	0
1368-605	3(92% D + 8% Q)2(Q)0	605	2
800-1168	3(D)2(Q)0	1168	2
1040-605	3(95% D + 5% Q)2(Q)0	1402	4
563-605	2(DQ)2(Q)0	1568	2
432-797	4(Q)4(Q)2	1645	3
963-605	2(75% D + 25% Q)2(Q)0	1834	4
		1973	3

The gamma-gamma directional correlation measurements are carried out in the decay of $\text{Cs}^{134} \rightarrow \text{Ba}^{134}$ for the above mentioned cascades. The corresponding correlation coefficients are given above in a tabular form along with the results of previous investigators.

The angular correlation function $W(\theta)$ versus the angle subtended by the two detectors is plotted for all the seven cascades. The plots are shown in figs. 3 to 6.

The proposed spin sequence for the cascades along with the admixture content that are resulted in the present directional correlation studies and the spins of all excited levels are represented in the Table II.

DISCUSSION

The gates setting at 600 keV in one channel is to enclose the photopeaks comprised of the 605, 569 and 563 keV lines and 800 keV in another channel to bracket the peaks containing the 797 and 802 keV components. Therefore the

gates at these energies comprise the following cascades : 797-605 keV, 569-797 keV, 802-563 keV and 802-(563)-605 keV triple cascade. The percentage contributions of all these cascades are given as 797-605 keV (71%), 569-797 keV (1.4%), 802-563 keV (8.2%) and 802-(563)-605 keV (8.8%). The 605-797 keV cascade is

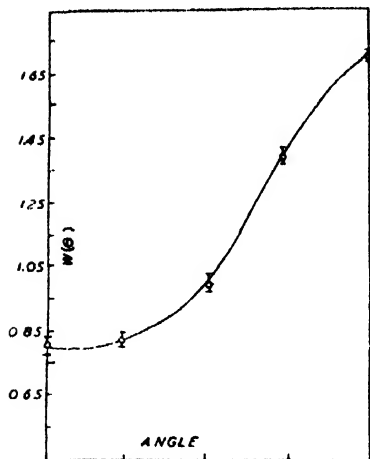


Fig. 3. Correlation plot between $W(\theta)$ vs. angle θ for 963-605 keV cascade.

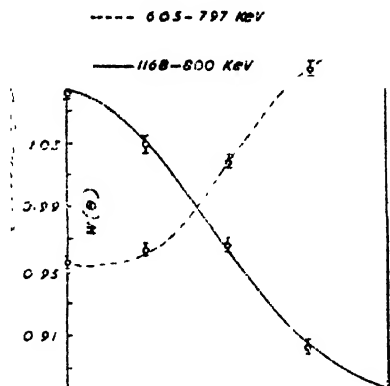


Fig. 4. Correlation plot between $W(\theta)$ vs. angle θ for 1168-605 keV and 605-797 keV (separated).

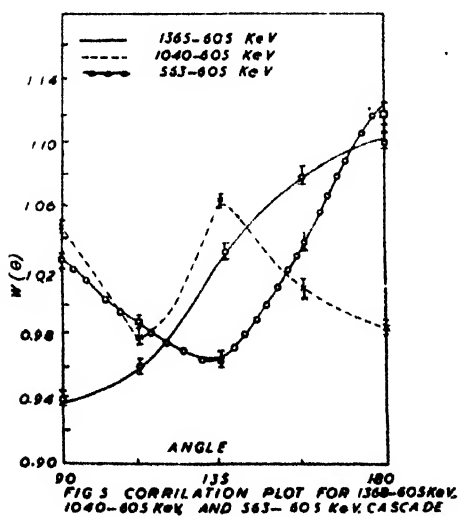


FIG. 5. CORRELATION PLOT FOR 1368-605 keV, 1040-605 keV AND 563-605 keV CASCADE

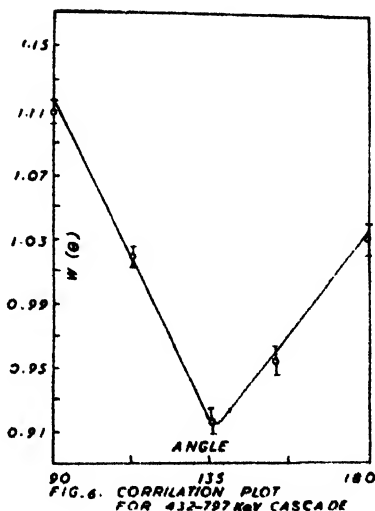


FIG. 6. CORRELATION PLOT FOR 432-797 keV CASCADE

separated from the others by shifting the analyzer window of the first channel to the high energy side of the 605 keV peak to eliminate the contributions of 569 and 663 keV radiations. The values of the correlation coefficients thus obtained after eliminating the interference effects of other adjacent cascades are in agreement

with those theoretically computed values with the sequence $4(Q)2(Q)0$. Further interpretation of angular correlation coefficients is difficult in view of the fact that there are various interfering cascades.

The angular correlation study with gates set at 565 and 605 keV comprise the double cascade 563-605 keV and triple cascade 569-(797)-605 keV. The percentage contributions reported by Munnich *et al* are 64% and 36% respectively. Taking the percentage compositions into consideration, the spin sequence $2(DQ)2(Q)0$ resulted for the 563-605 keV cascade and either $3(D)4(Q)2(Q)0$ or $4(D)4(Q)2(Q)0$ for the 569-(797)-605 keV cascade.

The theoretical correlation coefficients for $2(DQ)2(Q)0$ sequence with mixing ratio 0.5768 and with 75% dipole content are in close agreement with the experimentally obtained coefficients for 963-605 keV cascade. The admixture content in 963 keV transition is obtained from the extrapolated plot of fig 7. The correlation coefficients for 1040-605 keV are consistent with $3(DQ)2(Q)0$ sequence with 95% dipole admixture in 1040 keV transition. Segaert *et al* (1963) reported the

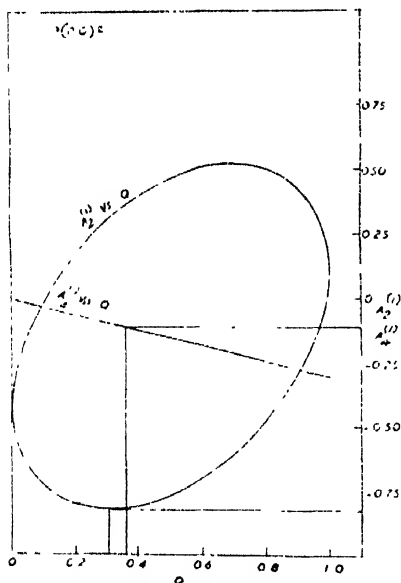


Fig. 7. Multipole admixture plot for the 963 keV transition.

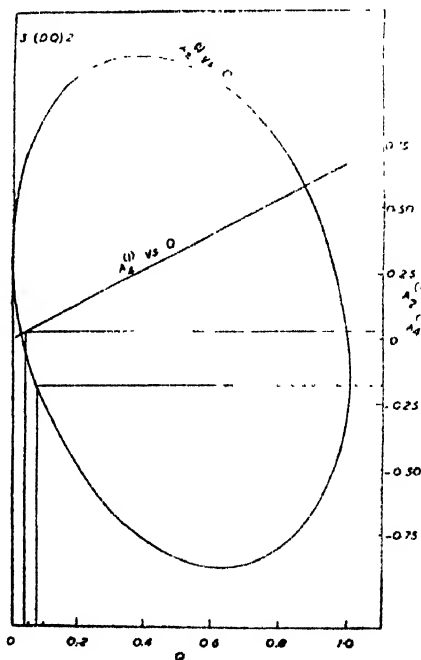


Fig. 8. Admixture content in 1040 keV gamma transition. ■

spin sequence for this cascade as $4(Q)2(Q)0$ due to the fact that they could not observe the ground state transition with 1645 keV which, in turn, if observed supports $3(DQ)2(Q)0$ sequence. However in the present analysis a radiation with energy 1645 keV is observed and the angular correlation coefficients are consistent with the $3(DQ)2(Q)0$ sequence. The mixing ratio obtained after

calculation is $\delta = \pm 0.2949$. The 95% dipole content in the 1040 keV transition is represented in the multipolarity graph for 3(DQ)2 as shown in fig. 8.

After comparing the values of a_2 and a_4 obtained from the present experimental investigation with theoretical coefficients for different spin sequences for 432-797 keV cascade, it is found that only 4(Q)4(Q)2 sequence agrees well with the present values. From this investigation a spin value of 4 units is assigned to the 1834 keV excited level and the 432 keV gamma component results from a transition from the 1834 keV level to 1402 keV level which is considered as pure transition. This cascade is considered as only due to the coincidences observed between 432 keV and 797 keV radiations. A further investigation on this transition will be useful in establishing the properties of the 1834 keV excited level.

The spin value of the ground state of Cs^{134} has been reported as 4 by Klema and the change of spin for 80 keV beta transition has been reported as 0, ± 1 . the 605 keV transition has been established predominantly as E_2 and life time of the first excited state was found to be 3×10^{-9} sec. (Bell *et al*, 1949). Hence it is assumed that correlation is not affected by external fields. From these results it is evident that 1973 keV level of Ba^{134} must have any one of the values 3, 4 or 5 for its spin. If a value of 5 is to be assigned for the spin of 1973 keV level, an admixture of $M3 + E4$ would result in the 1368 keV transition which is ruled out on the basis of life time considerations of the levels.

In the experimental analysis of the present investigation the correlation coefficients are in agreement with the theoretical coefficients of the 4(Q)2(Q)0

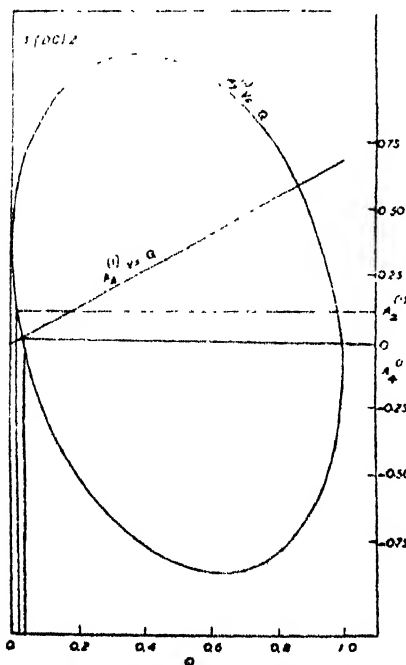


Fig. 9. Quadrupole content in 1368 keV transition.

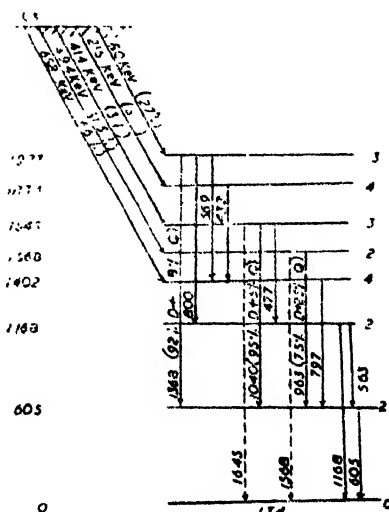


Fig. 10. Final decay scheme of Cs^{134} .

sequence with a spin value of 4 units for the level at 1973 keV. On this basis the 1168 keV transition should be E3 or E3+M4, but the conversion coefficients for such a transition are not in agreement with the measured conversion coefficients for this transition. Hence the 1368 keV transition is a pure quadrupole for which also the conversion coefficient is not in agreement with the measured values. From these considerations the assumption of spin 4 makes a poorer fit. Next considering the spin value of 3 units for the 1973 keV level, the coefficients are in good agreement with theoretical coefficients of 3(DQ)2(Q)0 sequence with large dipole admixture in 1368 keV transition. (fig. 9.). The conversion coefficients for this sequence are consistent with the measured values.

The cascade 800-1168 keV is studied in order to assign the spin value of the level at 1973 keV. As a result the values of a_2 and a_4 lead to the spin sequence 3(DQ)2(Q)0. From the results obtained on the study of the two cascades mentioned above, it may be concluded that the excited level with energy 1973 keV be assigned with a spin value of 3 units and the transition with energy 1368 keV has 92% dipole radiation as can be noted from fig. 9.

From the results of the present investigation on Cs¹³⁴, a decay scheme is proposed as shown in fig. 10. The spin assignments for 605 and 1168 keV levels obtained in the present work are consistent with the values of Mallman (1961) and Davydov *et al*, (1960). The spin 3 of the 1645 keV level can be said to be consistent with the assumptions of vibrational model of Wilets *et al*, 1956.

According to Mallman's theoretical calculations the spin value for the level at 1568 keV is either 1 or 3 and the level at 1645 keV is 3 or 4. In the present investigation the spin at these levels are not in agreement with the predictions of any other except of Mallman. The spin value 3 for the 1973 keV excited level is not in agreement with any one of the theoretically computed values on the basis of the existing models (see references). Hence the results of this excited state is open for further study and discussion.

REFERENCES

- Bell, R. E. and Jeans, M. 1949. *Phy. Rev.* **76**, 1409.
 Bell, R. E., Graham, R. L. and Petch, H. E. 1952. *Canad. Jour. Phys.* **30**, 35.
 Bohr, A. and Mottelson, B. 1953. *Mat. Phy. MeddDon. Vid Selskab.* **27**, no. 3.
 Coleman, L. W. and Schectel, L. 1963. *Nucle. Phys.* **20**, 661.
 Cork, J. M., LeBlanc, J. M., Neslie W. H., Martin, D. W. and Brice, M. K. 1953. *Phy. Rev.* **90**, 444.
 Davydov, A. and Chaban, A. 1960. *Nucl. Phys.* **20**, 499.
 Davydov, A. and Filippov, G. 1958. *Nucl. Phys.* **8**, 237.
 Goldhaber, M. and Hill, R. 1952. *Rev. Mod Phys.* **24**, 179.
 Klema, E. 1955. *Phy. Rev.* **90**, 66.
 Mallman, G. 1961. *Nucl. Phys.* **24**, 533.
 Munnich, F., Fricke, K. and Welloner. 1963. *Z. Fur. Physik* **174**, 68.
 Scharff-Golchaber, G. and Wenner, J. 1955. *Phy. Rev.* **98**, 212.
 Schrubur, S. O. and Hogg, B. G. 1963. *Nucl. Phys.* **48**, 647.
 Seagart, G. L., Demuynek, J. L., Dorikens-Vanfraet, L. V. and Dorikens, M. 1963. *Nucl. Phys.* **48**, 76.
 Stewart, M. G., Scharenberg, R. P. and Wiedenbeck, M. L. 1955. *Phy. Rev.* **99**, 691.
 Raz, B. 1959. *Phy. Rev.* **114**, 1116.
 White, W. H. 1963. *Nucl. Inst. and Methods* **21**, 209.
 Wilets, L. and Jeans, M. 1956. *Phy. Rev.* **102**, 788.

AN ISOTOPE EFFECT IN THE COLLECTION OF RECOILED PRODUCTS OF C_2H_5Br , $C_2H_4Br_2$ AND CH_2Br_2

A. LAL

DEPARTMENT OF PHYSICS,
BANARAS HINDU UNIVERSITY,
VARANASI-5.

(Received February 19, 1966)

ABSTRACT. The present work reports a study of the collection of the recoil products of ethyl bromide, ethylene dibromide and methylene dibromide and the associated isotope effect. The effect has been observed on both the anode and the cathode using a Ra + Be source of 300 mC. A possible explanation for the higher enrichment on the anode and for the isotope effect has been attempted on the basis of 'Auger Electron Hypothesis' recently suggested by Geissler and Willard.

INTRODUCTION

In an earlier paper henceforth referred to as I, Arnikaar and Lal (1960) reported the isotope effect in case of the compound bromo-benzene following purely a physical method. The characteristic values ($\gamma/\sigma n$) were calculated with the help of cross-section (σ), abundance (n) and the yield (γ) of the bromine isotopes collected on the electrodes. The yields obtained on one of the electrodes showed the occurrence of a notable isotope effect in the formation and collection of the isotopes Br-80 and Br-82 in contrast with its absence between the two isomers Br-80 and Br-80m as shown by their characteristic values ($\gamma/\sigma n$).

There is lack of agreement in respect of whether or not an isotope enrichment occurs in the products of recoil processes. Fox and Libby (1952), Rowland and Libby (1953) and Chien and Willard (1954) find no isotopic effect in the retention in the case of iso- and *n*-propyl bromide, while Shaw (1951, 1956) as well as Capron *et al* (1952, 1953) observe the isotopic effect at least in the case of aromatic compounds. Capron *et al* (1958) were the first to report isotope effect in liquid phase using the radio chromatographic technique.

The spectrum of gamma rays of neutron capture is different for the isotopes Br-80 and Br-82 therefore, it is natural to expect variations in the behaviour of isotopes of bromine activated by (n, γ) process. The success with bromobenzene encouraged to investigate the isotope effect in liquid phase with other organic compounds such as C_2H_5Br , $C_2H_4Br_2$ and CH_2Br_2 following the charged plate technique. The reason behind adopting the charged plate technique is not only its simplicity, but also the fact that one of the best methods of collecting radioelements

free from any inactive material is the application of an electric field either to the gaseous or to the liquid phase. The failure of the chemical method in observing the isotope effect with ethyl bromide and methylene dibromide is well known (Nesmeyanov *et al* 1959, Shaw 1957) while we have succeeded in observing the effect with the charged plate technique. Further, in our experiments it was unnecessary to have the presence of any foreign halogen atoms to observe the effect as mentioned by Nesomeyanov *et al* (1961). The present paper deals with the results for the collection on charged plates of radioisotopes of bromine in a state of high specific activity and the associated isotope-effect.

EXPERIMENTAL

About 350 ml. of the organic compound was irradiated in a silica glass beaker with a 300 mC Ra-Be neutron source with an integral intensity of 3.2×10^6 N cm²/sec plunged in the liquid. The neutron source was surrounded with 2.2 cm of paraffin and a thin walled glass tube. The electrodes consisting of two parallel plates of silver with a trace of AgBr were placed nearly 6 cms apart and symmetrically with respect to the plunged neutron source. The beaker, containing the

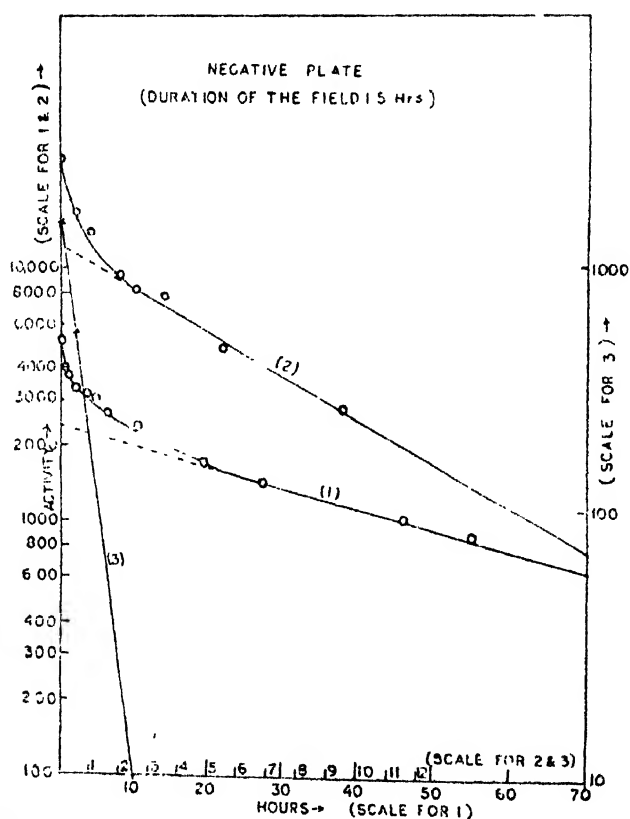


Fig. 1. Analysis of the decay curves of the activity collected on the cathode.
1. Decay curve : Br-80, Br-80m & Br-82 ; 2. Decay curve : Br-80 & Br-80m,
3. Half line : Br-80.

organic substance for irradiation was sealed with a circular glass plate. Further the system was completely surrounded, from all sides, with paraffin blocks of 1.5" thickness in order to check the escaping neutrons. The target substance was put for irradiation for a period of 9 days, in every experiment, corresponding to six times the half-life of the longest lived isotope. During the end of irradiation the electric field was applied for one and half hours or for five hours as required.

The electrodes, after drying, were put beneath a G.M. counter for measurement of the activities. Normally the counting was done by introducing the silver plates in the grove of the lead castle mounted along with the end window Saip counter. Liquid activity was also determined, with the help of a Mullard liquid G.M. counter, by measuring the activities before and after applying the electric field. Thus it gave a measure of 'retentivity' which was found to vary between 60 and 70% for all the isotopes considered together.

RESULTS

The activities collected on the electrodes were measured with the help of a thin end window Saip G.M. counter separately. They were plotted on a semilog paper against time and the analysis of the decay curves so obtained gives the

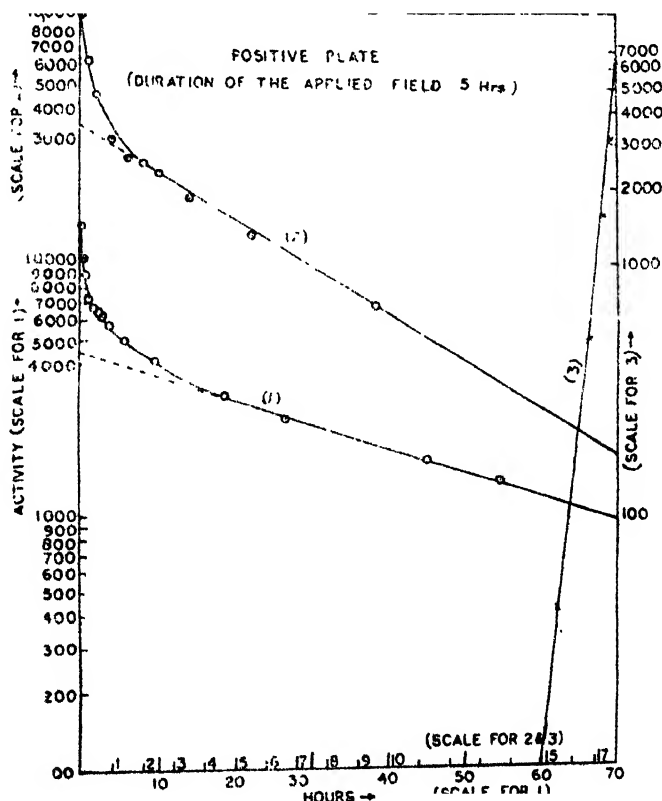


Fig. 2. Analysis of the decay curves of the activity collected on the anode.
 1. Decay curve : Br-80, Br-80m & Br-82 ; 2. Decay curve : Br-80 & Br-80m,
 3. Half life line : Br-80.

fractional yield of the various species of radio-isotopes present during the application of the field. These decay curves (figs. 1 and 2) which are the typical of numerous observations show that the activities produced are Br-80, Br-80m and Br-82. It is quite probable that some of the last activities were directly formed from the target Br-79.

The relative yields of the different activities collecting on the electrodes are given in Table I and II are typical of a series of experiments.

TABLE I(A)
Duration of the Applied Field-1.5hrs.

Irradiated Compound	Activity	Anode	Cathode
$C_2H_4Br_2$	Total	9,200	5,173
	36 hr.	3,800	2,450
	18 min.	2,300	1,573
	4.4 hr.	3,100	1,150
CH_2Br_2	Total	10,580	5,948
	36 hr.	4,200	3,000
	18 min.	3,180	1,748
	4.4 hr.	3,200	1,200
C_2H_5Br	Total	6,339	3,572
	36 hr.	2,400	1,800
	18 min.	2,139	1,112
	4.4 hr.	1,800	660

TABLE I(B)
Duration of the applied field -5 hrs.

Irradiated Compound	Activity	Anode	Cathode
$C_2H_4Br_2$	Total	14,076	5,692
	36 hr.	4,200	3,800
	18 min.	5,976	777
	4.4 hr.	3,900	1,115
CH_2Br_2	Total	14,764	6,375
	36 hr.	4,600	4,200
	18 min.	6,364	1,000
	4.4 hr.	3,800	1,180
C_2H_5Br	Total	3,308	1,586
	36 hr.	1,080	575
	18 min.	1,328	841
	4.4 hr.	900	170

The periods of the Br-80 isomers are such that they reach transient equilibrium during the irradiation period. Hence one half of the total 4.4 hr. activity measured is due to the daughter product. This 'half' value together with the 18 min. activity directly formed from the target represents the total Br-80 collected.

Table II(A and B) shows the net values of the different radio-isotopes directly formed from the target.

TABLE II(A)

Compound	Isotopes	Anode	Cathode
$C_2H_4Br_2$	Br-82	3,800	2,450
	Br-80	2,300	1,573
	Br-80m	1,550	575
CH_2Br_2	Br-82	4,200	3,000
	Br-80	3,150	1,748
	Br-80m	1,600	600
C_2H_5Br	Br-82	2,400	1,800
	Br-80	3,135	1,112
	Br-80m	900	330

TABLE II(B)

Compound	Isotopes	Anode	Cathode
$C_2H_4Br_2$	Br-82	4,200	3,800
	Br-80	5,976	777
	Br-80m	1,950	557
CH_2Br_2	Br-82	4,600	4,200
	Br-80	6,364	1,000
	Br-80m	1,900	590
C_2H_5Br	Br-82	1,080	575
	Br-80	1,328	841
	Br-80m	450	85

DISCUSSION

The maximum energy of the recoiled atoms of bromine, after (n, γ) reaction, carried out on thermal neutrons is equal to 174 ev. The capture of a neutron is accompanied by 3-4 gamma quanta, therefore it can be expected that the average energy of the recoil atoms of bromine will be of the order of 40-50 ev. On the attainment of this much of energy reactions with the participation of recoil atoms become possible. These reactions leading to stable end products are responsible for the reaction of the type (I).



In gaseous state, bromine atoms or ions produced, as a result of (n, γ) reaction, are able to undergo bimolecular displacement reaction (Willard, 1961). But it is difficult to say accurately about the history of a hot atom in a liquid. It will be also difficult to predict about the effect of the dense molecular environment of the liquid upon the bromine species from the information of the mechanism of such reactions. But the high retention observed in Szilard Chalmers' reaction suggests the above reaction,

The result of Capron *et al* (1946) point to the appearance of ionization at some stage in the process of recoil. Both positively and negatively charged species of Br-80 and Br-82 have been found in our experiments. Whatever may be the duration of the applied field, it is observed invariably that there is a higher enrichment of negatively charged species than the positive ones. Not only the negatively charged species of Br-80 are more compared to positively charged Br-80 but a similar occurrence of Br-82 species has also been observed. This suggests, probably, that there is a similarity in the behaviour of Br-82 and Br-80 recoiled atoms at least regarding their collection on the electrodes. We know that Br-80 exists in two states i.e. Br-80m and Br-80. The meta-stable state Br-80m decays with a half life of 4.4 hrs with the emission in series of two gamma quanta of energies 49 keV and 37 keV respectively to ground state of 18 minutes half life (Strominger *et al* 1958). Emery (1965) and Anders (1965) have found out recently that Br-82 exists in a metastable state with a half life of nearly 6 minutes. The metastable state of Br-82 i.e. Br-82m decays with the emission of a gamma quanta of energy 43 keV to ground state of 36 hrs. half life. Due to high factor of internal conversion associated with the transitions of Br-80m \rightarrow Br-80 and Br-82m \rightarrow Br-82 a good fraction of the initially formed Br-80 and Br-82 are expected to be in the positively charged state following considerable electron loss due to Auger effect. The accumulation of charge due to Auger effect may lead to molecular dissociation as shown by Goldsmith and Bluerer (1950). The occurrence of such molecular dissociations were considered theoretically by Cooper (1942) on the basis of Franck-Condon principle. Studies in the field of (n, γ) reaction on the halogen molecules have demonstrated that the C-Br bond ruptures in virtually every event (Suess 1940, Libby 1941 and Wexler and Davies 1952). In most of the cases the halogens are found to bear a positive charge. These considerations account for the positively charged species and of the concentration of Br-80 and Br-82. Consequently, under a high electric field there should be a higher enrichment on the cathode. But the results obtained point that it is not the initial charge of the fragments, but their subsequent history that determines on which electrode they will be deposited.

Considering the results of isomeric transition Geissler and Willard (1963) have put forward a new hypothesis known as 'Auger Electron Hypothesis'. According to them, the reaction



does take place. This arises because of the localised radiation chemistry created by the internal conversion and the Auger electrons emitted by the recoil atoms. On the basis of this hypothesis the higher yield observed on the anode is easily computable. Further the contribution to the high activity of negatively charged species of Br-80m can be accounted to their high cross-section. It is found during the course of experiments that the activity of the positive electrode is much affected

compared to that of the cathode when the duration of the applied field is small (i.e. 1.5 hrs.) This observation points out that the negatively charged species develop during the collection. This supports the reaction suggested by Geissler and Willard.

The occurrence of an isotope effect on the relative yields of radioisotopes Br-80, Br-80m and Br-82 collected on an electrode has already been reported in case of bromobenzene following charged plate technique. As given earlier the relative yields (γ_i) for a given species is

$$\gamma_i = \theta_i n_i \sigma_i$$

where σ_i , n_i and θ_i are the capture cross-section, the amount of target nuclei and the fraction of the given products finally collecting on an electrode respectively. This would be the same for all species in the absence of an isotope effect. Tables III(A) and III(B) show the relative yield together with the available data for percentage natural abundance and capture cross-section (σ) of the corresponding target nuclei Br-79 and Br-81.

TABLE III(A)
Duration of the Applied field -1.5 hr.

Irradiated Substance	Target data	σ (barns)	Abundance n%	Product Yields			
				γ	Anode $\gamma/\sigma n$	γ Cathode	$\gamma/\sigma n$
C ₂ H ₄ Br ₂	Br-79 (18 min)	8.5	50.5	2,300	5.3	1,573	3.6
	Br-79 (4.4 hr.)	2.9	50.5	1,550	10.0	575	2.9
	Br-81 (36 hr.)	3.5	49.5	3,800	22.2	2,450	15.0
CH ₂ Br ₂	Br-79	8.5	50.5	3,180	7.5	1,748	4.0
	Br-79	2.9	50.5	1,600	10.9	600	4.1
	Br-81	3.5	49.5	4,200	24.5	3,000	17.5
C ₂ H ₅ Br	Br-79	8.5	50.5	2,139	5.0	1,112	2.5
	Br-79	2.9	50.5	900	6.1	330	2.2
	Br-81	3.5	49.5	2,400	14.0	1,800	10.5

TABLE III(B)
Duration of the applied field -5 hours

Irradiated Substance	Target data	σ (barns)	Abundance n%	Product Yields			
				γ	Anode $\gamma/\sigma n$	Cathode γ	$\gamma/\sigma n$
C ₂ H ₄ Br ₂	Br-79 (18 min)	8.5	50.5	5,976	13.9	777	1.8
	Br-79 (4.4 hr.)	2.9	50.5	1,950	13.3	557	3.8
	Br-81 (06 hr.)	3.5	49.5	4,200	24.2	3,800	22.2
CH ₂ Br ₂	Br-79	8.5	50.5	6,364	14.8	1,000	2.3
	Br-79	2.9	50.5	1,900	13.0	590	4.0
	Br-81	3.5	49.5	4,600	26.8	4,200	24.5
C ₂ H ₅ Br	Br-79	8.5	50.5	1,328	3.4	841	1.9
	Br-79	2.9	50.5	450	3.1	85	0.5
	Br-81	3.5	49.5	1,080	6.3	575	3.3

It is obvious from these tables that isotope effect can be visualised on either electrode under different durations of the applied electric field. From Table III(A) the effect is found on the cathode when the applied field is for a duration of 1.5 hr. The fractions of the positively charged atoms may differ among the different isotopes of a given element on account of the variation in their coefficients of internal conversion with the capturing nuclides. This accounts in part the occurrence of isotope effect. Under a high electric field these species are collected on one of the electrodes and as a result we get isotope effect on the cathode as it is clear from the characteristic values of the cathode from Table III(A). However, the effect is observed as well on the anode plate when the field is applied for a duration of five hours. We have already pointed out that the Br^- ions develop during the course of applied field. From the duration of the applied field and absence of the effect on the cathode in table III(B) indicates that probably the positively charged species might have undergone reactions on account of their high reactivity. It is interesting to note that the isotope effect is observed only on one plate at a time. Probably the species formed as a result of (n, γ) reaction and isomeric transition undergo the reaction (2) suggested by Geissler and Willard, thus giving rise to isotope effect on the anode. A surprising similarity between the isotopes Br-80 and Br-82 is that both of them have got a metastable state and a high transition probability to their ground states.

An interesting feature of the experiment was that during the last 3.5 hours of the collection the increase in the activity on the cathode is mainly due to the contribution of positive species of Br-82 atoms as compared to Br-80 which indicates that the rate of reaction is different for Br-80 and Br-82, Showing thus that Br-82 positive ions preserve their entity in the liquid for a longer time than Br-80 ones. This may raise a point that the charge developed on the Br-82 ions is not as much as in case of Br-80 ions.

ACKNOWLEDGMENTS

The author is grateful to Dr. B. M. Shukla, Reader, Department of Chemistry for the valuable guidance and to Dr. G. B. Singh, Professor and Head of the Department of Chemistry for providing the laboratory facilities.

REFERENCES

- Anders, O. U. 1965. *Phys. Rev.* 138, No. 1B, B-1-B8.
 Arnikaar, H. J., and Lal, A., 1960. *Indian J. Phys.* 34, 441.
 Capron, P. C., Stokkink, G. and Van Meerssche, M., 1946. *Nature*, 157, 806.
 Capron, P. C. and Crevecoeur, 1952. *J. Chim. Phys.*, 20, 1403.
 ————— 1953. *J. Chem. Phys.*, 21, 1843.
 Capron, P. C., and Oshima, 1952. *J. Chem. Phys.*, 20, 1403.
 Capron, P. C., Colas, P., Gilly and Deblasieux, J., 1958. *Proc. Second Int. Conf. Peaceful Uses of Atomic Energy*, Geneva, 20, 240.
 Chien, R. S. H., and Willard, J. E., 1954. *J. Am. Chem. Soc.*, 76, 4735.
 Cooper, E., 1942. *Phys. Rev.* 61, 1.

An Isotope Effect in the Collection of Recoiled Products, etc. 47

- Emery, J. F., 1965. *J. Inorg. Nucl. Chem.* **27**, 903.
- Fox, M., and Libby, W. F., 1952. *J. Chem. Phys.*, **20**, 487.
- Geissler, P. R., and Willard, J. E., 1963. *J. Phys. Chem.* **67**(8), 1675.
- Goldsmith, G. J. and Bluerer, E., 1950. *J. Phys. and Colloid Chem.*, **54**, 717.
- Libby, W. F., 1941. *Science*, **97**, 283.
- 1947. *J. Am. Chem. Soc.*, **69**, 2523.
- Milman, M., and Shaw, P. F. D., 1956. *J. Chem. Soc.* 2101.
- 1957. *J. Chem. Soc.* 1303.
- Nesmeyanov, A. N., and Borisov, E. A., 1959. *Radiokhimiya*, **1**, 86.
- Nesmeyanov, A. N., Filatov, E. S., Borisov, E. A., and Shukla, B. M., 1961. *Proc. Symp. Chem. Effects of Nucl. Trans. I.A.E.A., Vienna* **1**, 259.
- Rowland, F. S., and Libby, W. F., 1953. *J. Chem. Phys.*, **21**, 1495.
- Shaw, P. F. D., 1951. *J. Chem. Soc.*, 443.
- Shaw, P. F. D., and Collio, 1956. *J. Chem. Soc.*, 434.
- Strominger, D., Hollander, J. M., and Seaborg, G. T., 1958. *Rev. Mod. Phys.* **30**, Pt II, 649.
- Suess, H., 1940. *Z. Physik, Chem., B-45*, 297., 312.
- Wexler, S., and Davies, T. H., 1952. *J. Chem. Phys.* **20**, 1688.
- Willard, J. E., 1961. *Proc. Symp. Chem. Effects of Nucl. Trans. I.A.E.A. Vienna*, **1**, 215.

GAMMA-GAMMA DIRECTIONAL CORRELATIONS IN Pr^{144}

S. L. GUPTA AND N. K. SAHA

DEPARTMENT OF PHYSICS AND ASTROPHYSICS

UNIVERSITY OF DELHI, DELHI-7.

(Received March 25, 1966)

ABSTRACT. The gamma rays of energy region 34-100 keV, following the beta decay of Ce^{144} , have been studied using coincidence and directional correlation methods, taking care of the highly disturbing scattering effects in this region. The correlation function found for the 54-80 keV cascade supports the spin assignment of 0^- for the Pr^{144} ground state. It is further shown that the direct angular correlation measurement of the 34-100 keV cascade cannot lead to any unambiguous spin assignment of the ground state.

INTRODUCTION

The spin of the Pr^{144} ground state has been the subject of considerable controversy in recent years. 0^- spin and parity assignment was made to this state in the level scheme (Fig. 1) of Pr^{144} deduced by Geiger *et al.* (1960) from a careful measurement of the conversion electron spectrum and the conversion line intensity ratios following the beta decay of Ce^{144} . This was later supported by conversion electron-gamma and gamma-gamma coincidence studies (Geiger *et al.*, 1961) of the Pr^{144} gamma transitions. Several other authors (Raghavan and Steffen, 1963; Porter and Day, 1959; Hess *et al.*, 1963), on the basis of studies of the beta-gamma directional correlation and the beta spectrum shape in the Pr^{144} — Nd^{144} decay, have also confirmed the 0^- spin assignment. On the other hand, the results of the beta-gamma circular polarization and directional correlation measurements (Graham *et al.*, 1958; Eman and Tadic, 1963; Hess *et al.*, 1963; Collin *et al.*, 1963; Lobashov and Nazarenko, 1961) in the Pr^{144} — Nd^{144} decay do not completely rule out an 1^- spin for the ground state of Pr^{144} . The whole situation has been carefully analysed by Singru *et al.* (1963) who conclude: "No unique spin assignment to the Pr^{144} ground state is possible on the basis of the available measurements on the Pr^{144} — Nd^{144} beta-transitions. A unique spin assignment to the Pr^{144} ground state is possible, however, if the available experimental data on the beta and gamma transitions in the Ce^{144} — Pr^{144} decay are properly interpreted". Moreover, controversy existed also about the spin of the 134 keV excited state of Pr^{144} , as the beta decay data (Hickock *et al.*, 1958) allowed three spin values, namely, 0, 1 and 2. A spin assignment of 1^- to the 134 keV excited state has been possible now from Geiger's decay scheme (Fig. 1) as well as from the beta-

gamma directional correlation measurements made by Collin *et al.* (1963), following the Ce^{144} beta decay.

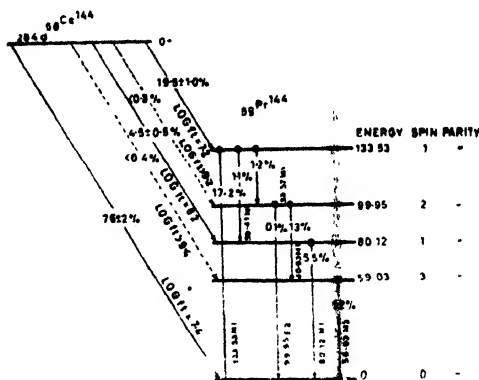


Fig. 1. Decay scheme of Ce^{144} as proposed by Geiger *et al.*

The two gamma-gamma cascades following the Ce^{144} — Pr^{144} decay, namely, 34-100 keV and 54-80 keV both involve the ground state as well as the 134 keV excited state of Pr^{144} . The 80 and the 100 keV gamma transitions feed the ground state of Pr^{144} (Fig. 1) and are expected to be pure multipoles, if the ground state spin were to be 0^- . From the internal conversion studies of Geiger *et al.* (1960, 1961), it is clear that the 80 keV transition is $>99\%$ M1. As regards the 100 keV transition, the internal conversion measurements (Geiger *et al.*, 1960; Geiger *et al.*, 1961), though consistent with its pure E2 character, do not rule out the possibility of an appreciable M1 admixture ($\sim 25\%$) in this transition.

The original aim of this work was to analyse the multipole mixing of the 100 keV transition by carrying out the gamma-gamma directional correlation of the 34-100 keV cascade, for which very scanty data (Bhattacharyya and Shastry, 1963) exist at present. This would also clarify the ground state spin of Pr^{144} . Strongly interfering coincidence counts from this energy region and the extremely low intensity of the 100 keV transition, however, made such a measurement inconclusive. The results of our coincidence and directional correlation measurements on this cascade as well as those of other authors (Sengupta *et al.*, 1959; Bhattacharyya and Shastry, 1963) are discussed here and their inconclusive character brought out. Alternatively, we considered it worthwhile to examine the ground state spin of Pr^{144} from the gamma-gamma directional correlation measurement of the 54-80 keV cascade, which has so far been investigated only by Zuk *et al.* (1963). This measurement promises to decide finally the spin and parity assignment to the Pr^{144} ground state.

EXPERIMENTAL PROCEDURE

The gamma ray scintillation spectrum of Ce^{144} is shown in Fig. 2. A perspex disc of suitable thickness was interposed in front of the crystal to reduce beta

contribution from the decay of Pr^{144} . All coincidence measurements were carried out using a fast-slow coincidence assembly with an effective resolving time of

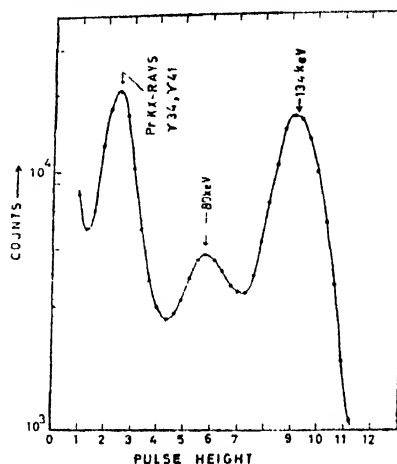


Fig. 2. Gamma ray scintillation spectrum of Ce^{144} .

≈ 30 ns. The coincidence spectra are recorded by setting one spectrometer first on the 34 and then on the 80 keV region. The results of the gamma-gamma coincidence and the gamma-gamma directional correlation measurements of the 54-80 keV cascade are discussed in the following sections.

GAMMA-GAMMA COINCIDENCE MEASUREMENTS

The observed gamma ray spectrum coincident with the Pr K X-rays (~ 35 keV) is shown in Fig. 3. The spectrum is similar to that obtained by Sengupta *et al.* (1959). It shows a strong peak at 100 keV of intensity comparable to that of γ -80. The same spectrum recorded by Geiger *et al.* (1961), with properly shielded crystals, shows, however, an almost complete absence of a peak at 100 keV.

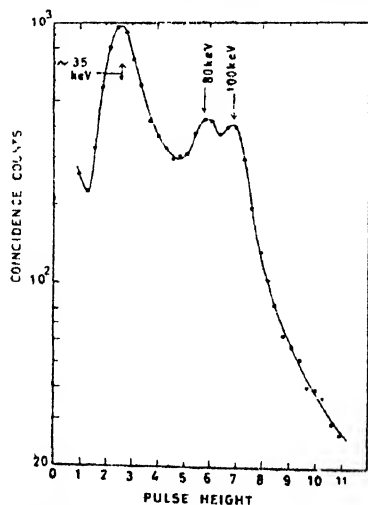


Fig. 3. Gamma ray spectrum in coincidence with the Pr K X-rays.

The computed relative photopeak intensities in this coincidence spectrum based on their decay scheme (Fig. 1), assuming that the gate includes the Pr K X-rays, γ -34 and γ -41, are in reasonable agreement with their observed coincidence spectrum. The computed relative photopeak intensity expected at 100 keV is only $\sim 4\%$ of the observed photopeak intensity at 80 keV and is not expected to be resolved in the spectrum. The relatively strong peak at 100 keV in the coincidence spectrum observed in the present work and that of Sengupta *et al.* (1959) is, therefore, not explained. It may presumably arise as a result of the contribution from (a) the Compton scattering of the 134 keV quanta from one crystal to the other, (b) the escape of the Iodine K X-rays from one crystal to the other and (c) the neighbouring peak at the 80 keV. The presence of interfering coincidences due to (a) is directly confirmed by us by taking a Ce^{144} source and observing that false coincidences are produced by Compton scattering of its 142 keV gamma ray at the same channel settings as in the actual experiment.

It is clear that with the two counters mutually shielded from each other, the actual number of 34-100 keV coincidences would indeed be extremely small because of the very weak intensity of the 100 keV transition. Consequently, these would not be resolved in the coincidence spectrum in the presence of the strong neighbouring peak at 80 keV.

The directional correlation of the 34-100 keV cascade has been measured by Bhattacharyya and Shastri (1963) who seem to have observed a measurable area under the 100 keV peak in the coincidence spectrum of the Pr K X-rays. The correlation function obtained by them is

$$W(\theta) = 1 - (0.226 \pm 0.030) P_2(\cos \theta) + (0.018 \pm 0.030) P_4(\cos \theta). \quad \dots (1)$$

The directional correlation measurement carried out by us for this cascade also showed an A_2 value $[-(0.270 \pm 0.038)]$ comparable to the above $[-(0.226 \pm 0.030)]$. The theoretical values of the expansion coefficients A_2 and A_4 for the $1(M1)2(E2)0$ cascade are -0.250 and 0 , respectively. These directional correlation results, therefore, apparently support a 0^- spin assignment to the Pr^{144} ground state and an E2 multipolarity of the 100 keV transition. Both these measurements, however, have been made without correcting for the various contributions to the coincidence counts as explained above. It is, therefore, difficult to attach any significance to these measurements, as the results obtained may arise almost entirely from the spurious coincidences expected in this energy region. We would rather conclude that a reliable measurement of the directional correlation of the 34-100 keV cascade is not feasible and thus nothing definite can be said about the multipole character of the 100 keV transition from this directional correlation experiment.

GAMMA-GAMMA DIRECTIONAL CORRELATION OF THE 54-80 keV CASCADE

Using double the voltage gain to allow adequate separation between the various gamma rays, the observed gamma spectrum coincident with the γ -80 is reproduced in Fig. 4. The estimated shape of the 54 keV gamma line is also indicated by the dashed line in this figure. The broadening of the K X-rays photopeak on its higher energy side seems to indicate the contribution of Compton scattering of the 134 keV quanta.

For measuring the directional correlation of the 54-80 keV cascade, one of the spectrometers was set on the lower half of the 80 keV photopeak and the other on the high energy side of the 54 keV peak, as obtained in the coincidence spectrum of Fig. 4. The windows thus selected are intended to suppress almost

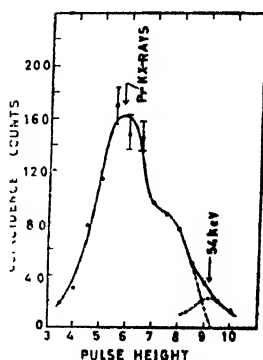


Fig. 4. Gamma ray spectrum in coincidence with the 80 keV photopeak.

completely the effect of Compton scattering of the 134 keV quanta. The interference from the neighbouring Pr K X-rays peak (Fig. 4) is thereby also eliminated. A test coincidence measurement carried out with a Ce^{141} -source at these window settings proved the effectiveness of protection against the spurious coincidences due to Compton scattering.

The data were collected at 90° , 135° , 180° , 225° and 270° with respect to the fixed detector in a total of ~ 50 counting hours. The normalized expansion coefficients, after correcting for finite angular resolution, are :

$$A_2 = -0.168 \pm 0.030, \quad A_4 = 0.022 \pm 0.077. \quad \dots (2)$$

As already stated, the spin of the 134 keV state of Pr^{144} is convincingly established as 1^- from the available experimental data (Geiger *et al.* 1961; Collin *et al.* 1963). We also know that all the gamma transitions in Pr^{144} , with the exception of γ -59 and γ -100, are M1 transitions with less than 1% E2 admixture. As explained earlier, the ground state spin of Pr^{144} can be either 0^- or 1^- . Three possible spin sequences for the 54-80 keV cascade then follow. Assuming $\sim 1\%$ E2 admixture in both the 54 and the 80 keV transitions, the probable limits of

the expansion coefficient A_2 , computed theoretically, corresponding to the three possible spin sequences are as follows :

- (i) $1(D, Q) 1(D) 0 \rightarrow$ $-0.37 < A_2 < -0.08$,
- (ii) $1(D, Q) 1(D, Q) 1-$ $+0.016 < A_2 < +0.28$,
- (iii) $1(D, Q) 2(D, Q) 1-$ $+0.09 < A_2 < +0.36$.

where D and Q denote the dipole and quadrupole contents in a transition. The experimental $A_2 = -(0.168 \pm 0.030)$ value, obtained by us, is only consistent with the spin sequence (i) and provides a most convincing evidence for a 0^- ground state spin assignment of Pr^{144} . Conclusions drawn earlier by Zuk *et al.* (1963) from the directional correlation measurement of this cascade also favour a 0^- spin assignment. Their experimental value $A_2 = -(0.102 \pm 0.020)$ is also compatible only with the spin sequence (i).

CONCLUSION

It is thus possible to make an independent check of the ground state spin assignment of Pr^{144} from the gamma-gamma directional correlation of the 54-80 keV cascade only. The 34-100 keV cascade leads to inconclusive results. Also the contradiction existing in the gamma ray spectrum in coincidence with the Pr K X-ray observed by Geiger *et al.* (1961) and by Sengupta *et al.* (1959) is explained.

Geiger *et al.* have tried to explain the 0^- ground state spin of Pr^{144} on the theoretical grounds. Although the situation is quite complex in odd-odd nuclei, they have proposed an interpretation on the unified model in terms of the intrinsic odd nucleon level assignments of Mottelson and Nilsson, which seems to account at least qualitatively for the said ground state spin assignment.

ACKNOWLEDGMENT

We are thankful to Professor R. C. Majumdar, Head of the Department of Physics and Astrophysics, University of Delhi, Delhi, for giving us excellent facilities to carry out this work and for his constant encouragement. We are grateful to Professor R. M. Steffen of Purdue University, USA, for many helpful discussions in connection with the present work.

REFERENCES

- Bhattacharyya, R. and Shastry, S., 1963. *Indian J. Phys.*, **37**, 357.
- Collin, W., et al., 1963. *Physics Letters*, **5**, 329.
- Eman, B. and Tadic, D., 1963. *Physics Letters*, **4**, 13.
- Geiger, J. S., Graham, R. L. and Ewan, G. T., 1960. *Nuclear Physics*, **16**, 1.
- Geiger, J. S., Graham, R. L. and Ewan, G. T., 1961. *Nuclear Physics* **28**, 387.

- Graham, R. L., Geiger, J. S. and Eastwood, T. A., 1958. *Can. Jour. Phys.* **36**, 1084.
- Hess, R., Lipnik P. and Sunnier, J. W., 1963. *Physics Letters*, **5**, 327.
- Hickock, R. L., McKinley, W. A., and Fultz, S. C., 1958. *Phys. Rev.* **109**, 113.
- Lobashov, V. M., and Nazarenko, V. A., 1961. *JETP (USSR)*, **41**, 1433.
- Porter, F. T. and Day, P. P., 1959, *Phys. Rev.*, **114**, 1286.
- Raghavan, R. S. and Steffen R. M., 1963. *Physics Letters*, **5**, 198.
- Sengupta, A. K., Bhattacharyya, R., Lahiri, J., and Mukherjee, P. N., 1959. *Indian J. Phys.*, **33**, 388.
- Singru, R. M., Raghavan, R. S., and Steffen, R. M., 1963. *Physics Letters* **6**, 319.
- Zuk, W. and Gustafsson, S., 1963. *Ark. Fys.*, **24**, 69.

THE MEASUREMENT OF THE ICC OF THE 192 keV TRANSITION IN In-114m.

M. RAJA RAO AND SWAMI JNANANANDA

LABORATORIES FOR NUCLEAR RESEARCH, ANDHRA UNIVERSITY, WALTAIR.

(Received April 20, 1966)

ABSTRACT. A method employing internal-external-conversion technique using a well-type plastic scintillation spectrometer (Raja Rao and Jnanananda, 1965) is adapted for the measurement of the ICC for the 192 keV transition in In-114m with foils of Ta and Cd as external converters. The average value obtained for the deduced $\alpha_k = 1.95 \pm 0.29$ which is compared with the theoretical values of Rose and Sliv.

INTRODUCTION

Measurements of Steffen (1951) have shown that for α_k values the multipole assignment for this 192 keV transition could be E4 while for K/L ratio the assignment could be E5. This discrepancy had been resolved by other measurements (Grabowski *et al.*, 1962, Daniel *et al.*, 1963 and Kleinheinz *et al.*, 1964) on K/L ratio which support the E4 assignment. However, the K/M , $K/M+N$ and $K/L+M+N$ ratios as determined by a precision method (Daniel *et al.*, 1963) are found to be considerably higher than the theoretical computed values. Therefore a remeasurement of α_k , possibly with a different technique, serves as a check in establishing the multipole assignment. The present internal-external-conversion technique employing a beta scintillation spectrometer enables an independent measurement of the total ICC, α . The multipole assignment is fixed on comparing the deduced α_k value with the theoretical values (Sliv and Band, 1965, Rose 1958).

EXPERIMENTAL

The In-114m isotope, having a half-life of 50 days, is obtained in liquid form with an activity of 1.5 mC/ml from the Atomic Energy Est., Trombay. The source is spread over a circular area of diameter ~ 5 mm on a thin alkathene film of thickness ~ 2 mg/cm². On evaporation the source thickness is ~ 200 micro gms/cm². The mounting of the source, the collimator, the geometry and the rest of the experimental arrangements are described in the author's earlier paper (Raja Rao and Jnanananda, 1965) in which the experimental procedure also is described in detail.

The observed electron spectra for low gain and high gain adjustments of the amplifier are plotted as shown in Fig. 1. In order to arrive at the value of the intensity of the conversion electrons (whose average energy indicated by the peak being 175 keV), the underlying beta continuum had to be subtracted. The spectral

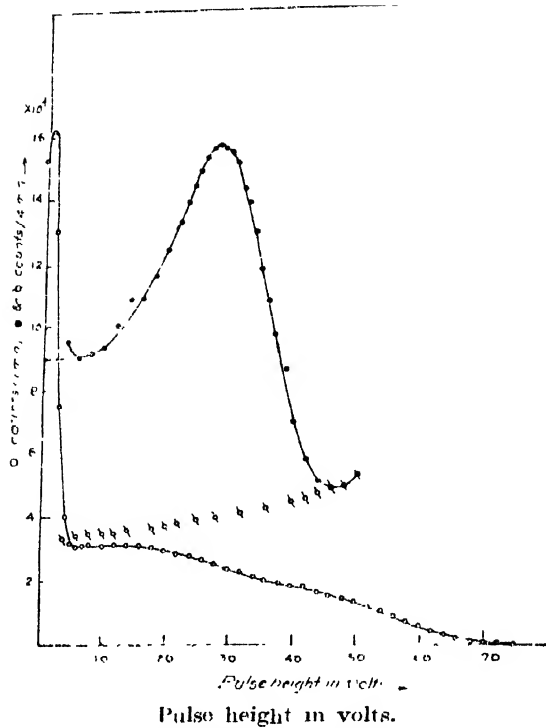


Fig. 1. Beta and conversion electron spectra of In-114m source. The points \circ represent the total spectrum for low gain of the amplifier. The points \bullet represent the conversion electrons at high gain. The points \odot represent the extrapolated beta spectrum obtained from Fig. 2.

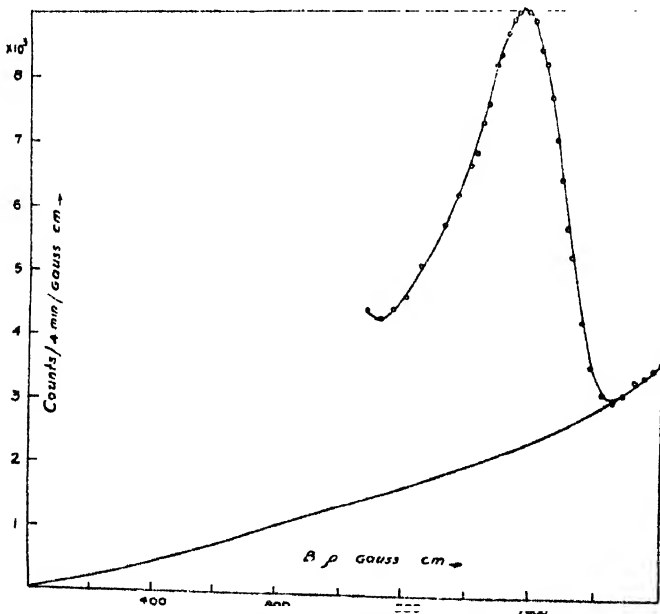


Fig. 2. Beta spectrum of In-114m source translated into momentum distribution. The recorded spectrum is represented by \circ and the continuous line is the extrapolation to the origin.

shape of the continuum in the low energy region is found by the following method: The observed spectrum is transferred into that of a momentum distribution, i.e., $B\rho$ vs counting rate per unit $B\rho$, employing published tables (Gerholm, 1955), as shown in Fig. 2. Assuming that in such a momentum distribution a beta continuum starts from the origin, the observed continuum is smoothly joined to the origin. This extrapolated part, on transformation back into the corresponding counts/channel width in the energy scale and then again into the pulse height in volts vs counts/channel width, indicates the spectral shape of the continuum in the low energy region as shown in Fig. 1. The observed conversion line, area (a_e), occupied by the conversion peak, is measured twice on different days A and B as 69.6 cm² and 69.1 cm² respectively when plotted to a scale of 5 volts/cm on the X-axis (X_e) and 10⁴c/4 min/cm on the Y-axis (Y_e). These values of a_e are corrected (ref. 7) employing the factors (i) for geometry, $f_g = G_r/G_e = 0.0053/0.0038$, (ii) for air + window absorption, $f_w = 1.18$ and (iii) for phosphor-back-scattering of electron, $f_{pb} = 1.365$. The values for the true conversion electron intensity per min. $N_e = a_e X_e Y_e f_g f_w f_{pb}$ for A and B are 19.495×10^5 and 19.362×10^5 respectively. In view of the above mentioned extrapolation and the small inaccuracies in the corrections as well as the negligence of other not very significant corrections at this energy region, the N_e values are accurate limited to an estimated error of 10%.

Gamma ray measurement is made by recording the photoelectron liberated, on external conversion, in foils of tantalum (8.73 mg/cm²) and cadmium (11.97

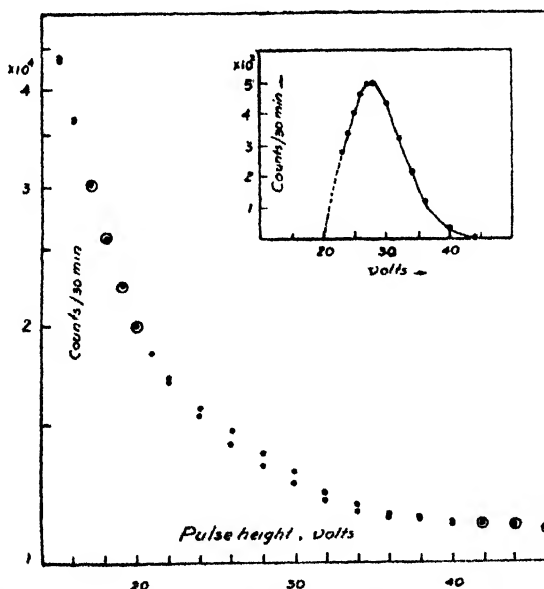


Fig. 3. Gamma spectra of In-114m source. The points o represent the spectrum with a Cd external converter and the points ● that with the compton-equivalent Al target. The insert shows the photoelectron distribution.

mg/cm²) of diameter 1.039 cm. after having stopped all the beta groups from entering the detector with a suitably thick Al stopper. The converter is located inside the well of the phosphor as described in a previous paper (Raja Rao *et al.* 1965). The observed spectra with the cadmium converter and a Compton equivalent aluminium target as well as the resulting photoelectrons spectrum are shown in Fig. 3. The photoelectron line area (a_p) as measured on the plots scaled to 5 volts/cm (X_p) and 100c/30min/cm (Y_p) are obtained as 25.1 cm² (Ta, A) and 10.89 cm² (Cd, B). The corresponding values for gamma intensity $N_r = a_p X_p Y_p f_{Al} f_{ad} f_{sa} f_{pb} / \sigma N$ are obtained applying the factors for (i) the gamma ray attenuation in the Al stopper $f_{Al} = 1.131$, (ii) the angular distribution of the emitted photoelectrons $f_{ad} = 1.075$, (iii) the absorption of photoelectrons within the converter $f_{sa} = 3.09$ (Ta) and 3.094 (Cd) and (iv) for the phosphor backscattering of the photoelectrons $f_{pb} = 1.516$ (Ta) and 1.389 (Cd). The values for N_r per min are obtained as 4.718×10^5 (A) and 4.587×10^5 (B) on substituting the values 205 (Ta) and 38 bn/atom (Cd) for the photoelectric cross-section σ (Grodstein, 1953), and for N , the number of atoms in the converter. The error in the N_r value is estimated to be 10% because of the small inaccuracies in the several factors involved and also in view of the negligence of the coherent and bound electron scattering effects.

TABLE I

Trial	Converter	Total ICC $\alpha = N_c/N_r$	Average α	Accepted K/L (ref. 1, 2)	Exptl. α_k $\alpha/(1 + \frac{1}{3}L/K)$	Theor. α_k for E4 Rose Sliv	Other exptl. α values
I	Ta	4.132	4.176 ± 0.044	1.16	1.94 ± 0.29	2.5 2.25	4.2 ± 0.4 (ref. 3)
	Cd	4.22					4.0 (ref. 4)
II	Ta	4.164	4.211 ± 0.047		1.96 ± 0.29		4.3 ± 0.04 (ref. 5)
	Cd	2.58					

1. Grabowski *et al.*, 1962
2. Kleinheinz *et al.*, 1964
3. Steffen, 1951
4. Boehm *et al.*, 1949
5. Hoffman, 1957.

The present values of conversion coefficients (α and α_k) along with the theoretical K-conversion coefficients are presented in Table I. The deduced α_k expt. values in the table are limited in accuracy having a total error of 15%. As can be seen the α_k values are in agreement with Sliv's theoretical value for 192 keV E4 radiation.

ACKNOWLEDGMENT

The authors gratefully acknowledge the financial assistance rendered by the Department of Atomic Energy, Government of India.

REFERENCES

- Boehm, F. and Preisswork, P., 1949. *Helv. Phys. Acta* **22**, 331.
- Gerholm, T. R., 1955. Appendix VIII, "*Beta-and Gamma-Ray Spectroscopy*" Ed. K. Siegbahn, N.-H.P.C., Amsterdam.
- Grabowski, Z., Gustafsson, S. and Backstrom, G., 1962. *Nucl. Phys.* **38**, 648.
- Grodstein, G. W., 1953. *X-ray attenuation coefficients*, N.B.S. Circ. No. 583, Washington D. C.
- Hoffman, K. W., 1957, *Z. Phys.* **148**, 298.
- Kleinheinz, P., Samuelsson, L., Vukanovic, R. and Siegbahn, K. 1964, *Nucl. Phys.* **59**, 673.
- Raja Rao, M., and Jnanananda, S., 1965. *Nucl. Instr. & Methods* **36**, 261.
- Rose, M. E., 1958. "*Internal Conversion Coefficients*", N.-H.P.C., Amsterdam.
- Sliv, L. A., and Band, I. M., 1965. Appendix V, *Alpha-Beta-and Gama-Ray Spectroscopy*, Ed. K. Siegbahn, N.-H.P.C., Amsterdam.
- Steffen, R. M., 1951. *Phys. Rev.* **83**, 166.

GENERATION OF NON-LINEAR DIPOLE MOMENT IN A TWO LEVEL SYSTEM

B. K. MOHANTY

DEPARTMENT OF PHYSICS, INDIAN INSTITUTE OF TECHNOLOGY, KHARAGPUR

(Received May 3, 1966 ; Resubmitted August 29, 1966)

ABSTRACT. With the availability of intense sources it has been possible to observe non linear effects in dipole moments in interactions where only two energy levels take part. Using the geometrical representation for Schrodinger equation the expectation value for non-linear component of dipole moment has been obtained. It has been demonstrated that a permanent dipole moment must be present in the system for generating this effect. The non-linear component is seen to be appreciable for $\omega = \omega_{12}$ and $\omega \approx \omega_{12}/2$. The dependance of this component on the angle between the induced dipole moment and the oscillating field is shown to be $\sim \cos^2 \theta \sin \theta$

INTRODUCTION

The dipole moment induced in an atom, designated as a system, is seen, in general, to be linear in the frequency of the applied field. But it is possible to observe dipole moment which is not linear in the frequency of the applied field by using more intense sources than ordinarily available ones.

This generation of the higher harmonics of the frequency of an electromagnetic field interacting with a material system (or an atom) has been of much interest to physicists in recent times. (Franken and Ward, 1963). These processes, involving multiphoton transitions, may be explained by higher order perturbation theory. The field required to produce these effects must be highly intense and recently optical maser sources have been used to demonstrate this phenomena (Franken *et al.* 1961). In fact the order of magnitude of the optical maser sources to demonstrate this effect is of the order of 10^6 joules with a peak power of the order of 10^9 watts (Franken and Ward, 1963). These sources are highly monochromatic and so it is reasonable to assume that only two stationary energy states of the system (involving one transition frequency, which is more or less equal to the frequency of the applied field) will be principally involved in such an interaction. Reports are available where only two energy levels have indeed been associated in generating optical harmonics. The investigation of such multiple photon transition has been reported (Voskonyan, Klyshko and Tusmanov 1964; Klyshko and Tusmanov 1965) These investigators have used a magnetic dipole transition of the sublevels of the ground state of the free radical diphenyl picryl hydrazyl (DPPH).

The object of this article is to demonstrate the generation of harmonics of the applied field frequency in the cases where only two levels are involved in the interaction and study the characteristics of the non-linear dipole moment.

In the case of a two level system, a higher harmonic generation will be possible only if (i) there is a permanent dipole moment present in the system or (ii) if the induced dipole moment itself is non-linear in terms of the field. We shall discuss only the case (i). The fact that a permanent dipole moment is a necessity for the above mentioned processes has also been discussed in the restricted case of a magnetic dipole transition by Voskonyan, Klyshko and Tusmanov (previous reference). We shall presently demonstrate a model, which is capable of explaining the phenomenon for a more general situation.

FORMULATION OF THE PROBLEM

We start with a system of which only two non-degenerate energy levels are involved. The levels are designated as level 1 with energy E_1 and level 2 with energy E_2 . Their transition frequency is ω_{12} which is always positive.

$$\omega_{12} = \frac{E_1 - E_2}{\hbar}$$

Only a monochromatic field is considered. The interaction coupling the system to the electromagnetic field is of electric dipole type (Senitzky 1962; Bonch Bruevich *et al.*, 1965); the interaction hamiltonian being :

$$V(t) = -\vec{\mu} \cdot \vec{E}_0(t) \quad \dots \quad (2.1)$$

where $\vec{\mu}$ is the electric dipole moment operator and \vec{E}_0 is the applied field. The field has been regarded as classical, but a quantum theoretical consideration does not change the results (Mandel and Wolf 1963). The dipole moment operator is assumed real for convenience.

The wave function of a two level system is written down as :

$$\psi(t) = a_1(t)\psi_1 + a_2(t)\psi_2 \quad \dots \quad (2.2)$$

where ψ_1 is the wave function for state 1 and ψ_2 is the wave function for state 2, a_1 and a_2 being the coefficients associated with them. The phase of ψ is of little importance when only two energy levels are being considered.

The Schrodinger equation is then written down

$$(H + V) \psi = i\hbar \frac{d\psi}{dt} \quad \dots \quad (2.3)$$

H is the hamiltonian for stationary states, with the exactly solvable eigen value equations

$$H\psi_i = E_i\psi_i \quad (i = 1, 2) \quad \dots \quad (2.4)$$

Substituting eqn. (2.2) into eqn. (2.3) we get

$$a_1 E_1 \psi_1 + a_2 E_2 \psi_2 + a_1 V \psi_1 + a_2 V \psi_2 = i\hbar \frac{da_1}{dt} \psi_1 + i\hbar \frac{da_2}{dt} \psi_2$$

Multiplying this equation with ψ_1 from left, substituting eqn. (2.4) and using the property of orthonormality of ψ_i 's ($\int \psi_i^* \psi_j d\tau = \delta_{ij}$) we obtain :

$$\frac{da_1}{dt} = \frac{E_1}{i\hbar} a_1 + \frac{V_{11}}{i\hbar} a_1 + \frac{V_{12}}{i\hbar} a_2 \quad \dots (2.5)$$

and similar equations for a_2 , a_1^* and a_2^* can be obtained. V_{ij} is nothing but the expectation value of V and is given by $\int \psi_i^* V \psi_j d\tau$ ($i, j = 1, 2$).

To find the expectation value of the dipole moment operator $\vec{\mu}$ directly, the geometrical representation of the Schrodinger equation (Feynman, Vernon, and Hellworth 1958) is used.

We construct the three real components of a 3-vector \vec{r} :

$$\begin{aligned} r_1 &= a_1 a_2^* + a_1^* a_2 \\ r_2 &= i(a_1 a_2^* - a_1^* a_2) \\ r_3 &= a_1 a_1^* - a_2 a_2^* \end{aligned} \quad \dots (2.6)$$

and also $r_4 = a_1 a_1^* + a_2 a_2^*$, which is not independant.

For a normalised ψ the value of r_4 is equal to 1 (Feynman *et al*, previous reference)

So the equation of motion for \vec{r} is, using eqn. (2.5)

$$\frac{d\vec{r}}{dt} = \vec{\omega} \times \vec{r} \quad \dots (2.7)$$

where $\vec{\omega}$ is a vector in the same hypothetical coordinate system, with

$$\begin{aligned} \omega_1 &= (V_{12} + V_{21})/\hbar \\ \omega_2 &= i(V_{12} - V_{21})/\hbar \\ \omega_3 &= \omega_{12} + (V_{11} - V_{22})/\hbar \end{aligned} \quad \dots (2.8)$$

The expectation value of the electric dipole moment operator is directly given by :

$$\begin{aligned} \langle \vec{\mu} \rangle &= \int \psi^* \vec{\mu} \psi d\tau \\ &= \int (a_1^* \psi_1^* + a_2^* \psi_2^*) \vec{\mu} (a_1 \psi_1 + a_2 \psi_2) d\tau \\ &= a_1^* a_1 \int \psi_1^* \vec{\mu} \psi_1 d\tau + a_1^* a_2 \int \psi_1^* \vec{\mu} \psi_2 d\tau + a_2^* a_1 \int \psi_2^* \vec{\mu} \psi_1 d\tau \\ &\quad + a_2^* a_2 \int \psi_2^* \vec{\mu} \psi_2 d\tau \\ &= \vec{\mu}_{11} r_1 + \frac{1}{2}(\vec{\mu}_{11} - \vec{\mu}_{22}) r_3 + \frac{1}{2}(\vec{\mu}_{11} + \vec{\mu}_{22}). \end{aligned} \quad \dots (2.9)$$

where $\vec{\mu}_{12}$ is understood to be $\int \psi_1^* \vec{\mu} \psi_2 d\tau = \vec{\mu}_{21}$ when $\vec{\mu}$ is real and hermitian (Feynman *et al.*, 1958, Previous Ref.) When the field is applied the contribution to the eqn. (2.9) is predominantly due to the first term, i.e., that component of $\vec{\mu}$ which accounts for the transition between the two stationary levels.

THE SOLUTION

We assume the field to be sinusoidal ($\vec{E}_0 = \vec{E} \cos \omega t$), then the form of the interaction is :

$$\begin{aligned} V &= -\vec{\mu} \cdot \vec{E} \cos \omega t \\ &= -\text{Re} \cdot \vec{\mu} \cdot \vec{E} e^{-i\omega t} \end{aligned} \quad \dots (3.1)$$

The equation (2.7) reduces to :

$$\begin{aligned} \frac{dr_1}{dt} &= -r_3 \frac{2\vec{\mu}_{12} \cdot \vec{E}}{\hbar} \sin \omega t - [\omega_{12} - (\mu_{11} - \mu_{22}) \cdot \vec{E}/\hbar \cos \omega t] r_2 \\ \frac{dr_2}{dt} &= [\omega_{12} - (\mu_{11} - \mu_{22}) \cdot \vec{E}/\hbar \cos \omega t] r_1 + r_3 \frac{2\vec{\mu}_{12} \cdot \vec{E}}{\hbar} \cos \omega t \\ \frac{dr_3}{dt} &= r_2 \frac{2\vec{\mu}_{12} \cdot \vec{E}}{\hbar} \cos \omega t - r_1 \frac{2\vec{\mu}_{12} \cdot \vec{E}}{\hbar} \sin \omega t \end{aligned} \quad \dots (3.2)$$

If one neglects μ_{11}/\hbar and μ_{22}/\hbar in comparison with ω_{12} , equation (3.2) are formally similar to Bloch equations of magnetic susceptibility (Bloch 1946), but are more general, and can be solved exactly by the rotating coordinate method, (Archibald 1952) to find the value of linear dipole moment. But the presence of a time dependance in ω_3 component complicates the situation.

The rotating coordinate transformation

$$\begin{aligned} r'_1 &= r_1 \cos \omega t + r_2 \sin \omega t \\ r'_2 &= -(r_1 \sin \omega t - r_2 \cos \omega t). \\ r'_3 &= r_3 \end{aligned} \quad \dots (3.3)$$

with its inverse

$$\begin{aligned} r_1 &= r'_1 \cos \omega t - r'_2 \sin \omega t \\ r_2 &= r'_1 \sin \omega t + r'_2 \cos \omega t \\ r_3 &= r'_3 \end{aligned} \quad (3.4)$$

gives us the equations :

$$\frac{dr'_i}{dt} = \omega' \times r' \quad \dots (3.5)$$

where

$$\omega'_1 = \gamma = -\frac{2\vec{\mu}_{12} \cdot \vec{E}}{h}$$

$$\omega'_2 = 0$$

$$\omega'_3 = \Delta + \delta \cos \omega t \text{ with } \Delta = \omega_{12} - \omega; \delta = -(\vec{\mu}_{11} - \vec{\mu}_{22}) \cdot \vec{E}/\hbar$$

We proceed by writing for the \vec{r}' components :

$$\begin{aligned} dr'_1/dt + [\Delta + \delta \cos \omega t]r'_2 &= 0 \\ dr'_2/dt - [\Delta + \delta \cos \omega t]r'_1 + \gamma r'_3 &= 0 \\ dr'_3/dt - \gamma r'_2 &= 0 \end{aligned} \quad \dots (3.6)$$

This set of equations is not exactly solvable, but it is possible to solve them by an approximation.

To solve the equations (3.6) the following substitutions are made .

$$\begin{aligned} r'_1 &= \sum_{n=-\infty}^{+\infty} u_n(\gamma, \delta) e^{-in\omega t} \\ r'_2 &= \sum_{n=-\infty}^{+\infty} v_n(\gamma, \delta) e^{-in\omega t} \\ r'_3 &= \sum_{n=-\infty}^{+\infty} r_n(\gamma, \delta) e^{-in\omega t} \end{aligned} \quad \dots (3.7)$$

It is easy to see that ($n = 0$) terms are nothing but the contributions to r_1 and r_2 which are linear in the applied field, whereas ($n = 0$) term in r_3 is non-oscillatory.

Substituting the equation (3.7) into equation (3.6) one gets :

$$\begin{aligned} -\frac{in\omega}{\gamma} u_n + \frac{\Delta}{\gamma} v_n + \frac{1}{2} \frac{\delta}{\gamma} (v_{n-1} + v_{n+1}) &= 0 \\ -\frac{in\omega}{\gamma} v_n - \frac{\Delta}{\gamma} u_n - \frac{1}{2} \frac{\delta}{\gamma} (u_{n-1} + u_{n+1}) + r_n &= 0 \\ -\frac{in\omega}{\gamma} r_n - v_n &= 0 \end{aligned} \quad \dots (3.8)$$

We substitute $q = \frac{\delta}{\gamma}$ and $s = \frac{\Delta}{\gamma}$ and assume $q \ll 1$. This assumption is quite justified as the necessity of having a highly intense field to observe the

non linear effects points out that δ is indeed very much smaller than γ . We now expand u_n , v_n and r_n in powers of q to see how these terms depend on this parameter

$$\begin{aligned} u_n(q) &= \sum_{\nu=0}^{\infty} u_{n\nu} q^{\nu} \\ v_n(q) &= \sum_{\nu=0}^{\infty} v_{n\nu} q^{\nu} \\ r_n(q) &= \sum_{\nu=0}^{\infty} r_{n\nu} q^{\nu} \end{aligned} \quad \dots \quad (3.9)$$

These equations allow us to write equations (3.8), after picking up similar coefficients of q , in the form :

$$\begin{aligned} -\frac{in\omega}{\gamma} u_{n\nu} + sv_{n\nu} + \frac{1}{2}(v_{n-1, \nu-1} + v_{n+1, \nu-1}) &= 0 \\ -\frac{in\omega}{\gamma} v_{n\nu} - su_{n\nu} - \frac{1}{2}(u_{n-1, \nu-1} + u_{n+1, \nu-1}) + r_{n\nu} &= 0 \quad \dots \quad (3.10) \\ -\frac{in\omega}{\gamma} r_{n\nu} - v_{n\nu} &= 0 \end{aligned}$$

We shall also consider the symmetry properties of u_n , v_n and r_n , which are :

$$\begin{aligned} u_n(-q) &= (-1)^n u_n(q) \\ v_n(-q) &= (-1)^n v_n(q) \end{aligned} \quad \dots \quad (3.11)$$

and

$$r_n(-q) = (-1)^n r_n(q)$$

which means in equations (3.9) only even terms of the combination $n+\nu$ will exist. An additional fact must also be considered : when q is zero, r_n cannot have an oscillatory term dependant on ω , as under such a circumstance the equations (3.6) can be shown to be exactly solvable. So the terms like r_{20} , r_{40} are nonexistent.

$$r_{n0} = r_{n0} \delta_{n0} \quad \dots \quad (3.12)$$

Now we shall solve equations (3.10) for specific n and ν .

For $\nu = 0$, the equations are independant of q , and reduce to the simpler case where there is no permanent dipole moment. So the equations reduce to :

$$\begin{aligned} -\frac{in\omega}{\gamma} u_{n0} + sv_{n0} &= 0 \\ -\frac{in\omega}{\gamma} v_{n0} - su_{n0} + r_{n0} &= 0 \quad \dots \quad (3.13) \\ -\frac{\omega}{\gamma} r_{n0} - v_{n0} &= 0 \end{aligned}$$

It can be clearly seen, using equation (3.12) that for $n \neq 0$,

$$u_{n0} = u_{n0}\delta_{n0} \quad \text{and} \quad v_{n0} = v_{n0}\delta_{n0}$$

which means no higher order solution will exist unless there is a permanent dipole moment present ($\delta \neq 0$).

THE NON LINEAR DIPOLE MOMENT

The first order solutions of u_n and v_n with $n = 1$ give rise to $u_{n\nu}$ and $v_{n\nu}$ values which give a contribution to the value of dipole moment which oscillates with a frequency 2ω .

The same approximation also gives a contribution to the linear part of the dipole moment expectation value $\langle \vec{\mu} \rangle$ through $r_{n\nu}$.

Writing equations (3.10) for $n = 1$, $\nu = 1$

$$\begin{aligned} -\frac{i\omega}{\gamma} u_{11} + s v_{11} + \frac{1}{2} r_{00} &= 0 \\ -\frac{i\omega}{\gamma} v_{11} - s u_{11} - \frac{1}{2} u_{00} + r_{11} &= 0 \quad \dots (4.1) \\ -\frac{i\omega}{\gamma} r_{11} - v_{11} &= 0 \end{aligned}$$

We substitute the value of u_{00} and v_{00} from equations (3.13) ($u_{00} = \gamma/\Delta r_{00}$, $v_{00} = 0$) and get :

$$\begin{aligned} u_{11} &= \frac{\gamma^2}{2(\omega^2 - \Delta^2 - \gamma^2)} r_{00} \\ v_{11} &= \frac{i\omega\gamma^2}{2\Delta(\omega^2 - \Delta^2 - \gamma^2)} r_{00} \quad \dots (4.2) \end{aligned}$$

These two terms give the major contribution to the part of dipole moment which has a frequency of 2ω . The value of r_{11} may also be noted and this will give a correction to the expectation value of dipole moment with a frequency of ω :

$$r_{11} = -\frac{\gamma^3}{2\Delta(\omega^2 - \Delta^2 - \gamma^2)} r_{00} \quad \dots (4.3)$$

Similarly we may carry on the higher order calculations, and get 3ω , 4ω , ... dependant values of dipole moment expectation value.

Now collecting the u_{11} , v_{11} values and tracing back the substitutions

$$\begin{aligned} r_1' &= u_{00} + u_{11} q e^{-i\omega t} + \dots \\ r_2' &= v_{11} q e^{-i\omega t} + \dots \\ r_3' &= r_{00} + r_{11} q e^{-i\omega t} \end{aligned} \quad \dots \quad (4.4)$$

Collecting only the real values and operating the inverse transformation eqn. (3.4)

$$\begin{aligned} r_{1dc} &= \frac{\gamma\delta}{4(\omega^2 - \Delta^2 - \gamma^2)} \left[1 - \frac{\omega}{\Delta} \right] r_{00} + \frac{\gamma\delta}{4(\omega^2 - \Delta^2 - \gamma^2)} \left[1 + \frac{\omega}{\Delta} \right] r_{00} \cos 2\omega t \\ r_{22\omega} &= \frac{\gamma\delta}{4(\omega^2 - \Delta^2 - \gamma^2)} \left[1 - \frac{\omega}{\Delta} \right] r_{00} \sin 2\omega t \end{aligned} \quad \dots \quad (4.5)$$

DISCUSSION

The equations (4.5) give us the value of non linear dipole moment, both the non oscillatory part and the part which has a dependance on 2ω . The non oscillatory contribution to the expectation value, using eqn. (2.9) is

$$\langle \vec{\mu} \rangle_{dc} = \frac{\gamma \delta \vec{\mu}_{12} (\omega_{12} - 2\omega)}{4(\omega_{12} - \omega)(\omega^2 - \Delta^2 - \gamma^2)} r_{00} + \frac{1}{2} (\vec{\mu}_{11} - \vec{\mu}_{22}) r_{00} + \frac{1}{2} (\vec{\mu}_{11} + \vec{\mu}_{22}) \quad (5.1)$$

The 2ω dependant part is, neglecting the second order term in r_3 :

$$\langle \vec{\mu} \rangle_{2\omega} = \frac{\gamma \delta \vec{\mu}_{12} \omega_{12}}{4(\omega_{12} - \omega)[\omega^2 - (\omega_{12} - \omega)^2 - \gamma^2]} r_{00} \cos 2\omega t \quad \dots \quad (5.2)$$

As we are dealing with high frequencies, one can neglect γ^2 in comparison with ω^2 in equations (5.1) and (5.2). This only means that field saturation is not considered. Then equations (5.1) and (5.2) reduce to :

$$\begin{aligned} \langle \vec{\mu} \rangle_{dc} &= - \left[\frac{\gamma \delta \vec{\mu}_{12}}{4(\omega_{12} - \omega)\omega_{12}} - \frac{1}{2} (\vec{\mu}_{11} - \vec{\mu}_{22}) \right] r_{00} + \frac{1}{2} (\vec{\mu}_{11} + \vec{\mu}_{22}) \\ \langle \vec{\mu} \rangle_{2\omega} &= \frac{\gamma \delta \vec{\mu}_{12}}{4(\omega_{12} - \omega)(2\omega - \omega_{12})} r_{00} \cos 2\omega t \end{aligned} \quad \dots \quad (5.3)$$

In general, for a complex value of dipole moment, the value of $\langle \vec{\mu} \rangle$ must contain r_2 contribution, which is :

$$\langle \vec{\mu} \rangle_{2\omega} = \frac{\gamma \delta \vec{\mu}_{12}}{4(\omega_{12} - \omega)\omega_{12}} r_{00} \sin 2\omega t \quad \dots \quad (5.4)$$

These two equations, eqn. (5.3) and (5.4), show an interesting property of the 2ω dependant part of $\langle \vec{\mu} \rangle$ that is, $\langle \vec{\mu} \rangle_{2\omega}$. One gets the maximum value for $\langle \vec{\mu} \rangle_{\omega}$ for two values of ω : $\omega = \omega_{12}$ and $\omega = \omega_{12}/2$. In the second case the value of $\langle \vec{\mu} \rangle_{\omega}$ has already fallen off, so that at $\omega_{12} = 2\omega$ the effect of $\langle \vec{\mu} \rangle_{2\omega}$ will be easily observed. Both the effects-giving rise to an absorption of second harmonic power can be in principle observed.

The equations (5.3) and (5.4) do not immediately display saturation due to finite width of energy levels. But as pointed out by Haaken *et al.* (Haaken, der Agobian and Pauthier 1965), one can directly take into account this effect by replacing ω_{12} by a complex quantity $\omega_{12}' + i/\Gamma$; where Γ has the significance of a relaxation time. The equations (5.3) and (5.4) also point out that the orientation of the oscillating field affects the value of $\langle \vec{\mu} \rangle_{2\omega}$ in a very different manner than the value of $\langle \vec{\mu} \rangle_{\omega}$. $\langle \vec{\mu} \rangle_{\omega}$ directly depends on $\vec{\mu}_{12} \cdot \vec{E}$, so that if the angle between $\vec{\mu}_{12}$ and \vec{E} is Θ ; then the angular dependance of $\langle \vec{\mu} \rangle_{\omega}$ is

$$\langle \vec{\mu} \rangle_{\omega} \sim \cos^2 \Theta$$

when we consider it in the direction of the applied field. It will show a maximum at $\Theta = 0$ and drop off to zero at $\Theta = \pi/2$. But the dependance of $\langle \vec{\mu} \rangle_{2\omega}$ is as follows :

$$\langle \vec{\mu} \rangle_{2\omega} \sim (\vec{\mu}_{12} \cdot \vec{E})[(\vec{\mu}_{11} - \vec{\mu}_{22}) \cdot \vec{E}](\vec{\mu}_{12} \cdot \hat{n})$$

\hat{n} is the unit vector in the direction of \vec{E} .

If one uses a static (non oscillating) field to separate the levels (as the strong static magnetic field in a Bloch system) $\vec{\mu}_{12}$ will be in the direction of this field and $(\vec{\mu}_{11} - \vec{\mu}_{22})$ will be perpendicular to it. This is evident from the fact that the transition inducing dipole moment may be denoted by Pauli σ_x, σ_y matrices and the permanent dipole moment may then be denoted by the perpendicular σ_z matrix, as pointed out by Dicke (Dicke 1954). Then the angular dependance of $\langle \vec{\mu} \rangle_{2\omega}$ is:

$$\langle \vec{\mu} \rangle_{2\omega} \propto \sin \Theta$$

This is, of course, strictly true for the part of $\langle \vec{\mu} \rangle_{2\omega}$ when $\omega = \omega_{12}/2$. In the case $\omega = \omega_{12}$; r_2 value has to be considered and the expression is expected to be more involved.

The expression for $\langle \vec{\mu} \rangle_{2\omega}$, where $2\omega = \omega_{12}$, now shows that the maximum does not occur at $\Theta = 0$. In fact $\langle \vec{\mu} \rangle_{2\omega}$ is equal to zero for $\theta = \pi/2$ and

$\ominus = 0$. The maximum occurs at about $\ominus \sim 35^\circ$. Such a result has been verified in the case of a magnetic dipole transition by Voskonyan *et al.* (Voskonyan *et al.* 1964).

ACKNOWLEDGMENTS

The author thanks Prof. H. G. Venkates for his guidance in carrying out the work and Dr. S. K. Duttaray for many useful and critical discussion. He is also indebted to Prof. H. N. Bose for his kind interest in the work.

REFERENCES

- Archibald, W. J., 1952. *Am. Jour. of Phys.* **20**, 368.
Bloch, F., 1946. *Phys. Rev.* **70**, 46.
Bonch-Bruevich, A. M., and Khodovoi, V. A., 1965. *Soviet Phys. USPEKHI*, **8**, 1.
Dicke, R. H., 1954. *Phys. Rev.* **96**, 99.
Feynman, R. P., Vernon, F. L., and Hellworth, R. W., 1958. *Jour. of Appl. Phys.* **29**, 49.
Franken, P. A. *et al.*, 1961. *Phys. Rev. Letters* **7**, 118.
Franken, P. A. and Ward, J. F., 1963. *Rev. of Mod. Phys.* **35**, 23.
Haaken H., der Agobian, R., and Pauthier, M., 1965. *Phys. Rev.* **140**, A 437.
Klyshko, D. and Tusmanov, V., 1965. *Soviet Phys. JETP*, **20**, 1367.
Mandel, L., and Wolf, E., 1963. *Phys. Rev. Letters*, **10**, 276.
Senitzky, I. R., 1962, *Phys. Rev.* **127**, 1638.
Voskonyan, A. V., Klyshko, D., and Tusmanov, V., 1964. *Soviet Phys. JETP*, **18**, 967.

ELECTRON AFFINITY OF HALOGEN ATOMS

S. P. TANDON, M. P. BHUTRA* AND K. TANDON**

PHYSICAL LABORATORIES, UNIVERSITY OF JODHPUR, JODHPUR, INDIA.

(Received May 16, 1966, Resubmitted August 12, 1966)

ABSTRACT. Electron affinities of Fluorine, Chlorine, Bromine and Iodine have been evaluated in the case of twenty monomers of alkali metal halides, using the relation

$$E = D_e + I - \frac{e^2}{r_e} \left[1 - \left\{ \frac{k_e r_e^3}{e^2} + 3 \right\}^{-1} \right]$$

where D_e is the dissociation energy of polar diatomic molecules AX , I is the ionization potential of atom A , e is the electronic charge, k_e is the force constant for infinitesimal amplitude and r_e is the equilibrium internuclear distance.

These E values have been compared with those obtained by other experimental and theoretical methods.

INTRODUCTION

In a recent communication (Tandon *et al.*, 1966) it has been shown that the relation between electron affinity and other molecular constants deduced from potential function having gaussian form repulsion term, leads to results much better than ones obtained by other theoretical methods of evaluating electron affinities. This is due to the fact that such a potential function adequately includes the polarizability, Van der waal and short range repulsion effects (Bleick and Mayer, 1934; Kunimuni, 1950; Rice and Klemperer, 1957; Varshni and Shukla, 1961), which are important in the case of polar diatomic molecules. In the present communication this relation has been used to calculate the electron affinities of halogen atoms in the case of monomers of alkali metal halides. The results have been discussed in the light of those obtained by other theoretical and experimental methods.

CALCULATION OF ELECTRON AFFINITIES

The following relation between electron affinity and the molecular constants deduced earlier by authors (1966), has been used to evaluate E , the electron affinity of halogen atoms (X).

$$E = D_e + I - \frac{e^2}{r_e} \left[1 - \left\{ \frac{k_e r_e^3}{e^2} + 3 \right\}^{-1} \right] \quad \dots (1)$$

where D_e is the dissociation energy of polar diatomic molecule AX , I is the ionization

*Physics Department, Lachoo Memorial College of Science, Jodhpur, India.

**Chemical Laboratories, University of Jodhpur, Jodhpur, India.

ization potential of atom A , e is the electronic charge, k_e is the force constant for infinitesimal amplitude and r_e is the equilibrium internuclear distance.

DATA AND PROCEDURE

The observed values of dissociation energy D_e , referred to 0°K , are expressed in electron volts and collected in Table I, values followed by “(H)” are taken from Herzberg’s molecular data (1950). Similarly “(G)” refers to data taken from Gaydon’s book (1953) and that referred by Herzberg (1950) as Gaydon’s data.

The ionization potential (I) values for alkali metals, expressed in e.v. (Table I) are those given by Hodgman (1963).

The values of equilibrium internuclear distance (r_e) are expressed in Å (Table I) and are taken from the “Tables of Interatomic distances and configuration of molecules and ions” (The Chemical Society, London, England, 1958) except where indicated. The r_e values in paranthesis are roughly estimated ones.

The values of force constant for infinitesimal amplitude k_e expressed in md/Å have been calculated from molecular data given by Herzberg (1950) unless stated otherwise.

Using these values of the molecular constants the electron affinities of halogen atoms have been calculated from equation (1). These values have been collected in Tables II–V along with values obtained by other theoretical and experimental methods for comparison.

DISCUSSION

Study of equation (1) reveals that r_e values must be very accurately known, since higher powers of r_e appear. While accurate k_e values, except in few cases, are available for a large number of molecules, accurate r_e values are available for few. In such cases divergence from observed values is expected.

The experimental methods which have so far been used for estimating the electron affinities of atoms use electron attachment phenomena, electron impact measurements, equilibrium measurements and kinetics of electrodes processes and the theoretical ones involve calculation of lattice energies, heats of solvation of ions, and extrapolation of ionization potentials. For details of these methods reference may be made to the review by Pritchard (1953). It is of interest to note that these methods often yield very conflicting values. The values of E obtained by these methods have been collected for Fluorine, Chlorine, Bromine and Iodine in Tables II, III, IV and V, respectively. In nearly all cases the extrapolation methods yield E values much different from observed ones. The E values calculated for different halogen atoms using equation (1) agree with those obtained by other methods (Table II to V). However, the difference may

be due to the approximations involved in different methods and the use of inaccurate r_e values.

TABLE I
Electron affinities of halogen atoms

Atom	Molecule	k_e	r_e	I	D_e	$E(ev)$	E Mean (ev)
F	LiF	(2.36) ^a	(1.59) ^b	5.363	5.95±0.2(G) ≤6.6(H)	3.431±0.2 ≤4.081	3.843
	NaF	(1.465) ^a	(2.0) ^c	5.12	4.65±0.2(G) ≤5.3(H)	3.462±0.2 ≤4.112	
	KF	1.205 ^b	2.55 ^d	4.318	5.0±0.25(G)	4.158±0.25	
	RbF	1.39 ^b	(2.31) ^c	4.159	5.35±0.2(G)	3.876±0.2	
	CsF	1.451	2.345 ^e	3.89	5.5±0.2(G)	3.782±0.2	
Cl	LiCl	1.499 ^f	(1.97) ^c	5.363	5.0±0.3(G)	3.973±0.3	3.88
	NaCl	1.1 ^f	2.3606 ^e	5.12	4.24±0.05(G)	3.918±0.05	
	KCl	1.02 ^b	2.667 ^e	4.318	4.4±0.05(G) 4.42(H)	3.793±0.05 3.813	
	RbCl	1.076	2.787 ^g	4.159	4.5±0.2(G)	3.891±0.2	
	CsCl	0.95 ^b	2.906 ^e	3.87	4.6±0.2(G)	3.894±0.2	
Br	LiBr	1.248 ^f	2.17 ^e	5.363	4.35±0.3(G)	3.856±0.3	3.717
	NaBr	0.959 ^f	2.502 ^e	5.12	3.80±0.1(G) 3.85(H)	3.77±0.1 3.82	
	KBr	0.83 ^b	2.821 ^c	4.318	3.94±0.05(G) 3.96(H)	3.619±0.05 3.639	
	RbBr	0.788 ^b	2.945 ^c	4.159	4.0±0.25 (G)	3.692±0.25	
	CsBr	0.86 ^b	3.072 ^e	3.87	4.1±0.25(G)	3.623±0.25	
I	LiI	0.9727 ^h	2.392 ^c	5.363	3.5±0.2(G)	3.531±0.2	3.355
	NaI	0.7631 ^f	2.7115 ^c	5.12	3.07±0.1(G) 3.16(H)	3.434±0.1 3.524	
	KI	0.704 ^b	3.048 ^c	4.318	3.32±0.05(G) 3.33(H)	3.321±0.05 3.331	
	RbI	0.633 ^b	3.177 ^c	4.159	3.5±0.1(G) 3.29(H)	3.362±0.1 3.302	
	CsI	(0.665) ^a	3.315 ^c	3.87	3.4±0.1(G) 3.31(H)	3.248±0.1 3.148	

(a) Somayajulu (1960). (b) Barrow (1963). (c) Rittner (1951). (d) Grabner and Hughes (1950). (e) Hening *et al* (1954). (f) Rice and Klemperer (1957). (g) Tirschka Braunstein (1954). (h) Klemperer and Rice (1957).

TABLE II

Comparison of electron affinity of fluorine atom

E(e.v.)	Methods	Authors
3.843	Equation(1)	Present
3.622	Surface ionization	Dukel's kil and Ionov.*
3.62	Dissociation of alkali fluorides	Stamper and Barrow (1958)
3.567	Magnetron	Bernstein and Metly (1961)
3.557	Spectrophotometric	Jortner <i>et al</i> (1959)
5.0	Linear extrapolation	Pritchard (1953)
4.133	Borneyles	Mayer and Helmholtz (1932)
3.94	Quadratic extrapolation	Glockler*
3.47	Lattice energy	Cubieciotti. (1959)

*From Pritchard (1953)

TABLE III

Comparison of electron affinity of chlorine

E(e.v.)	Methods	Authors
3.88	Equation(1)	Present
4.021	Magnetron	Mitchell and Mayer (1940)
3.757	Surface ionization	Dukel' skil and Ionov.*
3.723	Magnetron	McCallum and Mayer (1943)
3.005	Electron impact	Hanson (1937)
4.8	Linear extrapolation	Pritchard (1953)
3.874	Lattice energy	Pritchard (1953)
3.68	-do-	Cubieciotti. Jr. (1959)
3.70	Quadratic extrapolation	Glockler*
3.10	-do-	Bates*

*Pritchard (1953)

TABLE IV
Comparison of electron affinity of bromine atom

E(e.v.)	Methods	Authors
3.717	Equation (1)	Present
3.83	Dissociation of alkali halides	Mayer and Helmholtz (1932)
3.818	Space Charge	Glockler and Calvin (1936)
3.805	Electron impact	Blewett (1936)
3.773	Mass spectrograph	Blewett (1936)
3.761	Flame	Piccardi (1926)
3.64	Surface ionization	Ionov (1940)
3.47	-do-	Weisblatt (1938)
3.556	Absorption spectra	Lederie (1933)
3.49	Magnetron	Doty and Mayer (1944)
3.47	Dissociation of alkali Halides	Saha and Tandon (1937)
3.799	Borneyles	Van Arkel, and De Boer (1927)
3.53	Lattice energy	Mayer and Helmholtz (1932)
3.526	Borneyles	Huggins (1937)

TABLE V
Comparison of electron affinity of iodine

E(e.v.)	Methods	Authors
3.355	Equation (1)	Present
3.557	Flame	Piccardi (1926)
3.31	Surface ionization	Ionov*
3.236	Space charge	Glockler and Calvin (1935)
3.141	Magnetron	Sutton and Mayer (1934, 1935)
3.002	Electron impact	Buchdahl (1941)
3.258	Lattice energy	Pritchard (1953)
3.14	-do-	Cubieciotti, Jr. (1959)

*Pritchard (1953)

REFERENCES

- Barrow, R. F. and Caunt, A. D., 1953. *Proc. Roy. Soc., London*, **A219**, 120.
- Bernstein, R. B. and Motlay, M., 1951. *J. Chem. Phys.* **19**, 1612.
- Bleick, W. E. and Mayer, J. E., 1934. *J. Chem. Phys.* **2**, 252.
- Blewett, J. P., 1936. *Phys. Rev.* **49**, 900.
- Buchdahl, R., 1941. *J. Chem. Phys.* **9**, 146.
- Cubieciotti D. D. Jr., 1959. *J. Chem. Phys.* **31**, 1945.
- Doty, P. M. and Mayor, J. E., 1944. *J. Chem. Phys.* **12**, 323.
- Gaydon, A. G., 1953. *Dissociation Energies*, (Chapman and Hall Ltd., London).
- Glockler, G. and Calvin, M., 1935. *J. Chem. Phys.* **3**, 771.
- , 1936. *J. Chem. Phys.* **4**, 492.
- Grabner, L. and Hughes, V., 1950. *Phys. Rev.* **79**, 819.
- Hanson, E. E., 1937. *Phys. Rev.* **51**, 86.
- Herzberg, G., 1950. *Molecular Spectra and Molecular Structure I. Spectra of Diatomic molecules*, 2nd ed. D. Van Nostrand Company, New York.
- Hodgman, C. D., 1963. *Hand Book of Chemistry and Physics*, The Chemical Rubber Publishing company, Ohio, Ed-44.
- Honig, A. Mandol, M. Stich, M. L., and Townes, C. H. 1954. *Phys. Rev.* **96**, 629.
- Huggins, M. L., 1937. *J. Chem. Phys.* **5**, 143.
- Ionov, N. I., 1940. *Comptes rendus Acad. Sci. U.S.S.R.* **28**, 512.
- Jortner, J., Stein, G. and Treinin, A., 1959. *J. Chem. Phys.* **30**, 1110.
- Klemperer, W. and Rice, S. A., 1957. *J. Chem. Phys.*, **26**, 618.
- Kunimune, M., 1950. *Prog. Theoret. Phys.* (Kyoto), **5**, 412.
- Lederle, E., 1933. *Zeits. f. Physik*, **7**, 328.
- Mayer, J. E. and Helmholtz, L., 1932. *Z. Physics* **75**, 19.
- McCallum, K. J. and Mayer, J. E., 1943. *J. Chem. Phys.* **11**, 56.
- Mitchell, J. J. and Mayer J. E., 1940. *J. Chem. Phys.* **8**, 282.
- Piccardi, G., 1926. *Atti accad. Lincei*, **3**, 566.
- Pritchard, H. O., 1953. *Chem. Rev.*, **52**, 529.
- Rice, S. A. and Klemperer, W., 1957. *J. Chem. Phys.*, **27**, 573.
- Rittner, E. S., 1951. *J. Chem. Phys.*, **19**, 1030.
- Saha, N. K. and Tondon, A. N., 1937. *Proc. Nat. Inst. Sci. Ind.*, **3**, 387.
- Somayajulu, G. R., 1960. *J. Chem. Phys.*, **33**, 1541.
- Stamper, J. G. and Barrow, R. F., 1958. *Trans. Faraday Soc.* **54**, 1952.
- Sutton, P. P. and Mayer, J. E., 1934. *J. Chem. Phys.*, **2**, 145.
- , 1935. *J. Chem. Phys.* **3**, 20.
- Tandon, S. P., Bhutra, M. P. and Tandon, K., 1966. *Indian J. Phys.* **40**, 49.
- Trischka, J. W. and Braunstein, B., 1954. *Phys. Rev.* **96**, 968.
- Van Arkel, A. E. and De Boer, J. H., 1927. *Physica*, **7**, 12.
- Varshni, Y. P. and Shukla, R. C., 1961. *J. Chem. Phys.* **35**, 582.
- Weisblatt, H. D., 1938. *Dissertation*, Johns Hopkins University.

BOOK REVIEW

THERMOELECTRICITY : SCIENCE AND ENGINEERING —by Roberk R. Heikes and Roland W. Ure, Jr. of the Westinghouse Research Laboratories and fourteen other Collaborators mostly from the Westinghouse Research Laboratories. Interscience Publishers, New York and London; 1961.

In recent years various methods have been developed for energy conversion of which thermoelectric devices are the most important. The materials necessary for production of such devices of appropriate efficiencies are obviously the semiconductors and the semimetals. The present volume which aims at giving a systematic presentation of the different aspect of the thermoelectric devices, rightly starts with a through discussion of the basic physical principles of semiconductors and semi-metals and methods of their controlled production. Properties of different such materials which have been found suitable for thermoelectric devices have also been exhaustively discussed. The technological and applied aspects have then been presented and can evidently be very easily followed by the reader. The future possibilities of such devices have also been discussed and in this connection the authors have briefly indicated the possibility of direct conversion of the heat of a nuclear reactor into electricity utilising such thermoelectric devices whereby the necessity of external generators or turbines is eliminated.

The volume though primarily meant for discussion of the different aspect of thermoelectric devices, in the investigation of which not many of the Indian laboratories are at present interested yet the method in which the basic physical principles of semiconductors and semimetals are discussed and the through review of the properties of thermoelectrically important materials, makes it worth reading by all workers on solid state physics.

A. K. Dutta

ELEMENTARY PARTICLES by Soklov; published by Pergamon Press. Oxford.

The book is a short review of the recent ideas and the phenomenology of the elementary particles siting prediction and discoveries. The book cannot claim any sort of completeness or a writing for the novice or any status of a text book. Yet the book is valuable as it mentions the landmarks and some of the crucial expressions in the analysis of the elementary particles. The author is successful in kindling interests of further study for serious readers of his book.

T. Roy

AN INTRODUCTION TO LAPLACE TRANSFORMATION—by J. C. Jaeger.
Published by Methuen and Co., Ltd. London.

It is a neat monograph on Laplace transform. In the first few pages he has given the rudiments of theory. Besides this the whole of the book has devoted to problems of communication engineering. The examples the author has chosen are very pertinent. Prof. Jaeger has not practically touched the inverse problem in the true sense of the term. Though it seems that Laplace transform is superior to Heavisides operational methods but failure of L. T. to problems again invites methods like Migusinski's, a point which communication engineers should know.

T. Roy

SYMPOSIUM OF PHOTOELASTICITY—Edited by M. M. Frocht. Published by Pergamon Press.

Photoelasticity by M. M. Frocht is the compilation of the papers presented at the International Symposium at the Illinois Institute of Technology in 1961. The use of Photoelastic method for the study stress distribution in various specimens are being used widely now-a-days in industrial problems. Due to its great practical importance a much greater attention is being devoted to improve the methods. The papers report the various new techniques and improvement of older methods for the determination stress and strain characteristics in various model specimens. One section contains survey of the recent activities in Japan on photoelasticity, a bibliography of recent works in photoelasticity in Britain and a paper on the recent developments in the field of photo-thermo-elasticity i.e. the study of the stress pattern developed due to thermal gradient. In other sections cover a wide field of interest e.g. two-dimensional methods using coatings, methods for the three dimensional photoelasticity, investigation of the elastic-plastic strain distribution around cracks in sheet materials, the potentiality of the method of scattered light etc. On reading the papers one can realise the vastness of the domain of application of photoelastic methods in science and engineering.

The papers are of highly technical nature and is suitable for the specialists. For the specialists the book will be very useful and informative. It gives an idea of the extent of the development going on in the field of photo-elasticity and the various recent prospective lines of developments. The bulk of the book do not seem to contain such a vast amount of informations on photoelasticity.

The editor and the publishers are to be congratulated for catering such a neat, small but informative publication on a topic of great interest. The book is worth of collection in any modern library of scientific and technical books.

R.K.S.

TURBULENCE—CLASSIC PAPERS ON STATISTICAL THEORY—Edited by S. K. Friedlander and Leonard Topper. Published by Interscience Publishers, N. V.

The volume contains a dozen of papers in statistical theory of turbulence ranging from 1921 to 1949. A brief historical background and references to same comparatively recent work appears in the preface. The papers are confined to theoretical work only e.g. the work of Simon and Slater to which G. I. Taylors paper refers (p. 100) is omitted. The papers reprinted are : 1. Diffusion by Continuous movement by G. I. Taylor (1921), (from proc. Lond. Math. Soc. Series 2, **20**, 196-211 (1921). 2. Richardson, L. F., "Note on a Theorem by G. I. Taylor" (from proceedings of the London Mathematical Society, Ser. 2, **20**, 211-212 (1921) 3. Taylor, G. I. "Statistical Theory of Turbulence. Parts I-IV" (from Proceedings of the Royal Society **A151**, 421-478, (1935). 5. Von Karman, T., and Howarth, L., "On the Statistical Theory of Isotropic Turbulence", (from Proceedings of the Royal Society **A164**, 192-215 (1938). 6. Taylor, G. I. "The Spectrum of Turbulence" (from proceedings of the Royal Society, **A164**, 476-490. (1938). 6. Dryden, H. L. "A Review of the Statistical Theory of Turbulence (from the Quartley of Applied Mathematics **1**, 7-42 (1943). 7. Kolmogoroff, A. N., "The Local Structure of Turbulence in Incompressible Viscous Fluid for very large Reynolds Numbers" (from Comptes rendus (Doklady) de Academie des Sciences de l' U.R.S.S. **30**, 301-305 (1941). 8. Kolmogoroff, A.N. "On Degeneration of Isotropic Turbulence in an Incompressible Viscous Liquid" (from Comptes rendus (Doklady) de academie des sciences de l'U.R.S.S. **31**, 538-540 (1941). 9. Kolmogoroff, A. N. "Dissipation of Energy in locally Isotropic Turbulence," (from Comptes rendus (Doklady) de l'academie des science del' U.R.S.S. **32**, 16-18(1941). 10. Von Karman, T. "Progress in the Statistical Theory of Turbulence", (from Journal of Marine Research **7**, 252-264 (1948). 11. Lin, C. C. "Note on the Law of Decay of Isotropic Turbulence" (from Proceedings of the National Academy of Science **34**, 540-543, (1948). 12. Von Karman, T. and Lin .C., "On the concept of Similarity in the Theory of Isotropic Turbulence." (from Reviews of Modern Physics, **21**, 516-519, (1949).

Of these No. 6, 10, and 12 are of the character of review

G. Bandyopadhyay

INDIAN JOURNAL OF PHYSICS

VOL. 41

No. 2

AND

VOL. 50

PROCEEDINGS

No. 2

OF THE

INDIAN ASSOCIATION FOR THE CULTIVATION OF SCIENCE

(Edited in collaboration with the Indian Physical Society).

FEBRUARY 1967

PUBLISHED BY THE
INDIAN ASSOCIATION FOR THE CULTIVATION OF SCIENCE
JADAVPUR, CALCUTTA-32

INSTRUCTIONS TO AUTHORS FOR PREPARATION OF MANUSCRIPTS

Original scientific papers on all branches of Physics and allied subjects such as Chemical Physics, Mathematical Physics, Applied Physics, Geophysics, Biophysics, Crystallography and Mineralogy etc.; are accepted for publication in Indian Journal of Physics provided these are not merely records of routine laboratory tests and contain original contributions to the knowledge of these Sciences. Normally, the author or at least one of the joint authors should be a member of the Indian Association for the Cultivation of Science or of the Indian Physical Society. Papers from authors other than members will be also accepted under special circumstances. Mss. for publication, in duplicate should be sent to the Assistant Secretary, Indian Journal of Physics, Indian Association for the Cultivation of Science, Jadavpur, Calcutta-32. Mss. submitted should be typewritten with double space, on one side of good quality paper, with sufficient margin on the left and at the top. Each paper should begin with an abstract just after the title of the paper and the name and full address of the author or authors. References in the text should be given either by quoting the year of publication within parantheses, if the surname of the author occurs in the text, or by quoting the surname of the author followed by the year within parantheses at the proper place. In case the reference has more than one name, all names other than the first should be replaced by *et al* in the text as shown. For example, "Thermal transformation..... was studied by Bernal *et al* (1959) and Das Gupta (1960)". Or "Thermal decomposition ... studied by different workers (Cuthbert, 1947 ; Weiden, 1954)". The full references should be given at the end of the paper, under head *References*, arranged alphabetically by surname, followed by initials, year of publication, standard abbreviated name of journal with single underline, volume with double underline, and the page *e.g.* : Perkins, H.D., 1950, *Proc. Royal Soc.* **A203**, 309. If more than one paper by the same authors occur in the same year, in the same journal or not, both in the text and in the *References* these should be chronologically signified by adding *a, b, c*, etc., to the year. Names of same author or authors successively coming in *References* may be replaced by a long 'dash'. Name of same journal coming in *References* successively may be also replaced by long dashes similarly. Positions for text figures and diagrams should be indicated in margin. Line diagrams should be drawn on white Bristol board or tracing paper with black Indian Ink and interior of the diagrams should contain the minimum number of index letters (preferably of simple Gothic style) or numerals (preferably Roman type). Where possible different graphs in the same diagram should only be differentiated by, full line, dotted line, dashed line, crosses, circles, squares etc. Full captions of all figures with serial numbers should be given in a separate sheet. Numerals for scales and description of coordi-

(Contd. to 3rd cover)

ON THE THERMAL EXPANSION OF γ -PHASE Cu-Mn ALLOYS AT HIGH TEMPERATURES

M. DE

INDIAN ASSOCIATION FOR THE CULTIVATION OF SCIENCE,
CALCUTTA-32, INDIA.

(Received June 25, 1966)

ABSTRACT. Photographs, using a 19 cm. diameter Unicam high temperature camera and filtered CuK_α radiation, were taken of powders from γ -phase Cu-Mn alloys with 4.53, 13.56 and 22.34 atomic percentage manganese upto 450°C . The linear thermal expansion coefficients have been determined from lattice parameter vs. temperature curves for all these alloys and the results have been compared with Grüneisen theory. It is found that the Grüneisen relation is valid for these solid solutions.

INTRODUCTION

The linear thermal expansion of solids is said to be due to the anharmonicity of interatomic forces and no complete theory of lattice vibrations that takes proper account of the anharmonic effects has yet been carried out satisfactorily for a 3 dimensional dielectric crystal and much less for a 3-dimensional metal. The lattice dynamics of Born is only quasi-harmonic. However, the theory of the equation of state is mainly due to Mie (1903) and Grüneisen (1912). This theory in its usual form (Grüneisen 1926) is based on the well known Debye approximation, leading to Grüneisen rule that the thermal expansion coefficient and the specific heat of a crystal are proportional. It implies a simple relation between the value of the constant γ (given by $\gamma = \alpha V/C_v K$ where α is the coefficient of volume expansion, C_v , V and K are the specific heat, volume and compressibility of the solid) and the sum of the exponents of the attractive and repulsive terms of the interatomic potential for central forces between atoms of Mie-Lennard-Jones type. Grüneisen theory was found to show correct type of expansion at least above the characteristic temperature θ by a number of workers—Nix and MacNair (1941, 1942), Hume-Rothery (1945), Thowlis *et al.* (1956), Quader and Dey (1962), Nicklow and Young (1963). However, the low-temperature works of Bijl and Pullan (1954, 1955), Rubin *et al.* (1954), Figgins *et al.* (1956), Simons *et al.* (1957) showed that the theory breaks down at a temperature below about $.3\theta$, the thermal expansion becoming bigger than the values predicted by the law. On the contrary Rubin *et al.* (1962) showed that the law holds good between 25° to 300°K in the case of Pb. Following low temperature experiments, Barron (1955) made an investigation of the variation of γ with temperature according to the lattice dynamics of Born and Karman and showed that for a cubic close packed

lattice the behaviour of γ is qualitatively similar to that found experimentally in monatomic metals.

Although there exists a considerable amount of work on the thermal expansion measurements for many of the metals and ionic crystals and the application of the Grüneisen theory to certain cases, for most of the alloys these have not been undertaken. So the present investigation is intended for the thermal expansion measurement in γ -CuMn alloys from x-ray powder photographs and also to test the validity of Grüneisen theory in these cases.

EXPERIMENTAL PROCEDURE

Copper manganese alloys with 4.53, 13.56 and 22.34 atomic percent manganese were prepared from spectrographically standardised copper and manganese supplied by Messrs. Johnson, Mathey and Co., London. Accurately weighed quantities of the component metals were melted together in evacuated and sealed quartz capsules; after melting the alloys were homogenized for a week in the temperature range 800–850°C. Weight changes during preparation were negligible.

Powder samples were obtained by hand-filing at room temperature. To remove the effect of cold-working and to obtain strain-free samples, powders were annealed at 600°C for 6 hours in pyrex glass capsules sealed under vacuum. This is also necessary to arrest the future grain-growth during heating in the high temperature camera. The filings were then sieved through a 250 mesh screen. To minimize thermal gradients small specimens about 4 mm. in length and .5 mm in diameter were prepared by taking the annealed powder in thin-walled pyrex capillaries with both ends sealed.

Using filtered CuK_α radiation and the standard 19 cm. Unicam high temperature camera, powder photographs were taken at temperatures lying between room temperature and 450°C. The temperature of the specimen was controlled manually within $\pm 1^\circ\text{C}$ by adjusting the variac of the circuit. The temperatures of the specimen were measured by a Pt-Pt Rh Thermocouple which was calibrated accurately by measuring the lattice parameter of pure Ag.

RESULTS AND DISCUSSIONS

(a) *Lattice parameter and coefficient of thermal expansion*

The lattice parameters of the alloys were determined from the high angle lines $(331)_{\alpha_1, \alpha_2}$ and $(420)_{\alpha_1, \alpha_2}$ and corrected by the standard extrapolation method of Taylor and Sinclair (1945). The values are given in Table I and the accuracy of the values lies within $\pm .0005 \text{ \AA}$. Curves giving the variation of lattice parameters with temperature are shown in Fig. 1. It is found that for all these three compositions they are linear which is in accordance with the recent thermal expansion

works of Rao *et al* (1964) on some compositions of AgPd alloys and Uma Devi *et al.* (1965) on Au-Pd alloys. These curves were extrapolated to 0°C and the linear

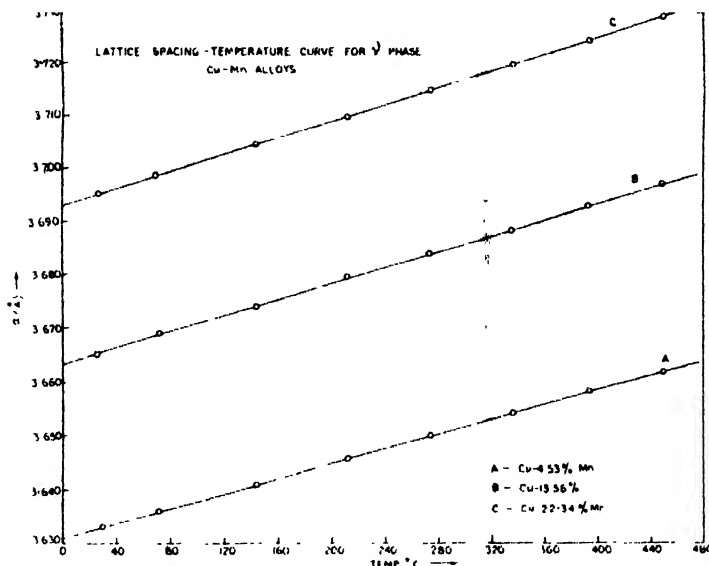


Fig. 1. Lattice Spacing - Temperature Curve for γ -phase Cu-Mn Alloys.

thermal expansion coefficients $\alpha_{200}^\circ\text{C}$ and $\alpha_0^\circ\text{C}$ were determined from the relation

$$\alpha = \frac{1}{a} \frac{da}{dT} \text{ for the three compositions. These values are inserted in Table II.}$$

In Table I data for the lattice parameters for pure copper are given from the works of Hume-Rothery and Andrews (1942). From those values, $a_{273}^\circ\text{K}$ and $\alpha_{273}^\circ\text{C}$ for pure copper were determined and are inserted in Table II. From Table II, α_{273} values of the three Cu-Mn alloys were plotted against composition of manganese (Fig. 2) and from this curve, by extrapolation, α_{273} for pure Cu was found to

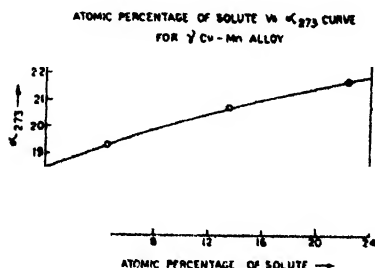


Fig. 2. Atomic percentage of solute vs. α_{273} curve for γ -Cu-Mn Alloys.

be $18.4 \times 10^{-6}/^\circ\text{C}$ which is in good agreement with that from Hume-Rothery and Andrews (Table II). It is evident that the thermal expansion coefficient increases with the increase of manganese concentration.

(b) *Comparison with Grüneisen theory*

Grüneisen (1912, 1926) has given an approximate theory of thermal expansion based on the Debye model of monatomic solids with a single Debye temperature θ . This theory relates the volume expansion of solids, whose atoms exert nearly harmonic vibrations in an asymmetrical force field, due to rise in temperature with the atomic heat of solid and its compressibility at absolute zero. The theory may be expressed as recommended by Hume-Rothery, in the following form,

$$3 \frac{a_T - a_0}{a_0} = \frac{V_T - V_0}{V_0} = \frac{E_T/Q}{1 - p \cdot E_T/Q} \quad \dots (1)$$

where V_0 and V_T are the volumes of the solids at 0°K and $T^\circ\text{K}$ respectively, E_T is the vibrational energy of the solid, a_0 and a_T are the lattice parameters at 0°K and $T^\circ\text{K}$, Q and p are constants given by

$$Q = \frac{V_0}{\gamma K_0} \quad \dots (1a)$$

where V_0 and K_0 are the molar volume and compressibility at absolute zero and γ is called Grüneisen constant, and

$$p = \frac{m+n+3}{6} \quad \dots (1b)$$

where m and n are the powers of the Mie potential function,

$$\phi = \frac{A}{r^m} - \frac{B}{r^n}, \quad r \text{ being interatomic distance.}$$

Relation (1) may again be written as,

$$\frac{a_0}{a_T - a_0} = \frac{3V_0}{V_T - V_0} = \frac{3Q}{E_T} - 3p \quad \dots (2)$$

In order to find out the value of the left hand side of Eq. (2) which is the reciprocal of the expansion at absolute zero we shall have to know a_0 which can be obtained if we can find out that at 273°K i.e. $\frac{a_{273} - a_0}{a_0}$ from our experimental data. This can be done by applying Fischmeister's low-temperature approximation (1956) to eq. (2) :

$$\frac{a_{273} - a_0}{a_0} = \frac{1}{3} \frac{E_T}{Q} = \frac{\alpha_{273} \cdot E_{273}}{C_{v273}} \quad \dots (3)$$

Assuming $Q = \frac{C_v}{3\alpha}$ at low temperatures, from eq. (3) a_0 can be determined

and thereby Q and p if we take a_{273} , α_{273} from Table II and if we can determine C_{v273} and thereby $E_{273} \left(E_T = \int_0^T C_v dT \right)$ for the alloys.

TABLE I
Lattice parameter of pure copper and γ -phase Cu-Mn alloys

Pure Copper*		Cu 4.53% Mn Alloy.		Cu 13.56% Mn Alloy.		Cu 22.34% Mn Alloy.	
Temp. °C	Lattice parameter. Å	Temp. °C	Lattice parameter. Å	Temp. °C	Lattice parameter. Å	Temp. °C	Lattice parameter. Å
18	3.6146	30	3.6328	26	3.6651	29	3.6952
300	3.6333	172	3.6357	72	3.6690	72	3.6986
500	3.6471	144	3.6410	144	3.6741	144	3.7046
671	3.6599	212	3.6454	212	3.6797	212	3.7100
771	3.6676	274	3.6500	274	3.6844	274	3.7149
871	3.6756	336	3.6542	336	3.6889	336	3.7200
		393	3.6584	393	3.6933	393	3.7246
		450	3.6623	450	3.6975	450	3.7291

*Hume-Rothery and Andrews (1942)

TABLE II
Data for the calculation of ' a_0 ' and ' α '

Composition	a_{273} Å	$\alpha_{273} \times 10^6$	C_{v273} cal. mol ⁻¹ °C ⁻¹	E_{273} cal mol ⁻¹	a_0 Å	$\alpha_{473} \times 10^6$
Cu	3.6133	18.30	7.62	1503.2	3.6003	
Cu- 4.53% Mn	3.6306	19.28	7.65	1507.4	3.6169	19.21
Cu-13.56% Mn	3.6633	20.70	7.68	1512.8	3.6484	20.62
Cu-22.34% Mn	3.6928	21.66	7.71	1517.7	3.6771	21.57

From N. B. S. monograph No. 21,1960 which provides the specific heat data for pure copper and manganese upto 300°K, the C_p values for the alloys from 0°K to 300°K were determined applying Neumann-Kopp's approximation rule. From these C_p values, C_v values were calculated from the relation, $C_p - C_v =$

$0.0214T \frac{C_p^2}{T_m}$, where T_m is the melting point of the substances in absolute scale.

Using these C_v values, E_T values were determined from the relation $E_T = \int_0^T C_v dT$

by calculating the area of the graph applying Simpson's rule.

From Eq. (2) $\frac{a_0}{a_T - a_0}$ and $\frac{1}{E_T}$ values were calculated and are plotted in Fig. 3

for the three γ -phase alloys and also for pure copper taking data for the latter from Hume-Rothery and Andrews (1942). These are called 'Grüneisen plots' and are inserted in Table II. It is found that for the alloys and also for pure Cu these plots give straight line curves. Similar straight line curves were obtained by Fischmeister (1956) for ionic crystals like NaCl, KCl, LiF, Potassium and Caesium bromides and iodides. Quader and Dey (1962) got straight line curves from these plots in the case of Ag and α -phase Ag-Cd alloys. Recently Nicklow and Young (1963) have also obtained the same nature of curves for Al and AgCl.

TABLE III

Data for Grüneisen plot for Cu and Cu-Mn alloys

Pure Copper		Cu 4.53% Mn Alloy.		Cu 13.56% Mn Alloy.		Cu 22.34% Mn Alloy.	
$\frac{1}{E_T} \times 10^4$	$\frac{a_0}{a_T - a_0}$	$\frac{1}{E_T} \times 10^3$	$\frac{a_0}{a_T - a_0}$	$\frac{1}{E_T} \times 10^3$	$\frac{a_0}{a_T - a_0}$	$\frac{1}{E_T} \times 10^3$	$\frac{a_0}{a_T - a_0}$
.610	251.8	.576	227.5	.584	218.5	.574	203.2
.264	109.1	.486	192.4	.484	177.1	.482	171.0
.188	76.9	.383	150.1	.382	142.0	.381	134.2
.151	60.4	.320	126.9	.318	116.6	.317	111.8
.136	53.5	.278	109.3	.277	101.3	.275	97.3
.123	47.8	.245	97.0	.244	90.1	.243	85.7
		.222	87.2	.221	81.3	.220	77.4
		.202	79.7	.201	74.3	.200	70.7

TABLE IV

Values of the constants 'Q' and 'p'

Compositions at %.	'Q'	'p'
Pure Copper.	139845	1.33
Cu 4.53% Mn.	133333	0.6667
Cu 13.56% Mn.	126984	1.46
Cu 22.34% Mn.	120000	0.6667

From Fig. 3 and Eq. (2), Q and p values for the three γ -phase alloys and also for Cu were determined and are inserted in Table IV. These values are supposed to

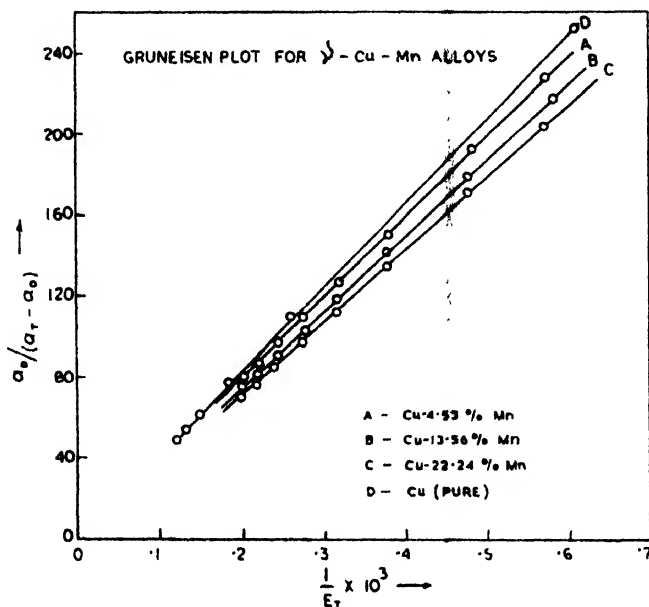


Fig. 3. Grüneisen plot for γ -Cu-Mn Alloys.

be correct within 10%. However, for pure Cu the value of Q is nearly 15% higher than the value given by Hume Rothery (1945) viz. 117,000. The value of α affects the values of Q and p to some extent but exactly the same value of Q for Cu as given by him cannot be obtained by applying Fischmeister method of calculation to his experimental data (1942). It is evident from these experiments that the values of Q for these alloys increase with the decrease of manganese concentration. However, from the rectilinearity of the curves obtained from Grüneisen plots it appears that within the limits of experimental error and the temperature range concerned Grüneisen Theory, as it stands, is valid for these solid solutions.

ACKNOWLEDGMENTS

The author is indebted to Prof. B. N. Srivastava, D.Sc., F.N.I., for his keen interest in the work and also to Dr. M. A. Quader for suggesting the problem and for valuable discussions.

REFERENCES

- Bijl, D., and Pullan, H., 1954. *Phil. Mag.*, **45**, 290.
 ———, 1955. *Physica*, **21**, 285.
 Barron, T. H. K., 1955. *Phil. Mag.*, **46**, 720.
 Corruccini, R. J., and Gniewek, J. J., 1960. *N.B.S. Monograph* No. 21.
 Devi, U., Rao, C. N., and Rao, K. K., 1965. *Acta Met.*, **13**(1), 44-5.

- Figgins, B. P., Jones, G. O., and Riley, D. P., 1956. *Phil. Mag.*, **1**, 747.
- Fischmeister, H. F., 1956. *Acta Cryst.*, **9**, 416.
- Gruneisen, E., 1912. *Ann. Phys. Leipzig*, **39**, 279.
- 1926. *Handbuch der Physik*, **10**, 1.
- Hume-Rothery, W., 1945. *Proc. Phys. Soc.*, **57**, 209.
- Hume Rothery, W. and Andrews, K. W., (1942), *J. Inst. Metals*. **68**, 19.
- Nicklow, R. M., and Young, R. A., 1963. *Phys. Rev.*, **129**, 1936.
- Nix, F. C., and McNair, D., 1941. *Phys. Rev.*, **60**, 597.
- Quader, M. A., and Dey, B. N., 1962. *Indian J. Phys.*, **36**, 43.
- Rao, C. N., and Rao, K. K., 1964. *Phil. Mag.*, **9(99)**, 527-8.
- 1964, *Canad. J. Phys.*, **42**, (7), 1336-42.
- Rubin, T., Altman, H. W., and Johnston, H. L., 1962, *J. Phys. Chem.*, **66**, 266.
- , 1954. *J. Am. Chem. Soc.*, **76**, 5289.
- Simmons, R. O., and Balluffi, R. W., 1957. *Phys. Rev.*, **108**, 278.
- Smclair, H., and Taylor, A., 1945, *Proc. Phys. Soc.*, **57**, 108., 126.
- Thewlis, J., and Davey, A. R., 1956. *Phil. Mag.*, **1**, 409.

DIVERSITY COMBINING USING CARRIER LOCK AND SIDE BAND LOCK TECHNIQUES*

PART II

N. B. CHAKRABARTI⁺ AND A. K. DATTA⁺⁺

INSTITUTE OF RADIO PHYSICS AND ELECTRONICS, UNIVERSITY OF CALCUTTA.

(Received January 15, 1966; Resubmitted May 25, 1966)

ABSTRACT. In this paper the design and performances of a diversity combining system using carrier lock and sideband lock techniques have been discussed. The effects of noise have been studied with particular reference to the loop phase equation, signal to noise ratio, RMS phase error and limiting of the sum of signal and noise on the threshold value in a two channel predetection diversity combining system. The results of combining two modulated r.f. carriers bearing the same information are also stated. A calculation for the first order probability density function of the instantaneous phase for a carrier phase lock circuit is given. A scheme is suggested to correct the Doppler frequency shift of the received signal.

INTRODUCTION

In fading channels it is often found necessary to incorporate some kind of diversity for reliable communication. An essential requirement in diversity system is that the signals on the different independent channels be combined coherently. It should be clear that diversity combination requires locking of the carrier of each channel to its signal and also locking of the different signals on the various channels. Now it may so happen that the received signal power on a given channel may not be adequate to ensure satisfactory locking of its own demodulating carrier, while the total channel power may be large enough. An efficient locking technique should, therefore, make use, if possible, of the total channel power to establish lock (in AM one should utilise both carrier and sideband powers). We shall discuss the problem of diversity combination in section 2, with particular reference to the philosophy of inter and intra channel coherence to secure gain in the SNR of the combined output. Locking techniques in diversity reception with particular reference to (i) a pre-detection combiner and (ii) a post-detection combiner have also been discussed in this section (Chakrabarti, *et al.*, 1966).

*This work has been carried out in the Institute of Radio Physics and Electronics, University of Calcutta.

⁺Now with the Department of Electronics and Electrical Communication Engineering, Indian Institute of Technology, Kharagpur.

⁺⁺Department of Physics, University of Burdwan, West Bengal.

Section 3 is devoted to a discussion on the effects of noise on the loop phase equation, SNR at the output of the combiner, RMS phase perturbation of the locking loop and limiting of the received signal on the threshold value.

Experimental set-up and results of combining two modulated r.f. carriers, are given in section 4.

LOCKING TECHNIQUE IN DIVERSITY RECEPTION

To satisfy the increasingly greater demand for long distance communication through radio waves is not only to provide additional communication channels but also to provide a reliable and efficient communication technique. Considerations of noise, interference and fading within the communication band and the time varying character of the propagation media call for the transmission of the same message in a number of frequency channels simultaneously.

It is known that for certain communication applications it is desirable to use broad band signals in conjunction with coherent reception and that linear wide band systems (like frequency diversity of DSB, SSB) can be designed to operate reliably for low input signal to noise ratios. The argument can be stated as follows. In a linear system the output SNR equals the input SNR. Suppose that there are a number of such channels carrying the same signal. If the outputs of the different channels can be so combined that the signals add coherently and the weights used in combination are proportional to the signal to noise ratio of the corresponding channels then it can be shown that the SNR of the sum is equal to the sum of the SNR's (Kahn, L. R., 1954). This is optimum diversity combination. Even if the weights are unity, there is considerable gain in SNR, for now the output SNR is equal to $\Sigma s_k^2 / \Sigma n_k^2$ where s_k and n_k are the signal and noise powers in the k -th channel. Two advantages arise. Firstly, the statistics of the combined noise and interference powers, which individually may have high ratios of the peak to r.m.s. assume after addition a fairly smooth character. Secondly, the output SNR shows considerable improvement over that of a single channel carrying an amount of power equal to the sum of the powers in the component channels. Such wide band systems thus have an inherent resistance to interference.

To establish Phase coherence inter and intra channels

If we have a frequency diversity of order two, there will be two r.f. signals carrying the same message although their input signal to noise ratio (SNR) will in general be different. Since the two inputs are at two different frequencies they will have to be brought back to the same frequency by appropriate local oscillators. Further since the r.f. phases after heterodyning will be different the modulation phase of the output of any coherent type detector will also be different. The phasing of the two r.f. signals to bring them into coherence can be done at r.f. (Brennan, D. G., 1959) and also at base band for linear demodulation systems.

Figs. (1) and (2) show the block representations to implement these techniques. For r.f. phase locking one would need a phase comparator or discriminator for measuring the difference in phase between the two r.f. signals and actuate the local oscillator in such a way as to reduce and if possible eliminate the phase difference between the two signals. For phasing at base band the demodulated outputs in the two channels can be compared by means of an audio frequency phase discriminator, the detected output of the discriminator controlling the r.f. phase of one of the channels.

The above mentioned differentially coherent technique enable one to bring the two inputs to a common reference. (It should be obvious that predetection phasing is the optimum technique if the demodulation is non-linear).

Locking through use of IF phase information

Fig. (1) shows the block diagram for a diversity combiner where relative phasing is accomplished at RF for a frequency diversity of order three. The intermediate frequency (i.f.) outputs of the three mixer stages are the same and the three i.f. outputs are brought in phase coherence before they are added and fed to a sideband lock receiver of the proper kind. Let us consider the input to the combiner is a frequency diversity of DSB signals of order three. Three frequency channels are separated using three frequency selective networks preceding the three mixer stages. Of the three local oscillators associated with the three mixer stages in the receiving system, two are of voltage controlled type and the third one along with its mixer is recognised as the reference chain and the corresponding i.f. output may be called as the reference i.f. output. The phase of the other two outputs are compared with it using two phase discriminators and d.c. controlling voltages are obtained in proportion to the phase departure between them. This d.c. controlling voltage is used to change the reactance offered by

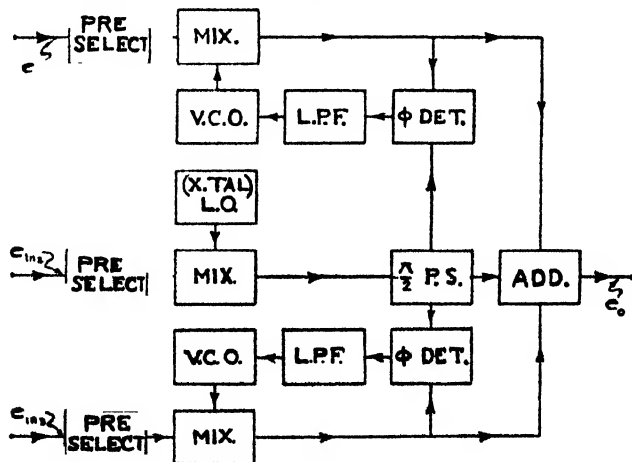


Fig. 1. Block diagram for coherent combination of the signals in a three channel frequency diversity system using r.f. phase information

a voltage sensitive diode which forms a frequency determining parameter in each of the VCO's. The d.c. controlling voltage is utilised in such a sense as to make the phase discrepancies between the i.f. outputs a minimum. It is seen that the reference i.f. output is given a phase shift of $\pi/2$ radians before multiplication. In the phase discriminator the low frequency output is proportional to the sine of the phase difference between its two inputs. Thus if the two i.f. outputs are in phase the product demodulator output is zero and the magnitude and polarity of this output depend on the magnitude of the phase difference between the two and whether one leads or lags the other.

The abovementioned technique is also suitable for combining diversity signals resulting from other types of modulations, linear as well as nonlinear.

To derive the expression for the control voltage in this case we note first that the IF output of the reference channel may be written to be

$$e_{Ref} = A \cos (\omega_i t + \phi_1 + \pi/2) \quad \dots (1)$$

and that of the other channel

$$e_{oc} = B \cos (\omega_i t + \phi_2) \quad \dots (2)$$

When these two IF outputs are multiplied one gets

$$e_d(t) = kAB \sin (\phi_1 - \phi_2) \quad \dots (3)$$

as the controlling d.c. voltage.

Locking through use of modulation phase information

The combination of a diversity of signals can also be achieved using phase information from the detected modulation components. This technique is particularly suited for linear modulation systems. Fig. (2) shows the block diagram of such a Phasing Scheme. The input to such a combiner can be taken to be a frequency diversity DSB (since the modulation is linear) signal of order three. The three i.f. outputs in this case are fed to three DSB modulation receivers. It is known that the inphase channel output for such a receiving system corresponds to the modulation components. Before adding the three P channel outputs together it must be ascertained that they have been brought in phase coherence. Phase coherence between the modulation components is achieved by comparing the phase of the modulation output in the reference chain with those at the other two chains using two low frequency phase discriminators. The d.c. outputs of these phase detectors are used to control the phase of the VCO's in the respective chain. The phase detector output in this case is also proportional to $\sin \phi_s$, where ϕ_s stands for the phase discrepancy between its two inputs. Each P channel output is fed to a wide band phase shifter associated with it. The outputs of each of the phase shifter are in phase quadrature with each other. So from the reference P channel two outputs are derived which are in phase quadrature and are applied to the two phase detectors as one of the two inputs.

The techniques mentioned above are meant for correcting phase perturbations between the signals in the different channels. There may sometimes be some disturbances common to all the channels e.g. Doppler shift. In such cases it is desirable to correct these common disturbances by means of a control circuit operated by the average value of a sum of the instantaneous phases in the different channels. Schematic diagram of such a control circuit is given in Fig. (3).

PHASE EQUATION AND SIGNAL TO NOISE RATIO IN A TWO-CHANNEL PREDETECTION COMBINER DIVERSITY SYSTEM

Let us consider the system of Fig. (1). If the inputs (1) and (2) are represented by

$$e_{i1}(t) = \Sigma A_u \cos(\omega_0 t + ut + \phi_u) + n_1 \cos(\omega_0 t + \phi_{n1}) \quad \dots (7)$$

$$\text{and} \quad e_{i2}(t) = \Sigma A_v \sin(\omega_0 t + vt + \phi_v) + n_2 \sin(\omega_0 t + \phi_{n2}) \quad \dots (8)$$

the output of the product modulator will be

$$e_d(t) = \Sigma \Sigma A_u A_v \sin(vt - ut + \phi_v - \phi_u) + \Sigma A_k n_2 \sin(\phi_v - \omega_k t - \phi_k) \quad \dots (9)$$

In the particular case when the signals are of the CW type the expression for the output may be written more simply as

$$e_d(t) = [A_1 A_2 \sin(\phi_1 - \phi_2) + n_1 A_2 \sin(\phi_2 - \phi_{n1}) \\ + n_2 A_1 \sin(\phi_{n2} - \phi_1) + n_1 n_2 \sin(\phi_{n1} - \phi_{n2})] \quad (10)$$

It will be seen that this output contains a term proportional to the sine of the difference between the phases of the two signals, a term representing intermodulation between the signal and noise and the third term representing intermodulation between the noise components.

In general the difference in phase $\phi_1 - \phi_2$ will be a slowly varying function of time and one can therefore use a low pass filter of narrow bandwidth to accept only the slowly varying components. The detected output thus filtered has been contaminated with noise and intermodulation components in the band of this filter.

The filtered output as shown in the diagram controls the instantaneous frequency of the VCO. The phase equation that results is

$$\frac{d\phi}{dt} = Kf(p) \sin(\phi_1 - \phi_2 - \psi_0) \quad \dots (11)$$

If the effective signal to noise ratio in the closed loop bandwidth of the controlled loop be adequate then it is reasonable to assume that the magnitude of the

phase $(\phi_1 - \phi_2 - \psi_0)$ will be small and one can write the phase equation in the linearised form as

$$\frac{d\phi}{dt} = Kf(p)(\phi_1 - \phi_2 - \psi_0) \quad \dots \quad (12)$$

It should be mentioned that although there will be steady state phase error the phase difference $\phi_1 - \phi_2$ will be perturbed by the noise terms present. The summed output can be written as

$$e_T(t) = [A_1 \exp j(\omega_0 t + \phi_1 - \psi_0) + A_2 \exp j(\omega_0 t + \phi_2 - \psi_0 - \phi_e) + n_1 \exp j(\omega_0 t + \phi_{1n}) + n_2 \exp j(\omega_0 t + \phi_{2n})] \quad \dots \quad (13)$$

where ϕ_e is the phase error. The amplitude of the instantaneous signal will thus be

$$S = [A_1^2 + A_2^2 + 2A_1 A_2 \cos \phi_e]^{\frac{1}{2}} \quad \dots \quad (14)$$

If the noises appearing in the two channels have a correlation coefficient ρ then the total noise voltage will be given by

$$N = [n_1^2 + n_2^2 + 2\rho n_1 n_2]^{\frac{1}{2}} \quad \dots \quad (15)$$

In the case of three channels the corresponding signal and noise outputs are

$$S = [A_1^2 + A_2^2 + A_3^2 + 2(A_1 A_2 \cos \phi_{12} + A_2 A_3 \cos \phi_{23} + A_3 A_1 \cos \phi_{31})]^{\frac{1}{2}} \quad (16)$$

$$N = [n_1^2 + n_2^2 + n_3^2 + 2(\rho_{12} n_1 n_2 + \rho_{23} n_2 n_3 + \rho_{31} n_3 n_1)]^{\frac{1}{2}} \quad \dots \quad (17)$$

Effect of limiting the sum of signal and noise on the threshold value

Threshold : Threshold SNR is defined as the value of the signal to noise ratio at which the rate of change of output SNR with the input SNR shows an abrupt break. Threshold phenomenon is due to nonlinear processes occurring in demodulation which cause through intermodulation a rise in the value of the noise appearing in the output.

In CPL threshold SNR (power) in the effective bandwidth of the system is about 5 or 7 db.

Limiting : It is known that if a sum of two signals is limited and the limited signal is passed through a bandpass filter there is a general suppression of the weaker component. The amount of this suppression depends on the amplitude ratio and the difference in frequency. This result can be carried over to the analysis of the situation when one of the signals is replaced by a random noise.

The probability of the noise amplitude being above a certain value C , is given by

$$\frac{2}{\sqrt{\pi}} \int_0^C e^{-x^2/2N_0} \cdot dx \cdot \frac{1 + \operatorname{erf} \sqrt{R}}{2} .$$

This shows that at a signal to noise ratio of R the favourable period is more than the unfavourable by a factor equal to $\frac{1+\operatorname{erf}\sqrt{R}}{1-\operatorname{erf}\sqrt{R}}$. If we assume that the average suppression during the favourable period is the same as that in the unfavourable period, the average SNR at the output will show an apparent improvement.

This improvement in SNR is however of no consequence in binary PSK reception if the error probability is less than the minimum desired value before limiting. This is so because the error probability is determined essentially by the condition that the value of the in phase component of noise be less than a certain maximum in order that the number of times the r.f. phase is modified by the noise is less than a prescribed minimum. Limiting filtering cannot alter this condition and therefore has no effect on the threshold value.

R.M.S. Phase Error : It is of interest to form an estimate of the perturbation produced by noise in the feedback loop. In fact the effective signal strength is always found to be multiplied by the term $\cos \phi_e$ where ϕ_e is the phase error due to noise. Further there may be instant of time when the phase disturbance due to noise might cause loss of synchronisation.

An examination of the noise terms in the loop phase equation (Refer Eq. 9) shows that the output noise is in general a nonlinear function of the input noise except when the signal to noise ratio is high. One of the terms in this equation can be considered to have arisen due to phase modulation of the noise in the band by a voltage proportional to the carrier phase. It is therefore expected that the spectrum of this intermodulation will spread over the band equal to the sum of the noise band and the band of the carrier phase modulation. If the latter is small the spectral character of this intermodulation term can be considered to be the same as that of the input noise. The effect of another term which is due to intermodulation between noise components will also have to be considered unless the signal to noise ratio is adequate.

To analyse the phase equation it is convenient to lump all the noise terms together as a single noise term having approximately the same spectral character as the input noise. However, its magnitude increases more sharply than the input. The equivalent equation is

$$\frac{d\phi}{dt} = \Omega - Kf(p)[A \sin \phi + N] \quad (18)$$

To find the probability distribution of the loop phase the above equivalent equation must first be converted into corresponding equation for the probability density, W . This equation when $f(p) = 1$ and $\Omega = 0$, is known to be given by

$$\frac{\partial W}{\partial t} = \frac{N_0 K^2}{4} \frac{\partial^2 W}{\partial \theta^2} + K \frac{\partial}{\partial \theta} (A \sin \theta \cdot W) \quad (19)$$

where N_0 is the noise power.

It is easy to verify that the solution to this equation in the steady state $\frac{\partial W}{\partial t} = 0$ is

$$W(\theta) = \frac{\exp(a \cos \theta)}{2\pi I_0(a)}, \quad \text{where } a = \frac{4A}{KN_0}.$$

An approximate solution of the derived equation for a general $f(p)$ can be found by first linearising the equation and solving it, and replacing the first power of θ by $\sin \theta$ and θ^2 by $2(1 - \cos \theta)$ in the solution. Once the probability density is determined, the square phase error and the mean value of $\cos \phi$ can be readily found by evaluating the integrals

$$\overline{\phi^2} = \frac{1}{2\pi} \int_{-\pi}^{\pi} \phi^2 W(\phi) \cdot d\phi \quad \dots (20)$$

$$\overline{\cos \phi} = \frac{1}{2\pi} \int_{-\pi}^{\pi} \cos \phi W(\phi) \cdot d\phi \quad \dots (21)$$

In the particular cases when $f(p) = 1$ or $f(p) = \frac{1}{1+p^2}$, the value of $\overline{\cos \phi}$ is

$$\frac{I_1(a)}{I_0(a)}, \quad \text{where } a = \frac{A^2}{\text{Noise density} \times \text{noise bandwidth}}.$$

EXPERIMENTAL SET-UP, RESULTS AND DISCUSSIONS

Fig. 4. shows the block diagram of the experimental arrangements for the coherent combination of two r.f. carriers at frequencies 1.55 mc/s and 1.85 mc/s

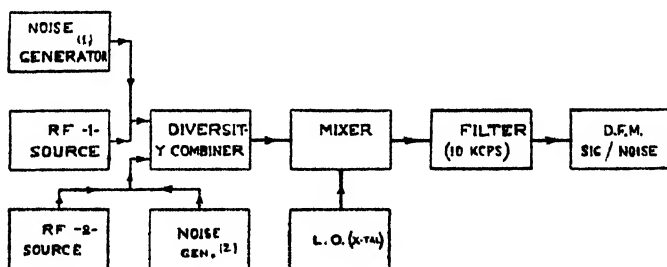


Fig. 4. Block diagram of the experimental set-up for coherent combinations of two r.f. carriers.

respectively. The frequencies of the oscillators in the respective mixers are higher than the incoming carriers by 500 Kc/s. One of the oscillator is a V.C.O. and a V-33 type varactor is used in the frequency determining circuit. The voltage sensitivity of the VCO is 15 Kc/s per volt. The reference oscillator is that of a Clapp's type. A crystal controlled oscillator may preferably be used as a reference one.

In the design of the phase control loop, consideration has been given to the correlation time, maximum fading rate and noise bandwidth.

For the purpose of simulation of multiplicative noise caused by the propagation medium, one has to take into account, besides a nearly steady Doppler shift due to a regular drift, (i) flat fading, where the band of interest is subject, as a whole, to variations of amplitude and phase; (ii) selective fading where the fluctuations of amplitude and phase of different groups of frequencies in the band are relatively independent and (iii) multipath phenomena where a large number of identifiable paths having distinct time delays and amplitude-phase fluctuations contribute to the total received signal. For the first case one may multiply the input with the sum of a carrier and a narrowband noise around it. For the second the input is distributed to several bandpass channels and amplitude-phase fluctuations are introduced from narrowband noise sources. For multipath simulation provision is made for fixed and variable time delays and amplitude-phase variations of the different outputs from the tapped delay line. The bandwidth of the noise sources will have to be consistent with the fading rate both in amplitude and phase in the frequency band of interest. (The rms fading rate at H.F. determined essentially by the random velocity distribution of the scattering sources is known to be about $10/\lambda$ c/s where λ is in meters)

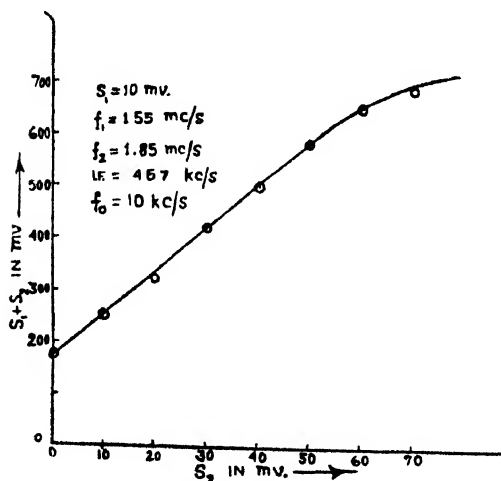


Fig. 5. Figure shows the variation of the combined output after coherent combination of two r.f. carriers with the change in level of either of the two carriers, the level of the other is held constant.

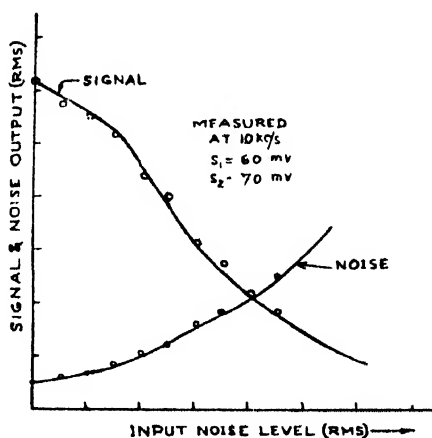


Fig. 6. Figure shows the variation of the signal and noise output in the combined output with the change in noise levels at the input to the combiner, the levels of the carriers are held constant.

The experimental result presented in Fig. (5) shows that the combined output due to two R.F. inputs increases linearly over a certain range of the inputs. The minimum acceptable value is determined by the total noise while the maximum value is controlled by the system non-linearity. From the results shown in Fig. (6) we note that as the input SNR deteriorates there is a reduction in the

summed output. This is due as mentioned in Sec. 3 to partial incoherence at the summing point due to inadequacy of the phase following loop. The noise output at the summing point shows a linear variation upto certain level of input noise after which there is a marked increase in the slope. This is due to the threshold phenomenon setting in as discussed in Sec. 3.

It should be emphasised that for the success of any diversity system a knowledge of such medium properties as correlation bandwidth in respect of envelope and phase, amount of correlation between the signal as well as noise fluctuations in the component channels and the fading spectrum is essential. Such data requiring analysis of observations over a long period, unfortunately, are not readily obtainable. This problem of channel estimation will be considered in a future communication.

ACKNOWLEDGEMENTS

The authors wish to thank Prof. J. N. Bhar, D.Sc., F.N.I., for his kind interest and encouragement. Thanks are also due to Messrs. P. Dharbhowmick and B. N. Biswas for helpful suggestions.

REFERENCES

- Brennan, D. G., 1959. *Proc. IRE*, **47**, 1075.
 Chakravarti, N. B. and Datta, A. K., 1966, *Indian. J. Phys.* **41**, 501.
 Davenport and Root 1958 *Random Signals and Noise*, Mc-Graw Hill Book Company, Inc.
 Kuhn, L. R., 1954. *Proc. IRE*, **42**, 1704.
 Middleton, D., 1960, Mc-Graw Hill Book Company, Inc. Chap. 10, 17.
 Montgomery, 1954. *Proc. IRE*, **42**, 447.
 Smith, R. A., 1951. *Proc. IRE*, **III**, **98**, 401.

APPENDIX

First order probability density function of instantaneous phase for a CPL circuit

To find the probability density of the instantaneous phase in a phase locking loop one may first develop the loop dynamical equation into the corresponding Fokker Planck equation. In the case when the loop filter is given by

$$f(p) = \frac{1}{1+p\tau}$$

the loop equation becomes

$$(1+p\tau) \frac{d\theta}{dt} + KA \sin \theta = K(\Omega_1 - \omega)$$

$$\text{where} \quad \Omega_1 = \frac{1}{K} [(1+p\tau)\Omega] \quad \dots \quad (A1)$$

Now the frequency deviation Ω may be a random variable with or without a steady component. If it has no steady component R.H.S. of A1 may be replaced

by a random variable having a power density determined by Ω_1 and n . The Fokker Planck equation for the steady state probability distribution in such a case can be written as

$$0 = - \frac{\partial}{\partial \theta} (x_1, W) + \frac{\partial}{\partial x_1} \left[\left(\theta + \frac{KA \sin \theta}{\tau^2} \right) W \right] + \frac{K^2 N_0}{4\tau^2} \cdot \frac{\partial^2 W}{\partial x_1^2} \quad \dots \quad (\text{A2})$$

where $x_1 = \dot{\theta}$.

It can be readily verified that the solution of the above equation is given by

$$W(\theta, \dot{\theta}) = c \exp \left((a \cos \theta + \frac{\beta}{2} \dot{\theta}^2) \right) \quad \dots \quad (\text{A3})$$

where
$$a = \frac{4A}{K^2 N_0} ; \quad \beta = - \frac{4\tau}{K^2 N_0}$$

Now if
$$f(p) = \frac{1+p\tau_0}{1+p\tau}$$

$$\frac{d\theta}{dt} = \Omega - Kf(p)(A \sin \theta + n)$$

or,
$$p\theta = \Omega - K \frac{1+p\tau_0}{1+p\tau} \cdot (A \sin \theta + n)$$

Writing $(1+p\tau_0)x = \theta$ one gets

$$px_1 = \frac{\Omega}{1+p\tau_0} - \frac{K}{1+p\tau} (A \sin \theta + n) \quad \dots \quad (\text{A4})$$

or,
$$(1+p\tau) \frac{\partial x_1}{\partial t} + KA \sin \theta = K \left[\frac{\Omega}{K} \frac{1+p\tau}{1+p\tau_0} - n \right]$$

If $\Omega = 0$, the Fokker Planck equation in the steady state is

$$x_1 \frac{\partial W}{\partial x_1} = \frac{\partial}{\partial x_1} \left[\left(x_1 + \frac{KA \sin \theta}{\tau} \right) \cdot W \right] + \frac{K^2 N_0}{4\tau^2} \cdot \frac{\partial^2 W}{\partial x_1^2} \quad \dots \quad (\text{A5})$$

where as usual $x_1 = \dot{\theta}$

The solution to the equation obtained by linearising the F - P equation can be found by noting that the solution in the linear case is given by

$$W(\theta, \dot{\theta}) = c \exp \left(\frac{\alpha \theta^2}{2} + \frac{\beta x_1^2}{2} \right) \quad \dots \quad (\text{A6})$$

where
$$\alpha = \frac{\text{Signal Power}}{\text{Noise power in the Noise band width}}$$

and
$$\beta = \frac{\alpha}{4\pi^2} \frac{1}{\text{Second moment of the noise spectrum}}$$

ELECTRICAL PROPERTIES OF SINGLE CRYSTALS OF TUNGSTENITE (WS_2)

S. R. GUHATHAKURTA

DEPARTMENT OF MAGNETISM

INDIAN ASSOCIATION FOR THE CULTIVATION OF SCIENCE, JADAVPUR, CALCUTTA-32.

(Received June 6, 1966)

ABSTRACT. The principal electrical conductivities of the naturally occurring single crystals of tungstenite have been studied from room temperature upto about 950°K in vacuum. The study reveals that (i) the substance has negative temperature coefficient of resistance; (ii) the conductivities increase permanently after preliminary heat treatment; (iii) the substance is a symmetrical varistor for currents along the basal plane; (iv) for currents perpendicular to the basal plane and at room temperature WS_2 is not only a symmetrical varistor but a thermistor also; the varistor and thermistor properties becoming less prominent with the rise of temperature; and (v) $\log \sigma$ vs $1/T$ curve is straight within the temperature range of 400°K to 950°K , and at lower temperatures (below 400°K) it departs from linearity.

INTRODUCTION

Tungstenite (WS_2) which is isomorphous with molybdenite (MoS_2) (Wyckoff, 1963) occurs in nature as blocks of single crystal but is of rare occurrence than the latter. Like Mo-atoms in molybdenite the W-atoms in the tungstenite crystal are arranged in layers parallel to the basal plane and each such layer is sandwiched between two parallel layers of sulphur atoms. The unit cell structure is built up by the repetition of the composite layer, made up of the above three layers. The hexagonal unit cell, which contains two molecules of tungstenite (WS_2), has the following dimensions as compared to molybdenite :

$$WS_2 : a = 3.18 \text{ \AA}, c = 12.50 \text{ \AA}, c/a = 3.93$$

$$MoS_2 : a = 3.1604 \text{ \AA}, c = 12.295 \text{ \AA}, c/a = 3.89$$

Compared to crystals of molybdenite which are very soft (hardness varying from 1 to 1.5 Mohs) (Berry *et al.*, 1959), those of tungstenite are harder (hardness 2.5 Mohs) (K. C. Li *et al.*, 1947). Also, where as molybdenite can be very easily cleaved to flakes of few Angstrom thickness, presumably due to the large distance, 3.66 \AA , between the basal layers, this is not so easy for tungstenite (interlayer distance 3.13 \AA) and flakes of thickness varying from 0.1 cm to 0.05 cm can be obtained by grinding with alundum powder or similar other abrasive powders. Most interesting fact is that, while molybdenite is diamagnetic (Dutta, 1944),

*The author expresses his gratefulness to Dr. R. K. Dutta Roy, formerly Chief chemist of Geological Survey of India, for kindly presenting us with some crystals of WS_2 .

with an approximately inverse temperature dependence of susceptibility (Dutta, 1945), tungstenite shows strong paramagnetism (Dutta and Roy Chowdhury, 1949) with a complicated temperature dependence of susceptibility. MoS_2 crystals are known to be very good semiconducting varistors (Dutta, 1947; Dey 1944) having rectifying properties along c -axis, its electrical conductivities along and perpendicular to the hexagonal axis being of the order 1 and $10^{-4} \text{ ohm}^{-1} \text{ cm}^{-1}$ respectively. But no measurements on the electrical conductivities of single crystals of WS_2 has yet been reported. Only some data on electrical conductivity, Hall effect etc. of powdered WS_2 by Decrue (1956) and Lagrenaudie (1952, 1954) are available. From these it was concluded that WS_2 is a p -type semiconductor having an electrical conductivity of the order of $10^{-8} \text{ ohm}^{-1} \text{ cm}^{-1}$ at room temperature and that it is a p -type rectifier with almost all metals.

To obtain reliable information regarding the electrical and other allied properties of WS_2 we have therefore carried out measurements with single crystals of WS_2 extended over as wide a range of temperature as possible. We had to use naturally occurring crystals* which often contain impurities, and only a very careful choice of the samples, could give us sufficiently reproducible results. It is needless to point out here that observations with crystals are more reliable than those with powdered samples since, in the latter case the surface effects between the different grains are sure to modify the electrical properties appreciably.

EXPERIMENTAL

Preparation of the working specimens

Small blocks of the specimens were fractured out from a large block of single crystal. These were then ground with alundum powder to rectangular tablets of suitable thicknesses having the flat faces parallel to c -plane. For measuring the electrical conductivity along the basal plane, small regions covering a distance of about 2 to 3 mm from each end along the length of the specimen were electroplated with copper. For measurement along directions perpendicular to the basal plane the two flat surfaces were electroplated. It may be noted that good copper plating is obtained only if the regions to be plated are first chemically mirrored with silver.

Methods of Measurement

The holders for measurement of electrical conductivities along and perpendicular to the basal plane were in principle the same as those used by earlier workers of this laboratory (Dutta, 1953; Mukherjee, 1964). The electrical conductivities were measured by the usual potentiometric method using a Pye Precision Potentiometer reading down to 1 micro volt. For measurements at high temperatures the samples were placed in a tubular electric furnace, and the temperatures were measured by a calibrated chromel-alumel thermocouple. All measurements

were made by evacuating the furnace tube to 10^{-2} mm of Hg with a two stage rotary oil pump.

RESULTS

In figure 1 are shown the current voltage characteristics at room temperature. From a linear extrapolation of such curves at low currents, the resistances or

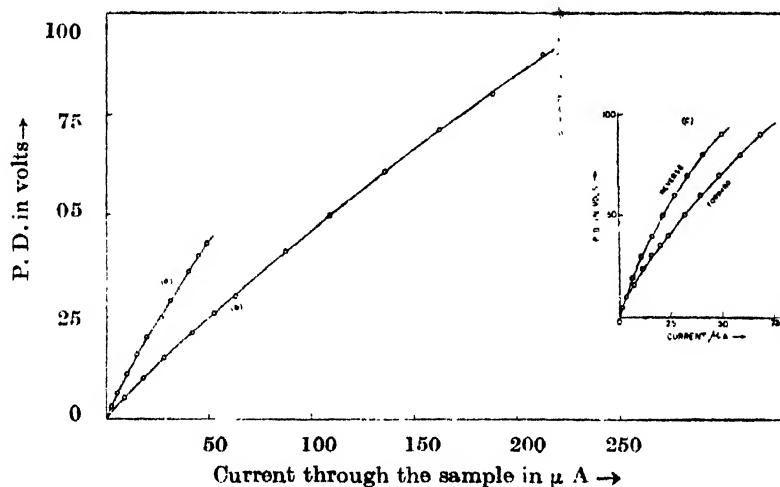


Fig. 1. Current voltage characteristics at 303°K.

- (a) Current along basal plane with broad contacts.
- (b) Current \perp to basal plane with broad contacts.
- (c) Current \perp to basal plane with one point contact and one broad contact.

conductivities of the crystal are calculated. In table I are shown such conductivities, σ_{\perp} and σ_{\parallel} for currents along and perpendicular to the basal plane respectively for three different fresh samples, which have not undergone any heat treatment.

TABLE I

Principal electrical conductivities of fresh samples of WS_2 at room temperature

Samples	Mean σ_{\perp}		Mean σ_{\parallel}	
	σ_{\perp} ohm $^{-1}$ cm $^{-1}$	ohm $^{-1}$ cm $^{-1}$	σ_{\parallel} ohm $^{-1}$ cm $^{-1}$	ohm $^{-1}$ cm $^{-1}$
1	3.86×10^{-6}		7.38×10^{-7}	
2	3.31×10^{-6}	3.9×10^{-6}	6.70×10^{-7}	7.3×10^{-7}
3	4.53×10^{-6}		7.82×10^{-7}	

Observation at higher temperatures

When the above mentioned measurements were first carried out at higher temperatures, it was found that the values of conductivity observed at different

temperatures including room temperature when the sample was heated up, were not reproduced while it was cooled down (Fig. 2 and Table II).

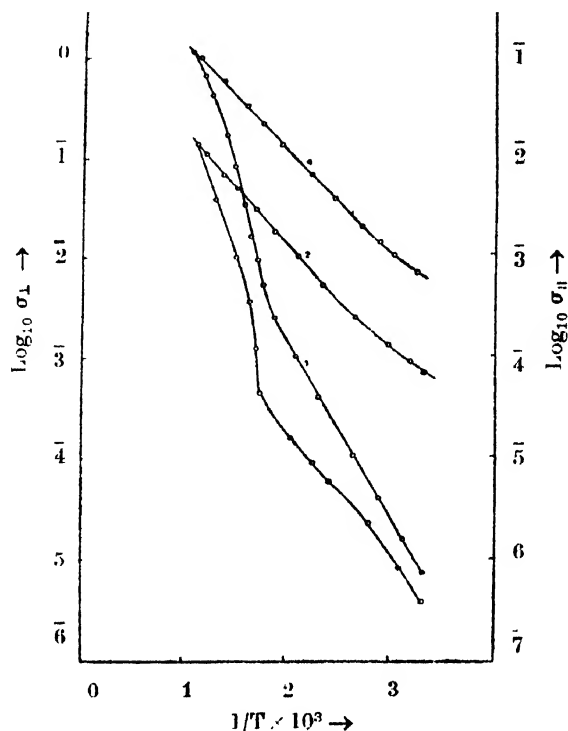


Fig. 2. Temperature variation of σ_{\parallel} and σ_{\perp} , conductivities \parallel and \perp to the c -axis respectively. Curves 1 and 3 for initial heatings of samples. Curves 2 and 4 after attainment of steady state.

TABLE II

Principal conductivities at room temperature of the samples of Table I after attaining steady state

Samples	Mean σ_{\perp}		Mean σ_{\parallel}	
	σ_{\perp} ohm ⁻¹ cm ⁻¹	ohm ⁻¹ cm ⁻¹	σ_{\parallel} ohm ⁻¹ cm ⁻¹	ohm ⁻¹ cm ⁻¹
1	3.78×10^{-4}		5.13×10^{-4}	
2	4.82×10^{-4}	5.05×10^{-4}	5.75×10^{-4}	5.85×10^{-4}
3	6.56×10^{-4}		6.67×10^{-4}	

However, after one or two heating and cooling cycles in vacuum the values become perfectly reproducible. Such a behaviour is not uncommon with semiconductors under similar conditions and possibly arises from absorbed gases and internal stresses. In figure 2 are also shown the temperature variation of the principal conductivities of a typical sample of WS_2 after the attainment of the steady state.

In figures 3 and 4 are represented the current-voltage characteristics at different temperatures of samples which have attained the steady state.

In order to study the phenomena which might be taking place during the process of attaining the steady state, an experiment was performed in which the sample is successively heated to different high temperatures, allowed to remain at those temperatures for sufficient time to attain steady temperatures, cooled to the room temperature and the change in resistance which has taken place at the room

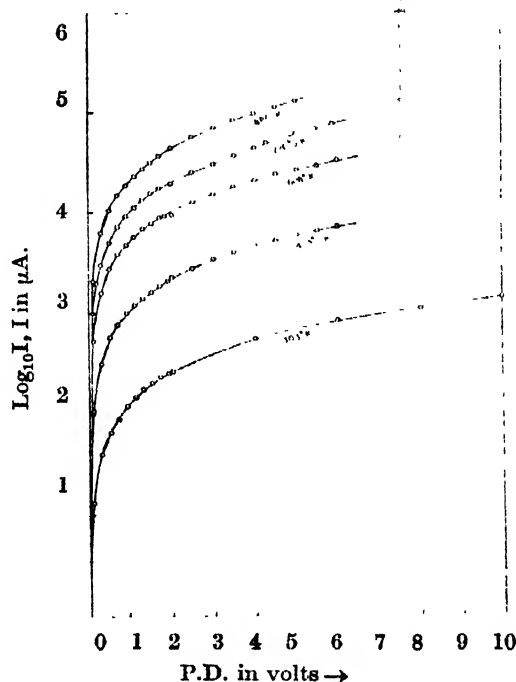


Fig. 3. Current voltage characteristics at different temperatures for currents along the basal plane with broad contacts. Curves are symmetrical for currents in reverse direction.

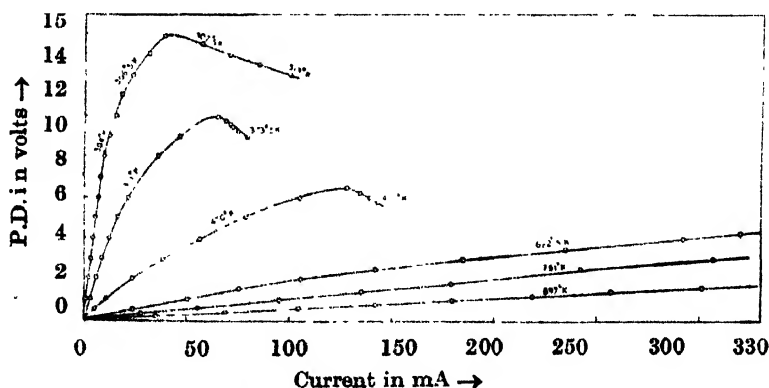


Fig. 4. Current voltage characteristics at different temperatures for current perpendicular to basal plane with broad contacts. Curves symmetrical for reverse current.

temperature is observed. The results of these observations are represented in figure 5.

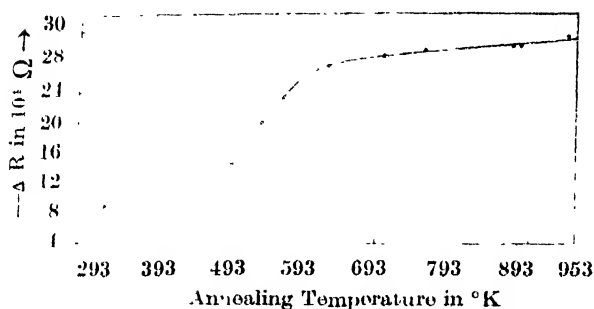


Fig. 5. Annealing effect of temperature on resistance of fresh samples.

DISCUSSIONS

1) Chemical binding and conductivity in WS_2

From a consideration of the paramagnetic properties of WS_2 it has been suggested (Dutta and Roy Chowdhury, 1949) that the bindings in it are of the type which are present in the salts of the iron group of elements. These are distinctly different from bindings in MoS_2 where there are strong covalent bonds between dissimilar atoms and a partial metallic type of planar bonds between similar atoms (Dutta, 1944). As a consequence MoS_2 possesses high diamagnetic anisotropy combined with fairly high electrical conductivity in the basal plane (Dutta, 1945). It is therefore evident that owing to the distinct ionic nature of bond in WS_2 , it should have much poorer electrical conductivity than MoS_2 . This is exactly what has actually been observed (Table III).

TABLE III

Magnetic susceptibilities $\chi_{||}$ and χ_{\perp} along and perpendicular to the c -axis, $\Delta\chi = \chi_{\perp} - \chi_{||}$ and $\sigma_{||}$ and σ_{\perp} corresponding electrical conductivities of MoS_2 and crystals of WS_2 before heat treatment

Specimen	Electrical properties			Magnetic properties			
	$\eta, \Omega^{-1} \text{ cm}^{-1}$	$\sigma_{\perp}, \Omega^{-1} \text{ cm}^{-1}$	$\Delta\chi, 10^6/\text{gmmol}$ c.g.s.e.m.u.	$\chi_{ }, 10^6/\text{gmmol}$ c.g.s.e.m.u.	$\chi_{\perp}, 10^6/\text{gmmol}$ c.g.s.e.m.u.	Aniso- tropy	
WS_2	7.3×10^{-7}	3.9×10^{-6}	1397.4	4916.8	6314.2	24%	
MoS_2	3.1×10^{-1}	1.2	-42.8	-87.1	-44.3	72%	

(2) Origin and nature of conductivity in WS_2

In view of the type of bindings proposed for WS_2 its conductivities should have, evidently, been much lower than what has been experimentally obtained. Therefore to explain this appreciable conductivity, the obvious suggestion is that

impurities are contributing to electrical conduction. This suggestion is further corroborated by the following considerations.

The small electrical anisotropy of WS_2 ($\frac{\sigma_1}{\sigma_{\parallel}} \approx 5.3$) observed on a fresh sample at room temperature disappears permanently when the sample is heated to higher temperature (figure 2) and considerable permanent increments take place in the actual values of conductivities also ($\sigma_1 = \sigma_{\parallel} \approx 10^{-4} \text{ ohm}^{-1} \text{ cm}^{-1}$) by these treatments. But the magnetic anisotropy only changes from 24% to about 18% (Dutta, 1949) in course of such treatments. The obvious conclusion is that electrical conduction phenomena in WS_2 is not a regular contribution from the crystal lattice but from sources in the crystal external to regular lattice positions. In other words WS_2 is an extrinsic semiconductor. From results of our preliminary measurements of Hall effect of single crystals, as also from those of earlier measurements with powders of WS_2 , we find that WS_2 is a *p*-type semiconductor.

(3) *Permanent changes in conductivities by heat treatments*

The observed permanent changes in conductivities (fig. 2), as stated above, may be explained if it is assumed that initially there had been a number of scattering or trapping or both kinds of centres in the crystal, which go to add to its resistance and that these centres are annealed out at higher temperatures. Existence of such an annealing effect in respect to these centres which may be foreign atoms, dislocations, or interstitials, vacancies etc. and possible combinations of some of these, is evident from figure 5⁺. It is to be noted, however, that similar annealing effects might also be caused by structural or chemical changes. But since no such effects are observed with magnetic properties, these (structural or chemical) may be ruled out. It may also be mentioned here that these centres which affect the transport properties considerably are evidently so low in number that their magnetic contributions would be very feeble, and hence these can not in any way appreciably affect the high paramagnetic contribution of the host crystal. Therefore their removal, by heat treatment, will not affect the magnetic properties.

(4) *Activation energies*

From fig. 2 where $\log \sigma$ has been plotted against $1/T$ where T is the absolute temperature, we find that the plots are straight lines within the temperature range 400°K to 950°K (below 400°K there being a slight departure from linearity) indicating that a single type of carrier is effective in this temperature range (400°K

⁺ From a study of such curves one can obtain information regarding the nature and kinetics of such scattering centres, a line of investigation which we propose to undertake in future.

to 950°K). Within this range the variation of σ with T can therefore be expressed by a relation of the type

$$\sigma = \sigma_0 e^{-\frac{\Delta E}{2KT}}$$

where σ is the observed electrical conductivity, σ_0 , a constant, and ΔE the activation energy and the rest of the symbols have their usual significances. The values of ΔE (Table IV) obtained from the figure 2 represent the energy gap between the valence and the acceptor level in the forbidden region—the current being mainly carried by the holes in the valence band as already indicated. The values of ΔE obtained by other workers are also included in the table IV and are found to be lower than those obtained by us. The reason for this may be (i) the samples were in the form of powders and (ii) the temperature ranges were much lower, to cause proper annealing so that carriers of lower excitation energies might be effective in producing conduction. The trend of our curves (figure 2) at lower temperatures (below 400°K) also indicates the existence of such low energy carriers.

Table IV

Activation energy, ΔE of WS_2 , ΔE_{\parallel} and ΔE_{\perp} refer to current directions parallel and perpendicular to c -axis respectively

Author	Nature of the specimen	Temperature range	ΔE_{\perp} in e. volts		ΔE_{\parallel} in e. volts
Present author	Single crystal (Natural)	400°K—950°K	0.45		0.45
			ΔE in e. volts		
Lagronaudie (1954)	Powder (artificial)	77°K—293°K	0.04,	0.11,	0.18
Deerue (1956)	Powder (artificial)	297°K—373°K	0.17		

(5) Current—voltage characteristics

Current voltage characteristics after the specimen had attained steady state through preliminary heat treatments are represented in figures 3 and 4.

From these curves, it is observed that at room temperature and for currents along the basal plane WS_2 behaves like a symmetrical varistor i.e. curves remain symmetrical for both direct and reverse currents. At higher temperatures also this behaviour persists. For currents perpendicular to the basal plane, the said characteristics are shown in figure 4, wherein it is observed that at room temperature WS_2 is not only a symmetrical varistor but its resistance also decreases due to self heating by the passage of current through it i.e. it behaves as a thermistor also. Both these properties, however, become gradually less prominent as the temperature is raised. These interesting observations are being theoretically analysed and the results will be published in a subsequent communication.

Under proper conditions i.e. with one broad contact and one point contact rectification in single crystals of WS_2 has been observed at room temperature for currents perpendicular to the basal plane only. From fig. 1 where the current-voltage characteristics for both forward and reverse currents along the c -axis of a fresh sample of WS_2 are represented, one finds that the rectification ratio, is rather poor suggesting that 'spreading resistance' due to radial distribution of current in this case is very small (Lagrenaudie 1952)

ACKNOWLEDGMENT

The author expresses his best thanks to Shri A. K. Dutta for suggesting the problem and constant guidance throughout the course of the work and to Prof. A. Bose for his kind interest in the work.

REFERENCES

- Berry, L. G., and Manson, B., 1959. *Mineralogy*, W. H. Freeman & Company, California 337.
- Deerue, J., 1950. *Helv. Chim. Acta.* **39**, 619, 812.
- Dey, A. P., 1944. *Proc. Nat. Ac. Sc. India*, **14**, 47.
- Dutta, A. K., 1944. *Indian, J. Phys.*, **18**, 249.
- , 1945. *Indian J. Phys.*, **19**, 225.
- , 1945. *Nature*, **156**, 240.
- , 1947. *Nature*, **159**, 477.
- , 1953. *Phys. Rev.*, **90**, 187.
- Dutta, A. K. and Roy Chowdhury, B. C., 1949. *Indian. J. Phys.* **23**, 131.
- Lagrenaudie, J., 1952. *J. Phys. Rad.* **13**, 311.
- , 1954. *J. Phys. Rad.* **15**, 299.
- Li, K. C., and Wang, C. Y., 1947. *Tungsten*, Reinhold Publishing corporation, New York, 9.
- Mukherjee, A. K., 1964. *Indian J. Phys.* **38**, 10.
- Wycoff, W. G., 1963. *Crystal Structures*, Inter Science, publishers, New York, **1**, 280, 408.

INFRARED STUDY OF EFFECT OF ENVIRONMENTS ON HYDROGEN BONDING IN CATECHOL, RESORCINOL AND QUINOL

D. K. MUKHERJEE AND S. B. BANERJEE

OPTICS DEPARTMENT,

INDIAN ASSOCIATION FOR THE CULTIVATION OF SCIENCE,
CALCUTTA-32.

(Received June, 13, 1966)

ABSTRACT. The infrared absorption spectra of catechol, resorcinol and quinol have been measured in the solid state and in solution in different solvents. The results confirm the existence of *cis* and *trans* molecules of catechol postulated by previous workers. It has been concluded that in the solid state the catechol molecules are intermolecularly linked with each other through hydrogen-bonding while in the case of solutions intermolecular hydrogen bonds of different strengths are formed between catechol and solvent molecules. The intramolecular bond is, however, found to persist with sufficient strength in solutions. The observed solvent effects on the OH vibrational frequencies of resorcinol and quinol have also been explained in terms of formation of intermolecular hydrogen bonds of varying strengths between the solvent and the solute molecules. In the case of resorcinol in the solid state, existence of strongly associated polymeric groups of molecules formed through intermolecular hydrogen bond of bent type as indicated by the structure of the crystal reported by previous workers has been confirmed.

INTRODUCTION

The infrared absorption spectra of catechol and resorcinol were studied in the first harmonic region of OH vibration by Wulf and Liddel (1935), who observed two peaks at 7060 and 6770 cm^{-1} in the case of catechol. In explaining the two peaks Pauling (1936) suggested the existence of *cis* and *trans* molecules of catechol. For resorcinol Wulf and Liddel observed only one peak at 7050 cm^{-1} . Ingraham *et al.* (1952) identified the two absorption bands due to free and intramolecularly bonded OH groups in catechol at 3611 and 3568 cm^{-1} respectively. Bellamy *et al.* (1966) observed a new peak due to OH vibration at 3535 cm^{-1} in the infrared absorption spectrum of resorcinol in ether and concluded that resorcinol molecules form complexes with ether molecules. Stanevich (1964) found that crystals of resorcinol and quinol exhibit peaks at 3270 cm^{-1} and 3275 cm^{-1} respectively. However, he apparently did not discuss the result for resorcinol by considering the crystal structure of this compound reported by Robertson (1936). It also appears that no systematic comparative study of the influence of different solvents on the OH vibrational frequencies of the three hydroxy phenols, viz., catechol, resorcinol and quinol has been made by previous workers. The importance of

specific local interaction in accounting for changes in the frequencies and intensities of bands due to groups like OH, C = O, etc., has recently been emphasised by different authors (e.g. Bellamy *et al*, 1958; Caldow and Thompson, 1960). Such a study of solvent effect on OH vibration of the hydroxyphenols would be helpful in ascertaining the nature and strength of intramolecular hydrogen bond in pure substances and would furnish interesting information about specific groups involved in intermolecular bond formation in the case of solutions. The infrared spectra of catechol, resorcinol and quinol have therefore been examined in the pure state and in solutions in different solvents and the results, with probable interpretation, have been presented in this paper.

EXPERIMENTAL

The compounds were obtained from E. Merck and were of AR quality. They were further purified by repeated crystallisation from ether solution and later by sublimation under vacuum. The solvents were carefully purified and dried before use. Thin solid films of catechol and resorcinol were used to record the absorption spectra while the spectrum of quinol in the solid state was measured in nujol mull.

The spectra were recorded with a Perkin Elmer Model 21 spectrophotometer fitted with rocksalt optics. The calibration was checked by recording the atmospheric water vapour band at 3740 cm^{-1} .

RESULTS AND DISCUSSION

The observed vibrational frequencies are given in Tables I, II and III. The absorption spectra of the compounds in pure state and in different solutions are

TABLE I
Catechol : O-H vibrational frequencies in cm^{-1}

Solid at 70°C (thin film)	Solution in				
	C_2Cl_4 (Ingraham <i>et al.</i> 1952)	CHCl_3	C_6H_6	$\text{C}_6\text{H}_5\text{NO}_2$	$(\text{C}_2\text{H}_5)_2\text{O}$
	3611	3614	3590		
3545	3568	3565	3560	3560	3565
				3525	
3440					3320

TABLE II
Resorcinol : O-H vibrational frequencies in cm^{-1}

Solid (Stancovich, 1964)	Solid at 25°C (present authors)	Solution in			Ether- resorcinol soln. dissolved in benzene
		$(\text{C}_2\text{H}_5)_2\text{O}$	C_6H_6	CHCl_3	
			3580	3595	3580 3515
3270	3270	3335			3325

TABLE III
Quinol : O-H vibrational frequencies in cm^{-1}

Solid (Stancovich, 1964)	Solid in Nujol mull (present authors)	Solution in $(\text{C}_2\text{H}_5)_2\text{O}$	Ether-quinol solution dissolved in benzene
3275	3260	3385	3595 3360

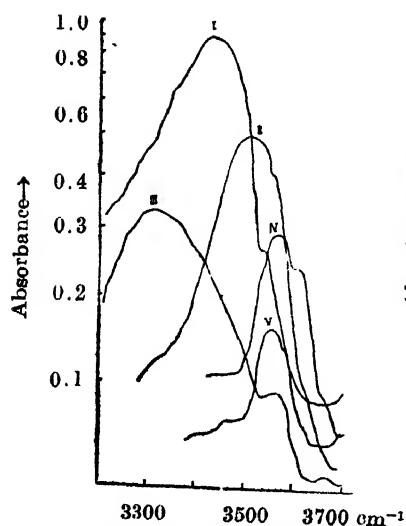


Fig. 1. Infrared absorption bands of catechol.

- I. Solid at 70°C (thin film).
- II. 0.6 M Solution in nitrobenzene
- III. 0.8 M " " ether
- IV. 0.3 M " " chloroform
- V. 0.8 M " " benzene

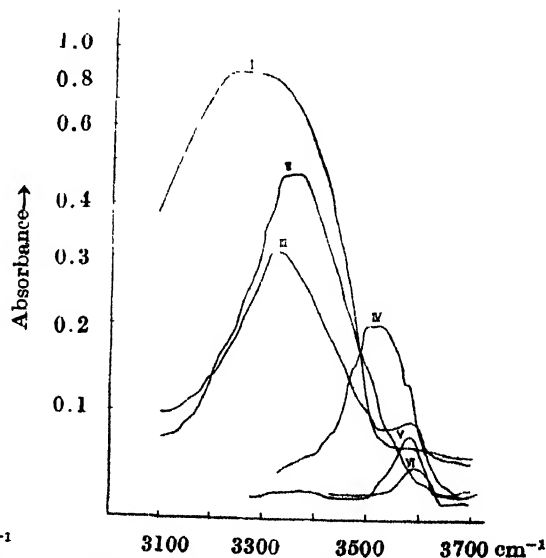


Fig. 2. Infrared absorption bands of resorcinol.

- I. Solid at 25°C (thin film)
- II. 0.8 M Solution in ether
- III. 3% ether-resorcinol complex in benzene
- IV. 0.6 M Solution in nitrobenzene
- V. 0.8 M " " benzene
- VI. 0.3 M " " chloroform

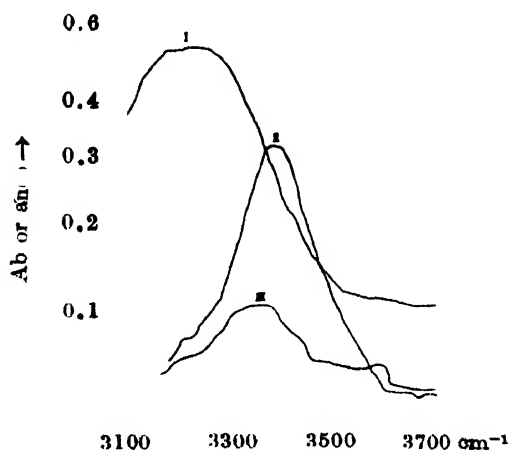


Fig. 3. Infrared absorption bands of quinol.

- I. Solid in nujol mull
- II. 0.6 M Solution in ether
- III. 1% ether-quinol complex in benzene.

reproduced in Figs. 1, 2 and 3. The results for the three compounds are discussed separately in the following paragraphs.

Catechol :

In dilute solutions in chloroform and benzene two peaks due to the stretching frequencies of free and intramolecularly bonded OH group corresponding to the *trans* and *cis* configurations postulated by Pauling (1936) could be identified. In chloroform solution the former is at 3614 cm^{-1} and the latter is at 3565 cm^{-1} while in the benzene solution the free OH stretching band is at about 3590 cm^{-1} , the frequency of the bonded OH being 3560 cm^{-1} . The slight decrease of the stretching frequency of the free OH vibration probably indicates slight basic behaviour of benzene to the hydroxyphenol. In ether solution, the band due to free OH vibration is absent and a new strong peak at 3320 cm^{-1} is observed. Evidently, this new band arises from association of molecules of ether with catechol through hydrogen-bonding between oxygen of ether and an O-H of catechol. In nitrobenzene also, the proton acceptor NO_2 group forms weak hydrogen bond with catechol molecule as is evident from the disappearance of the free OH vibrational band and appearance of a new band at 3525 cm^{-1} . In both ether and nitrobenzene solutions, the band due to intramolecularly bonded OH vibration persists with sufficient strength to indicate that the intramolecular OH ... O bond in catechol is strong enough to resist the influence of strong proton-accepting groups in solvents tending to break it up and that the intermolecular hydrogen

bond between the solvent and solute molecules is formed through the free OH group of the catechol molecule (Figs. 4 and 5).

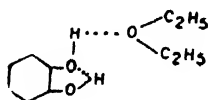


Fig. 4

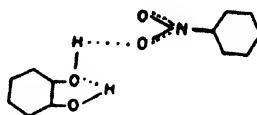


Fig. 5

In the case of crystals of catechol at 25°C only a broad strong band at 3440 cm^{-1} is observed. When the temperature is raised to about 70°C a second weak hump at about 3545 cm^{-1} is observed. This latter band obviously represents the stretching mode of the intramolecularly bonded OH. The new band at 3440 cm^{-1} can then be attributed to the formation of intermolecular OH ... O bond between neighbouring molecules in the solid state (Fig. 6).

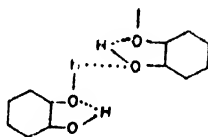


Fig. 6

The above findings apparently corroborate the views of previous authors (e.g. Bellamy and Pace, 1966) that formation of an O-H ... O-H bond makes the hydrogen attached to the acceptor oxygen more acidic and the oxygen of the donor OH group more basic, thus increasing the probability of formation of hydrogen bond at either end.

Resorcinol

In this molecule with two hydroxyl groups in the meta position there is no possibility of formation of intramolecular hydrogen bond and in chloroform solution the absorption band due to the free OH vibration appears at 3595 cm^{-1} , while in benzene solution this band is at 3580 cm^{-1} , which again shows slight displacement towards lower energies. In ether solution only a strong broad band with its centre at about 3335 cm^{-1} is observed. This band could be readily identified with the stretching vibration of the hydroxyl group hydrogen-bonded with oxygen of the ether molecule. This result is in agreement with that of Bellamy *et al.* (1966). When the resorcinol-ether complex is dissolved in benzene, probably some of the intermolecular bonds break up, as is apparent from appearance of a weak band at 3585 cm^{-1} due to free OH group. In nitrobenzene solution the existence of both free OH group and intermolecularly associated OH group weakly

bonded with the nitro group is evident from the appearance of two peaks at 3580 and 3515 cm^{-1} respectively. The absorption band of thin solid film is very broad with its centre at about 3270 cm^{-1} , which shows that the OH groups of neighbouring molecules are intermolecularly linked through OH ... O bond. The frequency of the intermolecularly bonded OH group in the solid state is lower than that of the OH group linked with oxygen of the ether molecule in ether solution. This fact and the large width of the OH band could evidently be attributed to the presence of polymeric chain of intermolecularly OH ... O bonded resorcinol molecules in the solid state. It would be interesting to note that from an investigation of crystal structure of resorcinol Robertson (1936) concluded that in the crystal, the molecules of resorcinol are grouped in spiral arrays about the two-fold screw axes and the hydroxyl groups of successive pairs of molecules approach each other to within a remarkable short distance of 2.7Å, which indicates presence of hydroxyl bonds, the angles between the bonds being fairly near the tetrahedral value of 109.5°. The results of the present investigation are thus in good qualitative agreement with Robertson's conclusion. The structure of the crystal further shows that the intermolecular OH ... O bond is of bent type. In that case the strong hydrogen bond which is responsible for the large frequency-shift could be attributed to the special cyclic structure of the associated molecules as discussed by Bellamy and Pace (1966).

Quinol

The infrared absorption spectrum of this compound in dilute solution should contain only one band due to free OH vibration, as there is no possibility of intramolecular hydrogen-bonding between OH groups which are in para position in the molecule. In ether solution a strong absorption band at 3385 cm^{-1} is observed. From a comparison with spectra of the other two hydroxyphenols this band could be attributed to the vibrational frequency of the OH group hydrogen-bonded with the oxygen of ether which forms a complex with quinol. When the ether-quinol complex is dissolved in a very dilute solution in benzene this band shifts slightly towards lower frequencies and a very weak band at about 3595 cm^{-1} is just discernible. This last band probably represents the frequency of free OH vibration. In the absorption spectrum due to the crystals dispersed in nujol mull a very broad absorption band with its centre at about 3260 cm^{-1} is observed. A similar maximum at 3275 cm^{-1} was reported by Stanevich (1964) for the quinol crystals. As for resorcinol, such absorption points to the presence of intermolecularly hydrogen-bonded polymeric molecules of quinol in the solid state.

ACKNOWLEDGMENT

The authors' thanks are due to Professor S. C. Sirkar, D.Sc., F.N.I. for helpful discussion and to Professor G. S. Kastha, D.Sc. for kindly offering facilities for

the work. Financial support to one of the authors (S.B.B.) as Pool Officer by the C.S.I.R., India is acknowledged.

REFERENCES

- Bellamy, L. J., Hallam, H. E., and Williams, R. L., 1958, *Trans. Faraday Soc.*, **54**, 1120.
Bellamy, L. J. and Pace, R. J., 1960, *Spectrochim Acta*, **22**, 525.
Caldow, G. L. and Thompson, H. W., 1960, *Proc. Roy. Soc. (London)*, **A 254**, 1.
Ingraham, J. L., Corse, J. and Bailey, G. T., 1952, *J. Am. Chem. Soc.*, **74**, 2297.
Pauling, L., 1936, *J. Am. Chem. Soc.*, **58**, 94.
Robertson, J. M., 1936, *Proc. Roy. Soc. (London)*, **A157**, 79.
Stanevich, A. E., 1964, *Optik i Spektros.*, **16**(6), 998.
Wulf, O. R. and Liddel, U., 1935, *J. Am. Chem. Soc.*, **57**, 1464.

LUMINESCENT DECAY OF VARIOUSLY PRETREATED KCl: Tl PHOSPHORS

R. V. JOSHI AND A. K. MENON

PHYSICS DEPARTMENT, M. S. UNIVERSITY, BORDA, INDIA.

(Received July 9, 1966 · Resubmitted November 12, 1966)

ABSTRACT. Room temperature measurements of the phosphorescence decay are made in untreated and pretreated KCl: Tl phosphors. Pretreated phosphors consist of specimens prepared with different heat treatments followed by deformation or in the undeformed state. The results obtained are analysed in terms of the concept that in the room temperature region the electron traps are due to negative ion vacancies. It is suggested that various types of negative ion vacancies exist depending on their location in the normal and distorted regions of the lattice. In the latter types the charged dislocations are presumed to play an important role.

INTRODUCTION

There have been a number of attempts at offering interpretations which would adequately explain the room temperature phosphorescence decay in KCl: Tl. Seitz (1938) interpreted it on the basis of the internal metastable states of the Tl^+ ions occupying substitutional positions in the host lattice. This was supported by Johnson and Williams (1953). Later work however showed that the electron traps are independent of the impurity ions and are formed by other crystalline imperfections in the host lattice (Ewles and Joshi 1960).

In all the earlier decay studies of the phosphor no particular attention has been given to the previous history of the sample. Therefore it is considered worthwhile to study the decay characteristics of the phosphor intensively under the influence of as many different factors as possible. The present work, concerned primarily with obtaining necessary data, specifically deals with the effects of thermal treatment, of deformation and of thermal treatment followed by deformation, on the decay of the phosphor at room temperature. Interpretations of the results obtained are offered on the basis of the concept advanced earlier that electron traps are due to single negative ion vacancies in different environments (Joshi 1964). It has been suggested before that the electrostatic interaction between dislocations, presumed to be charged, and negative ion vacancies may be important (Joshi and Menon 1965). This analysis is extended to the present work. The various components of the decay are considered to be due to differences in the degree of electrical interaction.

EXPERIMENTAL PROCEDURE

All the KCl : Tl specimens used in the experiment were prepared from potassium chloride of 'analar' grade by crystallisation from aqueous solution. The results presented are for KCl : Tl phosphors containing 0.0015 and 0.003 mol. of Tl. Measurements were made on the following samples : (i) as—obtained from solution (ii) annealed and slowly or rapidly cooled (iii) as—obtained and deformed and (iv) heat-treated and deformed. Annealing of the samples was carried out in a 'muffle' furnace, held at 300°C for 100 hours. With a suitable temperature control, the sample could be cooled very slowly at a rate of 1.5°C/hr. In the case of rapid cooling, the sample was withdrawn from the furnace after anneal at 300°C for 100 hours and then air-cooled. All annealings were carried out in evacuated and sealed Pyrex tubes. The sample, either *as*-obtained or heat-treated, was compressed to tablet in a chromium plated stainless steel press under a pressure of about 2000 kg/cm².

An account of the experimental technique has been presented previously (Joshi 1964). The sample was excited with ultraviolet light from a high pressure mercury discharge lamp, the excitation time in each case being 1.5 min. Phosphorescence decay measurements, following irradiation, were made using RCA

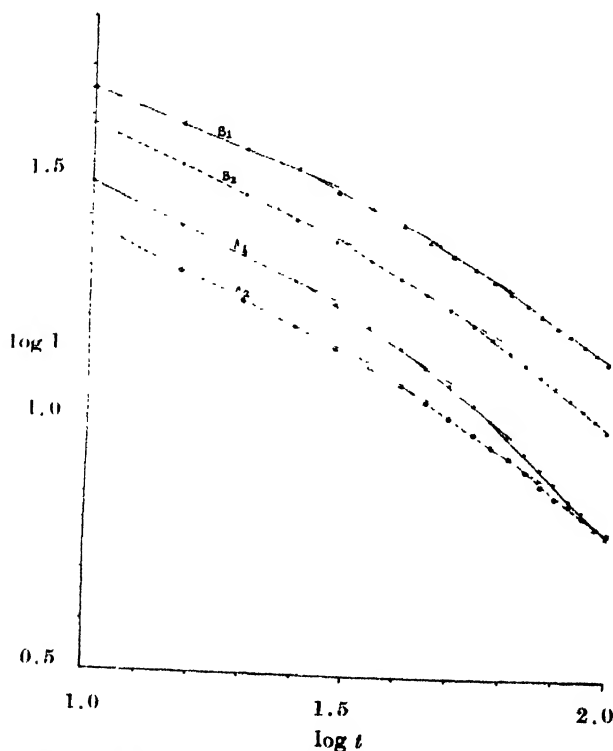


Fig. 1. Decay curves for samples A and B

Curves : A₁ and B₁ for Tl conc. 0.0015 ml.f.

„ : A₂ and B₂ „ „ „ 0.003 ml.f.

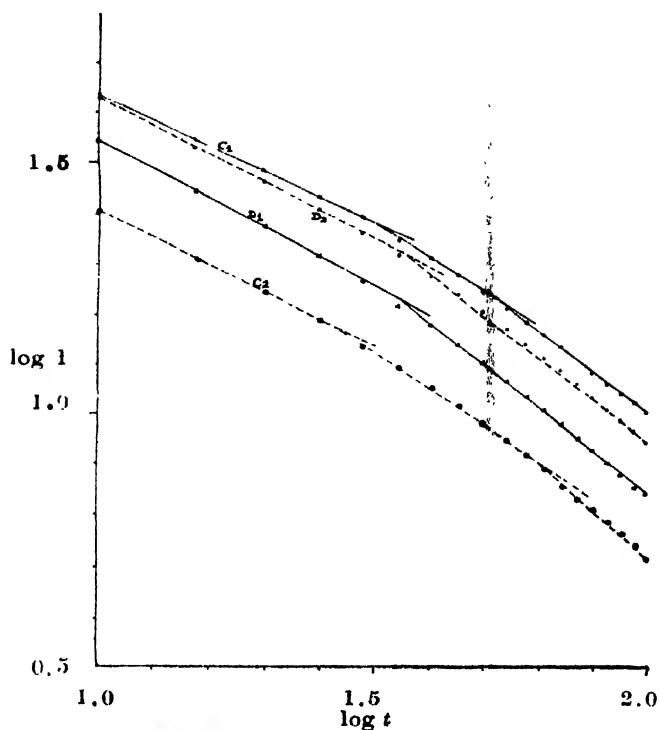


Fig. 2. Decay Curves for samples C and D Curves : C_1 and D_1 for Tl conc. 0.0015 m.f.
: C_2 and D_2 " " " 0.003 m.f.

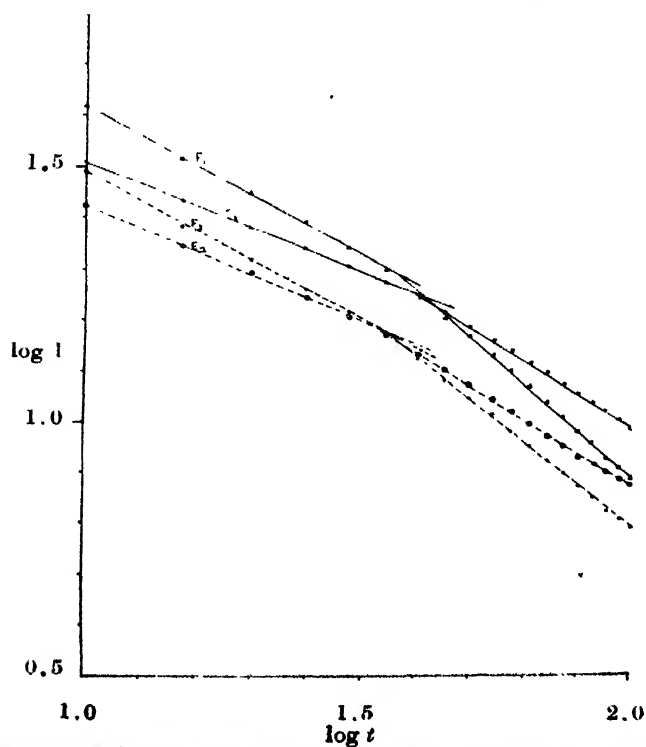


Fig. 3. Decay curves for samples E and F Curves : E_1 and F_1 for Tl conc. 0.0015 m.f.
: E_2 and F_2 " " " 0.003 m.f.

galvanometer. All the measurements were made at room temperature in total darkness.

EXPERIMENTAL RESULTS

Figures 1 to 3 indicate the results of the experiments performed with as-obtained and variously pre-treated KCl : Tl specimens. In all the figures log-log 931A photomultiplier the output of which, after amplification, was fed to a mirror plots of intensity (I) against time (t) show that the results can be fitted very well to the power law decay $I = I_0 t^{-n}$. Measurements were made on two KCl : Tl phosphors differing in their Tl content. Apparently there is no difference in the decay behaviour of the two phosphors. The decay curves for as-obtained or heat-treated samples show distinct curvatures. These curves can be fitted to suggest 3 to 4 independent first order processes. The noteworthy feature of the data presented in the figures is that in general, the number of decay components reduces to two if as-obtained or heat-treated specimen is deformed by stressing. A list of the samples used in the experiments, then nature of the physical treatment received by each sample and the values of the decay constants (n) for ultraviolet emission are indicated in Table I. Similar results were obtained for visible emission.

TABLE I

- Sample : A - As obtained from solution
 B - Sample A annealed at 300°C for 100 hrs., slowly cooled.
 C - Sample A annealed at 300°C for 100 hrs., rapidly cooled.
 D - Sample A compressed into tablet
 E - Sample B compressed into tablet
 F - Sample C compressed into tablet

Decay constant (n) values for different stages (U.V. emission)

Sample	Tl Content 0.0015 mol.		Tl Content: 0.003 mol.		n
A	A ₁	0.47, 0.65, 0.82, 1.0	A ₂	0.48, 0.54, 0.68, 0.82	
B	B ₁	0.39, 0.52, 0.61, 0.73	B ₂	0.46, 0.61, 0.82	
C	C ₁	0.51, 0.65, 0.84	C ₂	0.54, 0.72, 0.96	
D	D ₁	0.58, 0.85	D ₂	0.57, 0.85	
E	E ₁	0.43, 0.65	E ₂	0.46, 0.66	
F	F ₁	0.58, 0.92	F ₂	0.58, 0.85	

DISCUSSION

It is seen from the results that the decay curve for as-obtained or heat-treated specimens can be resolved into more than two concurrent first order processes. In general, the number of decay stages reduces to two if the as-obtained or heat-treated specimen is compressed by stressing. Similar results have been reported earlier by Morlin (1957). In a log-log plot he observed two linear stages for decay in the case of NaCl : Tl phosphors either in the form of discs prepared from powder or in the form of single crystals deformed by stressing. On the other hand, he found the plot for an undeformed single crystal phosphor to be a non-linear curve in the same diagram. These results can be understood if one attempts an explanation in terms of the electron traps due to single negative ion vacancies in different surroundings. It is suggested that the fastest component of the decay is due to phosphorescence Centres each of which consists of a combination of a negative ion vacancy (trap) with an adjacent substitutional Tl^+ ion (emission centre). Such phosphorescence centre form one category. The remaining components of the decay are due to phosphorescence centres each of which is composed of a similar combination as stated above but in the vicinity of an edge dislocation presumed to be negatively charged. This phosphorescence centres fall in second category. In the second category the phosphorescence centres are further differentiated on the basis of the distance of separation between the dislocation and the negative ion vacancy— Tl^+ ion complex. Variation in the distance of separation would lead to the difference in the degree of electrical interaction between them and correspondingly the lifetimes of the traps belonging to the second category would differ. It is suggested that the charge on the dislocation is small. That is a dislocation will not measurably influence the decay process if the distance of separation between it and the vacancy — Tl^+ ion complex is large say, fifty lattice spacings or more.

During plastic deformation a small stress can give rise to dislocation motion in the microcrystals of the phosphor. If during motion a dislocation comes in the close vicinity of a Tl^+ ion it will be pinned or immobilised by its interaction with the impurity ion. It is believed that as a result of plastic deformation the dislocation is pinned at the Tl^+ ion in majority of the phosphorescence centres of the second category. Hence the phosphorescence centres obtained after deformation would involve either a combination of a Tl^+ ion and adjacent negative ion vacancy or a similar combination closely associated with a charged dislocation. The rate of release of electron in any of the latter species of phosphorescence centres will be affected by dislocation more or less to the same extent. It is suggested that the two components of the decay observed after plastic deformation in all the samples are due to the above two types of the phosphorescence centres.

ACKNOWLEDGMENTS

We wish to express our thanks to Dr. N. S. Pandya for encouragement. One of us (A.K.M.) gratefully acknowledges the award of a Fellowship from the Council of Scientific and Industrial Research, New Delhi.

REFERENCES

- Ewles, J., and Joshi, R. V., 1960, *Proc. Roy. Soc.* **A254**, 358.
Johnson, P. D., and Williams, F. E., 1953, *J. Chem. Phys.* **21**, 125.
Joshi, R. V., 1964, *J. Phys. Chem. Solids*, **25**, 135.
Joshi, R. V., and Menon, A. K., 1965, *Phil. Mag.*, **12**, 963.
Morlin, Z., 1957, *Nature*, **189**, 89.
Seitz, F., 1938, *J. Chem. Phys.*, **6**, 150.

TRI-HARMONIC STRESS FUNCTION

SHINICHI SEIKE

DEPARTMENT OF MECHANICAL AND AGRICULTURAL ENGINEERING, UNIVERSITY OF IBARAKI,
AMI-MACHI, IBARAKI PREFECTURE, JAPAN

(Received July 16, 1966)

ABSTRACT. Airy's bi-harmonic Eqs. governs stress function in two dimensional isotropic elastic continuum. We find new Eqs. to determine stress functions in three dimensional isotropic elastic continuum. They are found to obey tri-harmonic Eqs.

VECTOR POTENTIAL TO STRESS TENSOR

Equilibrium of internal force in three dimensional elastic continuum reads

$$\partial_k f^{jk} = 0, \quad \dots \quad (1.1)$$

($j, k = 1, 2$ and 3 ; contracted over k),

with

$$f^{jk} = f^{kj},$$

where f^{jk} stands for stress tensor. We may take vector potential ϕ^1, ϕ^2 and ϕ^3 to them as

$$f^{jj} = -(\partial_k^2 \phi^m + \partial_m^2 \phi^k),$$

(j, k and $m = 1, 2$ and 3 ; cyclic),

$$f^{jk} = \partial_j \partial_k \phi^m (j \neq k \neq m), \quad \dots \quad (1.2)$$

so that (1.1) may identically be satisfied. We also take displacement potential by

$$e = (\partial_1 \psi_1, \partial_2 \psi_2, \partial_3 \psi_3), \quad \dots \quad (1.3)$$

where

$$e = (e^1, e^2, e^3)$$

means displacement. Stress potential and displacement potential are related by

$$\phi^m(\vec{r}) = G[\psi^j(\vec{r}) + \psi^k(\vec{r})] + \chi(x^m), \quad \dots \quad (1.4)$$

with reference to the well known relations

$$f^{jk} = G(\partial_j e^k + \partial_k e^j). \quad \dots \quad (1.5)$$

$2G = mE/(m+1)$ stands for modulus of shearing elasticity, with

$$\vec{r} = (x^1, x^2, x^3).$$

E and m are modulus of longitudinal elasticity and Poisson's number, respectively. The function $\chi(x^m)$ depends only upon x^m , and vanishes if we take the boundary condition of

$$\psi^j(\pm\infty) = 0.$$

$$(j = 1, 2 \text{ and } 3).$$

TRI-HARMONIC STRESS FUNCTION

In the previous section, we found displacement potential to be related by the relation

$$2G\psi^j = \phi^k + \phi^m - \phi^j, \quad \dots \quad (2.1)$$

Substituting (2.1) into fundamental Eqs. of elasticity

$$\partial_j \sigma^j = (1/E)[\sigma^j - (\sigma^k + \sigma^m)/m],$$

one finds secular Eqs. of

$$\begin{pmatrix} \partial_1^2 + \Delta/m, & -(\partial_3^2 + \partial_1^2), & -(\partial_1^2 + \partial_2^2) \\ -(\partial_2^2 + \partial_3^2), & \partial_2^2 + \Delta/m, & -(\partial_1^2 + \partial_2^2) \\ -(\partial_2^2 + \partial_3^2), & -(\partial_3^2 + \partial_1^2), & \partial_3^2 + \Delta/m \end{pmatrix} \begin{pmatrix} \phi^1 \\ \phi^2 \\ \phi^3 \end{pmatrix} = 0 \quad \dots \quad (2.2)$$

which leads us to

$$[(1+m)(1-m^2)/m^3]\Delta^3\phi^j = 0. \quad \dots \quad (2.3)$$

We finally obtain

$$\Delta^3\phi^j = 0, \quad \dots \quad (2.4)$$

$$(j = 1, 2 \text{ and } 3)$$

for

$$m \neq 1.$$

$$\sigma = (\sigma^1, \sigma^2, \sigma^3) = (f^{11}, f^{22}, f^{33})$$

means stress. Stress functions in three dimensional elastic continuum are governed by tri-harmonic Eqs.. There are six unknown functions f^{jk} and as many Eqs. of (1.1) and (2.4). f^{jk} can uniquely be determined by choosing three independent solutions of tri-harmonic Eqs. This is a generalization of Airy's bi-harmonic Eqs. into three dimensional isotropic elastic continuum.

SECOND VIRIAL AND ZERO-PRESSURE JOULE-THOMSON COEFFICIENTS OF POLAR AND NONPOLAR GASES AND GAS MIXTURES

M. P. SAKSENA, V. P. S. NAIN AND S. C. SAXENA

DEPARTMENT OF PHYSICS, UNIVERSITY OF RAJASTHAN, JAIPUR, INDIA

(Received June 15, 1966; Resubmitted September 19, 1966).

ABSTRACT. The second virial data of a few binary mixtures involving polar gases have been interpreted on the basis of rigorous theory in conjunction with the Stockmayer potential. The two forms have been used which differ from each other in the overlap part. Conventional combination rules have been used to approximate the unlike interaction from the knowledge of related like interactions. The interpretation is made less ambiguous by suitably categorising the mixtures. The data of second virial of some nonpolar and polar gases, and Joule-Thomson coefficient of ammonia are discussed.

INTRODUCTION

Hirschfelder, McClure and Weeks (1942), and Rowlinson (1949) employed the following Stockmayer (12-6-3) potential :

$$\phi(r) = 4\epsilon \left[\left(\frac{\sigma}{r} \right)^{12} - \left(\frac{\sigma}{r} \right)^6 \right] - \frac{\mu^2}{r^3} g(\theta_1, \theta_2, \psi), \quad \dots (1)$$

where

$$g(\theta_1, \theta_2, \psi) = 2 \cos \theta_1 \cos \theta_2 - \sin \theta_1 \sin \theta_2 \cos \psi \quad \dots (2)$$

to compute the second virial coefficient of polar gases. Here $\phi(r)$ is the interaction potential energy of the molecules at a separation distance r , θ_1 and θ_2 are the inclinations of the two dipole axes to the intermolecular axis, ψ is the azimuthal angle between them, μ is the permanent dipole moment, and ϵ and σ are the two potential parameters. Saxena and Joshi (1962) suggested another potential differing from that of Eq.(1) in its steepness for the overlap part of the potential. It has the explicit form similar to that of Eq.(1) except the repulsive force index is chosen to be eighteen and ϵ_0 has been preferred for ϵ . The two are simply related as,

$$\epsilon = \delta \epsilon_0 / 3\sqrt{3}. \quad \dots (3)$$

The potential parameters ϵ or ϵ_0 and σ are determined by analysing the experimental data of second virial, $B(T)$, as a function of temperature, while those for mixtures can be obtained by the geometric mean rules for ϵ or ϵ_0 , and arithmetic mean rule for σ . The expressions for $B(T)$ of pure gases, B_{mix} for binary mixtures and Joule-Thomson coefficient μ^0 for pure gases are given by Hirschfelder, Curtiss

and Bird (1964). The potential parameters from the literature *as well as* determined afresh by us are recorded for pure gases in Table I and for mixtures in Table II.

In this article we interpret the second virial data for pure gases and mixtures on the above two potentials. The gas systems considered involve both polar as well as nonpolar gases. A special effort has been made to present as far as possible an unambiguous interpretation and in many cases such conclusions are possible while for the remaining this will be possible only after a clearer knowledge of the association properties of the polar molecules is acquired.

$B(T)$ and $\mu^0 C_p^0$ for pure gases

The calculated and experimental values of $B(T)$ for the three nonpolar gases C_6H_6 , C_6H_{12} and $n-C_6H_{14}$, as a function of temperature in the range where experimental data exist are shown in Fig. 1. The comparison of theory and experiment for the two polar gases chloroform and diethyl-ether is shown in Fig. 2. In Figures 1 and 2 the continuous line represents the $B(T)$ values calculated according to the (18-6) and (18-6-3) potentials respectively, while the dotted line similarly corresponds to the (12-6) and the (12-6-3) potentials respectively. A similar comparison for the three remaining polar gases has already been given earlier by Saxena and Joshi (1962a). The experimental data of μ^0 are very scarce and of all the gases discussed here experimental values are available only for ammonia. We show in Fig. 3 these experimental points compared with the theoretical values on (12-6-3) and (18-6-3) potentials. A critical look of these three figures along with similar earlier studies reveal some interesting and useful information. In what follows below we discuss such aspects.

For the three gases of Fig. 1 we find that the scatter in the experimental points is appreciable. This particularly bothers us, for all these three gases there

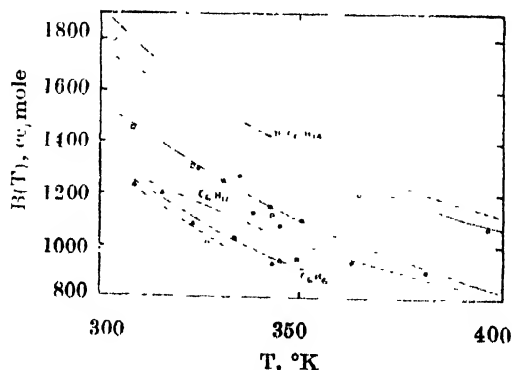


FIGURE 1. Comparison of experimental and calculated $B(T)$ values for pure nonpolar gases as a function of temperature θ , \bullet , \square , \blacksquare , Δ and Δ are experimental points, continuous and dashed curves refer to (18-6-3) and (12-6-3) potentials respectively.

is also appreciable difference between the two sets of computed values. Still if one tries to compare the theoretical curves with a sort of mean experimental curve some preference follows for the (18-6) potential. Saxena and Joshi (1962b) studied seven gases (neo- C_5H_{12} , C_2N_2 , C_3H_4 , SiF_4 , SiF_6 , C_2H_6 and CH_4) and found that except for neo- C_5H_{12} where (12-6) potential is inferior, both the potentials are equally well in reproducing the experimental data which are also more consistent than that of Fig. 1. Saksena and Saxena (1966) further studied the gases CO_2 , N_2O , C_2H_4 and N_2 and found that the two potentials are almost equally good. This however is as expected, for in almost all cases we are sufficiently below the Boyle point and in this region only the attractive part of the potential plays a significant role and that happens to be common in form and approximately equal in magnitude for both these potentials. We should expect that for temperatures above Boyle point the two potentials will appreciably differ and here (18-6) potential is likely to give a lead.

Saxena and Joshi (1962a) studied ten polar gases (CH_3Cl , C_2H_5Cl , $(CH_3)_2CO$, CH_3OH , CH_3F , CH_3NO_2 , CH_3CHO , NH_3 , H_2O and CH_3CN) on the (18-6-3) potential. This work has been extended to include two more gases here viz., $CHCl_3$ and $(C_2H_5)_2O$. Fig. 2 indicates that both the potentials are almost equally good

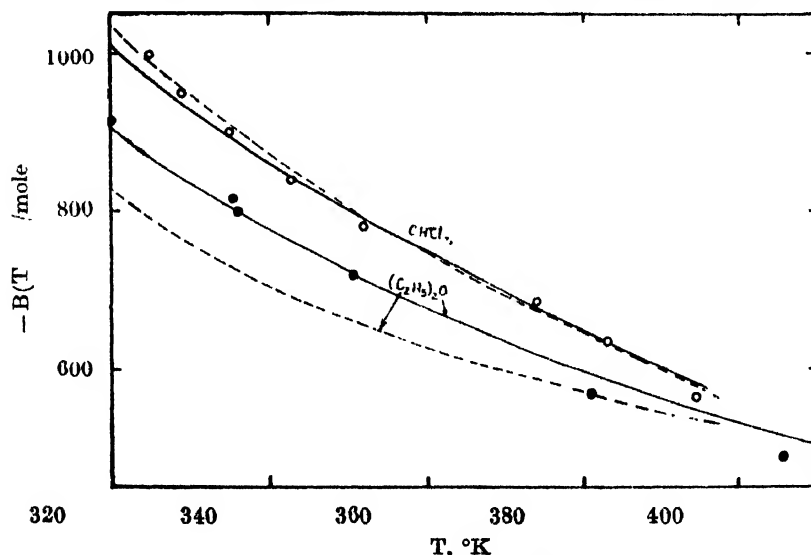


Fig. 2. Comparison of experimental and calculated $B(T)$ values for pure polar gases as a function of temperature T and \bullet are experimental points, continuous and dashed curves refer to (18-6-3) and (12-6-3) potentials respectively.

in reproducing the experimental data. The differences in the two sets of computed values, here as well as in the earlier work, are insignificant. This however should not be regarded as disappointing for the same reasons as mentioned above for the nonpolar gases.

In discussing the second virial of nonpolar and polar gases above we have not taken into account the effect of association between the molecules. The

formation of dimers and assemblies involving still larger number of a molecules is more pronounced for polar than for nonpolar molecules. Lambart *et al* (1949) and Fox and Lambert (1951) have suggested that the degree of association and its influence on the second virial should be estimated from the difference of the observed values and that obtained on the basis of Berthelot's equation. Lambert *et al* (1949) have shown that the degree of association is appreciable for acetonitrile and acetone only while chloroform and diethyl ether hardly show any such tendency. These authors (1949) and Rowlinson (1949) have further shown that the potential energy curve is seriously altered in presence of association. The depth of the potential energy, the position of the minimum and the general shape all get changed. This has a serious impact with out work described here as also with the large amount of work available in the literature which are also based on a similar approach. These efforts derive incentive from the possible facts that association and its effect on $B(T)$ may be small and more in the plausibility of finding such effective values of the potential parameters which can approximate the observed facts tolerably well. This has its own practical utility. Though some work has been done to disentangle the contributions to virial by the association over the free molecule, still much remains to be done to permit any accurate assesment.

A more sensitive property for finding out the appropriateness of a potential is the zero pressure Joule-Thomson coefficient. This theoretical possibility is completely offest by the unavailability of appropriate data. The experimental data are available only for water and ammonia. Both these systems have large dipole and appreciable quadrupole moments and therefore the potential so far discussed are inappropriate. Saxena and Joshi (1962) therefore extended the rigid dipole model of equation (1) by considering the term arising from the interaction of the permanent dipole and its induced dipole. This point polarizable model was considered by them to explain the second virial coefficient of a

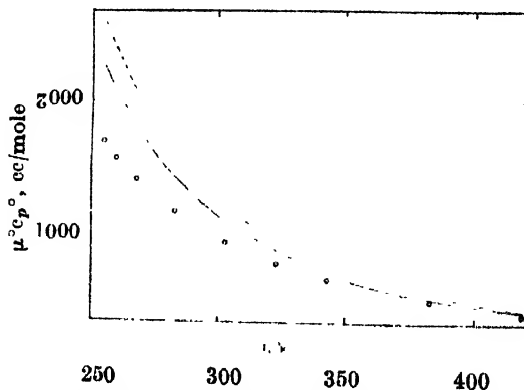


Fig. 3. Comparison of experimental and theoretical $\mu^\circ C_p^\circ$ values for ammonia as a function of temperature. \circ are experimental points, continuous and dashed curves refer to (18-6-3) and (12-6-3) potentials respectively.

few gases. They found a real change in the values of the potential parameters. Saxena, Joshi and Ramaswamy (1963) found it impossible to correlate $B(T)$ and $\mu^{\circ}c_p$ data for water on the basis of a single (12-6-3) or (18-6-3) potential. The reason is obvious. Here also we find from Fig. 3 that $\mu^{\circ}c_p$ experimental values for ammonia are not well reproduced by theory. It may be noted that (18-6-3) potential leads to better agreement with the experiment than the (12-6-3) potential. This may not be regarded as enough proof for the superiority of the (18-6-3) over the (12-6-3) but due regard may be given of the likely better competence of (18-6-3) potential for correlation. This point which looks rather trivial is important when one recalls that the computation of $B(T)$ on a potential appropriate for this gas will not be an easy job even for present age fast speed computers

$B(T)$ for gas Mixtures

The second virial coefficient for binary gas mixtures involving polar gases have not been studied so far on the basis of the rigorous kinetic theory. There are many reasons for this indifference. The important ones are the scarcity of experimental data and lack of theoretical elegance to account for the association effects in polar molecules which now appear in a more complicated fashion than for pure gases. We endeavour to cut through this inertia and see how best this comparison of theory and experiment can be made. We find that experimental data are available on six binary gas pairs permuting out of the polar and nonpolar gases discussed in the last section. The systems are *n*-hexane-diethyl ether, *n*-hexane-chloroform, chloroform-diethyl ether, cyclohexane-acetonitrile, cyclohexane-acetone and benzene-chloroform. The data on the first two systems are of Fox and Lambert (1951), for the next three systems of Lambert, Murphy and Sanday (1954), and for the last pair of Francies and McGlashan (1955) as reported by Huff and Read (1963). We next propose to investigate these data in following arbitrarily chosen categories :

1. In this we will consider those mixtures which include a combination of nonpolar gas with such a polar gas which does not exhibit any tendency to associate.

2. Those pairs which comprise a nonpolar and such a polar gas which dimerizes only.

3. And here such gas pairs in which both the components are polar but the gases are such which do not exhibit the tendency of association individually i.e. in the pure state but do so when two different gases interact.

4. There are other categories also possible. For example when two polar gases form a mixture these individually dimerize but may or may not do so in the mixture form. The six gas pairs mentioned above fall in the first three categories *n*-hexane-diethyl ether, *n*-hexane-chloroform and benzene-chloroform belong to

the first category, cyclohexane-acetonitrile and cyclohexane-acetone to the second category while diethyl ether-chloroform to the third category. There are some measurements available also on such gas pairs which fall in the categories mentioned in 4 above. We defer any consideration of such systems for the time being because a lot of ambiguity gets involved due to the polymerisation of like and unlike molecules. As soon as our understanding is improved about the association properties of molecules it will be profitable to study such systems and derive some inferences from this somewhat resolved and unambiguous study.

In Table III are reported the experimental and theoretically calculated values of the quantity B_{12} on both the potentials. It is known that in such studies B_{12} is preferred than B_{mix} because the former is independent of composition and is sensitively controlled by the nature of unlike interaction. Of all the possible combinations such mixtures which fall in the first category are easiest to interpret and the calculations approximate the ideal requirements as far as possible. In general, the agreement between both the sets of calculated and experimental values may be regarded as satisfactory. However, there are some interesting details which deserve special mention, here again the limitation of the data as regards the temperature range comes as a serious handicap. The agreement between theory and experiment for pure gases is usually better than for B_{12} obtained in these cases. The improvement here also can be easily obtained in case the unlike parameters are determined from B_{12} instead of the combination rules as is done for the case of pure gases. The principle reason for not following this approach and instead employ the combination rules is however obvious and as mentioned earlier lies in the limited information of the mixture virials. It would be a great valuable contribution to produce such data over an extensive temperature range so that unlike interaction may be directly determined and thence the adequacies of combination rules. This approach will have a sound backing and will have the competence to throw some real genuine light on the suitability of an intermolecular potential. For the first two systems of Table 3 we find that (12-6-3) potential is somewhat preferable than (18-6-3) potential. This is somewhat of an illusion when one recalls that for the common constituent of these two mixtures, *n*-hexane, (18-6-3) potential was distinctly superior over the (12-6-3) potential as was also for diethyl ether though for chloroform the difference is not very pronounced. These comments then suggest that the fault lies probably with the combination rules for the (18-6-3) potential. But as the rules for these two potentials are likely to be identical in nature the alteration in one to improve the agreement with experiment will spoil in the other. We strongly feel that it is not advisable to make an attempt to alter these combination rules which have withstood many crucial tests but to feel satisfied with the general overall success achieved. This suggestion which may be regarded as provisional at the moment should be thoroughly investigated as soon as the experimental data have become

available. For the third system of Table III where five directly observed points are available we find that (18-6-3) potential leads to a better agreement with the experiment than the (12-6-3) potential. Thus, in view of the present work for the three binary systems and the related pure gases we find that (18-6-3) potential seems a bit more promising for correlation than the (12-6-3) potential.

Fox and Lambert (1951) have studied the first two systems of Table III using Berthelot equation for the second virial coefficient derived on the basis of the principle of corresponding states. They concluded that these systems do not exhibit any tendency for association. A similar remark holds for the pure components involved. Thus the theory of virials applied adequately for such nonpolar combinations and theoretical calculations may be given as much reliance as mixtures of nonpolar gases.

TABLE I
Like interaction parameters for the (18-6-3) and (12-6-3) potentials*

Gas	μ Debye	r^*	ϵ/k or ϵ_0/k °K	σ Å	b cc/mole	Reference
n-hexane	(a)	—	639	4.07	85.05	Present work
	(b)	—	643.5	5.01	158.11	
Cyclohexane	(a)	—	562	4.40	107.5	Present work
	(b)	—	680	4.60	122.82	
Benzene	(a)	—	567	4.26	97.44	Present work
	(b)	—	974	3.50	54.1	
Chloroform	(a)	0.10	633	3.57	57.62	Present work
	(b)	1.05	1060	2.98	33.45	H.C.B. (1964)
Diethyl ether	(a)	0.11	595	3.62	59.73	Present work
	(b)	0.10	888	3.36	43.08	
Acetone	(a)	0.88	389	3.83	70.85	Saxena & Joshi (1962a)
	(b)	2.74	520	3.76	66.87	H.C.B. (1964)
	(c)	1.60	349	4.10	86.94	Saxena & Joshi (1962a)
Acetonitrile	(a)	3.5	—	—	—	—
	(b)	1.2	400	4.02	82.04	H.C.B. (1964)
Ammonia	(a)	1.47	257	2.70	24.83	Saxena & Joshi (1962a)
	(b)	1.0	320	2.60	22.12	H.C.B. (1964)

* (a) indicates the potential parameters for the (18-6-3) while (b) for the (12-6-3).
 $b = (2/3) \pi N \sigma^3$, N being Avagadro number.

TABLE II

Unlike interaction parameters for the (18-6-3) and (12-6-3) potentials.*

Gas system	<i>t</i> *	$(\epsilon_0)_{12}/k$ °K	$(\epsilon_0)_{12}/k$ or	σ_{12}	b_{12} cc/mole
				Å	
<i>n</i> -hexane- Chloroform	(a)	—	634	3.82	70.3
	(b)	—	826	3.99	80.2
<i>n</i> -hexane- Diethyl ether	(a)	—	617	3.85	56.8
	(b)	—	756	4.18	92.2
Cyclohexane- Acetone	(a)	—	468	4.12	87.9
	(b)	—	595	4.18	92.2
Cyclohexano- Acetonitrile	(a)	—	443	4.25	96.8
	(b)	—	522	4.31	101
Chloroform- Diethyl ether	(a)	0.105	614	3.60	58.6
	(b)	0.10	970	3.17	40.2
Benzene- Chloroform	(a)	—	599	3.91	75.4
	(b)	—	1016	3.24	42.9

*(a) indicates the potential parameters for the (18-6-3) while

(b) for the (12-6-3). $b_{12} = (2/3) \pi N \sigma_{12}^3$.

TABLE III

Comparison of the calculated and experimental $-B_{12}$ (cc/mole) values

Gas System	<i>T</i> °K	Experimental	Calculated	
			(18-6-3)	(12-6-3)
<i>n</i> -Hexano-Diethyl ether	326.2	1130	1067	1090
	352	940	879	928
<i>n</i> -hexane-Chloroform	326.2	1190	1131	1134
	352	960	937	970
Benzene-Chloroform	315.7	1300	1131	1103
	323.2	1130	1071	1039
	333.7	1040	988	957
	343.2	960	928	884
	349.3	950	890	843

TABLE IV

Comparison of the calculated and experimental $-B_{mix}$ (cc/mole) values

Gas system	T °K	Mole-fraction of non-polar component	Experimental	Calculated	
				(18-6-3)	(12-6-3)
Cyclohexano-Acetonitrile	326	0.2	2445	2530	2637
		0.5	1500	1558	1549
		0.8	1250	1210	1158
	349	0.2	1795	1819	1870
		0.5	1130	1172	1173
		0.8	960	935	892
Cyclohexane-Acetone	326	0.2	1267	1266	1241
		0.5	1146	1054	1040
		0.8	1169	1077	1100
	349	0.2	1023	1036	1027
		0.5	961	898	875
		0.8	1026	960	926

TABLE V

Comparison of the calculated and experimental $-B_{12}$ (cc/mole) values for Chloroform-Diethyl ether mixtures

T °K	Experimental	Calculated		
		(18-6-3)	(Corresponding states)	(12-6-3)
326.2	1520	906	860	840
338	1290	827	800	764
352	1030	750	730	693
363	870	697	680	643
393	500	581	550	539

The two systems elaborated in Table IV form the second category and here the two polar gases involved viz., acetonitrile and acetone polymerise but such effects are absent between the cyclohexane-acetonitrile and cyclohexane-acetone molecules in combination. This assumption which conforms the actual state for both these pairs offers a simplified procedure for an unambiguous interpretation of the experimental results. The pure polar gases no doubt have large association as pointed out by Lambert *et al*(1949). but in the calculation of B_{mix} this is easily taken care of by putting the observed value for the pure virial. As there is no association between the unlike molecules B_{12} remains unaffected. Computed values of B_{mix} for both the potentials are recorded in Table IV as function of composition at a particular temperature. We have for these systems considered B_{mix} values instead of B_{12} because it was found that it is not possible to uniquely

choose a single value of B_{12} for the entire of composition. This is an important observation and may have its bearing on the fact that one component of the mixture polymerises individually and consequently this is a property of all systems which belong to this category. It is pleasant to note in the Table that in all cases theory and experiment are in good agreement. This we regard as particularly important and a good support for the assumptions made to explain the behaviour of systems falling in this group. The two potentials in almost all cases lead to fairly identical results though if we critically examine (18-6-3) potential is a bit superior.

The data for one system, chloroform-diethyl ether, where both the components are polar, conform to the category third. They however show association when in combination. The estimation of B_{12} therefore from theory will not be directly comparable to the observed values because in theory we have not taken into account such effects. In fact the computed values should fall short to the directly observed values. In Table V we have listed the experimental B_{12} values as a function of temperature along with the computed values on the two potentials for the system. Indeed it will be noticed that the experimental values are always much higher than the calculated values and are in complete conformity with the prediction of the Berthelot's equation.

CONCLUSIONS

This study reveals several very interesting indications and inferences. The limitations of the availability of the appropriate type of data came in the way to extend the comparison of theory and experiment on a more elaborate level. This naturally puts an hesitation in emphasizing the particular features this paper has brought into light but still it is worthwhile as well as advisable to sum up what may be called as provisional conclusions to which future investigations should purport to strengthen. These are,

1. Properties of mixtures involving polar gases are not amenable to that straightforward interpretation as in the case of nonpolar gases. Some caution and care however in many cases may enable a thorough dependable interpretation. The knowledge of dipole and higher order moments, and the association properties of the molecules are big help for such a study.
2. The two potentials (12-6-3) and (18-6-3) used for the first time to interpret the mixture data are found as successful as the corresponding potentials for non-polar gases in all those cases where their applicability is permissible.
3. Partly enlightened by our experience of (18-6) and (12-6) potentials for nonpolar gases and gas mixtures, we find the symptoms suggesting that the steeper (18-6-3) potential may prove better for correlation of polar gas behaviour also at high temperatures and we look forward to put this prediction to an actual

test as soon as the proper data become available. This belief stems out from several indications where (18-6-3) is found superior to (12-6-3).

4. The categorisation of mixtures involving polar gases suggested here is arbitrary and artificial but has its basis in great convenience of interpretation and similarity of behaviour. It makes possible to think that combinations of polar and nonpolar gases which do not associate individually or in combination are easily interpretable like mixtures of nonpolar gases. Such combinations in which polar component associates while its other nonpolar partner as well as the combination do not, we find correlation of B_{mix} is possible. This approach is not quite free from objection for the representation of the polar gas behaviour by such an approach is an approximation. How to modify the theory to use the association effects is still a problem to solve adequately. However the present effort suggests a bold easy way out for the time being. We also find that the contribution to virial is very large when the combination of two pure components only exhibits association. Obviously the situation will become still more delicate when pure molecules will also show such association individually.

5. In interpreting the results we find that it is of great importance to know how far association effects are possible in individual molecules and when they combine. Unfortunately at the moment no definite procedure exists to do such a calculation though some efforts in this direction are being made recently. The use of Berthelot's equation to estimate qualitatively the presence of association is also only a rough approximation.

ACKNOWLEDGMENTS

We are thankful to the Ministry of Defence and the Council of Scientific and Industrial Research, New Delhi, for supporting this work. The awards of senior and junior research fellowships to M.P.S and V.P.S. respectively are also gratefully acknowledged.

REFERENCES

- Buckingham, A. D. and Pople, J. A., 1955 *Trans. Farad. Soc.*, **51**, 1173.
 Fox, J. H. P. and Lambert, J. D., 1957, *Proc. Roy. Soc. (London)* **A201**, 557.
 Francis, P. G. and McGlashan, M. L., 1955, *Trans. Farad. Soc.* **51**, 593.
 Hirschfelder, J. O., McClure, F. T. and Weeks, I. F., 1942, *J. Chem. Phys.* **10**, 201.
 Hirschfelder, J. O., Curtiss, C. F. and Bird, R. B., 1964, *Molecular Theory of Gases and Liquids*, John Wiley & Sons, Inc., New York.
 Huff, J. A. and Reed, T. M., 1963, *J. Chem. Eng. Data* **8**, 306.
 Lambert, J. D., Murphy, J. J. and Sanday, A. P., 1954, *Proc. Roy. Soc. (London)* **A226**, 1954.
 Lambert, J. D., Roberts, G. A. H., Rowlinson, J. S. and Wilkinson, V. J., 1949, *Proc. Roy. Soc. (London)* **A196**, 113.
 Rowlinson, J. S., 1949, *Trans. Farad. Soc.* **45**, 974.
 Saxena, M. P. and Saxena, S. C., 1966 *Proc. Natl. Inst. Sci. (India)*, **32**, 170.
 Saxena, S. C. and Joshi, K. M., 1962a, *Phys. Fluids*, **5**, 1217.
 ———, 1962b, *Indian J. Phys.*, **36**, 422.
 Saxena, S. C., Joshi, K. M. and Ramaswamy, S., 1963, *Indian J. Pure and Appl. Phys.* **1**, 420.

BAND ENERGY OF GOLD

S. CHATTERJEE AND D. K. CHAKRABORTY

INDIAN ASSOCIATION FOR THE CULTIVATION OF SCIENCE,
CALCUTTA-32.

(Received June 9, 1966)

ABSTRACT. The band energy of gold has been calculated for the point of the Brillouin Zone by the Augmented Plane Wave (A.P.W.) method with the help of the universal potential given by Gaspar for the noble metals. The convergence was tested for the state Γ_1 and is seen to be quite rapid.

INTRODUCTION

The problem of finding the energy levels in a solid is essentially a manybody one the solution of which is practically impossible without the help of some approximation methods. In practice, one starts with one electron Schrodinger equation with a potential which is periodic with the period of the crystal lattice. The energy is then calculated by a proper choice of the one electron wave function which must satisfy the Bloch's condition

$$\psi_{\vec{k}}(\vec{r}) = e^{i\vec{k} \cdot \vec{r}} u_{\vec{k}}(\vec{r})$$

where \vec{k} is a vector of the momentum space and the function $u_{\vec{k}}(\vec{r})$ has the periodicity of the crystal lattice. There are various methods to find out the form of $u_{\vec{k}}(\vec{r})$ of which the simplest one is to expand $u_{\vec{k}}(\vec{r})$ in terms of plane waves whose wave vectors are the reciprocal lattice vectors. But this method has the disadvantage that the lowest value of the secular equation may converge to the lowest eigen value of the atomic states thus necessitating large number of terms in the expansion. This difficulty has been overcome by Herring (1940) in his Orthogonalized Plane Wave (O.P.W.) method by orthogonalizing the plane waves with atomic core states. Although this method has become very successful in the case of simple metals and semi conductors, its success depends on the accurate knowledge of the atomic eigen values and eigen functions in advance. Another serious difficulty of this method is that for some symmetry states the opw's may be automatically orthogonal to the core states and hence the convergence will be poor. This point has been discussed by Hermann (1954) who suggests that in order to improve the convergence, one must add some function to the opw's which will be rapidly varying near the nucleus of the atoms forming the solid. But in the present formalism of the O.P.W. method, there is not much scope in adding rapidly varying functions near the nucleus.

There is yet another method, the Augmented Plane Wave Method, which takes into account many of the above discrepancies. In fact Slater (1964) has pointed out that the Augmented Plane Wave method is a direct answer to Herman's problem of addition of rapidly varying function near the nucleus. Another disadvantage of the O.P.W. method is that it requires the accurate knowledge of eigenvalues and eigen functions in addition to the knowledge of the potential. That is why the O.P.W. method has not been tried in case of heavier metals such as gold because of the nonavailability of Hartree-Fock solution of the atomic states.

The Augmented Plane Wave method was originally proposed by Slater (1937) and later modified by Slater and Saffren (1953). Since then there have been many applications of the method by various authors. Among them the most notable ones are Howarth (1955) and Burdick (1963). Both of them have applied the method to copper with different potentials but very little has been attempted in the case of the other two noble metals e.g. silver and gold. Since there is already one calculation on silver by the O.P.W. method (Chatterjee and Sen, 1966), we have attempted in this paper to calculate the energy bands in gold by the Augmented Plane Wave Method.

OUTLINE OF THE METHOD

The augmented plane wave method has been originally proposed by Slater (1937) and later modified by Slater Saffren and (1953), and successfully applied to copper by Howarth (1955). Following these authors each augmented plane wave may be written as

$$\phi_{\vec{k}} = a_0 \left[\epsilon(r-r_0) e^{i\vec{k} \cdot \vec{r}} + \epsilon(r_i-r) \sum_{l,m} 4\pi i^l \frac{j_l(kr_i)}{R_l(E, r_i)} Y_{lm}^*(\theta_k, \phi_k) Y_{lm}(\theta, \phi) R_l(E, r) \right] \quad (1)$$

where ϵ is a step function

$$\epsilon(x) = 1 \quad \text{for } x \geq 0$$

$$\epsilon(x) = 0 \quad \text{for } x < 0$$

Here \vec{k} is the reduced wave vector, r_i is the radius of the inscribed sphere on which the plane wave are joined with the spherical waves and $R_l(E, r)$ is the solution of the radial equation.

$$\frac{1}{r^2} \frac{d}{dr} \left(r^2 \frac{dR_l}{dr} \right) + \left[E - V(r) - \frac{l(l+1)}{r^2} \right] R_l = 0 \quad (2)$$

with the energy E which is the expectation energy of the augmented planes wave. Thus, in the construction of each augmented plane wave one computes the radial

wave functions $R_l(E, r)$ for a number of energies and l and then finds out the correct value of E and $R_l(E, r)$ from the following equation where ω is the volume of the unit cell outside the inscribed sphere.

$$(E - k^2)\omega = 4\pi r_i^2 \sum_l (2l+1) j_l^2(kr_i) \left[\frac{d}{dr} \ln R_l(E, r) \right]_{r=r_i} \quad \dots (3)$$

Equation (3) is the condition for the expectation energy. The equation is satisfied by means of trial and is quite laborious. But once the augmented plane waves are constructed accurately the problem becomes quite easy. One then utilises the variational procedure based on the linear combination of ϕ_{ks} to obtain the secular equation. The matrix elements of the secular equation are given by

$$\begin{aligned} \langle k_1/k_2 \rangle &= \omega \delta k_1 k_2 - 4\pi r_i^2 \left\{ \frac{(j_l |\vec{k}_1 - \vec{k}_2| r_i)}{|\vec{k}_1 - \vec{k}_2|} (1 - \delta k_1 k_2) \right\} \\ &\quad - \sum_l (2l+1) j_l(k_1 r_i) j_l(k_2 r_i) P_l(\cos \theta_{k_1 k_2}) I_l \quad \dots (4a) \end{aligned}$$

$$\text{where } I_l = \left[\frac{d}{dr} \ln R_l(E_2, r_i) - \frac{d}{dr} \ln R_l(E_1, r_i) \right] [E_1 - E_2]^{-1} \text{ for } E_1 \neq E_2$$

$$= - \frac{d}{dE} \left[\frac{d}{dr} \ln R_l(E, r) \right]_{r=r_i} \text{ for } E_1 = E_2$$

and

$$\begin{aligned} \langle k_1 | H | k_2 \rangle &= \frac{\vec{k}_1 \cdot \vec{k}_2}{|\vec{k}_1 - \vec{k}_2|} \left[\omega \delta k_1 k_2 - 4\pi r_i^2 j_l \frac{(|\vec{k}_1 - \vec{k}_2| r_i)}{|\vec{k}_1 - \vec{k}_2|} (1 - \delta k_1 k_2) \right] \\ &\quad + 4\pi r_i^2 \sum_l (2l+1) j_l(k_1 r_i) j_l(k_2 r_i) P_l(\cos \theta_{k_1 k_2}) J_l \quad (5) \end{aligned}$$

where

$$J_l = \left[E_1 \frac{d}{dr} \ln R_l(E_2, r) - E_2 \frac{d}{dr} \ln R_l(E_1, r) \right]_{r=r_i} (E_1 - E_2)^{-1} \text{ for } E_1 \neq E_2$$

$$= -E \frac{d}{dE} \left[\frac{d}{dr} \ln R_l(E, r) \right]_{r=r_i} + \left[\frac{d}{dr} \ln R_l(E, r) \right]_{r=r_i} \text{ for } E_1 = E_2$$

RESULTS AND DISCUSSION

In the present calculation on gold, the radial equation (2) is solved numerically by means of the Numerov method (Pratt, 1952) with the universal potential given

by Gaspar (1953). Since at present we are concerned with the power of convergence of the method, we have taken nine augmented plane waves for the point Γ of the Brillouin zone corresponding to the wave vectors (000) and (111). We have solved the radial wave equation (2) for $l = 0$ to $l = 6$. For $l > 6$ the contribution to the right hand side of equation (3) become negligible. The value of $\left[\frac{dr}{dr} \ln R_l(E, r) \right]_{r=r_i}$ are given for the augmented plane wave with the reduced wave vector (111).

TABLE I

Energy E	l	$\left[\frac{d}{dr} \ln R_l \right]_{r=r_i}$	$\frac{d}{dE} \left[\frac{d}{dr} \ln R_l \right]_{r=r_i}$
- .85 ryd.	0	-0.25659	-0.93825
	0	-9.91597	-38.50300
	1	- 1.82468	- 0.24450
	2	+ 0.09992	- 0.71450
1 ryd.	3	- 0.09391	- 0.89400
	4	- 0.77379	- 0.36050
	5	+ 1.31446	+ 0.19900
	6	+ 1.28000	- 0.22800

The nine by nine secular determinant has been factorised by the group theoretical consideration to give the states Γ_1 , Γ_{15} , Γ_{25}' and Γ_2' of which the determinant for Γ_1 is two by two and all the other states are one by one. The values are given in Table II from which the convergence for the state Γ_1 can be seen to be quite rapid.

TABLE II
Value of the energy in ryd

States	1st order	2nd order
Γ_1	- .84908	- .85004
Γ_{15}	.76034	
Γ_{25}'	1.34997	
Γ_2'	1.48467	

The calculation for the other symmetry points L and X and for the higher waves for the point is under progress.

ACKNOWLEDGMENTS

The authors are grateful to Prof B. N. Srivastava for his keen interest in the problem. Authors are also grateful to C.S.I.R. for financial assistance.

REFERENCES

- Burdick, G. A., 1963, *Phys. Rev.*, **129**, 138.
Chatterjee, S, and Sen, S. K., 1966, *Proc. Phys. Soc.*, **87**,
Gáspár, R., 1953, *Acta Phys. Acad. Sc. Hung.*, **3**, 263.
Herman, F., 1954, *Phys. Rev.*, **93**, 1214.
Herring, C, 1940, *Phys. Rev.*, **57**, 1169.
Howarth, D. J., 1955, *Phys. Rev.*, **99**, 469.
Pratt, G. W., 1952, *Phys. Rev.*, **88**, 1217.
Saffren, M. M., and Slater, J. C., 1953, *Phys. Rev.*, **92**, 1126.
Slater, J. C., 1937, *Phys. Rev.*, **51**, 486.
——— — 1964, *Adv. Qnt. Chem.*, **35**, 1964.

ON THE GROWTH OF SINGLE CRYSTALS OF NAPHTHALENE

S. C. DATT*, J. K. D. VERMA AND B. D. NAG

SAHA INSTITUTE OF NUCLEAR PHYSICS, CALCUTTA.

(Received May 30, 1966; Resubmitted July 4, 1966)

ABSTRACT. A glass furnace for the growth of single crystals of naphthalene (m.p. 80°C) from the melt by Bridgman-Stockbarger method is described. Crystals upto 1 in. in diameter and 8 in. in length can be easily grown. Different parameters affecting the growth of single crystals and various laboratory procedures have been outlined. The furnace, with suitable alterations, can also be used to grow single crystals of anthracene (m.p. 217°C).

INTRODUCTION

The increasing amount of interest in the studies of semiconducting, optical and ultrasonic properties of naphthalene and anthracene have prompted various workers in growing single crystals of these materials. A large number of methods are available for growing crystals of various materials (Buckley, 1951; Lawson and Nielsen, 1958; Gilman, 1963; Reynolds, 1963). Many theories have been developed to account for the various phenomena observed in crystal growth, but these are of very little assistance in the actual crystal growth in laboratories. For convenient operation and handling, every material requires a particular method for crystal growth, the selection of which depends much upon the melting point, chemical properties and crystal structure of the material. A method suitable for one material may be totally unsuitable for the growth of another material because of differences in melting point or chemical properties.

Although it appears that Bridgman (1925)-Stockbarger (1936) method is more frequently used, it is not the only available and not necessarily even the best method. Vapour phase or sublimation method (Volmer and Schultze, 1931; Obreimov and Prikhotjko, 1932; Lipsett, 1957; Mark, 1961) has been successfully used for growing single crystals of naphthalene in the form of flat platelets. Stober's method (1925) in which the crystal container is kept stationary and the temperature gradient varied, has been used by Belyaev *et al* (1959) and in a modified form by Roussett and Lochet (1942) to obtain good crystals of naphthalene. Kyropoulos (1926) method has also been used for obtaining large single crystals of naphthalene (Lawson and Nielsen, 1958).

Hendricks and Jefferson (1933) were probably the first to grow naphthalene crystals from melt. They adopted the method of Obreimov and Shubnikov

*On leave of absence from Education Department, Government of Madhya Pradesh, Bhopal.

(1924) which is a modification of methods devised by Tamman (1923) and also very much identical to Bridgman's method for growing inorganic crystals from melt. Bridgman's method has been extended by many workers (Feazle and Smith, 1948; Pimentel and McClellan, 1952; Pick and Wissman, 1954; Riehl, 1955; Sangster and Irvine, 1956; Lipsett, 1957, 1958; Yun and Beyer, 1964) for the preparation of large naphthalene crystals and is now mostly used.

REQUIREMENTS FOR THE GROWTH OF LARGE SINGLE CRYSTALS OF NAPHTHALENE BY BRIDGMAN-STOCKBARGER METHOD

In this method the material is melted in an evacuated glass capsule and very slowly lowered through a furnace which should have a sharp vertical temperature gradient near the crystal solid-liquid interface. A good large single crystal can be obtained depending upon the following parameters.

(a) *Furnace design*

The two essential points in designing a furnace for Bridgman-Stockbarger method are, achievement of good temperature gradient and convenience in operating and handling the furnace. The best form of temperature gradient is shown schematically in Fig 1. The maximum temperature should be kept 25° to 40°C

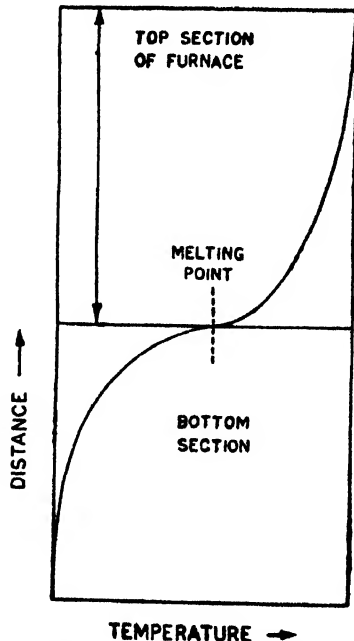


Fig. 1. Temperature gradient desired in a furnace for the growth of naphthalene single crystals.

above the melting point of naphthalene (80°C) to get rid of all traces of crystallinity in the melt. The temperature should fall gradually until the lowest part

of the top section is reached, and then it should drop abruptly, preferably to 65° or 70°C from 80°C.

(b) *Lowering rate*

The difficulties in growing large naphthalene crystals are mainly because of its great supercooling tendencies and low thermal conductivity. Almost all the heat of fusion of the growing crystal must be removed through the solid, which means that naphthalene due to poor thermal conductivity will take much time to solidify. Hence, lowering rate should be very slow, of the order of 0.1 in./hr or even less. The container is usually moved through the furnace by an electrically driven geared motor.

(b) *Shape of crystal container*

The super cooling tendencies of naphthalene and other organics required considerable care in the construction of crystal container. In designing the containers, the attempt is to initiate the growth of a single crystal at a point or constriction. A number of crystal containers of various shapes, as shown in Fig. 2.

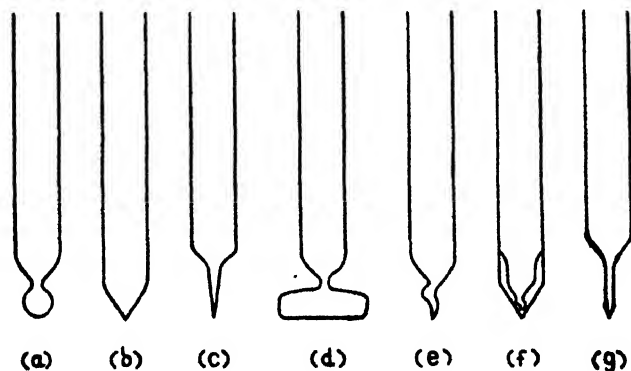


Fig. 2. Containers employed by various workers for the growth of single crystals : (a), Constricted bulb (Bridgman, 1925 and others); (b), Conical tip (Stockbarger (1936); (c), pointed capillary (Huber, et al., 1949; Loninger, 1952); (d), constructed bulb of large area (Lipsett, 1957); (e), Spiral tip (Spendiarov and Aleksandrov, 1959); (f), baffle tip (Sherwood and Thompson, 1960); and (g), ordinary thin capillary tip.

have been used by various workers. The authors have tried all these crystal containers and found type (d) and (e) the most suitable for naphthalene.

(d) *Purity of naphthalene*

When growing crystals by the Bridgman method, it is essential to use only material of the highest purity. Various methods are available for purification which include chromatography, multiple vacuum sublimation, vacuum sublimation with sulphuric acid treatment (Okamoto, et al., 1962), normal freezing (Lipsett, 1957) and zone refining (Wolf and Deutsch, 1954; Herington et al., 1956; Hayakawa, 1966; Inokuchi, 1966). In general, it has not been proved that any one of the

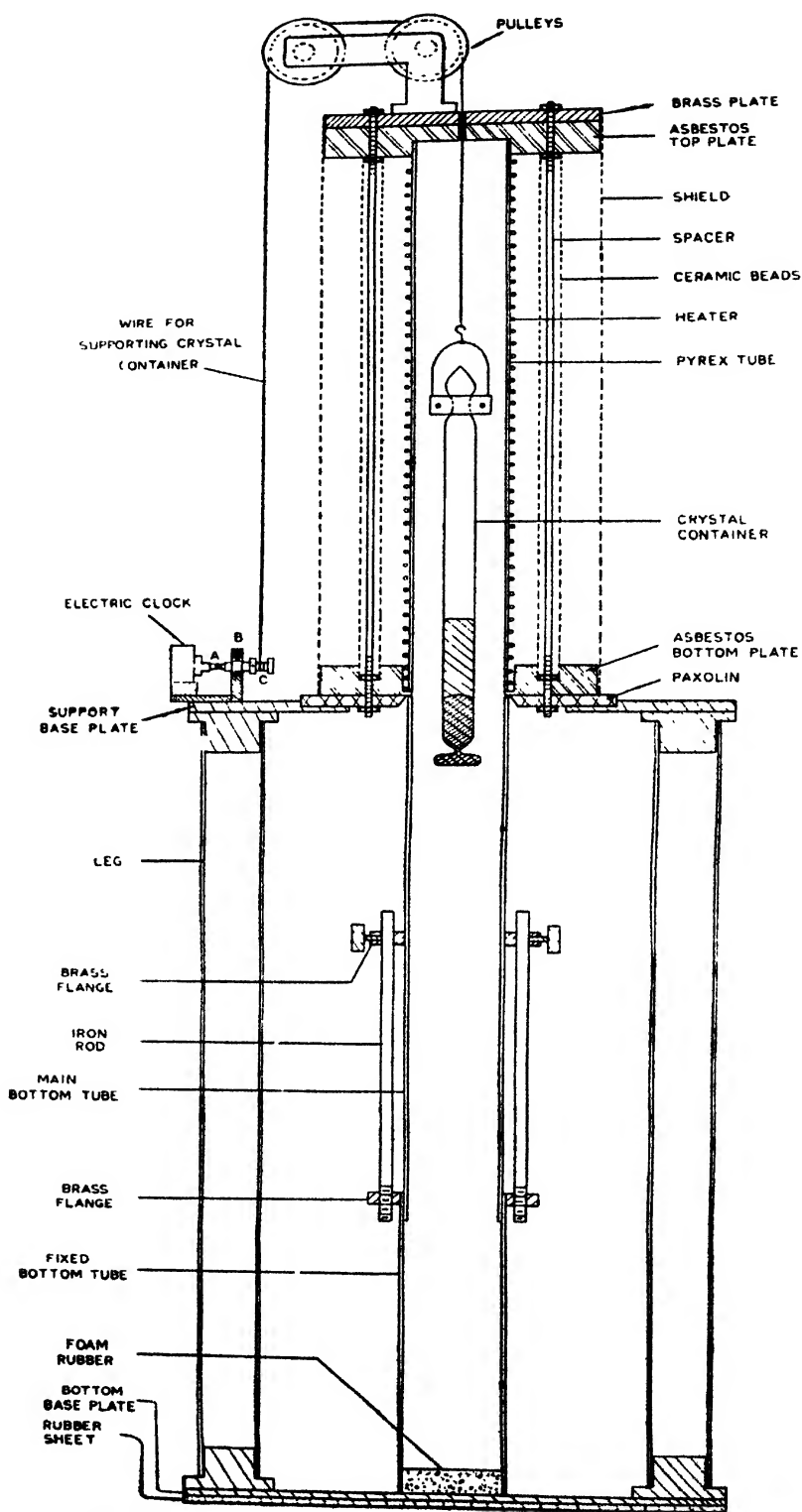


Fig. 3. Schematic diagram of the furnace.

above methods (excluding zone refining) possess advantages over others. Thus, one must carry out the purification by a combination of more than one of these methods. However, zone refining gives extremely pure naphthalene.

FURNACE FOR CRYSTAL GROWTH

A furnace incorporating the salient features discussed in the last section has been constructed in this laboratory. It is some what similar in design to that of Lipsett (1958).

The furnace, shown in Fig. 3, consists of two main sections—an upper Pyrex glass tube on which heater wire is wound and the lower brass tubes which are left at room temperature. The pyrex tube is 18 in. long and 60 mm in diameter. The tube rests on a thin (2 mm) asbestos projection which is supported by $\frac{1}{4}$ in. thick paxolin disc. The paxolin disc sits in a groove in support iron base plate, 14 in. square, and is fixed by three screws (not shown in the figure). The upper end of the pyrex tube fits tightly in a asbestos disc. A brass disc rests on the top of this asbestos disc. The top asbestos and the brass discs are secured in position by three iron spacers. This keeps the pyrex tube permanently in fixed position. The spacers are covered throughout their length by ceramic beads to prevent the heat being conducted to the top brass disc. This furnace is covered by galvanized iron sheet. The bottom section of the furnace consists of two tight fitting brass tubings. The lower tube is fitted to bottom iron base plate. This tube is 10 in. long and of $2\frac{3}{8}$ in. inner diameter and has a circular flange attached to it at the top. Two iron rods are firmly screwed in the top flange of the tube. The other tube which can slide up and down the iron rods is of $2\frac{3}{8}$ in. outer diameter and is 17 in. long. This tube can be fixed in any position on the rods by means of two set-screws. These brass tubes have been chromium plated. A piece of sponge rubber is placed inside the fixed bottom tube so that the crystal container is not broken due to some accidental release. The support base plate rests on four legs, made of $1\frac{1}{2}$ in. iron pipes. The complete unit is placed on a rubber sheet so as to reduce the effect of building and other vibrations to the furnace. The electric clock mechanism, etc., are mounted on the support base plate.

Two independent heaters have been used. The heater wires are insulated by small ceramic beads. The two heaters are connected together by means of a small ceramic connecting terminal strip so that they are arranged mechanically as a single wire, but are electrically insulated from each other. Stainless steel strips are used as anchors for the heater wire terminals. The wire is wound on the pyrex tube which is wrapped with asbestos paper to prevent slipping of the windings. The four heater leads are taken out through four small holes in the shield. Care is taken that no air leaks through these holes. All the leads are connected by means of screws and nuts, as hard soldering of the heater wires to the terminal leads in the furnace have a tendency to break after some heating

and cooling cycle. Power to both the top and bottom heater is supplied from two variable transformers fed from an A.C. line stabilizer. The temperature of the top portion of the furnace is nearly 110°C while it has been adjusted to 80°C at the bottom. A thermocouple has been permanently fitted to record the temperature of the furnace.

An electric clock mechanism has been used for lowering the crystals container. Care is taken to see that no undue strain is being exerted on the clock's gear train. A brass shaft of $\frac{1}{4}$ in. diameter passes through a ball bearing fitted in a brass hanger (B in Fig. 3) and projects on either side. One side of the shaft is coupled to the hour hand of the clock through a universal joint (A) which is bushed at one end to fit the clock. On the other end of the shaft, small wheel (C) with a groove of nearly $3/16$ in. diameter is placed with the help of two setscrews. The wire supporting the crystal container is wound on this wheel. This wire passes from the wheel over two other ball-bearing pulleys through a small hole drilled in the top discs and is attached to a hanger which keeps the wire taut when no crystal container is suspended in the furnace. The crystal container is fastened to a collar at the bottom of this hanger. The usual rate of descent of the crystal container with $3/16$ in. diameter wheel is about 0.049 in. in an hour. This could be made less by employing a wheel of smaller diameter.

LABORATORY PROCEDURES

The actual growth of a crystal is only a small part in the production of a final finished crystal. Many laboratory procedures have to be carried on before and after the growth. The crystal container is thoroughly cleaned (Rosebury, 1956), then filled with naphthalene, evacuated upto a pressure of 10^{-5} torr and sealed.

After crystal is grown, it is carefully taken out by cutting the container (Lipsett, 1957). It is then examined for principal cleavage plane (Lipsett, 1957). Naphthalene crystallizes in the $C_{2h}^2-P2_1/a$ space group (monoclinic crystal structure) and the principal cleavage plane is the *ab*-plane (Bannerjee, 1930; Abrahams, *et al.*, 1949; Robertson, 1953; Winchell, 1954). Since solid naphthalene forms a biaxial crystal, it is possible to identify a single crystal and the location of *b*-axis by using a polarizing microscope (Winchell, 1947; Menzies and Skinner, 1949; Pimentel and McClellan, 1952; Lipsett, 1957; Bloss, 1961). The polishing of crystals is an important part in the production of crystals and standard techniques (Lipsett, 1957; Yun and Beyer, 1964) have been used. The polished surfaces of naphthalene crystals deteriorate by sublimation. To preserve the surfaces, one should keep naphthalene crystals either in an inert atmosphere or in a frigidare.

REMARKS

The furnace described above has proved very successful in growing naphthalene single crystals. Insertion or removal of a crystal container hardly takes a few minutes. Naphthalene single crystals upto 1 in. in diameter and 8 in. long have been grown in the furnace. Large diameter naphthalene single crystals upto 2 in. can be grown if the pyrex tube diameter is 5 in. or more. The rate of descent of the crystal container then should also be reduced to 0.01 in. per hour. Longer crystals can be obtained simply by using longer furnaces. The furnace described above can also be conveniently used for growing single crystals of anthracene (m.p. 217°C) by suitably altering the power input to the two heaters. Anthracene powder has, however, to be sealed in the container at a pressure of 10^{-8} torr to avoid degassing. Moreover, no light should fall during crystal growth, otherwise photochemical reactions will take place.

It should be mentioned that cutting and polishing of crystals occupies an important place in the production of single crystals. It is more difficult to cut and polish a crystal without fracturing it than to grow the crystal initially unfractured.

These crystals are being used for studying electrical properties of naphthalene. These results would be reported elsewhere.

ACKNOWLEDGMENT

One of the authors (S.C.D.) is grateful to Education Department, Government of Madhya Pradesh, Bhopal, for granting him leave.

REFERENCES

- Abrahams, S. C., Robertson, J. M. and White, J. G., 1949, *Acta Cryst.*, **2**, 233.
Bannerjee, K., 1930, *Nature*, **125**, 456.
———, 1930, *Indian J. Phys.*, **4**, 557.
Bolyaev, L. M., Belikov, G. S. and Dobrzhanskii, G. F., 1959, *Rost Kristallov*, **2**, 102 ; transl. in *Growth of crystals*, **2**, 77. (1959).
Bloos, F. D., 1961, "An Introduction to the Methods of Optical Crystallography" Holt, Rinehart, and Winston, New York.
Bridgman, P. W., 1925, *Proc. Am. Acad. Arts Sci.*, **60**, 305.
Buckley, H. E., 1951, "Crystal Growth", John Wiley & Sons., Inc., New York.
Feazel, C. E. and Smith, C. D., 1948, *Rev. Sci. Instr.*, **19**, 817.
Gilman, J. J., 1963, "The Art and Science of Growing Crystals", John Wiley and Sons, Inc., New York.
Hayakawa, S., 1966, *Private communication*.
Hendricks, S. B. and Jefferson, M. E., 1933, *J. Opt. Soc. Am.*, **23**, 299.
Herington, E. F. G., Handley, R. and Cook, A. J., 1956, *Chem. & Ind. (London)*, 292.
Huber, O., Humble, F., Schneider, H. and Steffen, R., 1949, *Helv. Phys. Acta*, **22**, 418.
Inokuchi, H., 1966, *Private communication*.
Kyropoulos, S., 1926, *Z. anorg. Chem.*, **154**, 308.

- Lawson, W. D. and Nielsen, S., 1958, "*Preparation of single crystals*", Butterworths, London, 11.
- Leninger, R. F., 1952, *Rev. Sci. Instr.*, **23**, 127.
- Lipsett, F. R., 1957, *Can. J. Phys.*, **35**, 284.
- 1958, *Rev. Sci. Instr.*, **29**, 423.
- Mark, P., 1961, *Z. Naturforschg.*, **16a**, 950.
- Menzies, A. C. and Skinner, J., 1949, *Discussions Faraday Soc.*, **5**, 306.
- Obreimov, I. W. and Shubnikov, L., 1924, *Zeits. f. Physik*, **25**, 31.
- Obreimov, I. W. and Prikhotjko, A., 1932, *Phys. Z. Sowjetunion*, **1**, 203.
- Okumoto, Y., Huang, F. T., Gordon, A., Brenner, W. and Rubin, B., 1962, "*Organic Semiconductors*", Proceedings of an Inter Industry Conference, Chicago, April 1961, Eds., J. J. Brophy and J. W. Buttry, The MacMillan Co., New York.
- Pick, H. and Wissman, G., 1954, *Z. Physik*, **138**, 436.
- Pimentel, G. C. and McClellan, A. L., 1952, *J. Chem. Phys.*, **20**, 270.
- Reynolds, G. F., 1963, "*Physics and Chemistry of the Organic Solid State*", Vol. I, Eds., D. Fox, M. M. Labes and A. Weissberger, Interscience, New York, London.
- Riehl, N., 1955, *J. Phys. Chem. (U.S.S.R.)*, **29**, 959.
- Robertson, J. M., 1953, "*Organic crystals and Molecules*", Cornell University Press, Ithaca, New York.
- Rosebury, F., 1956, "*Tube Laboratory Manual*", Second Edition, Research Laboratory of Electronics, M.I.T., Cambridge, Mass.
- Roussett, A. and Lochet, M. R., 1942, *J. Physique*, **C3**, 146.
- Sangster, R. C. and Irwine, J. W., Jr., 1956, *J. Chem. Phys.*, **24**, 670.
- Sherwood, J. N. and Thomson, S. J., 1960, *J. Sci. Instr.*, **37**, 242.
- Spendiarov, N. N. and Aleksandrov, B. S., 1959, *Rost Kristallov*, **2**, 78; transl. in *Growth of Crystals*, **2**, 61, (1959).
- Stober, F., 1925, *Z. Krist.*, **61**, 299.
- Stockbarger, D. C., 1936, *Rev. Sci. Instr.*, **7**, 133.
- Tammann, G., 1923, "*Lehrbuch der Metallographie*" Leipzig.
- Volmer, M. and Schultze, W., 1931, *Z. Physik. Chem.*, **A156**, 1.
- Winchell, A. N., 1947, "*Elements of Optical Mineralogy, Part I, Principles and methods*", 5th ed., John Wiley & Sons, Inc., New York.
- 1954, "*The Optical Properties of Organic Compounds*", 2nd ed. The Academic Press, Inc., New York.
- Wolf, H. C. and Deutsch, H. P., 1954, *Naturwiss.*, **41**, 425.
- Yun, S. S. and Beyer, R. T., 1964, *J. Chem. Phys.*, **40**, 2538.

Letters to the Editor

The Board of Editors does not hold itself responsible for opinions expressed in the letters published in this section. The notes containing short reports of original investigations communicated to this section should not contain many figures and should not exceed 500 words in length. The contributions reaching the Secretary by the 15th of any month may be expected to appear in the issue for the next month. No proof will be sent to the author.

1

IMAGE INVERSION OF GEIGER PULSE

R. C. SASTRI AND S. D. CHATTERJEE

JADAVPUR UNIVERSITY, CALCUTTA, 32, INDIA.

(Received January 25, 1967)

In a normal Geiger counter operation, it is customary to maintain the axial wire at a positive potential, as suggested in the original paper of Geiger and Müller (1928). Such an arrangement yields a negative pulse at the wire due to the collection of electrons. The mechanism of pulse formation due to the motion of ions in an ion-chamber or a counter and its effect on external circuits has been discussed in some details by Curran and Craggs (1949). Curran and Reid (1948) have also described properties of some new types of counters, viz., (1) rectangular cathode with symmetrical and non-symmetrical wires and (2) circular cylindrical cathode with non-axial wire. In either case, such counters have shown improved dead time and reduced coincident cosmic-ray background.

Using the second type of counter, having both an axial and a non-axial wires situated within the same circular cylindrical cathode, an interesting new feature has been observed. The circuit arrangement is depicted in Fig. 1.

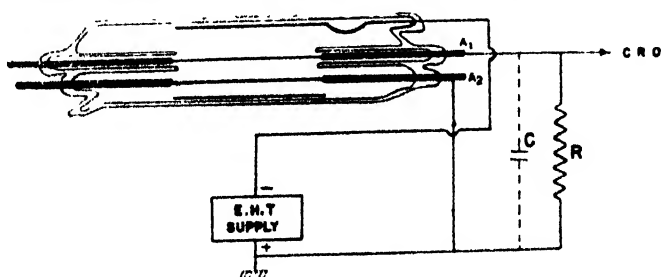


Fig. 1. Circuit arrangement for the study of image inverted pulses in a Geiger counter.

Case A : Negative potential is applied to the cylinder. The axial wire A_1 has a bigger diameter (~ 12 mil) than that of the offset wire A_2 (~ 4 mil). The former is connected to ground through a resistance R so that the pulse could be transferred to a Tektronix oscilloscope; C is the distributed capacity of the wire

and anything attached electrically to it. The offset wire A_2 is normally grounded either directly or through an auxiliary battery.

The axial wire A_1 having a relatively large diameter, does not promote Townsend avalanche in its neighbourhood and is in a quiescent state with a moderate cathode voltage, when the offset wire is left floating. However, when the latter is grounded, positive pulses simulating Geiger pulses appear at the terminal of the axial wire. The rise time and dead time of these pulses are of the same order of magnitude as of Geiger pulses, although the amplitude is correspondingly less. The latter can be varied within limits by varying the voltage of an auxiliary battery connected to the offset wire A_2 . Fig. 2 gives a photographic reproduction of such positive pulses.

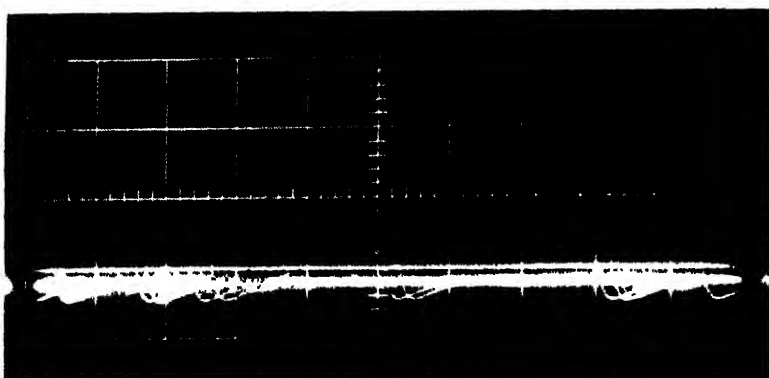


Fig. 2. Image inverted (positive) pulses at the terminal of the axial wire.

Case B: The operating condition of the counter is kept the same as before, excepting that the two wires are made identical in diameter (~ 4 mil.). Under such conditions, the counter appears to behave as two separate counters. However, the pulses appearing at the axial wire consist of both positive and negative pulses as shown in Fig. 3. The reflected positive pulses look sharper, because of smaller time-constant of the offset wire assembly.

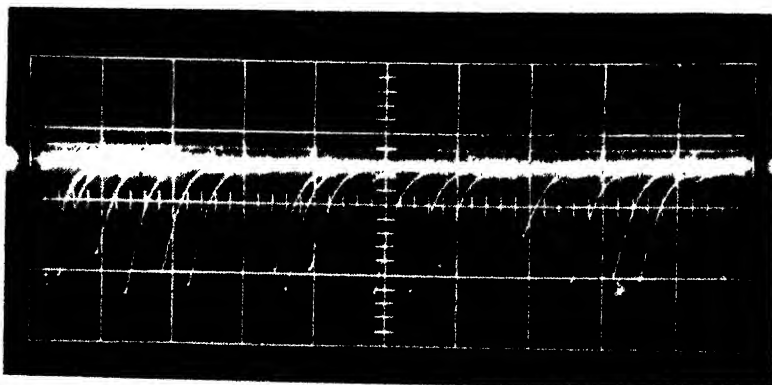


Fig. 3. Image inverted (positive) pulses, superimposed on normal Geiger (negative) pulses.

With slight modification of the circuit parameters, the behaviour of the axial and non-axial wires can be made mutually reversible. It may, however, be noted that the field-strength in the multiplicative region of the non-axial wire is about 15 per cent higher (Curran *et al.* 1948) than the field-strength at the corresponding region of the axial wire, resulting in a lower threshold potential of the former.

Looking at the results, it seems reasonable to suppose that case A represents the physical situation of a charged hollow cylinder enclosing two parallel cylindrical conductors of same finite lengths and having different diameters. The axial wire is grounded through a resistor, while the non-axial one is subjected to intermittent and transient charges. Accordingly, the positive pulses may possibly be identified with image inverted pulses, whose amplitude depends upon image attenuation factors (Harnwell, 1949).

REFERENCES

- Geiger, H. and Muller, W. 1928, *Phys. Zeit.* **29**, 839.
Curran, S. C. and Craggs, J. D. 1949, *Counting Tubes* Academic Press Inc. London, 36.
Curran, S. C. and Reid, J. M. 1948, *Rur. Sci. Inst.* **19**, 67.
Harnwell, G. P. 1949, *Principles of Electricity and Electromagnetism* Mc-Graw Hill Book Co. Inc., New York, 511.

TEMPERATURE VARIATION OF THE PHOTOELASTIC CONSTANTS OF AMMONIUM CHLORIDE

K. V. KRISHNA RAO AND V. G. KRISHNA MURTY

PHYSICS DEPARTMENT, OSMANIA UNIVERSITY, HYDERABAD, -7.

(Received November 19, 1966).

In a recent paper (Rao and Murty, 1966) from this laboratory, the temperature dependence of the photoelastic behaviour of a number of cubic crystals of NaCl type has been described. As ammonium chloride belongs to CsCl type and is found to show a behaviour different from NaCl type crystals with regard to variation of elastic constants with temperature (Bhagavantam, 1955), it is thought worthwhile to study the temperature dependence of its photoelastic constants also.

Using the same procedure as described earlier (Rao and Murty, 1966), the photoelastic constants of ammonium chloride have been determined at various temperatures in the range 35°C to 100°C. It was not possible to make observations above 100°C, as the crystal became translucent beyond 100°C, probably due to the onset of sublimation. The data on the thermal expansion and the thermoelastic behaviour, needed for evaluating the photoelastic constants at various temperatures, have been taken from literature (Sharma, 1950 and Subrahmanyam, 1954). As the data on the thermoelastic behaviour is not available, the value of dn/dt is calculated using Ramachandran's theory (1947) on the thermo-optic behaviour of solids.

Table I shows the values of the photoelastic constants obtained at different temperatures. The stress and the strain optical constants are found to increase numerically with temperature. In the temperature range studied, the variation in $(q_{11} - q_{12})$ is only 14.6%, whereas the variation in q_{44} is much larger, being 24.7%. Thus the behaviour of ammonium chloride, with respect to photoelastic-

TABLE I

Temperature °C	$-(q_{11} - q_{12}) \times 10^{13}$ C.G.S.	P_{11}	P_{12}	$q_{44} \times 10^{13}$ C.G.S.	P_{44}
35	2.95	0.161	0.251	4.28	0.032
60	3.11	0.169	0.263	4.70	0.034
80	3.25	0.176	0.274	5.03	0.035
100	3.38	0.182	0.284	5.35	0.036

city also, is different from NaCl type crystals, in which the variation in $(q_{11}-q_{12})$ is larger than in q_{44} . It will be interesting to study whether other CsCl type crystals also behave in the same manner.

REFERENCE

- Bhagavantam, S. 1955, *Proc. Ind. Acad. Sci.* **A41**, 72.
Ramachandran, G. M. 1947, *Proc. Ind. Acad. Sci.* **A23**, 266.
Rao, K. V. K. and Murty, V. G. K. 1966, *Proc. Ind. Acad. Sci.* **A64**, 24.
Sharma, S. S. 1950, *Proc. Ind. Acad. Sci.* **A32**, 268.
Subrahmanyam, S. V. 1954, *Ph. D. Thesis*, Osmania University.

BOOK REVIEWS

ROENTGENOGRAPHISCHE CHEMIE. By Brandenberger and Epprecht
Publisher : Birkhauser Verlag, Switzerland.

“Roentgenographische Chemie” by Brandenberger and Epprecht is a monograph on the application of X-ray diffraction methods in chemistry. At first it gives in short the various experimental methods in X-ray studies of crystalline materials. A short chapter is added to describe the electron diffraction and neutron diffraction studies of crystals. The application of X-ray diffraction studies to identify the type of the crystalline materials are explained subsequently. The authors then elaborate the distinction between the X-ray diffraction patterns of mixed crystals and explain how this can be used to analyse the mixtures of various crystalline materials. Another chapter gives the methods that may be used to follow chemical reactions. The characterisation of the condition of perfection in the crystals by X-ray and electron diffraction method is also described in some details. The last chapter describes in short the general method of determination of atomic arrangements in crystals. The monograph is useful so far as the practical application of X-ray diffraction methods for the identification and analysis of crystalline phases in various types of materials are concerned. The subject matter is presented without the details of the mathematical theories of X-ray diffraction. Every chapter contains at the end, a list of references which is the best asset of the book. In the chapter on identification and analysis of mixtures, it would have been more useful for the beginners to have some practical examples indicating the whole procedures as applied to a few typical unknown mixtures. The book is a lucid and easy reading presentation of the topics mentioned above for which the authors are to be congratulated. The printing and the paper is very good. The photographs and figures are well reproduced.

R. K. Sen

MATHEMATICAL APPARATUS OF THE THEORY OF ANGULAR MOMENTUM. By A. P. Yutsis, I. B. Levinson and V. V. Vanagas, Published by the Israel Program for Scientific translation : Price...

The book under review, an English translation from the original Russian, is an important and fruitful contribution to the current literature on the highly useful and specialized branch of quantum mechanics—the theory of angular momentum. It starts with a brief discussion of the relation between angular momentum operators and spatial rotations. The subsequent chapters mainly deal to begin with the problem of vector addition of two angular momenta, then with the problem of addition of an arbitrary number of angular momenta, and

finally discuss the various properties of vector coupling co-efficients. A major part has been devoted to the highly useful graphical methods for operations with J_m - and $3nJ$ -coefficients, and properties of irreducible tensor operators and their matrix elements. The book, thus, may be considered as a review of the properties of vector coupling co-efficients—the so-called Clebs-Gordon and Wigner co-efficients, an important mathematical apparatus in the quantum mechanical calculations involving the coupling of a number of angular momentum operators. In vector coupling problem, one usually finds various terminologies, used by different workers such as Clebs-Gordon coefficients, Wigner coefficients, Racah's W -coefficients, $3J$ -coefficients, J_m -coefficients, $3nJ$ -coefficients etc., between which confusion in definitions is often met with in literature. The authors have, carefully preserved their distinction to their as well as readers' convenience with specific definition for each of them.

The authors appear to have assumed the reader's preliminary acquaintance with the methods of group theory and the properties of quantum mechanical angular momentum operator and one encounters the frequent reference to Condon and Shortby's book "The Theory of Atomic Spectra". Wigner's book "Group theory" and Racah's work (1942, *Phys. Rev.*). Moreover, many of the results and mathematical inferences have been simply quoted without giving their proofs, perhaps to avoid cumbrous and tedious algebraic computation. Stress has been laid on the methods of calculation rather than on the derivation of these methods. Of course, the authors did not fail to give the complete references of the original works where an inquisitive reader may find the necessary proofs to his satisfaction. On the whole, the book will be highly useful to the scientific workers engaged in advanced research in many branches of Theoretical Physics, and interested more in having the ready formulae and methods of calculation rather than in their complicated derivations.

As stated earlier, the present contribution is a translation from the original Russian and the reviewer is unable to assure the faithfulness to the translations. However, the translator in his note admits that "translation, unlike rotation, cannot be always represented in a 'unitary' form". Even assuming unavoidable deviations from the original Russian, the translation lacks no clarity, continuity and lucidity of exposition.

U. S. Ghosh

INTRODUCTION TO PHYSICS—A. Kitaigorodsky; Foreign Languages Publishing House, Moscow; 720 pages. Translated from Russian by O. Smith.

The book is meant for those who after leaving the secondary school have taken up engineering as their subject of study. It covers the entire field of Physics except those which are taught in high schools. The book is divided into three main parts. Part one deals with mechanical and thermal motion and includes

in it the fundamental laws of mechanics, mechanical energy, momentum, rotation of a rigid body, vibrations, travelling and standing waves, accoustics, temperature and heat, thermodynamic processes and entropy, kinetic theory of gases and processes of transition to equilibrium. Part two deals with electromagnetic fields which includes electric and magnetic fields, electromagnetic fields, energy transformation in electromagnetic fields, electromagnetic radiation, phenomena of interference and scattering, diffraction of X-rays by crystals, double refraction, theory of relativity and the quantum nature of a field. The third part deals with structure and properties of matter and includes in it motion of charged, particles, wave properties of microparticles, atomic structure, molecules, atomic nuclei, nuclear transformations, atomic structure of bodies, phase transformatins, deformation of bodies, dielectrics, magnetic substances and effect of electronic structure on properties of bodies. The book thus covers practically the whole of Physics and the different basic aspects of it have been developed in a fairly logical sequence. But attempt has nowhere been made to make the treatments of different subjects exhaustive obviously because it is not meant for students of Physics degree course. Experimental physics and the historical development of different physical ideas have also not been considered in this book. The omission was intentional because firstly the author feels that in understanding of the modern techniques employed for an experiment in any branch of physics, knowledge of practically all the branches of physics is required and in consequence, 'experimental physics can not be subdivided' but should be treated as a separate subject; secondly since the book is not meant for those who want to be physicists inclusion of historical development was thought to be unnecessary. In spite of the omissions the basic physical ideas of the different branches have been explained in sufficiently clear and concise language. The book is undoubtedly a useful text book for students for the engineering degree courses and a helpful book for subsidiary reading by the students of physics honours courses.

A. K. D.

INDIAN JOURNAL OF PHYSICS

VOL. 41

No. 3

AND

VOL. 50

PROCEEDINGS

No. 3

OF THE

INDIAN ASSOCIATION FOR THE CULTIVATION OF SCIENCE

(Edited in collaboration with the Indian Physical Society).

MARCH 1967

PUBLISHED BY THE
INDIAN ASSOCIATION FOR THE CULTIVATION OF SCIENCE
JADAVPUR, CALCUTTA-32

INSTRUCTIONS TO AUTHORS FOR PREPARATION OF MANUSCRIPTS

Original scientific papers on all branches of Physics and allied subjects such as Chemical Physics, Mathematical Physics, Applied Physics, Geophysics, Biophysics, Crystallography and Minerology etc.; are accepted for publication in Indian Journal of Physics provided these are not merely records of routine laboratory tests and contain original contributions to the knowledge of these Sciences. Normally, the author or at least one of the joint authors should be a member of the Indian Association for the Cultivation of Science or of the Indian Physical Society. Papers from authors other than members will be also accepted under special circumstances. Mss. for publication, in duplicate should be sent to the Assistant Secretary, Indian Journal of Physics, Indian Association for the Cultivation of Science, Jadavpur, Calcutta-32. Mss. submitted should be typewritten with double space, on one side of good quality paper, with sufficient margin on the left and at the top. Each paper should begin with an abstract just after the title of the paper and the name and full address of the author or authors. References in the text should be given either by quoting the year of publication within parantheses, if the surname of the author occurs in the text, or by quoting the surname of the author followed by the year within parantheses at the proper place. In case the reference has more than one name, all names other than the first should be replaced by *et al* in the text as shown. For example, "Thermal transformation..... was studied by Bernal *et al* (1959) and Das Gupta (1960)". Or "Thermal decomposition ... studied by different workers (Cuthbert, 1947 ; Weiden, 1954)". The full references should be given at the end of the paper, under head *References*, arranged alphabetically by surname, followed by initials, year of publication, standard abbreviated name of journal with single underline, volume with double underline, and the page *e.g.* : Perkins, H.D., 1950, *Proc. Royal Soc.* **A203**, 309. If more than one paper by the same authors occur in the same year, in the same journal or not, both in the text and in the *References* these should be chronologically signified by adding *a, b, c*, etc., to the year. Names of same author or authors successively coming in *References* may be replaced by a long 'dash'. Name of same journal coming in *References* successively may be also replaced by long dashes similarly. Positions for text figures and diagrams should be indicated in margin. Line diagrams should be drawn on white Bristol board or tracing paper with black Indian Ink and interior of the diagrams should contain the minimum number of index letters (preferably of simple Gothic style) or numerals (preferably Roman type). Where possible different graphs in the same diagram should only be differentiated by, full line, dotted line, dashed line, crosses, circles, squares etc. Full captions of all figures with serial numbers should be given in a separate sheet. Numerals for scales and description of coordi-

(Contd. to 3rd cover)

THE EMISSION SPECTRUM OF THE CdBr MOLECULE (THE VISIBLE SYSTEM)

M. M. PATEL AND S. P. PATEL

DEPARTMENT OF PHYSICS, FACULTY OF SCIENCE

M. S. UNIVERSITY OF BARODA, BARODA, INDIA

(Received July 8, 1965; Resubmitted May 10, 1966)

ABSTRACT. The spectrum of CdBr was reinvestigated in emission using a high frequency discharge from a 125 Watt oscillator working in the frequency range 10 to 15 M.c/sec. A system of bands degraded to red, designated as $B^2\Sigma \rightarrow X^2\Sigma$ and occurring in the region $\lambda\lambda 4900-3900$ has been photographed with Hilger medium quartz and E_2 glass spectrographs. In addition to the bands already observed by various investigators, a number of new bands have been recorded in the present investigation. The existence of isotopic effect of Br^{79} and Br^{81} is established for about ten bands. The vibrational analysis of the band system is given and the following vibrational quantum formula is derived.

$$\nu_{head} = 24822.6 + [105.4(v' + \frac{1}{2}) - 1.70(v' + \frac{1}{2})^2] - [229.9(v'' + \frac{1}{2}) - 0.47(v'' + \frac{1}{2})^2]$$

INTRODUCTION

The spectra of halides of zinc, cadmium and mercury have been investigated in various degrees of detail by different workers. [Wieland (1929, 1941), Oeser (1935), Ramasastry and Rao (1946), Ramasastry (1947), Ramasastry and Sreeramurthy (1950)]. These molecules show systems of two general types. One type is a short wavelength range system on the longer wavelength side of Zn, Cd or Hg lines in the ultraviolet region. The other type is a group of crowded bands, degraded to red, on a continuum with pronounced intensity maxima in the red region. In the short wavelength region of the visible spectrum, however, progression type of bands with a partial resolution into rotational lines are observed in a number of these molecules.

Two previous investigations have been made on the spectrum of CdBr. Wieland (1929) obtained the vibrational spectrum of this molecule in a high-frequency discharge in the region $3250-3120\text{\AA}$, consisting of violet degraded bands. Howell (1943) suggested that these bands form one of the components of the $^2\Pi \rightarrow ^2\Sigma$ transition but could not succeed in observing the other one. Ramasastry (1949) obtained some additional bands and attributed these to the missing component of the Wieland system. Wieland (1929) also mentioned the occurrence of the diffuse bands extending from 6400 to 3300\AA . Using a high-frequency source, later, Ramasastry (1949) obtained these visible bands extending from $4900-3850\text{\AA}$. Measurements of about fifty bands were reported and a regularity of intervals was indicated which was of the order of about 110 cm^{-1} .

In continuation of our work on the spectrum of CdCl (1966), a reinvestigation of the bands of CdBr in this region was also undertaken and the results obtained are reported here.

EXPERIMENTAL

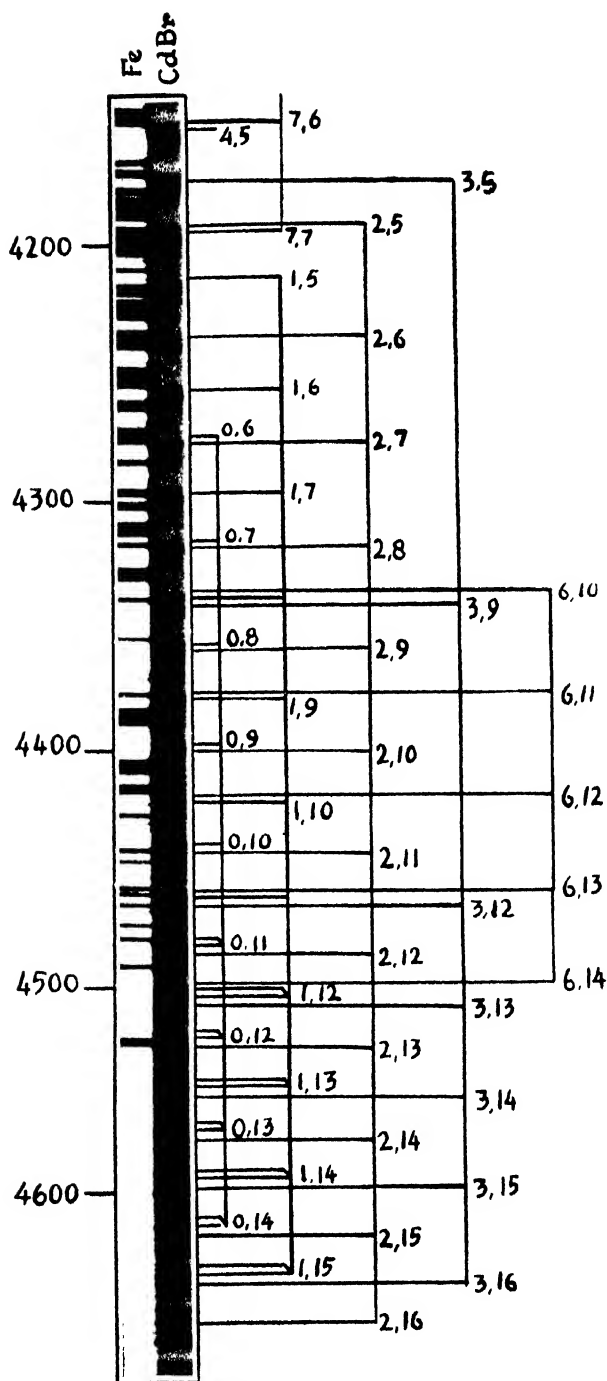
The spectrum of cadmium bromide was excited in a high frequency discharge from a 125 Watt oscillator working in the frequency range 10–15 Mc/sec. A pure sample of the substance was kept in a small quartz boat at the centre of a straight tube of quartz of about 25 cm. in length and 1.5 cm. in diameter. The discharge was established by external electrodes and was maintained bright-white in colour by strong heating. Continuous evacuation of the discharge tube with a high vacuum pump was necessary. Photographs of the spectra in the visible region were taken with the Hilger medium quartz spectrograph and with Hilger E_2 glass spectrograph, the latter having a dispersion of about 16 Å/mm. at 4300Å. An exposure of about 20 to 30 minutes was found adequate to record the spectrum with Ilford process plates. Iron arc lines were used as standards for determining the wavelengths. The wavelengths of the band heads reported here are averages of several independent settings of different plates.

RESULTS

The spectrum of cadmium bromide bands is reproduced in figs. 1 and 2. The bands are degraded towards the red. The bands on the longer wavelength side have sharp edges getting diffuse and broad towards shorter wavelength. Some of the bands in the region 4800-4400 Å show sharp double heads. In table I the wavelengths, wave numbers in vacuum and visually estimated values of intensities of the bands obtained in the present investigation are given. In the fifth column the wave numbers of the bands reported by Ramasastry (1949) are given for comparison. The classification of bands is given in column 4. The calculated values along with observed isotopic shifts for about ten bands have been given in table II.

DISCUSSION

In addition to forty nine bands already reported by Ramasastry (1949), nearly ninety bands have been observed and measured in the present investigation. When the most intense bands taken alternately are arranged in a row, the wave number intervals show a regular decrease for about three groups of bands. Hence they are considered as members of a progression of the lower state of this molecule. When the bands in this region were assigned to three different v' -progressions, it was possible to get the lower state difference of about 230 cm^{-1} . Following the standard procedure (Herzberg, 1950) for calculating the vibrational constants, the band head equation given below, was derived, and this accounts in a satis-

Fig 1. CdBr bands taken with a E_c^+ glass spectrograph

M. M. Patel and S. P. Patel

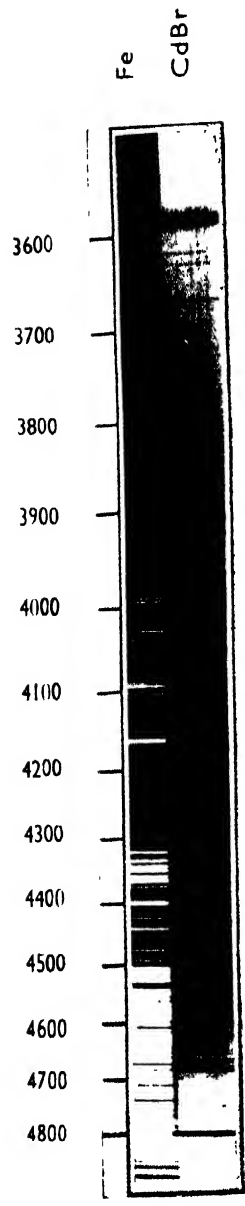


Fig 2. CdBr bands taken with low dispersion spectrograph

factory manner for all the observed bands. The agreement of ν_{obs} and ν_{cal} is shown in Column 6, table 1.

$$\nu_{head} = 24822.6 + [105.4(v' + \frac{1}{2}) - 1.70(v' + \frac{1}{2})^2] \\ - [229.9(v'' + \frac{1}{2}) - 0.47(v'' + \frac{1}{2})^2].$$

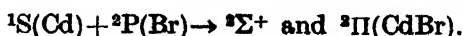
When the bands are arranged in a Deslandres table, the intensity distribution bears a close resemblance to that observed in the corresponding systems of the halides of zinc and mercury. The Condon parabola for the system appears to be sufficiently wide which probably accounts for the poor intensities of the bands having lower v' and v'' values.

As the two isotopes of bromine (Br^{79} and Br^{81}) occur in the ratio of 50.57 : 49.43 one may expect the intensities of the corresponding isotopic bands to be nearly the same. In the region 4700 to 4400 Å this isotope effect gives the bands a double headed appearance. The isotopic shift for the band (v', v'') is given by

$$\nu_{v_i} - \nu_v = \Delta\nu = (\rho - 1)[\omega'_e(v' + \frac{1}{2}) - \omega''_e(v'' + \frac{1}{2})] \\ - (\rho^2 - 1)[\omega'_e x'_e(v' + \frac{1}{2})^2 - \omega''_e x''_e(v'' + \frac{1}{2})^2]$$

where ν_{v_i} refers to CdBr^{81} and ν_v to CdBr^{79} . The isotopic factors $(\rho - 1)$ and $(\rho^2 - 1)$ come out to be -0.00723 and -0.01443 respectively. Using these values the isotopic shifts for about ten bands were calculated. The observed separations were then compared with the calculated values. The agreement is quite close and is shown in Table II.

If the molecule cadmium bromide is formed from cadmium and bromine atoms, both taken in their normal states, the possible electronic states are $^2\Sigma^+$ and $^2\Pi$



As the lowest electronic states of a molecule are usually those that dissociate into their normal atoms, these $^2\Sigma^+$ and $^2\Pi$ states may be taken as the low levels of cadmium bromide molecule. These two states represented in the usual notation can be expressed as

$$\sigma^2\sigma^2\pi^4\sigma, ^2\Sigma^+ \\ \sigma^2\sigma^2\pi^3\sigma^2, ^2\Pi_i$$

The inverted $^2\Pi$ state will be one of the low lying states and may be nearer to $^2\Sigma^+$ state. A band system expected due to the transition $\sigma^2\sigma^2\pi^3\sigma^2, ^2\Pi_i \rightarrow \sigma^2\sigma^2\pi^4\sigma, ^2\Sigma^+$ should be of very low energy and may appear in the infra-red region, or the non-appearance of the above transition may be due to the fact that $^2\Pi_i$ may be a repulsive state.

The system B lying in the region 3900–4900 Å consists of red degraded bands. As most of the bands excepting those in the region 4400–4700 Å are single headed and that these double headed bands are due to isotope effect the transition may

TABLE I

Band heads of CdBr in the region 4900 to 3900 Å

Intensity	Wavelength	Observed Wave Number in vacuum	v', v''	Value observed by Ramasastry	$\nu_{obs} - \nu_{cal}$ in cm^{-1}
2	4908.53	20367	0, 20	—	-1
1	4884.55	20467	1, 20	—	-3
1	4867.19	20540	4, 21	—	-5
1	4861.28	20565	2, 20	—	-3
2	4834.24	20680	1, 19	20691	0
2	4808.43	20791	0, 18	20793	+1
3	4785.65	20890	1, 18	20905	-2
1	4768.52	20965	4, 19	—	-1
2	4762.62	20990	2, 18	—	-1
3	4759.67	21004	0, 17	21014	+1
3	4734.98	21118	—	21120	—
1	4729.05	21140	6, 19	—	+4
2	4720.79	21177	4, 18	—	-1
3	4714.78	21204	2, 17(79)	21215	+1
2	4709.03	21230	2, 17(81)	—	—
1	4700.81	21267	5, 18	—	+1
2	4693.75	21299	3, 17(79)	—	+1
2	4688.02	21325	3, 17(81)	21319	—
4	4668.10	21416	2, 16(79)	—	-1
3	4662.88	21440	2, 16(81)	21444	—
3	4647.70	21510	3, 16	—	-2
4	4642.74	21533	1, 15(79)	21531	0
4	4638.04	21555	1, 15(81)	21555	—
4	4631.77	21584	9, 18	—	-2
5	4622.13	21629	2, 15	—	-2
4	4618.72	21645	0, 14(79)	21644	-1
4	4614.03	21667	0, 14(81)	21668	—
4	4608.92	21691	5, 16	—	-1
5	4601.71	21725	3, 15	—	-1
5	4597.26	21746	1, 14(79)	—	-2

TABLE I (contd.)

Intensity	Wavelength	Observed Wave Number in vacuum	ν', ν''	Value observed by Ramasastry	$\nu_{obs} - \nu_{cal}$ in cm^{-1}
4	4592.62	21768	1, 14(81)	21758	—
3	4586.93	21795	9, 17	—	-3
6	4576.63	21844	2, 14	—	-3
6	4573.29	21860	0, 13(79)	—	-2
5	4568.92	21881	0, 13(81)	21874	—
3	4563.89	21905	5, 15	—	-2
6	4556.40	21941	3, 14	—	-1
7	4551.43	21965	1, 13(79)	—	+1
6	4547.49	21984	1, 13(81)	21979	—
4	4542.12	22010	9, 16	—	-2
7	4531.83	22060	2, 13	—	-3
8	4528.13	22078	0, 12(79)	—	-2
7	4524.44	22096	0, 12(81)	22090	—
4	4519.32	22121	5, 14	—	-1
8	4512.19	22156	3, 13	—	-2
9	4507.30	22180	1, 12(79)	—	-2
9	4503.85	22197	1, 12(81)	22194	—
3	4501.83	22207	6, 14	—	0
4	4495.95	22236	—	—	—
9	4487.68	22277	2, 12	—	-3
9	4484.06	22295	0, 11(79)	22295	-3
9	4480.84	22311	0, 11(81)	—	—
9	4468.42	22373	3, 12	—	-2
9	4463.04	22400	1, 11	22407	0
4	4459.06	22420	6, 13	—	-3
9	4444.19	22495	2, 11	—	-3
10	4440.63	22513	0, 10(79)	22522	-4
9	4437.68	22528	0, 10(81)	—	—
3	4432.95	22552	5, 12	—	-4
10	4420.41	22616	1, 10	—	-3

TABLE I (contd.)

Intensity	Wavelength	Observed Wave Number in vacuum	ν', ν''	Value observed by Ramasastry	$\nu_{obs} - \nu_{cal}$ in cm^{-1}
8	4416.30	22637	6, 12	—	-4
9	4400.95	22716	2, 10	—	-2
8	4397.27	22735	0, 9	22731	-2
9	4377.63	22837	1, 9	22844	-2
7	4374.38	22854	6, 11	—	-5
8	4359.50	22932	2, 9	—	-3
7	4354.94	22956	0, 8	22954	-2
8	4340.57	23032	3, 9	—	-1
8	4335.68	23058	1, 8	23057	-2
4	4332.85	23073	6, 10	—	-5
8	4317.51	23155	2, 8	—	-4
7	4313.42	23177	0, 7	23168 23213 (Chlorine atomic-line) 23278	-3
7	4294.51	23279	1, 7	—	-3
7	4276.33	23378	2, 7	—	-3
3	4272.30	23400	0, 6	23390	-3
6	4253.58	23503	1, 6	23496	-2
6	4235.99	23601	2, 6	23609	-3
7	4218.76	23697	3, 6	—	-2
3	4213.60	23726	1, 5	23723	-3
5	4197.32	23818	7, 7	—	-5
4	4196.27	23824	2, 5	23826	-3
5	4179.08	23922	3, 5	—	0
4	4175.76	23941	—	23942	—
4	4163.24	24013	4, 5	—	-1
3	4158.40	24041	7, 6	24039	-5
3	4140.31	24146	3, 4	24149	-1
2	4120.68	24261	10, 6	24267	-9
3	4105.96	24348	8, 5	24364	0
+3	4086.66	24463	4, 3	24469	-3

TABLE I (contd.)

Intensity	Wavelength	Observed Wave Number in vacuum	ν', ν''	Value observed by Ramasastry	$\nu_{obs} - \nu_{cal}$ in cm^{-1}
+2	4068.53	24572	8, 4	24580	0
+2	4049.08	24690	4, 2	24694	-2
+2	4031.77	24796	8, 3	24803	-2
+2	4012.52	24915	4, 1	24908	-4
+2	3997.75	25007	5, 1	25010	-1
+2	3978.82	25126	13, 3	25129	—
+1	3961.48	25236	5, 0	25230	0
+1	3943.20	25352	13, 2	25346	—
+1	3927.08	25457	11, 1	25448	—
+0	3917.10	25522	12, 1	—	—

+ Measurements made on the plate taken with a medium quartz Spectrograph.

TABLE II

Assignment ν', ν''	Observed shift in cm^{-1}	Calculated shift in cm^{-1}
0, 10	15	15
0, 11	16	17
0, 12	18	19
0, 13	21	20
0, 14	22	22
1, 12	17	18
1, 13	19	19
1, 14	22	21
1, 15	22	23
2, 16	24	24
2, 17	26	25
3, 17	26	25

Fig. 1. CdBr bands taken with a E₂ glass spectrograph.

Fig. 2. CdBr bands taken with low dispersion spectrograph.

in all probability be $^2\Sigma^+ \rightarrow ^2\Sigma^+$. The electron configuration $\sigma^2\sigma\pi^4\sigma^2$ gives rise to $^2\Sigma^+$ state which will also be one of low energy. The upper state of the visible bands may hence be identified with this state. The change of an electron from an inner σ to an outer σ orbit is consistent with the expected decrease in the vibrational frequency of the red degraded band system. This $^2\Sigma^+$ and the other excited states of the molecule will be those which could be derived from cadmium and bromine atoms, with one, or the other, or both of them, in their excited atomic states. If the cadmium atom is taken in the first excited state and the bromine atom is taken in the normal state it gives rise to $\Sigma^+(2)$, Σ^- , $\Pi(2)$ and Δ doublet and quartet states. The doublet levels alone should be considered here. Selection rules do not permit the levels $^2\Sigma^-$ and $^2\Delta$ to combine with the ground state. A $^2\Sigma^+ \rightarrow ^2\Sigma^+$ transition in this region is therefore expected.

A group of bands in the region 5000 to 6400 Å have also been recorded in the present investigation. They are degraded to red but are diffuse in appearance. Attempts are being made to analyse them.

ACKNOWLEDGMENTS

The authors wish to express their thanks to Prof. N. S. Pandya for his keen interest in this work. One of the authors (S.P.P.) is grateful to the Council of Scientific and Industrial Research, New Delhi, for the award of a Research Fellowship.

REFERENCES

- Herzberg, G., 1950, *Spectra of Diatomic Molecules*, D. Van Nostrand Co., Inc., New York.
 Howell, H. G., 1943, *Proc. Roy. Soc., A* **182**, 95.
 Patel M. M., and Patel S. P., 1966, *Indian J. Pure. Appl. Phys.* **4**, 388,
 Oeser, E., 1935, *Z. P.*, **95**, 699.
 Ramasastry, C., and Rao, K. R., 1946, *Indian J. Phys.*, **20**, 100.
 Ramasastry, C., 1947, *Indian J. Phys.*, **21**, 265.
 Ramasastry, C., and Sreeramurthy K., 1950, *Proc. Nat. Inst. Sci., Indian*, **16**, 305.
 Ramasastry, C., 1949, *Indian J. Phys.*, **23**, 453.
 Wieland, K., 1929, *Helv. Phys. Acta.*, **2**, 46 and 77.
 ———, 1941, *Helv. Phys. Acta.*, **14**, 420.

ELASTIC SCATTERING OF ELECTRONS BY HYDROGEN ATOM

S. B. GUPTA* AND N. C. SIL

DEPARTMENT OF THEORETICAL PHYSICS,

INDIAN ASSOCIATION FOR THE CULTIVATION OF SCIENCE,

JADAVPUR, CALCUTTA-32

(Received July 16, 1966).

ABSTRACT. The total cross sections of elastic scattering of electrons by hydrogen atom at the incident energies of 13.6 ev, 54.4 ev, 122.4 ev, 217.6 ev have been calculated in the Born-Oppenheimer (B.O.) approximation with the neglect of the core interaction term and taking into account the distortion of the plane incident wave in the field of the target atom.

INTRODUCTION

The cross sections of elastic scattering of electrons by atoms are easily calculated with the Born approximation which, however, is valid only at high incident energies; if we include exchange effect in the above, we get the Born Oppenheimer formula which leads generally to poor results at low energies for exchange scattering amplitudes. As the derivation of the B.O. formula is not logically perfect, a number of modifications of the B.O. approximation have been proposed (Feenberg 1932, Mittleman 1962, Bell and Moiseiwitsch 1963, Ochkur 1964). Ochkur suggests that as the first order Born approximation has been derived according to the first order perturbation theory, the first order B.O. formula for exchange scattering amplitude should not contain terms which are not within the frame work of the first order approximation. So he retains only the first term in the expansion of the B.O. formula in the powers of k_0^{-2} (k_0 = wave number of the incident electron). As a result the effect of the core potential term is neglected. Kang and Sucher (1966) have justified this omission by proving that in the exchange amplitude for electron-atom collision, the core interaction term vanishes identically when the core (proton) is infinitely heavy.

Again in the first Born and B.O. formulae the wave function for the colliding electron is approximated by the incident plane wave on the supposition that the incident energy is high. At low energies, the distortion of the plane waves should be considered. This is generally done by having recourse to higher order approximations. In his investigation of the elastic scattering of electrons by helium and hydrogen atoms, Sachl (1958) has given a formulation for taking into account

*Department of Mathematics, M. B. B. College Agartala.

the distortion of the s -wave part of the incident wave. The present paper is an extension of Sachl's work in that here we consider the distortion of higher waves. However Sachl's distorted wave is singular at the origin, while our function is free from this singularity. We have omitted the core interaction term from the B.O. formula as suggested by Kang and Sucher (1966). With the neglect of this term, the elastic cross section for collision becomes very large compared to the theoretical results obtained by the close coupling method of Burke, Schey and Smith (1963) and by the first order exchange approximation of Bell and Moiseiwitsch (1963). The inclusion of the effect of distortion of the incident waves considerably improves the result except at $k_0 = 1$ where the validity of the Born or B.O. approximation is questionable and where distortion and polarization of the atom play an important role.

DIRECT AND EXCHANGE SCATTERING AMPLITUDES

The wave equation for the scattering of an electron by a H atom (in atomic units) is

$$\left(-\frac{1}{2}\Delta_1^2 - \frac{1}{2}\Delta_2^2 - \frac{1}{r_1} - \frac{1}{r_2} + \frac{1}{r_{12}} - E \right) \psi(\mathbf{r}_1, \mathbf{r}_2) = 0 \quad \dots (1)$$

where $\psi(\mathbf{r}_1, \mathbf{r}_2)$ and E are respectively the wave function and the total energy of the system. The boundary conditions on $\psi(\mathbf{r}_1, \mathbf{r}_2)$ are

$$\psi(\mathbf{r}_1, \mathbf{r}_2) \sim \exp i\mathbf{k}_0 \cdot \mathbf{r}_1 \psi_0(\mathbf{r}_2) + \sum_n \frac{\exp ik_n r_1}{r_1} f_n(\theta_1, \phi_1) \psi_n(\mathbf{r}_2) \text{ as } r_1 \rightarrow \infty \quad \dots (2)$$

$$\sim \sum_n \frac{\exp ik_n r_2}{r_2} g_n(\theta_2, \phi_2) \psi_n(\mathbf{r}_1) \text{ as } r_2 \rightarrow \infty \quad \dots (3)$$

Here $\psi_n(\mathbf{r})$ is the wave function of the n -th state of the H atom with eigen energy E_n ; \mathbf{k}_0 and \mathbf{k}_n are the momenta of the incident and scattered electrons.

It is usual to expand the wave function $\psi(\mathbf{r}_1, \mathbf{r}_2)$ in the form

$$\psi(\mathbf{r}_1, \mathbf{r}_2) = \left(\sum_n + \int \right) \psi_n(\mathbf{r}_2) F_n(\mathbf{r}_1) \quad \dots (4)$$

where \sum_n is the summation over discrete states and \int denotes integration over functions of continuous spectrum. The function $F_n(\mathbf{r})$ in (4) satisfies the integral equation

$$F_n(\mathbf{r}) = e^{i\mathbf{k}_n \cdot \mathbf{r}} \delta_{0n} - \frac{1}{2\pi} \int \int \frac{e^{i\mathbf{k}_n \cdot |\mathbf{r} - \mathbf{r}_1|}}{|\mathbf{r} - \mathbf{r}_1|} \cdot \left(\frac{1}{r_{12}} - \frac{1}{r_1} \right) \\ \times \psi(\mathbf{r}_1, \mathbf{r}_2) \psi_n^*(\mathbf{r}_1) d^3\mathbf{r}_1 d^3\mathbf{r}_2 \quad \dots (5)$$

Then comparing the asymptotic form of $\psi(\mathbf{r}_1, \mathbf{r}_2)$ in the equation (4) with the right hand side of the equation (2) one easily obtains for the direct scattering amplitude for elastic scattering

$$f_0(\theta, \phi) = -\frac{1}{2\pi} \int \int e^{-i\mathbf{k} \cdot \mathbf{r}_1} \left(\frac{1}{r_{12}} - \frac{1}{r_1} \right) \psi(\mathbf{r}_1, \mathbf{r}_2) \psi_0^*(\mathbf{r}_1) d^3\mathbf{r}_1 d^3\mathbf{r}_2 \quad \dots (6)$$

where \mathbf{k} is the momentum of the scattered electron.

In an analogous manner, we derive the formula for exchange amplitude $g_0(\theta, \phi)$ for elastic scattering in the form

$$g_0(\theta, \phi) = -\frac{1}{2\pi} \int \int e^{-i\mathbf{k} \cdot \mathbf{r}_2} \left(\frac{1}{r_{12}} - \frac{1}{r_2} \right) \psi(\mathbf{r}_1, \mathbf{r}_2) \psi_0^*(\mathbf{r}_2) d^3\mathbf{r}_1 d^3\mathbf{r}_2 \quad \dots (7)$$

Therefore the total elastic scattering cross section for e^-H collision is

$$\sigma = 2\pi \int_0^\pi \left\{ \frac{1}{4} |f_0 + g_0|^2 + \frac{3}{4} |f_0 - g_0|^2 \right\} \sin \theta d\theta \quad \dots (8)$$

In the usual Born approximation one substitutes

$$F_0(\mathbf{r}) = e^{i\mathbf{k}_0 \cdot \mathbf{r}} \quad \dots (9)$$

$$\text{and} \quad F_n(\mathbf{r}) = 0, \quad n \neq 0 \quad \dots (10)$$

This approximation called the zero order approximation is justified when $k_0 \gg 1$

The second term on the right hand side of (5) when $n = 0$ measures the distortion of the incident plane wave in the presence of the atom. One gets series expansions for $f_0(\theta, \phi)$ and $g_0(\theta, \phi)$ by iteration using (5). The convergence of these series is very poor at low energies. Moreover the higher order terms of f_0 and g_0 cannot be evaluated without great computational efforts.

We shall, however, take for $F_0(\mathbf{r})$ an approximate solution of the following equation derived from the equations (1), (4) and (10).

$$(\Delta_1^2 + k_0^2) F_0(\mathbf{r}_1) = 2V_{00}(\mathbf{r}_1) F_0(\mathbf{r}_1) \quad \dots (11)$$

$$\text{where} \quad V_{00}(\mathbf{r}_1) = \int \left(\frac{1}{r_{12}} - \frac{1}{r_1} \right) \psi_0^*(\mathbf{r}_2) \psi_0(\mathbf{r}_2) d^3\mathbf{r}_2$$

$$= -e^{-2\mathbf{r}_1} \left(1 + \frac{1}{r_1} \right) \quad \dots (12)$$

DERIVATION OF AN APPROXIMATE EXPRESSION FOR $F_0(\mathbf{r})$

Let us expand $F_0(\mathbf{r})$:

$$F_0(\mathbf{r}) = \sum_{l=0}^{\infty} r^{-l} f_l(r) P_l(\cos \theta)$$

where $P_l(\cos \theta)$ is the Legendre polynomial of the order l . Then $f_l(r_1)$ satisfies the equation

$$\frac{d^2 f_l}{dr_1^2} + \left[k_0^2 - 2V_{00}(r_1) - \frac{l(l+1)}{r_1^2} \right] f_l(r_1) = 0$$

and
$$f_l(r_1) \xrightarrow{r_1 \rightarrow \infty} \frac{e^{-i\eta_l}}{k_0} \sin \left(k_0 r - \frac{l\pi}{2} + \eta_l \right),$$

the scattering phaseshift η_l of the l -th order partial wave being assumed to be known from the formula (Mott and Massey 1965, p. 464)

$$\eta_l = -\pi \int_0^\infty J_{l+1/2}^2(k_0 r) V_{00}(r) r dr \quad \dots \quad (13)$$

where $J_{l+1/2}(k_0 r)$ is an ordinary Bessel function. The equation (11) is the scattering wave equation in the static field approximation. Then an approximate solution of the equation (11) has the asymptotic form

$$F_0(\mathbf{r}) \sim e^{ik_0 \cdot \mathbf{r}} + f(\theta) r^{-1} e^{ik_0 \mathbf{r}}.$$

where $f(\theta)$ is the corresponding scattering amplitude defined by

$$f(\theta) = (2ik_0)^{-1} \sum_{l=0}^{\infty} (2l+1)(e^{2i\eta_l} - 1) P_l(\cos \theta) \quad \dots \quad (15)$$

Using the expansion

$$e^{ik_0 \cdot \mathbf{r}} = \sum_l (2l+1) i^l j_l(k_0 r) P_l(\cos \theta)$$

and identifying the equation (14) with the asymptotic solution of the equation (11) in terms of the spherical Bessel and Neumann functions, $j_l(k_0 r)$ and $n_l(k_0 r)$, one easily proves that

$$F_0(\mathbf{r}) \sim e^{ik_0 \cdot \mathbf{r}} + \sum_{l=0}^{\infty} (2l+1) i^{l+1} e^{i\eta_l} \sin \eta_l [j_l(k_0 r) + i n_l(k_0 r)] \quad \dots \quad (16)$$

In order that we may use the expression (16) for the complete wave function $F_0(\mathbf{r})$ valid for all r , we remove the singularity at $r = 0$ by multiplying the Neumann function n_l by the correction factor $(1 - e^{-\alpha r})^{2l+1}$ where α is a quantity dependent on l and k_0 . We however have taken $\alpha = 1$. This value of α should however be obtained variationally using

$$F_0(\mathbf{r}) = e^{ik_0 \cdot \mathbf{r}} + \sum_{l=0}^{\infty} (2l+1) i^{l+1} \left(\frac{1}{2} \sin 2\eta_l + i \sin^2 \eta_l \right) \times [j_l(k_0 r) + i(1 - e^{-\alpha r})^{2l+1} n_l(k_0 r)] \quad \dots \quad (17)$$

as the trial wave function of the equation (15) with η_l given by the equation (13). Since we use the approximate values of the phase shifts η_l given by the equation (13), we obtain an approximation for $F_0(\mathbf{r})$ which takes some account of the distortion of the plane waves. We now calculate $f_0(\theta, \phi)$ and $g_0(\theta, \phi)$ from the integral equation (6) and (7) using the above value of $F_0(\mathbf{r})$

CALCULATION OF SCATTERING AMPLITUDES

4.1. Direct scattering amplitude

Substituting the approximate wave function $F_0(\mathbf{r})$ given by (17) in (6) we obtain

$$f_0(\theta, \phi) = f_0^{(1)} + f_0^{(2)} + f_0^{(3)}$$

where
$$f_0^{(1)} = -\frac{1}{2\pi} \int e^{i\mathbf{q} \cdot \mathbf{r}_1} V_{00}(r_1) d^3\mathbf{r}_1 \quad \text{with } \mathbf{q} = \mathbf{k}_0 - \mathbf{k}, \quad \dots \quad (18)$$

$$f_0^{(2)} = -\frac{1}{2\pi} \sum_{l=0}^{\infty} \left(\frac{1}{2} \sin 2\eta_l + i \sin^2 \eta_l \right) i^{l+1} \\ \times \int e^{-i\mathbf{k} \cdot \mathbf{r}_1} V_{00}(r_1) j_l(k_0 r_1) P_l(\cos \theta_1) d^3\mathbf{r}_1 \quad \dots \quad (19)$$

and
$$f_0^{(3)} = -\frac{1}{2\pi} \sum_{l=0}^{\infty} \left(\frac{1}{2} \sin 2\eta_l + i \sin^2 \eta_l \right) i^{l+2} \\ \times \int e^{-i\mathbf{k} \cdot \mathbf{r}_1} V_{00}(r_1) (1 - e^{-r_1})^{2l+1} n_l(k_0 r_1) P_l(\cos \theta_1) d^3\mathbf{r}_1 \quad \dots \quad (20)$$

Utilizing the identities (Magnus and Oberhettinger 1954, p. 77) :

$$\int_0^{2\pi} e^{ik_0 r_1 \sin \phi \sin \theta_1 \cos \phi_1} d\phi_1 = 2\pi J_0(k_0 r_1 \sin \phi \sin \theta_1) \quad \dots \quad (21)$$

$$\int_0^\pi e^{ik_0 r_1 \cos \phi \cos \theta_1} J_0(k_0 r_1 \sin \phi \sin \theta_1) P_l(\cos \theta_1) \sin \theta_1 d\theta_1 \\ = \left(\frac{2\pi}{k_0 r_1} \right)^{\frac{1}{2}} i^l P_l(\cos \phi) J_{l+\frac{1}{2}}(k_0 r) \quad \dots \quad (22)$$

and the equation (13),

we obtain

$$f_0^{(2)} = -\frac{1}{k_0} \sum_{l=0}^{\infty} (2l+1) (\sin^2 \eta_l - i \frac{1}{2} \sin 2\eta_l) \eta_l P_l(\cos \theta) \quad \dots \quad (23)$$

In order to obtain the expansion of $f_0^{(3)}$ we use the relations (21) and (22) and

(Magnus and Oberhettinger 1954, p. 37)

$$\int_0^{\infty} e^{-2at} J_{l+\frac{1}{2}}(k_0 r) J_{-l-\frac{1}{2}}(k_0 r) dr$$

$$= \frac{1}{\pi} \int_0^{\pi/2} \frac{\cos(2l+1)\phi}{(a^2 + k_0^2 \cos^2 \phi)^{\frac{1}{2}}} d\phi \quad \dots (24)$$

EXCHANGE SCATTERING AMPLITUDES

Kang and Sucher (1966) have shown that in the exchange amplitude for electron-atom collision, the core potential term vanishes identically when the proton is heavy. Accordingly we have omitted this term from the B.O. formula (7).

On substitution of the approximate wave function $F_0(\mathbf{r})$ defined in (17) in the B.O. formula thus modified, we get

$$g_0(\theta, \phi) = g_0^{(1)} + g_0^{(2)} + g_0^{(3)} \quad \dots (25)$$

where
$$g_0^{(1)} = -\frac{1}{2\pi} \int \int \frac{1}{r_{12}} e^{i(\mathbf{k}_0 \cdot \mathbf{r}_1 - \mathbf{k} \cdot \mathbf{r}_2)} (\psi_0^*(\mathbf{r}_1) \psi_0(\mathbf{r}_2) d^3\mathbf{r}_1 d^3\mathbf{r}_2 \quad \dots (26)$$

$$g_0^{(2)} = -\frac{1}{2\pi} \sum_{l=0}^{\infty} i^{l+1} (2l+1) \left(\frac{1}{2} \sin 2\eta_l + i \sin^2 \eta_l \right) \times$$

$$\times \int \int \frac{1}{r_{12}} e^{-i\mathbf{k} \cdot \mathbf{r}_2} \psi_0^*(\mathbf{r}_1) j_l(k_0 r_1) \psi_0(\mathbf{r}_2) P_l(\cos \theta_1) d^3\mathbf{r}_1 d^3\mathbf{r}_2 \quad \dots (27)$$

and
$$g_0^{(3)} = -\frac{1}{2\pi} \sum_{l=0}^{\infty} i^{l+2} (2l+1) \left(\frac{1}{2} \sin 2\eta_l + i \sin^2 \eta_l \right)$$

$$\times \int \int \frac{1}{r_{12}} e^{-i\mathbf{k} \cdot \mathbf{r}_2} \psi_0^*(\mathbf{r}_1) (1 - e^{-\mathbf{r}_1})^{2l+1} n_l(k_0 r_1) \psi_0(\mathbf{r}_2) P_l(\cos \theta_1) d^3\mathbf{r}_1$$

$$\times d^3\mathbf{r}_2 \quad \dots (28)$$

$g_0^{(1)}$ is the contribution to $g_0(\theta, \phi)$ from the unperturbed incident wave function $e^{i\mathbf{k}_0 \cdot \mathbf{r}}$ and is given in the following closed analytical form (Corinaldesi and Trainor 1952, Kang 1966) :

$$g_0^{(1)} = -\frac{8(4k_0^2 + q^2)}{q^3(1+k_0^2)^3} \sin^{-1} \frac{q}{(q^2+4)^{\frac{1}{2}}} - \frac{16}{(1+k_0^2)^2(q^2+4)}$$

$$+ \frac{16k_0^2}{(1+k_0^2)^3 q^2} - \frac{32}{(1+k_0^2)(q^2+4)^2} \quad \dots (29)$$

where $q = 2k_0 \sin \theta/2$.

Using the expansion

$$\frac{1}{r_{12}} = \sum_{n=0}^{\infty} \sum_{m=-n}^n \frac{(n-|m|)!}{(n+|m|)!} \delta_n(r_1, r_2) P_n^{|m|}(\cos \theta_1) P_n^{|m|}(\cos \theta_2) \cos m(\phi_1 - \phi_2)$$

where $\delta_n(r_1, r_2) = r_1^n/r_2^{n+1}$ or r_2^n/r_1^{n+1} according as $r_1 < r_2$ or $r_1 > r_2$,

and integrating over the angular coordinates with the help of the relations (21) and (22) we easily show that

$$g_0^{(2)} = 8 \sum_{l=0}^{\infty} (\sin^2 \eta_l - i \frac{1}{2} \sin 2\eta_l) P_l(\cos \theta) \int_0^{\infty} r_1^2 e^{-r_1} j_l(k_0 r_1) \\ \times \left[\int_0^{\infty} \delta_l(r_1, r_2) r_2^2 e^{-r_2} j_l(k_0 r_2) dr_2 \right] dr_1 \quad \dots \quad (30)$$

$$\text{and } g_0^{(3)} = 8 \sum_{l=0}^{\infty} \left(\frac{1}{2} \sin 2\eta_l + i \sin^2 \eta_l \right) P_l(\cos \theta) \cdot \int_0^{\infty} r_1^2 e^{-r_1} (1 - e^{-r_1}) \\ \times n_l(k_0 r_1) \left[\int_0^{\infty} \delta_l(r_1, r_2) r_2^2 e^{-r_2} j_l(k_0 r_2) dr_2 \right] dr_1 \quad (31)$$

To obtain analytical expressions for $g_0^{(2)}$ and $g_0^{(3)}$ we substitute the values of j_l and n_l and integrate (30) and (31) over r_2 and r_1 .

RESULTS AND DISCUSSION

The calculations of the integrals involving j_l and n_l in $f_0^{(2)}$, $g_0^{(2)}$ and $g_0^{(3)}$ are straightforward but become tedious as the value of l increases. Fortunately the contribution to the direct and exchange scattering amplitudes $f_0(\theta, \phi)$ and $g_0(\theta, \phi)$ from these integrals for $l \geq 2$ are negligibly small when $k_0 \geq 2$. So in our work we have considered the s -, p - and d -wave distortions of the incident wave. When the core interaction term is omitted from the B.O. formula, the total cross section becomes very large compared to those obtained by Wu (1960) with the usual B.O. formula. However when we use the distorted wave function $F_0(r)$ in the modified B.O. formula, the values of the scattering cross sections drop considerably. As there are no experimental data on the elastic scattering of electrons by H atoms at high energies in the table below we compare our results with some

TABLE
Total cross-sections of e - H elastic collisions
(in units of)

Incident energy wave numbers k_0 (in a_0^{-1})	B.O. approxi- mation (Wu (1960))	Close coupling approx. [Burke <i>et al.</i> (1963)]	First Order approx. [Bell and Moiseiwitch (1963)]	Present Without distortion	Calculation with distortion
1	2.105	4.748	2.710	14.78	12.46
2	.680	.795	.797	.99	.81
3	.290	—	.300	.40	.35
4	.157	—	.158	.29	.27

recent theoretical findings of others. At $k_0 = 2$ there is some agreement between our result with the distortion of the plane incident wave taken into account and that of Burke *et al.* (1963) or of Bell and Moiseiwitsch (1963). The cross sections at other energies deviate substantially from those of Wu (1960) or Bell and Moiseiwitsch (1963), mainly due to our neglect of core interaction term. The very large cross section at $k_0 = 1$ may be due to the failure of our approximation method at this energy. Moreover at such a low energy the polarization potential due to the distortion of the atom plays an important role. With Oehkur's modification which retains only the leading term in the expansion of the formula for the exchange scattering amplitude in powers of k_0^{-2} and virtually neglects the effect of the core potential terms in the formula, Jha *et al.* (1967) have obtained total cross section for e-H elastic collision at $k_0 = 1$ in close agreement with that of Burke *et al.* (1963). This suggests further examination of the derivation of the B.O. formula.

ACKNOWLEDGMENTS

It is a pleasure to acknowledge our indebtedness to Professor D. Basu for helpful discussions and valuable suggestions.

REFERENCES

- Bell, K. L. and Moiseiwitsch, B. L., 1963, *Proc. Roy. Soc. (London)* **276**, 346.
 Burke, P. G., Schey, H. M. and Smith, K., 1963, *Phys. Rev.* **129**, 1288.
 Corinaldesi, E. and Trainor, R., 1952, *Nuovo Cim*, **9**, 940.
 Feenberg, E., 1932, *Phys. Rev.* **40**, 40.
 Jha, R., Banerjee, S. N. and Sil, N. C. (to be published in *Indian J. Phys.*)
 Kang, Ik-Ju, 1966, *Phys. Rev.* **144** (1), 29.
 Kang, Ik-Ju and Sucher, J., 1966, *Phys. Letters*, **20**, 22.
 Magnus, W., and Oberhettinger, F., 1954, *Formulas and Theorems for the Mathematical Physics*, Chelsee Publishing Company, New York.
 Mittleman, M. H., 1962, *Phys. Rev. Letters*, **9**, 495.
 Mott, N. F. and Massey, H. S. W., 1965, *Theory of Atomic Collisions*, 3rd edition, Clarendon Press, Oxford.
 Oehkur, V. I., 1964, *J. Expl. Theor. Phys.* (English edition) **18**, 503.
 Sechl, V., 1958, *Phys. Rev.*, **110**, 891.
 Wu, T. Y., 1960, *Canad. J. Phys.* **38**, 1064.

CHERENKOV RADIATION IN A MEDIUM OF VARIABLE DIELECTRIC CONSTANT

R. M. KHAN

DEPARTMENT OF MATHEMATICS, CITY COLLEGE, CALCUTTA

(Received May 25, 1966)

ABSTRACT. Cherenkov effect in a medium with a variable dielectric constant alters the amplitude of each component of the field variable and the output of radiation compared to the usual Cherenkov radiation as obtained by Frank and Tamn (1937). Even if asymptotically the specific inductive capacity becomes a constant, the radiation still then remains different. Semi-vertical angle of the cone of radiation fluctuates with the change of dielectric constant.

INTRODUCTION

Generally we consider the dielectric constant as a scalar constant for isotropic substance or a tensor for anisotropic medium. Besides these two there are substances where the dielectric constants are scalar variables. So it is important to observe the behaviour of the field variables and Cherenkov radiation for a high energy particle through this type of medium.

From Maxwell's equations of field variables with Fourier transformation

$$\left. \begin{aligned} \text{rot } H &= \frac{i\omega\epsilon}{c} E + \frac{4\pi}{c} j \\ \text{rot } E &= -\frac{i\omega}{c} H \\ \text{div } (\epsilon E) &= 4\pi\rho \\ \text{div } H &= 0, \end{aligned} \right\} \dots (1)$$

where ω is the frequency and ϵ is the dielectric constant.

Eliminating H ,

$$ic/\omega \text{ rot rot } E = \frac{i\omega\epsilon}{c} E + \frac{4\pi}{c} j \dots (2)$$

Let the electron move along the z axis with the velocity v and in cylindrical co-ordinates (ρ, ϕ, z) , E is independent of ϕ and $E_\phi = 0$.

$$\text{From (2)} \quad -\frac{\partial}{\partial z} \left(\frac{\partial E_\rho}{\partial z} - \frac{\partial E_z}{\partial \rho} \right) = \frac{\omega^2}{c^2} \epsilon E_\rho$$

and
$$\frac{1}{\rho} \frac{\partial}{\partial \rho} \left\{ \rho \left(\frac{\partial E_\rho}{\partial z} - \frac{\partial E_z}{\partial \rho} \right) \right\} = \frac{\omega^2}{c^2} \epsilon E_z - \frac{i e \omega}{\pi c^2 \rho} e^{-\frac{i \omega z}{v}} \delta(\rho).$$

Let
$$E_\rho = f_1(\rho) e^{-\frac{i \omega z}{v}}, \quad E_z = f_2(\rho) e^{-\frac{i \omega z}{v}}$$

Then
$$s^2 f_1 = -\frac{i \omega}{v} \frac{\partial f_2}{\partial \rho} \quad \dots (3)$$

and
$$\frac{\partial^2 f_2}{\partial \rho^2} + \frac{1}{\rho} \frac{\partial f_2}{\partial \rho} + s^2 f_2 - \frac{1}{\epsilon(\epsilon \beta^2 - 1)} \frac{\partial \epsilon}{\partial \rho} \frac{\partial f_2}{\partial \rho} = \frac{i e s^2}{\pi \epsilon \omega} \frac{\partial(\rho)}{\rho} \quad \dots (4)$$

where
$$s^2 = \frac{\omega^2}{v^2} (\epsilon \beta^2 - 1), \quad \beta^2 = \frac{v^2}{c^2}.$$

If we put $f_2(\rho) = u(\rho) H_1^{(2)}(s\rho)$ in (4) and also we consider as $u = u_0 + u_1$, $\epsilon = \epsilon_0 + \epsilon_1$, where u_0 and ϵ_0 are absolute constants, u_1 and ϵ_1 are functions of ρ only but they are small. In this case neglecting second order small quantities we get

$$\begin{aligned} \frac{\partial^2 u_1}{\partial \rho^2} + \left(\frac{1}{\rho} - 2s_0 \frac{H_1}{H_0} \right) \frac{\partial u_1}{\partial \rho} - \left\{ \frac{1}{2} \frac{\omega^2 u_0}{c^2 s_0} \frac{H_1}{H_0} - \rho \frac{\partial^2 \epsilon_1}{\partial \rho^2} \right. \\ \left. + \left(\frac{\omega^2 u_0}{c^2} \rho + \frac{1}{2} \frac{\omega^2 u_0}{c^2 s_0} \frac{H_1}{H_0} - \frac{\omega^2}{\epsilon_0} \frac{u_0}{v^2 s_0} \frac{H_1}{H_0} \right) \frac{\partial \epsilon_1}{\partial \rho} \right\} = 0 \quad \dots (5) \end{aligned}$$

Here $H_1 = H_1^{(2)}(s\rho)$, $H_0 = H_0^{(2)}(s\rho)$ (Hankel's functions)

From (5) $u_1 = \int \left\{ \frac{1}{\rho \chi_1(\rho)} \int \rho \chi_1(\rho) \chi(\rho) d\rho \right\} d\rho + C_1 \int \frac{d\rho}{\rho \chi_1(\rho)} + C_2 \quad \dots (6)$

where C_1 and C_2 are constants and

$$\chi_1(\rho) = e^{-2s_0} \int \frac{H_1}{H_0} d\rho,$$

$$\chi(\rho) = \frac{1}{2} \frac{\omega^2 u_0}{c^2 s_0} \frac{H_1}{H_0} \rho \frac{\partial^2 \epsilon_1}{\partial \rho^2} + \left(\frac{\omega^2 u_0}{c^2} \rho + \frac{1}{2} \frac{\omega^2 u_0}{c^2 s_0} \frac{H_1}{H_0} - \frac{\omega^2 u_0}{\epsilon_0 s_0 v^2} \frac{H_1}{H_0} \right) \frac{\partial \epsilon_1}{\partial \rho},$$

$$s_0^2 = \frac{\omega^2}{v^2} (\epsilon_0 \beta^2 - 1).$$

There is a singularity at $\rho = 0$ in (4).

From (4) we have

$$\lim_{\rho \rightarrow 0} \rho \frac{\partial f_2}{\partial \rho} = \left[\frac{i e s^2}{\pi \epsilon \omega} \right]_{\rho=0}$$

or

$$\begin{aligned} \lim_{\rho \rightarrow 0} \left[-\frac{2i}{\pi} (u_0 + u_1) + \rho \frac{\partial u_1}{\partial \rho} \left(1 - \frac{i2}{\pi} \log \frac{s_0}{2} \right) \right. \\ \left. - \frac{i2}{\pi} \rho \log \rho \frac{\partial u_1}{\partial \rho} \right] = \frac{i e}{\pi \omega \epsilon_0} \left(s_0^2 + \frac{\omega^2}{v^2} \cdot \frac{k_0}{\epsilon_0} \right) \quad \dots (7) \end{aligned}$$

where k_0 is the value of ϵ_1 at $\rho = 0$.

Here
$$u_0 = -\frac{es_0^2}{2\omega\epsilon_0} \quad \dots \quad (8)$$

If u_1 is constant then
$$u_1 = -\frac{e\omega k_0}{2v^2\epsilon_0^2} \quad \dots \quad (9)$$

From (7),

$$\begin{aligned} \lim_{\rho \rightarrow 0} \left[-\frac{i2}{\pi} \left(\int \left\{ \frac{1}{\rho\chi_1(\rho)} \int \rho\chi_1(\rho)\chi(\rho)d\rho \right\} d\rho + C_1 \int \frac{d\rho}{\rho\chi_1(\rho)} + C_2 \right. \right. \\ \left. \left. + \left(1 - 5772i - \frac{i2}{\pi} \log \frac{s_0}{2} \right) \left\{ \frac{\int \rho\chi_1(\rho)\chi(\rho)d\rho}{\chi_1(\rho)} + \frac{C_1}{\chi_1(\rho)} \right\} \right. \right. \\ \left. \left. - \frac{i2}{\pi} \log \rho \left\{ \frac{\int \rho\chi_1(\rho)\chi(\rho)d\rho}{\chi_1(\rho)} + \frac{C_1}{\chi_1(\rho)} \right\} \right] = \frac{ie\omega k_0}{\pi v^2\epsilon_0^2} \quad \dots \quad (10) \end{aligned}$$

Again at a large distance u_1 and ϵ_1 must be bounded for physical solution. Thus

$$\begin{aligned} \lim_{\rho \rightarrow \infty} \left[\int \left\{ \frac{1}{\rho\chi_1(\rho)} \int \rho\chi_1(\rho)\chi(\rho)d\rho \right\} d\rho + C_1 \int \frac{d\rho}{\rho\chi_1(\rho)} + C_2 \right] \\ = \text{a bounded quantity.} \quad \dots \quad (11) \end{aligned}$$

From (10) and (11) C_1 and C_2 can be found out.

The components of the field variables are

$$\left. \begin{aligned} E_\rho(\omega) &= -\frac{i\omega}{vs^2} \frac{\partial E_z}{\partial \rho} \\ &= \left\{ \frac{i\omega}{vs_0} (u_0 + u_1) H_1 - \frac{i\omega}{vs_0^2} H_0 \frac{\partial u_1}{\partial \rho} - \frac{i}{2} \frac{\omega^3 u_0}{c^2 v s_0^3} \epsilon_1 H_1 \right. \\ &\quad \left. + \frac{i}{2} \frac{\omega^3 u_0}{c^2 v s_0^3} \rho H_1 \frac{\partial \epsilon_1}{\partial \rho} \right\} e^{i\omega \left(t - \frac{z}{v} \right)} \\ E_z(\omega) &= (u_0 + u_1) H_0 e^{i\omega \left(t - \frac{z}{v} \right)} \\ H_\rho(\omega) &= -\frac{ic}{\omega} \left(\frac{\omega^2}{v^2 s^2} + 1 \right) \frac{\partial E_z}{\partial \rho} \\ &= \left(\frac{i\omega}{c} \frac{u_0}{s_0} \epsilon_0 H_1 + \frac{i\omega}{c} \frac{\epsilon_0}{s_0} u_1 H_1 - \frac{i}{2} \frac{\omega^3}{c^3 s_0^3} \epsilon_0 u_0 \epsilon_1 H_1 + \frac{i\omega u_0}{c s_0} \epsilon_1 H_1 \right. \\ &\quad \left. - \frac{i\omega \epsilon_0}{c s_0^2} H_0 \frac{\partial u_1}{\partial \rho} + \frac{i}{2} \frac{\omega^3 u_0}{c^3 s_0^3} \epsilon_0 \rho H_1 \frac{\partial \epsilon_1}{\partial \rho} \right) e^{i\omega \left(t - \frac{z}{v} \right)} \end{aligned} \right\} \quad \dots \quad (12)$$

$$\text{For } \left. \begin{aligned} \omega > 0, \quad ReE_\rho &= 2 \int ReE_\rho(\omega) d\omega \\ ReE_z &= 2 \int ReE_z(\omega) d\omega \\ ReH_\phi &= 2 \int ReH_\phi(\omega) d\omega \end{aligned} \right\} \dots (13)$$

(i) The results of (12) reveal that the components of electromagnetic intensities are different from usual forms of them. The expressions of them are rather unwieldy, but we can compute them numerically upto a certain order.

(ii) At large distance

$$\begin{aligned} E_z(\omega) &= \left[-\frac{es_0^2}{2\omega\epsilon_0} + \frac{e}{8} \frac{\omega}{c^2\epsilon_0} k_1 + (a+ib) \right] \sqrt{\frac{2}{\pi s_0 \rho}} e^{i\omega\lambda} \\ H_\phi(\omega) &= \left[\frac{es_0}{2c} - \frac{3}{8} \frac{e\omega^2}{c^3 s_0} k_1 + \frac{es_0}{2c\epsilon_0} k_1 - \frac{e\omega^2}{4s_0 c^3} k_2 - \frac{\omega\epsilon_0}{cs_0} (a+ib) \right. \\ &\quad \left. - \frac{i\omega}{c} \frac{\epsilon_0}{s_0^{\frac{3}{2}}} (a_1+ib_1) \right] \sqrt{\frac{2}{\pi s_0 \rho}} e^{i\omega\lambda}, \end{aligned}$$

where

$$\lim_{\rho \rightarrow \infty} \epsilon_1 = k_1, \quad \lim_{\rho \rightarrow \infty} \left(\rho \frac{\partial \epsilon_1}{\partial \rho} \right) = k_2, \quad \lim_{\rho \rightarrow \infty} u_1 = a+ib,$$

$$\lim_{\rho \rightarrow \infty} \frac{\partial u_1}{\partial \rho} = a_1+ib_1, \quad \lambda = t - \frac{z}{v} - \frac{s\rho}{\omega} + \frac{\pi}{4\omega}.$$

(iii) Cherenkov radiation W through the surface of a cylinder of length l is

$$W = 2\pi\rho l \int_{-\infty}^{\infty} \frac{c}{4\pi} [EH] dt$$

$$\text{or } \frac{dW}{dl} = -\frac{c\rho}{2} \int_{-\infty}^{\infty} R_e E_z \cdot R_e H_\phi dt$$

$$\begin{aligned} &= \int_0^{\omega_{max}} \left[\frac{e^2}{c^2} \left(1 - \frac{1}{\epsilon_0 \beta^2} \right) \omega - \frac{e^2}{c^2} \frac{k_1}{\epsilon_0} \omega + \frac{e^2 s_0^2}{\omega \epsilon_0^2} k_1 \right. \\ &\quad \left. - \frac{e^2}{2c^2} \frac{\omega}{\epsilon_0} k_2 - 4e(a-b) + \frac{e}{2s_0} (a_1+b_1) \right] d\omega \end{aligned}$$

If ϵ_1 is constant then $k_1 = k_0 = \epsilon_{01}$ (say), $k_2 = 0$,

$$u_1 = a = -\frac{e\omega\epsilon_{01}}{2v^2\epsilon_0^{\frac{3}{2}}}, \quad b = 0, \quad a_1 = 0 = b_1.$$

In this case

$$\frac{dw}{dl} = \frac{e^2}{c^2} \int \left[\left(1 - \frac{1}{\epsilon_0 \beta^2} \right) + \frac{c^2 \epsilon_{01}}{v^2 \epsilon_0^2} \right] \omega dw$$

(iv) If θ is the semi-vertical angle of the cone of radiation then

$$\cos \theta = \frac{1}{\sqrt{\epsilon_0} \beta} \left(1 - \frac{\epsilon_1}{2\epsilon_0} \right)$$

If now $v < \frac{c}{\sqrt{\epsilon_0}}$, θ may still have a real value which means that radiation can exist even then. As ϵ_1 is a variable quantity, i.e. a function of distance, the semi-vertical angle of the above cone also varies with distance.

ACKNOWLEDGMENT

I express my thanks to Dr. T Roy of Jadavpur University, for his kind help in the preparation of this paper.

RADIOACTIVE DECAY OF Nd^{147}

M. S. RAJPUT AND M. L. SEHGAL

DEPARTMENT OF PHYSICS, ALIGARH MUSLIM UNIVERSITY, ALIGARH, U.P. (INDIA)

(Received, July 31, 1965; Resubmitted September 31, 1966)

ABSTRACT. The decay of Nd^{147} to the levels of Pm^{147} has been studied using scintillation and coincidence techniques. To confirm the existence of the second 91 keV gamma ray originating from the level at 182 keV, the detection efficiency of the NaI(Tl) crystal for the 91 keV gamma ray was measured in the 91 keV-91 keV coincidences in the fixed geometry. By comparing the experimental value of the detection efficiency with the standard value, it was found that the percentage of the second 91 keV gamma ray is about $(10 \pm 2)\%$. The K-conversion coefficient of the 91 keV gamma ray, which is in coincidence with the 599 keV gamma ray has been measured to be 1.6 ± 0.2 . The K-conversion coefficient of the 91 keV gamma ray originating from the 182 keV level is estimated to 0.92 ± 0.53 .

INTRODUCTION

The decay of Nd^{147} to the levels of Pm^{147} has been studied by Hans (1955), Cork (1958), Gunye (1961), Bernye (1958), Mitchel (1958), Wendt (1960, Bodensstedt (1960) and Shastri (1964). A tentative decay scheme has been proposed by Hans (1955) and Gunye (1961). There are still some discrepancies regarding the second 91 keV gamma ray in the decay scheme of Nd^{147} . Wendt (1960) proposed a level at 182 keV on the basis of their measured log ft values and beta intensity ratios. The beta group feeding this level was about 10.4%. According to their level scheme, this level decays by the emission of two 91 keV gamma rays in cascade. Gunye (1961) put an upper limit of 1% to the population of this level by the beta decay of Nd^{147} on the basis of their gamma-gamma coincidence and absorption experiments. We have measured the efficiency of NaI(Tl) crystal for the 91 keV gamma ray in the 91 keV-91 keV coincidences so as to see the existence of the second 91 keV gamma ray which comes from the level at 182 keV. By comparing the experimental value of the detection efficiency with the value given in the literature for the standard geometry we find that there are two 91 keV gamma rays in cascade and the percentage of the beta group feeding the level at 182 keV is $(10 \pm 2)\%$.

EXPERIMENTAL TECHNIQUES

The Isotope Nd^{147} was obtained from Isotope Division, Atomic Energy Establishment Trombay, Bombay. The sources were prepared in perspex cells thick enough to absorb all betas. The internal diameter of the cylindrical cell was 1 mm. For studying the gamma-gamma coincidences two cylindrical

NaI(Tl) crystals of 4.4 cm dia and 5.1 cm height were coupled with 6292 Dumont Photomultiplier tubes. A conventional slow-fast coincidence circuit of resolving time $2\tau = 0.15\mu\text{sec}$ was used to study the coincidences. A single channel analyzer was used to select the gating pulses and the coincidence pulses were analysed with an Eldorado PA400 type twenty channel analyser. The source was placed at the intersection of the axes of the two crystals which are at 90° to each other.

INTENSITY MEASUREMENTS

The gamma ray spectrum of Nd^{147} was studied with a scintillation spectrometer and is shown in fig. 1. The most intense peaks are due to the K X-ray at 38 keV and a peak at 91 keV. All the gamma rays reported by Gunye *et al*, (1961) can be seen in the singles spectrum. By the stripping analysis of the singles spectrum an estimate of the intensities of the unconverted gamma rays has been made after applying proper corrections. The intensities thus obtained are given in table I.

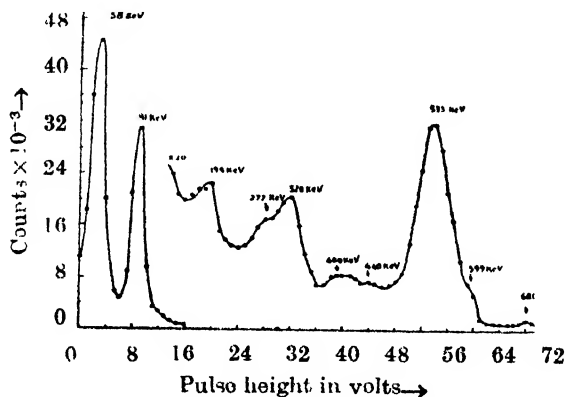


Fig. 1. The Nd^{147} gamma spectrum taken with a NaI(Tl) scintillator coupled with a 6292 photomultiplier tube.

GAMMA-GAMMA COINCIDENCES

The coincidence studies of the various gamma rays were carried out with two scintillation spectrometers. The resolution of the spectrometers was about 9% for the 662 keV gamma rays. The coincidences were observed by placing the two crystals at right angle to each other at a distance of 5 cm from the source.

Fig. 2 shows the results obtained by gating the 91 keV gamma rays. It is clear from coincidence spectrum that there is another 91 keV gamma ray in coincidence with the 91 keV gamma ray. Gunye *et al* (1961) have suggested that the peak at 91 keV in the coincidence spectrum is due to the triggering of the Compton of the high energy gamma rays sitting under the photopeak of the 91 keV gamma ray in coincidence. Since their absorption coefficient did not correspond to the 91 keV gamma ray, they therefore concluded that there is only one gamma ray and put an upper limit of 1% to the upper 91 keV gamma ray if it exists. To look for the second 91 keV gamma ray we measured the

total detection efficiency of the NaI(Tl) crystal for the 91 keV gamma ray in the 91 keV-91 keV coincidences.

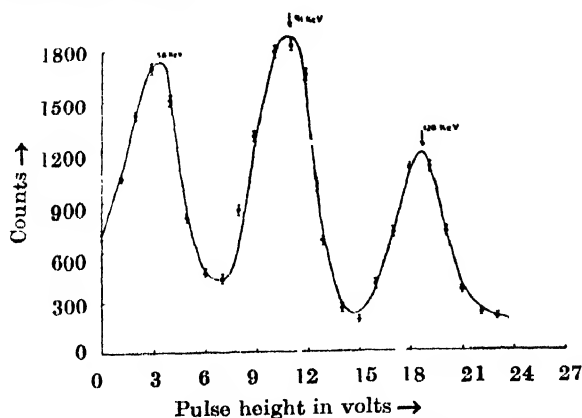


Fig. 2. Low-energy side gamma ray spectrum in coincidence with the 91 keV gamma ray.

It was pointed out by Wendt (1960) that the level at 182 keV is fed only through the beta decay of Nd^{147} . Let x and y be the fractions of the beta transition feeding the levels at 182 keV and 91 keV respectively as shown in fig. 3. The number of 91 keV gamma rays in the triggering gate channel is :

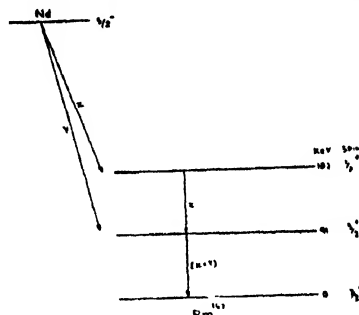


Fig. 3. Lower excited states of Pm^{147} , populated by the beta decay of Nd^{147} .

$$N_{\gamma^{91}} = N_0 f_1 \epsilon_1 \omega_1 \left[\frac{x}{1 + \alpha_{\tau_1}} + \frac{x+y}{1 + \alpha_{\tau_2}} \right] \quad \dots (1)$$

where f_1 is the fraction of the total 91 keV gamma rays in the gate channel, ω_1 is the solid angle subtended by the source at the crystal, ϵ_1 is the intrinsic detection efficiency of the NaI(Tl) crystal and α_{τ_1} and α_{τ_2} are the total conversion coefficients of the upper and lower 91 keV gamma rays respectively. Similarly the coincidence counting rate between the two 91 keV gamma rays is :

$$N_{\gamma-\gamma^{91-91}} = 2N_0 x f_1 \frac{\epsilon_1 \omega_1}{1 + \alpha_{\tau_1}} \frac{\epsilon_2 \omega_2}{1 + \alpha_{\tau_2}} \quad \dots (2)$$

here $\epsilon_2 \omega_2$ is the total detection efficiency of the second crystal in the display channel for the 91 keV gamma rays. If the upper 91 keV gamma ray is channelled

TABLE I

Gamma ray Energy (keV)	Unconverted gamma-ray intensities per thousand disintegrations	
	Present work	Ganye et al (1961)
91 ($\alpha + \gamma$)	310	275
120	10	8
199	8	6
277	13	14
310	4	6
322	28	32
400	12	16
413	10	7
442	18	20
491	3	3
533	115	126
609	8	6
680	9	10

TABLE II

S.N.	x	N_S^{01-H}	Total detection efficiency ($\epsilon_2 \omega_2$)	
		$N_{\gamma-\gamma}^{01-01}$	Experimental	Theoretical
1	4	0.173	0.0824	
2	6	0.123	0.064	
3	8	0.099	0.050	
4	10	0.082	0.043	0.042
5	12	0.071	0.038	
6	14	0.065	0.034	
7	15	0.063	0.032	

the lower gamma ray is displayed and vice versa. So the coincidence counting rate is doubled. Dividing eq. 2 by eq. 1 we get :

$$\frac{N_{\gamma-\gamma}^{01-01}}{N_{\gamma}^{01}} = \frac{2x\epsilon_2\omega_2}{x(1+\alpha_{\tau_2})+(x+y)(1+\alpha_{\tau_1})} \quad \dots (3)$$

In the above equation $N_{\gamma^{91}}$ are the true counts of the gate channel of the coincidence circuit. In the observed counts, a part of them are due to the Compton of the high energy gamma rays sitting under the photopeak at 91 keV, that is;

$$N_{obs}^{91} = N_{\gamma^{91}} + N_S^H \quad \dots (4)$$

where N_S^H corresponds to the counts due to the Compton of the high energy gamma rays and $N_{\gamma^{91}}$ to the counts due to the 91 keV gamma ray. Similarly we have,

$$N_{obs}^{91-91} = N_{\gamma-\gamma}^{91-91} + N_S^{91-H} \quad \dots (5)$$

where N_S^{91-H} corresponds to the coincidence counts between the 91 keV gamma ray and the Compton due to the high energy gamma rays which are in coincidence with 91 keV gamma ray and $N_{\gamma-\gamma}^{91-91}$ to the true 91 keV—91 keV coincidences.

From the analysis of the singles spectrum it is possible to find the value of N_S^H which is given by the following expression :

$$N_S^H = N_0 \alpha f_2 \frac{\epsilon_1^{ave} \omega_1}{1 + \alpha \tau_{ave}} \quad \dots (6)$$

where α is the fraction of gamma rays having energy higher than 91 keV and $\alpha \tau_{ave}$ the average value of their total conversion coefficient. It is interesting to note that $\alpha \tau_{ave}$ which appears in eq. 6 cancels out in the final equation 9. The quantity f_2 is the fraction of these high energy gamma rays which are lying under the photopeak at 91 keV and $\epsilon_1^{ave} \omega_1$ is the average value of the total detection efficiency for these high energy gamma rays; it is also satisfying to note that this quantity also does not appear, in the final expression. Similarly N_S^{91-H} is given by the following equation :

$$N_S^{91-H} = N_0 \alpha f_2 f_3 \frac{\epsilon_1^{ave} \omega_1}{1 + \alpha \tau_{ave}} \cdot \frac{\epsilon_2 \omega_2}{1 + \alpha \tau_2} \quad \dots (7)$$

Here f_3 is the fraction of the total high energy gamma rays which are in coincidence with the 91 keV gamma ray. Hence

$$\frac{N_S^{91-H}}{N_S^H} = \frac{N_0 \alpha f_2 f_3 \frac{\epsilon_1^{ave} \omega_1}{1 + \alpha \tau_{ave}} \cdot \frac{\epsilon_2 \omega_2}{1 + \alpha \tau_2}}{N_0 \alpha f_2 \frac{\epsilon_1^{ave} \omega_1}{1 + \alpha \tau_{ave}}} \quad \dots (8)$$

$$= \frac{\epsilon_2 \omega_2}{1 + \alpha \tau_2} \cdot f_3 \quad \dots (9)$$

From eqs. 3 and 8 we get

$$\frac{N_S^{91-H}}{N_{\gamma-\gamma}^{91-91}} = \frac{f_3 \cdot N_S^H [x(1 + \alpha \tau_2) + (x+y)(1 + \alpha \tau_1)]}{(1 + \alpha \tau_2) \cdot N_{\gamma^{91}} \cdot 2x} \quad \dots (10)$$

By the analysis of the singles spectrum, the value of $\frac{N_S^H}{N_{\gamma}^{91}}$ can be calculated. The value of f_3 was calculated from the decay scheme of Nd^{147} . In the present case it came out to be 0.38. The values of $\frac{N_S^{91-H}}{N_{\gamma}^{91-91}}$ were calculated by taking y equal to 65% and varying x from 4% to 15% as shown in Table II. Knowing this ratio the values of N_S^{91-H} and N_{γ}^{91-91} were calculated from eq. 5 as a function of x . Using eq. 3, the value of total detection efficiency $\epsilon_2\omega_2$ was calculated as shown in Table II. In calculating $\epsilon_2\omega_2$ the values of conversion coefficients α_{τ_1} and α_{τ_2} were calculated from the tables of Rose (1958) assuming

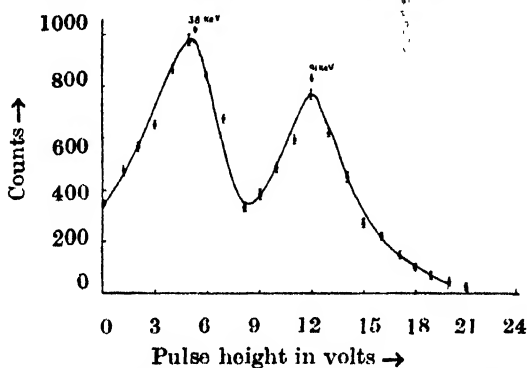


Fig. 4. Gamma ray spectrum in coincidence with the 599 keV gamma rays.

the upper 91 keV gamma ray as 100% M_1 and the lower 91 keV as a mixture of 95% M_1 and 5% E_2 as discussed in section 5. For comparison the theoretical value of the detection efficiency for the crystal used was taken from the Nuclear Data Tables (1960). This value agrees with the experimental value when the value of x is $(10 \pm 2)\%$.

V. THE α_k MEASUREMENTS

To measure the K -conversion coefficient of the lower 91 keV gamma ray the fixed channel was set around 599 keV and the sliding channel was run at low energies. The photo-areas under the K -X-ray peak and the 91 keV peak (Fig. 4) were corrected for absorption, detection efficiency of the crystal, escape peak correction etc. The fluorescence yield correction, Wapstra (1959) was also applied to the X-ray peak. A value of 1.6 ± 0.2 was obtained for the K conversion coefficient. This value is in agreement with the value measured by Hans (1955).

To have an estimate about the K -conversion coefficient of the upper 91 keV gamma ray, coincidences were recorded on the low energy side by triggering with the 91 keV gamma ray as shown in fig. 2. K -conversion coefficient was measured from the coincidence spectrum as described earlier, after applying various corrections, and came out to be 1.26 ± 0.25 . This value nearly corresponds to the average value of the conversion coefficients for the upper and the lower 91 keV

gamma rays. The conversion coefficient for the lower 91 keV gamma ray is 1.6 ± 0.2 as stated above. The conversion coefficient for the upper 91 keV gamma ray comes out to be 0.92 ± 0.53 . The theoretical value for the K -conversion coefficients for E_1 , M_1 and E_2 type of transitions are 0.29, 1.62 and 1.31 respectively. Thus we conclude that the upper 91 keV gamma ray is most probably $E_2 + M_1$ and the lower 91 keV gamma ray is either M_1 or $M1$ with a small admixture of E_2 . From the preliminary study of the 91-91 keV cascade angular correlation we have found that the lower 91 keV gamma ray contains a quadrupole admixture of 5% assuming the upper 91 keV gamma ray as 100% M_1 .

The authors are thankful to Professor Rais Ahmed for his stimulating interest through out this work. One of the authors (M.S.R.) is thankful to the Aligarh Muslim University for providing him a research fellowship.

REFERENCES

- Bernyo, D. 1958, *Nuclear Physics* **8**, 607.
 Bodendstedt, E. et al., 1960, *Z. Phys.* **160**, 33.
 Cork, J. M. et al 1958, *Phys. Rev.* **110**, 526.
 Gunyo, M. R., Jambunathan, R. and Saraf, B. L. 1961, *Phys. Rev.* **124**, 172.
 Hans, H. S., Saraf, B. L. and Mandeville, C. E. 1955, *Phys. Rev.* **97**, 1267.
 Marion, J. B., 1960, *Nuclear Data Tables*, National Academy of Sciences-National Research Council, Washington 25, D. C. Part 3, page 53.
 Mitchell A. C. G., et. al 1958, *Phys. Rev.* **111**, 1343.
 Rose, M. E. 1958, *Internal conversion coefficients*, North Holland Publ. Co. Amsterdam.
 Shastri, W. V. G. et al 1964, *Indian J. Pure and Appl. Phys.* **2**, 307.
 Wandt, H. D. and Kleinhentz, P. 1960. *Nuclear Physics* **20**, 167.
 Wapstra, A. H. et al 1959, *Nuclear Spectroscopy tables*, North Holland Publ. Co. Amsterdam.

ON THE RELATION BETWEEN THE ENERGY OF ACTIVATION FOR DIELECTRIC RELAXATION AND THE INTERACTION ENERGY OF POLAR ORGANIC MOLECULES IN DILUTE SOLUTIONS IN NON-POLAR SOLVENTS

(Miss) B. SINHA, S. B. ROY AND G. S. KASTHA

OPTICS DEPARTMENT,

INDIAN ASSOCIATION FOR THE CULTIVATION OF SCIENCE,
CALCUTTA-32.

(Received August 8, 1966)

ABSTRACT. The results of measurement in the 7 mm. microwave region on the temperature dependence of the time of relaxation (τ) of a number of polar organic molecules of different shape, size and dipole moment dispersed in very dilute solutions in non-polar solvents have been reported. It has been shown that the dependence of τ at any temperature (T) on the viscosity (η) of the solution may be represented by $\tau.T = \text{const. } \eta^\gamma$ where γ is the ratio of the experimentally determined heats of activation for dielectric relaxation and viscous flow. The relation between the activation energy for dipole rotation for a large number of polar organic molecules in dilute solution in CCl_4 and the total energy due to dipole-dipole, dipole-induced dipole and London dispersion forces between the solute and solvent molecules has been discussed. It is found that the agreement between the experimental and the calculated energy values is fairly satisfactory for many of the compounds and the probable causes for somewhat large discrepancies in a few cases have been suggested.

INTRODUCTION

Recently (Sinha *et al.*, 1965, 1966) it has been shown that the time of relaxation (τ) of organic polar molecules in very dilute solutions in non-polar solvents at any temperature (T) is not dependent linearly on the viscosity (η) of the solutions, but may be expressed as $\tau.T = \text{const. } \eta^\gamma$ where γ is the ratio of the experimentally determined values of the heat of activation for dielectric relaxation and viscous flow. However, no attempt was made to correlate the values of the heat of activation for dipole orientation with the energies of various intermolecular interactions between the solvent and solute molecules. Bhanumati (1963) had shown that in the case of some pure polar organic liquids the experimental values of the activation energy for dipole-orientation agree fairly well with the total interaction energies calculated from the dipole-dipole and dipole-induced dipole forces. In

the case of dilute solutions of polar molecules in nonpolar solvents it will be interesting to find out the contributions made by different intermolecular interactions to the total activation energy required for the process of the orientation of the dipoles. For this purpose, use has been made of the results of measurements of the temperature dependence of the time of relaxation of a number of polar organic compounds, having molecules of different shape, size and dipole moment, in solutions in different non-polar solvents and those reported in the papers mentioned above.

EXPERIMENTAL

The chemicals nitromethane, nitroethane, chloroform, acetone, ethyl acetate α -bromonaphthalene and methyl, ethyl and benzyl esters of benzoic acid used in, this investigation were of chemically pure quality and the samples were subjected to fractional distillation and distillation under reduced pressure before use. Carefully dehydrated carbon tetrachloride, benzene and *n*-hexane used as solvents, showed slight losses in a path-length of 24 cm in the frequency region of 7.7 mm and these were properly taken into account for determining the overall losses due to the solutions. The experimental arrangements and the method of calculation of loss tangent ($\tan \delta$) were the same as described in a previous paper (Bhattacharyya *et al.*, 1964). The values of the viscosity of the solvents were taken from the data published in the standard literatures.

RESULTS AND DISCUSSION

The time of relaxation (τ) for the molecules of the various polar compounds in very dilute solution in the different solvents at different temperatures (T) were calculated from the experimental $\tan \delta$ -values with the help of the following equation,

$$\tan \delta = \frac{(\epsilon' + 2)^2}{\epsilon'} \cdot \frac{4\pi NC\mu^2}{27kT} \cdot \frac{\omega\tau}{1 + \omega^2\tau^2} \quad \dots (1)$$

where C is the concentration in moles/cc, ϵ' is the dielectric constant of the solution at the angular frequency of measurement (ω), μ is the dipole moment of the polar molecule and the other symbols have their usual meanings. The values of ϵ' were taken to be the same as the static dielectric constant of the pure solvents and the dipole moments of the molecules of ethyl and benzyl benzoates, and α -bromonaphthalene were taken from the published data and those of the remaining compounds were determined experimentally (see Section a). The values of T , $\tan \delta$, τ and $\frac{\tau T}{\eta}$ are given in Tables I-IX

TABLE I
Nitromethane

1.84 × 10 ⁻⁴ moles/cc in CCl ₄				1.84 × 10 ⁻⁴ moles/cc in C ₆ H ₆				1.86 × 10 ⁻⁴ moles/cc in C ₆ H ₁₄			
T°K	tan δ	$\tau \times 10^{12}$ Sec	$\frac{\tau \cdot T}{\eta} \times 10^7$	T°K	tan δ	$\tau \times 10^{12}$ Sec	$\frac{\tau \cdot T}{\eta} \times 10^7$	T°K	tan δ	$\tau \times 10^{12}$ Sec	$\frac{\tau \cdot T}{\eta} \times 10^7$
275	.0392	2.42	4.78	275	.0440	4.75	5.83	276	.0280	1.45	2.93
284	.0370	2.30	4.79	285	.0430	4.35	5.88	282	.0268	1.41	2.96
296	.0345	2.18	4.85	293	.0420	3.99	5.83	289	.0254	1.36	2.96
305	.0327	2.09	4.86	303	.0400	3.62	5.76	296	.0240	1.31	2.97
315	.0305	1.97	4.82	313	.0383	3.40	5.88	305	.0224	1.24	2.98
325	.0286	1.87	4.78	323	.0367	3.20	5.96	315	.0208	1.18	2.99
335	.0268	1.77	4.73	333	.0345	2.87	5.74	325	.0191	1.12	2.97
345	.0250	1.67	4.67	343	.0330	2.71	5.82	335	.0178	1.06	2.97

 $\Delta H_{\tau} = 0.31$ K.Cal/mole $\Delta H_{\eta} = 2.44$ K.Cal/mole $\gamma = 0.13$ $\Delta H_{\tau} = 0.95$ K.Cal/mole $\Delta H_{\eta} = 2.53$ K.Cal/mole $\gamma = 0.37$ $\Delta H_{\tau} = 0.43$ K.Cal/mole $\Delta H_{\eta} = 1.84$ K.Cal/mole $\gamma = 0.23$

TABLE II
Nitroethane

1.4 × 10 ⁻⁴ moles/cc in CCl ₄				1.4 × 10 ⁻⁴ moles/cc in C ₆ H ₆				1.4 × 10 ⁻⁴ moles/cc in C ₆ H ₁₄			
T°K	tan δ	$\tau \times 10^{12}$ Sec	$\frac{\tau T}{\eta} \times 10^7$	T°K	tan δ	$\tau \times 10^{12}$ Sec	$\frac{\tau T}{\eta} \times 10^7$	T°K	tan δ	$\tau \times 10^{12}$ Sec	$\frac{\tau T}{\eta} \times 10^7$
274	.0324	7.04	2.47	275	.0321	6.89	5.84	274	.0344	2.89	4.17
279	.0330	6.50	2.48	283	.0327	6.17	5.77	282	.0327	2.73	4.22
828	.0336	5.68	2.54	290	.0333	5.41	5.53	290	.0311	2.59	4.28
296	.0339	4.83	2.44	295	.0330	5.25	5.69	297	.0293	2.47	4.32
306	.0333	4.10	2.37	305	.0324	4.90	5.89	307	.0277	2.28	4.31
316	.0321	3.65	2.42	315	.0318	4.40	5.89	317	.0256	2.10	4.31
326	.0305	3.27	2.44	325	.0309	4.27	6.29	327	.0235	1.92	4.22
336	.0289	3.00	2.53	335	.0296	3.52	5.69	333	.0224	1.83	4.21
				345	.0284	3.28	5.81				

$\Delta H\tau = 1.94$ K.Cal/mole
 $\Delta H\eta = 2.44$ K.Cal/mole
 $\gamma = 0.79$

$\Delta H\tau = 1.38$ K.Cal/mole
 $\Delta H\eta = 2.53$ K.Cal/mole
 $\gamma = 0.55$

$\Delta H\tau = 0.87$ K.Cal/mole
 $H\eta = 1.84$ K.Cal/mole
 $\gamma = 0.47$

TABLE III
Acetone

1.35 × 10 ⁻⁴ moles/cc in CCl ₄				1.35 × 10 ⁻⁴ moles/cc in C ₆ H ₆				2.71 × 10 ⁻⁴ moles/cc in C ₆ H ₁₄			
T°K	tanδ	τ × 10 ¹² Sec	$\frac{\tau \cdot T}{\eta \gamma} \times 10^7$	T°K	tanδ	τ × 10 ¹² Sec	$\frac{\tau \cdot T}{\eta \gamma} \times 10^7$	T°K	tanδ	τ × 10 ¹² Sec	$\frac{\tau \cdot T}{\eta \gamma} \times 10^7$
274	.0258	4.44	3.52	274	.0241	2.75	5.51	274	.0396	1.90	2.63
282	.0252	4.10	3.58	282	.0229	2.61	5.49	281	.0372	1.79	2.62
289	.0243	3.56	3.37	289	.0220	2.51	5.50	288	.0348	1.69	2.65
297	.0233	3.24	3.34	296	.0211	2.41	5.50	295	.0324	1.58	2.63
307	.0222	3.06	3.47	306	.0199	2.30	5.52	305	.0297	1.47	2.66
317	.0211	2.88	3.59	316	.0188	2.19	5.54	315	.0270	1.36	2.68
325	.0200	2.68	3.58	326	.0180	2.07	5.49	325	.0243	1.24	2.62
$\Delta H\tau = 1.17$ K.Cal/mole				$\Delta H\tau = 0.36$ K.Cal/mole				$\Delta H\tau = 0.92$ K.Cal/mole			
$\Delta H\eta = 2.44$ K.Cal/mole				$\Delta H\eta = 2.53$ K.Cal/mole				$\Delta H\eta = 1.84$ K.Cal/mole			
$\gamma = 0.48$				$\gamma = 0.14$				$\gamma = 0.50$			

TABLE IV
Chloroform

3.73 × 10 ⁻⁴ mole/cc in CCl ₄				3.72 × 10 ⁻⁴ moles/cc in C ₆ H ₆				3.73 × 10 ⁻⁴ moles/cc in C ₆ H ₁₄			
T°K	tanδ	τ × 10 ¹² Sec	$\frac{\tau \cdot T}{\eta \gamma} \times 10^7$	T°K	tanδ	τ × 10 ¹² Sec	$\frac{\tau \cdot T}{\eta \gamma} \times 10^7$	T°K	tanδ	τ × 10 ¹² Sec	$\frac{\tau \cdot T}{\eta \gamma} \times 10^7$
274	.0101	8.52		278	.0103	8.07	1.60	275	.0125	3.19	3.81
285	.0106	7.41	1.14	288	.0109	6.77	1.72	283	.0118	2.89	3.72
295	.0110	6.38	1.12	298	.0113	5.55	1.76	289	.0113	2.74	3.76
305	.0114	5.00	1.07	306	.0115	4.10	1.52	295	.0108	2.61	3.81
317	.0112	4.10	1.08	315	.0111	3.59	1.59	305	.0099	2.32	3.73
325	.0108	3.46	1.10	325	.0105	3.12	1.66	315	.0092	2.15	3.80
333	.0103	3.20	1.14					325	.0085	1.99	3.82

 $\Delta H\tau = 3.07$ K.Cal/mole $\Delta H\eta = 2.44$ K.Cal/mole $\gamma = 1.26$ $\Delta H\tau = 3.17$ K.Cal/mole $\Delta H\eta = 2.53$ K.Cal/mole $\gamma = 1.25$ $\Delta H\tau = 1.13$ K.Cal/mole $\Delta H\eta = 1.84$ K.Cal/mole $\gamma = 0.62$

TABLE V
Ethyl acetate

3.06 × 10 ⁻⁴ moles/cc in CCl ₄				2.05 × 10 ⁻⁴ moles/cc C ₆ H ₆				2.05 × 10 ⁻⁴ moles/cc in C ₆ H ₁₄			
T°K	tan δ	$\tau \times 10^{12}$ Sec	$\frac{\tau \cdot T}{\eta \gamma} \times 10^7$	T°K	tan δ	$\tau \times 10^{12}$ Sec	$\frac{\tau \cdot T}{\eta \gamma} \times 10^7$	T°K	tan δ	$\tau \times 10^{12}$ Sec	$\frac{\tau \cdot T}{\eta \gamma} \times 10^7$
274	.0196	6.55	2.23	274	.0130	6.38	4.04	274	.0159	2.09	3.76
283	.0200	5.74	2.28	281	.0135	5.39	3.75	281	.0150	1.98	3.72
291	.0203	4.73	2.16	289	.0133	5.14	4.06	288	.0143	1.91	3.78
298	.0200	4.49	2.28	305	.0128	4.59	4.43	295	.0136	1.83	3.79
308	.0193	3.65	2.09	315	.0124	3.69	4.03	306	.0125	1.70	3.78
318	.0186	3.51	2.30	325	.0118	3.24	3.96	316	.0115	1.60	3.78
328	.0175	3.09	2.30	335	.0111	2.95	4.02	326	.0110	1.49	3.73
338	.0168	2.98	2.48	345	.0105	2.71	4.10	336	.0097	1.38	3.66
$\Delta H\tau = 1.97$ K.Cal/mole				$\Delta H\tau = 1.71$ K.Cal/mole				$\Delta H\tau = 0.57$ K.Cal/mole			
$\Delta H\eta = 2.44$ K.Cal/mole				$\Delta H\eta = 2.53$ K.Cal/mole				$\Delta H\eta = 1.84$ K.Cal/mole			
$\gamma = 0.81$				$\gamma = 0.68$				$\gamma = 0.31$			

TABLE VI
Methyl benzozte

2.29 × 10 ⁻⁴ moles/cc in CCl ₄				3.05 × 10 ⁻⁴ moles/cc in C ₆ H ₆				2.29 × 10 ⁻⁴ moles/cc in C ₆ H ₁₄			
T°K	tan δ	$\tau \times 10^{12}$ Sec	$\frac{\tau \cdot T}{\eta \gamma} \times 10^7$	T°K	tan δ	$\tau \times 10^{12}$ Sec	$\frac{T \cdot \tau}{\eta \gamma} \times 10^7$	Tsk	tan δ	$\tau \times 10^{12}$ Sec	$\frac{T \cdot \tau}{\eta \gamma} \times 10^7$
275	.0086	23.24	12.09	276	.0173	1240	6.26	276	.0162	9.51	7.23
285	.0096	19.29	11.61	285	.0188	10.77	6.30	286	.0172	8.28	7.31
294	.0104	17.06	11.56	294	.0203	9.26	6.28	295	.0177	7.39	7.32
304	.0110	15.38	11.91	304	.0218	7.82	6.14	304	.083	6.44	7.15
317	.0116	13.77	12.27	316	.0222	6.87	6.31	313	.0186	5.78	7.18
330	.0126	11.85	12.10	328	.0229	5.86	6.27	329	.0186	4.66	7.10
343	.0132	10.60	12.40	338	.0237	4.85	—	336	.0181	3.54	—
$\Delta H_\tau = 1.58$ K.Cal/mole				$\Delta H_\tau = 2.01$ K.Cal/mole				$\Delta H_\tau = 1.76$ K.Cal/mole			
$\Delta H_\eta = 2.44$ K.Cal/mole				$\Delta H_\eta = 2.53$ K.Cal/mole				$\Delta H_\eta = 1.84$ K.Cal/mole			
$\gamma = 0.65$				$\gamma = 0.79$				$\gamma = 0.96$			

TABLE VII
Ethyl benzoate

2.07 × 10 ⁻⁴ moles/cc in CCl ₄				2.07 × 10 ⁻⁴ moles/cc in C ₆ H ₆				2.07 × 10 ⁻⁴ moles/cc in C ₆ H ₁₄			
T°K.	tan δ	$\tau \times 10^{12}$ Sec	$\frac{\tau \cdot T}{\eta \gamma} \times 10^7$	T°K.	tan δ	$\tau \times 10^{12}$ Sec	$\frac{\tau \cdot T}{\eta \gamma} \times 10^7$	T°K.	tan δ	$\tau \times 10^{12}$ Sec	$\frac{\tau \cdot T}{\eta \gamma} \times 10^7$
275	.0069	25.05	15.01	276	.0081	21.09	—	276	.0135	11.67	10.48
285	.0077	21.69	14.93	285	.0090	18119	16.82	287	.0143	10.21	10.40
295	.0081	19.29	15.44	294	.0096	16.30	16.90	295	.0150	9.22	10.52
304	.0088	17.39	15.03	303	.0103	14.62	16.77	304	.0156	8.22	10.40
317	.0095	15.11	15.05	313	.0109	13.08	16.60	318	.0163	7.05	10.54
331	.0103	13.12	14.98	323	.0113	11.99	16.90	335	.0169	5.63	—
345	.0110	11.42	15.00	333	.0120	10.73	16.58				
				343	.0124	9.81	16.60				
$\Delta H\tau = 1.45$ K. Cal./mole				$\Delta H\tau = 1.43$ K. Cal./mole				$\Delta H\tau = 1.54$ K. Cal./mole			
$\Delta H\eta = 2.44$ K. Cal./mole				$\Delta H\eta = 2.53$ K. Cal./mole				$\Delta H\eta = 1.84$ K. Cal./mole			
$\gamma = 0.59$				$\gamma = 0.56$				$\gamma = 0.84$			

TABLE VIII
Benzyl benzoate

2.08 × 10 ⁻⁴ moles/cc in CCl ₄				1.56 × 10 ⁻⁴ moles/cc in C ₆ H ₆				1.56 × 10 ⁻⁴ moles/cc in C ₆ H ₁₄			
T°K	tan δ	$\tau \times 10^{12}$ Sec	$\frac{\tau \cdot T}{\eta} \times 10^7$	T°K	tan δ	$\tau \times 10^{12}$ Sec	$\frac{\tau \cdot T}{\eta} \times 10^7$	T°K	tan δ	$\tau \times 10^{12}$ Sec	$\frac{\tau \cdot T}{\eta} \times 10^7$
278	.0053	38.04	15.53	274	.0050	29.93	18.47	278	.0087	16.42	13.47
288	.0059	32.79	15.81	283	.0053	25.88	18.24	288	.0092	14.90	13.98
298	.0065	28.56	16.04	292	.0061	22.56	18.17	298	.0096	13.50	14.45
308	.0072	25.10	16.01	300	.0067	19.97	17.96	308	.0100	12.27	14.85
317	.0076	22.89	16.46	311	.0072	17.47	18.01	318	.0107	10.87	14.87
326	.0080	20.82	16.64	323	.0078	15.9	18.27	328	.0114	9.56	14.56
335	.0084	19.32	17.14	333	.0082	14.15	18.53	335	.0118	8.744	14.41
343	.0088	17.88	—	346	.0089	12.10	18.21				
$\Delta H\tau = 1.85$ K.Cal/mole				$\Delta H\tau = 1.73$ K.Cal/mole				$\Delta H\tau = 1.69$ K.Cal/mole			
$\Delta H\eta = 2.44$ K.Cal/mole				$\Delta H\eta = 2.53$ K.Cal/mole				$\Delta H\eta = 1.84$ K.Cal/mole			
$\gamma = 0.76$				$\gamma = 0.69$				$\gamma = 0.92$			

TABLE IX
 α -bromonaphthalene

2.82×10^{-4} moles/cc in CCl_4				2.82×10^{-4} moles/cc in C_6H_{14}			
T°K	$\tan \delta$	$\tau \times 10^{12}$ Sec	$\frac{\tau \cdot T}{\eta \gamma} \times 10^7$	T°K	$\tan \delta$	$\tau \times 10^{12}$ Sec	$\frac{\tau \cdot T}{\eta \gamma} \times 10^7$
276	.0044	34.38	22.5	276	.0090	15.94	22.09
286	.0048	30.32	22.7	286	.0094	14.49	22.02
296	.0052	26.80	22.7	296	.0099	13.19	21.84
306	.0056	23.99	22.6	306	.0100	12.01	21.65
319	.0060	21.29	22.9	316	.0105	11.22	21.95
333	.0064	18.96	23.3	326	.0107	10.48	22.05
343	.0066	17.72	23.9				

$$\Delta H\tau = 1.37 \text{ K.Cal/mole}$$

$$\Delta H\eta = 2.44 \text{ K.Cal/mole}$$

$$\gamma = 0.56$$

$$\Delta H\tau = 0.94 \text{ K.Cal/mole}$$

$$\Delta H\eta = 1.84 \text{ K.Cal/mole}$$

$$\gamma = 0.51$$

TABLE X

Compound	Dipole moment in Debye Unit (μ_D) in soln. in			Other microwave measurement (μ_D) in	
	CCl_4	C_6H_6	C_6H_{14}	C_6H_6 solution	
Nitromethane		2.85		2.87 ^b	2.81 ^c
Nitroethane	3.00	2.97			
Chloroform	1.08	1.08		1.13 ^a	1.23 ^b
Acetone	2.54			(in heptano)	
Ethylacetate	1.55	1.54		2.58 ^b	2.6 ^c
Methyl benzoate			1.82	1.32 ^c	

(a) Jackson and Powles (1946)

(b) Whiffen and Thompson (1946)

(c) Cripwell and Sutherland (1946)

TABLE XI

(α_s) Polarisability of CCl_4 molecule 105.0×10^{-25} cc.
 (I_s) Ionisation potential of „ 11.47 ev

$$f = \frac{I_p}{I_p + I_s}$$

Compound μ_D	Polarisa- bility α_p $\times 10^{25}$ cc	Ionisation potential I_p ev	Activation energy ΔH^\ddagger K. Cal/mole	$\frac{\Delta H}{f\alpha_p} \times 10^{-25}$	E_L^* K. Cal/mole calculated for	
					$r = 5.25 \text{ \AA}$	$r = 5.43 \text{ \AA}$
Nitro methane 2.85	49.0	11.00	0.31	.013	.48 (.61)	.39 (.50)
Nitro ethane 3.00	69.0	10.00	1.94	.064	.60 (.74)	.49 (.60)
Acetone 2.54	63.3	10.10	1.17	.038	.58 (.68)	.47 (.55)
Chloroform 1.08	82.3	11.50	3.07	.070	.82 (.84)	.67 (.68)
Ethylacetate 1.55	88.0	9.50	1.97	.049	.79 (.83)	.64 (.67)
Fluoro benzene 1.45	102.0	9.0.2	0.70	.015	.90 (.93)	.74 (.77)
Chloro benzene 1.56	122.5	8.80	0.90	.019	1.06 (1.10)	.86 (.89)
Bromo benzene 1.50	136.0	8.98	1.46	.025	1.16 (1.19)	.95 (.98)
nitro benzene 3.97	129.2	9.00	1.65	.029	1.15 (1.39)	.94 (1.13)
<i>o</i> -dichloro benzene 2.20	141.7	9.06	1.38	.022	1.24 (1.31)	1.02 (1.08)
<i>m</i> -dichloro benzene 1.48	142.3	9.00	1.52	.024	1.27 (1.30)	1.04 (1.07)
<i>o</i> -nitro toluene 3.66	149.0	8.0-9.0	1.55	.023-.026	1.19-1.33 (1.39-1.53)	.97-1.09 (1.13-1.25)
<i>m</i> -nitro toluene 4.14	149.0	8.0-9.0	0.78	.012-.013	1.17-1.33 (1.43-1.59)	.95-1.09 (1.15-1.29)
<i>p</i> -nitro toluene 4.42	134.0	8.0-9.0	0.85	.014-.016	1.07-1.20 (1.36-1.49)	.87-.98 (1.10-1.21)
Methyl benzoate 1.82	151.0	8.0-9.0	1.58	.023-.026	1.20-1.35 (1.25-1.40)	.98-1.10 (1.02-1.14)
Ethyl benzoate 1.88	171.0	8.0-9.0	1.45	.019-.021	1.36-1.53 (1.41-1.58)	1.11-1.25 (1.15-1.29)

TABLE XI (cont.)

Compound μD	Polarisability αp $\times 10$	Ionisation potential I_p ev	Activation energy ΔH_τ K.Cal/mole	$\frac{\Delta H_\tau}{f\alpha_p} \times 10^{-25}$	E_L K.Cal/mole calculated for	
					$r = 5.25 \text{ \AA}$	$r = 5.43 \text{ \AA}$
Benzyl benzoate 2 00	252.0	8.0-9.0	1.85	.016-.018	2.21 (2.27)	1.80 (1.85)
α -chloro naphthaleno 1 50	193.0	8.2	1.43	.018	1.61 (1.64)	1.32 (1.35)
α -bromo naphthalene 1 50	197.0	8.2	1.37	.017	1.64 (1.67)	1.35 (1.38)

*The quantities in the parentheses give the values of $E_L + E_D$ when the interaction energy due to dipole-induced dipole forces is considered. For $\mu < 2D$ the contribution due to E_D is less than 5% of E_L . Only for $\mu > 2$ is the contribution appreciable.

The molar heats of activation (ΔH_τ) for dielectric relaxation and (ΔH_η) for viscous flow were determined from the plots of $\log(\tau T)$ and $\log \eta$ against $1/T$ as usual. These values and also their ratio (γ) are given at the foot of the respective Tables.

(a) Determination of the dipole moment (μ)

It is seen from equation (1) that the graphs of $T \tan \delta/c$ against $\omega\tau$ and consequently T would show a maximum at a certain temperature T_{max} for which the condition $\omega\tau = 1$ is satisfied. Some of these curves are shown in figures 1(a)-(c). The μ -values have been calculated from the maximum value of $T \tan \delta/c$ obtained from the graph at the temperature T_{max} and are given in Table X. The μ -values reported by other workers from measurements in the microwave region are included in the table for comparison. The agreement between these values is seen to be satisfactory.

(b) Dependence of time of relaxation on viscosity and molecular size :

The results presented in Tables I-IX show that for a given polar molecule the τ -value at a temperature T increases with the increase in the viscosity of the solvent, while in the case of any of the solvents the τ -values of the different polar molecules arrange themselves roughly accordingly to the size of the molecules. This shows τ may be expressed as $\tau = f(\eta)f(v)$. In order to

determine the functional dependence of τ on η at any temperature T , the values of $\log (\tau.T)$ have been plotted against $\log \eta$ -values. The linear plots give

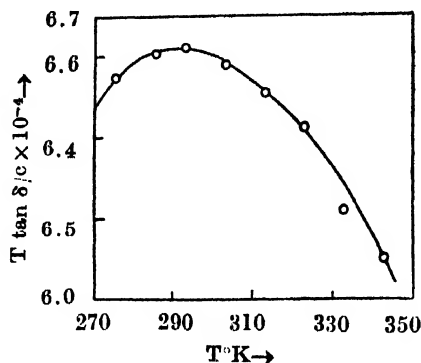


Fig. 1a. Plot of $\frac{T \cdot \tan \delta}{c}$ vs T

Nitromethane in solution in benzene.

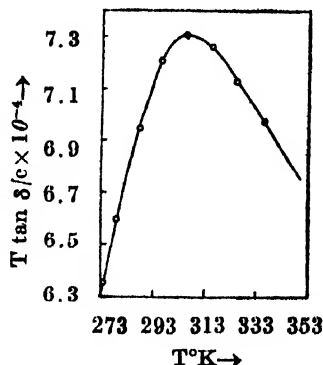


Fig. 1b. Plot of $\frac{T \cdot \tan \delta}{c}$ vs T .

Nitroethane in a solution in carbon tetrachloride.

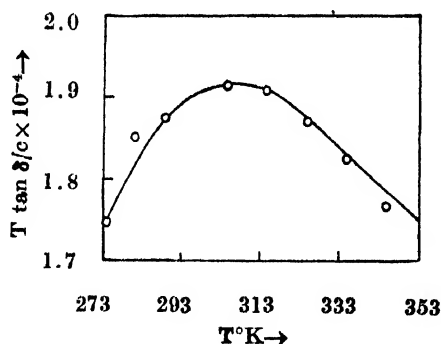


Fig. 1c. Plot of $\frac{T \tan \delta}{c}$ vs T

Ethylacetate in solution in benzene.

the required relation $\tau T = \text{const. } \eta^\gamma$ as obtained in an earlier paper (Sinha *et al.*, 1966). The constancy in the values $\tau \cdot T / \eta^\gamma$ are seen from the data in Tables I-IX.

(c) *Activation energy and intermolecular forces :*

In the case of solutions of polar organic compounds in non-polar solvents the three main types of intermolecular forces (Ketelaar, 1953) are :

(i) dipole-dipole interaction, the energy of interaction

$$E_{\pi} = -\frac{z}{3} \frac{\overline{\mu^2}}{R^3 k} \quad \dots (2a)$$

(ii) dipole-induced dipole interaction, the energy of interaction

$$E_D = -2 \frac{\alpha_s \mu^2}{R^3} \quad \dots (2b)$$

and

(iii) London dispersion forces, the energy being

$$E_L = -\frac{3}{2} \frac{\alpha_s \alpha_p}{r^6} \cdot \frac{I_s \cdot I_p}{I_s + I_p} \quad \dots (2c)$$

where μ is the dipole moment, α the polarisability, I the ionisation potential, R is the separation between dipoles and r the average distance between the solvent and solute molecules, the suffixes s and p denoting quantities of the solvent and solute molecule respectively.

If we neglect the possibility of other interactions e.g. hydrogen bond formation etc., then the sum of the above energies should be equal to the activation energy required for dipole orientation. However, we may note that for very dilute solutions since R is large E_k will be negligible while if μ is not very large and α not too small the contribution due to E_D will also be small (about 2.5% of E_L if $\mu < 2$). Thus the interaction energy due to London forces E_L would chiefly determine the activation energy. For this purpose the necessary values of α_p have been taken from the values published in the literature wherever available and in other cases these values have been calculated from the refractive index and molar volume data. The ionisation potential values have been taken from the published papers (Kandel, 1955; Watanabe, 1957; Vilesov and Terenin, 1957; Streiswieser, 1960). In case where the values for the substituted compounds are not available, the required ionisation potential have been estimated from that of the parent compound. The values of ΔH_τ for the different compounds in solution in carbon tetrachloride obtained in the present and previous investigations (Sinha *et al.*, 1965, 1966) have been used because the polarisability of the molecule of CCl_4 is the same in all directions. With these value E_L may be written as

$$E_L = -gf\alpha_p \quad \dots (3)$$

where

$$g = \frac{3}{2} \frac{I_s \cdot \alpha_s}{r^6}$$

is constant for the particular solvent if r is taken to be almost constant. $f = I_p / I_p + I_s$ varies between 0.4 and 0.5 for most of the molecules. If I_p , I_s are expressed in K.Cal/mole, r in cm and α_p , α_s in cc. then E_L would be expressed in K.Cal/mole. From equation (3) it is evident that for a given solvent if E_L is put equal to ΔH_τ then $\Delta H_\tau / f\alpha_p$ should be constant. These are shown in Table XI. The ratio $\Delta H_\tau / f\alpha_p$ are seen to be approximately constant for the different molecules,

On the other hand with the value of r estimated from the total number of molecules per cc. of the carbon tetrachloride solution the values of E_L have been obtained from equation (3) for two values of r . These are shown in the same table. The agreement between the experimental ΔH_T values and the calculated values of E_L is fairly satisfactory. This table also contains the values of the total interaction energy $E_L + E_D$ when the energy due to dipole-induced dipole forces is not neglected. Even then in some cases, however, there are somewhat large discrepancies between the two energy values. This might be due to the following reasons :

(1) In calculating the values of E_L the average values of the polarisability (α_P) has been used which in these cases may not be quite justified, and

(2) The value of r the average distance of separation has been taken to be approximately the same in all cases, but actually the value may be somewhat different in different cases.

(3) The calculated value of E_L shows the largest disagreement in the case of chloroform for which the experimental values of activation energy in solutions in CCl_4 and C_6H_6 are also larger than those for viscous flow. In the case of solution in C_6H_{14} however, the activation energy is smaller (see Table IV). These facts indicate that probably the proton donor chloroform molecules form weak intermolecular bounds with the solvent molecules of CCl_4 and C_6H_6 . The formation of such bonds, the possibility of which has been excluded from consideration, may account for the large deviation between the experimental and the calculated values in the case of chloroform.

REFERENCES

- Bhanumati, A. (Mrs.), 1963, *Ind. J. Pure. Appl. Phys.*, **1**, 79.
 Bhattacharyya, J., Sinha, B. (Miss), Roy, S. B., and Kastha, G. S., 1964, *Indian J. Phys.*, **38**, 413.
 Cripwell, F. J., and Sutherland, G. B. B. M., 1946, *Trans. Farad. Soc.*, **42A**, 149.
 Jackson, W., and Powles, J. G., 1946, *Trans. Farad. Soc.*, **42A**, 101.
 Kandel, R. J., 1955, *J. Chem. Phys.*, **23**, 84.
 Ketolaar, J. A. A., 1953, *Chemical Constitution*, Elsevier Publishing Company.
 Sinha, B. (Miss), Roy, S. B., and Kastha, G. S., 1965, *Indian J. Phys.*, **39**, 328.
 —, 1966, *Indian J. Phys.*, **40**, 101.
 Stroiswieser, A. (Jr.), 1960, *J. Am. Chem. Soc.*, **83**, 4123.
 Vilesov, F. I. and Terenin, A. N., 1957, *Dok. Akad. Nauk. U.S.S.R.*, **115**, 744.
 Watanabe, K., 1957, *J. Chem. Phys.*, **26**, 541.
 Whiffen, D. H. and Thompson, H. W., 1946, *Trans. Farad. Soc.*, **42A**, 114, 122.

SECOND VIRIAL COEFFICIENT OF NON-POLAR GASES AND GAS MIXTURES AND BUCKINGHAM-CARRA-KONOWALOW POTENTIAL

V. P. S. NAIN AND S. C. SAXENA

DEPARTMENT OF PHYSICS, UNIVERSITY OF RAJASTHAN, JAIPUR, INDIA

(Received August 8, 1966)

ABSTRACT. Second virial coefficient data of five rare gases, hydrogen and methane as a function of temperature have been interpreted on the three parameter intermolecular potential recently introduced by Carra' and Konowalow. Potential parameters have been determined for these seven pure gases. Combination rules have been derived which enable the determination of the unlike interactions from the knowledge of the related like interactions only. The second virial data of eight different binary gas pairs are also discussed. From these detailed investigations it has been concluded that this potential is somewhat superior to the two other widely studied three parameter potentials viz., the modified Buckingham exp-6 and Morse.

INTRODUCTION

A large number of intermolecular potentials have been used for computing the second virial coefficient, $B(T)$, of non-polar gases and gas mixtures. In this article we study in detail a three parameter potential recently introduced by Carra' and Konowalow (1964). This potential employs an exponential function to represent the repulsive overlap part of the intermolecular potential first suggested by Buckingham (1947) and is therefore more fully referred as Buckingham-Carra'-Konowalow potential. Hereafter this potential will be abbreviated as BCK. According to this the interaction potential energy, $\phi(r)$ is given by

$$\phi(r) = \epsilon \left(\frac{6+b}{b} \right) \left(\frac{r_m}{r} \right)^6 \left[\frac{6}{6+b} \exp \left\{ b \left(1 - \frac{r}{r_m} \right) \right\} - 1 \right] \quad \dots (1)$$

Here r is the molecular separation distance, ϵ the depth of the potential energy minimum, r_m is the value of r for which $\phi(r)$ is a minimum, and b is a parameter which controls the slope of the repulsive limb.

Carrá and Konowalow (1964) determined the parameters of the BCK potential for neon, argon, krypton and xenon by using the crystal energy data and one value of the second virial coefficient. We determine the potential parameters for the five rare gases, hydrogen and methane employing only the $B(T)$ data as a function of temperature. Making use of the expressions for the combination rules, also developed here, the $B(T)$ data of eight different gas pairs as a function of tempera-

On the other hand with the value of r estimated from the total number of molecules per cc. of the carbon tetrachloride solution the values of E_L have been obtained from equation (3) for two values of r . These are shown in the same table. The agreement between the experimental ΔH_T values and the calculated values of E_L is fairly satisfactory. This table also contains the values of the total interaction energy $E_L + E_D$ when the energy due to dipole-induced dipole forces is not neglected. Even then in some cases, however, there are somewhat large discrepancies between the two energy values. This might be due to the following reasons :

(1) In calculating the values of E_L the average values of the polarisability (α_P) has been used which in these cases may not be quite justified, and

(2) The value of r the average distance of separation has been taken to be approximately the same in all cases, but actually the value may be somewhat different in different cases.

(3) The calculated value of E_L shows the largest disagreement in the case of chloroform for which the experimental values of activation energy in solutions in CCl_4 and C_6H_6 are also larger than those for viscous flow. In the case of solution in C_6H_{14} however, the activation energy is smaller (see Table IV). These facts indicate that probably the proton donor chloroform molecules form weak intermolecular bounds with the solvent molecules of CCl_4 and C_6H_6 . The formation of such bonds, the possibility of which has been excluded from consideration, may account for the large deviation between the experimental and the calculated values in the case of chloroform.

REFERENCES

- Bhanumati, A. (Mrs.), 1963, *Ind. J. Pure. Appl. Phys.*, **1**, 79.
 Bhattacharyya, J., Sinha, B. (Miss), Roy, S. B., and Kastha, G. S., 1964, *Indian J. Phys.*, **38**, 413.
 Cripwell, F. J., and Sutherland, G. B. B. M., 1946, *Trans. Farad. Soc.*, **42A**, 149.
 Jackson, W., and Powles, J. G., 1946, *Trans. Farad. Soc.*, **42A**, 101.
 Kandel, R. J., 1955, *J. Chem. Phys.*, **23**, 84.
 Ketelaar, J. A. A., 1953, *Chemical Constitution*, Elsevier Publishing Company.
 Sinha, B. (Miss), Roy, S. B., and Kastha, G. S., 1965, *Indian J. Phys.*, **39**, 328.
 ———, 1966, *Indian J. Phys.*, **40**, 101.
 Stroiswieser, A. (Jr.), 1960, *J. Am. Chem. Soc.*, **83**, 4123.
 Vilesov, F. I. and Terenin, A. N., 1957, *Dok. Akad. Nauk. U.S.S.R.*, **115**, 744.
 Watanabe, K., 1957, *J. Chem. Phys.*, **26**, 541.
 Whiffen, D. H. and Thompson, H. W., 1946, *Trans. Farad. Soc.*, **42A**, 114, 122.

SECOND VIRIAL COEFFICIENT OF NON-POLAR GASES AND GAS MIXTURES AND BUCKINGHAM-CARRA-KONOWALOW POTENTIAL

V. P. S. NAIN AND S. C. SAXENA

DEPARTMENT OF PHYSICS, UNIVERSITY OF RAJASTHAN, JAIPUR, INDIA

(Received August 8, 1966)

ABSTRACT. Second virial coefficient data of five rare gases, hydrogen and methane as a function of temperature have been interpreted on the three parameter intermolecular potential recently introduced by Carra' and Konowalow. Potential parameters have been determined for these seven pure gases. Combination rules have been derived which enable the determination of the unlike interactions from the knowledge of the related like interactions only. The second virial data of eight different binary gas pairs are also discussed. From these detailed investigations it has been concluded that this potential is somewhat superior to the two other widely studied three parameter potentials viz., the modified Buckingham exp-6 and Morse.

INTRODUCTION

A large number of intermolecular potentials have been used for computing the second virial coefficient, $B(T)$, of non-polar gases and gas mixtures. In this article we study in detail a three parameter potential recently introduced by Carra' and Konowalow (1964). This potential employs an exponential function to represent the repulsive overlap part of the intermolecular potential first suggested by Buckingham (1947) and is therefore more fully referred as Buckingham-Carra'-Konowalow potential. Hereafter this potential will be abbreviated as BCK. According to this the interaction potential energy, $\phi(r)$ is given by

$$\phi(r) = \epsilon \left(\frac{6+b}{b} \right) \left(\frac{r_m}{r} \right)^6 \left[\frac{6}{6+b} \exp \left\{ b \left(1 - \frac{r}{r_m} \right) \right\} - 1 \right] \quad \dots (1)$$

Here r is the molecular separation distance, ϵ the depth of the potential energy minimum, r_m is the value of r for which $\phi(r)$ is a minimum, and b is a parameter which controls the slope of the repulsive limb.

Carrá and Konowalow (1964) determined the parameters of the BCK potential for neon, argon, krypton and xenon by using the crystal energy data and one value of the second virial coefficient. We determine the potential parameters for the five rare gases, hydrogen and methane employing only the $B(T)$ data as a function of temperature. Making use of the expressions for the combination rules, also developed here, the $B(T)$ data of eight different gas pairs as a function of tempera-

ture have been interpreted. Lastly, we present a comparative assessment of this potential in relation to the two other intermolecular potentials and show the supremacy of the BCK potential. The other two potentials are the familiar modified Buckingham exp-6 potential first used by Rice and Hirschfelder (1954) and the Morse potential exploited by Konowalow, Taylor and Hirschfelder (1961). These two potentials will be abbreviated as BRH and KTH respectively.

COMBINATION RULES

The development of such relations which may permit the determination of the unlike molecular interactions from the related like interactions is very useful for it then becomes possible to calculate the different properties of mixtures also. Such relations, usually referred as combination rules, are not known for the BCK potential. We present below the development of such expression. This has been done in brief for the pertinent arguments involved have been stated earlier in many papers. Equation (1) is easily transformed to the following convenient form :

$$\phi(r) = Ae^{-Br} - D/r^6, \quad \dots (2)$$

where

$$A = \frac{6\epsilon\epsilon^6}{b^{*6}}, \quad B = b/r_m, \quad \text{and} \quad D = \epsilon \left(\frac{6+b}{b} \right) r_m^6, \quad \dots (3)$$

and r^* is the reduced value of r such that $r^* = r/r_m$. As shown by Zener (1931) the value of B corresponding to the unlike molecules can be written in terms of the like molecules as,

$$B_{12} = (1/2)(B_{11} + B_{22}). \quad \dots (4)$$

The theories of dispersion forces first given by London (1930) and further approximated by Beattie and Stockmayer (1951) suggest the geometric mean rule for D so that

$$D_{12} = (D_{11} \cdot D_{22})^{1/2}. \quad \dots (5)$$

Theory provides no clue for suggesting a combination rule for the parameter A . Some empirical arguments and more the success achieved in connection with the other potentials prompt us to assume a geometric mean rule for A also. Consequently we get

$$A_{12} = (A_{11} \cdot A_{22})^{1/2} \quad \dots (6)$$

Substituting the values of different D_{ij} and A_{ij} from Eq. (3) in Eqs. (5) and (6) respectively, and then dividing the former by the latter we get the following transcendental equation for evaluating the parameter b_{12} ,

$$\frac{b_{12}+6}{e^{b_{12}}} = \left[\frac{b_{11}+6}{e^{b_{11}}} \cdot \frac{b_{22}+6}{e^{b_{22}}} \right]^{1/2}. \quad \dots (7)$$

Again the substitution of different B_{ij} in Eq. (4) from Eq. (3) leads directly to the following explicit relation for $(r_m)_{12}$ in terms of b_{12} and other constants characteristic of pure interactions. This is

$$(\gamma_m)_{12} = \frac{2b_{12}}{b_{11}/(r_m)_{11} + b_{22}/(r_m)_{22}} \quad (8)$$

Similarly the required relation for ϵ_{12} emerges when one substitutes in Eq. (6) the values of different A_{ij} from Eq. (3), which is

$$\epsilon_{12} = (\epsilon_{11} \cdot \epsilon_{22})^{\frac{1}{2}} \left(\frac{b_{12}}{(b_{11} \cdot b_{22})^{\frac{1}{2}}} \right)^{\frac{1}{2}} \left[\frac{(r_m)_{11} \cdot (r_m)_{22}}{(r_m)_{12}^2} \right]^{\frac{1}{2}} \cdot \frac{e^{\frac{b_{11} + b_{22}}{2} \frac{1}{b_{12}}}}{e^{\frac{1}{b_{12}}}} \quad \dots \quad (9)$$

The relations (7), (8) and (9) are to be employed for computing b_{12} , $(r_m)_{12}$ and ϵ_{12} respectively and hence the so called combination rules.

POTENTIAL PARAMETERS

The approach of Carra' and Konowalow (1964) for determining the three parameters b , ϵ/k and r_m of BCK potential is somewhat objectionable. This is because they have employed the crystal energy data and assumed the validity of the pairwise additivity rule. We have therefore evaluated the potential parameters from the temperature dependence of $B(T)$ data alone. The parameter b of the BCK potential is related with the parameter α of the modified exp-(6) potential, Carra' and Konowalow (1964), as

$$b = \alpha - 6. \quad (10)$$

This relation results by equating the values of $\phi(r)$ on the two potentials at the minimum. To start with we have also assumed the relation of Eq. (10) and determined the remaining two parameters ϵ/k and tr by adopting the familiar method of translation. A log-log plot of the reduced virial coefficient $B^*(b, T^*)$, is drawn against T^* the reduced temperature for a particular value of b characteristic of the gas under investigation. A similar log-log plot of experimental $B(T)$ against T is next prepared on a transparent graph paper employing the same scale as in the previous plot. The latter plot is next moved over the former and an effort is made to best coincide the two by translations parallel to the two axes. The magnitudes of translation along the X and Y axes yield the values for ϵ/k and r_m respectively. The values so obtained are recorded in Table I. The references to the experimental data employed are given in the last column of this very table.

The parameters for the unlike interactions can now be calculated according to the Eqs. (7), (8) and (9) and the like parameters recorded in Table I. The values of these unlike parameters are reported in Table II.

COMPARISON OF THEORETICAL AND EXPERIMENTAL
SECOND VIRIAL COEFFICIENT

The second virial coefficient of a pure gas, $B(T)$, as given by Hirschfelder, Curtiss and Bird (1954), is

$$B(T) = 2/3\pi N r_w^3 B^*(b, T^*), \quad \dots (11)$$

where N is the Avogadro number. Utiling the tabulations of Carra' and Konovalow for $B^*(b, T^*)$ in conjunction with the parameters given in Table II, $B(T)$ was calculated at all those temperatures where direct measured values are available. We do not report here all these calculations for the sake of brevity. However in Table III column 2 we list for all the gases average absolute deviations, \bar{X} . The latter being the difference of the experimental and calculated values of the second virial coefficient.

TABLE I
Potential parameters for like interactions

Gas	Parameters Parameters b	ϵ/K $^\circ K$	r_m $^\circ A$	References
He	6.5	4.53	3.084	
Ne	8.5	36.31	3.018	
Ar	8.0	125.9	3.828	
Kr	6.3	152.7	4.295	
Xe	8.0	231.2	4.585	
H ₂	8.0	32.61	3.263	
CH ₄	8.0	155.6	4.244	

TABLE II
Potential parameters for unlike interactions

Gas pairs	Parameter b_{12}	ϵ_{12}/K $^\circ K$	$(r)_{m12}$ $^\circ A$
He-Ne	7.5	12.97	3.047
He-Ar	7.25	23.14	3.456
Ne-Ar	8.25	71.94	3.363
Ne-Kr	7.41	91.1	3.458
Ar-Kr	7.15	144.9	4.029
He-H ₂	7.25	11.82	3.180
Ar-H ₂	8.0	64.50	3.523
Ar-CH ₄	8.0	140.7	4.013

TABLE III

 Comparison of average absolute deviations, \bar{X} , in cc/mole for pure gases

Gas	BCK set I	BCK set II	BRH	KTH
He	0.14	—	0.18	1.41
Ne	0.78	1.15	0.91	0.72
Ar	2.56	2.51	3.74	5.71
Kr	11.38	18.39	5.55	7.66
Xe	1.56	3.28	7.89	2.42
H ₂	0.31	—	0.42	0.36
CH ₄	0.10	—	0.37	1.31

TABLE IV

 Comparison of average absolute derivations, \bar{X} , in cc/mole for binary gas pairs

Gas pair	BCK	BRH	KTH
He-Ne	0.51	0.59	0.99
He-Ar	1.48	3.14	5.03
Ne-Ar	18.6 , 8.6	24.5 , 14.8	20.1 , 10.4
Ne-Kr	12.6	16.0	7.4
Ar-Kr	19.1	4.75	18.3
He-H ₂	0.76	0.68	1.66
Ar-H ₂	0.58	0.63	0.69
Ar-CH ₄	3.55	1.55	2.08

Set I refers to the values obtained on the basis of the potential parameters determined here, while set II employs those reported by Garra' and Konowalow.

The second virial coefficient of a binary mixture $B_{mix}(T)$, is given by the following expression (1954)

$$B_{mix}(T) = X_1^2 B_{11} + X_2^2 B_{22} + 2X_1 X_2 B_{12}. \quad \dots (12)$$

Here X_1 and X_2 are the mole fractions of the components 1 and 2 respectively, B_{11} and B_{22} are the $B(T)$ values for the components 1 and 2 respectively, and B_{12}

is the virial coefficient of a hypothetical pure gas whose molecules interact according to the potential law for (1, 2) interaction. $B_{mix}(T)$ values were computed for the eight gas pairs at all those temperatures where directly observed values are available. Again for conciseness we do not report all these calculations but instead are given in Table IV column 2 the average of the absolute differences between the observed and calculated values, \bar{X} . The experimental data used here are due to the authors Fender and Halsey (1962), Thomaes and Steenwinkel (1962), Gibby, Tanner and Masson (1929), Edwards and Rooserveare (1942), and Knobler and Beenakker (1959).

It will be noted from the entries of column 2 Table III that the reproduction of $B(T)$ values is satisfactory for helium, neon, argon, xenon, hydrogen and methane in as much as deviations are always within the limits of experimental uncertainties. The situation for the case of krypton is very unsatisfactory and the discrepancy is more than can be explained on the basis of experimental uncertainties. We have also calculated the $B(T)$ values for neon, argon, krypton and xenon utilising the potential parameters of Carra' and Konowalow (1964). The \bar{X} -values for all these gases are listed in Table III column 3. It is important to note that discrepancies in all cases except argon are now more than in the previous case and particularly for krypton this difference is appreciable.

Similarly we notice from Table IV that for the gas pairs helium-neon, helium-argon, helium-hydrogen, argon-hydrogen and argon-methane the agreement between the experimental and calculated $B(T)$ values is good. On the other hand for neon-argon, neon-krypton and argon-krypton the reproduction of $B(T)$ values is quite poor. According to Saxena and Gambhir (1963) experimental value for neon-argon gas pair is likely to be in error (1963). Thus, in binary gas pairs we find that agreement between theory and experiment is always satisfactory except when krypton constitutes as one of the components. The failure of the BCK potential to explain the data of krypton is not very strange and has been noticed earlier also in connection with other potentials, Bahethi and Saxena (1964).

In order to have an absolute assessment of this potential in relation with the BRH and KTH potentials it is essential to know the values of \bar{X} for these two potentials for systems of Tables III and IV. Employing the most commonly used parameters and suitable tabulations virials were calculated for all these gases and gas pairs and \bar{X} computed. These values are recorded directly in Tables III and IV. A critical study of the two tables reveals that leaving krypton in all cases BCK potential is better than the two other potentials. BHR potential also seems to be somewhat preferable over the KTH potential. The uniqueness of the behaviour of krypton seems to be inherent in all the three potentials. It is important to note that in BHR potential the parameters were determined by considering both the second virial, viscosity and crystal data but α was treated as a completely disposable parameter. In the case of KTH potential the parameters

were determined from $B(T)$ data alone or in combination with crystal data. Thus the comparison between BCK and KTH potentials may be regarded as equivalent in most of the cases. To get a more clear picture about the relative merits of BCK and BRH potentials we undertake certain more investigations in the next section.

DISCUSSION ON INTERMOLECULAR POTENTIALS

As pointed out in the last section BCK potential fails to reproduce the $B(T)$ data for krypton. The deviation between the experiment and theory is pronounced and somewhat alarming only at low temperatures ranging upto 170°K . It is important to note that at still higher temperatures upto 873°K the theory does succeed in reproducing the experimental data within the margin of experimental uncertainties. The situation is relatively superior for the BRH potential and even for the KTH potential to some extent. We therefore reexamine the krypton $B(T)$ data and make an attempt to determine the three parameters independently without assuming the relation of Eq. (10) for b . We include also argon data for a similar analysis though for this gas BCK potential has been found to be superior to both BRH and KTH potentials. Another consideration which weighed with us to include this gas is the availability of its $B(T)$ data over a very extensive temperature range $85\text{--}873^\circ\text{K}$.

The procedure adopted for determining the three parameters of the BCK potential is somewhat similar to that earlier described in section 3 except now the theoretical log-log plots are drawn for several probable values of b .

While moving the experimental log-log plot over the theoretical plots an attempt is made to fix the parameter b on the criterion of best fit. The values of the potential parameters so obtained for argon and krypton are reported in Table V. The reproduction of the $B(T)$ data on the basis of these parameters improves remarkably as compared to the one obtained on the basis of the parameters of Table I. To give an idea we quote the average absolute deviation of the computed values from the experimental values. These are 1.08 and 3.26 cc/mole for argon and krypton respectively. A further check is possible on the suitability of these parameters by performing calculations on binary systems which involve these gases. We investigated the systems argon-krypton and neon-krypton in this light. However the calculations revealed only inappreciable improvement. This of course should not be regarded as disappointing. As regards the absolute values of the potential parameters are concerned these are reported in Table VI and are appreciably different than those of Table II. The mixture $B(T)$ values for these systems are available only over a limited temperature range and it so happens that the changes produced in the computed $B(T)$ values from the variations in the values of the potential parameters cancel each other such that the overall values remain unaffected. We are of the opinion that in general it would be more appropriate to determine the three parameters of the BCK potential by treating all the three

parameters as completely disposable at least in those cases where elaborate experimental data are available.

TABLE V
Potential parameters for argon and krypton

Gas	b	ϵ/K $^{\circ}K$	r_m \AA°
Ar	8.5	128.8	3.828
Kr	7.0	156.7	4.362

TABLE VI
Potential parameters for gas pairs

Gaspair	b_{12}	ϵ_{12}/K $^{\circ}K$	(r_m) \AA°
Ar-Kr	7.75	149.7	4.053
Ne-Kr	7.75	102.4	3.506

TABLE VII
Values of parameters c' and b' as computed from Eqs. (13) and (14)

Gas Paramoter	He	Ne	Ar	Kr	Xe	H ₄	CH ₂
C*	4.0	5.1	5.0	4.5	4.9	5.0	4.9
C'	4.2	5.0	5.0	4.5	4.6	5.3	4.9
b	6.5	8.5	8.0	6.3	8.0	8.0	8.0
b' (set I)	17.7	7.3	6.6	7.1	7.9	8.4	7.1
b' (set II)	—	8.7	7.2	4.9	6.9	—	—

*These values are taken from Konowalow, and Hirschfelder, 1961.

In literature it has been often attempted to compare parameters on the basis that the plot of $\phi(r)$ versus r has the same curvature at the minimum for all. Thus a relationship between the parameter C of the KTH potential with that of the

BRH potential was given by Konowalow and Hirschfelder (1961). This leads finally to the result that

$$C' = \left[\frac{3\alpha(\alpha-7)}{(\alpha-6)} \cdot \frac{\epsilon(BRH)}{\epsilon(KTH)} \cdot \frac{\sigma^2}{r_m^2} \right]^{\frac{1}{2}} \quad \dots (13)$$

Similarly one can relate b of the BCK potential with α of the BRH potential to get

$$b' + 5 = \frac{\alpha(\alpha-7)}{(\alpha-6)} \cdot \frac{\epsilon(BRH)}{\epsilon(BCK)} \cdot \frac{r_m^2(BCK)}{r_m^2(BRH)} \quad \dots (14)$$

In Eqs. (13) and (14) C' and b' respectively are the values of c and b when the curvatures at the minimum for the KTH and BCK potentials are made equal to that for the BRH potential. These values of c' and b' are reported in Table VII. It will be noted from this table that for the KTH potential the agreement between the c' and c values is quite good indicating thereby a lot of similarity between the KTH and BRH potential. On the other hand the agreement between b' and b values is rather poor. This suggests that the BCK potential has somewhat different character in the short range intermolecular forces compared to the BRH potential. This further suggests that relation given by Eq. (10) should be assumed only when an independent accurate determination of b is not possible.

CONCLUSIONS

We wish to make the explicit mention of the following conclusions in view of the studies presented in this paper :

1. The BCK three parameter potential seems to be adequate enough to correlate the second virial data of pure gases and binary gas mixtures. At present the limitations of the available theoretical tabulations do not permit a check of this potential against other properties.

2. This potential completes favourably with the two other widely studied three parameter potentials. It is likely that it may supersede even the BRH potential which has been enjoying the status of being the best potential for correlating the different properties of gases and gas mixtures. Certainly this new BCK potential seems superior to the KTH potential.

3. In view of the great promise associated with the BCK potential we feel that the scope of work on this potential be increased by including the particular calculations relevant for the other equilibrium and non-equilibrium properties of gases and gas mixtures.

ACKNOWLEDGMENTS

We are thankful to Dr. D. D. Konowalow for his interest and encouragement in the work presented here. This research was supported by the Council of

Scientific and Industrial Research, New Delhi. The award of a research scholarship to one of us (V.P.S.) is also gratefully acknowledged.

REFERENCES

- Bahethi, O. P., and Saxena, S. C., 1964, *Indian J. Pure and Appl. Phys.*, **3**, 12.
 Beattie, J. A., and Stockmayer, W. H., 1942, *J. Chem. Phys.*, **19**, 473.
 ————— 1951, *States of matter* edited by H. S. Taylor and S. Glasstone (Princeton, New Jersey: D. Van Nostrand Co., Inc.).
 Beattie, J. A., Barrault, R. J., and Brierley, J. S., 1951, *J. Chem. Phys.*, **10**, 1222.
 Beattie, J. A., Brierley, J. S., and Barrault, R. J., 1952, *J. Chem. Phys.*, **20**, 1613.
 Buckingham, R. A., and Corner, J., 1947, *Proc. Roy. Soc.*, **A 189**, 118.
 Carra, S., and Konowalow, D. D., 1964, *Nuovo Cimento*, **34**, 205.
 Edwards, A. E., and Roseveare, 1942, *J. Am. Chem. Soc.*, **64**, 2816.
 Fender, B. E. F., and Halsey, G. D., 1962, *J. Chem. Phys.*, **36**, 1881.
 Gibby, C. W., Tanner, C. C., and Masson, L., 1929, *Proc. Roy. Soc. (London)*, **A 122**, 283.
 Hirschfelder, J. O., Curtiss, C. F., and Bird, R. B., 1954, *Molecular Theory of Gases and Liquids* Chapman and Hall, Ltd., London.
 Holborn, L., and Otto, J., 1920, *Ann. Physik.*, **63**, 674; 1924, *Z. Physik*, **23**, 77.
 ————— 1955, *Z. Physik.*, **33**, 1.
 ————— 1926, *Z. Physik.*, **38**, 359.
 ————— 1922, *Z. Physik*, **11**, 367.
 ————— 1924, *Z. Physik*, **23**, 77.
 Knobler, C. M., Beerakker, J. J. M., and Knapp, H. F. P., 1959, *Physica*, **25**, 909.
 Konowalow, D. D., Taylor, M. H., and Hirschfelder, J. O., 1961, *Phys. Fluids*, **4**, 622.
 Konowalow, D. D., Hirschfelder, J. O., 1961, *Phys. Fluids*, **4**, 629.
 London, F., 1930, *Trans. Farad. Soc.*, **33**, 222; 1930, *Zeits. Phys. Chem.*, **B 11**, 222.
 Michels, A., and Wouters, H., 1941, *Physica*, **8**, 923.
 Michels, A., and Goudekot, M., 1941, *Physica*, **8**, 347.
 Nijhoff, G. P., and Keesom, W. H., 1927, *Leiden Comm.*, 1880.
 Rice, W. E., and Hirschfelder, J. O., 1954, *J. Chem. Phys.*, **22**, 187.
 Saxena, S. C., and Gambhir, R. S., 1963, *Molecular Phys.*, **6**, 577.
 Schamp, Jr., H. W., Mason, E. A., Richardson, A. C. B., and Altman, A., 1958, *Phys. Fluids*, **1**, 329.
 Schneider, W. G., and Duffie, J. A. H., 1949, *J. Chem. Phys.*, **17**, 751.
 Thomaes, G. and Van Steenwinkel, R., 1962, *Nature*, **193**, 160.
 Thomaes, G. and Van Steenwinkel, R., and Stone, W., 1962, *Mol. Phys.*, **5**, 301.
 Whalley, E., Lupien, Y., and Schneider, W. G., 1953, *Canadian J. Chem.*, **31**, 722.
 Whalley, E., and Schneider, W. G., 1954, *Trans. Am. Soc., Mining Met. Engrs.*, **76**, 983; 1955, *J. Chem. Phys.*, **23**, 1644.
 Whalley, E., Lupien, Y., and Schneider, W. G., 1955, *Canadian J. Chem.*, **33**, 633.
 Witonsky, R. J., and Miller, J. G., 1963, *J. Am. Chem. Soc.*, **85**, 282.
 Yntema, J. L., and Schneider, W. G., 1950, *J. Chem. Phys.*, **18**, 641.
 Zener, C., 1931, *Phys. Rev.*, **37**, 556.

INTERRUPTED WAVE SYNCHRONISATION

B. N. BISWAS

DEPARTMENT OF PHYSICS,
BURDWAN UNIVERSITY,
BURDWAN, INDIA.

(Received March 21, 1966; Re-submitted June 8, 1966; January 17, 1967)

ABSTRACT. In this paper the phenomenon of interrupted wave synchronisation of an automatic phase control circuit has been studied. The response of such a circuit preceded by a tunable high Q circuit to an interrupted sinusoid has been analysed. Simple but not very accurate expressions for the locking range of the APC systems when the incoming signal is an interrupted one have been derived. When the APC circuit is not preceded by a tunable high Q circuit it has been found that the locking range increases with increasing values of the rate of interruption and duty cycle of the incoming wave. Necessary and sufficient conditions have been presented for sideband locking. It has been found that the locking of the local oscillator with any of the Fourier's Component becomes easy when the conventional APC circuit is preceded by a tunable high Q circuit. Experimental results regarding carrier and side-band locking range have been presented and found to be in good agreement with the conclusions of the analysis.

INTRODUCTION

Locking phenomena in an automatic phase control circuit with a CW signal have been studied by many authors (Richman, D., *et al* 1954). In this paper locking phenomena in an automatic phase control circuit with an interrupted continuous wave signal with a high value of carrier to noise ratio (CNR) will be examined. Direct synchronisation of a continuous wave oscillator with an interrupted sinusoid has, however, been studied in detail by Fraser, D. W. Injection synchronised oscillators, however, suffer from the defect that the independent control of the synchronisation range and the noise bandwidth of the system could not be achieved without affecting the stability of the local oscillator. As such method of indirect synchronisation—automatic frequency control (AFC) and automatic phase control (APC) of an oscillator were suggested. In an AFC system the frequency of the local oscillator is compared to a reference frequency and thus this system requires a finite error although small, in the frequency of the local oscillator for its required operation. The phase locked system (APC), on the other hand, requires no steady state error in the output frequency of the oscillator but instead utilises an error in the output phase which is the 'integral' of the controlled variable i.e. the output frequency. Thus, here these parameters can be controlled independent of one another.

This work was done at the Institute of Radio Physics and Electronics, University of Calcutta.

It has been shown that in the case of CW synchronisation an idea about the average network gain of the loop filter and maximum possible synchronising range gives a reasonable estimate of the locking range and locking time (Chakrabarti, N. B. *et al*, 1964). A typical block diagram of an APC circuit is shown in Fig. 1. The input to the system, in contrast to the case of CW synchronisation, consists of a single tone CW signal which is being interrupted at a suitable rate. The spectral

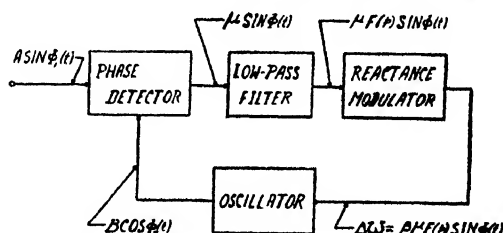


Fig. 1. A typical block diagram of an automatic phase control circuit incorporating a phase detector, a low-pass filter, a reactance modulator and an oscillator.

components of the input wave consist of a carrier and side-band components which are separated from the carrier frequency component by the frequency of interruption and its multiple thereof. From this one can easily conjecture that the local oscillator can be made to lock with any one of the Fourier Components (of course with proper choice of system parameters). If the input is a stable one that is if a CW wave being interrupted is derived from a crystal oscillator and the waveform causing interruption is also stable, then oscillation with stable phase and frequency can be obtained by locking an oscillator or oscillators with the different sideband components. Such a technique permits saving of crystals in a frequency synthesis. Another very important use to which this phenomenon of interrupted wave synchronisation may be put is to convert a PRF modulation into frequency modulation.

In section 2 the governing equations of an APC circuit with an interrupted CW signal as the input have been derived. In section 3 the simple APC circuit has been studied in detail and an equation for the locking range in terms of the duty cycle of the input wave and the system parameters has been derived.

Section 4 deals with the analysis of an APC circuit with a low-pass filter in the loop. In this section an expression for the locking ratio for the carrier frequency component has been presented.

Section 5 presents an analysis of this simple APC circuit when it is preceded by a tunable high Q circuit. Expressions for the locking range for the side-band components are also given.

Section 6 deals with the analysis of the APC circuit incorporating a low-pass filter in the loop and preceded by a high Q tuned circuit. This is followed by a description of the experimental set up and a discussion of the experimental results regarding carrier locking range and sideband locking in section 7. Experimental

results are in good agreement with the conclusion of the analysis presented in the text.

DERIVATION OF THE LOOP EQUATIONS

Let us consider the typical APC circuit, with a low-pass filter in the loop, for synchronisation with an interrupted sinusoid having a duty cycle of T/T_r (Fig. 1). During the on-period of the input wave the phase-detector acting as an error sensing device of the loop produces an output ($\mu \sin \phi$) that controls the instantaneous phase or frequency of the voltage controlled oscillator through the low-pass filter in the loop. Here μ is the sensitivity of the phase detector and ϕ is the instantaneous phase difference between the reference input and the local oscillator during the on-period. During the off-period the instantaneous phase or the frequency of the VCO is controlled by the stored energy in the low-pass filter in the loop during the on-period of the input wave. The governing equation of the APC loop for the on-period is given by

$$\frac{d\phi}{dt} = \Omega - KF(p) \sin \phi, \quad \dots (2.1)$$

and that for off-period is given by

$$\frac{d\phi}{dt} = \Omega - \beta e_d(t), \quad \dots (2.2)$$

where

$$e_d(t) = \int_0^t e(t_1) f(t-t_1) dt_1, \quad \dots (2.3)$$

and β is the sensitivity of the reactance tube; $F(p)$ is the filter transfer-function and K is the maximum possible synchronising range in radian per second and $e(t_1)$ is given by

$$e(t_1) = \mu \sin \phi(t_1) \quad \dots (2.4)$$

and $f(t-t_1)$ is the impulse response of the filter network at time $t = t_1$.

THE SIMPLE APC CIRCUIT

The simple APC circuit consists of a phase detector and a voltage controlled oscillator. The governing equation of such a simple circuit is given by

$$\frac{d\phi}{dt} = \Omega - K \sin \phi, \quad 0 \leq t \leq T \quad \dots (3.1)$$

and

$$\frac{d\phi}{dt} = \Omega, \quad T \leq t \leq T_r \quad \dots (3.2)$$

where the symbols have their usual significance. It is to be noted that locking can only occur when open loop frequency error is less than the maximum possible synchronising range K and the net phase shift between the local oscillator and the reference input is zero. Expressed analytically

$$\int_{-T_r}^{T_r} \left(\frac{d\phi}{dt} \right) dt = 0 \quad \dots (3.3)$$

$$\text{i.e. } \int_{-T}^T (\Omega - K \sin \phi) dt + \int_{-T_r}^{T_r} \Omega dt = 0 \quad \dots (3.3a)$$

which on comparison with Eq. (3.1) and on integration yield the following simple equation

$$\begin{aligned} & 2 \tan^{-1} \left[\frac{1}{x} - \frac{\sqrt{1-x^2}}{x} \tanh \left(K t_0 \frac{\sqrt{1-x^2}}{2} \right) \right] \\ & - 2 \tan^{-1} \left[\frac{1}{x} - \frac{\sqrt{1-x^2}}{x} \tanh K(t_0 + nT_r) \frac{\sqrt{1-x^2}}{2} \right] \\ & = x(1-n)KT, \end{aligned} \quad (3.4)$$

where x stands for the locking ratio Ω/K and n represents the duty cycle of the input interrupted wave and t_0 is the constant that determines the initial difference of phase between the local oscillation and the reference oscillation. The value of t_0 can be found from the fact that at the edge of the band of synchronisation it can be assumed with a fair degree of accuracy that the phase difference is very approximately equal to $\pi/2$ radians. Therefore, with this assumption one can write from Eq. (3.9)

$$\tanh \left[K t_0 \frac{\sqrt{1-x^2}}{2} \right] = \sqrt{\frac{1-x}{1+x}} \quad (3.5)$$

Therefore, comparing Eq. (3.4) with Eq. (3.5) one can easily show that the locking equation is given by

$$\begin{aligned} & \frac{1}{x} - \frac{\sqrt{1-x^2}}{x} \cdot \frac{\sqrt{\frac{1-x}{1+x}} + \tanh \left(nKT_r \frac{\sqrt{1-x^2}}{2} \right)}{1 + \frac{\sqrt{1-x}}{1+x} \tanh \left(nKT_r \frac{\sqrt{1-x^2}}{2} \right)} \\ & = \frac{1 - \tan[(1-n)xKT_r/2]}{1 + \tan[(1-n)xKT_r/2]} \quad \dots (3.6) \end{aligned}$$

In many practical situations the phase-difference between the local oscillator and the reference input is not very large and in this case the linearised version of the loop gives a reasonably accurate result. This is obtained when $\sin \phi$ is replaced by $\pi/2 \cdot \phi$ which can be done only when ϕ lies within $-\pi/2$ and $+\pi/2$. In such a case the governing equations of the loop are given by

$$\frac{d\phi}{dt} = \Omega - \frac{2}{\pi} K\phi, \quad (3.7)$$

and

$$\frac{d\phi}{dt} = \Omega \quad (3.8)$$

Thus the instantaneous value of the phase difference ϕ is given by $0 \leq t \leq T$

$$\phi = \phi_0 \exp \left(-\frac{2}{\pi} Kt \right) + \frac{\pi}{2} \cdot \frac{\Omega}{K} \left[1 - \exp \left(-\frac{2}{\pi} Kt \right) \right] \quad \dots (3.9)$$

and corresponding equation of lock-in can be written as

$$\left[1 - \exp \left(-\frac{2}{\pi} KT \right) \right] \left(\phi_0 - \frac{\pi}{2} \frac{\Omega}{K} \right) = \Omega (Tr - T) \quad \dots (3.10)$$

which on simplification yields,,

$$\frac{\Omega}{K} = \frac{1 - \exp \left(-\frac{2}{\pi} KT \right)}{1 - \exp \left(-\frac{2}{\pi} KT \right) + 4 \frac{K}{w_r} (1-n)} \quad \dots (3.11)$$

where w_r is the repetition rate of interruption measured in radians per second

THE APC LOOP WITH A LOW-PASS FILTER

In this section the behaviour of the automatic phase control circuit incorporating a low-pass filter in the loop will be discussed. The operation of this circuit is different from the APC circuit without filter. This is because of the fact that during the on-period of the input signal, the instantaneous phase or frequency of the local oscillator will be gradually pulled towards that of the reference input provided the open loop frequency error is less than the maximum permissible value of the locking range. If the open loop frequency error is less than the maximum permissible value of the locking range, the frequency or the instantaneous phase of the local oscillator will be locked in synchronism with the reference input within a very short time compared to the on-period of the incoming wave. The control signal, obtained as a result of comparison of the instantaneous phases of the local oscillator and reference input is a d.c. potential that manages to maintain the synchronism between them. This d.c. potential depends on the

time constant of the low-pass filter, the duty cycle of the incoming signal, open loop frequency error and the strengths of the oscillators and the reference input.

During the off-period the error signal is absent but the d.c. potential, which has been stored up in the low pass filter during the on-period, will try to hold the instantaneous phase of the local oscillator to the locked value during the off-period. However, the phase will drift away from the locked value and reach a value which will be governed by the duty cycle as well as by the characteristics of the filter. The local oscillator is said to be synchronised if either of the following conditions is satisfied viz.,

(i) the reduction of the phase difference between the local oscillator and the reference input during the on-period must compensate the drift of phase difference between them during the off-period,

(ii) the phase of the local oscillator should attain a steady value at the end of the successive on-period of the input wave.

In this section an expression for the carrier locking ratio Ω/K will be derived with respect to two filters one having no limiting high frequency and the other a finite high frequency gain.

FILTER WITH NO LIMITING HIGH FREQUENCY GAIN

Let us consider the APC loop with the low-pass filter as shown in Fig. 1. Assuming that the phase difference lies within $-\pi/2$ and $+\pi/2$ one can then with a reasonable degree of accuracy replace $\sin \phi$ by $\frac{2}{\pi} \cdot \phi$ and write the governing equation of the linearised APC loop as

$$\tau \frac{d^2\phi}{dt^2} + \frac{d\phi}{dt} + \frac{2}{\pi} K\phi = \Omega, \quad (4.1)$$

where τ is the time constant of the filter network. The solution of which is given by

$$\begin{aligned} \phi \cong \frac{\Omega}{K} + \frac{2}{\pi} \left[\left(\phi_0 - \frac{\pi}{2} \frac{\Omega}{K} \right) + \Omega\tau \right] \exp\left(-\frac{2}{\pi} Kt\right) \\ - \frac{2}{\pi} \left[\frac{2}{\pi} K\tau \left(\phi_1 - \frac{\pi}{2} \frac{\Omega}{K} \right) + \Omega\tau \right] \text{Exp}\left(-\frac{t}{\tau}\right), \end{aligned} \quad \dots (4.2)$$

$$\text{for } \frac{\Omega}{\pi} K\tau << 1$$

$$\text{and } \phi \cong \frac{\Omega}{K} + C \sin \left(\sqrt{\frac{2}{\pi} K\tau} \frac{t}{2\tau} + \theta \right) \exp\left(-\frac{t}{2\tau}\right), \frac{8}{\pi} K\tau >> 1 \quad \dots (4.3)$$

where

$$C \sin \theta = \phi_0 - \frac{\pi}{2} \frac{\Omega}{K},$$

$$C \cos \theta = \frac{\Omega + \frac{1}{2\tau} \left(\phi_0 - \frac{\pi}{2} \frac{\Omega}{K} \right)}{\sqrt{2/\pi \cdot \frac{K}{\tau}}} \quad \dots \quad (4.4)$$

and $\phi = \phi_0$ at time $t = 0$.

In this sub-section the equation for locking ratio will be derived. This is based upon the utilisation of the linearised solutions [vide Eq. (4.2) and Eq. (4.3) of Eq. (4.1) and the first condition of section 4]. Remembering this one can easily show (see Appendix A) that the governing equation of the loop during the off-period is given by

$$\frac{d\phi}{dt} \cong \Omega - K e^{-t/\tau} \left[\frac{\Omega}{K} \cdot \frac{T}{\tau} + \frac{1}{K\tau} \left\{ \left(\phi_0 - \frac{\pi}{2} \frac{\Omega}{K} \right) + \tau \Omega \right\} \right], \quad \dots \quad (4.5)$$

$$\frac{8}{\pi} K\tau < < 1$$

and

$$\begin{aligned} \frac{d\phi}{dt} \cong \Omega - K e^{-\tau/t} & \left[\frac{\Omega}{K} (e^{T/\tau} - 1) + 4C e^{-\frac{\tau}{2T}} \sin \left(\sqrt{\frac{8}{\pi} K\tau} \frac{T}{2\tau} - \tan^{-1} \sqrt{\frac{8}{\pi} K\tau} - \theta \right) \right. \\ & \left. + \frac{4C}{\sqrt{\frac{2}{\pi} K\tau}} \sin \left(\tan^{-1} \sqrt{\frac{8}{\pi} K\tau} - \theta \right) \right], \quad \frac{8}{\pi} K\tau > > 1 \quad \dots \quad (4.6) \end{aligned}$$

The solutions of Eq. (4.5) and Eq. (4.6) are respectively given by

$$\begin{aligned} \phi(t) \cong \Omega (t-T) + K\tau & \left[\frac{\Omega}{K} \cdot \frac{T}{\tau} + \frac{1}{K\tau} \left\{ \left(\phi_0 - \frac{\pi}{2} \frac{\Omega}{K} \right) + \Omega\tau \right\} \right] \\ & \times \left(\exp \left(-\frac{t}{\tau} \right) - \exp \left(-\frac{T}{\tau} \right) \right) + \phi(T), \quad \frac{8}{\pi} K\tau < < 1 \quad \dots \quad (4.7) \end{aligned}$$

and

$$\phi(t) \cong \Omega (t-T) + K T q \left(e^{-\frac{t}{\tau}} - e^{-\frac{T}{\tau}} \right) + \phi(T), \quad \frac{8}{\pi} K\tau > > 1 \quad \dots \quad (4.8)$$

where $\phi = \phi(T)$ at time $t = T$ and q stands for the right-hand side of Eq. (4.6). From these two equations one can easily show that the locking ratios Ω/K of the APC circuit with a low-pass in the loop are given by

$$\frac{\Omega}{K} \cong \frac{\pi}{2} \left[1 - \left\{ \left(e^{-\frac{T_r}{\tau}} - e^{-\frac{T}{\tau}} \right) + e^{-\frac{2KT}{\pi}} \right\} \right] / \left[KTr(1-n) + \frac{\pi}{2} nKTr \right. \\ \left. \left(e^{-\frac{T_r}{\tau}} - e^{-\frac{T}{\tau}} \right) + \frac{\pi}{2} \left(\frac{\pi}{2} - KT \right) \left\{ \left(e^{-\frac{T}{\pi}} - e^{-\frac{T}{\tau}} \right) + e^{-\frac{2}{\pi} KT} \right\} \right],$$

for $\frac{8}{\pi}K\tau \ll 1$... (4.9)

and for the case when $8/\pi K\tau \gg 1$

$$\frac{\Omega}{K} \cong \frac{1 - \left[\cos \left(\sqrt{\frac{2}{\pi}} K\tau \frac{T}{\tau} \right) + \sin \left(\sqrt{\frac{2}{\pi}} K\tau \frac{T}{\tau} \right) \right] e^{-T/2\tau}}{1 + \left[\left(\frac{4}{\pi} K\tau - 1 \right) \sin \left(\sqrt{\frac{2}{\pi}} K\tau \frac{T}{\tau} \right) - \cos \left(\sqrt{\frac{2}{\pi}} K\tau \frac{T}{\tau} \right) \right]} \quad \dots (4.10)$$

FILTER WITH FINITE HIGH FREQUENCY GAIN

In this sub-section carrier locking equation for the APC circuit with a low-pass filter with finite high frequency gain will be derived. This is based upon the reasonable assumption, although not a very accurate one, that at the end of the on-period of the input wave the instantaneous phase-difference ϕ attains a steady state value. The governing equations of such an APC circuit are given by (see Appendix B)

$$\frac{d\phi}{dt} \cong \Omega - \frac{2}{\pi} K \cdot \frac{1+xp\tau}{1+(1+x)p\tau} \cdot \phi \quad \dots (4.11)$$

$$\frac{d\phi}{dt} \cong \Omega - \frac{2}{\pi} \frac{x}{1+x} K\phi - \frac{2}{\pi} \left[\frac{\pi}{2} \frac{\Omega}{K} - \frac{x}{1+x} \phi(T) \right] e^{-\frac{t-T}{(1+x)\tau}}$$

The solution of Eq. (4.11) can be written for the case when

$$\frac{8}{\pi}(1+x)K\tau > (1 + \frac{2}{\pi} xK\tau)^2 \text{ as} \quad \dots (4.12)$$

$$\phi \cong \frac{\pi}{2} \frac{\Omega}{K} + C e^{-\alpha t} \sin(\beta t + \theta) \quad \dots (4.13)$$

where C and θ are constants to be determined from the boundary conditions, namely, at time $t = 0$, $\phi = \phi_0$ and at time $t = T$, $\frac{d\phi}{dt} = 0$, α and β are given by

$$\alpha = \frac{1 + \frac{2}{\pi} xK\tau}{2(1+x)\tau}$$

$$\beta = \frac{\sqrt{\frac{8}{\pi} (1+x)K\tau - (1 + \frac{2}{\pi} xK\tau)^2}}{2(1+x)\tau} \quad \dots (4.14)$$

The instantaneous value of the phase difference during the off-period of the signal is given by

$$\phi \simeq \frac{\pi}{2m} \cdot \frac{\Omega}{K} + \left[\Omega - \frac{2}{\pi} mK\phi(T) \right] \left[(1+x)\tau - \frac{\pi}{2mK} \cdot e^{-\frac{2}{\pi} mK\tau} \right] e^{-\frac{2}{\pi} mKt} - (1+x)\tau \left[\Omega - \frac{2}{\pi} mK\phi(\tau) \right] \exp \left(\frac{2}{\pi} mK\tau - \frac{t-\tau}{(1+x)\tau} \right), \quad \dots \quad (4.15)$$

where m is the ratio of a.c. to d.c. gain of the filter network. Comparing (4.13) Eq. (4.14) one can write the carrier locking equation as

$$\frac{\pi}{2} \simeq \frac{\pi}{2m} \cdot \frac{\Omega}{K} + \left[\Omega - \frac{2}{\pi} mK\phi(T) \right] \left[(1+x)\tau - \frac{\pi}{2mK} e^{-\frac{2}{\pi} mK\tau} \right] e^{-\frac{2}{\pi} mKt} - (1+x)\tau \left[\Omega - \frac{2}{\pi} mK\phi(T) \right] \exp -\frac{2}{\pi} mK\tau - \frac{T(1-n)}{(1+x)\tau} \quad (4.16)$$

Although it is not very difficult to find an expression for the locking ratio (Ω/K) in terms of the system parameters from Eq. (4.16) it is considered reasonable to mention the conclusion of the analysis which are evident from Eq. (4.16), viz., (i) the locking ratio (Ω/K) will increase with increasing value of the repetition frequency (f), (ii) it (Ω/K) will also increase with increasing value of the duty cycle (n).

SIDE-BAND LOCKING—SIMPLE APC CIRCUIT

In this section locking phenomena in a simple APC circuit with respect to sideband components of the input signal will be discussed. Following Fraser's argument (Fraser, D. W., 1957) it is easy to show that the synchronisation of local oscillation with any one of the sideband components is feasible. It seems that locking can be achieved with a few of the sideband components around the carrier if the incoming signal to noise ratio is not high. This is because of the fact that for higher order sideband components locking range will be correspondingly small—not only because of the low value of the particular synchronising component of the input signal but also due to the effect of the $R-C$ time constant of the self-bias circuit of the oscillator (op. cit. 2). Thus for synchronisation with higher order sideband components it is logical to expect that the local oscillator due to its inherent phase jitter may sometimes step out of synchronism with respect to the particular higher order spectral component of the input signal. In view of the above fact is preferable to use a tunable high Q circuit to be followed by the APC circuit as shown in fig. 2. As the input to the high Q tuned circuit consists of a series of pulsed sinusoid so the input to the APC circuit consists of the required sideband component to which the high Q circuit has been tuned plus a few side-

band components. For practical purposes one can ignore the effect of all the sideband components on the locking behaviour of the APC circuit except two adjacent

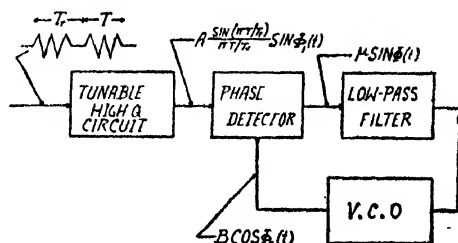


Fig. 2. Block diagram of an APC circuit preceded by a tunable high Q circuit. The high Q circuit has been assumed to be tuned to the first order sideband of the input interrupted sinusoids of on-period T , seconds and repetition period Tr seconds.

components around the tuned component. Therefore, care should be taken to see that frequency of the local oscillator lies comparatively close to that of the wanted component of the input spectrum; otherwise, the local oscillator may unnecessarily be pulled towards the unwanted component. In this section techniques of sideband locking of an APC circuit preceded by a high Q tuned circuit will be discussed.

Let us suppose that the carrier amplitude in relation to the duty cycle of the interrupted wave is chosen in such a way that the locking range due to the carrier component is not greater than half the repetition rate of interruption of the input wave. Let us consider the case of locking the local oscillator with the help of the first order upper sideband component of the input wave. In this case a sort of unwanted pulling of the local oscillator as stated elsewhere in the text may occur either due to the carrier component or to second order upper sideband component. Thus when the frequency of the local oscillator lies in between the carrier component and the first order upper sideband component, the governing equation of the loop can be written as

$$\frac{d\phi_{1u}}{dt} = \Omega_{1u} - xK \sin \phi_{1u} \quad \dots (5.1)$$

and

$$\frac{d\phi_{cu}}{dt} = \Omega_{cu} - y_{cu} K \sin \phi_{cu} \quad \dots (5.2)$$

where ϕ_{1u} and ϕ_{cu} are respectively the phase difference of the local oscillator of instantaneous angular frequency ω_{10} with respect to the first order upper sideband component and the carrier component and

$$x = \frac{\sin\left(\frac{\pi T}{Tr}\right)}{(\pi T/Tr)}, y_{cu} = \frac{(T/Tr)}{\sqrt{1 + 4Q^2\left(\frac{\omega_r}{\omega_c - \omega_r}\right)^2}} \quad \dots (5.3)$$

Again the corresponding loop equation for the case when the frequency of the local oscillator lies between the first order upper sideband component and the second order upper sideband component of the input wave can be written as

$$\frac{d\phi_{1u}}{dt} = \Omega_{1u} - xK \sin \phi_{1u}, \quad \dots (5.4)$$

and

$$\frac{d\phi_{2u}}{dt} = \Omega_{2u} - y_{2u} K \sin \phi_{2u}, \quad \dots (5.5)$$

where ϕ_{2u} is the phase difference of the local oscillator with respect to the second order upper sideband component of the input wave and

$$y_{2u} = \frac{\sin\left(\frac{2\pi T}{T_r}\right) / \left(\frac{2\pi T}{T_r}\right)}{\sqrt{1 + 4Q^2 \left(\frac{\omega_r}{\omega_c - \omega_r}\right)^2}} \quad \dots (5.6)$$

Now for the case when the frequency of the local oscillator lies between the carrier and the first order upper sideband, in order to avoid pulling by the carrier component, it is desirable to satisfy the following conditions

$$\begin{aligned} \Omega_{1u} &< xK, \\ \Omega_{cu} &> y_{cu}. \end{aligned} \quad \dots (5.7)$$

Similarly for the case when the frequency of the local oscillator lies between the first order and second order upper sideband components of the input wave it is advisable to choose the loop parameters in such a way as to satisfy the following conditions

$$\begin{aligned} \Omega_{1u} &< xK, \\ \Omega_{2u} &> y_{2u}K \end{aligned} \quad \dots (5.8)$$

Therefore, the maximum possible locking range for the first order sideband component is given by

$$\Omega_{1u} \simeq K \frac{\sin\left(\frac{\pi T}{T_r}\right)}{(\pi T/T_r)} \quad \dots (5.9)$$

APC CIRCUIT INCORPORATING A LOW-PASS FILTER AND PRECEDED BY A HIGH Q TUNED CIRCUIT

In this section the effect of incorporating a low-pass filter in the loop on the sideband locking behaviour of an APC circuit when it is preceded by a tunable high Q circuit will be discussed. Inclusion of the low-pass filter in the loop will,

however, introduces the so-called pull-in phenomena (Chakrabarti, *et al.* 1964). The response to transients may no longer be deadbeat even if the initial difference frequency lies within the locking range and instantaneous frequency may drift a few beat cycles of continuous decreasing frequency till equilibrium is reached. It has been shown (op. cit.) that in such a case the locking range of the APC circuit depends on the average gain of the filter network over the range d.c. to open loop frequency difference. Analytical expressions of locking range for different components can be written as

$$\Omega_{1u} \simeq K \frac{\sin \left(\frac{\pi T}{T_r} \right)}{\frac{\pi T}{T_r}} \bar{G}(\Omega_{1u}), \quad \dots (6.1)$$

$$\Omega_{2u} \simeq y_{2u} \bar{G}(\Omega_{2u}), \quad \dots (6.2)$$

$$\Omega_{cu} \simeq y_{cu} G(\Omega_{cu}) \quad \dots (6.3)$$

Therefore following the arguments of section 5, one can show that either of the following conditions is to be satisfied in order to avoid unnecessary pulling by the unwanted component

$$x \bar{G}(\Omega_{1u}) > y_{2u} \bar{G}(\Omega_{2u}) \quad \dots (6.4)$$

$$x \bar{G}(\Omega_{1u}) > y_{cu} \bar{G}(\Omega_{cu}) \quad \dots (6.5)$$

EXPERIMENTAL SET UP AND RESULTS

In this section we shall describe experimental set-up and discuss the experimental results in relation to the conclusions of the analysis presented in the text.

Fig. 3 shows the experimental set-up for taking measurements on the variation of locking range with the duty cycle of the input interrupted wave and for the

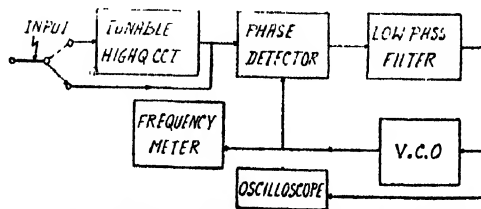


Fig. 3. Experimental set-up for taking measurements on the performance of the APC circuit with respect to an input interrupted sinusoids. For sideband locking the switch is to be placed at the dotted position.

side-band locking high Q -tuned circuit is to be used before the conventional APC loop. The circuit diagram of the high Q -tuned circuit is shown in the

Fig. 4. The interrupted wave is obtained by means of an electronic switch. As discussed in the text in order to observe accurately the phenomenon of

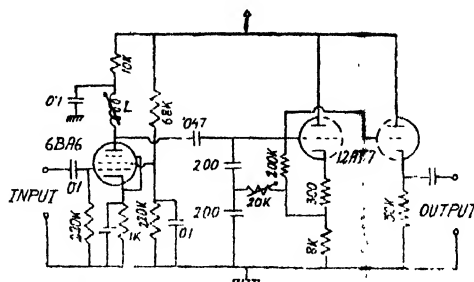


Fig. 4. The circuit diagram of a tunable high Q circuit. Tuning can be adjusted by the variable inductance L and the Q value of this tuned circuit can be continuously adjusted by the 20K potentiometer. In practice this 20K potentiometer consists of two potentiometers—one for coarse control and the other for fine adjustment.

sideband locking of the voltage controlled oscillator it is necessary that the locking range of the VCO for sideband component with respect to half the separation between the sidebands should be small. This, in effect, requires that the frequency stability of the local oscillator should be good. For this reason a Clapp's oscillator with a varactor (V 33) for its control of frequency has been used for the observation of sideband locking. Otherwise, there is possibility that the system may fall out of synchronism with respect to the particular sideband component of the input signal. This is because of the fact that the locking range of the particular sideband component is required to be small in order to avoid unnecessary pulling by the neighbouring sideband component. Thus the frequency instability of the local oscillator must be small compared to the locking range of the system for the particular sideband component of interest. The local oscillator with the varactor (V-33), which is known to have a reasonable frequency stability, is shown in Fig. 5. Care should be taken to see that the input amplifier feeding the phase detector should have a flat top response. Presence

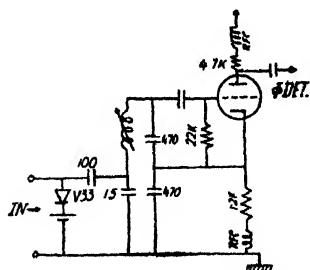


Fig. 5. A typical circuit diagram of a Clapp's oscillator with the varactor diode V-33 connected (with proper bias voltage) across the 15 pF capacitor for controlling the instantaneous frequency of the oscillator by means of a d.c. voltage to be applied in between the input terminals,

of dip anywhere in the characteristics may give rise to suprious effects (Biswas, 1964).

Fig. 6. shows the variation of the locking range with the ratio of the on-period to the off-period for two different carrier levels. From this curve one can conclude

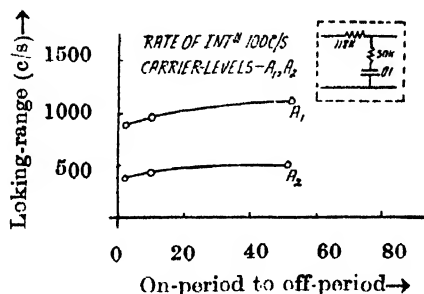


Fig. 6. Graphical representation of the variation of the locking range of the APC circuit with ON-OFF ratio of the input interrupted wave having carrier levels A_1 and A_2 and a repetition rate of 100 c/s. A_1 is greater than A_2 . The filter network of the APC loop is inset in the figure.

that the locking range of the phase locked oscillator with an interrupted wave input approaches to that of the phase locked oscillator with a CW input. Fig. 7

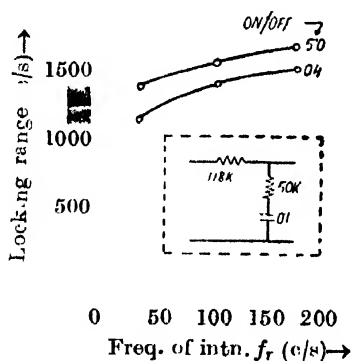


Fig. 7. Graphical representation of the dependence of the Locking Range of the APC circuit on the variation of the Frequency of interruption of the input wave for two different values of the on-off ratios of the input wave. The filter network is inset in the diagram.

gives a graphical representation of the variation of the locking range with repetition rate of the input wave for two different values of the duty cycle of the input. It is to be noted that these results are in good agreement with the conclusions of the analysis of section 4.2. The experimental results regarding the sideband locking of the phase locked oscillator is shown in the following Table I.

TABLE I

Centre frequency of the reference input 410 Kc/s; on/off ratio of the input wave is unity

Detuning of the reference input	Observed repetition frequency for locking	Inference from the observation for sideband locking experiment for different values of the carrier levels
+ 1000 cycles/second	Nearly 1000 cycles/sec.	The sideband locking experiment has been repeated for different carrier levels and it has been found that lower carrier levels give better results on the observation of sideband locking.
+ 750 cycles/second	Nearly 750 cycles/sec.	

CONCLUSIONS

The phenomenon of locking of an APC circuit with an interrupted wave have been discussed fully. Locking range equation (vide Eq. 3.11, Eq. 4.10 and Eq. 4.16) have been derived. These equations are simple as such simple analytical or graphical solutions are possible. Experimental results presented in this paper give an useful information regarding the variation of locking range of the VCO with the duty cycle of the input wave and the phenomenon of sideband locking technique of the APC circuit when it is preceded by a high Q tuned circuit. Experimental results are in good agreement with the simplified analysis presented in text. It has been found that the synchronisation of the local oscillator with any of the sideband components of the input wave becomes easier when it is preceded by a high Q tuned circuit.

ACKNOWLEDGEMENT

The author is greatly indebted to Prof. N. B. Chakrabarti of the Indian Institute of Technology, Kharagpur for suggesting the problem and supervision of work. The author takes the opportunity of thanking Prof. J. N. Bhar of the Institute of Radio Physics and Electronics, the University of Calcutta for providing the author with all the research facilities. The author wishes to thank Mr. A. K. Datta for helpful discussions.

REFERENCES

- Biswas, B. N., 1964, *Symposium on Telecommunications and Electronics*, held at the Institute of Radio Physics & Electronics, University of Calcutta, Feb. 27-28.
- , 1964, *Indian J. Phys.*, **38**, 561.
- Chakrabarti, N. B., and Biswas, B. N., 1964, *Indian J. Phys.*, **38**, 148.
- Fraser, D. W., 1957, *Proc. I.R.E.*, **44**, 1257.
- Richman, D., 1954, *Proc. I.R.E.*, **42**, 106.

APPENDIX

A. *Derivation of the Loop Equation of the APC circuit with a Low Pass Filter with No Limiting High Frequency gain during the off-period of the Input Wave*

On comparison of Eq. (2.3) with Eq. (2.4) one can write for the output of the low pass filter with no finite high frequency gain at the end of the on-period of the input wave as

$$e_d(t) = \frac{e^{-t/\tau}}{\tau} \int_0^{\tau} e^{t_1/\tau} e(t_1) dt_1, \\ \simeq \frac{2}{\pi} \frac{\mu}{\tau} e^{-t/\tau} \int_0^{\tau} \phi(t_1) e^{t_1/\tau} dt_1. \quad \dots \quad (\text{A.1})$$

Comparing Eq. (A.1) with Eq. (4.2) and Eq. (4.3) one can show that it can be written as

$$e_d(t) \simeq \frac{2}{\pi} \mu e^{-t/\tau} \left[\frac{\pi}{2} \frac{\Omega}{K} \frac{T}{\tau} + \frac{\pi}{2K\tau} \left\{ \left(\phi_0 - \pi/2 \right) \frac{\Omega}{K} + \Omega\tau \right\} \right]$$

for $\frac{8}{\pi} K\tau < 1$... (A.2)

and

$$e_d(t) \simeq \mu e^{-t/\tau} \left[\frac{\Omega}{K} \left(e^{\frac{T}{\tau}} - 1 \right) + \frac{4C e^{-\frac{T}{2\tau}}}{\pi \sqrt{\frac{2}{\pi} K\tau}} \sin \left(\sqrt{\frac{8}{\pi} K\tau} \frac{T}{2\tau} + \theta - \tan^{-1} \sqrt{\frac{8}{\pi} K\tau} \pi \right) \right. \\ \left. + \frac{4C}{\pi \sqrt{\frac{2}{\pi} K\tau}} \sin \left(\tan^{-1} \sqrt{\frac{8}{\pi} K\tau} - \theta \right) \right], \text{ for } \frac{8}{\pi} K\tau > 1 \quad \dots \quad (\text{A.3})$$

Substitution of $e(t)$ from (A.2) and (A.3) in Eq. (2.2) yields the loop equation for the off-period of the input signal for the APC circuit with the low-pass filter.

B. *Derivation of the Governing Equation of the Loop during the off-period of the Input wave for the Filter with finite high Frequency Gain*

Let us consider the low pass filter with limiting high frequency gain as shown in Fig. In this way it can be shown that the impulse response of the network is given by

$$f(t) = \frac{x}{1+x} \delta(t) + \frac{1}{\tau(1+x)^2} \exp \left(-\frac{t}{(1+x)\tau} \right), \quad \dots \quad (\text{B.1})$$

where $\delta(t)$ is the Dirac's delta function. Therefore the output of the filter at the end of the on-period of the filter network is given by

$$e_d(t) \cong \mu \frac{2}{\pi} \frac{x}{1+x} \phi(t) + \frac{2}{\pi} K_1 \exp \left(- \frac{t}{(1+x)\tau} \right), \quad \dots \quad (\text{B.2})$$

where K_1 is a constant to be found from the boundary condition. Therefore the governing equation of the loop during the off-period is given by

$$\frac{d\phi}{dt} = \Omega - \frac{2}{\pi} K_1 \frac{x}{1+x} \phi(t) - \frac{2}{\pi} K K_2 \exp \left(- \frac{t}{(1+x)\tau} \right), \quad \dots \quad (\text{B.3})$$

where K_2 is a constant to be determined from the boundary condition at time $t = T$,

$$\frac{d\phi}{dt} = 0.$$

Letters to the Editor

The Board of Editors does not hold itself responsible for opinions expressed in the letters published in this section. The notes containing short reports of original investigations communicated to this section should not contain many figures and should not exceed 500 words in length. The contributions reaching the Secretary by the 15th of any month may be expected to appear in the issue for the next month. No proof will be sent to the author.

3

CHERENKOV RADIATION BY LINE CHARGE

R. M. KHAN

CITY COLLEGE, CALCUTTA.

(Received August 23, 1966)

Problems of Cherenkov radiation of various aspects have been investigated in many papers. These are mainly concerned with the motion of a point charge or a beam of electrons. This paper deals with the case in which radiation is produced by a line charge rather than a point charge or a beam of electrons. The line charge consists of a continuous line density α moving with a constant velocity v perpendicular to the line within a dielectric medium. The medium is assumed to be a perfect dielectric and the absorption of radiation, dispersion and scattering are ignored. The medium is unbounded, so the sweeping plane is infinite.

Let the line charge be parallel to z axis and moving along the y axis. Maxwell's equations for field variables E and H after expanding in Fourier series (e.g.)

$$E = \int_{-\infty}^{\infty} E_{\omega} e^{i\omega t} d\omega, \dots \text{ are}$$

$$\left. \begin{aligned} \text{rot } H_{\omega} &= \frac{i\omega n^2}{c} E_{\omega} + \frac{4\pi}{c} j_{\omega} \\ \text{rot } E_{\omega} &= -\frac{i\omega}{c} H_{\omega} \\ \text{div } E_{\omega} &= \frac{4\pi}{n^2} \rho \\ \text{div } H_{\omega} &= 0, \end{aligned} \right\} \dots \quad (1)$$

where n is the refractive index of the medium at the frequency ω , c is the velocity of light, j is the current density and ρ is the density of free charges.

Introducing vector and scalar potentials A and ϕ we have

$$\nabla^2 A_u + \frac{n^2 \omega^2}{c^2} A_u = -\frac{4\pi}{c} j_u \quad \dots (2)$$

with the conditions

$$\left. \begin{aligned} H_w &= \text{rot } A_w \\ E_w &= -\frac{i\omega}{c} A_w - \text{grad } \phi_w \\ \text{div } A_w + \frac{i\omega n^2}{c} \phi_w &= 0 \end{aligned} \right\} \quad \dots (3)$$

Here $j_x = 0 = j_z$ and $j_y = \alpha v \delta(x) \delta(y - vt)$

$$\therefore j_y(\omega) = \frac{\alpha}{2\pi} \delta(x) e^{-i\omega \frac{y}{v}} \quad \dots (4)$$

From symmetry the motion is independent of z .

$$\text{Taking } A_x = 0 = A_z \text{ and } A_y = u(x) e^{-\frac{i\omega y}{v}} \quad \dots (5)$$

We obtain from (2)

$$\frac{\partial^2 u}{\partial x^2} + s^2 u = -\frac{2\alpha}{c} \delta(x) \quad \dots (6)$$

$$\text{where } s^2 = \frac{\omega^2}{v^2} (n^2 \beta^2 - 1), \quad \beta = \frac{v}{c}.$$

If $s^2 < 0$ the equation (6) does not contribute any wave solution. If $s^2 > 0$, i.e. the velocity of the line charge is greater than the phase velocity of light in the medium, then

$$u = B e^{-s x} \quad \text{when } x > 0$$

$$\text{and } u = B' e^{s x} \quad \text{when } x < 0 \quad \dots (7)$$

where B and B' are constants.

Considering the singularity at $x = 0$,

$$B = -\frac{i2\alpha}{cs} \quad \dots (8)$$

$$\therefore A_y(\omega) = -\frac{i2\alpha}{cs} e^{-isx - i\frac{\omega}{v}y + i\omega t} \text{ when } x > 0.$$

In this case

$$\left. \begin{aligned} H_z(w) &= -\frac{2\alpha}{c} e^{-isx - i\frac{\omega}{v}y + i\omega t} \\ E_x(w) &= \frac{2\alpha}{vn^2} e^{-isx - i\frac{\omega}{v}y + i\omega t} \\ E_y(w) &= -\frac{2\alpha s}{\omega n^2} e^{-isx - i\frac{\omega}{v}y + i\omega t} \end{aligned} \right\}$$

$$\left. \begin{aligned} ReH_z &= -\frac{4\alpha}{c} \int_0^{\infty} \cos \chi \, dw \\ ReE_y &= -4\alpha \int_0^{\infty} \frac{s}{\omega n^2} \cos \chi \, dw \end{aligned} \right\}$$

where

$$\chi = w \left\{ t - \left(\frac{sx}{w} + \frac{y}{v} \right) \right\}$$

when

$$x < 0,$$

$$H_z(\omega) = \frac{2\alpha}{c} e^{isx - i\frac{\omega}{v}y + i\omega t}$$

$$E_x(\omega) = -\frac{2\alpha}{vn^2} e^{isx - i\frac{\omega}{v}y + i\omega t}$$

$$E_y(\omega) = -\frac{2\alpha s}{\omega n^2} e^{isx - i\frac{\omega}{v}y + i\omega t}$$

CONCLUSION

(i) Equation (9) and (11) reveal that outgoing plane waves are propagating when $s > 0$. At a particular frequency planes are parallel to $sx + \frac{\omega}{v}y = 0$

and $sx - \frac{\omega}{v}y = 0$.

(ii) Radiation is confined between two planes perpendicular to the above planes similar to cone as in the case of a point charge. The angle between the planes of radiation is $2 \cos^{-1} \frac{1}{\beta n}$ which is identical with the Cherenkov relation.

(iii) Cherenkov radiation per unit time is

$$\begin{aligned} \frac{dw}{dt} &= 2 \int_{-\infty}^{\infty} \frac{c}{4\pi} [EH] dy \\ &= \frac{c}{2\pi} \int_{-\infty}^{\infty} (Re H_z \cdot Re E_y) dy \\ &= 8\alpha^2 \int_0^{\infty} \frac{1}{n^2} \sqrt{n^2 \beta^2 - 1} d\omega \end{aligned}$$

Thus per unit of frequency interval the amount of radiation is $\frac{8\alpha^2}{n^2} \sqrt{n^2 \beta^2 - 1}$.

It is interesting to note that the whole of the frequency dependence is via n .

ACKNOWLEDGMENT

I thank Dr. T. C. Roy, Jadavpur University, for encouragement in the preparation of this paper.

STUDY OF HYDROGEN BONDING IN 2,4- AND 3,5-XYLENOL

S. B. BANERJEE AND D. K. MUKHERJEE

OPTICS DEPARTMENT,

INDIAN ASSOCIATION FOR THE CULTIVATION OF SCIENCE,
CALCUTTA-32.*(Received February 6, 1967)*

Intermolecular hydrogen bonding exhibited by xyenols in different solvents was studied by infrared spectroscopy in the $700\text{--}1600\text{ cm}^{-1}$ region by Neuilly (1954) and by n.m.r. spectroscopy by Yamaguchi (1961), who noted that xyenols with one or more methyl group in the ortho position with respect to the OH group show weaker intermolecular hydrogen bonding than other xyenols. The difference in properties of xyenols was also commented on by Sears and Kitchen (1949), Buckingham (1960), Schaefer and Schneider (1960) and Bono (1956). The infrared absorption spectra of xyenols in different solutions in the fundamental OH frequency region were not apparently reported by any previous worker and an investigation was undertaken to record and compare the positions of OH stretching vibrational bands of xyenols in different environments in order to find out any evidence of difference in the hydrogen bonding behaviour of these compounds. In the present note preliminary results obtained in the case of 2, 4- and 3, 5-xyenol have been reported.

The spectra were measured with a Perkin Elmer Model 21 Spectrophotometer with rock salt optics and calibration of spectra was made by recording the 3741 cm^{-1} absorption band of atmospheric water vapour. The xyenols and the solvents used were carefully purified and dehydrated. The accuracy of measurement in the position of the bands is $\pm 5\text{ cm}^{-1}$.

The wave numbers of the OH vibrational bands due to 2, 4- and 3, 5-xyenol in the pure state and in different solvents are given in Table I. The infrared spectra of dilute solutions of 3, 5- and 2, 4-xyenol in CCl_4 show the free OH vibrational bands at 3622 and 3623 cm^{-1} respectively. In solution in benzene the band maximum shifts by about 57 cm^{-1} in the case of 3, 5-xyenol and about 45 cm^{-1} in the case of 2, 4-xyenol towards lower frequencies. This seems to indicate that in these cases some weak but definite intermolecular association takes place between molecules of xyenols and benzene, which is a π -electron donor, through the OH group and the π -electron.

In solutions in dioxane, ether and nitrobenzene, 3, 5-xyenol shows intermolecular hydrogen bonding of different strengths with proton acceptor groups in the solvents through the OH group, as is evident from the shift of the OH band

from 3622 cm^{-1} in CCl_4 solution to 3340, 3345 and 3495 cm^{-1} respectively. Similar intermolecular hydrogen bonding is also exhibited by 2, 4-xyleneol in which case the OH band shifts from 3623 cm^{-1} in CCl_4 solution to 3370, 3370 and 3518 cm^{-1} in solutions in dioxane, ether and nitrobenzene, respectively. The shifts in the OH vibrational band of 3, 5-xyleneol in different solvents with respect to its

TABLE I
Position of OH vibrational band in cm^{-1}

Substance	Solution in						Pure
	carbon tetra chloride	chloroform	dioxane	ether	nitro benzene	benzene	
2, 4-Xyleneol	3623	3613	3370	3370	3518	3578	3418
3, 5-Xyleneol	3622	3611	3340	3345	3495	3565	3330*

*solid

position in the CCl_4 solution are thus larger than those observed in the case of 2, 4-xyleneol. This may be due to the fact that in the latter molecule the CH_3 group which is in 2-position sterically hinders the OH group and affects the hydrogen bonding situation as suggested by Yamaguchi (1961) from n.m.r. studies. The corresponding shifts of the OH band in the cases of crystals of 3, 5-xyleneol and the liquid film of 2, 4-xyleneol indicate formation of intermolecular hydrogen bond in these states of aggregation also. The comparatively large shift in the case of 3, 5-xyleneol in the solid state probably indicates presence of polymeric groups of intermolecularly associated molecules formed through $\text{OH}\cdots\text{O}$ bonds.

Further detailed study with these and other xyleneols is in progress.

The authors are grateful to Professor S. C. Sirkar, D.Sc., F.N.I. for helpful discussions and to Professor G. S. Kastha, D.Sc., for kindly providing laboratory facilities. One of the authors (S.B.B.) acknowledges financial support by the C.S.I.R. (India) as a Pool Officer.

REFERENCES

- Bono, D., 1956, *Bull. Soc. Chim. France*, 1368.
 Buckingham, A. D., 1960, *Canadian J. Chem.*, **38**, 300.
 Neuilly, M., 1954, *Comp. rend.*, **238**, 781.
 Schaefer, T. and Schneider, W. G., 1960, *J. Chem. Phys.*, **32**, 1218.
 Sears, W. C. and Kitchen, J., 1949, *J. Am. Chem. Soc.*, **71**, 4110.
 Yamaguchi, I., 1961, *Bull. Chem. Soc.*, Japan, **34**, 744.

BOOK REVIEWS

FUNDAMENTALS OF MECHANICS—by Rais Ahmed, pp-235. price Rs. 15/- Asia Publishing House.

The small book on mechanics meant for Higher Secondary or Pre-University classes of the Indian Universities is written in usual American style, but thoroughly Indianized for the better understanding of Indian students. The English is indeed very simple, and conversational justifying the authors claims. But the introduction to units is too verbose considering the size of the book scarcely any justice has been done to fundamental instruments of measurement. The point on the accuracies of the instruments, which beginners quite often miss, has not been well made. The picture of sliding vernier calipers has been simply titled "The vernier", the micrometer screwgauge as simply "The micrometer". Thus many of the picture titles are insufficient and inaccurate and likely to be confusing *e.g.* fig. 3.1 "Approximate motion of a table" in the class room". That is meant perhaps is the motion relative to a fixed coordinate system in space. Fig. 3.2 "Motion of rigid body. All particles move the same distance with the same velocity". Obviously, again, a translational motion is meant. Such imperfect ideas as the titles indicate, inculcated in the tender minds may be dangerous for the future, mental get up as a physicist. Moreover, the "conversational approach" of the author has allowed a number of serious inexactness in definition and loose talk creep in on pp. 16, 17, 22, *e.g.* definitions of motion, speed velocity etc., "direction of angular speed" etc. On wonders on reading the statement (page 139): "raw material+energy=finished product", whether raw material—energy will be=unfinished product'.

The book bristles with such queer statements and one cannot recommend the book to the students.

A. Bose

CRYOPHYSICS -by K. Mendelssohn. Pp. 183 price cloth : \$ 4.50, paper \$ 2.50 Interscience Publishers Inc.

The author a veteran in the field of cryophysics is essentially a physicist and his aim in this small book is to raise before the readers a clear physical picture of the outstanding phenomena occurring at Low temperatures which have shock the foundations of Solid State Physics, laid down these very foundations. Time and again we come across in his writing, a new angle of observation, and a simple way of putting a complex phenomenon before the reader and what can be more apt than the very opening lines of the Introduction pointing to the crux of cryophysics.

The small section on cryogenics is nevertheless a compendium of all major and most modern cryogenic desires and informations. One may not, however, agree with the statement that $J-T$ method is generally used for liquefaction of H_2 because of the fear of explosion hazard; since all the hazard is already present in compressing H_2 and otherwise handling it, whichever method is adopted. A mention of spin lattice relaxation phenomenon would have been appropriate in connection with the magnetic cooling method.

In the chapter on thermometry, the paragraph on direct calibration of T^* against, would be better placed later, *i.e.* after a more basic method of comparing the magnetic scale to the thermodynamic scale has been discussed.

On page 52, it may suit for some purposes to speak that "In many cases especially in magnetically dilute salts Curie's Law has been found valid over a wide temperature range". But one actually finds that Curie's Law is an ideal case more observed in its breach than validity.

Apart from exchange interaction such deviations may arise from ligand field splittings of the ground level and is often present.

It is indeed at the extreme low temperature, where saturation effect is prominent that the deviation from Curie Law is also prominent, thus complicating the issue.

However, since the sp. heat anomalies corresponding to ligand field effects are usually of the Schottky type and the book is too small for niceties the author is justified in making certain approximations in his statements.

It is often sufficient to discuss the thermal variation of properties of the limiting cases of a theory e.g. the magnetic susceptibility, sp. heat, thermal conductivity etc. This may however sometimes prove to be limited particularly when the interaction are often dependent on temperature and on impurities or lattice defects. What happens in the intervening regions is then much more interesting than the limiting ranges.

The chapters on superconductivity and Helium Problem contain a wealth of information on these two baffling problems in cryophysics. This small book has no doubt made a very usefully place for itself in all Physics Libraries.

A. Bose

HANDBOOK OF VACUUM PHYSICS Edited by A. H. Beck. Vol. 1. Gases and Vacua; parts 1-3—Pp. 208, price 40s net. Pergamon Press.

This is not a hand book in the German sense, but is a handy book of reference for vacuum technicians. It does not deal with the fundamental theories or descriptions of vacuum processes and gives only the barest mention of some of these and is therefore not meant for a beginner or even a half backed research worker referring to vacuum technology as a side line. On the other hand it discusses in quite details working formulae for vacuum pumps and allied set ups, and gives a wealth of technical data for different commercially available pumps and vacuum materials.

The working formulae for vacuum pumps and vacuum systems including systematic leak detection programmes will be of considerable help to vacuum technologists, but for research laboratories facing daily problems in maintaining high vacua on moderate scale. I would still prefer some book giving lots of practical hints in vacuum practice, and including good details of a number of modernised vacuum pumps circuits, gadgets, leak detectors etc.

The book contains three longish articles by specialists on (1) Vacuum technology as applied to continuously pumped system (2) Properties of high vacuum pumps and design of vacuum pumping systems and (3) Leak detection and detectors.

The section on ion-pumps, getter pumps sorption-pumps and cryo-pumps is interesting, but again exasperatingly lacks in details. Several technical terms used in the book with hardly any explanation of the meaning. The author evidently assumes that all the readers have the necessary technological knowledge.

TABLE OF SINES AND COSINES TO TEN DECIMAL PLACES AT THOUSANDTHS OF A DEGREE—By H. E. Salzer and N. Levini, Pergamon Press, 1962, Price \$ 10.

This good sized volume may be considered as a standard table of references for sines and cosines and represents the results of an enormous amount of patient, laborious and accurate computation. Those of us, who are accustomed to using trigonometrical tables upto four or five significant figures at no more than 1 minute interval will hardly want to touch this volume with a pair of tongs. But to a large number of computationists in the field of

space technology not too speak of astronomy, geodesy etc. the book will prove to be invaluable, since it strikes a golden mean and fills up a gap in the existing standard tables which either go to too many decimal places without the necessary accuracy in interpolation or go to too few decimal places with too great fractional interpolation. Through other trigonometrical ratios could not be included in the book this is obviously not a fundamental need. Together with the explicit instructions for interpolations, direct and inverse, illustrated by examples, the book is sure to be of the utmost use to mathematicians, physicists and technicians alike in the field intended.

A. Bose

THEORY OF ELASTICITY—By M. Filonenko - Borodich p.p. 387 Price \$ 6/- Translated from Russian by M. Kohayeva. Foreign Languages Publishing House, Moscow.

Theory of elasticity has developed on a more or less purely mathematical basis from the time of its inception in 17th century and has become one of the most important of classical physico-mathematical formalising. Importance of elasticity in technological problems no doubt tended to develop it as a means of routine investigation of the elastic properties of constructional materials. But the attempts to correlate between bulk elasticity and molecular binding forces have been rather inconspicuous. The recognition of anisotropy in crystalline materials though further complicating the problem of elastic bodies, has done much to improve the liaison between theories of macroscopic and microscopic elastic forces in the solid state. However, the microscopic theory of elasticity, closely linked to the theory of thermal vibrations in solids, is the matter of discussion of a different nature and is not contemplated in the present book. The contents of the present book deals entirely with the classical theory of elasticity of solids, but deals with it in a very able and concise manner, explaining with sufficient working examples, each of the different methods and theorems employed in the sequence of development of the subject. It is of a necessity not as analytical or elaborate as Love's classical book, but takes many short cuts in the formalisms and assuming a sufficient knowledge of vectors and tensors in the reader. As such the book may be somewhat difficult for the honours class students to take in their first reading. Once over the initial hurdles of introduction into the subject *i.e.* for more advanced readers the book should prove to be very useful.

A. Bose

INDIAN JOURNAL OF PHYSICS

VOL. 41

No. 4

AND

VOL. 50

PROCEEDINGS

No. 4

OF THE

INDIAN ASSOCIATION FOR THE CULTIVATION OF SCIENCE

(Edited in collaboration with the Indian Physical Society).

APRIL 1967

PUBLISHED BY THE
INDIAN ASSOCIATION FOR THE CULTIVATION OF SCIENCE
JADAVPUR, CALCUTTA-32

MODIFIED VARSHNI-SHUKLA POTENTIAL FUNCTION FOR DIATOMIC ALKALI HALIDE MOLECULES

M. M. PATEL V. B. GOHEL* AND M. D. TRIVEDI*

PHYSICS DEPARTMENT, M. S. UNIVERSITY BARODA

(Received July 9, 1966).

ABSTRACT. The values of the rotational constants α_e , vibrational constants ω_e and $\omega_e x_e$ and dissociation energies have been calculated for eighteen diatomic alkali halide molecules by using modified form of the Varshni and Shukla potential function. The calculated values are in good agreement with the experimental values and the potential function is compared with the previously suggested potential function.

Different potential energy functions have been proposed for alkali halide diatomic molecules assuming the molecule to be constituted of ions. For earlier developments reference may be made to Rittner (1951) and Varshni (1957).

Rittner (1951) has presented a theory of alkali halide molecules in the spirit of the Born-Mayer lattice theory Varshni and Shukla (1961) have compared the following three functions :

$$U = -\frac{e^2}{r} + Be^{-r/\sigma} \quad \dots \quad \text{(Born-Mayer)} \quad \dots \quad (1)$$

$$U = -\frac{e^2}{r} - \frac{e^2(\alpha_1 + \alpha_2)}{2r^4} - \frac{2e^2\alpha_1\alpha_2}{r^7} - \frac{C}{r^6} + A \exp\left(\frac{-r}{\rho}\right) \quad \text{(Rittner)} \quad \dots \quad (2)$$

$$U = -\frac{e^2}{r} + P \exp(-kr^2) \quad \text{(Varshni-Shukla)} \quad \dots \quad (3)$$

B, σ, A, ρ, P and k are the constants α_1 and α_2 are the polarizability values of the ions.

By a comparative study of these functions Varshni and Shukla (1961) concluded that potential function (3) is superior to potential function (1) but slightly inferior to potential function (2).

However from the study of the calculated values of α_e , the rotational constant, and $\omega_e x_e$, the vibrational const., we have found that it is possible to account for α_e and $\omega_e x_e$ more satisfactorily, if we modify the Varshni and Shukla (1961) potential function. The modified form of the function is :

$$U = -\frac{e^2}{r} + P \exp(-kr^{3/2}) \quad \dots \quad (4)$$

*SHETH M. N. SCIENCE COLLEGE PATNA.

The constants P and k can be determined by using the following conditions :

$$\left(\frac{dU}{dr} \right)_{r=r_e} = 0 \quad \dots (5)$$

$$\left(\frac{d^2U}{dr^2} \right)_{r=r_e} = k_e, \quad \dots (6)$$

where k_e is the force constant and r_e is the equilibrium internuclear distance. The calculations for α_e and $\omega_e x_e$ and D_i the dissociation energies have been made. The method of calculating α_e and $\omega_e x_e$ has been explained by Varshni (1957-59). The relevant equations are :

$$\alpha_e = - \left[\frac{Xr_e}{3} + 1 \right] \frac{6B_e^2}{\omega_e} \quad \dots (7)$$

$$\omega_e x_e = \left[\frac{5}{3} X^2 - Y \right] r_e^2 \left(\frac{W}{\mu_A r_e^2} \right) \quad \dots (8)$$

where

$$W = 2.1078 \times 10^{-16},$$

$$X = U'''(r_e)/U''(r_e) \text{ and } Y = U^{IV}(r_e)/U''(r_e).$$

and

$$D_i = -U(r_e).$$

The experimental data are the same as those used by Varshni and Shukla (1961).

The values of α_e and $\omega_e x_e$ and D_i calculated by using the function (4) have been presented in tables I, II, and III. α_e and $\omega_e x_e$ and D_i values calculated by Varshni and Shukla (1961) from potential functions (2) and (3) have also been included in tables I, II, and III for comparison.

CONCLUSION

α_e : table (I) shows that a considerable improvement is obtained over the values calculated by using Varshni and Shukla potential function. In certain cases e.g. LiBr, NaCl, NaBr, NaI, KI etc., the values are rather better than the values calculated from Rittner's function. In some cases, the values are as good as those obtained from Rittners function.

However the proposed function is slightly inferior to Rittner's function in certain cases such as, RbCl, RbBr, etc. It is interesting to note that the proposed function fails miserably in the case of flourides. Excluding fluorides the percentage error is less than the Rittner's function.

TABLE I
 The rotational constants

Molecule	$\alpha_e \times 10^4$ obs. cm^{-1}	$\alpha_e \times 10^4$ Calc. Pot (2) cm^{-1}	% error	$\alpha_e \times 10^4$ Calc. Pot (3)	% error	$\alpha_e \times 10^4$ Calc. Pot (4)	% error
	(a)						
LiF	197.1	145.3	-26.3	100.7	-48.9	85.35	—
	(b)						
LiBr	56.41	50.41	-10.6	47.63	-15.6	57.33	+ 1.6
	(b)						
LiI	40.90	37.6	- 8.1	37.05	- 9.4	44.04	+ 7.7
	(b)						
NaCl	16.1	14.9	- 7.5	13.81	-14.2	16.04	- 0.4
	(b)						
NaBr	9.4	11.0	+17.0	8.45	-10.1	9.727	+3.5
	(b)						
NaI	6.5	7.67	+18.0	6.10	- 6.2	7.003	7.7
	(c)						
KF	23.35	19.91	-14.7	16.54	-29.2	2.015	—
	(b)						
KCl	7.90	7.70	-2.5	7.37	- 6.7	8.330	+ 5.4
	(b)						
KBr	4.05	3.87	- 4.4	3.67	- 9.4	4.185	+ 3.2
	(b)						
KI	2.70	2.51	- 7.0	2.37	-12.2	2.731	+1.1
	(d)						
RbF	15.18	14.40	- 4.5	13.61	-10.5	22.95	—
	(b)						
RbCl	4.50	4.42	- 1.8	4.29	- 4.7	4.833	+ 7.3
	(b)						
RbBr	1.86	1.83	- 1.6	1.80	- 3.2	2.033	+ 9.1
	(b)						
RbI	1.10	1.04	- 5.5	1.00	- 9.1	1.145	+ 3.6
	(b)						
CsF	11.00	12.49	+13.5	12.96	+17.8	14.34	—
	(b)						
CsCl	3.30	3.38	+ 2.4	3.41	+ 3.3	3.802	+15.16
	(b)						
CsBr	1.20	1.19	- 0.8	1.17	- 2.5	1.274	+ 6.2
	(b)						
CsI	0.68	0.75	+10.3	0.72	+ 5.9	0.8085	+17.65
Average %error excluding							
fluorides			7.0%		8%		6.4%

 (a) Vidale (1960) ; (b) Honig *et al.* (1954) ; (c) Green *et al.* (1958) ; (d) Lew *et al.* (1958),

TABLE II
The vibrational constants

Molecules	$\omega_e x_e$ est. Cm ⁻¹ .	$\omega_e x_e$ Calc. Pot. (2) cm ⁻¹	$\omega_e x_e$ Calc. Pot. (3) cm ⁻¹	$\omega_e x_e$ Calc. Pot. (4) cm ⁻¹
LiF	7.9(a)	6.896	6.62	4.826
LiRr	4.28(b)	3.66	4.12	4.373
LiI	3.35(b)	2.997	3.49	3.694
NaCl	2.05(b)	1.75	1.89	—
NaBr	1.50(b)	1.64	1.39	1.464
NaI	1.08(b)	1.25	1.10	1.163
KF	1.45(c)	1.99	1.96	2.075
KCl	1.30(b)	1.21	1.32	1.41
KBr	0.80(b)	0.727	0.792	0.8341
KI	—	0.507	0.553	0.5855
RbF	1.3(c)	1.95	2.09	18.4
RbCl	0.92(b)	0.83	0.916	1.08
RbBr	—	0.465	0.520	0.5512
RbI	—	0.292	0.323	0.7149
CsF	1.23(c)	1.97	2.31	2.39
CsCl ₂	0.75(b)	0.722	0.824	0.8654
CsBr	—	0.335	0.374	0.373
CsI	—	0.208	0.229	0.249

(a) Vidale (1960) ; (b) Klemperer (1957), Rice (1957) † (c) Barrow *et. al.* (1953).

$\omega_e x_e$: In table II, except for LiF, the reported values are estimated ones and it is not possible to draw any conclusions regarding the errors of the calculated results from the potential functions considered. Hence we have not given the percentage errors.

The values of $\omega_e x_e$ calculated with potential function (4), are nearer to the estimated values than those calculated by using Rittner's and Varshni-Shukla's functions in many cases.

TABLE III

The dissociation energies

Molecules	D_i observed* Kcal/mole	D_i Pot (2) Kcal/mole	% error	D_i Calc. from Pot (3) Kcal/mole	% error	D_i Calc. from Pot (4) Kcal/mole	% error
LiF	177.8	185.8	4.5	184.0	3.5	174.8	1.7
LiBr	142.1	142.1	0.4	132.7	7.0	133.9	6.2
LiI	130.7	130.6	0.1	123.0	5.9	122.0	6.7
NaCl	127.9	130.0	1.6	125.5	1.9	124.6	2.6
NaBr	124.4	127.7	2.7	118.8	4.5	117.9	5.2
NaI	114.5	118.9	3.8	109.8	4.1	109.0	4.8
KF	131.6	136.5	3.7	134.7	2.4	133.4	1.4
KCl	133.3	116.2	2.6	112.2	1.0	111.5	1.6
KBr	109.1	109.5	0.4	105.8	3.0	105.1	3.7
KI	101.9	101.1	0.8	97.5	4.3	96.97	5.0
RbF	135.8	135.7	0.1	131.8	2.9	141.7	4.3
RbCl	111.1	111.4	0.3	107.5	3.2	106.9	3.8
RbBr	106.7	106.0	0.7	102.0	4.4	101.5	4.8
RbI	98.7	97.6	1.1	94.0	4.8	93.3	5.5
CsF	133.3	135.4	1.6	128.9	3.3	128.2	3.8
CsCl	107.6	108.1	0.5	103.6	3.7	103.0	4.3
CsBr	103.2	101.3	1.8	97.5	5.5	97.2	5.8
CsI	93.2	88.3	5.3	85.4	8.4	84.9	8.9
Average % Error			1.8		4.1		4.6

*Gaydon (1953).

D_i : It is found from table III that % error in D_i values calculated by using pot. (4) is slightly greater than those calculated by using Rittner's and Varshni Shukla's potential function.

However, it should be noted that most of the experimental values are uncertain by above ± 4 kcal/mole, which corresponds to 3% hence no strict conclusion can be drawn about the relative performances.

To summarize, we may say that the results of α_e and $\omega_e x_e$ obtained with potential function (4) are superior to potential functions. (2) and (3).

From the discussion for the repulsive term by Varshni-Shukla (1961) we retain the conclusion drawn by them that the exponential term in Fn. (4) represents the combined effect of polarization and Van der Waal forces.

ACKNOWLEDGMENTS

The authors are grateful to H. C. Trivedi, Principal, Seth M. N. Science College for his inspiration and encouragement.

REFERENCES

- Barrow R. F. and Caunt, A. D. 1953, *Proc. Roy. Soc. (London)*, **A219**, 120.
Gaydon A. G., 1953. *Dissociation Energies and Spectra of Diatomic Molecules*
Chapman and Hall, Ltd., London
Green, G. W., Low. H. *Can. J. Physics*. 1958, 36, 171, *Phys. Rev.* **96**, 629.
Honig, A. Mandel, M. Stiech M. L. and Townes C. H. 1954, *Phys. Rev.* **96**, 629.
Klemperer W. and S. A. Rice. 1957, *J. Chem., Phys.* **26**, 618.
Low, Morris, Geiger, and Esinger. 1958, *Can. J. Phys.* **36**, 171.
Rice S. A. and W. Klemperer, 1957, *J. Chem. Phys.*, **27**, 573.
Rittner E. S., 1951, *J. Chem. Phys.*, **19**, 1030.
Varshni, Y. P., 1957, *Revs. Modern Phys.* **29**, 664 ; 1959, **31**, 839.
——— 1957, *Trans. Faraday Soc.* **53**, 132.
——— and Shukla R. C. 1961, *J. Chem. Phys.* **35**, 582.
Vidale, G.L., 1960, *J. Phys. Chem.* **64**, 314.

NUCLEAR MAGNETIC RELAXATIONS AND MOLECULAR REORIENTATION FREQUENCIES OF α -HYDROQUINONE AND γ -HYDROQUINONE

V. D. AGRAWAL AND R. C. GUPTA

DEPARTMENT OF PHYSICS, LUCKNOW UNIVERSITY, LUCKNOW.

(Received August 30, 1966; Resubmitted November 8, 1966)

ABSTRACT. The spin-lattice nuclear magnetic relaxations have been measured for stable (α) and meta-stable (γ) Hydroquinones or Quinols. The studies were carried out as a function of temperature from 94°K to 360°K, at the radio frequency of 25 Mc/sec. The N.M.R. relaxations show the molecular rotation with the rise of temperature in both the cases. The activation energies and molecular reorientation frequencies have also been calculated.

INTRODUCTION

The present work is an attempt to extend the work of Gupta (1963) on motion of α -Hydroquinone and γ -Hydroquinone molecules. His results of α -Hydroquinone for line-widths vs. temperature show first transition at about 341°K and second transition at about 388°K, with the specific heat anomaly which occurs at 325°K. In the case of γ -Hydroquinone first transition is found at about 365°K and second transition at about 375°K, with the heat anomalies occurring at temperatures 230°K and 336°K. These transitions are interpreted by him as being a reorientation of molecule about the molecular axis. The interchange of energy between nuclei and lattice may also be studied by means of spin-lattice relaxation time. The present N.M.R. relaxation measurements have been made on α -Hydroquinone and γ -Hydroquinone in an attempt to obtain more detailed informations concerning the nature of molecular motions.

EXPERIMENTAL ARRANGEMENT

The magnetic relaxations of solid α -Hydroquinone and γ -Hydroquinone have been measured at 25 Mc/sec using a proton resonance spectrometer in a field of about 5998 gauss. The records of T_1 have been recorded by one of us in University College of North Wales, Bangor, U. K. The records of T_1 at room temperature have been shown in fig. (1) and fig. (2).

THEORY

Bloembergen *et al* (1948) derived an expression for T_1 in terms of a correlation time τ_c , which sets a time scale to the random motion. τ_c can be roughly defined

as the time taken by a molecule to turn through a radian or to move through a distance comparable with its dimensions.

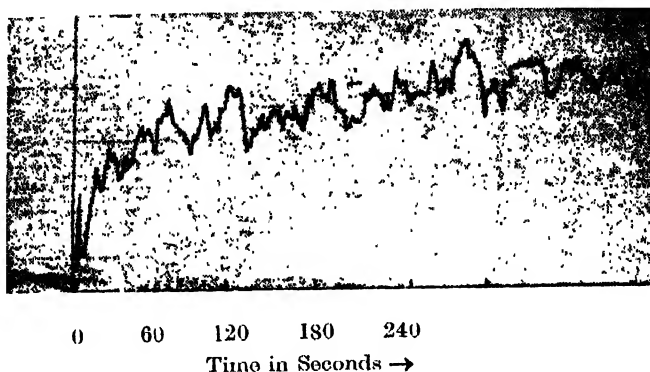


Fig. (1) Signal decay curve of T_1 for α -Hydroquinone at room temperature.

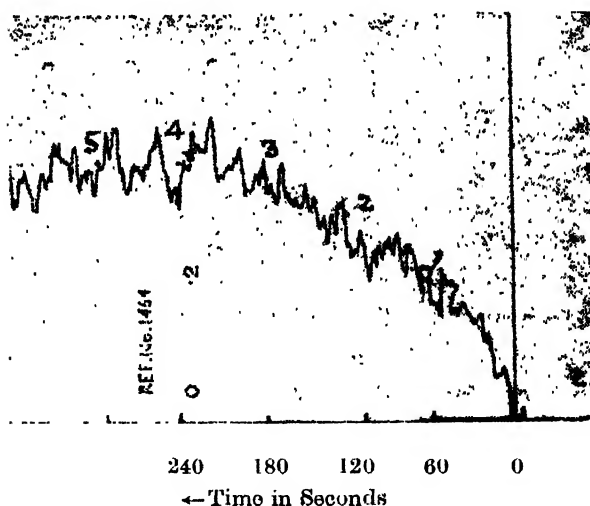


Fig. (2) Signal decay curve of T_1 for γ -Hydroquinone at room temperature.

The expression has been slightly modified by Kubo and Tomita (1954) and obtained :

$$\frac{I}{T_1} = C_1 \left[\frac{\tau_c}{I + \omega_0^2 \tau_c^2} \frac{4\tau_c}{I + 4\omega_0^2 \tau_c^2} \right]$$

where $\omega_0 = 2\pi\nu_0$ and C_1 is a constant.

Thus T_1 decreases as the value of τ_c increases, it reaches minimum when reorientation frequency and radio frequency become roughly equal, beyond which T_1 rises with temperature, such behaviour has in fact been found for three isotopic species of benzene by Andrew and Eades (1953b). With the help of above equation,

the values of T_1 at various temperatures can be converted in terms of τ_c . The plot of $\log \tau_c$ vs $1/T$ yields a straight line and its slope will give the activation energy E_R . This procedure is the only approach when the plot of T_1 against $1/T$ gives no minimum value of T_1 due to the intervention of solid-solid phase transition as in the case of Cyclohexane (Andrew and Eades, 1953a).

METHOD FOR MEASUREMENT OF T_1

In the present work for the measurements of relaxation times Linder's (1957) decay technique has been adopted. Measurement by this method is possible when T_1 is long compared to the constant of the recording apparatus. The principle of the method is that when spin system is saturated by the application of the radio-frequency amplitude H_1 , such that $\gamma^2 H_1^2 T_1 T_2$ is much greater than unity, the observed intensity falls until the signal vanishes completely. The radio-frequency field is lowered to the unsaturated value of nuclear system and regrowth of signal is recorded. The growth is exponential and governed by the formula :

$$S(t) = S_0 \left(1 - \exp \left(- \frac{t}{T_1} \right) \right)$$

where $S(t)$ and S_0 are the intensities of signals in saturated and unsaturated states. The slope of the curve $s_0 - s(t)$ against time (t) gives relaxation time T_1 .

ACTIVATION ENERGY AND ROTATIONAL-FREQUENCY

Gutowsky and Pake (1950) and Kubo and Tomita (1954) modified the theory of Bloembergen *et al* and modified expression is given as :

$$2\pi\nu_c = \alpha\gamma\delta H [\tan \{ \pi(\delta H^2 - B^2)/2(C^2 - B^2) \}]^{-1}$$

where ν_c is the correlation frequency for motion narrowing the line, C is the line-width at temperature below the transition region, δH is the linewidth in the Transition region, B is the line width at higher temperature, γ is the gyromagnetic ratio and α is $(\ln 2)^{-1}$ and its value is $(8 \times 0.6931)^{-1}$. $(C^2 - B^2)$ can be replaced by (C^2) if B^2 is too small as compared to C^2 . The correlation frequency ν_c is assumed to obey Arrhenius equation :

$$\nu_c = \nu_0 \exp \left[\frac{-E_R}{RT} \right]$$

where E_R is the activation energy and R is the gas constant/mole.

In the case of α -Hydroquinone the value of C is 09.53 gauss and value of B is 0.31 gauss. In γ -Hydroquinone the value of C and B are 8.40 gauss and 0.40 gauss respectively. These values have been calculated with experimental line-width vs temperature curve obtained by Gupta (1963).

The molecular reorientation frequencies for α Hydroquinone have been shown in Table II and for γ -Hydroquinone in Table III. The plot of $\log \nu_c$ vs $1/T$ yields a straight line and its slope will give activation energy E_R for molecular rotation.

RESULTS

The spin-lattice relaxation times measured by signal decay method for α -Hydroquinone and γ -Hydroquinone are quoted in Table I.

TABLE I

Spin-lattice relaxation times of stable and m -stable Hydroquinone

Temperature °K	Stable Hydroquinone	m -stable Hydroquinone
94°	5.0 minutes	1.20 minutes
293°	3.0 „	0.90 „
353°	—	0.83 „
360°	1.4 „	—

TABLE II

Molecular reorientation frequencies for stable (α) Hydroquinone

Temperature °K	δ H (gauss)	ν_c
366	7.81	3.41 Kc/sec.
374	6.56	5.48 Kc/sec.
388	1.52	30.48 Kc/sec.
400	0.43	—

TABLE III

Molecular reorientation frequencies for m -stable (γ) Hydroquinone

Temperature °K	δ H (gauss)	ν_c
350	8.06	0.8043 Kc/sec.
367	7.50	1.9272 Kc/sec.
370	5.00	6.2199 Kc/sec.
374	1.40	23.8720 Kc/sec.
380	1.00	36.6630 Kc/sec.

Thus with above results it is evident that T_1 is greater for stable Hydroquinone in comparison to meta-stable Hydroquinone. Also for both α -Hydroquinone and γ -Hydroquinone the values of T_1 are reduced with rise of temperature. Most likely this is due to rotation of molecule about the molecular axis. The activation energies for both have been calculated. For α -Hydroquinone it is found to be 5.26 K.cal/mole and for γ -Hydroquinone it is about 13.02 K.cal/mole which is a reasonable value to cross the potential barrier hindering rotation (Muzushima 1954). Furthermore, as obtained by Gupta (1963) the second moments and line-widths in both α - and γ -Hydroquinone show a remarkable reduction in its values with the rise of temperature, giving added support to the theory of molecular rotation.

ACKNOWLEDGMENT

Authors are highly indebted to Professor P. N. Sharma, D.Sc., Head of the Physics Department for his interest and encouragement throughout the work.

REFERENCES

- Andrew, E. R. and Eades, R. G., 1953a, *Proc. Roy. Soc. A*, **216**, 398.
 ————— 1953b, *Proc. Roy. Soc. A*, **218**, 537.
 Bloembergen, N., Purcell, E. M. and Pound, R. V., 1948, *Phys. Rev.*, **73**, 679.
 Gupta, R. C., 1963, *Ph.D. thesis*, University College of North Wales, Bangor, U.K.
 Gutowsky, H. S. and Pake, G. E., 1950, *J. Chem. Phys.*, **18**, 162.
 Kubo, R. and Tomita, K., 1954, *J. Physical Soc. Japan*, **9**, 888.
 Linder, S., 1957, *J. Chem. Phys.*, **26**, 900.
 Muzushima, S., 1954, *Structure of molecules and internat rotation*. Academic Press, Inc. New York, 7.

DIFFERENTIAL CAPTURE PROBABILITY OF ELECTRON IN PROTON-HYDROGEN COLLISION AT LOW ENERGIES

GURUDAS CHATTERJEE AND N. C. SIL

DEPARTMENT OF THEORETICAL PHYSICS,
INDIAN ASSOCIATION FOR THE CULTIVATION OF SCIENCE,
JADAVPUR, CALCUTTA, INDIA.

(Received August 17, 1966)

ABSTRACT. Electron capture in proton-hydrogen collision at 3° scattering angle (laboratory system) has been investigated, using a two state approximation. The system of two protons and an electron forms a hydrogen-molecular-ion, with variable internuclear distance. In the present paper only the lowest symmetric and anti-symmetric states of H_2^+ are considered and the protons with their associated electron-cloud are scattered differently in these two cases. The two different scattering amplitudes are each associated with a time dependent phase which develops differently for the symmetric and anti-symmetric states. Finally the amplitudes in different phases interfere and determine the probability of capture. The numerical computation of capture probability in the present paper shows a very good agreement with experiment regarding the position of maxima and minima, in the energy range 1.1 to 0.45 Kev. Below 0.45 Kev the present result shows more rapid fluctuations, in capture probability which are however, not found in the experimental curve.

INTRODUCTION

The proton-hydrogen atom charge transfer problem has been largely investigated, both theoretically and experimentally in recent years. Previous theoretical studies, on the differential cross sections at fixed scattering angle, were made by Bates and McCarroll (1962) and Mukherjee and Sil (1962), using a 'two-state approximation' in impact parameter method. Theoretical calculations show a resonant variation of capture probability against the incident energy of the proton. The probability reaches the value one at the peaks and zero at the valleys. The experimental findings of Helbig and Everhart (1965) show a similar variation of capture probability with several peaks and valleys, but the probabilities neither reach the maximum value one, nor drop to zero. This deviation from theoretical result was found more prominent near the lower energies. Moreover there is a marked disagreement between those theoretical results and experimental findings in respect of the position of maxima and minima.

The discrepancies were thought of as due to the neglect of the coupling of the excited states. Accordingly calculations were done by Bates and Williams (1964) using a 'three state approximation'. Another theoretical result was put forward

by Basu, Sil and Bhattacharyya (1965), using a variational method and taking four atomic states $1S$, $2S$ around each proton. Both of these calculations show a decrease of the capture probability at the peak and increase of the same at the valley, thus in qualitative agreement with the experiment of Everhart.

Recently, F. J. Smith (1964) pointed out the failure of the impact parameter method at low energies and developed the wave treatment of the same problem. Taking into consideration only two states in his calculations, he finds a considerable decrease in the oscillation of capture probability at low energies. Further, after introducing a correction due to coupling with the excited state $2p\pi_u$ (from the calculations of Bates and Williams) in this two state calculations, he finds a good agreement regarding the position of resonances.

Another theoretical treatment, in connection with the scattering problem of $\text{He}^+ - \text{He}$ system, has been introduced by Marchi and Smith (1965). They have emphasized the need for the separate treatment for the motion of the two nuclei in two separate fields due to symmetric and antisymmetric states of ion-atom pair. In our problem we allow the two protons to move in their respective classical orbits under the potential due to symmetric and antisymmetric states of hydrogen molecular ion. In order that the protons may be scattered through a fixed angle, each of the two potentials gives rise to a separate set of impact parameter, distance of closest approach and the classical cross section of scattering. The square root of the classical cross section is assumed to be the scattering amplitude in the respective state. Each amplitude is associated with a certain phase which is determined by the time dependent motion of the electrons in the field of the two protons. In the calculation of the phase, the effect of motion of the protons in their actual trajectory (rather than the approximate assumption that protons move in straight paths) has also been considered. Finally, the two amplitudes with their appropriate phase interfere and exhibits capture phenomena at a particular angle.

Atomic units are used in all calculations of this paper.

T H E O R Y

If Ψ is the wave function of a system composed of two protons A and B placed at the points \mathbf{R}_A and \mathbf{R}_B and an electron at \mathbf{r} , then we can expand Ψ in terms of molecular wave functions as

$$\Psi = \sum_i F_i(\mathbf{R}) \psi_i(\mathbf{R}, \mathbf{r}),$$

where,

$$R = |\mathbf{R}| = |\mathbf{R}_A - \mathbf{R}_B|, \text{ and } \Psi_i(\mathbf{R}, \mathbf{r})$$

is the molecular wave function with the nuclear separation distance R considered momentarily at rest.

The identity of A and B gives rise to two sets of wave functions, symmetric and antisymmetric, corresponding to the interchange of A and B in the hamiltonian.

For small velocities of the incident proton it is a reasonable approximation to take in the sum only two terms, viz., the lowest states in the symmetric and anti-symmetric distribution of electron cloud in hydrogen molecular ion.

Thus in this two state approximation Ψ is written as

$$\Psi = F_S(\mathbf{R})\psi_S(\mathbf{R}, \mathbf{r}) + F_a(\mathbf{R})\psi_a(\mathbf{R}, \mathbf{r})$$

For large R , the molecular wave functions transform to the linear combinations of the ground state atomic wave functions $\psi_{A,B}(\mathbf{r})$ i.e. wave functions of the electron around the proton A or the proton B . The functions $F_{S,a}(\mathbf{R})$ take up the form $\exp(i\mathbf{k} \cdot \mathbf{R}) + f_{S,a}(\theta)\{\exp(ikR)\}/R$ for large R , so that the scattered wave is given by

$$\begin{aligned} \psi_{SC} = \frac{1}{\sqrt{2}} \frac{e^{ikR}}{R} \left[\{\psi_A(\mathbf{r}) + \psi_B(\mathbf{r})\} f_S(\theta) e^{i\{\eta_S(t)\}}_{t \rightarrow \infty} \right. \\ \left. + \{\psi_A(\mathbf{r}) - \psi_B(\mathbf{r})\} f_a(\theta) e^{i\{\eta_a(t)\}}_{t \rightarrow \infty} \right] \quad \dots (1) \end{aligned}$$

We assume that the amplitude $f_{S,a}(\theta)$ is the positive square root of the classical cross section $\sigma_{S,a}^c(\theta)$ which is connected with impact parameter $b_{S,a}$ and scattering angle θ , by the relation,

$$\sigma_{S,a}^c(\theta) = b_{S,a} \left(\frac{db}{d\theta} \right)_{S,a} \csc \theta.$$

It is to be noted that we have introduced in the asymptotic form of Ψ the phase factors $\exp[i\{\eta_{S,a}(t)\}]$ which determine the dissociation of molecular wave functions $\psi_{S,a}(\mathbf{R}, \mathbf{r})$ to either $\psi_A(\mathbf{r})$ or $\psi_B(\mathbf{r})$ after infinite separation of the protons. The electron has been originally attached to the proton A before the collision starts and we may associate this initial condition to $[\eta_{S,a}(t)]_{t \rightarrow -\infty} = 0$ (Time is measured from the instant when the two protons are close to each other). The phase factors have been obtained from the time dependent wave equation of the electron in the field of the two protons, (cf. Smith, F. T. 1965)

$$\eta_{S,a}(t) = \int_{-\infty}^t \epsilon_{S,a}[R(t)] dt \quad \dots (2)$$

where $\epsilon_{S,a}$ is the electronic energy in the ground state of symmetric and antisymmetric cloud of hydrogen molecular ion.

Collecting the coefficient of ψ_B from the equation (1) and squaring it, we get the capture cross section. This capture cross section divided by the sum of the cross sections of scattering and capture gives the capture probability,

$$P_C = \frac{1}{2} \left[1 - \frac{2\sqrt{\sigma_S^c \cdot \sigma_a^c}}{\sigma_S^c + \sigma_a^c} \cos \{\eta_S(\infty) - \eta_a(\infty)\} \right] \quad \dots (3)$$

CALCULATIONS AND RESULTS

We have from (2)

$$\begin{aligned}\eta_{S,a}(\infty) &= \int_{r_0}^{\infty} \epsilon_{S,a}[R(t)] dt \\ &= 2 \int_{(r_0)_{S,a}}^{\infty} \epsilon_{S,a}[R] \left(\frac{dt}{dR} \right)_{S,a} dR \quad \dots (4)\end{aligned}$$

$\left(\frac{dR}{dt} \right)_{S,a}$ are given by the well known classical relation,

$$\left(\frac{dR}{dt} \right)_{S,a}^2 = v_0^2 \left[1 - \frac{2}{T} \left\{ \epsilon_{S,a}(R) + \frac{1}{R} + 0.5 \right\} - \frac{b_{S,a}^2}{R^2} \right]$$

and $(r_0)_{S,a}$ are the distances of closest approach, so that for $R = r_0$, $(dR/dt) = 0$. v_0^2 is the velocity and T the kinetic energy of the incident proton in laboratory system of coordinates.

The table of $\epsilon_{S,a}(R)$ at equal intervals of R has been calculated by H. Wind (1965), and $b_{S,a}$ have been plotted against energy by F. J. Smith (1965).

The integrand in (4) has a singularity at the lower limit. The behaviour of the integrand near the lower limit is like that of x^{-1} near the origin. We have employed a method, as given in the book 'Methods of Mathematical Physics' by Jeffreys and Jeffreys (1962) for the evaluation of the integral near the lower limit. The integration in the rest of the range is done by Simpson's method. Next we substitute the value of $[\eta_S(\infty) - \eta_a(\infty)]$ in (3). We also substitute the values of $\sigma_{S,a}^c$ from the work of F. J. Smith. This gives the expression for P_c .

The capture probability calculated in this paper is presented in fig. 1 in solid line. The experimental curve of Everhart and the curve giving the results of the theoretical calculations in two state approximation by F. J. Smith are also shown for comparison.

It is seen that regarding the positions of maxima and minima, good agreement with experiment is obtained in the range 0.45 to 1.1 Kev. Below 0.45 Kev, the calculated capture probability shows more frequent oscillations which have not been observed in the experiment of Everhart *et al.*, The more frequent oscillation of capture probability in our results in the energy range 0.45 to 0.1 Kev is due to the rapid variation of the phase difference $[\eta_S(\infty) - \eta_a(\infty)]$. This tendency of more rapid oscillations with decreasing energy is also found in the theoretical results of Bates and Williams (1964), down to 0.25 Kev.

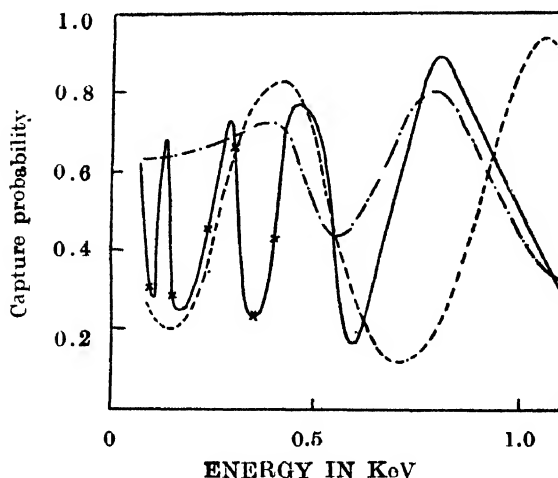


Fig. 1. Capture probability against the incident energy of the proton (in Lab. system).
 — — — — theoretical curve of F.J. Smith (1964) by two-state-calculations. His three state calculation with the inclusion of $2p\pi u$ shows better agreement with experiment.
 - - - - - experimental curve of Helbig and Everhart. (1965) States
 — · — · — theoretical curve by the present authors, with actual points of calculation indicated only below 0.5 keV energy to show extrapolation particularly at 0.12 KeV energy.

Above 1.1 Kev our theoretical curve begins to be out of phase with the corresponding experimental curve, this may be due to the neglect of the higher excited states of H_2^+ . F. J. Smith finds an encouraging agreement with experiment by considering the correction in capture probability due to the $2p\pi_u$ state. The work to incorporate the same effect in our method is in progress.

ACKNOWLEDGMENTS

The authors are thankful to Prof. D Basu for many valuable discussions during the progress of the work. Thanks are also due to Dr. A. C. Shamihoke, Head of the Department of Computation, C.M.E.R.I., Durgapur, for kindly accommodating our work in their Electronic Computer I.B.M. 1620.

REFERENCES

- Bates, D. R., and McCarroll, R., 1958, *Proc. Roy. Soc. (London)*, A **245**, 175.
 Bates, D. R. and Williams, D. A., 1964, *Proc. Phys. Soc., (London)*, **83**, 425.
 Basu, D., Sil, N. C. and Bhattacharya, D. M., 1966, *Phys. Rev.* **144**, 1, 56.
 Helbig, H. F., and Everhart, E., 1965, *Phys. Rev.* **140**, 715.
 Jeffreys and Jeffreys, 1962, *Methods of Mathematical Phys.*, Third Edition, 289.
 Mukherjee, S. C., and Sil, N. C., 1962, *Indian J. Phys.*, **36**, 622.
 Marchi, R. P. and Smith, F. T., 1965, *Phys. Rev.*, **139**, 1025.
 Smith, F. J., 1964, *Proc. Phys. Soc.*, **84**, 889.
 Wind, H., 1965, *J. Chem. Phys.*, **42**, 2371.
 ———, 1965, Thesis on "Electric Field Dissociation of H_2^+ ". (private communication by the courtesy of Dr. Wind.).

RADIO-FREQUENCY CONDUCTIVITY OF IONIZED GASES IN MAGNETIC FIELD

R. N. GUPTA AND S. K. MANDAL

DEPARTMENT OF PHYSICS, NORTH BENGAL UNIVERSITY,

RAJA RAMMOHUNPUR, DARJEELING.

(Received July 15, 1966 ; Resubmitted January 21, 1967)

ABSTRACT. The radio-frequency conductivity of ionized gases (air and Carbon dioxide) has been measured within a pressure range of a few microns of Hg to .3 mm of Hg in presence of a magnetic field varying from 0 to 700 Gauss, and a frequency of 10.6 Mc/sec, the discharge being excited by a transformer. It has been observed that conductivity decreases in presence of magnetic field for all values of pressure and the pressure at which the conductivity becomes a maximum increases with the increase of magnetic field. The results can be explained fairly well by an extension of the theory put forward by Gilardini (1959) and the quantitative agreement is also satisfactory. The introduction of the effect of equivalent pressure generally gives results in wide divergence with experimental results and hence it is concluded that for values of (H/P) employed in this case, the equivalent pressure concept does not hold. The reasons for the failure of equivalent pressure expression in this case have been discussed.

INTRODUCTION

In a previous paper (Sen and Ghosh, 1966) a method has been described to measure the radio-frequency conductivity of ionised gases and a study has been made regarding the interaction of radio-frequency waves with ionised gases. Since the presence of a magnetic field changes the various characteristics of a discharge, it is natural to suppose that the radio-frequency conductivity of an ionized gas will also change in presence of a magnetic field. Conductivity of ionized gases such as air, nitrogen and hydrogen in a magnetic field was measured by Ionescu and Mihul (1932) for pressure greater than 10^{-3} mm of Hg who found that maxima other than those due to free electrons could be obtained. With very intense fields, only the vibration due to free electrons remained, the others disappearing and the values of the magnetic field giving maximum conductivity varied with pressure. A theory regarding the variation of radio-frequency conductivity with magnetic field was proposed by Appleton and Boohariwala (1935) who showed that the real part of radio-frequency conductivity in a magnetic field is given by

$$\sigma_{rH} = \frac{ne^2}{m} \cdot \frac{\nu_c(\omega^2 + \omega_b^2 + \nu_c^2)}{(\omega^2 + \omega_b^2 + \nu_c^2)^2 - 4\omega^2\omega_b^2} \quad \dots (1)$$

n is the number of electrons per unit volume and ν_c the collision frequency, ω is the angular frequency of the applied field and $\omega_b = \frac{eH}{m}$; from graphical analysis,

it was shown by the authors that the value of v_e for which the conductivity becomes a maximum is obtained when $v_e = 0$ which is anomalous and further the experimental results obtained by the authors were not supported by the theory developed; but it was conclusively shown that the magnetic field has a marked influence on the pressure at which the conductivity becomes a maximum and the value of the conductivity changes when the magnetic field is applied. A general theory regarding the variation of radio-frequency conductivity of ionized gases and its variation with pressure and the magnetic field has been worked out by Gilardini (1959) who derived the expression for the conductivity of an ionized gas under the following assumptions:

(a) when the distribution function is predominantly spherically symmetrical in velocity space but not necessary Maxwellian.

(b) when the electron collision frequency is an arbitrary function of electron velocity. The value of the complex conductivity is given by

$$\sigma = \frac{e^2 n}{m} \cdot \frac{1}{v_e + j\omega}$$

In presence of magnetic field he has defined two conductivities; a conductivity σ_e for the right-handed polarization and a conductivity σ_0 for the left-handed polarization where

$$\sigma_e = \frac{e^2 n}{m} \left[\frac{1}{v_e + j(\omega - \omega_b)} \right],$$

and

$$\sigma_0 = \frac{e^2 n}{m} \left[\frac{1}{v_e + j(\omega + \omega_b)} \right]$$

and the conductivity in the direction of the field is given by

$$\sigma_H = \frac{1}{2} (\sigma_e + \sigma_0).$$

and

$$\begin{aligned} \sigma_H = \frac{e^2 n}{m} \left[\left\{ \frac{v_e}{v_e^2 + (\omega - \omega_b)^2} + \frac{v_e}{v_e^2 + (\omega + \omega_b)^2} \right\} \right. \\ \left. - j \left\{ \frac{(\omega - \omega_b)}{v_e^2 + (\omega - \omega_b)^2} + \frac{(\omega + \omega_b)}{v_e^2 + (\omega + \omega_b)^2} \right\} \right] \end{aligned}$$

so that real part of the conductivity is given by

$$\sigma_{rH} = \frac{e^2 n}{m} \left[\frac{v_e}{v_e^2 + (\omega - \omega_b)^2} + \frac{v_e}{v_e^2 + (\omega + \omega_b)^2} \right]$$

and after simplification it reduces to the result obtained earlier by Appleton and Boohariwalla (1935)

$$\sigma_{rH} = \frac{e^2 n}{m} \frac{\nu_0[\nu_0^2 + \omega_b^2 + \omega^2]}{(\nu_0^2 + \omega^2 + \omega_b^2)^2 - 4\omega^2\omega_b^2}$$

Though some measurements of radio-frequency conductivity have been carried out earlier it is felt necessary that a thorough and systematic experimental measurement of radio frequency conductivity of ionized gases in a magnetic field will yield some data which can be utilized for the verification of the theory advanced by Gilardini (1959) or by Appleton and Boohariwalla (1935). Also it will be of interest to study the variation of radio-frequency conductivity in a magnetic field and to see how the pressure at which the conductivity becomes a maximum varies with the application of the magnetic field. An idea regarding the interaction of the magnetic field with the ionized gases can thus be obtained. With this object in view the present work has been undertaken and the paper reports the results obtained experimentally in case of air and carbondioxide in presence of magnetic field varying from 0 to 700 gauss and the pressure varying from a few microns to 300 microns.

EXPERIMENTAL PROCEDURE

The radio-frequency conductivity of ionized gases such as air and carbondioxide has been determined in the same way as has been done by (Sen and Ghosh, 1966). Pure and dry air has been used and carbondioxide has been prepared by letting a saturated solution of oxalic acid (analytical grade) in water fall drop by drop in to a saturated solution of sodiumbicarbonate (analytical grade). The evolved carbondioxide was passed through phosphorus pentoxide to remove water vapour. The magnetic field has been supplied by an electromagnet and the lines of force are perpendicular both to the direction of the field and to the length of the discharge tube. Keeping the magnetic field constant at a particular value, the pressure of the gas has been varied and the conductivity of the gas determined for various values of the pressure, and the same procedure has been repeated for various values of the magnetic field. The experiment has been repeated a large number of times and the results have been found to be consistent. The pressure of the gas has been measured as was done in the previous papers, (Sen *et. al.*, 1962, a, b). The frequency of the applied field as measured by a wide band communication receiver was 10.6 Mc/sec and measurements were taken for the value of the discharge current of 20mA. The values of the magnetic field have been measured accurately by a calibrated Flux-meter.

RESULTS AND DISCUSSION

The variation of radio-frequency conductivity against pressure has been plotted in case of air and carbondioxide for different values of the magnetic field in Fig. 1 and Fig. 2; also the conductivity pressure curve without magnetic field

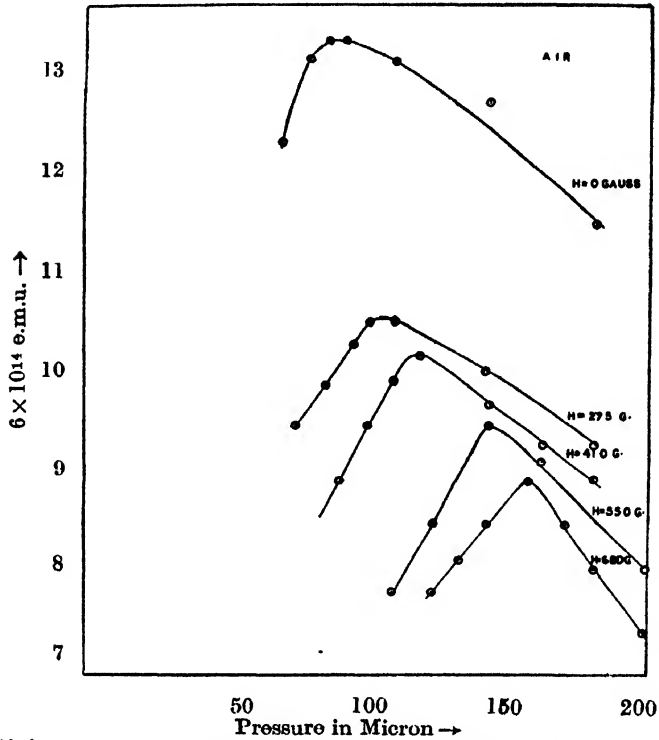


Fig. 1. Conductivity of ionised air against pressure for different values of the magnetic field.

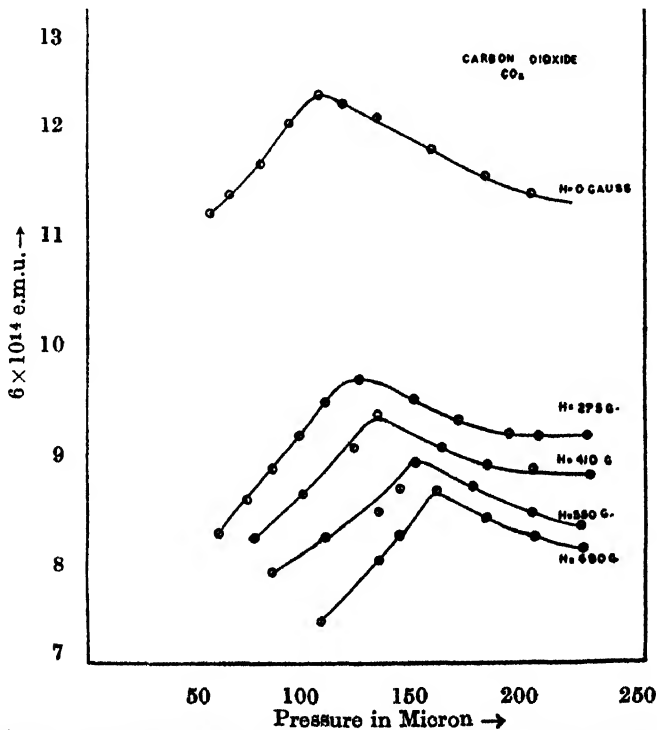


Fig. 2. Conductivity of ionised carbondioxide against pressure for different values of the magnetic field.

has been given for comparison. It is observed that the value of σ_r is smaller when magnetic field is present than that without field for all values of pressure and the pressure at which the conductivity becomes a maximum always shifts to higher pressure when the magnetic field is increased. That the real part of r.f. conductivity will be smaller in presence of magnetic field than when the field is absent is evident from the following considerations; we have

$$\sigma_r = \frac{ne^2}{m} \cdot \frac{\nu_c}{\nu_c^2 + \omega^2}$$

and

$$\sigma_{rH} = \frac{ne^2}{m} \cdot \frac{\nu_c(\nu_c^2 + \omega^2 + \omega_b^2)}{(\nu_c^2 + \omega^2 + \omega_b^2)^2 - \omega^2\omega_b^2}$$

so that when the magnetic field employed is of the order of 200 gauss, we get

$$\omega = 3.52 \times 10^9 \text{ radians}$$

and for $H = 300$ Gauss, $\omega = 5.28 \times 10^9$ radians

whereas the frequency of the applied field is of the order of 2.95×10^8 cycles/sec or 1.852×10^7 radians; we can therefore neglect ω in comparison to ω_b and hence obtain

$$\sigma_{rH} = \frac{ne^2}{m} \cdot \frac{\nu_c(\nu_c^2 + \omega_b^2)}{(\nu_c^2 + \omega_b^2)^2 - 4\omega^2\omega_b^2}$$

then

$$\frac{\sigma}{\sigma_{rH}} = \frac{(\nu_c^2 + \omega_b^2)^2 - 4\omega^2\omega_b^2}{(\nu_c^2 + \omega_b^2)(\nu_c^2 + \omega^2)}$$

and neglecting $4\omega^2\omega_b^2$ in comparison to $(\omega_b^2 + \nu_c^2)^2$ we get

$$\frac{\sigma}{\sigma_{rH}} = \left(\frac{1 + \omega_b^2/\nu_c^2}{1 + \omega^2/\nu_c^2} \right)$$

and since $\omega_b \gg \omega$, σ/σ_{rH} will be greater than unity as is actually found to be the case in the range of pressure investigated. Considering from the physical point of view it is seen that due to the presence of magnetic field the effective mean free path is shortened and now there is a greater number of collisions which results in a net reduction of the number of drifting electrons contributing to the conductivity current and hence the conductivity decreases. However, in the discussion which follows it will be assumed that the number of electrons per unit volume is the same in the presence of magnetic field as in its absence, because it is clearly observed in the course of experiment as well as from theoretical considerations that there is a gradation of concentrations of electrons in the path of the radio-frequency field but the average number approximately remains the same.

The values of pressure at which the conductivity becomes maximum in case of air and carbondioxide have been obtained from the curves of Fig. 1 and 2 and entered in Table I.

TABLE I

Gas	Magnetic field in gauss	Value of maximum conductivity $\times 10^{14}$ e.m.u.	Corresponding pressure as from experiment in micron.	(P_H) min from equ. (2) (microns)	(P_H) min from equn (4) in micron
Air	0	13.175	92		
	275	10.475	112	115.7	92.56
	410	10.125	123	118.8	95.04
	550	9.175	150	130.02	104.016
	680	8.923	170	136.66	109.33
Carbondioxide	0	12.6	108		
	275	9.85	125	140.7	112.56
	410	9.45	140	146.7	117.36
	550	9.00	155	154.0	123.2
	680	8.725	162	157.9	127.12

It is evident that the maximum value of conductivity diminishes and the pressure at which the conductivity becomes a maximum shifts to higher values with the application of the magnetic field. To explain this it is observed that since $\omega_b \gg \omega$ for the values of magnetic field employed,

$$\sigma_{rH} = \frac{ne^2}{m} \frac{1}{\nu_c^2 + \omega_b^2}$$

and putting

$$\nu_c = \frac{v_r}{\lambda} = \frac{v_r P}{L}$$

where L is the mean of free path of the electron in the gas at a pressure of 1 mm v_r the velocity of the electrons we get,

$$\sigma_{rH} = \frac{ne^2}{m} \cdot \frac{L}{v_r} \frac{1}{P^2 + C_1 H^2}$$

where

$$C_1 = \left(\frac{e}{m} \cdot \frac{L}{v_r} \right)^2$$

and σ_{rH} will be a maximum with respect to P

when
$$(P_H)_{max}^2 = C_1 H^2,$$

where $(P_H)_{max}$ is the pressure at which the conductivity becomes a maximum in presence of magnetic field.

then
$$(\sigma_{rH})_{max} = \frac{1}{2} \cdot \frac{ne^2}{m} \cdot \frac{L}{v_r} \cdot \frac{1}{(P_H)_{max}}.$$

and
$$(\sigma_r)_{max} = \frac{1}{2} \cdot \frac{ne^2}{m} \cdot \frac{L}{v_r} \cdot \frac{1}{P_{max}}.$$

so that
$$(P_H)_{max} = \frac{(\sigma_r)_{max}}{(\sigma_{rH})_{max}} \cdot P_{max}. \quad (2)$$

The values of $(\sigma_r)_{max}$ and $(\sigma_{rH})_{max}$ as well as P_{max} can be obtained from experimental data and hence $(P_H)_{max}$ can be calculated. The results calculated from equation (2) have been entered into the fifth column of the Table I; the agreement is quite satisfactory considering the simplifications involved in the deduction of the equation. The result also shows that the pressure at which the radio-frequency conductivity becomes maximum always shifts to higher values as the magnetic field is increased. The above deduction cannot be taken as rigorous because in presence of a magnetic field the actual pressure is changed to an effective pressure as has been shown by Blevin and Haydon, (1958)

$$P_H = P\sqrt{1+C_1H^2/P^2}.$$

where
$$C_1 = \left(\frac{e}{m} \cdot \frac{L}{v_r} \right)^2.$$

Due to this change of pressure the collision frequency also changes. Gilardini (1959) in developing his theory has not taken this change into consideration and assumed that the collision frequency is same both with the without magnetic field. Hence

$$\sigma_{rH} = \frac{ne^2}{m} \cdot \frac{L}{v_r} \cdot \frac{[P^2+C_1H^2]^{\frac{1}{2}}}{P^2+2C_1H^2} \quad \dots (3).$$

The condition for obtaining the maximum value of σ_{rH} when its variation with pressure is taken into consideration is obtained from equation (3). This occurs when $P = 0$ which is anomalous. It may be recalled that Appleton and Boohariwalla (1935), without taking into consideration the concept of equivalent pressure also came to the same conclusion from graphical analysis. Consequently if we

adopt the Blevin and Haydon expression in this case, it leads to result which is anomalous. Of course the validity of Belvin and Haydon's expression has previously been tested in case of air by Sen and Ghosh (1961) where it was shown that for values of pressure less than 150μ and magnetic field of the order of 100 gauss the expression gives values of equivalent pressure different from the actual pressure. Since the pressure at which maxima are occurring is in a region greater than 100μ , and the magnetic field employed is also large it can be conjectured that Blevin and Haydon's expression does not hold in the region of pressure where maxima are occurring.

Townsend and Gill (1937) on the otherhand deduced that

$$\mu_H = \frac{\mu}{1 + \omega_b^2 \tau^2}.$$

where μ_H is the mobility of electrons in the magnetic field H ; τ is the time between successive collisions and $\omega_b = eH/m$. It can be deduced from the above relation that

$$P_H = P \left[1 + C_1 \frac{H^2}{P^2} \right]$$

and hence

$$\sigma_{rH} = \frac{ne^2}{m} \cdot \frac{L}{v_r} \cdot \frac{P[P^2 + C_1 H^2]}{[(P^2 + C_1 H^2)^2 + C_1 H^2 P^2]}.$$

and σ_{rH} is maximum when $(P_H)_{max} = C_1 H^2$.

then

$$(\sigma_{rH})_{max} = \frac{ne^2}{m} \cdot \frac{L}{v_r} \cdot \frac{1}{(P_H)_{max}} \cdot \frac{2}{5}.$$

and as

$$(\sigma_r)_{max} = \frac{ne^2}{m} \cdot \frac{L}{v_r} \cdot \frac{1}{P_{max}} \cdot \frac{1}{2}.$$

we get

$$(P_H)_{max} = \frac{(\sigma_r)_{max}}{(\sigma_{rH})_{max}} \cdot \frac{4}{5} \cdot (P_H)_{max}. \quad \dots (4)$$

The results calculated from equation (4) are entered into the last column of Table I. It is observed that results obtained with equation (4) are in wide disagreement with the experimental results both in the case of air and carbondioxide. It is thus evident that the concept of equivalent pressure whether from Blevin and Haydon expression or from Townsend expression can not lead to any improvement in the theoretical deduction.

It can thus be concluded that in case of air and carbondioxide the simple theory put forward by Gilardini can explain the results quite well specially

when the gyro-frequency is far removed from the frequency of the measuring field but this treatment is over simplified. Further it has been shown that the inclusion of the concept of equivalent pressure does not lead to any better results. In fact Haydon (1961) has discussed the limitation of the equivalent pressure concept in which he found different values of C_1 for Hydrogen by plotting (α_H/α_0) where α is the first Townsend coefficient against values of (H/E) varying from 0 to 2.5 where E is the breakdown voltage. From this he has concluded that perhaps drift velocity is a linear function of (E/P) for small (E/P) values but varies as $(E/P)^n$ where $n > 1$ for large (E/P) values. The value of E/P in these experiments is of the order of 150 volts/cm mm of Hg and hence the linearity relation between the drift velocity and (E/P) on which the Blevin Haydon expression is based, may not hold good for the values of (E/P) used here. This may partly account for the failure of the conception of equivalent pressure in explaining the observed results. The limitations of equivalent pressure concept have also been discussed previously by Sen and Ghosh (1961) where it was shown that the expression is valid upto a pressure of 150μ when the magnetic field is of the order of 100 gauss. Since the magnetic field used here is much greater than 100 gauss, and the maxima are also occurring at pressures greater than 150μ , the Blevin Haydon expression cannot be expected to hold here. Experiments are in progress in this laboratory to measure the radio-frequency conductivity in other gases specially in inert gases and the results will be reported in future.

ACKNOWLEDGMENT

The authors are indebted to Prof. S. N. Sen, Head of the Department of Physics for his guidance through out the progress of the work.

REFERENCES

- Appleton, E. V. and Boohariwalla, D. B. 1935, *Proc. Phys. Soc. London*, **47**, 1374.
 Blevin, H. A. and Haydon, S. C. 1958, *Aust. J. Phys.* **11**, 18.
 Ionescu, V. and Mihul, C. J., *Phys. Radium (Paris)* **6**, 35.
 Gilardini, A. 1959, *Nuovo Cimento Suppl. Sermon* **10**, **13**, 9.
 Haydon, S. C. 1961, *Proc. Fifth Int. Conf. on Ionization Phenomena in Gases Munich*, **1**, 7, 63.
 Sen, S. N. and Ghosh, A. K. 1961, *Indian J. Phys.* **35**, 101.
 —————, 1962, a, *Proc. Phys. Soc. (London)* **70**, 108.
 —————, 1962, b, *Proc. Phys. Soc. (London)*, **89**, 909.
 —————, 1966, *Indian J. Pure & App. Phys.* **4**, 70.
 Townsend, J. S. and Gill, E. W. B., 1937, *Phil Mag.* **26**, 290.

CHERENKOV RADIATION IN DIELECTRIC MEDIUM WITH CONDUCTIVITY

R. M. KHAN

CITY COLLEGE, CALCUTTA.

(Received August 23, 1966)

ABSTRACT. Cherenkov radiation through dielectric medium having conductivity has been considered. It has been shown that Cherenkov radiation is obtained at any velocity of the particle through medium though the attenuation will be large for low velocities. Some features of penetration length has been discussed which are unlike those of usual electromagnetic radiation in conducting media. The opening angle also seems to be of interest.

The problem of Cherenkov radiation in nonconducting media has been discussed by many investigators (1953). In practice however materials generally have varied amount of conductivity and thus lead to attenuation. It is therefore interesting to see the relative importance of the conductivity and the particle velocity in the production of Cherenkov radiation.

We start with Maxwell's equations with Fourier components;

$$\left. \begin{aligned} \text{rot } H_{\omega} &= \frac{i\omega n^2}{c} E_{\omega} + \frac{4\pi}{c} j_{\omega} + \frac{4\pi}{c} \sigma E_{\omega} \\ \text{rot } E_{\omega} &= -\frac{i\omega}{c} H_{\omega} \\ \text{div } D_{\omega} &= 4\pi\rho \\ \text{div } H_{\omega} &= 0 \\ D_{\omega} &= n^2 E_{\omega} \end{aligned} \right\} \dots (1)$$

where ω is the frequency, n^2 is the dielectric constant of the medium and σ is the conductivity of the medium. n and σ in general depend on ω .

Introducing scalar and vector potentials ϕ and A as usual we have

$$\left. \begin{aligned} H_{\omega} &= \text{rot } A_{\omega} \\ E_{\omega} &= -\frac{i\omega}{c} A_{\omega} - \text{grad } \phi_{\omega} \\ \nabla^2 A_{\omega} + \frac{1}{c^2} (\omega^2 n^2 - i4\pi\sigma\omega) A_{\omega} &= -\frac{4\pi}{c} j_{\omega} \\ \nabla^2 \phi_{\omega} + \frac{1}{c^2} (\omega^2 n^2 - i4\pi\sigma\omega) \phi_{\omega} &= -\frac{4\pi}{n^2} \rho \end{aligned} \right\} \dots (2)$$

with the modified Lorentz condition

$$\text{div } A_{\omega} + \frac{1}{c} (4\pi\sigma + i\omega n^2) \phi_{\omega} = 0.$$

Let the particle be moving along the z direction with uniform velocity v . Then in cylindrical co-ordinates the components of vector potential are

$$A_\rho = 0 = A_\varphi \text{ and}$$

$$\frac{\partial^2 A_z}{\partial \rho^2} + \frac{1}{\rho} \frac{\partial A_z}{\partial \rho} + \frac{\partial^2 A_z}{\partial z^2} + \frac{1}{c^2} (\omega^2 n^2 - i 4\pi\sigma\omega) A_z = -\frac{e}{\pi c\rho} e^{-i\omega \frac{z}{v}} \delta(\rho) \quad \dots (3)$$

$$\text{Let } A_z = u(\rho) e^{-i\omega \frac{z}{v}} \quad \dots (4)$$

$$\text{From (3)} \quad \frac{\partial^2 u}{\partial \rho^2} + \frac{1}{\rho} \frac{\partial u}{\partial \rho} + s^2 u = -\frac{e}{\pi c\rho} \delta(\rho), \quad \dots (5)$$

$$\text{where } s^2 = \frac{w^2}{v^2} \left\{ (n^2 \beta^2 - 1) - i \frac{4\pi\sigma\beta^2}{\omega} \right\}, \quad \beta = \frac{v}{c}.$$

$$\text{If } s = s_1 + i s_2, \text{ then}$$

$$s_1^2 - s_2^2 = \frac{w^2}{v^2} (n^2 \beta^2 - 1) \quad \dots (6)$$

$$s_1 s_2 = -\frac{2\pi\sigma\omega}{c^2} \quad \dots (7)$$

From these we have

$$\left. \begin{aligned} s_1 &= \pm \frac{\omega}{\sqrt{2v}} \left[\left\{ (n^2 \beta^2 - 1)^2 + \frac{16\pi^2 \sigma^2 \beta^4}{\omega^2} \right\}^{\frac{1}{2}} + (n^2 \beta^2 - 1) \right]^{\frac{1}{2}}, \\ s_2 &= \pm \frac{\omega}{\sqrt{2v}} \left[\left\{ (n^2 \beta^2 - 1)^2 + \frac{16\pi^2 \sigma^2 \beta^4}{\omega^2} \right\}^{\frac{1}{2}} - (n^2 \beta^2 - 1) \right]^{\frac{1}{2}} \text{ when } n^2 \beta^2 - 1 \geq 0 \\ \text{and} \\ s_1 &= \pm \frac{\omega}{\sqrt{2v}} \left[\left\{ (1 - n^2 \beta^2)^2 + \frac{16\pi^2 \sigma^2 \beta^4}{\omega^2} \right\}^{\frac{1}{2}} - (1 - n^2 \beta^2) \right]^{\frac{1}{2}}, \\ s_2 &= \pm \frac{\omega}{\sqrt{2v}} \left[\left\{ (1 - n^2 \beta^2)^2 + \frac{16\pi^2 \sigma^2 \beta^4}{\omega^2} \right\}^{\frac{1}{2}} + (1 - n^2 \beta^2) \right]^{\frac{1}{2}} \text{ when } n^2 \beta^2 - 1 < 0. \end{aligned} \right\} \quad \dots (8)$$

The right hand side of (7) is independent of v and it represents rectangular hyperbola with v varying. In (8) there is an ambiguity in sign and it may lead to different values of s_1 and s_2 . But from (7) s_1 and s_2 have opposite signs, so only two cases are possible.

Case I : $s_1 > 0$ and $s_2 < 0$.

s_1 and s_2 lie on the same branch of the hyperbola (7). For the outgoing wave $u = BH_0^{(2)}(s\rho)$ and $B = -(ie/2c)$ which is fixed by the strength of the singularity at $\rho = 0$.

Here $A_z(\omega) = BH_0^{(2)}(s\rho) e^{-\frac{i\omega z}{v} + i\omega t}$

Using the asymptotic form of $H_0^{(2)}(s\rho)$ for $|s\rho| \gg 1$,

$$A_z(\omega) = -iB_1(\alpha_1 + i\beta_1) \frac{1}{\sqrt{\rho}} e^{s_2\rho} e^{i\omega\chi}, \quad \dots (9)$$

where

$$B_1 = \frac{e}{2c} \sqrt{\frac{2}{\pi(s_1^2 + s_2^2)}},$$

$$\alpha_1 = \frac{1}{\sqrt{2}} (\sqrt{s_1^2 + s_2^2} + s_1)^{\frac{1}{2}}, \quad \beta_1 = \frac{1}{\sqrt{2}} (\sqrt{s_1^2 + s_2^2} - s_1)^{\frac{1}{2}}$$

and

$$\chi = t - \left(\frac{z}{v} + \frac{s_1}{\omega} \rho \right) + \frac{\pi}{4\omega} \quad \dots (10)$$

Case II. $s_1 < 0$ and $s_2 > 0$.

In this case s_1 and s_2 lie on the opposite branch of the hyperbola (7).

For the outgoing wave $u = \frac{ie}{2c} H_0^{(1)}(s\rho)$

and

$$A_z(\omega) = \frac{ie}{2c} H_0^{(1)}(s\rho) e^{-i\omega \frac{z}{v} + i\omega t}$$

In the asymptotic form when $(s\rho) \gg 1$,

$$A_z(\omega) = -iB_1(\alpha_1 + i\beta_1) \frac{1}{\sqrt{\rho}} e^{-s_2\rho} e^{i\omega \left\{ t - \left(\frac{z}{v} - \frac{s_1}{\omega} \rho \right) + \frac{3\pi}{4\omega} \right\}} \quad \dots (11)$$

The expression of $A_z(\omega)$ in (9) and (11) are identical. There is only a phase difference of π . More over there is no discontinuity of s_1 and s_2 in either case.

By (2) and (9) the field strengths are

$$\left. \begin{aligned} H_{\varphi}(\omega) &= -iB_1(\alpha_1 + i\beta_1) \left[\frac{1}{2\rho} - s_2 + is_1 \right] \frac{1}{\sqrt{\rho}} e^{s_2\rho} e^{i\omega\chi} \\ E_{\rho}(\omega) &= B_1 \frac{wc}{v} (\alpha_1 + i\beta_1) \frac{4\pi\sigma - i\omega n^2}{16\pi^2\sigma^2 + \omega^2 n^4} \left[\frac{1}{2\rho} - s_2 + is_1 \right] \frac{1}{\sqrt{\rho}} e^{s_2\rho} e^{i\omega\chi} \\ E_z(\omega) &= -iB_1(\alpha_1 + i\beta_1) \left[\frac{i\omega}{c} + \frac{\omega^2 c}{v^2} \frac{4\pi\sigma - i\omega n^2}{16\pi^2\sigma^2 + \omega^2 n^4} \right] \frac{1}{\sqrt{\rho}} e^{s_2\rho} e^{i\omega\chi} \end{aligned} \right\} \dots (12)$$

$$\left. \begin{aligned} ReH_{\varphi}(\omega) &= B_1 \frac{1}{\sqrt{\rho}} e^{s_2\rho} \left[\left\{ \beta_1 \left(\frac{1}{2\rho} - s_2 \right) + \alpha_1 s_1 \right\} \cos \omega\chi \right. \\ &\quad \left. + \left\{ \alpha_1 \left(\frac{1}{2\rho} - s_2 \right) - \beta_1 s_1 \right\} \sin \omega\chi \right] \\ ReE_{\rho}(\omega) &= B_1 \frac{wc}{v(16\pi^2\sigma^2 + \omega^2 n^4)} \frac{1}{\sqrt{\rho}} e^{s_2\rho} \left[\left\{ (4\pi\sigma\alpha_1 + \omega n^2\beta_1) \left(\frac{1}{2\rho} - s_2 \right) \right. \right. \\ &\quad \left. \left. - (4\pi\sigma\beta_1 - \omega n^2\alpha_1) s_1 \right\} \cos \omega\chi - \left\{ (4\pi\sigma\alpha_1 + \omega n^2\beta_1) s_1 + (4\pi\sigma\beta_1 - \omega n^2\alpha_1) \right. \right. \\ &\quad \left. \left. \left(\frac{1}{2\rho} - s_2 \right) \right\} \sin \omega\chi \right] \end{aligned} \right\} \dots (13)$$

$$\left. \begin{aligned} ReE_z(\omega) &= -B_1 \frac{1}{\sqrt{\rho}} e^{s_2\rho} \left[\left\{ \frac{\beta_1}{v^2} \frac{4\pi\omega^2 c\sigma}{16\pi^2\sigma^2 + \omega^2 n^4} \right. \right. \\ &\quad \left. \left. + \alpha_1 \left(\frac{\omega}{c} - \frac{\omega^3 cn^2}{v^2} \frac{1}{16\pi\sigma^2 + \omega^2 n^4} \right) \right\} \cos \omega\chi \right. \\ &\quad \left. + \left\{ \frac{\alpha_1}{v^2} \frac{4\pi\omega^2 c\sigma}{16\pi^2\sigma^2 + \omega^2 n^4} - \beta_1 \left(\frac{\omega}{c} - \frac{\omega^3 cn^2}{v^2} \frac{1}{16\pi\sigma^2 + \omega^2 n^4} \right) \right\} \sin \omega\chi \right] \\ H_{\varphi} &= \int_0^{\infty} 2[ReH_{\varphi}(\omega)]d\omega \\ E_{\rho} &= \int_0^{\infty} 2[ReE_{\rho}(\omega)]d\omega \\ E_z &= \int_0^{\infty} 2[ReE_z(\omega)]d\omega \end{aligned} \right\} \dots (14)$$

CONCLUSION

(i) The value of A_z in (9) reveals that no restriction on the particle velocity is required for the outgoing wave propagation, though it is damped. Thus Cherenkov radiation takes place at any velocity of the particle in a medium having certain amount of conductivity.

(ii) The energy radiated through the surface of a cylinder per unit length whose axis is the line of motion of the electron is given by

$$\begin{aligned} \frac{dW}{dt} &= - \frac{1}{2} \int_{-\infty}^{\infty} E_z H_{\phi} dt \\ &= \frac{e^2}{c} \int_0^{\infty} \frac{1}{s_1^2 + s_2^2} \left[\{ \alpha_1(s_1 - s_2) - \beta_1(s_1 + s_2) \} \left\{ \frac{1}{v^2} (\alpha_1 + \beta_1) \frac{4\pi\omega^2 c \sigma}{16\pi^2 \sigma^2 + \omega^2 n^4} \right. \right. \\ &\quad \left. \left. + (\alpha_1 - \beta_1) \left(\frac{\omega}{c} - \frac{\omega^3 c b^2}{v^2} \frac{1}{16\pi^2 \sigma^2 + \omega^2 n^4} \right) \right\} \right] d\omega \quad \dots (15) \end{aligned}$$

This expression leads to the correct limiting case $\sigma = 0$ which is give by

$$\frac{dW}{dt} = \frac{e^2}{c^2} \int_0^{\infty} \left(1 - \frac{1}{\beta^2 n^2} \right) \omega d\omega.$$

(iii) From (10) the semi-vertical angle of the cone of radiation $\theta_1 = \tan^{-1}(vs_1/\omega)$. It is different from Chrenkov relation $\theta = \cos^{-1}(1/n\beta)$. Comparing the values of θ_1 with those of θ against v one can observe that the cone of Cherenkov radiation in a conducting medium is generally wider than that of a non-conducting medium. For the values of v between 0 and c/n , θ has no value (i.e. no Cherenkov radiation takes place) but θ_1 has singificant values which means that the Cherenkov radiation takes place in conducting medium.

(iv) The penetration length

$$\left. \begin{aligned} a &= \frac{\sqrt{2}v}{\omega \left[\left\{ (n^2 \beta^2 - 1)^2 + \frac{16\pi^2 \sigma^2 \beta^4}{\omega^2} \right\}^{\frac{1}{2}} - (n^2 \beta^2 - 1) \right]^{\frac{1}{2}}} \text{ when } n^2 \beta^2 - 1 \geq 0, \\ \text{or} \\ a &= \frac{\sqrt{2}v}{\omega \left[\left\{ (1 - n^2 \beta^2)^2 + \frac{16\pi^2 \sigma^2 \beta^4}{\omega^2} \right\}^{\frac{1}{2}} + (1 - n^2 \beta^2) \right]^{\frac{1}{2}}} \text{ when } n^2 \beta^2 - 1 < 0. \end{aligned} \right\} \dots (16)$$

The values of a for typical values of v are given below :

$$(I) \quad v = \frac{c}{n}, \quad a = \frac{c}{\sqrt{2\pi\omega\sigma}}$$

$$(II) \quad v = c \text{ and } n = 1, \quad a = \frac{c}{\sqrt{2\pi\omega\sigma}}$$

$$(III) \quad \text{when } v = c, n > 1 \text{ and } \sigma \text{ is very small, } a \approx \frac{c}{2\pi} \frac{\sqrt{n^2-1}}{\sigma} \dots \quad (17)$$

In the usual electromagnetic phenomenon the penetration length = $\frac{cn}{2\pi\sigma}$. It is interesting to compare (17) with this expression.

(v) There is a critical value of v depending on the medium. The penetration length changes rapidly with v until v attains critical value after which it changes very slowly.

(vi) The wave length of the radiation is given by

$$\left. \begin{aligned} \lambda &= \frac{2\sqrt{2\pi v}}{\omega \left[\left\{ (n^2\beta^2-1)^2 + \frac{16\pi^2\sigma^2\beta^4}{\omega^2} \right\}^{\frac{1}{2}} + (n^2\beta^2+1) \right]^{\frac{1}{2}}} \quad \text{when } n^2\beta^2-1 \geq 0, \\ \text{and} \\ \lambda &= \frac{2\sqrt{2\pi v}}{\omega \left[\left\{ (1-n^2\beta^2)^2 + \frac{16\pi^2\sigma^2\beta^4}{\omega^2} \right\}^{\frac{1}{2}} + (n^2\beta^2+1) \right]^{\frac{1}{2}}} \quad \text{when } n^2\beta^2-1 < 0. \end{aligned} \right\} \dots \quad (18)$$

One sees that a and λ are comparable when $n^2\beta^2-1 < 0$. At the first sight it may be seen that under these circumstances Cherenkov Radiation though produced it becomes unimportant. But that is actually not the case. Since if the conducting material be in the form of a thin wafer, a narrow cylinder or something of this sort then outside the medium, e.g. in vacuum one will have a substantial effect. Calculation stemming from these consideration are in progress and will be communicated elsewhere.

ACKNOWLEDGMENT

I express my sincere thanks to Dr. T. C. Roy of Jadavpur University, for his kind help in the preparation of this paper.

REFERENCE

Jelley, J. V., 1959 *Cherenkov Radiation and its application*. Pergamon Press.

EXCITATION OF 1^1S STATE TO 2^1S STATE OF HELIUM ATOM BY ELECTRON IMPACT IN OCHKUR APPROXIMATION

S. N. BANERJEE

DEPARTMENT OF THEORETICAL PHYSICS,
INDIAN ASSOCIATION FOR THE CULTIVATION OF SCIENCE,
JADAVPUR, CALCUTTA-32

(Received August 12, 1966)

ABSTRACT. The cross section for 1^1S - 2^1S transition of helium atom by electron impact has been investigated in Ochkur (1964) approximation near threshold for excitation. The total excitation cross-section in the energy range 20.6 eV to 24 eV of incident electron energy has been compared with the most recent experimental findings of Holt and Krotkov (1966).

INTRODUCTION

Several theoretical attempts have been made to calculate the cross section for the electronic excitation from the ground state of helium atom to the 2^1S state. Massey and Mohr (1933) have calculated the excitation cross-section in the Born approximation. Massey and Moiseiwitsch (1954) have used a distorted-wave method in which the coupling between the singlet and triplet metastable levels was neglected. Fox (1965) has applied Born approximation to calculate the above transition cross section in the high-energy region, using various analytical functions for the ground state and the wave function of Marriott and Seaton (1957) for the 2^1S state, which is made explicitly orthogonal to the different ground state functions. Marriott (1964) has carried out numerical computation of partial cross sections for $l = 0, 1, 2, 3$ for the elastic collision and the inelastic transitions to 2^1S and 2^3S states from the ground state wherein the electron exchange effect has been allowed for and all coupling terms between 1^1S , 2^1S and 2^3S states have been retained.

In the present work, we have used Ochkur (1963) approximation to calculate the 1^1S - 2^1S transition cross section. The ground state wave function of helium atom is taken to be that of Green *et al* (1954) and the 2^1S state wave function is taken as a linear combination of the form of Marriott and Seaton (1957) and that of Green (1954) so as to be explicitly orthogonal to ground state wave function.

We have carried out our calculation in the energy range near the threshold for excitation where recent experimental results of Holt and Krotkov (1966) are available for comparison.

T H E O R Y

The first Born approximation to the excitation amplitude for the transition from the ground state of helium atom with wave function $\psi_0(r_1, r_2)$ to the n th excited state $\psi_n(r_1, r_2)$ is given by (in atomic units)

$$f_B(k_0, k_n) = -\frac{2}{q^2} \int \int \psi_n^*(r_1, r_2) \left\{ e^{iq \cdot r_1} + e^{iq \cdot r_2} \right\} \\ \times \psi_0(r_1, r_2) dr_1 dr_2$$

Where k_0, k_n are the momenta of the incident and scattered electrons and $q = |k_0 - k_n|$.

The corresponding exchange transition amplitude in Ochkur approximation is given by

$$q(k_0, k_n) = \frac{q^2}{2K_0^2} f_B(k_0, k_n).$$

The wave-function for 2¹S state should be orthogonal to the original ground state wave function $\psi_0(r_1, r_2)$. However, the wave-function of Marriott and Seaton (1957) for 2¹S state is not orthogonal to the ground state wavefunction of Green *et al* (1954) to be used in our calculation. Following Fox (1965), we have chosen the wave-function of 2¹S state as a linear combination of the form of Marriott and Seaton (1957) and that of Green *et al* (1954) so that the resulting wave function is explicitly orthogonal to the above ground state wave function.

The ground state wave function of helium atom due to Green *et al* (1964) is

$$\psi_0(r_1, r_2) = \phi_0(r_1) \phi_0(r_2)$$

where

$$\phi_0(r) = N(e^{-Zr} + c e^{-2Zr})$$

with

$$Z = 1.4558$$

$$N = .837389$$

$$c = .60.$$

The orthogonalised 2¹S state wave function we have used is

$$\psi_2^{1s} = \frac{1}{\sqrt{1-\Delta^2}} [\psi_2^{MS}(r_1, r_2) - \Delta \psi_0]$$

where $\psi_2^{MS}(r_1, r_2)$ is the wave function for 2¹S state of Marriott and Seaton (1957)

$$\text{i.e. } \psi_2^{MS}(r_1, r_2) = \frac{2^{1/4} \times .478}{\pi} [e^{-2r_1} (e^{-1.136r_2} - .317r_2 e^{-.464r_2}) \\ + e^{-2r_2} (e^{-1.136r_1} - .317r_1 e^{-.464r_1})]$$

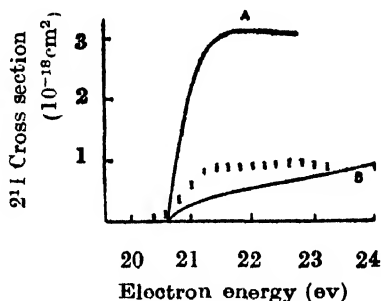
and

$$\Delta = \int \psi_2^{MS}(r_1, r_2) \psi_0(r_1, r_2) dr_1 dr_2$$

The total cross section Q on is obtained by integrating numerically the differential cross section $\frac{K_n}{K_0} |f-g|^2$ over all possible angles with the help of Gaussian Quadrature formula.

RESULTS AND DISCUSSION

We have calculated the excitation cross section for the transition 1^1S-2^1S in the energy range of 20.6 eV to 24 eV and have given a plot of the same against energy in the adjoining figure. The theoretical curve of Marriott (1964) and the experimental findings of Holt and Krotkov (1966) are shown in the figure for comparison. Here we notice that in the vicinity of threshold for excitation, our results compare favourably with the experimental results of Holt and Krotkov (1966). However, further away from threshold our cross-section values gradually increase with energy whereas the experimental values rise rapidly to a plateau $(1.0 \pm .3) \times 10^{-18} \text{ cm}^2$ at an energy 21.22 eV (approximately) and then remain almost constant.



The total cross-section for production of the 2^1S state. Curve A—Calculation by Marriott (1964); Curve B—present calculation. I—are the experimental data of Holt and Krotkov (1966).

It may be mentioned that we have compared our results of total excitation cross-sections with the most recent experimental findings of Holt and Krotkov (1966) who have measured the total cross-section for excitation of the 2^1S state in helium by electron bombardment, with the cross-section scale adjusted so that the 2^3S peak is exactly $3 \times 10^{-18} \text{ cm}^2$. The values of the excitation cross section calculated by Marriott though in fair agreement with the experimental findings of Schulz and Fox (1957), are higher than the present theoretical values as well as the experimental findings of Holt and Krotkov (1966).

In conclusion, we find that Ochkur approximation which is comparatively simple gives fairly good results when compared with other laborious and more complicated methods. The total cross section for 1^1S-3^1S state is under investigation.

ACKNOWLEDGEMENT

The author is thankful to Prof. D. Basu for his kind interest and valuable discussions throughout the progress of the work. Thanks are also due to Dr. Dr. N. C. Sil for helpful discussions.

REFERENCES

- Fox, M. A., 1965, *Proc. Phys. Soc.*, 86.
Holt, H. K., and Krotkov, R., 1966, *Phys. Rev.*, **144**, 82-93.
Marriott, R., 1964, *Atomic Collision Processes*, North-Holland Publishing Company, Amsterdam.
Marriott, R., and Seaton, M. J., 1957, *Proc. Phys. Soc.* **70**, 296.
Massey, H. S. W., and Moiseiwitsch, B. L., 1954, *Proc. Roy. Soc. (London)*, **A227**, 38.
Massey, H. S. W., and Mohr, C. B. O., 1933, *Proc. Roy. Soc. (London)*, **A**, **140**, 633.
Oehkur, V. I., 1963, *JETP* **45**, 734.
Schulz, G. J., and Fox, R. E., 1957, *Phys. Rev.*, **106**, 1179.

CHERENKOV RADIATION IN A SEMI-INFINITE DIELECTRIC MEDIUM WITH A CONDUCTING BOUNDARY

R. M. KHAN

DEPT. OF MATHEMATICS, CITY COLLEGE, CALCUTTA.

(Received September 9, 1966)

ABSTRACT. Cherenkov radiation due to the passage of a point charge moving parallel to the conducting boundary inside a semi-infinite dielectric medium has been studied. The formulae obtained are in agreement with the formulae for Cherenkov radiation of electron in an infinite homogeneous medium in the limiting case.

INTRODUCTION

Linhart (1955) and Danos (1955) worked out the problem of Cherenkov radiation emitted by an electron moving in vacuum with uniform motion on a straight line parallel to the plane face of semi-infinite dielectric medium. Here we propose to calculate electro-magnetic field and Cherenkov radiation due to a charge particle moving inside a semi-infinite dielectric medium with a constant velocity on a straight line parallel to the plane boundary. The other side is a semi-infinite conducting medium. The conductivity is assumed to be high and in fact taken to be infinite for simplicity of calculation.

STATEMENT OF PROBLEM

Let $x = 0$ be the equation of the boundary surface; $x > 0$, the dielectric medium and $x < 0$, the conducting medium. A particle of charge e is moving with a constant velocity v in a straight line parallel to z -axis at a distance a from the boundary surface. We are interested in the case when v is greater than the phase velocity of light in the dielectric medium.

Maxwell's equations for field variables E and H are

$$\left. \begin{aligned} \text{rot } H_{\omega} &= \frac{i\omega}{c} E_{\omega} + \frac{4\pi}{c} j_{\omega} \\ \text{rot } E_{\omega} &= -\frac{i\omega}{c} H_{\omega} \\ \text{div } E_{\omega} &= \frac{4\pi}{\epsilon} \rho_{\omega} \\ \text{div } H_{\omega} &= 0, \end{aligned} \right\} \dots (1)$$

where j is the current density, ρ is the density of free charges and ϵ is the dielectric constant. All quantities are used as Fourier Transform. Introducing vector and scalar potential A and ϕ we arrive at the following set :

$$\left. \begin{aligned} H_{\omega} &= \text{rot } A_{\omega} \\ E_{\omega} &= -\frac{i\omega}{c} A_{\omega} - \text{grad } \phi_{\omega} \\ \nabla^2 A_{\omega} + \frac{\epsilon\omega^2}{c^2} A_{\omega} &= -\frac{4\pi}{c} j_{\omega} \\ \text{with the condition } \text{div } A_{\omega} + \frac{i\epsilon\omega}{c} \phi_{\omega} &= 0 \end{aligned} \right\} \dots (2)$$

$$\text{Here } j_x = 0 = j_y \text{ and } j_z = ev\delta(x-a)\delta(y)\delta(z-vt) \dots (3)$$

SOLUTION

Taking $A_x = 0 = A_y$,

$$\nabla^2 A_z + \frac{c\omega^2}{c^2} A_z = -\frac{2e}{c} \delta(x-a)\delta(y)e^{-i\omega \frac{z}{v}} \dots (4)$$

To solve the equation (4) we assume that

$$A_z = u(x, y)e^{-\frac{i\omega z}{v}}.$$

From (4) we have

$$\frac{\partial^2 u}{\partial x^2} + \frac{\partial^2 u}{\partial y^2} + s^2 u = -\frac{2e}{c} \delta(x-a)\delta(y), \dots (5)$$

where

$$s^2 = \frac{w^2}{v^2} (\epsilon\beta^2 - 1), \quad \beta = \frac{v}{c}.$$

There is no electromagnetic field inside the conducting medium. On the boundary surface tangential components of E and normal components of H should be zero. To satisfy these conditions u and $\partial u/\partial y$ should be zero at $x = 0$. Besides there is a singularity at $x = a, y = 0$. Thus the solution of (5) is

$$u = -\frac{ie}{2c} [H_0^{(2)}(sq_1) - H_0^{(2)}(sq_2)], \dots (6)$$

where

$$q_1^2 = (x-a)^2 + y^2, \quad q_2^2 = (x+a)^2 + y^2.$$

$$\left. \begin{aligned} \therefore A_z(\omega) &= -\frac{ie}{2c} [H_0^{(2)}(sq_1) - H_0^{(2)}(sq_2)] e^{-i\omega \left(t - \frac{z}{v}\right)} \\ \text{and } \phi(\omega) &= -\frac{ie}{2v\epsilon} [H_0^{(2)}(sq_1) - H_0^{(2)}(sq_2)] e^{-i\omega \left(t - \frac{z}{v}\right)} \end{aligned} \right\} \dots (7)$$

The field components are

$$\left. \begin{aligned} H_x(\omega) &= \frac{ics}{2c} \left[\frac{y}{q_1} H_1^{(2)}(sq_1) - \frac{y}{q_2} H_1^{(2)}(sq_2) \right] e^{i\omega \left(t - \frac{z}{v} \right)} \\ H_y(\omega) &= -\frac{ies}{2c} \left[\frac{x-a}{q_1} H_1^{(2)}(sq_1) - \frac{x+a}{q_2} H_1^{(2)}(sq_2) \right] e^{i\omega \left(t - \frac{z}{v} \right)} \\ E_x(\omega) &= -\frac{ies}{2v\epsilon} \left[\frac{x-a}{q_1} H_1^{(2)}(sq_1) - \frac{x+a}{q_2} H_1^{(2)}(sq_2) \right] e^{i\omega \left(t - \frac{z}{v} \right)} \\ E_y(\omega) &= \frac{-ies}{2v\epsilon} \left[\frac{y}{q_1} H_1^{(2)}(sq_1) - \frac{y}{q_2} H_1^{(2)}(sq_2) \right] e^{i\omega \left(t - \frac{z}{v} \right)} \\ E_z(\omega) &= -\left[\frac{es^2}{2\omega\epsilon} [H_0^{(2)}(sq_1) - H_0^{(2)}(sq_2)] \right] e^{i\omega \left(t - \frac{z}{v} \right)} \end{aligned} \right\} \dots \quad (8)$$

One can easily verify that tangential components E_y and E_z and normal component H_x are zero at $x = 0$.

Surface charge and surface current : One notes that the normal component E_x and tangential component H produce surface charge and surface current on the boundary surface. If Σ and K are the surface charge density and surface current density then

$$4\pi\Sigma = Re(\epsilon E_x)_{x=0} = -\frac{ea}{v} \int \frac{s}{q} \left[J_1(sq) \sin \omega \left(t - \frac{z}{v} \right) + N_1(sq) \cos \omega \left(t - \frac{z}{v} \right) \right] dw \quad \dots \quad (9)$$

$$4\pi K = Re(H_y)_{x=0} = -ea \int \frac{s}{q} \left[J_1(sq) \sin \omega \left(t - \frac{z}{v} \right) + N_1(sq) \cos \omega \left(t - \frac{z}{v} \right) \right] dw$$

$$\text{where } q^2 = a^2 + y^2. \quad \dots \quad (10)$$

Equation (9) shows that $\Sigma \rightarrow 0$ and $a \rightarrow 0$, i.e. there will be no surface charge when the point charge moves very closely to the boundary surface. This may be understood if we imagine a particle of opposite charge at the image point of the real particle similar to the static case. If the distance between these two oppositely charged particles is very small, the medium is not effectively polarized due to equal amount of polarization by the oppositely charged particles.

Calculation of Radiation : We now calculate the total energy radiated by the point charge through the surface of a half cylinder of large radius with the axis as z -axis. In cylindrical co-ordinates (r, θ, z)

$$\begin{aligned} H_\theta &= -H_x \sin \theta + H_y \cos \theta \\ &= \frac{-ies}{2c} \left[H_1^{(2)}(sq_1) \frac{r - a \cos \theta}{q_1} - H_1^{(2)}(sq_2) \frac{r + a \cos \theta}{q_2} \right] e^{i\omega \left(t - \frac{z}{v} \right)} \end{aligned} \quad \dots \quad (11)$$

$$\text{where } q_1^2 = r^2 - 2ar \cos \theta + a^2, \quad q_2^2 = r^2 + 2ar \cos \theta + a^2.$$

For large values of r ,

$$\left. \begin{aligned} H_\theta(\omega) &= \frac{es}{2c} \sqrt{\frac{2}{\pi sr}} \left[e^{-is(r-a \cos \theta) + i\frac{\pi}{4}} - e^{-is(r+a \cos \theta) + i\frac{\pi}{4}} \right] e^{i\omega \left(t - \frac{z}{v} \right)} \\ E_z(\omega) &= -\frac{es^2}{2\omega\epsilon} \sqrt{\frac{2}{\pi sr}} \left[e^{-is(r-a \cos \theta) + i\frac{\pi}{4}} - e^{-is(r+a \cos \theta) + i\frac{\pi}{4}} \right] e^{i\omega \left(t - \frac{z}{v} \right)} \end{aligned} \right\} \quad (12)$$

Since $s > 0$, waves (partly reflected at the boundary) are propagated at a large distance from the boundary surface.

$$\left. \begin{aligned} ReH_\theta &= \int_0^\infty \frac{2es}{c} \sqrt{\frac{2}{\pi sr}} \sin \omega \left(t - \frac{z}{v} - \frac{sr}{\omega} + \frac{\pi}{4\omega} \right) \sin(sa \cos \theta) d\omega \\ ReE_z &= -\int_0^\infty \frac{2es}{\epsilon\omega} \sqrt{\frac{2}{\pi sr}} \sin \omega \left(t - \frac{z}{v} - \frac{sr}{\omega} + \frac{\pi}{4\omega} \right) \sin(sa \cos \theta) d\omega \end{aligned} \right\} \quad \dots \quad (13)$$

Radiation through the surface per unit length is

$$\begin{aligned} \frac{dW}{dt} &= \frac{c}{4\pi} \int_{-\infty}^\infty \int_{-\frac{\pi}{2}}^{\frac{\pi}{2}} (-R_\theta H_\theta \cdot R_\theta E_z) r \, d\theta \, dt \\ &= \frac{e^2}{c^2} \int_0^\infty \left(1 - \frac{1}{\epsilon\beta^2} \right) \omega [1 - J_0(2sa)] d\omega \end{aligned} \quad \dots \quad (14)$$

$$\text{In practice} \quad \frac{dW}{dt} = \frac{e^2}{c^2} \int_0^{\omega_{max}} \left(1 - \frac{1}{\epsilon\beta^2} \right) \omega [1 - J_0(2sa)] d\omega \quad \dots \quad (15)$$

DISCUSSION

Energy loss per unit frequency interval per unit length is given by

$$S = \frac{e^2}{c^2} \left(1 - \frac{1}{\epsilon\beta^2} \right) \omega [1 - J_0(2sa)] \quad \dots \quad (16)$$

In the limit when $a \rightarrow \infty$ the equation (16) should go to the expression of the homogeneous medium.

In infinite homogeneous dielectric medium Cherenkov radiation per unit frequency interval per unit path length is

$$S' = \frac{e^2}{c^2} \left(1 - \frac{1}{\epsilon\beta^2} \right) \omega \quad \dots \quad (17)$$

which obviously is the limit of S when $a \rightarrow \infty$.

When $a \rightarrow 0$, $S \rightarrow 0$, i.e. Cherenkov radiation does not take place, if the point charge moves closely to the boundary surface. It is due to the effect of a particle of opposite charge at the image point of the point charge.

If the distance of the particle from the boundary surface is increased, $J_0(2sa) < 1$ until the first zero of J_0 is obtained. In this case $S < S'$. Though the boundary surface reflects the waves, the point charge at the image point which is effectively the surface charge polarizes the medium in opposite direction and ultimately the total energy loss becomes less than the ordinary Cherenkov radiation. Thus in this situation the conducting barrier reduces the radiation. After the first zero of J_0 , $J_0 < 0$ until the second zero is obtained. In this case $S > S'$ i.e. by suitably adjusting the distance of the particle from the boundary surface the energy loss can be increased and it may be greater than ordinary Cherenkov radiation. Considering all these results we conclude that S oscillates with a and ultimately it converges to S' . A similar phenomenon though not exactly identical with the previous case occurs when variable of radiation intensity are considered as a function of w . These variations of intensity with a are to be traced to the phenomenon of interference.

ACKNOWLEDGMENT

The author expresses his thanks to Dr. T. C. Roy, Jadavpur University, for help in preparation of this manuscript.

REFERENCES

- Linhart, J. G. 1955, *J. App. Phys.* 26.
- Danos, M. 1955, *J. App. Phys.* 26.
- Jackson, J. D., *Classical Electrodynamics*.
- Jolley, J. V., *Cherenkov Radiation and its application*. Pergamon Press.

FLAME EMISSION SPECTRUM OF SnO MOLECULE IN THE VISIBLE REGION

M. M. JOSHI AND R. YAMDAGNI

DEPARTMENT OF PHYSICS, UNIVERSITY OF ALLAHABAD, INDIA

(Received August 20, 1965; Resubmitted August 20, 1966)

(Plate 2 and 3)

ABSTRACT. The emission from the flame containing tin halides or metallic tin has been investigated in the visible region. One hundred and thirteen bands have been photographed in the region $\lambda\lambda$ 6480-3500 and have been attributed to the diatomic oxide SnO . Most of these bands have been arranged into three systems—A, B and C, whose lower level has been identified to be the ground state. It has been found that Mahanti's systems B and C do not exist separately but are in fact parts of the present system $C \rightarrow X$. Vibrational schemes have been drawn according to the following expressions:

$$A \rightarrow X, v = 19073.8 + 453.0(v' + \frac{1}{2}) - 4.00(v' + \frac{1}{2})^2 - 822.4(v'' + \frac{1}{2}) + 3.73(v'' + \frac{1}{2})^2.$$

$$B \rightarrow X, v = 24312.8 + 595.0(v' + \frac{1}{2}) - 3.90(v' + \frac{1}{2})^2 - 0.25(v' + \frac{1}{2})^3 - 822.4(v'' + \frac{1}{2}) + 3.73(v'' + \frac{1}{2})^2.$$

$$C \rightarrow X, v = 25448.5 + 561.0(v' + \frac{1}{2}) - 1.20(v' + \frac{1}{2})^2 - 0.16(v' + \frac{1}{2})^3 - 822.4(v'' + \frac{1}{2}) + 3.73(v'' + \frac{1}{2})^2.$$

The $v''=2$ level has been found to be perturbed in both the systems B and C. Some bands have also been added to the already known system D.

INTRODUCTION

While studying the emission spectrum of the oxy-coal-gas flame containing tin sulphide or tin chloride, Eder and Valenta (1924) for the first time reported the presence of all marked red degraded bands which extended through the blue and the near ultraviolet regions. Later on, these bands are also recorded in the arc spectrum of metallic tin on carbon poles by Mahanti (1931), who attributed them to the diatomic molecule SnO . Mahanti arranged these bands in three systems and termed them as A, B and C. The system A occurring in the region $\lambda\lambda$ 4490-3200 was the most intense one and all the principal bands fitted into it. System B and C were, however, weak and fragmentary. Connelly (1933) photographed the emission and absorption spectrum of SnO in $\lambda\lambda$ 4660-3070 region, and furnished an extended and revised vibrational scheme for Mahanti's A system which he designated as $D \rightleftharpoons X$. Connelly, however, questioned the separate existence of the B and C systems while, Pearce and Gaydon (1941) have referred their vibrational analyses as uncertain. The ultraviolet absorption was studied in emission by Loomis and Watson (1934); in absorption by Sharma (1944); and an extensive study of this region was also made by Eisler and Barrow (1949). Barrow and Rowlinson (1954) studied the absorption in the Schumann region. Jevons (1938) removed certain anomalies in the values of the anharmonic coefficients by proposing

a new expression for Connolly's D system. The rotational analysis of the (1, 0), (0, 0) and (0, 1) bands of the D system was performed by Lagerquist, Nilsson and Wigartz (1959) and according to them the system corresponds to $^1\pi-^1\Sigma$ transition. It is evident from the foregoing that while the spectroscopic constants for the D system are well established, and fairly reliable information is available for the ultraviolet and Schumann region, no satisfactory data for the visible region, on the longer wavelength side of $\lambda 4660$ region, exist. Whatever little information we possess is insufficient to draw any definite conclusions. On the other hand several well marked band systems, stretching almost through the entire visible region are known to exist for the PbO molecule; Mecke (1929); Bloomenthal (1930); Shawhan and Morgan (1935); Howell (1936); and Barrow, Deutsch and Travis (1961). Similar band systems for SnO molecule can therefore be reasonably expected. The aim of the present communication is to report the fresh results obtained by the authors in the $\lambda\lambda 6480-3200$ region of the flame spectrum of the SnO molecule.

EXPERIMENTAL

The flame apparatus, described in figure 1 was used as the source of emission. A solution of pure stannic chloride, sucked through *T*, was fed into the burner

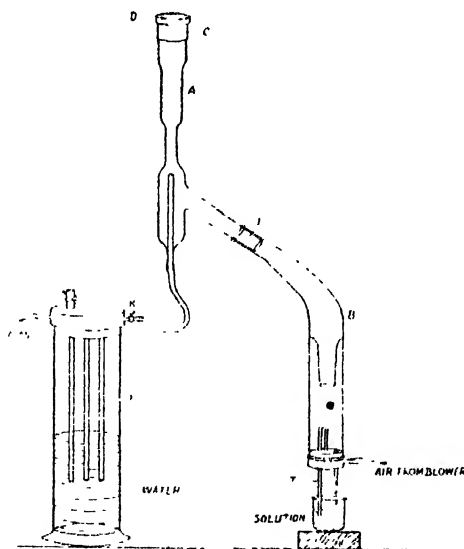


Fig. 1.

A, in the form of a fine spray obtained by blowing air under pressure. The pressure of the gas was controlled with the mechanism *S* and it was let into the burner through the cock *K*. The mixture gave a blue bright flame with a faint yellow centre which appeared occasionally. The intensity of the light source could be increased with the concentration of the solution. The spectrum of the flame obtained in this manner was photographed on Hilger E612 glass and Hilger E492 quartz spectrographs. Investigations were also made by feeding stannous

chloride, stannic bromide, stannic oxide and tin metal powder. Exactly similar bands lying in the region $\lambda\lambda 6480-3200$ were recorded in each case. The brightest emission was obtained either by putting the tin metal powder over the porcelain disc *D*, fitted at the top of the apparatus, or by feeding the stannous bromide solution. However, the intensity of the flame emission was found to be markedly different in different regions. While with the glass spectrograph, bands in the different regions could be photographed in two to four hours, prolonged exposures were needed to record them with the quartz spectrograph. Spectrograms were obtained by using Ilford R40 rapid process panchromatic and N40 process plates. Copper, iron d.c. arcs and neon discharge tube were used as source of comparison standards in different regions.

RESULTS

The flame emission described above and attributed to SnO has yielded a large number of bands in the region $\lambda\lambda 6480-3200$ stretching practically without a break. Out of these bands, 86 have been recorded for the first time while the rest include the prominent SnO bands reported by Connelly and others in this region. Almost all of the new bands have been arranged into three systems *A*, *B* and *C*, different from those of Mahanti, seven new bands have been added to the system *D* and the remaining few are left unclassified.

System A ($\lambda\lambda 6480-5250$)

This system consists of 19 entirely new bands. Most of these are sharp and only a few are somewhat diffuse. The system can be satisfactorily represented by the following expression :

$$\nu = 19073.8 + 453.0(\nu' + \frac{1}{2}) - 4.00(\nu' + \frac{1}{2})^2 - 822.4(\nu'' + \frac{1}{2}) + 3.73(\nu'' + \frac{1}{2})^2 \quad \dots (1)$$

The wavelengths of bands, their wavenumber equivalents in vacuum, together with the visual estimates of intensity on a scale of 10, and vibrational assignments for the system have been incorporated in Table I. It is to be noted that the intensity measurements are on a scale of 10 taking all the three systems together. Diffuse bands with uncertain measurements are marked as *d*. The bands (1,3) and (3,4) are presumably masked by the broadening of the yellow doublet of sodium occurring as an impurity. Figure 2, (plate 2A) reproduces the spectrogram.

System B ($\lambda\lambda 5840-3930$)

Thirty three bands have been incorporated in this system. They include twenty eight entirely new bands, while 5 unclassified bands reported by Connelly have also been accounted for. The proposed system is entirely different from the one suggested by Mahanti. Equation (2) explains the vibrational analysis within limits of experimental error :

$$\begin{aligned} \nu = 24312.8 + 595.0(\nu' + \frac{1}{2}) - 3.90(\nu' + \frac{1}{2})^2 - 0.25(\nu' + \frac{1}{2})^3 - 822.4(\nu'' + \frac{1}{2}) \\ + 3.73(\nu'' + \frac{1}{2})^2 \quad \dots (2) \end{aligned}$$

It is to be noted that the system in general is weak and the level $v' = 2$ is found to be perturbed by about 9 cm^{-1} . Like Table I, Table II explains the data for $B \rightarrow X$ system. Spectrogram is reproduced in figures 3 and 4, (plate 2).

System C ($\lambda\lambda 5010-3700$)

The proposed system C, consisting of 41 bands, is well developed and quite intense. Besides eighteen new bands, it includes 15 prominent bands of Mahanti's B and C systems and 8 of Connelly's unclassified bands as well. Compared with systems A and B the sequences are better marked in this case. The level $v' = 2$ is found to be perturbed by about 12 cm^{-1} .

Within the limits of experimental error the following expression explains the vibrational scheme for system C^2 :

$$v = 25448.5 + 561.0(v' + \frac{1}{2}) - 1.20(v' + \frac{1}{2})^2 + 0.16(v' + \frac{1}{2})^3 - 822.4(v'' + \frac{1}{2}) + 3.73(v'' + \frac{1}{2})^2 \quad \dots (3)$$

Figures 5 and 6 in plate 3 display the bands of the system, and Table II describes the relevant data about it. Bands marked with (+) were reported by Connelly as unclassified.

Table IV indicates the new bands added to the system D , while the bands left unclassified have been entered in table V.

TABLE I

λ_{atr} in A	Int.	ν_{vac} Obs.	in cm^{-1} calc.	Classification
6479.8	4	15428	15422	(3,6)
6456.3	1	15485	15486	(5,7)
6378.6	4	15673	15674	(0,4)
6335.8	3	15779	15771	(2,5) d
6309.8	1	15844	15843	(4,6)
6202.2	3	16119	16119	(1,4)
6172.6	4	16196	16200	(3,5)
6069.9	6	16470	16467	(0,3)
6039.5	2	16553	16556	(2,4)
6015.2	1	16620	16621	(4,5)
5789.6	8	17268	17267	(0,2)
5643.9	5	17713	17712	(1,2)
5612.5	0	17812	17819	(5,4) d
5532.4	3	18071	18074	(0,1)
5399.8	2	18514	18519	(1,1)
5371.5	2	18612	18612	(5,3)
5292.0	1	18891	18889	(0,0)
5276.5	0	18947	18956	(2,1) d
5256.5	1	19019	19017	(6,3)

d-Diffuse, measurement uncertain.

TABLE II

λ_{atr} in Å	Int.	ν_{vac} Obs.	in cm^{-1}		Classification
			Calc.		
5838.1	1	27124	17133		(0,9) d
5590.0	3	17884	17884		(0,8)
5409.5	1	18481	18475		(1,8)
5360.1	3	18651	18651		(0,7)
5302.0	5	18856	18861		(3,9)
5250.4	0	19041	19051		(2,8) p
5196.8	0	19237	19238		(1,7)
5148.0	6	19420	19421		(0,6)
5096.3	3	19617	19616		(3,8)
5047.9	2	19805	19814		(2,7) p
4949.7	3	20198	20199		(0,5)
4904.7	1	20382	20379		(3,7)
4859.3	0	20573	20584		(2,6) p
4810.9	2	20780	20785		(1,5)
4763.9	5	20985	20984		(0,4)
4727.5	1	21147	21149		(3,6)
4681.0	1	21352	21362		(2,5) p,d
4634.6	3	21571	21570		(1,4) +
4590.7	5	21777	21777		(0,3) +
4557.4	0	21936	21926		(3,5) d
4470.5	4	22363	22363		(1,3)
4428.3	4	22576	22577		(0,2) +
4360.2	1	22928	22939		(2,3) p
4316.0	1	23163	23163		(1,2)
4297.3	0	23264	23263		(4,4)
4275.8	0	23381	23384		(0,1) AM
4253.4	2	23504	23504		(3,3)
4212.3	2	23733	23739		(2,2) p
4112.9	3	24307	24304		(2,2) BM +
4074.3	0	24537	24547		(2,1) p
4022.0	1	24856	24856		(4,2)
3942.9	0	25355	25362		(2,0) p
3936.5	1	25396	25393		(5,2) CM +

d —Diffuse, measurement uncertain.

p —Perturbation.

+ —Observed by Connelly also.

AM, BM, CM—Bands of Mahanti's A, B and C systems.

TABLE III

λ_{atr} in Å	Int.	ν_{vac} Obs.	in cm^{-1} Calc.	Classification
5009.2	1	19958	19959	(7,12)
4923.6	0	20305	20300	(5,10) d
4879.8	1	20487	20487	(4,9)
4833.5	2	20679	20683	(3, 8)
4783.1	1	20901	20888	(2,7) p
4749.7	0	21048	21048	(5,9)
4738.0	0	21100	21100	(1, 6)
4706.4	3	21242	21242	(4, 8)
4662.0	3	21444	21446	(3, 7) +
4623.6	0	21622	21612	(6, 9) d
4612.1	2	21676	21658	(2, 6) p, +
4569.5	2	21878	21878	(1, 5) C
4543.1	2	22005	22005	(4, 7) -
4522.6	2	22105	22104	(0, 4) +
4499.1	3	22220	22216	(3, 6) +
4452.5	7	22453	22436	(2, 5) p, CM
4411.6	7	22661	22663	(1, 4) C
4389.1	2	22777	22775	(4, 6) +
4366.1	4	22897	22896	(0, 3) BM
4347.9	1	22993	22994	(3, 5)
4302.2	6	23237	23221	(2, 4) p, CM
4262.3	9	23455	23455	(1, 3) C
4218.8	8	23697	23690	(0, 2) BM
4160.8	2	24027	24013	(2, 3) p, CM
4145.9	1	24113	24114	(5, 5)
4121.9	7	24254	24255	(1, 2) C
4107.7	2	24338	24338	(4, 4) d
4079.9	10	25404	24504	(0, 1) BM
4068.5	2	24572	24572	(3, 3) +
4026.9	3	24826	24813	(2, 2) p, CM
4014.3	1	24904	24899	(5, 4) d, BM

TABLE III (contd.)

λ_{atr} in Å	Int.	ν_{vac} Obs.	in cm^{-1} Calc.	Classification
3978.8	6	25126	25131	(4, 3) BM
3948.5	8	25319	25319	(0, 0) BM
3899.3	6	25638	25621	(2, 1) p
3863.5	9	25876	25878	(1, 0)
3855.4	2	25930	25931	(4, 2) d, BM
3818.8	5	26179	26179	(3, 1)
3779.9	4	26448	26436	(2, 0) p, +
3773.1	1	26496	26492	(5, 2)
3738.9	1	26738	26738	(4, 1)
3703.2	2	26996	26994	(3, 0)

d — Diffuse.

p — Perturbation.

+ — Observed by Connelly also.

BM, CM—Bands of Mahanti's B and C systems.

TABLE IV

λ_{atr} in Å	Int.	ν_{vac} Obs.	in cm^{-1} Calc.	Classification
4048.3	1	24695	24696	(4, 9)
3879.6	2	25769	25768	(5, 8)
3860.0	1	25994	25993	(6, 9)
3704.5	2	26986	26984	(4, 6)
3562.9	0	28059	28057	(6, 6)
3531.9	2	28305	28303	(5, 5)
3501.8	0	28549	28547	(4, 4)

TABLE V

λ_{atr} in Å	Int.	ν_{atr} in Å	Int.
5954.0	2	4463.1	1
5772.3	2	4139.2	0
5242.3	1	4056.4	1
5217.7	2	4039.6	0
5176.3	3	4005.3	1
4837.9	0	3762.3	0
4693.2	1		

DISCUSSION

The earlier work on the absorption spectrum of SnO molecule has established its ground state vibrational frequency to be 822.4 cm^{-1} , Herzberg (1950). A glance on the expressions (1), (2) and (3), pertaining to the systems A, B and C, immediately reveals that they involve a common lower electronic state with a vibrational frequency of 822.4 cm^{-1} . The new bands obtained in emission from the flame containing tin or tin compounds and arranged in the three systems referred to above, have therefore rightly been assigned to the diatomic oxide SnO.

It is quite evident from the reproductions of the spectrograms that the main feature of the visible spectrum of SnO is the presence of mutually overlapping systems. While systems A and B are weak, C appears to be fairly strong. The systems B and C exhibit perturbations and it is to be noted that the $v' = 2$ level is perturbed in both of them. The upper state vibrational frequencies of these systems are 453.0 cm^{-1} for A, 595.0 cm^{-1} for B and 561.0 cm^{-1} for C, respectively. Their comparison with the ground state vibrational frequency indicates that the Condon parabola for the system A is expected to be more wide than those for B and C and the intensity distribution of the system A demonstrates that it is indeed so. It is of interest to compare the results obtained by the authors with those of Mahanti (1931) and Connelly (1933). Mahanti proposed the formulae for the band heads, which he arranged in three different systems :

System A ($\lambda\lambda 4490-3200$)

$$\nu = 29630.5 + 586.0(v' + \frac{1}{2}) - 6.0(v' + \frac{1}{2})^2 - 824.0(v'' + \frac{1}{2}) + 4.0(v'' + \frac{1}{2})^2 \quad \dots (4)$$

System B ($\lambda\lambda 4525-3850$)

$$\nu = 25418.6 + 637.0(v' + \frac{1}{2}) - 8.0(v' + \frac{1}{2})^2 - 824.0(v'' + \frac{1}{2}) + 4.0(v'' + \frac{1}{2})^2 \quad \dots (5)$$

System C ($\lambda\lambda 4570-3930$)

$$\nu = 24370.4 + 582.0(v' + \frac{1}{2}) - 4.0(v' + \frac{1}{2})^2 - 813.5(v'' + \frac{1}{2}) + 5.5(v'' + \frac{1}{2})^2 \quad \dots (6)$$

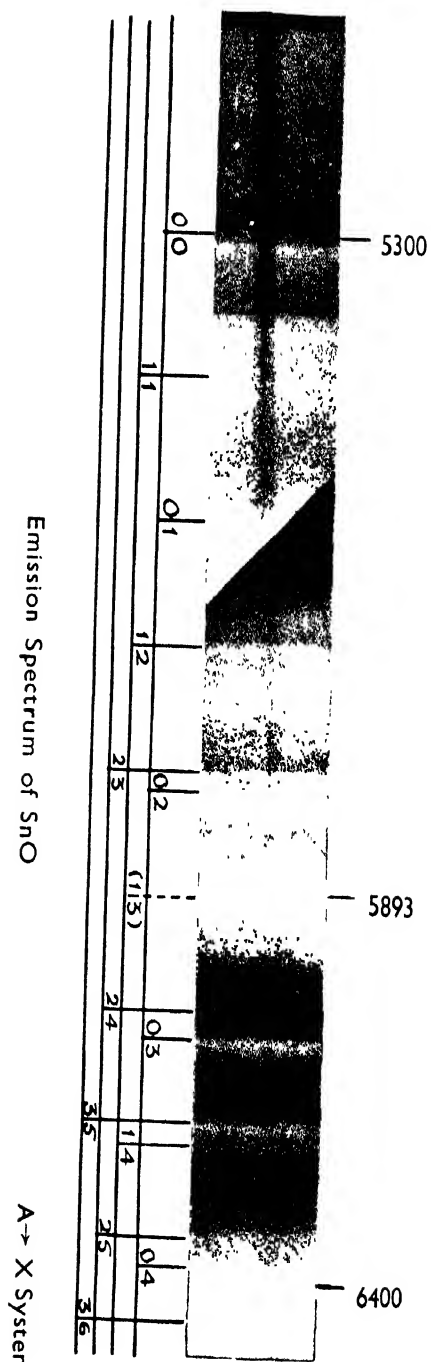
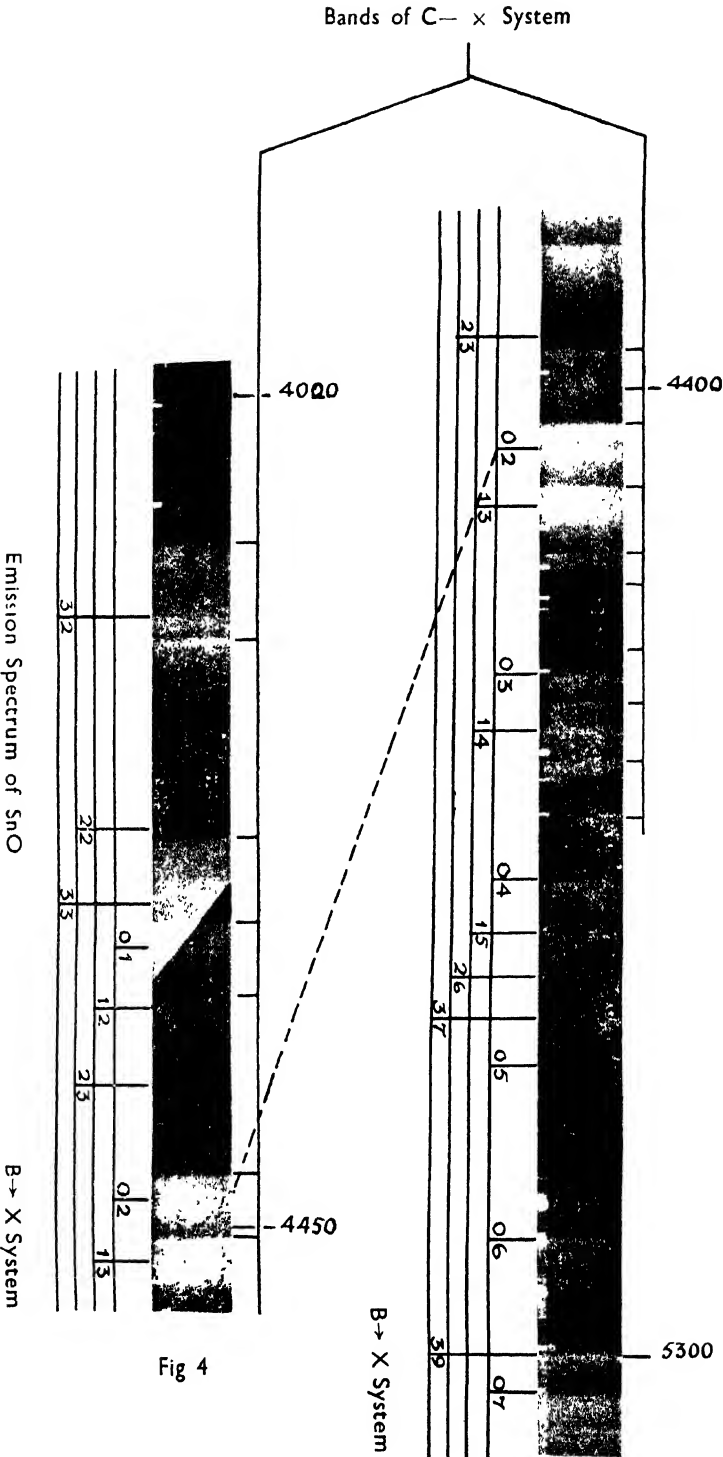
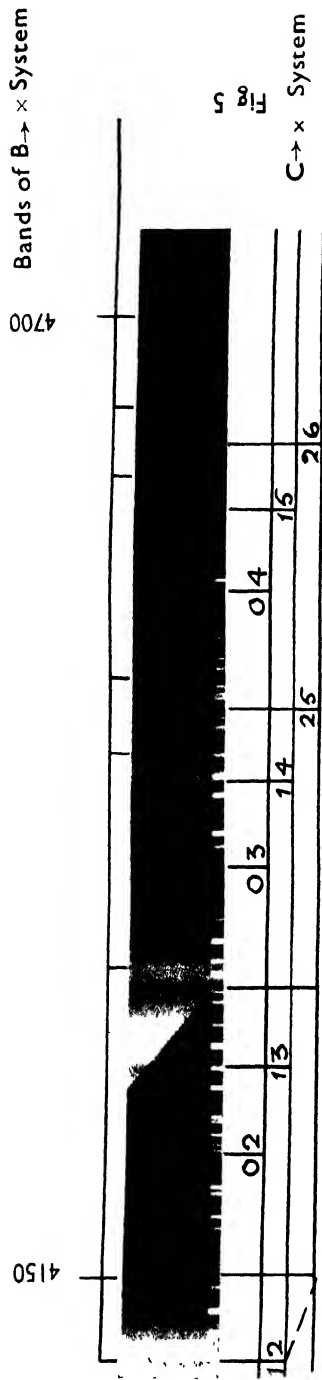
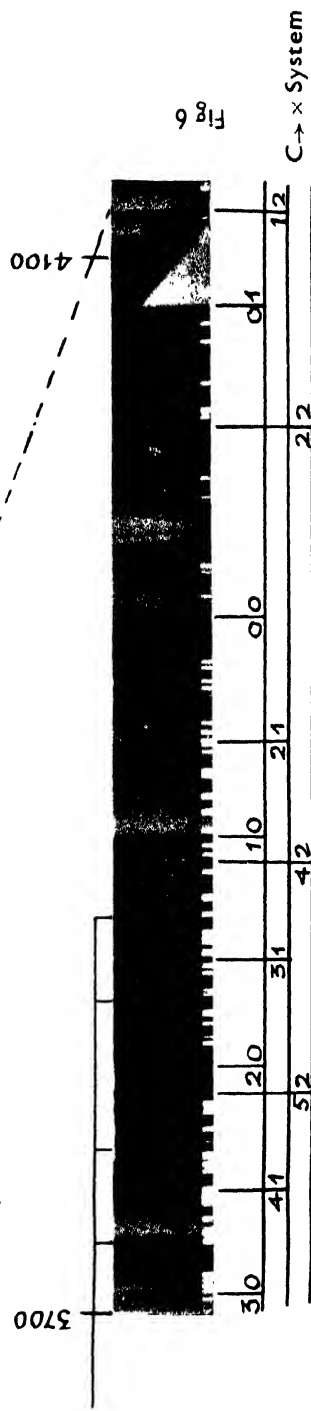


Fig 2





Bands of $E - \times$ System



Emission Spectrum of SnO ($C \rightarrow \times$ System)

It is to be noted that Mahanti's designation of various systems is not in conformity with the modern spectroscopic usage. The transitions corresponding to the above systems are shown at (a) in figure 7.

It is evident from Mahanti's classification that the systems A and B arise from the common lower level described by him as 'a', the lower level of the system C was called as X and none of the electronic states of this system were in common with those of A and B. As regards the ground state, Mahanti, on the basis of certain thermochemical considerations, decided in favour of X, a situation however not substantiated by any reliable spectroscopic evidence. Obviously the confirmation of this interpretation rested heavily on the absorption studies. Should the above genesis of the C system be correct, needless to say that it would be most natural to expect this transition in absorption.

Connelly, however succeeded in producing the SnO spectrum in absorption as well as in emission. Examination of the absorption spectrum obtained by Connelly revealed that only the bands of Mahanti's system A could be traced and those belonging to B and C systems of Mahanti were conspicuous by their absence. As already remarked, according to Mahanti's scheme of transitions, his system C must appear in absorption. Evidently, this fact is not observed by Connelly. It should further be noted that out of Mahanti's A and B systems, both of which involve the common lower state, if the former appears in absorption the latter should also appear. This situation is also not obtained by Connelly. It is therefore obvious that Mahanti's interpretation of facts is not in conformity with the absorption studies due to Connelly. It is to be noted that although Connelly observed a much larger number of bands than Mahanti did, but he arranged most of them into only one system which was termed as D in order to distinguish it from Mahanti's nomenclature. The system is well represented by the following expression due to Jevons (1938) :

System D ($\lambda\lambda 4490-3070$)

$$\nu = 29624.9 + 582.6(\nu' + \frac{1}{2}) - 3.08(\nu' + \frac{1}{2})^2 - 0.135(\nu' + \frac{1}{2})^3 - 822.4(\nu'' + \frac{1}{2}) + 3.73(\nu'' + \frac{1}{2})^2 \quad \dots (8)$$

Besides explaining a considerable number of new bands, the above expression also provides a satisfactory account of Mahanti's A system. The scheme of transitions suggested by Connelly is depicted as (b) in Fig. 7.

As regards Mahanti's B and C systems, although Connelly confirmed the presence of their principal bands in emission, yet he was doubtful about their existence as parts of two separate systems, and he also questioned their associations with the ground state of the molecule. To the best of our information these points have remained unresolved uptill now. However, due to the additional information furnished by the present investigations a better picture of the situation can now be presented.

The levels obtained by the authors have been displayed in part (c) of figure 7 where four transitions all terminating in the ground state have been observed.

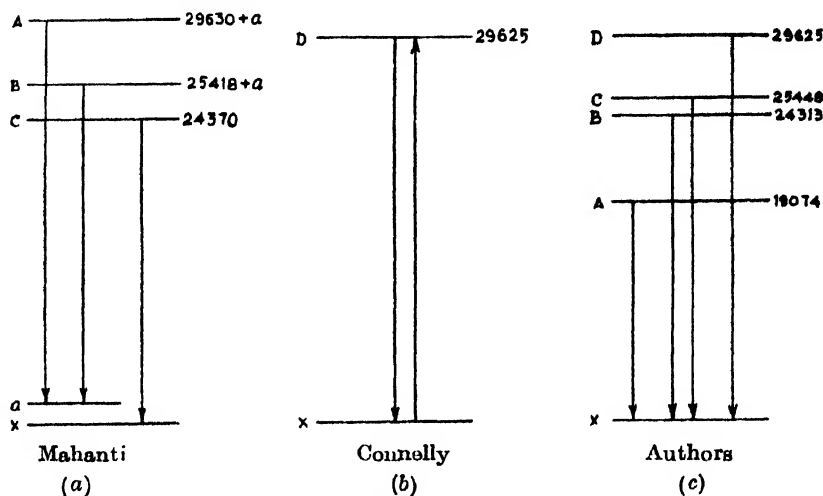


Fig. 7.

The state designated as D is the same as observed by Connolly and in addition three more levels C, B and A have been discovered. It is to be remembered that Mahanti's level A corresponds to the present level D.

From Table III it can be observed that almost all the prominent progressions belonging to Mahanti's systems B and C have been satisfactorily incorporated in the present system C. Thus a single transition $C \rightarrow X$ accounts for both these systems and in fact they do not exist separately. Evidently, this is what Connolly had also suggested.

To complete the outline of the visible spectrum of SnO it will not be out of place to mention that Eisler and Barrow (1949) have referred to the unpublished work of Mrs. Richards who has observed the stronger bands of Mahanti's B and C systems in absorption. This significant observation confirms that the lower state of the present transition $C \rightarrow X$ has rightly been identified to be the ground state of the molecule and Connolly's apprehensions on this score were ill-founded. Thus all the major discrepancies in the interpretation of the visible spectrum of SnO appear to have been removed and the present work can be considered to offer a more rational explanation of experimental facts.

The unclassified bands in general are weak and do not form any progressions with constant differences. Although their interpretation at the moment is not possible, chances for another system of SnO in the visible region can, however, not be ruled out.

A comparison of the information regarding the states of SnO molecule with those of the other heavy diatomic molecules, arising out of the combination of

IVb and VIB subgroups of the periodic table, will form the part of a separate communication.

ACKNOWLEDGMENTS

The authors are grateful to the Council of Scientific and Industrial Research New Delhi for the financial assistance.

REFERENCES

- Barrow, R. F., Deutsch, J. L., and Travis, D. M., 1961, *Nature*, London, **191**, 374.
Barrow, R. F. and Rowlinson, H. C., 1954, *Proc. Phys. Soc.* **A224**, 374.
Bloomenthal, S., 1930, *Phys. Rev.* **35**, 34.
Connelly, F. C., 1933, *Proc. Phys. Soc.* **45**, 780.
Edor, J. M., and Valenta, E., 1924, *Atlas Typischer Spec.*
Eisler, B., and Barrow, R. F., 1949, *Proc. Phys. Soc.* **A62**, 740.
Herzberg, G. 1950, *Molecular Spectra and Molecular Structure*, Vol. I, D. Van Nostrand & Company, New York.
Howell, H. G., 1936, *Proc. Roy. Soc.* **153**, 683.
Jevons, W., 1938, *Proc. Phys. Soc.* **50**, 910.
Largerqvist, A., Nilsson, N. E. L., and Wigartz, K., 1959, *Ark. Fys.* **15**, 521.
Loomis, F. W., and Watson, T. F., 1934, *Phys. Rev.* **45**, 805.
Mahanti, P. C., 1931, *Zeit. f. Phys.* **68**, 114.
Mahanti, P. C., and Sen Gupta, A. K., 1938, *Zeit. f. Phys.* **109**, 39.
———, 1939, *Indian J. Phys.* **13**, 331.
Mecke, R., 1929, *Die Naturwissenschaften* **17**, 122.
Sharma, D., 1944, *Proc. Nat. Acad. Sci. India* **A14**, 133.
Shawhan, E. N., and Morgan, F. 1935, *Phys. Rev.* **47**, 377.

ORTHORHOMBIC LIGAND FIELD THEORY OF THE MAGNETIC BEHAVIOURS OF $\text{Cu}(\text{NH}_4\text{SeO}_4)_2 \cdot 6\text{H}_2\text{O}$

U. S. GHOSH, R. N. BAGCHI, A. K. PAL AND S. N. MITRA

DEPARTMENT OF MAGNETISM

INDIAN ASSOCIATION FOR THE CULTIVATION OF SCIENCE

CALCUTTA-32.

(Received August 30, 1966)

ABSTRACT. The e.p.r. measurements on $\text{Cu}(\text{NH}_4\text{SeO}_4)_2 \cdot 6\text{H}_2\text{O}$ clearly indicate an orthorhombic distortion of the ligand field acting on the hexa-coordinated Cu^{2+} ion. Assuming an orthorhombic ligand field of both second and fourth order, the expression for the principal orthorhombic g -values and magnetic susceptibilities have been derived with due consideration of the presence of covalency overlap of the d -orbitals of the central metal atom with the electronic charge clouds of the ligand atoms. For reasons of completeness, the calculation has been extended upto the 3rd order correction terms in the perturbation procedure adopting Pryce's spin-Hamiltonian formalism, although these third order terms have been neglected while fitting the theory with the experiments. Attempts have been made to fit the theory with the experiments of optical absorption, principal g -tensors and magnetic anisotropies and mean susceptibility as best as possible by evaluating the values of certain parameters appearing in the theoretical expressions. Important inferences have been drawn regarding the remarkable variation of the anisotropic component of the ligand field with temperature and the anisotropic reduction of the orbital moment and S.O. coupling coefficient from their respective free ion values due to the covalency effect.

INTRODUCTION

Recent e.p.r. measurements at room temperature in four copper Tutton salts (Bose *et al* 1964; Ghosh *et al*, 1965) have shown that the symmetry of the ligand field acting on the central Cu^{2+} ion in these crystals is perceptibly orthorhombic. This is in general consistent with the findings of Bleaney *et al* (1949) and Bagguley and Griffiths (1952) though for the want of a convenient and accurate method of determining orthorhombic g -values and their orientations at that time, their e.p.r. data had to be often given in terms of g_{\parallel} and g_{\perp} , apparently indicating only an approximately uniaxial symmetry of the ligand field. The experiment of Bagguley and Griffiths on some dilute Cu^{2+} Tutton salts showed large changes in relative magnitudes of g_i 's between 300°K and 90°K.

Using a recent convenient method (Bose *et al*, 1964) for determining accurately the magnitudes and orientations of orthorhombic g_i 's in crystals, we have carried out e.p.r. measurements on $\text{Cu}(\text{NH}_4\text{SO}_4)_2 \cdot 6\text{H}_2\text{O}$ at both liquid oxygen ($\sim 90^\circ\text{K}$) and room temperature ($\sim 300^\circ\text{K}$). In this salt and a few others unlike $\text{Cu}(\text{NH}_4\text{SO}_4)_2 \cdot 6\text{H}_2\text{O}$, magnetic measurements (Bose *et al*, 1957) show very small changes with

temperature in the orientation of crystalline χ_1 and χ_2 axes in the (010) plane, but with a tetragonal approximation the ionic anisotropy deviates from Curie law and the ionic orientations appear to change to some extent as the temperature varies. It would be interesting then with the powerful e.p.r. method at our disposal to probe into the actual nature of these ionic deviations and changes which have so little outward manifestations in the crystalline behaviours.

Polder's theory (1942) of the susceptibility of Cu^{2+} ion assumed a purely electrostatic dipolar model of the octahedron which was considered to possess only a tetragonal distortion and could not properly assign the energy levels of the ligand field (Bose *et al*, 1957) primarily, owing to the inapplicability of the above model and the approximate nature of calculation from the available data on crystal structure, dipole moment and the radius of 3d orbit. Bleaney, Bowers and Pryce (1955) extended Abragam and Pryce's theory (1951) to the octahedrally co-ordinated Cu^{2+} ion under the second order orthorhombic field to interpret the results of e.p.r. measurements.

In the present work we have derived the theoretical expressions for the principal g -values and the susceptibilities for the octahedrally co-ordinated Cu^{2+} ion by assuming an orthorhombic field of both second and fourth order with due consideration of the presence of overlap between the central ion 3d-orbitals with the s - and p -orbitals of the neighbouring ligand atoms, resulting in the formation of molecular orbitals of the magnetic electrons in such complexes (Van Vleck, 1935, Stevens, 1953; Owen 1955). These theoretical expressions involve certain parameters, connected with the ligand co-efficients and the overlap effect and attempts are then made to fit the theory uniquely with the experimental data by evaluating the reasonable values of these parameters, consistent with the other independent observation from optical absorption. This procedure of interpreting the experimental data leads to important inferences regarding the remarkable variation of the anisotropic part of the ligand field with temperature, and the anisotropic reduction of the S.O coefficient and the orbital moment from their respective free ion values due to the effect of convalency overlap.

FINE STRUCTURE ENERGY LEVELS OF THE LIGAND FIELD

In a cubic field of O_h symmetry, the free ion ground state 2D of Cu^{2+} ion splits into an upper orbital triplet T_{2g} and a lower orbital doublet E_g . The superposed orthorhombic component of the ligand field lifts all the orbital degeneracies of both T_2 and E_g , but S.O interaction has no effect on the lower cubic doublet E_g in the first order. Hence in our perturbation procedure, we first apply the total ligand field inclusive of the anisotropic part on the free ion ground state and then adopt Pryce's (1950) Spin Hamiltonian formalism for the calculation of g -values and magnetic susceptibilities.

Electronic configuration of Cu^{2+} ion being $3d^9$, the system can be conveniently described in terms of a single hole in the completed $3d$ sub-shell. This hole is subjected to an orthorhombic potential given by

$$V = D'(x^4 + y^4 + z^4 - \frac{3}{8} r^4) + Ax^2 + By^2 - (A+B)z^2 + ax^4 + by^4 \\ - (a+b)z^4 + 6ay^2z^2 + 6bx^2z^2 - 6(a+b)x^2y^2 \quad \dots (1)$$

In case of tetragonal symmetry about z axis,

$$A = B \text{ and } a = b,$$

and the expression for V reduces to that given by Abragam and Pryce (1951) for tetragonal potential.

Putting,

$$\frac{A+B}{2} = -\sigma', \quad \frac{A-B}{2} = \delta' \\ \frac{a+b}{2} = -\gamma', \quad a-b = \epsilon'$$

We get a convenient expression for V as follows :

$$V = D'(x^4 + y^4 + z^4 - \frac{3}{8} r^4) + \sigma'(3z^2 - r^2) + \delta'(x^2 - y^2) \\ + \gamma'(2z^4 - x^4 - y^4 + 12x^2y^2 - 6y^2z^2 - 6x^2z^2) \\ + \epsilon'(x^4 - y^4 + 6y^2z^2 - 6x^2z^2) \quad (3)$$

In (1) and (3) first the term represents the cubic component of the potential and remaining terms arise from the orthorhombicity of the ligand field. The ligand field interaction for the d -hole is

$$H_v = +eV$$

To find the eigen values of H_v and the corresponding eigen functions, we need to evaluate the matrix elements of H_v between the orbitally five-fold degenerate free ion states of the d -hole which are denoted by $d_0, d_{\pm 1}, d_{\pm 2}$ the suffixes indicating the possible 1_z values. Matrix elements of the first four terms (i.e. with $D', \gamma', \sigma', \delta'$) in (3) can be easily calculated using Steven's equivalent operator technique (Stevens, 1952) and noting that

$$2z^4 - x^4 - y^4 + 12x^2y^2 - 6y^2z^2 - 6x^2z^2 \\ = 5(x^4 + y^4 + z^4 - \frac{3}{8} r^4) - 3(x^4 - 6x^2y^2 + y^4)$$

For the remaining term (i.e. with ϵ') in (3), we note that

$$\epsilon'(x^4 - 6x^2z^2 + 6y^2z^2 - y^4) = -\epsilon' \frac{8\sqrt{\pi}}{3\sqrt{10}} r^2(Y^2_4 + Y^{-2}_4)$$

Matrix element for this term can be easily calculated with the help of Wigner co-efficient formula (Stevens, 1952). Thus operating H_v on d_0 , $d_{\pm 1}$ and $d_{\pm 2}$, and solving the relevant secular equation we get the following eigen values

$$\left. \begin{aligned} E_1 &= 6D - [36(\sigma + 3\gamma)^2 + 3(2\delta - \epsilon)^2]^{\frac{1}{2}} \\ E_2 &= 6D + [36(\sigma + 3\gamma)^2 + 3(2\delta - \epsilon)^2]^{\frac{1}{2}} \\ E_3 &= -4D + 6\sigma - 24\gamma \\ E_4 &= -4D - 3\sigma + 12\gamma - (3\delta + 2\epsilon) \\ E_5 &= -4D - 3\sigma + 12\gamma + (3\delta + 2\epsilon) \end{aligned} \right\} \dots (4)$$

and the corresponding eigen functions are

$$\left. \begin{aligned} \psi_1 &= a_1 d_0 + b_1 \frac{1}{\sqrt{2}} (d_2 + d_{-2}) \\ \psi_2 &= b_1 d_0 - a_1 \frac{1}{\sqrt{2}} (d_2 + d_{-2}) \\ \psi_3 &= \frac{1}{\sqrt{2}} (d_2 - d_{-2}) \\ \psi_4 &= \frac{1}{\sqrt{2}} (d_1 - d_{-1}) \\ \psi_5 &= \frac{1}{\sqrt{2}} (d_1 + d_{-1}) \end{aligned} \right\} \dots (5)$$

$$\left. \begin{aligned} \text{where } D &= \frac{3}{5} e D' \beta \bar{r}^4 \\ \sigma &= e \sigma' \alpha r^2 \\ \delta &= e \delta' \alpha r^2 \\ \gamma &= e \gamma' \beta r^4 \\ \epsilon &= \frac{8}{3} \sqrt{\pi} e \rho \epsilon' \bar{r}^4 \end{aligned} \right\} \begin{aligned} \alpha &= -\frac{2}{21}, \quad \beta = +\frac{2}{63} \\ \text{corresponding to the configuration } 3d^1, \\ \text{since the system has been described in} \\ \text{terms of hole.} \end{aligned}$$

in which α and β are the numerical factors appearing in Stevens' equivalent operators and ρ is the numerical factor appearing in Wigner coefficient formula for the matrices of the type

$$\langle L = 2, M | r^4 [Y_4^2 + Y_4^{-2}] | L = 2, M = \pm 2 \rangle$$

$$\text{and } \frac{b_1}{a_1} = \frac{6(\sigma + 3\gamma) - [36(\sigma + 3\gamma)^2 + 3(2\delta - \epsilon)^2]^{\frac{1}{2}}}{\sqrt{3}(2\delta - \epsilon)},$$

$$a_1^2 + b_1^2 = 1$$

For octahedral co-ordination the cubic field parameter D is negative (D' being negative and β positive). Moreover under cubic field alone ($\sigma = \delta = \gamma = \epsilon = 0$), it is evident from (4) that the original five fold degenerate free ion states of the d -hole split up into lower orbital doublet E_g of energy $6D$ and an upper orbital triplet T_{2g} of energy $-4D$, the overall cubic field separation being $10D$. In the superposed orthorhombic field the cubic orbital doublet and triplet levels split up into two and three levels respectively, the orbital degeneracy being thus completely removed. Further it will be seen from (4) that in the orthorhombic field, mean centre of the three split components (ψ_3, ψ_4, ψ_5) of the cubic triplet T_{2g} lies at $-4D$ which is also the energy value of the cubic triplet T_{2g} and that of the two split components (ψ_1, ψ_2) of the cubic doublet E_g lies at $6D$, the energy value of the cubic doublet E_g . This has resulted from the particular choice of the form of expression for the orthorhombic potential V . Thus the separation of the mean centres mentioned above, is $10D$ which is also the cubic field splitting and this fact will be taken into consideration while evaluating the parameter D from optical absorption spectrum.

Assuming the orthorhombic distortion of the octahedron to be small, ψ_1 with energy E_1 is evidently the lowest level, ψ_2 lies next and the relative order of ψ_3, ψ_4, ψ_5 depends on the sign and magnitudes of the parameters $D, \sigma, \delta, \gamma$ and ϵ . The fitting of experimental data, shown later also justifies our assumption regarding the relative order of the ligand field levels

Calculation of g -values

The ligand field energy states (5) can be expressed in term of real d -orbitals which can replace the combination of d function in (5) as follows :

$$\frac{1}{\sqrt{2}} (d_2 + d_{-2}) \equiv d_{x^2-y^2}$$

$$d_0 = d_{3z^2-r^2}$$

$$\frac{1}{\sqrt{2}} (d_2 - d_{-2}) = d_{xy}$$

$$\frac{1}{\sqrt{2}} (d_1 + d_{-1}) = d_{yz}$$

$$\frac{1}{\sqrt{2}} (d_1 - d_{-1}) = d_{xz}$$

The suffixes (x^2-y^2) etc. on the R.H.S. represent the angular parts of the real d -orbitals. Now, the orbitals in the complex are not pure atomic d -orbitals, they are considerably modified by appropriate combination of ligand σ and π orbitals. These modifications are now taken into consideration while calculating the g -values and magnetic susceptibility.

Denoting a molecular orbital by a ϕ -function with the suffix same as that for the original real d -orbital, the fine structure energy states (5) is now written as

$$\begin{aligned}\Psi_1 &= a_1\phi_{3z^2-r^2}^2 + b_1\phi_{x^2-y^2}^2 \\ \Psi_2 &= b_1\phi_{3z^2-r^2}^2 - a_1\phi_{x^2-y^2}^2 \\ \Psi_3 &= \phi_{xy} \\ \Psi_4 &= \phi_{yz} \\ \Psi_5 &= \phi_{xz}\end{aligned}\quad \dots \quad (6)$$

The S.O. interaction has no effect in the first order on the lowest orbital singlet Ψ_1 and hence for the calculation of g -value and magnetic susceptibility we adopt Pryce's Spin Hamiltonian formalism (Pryce, 1950). The Spin Hamiltonian is given by

$$\begin{aligned}H_s &= \langle \Psi_1 | H' | \Psi_1 \rangle - \sum_{n \neq 1} \frac{\langle \Psi_1 | H' | \Psi_n \rangle \langle \Psi_n | H' | \Psi_1 \rangle}{E_n - E_1} \\ &+ \sum_{n \neq 1} \sum_{m \neq 1} \frac{\langle \Psi_1 | H' | \Psi_m \rangle \langle \Psi_m | H' | \Psi_n \rangle \langle \Psi_n | H' | \Psi_1 \rangle}{(E_n - E_1)(E_m - E_1)} \\ &- \sum_{n \neq 1} \frac{\langle \Psi_1 | H' | \Psi_n \rangle \langle \Psi_n | H' | \Psi_1 \rangle \langle \Psi_1 | H' | \Psi_1 \rangle}{(E_n - E_1)^2} \quad \dots \quad (7)\end{aligned}$$

where H' stands for the perturbation $\vec{\zeta} \vec{L} \cdot \vec{S} + \beta \vec{H}(\vec{L} + 2\vec{S})$ in which ζ is the S.O. coupling coefficient for the free ion, and the various matrix elements of the type $\langle \Psi_j | H' | \Psi_k \rangle$ occurring in (7) imply that states Ψ 's are acted on only by the orbital operators appearing in the expression for the perturbation H' . While evaluation various matrices of the type $\langle \Psi_j | H' | \Psi_k \rangle$, the relationship between two types of matrices of the operators \vec{L} and $\vec{\zeta} \vec{L}$, one calculated between the atomic d -orbitals and the other between the corresponding molecular orbitals, are given as follows (Low, 1960) :

$$\begin{aligned}\langle \phi(\rho) | L_i | \phi(\rho) \rangle &= \langle d(\rho) | L_i | d(\rho) \rangle = 0 \\ \langle \phi(\tau) | L_i | \phi(\tau) \rangle &= k_i \langle d(\tau) | L_i | d(\tau) \rangle \\ \langle \phi(\rho) | L_i | \phi(\tau) \rangle &= k_i' \langle d(\rho) | L_i | d(\tau) \rangle \\ \langle \phi(\rho) | \zeta L_i | \phi(\rho) \rangle &= 0 \\ \langle \phi(\tau) | \zeta L_i | \phi(\tau) \rangle &= R_i \langle d(\tau) | \zeta L_i | d(\tau) \rangle \\ \langle \phi(\rho) | \zeta L_i | \phi(\tau) \rangle &= R_i' \langle d(\rho) | \zeta L_i | d(\tau) \rangle\end{aligned}$$

where $i = x, y, z$; $\phi(\tau)$ and $\phi(\rho)$ represent the molecular orbitals ($\phi_{xy}, \phi_{yz}, \phi_{xz}$) and ($\phi_{3z^2-r^2}, \phi_{x^2-y^2}$) resulting from the modification of the corresponding atomic

orbitals $d(\tau)(d_{xy}, d_{yz}, d_{zx})$ and $d(\rho)(d_{3z^2-r^2}, d_{x^2-y^2})$ respectively. The k_i 's and R_{is} are known as the orbital reduction and S.O. coupling reduction factors respectively arising from the covalency effect, and these are considered to partake of the symmetry of the ligand field. Evaluating the matrices in (7) we finally get the expression for the Spin Hamiltonian expressed as a polynomial in spin variables only and this will operate on the spin states $|S_z = \frac{1}{2}\rangle$ and $|S_z = -\frac{1}{2}\rangle$. Thus the Spin Hamiltonian for $H||z$ becomes

$$H_s(z) = 2\beta H[S_z(1-u_3R'_z k'_z + \lambda_1 R'_y R_x k'_z - \lambda_2 R'_x R_y k'_z + \lambda_3 R'_y R'_x k_z) + 2i(\lambda_4 R'_x{}^2 S_x S_y - \lambda_5 R'_y{}^2 S_y S_x)] - v_z \beta^2 H^2 \quad \dots (8)$$

For $H||x$

$$H_s(x) = 2\beta H[S_x(1-u_1R'_x k'_x - \lambda_1' R'_y R'_z k_x - \lambda_2 R'_y R_z k'_x - \lambda_3 R'_y R_z k'_x) + 2i(\lambda_5 R'_y{}^2 S_y S_z - \lambda_6 R'_z{}^2 S_x S_z)] - v_x \beta^2 H^2 \quad \dots (9)$$

and for $H||y$

$$H_s(y) = 2\beta H[S_y(1-u_2R'_y k'_y + \lambda_1 R_x R'_z k_x + \lambda_2 R'_x R'_z k_y - \lambda_3 R_z R'_x k'_y) + 2i(\lambda_6 R'_z{}^2 S_z S_x - \lambda_4 R'_x{}^2 S_x S_z)] - v_y \beta^2 H^2 \quad \dots (10)$$

$$\text{where } u_1 = \frac{(a_1\sqrt{3}+b_1)^2\zeta}{E_3-E_1}, \quad u_2 = \frac{(a_1\sqrt{3}-b_1)^2\zeta}{E_5-E_1}, \quad u_3 = \frac{(a_1\sqrt{3}-b_1)^2\zeta}{E_4-E_1},$$

$$\lambda_1 = \frac{b_1(a_1\sqrt{3}-b_1)\zeta^2}{(E_3-E_1)(E_4-E_1)}, \quad \lambda_2 = \frac{b_1(a_1\sqrt{3}+b_1)\zeta^2}{(E_3-E_1)(E_5-E_1)}, \quad \lambda_3 = \frac{(3a_1^2-b_1^2)\zeta^2}{2(E_5-E_1)(E_4-E_1)}$$

$$\lambda_4 = \frac{(a_1\sqrt{3}+b_1)^2\zeta^2}{2(E_5-E_1)^2}, \quad \lambda_5 = \frac{(a_1\sqrt{3}-b_1)^2\zeta^2}{2(E_4-E_1)^2}, \quad \lambda_6 = \frac{b_1^2\zeta^2}{(E_3-E_1)^2}$$

$$v_x = \frac{(a_1\sqrt{3}+b_1)^2k_x'^2}{E_5-E_1}, \quad v_y = \frac{(a_1\sqrt{3}-b_1)^2k_y'^2}{E_4-E_1}, \quad v_z = \frac{4b_1^2k_z'^2}{E_3-E_1}$$

In equations (8), (9) and (10), terms independent of H have been omitted since they do not produce any zero field splitting of the Kramers degenerate spin states of $S_z = \pm 1/2$. The last term in each of the above equations also does not produce any splitting of the degenerate components and is not important in the calculation of g -values, but this being dependent on H^2 assumes much importance in the calculation of susceptibility constituting the temperature independent paramagnetism and hence is retained.

Operating on the spin states $|\frac{1}{2}\rangle$ and $|\frac{-1}{2}\rangle$ with the Hamiltonian $H_s(x)$ we get a secular matrix which on diagonalization gives the following energy values for $H||x$.

$$W_{\pm}(x) = -v_x \beta^2 H^2 \pm [1 - u_1 R'_x k'_x - \lambda_1 R'_y R'_z k_x - \lambda_2 R_y R'_z k'_x - \lambda_3 R'_y R_z k'_x - \lambda_5 R'_y{}^2 - \lambda_6 R'_z{}^2] \beta H$$

Thus g_x is given by

$$g_x = \frac{W_+(x) - W_-(x)}{\beta H} = 2[1 - u_2 R'_x k'_x - \lambda_1 R'_y R'_z k'_x - \lambda_2 R_y R'_z k'_x - \lambda_3 R'_y R'_z k'_x - \lambda_5 R'_y{}^2 - \lambda_6 R'_z{}^2] \quad \dots (11)$$

The expression for energy values $W_{\pm}(x)$ are now suitably written as

$$W_{\pm}(x) = -v_x \beta^2 H^2 \pm \frac{1}{2} g_x \beta H \quad \dots (12)$$

Similar calculation for $H||y$ gives

$$W_{\pm}(y) = -v_y \beta^2 H^2 \pm \frac{1}{2} g_y \beta H \quad \dots (13)$$

$$g_y = 2[1 - u_2 R'_y k'_y + \lambda_1 R_x R'_z k'_y + \lambda_2 R_x R'_z k'_y - \lambda_3 R'_x R'_z k'_y - \lambda_4 R'_x{}^2 - \lambda_6 R'_z{}^2] \quad (14)$$

and for $H||z$

$$W_{\pm}(z) = -v_z \beta^2 H^2 \pm \frac{1}{2} g_z \beta H \quad \dots (15)$$

$$g_z = 2[1 - u_3 R'_z k'_z + \lambda_1 R'_y R'_x k'_z - \lambda_2 R_y R'_x k'_z + \lambda_3 R'_y R'_x k'_z - \lambda_4 R'_x{}^2 - \lambda_5 R'_y{}^2] \quad \dots (16)$$

Calculation of susceptibility

The general expression for g_m -ionic susceptibility is given by

$$K_i = \left[-\frac{N}{H} \frac{\sum \frac{\partial W(i)}{\partial H} \exp\left(-\frac{W(i)}{kT}\right)}{\sum \exp\left(-\frac{W(i)}{kT}\right)} \right] \quad \dots (17)$$

$\lim_{H \rightarrow 0}$
 $(i = x, y, \text{ or } z)$

The limit can be easily evaluated using L' Hospital's rule in our case since the expression reduces to the indeterminate form $\frac{0}{0}$ if we put $H = 0$. Thus the expression for susceptibility along the three directions x, y and z reduces to

$$K_i = \frac{N\beta^2}{KT} \cdot \frac{g_i^2}{4} + 2N\beta^3 v_i \quad (i = x, y \text{ or } z) \quad \dots (18)$$

The mean susceptibility is then given by

$$\bar{K} = \bar{K} = 1/3(K_x + K_y + K_z) \quad \dots (19)$$

RESULTS AND DISCUSSIONS

$\text{Cu}(\text{NH}_4\text{SeO}_4)_2 \cdot 6\text{H}_2\text{O}$ belongs to the monoclinic system (space group $P2_1/a$) and contains two magnetically inequivalent ions in the unit cell as known from c.p.r. experiments and also from the recent X-ray structure analysis of the isomorphous nickel, Tutton salts (Morosin and Lingafelter, 1964). Orientation of one

ion (the paramagnetic complex) can be derived from the other by reflection in the (010) plane. The mean magnetic susceptibility $\bar{\chi}$ and principal crystalline anisotropies ($\chi_1 - \chi_2$) and ($\chi_1 - \chi_3$) have been accurately determined between 300°K and 90°K in our laboratory (Bose *et al*, 1957 Ghosh- to be published). Further, the principal g -tensors and their orientations have been determined here by the accurate e.p.r. technique (described elsewhere, Bose *et al*, 1964) both at room temperature and 90°K (Table I). The calculated values of crystalline anisotropies and mean susceptibility in Table II have been obtained by using equations (18), (19) and the following relation :

$$\chi_j = \sum_{i=x,y,z} K_i \mu_{ij}^2 \quad (j = 1, 2, 3)$$

where μ_{ij} is the direction cosine of K_i with χ_j . The values of μ_{ij} at room temperature and 90°K are furnished by our e.p.r. measurements at the two temperatures, presuming of course that the direction of K_i 's are coincident with those of g_i 's. The overall changes of μ_{ij} 's are found to be not very large. Therefore, at intermediate temperatures they have been assumed to have intermediate values between those at 90°K and 300°K, obtained by linear interpolation, consistent with the orthogonality relations between them.

TABLE I

The principal g -tensors and their orientations in $\text{Cu}(\text{NH}_4\text{SeO}_4)_2 \cdot 6\text{H}_2\text{O}$ crystals from e.p.r. measurements (a, b , are the principal crystallographic axes).

a. Temperature 300°K

Principal g -tensors	angles with respect to			
	χ_1	χ_2	$\chi_3 \equiv b$	a
$g_x = G_2 = 2.12_3$	64°.9	40°.6	119°.3	36°.6
$g_y = G_1 = 2.05_2$	63°.1	130°.1	128°.0	92°.2
$g_z = G_3 = 2.39_6$	38°.3	85°.9	51°.9	53°.5

b. Temperature 90°K

Principal g -tensors	angles with respect to			
	χ_1	χ_2	$\chi_3 \equiv b$	a
$g_x = G_2 = 2.12_0$	60°	62°.4	137°	47°.2
$g_y = G_1 = 2.06_8$	71°.4	157°.1	110°.3	107°.6
$g_z = G_3 = 2.40_0$	36°.3	85°.4	53°	48°

The x , y and z axes of the ion have been chosen in such a way that it gives the closest fit of the theory with the experimental results (Table II). The z and y axes are thus found to correspond to the directions of the highest and lowest g -tensors respectively. This is quite consistent with the previously observed fact that under tetragonal approximation $g_{||}(=g_z)$ is greater than $g_{\perp}(\approx \sqrt{\frac{1}{2}(g_x^2 + g_y^2)})$ (Bleaney *et al*, 1949; Bose *et al* 1957).

It has been found on actual calculation that the third order terms in g -values are very small contributing less than 0.5 per cent of the total and hence those are neglected. Then the number of parameters appearing in the theoretical expressions for g -values, magnetic susceptibilities and ligand field energy levels reduces to eleven viz. D , σ , δ , γ , ϵ , k'_x , k'_y , k'_z , R'_x , R'_y and R'_z . The relative values of k_i 's and those of R_i 's ($i = x, y, z$) are, of course, dependent on the lower symmetric field parameters σ , δ , γ and ϵ although they may not be explicitly expressible in terms of the latter. The cubic field parameter D is readily furnished by the optical absorption experiment on aqueous solution of some cupric salts (Dreisch and Trommer, 1937; Mookerjee *et al*, 1959) in which the Cu^{2+} ion is also co-ordinated by six water molecules as in copper Tutton salts. The experiments show a broad peak at $12,300 \text{ cm}^{-1}$ which does not vary much from salt to salt and with temperature and may be considered to correspond approximately to a transition from the mean centre of the split components of E_g to that of the split component of T_{2g} in the orthorhombic field, the separation between the mean centres being $10D$. The few other peaks occurring at much higher frequencies such as 17000 cm^{-1} , $35,000 \text{ cm}^{-1}$ etc. are supposed to arise from charge transfer processes and not from transitions between ligand field levels. Having thus found the parameter D , the remaining ten parameters are then adjusted by trial so as to fit the experiments of susceptibility, anisotropy and g -values as best as possible, taking the values at 90°K to be the standard and making the deviations between calculated and observed values at other temperatures as small as possible. The flexibility of the choice of covalency parameters k_i 's and R_i 's is limited by the condition that they lie between 0.5 and 1. Extensive trial and error computations have shown that it is possible to fit the theory exactly with the experiments only at one temperature and not at all temperatures. The reason for the particular choice of the temperature 90°K at which the theory has been made to fit the experiments almost exactly is that at this temperature the experimental results are very accurate; the signal to noise ratio and the sharpness of resonance signal as well as the percentage accuracy of the anisotropy and susceptibility measurements are very high. In this procedure of evaluation of the parameters, we assume them to be constant with temperature. However, some of them, especially the anisotropic field parameters σ , δ , γ and ϵ may change by a large amount as the temperature varies but for the moment we consider them to remain the same, as otherwise the solution of the parameters from the given experimental data become non-unique.

TABLE II

Values of the parameters showing the closest fit between the calculated and observed results for $\text{Cu}(\text{NH}_4\text{ScO}_4)_2 \cdot 6\text{H}_2\text{O}$

$$D = -1230 \text{ cm}^{-1}, \quad \sigma = -98 \text{ cm}^{-1}, \quad \gamma = -5 \text{ cm}^{-1}, \quad \delta = 14 \text{ cm}^{-1}, \quad \epsilon = 54 \text{ cm}^{-1}$$

$$k'_x = 0.86, \quad k'_y = 0.85, \quad k'_z = 0.84, \quad R'_x = 0.91, \quad R'_y = 0.80, \quad R'_z = 0.84$$

$$\zeta = -829 \text{ cm}^{-1} \text{ (free ion value)}$$

a. Spectroscopic splitting factors

	Theoretical (Best fitting at 90°K)	Experimental	
		at 300°K	at 90°K
g_x	2.113	2.12 ₃	2.12 ₀
g_y	2.073	2.05 ₂	2.06 ₈
g_z	2.400	2.39 ₆	2.40 ₀

b. Susceptibilities

Temperature	$(\chi_1 - \chi_2) \times 10^6$		$(\chi_1 - \chi_3) \times 10^6$		$\bar{\chi} \times 10^6$	
	Theo	Experi*	Theo	Experi*	Theo	Experi*
90°K	1053	1054	443	445.5	5103	5101
140°K	685	692.1	270	276.5	3285	3281
200°K	475	486.6	197	182.1	2330	2326
240°K	397	405.3	154	146	1949	1943
300°K	317	322	128	112	1574	1566

*Experimental results for crystalline anisotropies are taken from the measurements of Bose *et al* (1957)

† Experimental values of mean susceptibilities are taken from the magnetic measurements (unpublished) of P.K. Ghosh.

The parameters best suited to fit the theory with the experimental results are shown in table II. The results indicate an appreciable anisotropic covalency overlap of the ligand charges with the charge cloud of the central metal atom as indicated by the values $k'_x = 0.86$, $k'_y = 0.85$, $k'_z = 0.84$ for the orbital reduction as also $R'_x = 0.91$, $R'_y = 0.80$, $R'_z = 0.84$ for the S.O. reduction factors. Due to the covalency effect, the orbital moment is reduced by 14, 15 and 16 percent and S.O. coupling coefficient by 9, 20 and 16 per cent along x , y and z directions respectively, from the free ion values. It is to be noted that while the calculated values of mean susceptibility at different temperatures agree to within 0.6 per cent of the experimental results, those of magnetic anisotropy systematically deviate by an amount changing from zero at 90°K up to a maximum of about 12.5 per cent

at 300°K from the experimental values. The agreement between theoretical and experimental values has been made closest at 90°K in our investigation for reasons mentioned earlier. But there still exist systematically increasing discrepancies for both the mean as well as the anisotropy as the temperature rises and these must be attributed to the fact that the lower symmetric field parameters σ , δ , γ and ϵ which have been considered so far as temperature independent must be appreciably varying with temperature. This is also corroborated by the earlier findings of Bose *et al* (1957) on copper Tutton salts. As a matter of fact, the variation of anisotropic field parameters with temperature is quite evident from our measurement of g -values at the two temperatures 90°K and 300°K. The paramagnetic resonance experiment which offers a direct probe into the paramagnetic complex clearly shows the variation although small of the principal g -values and hence the variation of anisotropic ligand field splittings with temperature. Moreover, the e.p.r. measurement shows that the paramagnetic complex changes its orientations with temperature very perceptibly at least in the xy -plane. With orientational changes, the packing in the lattice must be changing and hence the anisotropic part of the ligand field (Van Vleck, 1939 Bose *et al* 1957). The effect may be vice versa in the sense that the change of the ligand field may also cause orientational changes.

In the absence of sufficient data at different temperatures from other independent sources it is not possible to fit uniquely the experimental magnetic data alone assuming the anisotropic field parameters to vary with temperature. It is, however, enough for the present purpose in spite of several simplifying approximations to indicate the systematic change in the anisotropic component of the ligand field with temperature. It may be mentioned in closing that the ionic anisotropy vs. inverse temperature curve theoretically follows a straight line but experimentally deviates from linearity. The neglect of the 3rd order terms in g_i mentioned earlier will cause a constant but small difference in the values of g_i at all temperatures and hence only a slight change in the inclination of the above theoretical curve without introducing any curvature. Thus, the neglect of third order terms in no way can explain the systematically increasing deviation from the expected Curie law. Moreover resonance line-width experiments (Bleaney *et al*, 1949) show that exchange interaction in these dilute Cu^{2+} salts is too small ($<0.1\text{K}$) to explain the deviation.

ACKNOWLEDGMENT

The authors are grateful to Prof. A. Bose, D.Sc., F.N.I. for his valuable guidance and helpful criticism of the work.

REFERENCES

- Abraham, A. and Pryce, M. H. L., 1951, *Proc. Roy. Soc.* **A205**, 135.
Bagguley, D. M. S. and Griffiths, J. H. E., 1952, *Proc. Phys. Soc.* **A65**, 594.

- Bloaney, B., Bowers, K. D. and Pryce, M. H. L., 1955, *Proc. Roy. Soc.* **A228**, 166.
- Bloaney, B., Penrose, R. P. and Plumpton, Betty, 1949, *Proc. Roy. Soc.* **A198**, 406.
- Bose, A., Ghosh, U. S., Bagchi, R. N. and Pal, A. K., 1964, *Indian J. Phys.* **38**, 361.
- Bose, A., Mitra, S. C. and Dutta, S. K., 1957, *Proc. Roy. Soc.* **A239**, 165.
- Dreisch, T. and Trommer, W., 1937, *Z. Phys. Chem.* **B87**, 37.
- Ghosh, P. K., 1966, *Thesis, Calcutta University*.
- Ghosh, U. S., Pal, A. K. and Bagchi, R. N., 1965, *J. Phys. Chem. Solids* **26**, 2041.
- Low, W., 1960, *Paramagnetic resonance in solid (Solid state Physics, suppl. 2)*, Academic Press, N.Y.
- Montgomery, H. B. and Lingafelter, E. C., 1964, *Acta Cryst.* **17**, 1478.
- Mookerjee, A. and Chhonkar, N. S., 1959, *Indian J. Phys.* **33**, 74.
- Owen, J., 1955, *Disc. Farad. Soc.* No. 19, 127.
- Polder, D., 1942, *Physica* **9**, 709.
- Pryce, M. H. L., 1950, *Proc. Phys. Soc.* **A63**, 25.
- Stevens, K. W. H., 1952, *Proc. Phys. Soc.* **A65**, 209.
- 1953, *Proc. Roy. Soc.* **A219**, 542.
- 1935, *J. Chem. Phys.* **3**, 807.
- Van Vleck, J. H., 1939, *J. Chem. Phys.* **7**, 61.

ELECTRONIC ABSORPTION SPECTRA OF 2-, 4-, 6- AND 7-METHYL QUINOLINE VAPOURS

M. A. SHASHIDHAR AND K. SURYANARAYANA RAO

DEPARTMENT OF PHYSICS, KARNATAK UNIVERSITY, DHARWAR

(Received March 21, 1966; Resubmitted November 8, 1966)

(Plate 4 and 5)

ABSTRACT. The near ultraviolet absorption spectra of four methyl-substituted quinolines, namely, 2-, 4-, 6- and 7-methyl quinolines, have been photographed for the first time in the vapour state. The spectra of these molecules occur approximately in the region $\lambda 3200 - \lambda 2800 \text{ \AA}$ and consist in each molecule of 10 to 15 rather broad, red-degraded bands. With the Raman and infra-red data on these molecules available in the literature, the spectra have been analysed. The most intense bands at the longest wavelength side are chosen as (0,0) bands and their wave numbers are 31999, 32152, 31759 and 31836 cm^{-1} for 2-, 4-, 6- and 7-methyl quinolines respectively. No ground state frequencies have been recorded in these molecules despite the wide range of experimental conditions of study of the spectra, except for three weak fundamentals in 2-methyl quinoline. The fundamentals obtained in this work in each molecule account for most of the bands in the spectrum. The results obtained are reported and discussed.

INTRODUCTION

Although a good deal of work has been done on the ultraviolet absorption spectra in the vapour state of benzene and substituted benzenes, relatively not much work has been done on two-ring molecules and, in particular, on heteroatomic two-ring compounds. Therefore it was thought worth while to investigate in the vapour state the electronic absorption spectra of some of these heteroatomic molecules with two fused six-membered rings. As a first step in that direction, the near ultraviolet absorption spectra of four methyl-substituted quinolines, namely, 2-, 4-, 6- and 7-methyl quinolines have been investigated in the vapour state for the first time. The ultraviolet absorption spectra of these methyl quinolines have been studied in solution before (Knight *et al.* 1955; Pickard *et al.* 1947) and λ_{max} (wavelength of maximum absorption) and ϵ (extinction coefficient) reported. The infra-red spectra of all these molecules have been investigated by Shindo and Ikeawa, (1956), Shindo, (1960) and Katritzky and Alan Jones (1960), while the Raman spectra of only 2- and 4-methyl quinolines have been reported in the literature Luther and Reichol, 1950; Jatkari Kulkarni 1936). A preliminary note reporting the results of our investigation of the ultraviolet spectra in the vapour state of these four molecules has been published (Shashidhar *et al.* 1966). In this paper are reported the details of the investigation.

EXPERIMENTAL

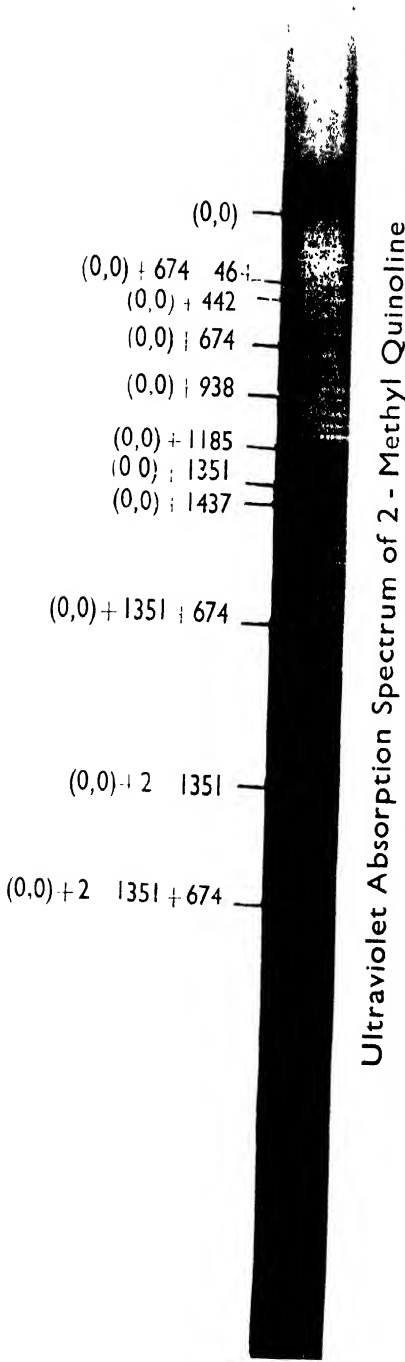
The samples of 2-, 4-, 6- and 7-methyl quinolines used in this investigation were supplied by Light and Co, England and were stated to be very pure. The boiling points of 2-, 4-, 6- and 7-methyl quinolines were 246°C, 258°C, 252°C, 248°C respectively. They were further purified by distillation in vacuum and the distilled products were used for work. Using absorption cells of lengths 5, 10, 25, 50, 75, 100, 150, 175 and 200 cm (the cells of the first three lengths were of quartz and the longer ones were of pyrex with pyrex to quartz graded seals), varying the temperature from that of the room to 200°C and eliminating the possibility at higher temperatures of the vapour condensing on the windows by keeping the main body of the absorption cell at about 10°C higher in temperature than the liquid container, spectra were photographed under conditions of saturated vapour pressure on a Hilger medium quartz spectrograph using Ilford R-40 and G-30 plates. A Hilger deuterium-filled lamp run on a stabilized power supply served as the source of continuum. The exposure time varied from about half an hour to a few hours. The bands were measured on five different spectrograms with reference to iron standards and the wavelengths computed with Hartmann's dispersion formula. The mean value of the different determinations was taken for the wavelength of each band. Because the bands are rather broad, the accuracy is estimated to be in general about 10 cm⁻¹.

RESULTS AND ANALYSIS

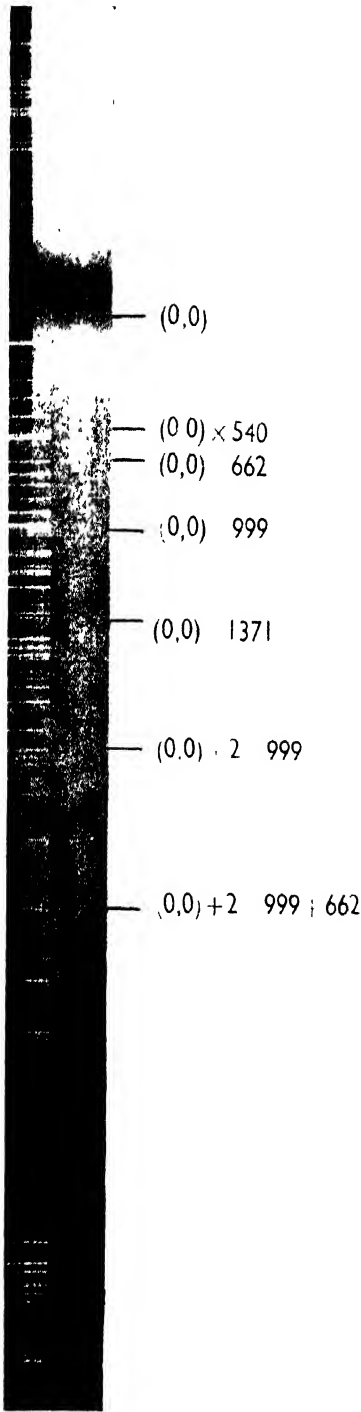
The electronic absorption bands of the methyl quinolines studied occur approximately in the region λ 2800 to λ 3200 Å. The bands are rather broad and degraded to the red. In all these molecules the minimum number of bands was obtained at room temperature with a path length of 25 cm. The most intense band at the longest wavelength in each molecule has been taken as the (0,0) band. With the (0, 0) band chosen in this way the bands of each molecules have been analysed with the help of the existing Raman and infra-red data. The wave numbers of the bands in vacuum, the visual estimates of their relative intensities, their separations in cm⁻¹ from the (0,0) band and their assignments are given in tables I, II, III and IV for 2-, 4-, 6- and 7-methyl quinolines respectively. Plates (4A, 4B, 5A and 5B) give enlarged reproductions of the spectra of the molecules investigated.

DISCUSSION

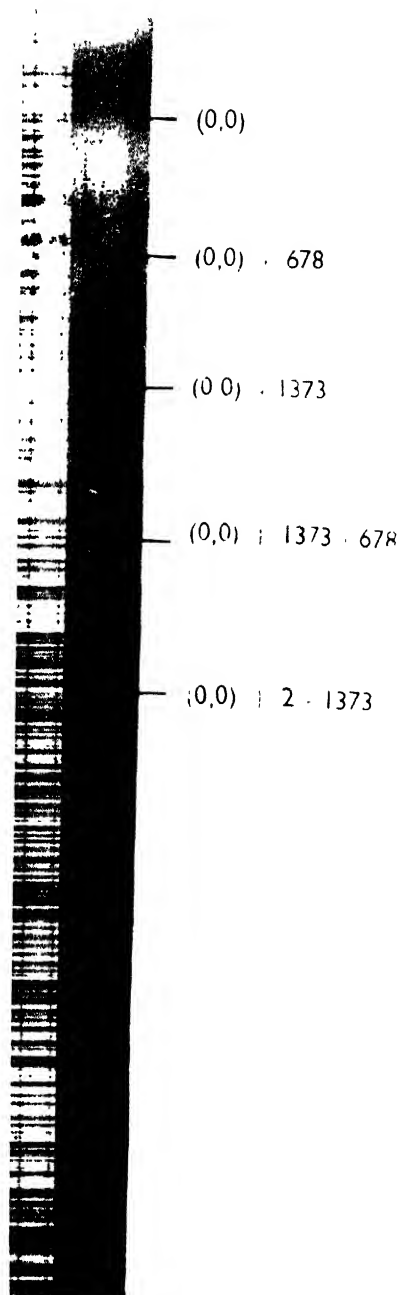
Each of the molecules studied in this work has a plane of symmetry which is the plane of the molecule, assuming the methyl group to be a single unit and therefore, they all belong to the point group, C_s . The observed band system in each of these molecules which corresponds to the forbidden transition in benzene, $^1A_{1g} \rightarrow ^1B_{2u} (^1L_b \rightarrow ^1A)$ is ascribed to $^1A' \rightarrow ^1A'$, which becomes allowed because of reduction in symmetry. It seems probable that in these molecules just as in the

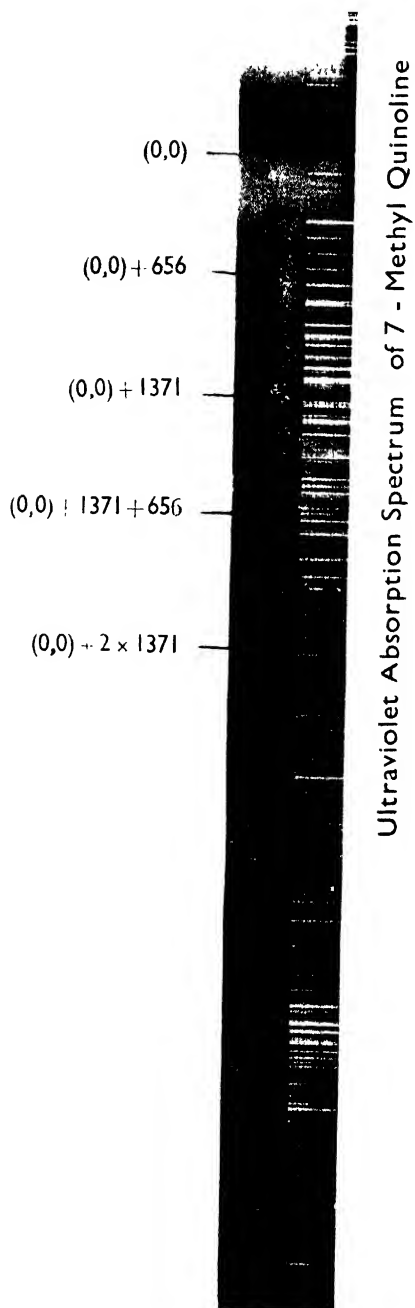


Ultraviolet Absorption Spectrum of 4 - Methyl Quinoline



Ultraviolet Absorption Spectrum of 6-Methyl Quinoline





case of quinoline vapour, there may also occur an $n-\pi^*$ system almost in the same region. We think, however, that the bands of the $n-\pi^*$ transition may be masked by the stronger, observed $\pi-\pi^*$ bands and that they are likely to contribute more to the background absorption in this region.

Ultra-violet absorption spectra of Methyl Quinolines in the vapour state

TABLE I
2-methyl Quinoline

Wave number in cm^{-1}	Intensity	Separation in cm^{-1} from (0,0) band	Assignment
31280	0	-719*	0,0-719
31473	0	-526	0,0-526
31535	0	-464	0,0-464
31659	0	-340	0,0-719+442
31999	6	0	0,0
32212	0	213	0,0+614-464
32441	1	442	0,0+442
32673	2	674	0,0+674
32937	1	938	0,0+938
33184	0	1185	0,0+1185
33350	2	1351	0,0+1351
33436	3	1437	0,0+1437
34035	1	2036	0,0+1351+674
34718	1	2719	0,0+2×1351
35390	0	3391	0,0+2×1351+674

*The error in measurement of this band is believed to be more because of its diffuseness and low intensity.

In all these molecules, there are two strong upper state frequencies which are progression-forming and also occur in combinations, the higher frequency being more intense. Each of them has about the same value in all the four molecules and they are : 674, 1351; 662, 1371; 678, 1373 and 656, 1371 in 2-, 4-, 6- and 7-methyl quinolines respectively. The more intense one around 1370 cm^{-1} may be a totally symmetric C-C stretching vibration (Gama C stretching) corresponding to the strong Raman frequencies 1376 cm^{-1} in naphthalene and 1372 cm^{-1} in quinoline. The other one around 670 cm^{-1} may be a totally symmetric vibration corresponding to the strong in-plane skeletal-distortion Raman frequencies 760

TABLE II
4-methyl Quinoline

Wave number in cm^{-1}	Intensity	Separation in cm^{-1} from (0,0) band	Assignment
31871	0	-281	
32032	0	-120	
32152	6	0	0,0
32692	1	540	0,0 + 540
32814	0	662	0,0 + 662
33150	1	999	0,0 + 999
33347	0	1195	0,0 + 1195
33523	2	1371	0,0 + 1371
34144	1	1992	0,0 + 2 \times 999
34804	0	2652	0,0 + 2 \times 999 + 662

TABLE III
6-methyl quinoline

Wave number in cm^{-1}	Intensity	Separation in cm^{-1} from (0,0) band	Assignment
31415	0	-344	
31575	0	-184	
31759	6	0	0,0
32031	0	272	
32265	0	506	0,0 + 506
32437	1	678	0,0 + 678
32624	0	865	0,0 + 865
32826	0	1067	0,0 + 1067
33132	2	1373	0,0 + 1373
33636	0	1877	0,0 + 1373 + 506
33839	0	2080	0,0 + 1373 + 678
34498	0	2739	0,0 + 2 \times 1373

TABLE IV
7-methyl Quinoline

Wave number in cm^{-1}	Intensity	Separation in cm^{-1} from (0,0) band	Assignment
31503	0	—338	
31639	0	—197	
31836	6	0	0,0
31931	0	95	
32237	0	401	0,0 + 401
32492	1	656	0,0 + 656
32932	0	1096	0,0 + 1096
33207	2	1371	0,0 + 1371
33583	0	1747	0,0 + 1096 + 656
33854	0	2018	0,0 + 1371 + 656
34571	0	2735	0,0 + 2 × 1371
35208	0	3372	0,0 + 2 × 1371 + 656

TABLE V

Molecule	Ground state frequencies in cm^{-1} ultra-violet absorption (Present work)	Raman	Infra-red	upper state frequencies (Present work) in cm^{-1}
2-methyl quinoline	464(0) 526(0) 719(0) — — — —	455(4) 522(5) 769(6) 1011(3) 1270(1) 1372(7) 1465(2)	— — — 1015 1254 1380 1473	442(1) — 674(2) 938(1) 1185(0) 1351(3) 1437(3)
4-methyl quinoline	— — — — —	565(7) 705(8) 1068(6) — 1361(8)	— — — 1294 1361	540(1) 662(0) 999(1) 1195(0) 1371(2)
6-methyl quinoline	— — — — —	— — — — —	— — — 1145 1376	506(0) 678(1) 865(0) 1067(0) 1373(2)
7-methyl quinoline	— — — —	— — — —	— — 1139 1385	401(0) 658(1) 1096(0) 1371(2)

and 758 cm^{-1} in naphthalene and quinoline respectively. In the 2- and 4-methyl quinolines, the corresponding Raman frequencies are 769(6), 1372(7) and 705(8), 1361(8) respectively. While the lower frequency has decreased in the upper states of these molecules, the higher one seems to remain almost unchanged.

It has not been possible to assign two to three bands in three of these spectra because, despite the fact that the spectra have been taken under all possible experimental conditions, no ground state fundamentals have been obtained for these molecules.

The correlations between the frequencies obtained in this work and the Raman and the infra-red data where available are shown in Table V, in which are also given for comparison, the corresponding data of naphthalene, [*U, V*—absorption data : (Sporer and Cooper, 1955); Raman and Infra-red data : (Lippincott and O' Reilly, 1955)].

The infra-red data of these molecules in the literature are not available to us. The infra-red data given in the Table are solution data taken from Katritzky and Alan Jones. They are not actually of methyl quinolines but are values obtained by the authors from their infra-red solution measurements on many substituted quinolines including the different methyl quinolines. They are, however, believed to be useful enough for correlation purposes since the authors state that the positions of these bands are relatively constant for different substituents while their intensities vary with the substituent. Therefore their intensities are not given in the table

ACKNOWLEDGMENT

One of the authors (K.S.R.) wishes to thank the University Grants Commission, Delhi, for the kind financial assistance given towards the cost of the chemicals used in this investigation.

REFERENCES

- Jatkar, S. K. K., 1936, *Indian J. Phys.* **10**, 23.
Katritzky, A. R. and Alan Jones, R., 1960, *J. Chem. Soc.* 2942.
Knight, S. B., Wallick, R. H. and Blach, 1955, *J. Am. Chem. Soc.* **77**, 2577.
Lippincott, E. R. and O' Reilly Jr. E. J., 1955, *J. Chem. Phys.* **23**, 238.
Luther H., and Reichel, C., 1950, *Z. Physik. Chem.* **195**, 103.
Pickard, P. L. and Lochte, H. L., 1947, *J. Am. Chem. Soc.* **69**, 14.
Samuel, B. K., Wallick, R. H. and Caroly, B., 1955, *J. Am. Chem. Soc.* **77**, 2577.
Shashidhar, M. A. and Suryanarayana Rao, K., 1966, *Curr. Sci.*, **35**, 230.
Shindo H., and Ikeawa, N., 1956, *Pharm. Bull (Japan)* **4**, 292.
Shindo, H., 1960, *Chem. Pharm. Bull. (Tokyo)* **8**, 845.
Sponer, H. and Cooper, C. D., 1955, *J. Chem. Phys.* **23**, 646.

Letters to the Editor

The Board of Editors does not hold itself responsible for opinions expressed in the letters published in this section. The notes containing short reports of original investigations communicated to this section should not contain many figures and should not exceed 500 words in length. The contributions reaching the Secretary by the 15th of any month may be expected to appear in the issue for the next month. No proof will be sent to the author.

5

ON THE CLASSICAL RADIATION BY AN ELECTRON IN UNIFORM CIRCULAR MOTION IN THE FORM OF MULTIPOLES

T. P. KHAN

D. A. COLLEGE, GARIA, 24-PARGANAS, WEST BENGAL, INDIA.

(Received September 16, 1966).

INTRODUCTION

The problem of classical radiation by electron in uniform circular motion was extensively discussed by Schott (1912). While Schott's interest was to explain atomic structure Schwinger (1912) repeated that analysis of the same problem to find out the maximum energy limit to be obtained by synchro-cyclotron. In this paper attempt has been made to obtain classical radiation by electron in uniform circular motion in the form of multipoles. An electric charge within the medium of dielectric constant ϵ is moving in a circular orbit of radius R with constant angular velocity ω_0 . The motion is assumed to be confined in a plane and the angular distributions of the radiation have been obtained after integration of the usual energy term on the surface of a sphere.

Spherical wave solution of Maxwell's Equation :

The Maxwell's equations for a source moving in a circular orbit of radius R and constant angular velocity ω_0 in the medium of dielectric constant ϵ ,

$$\nabla^2 \phi - \frac{\epsilon}{c^2} \frac{\partial^2 \phi}{\partial t^2} = \frac{4\pi}{\epsilon} \rho \quad \dots (1)$$

$$\nabla^2 A - \frac{\epsilon}{c^2} \frac{\partial^2 A}{\partial t^2} = \frac{4\pi}{c} J \quad \dots (2)$$

where ϕ , A , ρ , J have their usual meaning. Out of these two equations (1) and

(2) solution of single equation is enough to determine the two quantities ϕ , A , since ϕ , A are related by the Gauge

$$A = \frac{\epsilon v}{c} \phi$$

The potentials ϕ , A , and the source density $\rho(x)$, $J(x)$ are transformed in space and time according to the general rule of Fourier transforms.

$$F(x, t) = \frac{1}{(2\pi)^2} \int d^3K \int d\omega F(K, \omega) e^{ik \cdot x - i\omega t}$$

and the equations (1) and (2) are transformed into

$$\left[K^2 - \frac{\epsilon \omega^2}{c^2} \right] \phi(K, \omega) = \frac{4\pi}{\epsilon} \rho(K, \omega) \quad \dots (3)$$

$$\left[K^2 - \frac{\epsilon \omega^2}{c^2} \right] A(K, \omega) = \frac{4\pi}{C} J(K, \omega) \quad \dots (4)$$

with reference to a spherical polar co-ordinate system we assign the position of the charged particle at any instant to be at $(R, \omega_0 t, \pi/2)$ while the position of observation point has the co-ordinate (r, ϕ, θ) .

From the knowledge of Fourier transforms (Morse *et al*).

$$\rho(K, \omega) = \frac{e}{2\pi} \int e^{-ikR[\sin u \cos(\omega_0 t - v)] - i\omega t} dt \quad \dots (5)$$

substituting (5) in (3) and applying the same technique of Fourier transforms, we obtain

$$\begin{aligned} \phi(\omega) &= \frac{2e}{\epsilon(\omega)} \frac{1}{(2\pi)^{3/2}} \int \int e^{iK \cdot x - iKR[\sin u \cos(\omega_0 t - v)] - i\omega t} d^3K dt \\ &= \frac{2e}{\epsilon(\omega)} \frac{1}{(2\pi)^{3/2}} \sum \sum \alpha_{mn} \delta(\omega - m\omega_0) e^{im\phi} \rho_n^m(\cos \theta) j_n \left(\frac{\sqrt{\epsilon\omega}}{c} R \right) h_n \left(\frac{\sqrt{\epsilon\omega}}{c} r \right) \dots (6) \end{aligned}$$

Multipole Expansion of the Electromagnetic fields

The components of the Electromagnetic fields in (r, ϕ, θ) directions

$$E_r = -\frac{\partial \phi}{\partial r} \quad \because A_r = 0$$

$$E_\phi = -\frac{1}{C} \frac{\partial A\phi}{\partial t} - \frac{1}{r} \frac{\partial \Phi}{\partial \phi} = -\frac{\epsilon v}{c^2} \frac{\partial \Phi}{\partial t} - \frac{1}{r} \frac{\partial \Phi}{\partial \phi}$$

$$E_\theta = -\frac{1}{r \sin \phi} \frac{\partial \Phi}{\partial \theta} \quad \because A_\theta = 0$$

$$H_r = -\frac{1}{r \sin \phi} \frac{\partial A\phi}{\partial \theta} = -\frac{\epsilon}{C} \frac{v}{r \sin \phi} \frac{\partial \Phi}{\partial \theta}$$

$$H_\phi = 0$$

$$H_\theta = \frac{1}{r} \frac{\partial}{\partial r} (r A\phi) = \frac{\epsilon v}{cr} \frac{\partial}{\partial r} (r \Phi)$$

From (6) $\Phi(t)$ is obtained from the rule of Fourier transform

$$\Phi(t) = \frac{1}{\sqrt{2\pi}} \int \Phi(\omega) e^{-i\omega t} d\omega \quad \text{as}$$

$$\Phi(t) = \frac{2e}{\epsilon} \frac{1}{(2\pi)^2} \sum \sum \alpha_{mn} e^{im\phi} \rho_n^m (\cos \theta) e^{-im\omega_0 t} j_n(\sqrt{\epsilon m \beta}) h_n \left(\frac{\sqrt{\epsilon m \omega_0} r}{c} \right)$$

For energy transfer in the radial direction we require only E_ϕ and H_θ , which are when expanded in multipoles,

$$E_\phi n, m = +im \left[\frac{\epsilon v}{c^2} \omega_0 - \frac{1}{r} \right] \phi_{nm}(t)$$

$$\sum \sum E_{\phi nm} = \frac{2eim}{\epsilon(2\pi)^2} \left[\frac{\epsilon v}{c^2} \omega_0 - \frac{1}{r} \right] \sum \sum \alpha_{mn} e^{-im\omega_0 t} \times e^{im\phi} P_n^m(\cos \theta)$$

$$\times j_n(\sqrt{\epsilon m \beta}) \frac{e^{i\sqrt{\epsilon m \omega_0} r}}{\sqrt{\epsilon m \omega_0}} \frac{1}{r} \quad \dots \quad (7)$$

$$H_{\theta n, m} = \frac{\epsilon v}{c} \frac{\partial}{\partial r} \phi_{nm}(t) \text{ neglecting other terms.}$$

$$\sum \sum H_{\theta nm} = \frac{\epsilon v}{c} \frac{\partial}{\partial r} \sum \sum \phi_{nm}(t) \alpha_{mn} \quad \dots \quad (8)$$

Angular distribution of multipole radiation

The electromagnetic fields as obtained from (7) and (8) when terms upto $\left(\frac{1}{r}\right)$ are retained

$$E_\phi \rightarrow \frac{2e}{\sqrt{\epsilon}} \cdot \frac{\beta}{(2\pi)^2} \sum \sum \alpha_{mn} i^{-n} \frac{e^{i\sqrt{\epsilon m \omega_0} r - im\omega_0 t}}{r} j_n(\sqrt{\epsilon m \beta}) e^{im\phi} P_n^m(\cos \theta)$$

$$H_\theta \rightarrow 2e \cdot \frac{\beta}{(2\pi)^2} \sum \sum \alpha_{mn} i^{-n} \frac{e^{i\sqrt{\epsilon m \omega_0} r - im\omega_0 t}}{r} j_n(\sqrt{\epsilon m \beta}) e^{im\phi} P_n^m(\cos \theta)$$

The time averaged power radiated per unit solid angle is

$$\frac{d\rho}{d\Omega} = \frac{e^2\beta^2}{\sqrt{\epsilon(\pi)^2}} j_n^2(\sqrt{\epsilon m}\beta) |X_{m,n}(\theta, \phi)|^2$$

The table lists some of the simpler angular distributions.

$X_{m,n}(\theta, \phi)^2$		
<hr/>		
m		
<hr/>		
	± 1	± 2
<hr/>		
1 Dipole	$\frac{3}{16\pi}(1+\cos^2\theta)$	
<hr/>		
2 Quadrupole	$\frac{5}{16}(1-3\cos^2\theta$ $+4\cos^4\theta)$	$\frac{5}{16\pi}(1-\cos^4\theta)$
<hr/>		

The author expresses thanks to Dr. T. Roy of Jadavpur University for guidance and encouragement.

REFERENCES

- Jackson, *Classical Electrodynamics*, John Wiley & Sons, Inc., Page 550.
 Morse & Feschbach *Methods of Theoretical Physics*, : **I & II**, McGRAW—HILL BOOK Company Inc., Page 621, 827, 1325, 1362.
 Schwinger, 1949, *On Classical Radiation of accelerated electrons*, *Phys. Rev.* **75**, 1912.
 Schott, 1912, *Electromagnetic Radiation*, Cambridge University Press,

POSSIBILITY OF A REAL DEVIATION FROM FARADAY'S LAW OF ELECTROLYSIS

S. R. PALIT

DEPARTMENT OF PHYSICAL CHEMISTRY, INDIAN ASSOCIATION FOR THE
CULTIVATION OF SCIENCE, JADAVPUR, CALCUTTA-32

(Received April 15, 1967)

It has been observed by the author (Palit 1962a, b, 1963) that at a fixed voltage the current changes considerably on making the electrolyte flow past the electrodes, particularly so, if the electrolyte is a weak conductor. It appears that some conducting zone which probably is of different structure from the main bulk of the solution forms near the electrodes. Since structure promotes electronic conduction it was considered of interest to check the possibility of existence of non-electrolytic conduction in such weakly conducting systems. This was considered more worthwhile by the fact that practically all checks on Faraday's law have been carried out with fairly conducting electrolytes and no work appears to have been done with poor conductors, say, water itself. Our results throw considerable doubt on the validity of Faraday's law in such systems.

The experimental set-up is a very simple one, consisting of a beaker with two platinum wire electrodes inserted from the bottom. Two (or more) such are connected in series, one containing freshly distilled conductivity water and another containing a 0.5 N potassium sulphate solution serving as a coulometer (Abresh *et al.* 1960). The evolved gas is collected in graduated test tubes inverted over the electrodes. About 20 to 30 milliamperes D.C. current is sent through the system for a couple of hours or so to pre-saturate the electrolytes with hydrogen and oxygen. Electrolysis is now allowed to occur with 50 to 100 microampere current for three to five days or more until a few cc (usually 3 to 5 cc) of gas collects in the coulometer. The results are most unexpected.

If Faraday's law holds good, it is expected that equal volume of gas would collect in the two vessels. It is, however, observed (vide table) that the volume of gas collected over conductivity water at a particular electrode is much less than that collected over the coulometer at the same electrode. This occurs both at the anode and at the cathode. It was first thought that this may be due to the unequal solubility of the gas in the two electrolytes. To offset the effect of any such complicating factor, the electrolytes were not only presaturated with electrolytic gas by prolonged electrolysis as mentioned above, but the same sample of electrolyte was used in a number of consecutive experiments; this, however, made no difference in the results. Our observations can be summarised as follows.

(i) Wide deviation from Faraday's law is observed on electrolysis of conductivity water, provided the current is kept quite low say, of the order of a fraction of a milliampere or still lower.

(ii) The departure from Faraday's law tends to disappear with increasing concentration of electrolytes and somewhere in the range 0.01N to 0.1N the deviation becomes hardly detectable.

(iii) The lower the current and consequent less physical disturbance near the electrodes, the higher is the departure from Faraday's law.

More than a hundred experiments under varied conditions were made and they all confirmed the above results. The results were further confirmed by collecting electrolytic gas (hydrogen and oxygen together) in a closed apparatus similar to that recommended for use in coulometry (Abresh *et al.* 1960). The following is a typical set of results of one experiment with five cells and a coulometer in series.

TABLE

Electrolyte	Current milliamp	Volume of gas collected in the cell over cathode	Volume of gas collected in the coulometer in series over cathode	Per cent non-electrolytic conduction
Conductivity Water	0.100	0.6 cc	3.3	82%
N/10,000 K ₂ SO ₄	0.100	1.8 cc	3.3	46%
N/1,000 K ₂ SO ₄	0.100	2.4 cc	3.3	27%
N/100 K ₂ SO ₄	0.100	3.1 cc	3.3	6%
N/10 K ₂ SO ₄	0.100	3.3 cc	3.3	0%

It has not been possible to find any source of error in the above results and so it is concluded that Faraday's law is of limited validity in poorly conducting systems. An almost complete break-down of Faraday's law is easily observed by carrying out electrolysis of conductivity water in a closed system (Abresh, *et al.* 1960) using platinum electrodes (0.5 × 1 cm) and a current of 25 microamperes. It is observed that hardly any gas collects over even a couple of weeks whereas according to Faraday's law more than 6cc should have collected by this time; even in the coulometer in series only about a couple of cc gas collects. It appears that when there is paucity of ionic current carriers, the current tends to pass by some other mechanism, which is probably electronic.

There have been many reports in the literature (Hampel, 1964) about less than 100 percent current efficiency and these are generally explained as due to side reactions and other causes. Non-electrolytic current conduction should now be included as one of the factors for lower than theoretical current efficiency. Whether the non-electrolytic passage of current is caused by electronic conduc-

tion, or by conduction by charged water molecules, or by some other mechanism is an open question and would be duly answered particularly by transference experiments now under way. Further work is in progress and detailed results will appear elsewhere.

Thanks are due to Sri Prithwish Kumar Basu for carrying out the experimental work.

REFERENCES

- Abresh, K. and Classen, I. 1960, *Coulometric Analysis* (Translated by L. L. Leveson), Chapman and Hall, p. 80.
- Hampel, C. A. 1964, *Encyclopedia of Electrochemistry*, Reinhold Publishing Corp., New York, p. 593.
- Lingane, J. J., 1945, *J. Amer. Chem. Soc.*, **67**, 1916.
- , 1963, *Electrochemistry, Proceedings of the First Australian Conference, Sydney and Hobart* Pergamon Press, p. 711.
- Palit, S. R., 1962*a, b*, *Indian J. Phys*, **36**, 51, 586.

BOOK REVIEWS

DIPOLE RADIATION IN THE PRESENCE OF A CODUCTING HALF-SPACE. By A. Banos, Jr., Pergamon Press, Vol. 9 of the International Series of Monographs in Electromagnetic Waves—Editors : A. L. Cullen, V. A. Fock, and J. R. Wait; 1966. 70s

Consider an infinite plane surface separating two media—one a conducting medium which for simplicity is assumed to have infinite conductivity and the other a dielectric; and now put an oscillating dipole anywhere and with its axis either parallel to the plane of separation or perpendicular to it and you will have the basic considered in this monograph. While the problem is, to be sure, of interest, yet the reviewer is afraid that except the few who are actively working in the line (to which group the reviewer does not belong) the average physicist will find a perusal of this book of some 250 pages a tough job demanding too much of his time, patience and mathematical skill. However the book will be a useful reference book for any mathematical physicist who may be interested in the saddle point method of integration.

A. K. Ray Choudhuri

ATOMS TO ANDROMEDA—Edited by S. T. Butler and H. Messel; Pergamon Press, Oxford, 1966, pp 301, Price 21s.

'Atoms to Andromeda' is a collection of lectures in a summer School for high school students arranged by the Sydney School of Physics in 1966. Perhaps in such a course of lectures, one would expect to find an introduction to the Maxwell field theory, something about the wave theory of light, photons and the so-called dual aspect of light and may be there would be something about mesons, the expanding universe, the quasars and nuclear energy. Well, you really find all these in this book but it goes much further. There is the Dirac hole theory (even a mention of Feynman's idea of a particle proceeding in the negative direction of time), a discussion of the magnetic mirror and the magnetic bottle in plasma physics, a fairly detailed discussion of the digital computers and lastly something on parity, strangeness, SU(3) and SU(6). The reviewer would consider it a real wonder if the school students had been able to appreciate and benefit from this survey over such a vast and advanced field of Physics in the short time span provided by a summer school. Indeed, the reviewer feels that the topics and the level of discussion would be more suitable for, say, a refresher course for school or college teachers.

Perhaps the few lines above give a fairly good idea about the book, but it must be mentioned that the reviewer has found it an extremely readable book and has himself learnt much about branches he cannot consider his own. However, the picture of two boys throwing balls or trying to snatch away balls as a model of exchange interaction (Pp 29-30) seems too naive and is perhaps likely to lead to misconception. Again the explanation in parenthesis of angular momentum as $\text{mass} \times \text{angular velocity}$ is simply wrong.

An accent throughout the book has been on what has been done and is being done by the Sydney school. That is no doubt interesting reading for in some fields Sydney is now 'leading and not just following' but the details of the Molonglo radio observatory or the stellar interferometer at Narrabri observatory are likely to be considered a little too elaborate by the average foreign reader.

The reviewer would recommend the book for off time reading by mature physicists as it would be both entertaining and would broaden the general knowledge of present day physics.

A. K. Ray Choudhuri

INDIAN JOURNAL OF PHYSICS

VOL. 41

No. 5

AND

VOL. 50

PROCEEDINGS

No. 5

OF THE

INDIAN ASSOCIATION FOR THE CULTIVATION OF SCIENCE

(Edited in collaboration with the Indian Physical Society).

MAY 1967

PUBLISHED BY THE
INDIAN ASSOCIATION FOR THE CULTIVATION OF SCIENCE
JADAVPUR, CALCUTTA-32

EYRING'S EQUATION OF RELAXATION TIME AND DIELECTRIC ABSORPTION OF 3.14 cm MICRO- WAVES IN POLAR LIQUIDS—PART III. SUBSTITUTED TOLUENES AND α -BROMONAPHTHALENE

G. S. KASTHA, J. BHATTACHARYYA AND S. B. ROY

OPTICS DEPARTMENT,

INDIAN ASSOCIATION FOR THE CULTIVATION OF SCIENCE,
CALCUTTA-32.

(Received September 2, 1966)

ABSTRACT. The results of measurement on the times of relaxation of *o*, *m* and *p*-chlorotoluenes, *p*-bromotoluene, 3, 4-dichlorotoluene and α -bromonaphthalene in the liquid state at different temperatures and also the experimental values of the activation energies (ΔH^\ddagger) for dipole orientation are reported. An attempt has been made to correlate the experimental activation energies with the total energy due to intermolecular forces operating in the polar liquids. Following Eyring's theory of rate process, an expression for the 'frequency factor' has been deduced. The theoretical values have been compared with the experimental values for the frequency factor in the case of a number of polar organic compounds.

INTRODUCTION

Both Debye's theory and Eyring's theory of rate process have been applied to the elucidation of the mechanism of dipole rotation accompanying the phenomenon of dielectric relaxation in polar liquids subjected to rapidly alternating electric fields. The Debye's theory and some of its modifications (Perrin, 1939; Writz, 1954; Hill, 1954) have been used, chiefly, to obtain information about the molecular unit taking part in the dipole rotation and the internal viscous forces hindering such rotations. Eyring's theory on the other hand have yielded experimental values of heats of activation and entropy of activation required for the orientation of dipoles (Whiffen and Thompson, 1946; Fong and Smyth, 1963; Bhattacharyya *et al.*, 1966). While the limitations of the Debye's theory in determining the dimensions of the rotating dipole are well-known, the relation of the activation energy and the entropy of activation with the molecular parameters of the dipole is not obtained from the rate equation itself. Very little attempt has been made to correlate the experimental activation energy with the energy of the intermolecular forces obtaining in the polar liquids. Moreover, no method exists for obtaining an estimate of the entropy change in the relaxation process, which, incidentally is contained in the so called "frequency factor" obtained experimentally, from the molecular properties of the polar liquids.

Bhanumathi (1963) made attempt to identify the activation energies for dipole orientation in some organic polar liquids with the energy of interaction due to dipole dipole (Keesom) and dipole-induced dipole (Debye) forces between the molecules of the liquids. She obtained a fair amount of agreement between the experimental and the calculated energy values. Recently, Sinha *et al.*, (1966) have shown that in the case of very dilute solutions of polar compounds in non-polar solvents, the values of the activation energy calculated from a consideration of the interaction energy due to London's dispersion forces and the Debye forces agree fairly well with the activation energies obtained experimentally.

In the present paper an attempt has been made to calculate (i) the values of the activation energy by considering the total contributions from London, Keesom and Debye forces existing in the polar liquids and (ii) the value of the "frequency factor" from the parameters of the polar molecules. In order to find out how far the calculated values agree with the experimental values, the data on the activation energies and frequency factors obtained experimentally for a number of polar organic liquids in the present investigation and in earlier investigations (Bhattacharyya *et al.*, 1964, 1966) have been used.

EXPERIMENTAL

Chemically pure samples of *o*-, *m*- and *p*-chlorotoluenes, *p*-bromotoluene, 3,4-dichlorotoluene and α -bromonaphthalene obtained from reputed chemical firms were first fractionated and the proper fractions were repeatedly distilled under reduced pressure. The samples were properly dried before being used in the investigations. The experimental arrangement for determining the dielectric loss at 3-cm at different temperatures and the method of obtaining the time of relaxation (τ) were the same as described in the previous paper (Bhattacharyya *et al.*, 1966). The viscosities (η) of all the liquids were determined experimentally.

RESULTS AND DISCUSSION

The values of ϵ' , ϵ'' , $\tan \delta$ and τ along with the macroscopic viscosities (η) of all the compounds at different temperatures (T) are given in Tables I-VI. The values of the heat of activation for dielectric relaxation (ΔH_τ) and viscous flow (ΔH_η) have been obtained respectively from the graphs of $\log (\tau.T)$ against $1/T$ and $\log \eta$ vs $1/T$ as usual. These values and their ratios (γ) are given at the foot of the tables. The tables also contain the values of $\tau.T/\eta^\gamma$ and the average value of the frequency factor A obtained from the rate equation $\tau = AT^{-1} \exp (\Delta H_\tau/RT)$ for all the compounds. It is seen from the Tables that in each case $\tau.T/\eta^\gamma$ remains almost constant with temperatures. Similar relation was also observed with other compounds reported previously (Bhattacharyya *et al.*, 1966). In the following sections attempts have been made to calculate the activation energy and the frequency factor.

TABLE I
o-Chlorotoluene
Wave length (λ) = 3.14 cm

Temp. °K	ϵ'	ϵ''	$\tan \delta$	$\tau \times 10^{12}$ Sec	η m.p.	$\frac{\tau \cdot T}{\eta^\gamma} \times 10^7$
288	3.80	1.20	0.317	13.6	11.2	15.31
298	3.81	1.13	0.297	12.7	9.9	15.52
313	3.99	1.13	0.283	11.3	7.8	15.92
328	4.08	1.04	0.255	9.7	6.3	15.81
343	4.02	0.88	0.220	8.7	5.4	15.44
358	4.05	0.84	0.208	8.1	4.5	16.17
$\Delta H\tau = 1.07$ K.Cal/mole				$\gamma = 0.39$		
$\Delta H\eta = 2.75$ K.Cal/mole				$A = 62.1 \times 10^{-11}$		

TABLE II
m-Chlorotoluene
Wave length (λ) = 3.14 cm

Temp. °K	ϵ'	ϵ''	$\tan \delta$	$\tau \times 10^{12}$ Sec	η m.p.	$\frac{\tau \cdot T}{\eta^\gamma} \times 10^7$
278	3.76	1.95	0.519	22.5	11.1	25.72
298	3.74	1.64	0.438	19.2	8.5	26.47
313	3.79	1.49	0.393	16.8	6.8	26.37
328	3.82	1.36	0.356	15.0	5.6	26.46
343	3.76	1.17	0.312	13.5	4.8	26.32
358	3.76	1.13	0.301	13.0	4.4	27.30
$\Delta H\tau = 0.89$ K.Cal/mole				$\gamma = 0.36$		
$\Delta H\eta = 2.50$ K.Cal/mole				$A = 126.5 \times 10^{-11}$		

TABLE III
p-Chlorotoluene
Wave length (λ) = 3.14 cm

Temp. °K	ϵ'	ϵ''	$\tan \delta$	$\tau \times 10^{12}$ Sec	η m.p.	$\frac{\tau \cdot T}{\eta^\gamma} \times 10^7$
298	3.79	2.18	0.575	24.6	8.9	37.21
313	3.83	1.93	0.504	21.2	7.0	36.29
328	3.86	1.83	0.474	19.7	5.7	37.68
343	3.84	1.71	0.445	18.6	4.9	38.98
358	3.89	1.56	0.401	16.4	4.3	37.36
$\Delta H\tau = 0.78$ K.Cal/mole				$\gamma = 0.31$		
$\Delta H\eta = 2.56$ K.Cal/mole				$A = 204.6 \times 10^{-11}$		

TABLE IV
p-bromotoluene
 Wave length (λ) = 3.14 cm

Temp °K	ϵ'	ϵ''	$\tan \delta$	$\tau \times 10^{12}$ Sec	η m.p.	$\frac{\tau \cdot T}{\eta \gamma} \times 10^7$
313	3.34	1.54	0.461	27.3	9.5	38.86
328	3.45	1.53	0.444	24.3	7.7	39.02
343	3.47	1.44	0.415	22.4	6.6	39.98
358	3.59	1.42	0.396	19.9	5.8	38.50
$\Delta H\tau = 0.89$ K.Cal/mole				$\gamma = 0.35$		
$\Delta H\eta = 2.51$ K.Cal/mole				$A = 209.9 \times 10^{-11}$		

TABLE V
 3, 4-dichlorotoluene
 Wave length (λ) = 3.14 cm

Temp °K	ϵ'	ϵ''	$\tan \delta$	$\tau \times 10^{12}$ Sec	η m.p.	$\frac{\tau \cdot T}{\eta \gamma} \times 10^7$
303	3.30	2.16	0.655	38.9	13.7	18.36
318	3.33	1.82	0.547	31.8	10.3	19.30
333	3.58	1.76	0.492	24.2	8.5	17.63
348	3.68	1.66	0.451	21.2	6.7	19.11
363	3.76	1.57	0.418	18.9	6.2	18.80
$\Delta H\tau = 2.20$ K.Cal/mole				$\gamma = 0.71$		
$\Delta H\eta = 3.10$ K.Cal/mole				$A = 29.6 \times 10^{-11}$		

TABLE VI
 α -bromonaphthalene
 Wave length (λ) = 3.14 cm

Temp. °K	ϵ'	ϵ''	$\tan \delta$	$\tau \times 10^{12}$ Sec	η m.p.	$\frac{\tau \cdot T}{\eta \gamma} \times 10^7$
303	2.93	0.96	0.328	88.9	40.5	43.89
313	2.99	1.03	0.344	71.3	31.6	37.93
328	3.05	1.07	0.351	59.4	22.4	42.29
343	3.12	1.11	0.356	50.0	16.6	43.30
358	3.19	1.21	0.379	45.8	12.6	47.40
$\Delta H\tau = 2.30$ K.Cal/mole				$\gamma = 0.49$		
$\Delta H\eta = 4.72$ K.Cal/mole				$A = 56.6 \times 10^{-11}$		

a) Calculation of interaction energy

In order to obtain an estimate of the energy due to various intermolecular forces existing in polar liquids, special type of interaction e.g. hydrogen bonding etc. has been left out of consideration. The three main types of intermolecular forces considered are (i) London dispersion forces, (ii) Dipole-Dipole (Keesom) forces and (iii) Dipole induced dipole (Debye) forces (Ketelaar, 1953). So that the

total interaction energy is the sum of the energies due to each of the forces. The energy of interaction per molecule for the three types of forces are given by :

$$(i) \text{ London energy } E_L = 3 I \alpha^2$$

$$ii) \text{ Keesom energy } E_K = -\frac{2}{3} \frac{\mu^4}{kT r_0^6}$$

$$iii) \text{ Debye energy } E_D = -2 \alpha \mu^2 / r_0^3 \quad \dots (1)$$

where I is the ionisation potential of the molecule, α and μ respectively are the polarisability and the dipole moment of the molecule, r_0 is the average distance of separation between the dipolar molecules and k is the Boltzmann constant. The total interaction energy per molecule, $-U_m = E_L + E_K + E_D = E_L(1 + f_1 + f_2)$

$$\text{where } f_1 = \frac{E_K}{E_L} = \frac{8}{9} \frac{\mu^4}{I \alpha^2 kT} \quad \text{and} \quad f_2 = \frac{E_D}{E_L} = \frac{8}{3} \frac{\mu^2}{I \alpha} \quad (2)$$

If I is expressed in e.v. μ in Debye unit, r_0 in Å and α in units of 10^{-25} cc., then for a temperature $T = 333.3^\circ\text{K}$

$$f_1 = 1208.1 \mu^4 / I \alpha_p^2, \quad f_2 = 16.67 \mu^2 / I \alpha_p$$

$$\text{and} \quad E_L = -\frac{1.2 I \alpha_p^3}{r_A^6} \times 10^{-14} \text{ ergs/molecule} \quad (3)$$

Further, if the average distance r_A is calculated from the equation $r_A = \beta R_A$ where β is a constant and $R_A = (1.66 V_M)^{1/3}$ Å, V_M being the molar volume in cc., E_L may be written as

$$N.E = -\frac{.0627 I_e}{\beta^6} (\alpha_p / V_M)^3 \text{ K.cal/mole} \quad (4)$$

Since the activation energy is $-(-U) = U = N U_m$, where, N = Avogadro Number

$$U = \frac{.0627 I_e}{\beta^6} \left(\frac{\alpha_p}{V_M} \right)^3 (1 + f_1 + f_2) \text{ K.cal/mole} \quad \dots (5)$$

If this value of U is identified with the heat of activation ΔH , it is possible to calculate the value of β and to find out how far this value remains constant for the

different compounds. The value of β may also be estimated from the ratio of the free volume to the molar volume of the compound given by the relation $\beta_e = \left(\frac{V_M - v_0}{V_M} \right)^{1/3}$ where v_0 is the total volume of all the molecules in a gram molecule of the compound. This value of β_e is expected to be equal to that of β for molecules having very small dipole moments where E_K and E_D are negligible.

In order to find out how far the above considerations are consistent with the experimental results, all the necessary data have been collected in Table VII. The ΔH^\ddagger -values for compounds other than those obtained in the present investigation have been taken from the previously published data (Bhattacharyya *et al.*, 1964, 1966). The dipole moment (μ_D) and the molecular polarisability values (α_p) whenever available, have been taken from published literatures. In other cases α_p -values have been calculated from the molar volume and refractive index data. The values of the Van der Waal's constant $b = 4v_0$ have been calculated from the data on critical constants given in "physical properties of chemical compounds (15)". The data on ionisation potential have been taken from the published works (Kandel, 1955; Watanabe, 1957; Vilesov and Terenin, 1957; Streiswieser, 1960) and in the cases of *m*-dichlorobenzene, α -chloro- and α -bromo naphthalenes, the ionisation potential have been taken to be almost equal to that of the parent compounds.

It is seen from Table VII that except for molecules whose dipole moment $\sim 2D$ the contributions due to Keesom and Debye forces are small. The value of β varies between 0.8–1.0. While the values of β_e estimated from $\left(\frac{V_M - v_0}{V_M} \right)^{1/3}$ agrees roughly with the calculated β -values in the case of the alkyl benzenes, the disagreement between the two values increases as the dipole moment of the molecule increases. Considering the highly approximate nature of the calculations, the agreement is fairly satisfactory.

b) Calculation of the 'frequency factor'

The experimental value of the 'frequency factor' A is obtained from the time of relaxation τ at a temperature $T^\circ K$ for a particular compound from the relation

$$\tau = AT^{-1} \exp (\Delta H^\ddagger / RT) \quad \dots (6)$$

The quantity A which has the dimension of sec. deg. is not equal to $h/k = 4.8 \times 10^{-11}$ as is sometimes assumed, but is given from the Eyring's rate equation by the expression $A = h/k \exp (-\Delta S/R)$ where ΔS is the entropy of activation for the process of dipole orientation. Since Eyring has given no theoretical expression for determining the quantity ΔS we proceed to obtain the value of A from Eyring's fundamental rate equation (Glasstone *et al.*, 1941) given by

$$K_1 = \frac{kT}{h} \frac{F^\ddagger}{F} \exp (-U/RT) \quad \dots (7)$$

TABLE VII

$$U = \Delta H_{\tau} = \frac{.0627 I_e}{\beta^6} \cdot \left(\frac{\alpha_p}{V_M} \right)^2 (1 + f_1 + f_2)$$

$$\beta_e = \left(\frac{V_M - v_0}{V_M} \right)^{1/3}, \quad b = 4v_0$$

Compound μ_D	Polarisability $\alpha_p \times 10^{25} \text{cc}$ (V_M)	Ionisation potential I_e ev (bcc/mole)	$f_1 = \frac{Ek}{E_L}$ $\times 10^2$	$f_2 = \frac{E_D}{E_L}$ $\times 10^2$	ΔH_{τ} K.Cal/mole	β	β_e
Toluene .30	122.6 (111)	9.03 (146.3)	.007	.136	1.60	.868	.878
<i>o</i> -Xylene .51	141.0 (125)	8.77 (175.5)	.047	.351	1.53	.877	.848
<i>m</i> -Xylene .30	141.8 (128)	8.79 (177.2)	.006	.120	1.44	.822	.808
Ethyl benzene .36	141.0 (128)	8.70 (166.7)	.011	.168	2.20	.833	.877
Isopropyl benzene .40	156.0 (145)	8.70 (202.5)	.013	.184	2.90	.790	.867
Chloro benzene 1.56	122.5 (102)	8.80 (145.3)	5.41	3.76	1.19	.951	.864
Bromo benzene 1.50	136.0 (106)	8.98 (153.9)	3.68	3.07	1.49	.933	.860
<i>m</i> -dichloro benzene 1.48	142.3 (115)	9.00 (183.3)	3.18	2.85	1.02	.982	.848
<i>o</i> -Chloro toluene 1.43	141.6 (117)	8.88 (178.1)	2.84	2.71	1.07	.965	.853
<i>m</i> -Chlorotoluene 1.94	142.4 (118)	8.88	6.59	4.12	0.89	.985	—
<i>p</i> -Chloro toluene 1.94	142.4 (118)	8.82	9.57	5.00	0.78	1.005	—
<i>p</i> -Bromo toluene 1.96	155.0 (123)	8.69 (186.4)	8.54	4.76	0.89	.995	.853
α -Chloro naphthalene 1.50	193.0 (135)	8.00	2.05	2.43	2.71	.851	—
α -bromo naphthalene 1.50	197.0 (140)	8.00	1.97	2.38	2.30	.870	—

where $K_1 = 1/\tau$, U is the activation energy per mole, F is the total partition function per unit volume of the normal molecule and F^* is that of the activated molecule, excluding the contribution of the degree of rotational freedom along the reaction co-ordinate i.e. the angle of rotation of the dipole. We may assume that the electronic and vibrational contributions to the partition functions for the normal and the activated molecules to be the same. As regards the rotational contribution it may be observed that in the normal molecule, the dipole moment makes rotational oscillation of small amplitude and small frequency about its instantaneous position of orientational equilibrium, which in the activated molecule is converted into one of free rotation, the contribution due to which has already been included in equation (7). It is also assumed that the rotation about the two other axes are non-existent both in the normal and in the activated molecule. In the case of the normal molecule the rotational oscillational contribution to the partition function is $\approx kT/h\nu_0$ where ν_0 is estimated from the relation $2\pi\nu_0 = (\Omega/J)^{1/2}$ where J is the moment of inertia of the molecules about an axis perpendicular to the dipole moment. If the dipole moment is along the a -axis of the ellipsoidal molecule then J is intermediate between J_B and J_C . Ω is the restoring potential and is of the order of $3(E_K + E_D)$ in the polar liquids.

The translational contribution per molecule to the partition function for the activated molecule which may be supposed to be moving freely in a volume v = (vol. of liquid per molecule) is $(2\pi mkT/h^2)^{3/2} \cdot v$ (Frenkel, 1946). In the case of the normal molecule, however, the translational degrees of freedom are replaced in the liquid state by translational oscillations in the three mutually perpendicular directions about the mean equilibrium position of the molecule and the contribution to the partition function is $(kT/h\nu_t)^3$ (Frenkel, 1946) where ν_t is given by the equation $2\pi\nu_t = (f/m)^{1/2}$ and $f = (\partial^2 U_m / \partial r^2)_{eqib}$. Since U_m is of the form B/r^6 , f is obtained as $f = 42U_m/r_0^2$, U_m is the potential energy per molecule and m is the mass of the molecule.

Substituting these values in Eqn (7) the following expression for τ is obtained.

$$\tau = \frac{h}{kT} \left[\left(\frac{2\pi RT}{U} \right)^{3/2} \frac{kT}{(42)^{3/2} v} \frac{1}{h\nu_0} \right] e^{U/RT} \quad (8)$$

If $r_0^3 \approx v$ and ν_0 is replaced by $\bar{\nu}_0 = \frac{\nu_0}{c}$, Eqn. (8) takes the form

$$\tau = \frac{h}{kT} \left\{ \left(\frac{2\pi RT}{U} \right)^{3/2} \frac{kT}{(42)^{3/2} h c \bar{\nu}_0} \right\} e^{U/RT} \quad \dots (8a)$$

Comparing Eqn. (8a) with Eqn. (6) the frequency factor A is given by

$$A = \frac{h}{k} \left\{ \left(\frac{2\pi RT}{U} \right)^{3/2} \cdot \frac{kT}{(42)^{3/2} h c \bar{\nu}_0} \right\} \quad \dots (9)$$

For $T = 333.3^\circ K$ substituting the values of R , h , k and c , A is finally given as

$$A = \frac{7.29}{\bar{\nu}_0 U^{3/2}} \cdot \frac{h}{k} \quad \dots (9a)$$

TABLE VIII

$$A = \frac{7.29}{U^{3/2} \bar{\nu}_0} \cdot \frac{h}{k}$$

Compound	$A \times 10^{11}$ (experimental)	A (calculated) $\times 10^{11}$	
		$\bar{\nu}_0 = 1 \text{ cm}^{-1}$	$\bar{\nu}_0 = 0.5 \text{ cm}^{-1}$
Toluene	14.3	18.1	36.3
<i>o</i> -Xylene	22.1	18.0	35.9
<i>m</i> -Xylene	31.3	22.3	44.6
Ethyl benzene	8.1	12.2	24.4
Isopropyl benzene	2.8	7.4	14.8
Chlorobenzene	40.2	27.0	53.9
Bromobenzene	36.4	19.2	38.5
<i>m</i> -dichloro benzene	71.6	34.0	67.9
1, 2, 4-Trichloro benzene	126.8	29.9	59.8
<i>o</i> -Chlorotoluene	62.1	31.6	63.2
<i>m</i> -Chlorotoluene	126.5	41.7	83.3
<i>p</i> -Chlorotoluene	204.6	50.8	101.6
<i>p</i> -bromotoluene	209.9	68.9	137.8
3, 4-dichloro toluene	29.6	10.7	21.4
α -Chloro naphthalene	15.5	6.9	13.8
α -bromo naphthalene	56.6	10.0	19.9

Eqn. (9a) shows that A does not have the value h/k but varies from molecule to molecule depending on U and $\bar{\nu}_0$. The value of $\bar{\nu}_0$ estimated in the case of toluene from the equation $2\pi c\bar{\nu}_0 = (\Omega/J)^{1/2}$ is of the order of 1 cm^{-1} . With halo substituted benzenes, toluenes and naphthalenes the values of $\bar{\nu}_0$ are expected to be smaller than 1 cm^{-1} because of the substantial increase in the values of the moment of inertia (J) of the molecules. The value of the frequency factor A calculated for two values of $\bar{\nu}_0$ are given in Table VIII along with the experimental values of A . It is seen from the table that the experimental value of A in the case of the alkyl benzenes agrees fairly with the calculated A -value if $\bar{\nu}_0 = 1 \text{ cm}^{-1}$, while in the case of chlorobenzene bromobenzene, *m*-dichlorobenzene, *o*-chlorotoluene, 3, 4-dichloro-toluene and α -chloronaphthalene fair agreement is obtained if $\bar{\nu}_0$ is taken to be

0.5 cm⁻¹. In the case of *m*-chloro toluene, *p*-chloro- and *p*-bromotoluene and α -bromonaththalene the assumed value of $\bar{\nu}_0$ is to be further reduced in order that the calculated *A*-values agree fairly with experimental values of *A*.

REFERENCES

- Bhanumathi, (Mrs.) A., 1963, *Ind. J. Pure Appl. Phys.*, **1**, 79.
Bhattacharyya, J., Roy, S. B. and Kastha, G. S., 1964, *Indian J. Phys.*, **38**, 545.
———, 1966, *Indian J. Phys.*, **40**, 187.
Fong, F. K. and Smyth, C. P., 1963, *J. Am. Chem. Soc.*, **85**, 548, 1565.
Fr nkel, J., 1946, *Kinetic Theory of Liquids*, Clarendon Press, Oxford.
Glasstone, S., Laidler, K. J. and Eyring, H., 1941, *The Theory of Rate Process*, McGraw-Hill Book Co. Inc. Newyork.
Hill, N. E., 1954, *Proc. Phys. Soc.*, **B67**, 149.
Kandel, R. J., 1955, *J. Chem. Phys.*, **23**, 84.
Katelaar, J. A. A., 1953, *Chemical Constitution*, Elsevier Publishing Company.
Perrin, F., 1934, *J. de Phys* (7), **5**, 497.
Sinha, (Miss) B., Roy, S. B. and Kastha, G. S., 1967, *Indian J. Phys.*, (in press).
Streiswiessor, A. (Jr.), 1960, *J. Am. Chem. Soc.*, **83**, 4123.
Vilesov, F. I. and Terenin, A. N., 1957, *Dok. Akad. Nauk.*, S. S.S.R., **115**, 744.
Watanabe, K., 1957, *J. Chem. Phys.*, **26**, 541.
Whiffen, D. H. and Thompson, H. W., 1946, *Trans. Farad. Soc.*, **42A**, 114, 122.
Wirtz, K. and Spornol, A., 1953, *Z. Naturf.*, **8A**, 522.
Wirtz, K. and Gierer, A., 1953, *Z. Naturf.*, **8A**, 532.

EFFECT OF CLUSTER FORMATION ON THE VISCOSITY OF DENSE GASES

ARUN K. PAL AND A. K. BARUA

INDIAN ASSOCIATION FOR THE CULTIVATION OF SCIENCE, CALCUTTA

(Received September 15, 1966)

ABSTRACT. The effect of dimerization on the viscosity of dense gases has been calculated for the rigid sphere molecules by utilising an extension of the Enskog theory for dense gases. This treatment as distinguished from the earlier ones, takes into consideration the effect of dimerization on the collisional transfer term. Sample calculations made for Argon show that the contribution of dimerization to the viscosity is negative at low pressure and it becomes positive with the increase of pressure.

INTRODUCTION

For the calculation of the transport properties of dense gases it is necessary to consider the collision transfer (Chapman and Cowling, 1952) in addition to the transfer by molecular interaction. Enskog (Chapman and Cowling, 1952) long ago, first formulated a theory for the dense gases by considering the molecules to be rigid spheres. The advantage of this assumption is that the probability of multiple encounters become negligible. It has subsequently been found (Hirschfelder, Curtiss and Bird, 1954) that the Enskog theory can represent the transport properties of dense gases only approximately. Several attempts have been made to improve the Enskog theory by introducing semi-empirical corrections. Recently, Snider and Curtiss (1958, 1960) and Snider and McCourt (1963) have made a significant advance in the theory of dense gases. They have modified the Boltzmann equation which is an approximation to the series development of Bogolubov (1946) and Hollinger and Curtiss (1960). Curtiss, McElroy and Hoffman (1964) have used numerical methods to consider the effect of three body collisions on the first density term by a generalization of the Enskog rigid sphere expression.

Another factor which is of importance in the dense gases is the formation of clusters or bound molecules. As has already been pointed out by Das Gupta and Barua (1965) at sufficiently high pressures the gas should be treated as a mixture of monomers and j -mers. Stogryn and Hirschfelder (1941) have considered the formation of dimers in non-polar gases on realistic potential models. The effect of dimerization on the transfer by interaction has been considered by them. This treatment has recently been improved by Kim and Ross (1965) who considered the presence of quasi-dimers. These treatments are valid only for the initial pressure dependence. For higher densities it is necessary to consider the change

in the collisional transfer term due to cluster formation. At not too high pressures it is sufficient to consider dimerization only. In this paper a start has been made in this direction. We have made a sample calculation of the effect of dimerization on the viscosity of argon on the rigid sphere model. The results will show if the contribution of dimerization is of significant magnitude.

METHOD OF CALCULATION

The co-efficient of viscosity of a dense gas η_p on the Enskog theory may be expressed as (Chapman and Cowling, 1952)

$$\eta_p = \eta_0 b \rho \left[\frac{1}{b \rho \chi} + \frac{4}{5} + 0.7614 b \rho \chi \right], \quad \dots (1)$$

where η_0 is the zero-pressure viscosity, ρ the density, $b \rho = \frac{2}{3} \pi n \sigma^3$, σ being the collision diameter. The quantity χ is given by,

$$\chi = 1 + \frac{5}{8} \rho b + 0.2869 \rho^2 b^2 + \dots, \quad \dots (2)$$

The Enskog theory for a pure dense gas has been extended to the case of a binary mixture (Chapman and Cowling, 1952) and the viscosity for such a mixture may be written as,

$$\begin{aligned} [\eta_p]_{mix} = & \frac{5}{3} kT [b_{-1-1} n_{12} (1 + \frac{2}{5} b_{1\rho_1} \chi_1 + \frac{4}{5} M_2 b'_{2\rho_2} \chi_{12})^2 \\ & - 2b_{1-1} (1 + \frac{2}{5} b_{1\rho_1} \chi_1 + \frac{4}{5} M_2 b'_{2\rho_2} \chi_{12}) (1 + \frac{2}{5} b_{2\rho_2} \chi_2 + \frac{4}{5} M_1 b'_{1\rho_1} \chi_{12}) \\ & + b_{11} n_{21} (1 + \frac{2}{5} b_{2\rho_2} \chi_2 + \frac{4}{5} M_1 b'_{1\rho_1} \chi_{12})^2] / [\chi_{12} (b_{11} b_{-1-1} - b_{1-1}^2) \\ & + \frac{4}{15} (\pi kT)^{\frac{1}{2}} \{m_1^{\frac{1}{2}} n_1^{\frac{1}{2}} \chi_1 \sigma_1^4 + 2(2m_0 M_1 M_2)^{\frac{1}{2}} n_1 n_2 \chi_{12} \sigma_{12}^4 + m_2^{\frac{1}{2}} n_2^{\frac{1}{2}} \chi_2 \sigma_2^4\}], \quad \dots (3) \end{aligned}$$

In this formula,

$$\chi_1 = 1 + \frac{5}{12} \pi n_1 \sigma_1^3 + \frac{\pi}{12} n_2 (\sigma_1^3 + 16 \sigma_{12}^3 - 12 \sigma_{12}^2 \sigma_1) + \dots \quad \dots (4)$$

$$\chi_{12} = 1 + \frac{\pi}{12} n_1 \sigma_1^3 (8 - 3 \sigma_1 / \sigma_{12}) + \frac{\pi}{12} n_2 \sigma_2^3 (8 - 3 \sigma_2 / \sigma_{12}) + \dots \quad \dots (5)$$

with a corresponding equation for χ_2 . The subscripts 1, 2 stand for the components, 1, 2 respectively. We have also the following relations viz :

$$b_{11} = b'_{11} + n_{12} \chi_1 b''_{11} / \chi_{12}, \quad \dots (6)$$

$$b_{-1-1} = b'_{-1-1} + n_{21} \chi_2 b''_{-1-1} / \chi_{12}, \quad \dots (7)$$

$$b_{1-1} = -5kT(\frac{2}{3} - A)/E, \quad \dots (8)$$

$$b'_{11} = 5kT(\frac{2}{3} + M_2 A / M_1) / E, \quad \dots (9)$$

$$b''_{11} = 5kT/2[\eta_1]_1, \quad \dots (10)$$

The constant A depends on the ratio of the collision integrals,

The percentage of dimers at any particular temperature and pressure may be obtained from the equilibrium constant for dimerization,

$$K_2(T) = -(B_b + B_m)n/V, \quad \dots \quad (11)$$

$$= n_2 V / n_1^2, \quad \dots \quad (12)$$

$B_b(T)$ and $B_m(T)$ being the contribution of the bound double molecules and metastably bound molecules which have been calculated on the Lennard-Jones (12:6) model by Stogryn and Hirschfelder (1959). n_1, n_2 are respectively the number densities of monomers and dimers.

In order to obtain σ_2 it is necessary to calculate the viscosity of dimers. On the Lennard-Jones (12:6) model it has been shown by Stogryn and Hirschfelder (1959),

$$\frac{\sigma_{12}}{\sigma_1} = 1.03; \quad \frac{\epsilon_{12}}{\epsilon_1} = 1.32 \quad \dots \quad (13)$$

We have also the combination rules

$$\sigma_{12} = \frac{1}{2} (\sigma_1 + \sigma_2); \quad \epsilon_{12} = (\epsilon_1 \cdot \epsilon_2)^{\frac{1}{2}} \quad \dots \quad (14)$$

Thus by knowing $\sigma_1, \epsilon_1, \sigma_{12}$ and ϵ_{12} it is possible to calculate σ_2 and ϵ_2 from Eqs. (13) and (14). With these force constants for the dimers on the Lennard-Jones (12:6) model the viscosity values were calculated from the expression

$$\eta \times 10^7 = 266.93 \frac{\sqrt{MT}}{\sigma^2 \Omega^{*(2,2)}(T^*)} \quad \dots \quad (15)$$

where $\Omega^{*(2,2)}(T^*)$ is a reduced collision integral which has been tabulated as a function of $T^* = kT/\epsilon$. From the values of viscosity at any temperature as obtained from Eq. (15) σ_2 was calculated on the rigid sphere model from the expression,

$$\eta \times 10^7 = 266.93 \frac{\sqrt{MT}}{\sigma^2}, \quad \dots \quad (16)$$

For sample calculation of the effect of dimerization we have chosen the viscosity data of argon at 25°C (Michels, Botzen and Schuurman, 1954) The results obtained are shown in the Table I. It may be seen from the table that at lower pressures the effect of dimerization is to lower the viscosity which is in agreement with the results obtained by Barua and Das Gupta (1963) for steam and ammonia. However, at higher pressures the dimerization makes a positive contribution to viscosity. This may be due to the effect of dimers on the collisional transfer which overshadows the effect on the transfer by interaction, which is evident from the columns 4-6 of Table I. We have not made the calculations at higher pressures which will need the consideration of larger clusters. In fact at the highest pres-

tures considered by us, the positive contribution becomes less which is probably due to the importance of larger clusters at that pressure. As our main purpose in this paper is to find the effect of cluster formation on the rigid sphere model, we have not compared with the experimental viscosity data. In a subsequent paper we propose to make more realistic calculations.

Pressure (Atm.)	Density (g./cc.)	% of Dimers	$[\eta_p] \times 10^4$ mix calculated from eqn. (13) Poise	$\eta_p \times 10^4$ calculated from eqn. (1) Poise	$(\eta_{mix} - \eta_{cal}) \times 10^4$ in %
65.9	0.1115	6.41	2.327	2.380	-2.23
105.4	0.1806	9.65	2.540	2.535	0.72
175.2	0.3016	14.50	3.055	2.985	2.35
351.2	0.5558	21.92	5.171	4.955	4.44
465.5	0.6728	24.90	6.754	6.505	3.80

The authors are grateful to Prof. B. N. Srivastava for his kind interest and encouragement.

REFERENCES

- Barua, A. K. and Dasgupta, A., 1963, *Trans. Faraday Soc.*, **59**, 2243.
 Bogolubov, N. N., 1946, *J. Phys. (U.S.S.R.)*, **10**, 265.
 Chapman, S., and Cowling, T. G., 1952, *The Mathematical Theory of Non-Uniform Gases*, Oxford University Press.
 Curtiss, C. F., McElroy, M. B., and Hoffman, D. K., 1964, *WIS TC* 1-46, May.
 Dasgupta, A., and Barua, A. K., 1965, *J. Chem. Phys.*, **42**, 2849.
 Hirschfelder, J. O., Curtiss, C. F. and Bird, R. B., 1954, *Molecular Theory of Gases and Liquids*, John Wiley & Sons, N. Y.,
 Hollinger, H. B., and Curtiss, C. F., 1960, *J. Chem. Phys.*, **33**, 1386.
 Kim, S. K., and Ross, J., 1965, *J. Chem. Phys.*, **42**, 263.
 Michels, A., Botzons, A., and Schuurman, W., 1954, *Physica*, **20**, 1141.
 Snider, R. F., and Curtiss, C. F., 1958, *Phys. Fluids*, **1**, 122.
 ———, 1960, *Phys. Fluids*, **3**, 903.
 Snider, R. F., and McCourt, F. R., 1963, *Phys. Fluids*, **6**, 1029.
 Stogryn, D. E., and Hirschfelder, J. O., 1959, *J. Chem. Phys.*, **31**, 1531.

ON THE STRUCTURE OF COMPLEX SILVER LUTIDINE PER CHLORATE

T. RATHO AND Mrs. M. KRISHNASWAMY

REGIONAL ENGINEERING COLLEGE,
ROURKELA

(Received September 14, 1966.)

ABSTRACT. The Debye Scherrer pattern of complex Silver Lutidine per Chlorate has been obtained and analysed. The data obtained indicates that the crystal belongs to the monoclinic system with the unit cell dimensions $a = 10.96$ A.U., $b = 12.04$ A.U., and $c = 6.933$ A.U. and $\beta = 101^\circ 26'$. There are two molecules per unit cell and the space group P_2 , P_2/m or Pm can be assigned to the crystal.

INTRODUCTION

The study of complex salts containing ligands is of importance for the study of stretching force constants between the various groups of atoms in the molecules. Diamagnetic properties of such complexes are also of interest. Silver Lutidine per Chlorate $[\text{Ag}(\text{C}_7\text{H}_9\text{N})_2 \text{ClO}_4]$, is available in microcrystalline form, white in colour. As it is not possible to obtain single crystals suitable for complete structural analysis, the powder method has been used to establish certain crystallographic data.

EXPERIMENTAL

Filtered CuK_α radiation was obtained from a Machlett A-2 X-ray Diffraction tube running at 35KV and 15 m.A. and the specimen was contained in a very fine capillary of Lindmann glass of 0.01 mm. wall thickness and 0.5 mm. diameter. The Debye Scherrer pattern was obtained in a photographic film using a Rigaku Camera of 9 cm. diameter. The time of exposure was 4 hours. Interplanar distances were calculated with great accuracy from measurements on the photographic film. Attempts were made to index the power lines with Cubic, Tetragonal and Hexagonal systems and the data did not fit with any one of these systems of higher symmetry. Lipson's (Lipson, 1949) method was then tried which did not give a good number of constant differences indicating there by that the crystal belongs clearly to the two systems of lower symmetry namely the monoclinic or the triclinic. In such cases the De Wolffes' (1957) method or the most general method due to Ito (1950) is applicable. Here we have tried the latter method.

In the Table are listed the experimental X-ray data. As all the six parameters were to be found out the Ito's method was used and the powder pattern was indexed, Azaroff and Buerger (1958). The d values and the corresponding Q values ($1/d^2_{hkl} = Q_{hkl}$) are all given in the Table. Here Q_{hkl} is given by

$$Q_{hkl} = h^2 a^{*2} + k^2 b^{*2} + l^2 c^{*2} + 2klb^*c^* \cos \alpha^* + 2hlc^*a^* \cos \beta^* + 2hka^*b^* \cos \gamma^*$$

where α^* , β^* , γ^* and a^* , b^* and c^* are the reciprocal angles and axes respectively.

TABLE

No. of lines	Intensity	dA	$Q = 1/d$ hkl observed	Q hkl computed	Indices
1.	s	8.071	0.0154	0.01557	110
2.	s	6.074	0.0271	0.0276	020
3.	s	5.382	0.0345	0.03468	200
4.	w	3.966	0.0636	0.0634	121
5.	vw	3.869	0.0668	0.0672	201
6.	w	3.747	0.07122	0.0708	130
7.	s	3.580	0.07801	0.07803	300
8.	w	3.405	0.0863	0.08664	002
9.	w	3.241	0.0952	0.0948	221
10.	m	3.009	0.1105	0.1104 0.1109	040 321
11.	w	2.756	0.1316	0.1320 0.1321	302 041
12.	vw	2.682	0.1390	0.1387 0.1386 0.1389	400 401 312
13.	w	2.606	0.1470	0.1465	132
14.	w	2.539	0.1552	0.1559	241
15.	m	2.458	0.1656	0.1662 0.1663	421 420
16.	w	2.406	0.1728	0.1725	050
17.	m	2.344	0.1820	0.1821 0.1819	401 402
18.	vvw	2.240	0.1978	0.1973	302
19.	m	2.152	0.2160	0.2165 0.2167	142 500
20.	m	2.114	0.2238	0.2237 0.2240	510 303
21.	m	2.066	0.2342	0.2346	223
22.	s	2.007	0.2486	0.2484 0.2490 0.2490 0.2491	060 441 502 440

TABLE—(contd).

No. of lines	Intensity	dA	$Q_{hkl}=1/d^2$		Indices
			observed	computed	
23.	w	1.928	0.2690	0.2691	233̄
				0.2689	402
				0.2685	403̄
24.	vvw	1.877	0.2838	0.2831	260
				0.2840	333̄
				0.2843	161
25.	m	1.823	0.3004	0.2999	223
26.	vvw	1.764	0.3211	0.3216	541̄
27.	w	1.714	0.3404	0.3404	114̄
				0.3404	612̄
28.	vvw	1.698	0.3467	0.3466	004
				0.3468	170
29.	w	1.646	0.3693	0.3698	352
30.	w	1.604	0.3887	0.3892	550
31.	vw	1.573	0.4042	0.40462	124
32.	vw	1.541	0.4214	0.4215	371̄
				0.4214	334̄
				0.4215	552̄
33.	vw	1.501	0.4437	0.4442	172
				0.4439	144̄
				0.4439	642̄
				0.4433	053
34.	w	1.444	0.4779	0.4774	181
35.	vw	1.410	0.5031	0.5026	553̄
36.	w	1.378	0.5262	0.5260	182̄
				0.5261	632
37.	vw	1.354	0.5448	0.5449	315
				0.5451	273
38.	w	1.323	0.5709	0.5714	453
				0.5715	405̄
39.	vvw	1.283	0.6073	0.6077	364̄
				0.6069	472
40.	vvw	1.240	0.6504	0.6502	670
				0.6069	525̄

After certain trials the second, third, and the eighth reflections were taken as Q_{020} , Q_{200} and Q_{002} . It was then possible to find out the reciprocal cell dimensions as

$$a^* = 0.0731 \text{ A.U.}$$

$$b^* = 0.0831 \text{ A.U.}$$

$$c^* = 0.1472 \text{ A.U.}$$

In order to select the reciprocal cell angles α^* , β^* , $\gamma^*(hko)$, (hol) and (okl) reflections were carefully examined and it was found that (hko) and (okl) reflections were present if α^* and γ^* were taken to be 90° . The angle β^* could then be calculated after studying some pairs of (hol) and $(ho\bar{l})$ reflections after the equation

$$\cos \beta^* = \frac{Q_{hol} - Q_{ho\bar{l}}}{4hla^*c^*}$$

Thus β^* was found out to be $78^\circ 34'$. The six parameters of the reciprocal cell having been thus found the direct cell dimensions are obtained as

$$a = 10.970 \text{ A.U.}$$

$$b = 12.04 \text{ A.U.}$$

$$c = 6.933 \text{ A.U.}$$

$$\alpha = 90^\circ$$

$$\beta = 101^\circ 26'$$

$$\gamma = 90^\circ$$

The Buerger test for the reduced cell dimensions has been applied and the dimensions are found to be the reduced ones.

The above data establishes the crystal to be monoclinic. Finally all the powder lines were indexed using the general formula given above and the pattern so indexed showed the following conditions :

hkl —no condition

hol —no condition

hko —no condition

oko —no condition

ool —even present

The probable space groups therefore are P_2 or $P_{2/m}$ or P_m . The observed density is 1.644 gms/cc. and the number of molecules per unit cell comes to be 2. The calculated density is 1.563 gms/cc.

ACKNOWLEDGMENTS

We are thankful to the Union Education Ministry for awarding a scholarship to one of us (Mrs. M. Krishnaswamy). We are also thankful to Dr. D. V. Raman Rao, Professor of Chemistry of this institute for supplying the chemically pure sample used in this work.

REFERENCES

- Azaroff, L. V. and Buerger, M. J., 1958, *Powder Method*, 150.
Ito, T., 1950, *X-ray studies in Polymorphism*, Maruzen Tokyo.
Lipson, H., 1949, *Acta. Cryst.* **2**, 43.
Wolffe, P. M. De., 1957, *Acta. Cryst.* **10**, 590.

ELECTRON IMPACT ON HYDROGENIC BOUND ELECTRON

J. N. DAS

CENTRE OF ADVANCED STUDY IN APPLIED MATHEMATICS,
CALCUTTA UNIVERSITY, CALCUTTA.

(Received September 9, 1966).

ABSTRACT. Cross-section for the excitation of a hydrogenic bound electron by electron impact has been calculated in a Field Theoretic way. For low impact energy this reduces to the usual Born approximation result. At higher energies the result is a relativistic generalization. Better approximations for Bethes approximate formulae for high energy excitation cross-section are also obtained.

In the following discussion we consider the excitation of hydrogenic atom by electron impact in a Field Theoretic way (Roy, 1960). Bound state wave function of a hydrogen atom may be written in the form

$$\phi(x, x') = \langle V | \psi(x) \psi(x') | V \rangle \quad \dots (1)$$

where ϕ is an igen-state solution of the equation

$$-\frac{1}{i} \frac{\partial \phi}{\partial t} = \left(H_D + \frac{e^2}{|\vec{x}_1 - \vec{x}_2|} \right) \phi \quad \dots (2)$$

H_D is the Dirac Hamiltonian in the configuration space of the electron and the proton. With sufficient accuracy proton mass is taken to be infinitely heavy. Now we may write the initial and final wave functions for the bound electron in the form

$$\psi_i(x) = \int g_i(k_1) u_{k_1}(x) d\vec{k}_1$$

$$\psi_f(x) = \int g_f(\lambda_1) u_{\lambda_1}(x) d\vec{\lambda}_1$$

Thus the wave function for a bound and a free electron is

$$u_p(x_2) \psi(x_1) = \int g(k_1) \delta(p - k_2) u_{k_1}(x_1) u_{k_2}(x_2) d\vec{k}_1 d\vec{k}_2 \quad (4)$$

Hence the initial and final state vectors are

$$| \psi_i \rangle = \int g_i(k_1) \delta(p_1 - k_2) a_{k_1}^* a_{k_2} d\vec{k}_1 d\vec{k}_2 | V \rangle \quad (5)$$

$$| \psi_f \rangle = \int g_f(\lambda_1) \delta(p'_1 - \lambda_2) a_{\lambda_1}^* a_{\lambda_2} d\vec{\lambda}_1 d\vec{\lambda}_2 | V \rangle$$

The matrix element for the excitation of the bound electron from the state ψ_i to ψ_f by an electron impact which in the process transits from state '1' to '1'' is given by

$$\langle \psi_f | S | \psi_i \rangle = -ie^2 \int [-\psi_f(x_2) \gamma^\mu \psi_i(x_2) D_c(x_2 - x_1) \bar{u}_{p'_1}(x_1) \gamma_\mu u_{p_1}(x_1) d^4x_1 d^4x_2 - (1' \rightleftharpoons 2')] \quad \dots (6)$$

In momentum space the matrix element is

$$M_{fi} = (2\pi)^4 e^2 \int d\vec{p} [\bar{u}(p'_1) \gamma^\mu u(p_1) \bar{V}_f(p) \gamma_\mu V_i(q) - \bar{V}_f(p) \gamma_\mu u(p_1) \bar{u}(p'_1) \gamma^\mu V_i(q)] \quad \dots (7)$$

where

$$P = (W_2', p)$$

$$\vec{q} = \vec{p} + \vec{p}_1' - \vec{p}_1$$

$V_i(p)$ and $V_f(p)$ are the Fourier transforms of bound state wave functions for the initial and final states.

i.e.

$$\begin{aligned} \psi_i(r) &= \int V_i(p) e^{i\vec{p} \cdot \vec{r}} d\vec{p} \\ \psi_f(r) &= \int V_f(p) e^{i\vec{p} \cdot \vec{r}} d\vec{p} \end{aligned} \quad \dots (8)$$

Non-relativistic approximation for the bound wave function :

In this approximation we used non-relativistic Schrodinger wave function. So we take

$$V(p) = \phi_{nlm}(p) U(0)$$

where $U(\vec{s})$ stands for the plane wave spinor for momentum \vec{s} . Here we take ϕ_{nlm} and $\phi_{n'l'm'}$ corresponding to the initial and final states. We sum over final spins and average over initial spins for the square of the matrix element and get

$$\begin{aligned} |\bar{M}_{fi}|^2 &= \int_f \int_i |\bar{M}_{fi}|^2 = \frac{(2\pi)^8 e^4}{4} \int d\vec{p} d\vec{p}' \left[\frac{A}{(P_1 - P'_1)^4} + \frac{B}{(P_1 - P)^2 (P_1 - \bar{P})^2} \right. \\ &\quad \left. - \frac{C}{(P_1 - P'_1)^2 (P_1 - P)^2} - \frac{D}{(P_1 - P'_1)^2 (P_1 - \bar{P})^2} \right] \end{aligned} \quad (9)$$

where

$$A = F \cdot \text{Tr} \{ \gamma^\mu \Lambda(p'_1) \gamma^\nu \Lambda(p_1) \} \text{Tr} \{ \gamma_\mu \Lambda(0) \gamma_\nu \Lambda(0) \}$$

$$B = F \cdot \text{Tr} \{ \gamma^\mu \Lambda(p'_1) \gamma^\nu \Lambda(0) \} \text{Tr} \{ \gamma_\mu \Lambda(0) \gamma_\nu \Lambda(p_1) \}$$

$$C = F \cdot \text{Tr} \{ \gamma^\mu \Lambda(0) \gamma_\nu \Lambda(p_1) \gamma_\mu \Lambda(p'_1) \gamma^\nu \Lambda(0) \}$$

$$D = F \cdot \text{Tr} \{ \gamma^\mu \Lambda(p_1) \gamma^\nu \Lambda(p_1) \gamma_\nu \Lambda(0) \gamma_\mu \Lambda(0) \}$$

(10)

where

$$F = \phi_i(q) \phi_i^*(\bar{q}) \phi_f(\bar{p}) \phi_f^*(p)$$

On evaluation of the traces

$$\begin{aligned}
 A &= F. \frac{1}{m^2} [4W_1W'_1 + 2(m^2 - p_1p'_1)] \\
 B &= F. \frac{1}{m^2} [2W_1W'_1 + 2p_1.p'_1 - 2mW_1 - 2mW'_1 + 4m^2] \quad \dots \quad (11) \\
 C &= D = F. \frac{1}{m^2} [(p_1p'_1) + 2mW_1 + 2mW'_1 - 2W_1W'_1 - m^2]
 \end{aligned}$$

Excitation cross-section is given by

$$d\sigma = \frac{(2\pi)^2}{(2\pi)^{12}} d\Omega'_1 W_1 p'_1 W'_1 dW'_1 |\vec{M}_{fi}|^2 \delta(W_1 + W_2 - W'_1 - W'_2) \dots \quad (12)$$

Integration with respect to W'_1 yields

$$\frac{d\sigma}{d\Omega'_1} = \left(\frac{e^2}{4\pi}\right)^2 \frac{W_1 W'_1}{p_1} p'_1 \left\{ \frac{A' I_1^2}{(P_1 - P'_1)^4} + B' I_2^2 - \frac{+2C' I_1 I_2}{(P_1 - P'_1)^2} \right\} \dots \quad (13)$$

where $A' = \frac{1}{m^2} \{4W_1W'_1 + 2(m^2 - p_1.p'_1)\}$ etc.

$$I_1 = \int \phi_i(q) \phi_f(p) d\vec{p} \quad \dots \quad (14)$$

and

$$I_2 = \int \frac{\phi_i(\vec{q}) \phi_f(\vec{p})}{(P_1 - P)^2} d\vec{p} \quad \dots \quad (15)$$

The following cases are now considered :

(1) *Low energy scattering*

For very low impact energy (near the threshold energy) we can confidently neglect higher powers of momenta. In this approximation $A', B' \rightarrow 4$ and $C' = D' \rightarrow 2$. The result is nothing but the non-relativistic Born term. The merits and demerits of these results have been investigated by many authors. Corinaldesi and Trainer (1952) have evaluated the integrals analytically for special values of nl and $n'l'$.

(2) *Moderately high impact energy*

In this case the nature of the cross-section may well be investigated from the formulae (13), (14) and (15) with the further replacement of $(P_1 - P)^2$ by $-(\vec{p}_1 - \vec{p})^2$ in expression (15). In this approximation I_1 and I_2 corresponds to integrals for direct and exchange amplitudes. Tables (Omidvar, 1965) for integrals I_1 and I_2 for different initial and final quantum numbers are available and hence it is a simple matter to find corresponding cross-sections using formula (13).

(3) *High energy cross-section for direct scattering*

For large impact energies the exchange term becomes negligible and the nature of the scattering cross-section is determined solely by the direct term.

Differential cross-section is

$$\frac{d\sigma}{d\Omega'_1} = \left(\frac{e^2}{4\pi}\right)^2 \frac{W_1 W'_1 p'_1}{p_1 m^2} \{4W_1 W'_1 + 2(m^2 - p_1 \cdot p'_1)\} \frac{I_1^2}{(P_1 - P'_1)^4} \quad \dots (16)$$

For high impact energy $W'_1 \sim W_1$ and $t = |\vec{p}_1 - \vec{p}'_1|$ is very small, of the order W_{ab}^2/p_1 for $\theta \rightarrow 0$. Most of the contribution come but from a very small angle about the forward direction. Bethe's (1950) approximation formulae are then slightly modified. These take the forms

$$\sigma_{Tot} \sim \pi a_0^2 \left\{ \frac{\pi W_1^2 (6W_1^2 - 2m^2)}{p_1^2 m^2} \right\} \left[\log \left(\frac{K^2_T - W_{ab}^2}{K_{min}^2 - W_{ab}^2} \right) + \frac{W_{ab}^2}{(K_{min}^2 - W_{ab}^2)} \right] |M_{12}^1|^2 \quad \dots (17)$$

for optically allowed transition, and

$$\sigma_{Tot} \sim \pi a_0^2 \frac{\pi W_1^2}{4p_1^2} (6W_1^2 - 2m^2) \left[(K_T^2 - K_{min}^2) + 2W_{ab}^2 \log \left(\frac{K_T^2 - W_{ab}^2}{K_{min}^2 - W_{ab}^2} \right) + \frac{W_{ab}^2}{(K_{min}^2 - W_{ab}^2)} \right] |M_{12}^2|^2 \quad \dots (18)$$

for optically forbidden transition.

ACKNOWLEDGMENT

The author wishes to thank Dr. T. Roy of Jadavpur University for his interest in preparing the manuscript.

REFERENCES

- Bates, D. R. *et al*, 1950, *Phil. Trans.*, **A243**, 93.
 Corinaldesi, E. and Trainor, R., 1952, *Nuovo Cim.* **9**, 940.
 Omidvar, Kev. 1965, *Phy. Rev.* **140**, A38.
 Roy, T., 1960, *Zeit. f. Phy.* **158**, 142.


CRYSTALLOGRAPHIC STUDIES ON HYDRAZOBENZENE



S. L. CHORGHADÉ

METEOROLOGICAL OFFICE, POONA-5.

(Received August 4, 1966 ; Resubmitted October 17, 1966)

ABSTRACT. Hydrazobenzene, $\text{—NH} \cdot \text{NH—}$ , crystallizes in the bipyramidal class of orthorhombic crystals. Its unit cell has the dimensions

$$a = 7.33, b = 7.51, c = 18.72 \text{ \AA}.$$

The crystal density of 1.18 gm./c.c., found by floatation method, gives 4 molecules of hydrazobenzene in the unit cell of the crystal.

Measurement of refractive indices along the three crystallographic axes gave the following values :



$$\alpha = 1.595 \text{ (along } b \text{ axis)}$$

$$\beta = 1.602 \text{ (along } a \text{ axis)} ; \text{ The optic axial angle } 2V = 31^\circ 20'$$

$$\gamma = 1.700 \text{ (along } c \text{ axis)}$$

The crystal shows strong positive birefringence. The optical data together with the dimensions of the unit cell of the crystal of hydrazobenzene show an approximate tetragonal symmetry for the crystal with c axis as the axis of symmetry. Measurements of magnetic susceptibilities along three crystallographic axes made by Krishnan, *et al.* (1933) support the optical studies on the crystal.

INTRODUCTION

Azobenzene, stilbene and tolane, which crystallize in the monoclinic prismatic class, form an interesting series. They all have C_{2h}^{52} as their space group. The unit cells, which contain 4 molecules each, have very similar dimensions. All the three crystals have been found to have a pseudo-orthorhombic structure with $(20\bar{1})$ plane, which is nearly perpendicular to the ' a ' axis as a plane of approximate symmetry geometrically, magnetically and optically. The orientations of benzene rings in the unit cell are also similar in all these three crystals (Banerjee, 1938). Hydrobenzene, —NH. NH—, which is related to azobenzene in the same way as stilbene is related to tolane, falls out of this series in an interesting way. Its crystals display an approximate tetragonal symmetry with c axis as the axis of symmetry, as can be seen from the crystallographic studies described below.

MORPHOLOGICAL DATA AND THE UNIT CELL OF
HYDRAZOBENZENE CRYSTAL

Hydrazobenzene crystallizes in the bipyramidal class of orthorhombic crystals with axial ratios (Groth, 1919).

$$a : b : c = 0.9787 : 1 : 1.2497$$

The crystals show an approximate tetragonal symmetry with angles between the $m\{110\}$ faces being nearly equal to 90° and with $a \approx b$.

X-ray rotation and oscillation photographs taken about the 'a', 'b' and 'c' axes, using K_α radiation of copper, gave for the unit cell of the crystal :

$$a = 7.33 \text{ \AA}$$

$$b = 7.51$$

$$c = 18.72.$$

These dimensions lead to the axial ratios $a : b : c = 0.9763 : 1 : 2.492$, which agree well with the goniometric determinations except that the c axis will have to be halved.

The crystal density of 1.18 gm./c.c. found by the floatation method gives 4 molecules of hydrazobenzene in the unit cell of the crystal.

These axial dimensions also point out to the pseudo-tetragonal symmetry displayed by the crystal, since $a \approx b \neq c$.

Becker and Jancke (1921) have given the dimensions of the unit cell of hydrazobenzene crystal as $a = 11.10$, $b = 9.93$, $c = 9.33 \text{ \AA}$ with four molecules of hydrazobenzene in the unit cell. These results are inconsistent with the morphological data on the crystal (Groth, 1919). They also do not agree with our determination of the dimensions of the unit cell of hydrazobenzene crystal.

MAGNETIC DATA ON THE CRYSTAL OF
HYDRAZOBENZENE

Krishnan, Guha and Banerjee (1933) determined the magnetic susceptibilities of the orthorhombic crystals of hydrazobenzene along its three crystallographic axes and found that

$$\chi_a = -115.4$$

$$\chi_b = -130.4$$

$$\chi_c = -81.9$$

(the unit for χ 's being 10^{-6} of a c.g.s. electromagnetic unit).

The mean susceptibility of -109.2 determined for this crystal differs from Pascal's additive value of -121.3 . The mean susceptibilities and pascal's additive values have generally been found to agree closely with each other in the case of many organic compounds; azobenzene and hydrazobenzene are, however, striking exceptions.

Assuming that the two benzene rings in the molecule of hydrazobenzene lie in the same plane or in planes parallel to each other, it would be easy to see that the anisotropy of hydrazobenzene molecule ($K_{\perp} - K_{\parallel}$) would be nearly that of two benzene rings. The direction-cosines l , m and n , with reference to the crystallographic a , b , c axes, of the normal to the plane of the benzene rings can be calculated from the following relations :

$$l^2 - m^2 = \frac{\chi_b - \chi_a}{K_{\perp} - K_{\parallel}}$$

$$l^2 - n^2 = \frac{\bar{\chi}_c - \chi_a}{K_{\perp} - K_{\parallel}}$$

$$l^2 + m^2 + n^2 = 1,$$

where

$$K_{\perp} - K_{\parallel} = 108.$$

Substituting the values obtained by Krishnan, Guha and Banerjee, we get

$$l = \cos 51^{\circ} 21'$$

$$m = \cos 43^{\circ} 20'$$

$$n = \cos 73^{\circ} 30'$$

OPTICAL MEASUREMENTS ON HYDRAZOBENZENE CRYSTAL

The magnetic susceptibilities would further suggest that of the three refractive indices α , β and γ , the highest refractive index, γ , should be along c -axis while α and β should be along b and a axes respectively, and that $\alpha \approx \beta \ll \gamma$.

The optical measurements made on the crystal of hydrazobenzene fully fulfil these anticipations. Determination of refractive indices with the help of Abbe-Pulfrich refractometer and by the Becke immersion method gave

$$\alpha = 1.595 \text{ (along } b \text{ axis)}$$

$$\beta = 1.602 \text{ (along } a \text{ axis)}$$

$$\gamma = 1.700 \text{ (along } c \text{ axis),}$$

$a(100)$ being the optic axial plane. The optic axial angle ($2V$) from these measurements comes out to be $31^{\circ} 20'$. The crystal shows positive birefringence. The near equality of the refractive indices along a and b axes of the crystal points out to the pseudo-tetragonal character of its structure with c -axis as the axis of symmetry.

ORIENTATIONS OF BENZENE RINGS IN THE
CRYSTAL OF HYDRAZOBENZENE, DEDUCED FROM
OPTICAL DATA

Taking the density of the crystal of hydrazobenzene as 1.18 gm./c.c., the gram-molecular refractivities along the crystallographic axes, defined by the Lorentz constant

$$\frac{n^2-1}{n^2+2} \cdot \frac{M}{\rho}, \text{ would be :}$$

$$R_a = 68.53$$

$$R_b = 68.03$$

$$R_c = 75.86$$

The gram-molecular refractivities of the benzene molecule for vibrations along the normal to its plane and along directions in its plane are 16.4 and 32.6 respectively (Krishnan 1929), so that the birefringence of the benzene molecule is 16.2. Then, assuming that the optical moments induced in different benzene rings exert no influence on one another, the birefringence ($R_{||}-R_{\perp}$) of the hydrazobenzene molecule which has two benzene rings in the same or parallel planes should not be much different from 32.4. The orientations of the benzene rings in the crystal of hydrazobenzene can then be calculated from the optical data using the relations :

$$l^2-m^2 = \frac{R_b-R_a}{R_{||}-R_{\perp}}$$

$$l^2-n^2 = \frac{R_c-R_a}{R_{||}-R_{\perp}}$$

$$l^2+m^2+n^2 = 1,$$

where l , m and n are the direction—cosines of the angles which the normal to the plane of the benzene rings in the molecule of hydrazobenzene makes with a , b and c axes of the crystal. Substituting the measured values of gram-molecular refractivities in the above equations, we get

$$l = \cos 49^{\circ} 36'$$

$$m = \cos 48^{\circ} 42'$$

$$n = \cos 67^{\circ} 42'$$

which are in fairly good agreement with the direction-cosines obtained from the magnetic data. The small difference observed between the orientations of benzene rings in the crystal of hydrazobenzene from the optical and magnetic data is due to the fact that the mutual influences between the optical dipole moments of neighbouring molecules are quite large and not negligible as assumed.

Verification of these conclusions regarding orientations of the benzene rings by a complete and quantitative study of the structure of the hydrazobenzene crystal by X-ray methods would be very interesting.

The author is grateful to the authorities of the Indian Association for the Cultivation of Science, Calcutta, for giving the necessary facilities for major portion of the present work several years ago.

REFERENCES

- Becker, K. and Jancke, W., 1921, *Z. Physik. Chem.*, **99**, 242, 247.
Banerjee, S., 1938, *Zeits. Kristallog.* **A100**, 342.
Groth, P., 1919, "*Chemische Krystallographie*", V, 59.
Krishnan, K. S., 1929, *Proc. Roy. Soc., London*, **126A**, 155.
Krishnan, K. S., Guha, B. C. and Banerjee, S., 1933, *Phil. Trans. Roy. Soc., London*, **231A**, 235.

STRETCHING AND THE DIFFERENCE IN THE INTERMOLECULAR POTENTIALS OF H_2 AND D_2 FROM LOW TEMPERATURE DATA

A. K. GHOSH AND A. K. BARUA

INDIAN ASSOCIATION FOR THE CULTIVATION OF SCIENCE, CALCUTTA-32.

(Received September 15, 1966)

ABSTRACT. By analysing the low temperature viscosity data of H_2 and D_2 the effect of stretching on the intermolecular potentials of H_2 and D_2 has been considered. In the calculations quantum effects have also been taken into account. The results confirm the suggestion by Barua and Saran regarding the temperature dependence of the difference in the intermolecular potentials of H_2 and D_2 .

INTRODUCTION

In recent years, the difference in the intermolecular potentials of H_2 and D_2 has received attention from a number of workers. Previously, the general convention was to assume the potentials of isotopes to be identical. However, Michels, de Graaf and Seldam (1960) from an analysis of the accurate second virial coefficient data of Michels *et al.* (1959) first observed a definite difference in the intermolecular potentials of H_2 and D_2 . This was corroborated by Saran and Barua (1965) from an analysis of the viscosity data of H_2 and D_2 reported by Barua, Afzal, Flynn and Ross (1964). From the theoretical side, Knaap and Beenakker (1961) suggested that difference in the intermolecular potentials of H_2 and D_2 was due to the difference in their polarizabilities. Subsequently, Barua and Saran (1963) from an analysis of the second virial coefficient data (Michels *et al.*, 1960) obtained a regular temperature dependence of the difference in the intermolecular potentials of H_2 and D_2 which they explained as due to the temperature dependence of the polarizabilities of these gases. This temperature dependence of the polarizability comes mainly due to the stretching of the molecules with the increase of temperature. More recently, Mason, Amdur and Oppenheim (1965) have analysed various transport properties data including viscosity data for H_2 and D_2 and confirmed the results obtained by Michels *et al.* (1960) and Saran and Barua (1965). Due to the non-availability of quantum corrections for the transport properties which become prominent for H_2 and D_2 for temperatures below the room temperature, Saran and Barua (1965) had to limit their calculations to 300°K. However, recently quantum corrections for the transport properties have been calculated for the Lennard-Jones (12 : 6) model (Imam-Rahajoe, Curtiss and Bernstein 1965). In this paper we have examined the viscosity data of H_2 and D_2 as reported by Rietveld, Itterbeek, and Velds (1959) down to 14.4°K.

THEORETICAL FORMULAE

For all our calculations we shall use the Lennard-Jones (12:6) potential, which may be written as,

$$\phi(r) = 4\epsilon \left[\left(\frac{\sigma}{r} \right)^{12} - \left(\frac{\sigma}{r} \right)^6 \right] \quad \dots (1)$$

where $\phi(r)$ is the potential energy between two molecules separated by a distance r , ϵ is the depth of potential minimum and σ is the value of r for which $\phi(r) = 0$. The Lennard-Jones (12 : 6) potential holds strictly for spherically symmetrical molecules, i.e. it is incapable of taking into account inelastic collisions. However, as pointed out by Mason *et al.* (1962), viscosity is unaffected (to the first approximation) by inelastic collisions and at least for this particular property it is justified to use spherically symmetric potential.

The reduced coefficient of viscosity, η^* (Saran and Barua, 1965) may be written as

$$\eta^* = \eta \sigma^2 / \sqrt{m\epsilon} \quad \dots (2)$$

which is a function of $T^* = kT/\epsilon$

From Eq. (2) we can obtain the expression,

$$\frac{\eta_H - \eta_D}{\eta_H} = 1 - \frac{\sqrt{m_D \epsilon_D}}{\eta_H} \sigma_D^{-2} \eta^*(T^*_D) \quad (3)$$

where the subscripts H and D stand for H_2 and D_2 respectively and m represents the mass.

Let

$$\rho = (\sigma_H - \sigma_D) / \sigma_H,$$

then neglecting the higher terms,

$$\sigma_D^{-2} = \sigma_H^{-2} (1 + 2\rho) \quad \dots (4)$$

By developing $\eta^*(T^*_D)$ around the corresponding values of $\eta^*_H(T^*_H)$, we get

$$\begin{aligned} \eta^*(T^*_D) &= \eta^*(T^*_H) + (T^*_D - T^*_H) \partial \eta^* / \partial T^*_H \\ &= \eta^*(T^*_H) + T \cdot \delta \cdot \partial \eta^* / \partial T, \end{aligned} \quad \dots (5)$$

where

$$\delta = (\epsilon_H - \epsilon_D) / \epsilon_D$$

The magnitude of ρ is small (Knaap and Beenakker, 1961) and we shall neglect it in our considerations. Eq. (3) may thus be written as,

$$\frac{\eta_H - \eta_D}{\eta_H} = 1 - \frac{\sqrt{m_D \epsilon_D}}{\eta_H} \sigma_H^{-2} \left[\eta^*(T^*_H) + T \cdot \delta \cdot \frac{\partial \eta^*}{\partial T} \right] \quad \dots (6)$$

$$\text{Since, } m_D = 2m_H \text{ and } \sqrt{\epsilon_D / \epsilon_H} \simeq (1 - \frac{1}{2}\delta) \quad \dots (7)$$

We obtain finally,

$$\begin{aligned} \frac{\eta_H - \eta_D}{\eta_H} &= 1 - \sqrt{2} \left(1 - \frac{\delta}{2} \right) \left[1 + \frac{T \cdot \delta}{\eta_H} \frac{\partial \eta_H}{\partial T} \right] \\ &\simeq 1 - \sqrt{2} + \delta \left[\frac{1}{\sqrt{2}} - \frac{\sqrt{2}}{\eta_H} \cdot T \cdot \frac{\partial \eta_H}{\partial T} \right] \quad \dots (8) \end{aligned}$$

neglecting higher orders in δ .

From the theoretical side, following the procedure of Knaap and Beenakker (1961) and neglecting the difference in the repulsive energy of H_2 and D_2 , we obtain

$$\delta = \left[\left(1 - \frac{2\Delta\alpha(T)}{\alpha_H(T)} \right)^{-1} \left\{ \left(1 - \frac{2\Delta\alpha(T)}{\alpha_H(T)} \right)^{-1} - 1 \right\} \frac{\alpha_H(T)}{2\Delta\alpha(T)} \right] - 1 \quad \dots (9)$$

where $\Delta\alpha(T) = \alpha_H(T) - \alpha_D(T)$, $\alpha(T)$ being the polarizability at temperature T .

However, polarizability of molecules depends on internuclear distance and the stretching of the molecules with the increase of temperature will affect polarizability and consequently the intermolecular potentials. For a diatomic molecule the stretching due to vibrations and rotations may be expressed as (Bell, 1942)

$$\Delta r = \frac{kT}{2\pi^2\mu r_e v^2} + \frac{1}{2\pi^2\mu r_e v^2} \frac{\sum k(k+1)(2k+1)\sigma e^{-k(k+1)\sigma/kT}}{\sum (2k+1)e^{-k(k+1)\sigma/kT}} \quad \dots (10)$$

where μ is the reduced mass, v the frequency of vibration, r_e the equilibrium internuclear distance and $\sigma = h^2/8\pi^2\mu r_e^2$. By knowing $\alpha' = (d\alpha/dr)$, the change of polarizability due to stretching can be calculated. α'_H has been calculated accurately by Ishiguro *et al.* (1952) α'_D can be obtained from the relation,

$$\alpha'_D = \frac{(I_R/I_0)_D}{(I_R/I_0)_H} \left\{ \frac{(\nu_0 - \nu)^4_H}{(\nu_0 - \nu)^4_D} \frac{\mu_D \nu_D}{\mu_H \nu_H} \frac{(\alpha'_H + \frac{7}{45} \gamma'_H)(\alpha_D + \frac{7}{45} \gamma_D)}{(\alpha_H + \frac{7}{45} \gamma_H)} - \frac{7}{45} \gamma'_D \right\} \quad \dots (11)$$

where I is the intensity of the incident radiation of frequency ν_0 , I_0 the intensity of Rayleigh scattering and I_R the intensity of Raman line of frequency $\nu_0 - \nu$, γ denotes the anisotropy and $\gamma' = d\gamma/dr$. We have taken α_H , γ_H , γ_D and α'_H as obtained by Ishiguro *et al.* (1952). From the measurements of I_R/I_0 for H_2 and D_2 by Bhagabantam (1931, 1932), α'_D can be calculated from Eq. (11). Taking the value of $\alpha'_H = 1.411 \times 10^{-16}$ we get $\alpha'_D = 3.354 \times 10^{-16}$.

METHOD OF CALCULATION

Since we are concerned with low temperature data, it is necessary to account for quantum effects for the application of the theoretical formulae given above. These quantum corrections arise from symmetry and quantum effects and are particularly prominent for the lighter gases at low temperatures. Recently, Imam-Rahajoe, Curtiss and Bernstein (1965) have calculated from the phase-shifts

the quantum mechanical collision integrals for the Lennard-Jones (12 : 6) potential. In order to correct the experimental viscosity data for the quantum effects we have utilized the relation

$$\Delta\eta = \eta_c - \eta_q = C \left[\frac{1}{\Omega_c^{(2,2)*}(T^*)} - \frac{1}{\Omega_q^{(2,2)*}(\Lambda^*, T^*)} \right] \quad (12)$$

where the subscripts c and q stand for classical and quantum mechanical values, $\Omega^{(2,2)*}$'s are the collision integrals, $T^* = kT/\epsilon$, $\Lambda^* = h/\sigma\sqrt{2\mu\epsilon}$, is the quantum parameter, C is a function of the molecular weight, collision cross-section and temperatures (Hirschfelder, Curtiss and Bird, 1954). The force constants required for the calculation were obtained by fitting the experimental viscosity data to the Lennard-Jones (12 : 6) potential by the method of translation of axes (Mason and Rice, 1954). The results obtained are shown in Table II and are in

TABLE I
Experimental and calculated values of δ

T °K	η_D/η_H	δ_{exp}	δ_{calc}
20.4	1.455	0.067	0.058
71.5	1.446	0.061	0.056
90.1	1.441	0.054	0.055
196.0	1.418	0.013	0.051
229.0	1.413	-0.004	0.051

TABLE II
Force constants of H_2 and D_2

	This work			Diller and Mason (1966)		
	ϵ/k (°K)	σ (Å)	Λ^*	ϵ/k (°K)	σ (Å)	Λ^*
H_2	38.9	2.89	1.71	37.2	2.97	1.70
D_2	35.08	2.959	1.24	35.0	2.976	1.238

good agreement with those reported by Diller and Mason (1966). It was, however, observed that the viscosity data of D_2 as reported by Rietveld *et al.* (1959) are systematically lower than the more precise data of Kestin and Nagashima (1964) at 20°C and 30°C and those of Barua, Afzal, Flynn and Ross (1964) in the range -50°C to 150°C. It appears that the lower viscosity values of Rietveld *et al.* (1959) may be due to the presence of hydrogen as impurity. In order to correct

for this we have calculated the percentage of hydrogen from the simple formula for the viscosity of gas mixtures

$$\frac{1}{\sqrt{[\eta_{mix}]_1}} = \frac{x_H}{\sqrt{[\eta_H]_1}} + \frac{1-x_H}{\sqrt{[\eta_{D_2}]_1}} \quad \dots (13)$$

By taking the viscosity data (at zero density) of Barua *et al.* (1964) as the correct data for D_2 and η_{mix} as the experimental values of viscosity of D_2 , we have x_H the molefraction of H_2 in D_2 from Eq. (13). From three overlapping temperatures the average percentage of H_2 in D_2 comes out to be 2.67. We have corrected the experimental values of the viscosity of D_2 for the presence of H_2 according to the rigorous formulae for the viscosity of gas mixtures on the Chapman-Enskog theory. In order to obtain $\partial\eta_H/\partial T$ we have fitted the viscosity data to the polynomial

$$\eta_H = a + bT + cT^2, \quad (14)$$

by the least square, the coefficients being $a = 2.8195\mu P$ $b = 0.43\mu P^\circ K^{-1}$ $c = -0.4584 \times 10^{-3}\mu P^\circ K^{-2}$. The polynomial fit the data within an average deviation of 2% and for the viscosity value at 14.4°K, the deviation is about 10% which may very well be due to experimental error. Consequently, we shall leave the data at 14.4°K out of our consideration. Experimental values of δ can be calculated from Eq. (8) and are recorded in column 3 of Table I. The theoretically calculated values of δ are also shown in the same table.

DISCUSSION OF RESULTS

It may be seen from Table I that the calculated and the experimental values of δ show the same trend of variation with temperature. At the lower temperatures the agreement is quantitative. It must be pointed out that in view of our approximations and the small magnitude of δ , even qualitative agreement between experimental and the calculated values of δ should be considered as satisfactory. The results confirm the previously observed temperature dependence of Barua and Saran (1963). It is relevant here to refer to the suggestion of Mason *et al.* (1965) that the temperature dependence of δ (Barua and Saran, 1963) may be due to the limitations of the Lennard-Jones (12:6) model. However, it has been shown that both viscosity and second virial data show a temperature dependence of δ (Saran and Barua, 1965). From physical principles as well, intermolecular potentials should change with temperature as polarizability changes with temperature. That this effect plays a prominent role in diatomic molecules has also been shown by Saran and Deb(1966). Consequently a variation in δ with temperature is expected. Since Lennard-Jones (12 : 6) potential gives results which are consistent from the experimental and theoretical viewpoints it is perhaps not quite justified to ascribe the temperature dependence of δ (Barua and Saran, 1963) as due to an artifact of the model used for intermolecular forces. If the potential

model fails to give expected results then perhaps one of the reasons for the failure may be ascribed to the limitation of the model used.

ACKNOWLEDGMENT

The authors like to thank Prof. B. N. Srivastava, D.Sc., F.N.I., for his kind interest.

REFERENCES

- Barua, A. K., Afzal, M., Flynn, G. P. and Ross, J., 1964, *J. Chem. Phys.*, **41**, 374.
Barua, A. K. and Saran, A., 1963, *Physica*, **29**, 1393.
Bell, R. P., 1942, *Trans. Faraday Soc.*, **38**, 422.
Bhagabantam, S., 1931, *Indian J. Phys.*, **6**, 319,
———, 1932, *Indian J. Phys.*, **7**, 549.
Diller, D. E., and Mason, E. A., 1966, *J. Chem. Phys.*, **44**, 2604.
Hirschfelder, J. O., Curtiss, C. F. and Bird, R. B., 1954, *Molecular Theory of Gases and Liquids*, John Wiley & Sons, Inc., N. Y.
Imam-Rahajoo, S., Curtiss, C. F. and Bernstein, R. B., 1965, *J. Chem. Phys.*, **42**, 530.
Ishiguro, E., Arai, T., Kotani, M., and Mizushima, M., 1952, *Proc. Phys. Soc., Japan*, **A 65**, 178.
Kestin, J., and Nagashima, A., 1964, *Phys. Fluids*, **7**, 730.
Knaap, H. F. P., and Beenakker, J. J. M., 1961, *Physica*, **27**, 523.
Mason, E. A., Amdur, I. and Oppenheim, I., 1965, *J. Chem. Phys.*, **43**, 4458.
Mason, E. A., and Rice, W. E., 1954, *J. Chem. Phys.*, **22**, 522.
Mason, E. A., and Monchick, L., 1962, *J. Chem. Phys.*, **36**, 1622.
Michels, A., de Graaf, W., Wassenaar, T., Lovelt, J. M. H., and Louwerse, R. 1959, *Physica*, **25**, 25.
Michels, A., de Graaf, W., and Ten Seldam, C. A., 1960, *Physica*, **26**, 393.
Rietveld, A. O., Van Itterbeek, A., and Velds, C. A., 1959, *Physica*, **25**, 205.
Saran, A., and Barua, A. K., 1965, *Canad. J. Phys.*, **43**, 2374.
Saran, A., and Deb, S. K., 1966, *Mol. Phys.*, **10**, 221.

SYMMETRIES OF HIGHER ORDER AND THEIR INVARIANCE

M. DUTTA*

TALLMAN VISITING PROFESSOR OF MATHEMATICS, BOWDOIN COLLEGE,
BRUNSEWICK MAINE 04011, U.S.A.

(Received September 16, 1966)

ABSTRACT. If the equation of entropy-generation, considered as phenomenological law, is taken as the starting-point, general symmetry-relations, which are generalisations of Onsager relation, can be obtained. For this, the fact that generalised forces are differences or gradients of some thermodynamic quantities is to be fully utilised. Then, by simple and straightforward calculations, these symmetry-relations can be seen to be invariant under the general group of linear transformations of forces or fluxes. So, these symmetry-relations are natural laws as the Onsager reciprocal relation.

INTRODUCTION

In the linear theory of irreversible phenomena, the Onsager reciprocal relation plays a very important role (Onsager 1931, de Groot, 1951) and is considered as a fundamental law. But it is seen that the linear theory is not suitable in some cases, particularly when the chemical reactions are important in the irreversible processes (de Groot, 1951). Some attempts have been made to formulate and develop a non-linear theory. In this theory, the symmetry relations of higher order are important.

Here, symmetry-relations of higher order have been deduced simply from the well-known fact that the thermodynamic generalised forces are differences or gradients of some thermodynamic quantities, (generally intensive variables). The equation of entropy generation, taken in the usual form, is considered as a basic law and the closed study of its implications has been made. From this study the invariance of symmetry-relation of higher order under a general group of linear transformations of forces or fluxes follows simply and straight-forwardly.

BASIC NOTIONS AND THEIR SIGNIFICANCES

As already stated, a generalised force, X^μ , is the difference of some thermodynamic quantity x^μ like temperature, concentration, some potentials, etc. and so we can write,

$$X^\mu = \Delta x^\mu \quad \dots (1)$$

The equation of entropy-generation is usually written as

$$\sigma = \Delta S_v = J_\mu X^\mu \quad (2)$$

* At present, Professor of Mathematics, Powai, Bombay-76, India.

where σ is known as entropy-generation and is really the change ΔS_t of the entropy of system due to internal changes, J_μ is the flux corresponding to the generalised force X^μ , and the summation-convention, i.e., when the prefix and the suffix are same, it means summation over all possible values, has been used. After de Groot (1951), we shall consider the generalised forces as of a components linear vector, i.e., any linear combination of the forces, X^μ 's, is also a generalised force. Then, as the consequence of the equation (2), the flux is also a vector. Of course, for general group of linear transformations, the generalised force is a contragradient vector and the flux a covariant vector. Thus if we consider a linear transformation of forces as

$$X^\mu = \beta_{\mu\nu} X'^\nu \quad \dots \quad (3)$$

then the law of transformation of the fluxes is

$$J_\mu' = \beta_{\mu\nu} J_\nu \quad \dots \quad (4)$$

From the equations (1) and (2), we also get,

$$J_\mu = \frac{\partial S_\nu}{\partial x^\mu} \quad (5)$$

Also from experience and also from simple physical considerations, we have,

$$J_\mu = f_\mu(X^\nu) \quad \dots \quad (6)$$

where $f_\mu(X^\nu)$ denotes a functions of X^ν 's (having finite continuous derivatives of first k -th order, k being a suitable number) with the usual conditions that at the equilibrium position, near about which all considerations are restricted, we have

$$X^\nu = 0, \quad J_\mu = 0 \quad \text{for all } \nu\text{'s and } \mu\text{'s} \quad (7)$$

LINEAR THEORY

For clear understanding of the present discussions, it appears that we should discuss the usual linear theory from the present stand point.

* Now, the equation (5) is only a form of the implicit assumption of perfect differentiability of the Pfaffian expression representing dS which deserves a close minute scrutiny. If equations (1), (2) and (7), which have been clearly mentioned by de Groot (1951) as facts of experience, are admitted, the Onsager reciprocal relation implies and is implied by the perfect differentiability of dS_t . If this fact is accepted to be valid in general, the entire theory becomes very simple. In the present development, symmetries of higher order have been deduced easily and straightforwardly from this fact. But, the invariance of symmetry-relations of any order (if they exist) under the general group of linear transformations does not depend on this fact and follows generally and directly from simple discussions of linear transformations as it can be seen here.

When the close neighbourhood of the equilibrium position, in which our consideration are restricted, is such that first approximation will suffice, from equation (6) we have

$$J_{\mu} = \frac{\partial J_{\mu}}{\partial x^{\nu}} \Delta x^{\nu} = L_{\mu\nu} X^{\nu} \quad \dots (8)$$

Then, from the relations (6), (7) and (8) we get

$$L_{\mu\nu} = \frac{\partial J_{\mu}}{\partial x^{\nu}} = \frac{\partial^2 S_t}{\partial x^{\nu} \partial x^{\mu}} = \frac{\partial^2 S_{\nu}}{\partial x^{\nu} \partial x^{\mu}} = \frac{\partial J_{\nu}}{\partial x^{\mu}} = L_{\nu\mu} \quad \dots (9)$$

If S satisfies the usual conditions of commutativity of the orders of partial differentiation. The relation

$$L_{\mu\nu} = L_{\nu\mu} \quad \dots (10)$$

is the usual reciprocal relation of Onsager.

Now from relations (3), (4) and (7), we have,

$$J'_{\mu} = \beta_{\mu}^{\nu} J_{\nu} = \beta_{\mu}^{\nu} L_{\nu\rho} X^{\rho} = \beta_{\mu}^{\nu} \beta_{\lambda}^{\rho} L_{\nu\rho} X' = L'_{\mu\lambda} X'^{\lambda} \quad \dots (11)$$

i.e.,

$$L'_{\mu\lambda} = L'_{\lambda\mu} \quad \dots (12)$$

Thus, from (10) and from the commutativity of β_{μ}^{ν} 's we get the invariance of symmetry-relation, viz,

$$L'_{\mu\lambda} = L'_{\lambda\mu} \quad \dots (13)$$

The relation (13) also shows that $L_{\mu\nu}$ is a covariant tensor of second order.

NON-LINEAR THEORY OF THE SECOND ORDER

When the neighbourhood of the equilibrium position is such that it is sufficient to retain terms of second order, we get, by Taylor's theorem after neglecting the error,

$$\begin{aligned} J_{\mu} &= \frac{\partial J_{\mu}}{\partial x^{\nu}} \Delta x^{\nu} + \frac{1}{2!} \left\{ \frac{\partial^2 J_{\mu}}{\partial x^{\nu_1} \partial x^{\nu_2}} \Delta x^{\nu_1} \Delta x^{\nu_2} \right\} \\ &= L_{\mu\nu} X^{\nu} + L_{\mu\nu_1\nu_2} X^{\nu_1} X^{\nu_2} \quad \dots (14) \end{aligned}$$

where, when $\nu_1 \neq \nu_2$

$$\begin{aligned} L_{\mu\nu_1\nu_2} &= \frac{\partial^2 J_{\mu}}{\partial x^{\nu_1} \partial x^{\nu_2}} = \frac{\partial^2 S_2}{\partial x^{\mu} \partial x^{\nu_1} \partial x^{\nu_2}} \\ &= \frac{\partial^2 S_1}{\partial x^{\nu_1} \partial x^{\mu} \partial x^{\nu_2}} = \frac{\partial^2 J_{\nu_1}}{\partial x^{\mu} \partial x^{\nu_2}} = L_{\nu_1\mu\nu_2}, \\ &= \frac{\partial^2 S_2}{\partial x^{\nu_2} \partial x^{\nu_1} \partial x^{\mu}} = \frac{\partial^2 J_{\nu_2}}{\partial x^{\nu_1} \partial x^{\mu}} = L_{\nu_2\nu_1\mu} \end{aligned}$$

and, when $v_1 = v_2 = v$,

$$\begin{aligned} L_{\mu\nu\nu} &= \frac{1}{2!} \frac{\partial^2 J_\mu}{\partial x^\nu \partial x^\nu} = \frac{1}{2!} \frac{\partial^3 S}{\partial x^\mu \partial x^\nu \partial x^\nu} \\ &= \frac{1}{2!} \frac{\partial^3 S}{\partial x^\nu \partial x^\mu \partial x^\nu} = \frac{1}{2!} \frac{\partial^2 J}{\partial x^\mu \partial x^\nu} = \frac{1}{2} L_{\nu\mu\nu} \\ &= \frac{1}{2!} \frac{\partial^3 S}{\partial x^\mu \partial x^\nu \partial x^\mu} = \frac{1}{2!} \frac{\partial^2 J}{\partial x^\nu \partial x^\nu \partial x^\mu} = \frac{1}{2} L_{\nu\nu\mu} \end{aligned}$$

provided S_f satisfies usual mathematical conditions of commutativity of orders of partial differentiation. Now, in expression (14), v_1 and v_2 are dummy suffices so commutation v_1 and v_2 will lead to no new result. So, we have the symmetry relations of second orders as

$$L_{\mu v_1 v_2} = L_{v_1 \mu v_2} = L_{v_2 v_1 \mu} \quad \dots (15)$$

and

$$L_{\mu\nu\nu} = \frac{1}{2} L_{\nu\mu\nu} \quad \dots (16)$$

When there are only two generalised forces and so two fluxes, we have

$$L_{122} = \frac{1}{2} L_{212} = \frac{1}{2} L_{221},$$

$$L_{211} = \frac{1}{2} L_{121} = \frac{1}{2} L_{112}$$

Shrivastava and Kartar Singh (1966) was able to write these relations from some simple considerations.

As before, from (3) and (4) and (14) we obtain

$$L'_{\lambda\mu\nu} = \beta_\lambda^\sigma \beta_\mu^\sigma \beta_\nu^\tau L_{\rho\sigma\tau} \quad \dots (17)$$

From relations (15) and (16) and from the commutativity of β_μ^ν 's which are real numbers, we get invariance of the symmetric-relation. From (17) we also get that $L_{\lambda\nu\nu}$ is a covariant affine tensor of third order.

NON-LINEAR THEORY OF k TH ORDER

Now, when the neighbourhood about the equilibrium position is such that it will be sufficient to retain upto k th order say, by Taylor's theorem after neglecting the error after k -th term, we get

$$\begin{aligned} J_\mu &= \frac{\partial J_\mu}{\partial x^\nu} \Delta x^\nu + \frac{1}{2!} \left(\frac{\partial^2 J_\mu}{\partial x^{\nu_1} \partial x^{\nu_2}} \Delta x^{\nu_1} \Delta x^{\nu_2} \right) + \dots + \frac{1}{k!} \left(\frac{\partial^k J_\mu}{\partial x^{\nu_1} \dots \partial x^{\nu_k}} \Delta x^{\nu_1} \Delta x^{\nu_2} \dots \Delta x^{\nu_k} \right) \\ &= L_{\mu\nu} X^\nu + L_{\mu\nu_1\nu_2} X^{\nu_1} X^{\nu_2} + \dots + L_{\mu\nu_1 \dots \nu_k} X^{\nu_1} \dots X^{\nu_k} \end{aligned} \quad \dots (18)$$

where

$$L_{\mu\nu_1 \dots \nu_k} = \frac{\pi_i \rho_i!}{\pi k!} \frac{\partial^k J_\mu}{\partial x^{\nu_1} \dots \partial x^{\nu_k}} \quad \dots (19)$$

where ρ_i is the number of the i th group of equal indices of the index set v_1, v_2, \dots, v_k . Now, as γ 's are dummy suffices, so no new result is obtained by interchanging them. So, we get symmetry-relations as

$$L_{\mu\nu \dots v_k} = L_{\nu_1 \nu_2 \dots \nu_k} = \dots = L_{\nu_k \nu_1 \dots \nu_{k-1} \mu}, \quad v_1 \neq v_2 \neq \dots \neq v_k \quad \dots \quad (20)$$

$$L_{\mu\nu_1\nu_2\nu_3 \dots \nu_k} = \frac{1}{2!} L_{\nu_1\nu_2\nu_3 \dots \nu_k \mu} = \dots = L_{\nu_k\nu_1\nu_2\nu_3 \dots \mu}, \quad v_1 \neq v_2 \neq \dots \neq v_k \quad (21)$$

$$L_{\mu\nu\nu \dots \nu} = \frac{1}{k} L_{\nu\mu\nu \dots \nu} = \dots = \frac{1}{k} L_{\nu\nu \dots \nu\mu}, \quad v_1 = v_2 = \dots = v_k = \nu \quad \dots \quad (22)$$

These are the symmetry-relations of k -th order. Proceeding as before, we have,

$$\begin{aligned} J'_\mu &= \beta_\mu^\nu J_\nu = \beta_\mu^\nu [L_{\nu\rho} X^\rho + L_{\nu\rho_1\rho_2} X^{\rho_1} X^{\rho_2} + \dots + L_{\nu\rho_1 \dots \rho_k} X^{\rho_1} \dots X^{\rho_k}] \\ &= \beta_\mu^\nu \beta_\sigma^\rho L_{\nu\rho} X'^\sigma + \beta_\mu^\nu \beta_\sigma^\rho \beta_{\sigma_1}^{\rho_1} \beta_{\sigma_2}^{\rho_2} L_{\nu\rho_1\rho_2} X'^{\sigma_1} X'^{\sigma_2} + \dots + \beta_\mu^\nu \beta_{\sigma_1}^{\rho_1} \dots \beta_{\sigma_k}^{\rho_k} \\ &\quad L_{\nu\rho_1 \dots \rho_k} X'^{\sigma_1} \dots X'^{\sigma_k} \\ &= L'_{\mu\sigma} X'^\sigma + L_{\mu\sigma_1\sigma_2} X'^{\sigma_1} X'^{\sigma_2} + \dots + L'_{\mu\sigma_1 \dots \sigma_k} X'^{\sigma_1} X'^{\sigma_2} \dots X'^{\sigma_k} \end{aligned}$$

So we get

$$L'_{\mu\nu_1 \dots \nu_2} = \beta_\mu^\rho \beta_{\nu_1}^{\sigma_1} \beta_{\nu_2}^{\sigma_2} \dots \beta_{\nu_k}^{\sigma_k} L_{\rho\sigma_1 \dots \sigma_k}, \quad j \leq k.$$

Arguing as in the preceding cases, we have the invariance of the symmetry-relation of j -th order, $j \leq k$.

CONCLUDING REMARKS

From our above discussion, it is clear that if in phenomenological theories, we proceed from slightly altered assumption, which are also facts of experience, we get not only our present-day linear theory but also its generalisation upto any higher order. The mathematical method used is simple and straightforward.

ACKNOWLEDGMENTS

The author expresses his gratitude to National Professor S. N. Bose, F.R.S. for the keen interest shown in the problem and also for taking this work as a part of his research scheme.

REFERENCES

- de Groot, S. R., 1951, *Thermodynamics of Irreversible Processes*, North.Holland Publishing Company Amsterdam.
 Onsager, L., 1931, *Phys. Rev.* **37**, 408.
 ———, 1931, *Phys. Rev.* **38** 2265.
 Shrivastava, H. and Singh, Kartar, (unpublished).

D. C. THREE WIRE ELECTRICAL POWER TRANSMISSION NETWORK AS SOLVED BY RELAXATION METHOD

S. N. DUTTA

DEPARTMENT OF APPLIED PHYSICS, CALCUTTA UNIVERSITY.

(Received September 26, 1966)

ABSTRACT. This paper reveals how the relaxation method can be suitably applied to determine some important quantities such as line currents in D. C. Three Wire Transmission System. The equivalent circuit of this network system is used and the problem is solved easily by applying the principle of relaxational solution of D.C. network, considering the heating effects of steady currents flowing in it. The values of the required quantities thus obtained are compared with those found out by the normal method of network analysis.

INTRODUCTION

D.C. Three Wire Transmission system (Starr, 1946) is used for having considerable economy in feeders and distributors, when the electrical energy to be supplied is fairly large. Although there are different methods for solving this problem the relaxation method proves to be of advantage for yielding many useful informations simultaneously.

In this problem an unbalanced D.C. Three Wire Transmission system, that means the outer lines carrying unequal currents resulting a flow of current in the neutral line, is considered as shown in Fig. 1. The equivalent circuit diagram can be conveniently drawn indicated in Fig. 2, which is then solved by the relaxation method.

First of all Southwell and Black (1938), and later on Dutta (1966), applied the relaxation method in the problem of D.C. networks and showed its usefulness in solving the network problem represented by Fig. 2.

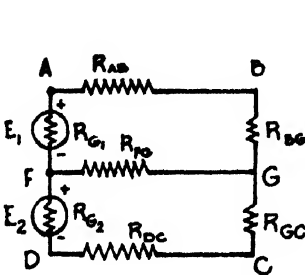


Fig. 1. Diagram for D.C. three wire Transmission-Network.

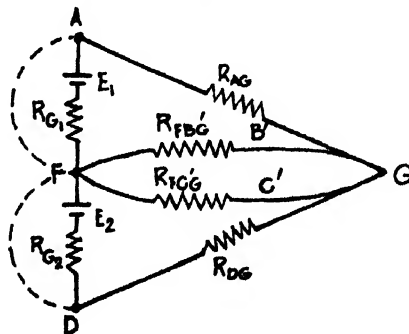


Fig. 2. Equivalent Circuit diagram for D.C. three wire Transmission Net-work.

THE METHOD

In the method described in this paper the heating effects of steady currents are considered. An electrical theorem in connection with the heating effects is used (Southwell and Black, 1938) and it can be enunciated as follows :

"In a network of conductors to which specified currents are supplied at two or more nodal points the actual distribution of currents is such that the total generation of heat less twice the energy expended in supplying the specified currents from a source at datum potential has its minimum value consistent with the satisfaction of Kirchoff's second law."

Two nodal points A and G of the network shown in Fig. 2, are considered and they are joined by a conductor of resistance R_{AG} . By Ohm's law a current of $\frac{V_A - V_G}{R_{AG}}$ will flow from A to G , (V_A and V_G are the potentials at A and G). If I_A and I_G be the currents flowing towards A and G respectively then $-I_A = I_G = g_{AG}(V_A - V_G)$, where $g_{AG} = 1/R_{AG}$. When all the conductors connected to A are considered, it can be put as,

$$\sum_A g_{AG}(V_A - V_G) + I_{AO} = 0 \quad \dots (1)$$

I_{AO} denoting the current supplied to A from outside. Then the heat generated in AG is $g_{AG}(V_A - V_G)^2$ and the total heat generated in the network can be written as,

$$2H = \sum_m g_{AG}(V_A - V_G)^2 \quad \dots (2)$$

\sum_m meaning the summation extending to every conductor. Also the rate of expenditure of energy is measured by $I_{AO}(V_A - V_O)$, if the current I_{AO} is supplied to A from an outside source at the datum potential V_O . Then the total expenditure of energy is given by,

$$\sum_n \{I_{AO}(V_A - V_O)\} = -E \quad \dots (3)$$

\sum_n denoting the summation extending to every nodal point. Hence the equation (1) is typical of the conditions for a minimum value of the quantity,

$$Q = H + E = \frac{1}{2} \sum_m \{g_{AG}(V_A - V_G)^2\} + \sum_n \{I_{AO}(V_A - V_O)\} \quad \dots (4)$$

because it is equivalent to,

$$-\frac{\partial Q}{\partial V_A} = -\frac{\partial}{\partial V_A} (H + E) = 0$$

Due to the presence of the source of E.M.F. (generators) the problem has to be modified as indicated below and then can be solved easily by relaxation method using the above theorem. It can be modified by assuming that the whole E.M.F. of each source is utilized to pass currents to earth through its own resistance

and the datum distribution of known currents to enter and to leave the network at nodal points is obtained. Then the effects of neutralising currents are simply to be calculated and superposed at those points.

Considering only the source of E.M.F. ' E_1 ' let A and F be supposed to be joined by a wire of zero resistance as shown by dotted line. Then the current passing through that source from A to F would return by that wire and hence in the datum distribution a current of $\frac{E_1}{R_{G_1}}$ enters the system at A and leaves at F , R_{G_1} being the internal resistance of the source (generator). Next the current distribution is to be calculated and superposed which will result when the neutralising currents $+\frac{E_1}{R_{G_1}}$ and $-\frac{E_1}{R_{G_1}}$ are supplied at F and A after the source of E.M.F. is removed.

Considering both the generators and all the branches of the network shown in Fig. 2, the expression for Q and the residuals can be written with the help of equation (4) as given below :

$$2Q = \frac{(V_G - V_A)^2}{R_{AG}} + \frac{(V_G - V_F)^2}{R_{FB'G}} + \frac{(V_A - V_F)^2}{R_{G_1}} + 2 \frac{E_1}{R_{G_1}} \{V_O - V_F - (V_O - V_A)\} \\ + \frac{(V_G - V_F)^2}{R_{FC'G}} + \frac{(V_G - V_D)^2}{R_{DG}} + \frac{(V_F - V_D)^2}{R_{G_2}} + 2 \frac{E_2}{R_{G_2}} \{V_O - V_D - (V_O - V_F)\} \dots \quad (5)$$

Hence,

$$\left. \begin{aligned} -\frac{\partial Q}{\partial V_G} &= -\frac{V_G - V_A}{R_{AG}} - \frac{V_G - V_F}{R_{FB'G}} - \frac{V_G - V_F}{R_{FC'G}} - \frac{V_G - V_D}{R_{DG}} = 0 = F_G \\ -\frac{\partial Q}{\partial V_A} &= \frac{V_G - V_A}{R_{AG}} - \frac{V_A - V_F}{R_{G_1}} - \frac{E_1}{R_{G_1}} = -\frac{E_1}{R_{G_1}} = F_A \\ -\frac{\partial Q}{\partial V_F} &= \frac{V_G - V_F}{R_{FB'G}} + \frac{V_A - V_F}{R_{G_1}} + \frac{V_G - V_F}{R_{FC'G}} - \frac{V_F - V_D}{R_{G_2}} = 0 = F_F \\ -\frac{\partial Q}{\partial V_D} &= \frac{V_G - V_D}{R_{DG}} + \frac{V_F - V_D}{R_{G_2}} + \frac{E_2}{R_{G_2}} = \frac{E_2}{R_{G_2}} = F_D \end{aligned} \right\} \quad (6)$$

If these residuals F_G , F_A , F_F and F_D obtained initially are liquidated, the potentials at the points A , G , F and D are found out and the corresponding currents can be calculated from them knowing the required resistances of different branches. In order to liquidate them the basic unit, group operation and the relaxation tables (Table I and II) are prepared (Allen, 1954; Dutta, 1966). All these procedures are elaborately shown in the following illustration.

The following example worked out by Christie (1952) using different method is taken for illustration.

In the D.C. Three Wire Transmission System shown in Fig. 1, the E.M.F. of the generators are $E_1 = E_2 = 110$ volts, the internal resistances of the generators are $R_{G_1} = R_{G_2} = 0.2$ ohm, the resistance of the neutral wire is $R_{FG} = 0.4$ ohm, the outer line resistances are $R_{AB} = R_{DC} = 0.1$ ohm, the load resistances are $R_{BG} = 8.0$ ohms and $R_{GC} = 10.0$ ohms. The currents flowing in the two outer and the neutral wires are to be found out.

From the supplied data, the values of the resistances of different branches of the network shown in Fig. 2, are $R_{AG} = R_{AB} + R_{BG} = 8.1$ ohms, $R_{DG} = R_{DC} + R_{CG} = 10.1$ ohms, $R_{FC'G} = R_{FG} = 2 \times R_{FG} = 0.8$ ohm.

With the substitution of the numerical values in the relation (5) and (6), it can be written as follows :

$$2Q = \frac{(V_G - V_A)^2}{8.1} + \frac{(V_G - V_F)^2}{0.8} + \frac{(V_A - V_F)^2}{0.2} + 2 \times 550(V_A - V_F) + \frac{(V_G - V_F)^2}{0.8} \\ + \frac{(V_G - V_D)^2}{10.1} + \frac{(V_F - V_D)^2}{0.2} + 2 \times 550(V_F - V_D) \\ \text{or } 2Q = \frac{(V_G - V_A)^2}{8.1} + \frac{(V_G - V_F)^2}{0.4} + \frac{(V_A - V_F)^2}{0.2} + \frac{(V_G - V_D)^2}{10.1} + \frac{(V_F - V_D)^2}{0.2} \\ + 2 \times 550(V_A - V_F) + 2 \times 500(V_F - V_D) \quad \dots (5a)$$

$$\left. \begin{aligned} -\frac{\partial Q}{\partial V_G} &= -\frac{V_G - V_A}{8.1} - \frac{V_G - V_F}{0.4} - \frac{V_G - V_D}{10.1} = 0 = F_G \\ -\frac{\partial Q}{\partial V_A} &= \frac{V_G - V_A}{8.1} - \frac{V_A - V_F}{0.2} - 550 = -550 = F_A \\ -\frac{\partial Q}{\partial V_F} &= \frac{V_G - V_F}{0.4} + \frac{V_A - V_F}{0.2} - \frac{V_F - V_D}{0.2} = 0 = F_F \\ -\frac{\partial Q}{\partial V_D} &= \frac{V_G - V_D}{10.1} + \frac{V_F - V_D}{0.2} + 550 = 550 = F_D \end{aligned} \right\} \quad \dots (6a)$$

On liquidating the residuals the potentials at different nodal points are obtained from the relaxation table. Then the required currents can be easily calculated from those values of potentials and the resistances of the outer and neutral wires as given below :

$$\begin{aligned} V_{GA} &= 106.4280 \text{ volts; where } V_{GA} \text{ is the potential of } G \text{ with respect to } A, \\ V_{DG} &= 108.7914 \text{ " ; } V_{DG} \text{ } D \text{ } G, \\ V_{FG} &= 0.9432 \text{ " ; } V_{FG} \text{ } F \text{ } G, \\ I_{GA} &= 13.13 \text{ amps; where } I_{GA} \text{ is the current flowing in the wire joining } G \text{ and } A, \\ I_{DG} &= 10.78 \text{ " ; } I_{DG} \text{ } D \text{ } G, \\ I_{FG} &= 2.46 \text{ } I_{FG} \text{ } G, \end{aligned}$$

TABLE I
Operational Table

Operation number	δV_G	δV_A	δV_F	δV_D	δF_G	δF_A	δF_F	δF_D
<i>Unit Operation</i> (1)	1	-	-	-	-2.7224	0.1234	2.5	0.099
(2)	-	1	-	-	0.1234	-5.1234	5.0	0
(3)	-	-	1	-	2.5	5.0	-12.5	5.0
(4)	-	-	-	1	0.099	0	5.0	-5.099
<i>Group Operation</i> (5) [(2) \times -1 + (3) \times -1.0247 + (4) \times -1.5617]	-	-1	-1.0247	-1.5617	-2.8397	0	0	2.8397

TABLE II
Relaxation Table

	δV_G	δV_A	δV_F	δV_D	F_G	F_A	F_F	F_D
	$V_G = V_A = V_F = V_D = 0$				0	-550	0	550
(a) [(3) \times 110]	-	-	110	-	275	0	-1375	1100
(b) [(4) \times 275]	-	-	-	275	302.225	0	0	-302.225
(c) [(5) \times 106.428]	-	-106.4280	-109.0568	-166.2086	0	0	0	0
0	0	-106.4280	0.9432	108.7914	0	0	0	0

The values of the currents in the wires GA , DG and FG thus found by relaxation method are compared with those calculated by conventional method of network analysis and they are found to be in good agreement as shown in the (Table III) below :

TABLE III
Comparison of values

Unknown quantities	Values calculated by	
	Relaxation Method	Conventional Method
I_{GA}	13.13 amps	13.30 amps
I_{DG}	10.78 amps	10.90 amps
I_{FG}	2.46 amps	2.40 amps

DISCUSSION

This method is seen to be a convenient one for having the values of all the unknown quantities obtained simultaneously, such as the potentials at the nodal points in the problem. With the increase of the number of branches of the network in the electrical problems, the conventional methods become laborious whereas this method can yield much quicker solution preferably with little practice of relaxation technique. In this method the internal resistances of the generators or the resistances of the paths AF and FD are to be known in order that the current in the datum distribution may be calculated.

ACKNOWLEDGMENT

The author is highly indebted to Prof. A. K. Sengupta, D.Sc., A.M.I.E.E. (London), Head of the Department of Applied Physics, Calcutta University, for his help and guidance throughout the progress of this work.

REFERENCES

- Allen, D. N. de G., 1954, *Relaxation Methods*, (McGraw-Hill Book Co., Inc., New York Chapter 1 and 2,
 Black, A. N. and Southwell, R. V., 1938, *Proc. Roy. Soc. A* **164**, 447.
 Christie, C. V., 1952, *Electrical Engineering*, McGraw-Hill Book Co. Inc. New York 91.
 Dutta, S. N., 1966, *Indian J. Phys.* **40**, 7, 163.
 Southwell, R. V., 1951, *Relaxation Methods in Engineering Science*, Oxford University Press, London Chapter VI..
 Starr, A. T., 1946, *Generation, Transmission and Utilisation of Electrical Power*, Sir Issac Pitman & Sons Ltd., London 33.

EFFECT OF HIGHER ORDER PARTIAL WAVE PHASE-SHIFTS IN ELASTIC ELECTRON SCATTERING BY HELIUM ATOM

S. N. BANERJEE AND N. C. Sil

DEPARTMENT OF THEORETICAL PHYSICS,

INDIAN ASSOCIATION FOR THE CULTIVATION OF SCIENCE,

JADAVPUR, CALCUTTA-32.

(Received September 29, 1966)

ABSTRACT. In elastic e^- -He scattering in the energy range of 13.6 ev to 54.4 ev we have computed in the Born approximation the higher order phase-shifts ($l \geq 3$); making use of lower order phase-shifts (i.e. for $l=0, 1, 2$) from the calculation of LaBahn and Callaway (1966), we find that the inclusion of the higher order phase-shifts considerably improves the value of the total and differential cross-sections in bringing them to better agreement with the experimental results.

INTRODUCTION

Recently LaBahn and Callaway (1966) have investigated the elastic scattering of electrons by helium atom in the energy range of 0 to 50 ev. Taking into account both the exchange and polarisation effects, they have calculated the S , P and D -wave phase-shifts in three different approximations viz. i) adiabatic-exchange (ii) Dynamic-exchange with all components and (iii) dynamic-exchange with only the dipole component. They have not, however, considered the phase-shifts for $l \geq 3$, which are expected to be of considerable importance specially at higher energies.

For scattering in the energy of 13.6 ev to 54.4 ev, we have computed in the Born approximation those higher order phase-shifts which contribute appreciably to the scattering cross-sections. For such energies and for such higher order phase-shifts, it will be enough to take only the asymptotic part of the potential which in effect will be a term of the form $-\alpha/r^4$ coming from the polarisation potential, the screened coulomb potential and other short-range potentials will have no appreciable contribution to it. As the exchange effect decreases with increase in energy and increase in order of phase-shifts, it will be consistent to neglect exchange terms. The fact that the higher order phase-shifts have small values gives us the reasonable justification for using the Born's approximation in calculating the phase-shifts.

THEORY

The Born approximation for the phase-shift is given by

$$\eta_l = -\frac{2mk_0}{\hbar^2} \int_0^\infty V(r)[j_l(r)]^2 r^2 dr$$

where
$$j_l(r) = \left(\frac{\pi}{2k_0 r}\right)^{\frac{1}{2}} \cdot J_{l+\frac{1}{2}}(k_0 r),$$

and the symbols have their usual significances, $V(r)$ is the total potential.

With potential $V(r) = -(\alpha/r^4)$, we may write (cf. Mott and Massey, 1965)

$$\begin{aligned} \eta_l &= -\frac{4\pi^2 m \alpha}{\hbar^2} \int_0^\infty \{J_{l+\frac{1}{2}}(kr)\}^2 \cdot r^{-3} dr \\ &= -\frac{4\pi^2 m \alpha}{\hbar^2} \cdot \left(\frac{k_0}{2}\right)^{4-1} \cdot \frac{\Gamma(3) \cdot \Gamma(l-2+3/2)}{[\Gamma(2)]^2 \cdot \Gamma(l+2+\frac{1}{2})} \end{aligned}$$

the constant α is the polarisability of the He atom and its value is $1.376 a_0^3$. The differential cross section $I(\theta)$ is given by

$$I(\theta) = \frac{1}{k_0^2} |\Sigma(2l+1)e^{i\eta_l} \cdot \sin \eta_l P_l(\cos \theta)|^2$$

and total cross section
$$Q = \frac{4\pi}{k_0^2} \Sigma(2l+1) \sin^2 \eta_l.$$

RESULTS AND DISCUSSIONS

The phase-shifts in radions for $l = 3, 4, 5$ and 6 waves are given in Table I for five different energies.

TABLE II

Energy in ev	$l=3$	$l=4$	$l=5$	$l=6$
13.6	.0374	.0124	.0067	—
21.25	.04285	.019493	.010496	.00629
30.60	.066834	.030379	.016358	.00981
41.65	.08439	.0383	.02065	.01239
54.40	.109786	.049903	.02687	.01622

LaBahn and Callaway (1966) have calculated S, P, D wave phase shifts in three different types of approximations, of which the dynamic exchange approxi-

mation with only the dipole component gives the best agreement with experiment. Hence we have calculated the total and differential cross sections by using the S , P , D wave phase-shifts of Labahn and Callaway (1966) dynamic exchange approximation with dipole component only and the higher order phase shifts computed here in the Born approximation.

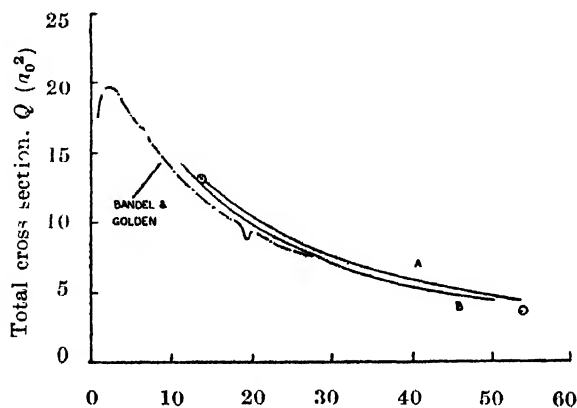


Fig. 1. Energy (ev). The total cross section Q is plotted against energy. Curve A—Present Calculation; Curve B—Calculation by LaBahn and Callaway (1966); —experimental results of Nermund (1930); dashed and dotted curve is that of Bandel and Golden (1965).

In fig. 1, we have plotted our calculated values of the total cross section Q against energy for the dynamic exchange case with the dipole component only.

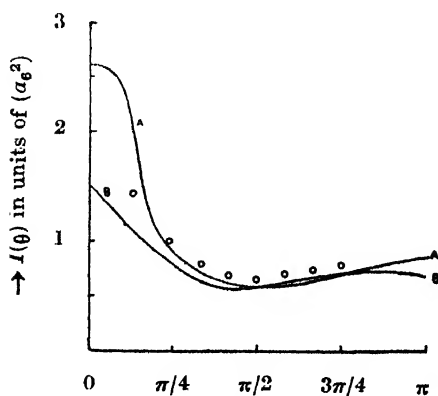


Fig. 2. $\rightarrow \theta$.

Differential cross section $I(\theta)$ is plotted against θ for 21.25 eV energy. Curve A—Present Calculation; Curve B—Calculation using only S , P , D wave phase-shifts of LaBahn and Callaway; \bigcirc —experimental results at 20 eV.

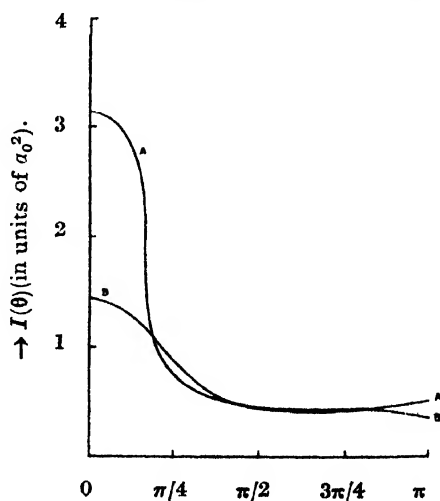


Fig. 3. $\rightarrow \theta$.

Differential cross section $I(\theta)$ is plotted against θ for 30.6 eV energy. Curve A—Present Calculation; Curve B—Calculation using the S , P , D wave phase-shifts of LaBahn and Callaway.

The theoretical results of LaBahn and Callaway (1966) in the dynamic exchange approximation with dipole component only and the experimental values of Bandel and Golden (1965) and Normand (1930) are shown for comparison. To get accurately Normand's experimental data of elastic scattering excitation cross section data of Gabriel and Heddle (1960) are added to those of ionisation cross section of Smith (1930) and the sum is subtracted from the total cross section data of Normand (1930), after increasing its value by 25% according to the suggestion of Gabriel and Heddle (1960). The discrepancy still left may be partially due to over simplification of the dynamics of the scattering electron in describing the distortion interaction and due to the influence of inelastic processes on the elastic scattering. In figs. 2 and 3, we have shown calculated differential cross section $I(\theta)$ for 21.25 ev and 30.6 ev electron energies respectively against scattering angles θ together with the available experimental results. These calculations have been done only for the dynamic exchange case in dipole approximation.

From the above figures, we see that the tendency of higher order phase-shifts is to give a sharp increase in the differential cross section for forward scattering angles. It should be mentioned that we have neglected exchange in the energy range of 13.6 ev to 54.4 ev in our computation of the phase shifts. This is justified because in the energy range concerned, influence of exchange decreases particularly for higher order partial waves.

ACKNOWLEDGMENT

The authors are thankful to Prof. D. Basu for his kind interest and valuable discussions throughout the progress of the work.

REFERENCES

- Bandel, H. W., and Golden, D. E., 1965, *Phys. Rev.* **138**, A14.
Gabriel, A. H. and Heddle, D.W.O., 1960, *Proc. Roy. Soc.*, **A258**, 124.
LaBahn, R. W. and Callaway, J., 1966, *Phys. Rev.*, **147**, 28.
Mott, N. F. and Massey, H. S. W., 1965, *The Theory of Atomic Collisions*, Oxford at the Clarendon Press, Third Edition.
Normand, C. E., 1930, *Phys. Rev.* **35**, 1217.
Smith, P. T., 1930, *Phys. Rev.*, **36**, 1293.

MAGNETIC SUSCEPTIBILITY OF SOME U^{+4} COMPOUNDS AT LOW TEMPERATURES

S. K. DUTTA ROY, B. GHOSH AND B. SAHOO*

DEPARTMENT OF PHYSICS, INDIAN INSTITUTE OF TECHNOLOGY,
KHARAGPUR

(Received September 29, 1966 ; Resubmitted January 6, 1967 and February 2, 1967)

ABSTRACT. Magnetic susceptibility of three U^{+4} compounds have been examined over a temperature range of 400°K to 100°K. Appreciable variation of magnetic moment for U^{+4} ion from salt to salt and also with temperature has been observed for all the compounds. A theory of magnetic susceptibility based on point charge model has been worked out for U^{+4} ion in crystalline state. The calculation yields a nonmagnetic singlet as the ground state and a doublet close to it. The experimental results are satisfactorily explained.

INTRODUCTION

The magnetic properties of the actinide group of elements have received rather limited attention. In the past both the experimental and theoretical workers focussed their interest on iron and rare earth group of salts and the fine details of their magnetic properties are now well understood. In the actinides the basic confusion arose with the ground state configuration of the magnetic electrons. Dawson (1952) reviewed the magnetic susceptibility data of some of the actinide complexes and concluded that for ions with one or two electrons the $6d$ rather than $5f$ shell electrons are the important magnetic ones. His suggestion was based on the fact that many of the ions of the actinide group of compounds indicate spin only moments similar to those found in the iron group of compounds. However, Hutchison and Candela (1957) indicated that the magnetic electrons in the $5f$ shell in crystalline environment can also give rise to effective spin only value of magnetic moment. This was also confirmed from the optical absorption studies which showed similarity in the absorption spectrum with the rare earth salts in which the magnetic electrons are in the $4f$ shell. Also an analysis of U^{+4} ion spectra (Satten, *et al.* 1960) reveals that the electronic energy levels are widely separated, indicating that the crystalline Stark splitting in the U^{+4} salts is large compared to the rare earth salts.

Dawson (1952), Hutchison and Candela (1957) observed a small temperature independent susceptibility for chloride complexes and a large temperature dependent susceptibility for fluoride complexes of uranium. The results were interpreted taking a six coordinated cubic field and an eight coordinated cubic field in chloride and fluoride complexes respectively. Six coordinated cubic field

*Department of Applied Chemistry, Indian Institute of Technology, Kharagpur.

acting on U⁺ ions splits the ground state $5f^2\ ^3H_4$ into four distinct levels $\Gamma_1, \Gamma_4, \Gamma_3, \Gamma_5$ (Bethe's notation, 1929) in which Γ_1 , a nonmagnetic singlet lies lowest. The next higher state Γ_4 is considerably removed from Γ_1 giving a temperature independent paramagnetic susceptibility. If the crystal field is of eight coordinated cubic symmetry then a degenerate state Γ_5 is lowest, and Γ_3, Γ_4 and Γ_1 are considerably removed from the ground level Γ_5 . The degenerate ground level contributes a temperature dependent paramagnetism and the quantitative expression is similar to a spin only value with effective spin $S' = 1$. But this simple theory does not predict a Curie-Weiss law dependence of susceptibility in UF_4 specimen observed by Leask, Osborne and Wolf (1961). Moreover, observed magnitude of the high frequency paramagnetism in UF_4 specimen has also not been confirmed by the theory. Therefore there is a discrepancy between the experimental result and the theoretical understanding of the origin of magnetism in UF_4 complexes. The present work is an extension of the earlier work of Hutchison and Candela (1957). The object has been to investigate the nature and symmetry of the crystalline field and their influence on magnetic properties of UF_4 complexes.

PREPARATION AND STRUCTURAL DATA

The complexes were prepared by photochemical reduction of uranyl ion in the presence of fluoride ion and also ammonia, hydroxylamine and hydrazine respectively, (chemicals used were of E. Merck quality). On chemical analysis they were found to possess the formula : (1) Ammonium uranium fluoride $UF_4NH_4F.H_2O$ (2) Hydrazine uranium fluoride $UF_4N_2H_4.HF(3)$, Hydroxylamine uranium fluoride $UF_4NH_2OH.HF$. They were all emerald green in colour and fine crystalline in form and insoluble in water. The coordination in the three double salts are the same as in UF_4 (Sahoo *et al.* 1961).

The x-ray crystallographic information is available for UF_4 . Zachariasen (1949) has shown that the space group is C_{2h}^6 . The compound is monoclinic with 12 stoichiometric molecules per unit cell. The choice of axis corresponds to a body centered translational group. The unit cell dimensions referring to a base centered translational group and space group setting $c2/c$ are

$$a_1 = 12.79 \pm 0.06$$

$$a_2 = 10.72 \pm 0.05$$

$$a_3 = 8.39 \pm 0.05$$

and $\alpha_2 = 126^\circ 10' \pm 30'$

The positions of uranium in unit cell are $4u_1$ in $\mp(0, u, 1/4)$ with $u = 0.20$ and $8u_{II}$ in $\pm(x, y, z), (x, \bar{y}, z+1/2)$ with $x = 0.208, y = 0.437$ and $z = 0.17$. The fluorine positions are unknown.

EXPERIMENTAL METHOD

The susceptibility balance with an electronic detection system and a pair of compensating coils for balancing the magnetic force was described by Subrahmaniam (1966) in an earlier communication. The sample capsule was suspended from one arm of the magnetic balance by means of a tungsten fibre (60 S.W.G.) and its vertical position was adjusted to within ± 0.05 mm. with the aid of the electronic detection system. The sample capsule was made of Pyrex glass. The capacity of the capsule was 1/8 inch in diameter and 3/16 inch long with external dimension of 1/4 inch in diameter and 9/32 inch in length. The diamagnetic susceptibility ($\sim 10^{-7}$) of Pyrex glass capsule at room temperature showed a reduction by 10% at 80°K. The capsule was annealed at 700°K for twenty-four hours. Even then the variation was observed (3%), hence this was considered as a correction to each point in temperature variation run.

The molar susceptibility of each compound was calculated from the expression,

$$\chi_M = \chi_{M(s)} \left[\frac{M}{M_S} \cdot \frac{\Delta I}{\Delta I_S} \cdot \frac{W_S}{W} \right] \quad \dots (1)$$

and that of the U^{+4} ion in each compound by

$$\chi_M(U^{+4}) = \chi_M - \sum_i \chi_M(i)$$

where χ_M is the molar susceptibility of uranium compound and $\chi_{M(s)}$ is the molar susceptibility of the powdered $KCr(SO_4)_2 \cdot 12H_2O$ used as standard. $\sum \chi_M(i)$ is the sum of the molar diamagnetic susceptibilities of the diamagnetic constituents of the compound including diamagnetic contribution for U^{+4} (Selwood, 1956), M is the molecular weight of the uranium compound and M_S is the molecular weight of the standard $KCr(SO_4)_2 \cdot 12H_2O$, ΔI is the increment of balance compensating current for the uranium compound corrected for the capsule increment, ΔI_s is the compensating current increment for the standard sample at the standardisation temperature and at the same field, W_s is the weight of the standard sample and W is the weight of the compound. As a check of the precision of the susceptibility measurement, data on ferric alum were obtained at several temperatures down to 80°K. The deviations from Onnes and Oosterhis' values of molar susceptibility were only 0.2% at 300°K and 0.5% at 80°K.

EXPERIMENTAL RESULTS

Susceptibility measurements were made at ten different temperatures of two independent preparations of ammonium uranium fluoride, hydrazine uranium fluoride and hydroxylamine uranium fluoride. The measurement on each preparation at a given temperature represents an average of at least three determinations differing by not more than 0.1%. The data on different independent preparations have coincided too closely to be distinguished.

The results are presented in table I and the curves are drawn in Fig. 1, where the square of the effective moment

$$p_e^2 = 8.00\chi_M T. \quad \dots (2)$$

is plotted against absolute temperature T .

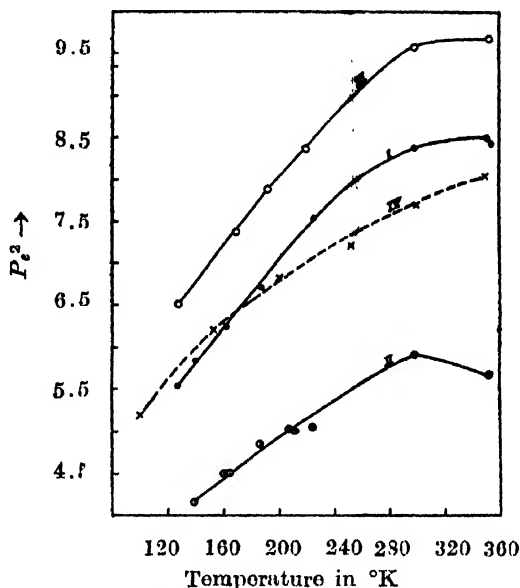


Fig. 1. Experimental curve
I. Hydrazine uranium fluoride.
II. Ammonium uranium fluoride.
III. Hydroxylamine uranium fluoride.
IV. Uf_4 data of Lensk, Osborne and Wolf. (1961)

TABLE I
Temperature variation of susceptibility of U^{+4} complexes

Hydrazine uranium fluoride mass of the sample = 0.0872 gm.			Ammonium uranium fluoride mass of the sample = 0.0680 gm.			Hydroxylamine uranium fluoride mass of the sample = 0.1952 gm.		
$T^{\circ}K$	$\chi_M(U^{+4}) \times 10^6$	p_e^2	$T^{\circ}K$	$\chi(U^{+4}) \times 10^6$	p_e^2	$T^{\circ}K$	$\chi_M(U^{+4}) \times 10^6$	p_e^2
353.0	2988	8.426	353.0	2003	5.652	352.5	3438.0	9.690
351.0	3030	8.506	299.0	2488	5.947	298.0	4029.1	5.594
						220.0	4769.1	8.387
299.0	3523	8.418	224.0	2813	5.037	218.0	4809.1	8.379
227.0	4155	7.491	213.0	2899	4.938	191.0	5161.1	7.879
223.0	4203	7.539	207.0	3030	5.013	169.0	5473.1	7.394
186.0	4506	6.701	186.0	3256	4.842	127.0	6412.1	6.510
162.0	4822	6.246	165.0	3409	4.495			
139.0	5246	5.829	160.0	3526	4.509			
127.0	5459	5.543	139.0	3739	4.155			

From the Table I it is observed that for all the three salts magnetic moment corresponds to a spin only value ($p_{spin}^2 = 8.00$) at room temperature. At low temperature appreciable departure from Curie law is observed. This departure varies from salt to salt. The experimental results show temperature dependence of the type $p_e^2 = 8.00 (AT+B+C/T)$ where A , B and C are constants, representing high frequency, Curie and Weiss term respectively. Values of A , B and C giving the best fit are shown in Table II. Table II shows that there is an appreciable

TABLE II

Sample	A	B	C
U F ₄ N ₂ H ₄ HF	10.21×10^{-4}	0.8833	-40.08
U F ₄ NH ₂ OH HF	9.250×10^{-4}	1.093	-49.35
U F ₄ NH ₄ F H ₂ O	3.339×10^{-4}	0.7099	-32.42
*U F ₄	6.625×10^{-4}	0.8996	-29.985

*(Calculated from :eask,
M.J.M. Darwell, W. (1961)
(data).

high frequency contribution as well as a somewhat large Weiss term in all the salts. The high frequency contribution as well as the Weiss term varies from salt to salt. The Curie term also changes from salt to salt.

THEORY

The electronic configuration of the two odd electrons in U^{+4} ion is $5f^2$ and the Russell-Saunders coupling is large compared to crystal field effect. The spin-orbit interaction gives ground state of U^{+4} ion as $3H_4$ with an excited state $3H_5$, considerably removed from the ground state ($\sim 5000 \text{ cm}^{-1}$). The symmetry of the crystal field of U^{+4} ion is not known precisely. However, Burbank (1951) has estimated theoretically the $F-F$ and $U-F$ spacing. From the estimated structure based on chemical and packing considerations it seems reasonable that the crystal field acting on U^{+4} ion is made up of two parts :

a) a dominant part of cubic symmetry due to a regular negative charges to which fluorine atoms approximate and (b) terms of lower symmetry on account of the displacement of fluorine atoms from regular cubic position surrounding each uranium ion. The total crystal field potential acting on the central U^{+4} ion is given by,

$$V = \sum_i V(x_i, y_i, z_i) = \left(\frac{G}{20} + \frac{I_1}{4} \right) \{ 35J_z^4 - 30J(J+1)J_z^2 + 25J_z^2 - 6J(J+1) + 3J^2(J+1)^2 \} + H_1 \{ 3J_z^2 - J(J+1) \} + \left(\frac{G}{8} - \frac{7}{8}I_1 \right) (J_+^4 + J_-^4) \dots \quad (3)$$

where the term containing G represents the part of the field with cubic symmetry and those containing H_1 and I_1 have tetragonal symmetry. Here we have neglected the sixth order cubic harmonic to simplify the calculation though this may have some contribution to the energy of the final levels. The final eigenstates and corresponding values are given by,

Wave functions	Energy
$\phi_6 = r 4> + s 0> + r -4>$	E_6
$\phi_5 = p -1> + q 3>$	E_5
$\phi_5' = p 1> + q -3>$	
$\phi_4 = \frac{1}{\sqrt{2}} 4> - \frac{1}{\sqrt{2}} -4>$	E_4
$\phi_3 = r 4> - s 0> + r -4>$	E_3
$\phi_2 = \frac{1}{\sqrt{2}} 2> + \frac{1}{\sqrt{2}} -2>$	E_2
$\phi_1 = p 3> - q -1>$	E_1
$\phi_1' = p -3> - q 1>$	
$\phi_0 = \frac{1}{\sqrt{2}} 2> - \frac{1}{\sqrt{2}} -2>$	E_0

where,

$$E_0 = -78G + 150I_1 - 8H_1$$

$$E_1 = \frac{1}{2}[(-36G - 180I_1 - 10H_1) - E_+]$$

$$E_2 = 12G - 480I_1 - 8H_1$$

$$E_3 = \frac{1}{2}[(96G + 480I_1 + 8H_1) - E_-]$$

$$E_4 = 42G + 210I_1 + 28H_1$$

$$E_5 = \frac{1}{2}[(-36G - 180I_1 - 10H_1) + E_+]$$

$$E_6 = \frac{1}{2}[(96G + 480I_1 + 8H_1) + E_-]$$

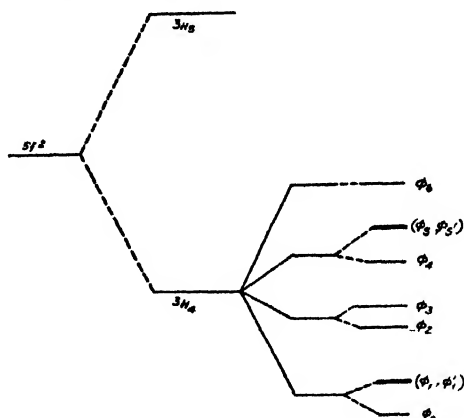
$$p = \frac{q(15\sqrt{7}G - 105\sqrt{7}I_1)}{E_1 - E_0} \quad \text{and} \quad p^2 + q^2 = 1$$

$$r = \frac{s(3\sqrt{70}G - 21\sqrt{70}I_1)}{E_3 - E_4} \quad \text{and} \quad 2r^2 + s^2 = 1$$

$$E_+ = \{(-90G - 450I_1 + 24H_1)^2 + 4(15\sqrt{7}G - 105\sqrt{7}I_1)^2\}^{\frac{1}{2}}$$

$$E_- = \{(-12G - 60I_1 + 48H_1)^2 + 8(3\sqrt{70}G - 21\sqrt{70}I_1)^2\}^{\frac{1}{2}}$$

The energy level diagram (Fig. 2) shows that the four cubic levels are split up into seven components, each triplet is breaking up into a singlet and a degenerate doublet. The cubic field leaves a degenerate triplet (ϕ_0, ϕ_1, ϕ_1') as the ground state.



Free ion + spin orbit coupling + cubic field + tetragonal field.

Fig. 2. Energy level diagram for U^{+4} ion in a tetrahedral coordination.

The tetragonal field splitting gives rise to singlet lowest (ϕ_0) and the doublet (ϕ_1, ϕ_1') is close to this ground state singlet. The other alternative of the doublet lying lowest with singlet above it is definitely ruled out because the $p_e^2 - T$ curve slopes down rapidly below room temperature (Fig. 1). p_e^2 values tend towards zero except for high frequency contribution which is an indication that ϕ_0 is lowest.

THE MAGNETIC SUSCEPTIBILITY

The first order Zeeman terms is obtained by finding

$$\langle \phi_i | H_m | \phi_j \rangle \text{ where } i, j = 0, 1, 1'$$

when

$$i = j \quad H_m = H_0 + \frac{4}{5} \beta H_z M_z$$

and when

$$i \neq j \quad H_m = H_0 + \frac{4}{5} \beta H_k M_k \quad (k = x, y)$$

where H_0 is the unperturbed Hamiltonian and β is the Bohr magneton. The second order Zeeman energy terms can be obtained from above by solving a secular determinant for $\phi_0, (\phi, \phi_1')$ in the usual way.

The energy in powers of the field strength H is given by

$$W_i = W_i^{(0)} + W_i^{(1)}H + W_i^{(2)}H^2 + \dots$$

where the first term is the unperturbed energy, the second and third terms are the first order and second order Zeeman energy terms respectively. Calculating the effect of the magnetic perturbation upto the second order we get the paramagnetic

gramionic susceptibility K_i ($i = \parallel$ or \perp to the tetragonal axis) using the well known formula of vanVleck.

The mean gramionic susceptibility is given by

$$\bar{K} = \frac{1}{3} (K_{\parallel} + 2K_{\perp}).$$

$$= \frac{N\beta^2 B_1}{3} \left[\frac{2A_1^2}{KT} + \frac{16D^2}{\Delta} (e^{\Delta/KT} - 1) \right] + A. \quad \dots (4)$$

where $\Delta = E_1 - E_0$ and $B_1 = \frac{1}{2 + e^{\Delta/KT}}$

and

$$A = \frac{1}{3} \frac{N\beta^2}{2 + e^{\Delta/KT}} \left[\left\{ \frac{2 \left(\frac{16}{5} pq \right)^2}{E_5 - E_1} + \frac{4 \left(\frac{2\sqrt{8}pr}{5} + \frac{2\sqrt{20}qs}{5} \right)^2}{E_3 - E_1} \right. \right.$$

$$+ \left. \frac{4 \left(\frac{2\sqrt{7}q}{5} - \frac{2\sqrt{9}q}{5} \right)^2}{E_2 - E_1} + \frac{4 \left(\frac{16}{25} p^2 \right)}{E_4 - E_1} + \frac{4 \left(\frac{4\sqrt{2}pr}{5} - \frac{4\sqrt{5}qs}{5} \right)^2}{E_6 - E_1} \right\}$$

$$+ \left\{ \frac{2 \left(\frac{64}{5} \right)}{E_2 - E_0} + \frac{4 \left(\frac{2\sqrt{7}q}{5} - \frac{2\sqrt{9}p}{5} \right)^2}{E_5 - E_0} \right\} e^{\Delta/KT} \right]$$

where

$$A_1 = \left(\frac{12}{5} p^2 - \frac{4}{5} q^2 \right)$$

$$D = \left\{ \frac{1}{2} \left(\frac{2\sqrt{7}p}{5} + \frac{2\sqrt{9}q}{5} \right)^2 \right\}^{\frac{1}{2}}$$

A is the susceptibility from the high frequency contribution. The square of the effective magnetic moment can be calculated combining equation (2) and (4). The equation (4) reduces to Hutchison and Candelas' (1957) expression if the three states ϕ_0, ϕ_1, ϕ_1' are taken to be a single degenerate ground state Γ_6 . The variation of p, q with T obtained theoretically from equation (4) using the values A_1^2

$=4.00$, $D^2 = 1$ and $\Delta = 200 \text{ cm}^{-1}$ and $A = 80 \times 10^{-6}$ (p, q, r, s are taken from the cubic wave functions; in fact both A_1^2 and D^2 deviate from the above values if the magnitude of the above parameters are obtained from tetragonal wave functions) are shown in Fig. 3. The theoretical curve (Fig. 3) has been drawn with $\Delta = 200$

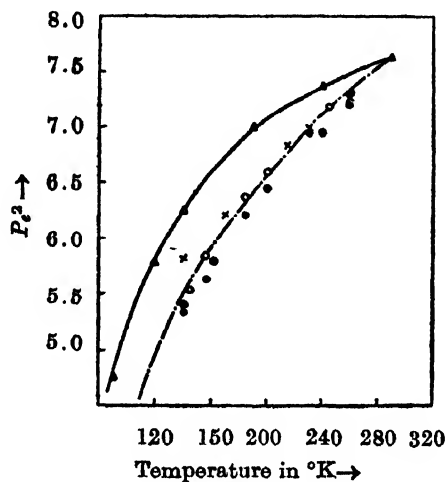


Fig. 3

————— Theoretical curve.
 - - - - - Experimental curve [room temperature value of
 all the four salts reduced to the theoretical one].

cm^{-1} as the experimental curves showed a bend near the room temperature suggesting this value of Δ . The experimental curves are redrawn in Fig. 3 reducing the room temperature values of all the three salts to the theoretical one. Points \odot , \times , \circ and \bullet given in Fig. 3 are corresponding to ammonium uranium fluoride, uranium fluoride, hydroxylamine uranium fluoride and hydrazine uranium fluoride. This procedure has been adopted because the temperature variation of p_e^2 is the same for all the three salts. The theoretical curve compares well with the temperature variation of p_e^2 for the three uranium salts (Fig. 3).

There is some divergence in the values of the Cuire constant for the three salts. It is possible that the cubic field is slightly different in them. Accurate parameter fitting can be done for the three salts; but in the absence of any magnetic anisotropy data we have not attempted such rigorous parameter fitting which in any case is not very meaningful, since the theory based on point charge model is too simple to justify a rigorous quantitative correspondence of the experimental results with the theory.

The optical absorption data of Satten, Young and Gruen (1960) refer to UCl_6 complexes which indicate that most of the excited levels lie between 5000 cm^{-1} to 29000 cm^{-1} . In all 18 pure electronic transitions are observed in the photographic region; four electronic levels are in the region 8325 cm^{-1} to 5000 cm^{-1} superimposed

with two vibronic levels. If we assign the first excited level as the most important level, the high frequency paramagnetism A is obtained to be 0.9×10^{-4} , which is one seventh of the experimentally observed value (Table II). In order to get the observed magnitude of the experimental high frequency term A at least the first excited level should be at about 1000 cm^{-1} . This difference is obviously due to the difference of coordination in chloride and fluorides as earlier indicated.

CALCULATION OF g VALUES

The values of g_{\parallel} and g_{\perp} (\parallel refers to magnetic field along Z direction which is the tetragonal axis and \perp refer to the magnetic field along the x or y direction \perp to the tetragonal axis) in terms of the admixtural coefficients are given by

$$g_{\parallel} = \frac{12}{5} p^2 - \frac{4}{5} q^2$$

$$g_{\perp} = 2 \left\{ \frac{1}{2} \left(\frac{2\sqrt{7}}{5} p + \frac{2\sqrt{9}}{5} q \right)^2 \right\}^{\frac{1}{2}}$$

The mean g value is very close to two. This compares well with resonance mean g observed at room temperature by Ghosh *et al* (1954) on powdered sample of UF_4 . g value arises from the doublet (ϕ_1, ϕ_1') states, therefore the intensity of the resonance line should drop with the lowering of temperature. Anisotropy is small and g_{\parallel} and g_{\perp} shows anisotropy if higher order admixing by the magnetic field is considered.

CONCLUSION

The most important feature of the present experimental result is that in UF_4 complexes a nonmagnetic singlet is lowest and at about 200 cm^{-1} a degenerate magnetic doublet contribute most of the susceptibility at high temperature. Such an energy spectrum evidently leads to a large temperature dependence of magnetic moment. The large high frequency paramagnetism arises from close lying levels between 1000 cm^{-1} to 5000 cm^{-1} . The g value is nearly isotropic at room temperature. The intensity of the resonance line is expected to diminish appreciably with the lowering of temperature. Up till now resonance measurements at low temperatures have not been reported.

REFERENCES

- Abragam, A. Pryce. M. H. L., 1951a, *Proc. Roy. Soc.* **A205**, 135.
 —————, 1951b, *Proc. Roy. Soc.* **A206**, 173.
 Bathe, H. A., 1929, *Ann. der. Phys.* **60**, 218.
 Burbank, R. D., 1951, *U.S.A.C.R.*, **AEC-D-3126**.
 Dawson, J. K., 1951, *Jour. Chem. Soc. (London)* **429**.

- Dawson, J. K., 1952, *Jour. Chem. Soc.* (London) 1185.
Ghosh, S. N., Gordy, W. and Hill, D. G., 1954, *Phys. Rev.* **96**, 32.
Hutchison, C. A., and Candela, G. A., 1957, *Jour. Chem. Phys.* **27**, 707.
Leask, M. J. M., Osborne, D. W. and Wolf, W. P., 1961, *Jour. Chem. Phys.* **34**, 209.
Sahoo, B. and Patnaik, D., 1961, *Curr. Sci.* **30**, 293.
Sutton, R. A., Young, D. and Gruen, D. M., 1960, *Jour. Chem. Phys.* **33**, 1140.
Subrahmaniam, A. V., 1966, *Indian J. Phys.*, **49**, 527.
Zachariasen, W. H., 1949, *Acta. Crys.* **2**, 390.

ELECTRON SCATTERING BY ATOMIC HYDROGEN IN OCHKUR APPROXIMATION

R. JHA*

DEPARTMENT OF THEORETICAL PHYSICS,
INDIAN ASSOCIATION FOR THE CULTIVATION OF SCIENCE,
JADAVPUR, CALCUTTA.

(Received October 5, 1966)

ABSTRACT. The elastic ($1s-1s$) and inelastic ($1s-2s$, $1s-2P$) scattering of electrons by atomic hydrogen have been investigated in ochkur approximation and the overall agreement with experiment obtained is better than the usual first Born approximation.

INTRODUCTION

The scattering of electron by hydrogen atom becomes complicated due to exchange and polarisation effects. The exchange effect is taken into account by properly antisymmetrising the wave function of the system of scattered electron and hydrogen atom. When the effect of exchange is small, the calculation is very easy in the B.O. approximation. But this yields, especially near threshold for excitation, spuriously large contribution to the total cross section on account of the lack of orthogonality between the initial and final states. To overcome this impasse, several modifications have been proposed. Thus, Bell and Moiseiwitsch (1963) applied their first order exchange approximation to \bar{e} -H scattering problem. Recently, Ochkur (1964) has made a modification in B-O approximation and have obtained satisfactory results in \bar{e} -He excitation and in ionisation processes. In our work we have applied the Ochkur approximation to the problems of elastic and inelastic ($1s-2s$, $1s-2P$) scattering of electrons by hydrogen atom.

THEORY

The first Born approximation in scattering amplitude (in a.u.) for the process of elastic scattering has the form

$$f(\theta) = -\frac{1}{2\pi} \iint e^{i\mathbf{q}\cdot\mathbf{r}_1} \psi_0(\mathbf{r}_2) \psi_0^*(\mathbf{r}_2) \left(\frac{1}{r_{12}} - \frac{1}{r_1} \right) d\mathbf{r}_1 d\mathbf{r}_2$$

where \mathbf{r}_1 and \mathbf{r}_2 are the co-ordinates of the scattered and bound electrons, and \mathbf{k}_0 and \mathbf{k} are the momentum vectors of the incident and scattered electron respectively and $|\mathbf{q}| = |\mathbf{k}_0 - \mathbf{k}| = 2k_0 \sin \theta/2$, θ being the scattering angle and $\psi_0(\mathbf{r}_2)$ is the ground state wave function of hydrogen atom.

* On leave from C. M. Chhleg, Darbhanga, Bihar University.

Similarly, the corresponding *B-O* approximation for the exchange scattering amplitude runs as

$$g(\theta) = -\frac{1}{2\pi} \iint e^{i(\mathbf{k}_0 \cdot \mathbf{r}_1 - \mathbf{k} \cdot \mathbf{r}_2)} \cdot \psi_0^*(\mathbf{r}_1) \left(\frac{1}{r_{12}} - \frac{1}{r_2} \right) \psi_0(\mathbf{r}_2) d\mathbf{r}_1 d\mathbf{r}_2$$

According to the suggestion of Ochkur, only the leading terms in powers of $1/k_0^2$ in $g(\theta)$ are to be retained in order to obtain better agreement with experimental results, consistent with the first order perturbation theory. Thus neglecting all higher order terms we get

$$g_{och}^{(\theta)} = \frac{q^2}{k_0^2} f_1(\theta)$$

where
$$f_1(\theta) = -\frac{1}{2\pi} \iint e^{i\mathbf{q} \cdot \mathbf{r}_1} \psi_0(\mathbf{r}_2) \psi_0^*(\mathbf{r}_2) \left(\frac{1}{r_{12}} \right) d\mathbf{r}_1 d\mathbf{r}_2$$

For excitation processes from ground state to n -th state, we get

$$f(\theta) = -\frac{1}{2\pi} \iint e^{i\mathbf{q} \cdot \mathbf{r}_1} \psi_n^*(\mathbf{r}_2) \left(\frac{1}{r_{12}} - \frac{1}{r_1} \right) \psi_0(\mathbf{r}_2) d\mathbf{r}_1 d\mathbf{r}_2$$

and
$$g_{och}^{(\theta)} = \frac{q^2}{k_0^2} f(\mathbf{k}_0, \mathbf{k}_n),$$

where
$$\mathbf{q} = \mathbf{k}_0 - \mathbf{k}_n$$

and other symbols have their usual meanings.

For elastic process, the differential cross section is given by

$$I(\theta) = \frac{1}{4} |f+g|^2 + \frac{3}{4} |f-g|^2$$

and for excitation processes,

$$I(\theta) = \frac{kn}{k_0} \left| \frac{1}{4} |f+g|^2 + \frac{3}{4} |f-g|^2 \right|$$

The total cross section
$$Q = 2\pi \int_0^\pi I(\theta) \sin \theta d\theta$$

For spinflip cross section in $1s-2s$ case, in which exchange effect is fundamental, we have $I(\theta) = \frac{kn}{k_0} |g|^2$ and this process provides a direct measure of the success of Ochkur approximation.

RESULTS AND DISCUSSIONS

In Fig. 1, calculated values of total cross section for the elastic scattering of electron by hydrogen is plotted against energy of the electron. Here we notice appreciable differences between the results of first Born approximation and

present calculations, particularly in the energy range of 13.6 ev to 60 ev, with further increase in energy our values tend towards those of first Born approximation results. For comparison we have shown also the experimental finding at 10 ev, which agrees more closely with the results of our present calculation than with the first Born approximation results.

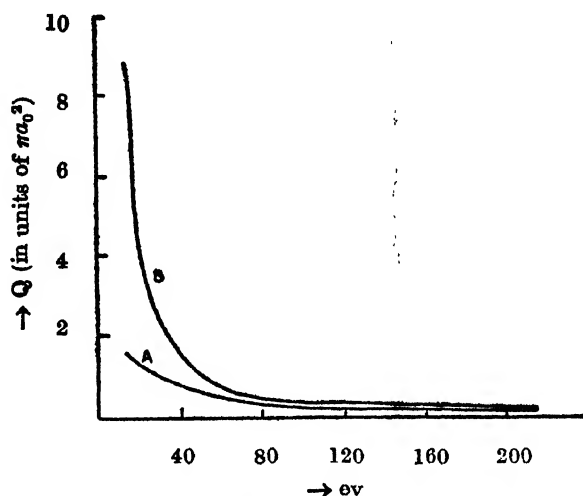


Fig. 1. Total elastic (1s—1s) cross section Q is plotted against energy. Curve B—present calculation; Curve A—Born results; O—experimental point.

In figs. 2 and 3 we have plotted 1s—2s total cross section and 1s—2s spin change cross section. In Fig. 2, the experimental points with error bars are from the measurements of Stebbings *et al.* (1960) and the full line curve is from the relative measurements of Lichten and Schulz (1959) fitted to the data of Stebbings *et al.* (1960). Fig. 2 shows that our results are lower than the first Born approximation results, in somewhat better agreement with experiment. In Fig. 3, our results

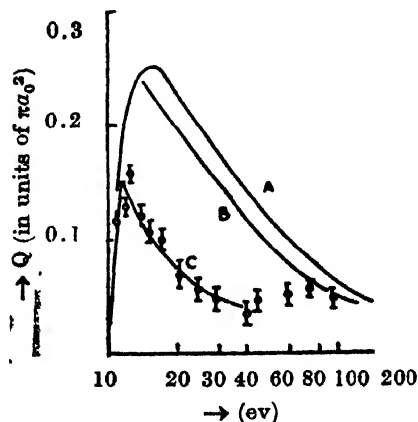


Fig. 2. Total inelastic 1s-2s cross section. Q is plotted against energy. Curve A—Born approximation; Curve B—present calculation; C—experimental points.

agree better with experimental results agreement than the close-coupling calculations of Burke *et al.*, (1963) from 13.6 ev to 35 ev. But in Fig. 2 and 3, there still remains a large discrepancy between experimental and theoretical results. In Fig. 4, where we have shown our calculated $1S-2P$ cross section together with

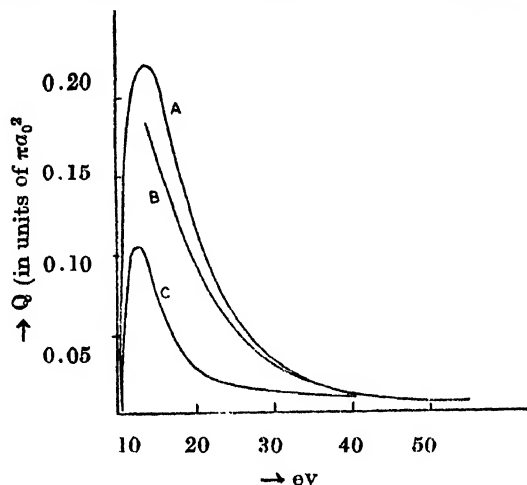


Fig.3. Total excitation cross section $1s-2s$ (spin flip) is plotted against energy. Curve A-calculations of Burke *et al.* (1963); Curve B-present calculations; Curve C-experimental curve.

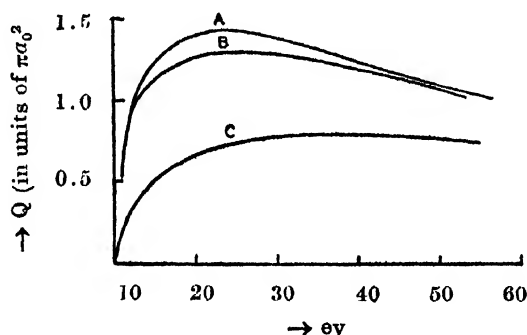


Fig. 4. Total excitation cross section $1s-2p$ is plotted against energy. Curve A. Born results; Curve B-present calculation; Curve C-experimental curve.

Born approximation cross section and experimental results, we find that Ochkur approximation does not show appreciable deviation from Born results in the energy range of 13.6 ev to 54.4 ev. At still higher energies, our cross section values converge towards the Born results.

In conclusion, we may say that in all the above processes of scattering, Ochkur approximation gives reasonable agreement with experiment. It is certainly better than Born approximation so far as its agreement with experiment is concerned. But even then there is a marked discrepancy between experimental and theoretical results. The polarization effect may partially account for this discrepancy.

ACKNOWLEDGMENT

The author is thankful to Prof. D. Basu for his kind interest and valuable discussions throughout the progress of the work. Thanks are also due to Dr. N. C. Sil for helpful discussions.

REFERENCES

- Bell, K. L. and Moiseiwitsch, B. L., 1963, *Proc. Roy. Soc. A* **276**, 346-53.
Burke, P. G., Schey, H. M. and Smith, K., 1963, *Phys. Rev.*, **129**, 1258-74.
Lichten, W. and Schulz, S., 1959, *Phys. Rev.*, **116**, 1132-9.
Ochkur, V. I., 1964, *Soviet Physics—JETP*, **18**, 503-8.
Stebbing, R. F., Fite, W. L., Hummer, D. G., and Brackman, R. T., 1960, *Phys. Rev.*, **119**, 1939-45.

ON A REPRESENTATION OF THE DIRAC MATRICES

N. D. SEN GUPTA

TATA INSTITUTE OF FUNDAMENTAL RESEARCH,
COLABA, BOMBAY-5.

(Received October 3, 1966)

ABSTRACT. The object of the paper is to construct a representation of the Dirac matrices adaptable to the free particle spinor.

INTRODUCTION

In order to obtain explicitly the solutions of the Dirac equation and to study their properties, it is the usual practice to start with suitable representation of the Dirac matrices, satisfying the anti-commutation relations. Conversely, one can ask the question whether one can build up a representation of the Dirac matrices adapted to the solution of the Dirac equation for a particular problem. The object of this short paper is to construct a representation of the matrices, in the spinor space of free particle. The construction of the matrices, in this way, is very instructive as it gives better insight to their characteristic properties related to the splitting up and mixing of the positive and negative energy states, as well as those of the spin states. The process is also interesting as it shows clearly where is the liberty of the choice and how the elements are determined. Finally, it also exhibits the natural role of the Pauli matrices in the representation and their invariance properties, which have been recently studied by the author (1965).

In the next section, the representation of the matrices in the space of free particle spinor has been developed. In the last section some of their properties, e.g. transposition operation, are discussed.

We will need frequently the Pauli matrices which we take as

$$\sigma_1 = \begin{vmatrix} 0 & 1 \\ 1 & 0 \end{vmatrix}, \quad \sigma_2 = \begin{vmatrix} 0 & -i \\ i & 0 \end{vmatrix}, \quad \sigma_3 = \begin{vmatrix} 1 & 0 \\ 0 & -1 \end{vmatrix}.$$

The very nature of the problem proposed will lead us to hermitian matrices. However, we do not lose any generality, as it is well-known that any non-hermitian representation may be made equivalent to a hermitian one by suitable similarity transformation (Pauli (1936)).

For any space vector \vec{q} we will use the notation α_q to denote $(\vec{\alpha} \cdot \vec{q})/|\vec{q}|$; so that $\alpha_q^2 = 1$. \sim over a matrix denotes its hermitian conjugate.

REPRESENTATION OF THE MATRICES

Let the free particle spinors be $U_+(\vec{p})$ and $U_-(\vec{p})$ corresponding to the positive and negative energies respectively. Hence

$$\left. \begin{aligned} \{\vec{\alpha} \cdot \vec{p} + \beta mc\} U_+(\vec{p}) &= -p_0 U_+(\vec{p}) \\ \{\vec{\alpha} \cdot \vec{p} + \beta mc\} U_-(\vec{p}) &= p_0 U_-(\vec{p}), \end{aligned} \right\} \quad \dots (1)$$

where $p_0 = +\{\vec{\alpha} \cdot \vec{p} + \beta mc\}^{1/2}$. Let us introduce the matrices α_+ and α_- defined by

$$\alpha_+ = -\frac{1}{p_0} \{\vec{\alpha} \cdot \vec{p} + \beta mc\} \quad \dots (2)$$

$$\text{and} \quad \alpha_- = \frac{1}{p_0} \{m\alpha_p - \beta |\vec{p}|\}; \quad \dots (3)$$

such that

$$\alpha_+^2 = 1, \quad \alpha_-^2 = 1 \quad \dots (4)$$

$$\text{and} \quad \alpha_+ \alpha_- + \alpha_- \alpha_+ = 0. \quad \dots (5)$$

Let \vec{j} and \vec{k} be two mutually orthogonal unit vectors in the plane perpendicular to \vec{p} , i.e.

$$(\vec{p} \cdot \vec{j}) = 0, \quad (\vec{p} \cdot \vec{k}) = 0 \quad \text{and} \quad (\vec{j} \cdot \vec{k}) = 0. \quad \dots (6)$$

It is clear that \vec{j}, \vec{k} are arbitrary up to a rotation in their plane.

Since α_+ is an involution and traceless one, it has two distinct pairs of eigen-vectors with eigen-values $+1, -1$. Let U_+^1 and U_-^2 be two mutually orthogonal eigen-vectors of α_+ with eigen-values $+1$ and similarly U_-^1 and U_+^2 be those with eigen-values -1 . These four vectors are mutually orthogonal and form the basis of our representation. Clearly in this basis α_+ is a diagonal matrix with elements $(+1, +1, -1, -1)$.

The matrices which commute with α_+ leave the subspaces of positive and negative energy states invariant. We can take any of the matrices which anti-commutes with α_+ to connect the positive energy states with those of negative energy and vice versa. In order that the representation is symmetric, with respect to positive and negative energy states, we take α_- as the matrix which just connects positive and negative energy states (without changing spin states) and conversely, as it is an involution. So that,

$$\left. \begin{aligned} \alpha_- U_+^s &= U_-^s \\ \alpha_- U_+^s &= U_+^s. \end{aligned} \right\} \quad (s = 1, 2) \quad (7)$$

and

Thus α_+ and α_- are given by

$$\alpha_+ = \begin{vmatrix} e, & 0 \\ 0, & -e \end{vmatrix} \quad \text{and} \quad \alpha_- = \begin{vmatrix} 0, & e \\ e, & 0 \end{vmatrix}, \quad \dots \quad (8)$$

where e is the 2×2 unit matrix.

Next let us consider the operator which interchanges only the spin states with same energy. The matrix Σ , for such an operator, is

$$\Sigma = \begin{vmatrix} \sigma_1, & 0 \\ 0, & \sigma_1 \end{vmatrix} \quad \dots \quad (9)$$

where σ_1 is the Pauli matrix given above. It clearly commutes with α_+ and α_- . The most general matrix which commutes with both α_+ and α_- is a linear combination of

$$\alpha_j \alpha_k, \quad \alpha_+ \alpha_- \alpha_k, \quad \alpha_+ \alpha_- \alpha_j.$$

Again for symmetry, let us take Σ to be proportional to $\alpha_j \alpha_k$ so that

$$\Sigma = i \alpha_j \alpha_k. \quad \dots \quad (10)$$

In order to find α_j, α_k separately we note that

$$\alpha_+ \alpha_j U_+^s = -\alpha_j U_+^s \quad \text{and} \quad \alpha_+ \alpha_j U_-^s = +\alpha_j U_-^s.$$

Thus the matrix α_j is of the form

$$\alpha_j = \begin{vmatrix} 0, & \sigma \\ \tilde{\sigma}, & 0 \end{vmatrix}, \quad \dots \quad (11)$$

where σ is any 2×2 matrix. It is easy to see that σ should satisfy the following conditions

$$\left. \begin{aligned} \sigma \bar{\sigma} &= e, \quad \sigma + \bar{\sigma} = 0 \\ \sigma \sigma_1 + \sigma_1 \sigma &= 0, \end{aligned} \right\} \quad \dots \quad (12)$$

and

such that $\alpha_j^2 = 1$, and α_j anti-commutes with α_- and α_+ . Hence

$$\sigma = i(\cos \theta \sigma_2 + \sin \theta \sigma_3), \quad \dots \quad (13)$$

where θ is any real parameter. Hence from Eq. (10), it follows that

$$\alpha_k = \begin{vmatrix} 0, & \sigma' \\ i', & 0 \end{vmatrix} \quad \dots \quad (14)$$

10

with

$$\left. \begin{aligned} \sigma' &= i(\sin \theta \sigma_2 - \cos \theta \sigma_3) \\ \sigma \sigma' + \sigma' \sigma &= 0. \end{aligned} \right\} \quad \dots \quad (15)$$

so that

As mentioned above \vec{j} and \vec{k} are indeterminate but for a rotation in the $(\vec{j} - \vec{k})$ plane, thus we can choose θ , in Eqs. (13) and (15), to be zero so that

$$\alpha_j = i \begin{vmatrix} 0 & \sigma_2 \\ -\sigma_2 & 0 \end{vmatrix}; \quad \alpha_k = i \begin{vmatrix} 0 & -\sigma_3 \\ \sigma_3 & 0 \end{vmatrix}. \quad \dots (16)$$

Finally the fifth mutually anti-commuting matrix

$$\alpha_+ \alpha_- \alpha_j \alpha_k = -i \alpha_+ \alpha_- \Sigma = i \begin{vmatrix} 0 & -\sigma_1 \\ \sigma_1 & 0 \end{vmatrix}. \quad \dots (17)$$

which is a matrix with only non-vanishing anti-diagonal elements.

DISCUSSIONS

The construction of the matrices shows how the Pauli matrices enter in the expression of the Dirac matrices in an obvious manner. The typical block character of all the four $\alpha_-, \alpha_j, \alpha_k, \alpha_+ \alpha_- \alpha_j \alpha_k$ is evident from their anti-commuting properties with α_+ , which is diagonal. All these four matrices connect positive energy states to the negative energy and vice versa. It is interesting to note that

$$i \alpha_j \alpha_k = \begin{vmatrix} \sigma_1 & 0 \\ 0 & \sigma_1 \end{vmatrix}, \quad i \alpha_+ \alpha_- \alpha_j = \begin{vmatrix} \sigma_2 & 0 \\ 0 & \sigma_2 \end{vmatrix}$$

and

$$-i \alpha_+ \alpha_- \alpha_k = \begin{vmatrix} \sigma_3 & 0 \\ 0 & \sigma_3 \end{vmatrix}. \quad \dots (18)$$

They are isomorphic to the Pauli matrices. It may be pointed out that these are also the only three linearly independent matrices which commute with α_+ and α_- . Thus our choice of $\Sigma = i \alpha_j \alpha_k$, in Eq. (10), is nothing but a choice of a particular representation of Pauli matrices. Any other choice would amount to a 3-dimensional real orthogonal rotation among these three matrices.

The representation constructed here is slightly different from those usually referred (Dirac (1928), Kronig (1938)). In this representation, α_p, β (obtained from α_+ and α_-) and α_j are real; α_k and $\alpha_p \beta \alpha_j \alpha_k$ are purely imaginary. Thus α_k and $\alpha_p \beta \alpha_j \alpha_k$ are anti-symmetric and α_p, β , and α_j are symmetric. The matrix B (Pauli (1936), which induces the transposition, is $\alpha_+ \alpha_- \alpha_j$. This representation is one of the second category of representation as noted by the author (1965).

ACKNOWLEDGMENT

The author acknowledges the support of the Atomic Energy Commission, Government of India.

REFERENCES

- Dirac, P. A. M., 1928, *Proc. Roy Soc.* **117**, 610.
 Kramers, H. A., 1937, *Proc. Acad. Amst.* **40**, 814.
 Pauli, W., 1936, *Ann. de l'Inst. H. Poincaré* **6**, 109.
 Sen Gupta, N. D., 1965, *Il. Nuo. Cim.* **36**, 1181.

ON THE PERFORMANCE CALCULATIONS OF THREE PHASE TRANSMISSION LINES BY RELAXATION METHOD

R. N. BASU* AND S. N. DUTTA

DEPARTMENT OF APPLIED PHYSICS, CALCUTTA UNIVERSITY

(Received October 10, 1966)

ABSTRACT. The application of relaxation technique in the nominal-T method of solution of transmission line problem is discussed with an illustration. The principle underlying the relaxational solution of a.c. networks having complex circuit constants (i.e., considering the reactances along with the resistances in different branches is utilised and the results thus obtained are compared with those calculated by normal method of solution. It also discusses about the application of the method to the solution of long transmission lines where the equivalent-T method is used instead of the nominal-T method normally used for medium lines.

INTRODUCTION

The performance calculations of three phase transmission lines under different given conditions at the receiving end and sending end are quite familiar in Electrical Engineering. Of the different methods available for such calculations, the nominal-T method is one. In the nominal-T method the line capacitance is assumed to be localised at the mid-point of the line as shown in Fig. 1. Depending

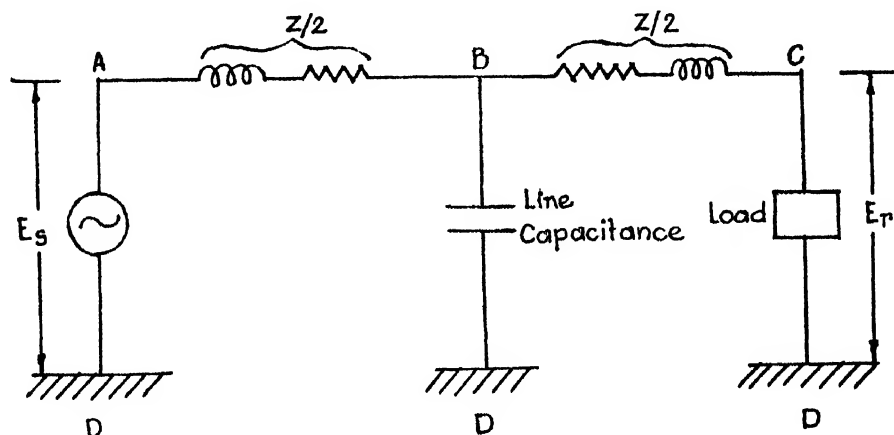


Fig. 1

Diagram for nominal T-method.

*Present address : Research and Development Department, Northern Electric Co., Ottawa, Canada.

on the available informations regarding the sending end and receiving end conditions, three distinct cases can be considered separately, viz.,

- (i) when receiving end voltage and load are known,
- (ii) when sending end voltage and receiving end impedance are known, and
- (iii) when sending end voltage and receiving end load are known.

When the receiving end terminals of the T -network, shown in Fig. 1, are terminated by the load-impedance, the same network can be represented in a convenient form as shown in Fig. 2a. The network thus formed is solved here with the help of relaxation method, and it is shown that such a relaxational solution yields a number of useful informations simultaneously.

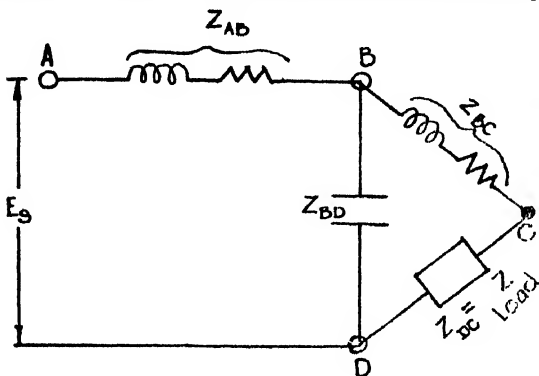


Fig. 2a

Equivalent impedance network diagram
nominal T-method.

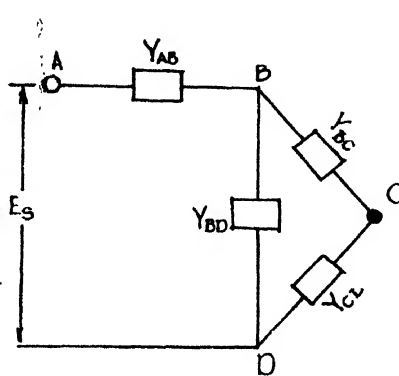


Fig. 2b

Equivalent admittance network diagram
for nominal T-method.

In using the technique of relaxation to the solution of a.c. networks, additional complications (in comparison with d.c. networks) arise due to the complex nature of the branch-impedances, which include resistances as well as reactances. Southwell and Black (1938) have applied relaxation method to the solution of an a.c. network having complex circuit constants. The principle underlying such a solution reveals the usefulness of the application of relaxation technique for solving the network shown in Fig. 2a, i.e., for the performance calculations of transmission lines.

PRINCIPLE OF THE METHOD

In Fig. 2b, Y_{AB} , Y_{BC} , ... etc. are equal to the reciprocals of the impedances Z_{AB} , Z_{BC} , ... etc. respectively, and the voltage between A and D stands for the sending end voltage measured between phase and neutral. Now writing the admittance of any branch, say BC , as—

$$Y_{BC} = g_{BC} + jb_{BC} \quad \dots (1)$$

and assuming the potentials at the points B and C to be

$$\left. \begin{aligned} v_B &= v_{x(B)} + jv_{y(B)} \\ v_C &= v_{x(C)} + jv_{y(C)} \end{aligned} \right\} \quad \dots (2)$$

and

the current flowing from B to C through the branch BC may be represented by

$$\begin{aligned} I_{BC} &= Y_{BC}(v_B - v_C) \\ &= [g_{BC}\{v_{x(B)} - v_{x(C)}\} - b_{BC}\{v_{y(B)} - v_{y(C)}\}] \\ &\quad + j[g_{BC}\{v_{y(B)} - v_{y(C)}\} + b_{BC}\{v_{x(B)} - v_{x(C)}\}] \end{aligned}$$

Let $-\sum_B I_{BC} = I_{B1} = \{i_{x(B)1} + ji_{y(B)1}\}$ be the total current flowing into B from all the branches attached to it, so that,

$$\begin{aligned} \text{and} \quad -i_{x(B)1} &= \sum_B [g_{BC}\{v_{x(B)} - v_{x(C)}\} - b_{BC}\{v_{y(B)} - v_{y(C)}\}] \\ -i_{y(B)1} &= \sum_B [g_{BC}\{v_{y(B)} - v_{y(C)}\} + b_{BC}\{v_{x(B)} - v_{x(C)}\}] \end{aligned} \quad \left. \vphantom{\sum_B} \right\} \dots \quad (3)$$

If $I_{B2} = i_{x(B)2} + ji_{y(B)2}$ stands for the current supplied to B from outside, then by Kirchoff's law—

$$\begin{aligned} \text{and} \quad i_{x(B)} &= i_{x(B)1} + i_{x(B)2} = 0 \\ i_{y(B)} &= i_{y(B)1} + i_{y(B)2} = 0 \end{aligned} \quad \left. \vphantom{i_{x(B)}} \right\} \dots \quad (4)$$

Supposing that the vector potential of D is unity and those of the points A, B, C to be zero, the currents passing from D along the branches DB and DC will be given by

$$\begin{aligned} \text{and} \quad I_{DB} &= Y_{BD} = g_{BD} + jb_{BD} \\ I_{DC} &= Y_{CD} = g_{CD} + jb_{CD} \end{aligned} \quad \left. \vphantom{I_{DB}} \right\} \dots \quad (5)$$

and no current will flow in any other branch of the circuit. In order that the assumed potential may be correct a current $-I_{D2} = I_{DB} + I_{DC} = i_{x(D)2} + ji_{y(D)2}$ will have to be supplied to D from outside. Under such a condition the currents I_{DB} and I_{DC} will leave the network at B and C respectively. But in fact no current passes to or leaves the network at B and C . Therefore it is required to superpose on the assumed potentials those which would result if currents $I_{B2}(=I_{DB})$ and $I_{C2}(=I_{DC})$ were supplied at B and C and allowed to leave the network at D and A the latter points being held at zero potential.

It is thus obtained initially

$$\begin{aligned} i_{x(B)} &= i_{x(B)2} = g_{BD}; \quad i_{x(C)} = i_{x(C)2} = g_{CD}; \\ i_{y(B)} &= i_{y(B)2} = b_{BD}; \quad i_{y(C)} = i_{y(C)2} = b_{CD}; \\ i_{x(D)} &= i_{x(D)2} = -(g_{BD} + g_{CD}); \\ i_{y(D)} &= i_{y(D)2} = -(b_{BD} + b_{CD}); \end{aligned}$$

$$\text{and} \quad i_{x(A)} = i_{y(A)} = 0.$$

For liquidating these initial values (viz. $i_{x(B)}$, $i_{y(B)}$, $i_{x(C)}$, and $i_{y(C)}$) by imposing suitable vector potentials at B and C only, a table of standard operations can be prepared by the use of the following :

$$\left. \begin{aligned}
 & \frac{\partial i_{x(C)}}{\partial v_{x(B)}} = g_{BC} = \frac{\partial i_{y(C)}}{\partial v_{y(B)}} ; \\
 & - \frac{\partial i_{x(C)}}{\partial v_{y(B)}} = b_{BC} = \frac{\partial i_{y(C)}}{\partial v_{x(B)}} ; \\
 \text{and} \quad & \frac{\partial i_{x(B)}}{\partial v_{x(B)}} = \frac{\partial i_{y(B)}}{\partial v_{y(B)}} = -\sum_B (g_{BC}) ; \\
 & - \frac{\partial i_{x(B)}}{\partial v_{y(B)}} = \frac{\partial i_{y(B)}}{\partial v_{x(B)}} = -\sum_B (b_{BC}) ;
 \end{aligned} \right\} \dots (6)$$

which are easily obtained from relations (3).

On liquidation of the residuals (i.e., the initial values of $i_{x(B)}$, $i_{y(B)}$, $i_{x(C)}$ and $i_{y(C)}$) the vector values of the currents at A and D , and also of the potentials at B and C will be obtained. These values will naturally correspond to the case when unit potential difference is applied between the terminals D and A .

The procedure involved in and the information available from such a method of solution will be apparent from the illustration given below :

ILLUSTRATION

For illustrating the method the following example which is worked out by Starr (1953), is considered.

Example. A three-phase transmission line 100 miles long has the following constants :

Resistance per mile = 0.25Ω ; Reactance per mile = 0.8Ω ; Susceptance per mile = 14×10^{-6} mho; Receiving end voltage = 66kv. It is required to determine (using nominal- T method),

(i) the sending end voltage and (ii) the sending end current when the line is delivering 15000 kw at 0.8 power factor lagging. The vector admittances of the different branches of the network (Fig. 2b), as calculated for the problem under consideration, are :

$$\begin{aligned}
 Y_{AB} &= 10^{-3}(7.1-j22.79), \\
 Y_{BC} &= 10^{-3}(7.1-j22.79), \\
 Y_{CD} &= 10^{-3}(3.446-j2.58), \\
 Y_{BD} &= 10^{-3}(0+j1.4).
 \end{aligned}$$

First of all it may be assumed for convenience that the potential at D is 1 kv (one kilovolt), and the potentials at A , B , and C are all zero. Then the currents in the branches DC and DB will be

$$I_{DC} = 3.446 - j2.58,$$

and

$$I_{DB} = 0 + j1.4.$$

Therefore, the current $-I_{D_2}$ to be fed from outside will be given by :

$$-I_{D_2} = 3.446 - j1.18.$$

Thus it is obtained initially,

$$i_{x(B)} = 0; \quad i_{x(C)} = 3.446; \quad i_{x(D)} = -3.446;$$

$$i_{y(B)} = 1.4; \quad i_{y(C)} = -2.58; \quad i_{y(D)} = 1.18;$$

and

$$i_{x(A)} = i_{y(A)} = 0.$$

Using the relations (6) and keeping in mind that all the ' g ' and ' b ' values mentioned there are to be multiplied by 10^3 (since here one kilo volt is considered in place of one volt mentioned previously) the unit operation table (Table I) is readily obtained for liquidating the initial values.

TABLE I
Unit operation table

	$\delta i_{x(A)}$	$\delta i_{x(B)}$	$\delta i_{x(C)}$	$\delta i_{x(D)}$	$\delta i_{y(A)}$	$\delta i_{y(B)}$	$\Delta i_{y(C)}$	$\delta i_{y(D)}$
$v_{x(B)}=1$	7.1	-14.2	7.1	0	-22.79	44.18	-22.79	1.4
$v_{x(C)}=1$	0	7.1	-10.546	3.446	0	-22.79	25.37	-2.58
$v_{y(B)}=1$	22.79	-44.18	22.79	-1.4	7.1	-14.2	7.1	0
$v_{y(C)}=1$	0	22.79	-25.37	2.58	0	7.1	-10.546	3.446

With the help of the procedure suggested previously by Basu (1958), the final operation table (Table II) is prepared which enables complete liquidation of the initial values in three steps only. It may, however, be mentioned that this procedure is not an essential one for the method under consideration. The relaxation table is then worked out as shown in Table III.

Thus when v_{DA} (i.e., sending end voltage) is 1 kv,

(i) the receiving end voltage,

$$v_{DC} = v_D - v_C = (0.788 - j0.143) \times 10^3 \text{ volts} = 0.8 / \angle -10^\circ 18' \text{ kv.}$$

and

(ii) the sending end current,

$$\begin{aligned} I_A = I_D &= 2.458 - j1.25 \\ &= 2.821 / \angle -26^\circ 57' \text{ amps.} \end{aligned}$$

TABLE II
Final operation table

$\delta v_{x(B)}$	$\delta v_{x(C)}$	$\delta v_{y(B)}$	$\delta v_{y(C)}$	$\delta i_{x(A)}$	$\delta i_{x(B)}$	$\delta i_{x(C)}$	$\delta i_{x(D)}$	$\delta i_{y(A)}$	$\delta i_{y(B)}$	$\delta i_{y(C)}$	$\delta i_{y(D)}$
.1	.2	0	0	.71	0	-1.4	.689	-2.279	-.14	2.795	-.376
-.188	-.377	.1	.194	.941	0	0	-.938	5.004	.22	-6.6	1.376
.275	.227	-.114	-.11	-.641	0	0	.636	-7.068	7.689	0	-.62

TABLE III
Relaxation table

$\delta v_{x(B)}$	$\delta v_{x(C)}$	$\delta v_{y(B)}$	$\delta v_{y(C)}$	$i_{x(A)}$	$i_{x(B)}$	$i_{x(C)}$	$i_{x(D)}$	$i_{y(A)}$	$i_{y(B)}$	$i_{y(C)}$	$i_{y(D)}$
Initial values				0	0	3.446	-3.446	0	1.4	-2.58	1.18
.246	.492	0	0	1.747	0	0	-1.751	-5.606	1.055	4.296	.255
-.122	-.245	.065	.126	2.359	0	0	-2.361	-2.353	1.198	0	1.149
-.043	-.035	.018	.017	2.458	0	0	-2.46	-1.257	0	0	1.242
.081	.212	.083	.143	2.458	0	0	-2.46	-1.257	0	0	1.242

Therefore for a receiving end voltage of $66/\sqrt{3}$ (between phase and neutral) the following quantities will be obtained,

Sending end current , $I_A = 134.4$ amps.[132.2 amps];

Sending end voltage, $v_{AD} = 82.5$ kv[82.3 kv];

and the sending end power factor = $\cos 26^\circ 57'$ lagging [$\cos 26^\circ 58'$].

The corresponding values of I_A , v_{AD} and the power factor as obtained by normal method of calculation (Starr, 1953) are given side by side within the brackets [], and it appears that they agree fairly well with each other.

DISCUSSION

The utility of the method described in this paper is appreciated when one considers that a relaxational solution as explained, readily yields a number of informations at a time viz., (i) vector currents at the sending and receiving ends, (ii) phase angle between the sending end and receiving end voltages together with the ratio between the two voltages, the ratio being constant for a given load-impedance, etc. Moreover the fact that the number of initial values to be liquidated in such problems will never exceed four, always brings forth a limitation in the labour associated with the process of liquidation. It may, however, be borne in mind that this method always requires a prior knowledge of the load admittance or the load impedance (which may be given directly or may be obtained from the given data). But as a rule the value of the receiving end impedance is not known

unless the load, its power factor and the receiving end voltage are known. Under such conditions Case (ii), as mentioned earlier in the introduction, becomes identical with Case (i).

So far as the application of relaxation technique is concerned, the solution of long transmission lines by equivalent- T method is in no way different from the nominal- T method of solution of medium transmission lines. In the former case the branch impedances (i.e., Z_{AB} , Z_{BC} , and Z_{BD} of Fig. 1) only will have some changed values which can be calculated by using proper expressions given in standard text books.

ACKNOWLEDGMENT

The authors take this opportunity to express their gratefulness to Prof. A. K. Sengupta, D.Sc., A.M.I.E.E. (London), Head of the Department of Applied Physics, Calcutta University, for his guidance throughout the progress of this work.

REFERENCES

- Black, A. N., and Southwell, R. V., 1938, *Proc. Roy. Soc.* **164**(A), 447.
Basu, R. N., 1958, *Journ. Assn. Applied Phys.* **5**, 30.
Southwell, R. V., 1951, *Relaxation Methods in Engineering Science*, Oxford University Press, London, Chapter VI.
Starr, A. T., 1953, *Generation, Transmission and Utilisation of Electrical Power*, Chapter VI., Sir Issac Pitman & Sons Ltd., London.

INDIAN JOURNAL OF PHYSICS

VOL. 41

No. 6

AND

VOL. 50

PROCEEDINGS

No. 6

OF THE

INDIAN ASSOCIATION FOR THE CULTIVATION OF SCIENCE

(Edited in collaboration with the Indian Physical Society).

JUNE 1967

PUBLISHED BY THE
INDIAN ASSOCIATION FOR THE CULTIVATION OF SCIENCE
JADAVPUR, CALCUTTA-32

Two stage, Rotary Vacuum Pump, suitable only for power drive through V-Belt, mounted on C.I. Base Plate with Electric Motor.

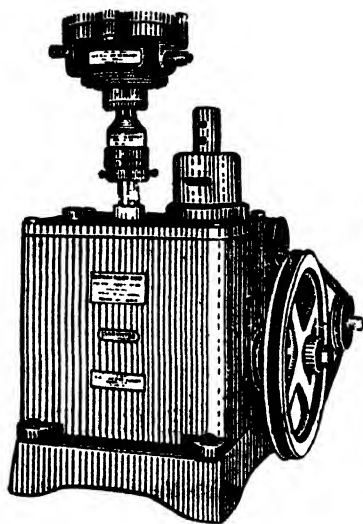
*Ultimate no-load Vacuum : 0.005 mm. of Mercury (McLeod Gauge) with closed Ballast & 0.5 mm. of Mercury with open Ballast

OTHER AVAILABLE MODELS

- * DRY/20 * SSRP/20 * TSRP/20
- * SSRP/30 * TSRP/30
- * SSRP/50 * TSRP/50 * DRY/100
- * DRY/80 * SSD/150
- * TSRP/150 * SSRP/325
- * TSRP/325 * SSD/750

Also five items of Vacuum Accessories—

- Moisture Trap, Type MT/30 & MT/50
- Non-return Valve, Type NRV/30 & NRV/50
- Surface Plate Type RSP/20



BASYNTH TSRP/75 ROTARY VACUUM PUMP

OIL SEALED TYPE

Manufactured by

BASIC & SYNTHETIC CHEMICALS PRIVATE LIMITED

25, EAST ROAD * JADAVPUR * CALCUTTA-32

Progressive/BSC-6

NON-AQUEOUS TITRATION

A monograph on acid-base titrations in organic solvents

By

PROF. SANTI R. PALIT, D.Sc., F.R.I.C., F.N.I.

DR. MIHIR NATH DAS, D.Phil.

AND

MR. G. R. SOMAYAJULU, M.Sc.

This book is a comprehensive survey of the recently developed methods of acid-base titrations in non-aqueous solvents. Acid-base concept, as developed by Lowry-Brönsted and Lewis is succinctly presented in this slender volume. The subject is divided into two classes, viz. titration of weak bases and titration of weak acids. The method of 'glycolic titration' is described at a great length as also the method of 'acetous titration' including its recent modifications for the estimation of weak bases. Various methods for the titration of weak acids are duly described. A reference list of all pertinent publications is included in this book.

122 pages with 23 diagrams (1964)

Inland Rs. 3 only. Foreign (including postage) \$ 1.00 or 5s.

Published by

**INDIAN ASSOCIATION FOR THE CULTIVATION OF SCIENCE
JADAVPUR, CALCUTTA-32, INDIA**

TEST OF VISCOSITY THEORIES OF FLORY, KURATA, PTITSYN AND PALIT FOR DILUTE POLYMER SOLUTIONS

DILIP K. SARKAR AND S. R. PALIT

DEPARTMENT OF PHYSICAL CHEMISTRY,
INDIAN ASSOCIATION FOR THE CULTIVATION OF SCIENCE, JADAVPUR,
CALCUTTA-32, INDIA.

(Received October 18, 1966)

ABSTRACT. The linear expansion factor α for the fractions of different types of macromolecules in a number of solvents at different temperatures have been determined using Stockmayer-Fixman's and in some cases Kurata's relationship. The validity of (1) Flory, (2) Kurata et al and (3) Ptitsyn theories have been tested in terms of the dependence of the function α on molecular weight. From available research data it has been found that Flory's theory is of limited applicability, while Kurata and Ptitsyn theories are in good agreement. The same data have been utilised to test Palit's theory which predicts linear dependence of $100\rho_0[\eta] + \ln M$ on $M^{2/3}$ with a slope of the order of 10^{-2} . Palit's equation has been found to be in very good agreement in practically all cases.

INTRODUCTION

Flory (1948, 1949, 1951) treated the interaction of chain segments with their environment as a mixing problem and was led to the following equation

$$\alpha^5 - \alpha^3 = 2\psi_1 C_M (1 - \theta/T) M^\dagger \quad (1)$$

where α is the linear expansion factor, defined as the ratio of the root-mean-square values of perturbed and unperturbed radii of gyration, ψ_1 is an entropy of dilution factor, θ represents the temperature at which the second virial coefficient vanishes for the solvent-polymer pair, and

$$C_M = (27/2.5/2.\pi^{3/2}N)(\bar{v}^2/V_1)(M/\bar{r}_0^2)^{3/2}$$

where N is Avogadro's number and \bar{v} and V_1 are the partial specific volume of the polymer and molar volume of the solvent respectively. In this theory the macromolecule is considered to be equivalent to a cluster of unconnected segments for which there is a spherically symmetrical Gaussian distribution around the centre of mass.

Kurata, Stockmayer and Roig (1960) proposed a new theory of excluded volume effect assuming an equivalent ellipsoid model, in which the polymer chain with fixed ends is replaced by a uniform distribution of unconnected segments within an ellipsoid whose dimensions are chosen to give the correct principal

radii of gyration of the chain and derived the following relationship for a Gaussian chain

$$\alpha^3 - \alpha/N^{\frac{1}{2}} = 1/(1 + 1/3\alpha^2)^{3/2} \cdot (4/3)^{5/2} (3/2\pi)\beta/a^3 \quad (2)$$

where a is the effective bond length, β the binary cluster integral, and N is the number of segments in the polymer chain.

Taking into account segment-segment interaction and on consideration of a non-Gaussian distribution function for α , Ptitsyn (1962) derived the following equation

$$[(4.68\alpha^2 - 3.68)^{3/2} - 1] = C'N^{\frac{1}{2}} \quad \dots (3)$$

The validity of eqs. (1), (2) and (3) is tested in this paper in terms of available literature values of α calculated for solutions of well defined fractions of a number of polymers in different solvents of varying solvent power at different temperatures.

Based on Eyring's Rate Theory and the 'hole' theory of liquids, Palit (1955, 1963) derived the following equation correlating intrinsic viscosity, $[\eta]$ and molecular weight of polymers.

$$100\rho_0[\eta] = K_1M^{2/3} - \ln M + K_2 \quad \dots (4)$$

where ρ_0 is the density of the polymer at infinite dilution and $K_1 = 1.09N^{1/3}\gamma v_p^{2/3}/RT \simeq$ order of 10^{-2} and K_2 are constants. We have used $\rho_0 = 1$ as a rough approximation.

The same literature data have been utilised to test equation (4).

DETERMINATION OF α

The linear expansion factor α , is obtained by either of the following three procedures :

Procedure (1) depends on the Flory-Fox (1951) relationship

$$[\eta] = KM^{\frac{1}{2}}\alpha^3 \quad \dots (5)$$

$$\frac{[\eta]}{[\eta]_\theta} = \alpha^3 \quad (6)$$

where $[\eta]_\theta$ is the intrinsic viscosity in θ -solvent. Eq. (6) is directly used if $[\eta]_\theta$ values are known.

Procedure (2) where data on $[\eta]_\theta$ are not available α is calculated by a modified relationship proposed by Kurata *et al* (1963) :

$$[\eta]^{2/3}/M^{1/3} = K^{2/3} + 0.363B\phi_0g(\alpha_\eta)(M^{2/3}/[\eta]^{1/3}) \quad \dots (7)$$

where $\phi_0 = 2.87 \times 10^{21}$ and $B = \beta/m_0^2$ in which β represents the binary cluster integral and m_0 is the molar weight of a polymer segment, and

$$g(\alpha_\eta) = 8\alpha_\eta^3(3\alpha_\eta^2 + 1)^{-3/2}$$

A rough value of $K^{2/3}$ is obtained from eq. (7) graphically after assuming $g(\alpha_\eta)$ to be unity. Using this value of K , values of α_η for all the fractions are obtained from eq. (5). With the help of these values of α_η and consequently of $g(\alpha_\eta)$ a more accurate value of $K^{2/3}$ is obtained by a second graphical intercept method.

Procedure (3) involves a more direct evaluation of K as suggested by Stockmayer and Fixman (1963). Their equation reads

$$[\eta] = KM^\dagger + 0.51\phi_p BM \quad \dots (8)$$

in which B is the polymer-solvent interaction parameter. Because of the simplicity of eq. (8), K values were obtained in most cases from the ordinate intercept of $[\eta]/M^\dagger$ vs. M^\dagger graphs. Unless otherwise indicated procedure (3) has been utilised for evaluation of K .

EXPERIMENTAL RESULTS AND DISCUSSION

A. ADDITION POLYMERS

1. *Poly-p-Chloro Styrene*. Our method of treatment of the experimental data is illustrated here in this case, in some details. The \bar{M}_n and $[\eta]$ values (Table I) of Kuwahara *et al* (1965) at 30°C are utilised to calculate K and α values of Table II.

TABLE I
Results for Poly-p-Chloro Styrene fractions

Fraction	$\bar{M}_n \times 10^{-4}$	$[\eta]$, dl./g.		
		Chlorobenzene	M.E.K.	Toluene
1	268	3.18	2.40	2.06
2	107	1.53	1.22	1.07
3	59.0	0.888	0.76	0.676
4	46.9	0.756	0.623	0.550
5	28.4	0.486	—	0.406
6	17.0	0.327	0.296	0.274

TABLE II
Values of K and α

Solvent	Temp. °C	α						$K \times 10^5$ (Procedure 2)
		1	2	Fraction 3	4	5	6	
Chlorobenzene		1.571	1.435	1.322	1.302	1.222	1.166	
M.E.K.	30	1.431	1.330	1.255	1.221	—	1.128	50
Toluene		1.360	1.274	1.207	1.170	1.148	1.100	

The values of α are found to increase with increase of M and solvent power in all the solvent-polymer pairs studied, indicating increased expansion of the molecule.

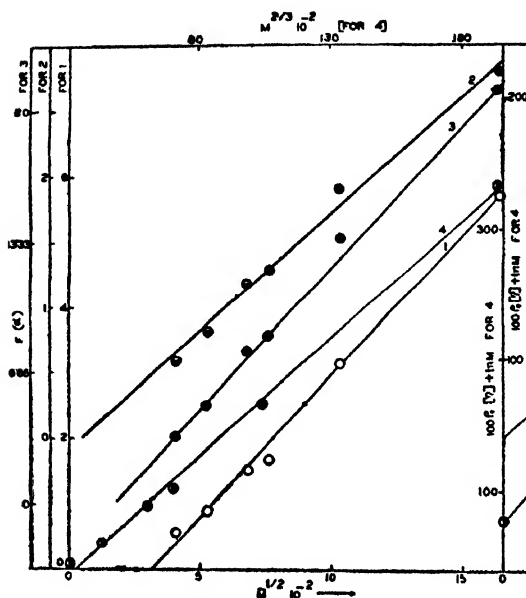


Fig. 1. Poly-p-Chlorostyrene in Chlorobenzene at 30°C

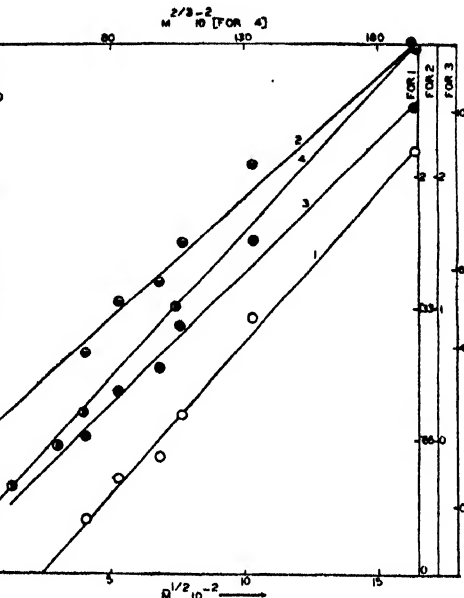


Fig. 2. Poly-p-Chlorostyrene in Toluene at 30°C.

GRAPHICAL TEST OF THE FOUR EQUATIONS

Analysis of Flory Relation : According to eq. (1) plots of $\alpha^5 - \alpha^3$ ag. $M^{1/2}$ are expected to give straight lines passing through the origin. Graphs of $\alpha^5 - \alpha^3$ vs. $M^{1/2}$ in all the solvents show a good linear monotonic increase but they do not pass through the origin. Abscissa intercepts correspond to about 99000, 57000 and 60000 Ms with chlorobenzene (Fig. 1), toluene (Fig. 2) and M.E.K. (Fig. 3) as respective solvents. This is in contradiction to Flory's eq. (1) according to which α should approach unity as the M approaches zero. Again from eq. (1) one can expect that $\alpha^5 - \alpha^3 / M^{1/2}$ values should be invariant with M ; evidently they increase with M . So, Flory's equation is inadequate for these systems.

Analysis of Kurata et al's relation : Plots of $(\alpha^3 - \alpha) (1 + 1/3\alpha^2)^{3/2}$ vs. $M^{1/2}$ (eq. 2) are fairly good linear in case of chlorobenzene, poorly linear in case of toluene and very poorly linear in case of M.E.K. and pass through the origin in case of M.E.K. and toluene. In case of chlorobenzene, however, a small abscissa intercept corresponding to 2500M is obtained by the least square method. It is apparent that the data fit better in the K-S-R. equation.

Analysis of Ptitsyn's Relation : According to eq. (3) plots of $[(4.68\alpha^2 - 3.68)^{3/2} - 1]$ ag. $M^{1/2}$ are expected to give straight lines passing through the origin. Such graphs although very good linear, in case of chlorobenzene, fairly good linear in

case of toluene and good linear in case of M.E.K., do not pass through the origin but give abscissa intercepts, as obtained by the least square method, corresponding to about 28000, 13000 and 10000 Ms in chlorobenzene, toluene and M.E.K. as respective solvents. This indicates that like Flory's eq., Pittsyn eq. has also got limited applicability in this case but in a sense it is better as its range of applicability is greater.

Analysis of Palit's Relation : According to eq. (4) plots of $100\rho_0[\eta] + \ln M$ ag. $M^{2/3}$ are expected to give straight lines. Good linear plots are obtained with chlorobenzene and very good liner plots are obtained with toluene and M.E.K. with 1.79×10^{-2} , 1.10×10^{-2} and 1.97×10^{-2} as corresponding slopes.

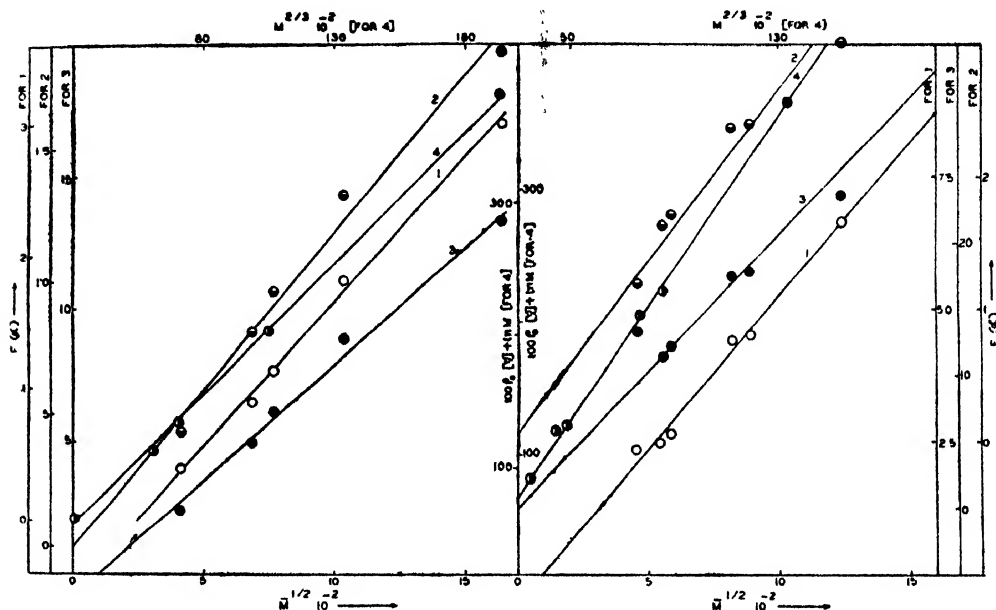


Fig. 3. Poly-p-Chlorostyrene in M.E.K., at 30°C.

Fig. 4. Poly-p-Methylstyrene in Toluene at 30°C.

2. **Poly-p-Methyl Styrene:** The \bar{M}_n and $[\eta]$ data of Kuwahara *et al.* (1965) at 30°C are utilised. K is evaluated by procedure 2. The Flory eq. gives fairly good, good and poorly linear plots in case of toluene (Fig. 4), cyclohexane (Fig.5) and M.E.K. (Fig. 6) as respective solvents but it has got an abscissa intercept of about 9000, 63000 and 53000 Ms respectively with these three solvents. The K-S-R eq gives poor linear plot in the case of toluene as solvent while good linear plots are obtained in the case of the other two solvents. In case of poorer solvents such as cyclohexane and M.E.K. it passes through the origin whereas, with a better solvent such as toluene a small ordinate intercept is obtained. The Ptitsyn eqn. gives fairly good linearity in toluene and good linear plots in cyclohexane and M.E.K. as solvents and passes through the origin in case of toluene whereas

in cyclohexane and M.E.K. it has an abscissa intercept of about 9000 and 14000 Ms respectively. Palit's plot is excellently linear in all these cases with respective slopes of 2.9×10^{-2} , 2×10^{-2} and 1.35×10^{-2} .

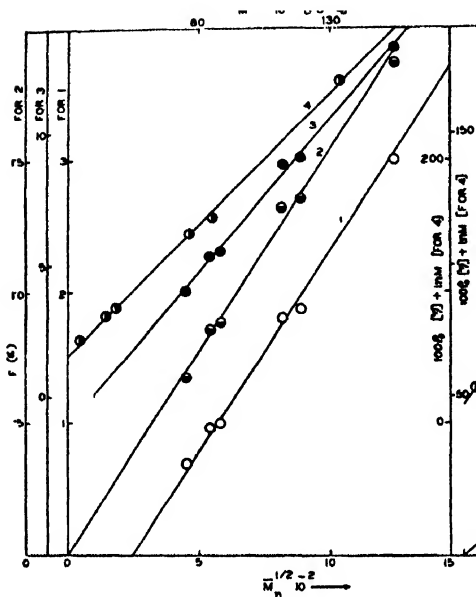


Fig. 5. Poly-p-Methylstyrene in Cyclohexane at 30°C.

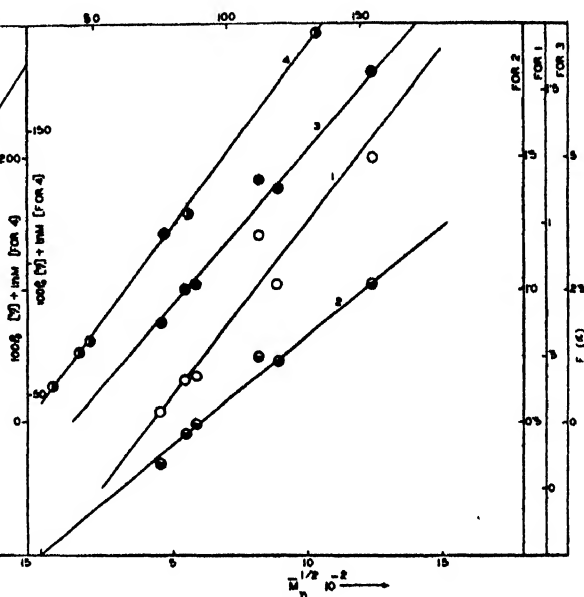


Fig. 6. Poly-p-Methylstyrene in M.E.K. at 30°C.

3. *Poly-m-Methyl Styrene* : Source of data is an unpublished work done by Choudhury *et al* (1967) in this laboratory. K is evaluated by procedure 2. At 30°C, Flory plot gives good, fairly good and poor linear plots with benzene (Fig. 7), cyclohexane (Fig. 8) and ethyl acetate (Fig. 9) as respective solvents but it has got an abscissa intercept corresponding to about 12000, 5000 and 8100 Ms. The K-S-R eq. gives poor linear plots in case of benzene and ethyl acetate whereas in case of cyclohexane it is out of linearity but all of them pass through the origin. Ptitsyn eq. gives poor linear plots in case of benzene and ethyl acetate whereas in case of cyclohexane as solvent fairly good linearity is obtained. However, all of them pass through the origin. At 40° and 50°C also K-S-R- and Ptitsyn theories are more or less satisfactory. Palit eq. gives good linearity in case of benzene and cyclohexane as solvents and in ethyl acetate also the linearity is fairly good with respective slopes of 2.75×10^{-2} , 1.83×10^{-2} and 1.35×10^{-2} .

4. *Poly-α-Methyl Styrene* (Fig. 10) : The \bar{M}_n and $[\eta]$ data of McCormick (1959) in toluene at 25°C are utilised. The Flory plot is too widely scattered to give any linearity. The K-S-R and Ptitsyn eqs. pass through the origin though

they give fairly good linear and poorly linear plots respectively. Palit's eq. gives very good linear plot with a slope of 1.88×10^{-2} .

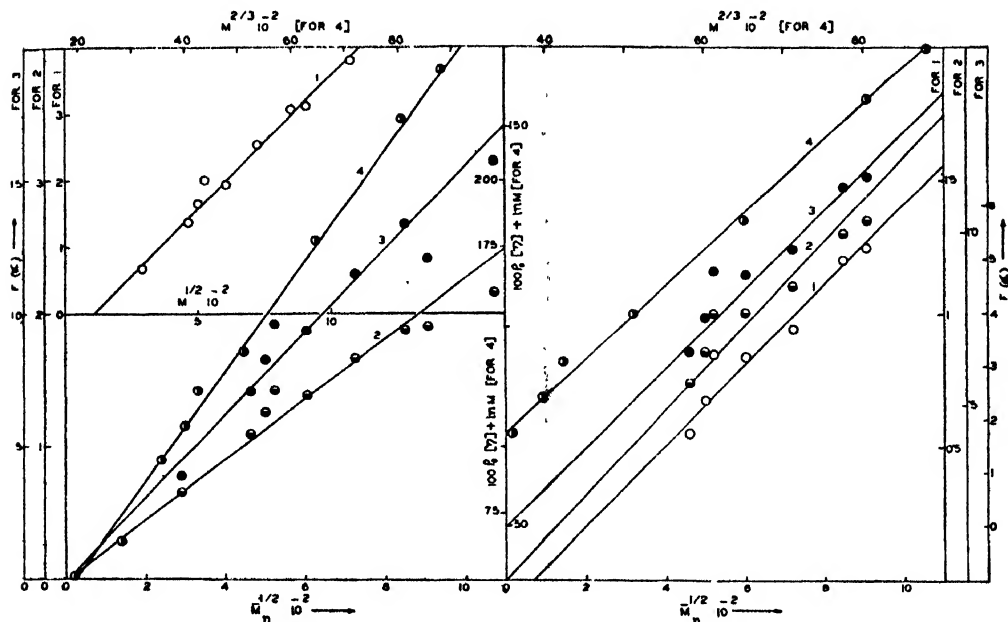


Fig. 7. Poly-m-Methylstyrene in Benzene at 30°C.

Fig. 8. Poly-m-Methylstyrene in Cyclohexane at 30°C.

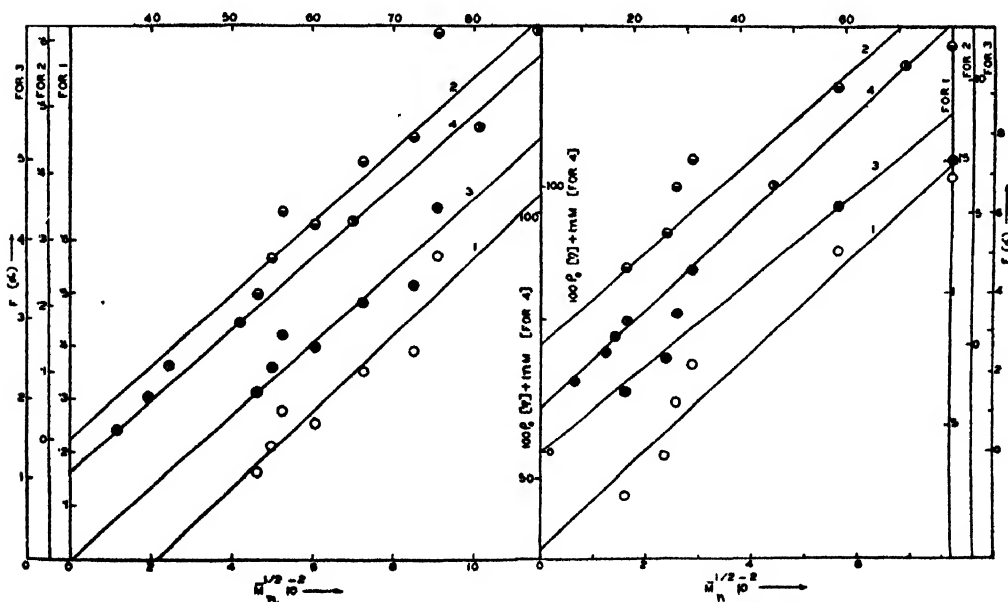


Fig. 9. Poly-m-Methylstyrene in Ethyl Acetate at 30°C.

Fig. 10. Poly-α-Methyl styrene in Toluene at 25°C.

5. *Polystyrene*: Fujita *et al* (1963) took eleven polystyrene fractions in toluene, in M.E.K. and in cyclohexane at 34.5°C. α is evaluated by procedure 1. With M.E.K. (Fig. 11) as solvent, poorly linear Flory plot is obtained with an abscissa intercept of about 40,000 M. The K-S-R and Ptitsyn plots are too much scattered to give any linearity. The least square straight lines have abscissa intercepts at about 12100 and 25600 Ms respectively. Excellent linear Palit plot is obtained with a slope of 1.45×10^{-2} .

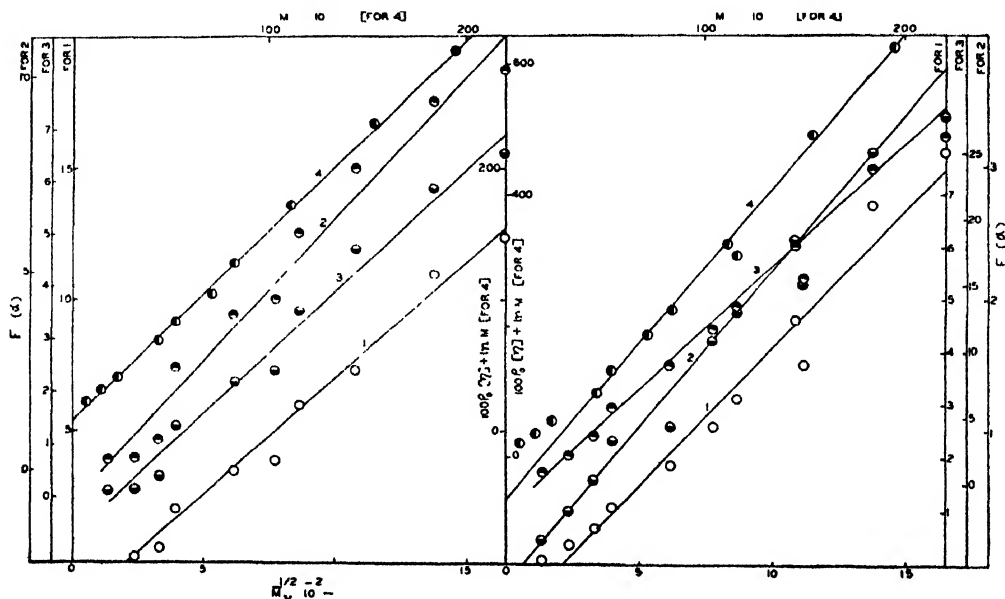


Fig. 11. Polystyrene in M.E.K., at 34.5°C. Ref. (12). Fig. 12. Polystyrene in Toluene at 34.5°C (Ref. 12).

With toluene (Fig. 12) as solvent very poorly linear Flory plot is obtained with an abscissa intercept at about 44100 M. Good linear K-S-R plot is obtained with an abscissa intercept at 4220 M. Excellent linear plot is obtained in case of Ptitsyn eq., but it has an abscissa intercept at about 12100 M. Good linear Palit plot is obtained with a slope of 2.56×10^{-2} .

When the data of Rossi *et al* (1965) in M.E.K. (Fig. 13) are utilised the Flory and Ptitsyn plots are found to be not linear at all. The least square straight lines give abscissa intercepts corresponding to about 1600 and 6400 Ms. Very poor linearity is observed in case of K-S-R eq., but the least square straight line passes through the origin. Fairly good linear Palit plot is obtained with a slope of 1.47×10^{-2} .

6. *Polymethyl Methacrylate*: The \bar{M}_w , $[\eta]_0$ and $[\eta]$ data of Chinai *et al* (1955) at 25°C are utilised. With toluene as solvent, the Flory plot is too much scattered to give any linearity (Fig. 14) and the least square straight line gives a small ordinate intercept while with M.E.K. fairly good linearity is obtained

(Fig. 15) with an abscissa intercept of about 96000 M. The K-S-R plot gives poor linearity with M.E.K. and passes through the origin while in case of toluene

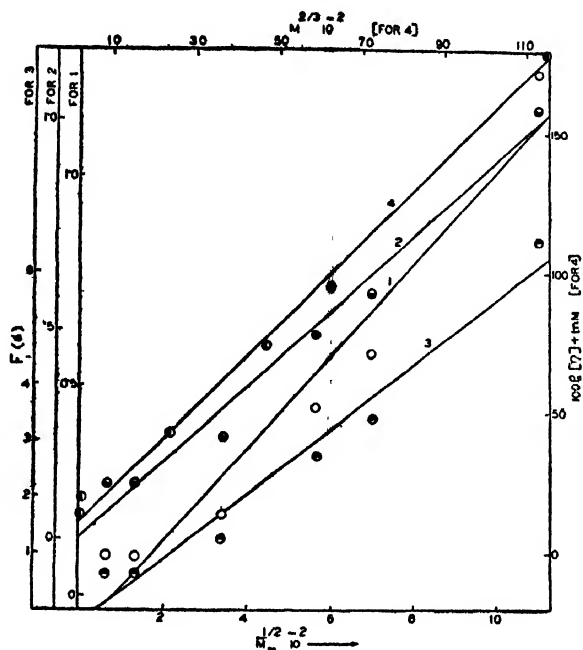


Fig. 13. Polystyrene in M.E.K., at 34.5°C (Ref. 13).

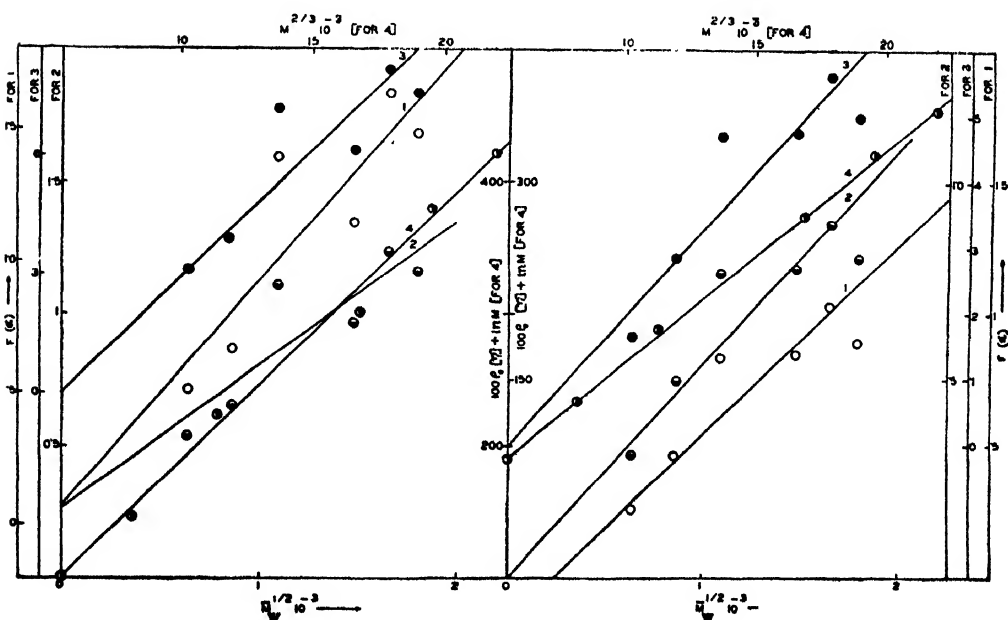


Fig. 14. Polymethyl Methacrylate in Toluene at 25°C.

Fig. 15. Polymethyl Methacrylate in M.E.K., at 25°C.

the plot is out of linearity and the least square straight line gives a large ordinate intercept. Ptitsyn plot passes through the origin though poor linearity is obtained in both the solvents. Palit's plot is fairly good linear with toluene and very good linear with M.E.K. with slopes of 1.94×10^{-2} and 1.62×10^{-2} respectively.

7. *Polyethyl-Methacrylate* (Fig. 16) : The \bar{M}_w , $[\eta]_0$ and $[\eta]$ data of Chinai *et al.*, (1956) in M.E.K. at 23°C are utilised. Poor linearity is obtained in case of Flory eq. while in case of K-S-R and Ptitsyn plots fairly good linearity is obtained and the linearity in case of Palit's plot is good with a slope of 1.86×10^{-2} . The K-S-R and Ptitsyn plots pass through the origin while Flory plot is found to give an abscissa intercept at about 68000 M.

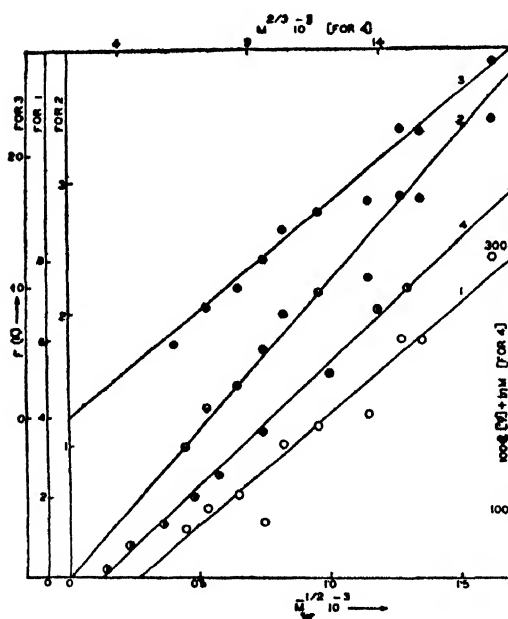


Fig. 16. Polyethyl Methacrylate in M.E.K. at 23°C .

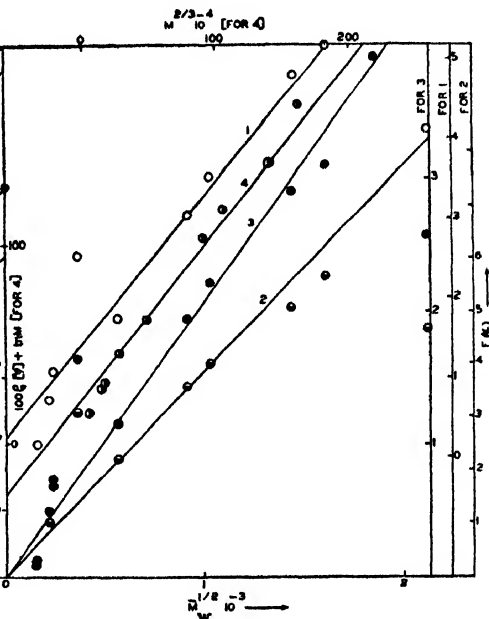


Fig. 17. Polyvinyl Carbazole in Benzene at 25°C .

8. *Polyvinyl Carbazole* (Fig. 17) : The M_{LS} and $[\eta]$ data of Ueberreiter *et al.* (1963) in benzene at 25°C are utilised. Very poor linearity is obtained in case of Flory plot and it gives an ordinate intercept. The K-S-R and Ptitsyn plots are poorly linear but they pass through the origin. Good linearity is obtained in case of Palit plot up to 2.07×10^6 M after which it exhibits curvature and it has a least square slope of 1.26×10^{-2} .

9. *Polyvinyl Acetate* (Fig. 18) : The M_{LS} and $[\eta]$ data of Varadaiah (1956) in benzene are utilised. In case of all the first three eqs. the plots are too much scattered to give any linearity. Ordinate intercepts are obtained by least square

method. Evidently none of the three equations is valid. Data may not be very reliable. However, the Palit plot is fairly satisfactory with a slope of 2.13×10^{-2} .

10. *Polyacrylonitrile*: The data of Bisschops (1955) are utilised. When $[\eta]$ and M_{SD} values are utilised, the Flory eq. in D.M.F. at 25°C (Fig. 19) is found

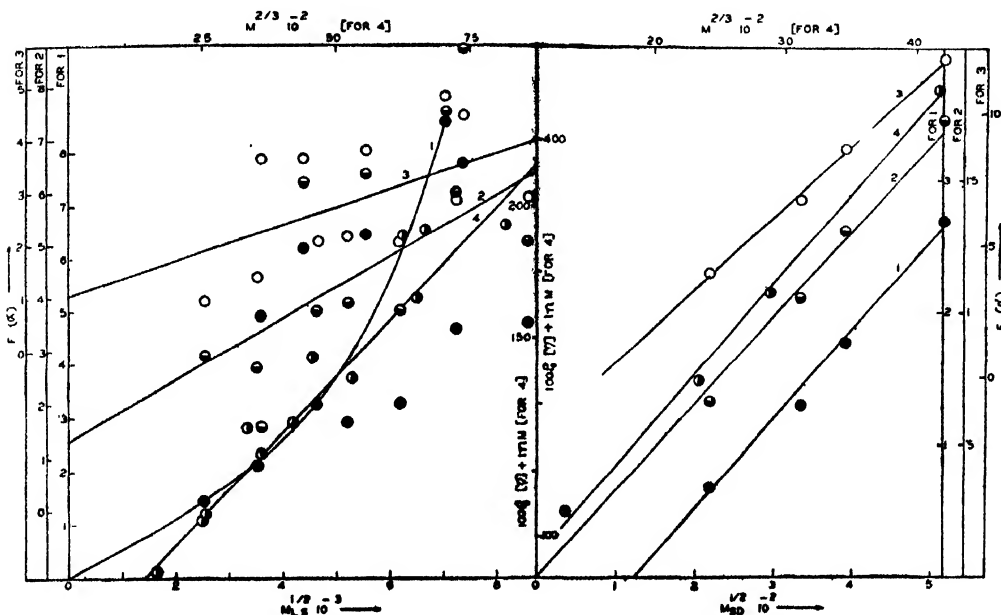


Fig. 18. Polyvinyl Acetate in Benzene at 30°C.

Fig. 19. Polyacrylonitrile in D.M.F. at 25°C.

to give good linearity with an abscissa intercept at about 15200 M. At 65°C upward curvature is noted. Very poor linearity is obtained in case of K-S-R eq., but it passes through the origin at all temperatures. The Ptitsyn plot at 25°C is excellently linear but it gives an abscissa intercept corresponding to about 5600 M. Fairly good linearity is obtained in case of Palit's eq. with a slope of 11.38×10^{-2} .

When $[\eta]$ and \bar{M}_W values of the same fractions are utilised the K-S-R plot is linear passing through the origin, while the Flory and Ptitsyn plots—though linear have got abscissa intercepts at about 16000 and 1200 Ms.

11. *Poly-N-N-Dimethyl Acrylamide*: The M_{LS} and $[\eta]$ data of Trossarelli *et al* (1962) are utilised. In methanol at 25°C (Fig. 20), the Flory plot is poorly linear with an abscissa intercept at about 6000 M. The K-S-R and Ptitsyn plots are poorly linear but they pass through the origin. Palit plot is good linear with a slope of 2.05×10^{-2} .

In water at 25°C (Fig. 21), fairly good linearity is obtained in case of Flory plot with an abscissa intercept at about 24000 and 8100 Ms at 25° and 40°C res-

pectively. Good linearity is obtained in case of K-S-R- plot and it passes through the origin. Fairly good linearity is obtained in case of Ptitsyn plot and it passes through the origin. Palit's plot is fairly good linear with a slope of 1.93×10^{-2} .

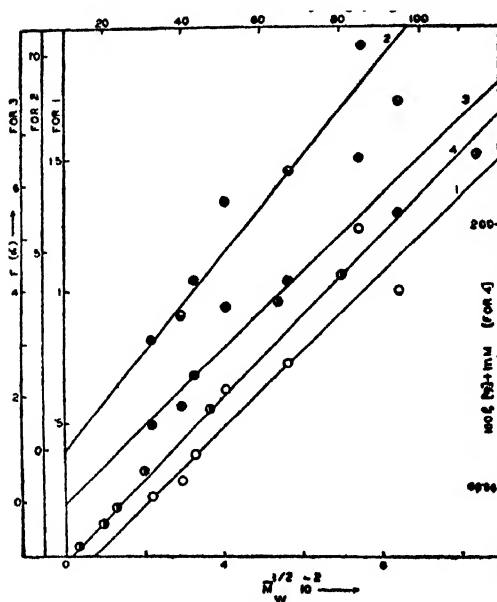


Fig. 20. Poly-N-N-Dimethylacrylamide in Methanol at 25°C.

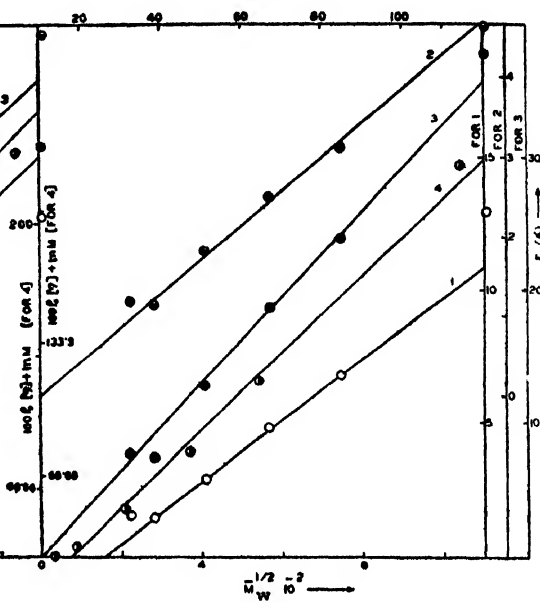


Fig. 21. Poly-N-N-Dimethylacrylamide in Water at 25°C.

12. *Polyacrylamide* (Fig. 22): The $M_{END\ GROUP}$ and $[\eta]$ data of Collinson *et al* (1957) in water at 25°C are utilised. Fairly good linearity is obtained in case of Flory, K-S-R and Ptitsyn plots with abscissa intercepts at about 5300, 900 and 4600Ms respectively. Very good linear Palit plot is obtained with a slope of 6.75×10^{-2} .

13. *Cis-Tactic Polybutadiene* (Fig. 23); The \bar{M}_n and $[\eta]$ data of Danusso (1961) in toluene at 30°C are utilised. Fairly good linearity is obtained in all the first three cases. The K-S-R plot passes through the origin, while the Flory and Ptitsyn plots have abscissa intercepts at about 4600 and 600Ms respectively. Good linearity is obtained in case of Palit plot with a slope of 6.51×10^{-2} .

14. *Polyvinyl Chloride* (Fig. 24): The \bar{M}_n and $[\eta]$ data of Ciampa *et al* (1956) in cyclohexanone at 25°C are utilised. Fairly good linearity is obtained in Flory plot with an abscissa intercept at about 8700 M . Poor linearity passing through the origin is obtained in K-S-R plot. Very poor linearity is obtained in Ptitsyn plot with an abscissa intercept at about 3000 M . Poor linearity with a slope of 9.05×10^{-2} is obtained in case of Palit plot. Data may not be very reliable,

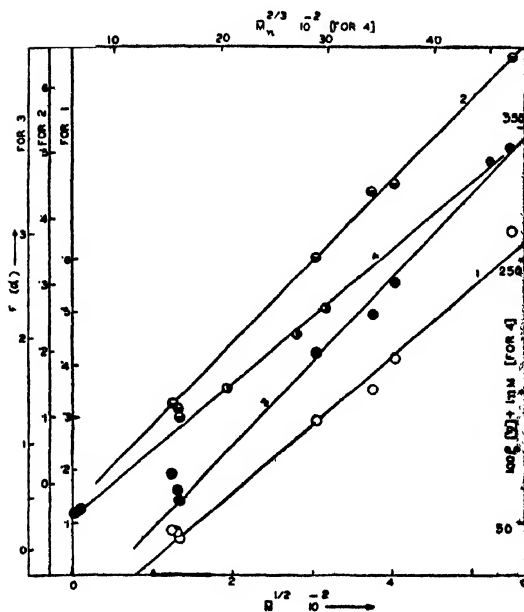


Fig. 22. Polyacrylamide in Water at 25°C.

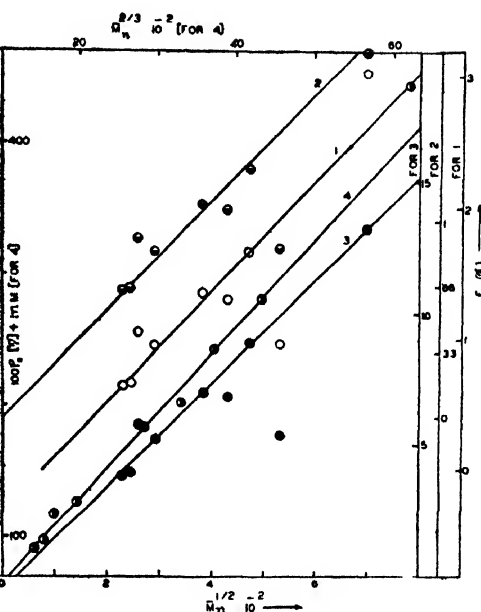


Fig. 23. Cis-Tactic Polybutadiene in Toluene at 30°C.

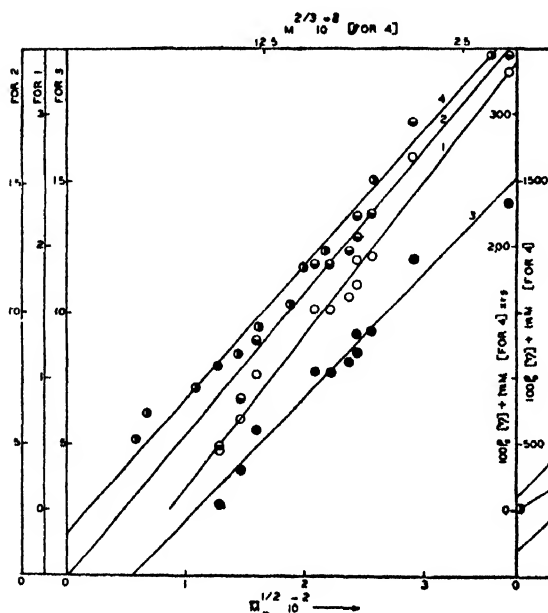


Fig. 24. Polyvinyl Chloride in Cyclohexanone at 25°C.

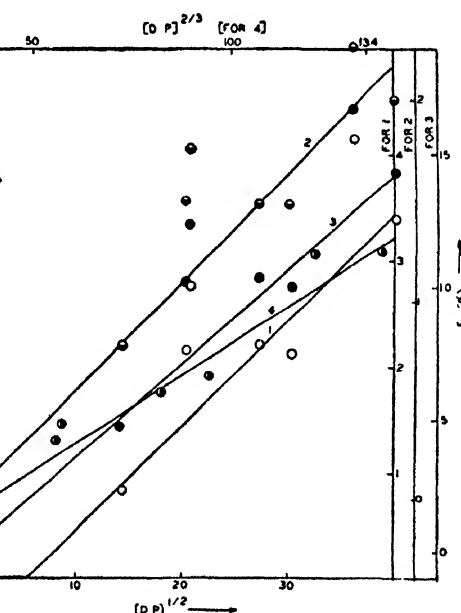


Fig. 25. Na-Carboxy Methyl Cellulose in aqueous solution at $I_E = 0.1M$ at 26°C.

B. SEMISYNTHETICS FROM CELLULOSE

1. *Na-Carboxy Methyl Cellulose* (Fig. 25): The M_{SD} and $[\eta]$ data of Sitaranaiiah *et al* (1962) in aqueous solution at $I_E = 0.1M$ at 26°C are utilised.

Linearity is poor in case of Flory plot while in case of K-S-R- and Pitsyn plots the linearity is very poor. The Flory plot has an abscissa intercept at about 29 D.P. while K-S-R- and Pitsyn plots pass through the origin. Palit plot is poor but is least poor, in comparison to the rest, having slope of 9.75×10^{-2} .

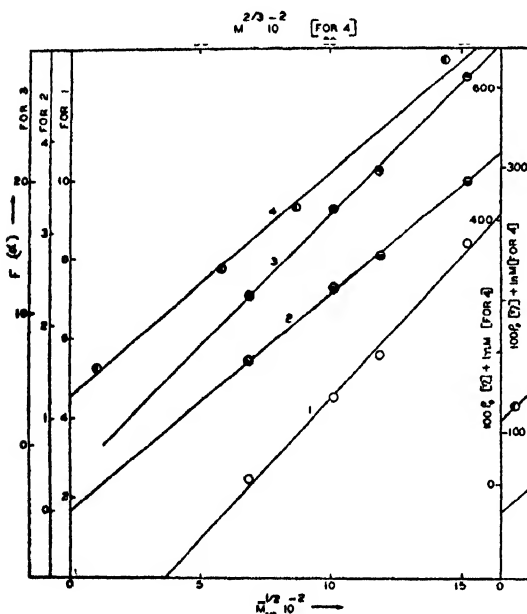


Fig. 26. Amylose Acetate in Chloroform at 30°C.

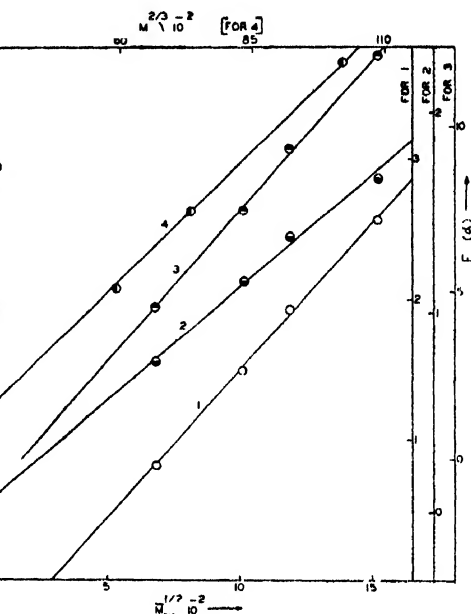


Fig. 27. Amylose Acetate in Nitromethane at 30°C.

2. *Amylose-Acetate* : The \bar{M}_w and $[\eta]$ data of Patel *et al* (1965) in chloroform and nitromethane at 25°C are utilised. K is evaluated by procedure 2. In Chloroform (Fig. 26) fairly good linear Flory plot is obtained with an abscissa intercept at about 133200 M. Good linear K-S-R- plot is obtained and it passes through the origin. Excellent linear plot is obtained in case of Pitsyn eq. and it has an abscissa intercept at about 16900 M. Fairly good linear Palit plot is obtained with a slope of 6.8×10^{-2} .

With nitromethane (Fig. 27), as solvent good linear Flory and Pitsyn plots are obtained with abscissa intercepts at about 84100 and 18900 Ms respectively. Fairly good linear K-S-R plot is obtained and it passes through the origin. Excellent linear plot is obtained in case of Palit eq. with a slope of 3.87×10^{-2} .

C. CONDENSATION POLYMERS

Polydimethyl Siloxane (Fig. 28) : The \bar{M}_v and $[\eta]$ data of Flory *et al* (1962) in M.E.K. at 30°C are utilised. The first three plots are too much scattered to give any linearity—the hand drawn curves appear to meet at a common point

on the abscissa corresponding to about 32400M. The least square straight lines give ordinate intercepts. Palit plot is slightly curved.

D. POLYETHER

Polyethylene Oxide (Fig. 29) : The $[\eta]_0$ and $[\eta]$ data of Rossi *et al* (1962) in benzene at 25°C are utilised. The Molecular weight determination on the fractions were made by the method of chemical titration in pyridine solution with well reproducible results. Fairly good linear plot is obtained in case of K-S-R- and Ptitsyn eqs. with abscissa intercepts at about 59 and 128 Ms. Good linearity is obtained with Flory plot with an abscissa intercept at about 196 M. Very good linearity is obtained in Palit's plot with a slope of 6×10^{-2} .

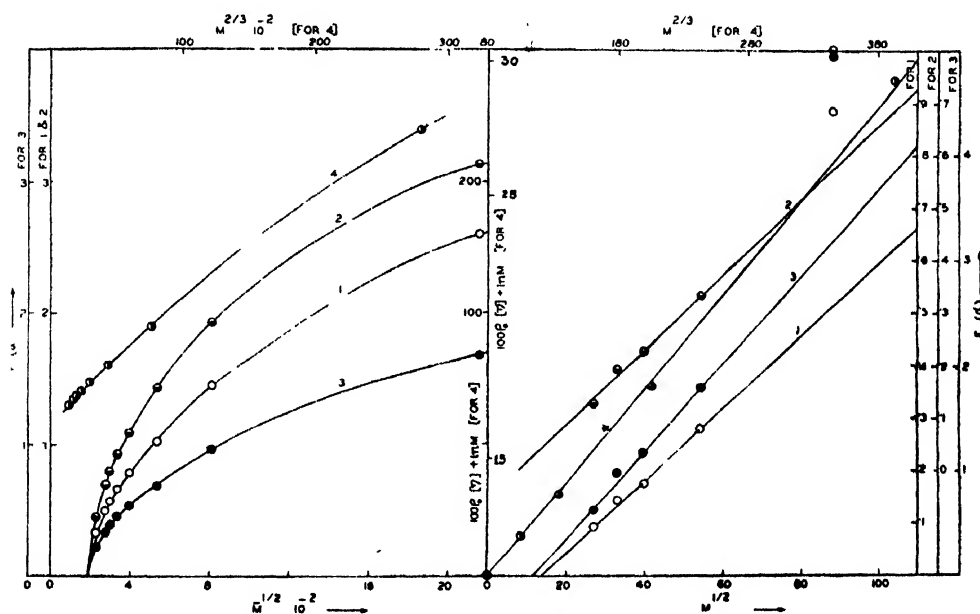


Fig. 28. Poly Dimethyl Siloxane in M.E.K. at 30°C.

Fig. 29. Polyethylene Oxide in Benzene at 25°C.

E. POLYESTER

Bisphenol A Polycarbonate : The \bar{M}_n and $[\eta]$ data of Sitaramaiah (1965) at 25°C are utilised. The Flory relation is found to be applicable only over 6000M. In tetrahydrofuran (Fig. 30), excellent linear plot is obtained in case of Flory eq. Fairly good linear plot passing through the origin is obtained in case of K-S-R- eq. Good linear plot passing through the origin is obtained in the case of Ptitsyn eq. Good linear Palit plot with a slope of 6.35×10^{-2} is obtained.

In ethylene dichloride (Fig. 31), poor linear Flory plot is obtained. Very poor linear plot is obtained in case of K-S-R eq., but it passes through the origin.

Fairly good linear plot with an abscissa intercept at about 225M is obtained in case of Ptitsyn eq. Poorly linear Palit plot with a slope of 6.51×10^{-2} is obtained.

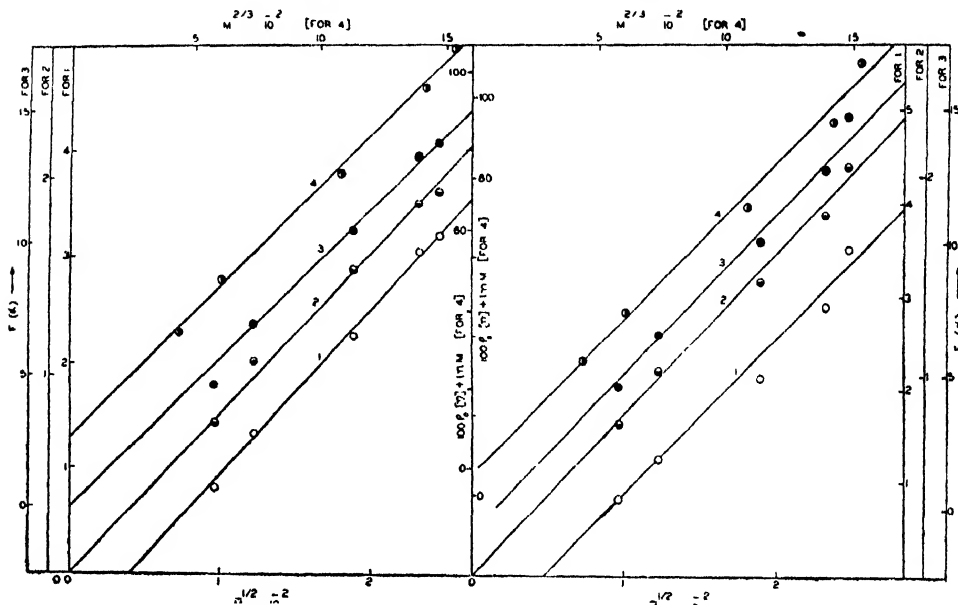


Fig. 30. Bisphenol A Polycarbonate in Tetrahydrofuran at 25°C.

Fig. 31. Bisphenol A Polycarbonate in Ethylene Dichloride at 25°C.

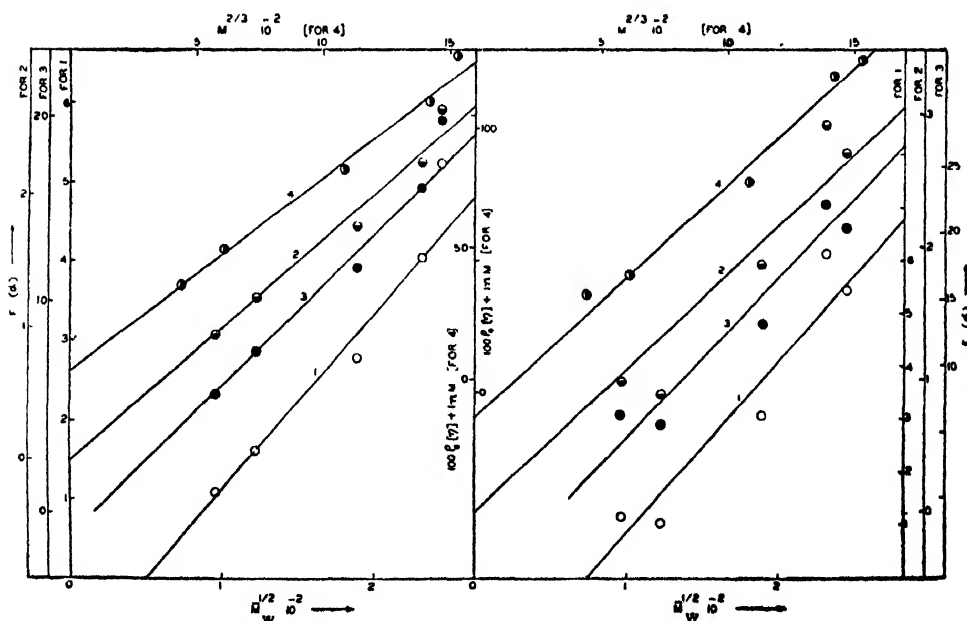


Fig. 32. Bisphenol A Polycarbonate in Chloroform at 25°C.

Fig. 33. Bisphenol A Polycarbonate in Tetrachloroethane at 25°C.

In chloroform (Fig. 32) fairly good linear plots are obtained in case of Flory and Ptitsyn eqs. the latter having an abscissa intercept at about 275 M. Poorly linear K-S-R plot—passing through origin is obtained. Good linear Palit plot with a slope of 7.29×10^{-2} is obtained.

In Tetrachloroethane (Fig. 33) very poor linearity is obtained in all the first three eqs. The K-S-R plot passes through the origin whereas the Ptitsyn plot gives an abscissa intercept at 3600M. Poor linearity is obtained in case of Palit's eq. with a slope of 8.84×10^{-2} .

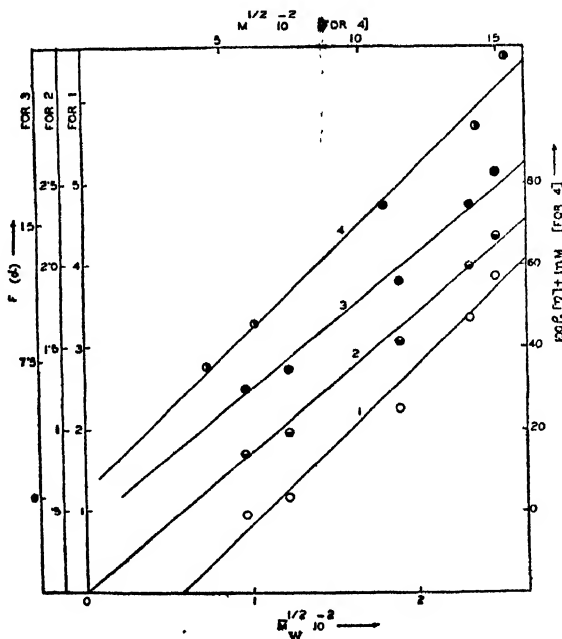


Fig. 34. Bisphenol A Polycarbonate in Methylene Chloride at 25°C.

In methylene chloride (Fig. 34) poorly linear plot is obtained in all the first three cases. K-S-R plot is found to pass through the origin. Ptitsyn plot has an abscissa intercept at about 400 M. Fairly good linear Palit plot is obtained with a slope of 6.58×10^{-2} .

F. POLYPEPTIDES

Poly- γ -Benzoyl-L-Glutamate The M_{LS} and $[\eta]$ data of Doty *et al* (1956) in dichloroacetic acid and D.M.F. at 25°C are utilised. In dichloroacetic acid (Fig. 35) very good linearity is obtained in case of Flory plot though it has an abscissa intercept at about 5000 M. Fairly good linear plot passing through the origin is obtained in case of K-S-R eq. Good linear plot is observed in case of Ptitsyn eq. though it gives a large ordinate intercept. Fairly good linear Palit plot with a slope of 4.05×10^{-2} is obtained.

In D.M.F. (Fig. 36) all the first three plots are much scattered. When least square method is applied the Flory and Ptitsyn eqs. are found to give abscissa

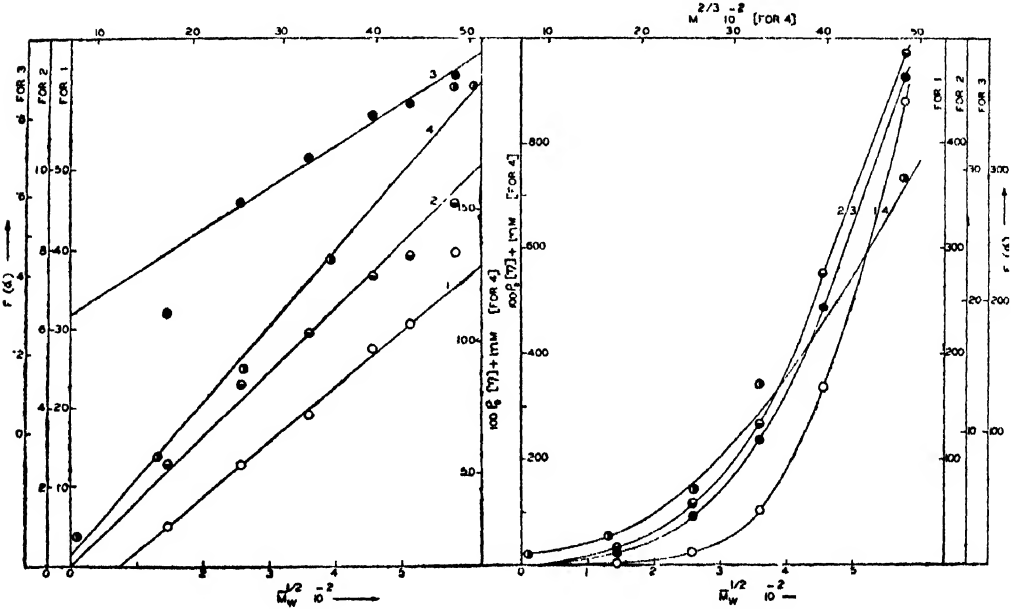


Fig. 35. Poly- γ -Benzoyl-L-Glutamate in Dichloroacetic acid at 25°C.

Fig. 36. Poly γ -Benzoyl-L-Glutamate in D.M.F. at 25°C.

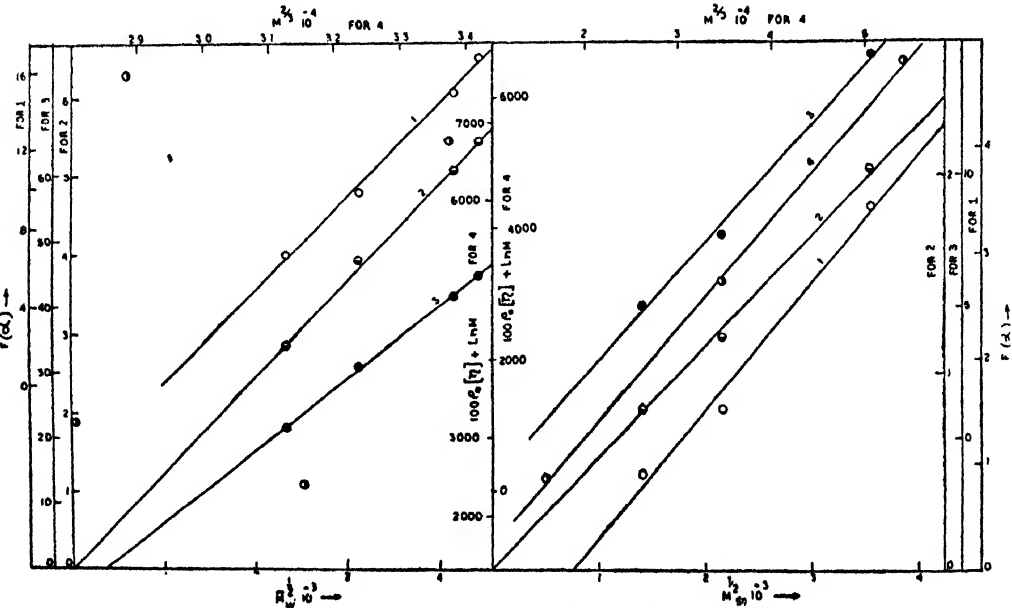


Fig. 37. D.N.A. in Water at 20°C.

Fig. 38. Renatured D.N.A. in water at 20°C.

TABLE III
Tabular Summary of Results

Polymer	Solvent	Temp. °C	LINEARITY AND ABSCISSA INTERCEPTS IN TERMS OF M				GENERAL REMARKS	
			Flory plot Eq. 1	K-S-R plot Eq. 2	Ptitsyn plot Eq. 3	Palit plot Eq. 4, $K_1 \cdot 10^2$	Best Linear eq.	Eq. that passes through the origin.
Poly-p-Chloro-Styrene	Chlorobenzene	30	good 99000	fairly good 2500	very good 28000	good 1.79	3	
	Toluene	"	good 60000	poor 0	fairly good 13000	very good 1.1	4	2
	M.E.K.	"	good 57000	very poor 0	good 10000	very good 1.97	4	2
Poly-p-Methyl Styrene	Toluene	"	fairly good 9000	poor *	fairly good 0	very good 2.91	4	3
	Cyclohexane	"	good 63000	good 0	good 9000	very good 2	4	2
	M.E.K.	"	poor 53000	good 0	good 14000	very good 1.35	4	2
Poly-m-Methyl Styrene	Benzene	"	good 12000	poor 0	poor 0	good 2.75	1 and 4	2 and 3
	Cyclohexane	"	fairly good 5000	scattered 0	fairly good 0	good 1.83	4	2 and 3
	Ethyl Acetate	"	poor 8100	poor 0	poor 0	fairly good 1.35	4	2 and 3

TABLE III—(contd).

Polymer	Solvent	Temp. °C	LINEARITY AND ABSCISSA INTERCEPTS IN TERMS OF M				GENERAL REMARKS	
			Flory plot Eq. 1	K-S-R plot Eq. 2	Ptitsyn plot Eq. 3	Palit plot Eq. 4, $K_1, 10^2$	Best Linear eq. passes through the origin	Eq. that passes through the origin
Poly- α -Methyl Styrene	Toluene	25	highly- scattered	fairly good 0	poor 0	very good 1.88	4	2 and 3
Polystyrene	M.E.K. (Ref. 12)	34.5	poor	highly scattered 12100	highly scattered 25600	very good 1.45	4	
		40000						
	Toluene (Ref. 12)	"	very poor 44100	good 4220	very good 12100	good 2.56	3	
	M.E.K. (Ref. 13)	"	highly scattered 6400	very poor 0	scattered 1600	fairly good 1.47	4	2
Polymethyl Methacrylate	Toluene	25	highly scattered small*	highly scattered large*	poor 0	fairly good 1.94	4	3
	M.E.K.	"	fairly good 96000	poor 0	poor 0	very good 1.62	4	2 and 3
	M.E.K.	23	poor 68000	fairly good 0	fairly good 0	good 1.86	4	2 and 3
Polyethyl Methacrylate	Benzene	25	very poor *	poor 0	poor 0	good 1.26	4	2 and 3
Polyvinyl Carbazole	Benzene	30	highly scattered *	highly scattered *	highly scattered *	fairly good 2.13	4	
Polyvinyl Acetate	Benzene							
Polyacrylonitrile	D.M.F.	25	good 15200	very poor 0	very good 5600	fairly good 11.38	3	2

TABLE III (contd.)

Polymer	Solvent	Temp. °C	LINEARITY AND ABSCISSA INTERCEPTS IN TERMS OF M					GENERAL REMARKS	
			Flory plot Eq. 1	K-S-R plot Eq. 2	Ptitsyn plot Eq. 2	Palit plot Eq. 4, $K_1 \cdot 10$	Best Linear eq.		
Poly-N,N-Dimethyl Acrylamide	Methanol	25	poor 6000	poor 0	poor 0	good 2.05	4	2 and 3	
	Water	"	fairly good 24000	good 0	fairly good 0	fairly good 1.93	2	2 and 3	
Polyacrylamide	Water	"	fairly good 5300	fairly good 900	fairly good 4600	very good 6.75	4		
Cis-Tactic Polybutadiene	Toluene	30	fairly good 4600	fairly good 0	fairly good 600	good 6.51	4	2	
	Cyclohexanone	25	fairly good 8700	poor 0	very poor 3000	poor 9.05	1	2	
Na-Carboxy Methyl Cellulose	Water $I_2 = 0.1M$.	26	poor 29 D.P.	very poor 0	very poor 0	least poor 9.75	4	2 and 3	
Amylose Acetate	Chloroform	30	fairly good 133200	good 0	very good 16900	fairly good 6.8	3	2	
	Nitromethane	"	good 84000	fairly good 0	good 18900	very good 3.87	4	2	
Poly Dimethyl Siloxane	M.E.K.	"	* highly curved	* highly curved	* highly curved	slightly curved	4		
Polyethylene Oxide	Benzene	25	good 196	fairly good 59	fairly good 128	very good 6	4		

TABLE III (contd.)

Polymer	Solvent	Temp. °C	LINEARITY AND ABSCISSA INTERCEPTS IN TERMS OF M					GENERAL REMARKS	
			Flory plot Eq. 1	K-S-R plot Eq. 2	Pittslyn plot Eq. 3	Pzlit plot Eq. 4, K_1 , 10	Best Linear eq.	Eq. that passes through the origin.	
Bisphenol A Polycarbonate	Tetrahydrofuran	25	very good 6000	fairly good 0	good 0	good 6.35	1		2 and 3
	Ethylene Dichloride	"	poor 6000	very poor 0	fairly good 225	poor 6.51	3		2
	Chloroform	"	fairly good 6000	poor 0	fairly good 275	good 7.29	4		2
	Tetrachloroethane	"	very poor 6000	very poor 0	very poor 3600	poor 8.84	4		2
	Methylene Chloride	"	poor 6000	poor 0	poor 400	fairly good 6.58	4		2
Poly- γ -Benzoyl L-Glutamate	Dichloro Acetic Acid	"	very good 5000	fairly good 0	good large*	fairly good 4.05	1		2
	D.M.F.	"	highly curved 48000	highly curved 0	highly curved 33000	curved	4		2
D.N.A.	Water	20	good 1000000	good 0	very good 360000	highly scattered	3		2
Renatured D.N.A.	Water	"	poor 640000	fairly good 0	fairly good 133000	good 16.47	4		2

* Stands for ordinate intercept

D.P. Stands for degree of polymerization.

intercepts at about 48000 and 33000 Ms respectively while the K-S-R eq is found to pass through the origin. The hand drawn curves can be made to pass through the origin. Palit plot is markedly curved but is least curved in comparison to the rest.

G. POLYNUCLEOTIDES

1. *D.N.A.* (Fig. 37) : The \bar{M}_w and $[\eta]$ data of Butler *et al* (1959) in water at 20°C are utilised. Good linear plot is obtained in case of Flory eq. with an abscissa intercept at about 1000000 M. Excellent linear Ptitsyn plot with an abscissa intercept at about 360000 M is obtained. Good linear plot is obtained in case of K-S-R eq. and it passes through the origin. Palit eq. is found to be not at all valid.

2. *Renatured D.N.A.* (Fig. 38) : The M_{Sn} and $[\eta]$ data of Doty *et al* (1965) in water at 20°C are utilised. Poor linearity is observed in case of Flory plot and it has an abscissa intercept at about 640000 M. Fairly good linearity is observed in case of K-S-R and Ptitsyn plots; the former passes through the origin while the latter gives an intercept at about 133000 M. Good linear plot with a slope of 16.47×10^{-2} is obtained in case of Palit's equation.

DISCUSSION

From Table III it will be observed that as regards linearity, out of 38 different polymer-solvent systems studied, Palit's plot is found to be best in 27 cases, Ptitsyn's eq. is found to be best in 6 cases, K-S-R eq. is best in 1 case and Flory eq. is best in 3 cases—there being a single case where it is difficult to ascertain whether Palit eq. or Flory eq. is best suited. From these statistics, it is evident that in so far as satisfaction of linearity is concerned, Palit's eq. is the best.

As regards the criteria of passing through the origin, the K-S-R and Ptitsyn eqs. are satisfied in 29 and 13 cases respectively, while the Flory eq. is not satisfied in a solitary case—it always gives either an abscissa intercept (in majority of cases) or an ordinate intercept (in a few cases). In cases where abscissa intercepts are given by all the three eqs., the intercept is always found to be the least in case of K-S-R eq. and it is always greatest in the case of Flory eq. So the K-S-R eq., based on an equivalent ellipsoid model, is best suited to interpret the molecular expansion of most of the polymers discussed. In cases where only K-R-S plot passes through the origin, the Ptitsyn eq. always gives smaller intercepts. So the Ptitsyn eq. is better suited to various polymer-solvent systems in comparison to Flory eq.

CONCLUSION

The general conclusion is that the Flory eq. suffers from a serious limitation—it is valid generally in the high molecular weight range. The K-S-R and Ptitsyn expressions are well suited to interpret the molecular expansion of most of the

polymers discussed. Palit's eq. excellently correlates intrinsic viscosity and molecular weight of polymers.

ACKNOWLEDGMENT

Thanks are due to C.S.I.R Govt. of India, for financial assistance to D.K.S.

REFERENCES

- Bianchi, E., Podemonte, E. and Rossi, C., 1965, *Macromol. Chem.*, **89**, 95.
 Bisschops, J., 1955, *J. Polymer Sci.*, **17**, 81.
 Bradbury, J. H., Doty, P. and Holtzer, A. M., 1956, *J. Am. Chem. Soc.*, **78**, 947.
 Butler, J. A. V., Laurence, D. J. R., Robins, A. B. and Shooten, K. V., 1959, *Proc. Roy. Soc. A*, **250**, I.
 Chinai, S. N., Matlack, J. D., Resmick, A. L. and Samuels, R. J., 1955, *J. Polymer Sci.*, **17**, 391.
 Chinai, S. N., and Robat, S. J., 1956, *J. Polymer Sci.*, **19**, 463.
 Choudhury, A. K., Sarkar, D. K. and Palit, S. R., 1967., *Macromol. Chem.*, (Communicated)
 Ciampa, G. and Schwindt, H., 1956, *Makromol Chem.*, **21**, 169.
 Collinson, E., Dainton, F. S., and McNaughton, G. S., 1957, *Trans. Faraday Soc.*, **53**, 489.
 Danusso, F., Gianotti, G. and Moraglio, G., 1961, *J. Polymer Sci.*, **51**, 475.
 Doty, P. and Eigner, J., 1965, *J. Mol. Biol.*, **12**, 549.
 Fixman, M. and Stockmayer, W. H., 1963, *J. Polymer Sci.*, **C1**, 137.
 Flory, P. J. and Schaeffgen, J. R., 1948, *J. Am. Chem. Soc.*, **70**, 2709.
 Flory, P. J., 1949, *J. Chem. Phys.*, **17**, 303.
 Flory, P. J. and Fox, T. G. Jr., 1951, *J. Am. Chem. Soc.*, **73**, 1904.
 Flory, P. J., Kinsinger, J. B., Mandelkern, L. and Shultz, W. B., 1962, *J. Am. Chem. Soc.*, **74**, 3364.
 Fujita, H., Okada, R. and Toyoshima, Y., 1963, *Makromol Chem.*, **59**, 137.
 Goring, D. A. I. and Sitaramaiah, G., 1962, *J. Polymer Sci.*, **58**, 1107.
 Kaneko, M. Kasai, A., Kuwahara, N., Ogino, K. and Ueno, S., 1965, *J. Polymer Sci.*, **3**, 985.
 Kurata, M., Roig, A. and Stockmayer, W. H., 1960, *J. Chem. Phys.*, **33**, 151.
 Kurata, M. and Stockmayer, W. H., 1963, *Fortschr. Hochpolymer Forsch.*, **3**, 196.
 Magnasco, V. and Rossi, C., 1962, *J. Polymer Sci.*, **58**, 977.
 McCormick, H. W., 1959, *J. Polymer Sci.*, **41**, 327.
 Meirone, M. and Trossarelli, L., 1962, *J. Polymer Sci.*, **57**, 445.
 Palit, S. R., 1955, *Indian J. Phys.*, **29**, 65.
 ———, 1963, *Jour. Indian Chem. Soc.*, **40**, 721.
 Patel, R. D. and Patel, R. S., 1965, *J. Polymer Sci.*, **3**, 2123.
 Ptitsyn, O. B., 1962, *Polymer Sci., U.S.S.R.*, **3**, 1061.
 Sitaramaiah, G., 1965, *J. Polymer Sci.*, **3**, 2743.
 Springer, J. and Ueberreiter, K., 1963, *Z. Physik Chem.*, **36(1-6)**, 299.
 Varadaiah, V. V., 1956, *J. Polymer Sci.*, **19**, 477.

ON THE REPRESENTATION OF THREE-BODY NON-ADDITIVE INTERACTIONS IN SOLIDS

YASHAWANT SINGH, ANIL SARAN AND A. K. BARUA

INDIAN ASSOCIATION FOR THE CULTIVATION OF SCIENCE, CALCUTTA-32

(Received October 18, 1966)

ABSTRACT. An attempt has been made to represent the three-body non-additive interactions empirically by a function which approximately represents the results obtained by quantum mechanical calculations. The results show that the Jansen's formula as such can not be utilized for the calculation of the second order crystal properties and the third virial coefficient of gases.

INTRODUCTION

The problem of representing the simultaneous interaction between more than two atoms or molecules has not yet been solved satisfactorily. The first attempt in this direction was made by Axilrod (1951) who obtained the interaction between three non-overlapping distributions of charge in the third-order perturbation theory. This so-called triple-dipole effect decreases the attraction compared to an additive sum-over pairs for an equilateral configuration of atoms and increases it for a linear array. The same type of third-order effect was evaluated by Muto (1943) for an oscillator model and later extended by Midzuno and Kihara (1956). These results have been applied to the calculation of the stability of inert gas solids and to the third virial coefficients of gases. The net effect summed over the hcp and the fcc lattices, however, favour the cubic configuration for the inert gas solids but its magnitude is too small to take care of the small pair potential difference between the two structures. Sherwood and Prausnitz (1964) have recently calculated the non-additive three-body contributions to the third virial coefficients of gases as obtained from the triple-dipole effect. Their calculations, however, reveal that at least for the dense gases it is essential to consider the non-additive repulsive forces in addition to the triple-dipole effect.

The first order forces (exchange, chemical or valence) which predominate at smaller inter-atomic distances are of the many-body type (Margenau 1939). These forces were evaluated for an equilateral triangle and a linear array of three helium atoms by Rosen (1953) and Shostak (1955) using molecular orbitals. Subsequently Jansen (1962, 1963) obtained the tri-atomic first-order and second-order three-body interaction for heavy rare gases by using a Gaussian effective electron model given by

$$\rho(r) = (\beta/\pi^{\frac{1}{2}})^3 \exp(-\beta^2 r^2), \quad \dots \quad (1)$$

where r is the distance from the effective electron to its nucleus, β is a parameter

and $\rho(r)$ is the charge distribution of effective electron. His results for the three-body interaction in first order, agree in sign with those of Rosen (1953) for helium. It should be pointed out that for the equilateral triangle configuration the relative three-body energy formula of Jansen remains almost constant for increasing interatomic distances (in terms of the dimensionless parameter βr) whereas the Rosen formula shows an exponential decrease. In the second-order the contribution to the relative three-body component is the sum of the effects due to diatomic and triatomic exchanges. Jansen's calculations explain satisfactorily the fcc structure and the energy of vacancy formation in solid argon (Jansen, 1963). Due to mathematical difficulties the quantum-mechanical calculations are not suitable for applying to a general case and for considering the effect on various properties. It seems that, at present the only way to consider simultaneously the effects of three-body interactions in both the attractive and the repulsive parts is to use a pair potential with the parameters adjusted to the theoretical results obtained for three-body interactions.

DETERMINATION OF THE THREE-BODY NON-ADDITIVE INTERACTION FUNCTION

The three-body non-additive interaction ϕ_{non} may be written as,

$$\phi_{non} = \phi_{total} - \frac{1}{2} \sum_{i \neq j} \phi_{ij}, \quad (2)$$

where ϕ_{total} represents the total interaction energy between three molecules forming a triangle and in the second term on the r.h.s. of eqn. (2), the summation extends over all the three pairs of the molecules. It has been shown by Kihara (1958) that the three-body non-additive interaction in the attractive part can be represented as

$$\phi_{non} = v(r_{12} r_{13} r_{23})^{-3} (1 + 3 \cos \theta_1 \cos \theta_2 \cos \theta_3), \quad \dots \quad (3)$$

where

$$v = \frac{\alpha}{4} \mu,$$

α is the polarizability and μ is the coefficient of two-body dispersion energy varying as r^{-6} . No convenient expression for ϕ_{non} including both the repulsive and the attractive parts is available. However, it is found that an expression

$$\phi_{non} = -\omega(r_{12}^* r_{13}^* r_{23}^*)^{-3} (1 + 10 \cos \theta_1 \cos \theta_2 \cos \theta_3) \frac{1}{2} \sum_{i \neq j} \phi_{ij} \quad (4)$$

represents fairly well the quantum mechanically obtained results by Jansen (1962, 1963) (Fig. 1). r_{ij}^* in the above equation are the reduced intermolecular distances. It is possible to determine ω from the cohesive energy in the solid state. The three-body non-additive contributions to the cohesive energy per lattice-point in a fcc lattice considering only the nearest neighbours are given by

$$\Delta E_{coh}/N = 8\Delta_{80} + 4\Delta_{90} + 8\Delta_{120} + 2\Delta_{180}, \quad (5)$$

where

$$\Delta_\theta = -\omega(r_{12}^* r_{13}^* r_{23}^*)^{-3} (1 + 10 \cos \theta_1 \cos \theta_2 \cos \theta_3) \sum_{i \neq j}^3 \phi_{ij} \quad \dots (6)$$

On the basis of the core-potential (Sherwood and Prausnitz 1964),

$$\phi(r) = 4\epsilon \left[\left(\frac{\sigma - 2a}{r - 2a} \right)^{12} - \left(\frac{\sigma - 2a}{r - 2a} \right)^6 \right], \quad \dots (7)$$

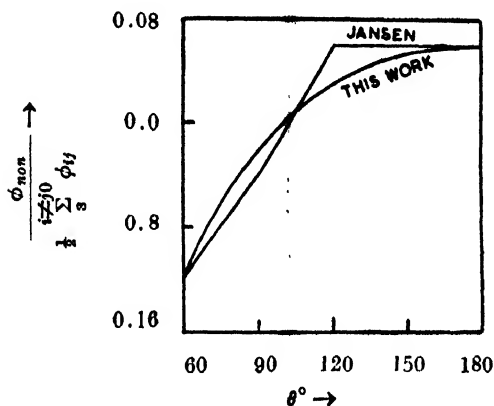


Fig. 1. The variation of $\phi_{non} / \sum_{i \neq j}^3 \phi_{ij}$ vs θ for solid argon.

(The interatomic distances are the nearest neighbour distances).

where a is the core radius, σ is the value of r for which $\phi(r) = 0$ and ϵ is the maximum energy of attraction, the pair cohesive energy per atom is given by

$$E'_{coh}/N = 2\epsilon \left[C_{12} \left(\frac{\sigma - 2a}{d_0 - 2a} \right)^{12} - C_6 \left(\frac{\sigma - 2a}{d_0 - 2a} \right)^6 \right] \quad \dots (8)$$

In the above expression C_{12} and C_6 are lattice sums for the fcc structure and d_0 is the distance of nearest neighbour.

The cohesive energy per atom corrected for the three-body interaction is then

$$E_{coh}/N = E'_{coh}/N + 8\Delta_{60} + 4\Delta_{90} + 8\Delta_{120} + 2\Delta_{180}. \quad \dots (9)$$

The value of ω calculated from eqn. (9) for inert gases are recorded in table I along with the force parameters (Sherwood and Prausnitz 1964) used in the calculation. The core-potential has been used due to its flexibility as shown by Barker (1964).

TABLE I

Gases	α^*	$\sigma \text{ \AA}$	$\epsilon / k^\circ K$	$d_0 \text{ \AA}$	$L_0 \text{ cal/mol}$	ω	$\frac{\Delta E_{coh}/N}{\phi_{ij}(\text{do})}$
Ar	0.125	3.314	147.2	3.756	1846	0.350	1.708
Kr	0.150	3.521	215.6	3.991	2666	0.400	1.679
Xe	0.175	3.878	298.8	4.335	3828	0.453	1.722

†Pollock, L., (1964) Rev. Mod. Phys., **36**, 748.

RESULTS AND DISCUSSION

In order to check the adequacy of eqn. (4), we have calculated the Debye characteristic temperature (Hirschfelder, Curtiss and Bird, 1954) given by

$$\theta_D(d_0) = \left(\frac{5}{3}\right)^{\frac{1}{2}} \frac{h\nu(d_0)}{k} \quad \dots (9)$$

where the fundamental frequency $\nu(d_0)$ for a molecule of mass m , moving in three-dimensional potential well corrected for three-body non-additive interaction on the core-potential is

$$\nu^2(d_0) = \frac{e}{\pi^2 m (\sigma - 2a)^2} \left[22(C_{14} - A) \left(\frac{\sigma - 2a}{d_0 - 2a} \right)^{14} - 5(C_8 - A) \left(\frac{\sigma - 2a}{d_0 - 2a} \right)^8 \right] \quad (10)$$

in which

$$A = \frac{\Delta E_{coh}/N}{\phi_{ij}(d_0)} \quad \dots (11)$$

The calculated and the experimental values of θ_D (Pollock, 1964) are given in Table II along with the values obtained on pair-potential ($A = 0$) and values determined from crystal properties (Singh and Barua, 1967). It can be seen from Table II that by considering three-body non-additive interaction the agreement between the experimental and the calculated values of θ_D becomes worse than that obtained on the pair-potential. However, no reliable quantitative conclusion on the three-body overlap forces based on the Jansen formulas which explain f.c.c. structure of inert gas solids with remarkable success, can be drawn from this simple analysis which shows a negative result (Table II). Recently, Bullough, Glyde, and Venables (1966) have measured the stacking fault energy in solid argon and have found it to be 1/15th of the value predicted by the Jansen formulas. It may be pointed out that the parameters for the pair-potential obtained from the crystal properties at 0°K represent the experimental θ_D value quite satisfactorily (Singh and Barua, 1967). This leads one to believe that the success of the additivity hypothesis may be due to an unexplained cancellation of the non-additive effects in the successive orders of the perturbation theory.

One of the best properties suitable for the study of non-additive interactions and which does not depend on more than three-body forces is the third virial coefficient of gases. In performing the theoretical calculation of the third virial coefficient $C(T)$, one must take into account of the following three types of three-body interactions;

- (a) the first-order triple overlap exchange interaction (Jansen, 1962),
- (b) the second-order single-overlap exchange interaction (Jansen and McGinnies 1956) and
- (c) the third-order triple-dipole interaction (Axilord and Teller, 1943).

The effect of the triple-dipole interaction on the third virial coefficient has been investigated by several workers (Koba, Kaneko and Kihara, 1956; Graben and Present 1962; Sherwood and Prausnitz 1964). In applying the Jansen formulas which include the interaction of types (a) and (b) to the theoretical calculation of non-additive third virial coefficient, Graben, Present and McCulloch (1966) find that Jansen's choice of the Gaussian parameter β is unreasonably large. The sensitive dependence of the non-additive correction to $C(T)$ on the parameter β limits the scope applying Jansen formulas as such in estimating the total non-additive effects in $C(T)$.

On the above arguments it seems that the Gaussian model and the Jansen formulas at best can be utilized to find a functional form of the non-additive correction of the types (a) and (b). In the present paper we have attempted in this direction and have found that the eqn. (4) which is independent of the parameter β is very close to the Jansen formulas.

TABLE II

Substance	Dobye Temp. ($^{\circ}$ K) at 0° K θ_{D0} calculated from			
	Dobye Temp. ($^{\circ}$ K) at 0° K θ_{D0} Exptl.	Pair- Potential	Three-body	Crystal Properties
Ar	93.3	67.7	62.3	94.1
Kr	71.7	52.7	48.6	72.4
Xe	55.0*	52.8	48.7	64.8

*This value is expected to be about 65° K. (Pollock 1964).

ACKNOWLEDGMENT

The authors wish to thank Prof. B. N. Srivastava, D.Sc., F.N.I., for his kind interest and encouragement.

REFERENCES

- Axilrod, B. M., 1951, *J. Chem. Phys.*, **19**, 719, 724.
 Axilrod, B. M., and Toller, E., 1943, *J. Chem. Phys.*, **11**, 299.
 Barker, J. A., Fock, W., and Smith, F., 1964, *Phys. Fluids*, **7**, 897.
 Bullough, R., Glyde, H. R., and Venable, J. A., 1966, *Phys. Rev. Letters*, **17**, 249.
 Graben, H. W., and Present, R. D., 1962, *Phys. Rev. Letters*, **9**, 247.
 Graben, H. W., Present, R. D., and McCulloch R. D., 1966, *Phys. Rev.*, **144**, 140.
 Hirschfelder, J. O., Curtiss, C. F., and Bird, R. B., 1964, *Molecular Theory of Gases and Liquids*, John Wiley & Sons, New York.
 Jansen, L., 1962, *Phys. Rev.*, **125**, 1798.

- Jansen, L., 1963, *Phys. Letters (Amsterdam)*, **4**, 91.
 Jansen, L., 1963, *Phil. Mag.*, **8**, 1305.
 Jansen, L., and McGinnies, R. T., 1956, *Phys. Rev.*, **104**, 961.
 Kihara, T., 1958, *Advances in Chemical Physics*, **1**, 267.
 Koba, S., Kaneko, S., and Kihara, T., 1956, *J. Phys. Soc., Japan*, **11**, 1050.
 Marganau, H., 1939, *Rev. Mol. Phys.*, **11**, 1.
 Midzuno, Y., and Kihara, T., 1956, *J. Phys. Soc., Japan*, **11**, 1045.
 Muto, Y., 1943, *Proc. Phys. Math. Soc., Japan*, **17**, 629.
 Rosen, P., 1953, *J. Chem. Phys.*, **21**, 1007.
 Sherwood, A. E., and Prusnitz, J. M., 1964, *J. Chem. Phys.*, **41**, 413, 429.
 Shostak, A., 1955, *J. Chem. Phys.*, **23**, 1808.
 Singh, Y., and Barua, A. K., 1967, *Indian J. Phys.* (to be published).

THERMAL CONDUCTIVITY OF SULPHURDIOXIDE AND DIETHYL ETHER AT DIFFERENT TEMPERATURES

A. DAS GUPTA

INDIAN ASSOCIATION FOR THE CULTIVATION OF SCIENCE,

CALCUTTA-32.

(Received October 18, 1966)

ABSTRACT. Thermal conductivity of sulphur dioxide and diethyl ether have been measured over the temperature range 39°-200.6°C with the help of thick-wire variant of the hot wire method. The observed data are in good agreement with the results obtained by earlier workers. Attempt has been made to interpret the observed data in the light of the recent theory developed by Mason and Monchick. It is found that relaxation phenomenon plays a significant role in the interchange of energy between translational and rotational degrees of freedom.

INTRODUCTION

Besides being of industrial and technological importance accurate measurements of thermal conductivity of polyatomic gases may serve as a source of information regarding the interchange of energy between internal and external degrees of freedom. Unlike monatomic gases which are devoid of internal motions, the heat conductivity of a polyatomic gas cannot be explained with the help of the classical theory. (Hirschfelder, Curtiss and Bird, 1954). The first attempt to take into consideration the transport of internal energy was made by Eucken (1913) according to whom,

$$\lambda M / \eta = f_{tr} C_{v_{tr}} + f_{int} C_{v_{int}} \quad \dots (1)$$

where λ = coefficient of thermal conductivity, η = coefficient of viscosity, M is the molecular mass, $C_{v_{tr}}$ and $C_{v_{int}}$ are the translational heat capacity and the internal heat capacity respectively. f_{tr} and f_{int} are the Eucken factors corresponding to the translational and internal degrees of freedom. For the noble gases f_{tr} was assigned a value 5/2 while from mean free path arguments f_{int} was taken to be equal to 1. Experiment, however, shows that f_{int} is temperature dependent for most of the polyatomic gases and varies from 0.7 to 1.3 over the temperature range 80°K — 380°K. It was suggested later by several workers that transport of internal energy takes place by some diffusion mechanism and f_{int} should be replaced by $\rho D / \eta$ where ρ is the gas density and D the self-diffusion coefficient. A more rigorous attempt to derive explicit expression for the thermal conductivity of polyatomic gases was made by Hirschfelder (1957) who considered the molecules in different quantum states as different chemical species. According

to him when the exchange of energy between translational and internal degrees of freedom is very fast so that a condition of local chemical equilibrium is maintained, one obtains the modified Eucken expression for the thermal conductivity of a polyatomic gas. Usually, however, for most of the polyatomic gases the condition of local chemical equilibrium is not maintained and it has been felt by several workers (Waelbroeck, and Zuckerbrodt, 1958; Srivastava and Barua, 1960) that some relationship must exist between thermal conductivity and the rate of exchange of energy between translational and the various internal degrees of freedom. The theory of heat conductivity therefore needs a better theoretical foundation so that it can be extended to the case of non-spherical molecules (both polar and nonpolar) undergoing inelastic collision.

Recently Mason and Monchick (1962) have derived explicit expressions for the thermal conductivity of both polar and non polar gases starting from the semi-classical theory of Wang Chang and Uhlenbeck (1964) and making some crude approximations. According to them in the case of nonpolar polyatomic gases a relaxation of energy transfer between translational and internal degrees of freedom affects the transport of heat energy. For polar gases, however, a second effect namely resonant exchange of energy between internal degrees of freedom plays a significant role. Mason and Monchick (1962) derived the following expressions for f_{tr} and f_{int} in the case of a polar gas;

$$f_{tr} = \frac{5}{2} \left[1 - \left(\frac{10}{3\pi} \right) \left(1 - \frac{2}{5} \frac{\rho D_{int}}{\eta} \right) \frac{1}{R} \sum \frac{C_k}{Z_k} \right] \quad \dots \quad (2)$$

$$f_{int} = \frac{\rho D_{int}}{\eta} \left[1 + \frac{5}{\pi} \left(1 - \frac{2}{5} \frac{\rho D_{int}}{\eta} \right) \frac{1}{C_{int}} \sum \frac{C_k}{Z_k} \right] \quad \dots \quad (3)$$

$$D_{int} = D[1 + Z'/Z_0]^{-1} \quad \dots \quad (4)$$

In the above expressions C_k is the heat capacity for the K -th internal mode and Z_k is the corresponding collision number. Z'/Z_0 is the correction due to the resonant exchange of internal energy. Generally, however, only the rotational modes are considered since Z is large for other modes. Finally the expression for the heat conductivity of a polar gas becomes,

$$\lambda M / \eta C_v = \frac{1}{C_v} \left[\frac{5}{2} C_{vtr} + \frac{\rho D_{int}}{\eta} C_{vint} - \frac{2}{\pi} \left(\frac{5}{2} - \frac{\rho D_{int}}{\eta} \right)^2 \frac{C_{rot}}{Z_{rot}} \right] = f_{M-M} \quad \dots \quad (5)$$

where f_{M-M} is the expression for Eucken factor according to Mason and Monchick's formulation.

In the present paper the observed thermal conductivity data have been utilised to determine the Z_{rot} values at different temperatures. In order to study the efficiency of transfer of translational as well as internal energies f_{tr} and f_{in} ,

values have been determined at different temperatures using the calculated values of Z_{rot} .

APPARATUS AND THEORY

In the present measurement the thick-wire variant of the hot-wire method has been utilised. The description of the conductivity cell has already been given in an earlier paper (Srivastava and Das Gupta, 1966). During experiment the cell was placed in oil bath whose temperature control was in general within $\pm 0.05^\circ\text{C}$. The constants of the cell used are given in Table I.

Gaseous Sulphurdioxide used in this experiment was prepared by the action of concentrated Sulphuric acid on Sodium sulphite. The gas was properly dried before use by passing it through Calcium Chloride. Gaseous diethyl ether was obtained by vaporizing chemically pure liquid ether.

The solution of the differential equation for the flow of heat along a wire has been shown by Kannuluik and Martin (1933, 1934) to be as follows,

$$f(\beta l) = (1/\beta l)^2 \left(1 - \frac{\tanh \beta l}{\beta l} \right) = \frac{2\pi r_1^2 \lambda J(R - R_0)}{R_0^2 I^2 \alpha l} \quad \dots (6)$$

$$\beta^2 = \frac{2h}{r_1 \lambda} - \frac{I^2 R_0 \alpha}{2\pi r_1^2 \lambda J l} \quad \dots (7)$$

$$h = \frac{K_u}{r_1 \ln(r_2/r_1)} \quad \dots (8)$$

where R is the resistance of the wire when a current I amp is flowing through it, R_0 is the resistance of the cell wire at the bath temperature for $I = 0$. K_u and λ are the thermal conductivities of the wire and the gas respectively.

In Table II a typical set of observations taken at 80.1°C for SO_2 and $(\text{C}_2\text{H}_5)_2\text{O}$ has been recorded. In this table K_u is the apparent thermal conductivity and K' is that obtained after reduction to the bath temperature and making correction for non-radial flow, radiation loss, temperature jump and wall effects. λ is the thermal conductivity obtained after correcting the mean value of K' for the assymetry in the cell construction by the relation $\lambda = K'(1-C)$. The factor $(1-C)$ was obtained by calibrating the cell with neon at 39° , 80° , 120.3° , 160.5° and 200.8°C taking the data of Kannuluik and Carman (1952) as standard. At every temperature the conductivity has been measured for three different currents and K_u values are found to agree within less than 1% on the average. The thermal conductivity values thus obtained are recorded in Table III. The variation of thermal conductivity with temperature has been shown graphically in Fig. 1. The results obtained for SO_2 and $(\text{C}_2\text{H}_5)_2\text{O}$ are found to be in good agreement with those obtained by Baker and De Haas (1964) and Vines and Bennett (1954) respectively.

TABLE I

Constants of thermal conductivity cell at different temperatures.

Constants/ $T^{\circ}\text{C} \rightarrow$	39	80	120.3	160.5	200.8
Thermal Conductivity ' λ ' of the wire in cal/cm. sec. $^{\circ}\text{C}$.	0.1670	0.1703	0.1731	0.1748	0.1756
Temperature coefficient of resistance ' α ' of the platinum wire in $^{\circ}\text{C}^{-1}$	0.00300	0.00264	0.00239	0.00217	0.00199
Resistance of the cell wire in ohms.	0.9705	1.0927	1.2081	1.3251	1.4416
Cell Constant (1-C)	.987	.985	.985	.985	.985
Length of the cell wire (2l)				6.290	cm.
Radius of the cell wire (r_1)				0.00506	cm.
Internal diameter of the cell ($2r_2$)				0.301	cm.
Outer diameter of the cell ($2r_3$)				0.590	cm.

TABLE II

Observations taken for the thermal conductivity in cal/cm.sec $^{\circ}\text{C}$ at 80.1 $^{\circ}\text{C}$

Substance	I in mA	(R-R ₀) in Ω	$K_u \times 10^5$	$K' \times 10^5$	$K'_{mean} \times 10^5$	$\lambda \times 10^5$
Sulphur dioxide	130.03	0.03178	0.032	2.908		
	129.29	0.03142	3.031	2.908	2.908	2.893
	128.25	0.03092	3.030	2.909		
Diethyl ether	127.23	0.01914	4.926	4.792		
	127.84	0.01928	4.938	4.803	4.804	4.774
	129.33	0.01967	4.956	4.818		

COMPARISON WITH THEORY

From eqn. (5) the expression for Z_{rot} becomes,

$$Z_{rot} = \frac{3}{\pi} \left(\frac{5}{2} - \frac{\rho D_{int}}{\eta} \right)^2 \frac{R}{C_v} \left[\frac{\rho D_{int}}{\eta} + \frac{3}{2} \left(\frac{5}{2} - \frac{\rho D_{int}}{\eta} \right) \frac{R}{C_v} - f_{M-M} \right]^{-1} \dots (9)$$

For the calculation of Z_{rot} from the above equation one must know the values of f_{M-M} , Z'/Z_0 , C_v and $\rho D/\eta$ at different temperatures. f_{M-M} occurring in the above expression has been replaced by f_{exp} ($= \lambda M/\eta C$) in the present calculation. The specific heats C_v for SO_2 and $(\text{C}_2\text{H}_5)_2\text{O}$ have been taken from the data of Lambert and Slater (1957) and Vines and Bennett (1954) respectively. It was shown by Baker and De Haas (1964) that for SO_2 Z'/Z_0 is very small and can be

neglected. There being no experimental data for the moment of inertia of diethyl ether, it is not possible to determine Z'/Z_0 in this case. This difficulty however, has been avoided by treating weakly polar diethyl ether as a nonpolar polyatomic gas for which D_{int} can be taken to be equal to D the self-diffusion coefficient.

For the calculation of $\rho D/\eta$ the force parameters on 12-6-3 potential given by Mason and Monchick (1961) have been utilised. The viscosity values for SO_2 have been taken from the recent measurements of Pal and Barua (1966) while for $(\text{C}_2\text{H}_5)_2\text{O}$ the data obtained by Craven and Lambert (1951) are utilised. The rotational collision numbers Z_{rot} thus determined have been recorded in column 4 of Table III. These values have been utilised to calculate f_{int} and f_{trans} using the equations (2) and (3).

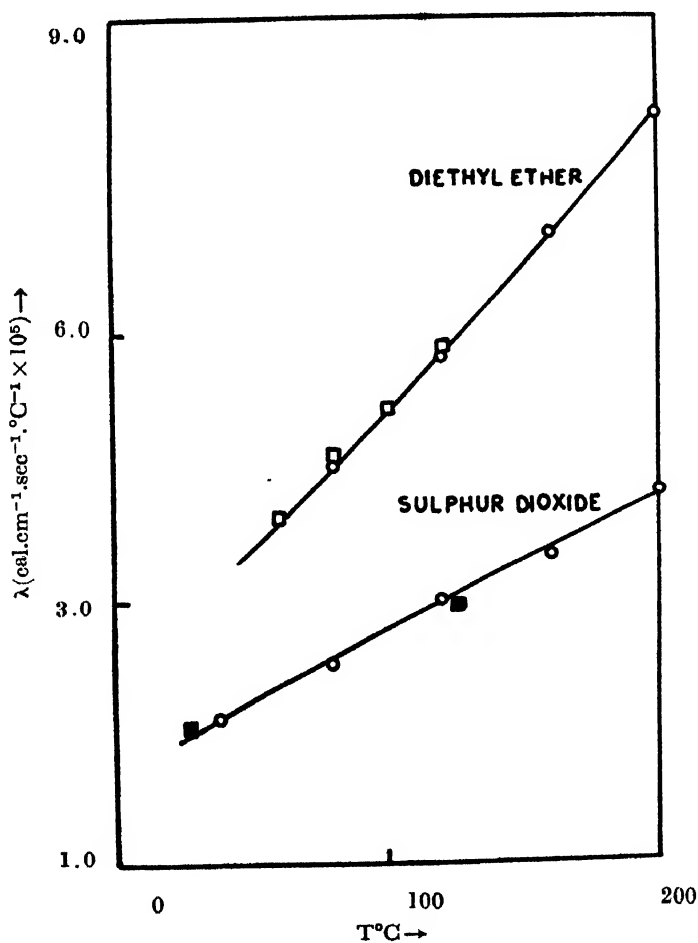


Fig. 1. O — Present Investigations.
 □ — Vines and Bennett (1954).
 Solid □ — Baker and De Haas (1964).

TABLE III

Rotational Collision number at different temperatures

Substance	T°C	$\lambda_{\text{expt}} \times 10$	Z_{rot}	f_{tr}	f_{int}
Sulphur dioxide	39.0	2.374	1.08	0.76	1.91
	80.1	2.893	1.13	0.84	1.80
	121.3	3.511	1.29	1.05	1.75
	161.1	3.989	1.49	1.24	1.67
	200.6	4.530	2.00	1.56	1.57
Diethyl ether	80.1	4.774	1.12	0.83	1.43
	120.2	5.806	1.36	1.13	1.40
	160.1	6.945	1.48	1.24	1.38
	200.1	8.095	1.56	1.30	1.37

DISCUSSION

It is evident from the present investigation that the Z_{rot} values obtained from the thermal conductivity measurements show an increase with temperature. This is, however, in accordance with the results obtained for Sulphur dioxide and ammonia by Baker *et al* (1964) and Srivastava and Das Gupta (1966) respectively. Recently Baker and Brokaw (1965) have obtained the reverse result regarding the temperature variation of Z_{rot} for a few polar gases including ammonia using thermal conductivity data. From the formulation of Mason and Monchick (1962) it appears that the rotational collision number is very much sensitive to thermal conductivity results. Hence a slight difference in the temperature dependence of thermal conductivity may yield an entirely different temperature variation for Z_{rot} . Recently, Zink, Bose and Itterbeck (1965, 1966) obtained a decrease in Z_{rot} values with the increase of temperature for Oxygen and Hydrogen-Helium systems, from ultrasonic measurements. In the case of polar gases however, no such experiments have yet been performed. For a polar gas it is rather difficult to predict anything regarding the temperature dependence of Z_{rot} since it involves long range dipole interaction which plays a significant role in energy interchange during collision. Moreover, the temperature variation of Z_{rot} for repulsive interaction is in the opposite direction from that for an attractive interaction. The different theories so far developed give conflicting results regarding the temperature dependence of rotational collision number. Therefore under the circumstances it appears that direct experiments are to be performed for polar gases over a wide range of temperature in order to get some idea about the temperature dependence of translational-rotational energy exchange.

From Table III it can be seen that f_{tr} values increase with the increase of temperature for both the gases whereas f_{int} shows a decrease. This implies that at high temperature the efficiency of translation-rotation energy interchange is reduced. Vines and Bennett (1954) however observed an increase of f_{int} with temperature for some polar and nonpolar polyatomic gases. They attached more importance to the translational-vibrational energy exchange which is usually significant at appreciably high temperatures. At moderate temperature, however the translational-rotational energy exchange plays a more prominent role. Moreover, in the treatment of Vines and Bennett (1954) there was no scope for taking into account the relaxation phenomena in the interchange of energy between external and internal degrees of freedom.

ACKNOWLEDGMENT

The author is thankful to Prof. B. N. Srivastava for his guidance and kind interest in the work.

REFERENCES

- Baker, C. B., and de Haas, N., 1964, *Phys. Fluids*, **7**, 1400.
 Baker, C. B., and Brokaw, R. S., 1965, *J. Chem. Phys.*, **43**, 3519.
 Craven, P. M., and Lambert, J. D., 1951, *Proc. Roy. Soc. (London)*, **A 205**, 439.
 Eucken, A., 1913, *Z. Physik*, **14**, 324.
 Hirschfelder, J. O., Curtiss, C. F., and Bird, R. B., 1954, *Molecular Theory of Gases and Liquids*, John Wiley & Sons, Inc., New York.
 Hirschfelder, J. O., 1957, Sixth Symposium (International) on Combustion. (Reinhold Publishing Corporation, New York), p. 361.
 Kannuluik, W. G., and Martin, L. H., 1933, *Proc. Roy. Soc. (London)*, **A 141**, 144; *ibid*, 1934, **A 144**, 496.
 Kannuluik, W. G., and Carman, E. A., 1952, *Proc. Phys. Soc.*, **B65**, 701.
 Lambert, J. D., and Slater, R., 1957, *Proc. Roy. Soc. (London)*, **A 243**, 78.
 Mason, E. A., and Monchick, L., 1962, *J. Chem. Phys.*, **36**, 1622.
 Monchick, L., and Mason, E. A., 1961, *J. Chem. Phys.*, **35**, 1676.
 Pal, A., and Barua, A. K., 1966, *Trans. Faraday Soc.*, **63**, 341.
 Srivastava, B. N., and Barua, A. K., 1960, *J. Chem. Phys.*, **32**, 427.
 Srivastava, B. N., and Das Gupta, A., 1966, *Phys. Fluids*, **9**, 722.
 Vines, R. G., and Bennett, L. A., 1954, *J. Chem. Phys.*, **22**, 360.
 Waelbroeck, F. G., and Zuckerbrodt, P., 1958, *J. Chem. Phys.*, **30**, 524.
 Wang Chung, C. S., Uhlenbeck, G. E., and de Boer, J., 1964, *Studies in Statistical Mechanics* (North Holland Publishing Company, Amsterdam), Vol. II, 249.
 Zink, H., Bose, T. K., and Itterbeck, A., 1965, *Phys. Letters*, **16**, 34.
 ———, 1966, *Phys. Letters*, **19**, 642.

CONTRIBUTION OF BOUND DOUBLE MOLECULES TO THE SECOND VIRIAL COEFFICIENT OF POLAR GASES

YASHWANT SINGH, ANIL SARAN AND A. K. BARUA

INDIAN ASSOCIATION FOR THE CULTIVATION OF SCIENCE,
CALCUTTA-32, INDIA.

(Received October, 18, 1966)

ABSTRACT. The contribution of the bound double molecules to the second virial coefficient $B(T)$ has been calculated for the polar gases. The calculation is valid for any 'effective' relative orientation between the dipoles of the two interacting molecules and is an improvement over the one made previously by Barua, Chakraborti and Saran.

I N T R O D U C T I O N

Due to the presence of long-range, angle-dependent, dipole-dipole forces, it is difficult to represent the intermolecular potential between two polar molecules in a suitable functional form. At present, the most commonly used potential energy function, the Stockmayer potential can be represented as :

$$\phi(r) = 4\epsilon[(\sigma/r)^{12} - (\sigma/r)^6] - \frac{\mu^2}{r^3} g(\theta_1, \theta_2, \phi), \quad \dots (1)$$

$$g(\theta_1, \theta_2, \phi) = 2 \cos \theta_1 \cos \theta_2 - \sin \theta_1 \sin \theta_2 \cos \phi, \quad \dots (2)$$

where μ is the dipole moment, θ_1 and θ_2 are the angles of inclination of the axes of the two dipoles to the line joining the centres of the molecules and ϕ is the azimuthal angle. When $\mu \rightarrow 0$, $\phi(r)$ is the commonly used Lennard-Jones (12 : 6) potential (Hirschfelder, Curtiss and Bird 1954) for nonpolar molecules.

The classical statistical expression for the second virial coefficient can be written as :

$$B(T) = \frac{N}{4} \int_0^\infty \int_\Omega (1 - e^{-\phi(r)/kT}) r^2 dr d\Omega \quad \dots (3)$$

where

$$\int_\Omega = \int_0^\pi \int_0^{2\pi} \int_0^{2\pi} \sin \theta_1 \sin \theta_2 d\theta_1 d\theta_2 d\phi \quad \dots (4)$$

Stockmayer (1941) and Rowlinson (1949) evaluated $B(T)$ for the polar gases from eqs. (1) and (3) by assuming equal probability for all the relative orientations of the dipoles of the interacting molecules.

Fortunately, physically more understandable and rigorous approach to the problem of calculating $B(T)$ can be achieved by breaking up $B(T)$ into three parts (Stogryn and Hirschfelder 1959) :

$$B(T) = B_f(T) + B_b(T) + B_m(T), \quad \dots (5)$$

where $B_f(T)$, $B_b(T)$ and $B_m(T)$ are respectively, the contributions of the free, bound and metastably bound double molecules to the second virial coefficient $B(T)$.

$B_b(T)$ and $B_m(T)$ are related to the equilibrium constant for dimerization. Recently Barua, Chakraborti and Saran (1965) have evaluated $B_b(T)$ mainly with the purpose of calculating the percentage of dimers in polar gases. In order to simplify the calculations, they have made certain approximations in evaluating the integrals. However, to calculate $B(T)$ accurately from eq. (5), all the parts should be calculated precisely. In the present paper we have made a refined calculation of $B_b(T)$.

OUTLINE OF FORMULATION

It has been recently pointed out by Semenov (1966) that the classical mechanics is not strictly valid in the range of states corresponding to bound particles where the Schrödinger equation allows only a number of discrete energy levels. Following his treatment the contribution of bound states to the second virial coefficient may be written as :

$$B_{q \text{ bound}} = -2^{3/2} N \lambda^{3/2} Z_q, \quad \dots (6)$$

where $B_{q \text{ bound}}$ includes the contribution of stable double molecules and

$$Z_q = \sum_{\rho} e^{-E_{\rho}^-/kT} = \sum_l (2l+1) \sum_n e^{-E_{nl}/kT}, \quad \dots (7)$$

where E_{ρ}^- is the energy of the bound particles, n and l are respectively the vibrational and rotational quantum numbers.

It is well known that the methods of classical statistical mechanics are applicable to the evaluation of the partitions function provided $\Delta E \ll kT$, where ΔE is the energy difference between two neighbouring quantum states of a system. The extensive study made by Stogryn and Hirschfelder (1959) and their evaluation of the maximum number of vibrational levels lead us to conclude that for heavy molecules (i.e. molecules except H_2 , He and Ne) and at not too low temperatures the difference between the classical and the quantum methods is insignificant. In the present paper we have followed the method of Hill (1955) applying classical statistical mechanics for obtaining the partition function for the bound double molecules.

For spherically symmetric potentials :

$$B_b(T) = -N\Lambda^3 Q_{2b}/V, \quad \dots (8)$$

where N is Avogadro's number, V is the volume, $\Lambda^3 = \frac{h^3}{2\pi m kT}$ and Q_{2b} is the partition function for bound double molecules. Following Hill (1955)

$$Q_{2b} = \frac{V}{2\Lambda^6} \int_{\phi(r) \leq 0}^{\infty} \exp [-\phi(r)/kT] 4\pi r^2 F(r) dr, \quad \dots (9)$$

where

$$F(r) = \frac{\Gamma\left\{\frac{3}{2}, -\frac{\phi(r)}{kT}\right\}}{\Gamma\left(\frac{3}{2}\right)}$$

From eqs. (9) and (10) one gets :

$$B_b(T) = -2\pi N \int_d^{\infty} r^2 \exp [-\phi(r)/kT] \left[\frac{\Gamma\left(\frac{3}{2}, -\frac{\phi(r)}{kT}\right)}{\Gamma\left(\frac{3}{2}\right)} \right] dr, \quad \dots (10)$$

where $\Gamma\left\{\frac{3}{2}, -\frac{\phi(r)}{kT}\right\}$ is incomplete gamma function and d is the value of r for which $\phi(r) = 0$.

The potential energy function given by eq. (1) can be written as :

$$\phi(r) = 4\epsilon[(\sigma/r)^{12} - (\sigma/r)^6 - A(\sigma/r)^3], \quad \dots (11)$$

where

$$A = \frac{\mu^2}{4\epsilon\sigma^3} g. \quad \dots (11a)$$

Let us define the following reduced quantities :

$$\phi^* = \phi/\epsilon, \quad r^* = r/\sigma, \quad T^* = kT/\epsilon,$$

$$d^* = d/\sigma, \quad B_b^* = B_b/b_0; \quad b_0 = \frac{2}{3}\pi N\sigma^3 \quad \dots (12)$$

In terms of the reduced quantities eq. (10) becomes :

$$B_b^*(T^*) = -3 \int_{d^*}^{\infty} r^{*2} \exp[-\phi^*/T^*] \left[\frac{\Gamma\left\{\frac{3}{2}, -\frac{\phi^*}{T^*}\right\}}{\Gamma\{3/2\}} \right] dr^* \quad \dots (13)$$

By applying certain mathematical transformations (Barua, Chakraborti and Saran 1965), we can obtain :

$$B_b^*(T^*) = -\frac{2}{\Gamma(3/2)} \sum_{n=0}^{\infty} \frac{\Gamma(1+n) \Gamma(5/2)}{\Gamma(1) \Gamma(\frac{5}{2}+n)} \cdot \frac{1}{n!} \int_{d^*}^{\infty} r^{*2} (-\phi^*/T^*)^{n+3/2} dr^* \quad (14)$$

Substituting the value of $\phi^*(r^*)$ from eq. (11) and putting $y = r^{*-3/2}$, the integral in eq. (14) reduces to :

$$\int_{d^*}^{\infty} r^{*2} (-\phi^*/T^*)^{n+3/2} dr^* = \left(\frac{4}{T^*} \right)^{n+3/2} \int_0^{y'} y^{2n} [A + y^2 - y^6]^{n+3/2} dy, \quad \dots (15)$$

where

$$y' = d^{*-3/2}.$$

Thus, finally we get :

$$B_b^*(T^*, A) = -\frac{16}{\pi^{\frac{1}{2}}} \sum_{n=0}^{\infty} \frac{4^{2n+3/2} \cdot (n+1)!}{(2n+3)!} \left(\frac{1}{T^*} \right)^{n+3/2} \times \int_0^{y'} y^{2n} [A + y^2 - y^6]^{n+3/2} dy. \quad \dots (16)$$

TABLE I

A	0.00	0.2	0.4	0.6	0.8	1.0	1.2	1.4	1.6
y'	1.000	1.043	1.077	1.105	1.129	1.151	1.170	1.188	1.204

TABLE II
Calculated values of $-B_0^*(T^*)$ for polar gases

T^*/A	0.0	0.2	0.4	0.6	0.8	1.0	1.2	1.4	1.6
0.4	10.7306	47.23870							
0.5	6.3247	23.38052	71.15254						
0.6	4.2679	14.37019	38.25175	96.16479					
0.7	3.1223	9.92758	24.32324	54.55975	124.03463				
0.8	2.4100	7.37405	17.09987	35.57824	73.54680				
0.9	1.9325	5.75356	12.83463	25.35370	47.99361	91.08378			
1.0	1.5940	4.65067	10.08723	19.18720	35.28832	61.82270	111.32201	198.62868	
1.25	1.0738	3.03080	6.28213	11.26657	19.15420	30.62958	49.29003	77.10798	129.76167
1.50	0.7857	2.17413	4.38854	7.61352	12.37489	18.83764	28.47653	41.49753	64.07642
1.75	0.6068	1.67673	3.28697	5.58409	8.82081	13.03356	18.96257	26.51244	38.72684
2.0	0.4868	1.31687	2.58136	4.32312	6.69729	9.70462	13.76776	18.75540	26.38593
2.5	0.3398	0.90538	1.74713	2.87350	4.34342	6.14638	8.45703	11.18268	15.02094
3.0	0.2531	0.67103	1.28240	2.08627	3.10745	4.33752	5.86431	7.63022	9.98015
4.0	0.1608	0.42242	0.79816	1.28250	1.87901	2.58373	3.42763	4.38600	5.57704
5.0	0.1135	0.29671	0.55707	0.88907	1.29102	1.76101	2.31315	2.93477	3.67862
10.0	0.0391	0.10120	0.18773	0.29594	0.42301	0.56881	0.73452	0.91818	1.12434

METHOD OF CALCULATION

The upper limit in the integral of eq. (16) is a function of A and can be calculated for a fixed value of A (which corresponds to an 'effective' relative orientation of the interacting dipoles) from the equation $\phi(y') = 0$. The values of y' for the different values of A are given in Table I. Recently Barua *et al*, (1965) have evaluated the integral by putting an average value of y within the bracket of eq. (15) so that for $A = 0$ each term in eq. (14) is equal to the corresponding term in the expression for the Lennard-Jones (12 : 6) potential (Stogryn and Hirschfelder 1959). With this approximation they obtained :

$$[\bar{y}_n^2 - \bar{y}_n^6]^{n+3/2} = \frac{4^n \cdot n! (2n+2)! (2n+3)! (2n+1)!}{(4n+5)! (n+1)!} \quad \dots (17)$$

As a further approximation, they had taken the upper limit of the integral as unity so that the eq. (16) reduces to

$$\begin{aligned} \int_{d^*}^{\infty} r^{*2} (-\phi^*/T^*)^{n+3/2} dr^* &= \int_1^{\infty} r^{*2} (-\phi^*/T^*)^{n+3/2} \cdot dr^* \\ &= \frac{2}{3} \left[\frac{4(A + \bar{y}_n^2 - \bar{y}_n^6)}{T} \right]^{n+3/2} \cdot \frac{1}{2n+1} \cdot \quad \dots (18) \end{aligned}$$

As the main purpose of Barua *et al* (1965) was to obtain the percentage of dimers for polar gases needed for the study of pressure dependence of transport properties, they were justified in making these approximations in order to simplify the calculations. However, as the main contribution to the total second virial coefficient $B(T)$, $B_v(T)$ must be evaluated precisely.

The summation in eq. (16) converges very rapidly for higher reduced temperatures and lower values of A . Otherwise, the convergence is slow and a large number of terms are needed in the series to obtain an accuracy of five significant figures. The integral of each term in the series of eq. (16) was divided into three equal intervals and for each interval a nine-point Gaussian integration was done. $B_v^*(T^*)$ has been calculated for T^* , ranging from 0.4 to 10 and for the values of A from 0 to 1.6 and are given in Table 2. We estimate the accuracy to be generally of the order of 0.01% and this is indicated by the good agreement with the results obtained by Stogryn and Hirschfelder (1959) for the Lennard-Jones (12:6) model (i.e. for $A = 0$).

ACKNOWLEDGMENT

The authors are grateful to Prof. B. N. Srivastava for his kind interest and encouragement.

REFERENCES

- Barua, A. K., Chakraborti, P. K. and Saran, A., 1965, *Mol. Phys.*, **9**, 9.
- Hirschfelder, J. O., Curtiss, C. F. and Bird, R. B., 1954, *Molecular Theory of Gases and Liquids*, John Wiley & Sons, Inc, New York.
- Hill, T. L., 1955, *J. Chem. Phys.*, **23**, 617.
- Hill, T. L., 1956, *Statistical Mechanics*, McGraw-Hill Book Co., Inc., New York.
- Rowlinson, J. S., 1949, *Trans. Faraday Soc.*, **45**, 974.
- Stockmayer, W. H., 1941, *J. Chem. Phys.*, **9**, 308.
- Stogryn, D. E. and Hirschfelder, J. O., 1959, *J. Chem. Phys.*, **31**, 1531.
- , 1960, *J. Chem. Phys.*, **33**, 942.
- Semenov, A. M., 1966, *High Temperature*, **3**, 598.

ON THE TEMPERATURE DISTRIBUTION OF A VISCOUS IN-COMPRESSIBLE FLUID IN A CIRCULAR PIPE UNDER UNSTEADY RATE OF HEAT ADDITION

S. N. DUBE

MATHEMATICS SECTION, ENGINEERING COLLEGE,
B. H. U., VARANASI-5, (INDIA)

(Received October 12, 1966; Resubmitted January 9, 1967)

ABSTRACT. In the present paper expressions for the temperature distributions in a circular pipe are derived when viscous incompressible fluid is flowing through it. The term of dissipation due to friction is not neglected and the rate of heat addition (i) varies linearly with time, and (ii) decreases exponentially with time. The difference in the temperature distribution introduced by the inclusion of the dissipation term has also been discussed.

INTRODUCTION

This paper consists of two parts. In Part A the temperature distribution in a circular pipe when viscous incompressible fluid is flowing through it with the rate of heat addition varying linearly with time is discussed. An expression for the temperature distribution is obtained in dimensionless form. This consists of two parts, the one varies linearly with dimensionless time Fourier modulus

$T_1 = \frac{k't}{R^2} (R \text{ radius})$ and the other is transient part of temperature, which vanishes in the limit as t tends to infinity. It is also seen that the contribution of the transient part is insignificant when $T_1 > 1$.

In part B the temperature distribution in the same pipe is studied when viscous incompressible fluid is flowing through it with the rate of heat addition decreasing exponentially with time. An expression for the temperature has been obtained taking

$$\frac{1}{\rho c_v} \frac{\partial Q}{\partial t} = \sum_{n=1}^{\infty} a_n e^{-n t},$$

which has been compared with that of Lal's result (1964) where he has obtained the expression by neglecting the dissipation term. Our expression contains some additional terms and the reason for this has been discussed. The result is in complete agreement with similar results obtained by Ballabh (1959) and Snnedon (1951) where Ballabh has obtained the expression for the velocity by using the method of superposability and Snnedon has discussed the heat flow under exponentially decreasing temperature gradient.

Here the expressions for the temperature distributions in both the parts are derived with the conditions that the surface $r = R$ (i) has zero initial temperature and (ii) is always being kept at zero temperature.

1. The energy equation (Pai, 1956) in the present case is

$$\frac{\partial T}{\partial t} = \frac{1}{\rho c_v} \frac{\partial Q}{\partial t} + k' \left(\frac{\partial^2 T}{\partial r^2} + \frac{1}{r} \frac{\partial T}{\partial r} \right) + cr^2, \quad \dots \quad (1.1)$$

where $k' = \frac{k}{\rho c_v}$ and $c = \frac{4\mu u_m^2}{\rho c_v R^4}$ are constants, and u_m represents the maximum velocity in the pipe. The last term in the equation (1.1) is dissipation due to friction and is not neglected in the present investigation.

PART A

2. Rate of heat addition varies linearly with time.

We, therefore, assume that

$$\frac{1}{\rho c_v} \frac{\partial Q}{\partial t} = at. \quad (2.1)$$

Equation (1.1) then becomes

$$\frac{\partial T}{\partial t} = at + k' \left(\frac{\partial^2 T}{\partial r^2} + \frac{1}{r} \frac{\partial T}{\partial r} \right) + cr^2. \quad (2.2)$$

Now let $\bar{T} = \int_0^\infty e^{-st} T dt$ be the Laplace transform of T and let T_0 be the initial value of T .

Multiplying equation (2.2) by e^{-st} and integrating between the limits 0 to ∞ , we get

$$\frac{\partial^2 \bar{T}}{\partial r^2} + \frac{1}{r} \frac{\partial \bar{T}}{\partial r} - \frac{s}{k'} \bar{T} = -\frac{1}{k'} \left(T_0 + \frac{cr^2}{s} + \frac{a}{s^2} \right). \quad \dots \quad (2.3)$$

Equation (2.3) can be solved by the method of variation of parameter and we get the solution as

$$\bar{T} = AI_0(rp) + BK_0(rp) + \phi(r, s), \quad \dots \quad (2.4)$$

where $p = \sqrt{\frac{s}{k'}}$, and

$$k' \phi(r, s) = K_0(rp) \int \left(T_0 + \frac{cr^2}{s} + \frac{a}{s^2} \right) \cdot I_0(rp) \cdot r dr \\ - I_0(rp) \int \left(T_0 + \frac{cr^2}{s} + \frac{a}{s^2} \right) \cdot K_0(rp) \cdot r dr.$$

Now we shall find T_0 .

Initially the rate of heat addition is zero and the temperature is steady in the pipe.

$$\text{Hence } \frac{\partial T_0}{\partial t} = 0 \text{ and we obtain } \frac{d^2 T_0}{dr^2} + \frac{1}{r} \frac{dT_0}{dr} = -\frac{c}{k'} r^2 \quad (2.5)$$

The boundary conditions are

$$T_0 = \text{finite when } r = 0$$

$$\text{and } T_0 = 0 \text{ when } r = R.$$

The solution of equation (2.5) under these boundary conditions is

$$T_0 = \frac{c}{16k'} (R^4 - r^4).$$

Substituting this value of T_0 in the expression for $\phi(r, s)$ and using certain recurrence relations of Bessel functions, we obtain

$$\phi(r, s) = \frac{c}{16k'} \left(\frac{R^4 - r^4}{s} \right) + \frac{a}{s^3}.$$

Then

$$\bar{T} = AI_0(rp) + BK_0(rp) + \frac{C}{16k'} \left(\frac{R^4 - r^4}{s} \right) + \frac{a}{s^3}. \quad (2.6)$$

The boundary conditions for \bar{T} are

$$\bar{T} = \text{finite when } r = 0$$

$$\text{and } \bar{T} = 0 \text{ when } r = R.$$

Applying these boundary conditions, we get

$$\bar{T} = \frac{C}{16k'} \left(\frac{R^4 - r^4}{s} \right) + \frac{a}{s^3} - \frac{a}{s^3} \cdot \frac{J_0(irp)}{J_0(iRp)}.$$

Now applying Laplace inversion theorem, we obtain

$$\begin{aligned} T = & \frac{C}{16k'} (R^4 - r^4) + \frac{1}{4k'} (R^2 - r^2) at - \frac{a}{64k'^2} (3R^2 - r^2)(R^2 - r^2) \\ & + 2a \sum_{m=1}^{\infty} \frac{R^4}{k'^2 \alpha_m^6} \cdot \frac{J_0\left(\frac{r\alpha_m}{R}\right)}{J_1(\alpha_m)} \cdot e^{-\frac{k'\alpha_m^2 t}{R^2}} \end{aligned} \quad (2.7)$$

where α_m are the positive roots of $J_0(\alpha) = 0$

At time $t = 0$, $T = \frac{C}{16k'} (R^4 - r^4)$. Hence from equation (2.7) by putting

$$t = 0, \text{ we get } \sum_{m=1}^{\infty} \frac{J_0\left(\frac{r\alpha_m}{R}\right)}{\alpha_m^5 J_1(\alpha_m)} = \frac{1}{128} \left(3 - \frac{r^2}{R^2}\right) \left(1 - \frac{r^2}{R^2}\right).$$

Writing $r/R = \eta$ so that η is less than 1, we get

$$\sum_{m=1}^{\infty} \frac{J_0(\eta\alpha_m)}{\alpha_m^5 J_1(\alpha_m)} = \frac{1}{128} (3 - \eta^2)(1 - \eta^2).$$

Putting $\eta = 0$, we get

$$\sum_{m=1}^{\infty} \frac{1}{\alpha_m^5 J_1(\alpha_m)} = \frac{3}{128}.$$

Now we make equation (2.7) dimensionless by introducing

$$\tau = \frac{T}{\theta}, \quad \frac{r}{R} = \eta, \quad T_1 = \frac{k't}{R^2},$$

where θ is a characteristic temperature.

We then get

$$\begin{aligned} \tau = b_0(1 - \eta^4) + bT_1(1 - \eta^2) - \frac{b}{16} (3 - \eta^2)(1 - \eta^2) \\ + 8b \sum_{m=1}^{\infty} \frac{1}{\alpha_m^5} \cdot \frac{J_0(\eta\alpha_m)}{J_1(\alpha_m)} \cdot e^{-\alpha_m^2 T_1}, \quad \dots \quad (2.8) \end{aligned}$$

where $b_0 = \frac{cR^4}{16k'\theta}$ and $b = \frac{aR^4}{4k'\theta}$ are clearly dimensionless numbers.

We now take

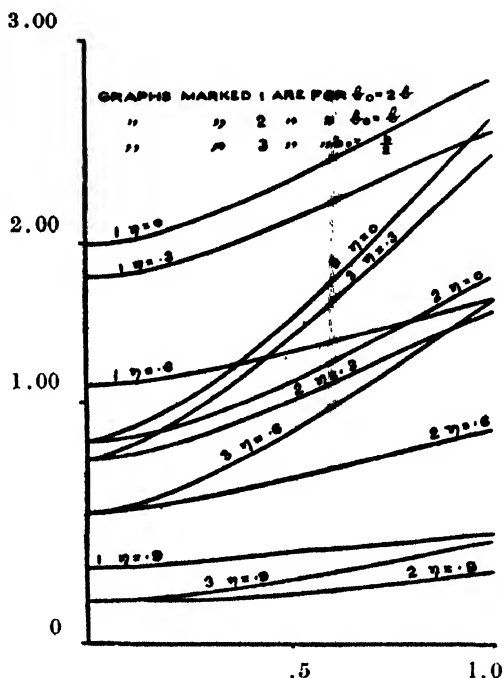
$$\tau = \tau_1 + \tau_2, \quad \text{where}$$

$$\tau_1 = b_0(1 - \eta^4) + bT_1(1 - \eta^2) - \frac{b}{16} (3 - \eta^2)(1 - \eta^2),$$

and

$$\tau_2 = 8b \sum_{m=1}^{\infty} \frac{1}{\alpha_m^5} \cdot \frac{J_0(\eta\alpha_m)}{J_1(\alpha_m)} \cdot e^{-\alpha_m^2 T_1}$$

The graphs for fixed η ($\eta = 0, 0.3, 0.6, 0.9$) showing the variation of τ with the parameter T_1 (dimensionless time Fourier modulus) have been drawn in three cases $b = 1, b_0 = 1$; $b = 2, b_0 = 1$; and $b = 1, b_0 = 2$ in the range $T_1 = 0$ to $T_1 = 1$.



Graph showing variation of τ with T_1

The graphs beyond $T_1 = 1$ have not been drawn because τ_2 is very small compared to τ_1 when $T_1 > 1$, hence the transient part is insignificant and τ varies linearly with T_1 in this range. From the graphs it is observed that τ increases with T_1 for fixed η . It is also seen that for any T_1 , τ decreases with the increase of η and it is maximum when $\eta = 0$. It means that points near the axis of the cylinder are having more temperature than the points which are far from the axis of the cylinder.

PART B

3. Rate of heat addition decreases exponentially with time.

We assume that
$$\frac{1}{\rho c_v} \frac{\partial Q}{\partial t} = \sum_{n=1}^{\infty} a_n e^{-n t} \quad (3.1)$$

Equation (1.1) then becomes

$$\frac{\partial T}{\partial t} = \sum_{n=1}^{\infty} a_n e^{-n t} + k' \left(\frac{\partial^2 T}{\partial r^2} + \frac{1}{r} \frac{\partial T}{\partial r} \right) + c r^2 \quad (3.2)$$

Let $\bar{T} = \int_0^{\infty} e^{-s t} \cdot T dt$ be the Laplace transform of T and let T_0 be the initial value of T .

Multiplying equation (3.2) by e^{-st} and integrating between the limits 0 to ∞ , we get

$$\frac{\partial^2 \bar{T}}{\partial r^2} + \frac{1}{r} \frac{\partial \bar{T}}{\partial r} - \frac{s}{k'} \bar{T} = -\frac{1}{k'} \left[T_0 + \frac{cr^2}{s} + \sum_{n=1}^{\infty} \frac{a_n}{(s+n)} \right].$$

The above equation can be solved by the method of variation of parameter and we get the solution as

$$\bar{T} = AI_0(rp) + BK_0(rp) + \phi(r, s), \quad \dots (3.3)$$

where

$$p = \sqrt{\frac{s}{k'}}, \quad \text{and}$$

$$\begin{aligned} k' \cdot \phi(r, s) = & K_0(rp) \int \left[T_0 + \frac{cr^2}{s} + \sum_{n=1}^{\infty} \frac{a_n}{(s+n)} \right] I_0(rp) \cdot r dr \\ & - I_0(rp) \int \left[T_0 + \frac{cr^2}{s} + \sum_{n=1}^{\infty} \frac{a_n}{(s+n)} \right] K_0(rp) \cdot r dr. \end{aligned}$$

Here $T_0 = \frac{c}{16k'} (R^4 - r^4)$ as obtained in Part A.

Substituting this value of T_0 in the expression for $\phi(r, s)$ and using certain recurrence relations of Bessel functions, we get

$$\phi(r, s) = \frac{c}{16k'} \left(\frac{R^4 - r^4}{s} \right) + \sum_{n=1}^{\infty} \frac{a_n}{s(s+n)}.$$

Then

$$\bar{T} = AI_0(rp) + BK_0(rp) + \frac{C}{16k'} \left(\frac{R^4 - r^4}{s} \right) + \sum_{n=1}^{\infty} \frac{a_n}{s(s+n)}. \quad \dots (3.4)$$

Applying the previous boundary conditions, we get

$$\bar{T} = \frac{C}{16k'} \left(\frac{R^4 - r^4}{s} \right) + \left[1 - \frac{J_0(irp)}{J_0(iRp)} \right] \sum_{n=1}^{\infty} \frac{a_n}{s(s+n)}. \quad \dots (3.5)$$

Now applying Laplace inversion theorem, we get

$$\begin{aligned} T = & \frac{c}{16k'} (R^4 - r^4) - \sum_{n=1}^{\infty} \frac{a_n}{n} \left[1 - \frac{J_0 \left\{ r \left(\frac{n}{k'} \right)^{\frac{1}{2}} \right\}}{J_0 \left\{ R \left(\frac{n}{k'} \right)^{\frac{1}{2}} \right\}} \right] e^{-nt} \\ & + 2 \sum_{n=1}^{\infty} \sum_{m=1}^{\infty} \frac{a_n}{\alpha_m \left[n - \frac{k' \alpha_m^2}{R^2} \right]} \cdot \frac{J_0 \left(\frac{r \alpha_m}{R} \right)}{J_1(\alpha_m)} \cdot e^{-\frac{k' \alpha_m^2 t}{R^2}} \\ & = T_1' + T_2' + T_3' \quad \dots (3.6) \end{aligned}$$

This expression for temperature does not agree with Lal's result (1964). His expression for the temperature with the present boundary conditions does not contain T_1' and T_3' because he has solved the energy equation by neglecting the dissipation term and by assuming

$$T = \sum_{n=1}^{\infty} T_n(r)e^{-nt},$$

where T_n is a function of r only whereas in our case the dissipation term has not been neglected. Our expression (3.6) for the temperature is in complete agreement with similar results obtained by Ballabh (1959) and Sneddon (1951). Ballabh (1959) in his paper has obtained the expression for the velocity by using the method of super-possibility and Sneddon (1951) has discussed the heat flow under exponentially decreasing temperature gradient.

Hence $T_1' + T_2' + T_3'$ is a more general solution of equation (1.1) and has been confirmed by Laplace Transform method.

A C K N O W L E D G M E N T

In the end, I wish to express my thanks to Dr. H. L. Agarwal for his valuable guidance in the preparation of this paper.

R E F E R E N C E S

- Ballabh, R., 1959, *Proc. of V Congress on Theo. and Appl. Mech India*.
 Goldstein, S., 1938, *Modern Developments in Fluid Dynamics*, Clarendon Press, Vol. II, Section 266.
 Lal, K., 1964, *Proc. Comb. Phil. Soc.*, **60**, 653.
 Lighthill, M. J., 1953, *Quart. J. Mech. Appl. Math.*, **6**, 398.
 McLachlan, N. W., 1934, *Bessel Functions for Engineers*, Clarendon Press.
 Pai, S., 1956, *Viscous Flow Theory, I-Laminar Flow*, D. Van Nostrand Company, Inc., 43.
 Sneddon, I. N., 1951, *Fourier Transform*, McGraw Hill Book Co., Inc.

CLASSICAL THEORIES OF DIELECTRIC CONSTANTS

C. M. KACHHVA AND S. C. SAXENA*

PHYSICS DEPARTMENT, RAJASTHAN UNIVERSITY, JAIPUR, INDIA

(Received October 14, 1966)

ABSTRACT. The equivalence of the two classical theories of dielectric constant one due to Mott and Gurney and the other due to Szigeti is discussed and established. This consists in the suggestion to identify the effective charge of the ion in the Szigeti's model with a factor in the theory of Mott and Gurney which determines the degree to which the neighbouring ions overlap. The effective charge of the different alkali halide crystals has been recalculated on the basis of the first relation of Szigeti employing the more recent data for dielectric constants and Reststrahlen frequency. The second relation is employed to compute compressibility and these are compared with the latest experimental data. Our interpretation of the Szigeti's theory also permits the calculation of low frequency dielectric constant from its first relation. We also discuss a procedure for evaluating infrared polarizability values from the basic knowledge of interatomic forces. Lastly, we correct and complete some of the earlier reported results, (Kachhava *et al.* 1966) on the theory of Mott and Gurney.

INTRODUCTION

We (1966) recently discussed the possibility of calculating the dielectric constant through the knowledge of interatomic forces. For this purpose the theory of Mott and Gurney (1948) was considered and specific calculations were presented for the alkali halide crystals having the NaCl-type of structure. Unfortunately some numerical error inadvertently got associated with these calculations. The purpose of the present paper, though is to examine and discuss the theory of dielectric constant as formulated by Szigeti (1949,50), we find it necessary to briefly summarize the corrected results of our previous effort so that a proper appraisal of the new work may be possible.

In addition we discuss a procedure for calculating the infra-red polarizability from the basic knowledge of interatomic forces. We report here the computed values of the effective charge on the basis of the first relation of Szigeti (1949) and most recent data of dielectric constants and Reststrahlen frequency. A link between the theories of Szigeti (1949, 50) and Mott and Gurney (1948) is established by identifying the effective charge in the former theory with the factor γ which determines the degree to which the neighbouring ions overlap in the latter theory. This has enabled the computation of the low frequency dielectric constant ϵ_0 through the use of the first relation of Sziegeti.

*Present address: Thermophysical Properties Research Center, Purdue University, Lafayette, Indiana, U.S.A.

CALCULATION OF ATOMIC POLARIZABILITY

The familiar relation between the dielectric constant ϵ_0 , and the polarizability α , is

$$\frac{\epsilon_0 - 1}{\epsilon_0 + 2} = \frac{4\pi\alpha}{3} \quad (1)$$

Further if the crystal does not possess permanent dipole moment, α is composed of the infrared polarizability α_i , and the ultraviolet polarizability α_u , the latter being known from the Drude's relation. We have then the well-known Clausius-Mossotti equation,

$$\frac{\epsilon_0 - 1}{\epsilon_0 + 2} = \frac{\epsilon_\infty - 1}{\epsilon_\infty + 2} + \frac{4\pi}{3} \alpha_i \quad (2)$$

in which ϵ_∞ is the high frequency dielectric constant.

For rigid non-overlapping ions α_i is related with the force constant A , Dekker (1962),

$$\alpha_i = \frac{Ne^2}{A} \quad (3)$$

Here N is the number of ions per unit cell, e the electronic charge and A is given by, Born and Huang (1956),

$$A = \frac{M}{3} \left[v''(r_0) + 2 \frac{v'(r_0)}{r_0} \right] \quad (4)$$

M being the coordination number and r_0 the equilibrium inter-ionic separation. Further we (1966) suggested that an appropriate form for $v(r)$ is,

$$v(r) = ae^{-r/\rho} - \frac{c}{r^6} - \frac{d}{r^8} \quad \dots \quad (5)$$

Here a and ρ are the potential parameters, c and d the Van der Waals constants and r the interatomic separation.

We have now two ways of calculating α_i . One from Eqn. (2) with the knowledge of ϵ_0 and ϵ_∞ , and another from Eqs. (3) to (5). The two sets of computed values are given in table I in columns 2 and 3. The values of ϵ_0 and ϵ_∞ are of Mott and Gurney (1948) and the details of the calculation of A are given by us (1966) earlier. The two sets of α values are in approximate agreement with each other and should be regarded as reasonable in view of the crude model and approximate nature of the theories.

TABLE I
The values of α_t , γ and s for alkali halide crystals

Crystal	α_t (10^{-24}cm^3)		γ		s
	Eq. (2)	Eq. (3)	Eq. (6)	Eq. (8)	
LiF	1.95	3.57	0.74	—	0.83
LiCl	3.26	4.51	0.68	0.54	0.74
LiBr	3.60	5.11	0.70	0.81	0.67
LiI	3.70	5.92	0.67	0.50	0.54
NaF	3.07	3.74	0.70	—	0.93
NaCl	3.35	4.77	0.70	0.37	0.74
NaBr	3.50	5.78	0.70	0.34	0.69
NaI	4.25	6.48	0.69	—	0.71
KF	3.66	4.50	0.74	—	0.91
KCl	4.13	6.34	0.71	—	0.80
KBr	4.29	6.74	0.69	0.25	0.76
KI	4.37	8.11	0.70	0.16	0.69
RbF	4.09	4.88	0.71	0.61	0.97
RbCl	4.90	6.52	0.71	0.37	0.84
RbBr	5.16	7.16	0.69	0.47	0.82
RbI	5.19	8.08	0.70	0.40	0.79
CsF	—	5.23	0.70	—	—
CsCl	5.46	6.99	0.72	0.68	0.84
CsBr	5.21	8.56	0.77	0.32	0.79
CsI	4.65	8.73	0.70	0.26	0.91

MOTT AND GURNEY THEORY OF DIELECTRIC CONSTANT

Mott and Gurney (1948) proposed that as a consequence of the overlap in the adjacent ions there is a reduction in the electric field due to polarization by a multiplicative factor γ . We (1966) have shown that

$$1-\gamma = \frac{\frac{r_0}{\rho}ae^{-r_0/\rho} - \frac{6c}{r_0^6} - \frac{8d}{r_0^8}}{e^2/r_0} \quad \dots (6)$$

The computed values of γ for the twenty alkali halides are given in column 4 of Table I.

Mott and Gurney (1948) have given the following relation for the low frequency dielectric constant,

$$\frac{\epsilon_0 - 1}{3 + (\epsilon_0 - 1)\gamma} = \frac{\frac{4\pi N}{3}(\alpha_1 + \alpha_2) - \frac{32\pi^2}{9}N^2\alpha_1\alpha_2(1-\gamma)}{1 - \frac{4\pi}{3}N(\alpha_1 + \alpha_2)(1-\gamma) + \frac{16}{9}\pi^2N^2\alpha_1\alpha_2(1-\gamma)^2} + \frac{\frac{4\pi}{3}\delta}{1 - \frac{4\pi}{3}\delta(1-\gamma)} \dots \quad (7)$$

Here α_1 and α_2 are the polarizabilities of the two ions and $\delta = Ne^2/A$. An alternative form of this equation is

$$\frac{\epsilon_0 - 1}{3 + (\epsilon_0 - 1)\gamma} = \frac{\epsilon_{cs} - 1}{3 + (\epsilon_{cs} - 1)\gamma} + \frac{\frac{4\pi}{3}\delta}{1 - \frac{4\pi}{3}\delta(1-\gamma)} \quad (8)$$

Equation (8) is utilized to compute γ with the known experimental values of ϵ_0 and ϵ_{∞} and of δ from Eq. (4). These values are recorded in column 5 of Table I. It is to be noted that this again tends to establish that Mott and Gurney theory of dielectric constant is inadequate to represent the facts.

Mott and Gurney (1948) also gave the following relation for the high frequency dielectric constant ϵ_{∞} :

$$\frac{\epsilon_{cs} - 1}{4\pi} = \frac{N(\alpha_1 + \alpha_2) - 8/3 \pi N^2 \alpha_1 \alpha_2 (1-\gamma)}{1 - \frac{4\pi}{3} N(\alpha_1 + \alpha_2) + \frac{16}{9} \pi^2 N^2 \alpha_1 \alpha_2 (1-\gamma)^2} \quad (9)$$

In the earlier work we (1966) reported ϵ_{∞} values for all except Caesium halides. We have now calculated ϵ_{∞} for these four halides employing the γ values as given by the relation of Eq. (6). These values also, like the remaining sixteen, are in good agreement with the experimental data. The average absolute deviation is 1.5 percent.

We now report the three sets of computed ϵ_0 values in Table II which supersede the earlier ones, Kachhava and Saxena (1966). In all calculations γ as obtained from Eq. (6) is used, while in the last it is identified with the effective charges as explained later. The other details are as given earlier by us (1966). We find that the relation of Eq. (7) is poor and inferior to that included in Eq. (8). We also notice that when γ is put equal to s the situation does not improve. All this simply confirms that the basic formulation is at fault.

S Z I G E T I T H E O R Y O F D I E L E C T R I C C O N S T A N T

Szigeti (1949, 50) attempted to improve the Born's wellknown relation for ϵ_0 obtained on the assumption of non-deformable and non-overlapping ions, viz.

$$\epsilon_0 = \epsilon_{cs} + \frac{4\pi N z^2 c^2}{\mu \omega_0^3} \dots \quad (10)$$

TABLE II

The low frequency dielectric constant ϵ_0 , of alkali halide crystals

Crystal	Experimental	Calculated		
		Eq. (7)	Eq. (8)	
			γ of Eq. (6)	$\gamma = s$
LiF	9.27	—	—	—
LiCl	11.05	21.5	13.9	15.1
LiBr	12.1	21.3	14.6	14.0
LiI	11.03	21.0	14.2	11.2
NaF	6.0	10.8	10.6	13.8
NaCl	5.62	8.75	7.05	7.29
NaBr	5.99	10.1	8.73	8.50
NaI	6.60	10.1	8.03	8.27
KF	6.05	8.30	8.65	5.43
KCl	4.68	6.72	6.26	6.72
KBr	4.78	6.36	6.20	6.47
KI	4.94	7.48	7.13	7.04
RbF	5.91	6.10	6.29	7.45
RbCl	5.0	5.79	5.67	6.19
RbBr	5.0	5.78	5.76	6.31
RbI	5.0	6.15	6.00	6.39
CsF	—	5.67	11.4	—
CsCl	7.20	7.52	7.49	8.46
CsBr	6.51	7.49	10.2	10.3
CsI	5.65	8.12	8.19	7.85

Here Z is the valency of the ions and μ the reduced mass of the two ions. He included the effect of the presence of other ions in the lattice and the fact that they overlap and cause deformation. He concludes that the net effect is that the dipole moment is reduced by a factor s and the Born's Eq. (10) assumes the following form as the first Szigeti's relation.

$$\epsilon_0 = \epsilon_{es} + \frac{4\pi N s^2 z^2 e^2}{\mu w_0^2} \left(\frac{\epsilon_{es} + 2}{3} \right)^2. \quad \dots (11)$$

Szigeti (1949) calculated the s values for the different crystals from Eq. (11) itself employing the experimental ϵ_0 , ϵ_{cs} and w_0 values. We have repeated these calculations for all the alkali halides in conjunction with the most upto date experimental information. These are listed in column 6 of Table I.

Szigeti (1949, 50) has shown that there are several factors which control the magnitude of s . Hanlon and Lawson (1959) have however shown that the major contribution to s comes from overlap. Thus we find that the actual ionic charge Ze gets changed to sZe , an effective value, due to the interaction of the neighbouring ions. Further s is the measure of the reduction of the dipole moment and hence of polarization and consequently it also can be regarded as directly controlling the effective field which is due to polarization. It is now interesting

TABLE III
The values of w_0 , β and ϵ_0 for alkali halide crystals

Crystal	(10^{-18}g^{-1})	β_{exptl}	β_{calc} Eq. (12)	$\frac{\beta_{\text{calc}}}{\beta_{\text{exptl}}}$	ϵ_0 Eq. (11) with $s=\gamma$
LiF	5.73	1.49	1.55	1.04	7.83
LiCl	3.84	3.36	3.69	1.10	10.7
LiBr	3.26	4.20	4.96	1.18	13.8
LiI	2.71	5.83	4.33	0.74	15.0
NaF	4.63	2.15	1.96	0.91	4.18
NaCl	3.09	4.17	4.68	1.12	5.13
NaBr	2.54	5.02	5.17	1.03	5.98
NaI	2.20	6.64	6.72	1.01	6.40
KF	3.62	3.28	2.98	0.91	4.36
KCl	2.71	5.73	5.04	0.88	4.31
KBr	2.18	6.75	5.97	0.88	4.36
KI	1.94	8.55	7.33	0.86	5.05
RbF	3.01	3.81	4.37	1.15	4.45
RbCl	2.24	6.40	5.73	0.89	3.75
RbBr	1.69	7.69	7.05	0.92	4.22
RbI	1.41	9.48	8.68	0.82	4.56
CsF	2.39	4.25	—	—	5.35
CsCl	1.86	5.55	5.12	0.92	5.05
CsBr	1.39	6.28	7.55	1.20	5.36
CsI	1.17	7.83	8.06	1.03	6.47

to recall that Mott and Gurney introduced the factor γ to take into account a similar effect. γ and s should therefore be identifiable with each other. This conclusion immediately provides a very pleasant correlating link between the two theories. This conclusion is indeed upheld by the records of columns 4 and 6 of Table I and many calculations of the properties described in this paper.

It is important to note that the s values vary between 0.70 to 0.95. The great success of the Born-Mayer theory of ionic crystals demands that s should not depart from unity by more than a couple of percent. Here we find the departure to be rather pronounced. In fact even Szigeti was quite alive to this trend and he has tried to explain it rather in detail. In passing we may however note as pointed out by Born and Haung (1956) that this anomaly is a consequence of simplifying in a crude fashion the physical picture involved in the phenomenon.

RELATION BETWEEN COMPRESSIBILITY, ϵ_0 AND w_0

Szigeti (1950) in the further development of his theory derived a relation between compressibility β , ϵ_0 and w_0 which is now commonly known as his second relation. It is

$$\frac{1}{\beta} = \frac{r_0^2 (\epsilon_0 + 2)}{3v (\epsilon_{cs} + 2)} \mu w_0^2. \quad \dots (12)$$

In parallel with Szigeti's original approach we recalculate β using the recent data. The w_0 values in particular are recorded in Table III column 2. The β values so obtained are listed in column 4 of this very Table. These should be compared with the experimental isothermal β values also recorded in this very Table in column 3. To make this comparison explicit we quote in column 5 the ratio β calc/ β expt. It will be seen that though in a few cases the disagreement is pronounced, yet on the whole the facts are well reproduced. This study provides a quantitative assessment of the success of Szigeti's theory and must be regarded as fairly encouraging.

CALCULATION OF ϵ_0

We again put a test to the Szigeti's theory on the basis of first relation, Eq. (11). The approach is unconventional inasmuch as it uses the suggestion developed in this paper of equating s with γ . Under this limitation the computation of ϵ_0 from Eq. (11) is straightforward when for all the other quantities we employ the experimental information. These values are recorded in column 6 of Table III. The deviations between the computed and experimental values are given in column 7. The agreement is certainly very encouraging when one notes that the average absolute deviation is only 10.2 percent for all the alkali halide crystals. This also provides an indirect proof for ascertaining the s values through γ and their complete equality.

CONCLUSIONS

We thus find that amongst the classical theories of dielectric constant Mott and Gurney theory fails to reproduce the experimental information, while that Szigoty theory is successful to a large extent. These detailed calculations performed for all the twenty alkali halide crystals and with the use of the latest experimental data provide the necessary background against which the more recent theories can be assessed. We do not mention any such details here but plan to report them in a separate article. These detailed and elaborate calculations, Kachhava (1966), simply tend to improve our faith in the Szigeti's theory to approximately understand the dielectric phenomenon inasmuch as the new values differ in general by a nominal amount and one further finds that these sophisticated calculations cannot be easily extended to all alkali halide crystals.

REFERENCES

- Born, M. and Huang, K., 1956, *Dynamical Theory of Crystal Lattices*, Clarendon Press, Oxford.
- Dekker, A. J., 1962, *Solid State Physics*, MacMillan and Co. Limited, London.
- Hanlon, J. E. and Lawson, A. W., 1959, *Phys. Rev.*, **113**, 472.
- Kachhava, C. M., 1966, *Ph.D. Thesis : Certain Problems of Solid State Physics*, Rajasthan University.
- Kachhava, C. M. and Saxena, S. C., 1966, *Indian J. Phys.* **40**, 225.
- Mott, N. F. and Gurney, R. W., 1948, *Electronic Processes in Ionic Crystals*, Clarendon Press, Oxford.
- Szigoti, B., 1949, *Trans. Faraday Soc.* **45**, 155.
- — —, 1950, *Proc. Roy. Soc. (London)* **A204**, 51.

ELECTRICAL CONDUCTIVITY OF NATURAL STANNIC OXIDE

S. C. MITRA

UNIVERSITY OF NIGERIA, NSUKKA, NIGERIA

(Received October 17, 1966)

ABSTRACT. The electrical conductivities of number of stannic oxide polycrystalline bars prepared from Nigerian cassiterite powder were measured in the temperature range 25°C to 650°C. The activation energy obtained in the high temperature range for three samples studied are 0.42, 0.48, 0.50 eV as against the activation energy of 0.72 eV obtained by Kohnke (1962) in the same temperature range for crystals of Bolivian cassiterite. For thin films of stannic oxide, Niloslavskii (1959) calculates an activation energy of 0.12 eV in the same temperature range.

INTRODUCTION

Cassiterite which is an important mineral of tin has stannic oxide, SnO_2 , as its main constituent, crystallises in the tetragonal rutile structure and is strongly resistant to chemical reagents and heat treatment in air or oxygen. It belongs to the structural space group $P4/m$ having two molecules per unit cell.

Earlier work on stannic oxide has been essentially limited to thin films and coatings (Bauer 1937, Aitchison 1954, Fischer 1954, Ishiguro *et al.* 1958), and powder samples (Ieblanc *et al.*, 1931; Guillery 1932, Foex 1944). The limitations inherent in these measurements due to grain boundaries, inhomogeneities and large surface-to-bulk ratio can be reduced by using polycrystalline solids or single crystals as study specimens. The only investigations reported in this direction are by Kohnke (1952) on three specimens from crystals of natural Bolivian cassiterite, studied in the temperature range 100°C to 500°C and by Lock (1963) on polycrystalline bars of stannic oxide, undoped and doped with antimony, in the temperature range 100°C to 900°C.

The object of the present communication is to give a preliminary report of conductivity measurements on polycrystalline bars of Nigerian cassiterite.

EXPERIMENTAL

(a) Preparation of samples

Polycrystalline solid rods were prepared from cassiterite powder by sintering at about 800°C in air. Rectangular slabs were sliced from the rod and ground to plane faces with fine emery powder. In the case of extended contacts, two opposite faces were copper plated. To test for rectification, one slab was prepared with

extended contact on one face, and a sharp point contact was maintained at the opposite face.

The sample holder used was made of porcelain base provided with brass electrodes, a modified form of the one used by Dutta (1953).

(b) *Electrical measurements*

Current voltage measurements up to 1.5 volts was made by potentiometer and above it by ammeter and voltmeter. Temperature variation was provided by an electrical furnace. Measurements were made both for forward and reverse currents in the temperature range 25°C to 650°C. Chromel Alumel thermocouple was used for measuring temperature.

RESULTS

The results of measurements are shown in Table I and II and graphs (figs. 1, 2, 3 and 4).

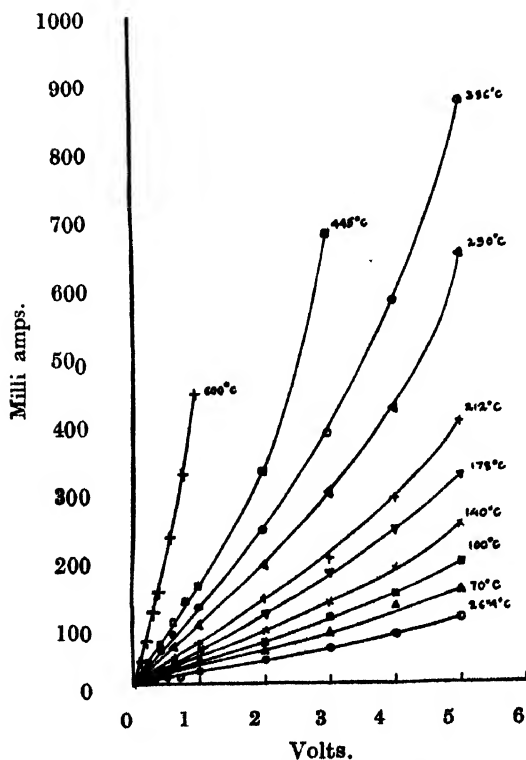


Fig. 1. Current-Voltage characteristic with extended contact at both ends.

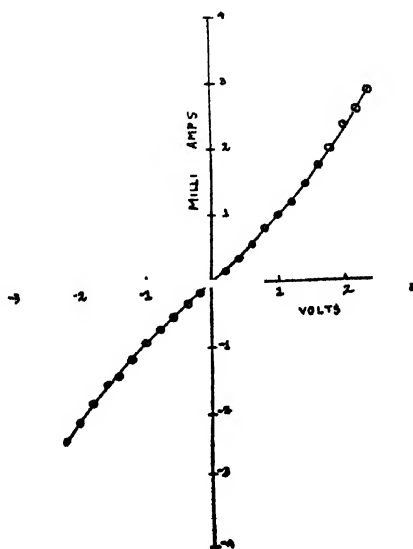


Fig. 2. Current-Voltage characteristic with extended contact at one end and point contact at the other.

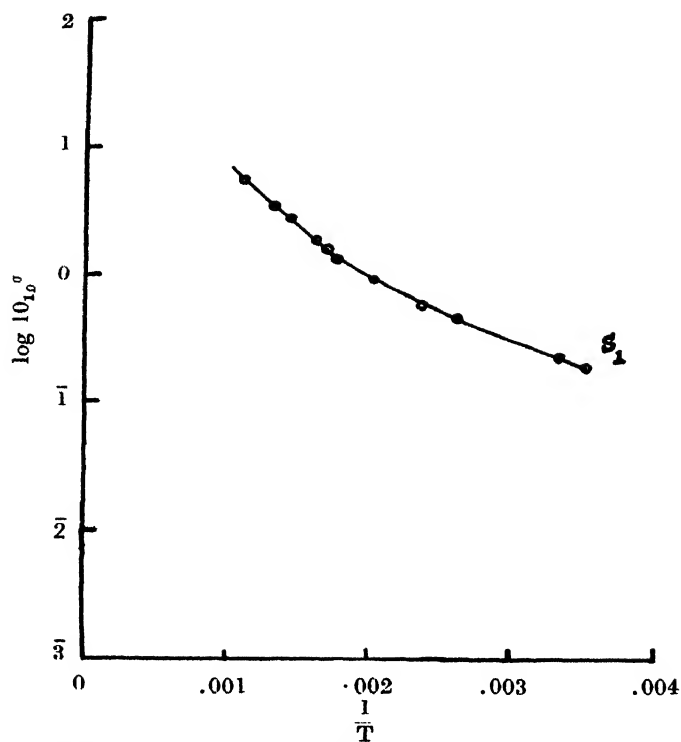


Fig. 3. Variation of conductivity with temperature. for specimen S_1 .

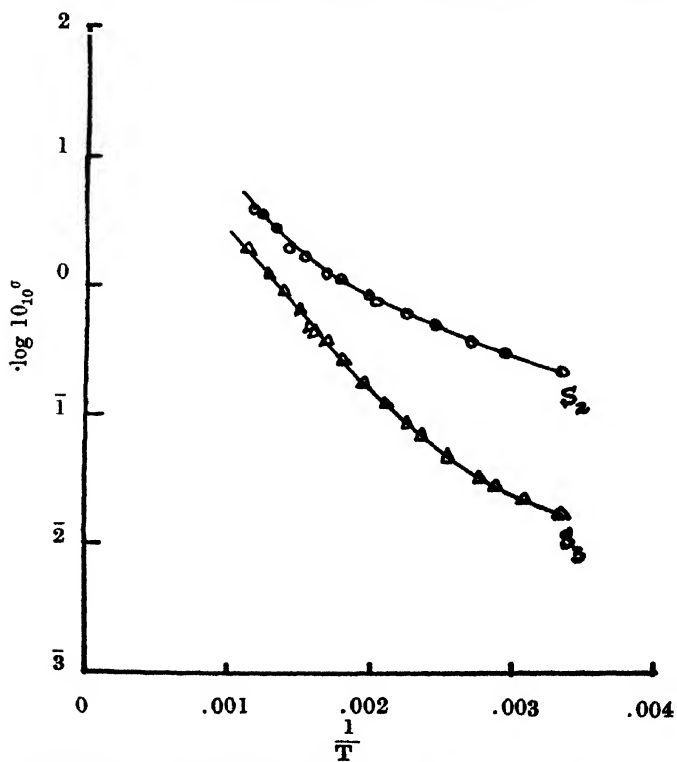


Fig. 4. Variation of conductivity with temperature for specimen S_2 and S_3 .

TABLE I

Sample	Density gm/cm ³	Dimonsion cm	Conductivity at room temperature ohm ⁻¹ cm ⁻¹
<i>S</i> ₁	5.180	2.154 × 0.711 × 0.52	0.216
<i>S</i> ₂	5.26	1.099 × 0.395 × 0.216	0.217
<i>S</i> ₃	4.861	1.924 × 0.489 × 0.349	0.017

TABLE II

The values of W_1 and W_2

Sample	W_1 eV	W_2 eV
<i>S</i> ₁	0.17	0.42
<i>S</i> ₂	0.17	0.48
<i>S</i> ₃	0.19	0.50

DISCUSSION

It is observed that both for extended as well as point contact, the current voltage characteristics are nonlinear and symmetrical. The non-ohmic nature increases with temperatures. No rectification occurs for point contact.

The electrical conductivity was calculated from the ohmic portion of the current voltage characteristics for low values of current and voltage.

The temperature variation conductivity plotted as $\log_{10}\sigma$ versus the inverse of temperature T°K shows two distinct linear portions, each of which can be fitted by a relation $\sigma = A \exp(-W/2kT)$ where the symbols have their usual significances. The values of activation energy W calculated for the specimens are listed in Table II. W_1 and W_2 refer to lower and higher temperature ranges of the curves.

Conductivity values of Kohnke (1952) at room temperature lie in the range 10^{-2} to 10^{-3} ohm⁻¹ cm⁻¹ whereas those of Lock (1963) lie in the range 10^{-1} to 10^2 ohm⁻¹ cm⁻¹ for doped specimen and is 10^{-2} for the undoped. Kohnke (1962) obtained 0.72 eV activation energy from the linear portion in the high temperature region for all three samples. No corresponding information is available from Locks's paper. Miloslavskii (1959) calculates an activation energy of 0.12 eV for thin films of stannic oxide in the same temperature range. These differences in the values of the conductivities and activation energies are due to differences

in the origin, nature and previous history of the specimens used by different investigators.

ACKNOWLEDGMENTS

The author wishes to thank Prof. A. V. Brancker, Head, Department of Physics and Prof. A. Singh, Head, Department of Chemistry of the University of Nigeria, for facilities provided and Mr. A. K. Dutta, Indian Association for the Cultivation of Science, Calcutta, for helpful discussions.

REFERENCES

- Aitchison, R. E., 1954, *Aust. J. appl. Sci.*, **5**, 10.
Bauer, G., 1937, *Ann. Phys. Lpz.* **3e**, 433.
Datta, A. K., 1953, *Phys. Rev.*, **90**, 187.
Fisher, A., 1954, *Z. Naturf.*, **9A**, 508.
Foex, M., 1944, *Bull. Soc. Chim. Fr.*, **11**, 6.
Guillery, P., 1932, *Ann. Phys. Lpz.*, **14**, 216.
Ishigaro, K., Sasaki, T., Arai, T., and Imai, I. J., 1958, *J. Phys. Soc. Japan*, **13**, 296.
Kohnko, E. E., 1962, *J. Phys. Chem. Solids*, **23**, 1557.
Leblanc, M., and Sachse, H., 1931, *Phys. Z.* **32**, 887.
Lock, L. D., 1963, *J. Electrochemical. Soc.*, **110**, 1081.
Moloslavskii, V. K., and Lyashenko, S. P., 1960, *Opt. Spectroc.*, **8**, 455.

ACOUSTIC FREE INDUCTION IN A QUADRUPOLEAR SPIN SYSTEM IN A CUBIC CRYSTAL

S. K. SINHA

SAHA INSTITUTE OF NUCLEAR PHYSICS, CALCUTTA-9

(Received May 30, 1966 ; Resubmitted February 2, 1967)

ABSTRACT. The bulk magnetisation vectors, excited by an acoustic pulse at magnetic resonance has been calculated in a cubic crystal, where each lattice site is assumed to be occupied by a nucleus of spin 1 (one). The Hamiltonian has been cast in a general form, for any

interaction of the form $\vec{I} \cdot \vec{D} \cdot \vec{I}$, and calculation has been done by setting up the Rabi-Bloch matrices, and neglecting, for simplicity, the spin-spin interactions. It is found that with a longitudinal excitation in one of the cubic axes, the transverse components of the average macroscopic moment vectors $\langle M_x \rangle_{av}$ and $\langle M_y \rangle_{av}$ are practically zero, being contributed by nuclei located at thin layers (of width equal to half wavelength of the acoustic waves) at the two ends of the sample. The results are identical with those of Kessel (Kessel, 1962) who analysed the above situation by a first order time-dependent perturbation method.

INTRODUCTION

The absorption of acoustic energy at magnetic resonance in solids, when the resonance is excited by an impressed acoustic field [Kastler (1952), Altshulen (1955), Jacobsen and Stevens (1963)], has been demonstrated both in pulsed [Jacobsen, Shiren and Tucker (1959), Tucker (1961), Shiren (1962), and Guermeur, Joffrin, Levelut and Penne (1964)] and CW [Proctor and Tantilla (1956), Proctor and Robinson (1956), Menes and Bolef (1958), Bolef and Menes (1959), and Bolef, de Klerk and Gosser (1962)] experiments. In such experiments one particular lattice mode is strongly excited, and the energy in the lattice mode is transmitted to the spin system via the spin-phonon interaction. There must be some relaxation mechanism (other than the so-called direct process) that will maintain the Boltzman population excess in the spin system. And since the excitation is strong, effectively equalising the upward and the downward transition probabilities of a spin, there will be a net absorption of energy from the excited lattice mode. The amount of the absorption is a measure of the direct spin-phonon interaction that couples the particular lattice mode with the magnetic spin system. This fact, together with the absence of "penetration depth" effect in metals leads to several interesting possibilities that can be explored by acoustic magnetic resonance experiments. Already, quite a few experiments have been done yielding important results [Bolef and Menes (1961), Shiren (1962), and Guermeur, Joffrin, Levelut and Penne (1965)]

However, there has not been any induction experiment in this field, so far. The possibility of such an experiment, using pulse technique, was analysed by Kessel (1962) a few years back. Although the method used in the analysis is sufficient for tackling the situation with simplifying assumptions, i.e. the neglect of spin-spin interaction, it is felt that a density matrix treatment of the phenomenon will be more convenient in more general cases*. We describe such a treatment which is similar to Lowe and Norberg's (1957) analysis of free induction in electromagnetically excited NMR. In our analysis we shall consider a cubic crystal, having lattice sites occupied by nuclei of spin 1 (one). The spin system will thus be coupled to the excited lattice mode by nuclear quadrupole interaction.

ACOUSTICALLY INDUCED NUCLEAR MAGNETIC INDUCTION IN A CUBIC CRYSTAL

(A) Spin-phonon interaction Hamiltonian in a quadrupolar spin system in an acoustically excited cubic crystal: Let us write the interaction term in the form,

$$H = -\hbar \vec{I} \cdot \vec{D} \cdot \vec{I} \quad \dots (1)$$

where \vec{I} is the nuclear spin vector, and \vec{D} is a tensor of rank two in three dimension, containing the lattice coordinates. In a rectangular coordinate system (X, Y, Z), where Z is the axis of quantisation of the spin system (that is, the direction of the D.C. magnetic field), it will be seen that the tensor, D , is symmetric for the particular spin-lattice system. Expanding (1), we can thus write :

$$\begin{aligned} H' = & -\hbar [\frac{1}{2}(D_{xx} + D_{yy})I_z^2 + \frac{1}{2}(2D_{zz} + D_{xx} - D_{yy})I_x^2 + \\ & + \frac{1}{2}(D_{xx} - D_{yy})(I_+^2 + I_-^2) + D_{xz}(I_x I_z + I_z I_x) + \\ & + D_{yz}(I_y I_z + I_z I_y) + D_{xy}(I_x I_y + I_y I_x)] \quad \dots (2) \end{aligned}$$

Dropping the terms that couple states with $\Delta m = 0$, we have :

$$\begin{aligned} H' = & -\hbar [\frac{1}{2}(D_{xx} - D_{yy})(I_+^2 + I_-^2) + D_{xz}(I_x I_z + I_z I_x) + D_{yz}(I_y I_z + I_z I_y) + \\ & + D_{xy}(I_x I_y + I_y I_x)] \quad \dots (3) \end{aligned}$$

We may note that the density-matrix method is effectively equivalent to the ordinary time-dependent perturbation method, upto certain degree of approximation. However, the former is different from the latter when the actual calculation is concerned. In the time-dependent perturbation method, one expands the time-dependent wave function in a complete set of time-independent basis functions, and solves for the expansion coefficients a_m, a_n etc. from a set of coupled differential equations. One popular way of doing this is to reduce these differential equations to a set of coupled algebraic equations by making use of Laplace Transforms. In general, it is difficult to obtain these transforms. However, in density-matrix method one avoids this difficulty by calculating the products ($a_n a_m$) which are more directly useful for calculating expectation values.

The components of D are functions of the local strain at the nuclear sites, and one can expand D in terms of the strain components e_{ij} in a Taylors series. Thus introducing the spin-phonon coupling constant G , we can write (in Voigt notation) :

$$D_j = D_j^{(0)} + \sum_i G_{ji} e_i + \text{higher order terms. } i, j = 1, 2, 3, \dots, 6.$$

where

$$G_{ji} = \left. \frac{\partial}{\partial e_i} (D_j) \right|_{e_i \rightarrow 0} \dots (4)$$

In order to define G uniquely, the (4) is written in the coordinate system (X_0, Y_0, Z_0) that coincides with the crystallographic axes. This also enables one to simplify the expansion (4) by using symmetry arguments. For example, in cubic symmetry, we have the expansion:

$$\begin{aligned} D_{x_0 x_0} &= \frac{G_{11}}{2} (2e_{x_0 x_0} - e_{y_0 y_0} - e_{z_0 z_0}), & D_{x_0 y_0} &= G_{44} e_{x_0 y_0} \\ D_{y_0 y_0} &= \frac{G_{11}}{2} (2e_{y_0 y_0} - e_{z_0 z_0} - e_{x_0 x_0}), & D_{y_0 z_0} &= G_{44} e_{y_0 z_0} \\ D_{z_0 z_0} &= \frac{G_{11}}{2} (2e_{z_0 z_0} - e_{x_0 x_0} - e_{y_0 y_0}), & D_{z_0 x_0} &= G_{44} e_{z_0 x_0} \end{aligned} \dots (5)$$

The components of D , used in the Hamiltonian (3) can then be obtained by using the following usual transformation relations :

$$\begin{aligned} D_{ii} &= \sum_{(\nu\mu)} \alpha_{i\nu} \alpha_{i\mu} D_{\nu\mu} \\ D_{ij} &= \sum_{(\nu\mu)} (a_{i\nu} a_{j\mu} + \alpha_{j\nu} a_{i\mu}) D_{\nu\mu} \end{aligned} \dots (6)$$

where

$$(\nu\mu) \equiv (x_0 x_0), (y_0 y_0), (z_0 z_0), (x_0 y_0), (y_0 z_0), \text{ and } (x_0 z_0).$$

and the coefficients a are given in table I.

TABLE I

Transformation coefficients. ' $a_{i\nu}$ ', for two Cartesian coordinate systems, i and ν , having the same origin and their mutual orientation being specified by the Eulerian angles θ , ϕ and ψ .

$i \setminus \nu$	x_0	y_0	z_0
x	$\cos \psi \cos \phi \cos \theta + \sin \psi \sin \phi$	$\cos \psi \sin \phi \cos \theta - \sin \psi \cos \phi$	$\cos \psi \sin \theta$
y	$\sin \psi \cos \phi \cos \theta - \cos \psi \sin \phi$	$\sin \psi \sin \phi \cos \theta + \cos \psi \cos \phi$	$\sin \psi \sin \theta$
z	$-\cos \phi \sin \theta$	$-\sin \phi \sin \theta$	$\cos \theta$

We will now consider a special case. Let us assume that a longitudinal acoustic wave of circular frequency ω has been impressed in the crystal with the propagation vector in the crystallographic (001) direction. We also assume that the laboratory Y -direction and the crystal (010) directions coincide, and the crystal has been rotated about the Y -axis such that the propagation vector \vec{k} (still in the crystal (001) direction) makes an angle θ with the D.C. magnetic field, ie. the Z -direction. This longitudinal wave will generate a standing wave pattern, and an axially symmetric strain field (time-dependent) in the crystal, the axis of symmetry being in the direction of \vec{k} . Let us also choose the laboratory X -axis such that it coincides with the projection of \vec{k} on the $X-Y$ plane. In such a case, we see that the only strain component is $e_{z_0z_0}$, where the direction z_0 is the crystal (001) and thus from (5), we get :

$$D_{z_0z_0} = G_{11}e_{z_0z_0}$$

$$D_{x_0x_0} = D_{y_0y_0} = -\frac{G_{11}}{2} e_{z_0z_0} \quad \dots (7)$$

$$D_{x_0y_0} = D_{y_0z_0} = D_{z_0x_0} = 0$$

Transforming (7) into the (XYZ) system (using (6), and the table I, with $\phi = \psi = 0$),

$$D_{zz} = \frac{G_{11}}{2} e_{z_0z_0}(3 \cos^2 \theta - 1), \quad D_{xx} = \frac{3}{2} G_{11}e_{z_0z_0} \sin \theta \cos \theta$$

$$D_{xx} = \frac{G_{11}}{2} e_{z_0z_0} (3 \sin^2 \theta - 1), \quad D_{xy} = D_{yz} = 0$$

$$D_{yy} = -\frac{G_{11}}{2} e_{z_0z_0} \quad \dots (8)$$

The Hamiltonian (3) then becomes :

$$H' = -\hbar \left[\frac{3}{8} G_{11} e_{z_0z_0} (I_+^2 + I_-^2) \sin^2 \theta + \frac{3}{4} G_{11} e_{z_0z_0} (I_x I_z + I_z I_x) \sin 2\theta \right] \quad \dots (9)$$

The above formulation holds for any interaction of the form (1). Nuclear quadrupolar interaction is also of this form and the Hamiltonian (9) is applicable to this case. The constants G_{11} etc. in (9) can be measured by suitable experiments,

However, to obtain the theoretical expression for G_{11} , one has to consider the particular interaction, in this case nuclear quadrupolar interaction, explicitly.

Writing

$$H' = -\hbar(\vec{Q}) : (\vec{\nabla}E)$$

where \vec{Q} is the nuclear quadrupole moment tensor, and $(\vec{\nabla}E)$, the electric field gradient tensor at the nuclear site, one obtains in this special case.

$$G_{11} = Ae \frac{\partial}{\partial ez_0z_0}(q)]_{ez_0z_0 \rightarrow 0} \quad \dots \quad (10)$$

where

$$A = \frac{eQ}{2I(2I-1)}$$

and

$$eq = \sum_j e_j(3 \cos^2 \theta_j - 1)r_j^{-3}$$

Q is the scalar quadrupole moment of the nucleus, and 'eq' is the axial electric field gradient with the symmetry axis along the z_0 -axis. In the definition of 'eq', j refers to the j th. charge-point external to the nucleus, and \vec{r}_j is the vector joining this charge-point with the origin (the center of the nucleus), and θ_j is the angle between \vec{r}_j and the symmetry axis.

(b) Total Hamiltonian for the spin-lattice system : The total Hamiltonian can thus be written as

$$H = H_0 + H_1 + H_2 + H'(t) \quad \dots \quad (11)$$

H_0 is the Zeeman Hamiltonian for the spin system, H_1 describes the magnetic dipole interaction between the spins, and H_2 stands for all other terms in the total Hamiltonian for the statistic spinlattice system. $H'(t)$ is given by the expression (9). If we neglect those parts of H_1 and H_2 that couples states with $\Delta m \neq 0$, we are left with the following Hamiltonian :

$$H = H_0 + H'(t) \quad \dots \quad (12)$$

where

$$H_0 = -\hbar \sum_n \omega_0 I z_n$$

and

$$H'(t) = -\hbar \sum_n [2\omega_n^{(1)}(I x_n I z_n + I z_n I x_n) + \omega_n^{(2)}(I^2_{+n} + I^2_{-n})] \cos \omega t$$

with

$$\begin{aligned} \omega_0 &= \gamma H_0 \\ \omega_n^{(1)} &= \frac{e}{\hbar} G_{11} e z_0 z_0(0) \sin 2\theta \\ \omega_n^{(2)} &= \frac{e}{\hbar} G_{11} e z_0 z_0(0) \sin^2 \theta \end{aligned} \quad \dots \quad (13)$$

It has been assumed that $ez_0z_0 = ex_0z_0(0) \cos \omega t$, and γ is the gyromagnetic ratio for the nucleus. We shall be concerned with the cases where $H'(t)$ can be treated as a small perturbation.

(C) Rabi-Bloch matrices for the system: The Schrodinger equation is :

$$i\hbar \frac{\partial}{\partial t} \psi(t) = H(t)\psi(t) \quad \dots (14)$$

If we write $\psi(t) = \exp\left(-\frac{it}{\hbar} H(0)\right) \psi'(t)$, the equation (14) transforms into

$$\exp\left(\frac{it}{\hbar} H(0)\right) H'(t) \exp\left(-\frac{it}{\hbar} H(0)\right) \psi'(t) = i\hbar \frac{\partial}{\partial t} \psi'(t) \quad \dots (15)$$

We now assume that the acoustic wave is impressed only for a duration t_ω , in the form of a square pulse of carrier frequency ω , and that t_ω is sufficiently small so that those terms in H_1 and H_2 which do not commute with $H'(t)$ or $H(0)$ have expectation values much less than 1 when multiplied by t_ω/\hbar . Their effect upon $H'(t)$ may then be ignored. Thus retaining only the terms H_0 in $H(0)$ the equation (15) is approximated as :

$$\exp(-i\omega_0 t \sum_n I_{zn}) H'(t) \exp(i\omega_0 t \sum_n I_{zn}) \psi'(t) = i\hbar \frac{\partial}{\partial t} \psi'(t). \quad \dots (16)$$

Using the transformation properties of the spin operators under the rotation about the Z -axis, the equation (16) reduces to

$$iL(t) \psi'(t) = \frac{\partial}{\partial t} \psi'(t) \quad \dots (17)$$

where

$$\begin{aligned} L(t) = & \sum [2\omega_n^{(1)} \{(I_{xn}I_{zn} + I_{zn}I_{xn}) \cos \omega_0 t + (I_{yn}I_{zn} + I_{zn}I_{yn}) \sin \omega_0 t\} \\ & + 2\omega_n^{(2)} \{(I_{xn}^2 - I_{yn}^2) \cos 2\omega_0 t + (I_{xn}I_{yn} + I_{yn}I_{xn}) \sin 2\omega_0 t\}] \cos \omega t \quad \dots (18) \end{aligned}$$

The solution of (17) is

$$\psi'(t_\omega) = \exp \left\{ i \int_0^{t_\omega} L(t) dt \right\} \psi'(0) \quad \dots (19)$$

which reduces to (neglecting small terms containing t_ω),

$$\psi(t_\omega) = R_{\omega=\omega_0}\psi(0), \quad \text{when } \omega = \omega_0$$

and

$$\psi(t_\omega) = R_{\omega=2\omega_0}\psi(0), \quad \text{when } \omega = 2\omega_0 \quad (20)$$

where

$$R_{\omega=\omega_0} = \exp\left(i\theta_1 \sum_n I_{z_n}\right) \exp\left\{i \sum_n \theta_{2n}(I_{y_n}I_{x_n} + I_{z_n}I_{x_n})\right\}$$

$$R_{\omega=2\omega_0} = \exp\left(i\theta_1 \sum_n I_{z_n}\right) \exp\left\{i \sum_n \theta_{3n}(I_{x_n}^2 - I_{y_n}^2)\right\}$$

$$\theta_1 = \omega_0 t, \quad \theta_2 = \omega^{(1)} t_\omega \text{ and } \theta_3 = \omega^{(2)} t_\omega. \quad \dots \quad (21)$$

In a representation in which I_z is diagonal, the matrices $R_{\omega=\omega_0}$ and $R_{\omega=2\omega_0}$ have been evaluated. The results for spin $I = 1$ are given in tables II and III.

(D) Computation of $\langle M_x \rangle_{av}$, $\langle M_y \rangle_{av}$ and $\langle M_z \rangle_{av}$: We know that if we assume that the solution of the time-dependent Schrodinger equation:

$$i\hbar \frac{\partial}{\partial t} \psi_n(t) = H_n(t) \psi_n(t)$$

is of the form

$$\psi_n(t) = R_n(t) \psi_n(0)$$

then

$$\langle I_{x_n} \rangle = \int \psi_n^+(0) R_n^+(t) I_{x_n} R_n(t) \psi_n(0) d\tau \quad (22)$$

Expanding

$$\psi_n(0) = \sum_p a_{pn}(0) u_{pn}$$

we have

$$\langle I_{x_n} \rangle = \text{Trace} \{ \rho_n(0) R_n^+(t) I_{x_n} R_n(t) \} \quad (23)$$

where

$$\langle u_{qn} | \rho_n(0) | u_{pn} \rangle = a_{pn}^*(0) a_{qn}(0) \quad \dots \quad (24)$$

For a system of N spins, if we neglect the mutual interactions between the spins, we obtain

$$\langle \vec{M} \rangle_{av} = \sum_n^{1,2,\dots,N} \text{Trace} \left\{ \frac{\exp(\xi I_{z_n}) R_n^+ \gamma \hbar (\vec{i} I_{x_n} + \vec{j} I_{y_n}) + \vec{k} I_{z_n} R_n}{\text{Trace} \{ \exp(\xi I_{z_n}) \}} \right\} \quad \dots \quad (25)$$

where $\exp(\xi I_{z_n}) / \text{Trace} \{ \exp(\xi I_{z_n}) \}$ has been taken as equal to $\rho_n(0)$. $\xi = \gamma \hbar H_0 / kT$, T being the temperature of the sample and k , the Boltzman factor. The spin

system is here assumed to be at thermal equilibrium before the application of the acoustic pulse.

We use the R matrices as given in tables II and III, and using the expression (25) we get the following expressions for the induced bulk nuclear magnetisation at the end of the acoustic pulse.

TABLE II

The matrix, $R_{\omega=\omega_0}$, for spin $I = 1$, in a representation in which I_z is diagonal. The elements are $\langle q | K | p \rangle$, and $S_\theta \theta_2 \equiv$ the sign of the angle θ_2 .

$q \backslash p$	1	0	-1
1	$\exp(i\theta_1)(1 + \cos \theta_2)/2$	$S_\theta \theta_2 (i \exp(i\theta_1) \sin \theta_2)/\sqrt{2}$	$\exp(i\theta_1)(1 - \cos \theta_2)/2$
0	$S_\theta \theta_2 (i \sin \theta_2)/\sqrt{2}$	$\cos \theta_2$	$S_\theta \theta_2 (-i \sin \theta_2)/\sqrt{2}$
-1	$\exp(i\theta_1)(1 - \cos \theta_2)/2$	$S_\theta \theta_2 (-i \exp(-i\theta_1) \sin \theta_2)/\sqrt{2}$	$\exp(-i\theta_1)(1 + \cos \theta_2)/2$

TABLE III

The matrix $R_{\omega=2\omega_0}$, for spin $I = 1$, in a representation in which I_z is diagonal. The elements are $\langle q | R | p \rangle$, and $S_\theta \theta_3 \equiv$ the sign of the angle θ_3 .

$q \backslash p$	1	0	-1
1	$\exp(i\theta_1) \cos \theta_3$	0	$S_\theta \theta_3 (i \exp(i\theta_1) \sin \theta_3)$
0	0	1	0
-1	$S_\theta \theta_3 (i \exp(-i\theta_1) \sin \theta_3)$	0	$\exp(-i\theta_1) \cos \theta_3$

Case I. $\omega = \omega_0$

$$\begin{aligned}
\langle M_x \rangle_{av} &= \gamma \hbar \frac{\cosh \zeta - 1}{1 + 2 \cosh \zeta} \sin \theta_1 \sum_n^{1,2,\dots,N} S_\rho(\theta_{2n}) \sin 2\theta_{2n} \\
\langle M_y \rangle_{av} &= \gamma \hbar \frac{\cosh \zeta - 1}{1 + 2 \cosh \zeta} \cos \theta_1 \sum_n^{1,2,\dots,N} S_\rho(\theta_{2n}) \sin 2\theta_{2n} \\
\langle M_z \rangle_{av} &= \gamma \hbar \frac{\sinh \zeta}{1 + 2 \cosh \zeta} \sum_n^{1,2,\dots,N} \cos \theta_{2n}
\end{aligned} \tag{26}$$

Case II. $\omega = 2\omega_0$

$$\begin{aligned}
\langle M_x \rangle_{av} &= 0 \\
\langle M_y \rangle_{av} &= 0 \\
\langle M_z \rangle_{av} &= \gamma \hbar \frac{2 \sinh \zeta}{1 + 2 \cosh \zeta} \sum_n^{1,2,\dots,N} \cos 2\theta_{3n}
\end{aligned} \tag{27}$$

After the withdrawal of the pulse, the time-dependence of $\langle M_x \rangle_{av}$ and $\langle M_y \rangle_{av}$ will be given as usual by the Fourier transform of the steady NMR line shape.

Referring to (26), and from the definitions of θ_2 as given in (21) and (13), we see that

$$\sum_n S_\rho(\theta_{2n}) \sin 2\theta_{2n} = \sum_n S_\rho\{a \cdot e^{(n)z_0 z_0(0)}\} \sin \left\{ \frac{a}{2} e^{(n)z_0 z_0(0)} \right\}, \quad \dots \tag{28}$$

where

$$a = \left\{ \frac{2}{3} G_{11} \sin 2\theta \right\} t_\omega.$$

$e^{(n)z_0 z_0(0)}$, for a standing wave pattern where end surfaces of the sample are at antinodes, may be written as

$$e^{(n)z_0 z_0(0)} = 2KA_0 \sin KZ_n.$$

and hence we see from (28) that the main contribution to the summation will come from the two layers at the ends of the sample, layers having a thickness " l " given by

$$kl = \pi/2 \text{ or } l = \lambda/4.$$

As an example, for experiment at 10 mc/s, $l \cong 10^{-2}$ cm. and an insignificantly small number of nuclei are taking effective part in contributing to $\langle M_x \rangle_{av}$ and $\langle M_y \rangle_{av}$.

ACKNOWLEDGMENT

I wish to thank A. Choudhury and S. K. Ghose for helpful discussions, and Professor A. K. Saha for his interest in the subject.

REFERENCES

- Altshuler, S. A., 1955, *Soviet Phys. JETP*. **1**, 37.
Barnes, D. J., 1963, *Nature*, **200**, 253.
Bolef, D. I., and Menes, M., 1959, *Phys. Rev.* **114**, 1441.
Bolef, D. I., de Klerk, J. and Gossor, R. B., 1962, *Rev. Sci. Instruments*. **33**, 631.
Bolef, D. I. and Menes, M., 1961, *J. Phys. Chem. Solids*. **19**, 79.
Guermeur, R., Joffrin, J., Levelut, A. and Penne, J., 1964, *Phys. Rev. Letters*. **13**, 107.
Guermeur, R., Joffrin, J., Levelut, A. and Penne, J., 1965, *Phys. Rev. Letters*. **15**, 203.
Jacobsen, E. H. and Stevens, K. W. H. 1963, *Phys. Rev.*, **129**, 2063.
Jacobsen, E. H., Shiren, N. S. and Tucker, E. B., 1959, *Phys. Rev. Letters*. **3**, 81.
Kastler, A., 1952, *Experientia*. **8**, 1.
Kossel, A. R., 1962, *Soviet Phys. JETP*. **14**, 895.
Lowe, I. J., and Norberg, R. E., 1957, *Phys. Rev.* **107**, 46.
Menes, M. and Bolef, D. I., 1958, *Phys. Rev.* **109**, 218.
Proctor, W. G. and Tantilla, W. H., 1956, *Phys. Rev.* **101**, 1757.
Proctor, W. G. and Robinson, W., 1956, *Phys. Rev.* **104**, 1344.
Shiren, N. S., 1961, *Phys. Rev. Letters*. **4**, 168.
Also, (1962), Bulletin Du Groupement d' informations mutuelles, AMPERE,
Compte Rendu, du 11^e colloque. Eindhoven 2-6 Juillet.
———, 1962, *Phys. Rev.* **128**, 2103.
Tucker, E. B., 1961, *Phys. Rev. Letters*. **6**, 183.

Letters to the Editor

The Board of Editors does not hold itself responsible for opinions expressed in the letter published in this section. The notes containing short reports of original investigations communicated to this section should not contain many figures and should not exceed 500 words in length. The contributions reaching the Secretary by the 15th of any month may be expected to appear in the issue for the next month. No proof will be sent to the author.

7

LIGHT SCATTERING BEHAVIOUR OF ACACIA CATECHUIC ACID IN COURSE OF ITS NEUTRALISATION WITH SODIUM HYDROXIDE

J. N. CHAKRAVORTY

RAMA KRISHNA MISSION RESIDENTIAL COLLEGE, NARENDRAPUR.

(Received April 12, 1967)

An weighed quantity of Acacia Catechuic Acid (ACA) was taken in a 50 ml casia flask and dissolved in a little quantity of distilled water and requisite amounts of NaOH solution was added so as to neutralise it to different extent as desired. The volume was made upto 50 c.c. after further addition of distilled water. The flask was kept in a refrigerator at 4°C and the liquid was allowed to settle for about 24 hours. The liquid was finally examined with the Brice Phoenix Light Scattering Photometer after repeating the entire process of clarification etc. as mentioned earlier (Chakravorty 1966). The experiments

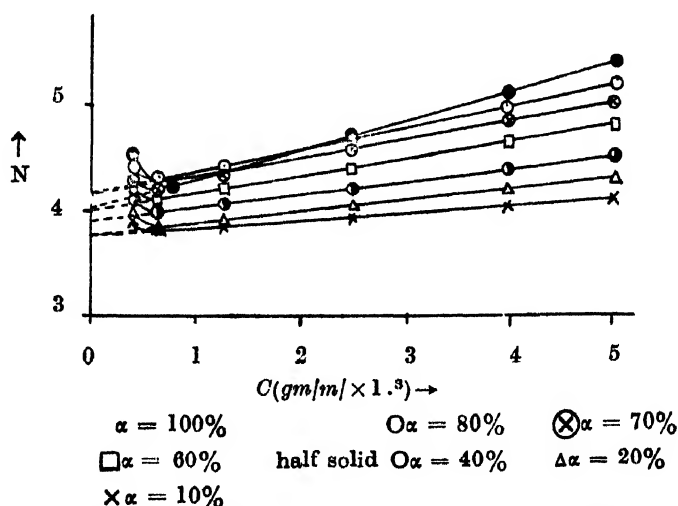


Fig. 1. Variation of dissymmetry with concentration at different degrees of neutralisation (α).

were performed with ACA solutions at different degrees of neutralisation and the results have been graphically represented in figs. 1 and 2.

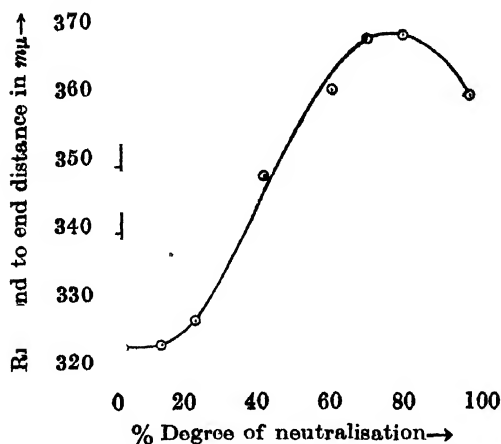


Fig. 2. Variation of root mean square end to end distance with degree of neutralisation.

The fig. 1 represents the variation of dissymmetry (Z) with concentration of ACA. There is a slight rise in the dissymmetry values at a very high dilution which may be attributed to high ionisation. The intrinsic dissymmetry values were obtained by extrapolating to zero concentration and the corresponding root mean square end to end distance $(\bar{h}^2)^{\frac{1}{2}}$ of the molecule (Stacey 1958) pertaining to the various degrees of neutralisation (α) has been represented in fig. 2. The rms end to end distance is 369 mμ and 360 mμ at $\alpha = 75\%$ and $\alpha = 100\%$ respectively as against 327 mμ in water (Chakravorty *et al*, 1963). It appears that the rms end to end distance increases with increase in the degree of neutralisation, becomes maximum at about $\alpha = 75\%$ and then decreases slightly at $\alpha = 100\%$. This behaviour can be explained as follows. With the addition of NaOH, ACA is gradually neutralised forming sodium salt which in its turn dissociates and increases the effective charge on the polymer thus leading to the gradual expansion of the polymeric coil. The little contraction observed beyond the point where $\alpha = 75\%$ appears to be due to the reduction of the charge density on the polyion owing to the increased rate of binding of counterions.

It may be useful to point out here that the dimensional change of the macromolecule has been expressed in terms of rms end to end distance $(\bar{h}^2)^{\frac{1}{2}}$. Zimm and Stockmeyer (1949) have shown that the radius of gyration ρ_g can be expressed as

$$\rho_g = a \sqrt{\frac{\sigma l_{av}^2}{6}} = a \sqrt{\frac{\bar{h}^2}{6}}$$

where σ and l_{av} represent respectively the number and average length of statistical segments, a is a constant, the value of which is equal to unity for linear polymer.

Under these conditions, therefore, the rms end to end distance may also be regarded as the relative measure of the radius of gyration.

My grateful thanks are due to late Prof. S. N. Mukherjee, Dr. M. N. Das and Dr. D. K. Chattoraj of Jadavpur University for their keen interest and valuable discussions. Thanks are also due to Danforth Foundation, America for financial assistance.

REFERENCES

- Chakravorty, J. N. and Mukherjee, S. N., 1963, *Jour. Indian Chem. Soc.*, **49**, 811-812.
Chakravorty, J. N., 1966, *Indian J. Phys.*, **40**, 605-608.
Stacey, K. A., 1958, *Light scattering in Physical Chemistry*, Bulterworths Scientific Publications, London.
Zimm, B. H. and Stockmeyer, W. H., 1949, *Jour. Chem. Phys.*, **17**, 1301.

8

MAGNETIC PROPERTIES OF NATURAL CRYSTALS
OF HEMATITE

A. K. MUKERJEE

DEPARTMENT OF MAGNETISM

INDIAN ASSOCIATION FOR THE CULTIVATION
OF SCIENCE, CALCUTTA 32, INDIA.

(Received June 1, 1967)

From magnetic measurements (Nèel *et al*, 1952; Lin, 1959) Within the temperature range 4°K to 950°K, of natural crystals of hematite (Elba), the presence of weak ferromagnetism and that of a transition in magnetic properties at about 250°K have been well established. From neutron diffraction studies (Shull *et al*, 1951) possibility of such a transition was ascribed to the change of the direction of the antiferromagnetic axis from that along the trigonal axis to that along the basal plane when the temperature is raised. Persistence of weak ferromagnetism even below 250°K which is contrary to the experimental observations with synthetic hematite (Guilaud, 1951), has been thought to be due to the presence of impurities, dislocations and non-uniformities in the lattice, which are usually present in the natural crystals. The magnetic behaviours of samples of hematite obtained from different origins are therefore expected to be different owing to the difference in the nature of the impurities and defects. But no experimental work has yet been reported to verify the suggestion. The study of the magnetic properties of a sample obtained from Brazil (Fe_2O_3 96.01% (with .5%FeO), SiO_2

1.7%, TiO_2 1.9%, MgO .2%, Al_2O_3 .13%, S .1%, H_2O .15%) has therefore been undertaken. Measurements along different directions were made with different crystals obtained from the same sample and within the range 100°K to 1000°K . Results of measurements on a particular crystal are shown in fig. 1.

It is observed that below 250°K , magnetisation along the plane of fresh sample is much larger than that along the axis which is contrary to earlier observations (Néel 1952, Lin 1959). Also at these temperatures the susceptibility along the axis, unlike earlier observation, is quite comparable to that along the plane. The changes in the magnetic properties in the transition region are none too sharp or large as found by earlier observers. Such flattening has also been observed by Morin (1950) with synthetic hematite containing 1% Ti as impurity. The heat

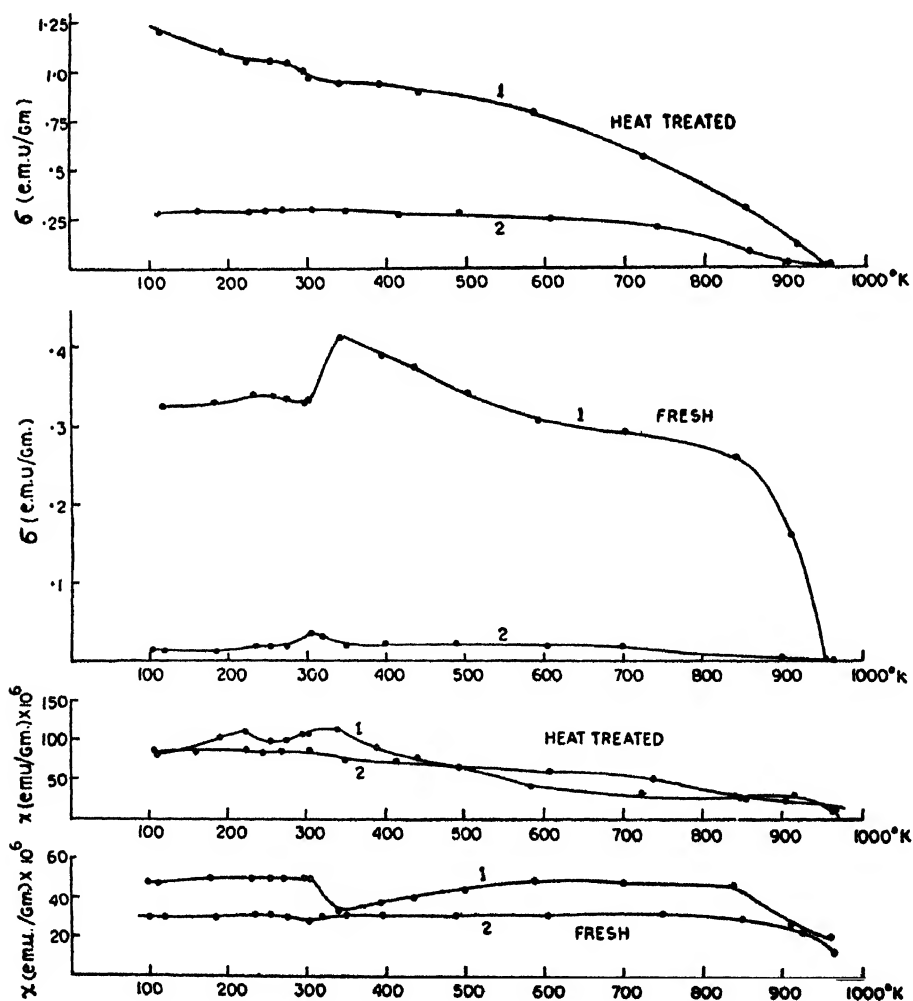


Fig. 1. Magnetisation (σ) and susceptibility (χ) at different temperatures of single crystals of hematite for fresh and heat treated samples. (1) along the basal plane (2) along the trigonal axis.

treatment of the samples during first cycle of measurement (in $\sim 10^{-3}$ mm) changed the absolute values of the magnetisation and susceptibility, along both the directions considerably, nature of temperature variation of these quantities not being very much affected, only the changes near the transition region becoming flatter. The susceptibility at the Néel temperature and the Néel temperature itself however remain nearly the same as earlier observed i.e. $\sim 20 \times 10^{-6}$ C.G.S., e.m.u and $955 \pm 5^\circ\text{K}$ respectively and are not affected by heat treatment.

Crystalline defects to which all these observations may be ascribed are presumably in the form of dislocations or substitutions in the sublattices rather than in the form of any ferromagnetic impurity such as magnetite etc., in which case there ought to have been a sharp discontinuity in the temperature variation of the magnetisation curve at the Curie temperature of the impurity.

Further investigations to explain the above observations in view of its structural and chemical aspects is in progress.

ACKNOWLEDGMENT

The author is thankful to Shri A. K. Dutta for constant guidance and to Professor A. Bose for his kind interest in the work. He also wishes to thank his colleague Mrs. D. Ghosh for help in setting up the low temperature device and to Dr. G. F. Claringbull, Keeper, Natural History Museum, London for kindly presenting the natural crystal of hematite.

REFERENCES

- Guilaud, C. 1951, *J. Phys. Rad.* **12**, 489.
 Lin, S. T. 1959, *Phys. Rev.* **116**, 1447.
 Morin, F. J. 1950, *Phys. Rev.* **78**, 819.
 Néel, L. and Pauthenet, R. 1952, *Compt. Rend.*, **234**, 2172.
 Shull, C. G., Strauser, W. A. and Woolan, E. O., 1951, *Phys. Rev.* **83**, 333.

9

MICROWAVE SPECTRA OF ETHYLAMINE MOLECULE

D. K. GHOSH, A. CHATTERJEE AND A. K. SAHA

SAHA INSTITUTE OF NUCLEAR PHYSICS, CALCUTTA

(Received April 10, 1967)

The ethylamine molecule is an asymmetric rotor. Exhaustive thermodynamic and infrared studies have not been made on this molecule. Some microwave absorption lines of ethylamine were observed by Matricon and Bonnet (1954). We have remeasured these lines and have extended the range of investigation.

The frequency range covered is 18.5 KMc/S to 26.0 KMc/S. Raytheon 2K 33B Klystron was used. In the region 20.5 K Mc/S—21.5 K Mc/S the klys-

tron presented a dead zone. The stark cell is an ordinary X-band wave guide section, about 8 ft. long. A variable amplitude square wave stark modulation at 100 Kc/s was used. The microwave power emerging from the cell was detected by a 1N26 crystal. The frequencies of the absorption lines were measured accurately by beating the Klystron frequency with standard markers in a 1N26 mixer crystal. Standard frequency at 100 kc/s was obtained from a primary frequency standard (General Radio AP 1100). More than sixty lines and their

TABLE I
Observed lines of Ethylamine

Frequency	Stark effect	Intensity	Frequency	Stark effect	Intensity
18511.95	1→2(+)	S	22564.26	2(+)	S
18625.30	2(+)	WW	22588.27	2(+)	WW
18655.63	1→2(+)	M	22603.46	2(+)	MS
18666.91	1→2(+)	M	22618.40	2(+)	S
18726.69	2(+)	M	22624.90	(?)	WW
18772.60	1→2(+)	W	22625.62	(?)	WW
18866.00	(?)	WW	22635.75	2(+)	S
19004.38	(?)	MS	22642.13	2(+)	S
19006.32	(?)	MS	22708.45	2(+)	M
19166.91	1→2(+)	MS	22751.49	2(+)	M
19187.43	1→2(+)	S	22752.32	2(+)	M
19254.43	1→2(+)	MS	22815.10	2(+)	WW
19329.01	2(+)	WW	22815.90	2(+)	WW
19343.03	2(+)	M	22909.39	2(+)	M
19497.10	1→2(+)	M	22975.50	2(+)	M
19700.86	2(+)	S	23195.67	2(+)	MW
19765.80	2(+)	M	23264.59	2(+)	or
19826.80	2(+)	M		1→2(+)	S
19900.55	1→2(+)	M	23369.67	2(+)	WW
20145.73	2(+)	M	23675.10	2(+)	WW
20237.69	2(+)	M	23928.30	1→2(+)	or
				2(+)	W
20311.52	2(+)	M			
21679.50	2(+)	WW	24027.49	2(+)	W
21729.20	2(+)	M	24261.88	2(+)	W
21730.25	2(+)	M	24291.00	2(+)	W
21736.25	2(+)	W	24418.40	2(+)	S
21767.10	2(+)	W	24802.64	2(+)	MS
21768.60	2(+)	W	24937.96	2(+)	M
21956.70	2(+)	M	25224.51	2(+)	W
22129.60	2(+)	S	25329.98	2(+)	S
22145.07	2(+)	MS	25396.85	2(+)	MS
22147.64	2(+)	MS	25562.15	2(+)	WW
			25977.37	2(+)	S

stark effects have been studied. The measured frequencies and intensities as well as the nature of their stark effects are listed in Table 1.

The intensities are termed S, MS, M, W and WW in order of their strengths. The nature of the stark effects observed on the various lines are : 1) 2(+) This denotes a second order stark effect, the stark components shifting to the higher frequency side of the line with increasing stark field. 2) $1 \rightarrow 2(+)$. This denotes lines which show a typical first order behaviour with the application of low stark fields and as the field is increased the second order stark effects sets in.

The presence of large number of absorption lines may be attributed to the splitting due to internal rotation in the molecule and due to inversion doubling. Detailed theoretical and experimental work is in progress and will be communicated later on with necessary details of the experimental set up.

REFERENCES

Matricon, M., and Bonnet, J., 1954, *J. Phys. Rad.*, **15**, 647.

BOOK REVIEWS

PROGRESS IN ELEMENTARY PARTICLE AND COSMIC RAY PHYSICS—Vol. VII, 1963. Edited by J. G. Wilson and S. A. Southuysen. Contributor: L. I. Dorman. Published by North-Holland Publishing Company, Amsterdam.

It is a single article by the Russian physicist L. I. Dorman of the Lebedev Physical Institute, Moscow. It contains an exhaustive accounts of general literature on Cosmic ray investigations covered upto the end of 1960 and publications in Russian upto the end of 1961.

In this volume, the contributor discusses the results on the primary Cosmic ray variations from the measurements of the secondary components over appropriate ranges of latitudes and describes exhaustively on the effects of Cosmic ray measurements of solar injected streams. All the established cosmic ray intensity variations are discussed with ample reference to published literature, especially during the I.G.Y. In particular, he has given a diagnostic interpretation of the "Forbush decrease" in terms of the Cosmic ray profile and in relation to the solar stream.

The introduction is followed by a description of the effects of the atmospheric and geomagnetic field on primary Cosmic radiation in second and third chapters. The fourth chapter deals with the time variations in Cosmic ray intensity and their theoretical interpretation in terms of the electromagnetic conditions in interplanetary space. Particles with energies between 10^9 and 10^{18} e.v. bombard the solar system with a practically isotropic intensity constant in time, but the number of low energy particles penetrating the weak fields in interplanetary space varies with the 11-year solar cycle. The last two chapters are concerned with the acceleration of Cosmic rays by the Sun, and possible anisotropies in the flux of particles from the galaxy. The last chapter, in particular, discusses the long term variation of the Cosmic ray intensity and the apparent 22-year variation.

Not unexpectedly, there is a heavy emphasis throughout this volume on the results and achievements of the Soviet investigators. However, a fairly comprehensive list of references is provided at the end of the volume.

Covering such a wide range of topics and spanning several years of investigations, especially over the past decade, this volume deserves the attention of Cosmic ray and Astrophysicists in general and other investigators in allied branches of Geophysics and Plasma physics.

S.D.C.

ELEMENTS OF PHYSICAL CHEMISTRY—by Samuel Glasstone and David Lewis. Macmillan & Co. Ltd. (1962), Papermac, Price 25s.

The book is practically a revised version of 'Elements of Physical Chemistry' by Glasstone. It differs from the previous one in ordering of chapters, relative emphasis on different topics, and new set of problems and reading references. On the whole the changes have been for the good. The language is clear, straightforward and precise, and unnecessary descriptive details have been avoided. The book will serve as a good text book for Honours undergraduates.

The ordering of chapters, however, is hard to understand. The philosophy with which the authors have approached the subject has not been made clear.

I think that elementary deductions of some basic equations of fundamental importance (such as Maxwell-Boltzman distribution law, Debye equation for dipole moment, Debye-Huckel Theory of strong electrolytes) display to the students the types of thought that played a part in development of Physical Chemistry. These deductions have been omitted in the book. Some elementary non-rigorous deduction could have been given just to enable the students to see how these results were arrived at.

According to the authors themselves Physical Chemistry is 'concerned with the elucidation or clarification of the principles underlying those transformations of matter known as chemical reaction'. This aim, however, could not be fully achieved in the book due to inadequate discussion on Quantum Theory. An explanation of chemistry can be achieved only from Quantum mechanics, which has been responsible for giving birth to most of the modern ideas in chemistry. The historical background and the reasonings by which Planck arrived at Quantum Theory could have been indicated, and the application of Schrödinger equation to a few simple cases could have been discussed (as done by Moore, for example). The authors have not tried to explain the change of physical properties with change in molecular architecture, which is one of the main aims of Physical Chemistry.

Apart from these minor points, the book is well balanced and well-written and will serve its purpose as a text book for Honours undergraduates.

M.C.

INDIAN JOURNAL OF PHYSICS

Vol. 41

No. 7

AND

Vol. 50

PROCEEDINGS

No. 7

OF THE

INDIAN ASSOCIATION FOR THE CULTIVATION OF SCIENCE

(Edited in collaboration with the Indian Physical Society).

JULY 1967

PUBLISHED BY THE
INDIAN ASSOCIATION FOR THE CULTIVATION OF SCIENCE
JADAVPUR, CALCUTTA-32

COSMIC RAY STARS IN PHOTOGRAPHIC EMULSION AT HIGH ALTITUDE

S. R. GANGULY, S. K. MONDAL AND S. D. CHATTERJEE

DEPARTMENT OF PHYSICS, JADAVPUR UNIVERSITY, CALCUTTA-32

(Received November 3, 1966)

ABSTRACT. Ilford G₅ photographic plates were sent in jet planes to an altitude of 7100 m and stars formed in the emulsion were investigated. 70.5% of the stars are found to be produced by neutrons; the size distribution of stars formed by charged and neutral primaries are represented in two histograms. The ratio of α -particles to protons released in a star is studied as a function of star size and this ratio is found to be constant at 0.43 for stars with 8 or more prongs. Energy distribution of α -particles from stars, as well as the variation of the number of grey particles with star size are presented graphically; mean energy of α -particles is found to be 13.4 Mev and the number of grey tracks is seen to increase linearly with star size. The size number distribution of all stars has been studied and this seems to be represented by two straight lines: $N(>n) = A \exp(-0.341n)$ for $n \leq 6$, and $N(>n) = B \exp(-0.256n)$ for $n > 6$. The distribution curve is compared with those obtained by other workers at 3460 m and 21000 m respectively and a steepening of slope with decrease of altitude is noted. A method of obtaining energy spectrum from the size distribution is indicated.

INTRODUCTION

The first experimental evidence for the nuclear disintegrations caused by cosmic rays in photographic emulsion is due to Blau and Wambacher (1937). They obtained pictures of sets of tracks radiating from a common origin, which came to be known as "stars". Such a star was caused by the simultaneous ejection of several ionizing particles from a disintegrating nucleus. These stars were subsequently investigated with improved types of emulsions by various workers like Perkins (1947, 1950), Lord and Schein (1949), Yagoda *et al.* (1949), George and Jason (1949), Camerini *et al.* (1949), Brown *et al.* (1949), Bernardini *et al.* (1950) and Page (1950).

Most of the previous observations were carried out at mountain altitudes. The present experiment was however undertaken to study the phenomenon of star formation in photographic emulsion at altitudes higher than that of mountain stations, in order to investigate their size distribution, the relative number of charged and neutral primaries among the star producing radiation and also some special features regarding the nature of secondaries from stars.

EXPERIMENTAL DETAILS

Sealed containers with Ilford G₅ plates, 100 μ thick, were sent up in military jet aircrafts flying on short trips at an average altitude of 7100 m, the total exposure time for each packet at this altitude being about 10 hours.

The tracks emanating from the stars were divided into three categories according to their grain densities, g :

- (1) "Thin" tracks, $g < 1.5g_{min}$,
- (2) "Grey" tracks, $1.5g_{min} < g < 5g_{min}$,
- (3) "Black" tracks, $g > 5g_{min}$,

where g_{min} is the grain density of a relativistic and singly charged particle.

The grey and black tracks have been classified together as "heavy" tracks. In case of protons, black tracks correspond to particles of energy less than about 40 Mev; grey tracks of energy between 40 and 330 Mev, and thin tracks of energy greater than about 330 Mev. A star size is usually expressed by the number of prongs emanating from the star.

Photomicrographs of a few typical stars recorded in the present experiment are shown in Fig. 1.

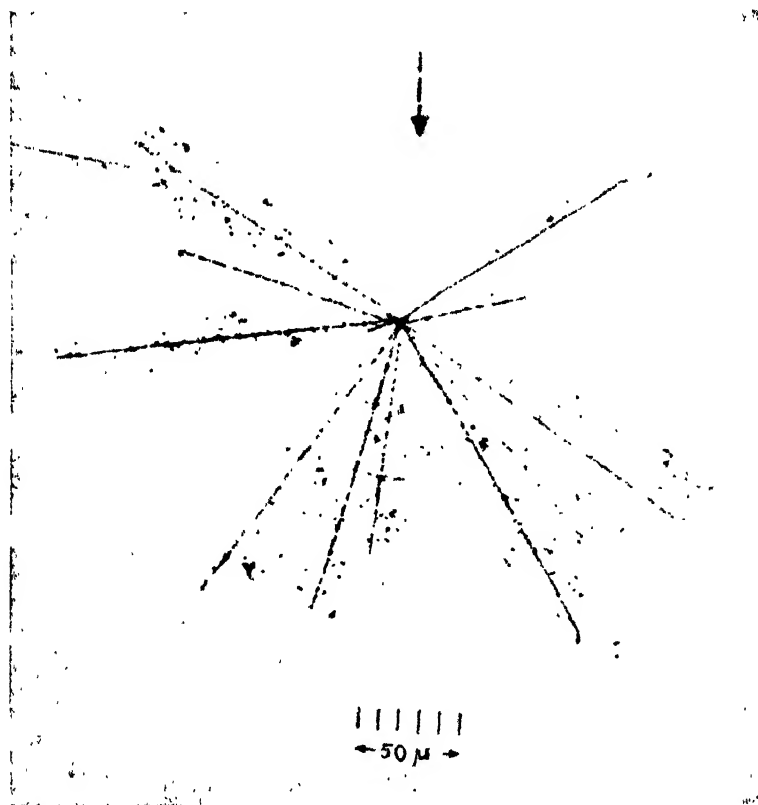


Fig. 1 (a) A star induced by a neutral particle. The probable direction of incidence of the primary is indicated roughly by the arrow.

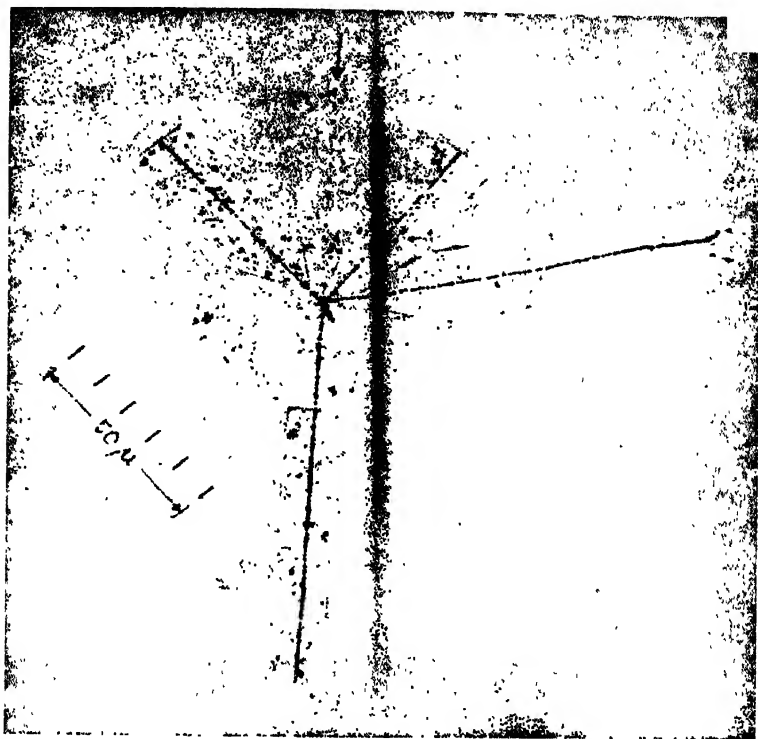


Fig. 1(b) A star induced by a charged particle. The path of the primary particle is indicated by the arrow.

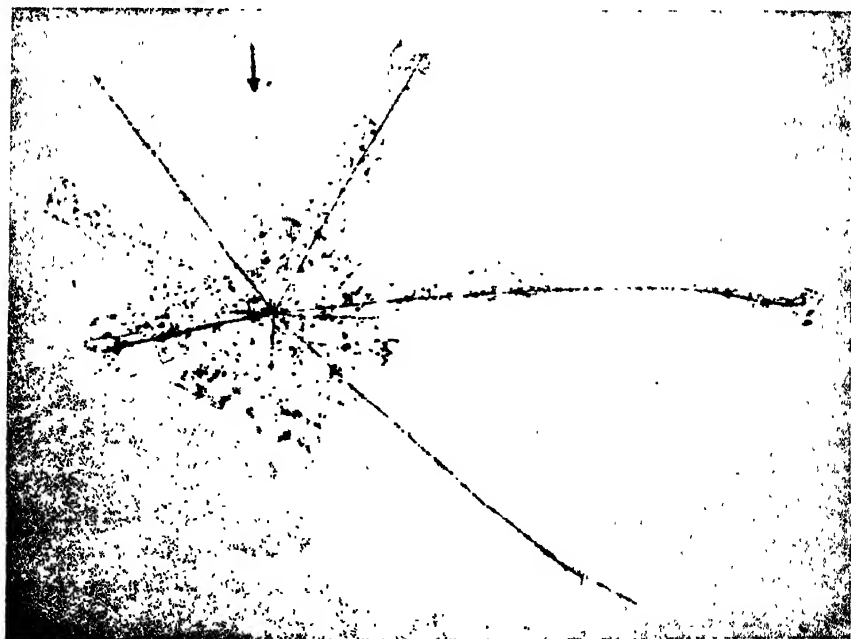


Fig. 1(c) A star induced by a charged particle. The arrow indicates the path of the primary particle.

RESULTS AND DISCUSSIONS

A. *Nature of the primaries producing stars*

During the exposure, the plates were kept in a definite orientation with the emulsion side lying in a vertical plane, the same end of the plate always facing upwards. It was thus possible to determine the direction of motion of a particle during its passage through the emulsion, relative to the vertical. It was observed that most of the thin tracks were inclined at small angles to the vertical. It was therefore reasonable to assume that most of the thin tracks "above" (i.e. in the upper hemisphere) the stars were due to initiating particles, whereas the thin tracks in the lower hemisphere were due to secondaries.

A second criterion for distinguishing the primary of a star was obtained from the following considerations. The disintegration of a heavy nucleus following the collision of a high energy particle proceeds in two separate steps. The first is the ejection from the nucleus of mesons and of high energy nucleons; the second is the "evaporation" of the residual excited nucleus. The first type of emitted particles produces thin tracks which are well collimated around the initial direction of motion of the primary, whereas the evaporation tracks do have almost isotropic distribution. The primary nucleon will, therefore, lie on the axis of symmetry of the emitted thin tracks and on the other hemisphere of the star.

Whenever a thin track was observed in the upper hemisphere of a star at a small angle with the vertical, and/or more or less in line with the axis of symmetry of the secondary fast particles, then that particular star was recognised as being produced by a charged primary; the absence of such a track would designate the star as being induced by a neutral primary. The primary particles, if charged, are mostly protons while the uncharged ones are usually neutrons. Somewhat similar discrimination was adopted by Brown *et al.* (1949) and Page (1950) to identify the primary of a star. Some of the stars, however, could not be recognised with regard to their primaries and they were left out of the following analysis.

(i) *Relative multiplicity of stars due to charged and uncharged primaries*

Stars were analysed according to whether they were induced by charged or uncharged primaries and it was found that 70.5% of the total number of stars recorded had been initiated by neutral particles.

This may be compared with the relative rate at 3460 m altitude as measured by Page (1950) and by Brown *et al.* (1949). These results are listed in Table I together with the results of the present investigation.

If it is assumed that the cross-section for star production is the same for charged (protons) and uncharged (neutrons) primary particles, the above results show that at the atmospheric depths considered, neutrons capable of producing stars are more numerous than the protons.

TABLE I

Author	Altitude	Percentage of stars formed by	
		Charged primaries	Neutral primaries
1. Pago	3460 m	17.0	83.0
2. Brown <i>et al.</i>	„	17.4	82.6
3. Present authors	7100 m	29.5	70.5

Most of the particles responsible for the stars at these depths are of secondary origin and their abundance in the atmosphere is determined by their rate of production and their rate of decay. The rate of production of protons and neutrons in air is mostly the same, but while neutrons disappear only by nuclear collisions, protons lose energy by ionization also. Therefore a comparatively smaller number of protons will be able to reach the lower atmosphere from an upper layer where they are produced.

Also, the relative number of protons will be smaller, with greater atmospheric depth of observation. This is illustrated from the rates at different altitudes as shown in Table I.

(ii) *Size distribution of stars due to charged and neutral primaries*

The number of stars induced by charged and uncharged primary particles as a function of star size are represented by the histograms shown in Fig. 2(a) and 2(b). The histograms clearly point out the difference in the size distribution in the two cases. In case of stars with fewer prongs, the neutron induced stars are much more in number than those induced by protons; whereas in case of larger stars both are about equally numerous. The same results were also obtained by Page (1950).

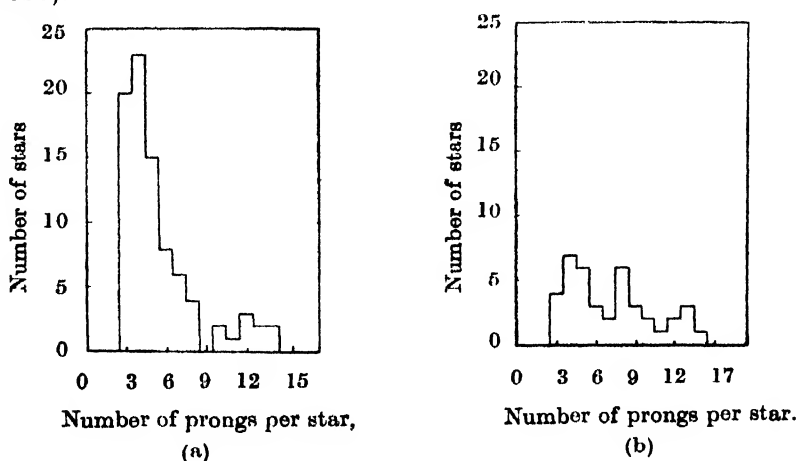


Fig. 2. Number of stars as a function of star size.

(a) Stars induced by charged primaries.

(b) Stars induced by neutral primaries.

The difference in the frequency of stars formed by neutrons and protons can be explained as being due to their varied energy spectrum. Compared to the neutrons, the protons are subject to an additional energy loss due to ionization. This effect becomes an important factor in the absorption of protons when the energy is sufficiently low. Thus at low energies there would be considerably more neutrons than protons, whereas at high energies, ionization loss is negligible and neutrons and protons will be present in comparable numbers. This explains why most of the low energy stars are neutron-induced.

B. *Some characteristics of the secondary particles emitted in a star*

In order to gain information regarding the process involved in the star formation, the measurements of some of the characteristics of the secondary particles were undertaken.

(i) *Alpha-proton emission ratio*

The low energy secondary particles emitted in a star are believed to be due to the "evaporation" process of the highly excited nucleus struck by the incident particle. The "evaporation" theory of nuclear disintegration was applied to the low energy particles from stars in photographic emulsion by Bagge (1946) and by Harding *et al.* (1949) and was extended further by Le Conteur (1950), who calculated the energy distribution of evaporated particles and also obtained the probability for the emission of different types of particles in a star as a function of the excitation energy of the nucleus.

One of the conclusions of the evaporation theory that can be easily checked against the experimental results is the ratio of alpha particles to protons among the secondaries of a star. The results of measurement of the mean proportion of alpha-particles in a star, for stars of different prong numbers are shown in Fig. 3. For larger values of prong number, particles heavier than alpha-particles were found to be emitted quite often. This phenomenon was also observed by Perkins (1950) and these prongs were excluded from the data plotted.

TABLE II

Authors	alpha to proton ratio
Perkins (1950)	0.50
Bernardini <i>et al.</i> (1950)	0.35
Page (1950)	0.37
Present authors	0.43

It is seen from Fig. 3 that the proportion of alpha-particles in a star decreases with increasing star size and for stars with greater than 8 prongs, the decrease is so slow that the ratio R of alpha-particles to the total number of heavy prongs

may be taken to be a constant at a value of $R = 0.30$. This datum gives for alpha-particles to proton ratio as 0.43 (taking all the singly charged secondaries to be protons).

The values for the average ratio of alpha-particles to protons emitted in larger stars obtained experimentally by different workers are shown in Table II. The results of calculations (using parameter 'd') of Le Couteur (1950) on the basis of evaporation theory are also plotted in dotted line in Fig. 3 for comparison. It

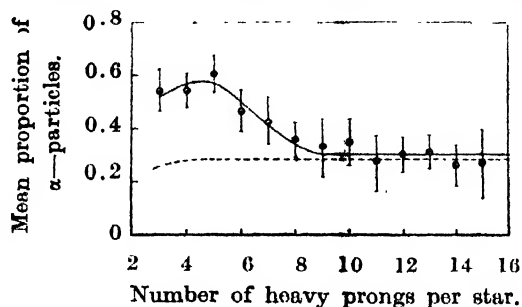


Fig. 3. Ratio of the number of alpha-particles to the total number of heavy prongs as a function of star size.

The dotted curve shows that calculated by Le Couteur (using his parameter 'd').

is seen that the calculated value of R is almost constant and equal to 0.28 and there is rough agreement between the theory and the present experimental results for larger stars.

The discrepancy for stars with small prong numbers are due to the stars formed in light C, O, N nuclei present in the emulsion, while Le Couteur's calculations refer to stars formed in Ag and Br nuclei. From the measurement of stars formed in pure gelatine, Perkins (1949) had shown that the alpha-proton ratio was much higher in stars formed in gelatine than in ordinary emulsion. It was also found that light C, N, O nuclei in emulsion contributed appreciably only to stars of less than about 6 to 8 prongs. This is also evident from the clear break at about prong number six in the size distribution curve of stars discussed later (in section C) in this paper. The above considerations explain the high value of alpha/proton ratio in smaller stars.

(ii) Energy distribution of alpha-particles from stars

The majority of alpha-particles emitted in stars stopped in emulsion. It was therefore possible to determine the distribution in energy of the alpha-particles by range measurement. The number of alpha-particles as a function of energy is represented in a histogram in Fig. 4 for stars with 6 or more heavy prongs (upto 15 prongs, which is the highest measured), only these stars being recognised as solely due to Ag and Br nuclei.

It is seen from Fig. 4 that the most probable energy of the α -particles is about 10 Mev while the average energy is 13.4 Mev. The general features of the

distribution is in agreement to the measurements of other workers viz. Harding *et al.* (1949) and Perkins (1950).

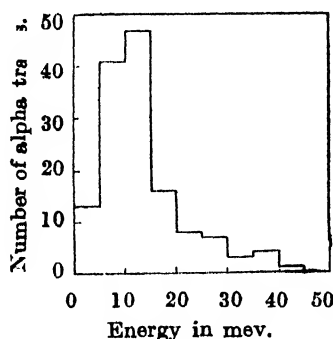


Fig. 4. Energy distribution of alpha particles from stars.

(iii) *Proportion of grey tracks*

Grey tracks are mostly due to protons of energy between about 40 MeV to 330 MeV and carry away most of the energy released in a star process. The average number of grey tracks was measured for stars with different number of heavy prongs and the results are shown graphically in Fig. 5. In order to reduce

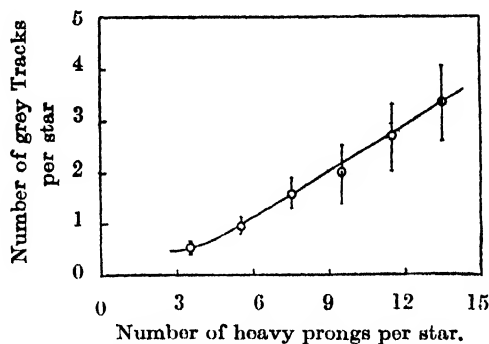


Fig. 5. Average number of grey tracks as a function of star size.

statistical errors, the star sizes have been grouped in twos, that is, grey tracks corresponding to stars of 3 and 4 prongs have been added together to give a single point in the graph, grey tracks from stars of 5 and 6 prongs are added to give the second experimental point, and so on.

It is seen from Fig. 5 that for the stars of 6 or more prongs, the number of grey tracks increases linearly with star size. The result is similar to that of Brown *et al.* (1949).

C. *Integral size distribution of stars*

The relative rate of occurrence of stars having different number of heavy prongs is represented in a semi-logarithmic plot in Fig. 6. In the present experiment, measurements were made only on stars having three or more prongs.

From the figure it is seen that the number (N) of stars decreases almost exponentially as the number (n) of heavy prongs per star increases. The experimental points, however, fall on two different straight lines in the semi-logarithmic plot, and the distribution can be expressed as :

$$N(>n) = A \exp(-0.341 n) \text{ for } n \leq 6$$

and
$$N(>n) = B \exp(-0.256 n) \text{ for } n > 6, \quad (1)$$

where $N(>n)$ represents the number of stars having more than n heavy prongs, and, A and B are constants.

Page (1950) and George and Jason (1949) also reported similar distribution in the number of stars with star size, represented by two straight lines with different slopes. The clear break at approximately $n = 6$ arises due to the fact that the light nuclei C, N, O in emulsion do not contribute appreciably to stars of more than six prongs. This fact had been verified by Perkins (1949) by making measurements with alternate layers of pure gelatine and normal emulsion as mentioned earlier. Thus the stars with more than six prongs can be recognised as almost solely due to Ag and Br. nuclei and these stars fall on a separate single straight line in Fig. 6.

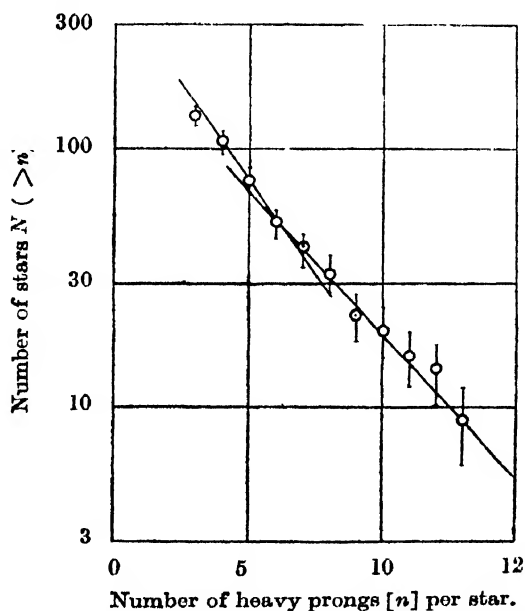


Fig. 6. Integral size distribution of stars.

When this size-number distribution found in the present experiment is compared with those obtained by other workers at different elevations, it is found that slope of the distribution curve changes with altitude, being steeper at lower elevations. To bring out this altitude variation of the power of the exponential distribution curve, integral size distribution of stars at three different elevations

has been shown together in Fig. 7. Curve A is taken from that obtained by Page (1950) at 3460m, curve B is that of the present experiment (at 7100m) re-plotted from Fig. 6 while curve C is computed from the data of Camerini *et al* (1949) obtained at 21000m, the three (smoothed) curves being normalised at $n = 14$. The decrease in slope with increasing altitude is clearly distinguishable. This result may be explained from the fact that the average energy of the star producing

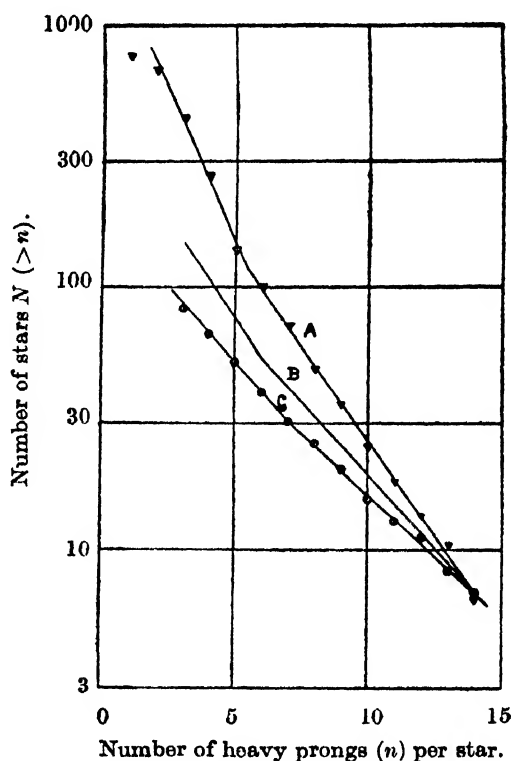


Fig. 7. Comparison of size distribution at different altitudes.

A—at 3460 m, obtained by Page (1950),

B—at 7100 m, present experiment,

C—at 21,000 m, obtained by Camerini *et al.* (1949).

radiation increases with elevation so that there are relatively more higher energy particles at upper elevation producing comparatively larger number of bigger stars.

The number of heavy prongs in a star is a measure of the energy of the initiating primary. The excitation energy of the evaporating Ag and Br nuclei disintegrating into slow particles (< 30 Mev) had been calculated by Le Couteur (1950) and was found to be a linear function of the number of black prongs per star. But if the total energy, including also those released in thin and grey tracks, is considered, the energy of the primary is no more a linear function of the star size.

Brown *et al.* (1949) have made extensive measurements of the energy of the different types of particles emanating from a star and have shown that the primary energy can be expressed as a function of the star size by an empirical relation :

$$E = 37n + 4n^2 \quad \dots (2)$$

where n is the number of heavy prongs in a star. Assuming the cross-section for star production to be independent of the energy within the limits concerned, the size distribution of stars given by relations (1) at the atmospheric depth of 420g cm^{-2} , combined with an energy-size relation like that of equation (2), would give the energy spectrum of the star producing radiation (N -component of cosmic rays) at this depth.

ACKNOWLEDGMENTS

We are grateful to the Eastern Air Command of the Indian Air Force for conducting the special flights for exposing the plates to cosmic radiation at high altitudes. Our thanks are also due to Sri N. C. Ghosh, M.Sc., of this department for his valuable help in processing the photographic plates.

REFERENCES

- Bagge, E., 1946, *Cosmic radiation* (Ed. by Heisenberg), Dover publications.
 Bernardini, G., Cortini, G. and Manfredini, A., 1950, *Phys. Rev.*, **79**, 952.
 Blau, M. and Wambacher, H., 1937, *Akad. Wiss. Wien.*, **146**, 623.
 ———, 1937, *Nature*, **140**, 585.
 Brown, R. H., Camerini, U., Fowler, P. H., Heitler, W., King, D. T. and Powell, C. F., 1949, *Phil. Mag.*, **40**, 862.
 Camerini, U., Coor, T., Davies, J. H., Fowler, P. H., Lock, W. O., Muirhead, H. and Tobin, N., 1949, *Phil. Mag.*, **40**, 1073.
 George, E. P. and Jason, A. C., 1949, *Colston Papers*, Butterworths Scientific Publications, London.
 Harding, J. B., Lattimore, S. and Perkins, D. H., 1949, *Proc. Roy. Soc.*, **A196**, 325.
 Le Couteur, K. J., 1950, *Proc. Phys. Soc.*, **A63**, 259, 498.
 Lord, J. J. and Schein, M., 1949, *Phys. Rev.*, **75**, 1956.
 Page, N., 1950, *Proc. Phys. Soc.*, **A63**, 250.
 Perkins, D. H., 1947, *Nature*, **160**, 707.
 ———, 1949, *Phil. Mag.*, **40**, 601.
 ———, 1950, *Phil. Mag.*, **41**, 138.

ELASTIC RESONANCE IN ELECTRON-HYDROGEN SCATTERING

S. N. BANERJEE, R. JHA AND N. C. SIL

DEPARTMENT OF THEORETICAL PHYSICS,

INDIAN ASSOCIATION FOR THE CULTIVATION OF SCIENCE, JADAVPUR, CALCUTTA-32, INDIA.

(Received December 16, 1967).

ABSTRACT. The singlet s -wave phase shifts in the elastic scattering of slow electrons by atomic hydrogen have been calculated in the energy range below the threshold for the excitation of second quantum level (10.2 eV) by Hulthén's variational method. The exchange effect has been allowed for and the polarisation effect has been considered through the process of virtual excitation to $2S$ and $2P_0$ levels. We obtain a resonance level at 9.55 eV energy, which agrees favourably with the recent experimental findings and the results of other theoretical calculations.

INTRODUCTION

Several experiments have been carried out on slow electron scattering by atomic hydrogen. Schulz (1964), Kleinpoppen *et al.* (1965) and McGowan *et al.* (1964) have found experimentally elastic resonances below the threshold for excitation of electronic states of atomic hydrogen.

A number of theoretical investigations has been made on $\bar{e}-H$ collision problem which has been discussed in our previous work (1965), where we have dealt with the same problem by Hulthén's variational method considering the polarisation effect through the virtual excitation to $2S$ and $2P_0$ level but neglecting the exchange effect. Here in the present paper, we have used the same variational method and have considered the exchange effect by explicitly antisymmetrising the wavefunction with respect to the atomic and incoming electrons, the polarisation effect has been taken into account in the same way as in our previous work (1965) so as to include virtual excitation to $2S$ and $2P_0$ levels. Recently, Geltman (1965) has applied variational method to investigate the $\bar{e}-H$ scattering with a particular choice of trial function so as to take into consideration the virtual excitation to higher excited states and has obtained very narrow resonances at electron energies below the first inelastic threshold. Burke and Taylor (1966) also have carried out close coupling calculations including correlation in their trial function on the resonances in $\bar{e}-H$ scattering.

Our calculations for singlet S -wave phase shifts indicate a resonance at an energy of 9.55 eV, which agrees satisfactorily with the experimental findings of Schulz (1964), Kleinpoppen *et al.* (1965), McGowan *et al.* (1965) and also with the results of other theoretical calculations.

THEORY

The wavefunction $\psi(r_1, r_2)$ of the system of two electrons moving in the field of a proton satisfies the wave equation $(H-E)\psi(r_1, r_2) = 0$... (1)

with
$$H = -\frac{\Delta_1^2}{2} - \frac{\Delta_2^2}{2} - \frac{1}{r_1} - \frac{1}{r_2} + \frac{1}{r_{12}}$$

in atomic units (i.e. $e = m = \hbar = 1 = a_0$), here r_1 and r_2 are the co-ordinates of the atomic and incoming electrons, relative to the proton and r_{12} is their mutual distance.

Since the total wave function of the system of two electrons must be anti-symmetric for exchange of their space and spin co-ordinates, we therefore choose for ψ the forms

$$\psi^\pm(r_1, r_2) = \frac{1}{\sqrt{2}} \sum_n \{ \psi_n(r_2) F_n^\pm(r_1) \pm \psi_n(r_1) F_n^\pm(r_2) \}$$

where $+$ and $-$ signs correspond to singlet and triplet states respectively and ψ_n represent the wave function for the n -th state of the hydrogen atom and satisfies the eigen value equation

$$(\Delta^2 - 2/r - 2E_n)\psi_n(r) = 0,$$

E_n represents the eigen energy of the n -th state of the atom.

If such functions can be had in which F^\pm_n have the asymptotic forms

$$F^\pm_n \sim e^{ik_0 r} \delta_{n0} + \frac{e^{iknr}}{r} f^\pm_n(\theta, \phi)$$

then the respective differential cross sections for excitations of the n -th state for antiparallel and parallel alignment of electrons are

$$\frac{K_n}{K_i} |f^\pm_n(\theta, \phi)|^2.$$

Here total energy $E = \frac{K_0^2}{2} + E_0 = \frac{K_n^2}{2} + E_n$ and E_0 represent the eigen energy of the ground state of the atom, K_0 , K_n represent respectively the momenta of the incident electron and scattered electron after excitation of the n -th state of the atom.

We shall consider only the symmetric wavefunction corresponding to the singlet case and neglect all states for $n \neq 0$. Henceforth we shall omit the superscript '+' for convenience.

Therefore,
$$\psi(r_1, r_2) = \frac{1}{\sqrt{2}} [\psi_0(r_1)F_0(r_2) + \psi_0(r_2)F_0(r_1)] \quad \dots (2a)$$

with

$$F_0(r) \sim e^{ik_0 r} + \frac{e^{ik_0 r}}{r} f(\theta, \phi) \quad (2b)$$

To solve eqn. (1) under the boundary conditions in (2b), we shall use Hulthén's variational method choosing our trial wave function $\psi(r, r_2)$ as

$$\psi(r_1, r_2) = \chi(r_1, r_2) F_0(r_2) + \chi(r_2, r_1) F_0(r_1) \quad \dots (3)$$

where
$$\chi(r_1, r_2) = \psi_{1a}(r_1) \left\{ 1 - \frac{\alpha^2 + \beta^2}{2} \cdot e^{-2\mu r_2} \right\} \\ + \alpha \psi_{2a}(r_1) \cdot e^{-\mu r_2} + \beta \psi_{2p_0}(r_1, r_2) e^{-\mu r_2} \quad \dots (3a)$$

the polar axis being along r_2 , $\mu = 1$

and
$$F_0(r_2) = \left\{ \frac{\sin K_0 r_2}{K_0 r_2} + (a + b e^{-r_2})(1 - e^{-r_2}) \frac{\cos k_0 r_2}{K_0 r_2} \right\} \quad \dots (3b)$$

It may be mentioned that we have considered only S -wave scattering and as in our previous work (1965) χ satisfies the normalisation condition $\int \chi^* \chi dr_1 = 1$ correct to terms of the order of α^2 and β^2 .

Substituting $\psi(r_1, r_2)$ from (3), (3a) and (3b) in the variational integral $L = \int \psi^*(H - E)\psi dr_1 dr_2$ and using Hulthén's variational method, the value of a is determined, the phase shift is related to a by $\eta_0 = \tan^{-1}a$ neglecting higher powers of α and β .

RESULTS AND DISCUSSIONS

We have evaluated only the singlet S -wave phase-shift values (η_0) for the case $b = 0$ in the trial function $F_0(r_2)$ for energies below the threshold for excitation of second quantum levels by using only the coupling of $1S$, $2S$ and $2P_0$ states.

We have plotted the phase-shifts η_0 against K_0^2 in Fig. 1, where we notice the peculiar resonating behaviour i.e. there is a sharp increase in phase-shift values above $K_0^2 = .70$.

We have shown Q_{res} as a function of K_0^2 in Fig. 2. By making use of Breit-Wigner cross-section formula

$$Q_{res} = \frac{4\pi}{K_0^2} \cdot \frac{\Gamma^2/4}{(E - E_{res})^2 + \frac{\Gamma^2}{4}}, \quad \text{we obtain}$$

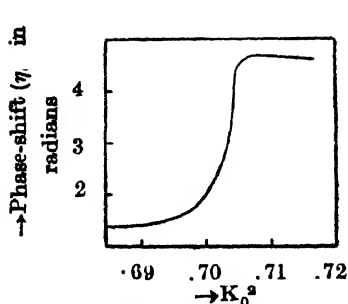


Fig. 1. The singlet S-wave phase shift is plotted as a function of K_0^2 in the neighbourhood of resonance.

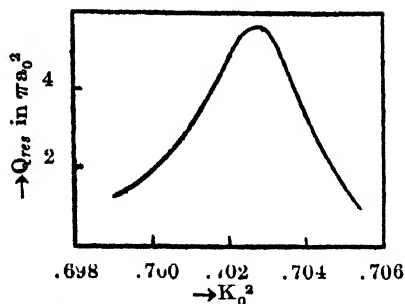


Fig. 2. The resonance part of S-wave cross section is plotted as a function of K_0^2 .

$E_{res} = (.7027 \text{ a.u.}) 9.55 \text{ ev}$, the width $\Gamma \sim .04 \text{ ev}$ and the resonance cross section $= 5.56\pi a_0^2$.

The first experimental report on a resonance in the scattering of electrons by atomic hydrogen has been made by Schulz (1964) at $(9.7 \pm .15) \text{ ev}$. Such a resonance has been further confirmed by the observations of Kleinpoppen and Raible (1965) who found that it is centred around $(9.73 \pm .12) \text{ ev}$. Recently McGowan et. al., (1965) have reported two resonances, one near 9.45 ev and the other near 9.68 ev.

Burke and Schey (1962) have obtained a resonance at 9.61 ev with a width of .109 ev in the 1S state and the corresponding resonance cross section being $5.66\pi a_0^2$. Nearly similar results were obtained by O'Malley and Geltman (1965), Temkin and Pohle (1965) and others. Most recently, Burke and Taylor (1966) have obtained two resonances, one at 9.560 ev and the other at 10.178 ev with widths of .0475 ev and .00279 ev respectively.

In conclusion, we may say that our present formulation yields satisfactory results for the position of elastic resonance in $\bar{e}-H$ scattering.

ACKNOWLEDGMENT

The authors are thankful to Prof. D. Basu for his kind interest and valuable discussions throughout the progress of the work.

REFERENCES

- Banerjee, S. N., Jha, R., Sil, N. C., 1965, *Indian J. Phys.*, **39**, 455.
- Burke, P. G. and Taylor, A. J., 1966, *Proc. Phys. Soc.*, **88**, 549.
- Burke, P. G. and Schey, H. M., 1962, *Phys. Rev.*, **126**, 147.
- Gailitis, M. and Damburg, R., 1963, *Proc. Phys. Soc.*, **82**, 192.
- Geltman, S., 1965, *Astro. Phys. J.*, **141**, 376.
- Herzenberg, A., Kwok, K. L. and Mandl, F., 1964, *Proc. Phys. Soc.*, **84**, 345.
- Kleinpoppen, H. and Raible, V., 1965, *Phys. Letters*, **18**, 24.
- McGowan, J. W., Clarke, E. M. and Curley, E. K., 1965, *Phys. Rev. Letters*, **15**,
- O'Malley, T. F. and Geltman, S., 1965, *Phys. Rev.*, **137**, 1344.
- Schulz, G. J., 1964, *Phys. Rev. Letters*, **13**,
- Temkin, A. and Pohle, R., 1963, *Phys. Rev. Letters*, **10**, 22.

ON THE ACOUSTICS OF SHOCKS GENERATED BY THE RUPTURE OF DIAPHRAGMS IN A TUBE

T. C. BHADRA*

NATIONAL CENTER FOR ATMOSPHERIC RESEARCH, BOULDER, COLORADO

(Received September 20, 1966)

ABSTRACT. The results are presented of the analysis of oscillograms due to shocks generated by the rupture of diaphragms in a shock tube. Shock overpressures p_0 and the duration t_0 of ceiling pressure to zero level transit have been determined from the oscillograms as functions of compression chamber pressures and distances. Shock velocities have been determined by the time of arrival method. The values of shock overpressures as determined by these two methods agree satisfactorily.

INTRODUCTION

Reiman (1880) and Hugoniot (1887) have already very early theoretically demonstrated that a pressure wave of finite amplitude changes its form during the propagation in such a manner that its front becomes increasingly steeper and its end increasingly flatter. A shock wave is characterized by a relatively large change in excess pressure across a very small region of space. Such shocks can result from explosions like the rupture of a membrane separating a region of high pressure from a region of low pressure in a tube or from a detonation of chemical explosives.

The literature on shock waves is extensive (Courant *et al.*, 1948) and here we shall content ourselves with the analysis of the pressure oscillograms of shock waves generated by breaking the diaphragm separating high and low pressure regions in a tube. The short duration of the shock makes an analysis of the direct measurements rather difficult, so that the analytical evaluation of the Furrer integral from the oscillograms has been pursued. In this respect the work of Furrer (1946) is an outstanding contribution to the physics and mathematics of explosions due to TNT explosives, cannon shot, and pistol shot. Leonard (1962) briefly discussed his work in a review article on explosive sound sources. In the present investigation, the method used by Furrer to analyse the pressure oscillograms due to the above mentioned explosions will be followed to analyse the pressure oscillograms due to the shock generated in a tube by the rupture of the membrane. Here no attempt has been made to introduce a correction term in the pressure distribution along the axis of the tube due to reflection, because of the complex mathematics involved to compute the reflection term. This is partly due to the irregular inside structure of the shock tube.

*Permanent address: Bose Institute, 93/1 Upper Circular Road, Calcutta 9, India.

In order to gain a clear insight into the physical characteristics of a shock, it is important to know the chronological sequence of the atmospheric pressure and its speed of propagation. The shock overpressure was measured by means of a calibrated piezoelectric transducer made by Kistler company, and speed of propagation was measured by the time of arrival method.

II. THEORETICAL CONSIDERATIONS

The most essential characteristics of a shock are the sudden onset and the short duration. In the case of a shock due to explosion, we have to expect a virtually discontinuous pressure leap. The parameters decisive for the effect of an explosion thrust, especially the pressure leap and the air speed, can be traced back to a single parameter, the wave velocity. In the vicinity of the explosion site, where the pressure leap and the air speed are high, the velocity of a wave is also very high. With increasing distance it approaches the velocity of sound asymptotically. As opposed to classical sound relationship a difference results in that the speed of propagation is no longer a pure material constant and the step pressure is added to the hydrostatic pressure, but these differences disappear very rapidly.

CHRONOLOGICAL PRESSURE DISTRIBUTION

In order to study the common form of the chronological pressure distribution of a shock in a cylindrical enclosure the following simple function which has been used by Furrer to study explosive waves in open atmosphere will be employed to analyse the pressure oscillograms in the present investigations :

$$p_t = p_0 / \cos \theta e^{-bt} \cos (\Omega t + \theta) \quad \dots (1)$$

where p_0 , the pressure ceiling, and t_0 , the duration of the pressure ceiling up to zero transit, will be introduced as two parameters from the oscillograms. Equation (1) has been found to fit the experimental shock tube data satisfactorily.

The following boundary conditions are to be satisfied for the determinations of b , Ω , and θ from the magnitude of p_0 and t_0 .

1. The chronological integral must be zero, i.e., physically the elastical procedure will be assumed and there will be no gas transport.

$$\int_0^{\infty} p_t dt = \frac{p_0}{\cos \theta} \int_0^{\infty} e^{-bt} \cos (\Omega t + \theta) dt = 0 \quad \dots (2)$$

$$\text{i.e.,} \quad \int_0^{\infty} e^{-bt} \cos (\Omega t + \theta) dt = 0 \quad \dots (3)$$

$$\text{which leads to } tg\theta = \frac{b}{\Omega} \quad \dots (4)$$

The maximum of $F(p_i) = \frac{p_{0i}}{2b}$, when $\omega^2 = \Omega^2 + b^2$ (12)

The shock itself can be interpreted as the sum of infinitely many vibrations with the assigned amplitudes of the Fourier integral

$$p_i = \frac{1}{2\pi} \int_{-\infty}^{+\infty} e^{j\omega t} F(p_i) d\omega \quad \dots (13)$$

APPARATUS

Figure 1(a) shows the photographs of the experimental arrangements and Figure 1(b) shows the schematic diagram of the shock tube in which the shocks were generated by rupturing AVISCO Cellophane Type 195 MSBO diaphragms with a metallic pointer activated by a solenoid. The number of sheets required

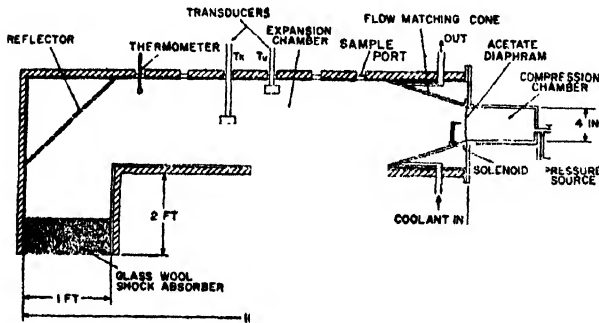


Fig. 1(b): Schematic diagram of the shock tube.

depends upon the ratio of the pressures on the two sides of the diaphragms. A minimum of 3, 5, and 8 sheets are required for the corresponding pressure ratios of 1.045, 1.758, and 3.515 (15, 25, and 50 psi). Air is used both for the driving and the driven gas. The flow of the gas from the compression chamber after the rupture of the membrane is matched by introducing a metallic cone 91.44 cms. long (3 feet) in between the compression and the expansion chambers. A pressure gauge is coupled to the compression chamber to read the air pressure in it.

The expansion chamber containing air at atmospheric pressure is cooled to about -10°C by circulating coolant from a constant temperature bath through a coil system incorporated in the chamber. The ratio of the cross-sectional areas of the compression and the expansion chambers is 3. Sample ports and observation windows are provided in the expansion chamber. The reflection of shock waves from the end of the expansion chamber is minimized with the help of a perforated acoustic reflector fixed at an angle of 45° to the axis of the shock tube assembly and a pad of glass wool enclosing the end of the tube. The outside of the expansion chamber is wrapped with a thick lining of glass wool in order to reduce heat transfer,

A calibrated quartz transducer T_k Model No. 601A, its associated electrostatic charge amplifier Model 566 made by the Kistler Instrument Corporation and a Tektronix Type 545A oscilloscope are used to measure the shock overpressure. The natural frequency and the rise time of the transducer are 140kc/s and 3 μ secs., respectively.

A second transducer T_g , made by Gulton Industries, and a H/P-400H VTVM are used in addition to the transducer, T_k , to measure the shock speed by the time of arrival method.

For further details about the shock tube and the results obtained on the interactions of shock waves with supercooled water (0.5 to 1 cc.) contained in glass and tygon tubings and with a single suspended supercooled droplet, reference is made to the papers by Goyer, Bhadra, and Gillin (1965) and Bhadra (1965).

EXPERIMENTS

In order to understand the mechanism of the interaction of shock waves with supercooled water, experiments were carried out to determine the following shock parameters as functions of distance and compression chamber pressure: (i) chronological pressure distribution, p_t , (ii) speed of shock wave, U_s , (iii) acoustic energy, W , (iv) frequency spectrum, $F(p_t)$.

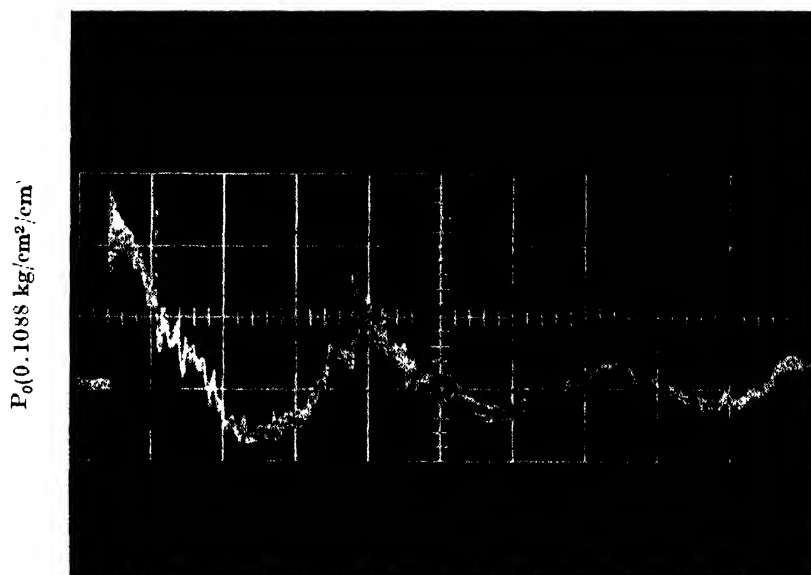
The chronological pressure distribution was determined by means of the transducer T_k in conjunction with the charge amplifier and the Tektronix oscilloscope. The oscilloscope was triggered by the signal picked up by the transducer, T_g , from the shock field. The transducer, T_g , was located ahead of the pressure amplitude measuring transducer, T_k , at a known distance from it. The transducer, T_g , was inserted into the shock field in such a way that the flow pattern in front of the transducer, T_k , was not disturbed to an appreciable amount. So the transducer T_g , was placed far off from the axial region as is shown in Figure 1. The axes of the transducers were aligned parallel to the direction of the gas flow.

The sensitivity of the transducer, T_k , is 1.0 μ Cb/psi and the charge amplifier is calibrated in terms of mv/ μ Cb.

From the oscillogram, the magnitude of the peak overpressure, p_0 , and the time, T , taken by the shock wave to travel the distance, D , between the two transducers, T_k and T_g , were estimated. The shock speed was determined from the measured values of the time, T , and the distance, D . p_0 and T were measured as functions of the compression chamber pressure and the distance from the diaphragm. Another parameter, t_0 , the time for the ceiling pressure to return to zero transit region was determined from the oscillogram. These values of p_0 and t_0 are used in determining the chronological pressure distribution, p_t , acoustic energy, W , and the frequency spectrum, $F(p_t)$.

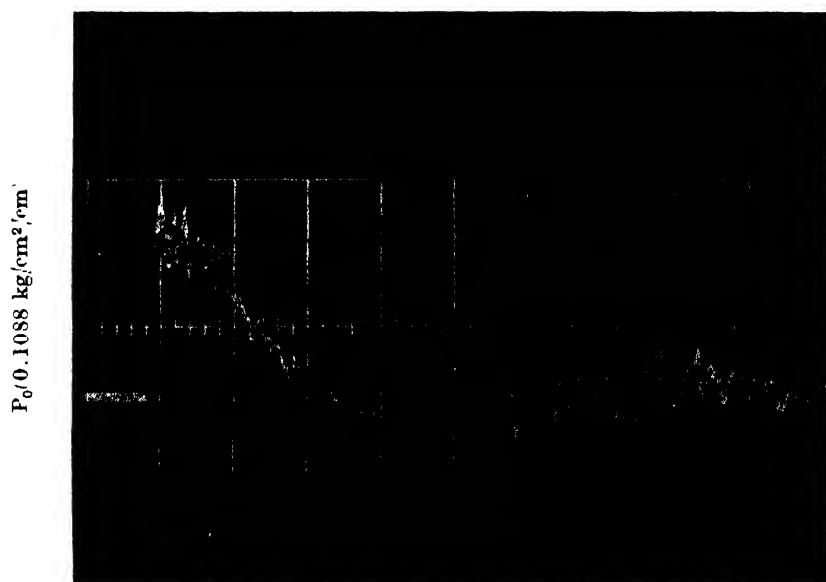
RESULTS AND DISCUSSIONS

Figures 2(a) and 2(b) show the two typical oscillograms of 3.515 Kg/cm^2 compression chamber pressure at distances 2.44 m and 1.83 m respectively. The



Time $\rightarrow 2\text{ms/division (Large)}$

Fig. 2: Pressure oscillogram of 3.515 Kg/cm^2 compression chamber pressure. Ordinate: p_0 in $0.1088 \text{ Kg/cm}^2/\text{cm}$. Abscissa: (a) Time in 2 ms/cm , at a distance of 2.44m .



Time $\rightarrow 1\text{ms/division (Large)}$

(b) Time in 1 ms/cm at a distance of 1.83m .

measured values of p_0 , the ceiling pressure, t_0 , the duration of the ceiling pressure up to zero level transition, U_x , the shock velocity, and the calculated values of W_1 the acoustic energy, p_c , the shock overpressure, M_x , the mach number, are presented in the table as functions of distance and compression chamber pressure. The velocity of sound in dry air at -10°C is 326 m/s. Column 'c' of the table shows the measured ceiling pressure, p_0 and Column 'd' shows the same as calculated from the ratio of shock velocity and sound velocity. The overall agreement between the measured and the calculated ceiling pressures is fairly satisfactory, but for 3.515 kg/cm² compression chamber pressure, the agreement is excellent. Column 'f' shows an appreciable increase of the shock velocities over the sound velocity at -10°C as shown in Column 'g'. Column 'i' shows the amount of acoustic energy/cm² available for each compression chamber pressure at different distances. Column 'h' shows the maximum value of the mach number using the minimum value of sound velocity. No correction for moisture content in air has been added.

For the pressure 3.515 Kg/cm² a minimum number of 8 diaphragms is required. However, at compression chamber pressures of 1.758 Kg/cm² and 1.045 Kg/cm² diaphragms cannot be ruptured by the metallic pointer so that 5 and 3 diaphragms are used respectively for these two cases. Since the number of diaphragms is changed when the compression chamber pressure is changed, it is difficult to relate correctly the ceiling pressure to the compression chamber pressure, but repeated experiments under similar conditions produced almost identical oscillograms.

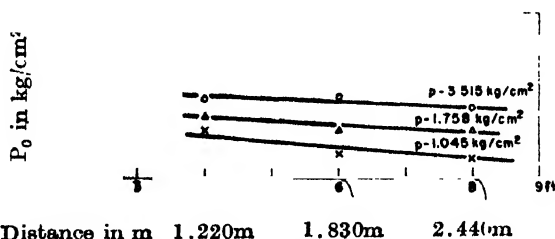


Fig. 3: p_0 → Overpressure plotted against distance as a function of the chamber pressure.

Figure 3 shows the measured ceiling pressure, p_0 , at various distances. p_0 decreases inversely with distance up to 1.22 m. It was not possible to measure the ceiling pressures at smaller distances, i.e., less than 1.22 m. In these regions the plots of p_0 against distance are shown by dashed lines indicating the uncertainty of the inverse relationship.

In Figure 4, the measured values of t_0 and p_0 are shown dependent on the compression chamber pressure. The measured values of t_0 from the oscillograms for compression chamber pressures of 1.758 Kg/cm² and 1.045 Kg/cm² at a distance of 1.22m have been found to be much smaller than those at 1.83m and 2.44m. The curve for t_0 against compression chamber pressure is steeper indicating, thereby, the rapid leveling down of the shock overpressure. In the region of 1.22m

the shock profile builds up and therefore it is difficult to visualise the mechanism involved for the lower values of t_0 .

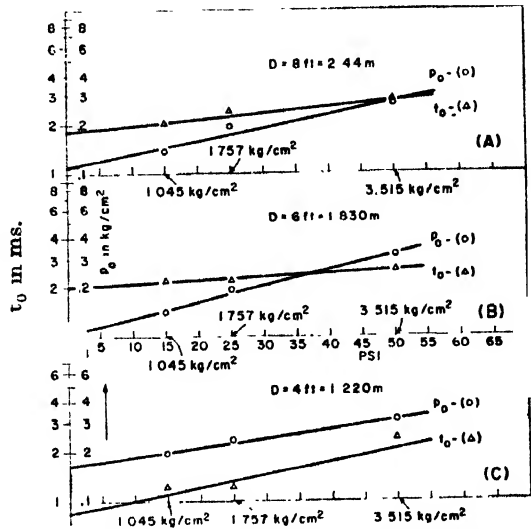
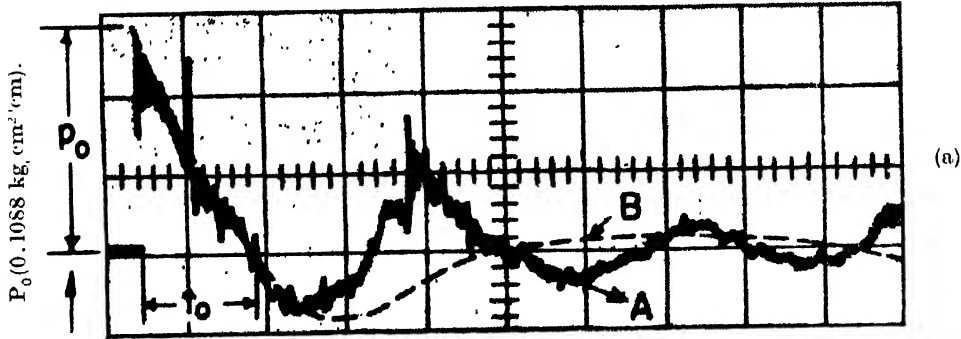
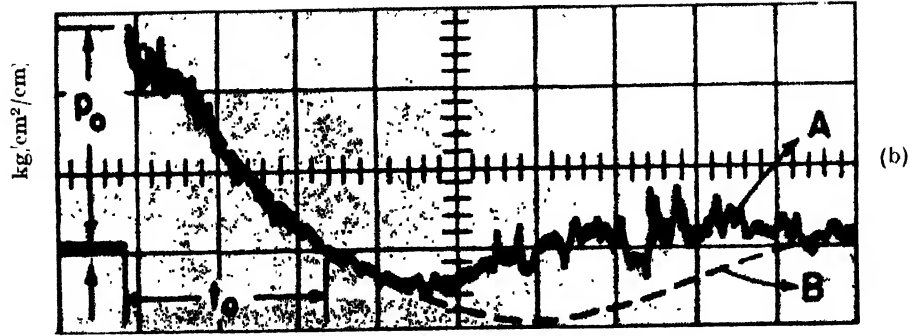


Fig. 4: p_0 and t_0 are plotted against the pressure in the compression chamber.



Time 2ms/division (Large).



Time 1ms/division (Large).

Fig. 5: Approximate function of the shock oscillogram of 3.515/Kg/cm² compression chamber pressure. (a) at 2.44 meter, (b) at 1.83 meter.

TABLE I
Results

Serial No.	*a in meters	b in Kg/cm ²	c Kg/cm ²	d Kg/cm ²	e in milli- sec.	f meter/ sec	g meter/ sec	h M _x	i in watts
1	1.22	3.515	0.305	0.374	2.4	373.99	326	1.15	0.0173
2	1.22	1.758	0.231	0.319	1.2	366.62	326	1.13	0.0050
3	1.22	1.045	0.196	0.218	1.2	356.22	326	1.09	0.0033
4	1.83	3.515	0.316	0.347	2.5	372.16	326	1.14	0.0193
5	1.83	1.758	0.196	0.245	2.2	358.75	326	1.10	0.0061
6	1.83	1.045	0.141	0.218	2.2	354.48	326	1.09	0.0029
7	2.44	3.515	0.267	0.272	2.8	363.02	326	1.11	0.0160
8	2.44	1.758	0.231	0.170	2.4	350.22	326	1.07	0.0067
9	2.44	1.045	0.196	0.143	2.2	345.95	326	1.06	0.0026

*a distance from the diaphragm

b compression chamber pressure

c measured shock ceiling overpressure p_0 d shock ceiling overpressure p_c calculated from ratios of shock velocity U_x and sound velocity a_x e duration of pressure ceiling up to zero level transition t_0 f shock velocity U_x as measured by time of arrival methodg sound velocity a_x in dry air at -10°C , velocity of sound increases by 0.05 m/s for addition of 0.10% by volume of moisture (in the present case air is not free from moisture).h m_x the mach number $= f/g = \frac{U_x}{a_x}$ i acoustic energy W in watts/unit area

In Figure 5, only two typical oscillograms of 3.515 Kg/cm² compression chamber pressure at 2.44m and 1.83m are represented by the curves A on which the curves B representing the approximate function

$$p_t = \frac{p_0}{\cos \theta} e^{-bt} \cos (\Omega t + \theta)$$

are superimposed. These curves present fairly good agreement between the theoretical and experimental values without correcting the theoretical values for reflection.

Figure 6 shows the frequency spectrum of the sound pulse from the shocks as calculated approximately from Fourier transform of the Equation (1). The Fourier transform is represented by Equation (10). In the figure, pressure amplitudes per 1 c.p.s. (Hz) at a distance of 2.44m for the compression chamber pressures of 3.515 Kg/cm², 1.758 Kg/cm², and 1.045 Kg/cm² are represented by the curves A, B, and C. The ordinate represents the pressure amplitudes in decibel/Hz. The 0 db has been defined to be equal to 1 $\mu\text{b}/\text{Hz}$. The maximum pressure amplitude is given by Equation (12). The pressure amplitude falls to zero at zero

frequency. The peak in the spectrums moves towards the lower frequency side of the spectrum as the pressure in the compression chamber is increased. This peak frequency, however, has no relationship whatsoever to the acoustical resonance frequency of the shock tube. For the three different cases, the peak frequencies are 454 Hz, 530 Hz, and 636 Hz for the compression chamber pressures of 3.515 Kg/cm², 1.758 Kg/cm², and 1.045 Kg/cm², respectively.

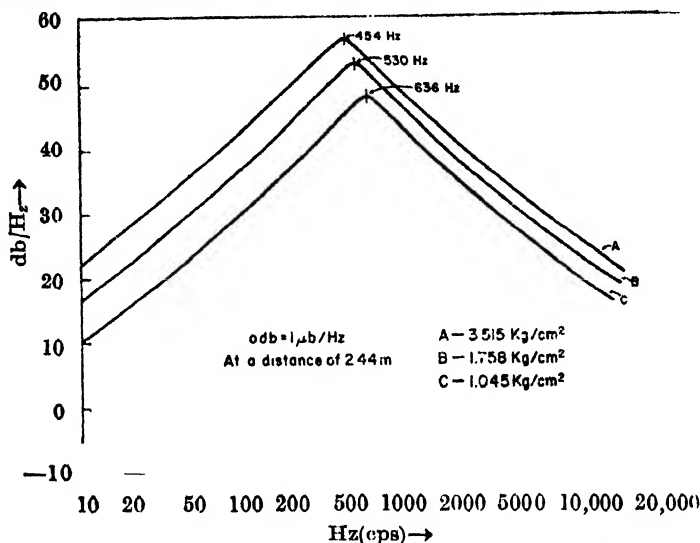


Fig. 6: Frequency spectrum as a function of compression chamber pressure.

Figure 7 represents sound pulse amplitude distribution as a function of frequencies at different distances for one compression chamber pressure. The pressure amplitudes of lower frequencies are higher at larger distances. The findings are in agreement with the theory of shock waves, i.e., shock waves decay into low frequency sound waves at larger distances.

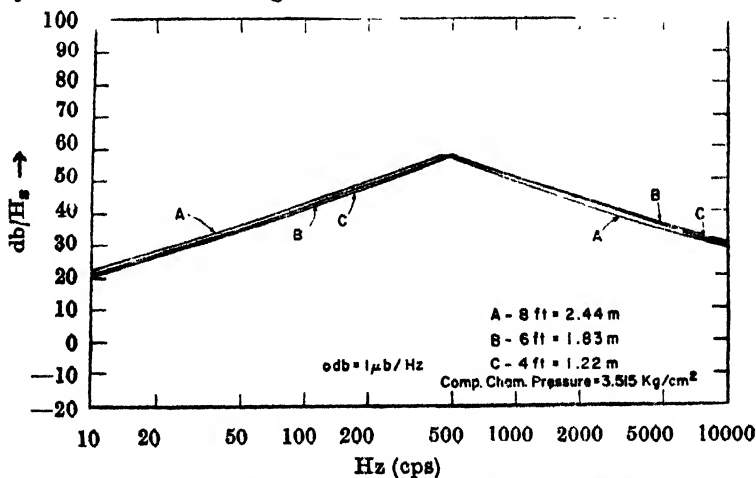


Fig. 7: Frequency spectrum at various distances.

CONCLUSION

It may be concluded here that Equation (1) can be used satisfactorily to analyze the shock tube data. Further, this analysis provides data in elucidating the mechanism involved to trigger freezing of supercooled water by shock waves for which this shock tube is designed.

ACKNOWLEDGMENT

The author expresses his sincere thanks to Dr. G. G. Goyer and Dr. Y Naga-kawa of NCAR and to Prof. R. W. Leonard, Physics Department, UCLA, for their valuable discussions and suggestions.

REFERENCES

- Bhadra, T. C. (to be published.)
Bradley, J. N., 1962, *Shock Waves in Chemistry and Physics*, John Wiley and Sons, Inc., N.Y.
Courant, R. and Friedrichs, K. O., 1948, *Supersonic Flow and Shock Waves*, Interscience Publishers, Inc., N.Y.
Furrer, W., 1946 *Schweizer Arch. Angew. Wiss. Techn.*, **12**, 213.
Furrer, W., and Weber, H., 1946, *Tehn. Mit. Schwiez, Telegr. U. Telph.*—Verio No. 6.
Goyer, G. G., Bhadra, T. C. and Gitlin, S., 1965, *J. Applied Meteor.*, **4**, 156.
Hugoniot, H., 1887, *Journ. del' ecole Polytechn.*, Paris, 57.
Leonard, R. W., 1962, *Handbuch Der Physik by S. Flugge*, Akustik II, Springer-Verlag, Berlin.
Reiman, B., *Nachr. Ges. Wiss*, 1880, *Goltingen*, 8.

A SIMPLE ANALYSIS OF THE NON-UNIFORM FIELD EFFECTS ON THE GUNN DEVICES

TAPAN BHATTACHARYA

ELECTRONICS DIVISION, COMPONENTS SECTION, ATOMIC ENERGY ESTABLISHMENT TROMBAY,
BOMBAY 74 (AS)

(Received December 6, 1966)

ABSTRACT. The effects of having a non-uniform field distribution on the efficiency of Gunn devices are studied from a device designer's viewpoint. Two means are suggested to achieve such field distributions: (i) resistivity gradient, and (ii) non-planar electrode geometry. Based on simplified mathematical models, both the cases are analysed for the output power and efficiency. The performance of those proposed devices is compared with the usual uniform-field Gunn devices, and the advantages, disadvantages and practicability of such devices discussed. It is shown that in certain ranges of the high-field domain width and the microwave frequency, the non-uniform field devices may be more efficient than their counterpart.

INTRODUCTION

There is much recent interest in the Gunn-effect oscillators (Gunn, 1964a, b) made of two-valley compound semiconductors. The differential-negative-conductance model, independently proposed by Ridley and Watkins (1961) and Hilsum (1962), predicts current instabilities in a two-valley semiconductor such as GaAs or InP when the applied electric field exceeds a threshold value. Ridley (1963) predicted the formation of a high-field domain and a low-field domain in the bulk once the applied field is in the region of negative differential conductivity. During and after its formation the high-field domain (HFD) propagates through the length of the sample with roughly the low-field electron drift velocity. The periodic nucleation and propagation of this HFD give rise to the microwave power output. The frequency of oscillation is given by the inverse of the domain transit time. McCumber and Chynoweth (1966) and Kroemer (1966) have shown that normal statistical fluctuations of the donor density in the semiconductor give rise to a dipole-domain formation. While the width of a pure accumulation-layer domain is directly proportional to the length of the sample (Ridley, 1963), no such simple relation exists in the case of a more practical dipole-layer domain, and it seems likely that the length of the sample does not have much influence on the width of a pure dipole-layer domain (Copeland, 1966a; Chynoweth, 1966). This is also borne out by the observation that coherent sinusoidal oscillations are obtained in shorter samples as compared to spiked oscillations in relatively longer samples (Foyt and McWhorter, 1966). However, the width of both types of domains is influenced strongly by the applied field, the width increasing with

increasing applied field (Allen *et al.*, 1966; Butcher *et al.*, 1966; Copeland, 1966a). Heeks (1966) observed that the field in the HFD saturates to around 75 KV/cm. and any excess applied voltage is absorbed by the domain by increasing in its width.

Gunn-effect oscillators have been successfully fabricated in the kilo-mega cycle frequency range with peak pulsed power output of about 100 watts (Dow *et al.*, 1966) and a few tens of milliwatts in the CW operation (Hakki and Knight, 1966). The efficiency of such devices is typically 3 to 10 percent, which compares well with the 2 percent efficiency of the present-day low-power single-cavity reflex klystrons. There have been some efforts made to calculate the efficiency of such devices (Hilsum, 1965; Copeland, 1966b). However, such calculations become extremely complicated because of the inherent non-linear nature of the device and computer solutions are usually resorted to. Hilsum (1965) considered an accumulation-layer domain equivalent to a charged capacitor and by considering the energy stored in this capacitor, arrived at a simple expression for the efficiency of the device.

In a series of experiments Heeks and coworkers (Heeks *et al.*, 1965; Heeks, 1966) demonstrated Gunn's original observation that only the nucleation of the HFD requires the applied field to be higher than the threshold field, but a much lower field is necessary to maintain the propagation of the HFD along the length of the sample. This demonstration immediately suggests that the efficiency of the Gunn device could possibly be increased by keeping the maintaining field low after the complete formation of the HFD, because then the Joule heat loss will be less. A further step ahead would be to convert the time variation of the applied field (Heeks, 1966) to a spatial variation in the sample, thus introducing a non-uniform field distribution. The purpose of this paper is to analyse this situation from a macroscopic viewpoint with the assumption of simplified mathematical models. Two different means are suggested to achieve such non-uniform field distributions and both the cases are analysed to obtain expressions for the efficiency. Comparison is made with the existing uniform-field Gunn devices and the advantages, disadvantages and the practicability of the proposed techniques are discussed.

RESISTIVITY GRADIENT

Kroemer (1966) suggested that intentional resistivity gradient may be used in the Gunn devices either to force the formation of a single depletion layer rather than a multiple of such layers, or, with a reverse gradient, to force the suppression of such depletion layers and formation of pure accumulation layers. Das and Maron (1966) analysed this situation and showed the desirability of having a non-uniform carrier distribution. We consider here an exponential distribution of the electron density :

$$n(z) = n_0 e^{(az/l)} \quad \dots (1)$$

where z is the distance along the sample of length l , and α is a constant. With an applied voltage V across the sample, the electric field $F(z)$ is given by :

$$F(z) = \frac{\alpha V e^{-(\alpha z/l)}}{(1 - e^{-\alpha})} \quad \dots (2)$$

where the built-in thermal field (of the order of $\frac{kT}{lq}$) is neglected. The low domain field F_L required to maintain the propagation of the HFD may be written as :

$$F_L = (F_T/m) \quad \dots (3)$$

where F is the threshold field and m is a constant greater than 1. For successful nucleation and propagation of the HFD we demand that :

$$\left. \begin{aligned} F(z) &= F_L; z = l \\ F(z) &\geq F_T; z \leq z_0 \end{aligned} \right\} \quad \dots (4)$$

Equations (2), (3) and (4) give :

$$V = (F_T l / \alpha m)(e^{\alpha} - 1), \quad \dots (5)$$

$$F(z) = (F_T/m) e^{\alpha} e^{-(\alpha z/l)}, \quad \dots (6)$$

$$z_0 = l(1 - \ln m/\alpha). \quad \dots (7)$$

The field distribution, as outlined above, is shown schematically in Fig. 1(a). Kroemer (1966) considered the formation mechanism of both an accumulation-layer and a dipole-layer HFD due to the statistical fluctuations in the carrier density. Applying Kroemer's argument in this case, with the existing non-uniform field, it is easily seen that the domain formation will be one of a dipole layer,

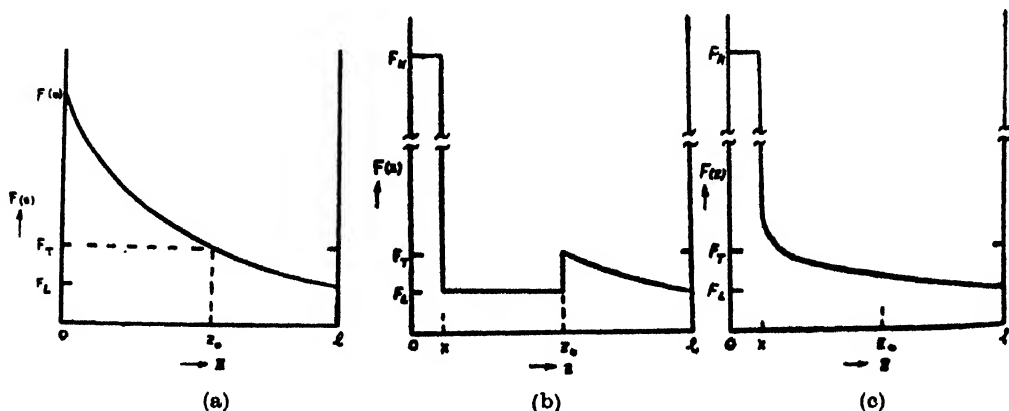


Fig. 1. Schematic diagram showing (a) the field distribution in the sample (Eq. (6)) immediately after the application of the external bias, (b) the assumed transient distribution at the time of the formation of the high-field domain, and (c) the final steady state distribution after the complete domain formation,

because the upstream field is higher than the down-stream field. We proceed with our calculations keeping in mind the salient features of a dipole-layer domain discussed in the Introduction.

In order to arrive at an expression for the efficiency of such a device, we make the following assumptions :

(i) The HFD is flat-topped, and the domain voltage is given reasonably accurately by :

$$V_H = F_H x \quad \dots (8)$$

where F_H , the field in the HFD, saturates to a value given by :

$$F_H = (F_T/s) \quad \dots (9)$$

where s is a constant less than 1 (Heeks, 1966). Any excess applied voltage is absorbed in the domain by increasing its width x .

(ii) The formation of the HFD takes place according to the Figs. 1(b) and 1(c). The potential drop in the region $0 < z < z_0$ is only responsible for the formation of the HFD (Fig. 1(b)), but after its formation, the potential gets redistributed as shown in Fig. 1(c).

(iii) The HFD is equivalent to a charged capacitor C , whose stored energy propagates through the length of the sample in time

$$\tau = (l/v) \quad \dots (10)$$

to deliver the microwave power (Hilsum, 1965). Here the low-field electron drift velocity v is given by :

$$V = F_L \mu = F_H \mu' \quad \dots (11)$$

where μ and μ' are the mobilities of the electrons in the lower and upper valleys respectively.

The weakest of the assumptions is (i) above. This assumption necessarily means that the wall thickness of the accumulation and depletion layers is negligible compared to the total width of the HFD. This, in turn, restricts the carrier density to rather high values (Allen *et al.*, 1966; Butcher *et al.*, 1966; Copeland, 1966a). Assumption (ii) is the basis of the mathematical model we use for analysing the situation, and in the absense of any contradictory evidence we are willing to base our calculations on this model.

Under these simplifying assumptions, the average power output of the device for a time large compared to τ is given by :

$$P_0 = \frac{\frac{1}{2} C V_H^2}{(l/v)} = \frac{K F_T^3 y \mu}{8 \pi s^2 m} \quad \dots (12)$$

where K is the dielectric constant of the material and the relative domain width is given by :

$$y \equiv (x/l). \quad \dots (13)$$

where z is the distance along the sample of length l , and α is a constant. With an applied voltage V across the sample, the electric field $F(z)$ is given by :

$$F(z) = \frac{\alpha V e^{-(\alpha z/l)}}{(1 - e^{-\alpha})} \quad (2)$$

where the built-in thermal field (of the order of $\frac{kT}{lq}$ α) is neglected. The low domain field F_L required to maintain the propagation of the HFD may be written as :

$$F_L = (F_T/m) \quad (3)$$

where F is the threshold field and m is a constant greater than 1. For successful nucleation and propagation of the HFD we demand that :

$$\left. \begin{aligned} F(z) &= F_L ; z = l \\ F(z) &\geq F_T ; z \leq z_0 \end{aligned} \right\} \quad (4)$$

Equations (2), (3) and (4) give :

$$V = (F_T l / \alpha m)(e^{\alpha} - 1), \quad (5)$$

$$F(z) = (F_T/m) e^{\alpha} e^{-(\alpha z/l)}, \quad (6)$$

$$z_0 = l(1 - \ln m/\alpha). \quad (7)$$

The field distribution, as outlined above, is shown schematically in Fig. 1(a). Kroemer (1966) considered the formation mechanism of both an accumulation-layer and a dipole-layer HFD due to the statistical fluctuations in the carrier density. Applying Kroemer's argument in this case, with the existing non-uniform field, it is easily seen that the domain formation will be one of a dipole layer.

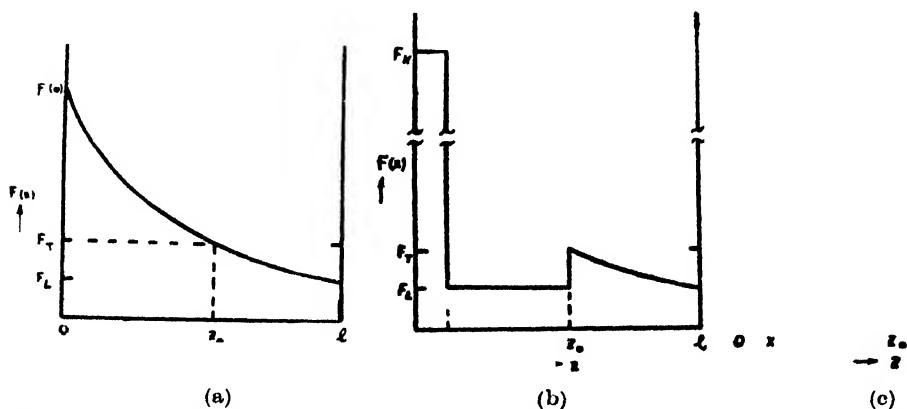


Fig. 1. Schematic diagram showing (a) the field distribution in the sample (Eq. (6)) immediately after the application of the external bias, (b) the assumed transient distribution at the time of the formation of the high-field domain, and (c) the final steady state distribution after the complete domain formation,

because the upstream field is higher than the down-stream field. We proceed with our calculations keeping in mind the salient features of a dipole-layer domain discussed in the Introduction.

In order to arrive at an expression for the efficiency of such a device, we make the following assumptions :

(i) The HFD is flat-topped, and the domain voltage is given reasonably accurately by :

$$V_H = F_H x \quad \dots (8)$$

where F_H , the field in the HFD, saturates to a value given by :

$$F_H = (F_T/s) \quad \dots (9)$$

where s is a constant less than 1 (Hecks, 1966). Any excess applied voltage is absorbed in the domain by increasing its width x .

(ii) The formation of the HFD takes place according to the Figs. 1(b) and 1(c). The potential drop in the region $0 < z < z_0$ is only responsible for the formation of the HFD (Fig. 1(b)), but after its formation, the potential gets redistributed as shown in Fig. 1(c).

(iii) The HFD is equivalent to a charged capacitor C , whose stored energy propagates through the length of the sample in time

$$\tau = (l/v) \quad \dots (10)$$

to deliver the microwave power (Hilsum, 1965). Here the low-field electron drift velocity v is given by :

$$V = F_L \mu = F_H \mu' \quad \dots (11)$$

where μ and μ' are the mobilities of the electrons in the lower and upper valleys respectively.

The weakest of the assumptions is (i) above. This assumption necessarily means that the wall thickness of the accumulation and depletion layers is negligible compared to the total width of the HFD. This, in turn, restricts the carrier density to rather high values (Allen *et al.*, 1966; Butcher *et al.*, 1966; Copeland, 1966a). Assumption (ii) is the basis of the mathematical model we use for analysing the situation, and in the absence of any contradictory evidence we are willing to base our calculations on this model.

Under these simplifying assumptions, the average power output of the device for a time large compared to τ is given by :

$$P_0 = \frac{\frac{1}{2} C V_H^2}{(l/v)} = \frac{K F_T^3 y \mu}{8 \pi s^2 m} \quad \dots (12)$$

where K is the dielectric constant of the material and the relative domain width is given by :

$$y \equiv (x/l). \quad \dots (13)$$

Equation (12) is derived with the help of Eqs. (3), (8), (9) and (11). Since the carriers in the HFD are in the upper valley of the conduction band, the resistance of this domain is approximately given by :

$$R_H = \int_0^y \frac{dz}{q\mu'n(z)} = \frac{l(1-e^{-\alpha y})}{\alpha n_0 q \mu'} \quad \dots (14)$$

where q is the electronic charge. For low values of the domain width, this resistance obviously reduces to :

$$R_H \approx (x/n_0 q \mu'). \quad \dots (15)$$

The resistance of the low field region is similarly given by .

$$R_L = \int_x^l \frac{dz}{q\mu'n(z)} = \frac{l}{\alpha n_0 q \mu'} (e^{-\alpha y} - e^{-\alpha}) \quad \dots (16)$$

The potential drop in the low-field region is given from Eqs. (5), (8) and (9) by .

$$V_L = V - V_H$$

$$F_T l [s(e^\alpha - 1) - \alpha m y]. \quad (17)$$

The power input to the device under these conditions is given by

$$P = \frac{V_H^2}{R_H} + \frac{V_L^2}{R_L} \quad (18)$$

and with the aid of Eqs. (8), (9), (14), (16) and (17) this becomes :

$$P = \frac{F_T^2 q n_0 \mu' l}{\alpha m^2 s^2} \left[ms(1-e^{-\alpha y}) + \frac{\{s(e^\alpha - 1) - \alpha m y\}^2}{\{e^{-\alpha y} - e^{-\alpha}\}} \right] \quad (19)$$

From Eqs. (12) and (19) the overall efficiency of the device is :

$$\eta = \frac{K F_T}{8 \pi q n_0 l} \left[\alpha m y \left\{ ms(1-e^{-\alpha y}) + \frac{[s(e^\alpha - 1) - \alpha m y]^2}{[e^{-\alpha y} - e^{-\alpha}]} \right\}^{-1} \right] \quad (20)$$

The efficiency thus calculated is plotted in Fig. 2 as a function of the relative domain width y with α as a parameter. The following values, typical of n -GaAs, are used for this purpose :

$$\begin{aligned} m &= 2 \\ s &= 0.043 \\ F_T &= 3.2 \times 10^3 \text{ volt/cm.} \\ K &= 1.1 \times 10^{-10} \text{ farad/meter,} \\ \mu &= 5000 \text{ cm}^2/\text{volt-sec.} \end{aligned} \quad \dots (21)$$

Also plotted in this figure is the efficiency of a uniform-field device (the curve marked $\alpha = 0$), the expression for which was derived by Hilsum (1965). The uniform carrier density assumed for this plot is equal to n_0 . Figure 2 clearly shows that for large values of y and relatively low α , the efficiency of the non-uniform field device, as described above, is larger than that for the uniform field device. The value of α cannot be much less than unity, because Eqs. (4) and (7) have to be simultaneously satisfied. Decreasing α automatically reduces z_0 , and since y cannot be larger than (z_0/l) , so the advantage obtained by decreasing α is lost. The minimum value of α , as seen from Eq. (7), is approximately 0.69, in which

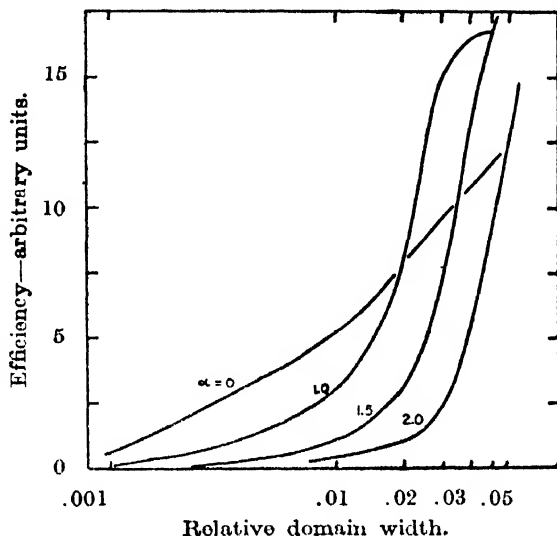


Fig. 2. The computed efficiency of the Gunn device plotted as a function of the relative domain width, for the uniform-field ($\alpha = 0$) and the non-uniform field ($\alpha > 0$) Gunn devices.

case there will not be any stable domain formation and oscillation. From known observations (Hilsum, 1965; Heeks, 1966) it can be safely assumed that the relative domain width y lies somewhere between 2 to 4 percent. With this range of values for y , Fig. 2 shows that having a non-uniform carrier distribution with $\alpha = 1$ does give a more efficient device than the uniform device of same length and having a carrier density of n_0 . It may not be possible to obtain such low gradient of carrier density ($\alpha = 1$) with the techniques of indiffusion. However, the usual donors in GaAs, such as Se and Te, have rather low diffusion constants, and the technique of out-diffusion could be employed to obtain the required carrier-density gradient.

NON-PLANAR ELECTRODE GEOMETRY

The second method to achieve the non-uniform field distribution in the Gunn devices is to use non-planar electrode geometry. We will consider here the case of concentric cylindrical electrodes as illustrated in Fig. 3. Such devices could

be fabricated by selective surface plating of the contact electrodes by the usual photolithographic techniques and then alloying. Similar surface-oriented Gunn devices with planar electrodes have been successfully used (Foxell *et al.*, 1965). The following analysis is made by adopting all the assumptions made in the previous case except (ii). With the symbols defined in Fig. 3, the average power output of the cylindrical device is given from Eqs. (8), (9), (10) and (11) as :

$$\begin{aligned}
 P_{oc} &= \frac{\frac{1}{2}C_c V_H^2}{(b-a)/F_L\mu} \\
 &= \frac{KdF_L\mu F_2^H x_c^2}{4(b-a)l_n(1+x_c/a)} \\
 &= \frac{KdF_3^T x_c\mu}{4(b-a)s^2m l_n(1+x_c/a)} \quad \dots (22)
 \end{aligned}$$

where the subscript *c* denotes the cylindrical case. Instead of calculating the power input to the device and the efficiency, as was done earlier, we will calculate the power output in the case of a planar-electrode device (case "p" in Fig. 3), and

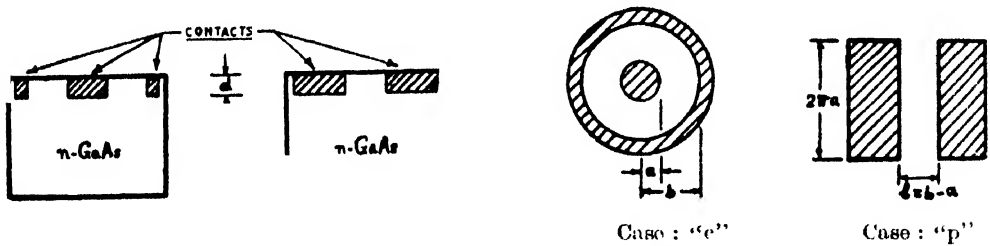


Fig. 3. Electrode configurations for the cylindrical (case "c") and the planar (case "p") devices.

assuming the same power input to both the devices, compare the output powers and hence the efficiencies. The latter case has been treated by Hilsum (1965), and in our notations the output power of the planar device is given by :

$$\begin{aligned}
 P_{op} &= \frac{\frac{1}{2}C_P V_2^H}{(b-a)/F_L\mu} \\
 &= \frac{KdaF_3^T x_{P'}}{4s^2m(b-a)} \quad \dots (23)
 \end{aligned}$$

As a basis for the comparison, we have assumed here that the depth of alloying *d* (see Fig. 3) is the same in both the cases and the width of the planar electrode

is $(2\pi a)$. With the same input power to both the devices, the ratio of the respective efficiencies is given from Eqns. (22) and (23) as :

$$\frac{\eta_C}{\eta_P} = \frac{P_{OC}}{P_{OP}} = \left(\frac{x_C}{x_P} \right) \ln \frac{(x_C/a)}{(1+x_C/a)} \quad \dots \quad (24)$$

Since for any positive x_C :

$$\left(\frac{x_C}{a} \right) > \ln \left\{ 1 + \left(\frac{x_C}{a} \right) \right\}, \quad \dots \quad (25)$$

hence from Eq. (24)

$$\frac{\eta_C}{\eta_P} > \frac{x_C}{x_P} \quad \dots \quad (26)$$

So, if $x_C > x_P$, then η_C will always be larger than η_P .

The field variation in the case "c" follows an inverse radial-distance law. With the boundary conditions enumerated in Eqs. (4) above (with the radial distance r substituted for z), we will have an identical situation here as in the previous case. Following the arguments given there and in the Introduction, it is possible that x_C will be larger than x_P , which will ensure that η_C is always larger than η_P . This was not unexpected, because the capacitance, and hence the energy stored in it with the same maximum field F_H , is larger in the case of cylindrical electrodes than that in the planar case with the same cross sectional area. Apart from this increase in the capacitance because of the geometry, there could be further increase in the efficiency of the cylindrical device because of the possible increase in the domain width due to the non-uniform field distribution.

Referring to Eqs. (25) and (26), it is noted that larger the value of (x_C/a) , larger will be the increase in η_C compared to η_P . With the present-day photolithographic techniques a could be as small as 3-5 microns, and with x_C presumably in the same range, there could be a substantial increase in the efficiency of the cylindrical device as compared to that in the planar device. Of course, the reduction in a will necessarily reduce the cross sectional area and hence the output power. Another interesting observation that can be made here is that the HFD travels radially through the active length $l = (b-a)$, and unlike the linear flow its width is reduced during its propagation. This will, therefore, tend to give rise to spiked waveform rather than sinusoidal ones (Foyt and McWhorter, 1966). This effect could conceivably be overcome by keeping the active length $(b-a)$ reasonably small. This reduction in the active length, which is one of the great advantages

of the surface-oriented devices (Foxell *et al.*, 1965), helps generating higher frequency.

ACKNOWLEDGMENT

The author wishes to thank M. B. Khambaty for introducing him to this field

REFERENCES

- Allen, J. W., Shockley, W., Pearson, G. L., 1966, *J. Appl. Phys.*, **37**, 3191.
 Butcher, P. N., Fawcett, W., Hilsaum, C., 1966, *Brit. J. Appl. Phys.*, **17**, 841.
 Chynoweth, A. G., 1966, *Private Communication*.
 Copeland, J. A., 1966a, *J. Appl. Phys.*, **37**, 3602.
 ———, 1966b, "Theoretical Study of a Gunn Diode in a Resonant Cavity" (to be published in *IEEE Trans. on Electron Devices*).
 Das, P., Maron, E., 1966, *Phys. Letters*, **20**, 444.
 Dow, D. G., Moshor, C. H., Vane, A. B., 1966, *IEEE Trans. on Electron Devices*, **ED-13**, 105.
 Foxell, C. A. P., Summers, J. G., Wilson, K., 1965, *Electronics Letters*, **1**, 217.
 Foyt, A. G., McWhorter, A. L., 1966, *IEEE Trans. on Electron Devices*, **ED-13**, 71.
 Gunn, J. B., 1964a, *IBM J. of Res. and Dev.*, **8**, 141.
 ———, 1964b, *Symposium on Plasma Effects in Solids*, Paris, France, p. 3.
 Hakki, B. W., Knight, S., 1966, *IEEE Trans. on Electron Devices*, **ED-13**, 94.
 Heeks, J. S., Woode, A. D., Sandbank, C. P., 1965, *Proc. IEEE (Correspond.)*, **53**, 55.
 Heeks, J. S., 1966, *IEEE Trans. on Electron Devices*, **ED-13**, 68.
 Hilsaum, C., 1962, *Proc. I.R.E.*, **50**, 185.
 ———, 1965, *Brit. J. Appl. Phys.*, **16**, 1401.
 Kroemer, H., 1966, *IEEE Trans. on Electron Devices*, **ED-13**, 27.
 McCumber, D. E., Chynoweth, A. G., 1966, *IEEE Trans. on Electron Devices*, **ED-13**, 4.
 Ridley, B. K., Watkins, T. B., 1961, *Proc. Phys. Soc. (London)*, **78**, 293.
 Ridley, B. K., 1963, *Proc. Phys. Soc. (London)*, **82**, 954.

A NOTE ON THE DISPERSION RELATION FOR VERY HIGH TEMPERATURE PLASMA

SAROJ K. MAJUMDAR

SAHA INSTITUTE OF NUCLEAR PHYSICS, CALCUTTA

(Received November 16, 1960)

ABSTRACT. The asymptotic expansion of the function $S_\nu(z)$ which completely describes the plasma dispersion law and introduced by Majumdar (1965) has been carried out for very high temperature and low magnetic field. From this expression the well-known results of zero magnetic field case are recovered.

INTRODUCTION

In an earlier work on the dispersion relation for electron plasma in an external magnetic field, (Majumdar, 1965), it was shown that the whole problem of plasma dispersion can be thoroughly solved in terms of a new function given by

$$S_\nu(Z) = \int_0^\infty e^{i\nu t + Z \cos t} dt. \quad \dots (1)$$

where

$$\left. \begin{aligned} \nu &= \omega/\omega_c \\ Z &= k_\rho^2 T/m\omega_c^2 \end{aligned} \right\}. \quad (2)$$

and

Here, $\omega_c = eH_0/mc$ is the cyclotron frequency of the plasma electrons, T is their kinetic temperature, ω and k_ρ are respectively the frequency and wave number (perpendicular to the applied magnetic field \vec{H}_0) of the disturbances.

It has been shown (Mazumdar 1965), that the whole problem of dispersion of waves in a magnetic plasma can be solved if one can find the various properties of $S_\nu(Z)$ as a function of ν and Z .

In this report, we wish to study the asymptotic behaviour of the function $S_\nu(Z)$ for very high temperature and low magnetic field. In that case both ν and Z assume large values, but ν/Z remains small. From the result so obtained, we shall recover the well-known case of zero magnetic field.

ASYMPTOTIC EXPANSION OF $S_\nu(Z)$

It has been discussed (Mazumdar, 1965) that the function $S_\nu(Z)$ can be thought as to belong to the family of Bessel's function. Calling ν as the order and Z as the argument of $S_\nu(Z)$, we need to find the asymptotic expansion for

large order and argument. For this purpose, we follow the method of steepest descent. To do this, we first transform the function $S_\nu(Z)$ in a suitable form. Setting $t = iw$ in eqn. (1), we get

$$S_\nu(Z) = i \int_0^{-i\infty} dw e^Z \cosh w - \nu w. \quad \dots (3)$$

The contour of the integral (3) runs from 0 to $-\infty$ along the imaginary axis as shown in fig. 1. We divide this contour at all points which correspond to odd

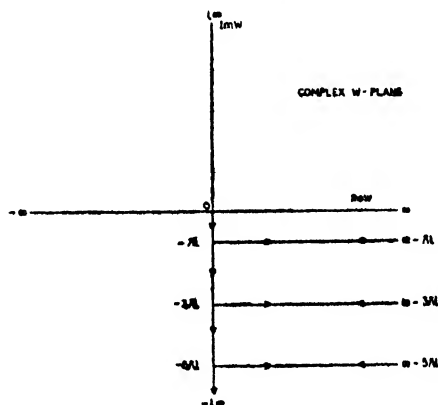


Fig. 1. Contour of integration in eqns, (3) and (4).

multiple of π . At each of these points we add and subtract straight line contours going to $+\infty$ in a direction parallel to the real axis, as shown in fig. 1. The result is that one can write the function $S_\nu(Z)$ in the following form :

$$\begin{aligned} S_\nu(Z) &= i \left[\int_0^{\infty - i\pi} + \int_{\infty - i\pi}^{\infty - 3i\pi} + \int_{\infty - 3i\pi}^{\infty - 5i\pi} + \dots \right] dw e^Z \cosh w - \nu w \\ &= -i \int_{\infty - i\pi}^0 e^Z \cosh w - \nu w dw + i \frac{e^{i\pi\nu}}{2 \sin \nu\pi} \int_{\infty - i\pi}^{\infty + i\pi} e^Z \cosh w - \nu w dw. \quad \dots (4) \end{aligned}$$

The form of the integrals in (4) is very similar to that of the integral representation of the modified Bessel function of the second kind. Therefore, following Watson (1952), we calculate the asymptotic expansion of $S_\nu(Z)$:

$$\begin{aligned} S_\nu(Z) &= ie^{ZB} \alpha \phi(1/2, 3/2; \alpha^2 A) \\ &+ \frac{i}{2} e^{ZB} \sum_{m=0}^{\infty} \frac{a_{2m+1}}{Z^{m+1}} \Gamma(m+1) + \frac{1}{2} (\cot \nu\pi) e^{ZB} \sum_{m=0}^{\infty} \frac{a_{2m}}{Z^{m+1}} \Gamma(m+\frac{1}{2}) \\ &= S_1 + S_2 + S_3 \quad \text{in the same order.} \end{aligned} \quad (5)$$

In (5), we have used the following :

$$\left. \begin{aligned} \alpha &= \sinh^{-1} v/Z \\ A &= (Z/2) \cosh \alpha \\ B &= \cosh \alpha - \alpha \sinh \alpha, \end{aligned} \right\} \quad (6)$$

the quantities α_m 's are certain coefficients of expansion whose values are tabulated by Watson, (1952). Here we shall use only the α_0 and α_1 terms, which have the following values :

$$\left. \begin{aligned} \alpha_0 &= (-\frac{1}{2} \cosh \alpha)^{-\frac{1}{2}} \\ \alpha_1 &= -\frac{2 \tanh \alpha}{3 \cosh \alpha} \end{aligned} \right\} \quad \dots \quad (7)$$

The function ϕ appearing in eqn. (5) is the confluent hypergeometric function (Erdelyi *et al* 1953.)

Eqn. (5) is the complete expression for the asymptotic expansion of $S_\nu(Z)$. This is a quite complicated expression, but in most cases of interest the summations over m can be replaced by their respective first terms. For example, in the case of high temperature plasma in a low magnetic field, the quantity Z is very large. In that case we are justified in using only the $m = 0$ term.

LOW MAGNETIC FIELD - HIGH TEMPERATURE PLASMA

In this case, $v/Z \ll 1$. Hence from eqns. (6) and (7) we can write,

$$\begin{aligned} \alpha_0 &\simeq v/Z; \quad A \simeq Z/2 + v^2/4Z; \quad B \simeq 1 - v^2/2Z \\ \alpha_0 &\simeq \frac{\sqrt{2}}{i} \left(1 - \frac{v^2}{4Z^2} \right); \quad \alpha_1 \simeq -\frac{2}{3} \frac{v/Z}{1 + v^2/Z^2}. \end{aligned}$$

Using these approximate values, the quantities S_1 , S_2 and S_3 whose sum is the asymptotic expression of $S_\nu(Z)$ given in eqn. (5), can be calculated. The result is

$$\begin{aligned} S_1 &\simeq i \frac{v}{Z} \phi(1/2, 3/2; v^2/2Z) e^{Z - v^2/2Z} \\ S_2 &\simeq -\frac{i}{3} \frac{v}{Z^2} \frac{1}{1 + v^2/Z^2} e^{Z - v^2/2Z} \\ S_3 &\simeq -\frac{1}{\sqrt{2}} \frac{\Gamma(\frac{1}{2})}{Z^{\frac{1}{2}}} (1 - v^2/4Z^2) e^{Z - v^2/2Z} \end{aligned} \quad (8)$$

and

$$S_\nu(Z) = S_1 + S_2 + S_3.$$

To check the result of the asymptotic expansion, we shall now show that this value of $S_\nu(Z)$ given by eqn. (8) leads to the correct expression of the dispersion relation for zero magnetic field. It has been shown (Mazumdar, 1965) that the dispersion law for plasma wave for zero magnetic field is given by

$$-\omega^2/c^2 + I_{xx} = 0, \quad \dots (9)$$

where

$$I_{xx} = \frac{\omega_p^2}{c^2} \frac{v^2}{Z} [1 + i\nu e^{-Z} S_\nu(Z)], \quad \dots (10)$$

ω_p is the electron-plasma frequency. Using eqns. (8) and (10) we calculate the limit of I_{xx} for $\omega_c \rightarrow 0$, and then use the resulting expression in (9). This gives us the following dispersion relation :

$$\begin{aligned} -\frac{\omega^2}{c^2} + \frac{\omega_p^2}{c^2} \frac{v^2}{Z} \left[-\phi(1, 3/2; -v^2/2Z) + \frac{2}{3} \frac{v^2}{Z} \phi(2, 5/2; -v^2/2Z) \right] \\ + \frac{i}{2} \frac{\omega_p^2}{c^2} \Gamma(1/2) \omega^3 \left[\frac{m}{k^2 T} \right]^{3/2} e^{-v^2/2Z} = 0. \end{aligned} \quad \dots (11)$$

Writing $\omega = \omega_r + i\omega_i$, where ω_r denotes the real part of the frequency and ω_i gives the imaginary part, and using the asymptotic form of the function ϕ , we separate the real and imaginary parts of eqn. (11). The final result is

$$\omega_r^2 = \omega_p^2 + k^2 \langle V^2 \rangle_{av}$$

$$\text{and} \quad \omega_i = \frac{1}{2} \left(\frac{\pi}{2} \right)^{\frac{1}{2}} \frac{\omega_p}{(k\lambda_D)^3} \exp - \left(\frac{1}{2k^2\lambda_D^2} \right) \quad \dots (12)$$

where $\langle V^2 \rangle_{av}$ is the average electron speed and λ_D is the well-known Debye length. The first equation of (12) is the dispersion relation in the familiar form, whereas the second relation is the well-known expression for Landau damping.

For a non-vanishing magnetic field one can, in a similar manner, calculate the dispersion law for high temperature plasma placed in a low magnetic field. It is also possible to extend the method for other values of the ratio v/Z and thus may cover a whole range of magnetic field.

ACKNOWLEDGMENTS

The author expresses his sincere gratitude to the Director Prof. B. D. Nag for providing him with the facilities to carry out the work.

REFERENCES

- Erdelyi, A., 1953, *Higher Transcendental Functions* Vol. 1, McGraw-Hill Book Company, Inc., [Chapter 6].
 Majumdar, S. K., 1965, *Indian J. Phys.*, **39**, 511.
 Watson, G. N., 1952, "*Theory of Bessel Functions*", 2nd Ed., Cambridge.

ON THE STRUCTURE OF COMPLEX SILVER QUINOLINE PERCHLORATE

T. RATHO AND MRS. M. KRISHNASWAMY

REGIONAL ENGINEERING COLLEGE, BOURKELA

(Received December 19, 1966)

ABSTRACT. The Debye Scherrer pattern of Silver Quinoline Per Chlorate has been studied and analysed. The unit cell dimensions are found to be $a = 15.15 \text{ \AA}$, $b = 11.91 \text{ \AA}$, $c = 13.08 \text{ \AA}$ and $\beta = 97.47^\circ$. There are four molecules in the unit cell. The space group $P2_1/m - C_{2h}^2$ can be assigned to the crystal.

INTRODUCTION

Silver Quinoline perchlorate $\text{Ag}[\text{C}_9\text{H}_7\text{N}]_2\text{ClO}_4$ crystals are obtainable in a microcrystalline form, white in colour. The study of crystal structure of these complex ligands throws light on their diamagnetic behaviour. It is also possible to know something about the stretching force constants between the various groups of atoms in these molecules. As it is not possible to grow large crystals we have tried to analyse the crystal by the wellknown powder methods.

EXPERIMENTAL

Copper radiation from a Machlett A-2 X-ray diffraction tube was made monochromatic by using a Ni filter. The apparatus was running at 20 m.A. and 30 K.V. The finely powdered specimen was contained in a Lindemann glass capillary of 0.01 mm. wall thickness and of 0.5 mm diameter. The Debye Scherrer photograph was obtained in a Rigaku camera of 9 cm. diameter. The time of exposure was 4 hours. In the usual manner the interplanar distances were calculated accurately. Methods applicable to the cubic, tetragonal and hexagonal systems were applied and the experimental data did not fit into any one of them. Therefore the crystal does not belong to the higher symmetry class. The Lipson's method (1949), when tried, did not give a good number of constant differences. Therefore the most general method of Ito (1950) applicable to crystals of lower symmetry, namely, the monoclinic and the triclinic was applied.

The experimental data relating to the d values and the corresponding Q values ($1/d_{hkl}^2 = Q_{hkl}$) are also given in the table. All the six parameters were found by using the Ito's method and the powder pattern was indexed after Azaroff and Bourger (1958).

We have after the above method of Ito,

$$Q_{hkl} = h^2 a^{*2} + k^2 b^{*2} + l^2 c^{*2} + 2klb^*c^* \cos \alpha^* + 2hlc^*a^* \cos \beta^* + 2hka^*b^* \cos \gamma^*$$

where $\alpha^*, \beta^*, \gamma^*$ and a^*, b^* and c^* are the reciprocal angles and axes respectively.

The first two reflections of very weak intensity, after some trials, could be taken as Q_{100} , Q_{001} and the seventh reflection was taken as Q_{020} . Using the above formula it was possible to find out the reciprocal cell dimensions. They are

$$a^* = 0.06664$$

$$b^* = 0.08397$$

$$c^* = 0.07714$$

It then became necessary to examine the (hko) , (hol) and (okl) reflections to select the reciprocal cell angles α^* , β^* and γ^* . If α^* and γ^* were taken to be 90° then (hko) and (okl) reflections could be detected. Therefore β^* was calculated after studying pairs of (hol) and $(ho\bar{l})$ reflections after the equation

$$\cos \beta^* = \frac{Q_{hol} - Q_{ho\bar{l}}}{4hla^*c^*}$$

The value of β^* so found was $82^\circ 13'$. The direct cell dimensions are therefore obtained from these six reciprocal parameters as

$$a = 15.15 \text{ A.U.}$$

$$b = 11.91 \text{ A.U.}$$

$$c = 13.08 \text{ A.U.}$$

$$\alpha = 90^\circ$$

$$\beta = 97^\circ 47'$$

$$\gamma = 90^\circ$$

The above dimensions were found to be the reduced ones after applying the Buerger test (1958). The above data speaks about the monoclinic structure of the crystal. After indexing all the powder lines in the light of the above formula the following conditions for the appearance of the lines were found.

$$hkl\text{—no condition}$$

$$hol\text{—no condition}$$

$$oko\text{—}k = 2n$$

The possible space group, therefore, is $P2_1/m-C_{2h}^2$. The observed density is 1.383 gms/cc. and the calculated density comes out to be 1.323 gms/cc. This gives four molecules per unit cell.

TABLE

No. of lines	Intensity	$d \text{ \AA}$	$Q_{hkl} = 1/d^2$ observed	Q_{hkl} computed	Indices
1.	vw	14.99	0.00444	0.00444	100
2.	vw	12.97	0.00595	0.00595	001
3.	s	8.024	0.0155	0.0160	11 $\bar{1}$
4.	m	7.463	0.0180	0.0178 0.0188	200 111
5.	s	6.977	0.0205	0.0209	20 $\bar{1}$
6.	vvw	6.511	0.0236	0.0238	002
7.	vvw	5.979	0.0280	0.0282 0.0280	020 21 $\bar{1}$
8.	s	5.537	0.0326	0.0326 0.0325	120 11 $\bar{2}$
9.	s	5.241	0.0364	0.0360 0.0372	20 $\bar{2}$ 12 $\bar{1}$
10.	m	5.021	0.0397	0.0399	300
11.	s	4.809	0.0432	0.0430	21 $\bar{2}$
12.	vvw	4.603	0.0472	0.0470 0.0471	310 202
13.	vw	4.314	0.0537	0.0536 0.0538 0.0537 0.0541	003 10 $\bar{3}$ 12 $\bar{2}$ 212
14.	s	4.131	0.0586	0.0592	122
15.	m	3.918	0.0651	0.0642	22 $\bar{2}$
16.	vw	3.649	0.0751	0.0754 0.0753	131 222
17.	w	3.457	0.0837	0.0837 0.0843 0.0836	40 $\bar{2}$ 23 $\bar{1}$ 32 $\bar{2}$
18.	m	3.318	0.0908	0.0904 0.0912 0.0908	123 22 $\bar{3}$ 41 $\bar{2}$
19.	w	3.237	0.0954	0.0952	004

TABLE—contd.

No. of lines	Intensity	$d \text{ \AA}$	$Q_{hkl} = 1/d^2$ observed	Q_{hkl} computed	Indices
20.	m	3.077	0.1057	0.1052 0.1060 0.1052 0.1052	104 303 402 33 $\bar{1}$
21.	w	2.975	0.1130	0.1128 0.1123 0.1135 0.1131 0.1130	040 114 331 313 412
22.	m	2.799	0.1276	0.1279	51 $\bar{2}$
23.	vw	2.663	0.1410	0.1413	403
24.	vvw	2.581	0.1501	0.1507 0.1510	513 414
25.	vw	2.519	0.1576	0.1574 0.1575	60 $\bar{1}$ 134
26.	m	2.436	0.1685	0.1678 0.1687 0.1682	305 134 34 $\bar{2}$
27.	m	2.322	0.1854	0.1854 0.1852 0.1849 0.1855 0.1856	503 151 342 514 62 $\bar{1}$
28.	w	2.214	0.2041	0.2047	433
29.	w	2.142	0.2180	0.2180 0.2180 0.2188 0.2187	144 351 343 442
30.	m	2.087	0.2295	0.2298 0.2291	053 306
31.	w	2.034	0.2418	0.2424 0.2411 0.2419	026 514 534
32.	w	1.962	0.2597	0.2598 0.2600 0.2589	061 452 416
33.	w	1.909	0.2746	0.2747 0.2749	261 615

TABLE—contd.

No. of lines	Intensity	$d \text{ \AA}$	$Q_{hkl} = 1/d^2$ observed	Q_{hkl} computed	Indices
34.	vw	1.844	0.2942	0.2938 0.2946 0.2948	360 505 354
35.	vw	1.791	0.3118	0.3121 0.3111 0.3116	236 435 526
36.	vw	1.729	0.3342	0.3335 0.3348 0.3337 0.3344	263 363 651 644
37	w	1.676	0.3562	0.3556 0.3567	264 255
38.	vw	1.628	0.3775	0.3779 0.3777	264 561, 562
39.	vw	1.589	0.3958	0.3951 0.3952 0.3962	463 526 546
40.	w	1.559	0.4116	0.4112	661
41.	vw	1.513	0.4372	0.4367	646
42.	vw	1.469	0.4633	0.4634 0.4632	365 645

ACKNOWLEDGMENTS

The authors wish to express their indebtedness to the Education Ministry, Government of India, for awarding a Research scholarship to one of us (Mrs. M. Krishnaswamy). They are also thankful to Dr. D. V. Ramana Rao and Mr. R. N. Patel of the Department of Chemistry, for supplying us the pure sample used in this work.

REFERENCES

- Azaroff, L. V. and Buerger, M. J., 1958, *Powder method*, Mc GrawHill, p. 150.
 Ito, T., 1950, *X-ray studies in Polymorphism*, Maruzen, Tokyo.
 Lipson, H., 1949, *Act. Cryst.*, **2**, 43.

ON HEAT TRANSFER IN NUCLEATE BOILING-(2)

S. P. BASU AND D. B. SINHA

DEPARTMENT OF APPLIED PHYSICS, CALCUTTA UNIVERSITY

(Received November 24, 1966)

ABSTRACT. Attempts have been made to measure the maximum heat flux attainable in the nucleate boiling range for di-ethyl ether boiling on horizontal platinum wires and copper tubes. The flux shows a dependence on the diameter of the heating surface. With smaller diameters of the wire the maximum heat flux increases. A full Nukiyama curve was also tried to be obtained. Though only the nucleate boiling range, and the film boiling and radiation zone were experimentally traced, the transition range from nucleate boiling to steady film boiling was also possible to be constructed with considerable definiteness. From the data a value for the Leidenfrost point for the liquid has also been suggested. The heat transfer coefficient at any given heat flux has been found to increase with the diameter of the heater wire decreasing. Moreover, the hysteresis effect has been found also to decrease with the diameter of the heater wire decreasing.

INTRODUCTION

The present day heat exchangers are being operated at higher and higher heat fluxes. The nucleate boiling phenomenon is very interesting in such a case because it offers very high rates of heat transmission. As the temperature difference between the heater surface and the bulk liquid increases, the rate of heat transmission gradually increases till it reaches a point when suddenly the heat transfer coefficient drops to very small value. Lang (1888) was the first to report this sudden drop in the rate of heat transmission. He reported on a sea water evaporator operated under pressure and heated by high pressure steam. His experiment clearly indicates that the overall coefficient attains a maximum when the temperature difference lies between 40 and 50°C and also shows a decrease in rate of boiling as ΔT is increased beyond this value. The experiment of Pridgeon and Badger (1924) on sea-water evaporators definitely show decreasing coefficients at temperature differences in excess of 25°C. Numerous experimenters have reported also that overall coefficients increase with ΔT less and less rapidly as higher value of the coefficient are reached.

Jacob and Linke (1933) obtained in the case of water a maximum heat transfer coefficient at a temperature difference of 15.5°C. Any attempt to reach a higher temperature difference caused the heater to burn out. However, no report of the maximum heat transfer coefficient was available from their experiments with Carbon tetrachloride.

Mosciki and Broder (1926) experimented with a wire heater. They found that when the wire had attained a certain temperature excess over the surrounding

liquid, a slight increase in power input caused a sudden rise in wire temperature and melted the wire. Nukiyama (1934) took up the steps followed by Moseiki and Broder and he seemed to be the first man who realized that maximum rate of boiling might occur at a moderate temperature difference. He boiled water at atmospheric pressure with electrically heated nichrome, nickel and platinum wires of various diameters (0.14-0.757 mm) and, by measuring the electrical resistance of the wire, determined its temperature for the various heat loads. However using a platinum wire of 0.014 mm. in diameter Nukiyama, was able to obtain a boiling curve which is reproduced in modified form in fig. 1. As the heat load increases the left hand branch of the curve is followed. At the point A, a slight increase in heat input causes a sharp rise in wire temperature and the

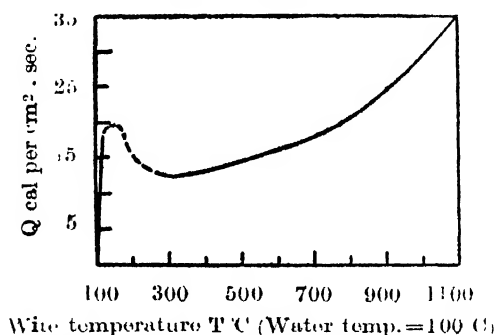


Fig. 1. Boiling curve of Nukiyama.

operating point jumps to B. If the heat load is increased still further the point B shifts to point D. But if the heat load is gradually decreased the right hand curve is followed upto C and then again a temperature jump occurs and the working point shifts to the left hand branch of the curve. Nukiyama stated that the dotted portion of the curve represents an unstable region, but his work clearly shows the existence of a maximum rate of boiling at a critical temperature difference of 40-50°C for water.

This method of experiment has the disadvantage that at higher temperatures the wire sags and the true heat transfer area becomes suspect as was rightly pointed out by the students of Prof. W. H. McAdams to Drew and Mueller (1937).

The experiments carried out on the line of Nukiyama also offer in addition to the determination of the maximum rate of heat transfer the minimum temperature of a steady spheroidal state for the liquid.

Moseiki and Broder found the limiting temperature of the wire to be independent of the main body temperature of the liquid. This seems to indicate that the limiting factor is primarily the temperature at the heating surface-liquid interface. Up to the breaking point the liquid adjacent to the wire, would, in all cases, be at the temperature of the latter, and the only essential change in local conditions caused by lowering of the bulk temperature would be a steepening of the temperature gradient in the liquid.

Though much has been said about the nature and orientation of the surface on the overall coefficient of it has been shown by Berenson (1962) that the maximum nucleate boiling heat flux is independent of the surface conditions.

The present set of experiments were undertaken to find data in the case of di-ethyl ether boiling on horizontal wires and tubes for investigation of the maximum heat flux, the critical temperature difference and the Liedenfrost point.

Experiments were performed with platinum wire heaters of 0.04 cm, .005 cm and 0.1 cm. diameter and thin walled (0.004") 3/16-th inch diameter copper tubes.

Experimental apparatus

Heater : The construction of the tube heater (copper tube) was described earlier (Basu, 1964). The heater cell using platinum wire as the heater was made on the same lines as by Ahsmann and Kronig (1951). It consists of a fine thermopure platinum wire placed along the axis of a horizontal cylinder made of brass. The end plugs are made of perspex. The detailed construction of the heater cell is shown in the fig. 2. At one end, the wire is screwed to a brass plug, fitting

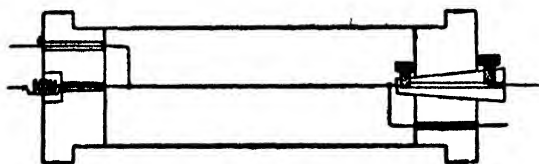


Fig. 2. Constructional details of the heater.

closely into the plug and passing centrally through it. The other end of the wire passes through the centre of the end plug and is soldered to a spring. This was done with a view to prevent sagging of the wire. One of the current leads is screwed to the outside end of the brass plug and the other is soldered to the spring. The potential leads were soldered to the platinum wire and taken out through holes drilled in the plugs. The internal diameter of the brass cylinder was 2.1 cm. and rows of 1/8" holes were drilled all over the body so as to ensure the free circulation of the liquid.

The details of purification of the liquid was described earlier (Basu 1964).

RELATION BETWEEN THE SURFACE TEMPERATURE OF THE HEATER WIRE AND ITS AVERAGE VOLUME TEMPERATURE.

The temperature of the wire was measured by resistance thermometry. The heating current was allowed to flow through a series circuit containing the heater cell and a standard 0.1 ohm resistance. Then by comparing the potential differences across the standard resistance and the heater length between the potential leads the resistance of the heater (platinum) was determined at each

heat load. Then from the temperature coefficient of platinum the temperature of the wire was determined. The potential differences were measured by a Diesselhorst thermoelectric-free potentiometer capable of measuring down to 0.1 micro volt. The actual measurements were taken down to 1 micro volt only. The bulk temperature was measured by three welded type single junction thermocouples (Copper-constantan).

The temperature measured in this way is the average volume temperature of the wire. In our calculation we have assumed this temperature to be equal to the surface temperature following the lines of Sato *et al* (1962) who have also shown that for very thin wires, as in our case, the average volume temperature is only slightly higher than the surface temperature.

In the boiling range the temperature change ($\Delta T'$) of the heater wire is small. For unit length of the platinum wire heat balance is given by ,

$$-2\pi k \frac{dT}{dr} dr - 2\pi k r \frac{d^2T}{dr^2} dr = 2\pi Q r dr \quad \dots (1)$$

where T = temp. of the platinum wire at radius r ,

K = Thermal conductivity of the platinum wire and

Q = Heat produced per unit time per unit volume.

Boundary conditions here are,

$$\left(\frac{dT}{dr} \right) = 0 \quad \text{at} \quad r = 0$$

$$-K \left(\frac{dT}{dr} \right)_{r=r_1} = h(T_s - T_B), \text{ at } r = r_1 \text{ (surface)}$$

where, h = heat transfer coefficient at surface,

T_s = Surface temp. of the wire and

T_B = Bulk temp. of the liquid.

Under these boundary conditions, equation (1) reduces to

$$T = \frac{Q}{4K} (r_1^2 - r^2) + \frac{Qr_1^2}{2h} + T_B \quad \dots (2)$$

where r_1 is the radius of the wire.

On the other hand, the average volume temperature is given by,

$$T_V = \frac{1}{\pi r_1^2} \int_0^{r_1} 2\pi T r dr = \frac{Qr_1^2}{8K} + \frac{Qr_1^2}{2h} + T_B \quad \dots (3)$$

Putting in equation (2) $T = T_S$ for $r = r_1$

$$T_S = \frac{Qr_1}{2h} + T_B$$

Therefore,

$$T_V - T_S = \frac{Qr_1^2}{8K} \quad \dots (4)$$

Now Q , the heat produced per unit time per unit volume, and q , the heat flux are related as

$$Q = \frac{2q}{r_1},$$

So, equation (4) becomes,

$$T_V - T_S = \frac{r_1}{4K} \cdot q \quad \dots (5)$$

Equation (5) enables one to calculate the surface temperature. From the above equation it is also evident that the departure of the surface temperature from the average volume temperature is a maximum when the heat flux q is a maximum.

RESULTS

Experiments were performed with wires of platinum of diameter 0.004 cm, 0.005 cm., 0.1 cm. and thin walled copper tubes (wall thickness .004") having a diameter of 3/16th inch.

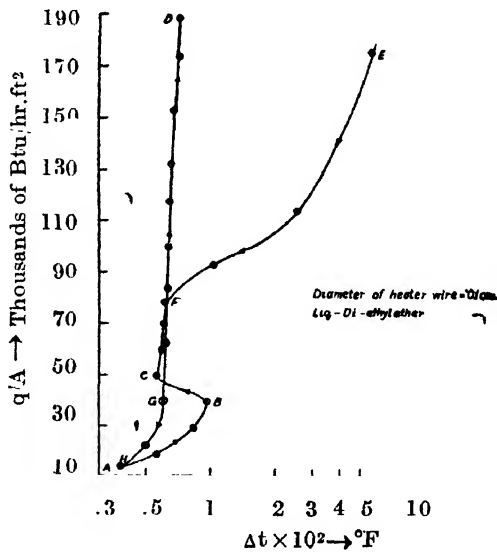


Fig. 3. q/A Vs Δt curves.

In the present set of experiments the values of critical heat flux, the critical ΔT and the maximum heat transfer coefficient are obtained for di-ethyl ether boiling on horizontal platinum wires. Data are also presented for ether boiling on horizontal copper tubes. The value of heat transfer coefficient is only stated in the latter case at a particular value of heat flux.

Fig. 3 shows the boiling curve obtained with platinum wire of diameter .01 cm. In this case the heat flux was increased and the curve ABCD was traced and then the temperature jump occurred and the operating point shifted to *E*. Decreasing the heat flux the curve EFGH was traced.

Fig. 4 gives the boiling curves for .004, .005 and .01 cm. diameter wires. The maximum heat flux values in these cases were slightly below that at which the temperature jump occurs. The hysteresis effect is present in all the cases. For decreasing values of heat flux the curves become almost straight lines.

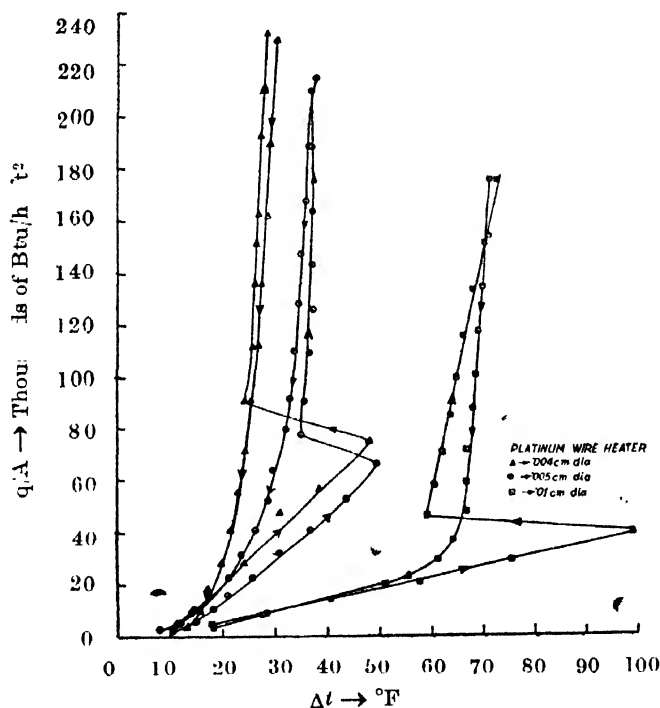


Fig. 4. q/A vs Δt curves.

Fig. 5 show the variation of heat transfer coefficient h , with ΔT for .004, 0.005 cm and .01 cm. platinum heaters respectively.

Fig. 6 shows in the case of 0.004 cm, 0.005 cm, 0.01 cm diameters, the nature of variation of heat flux with T in the radiation zone to the nucleate range across the unstable film boiling region drawn to the same scale.

Table 1 shows the difference between the average volume temperature of the wires, as measured in our experiment, and the surface temperature of the wires.

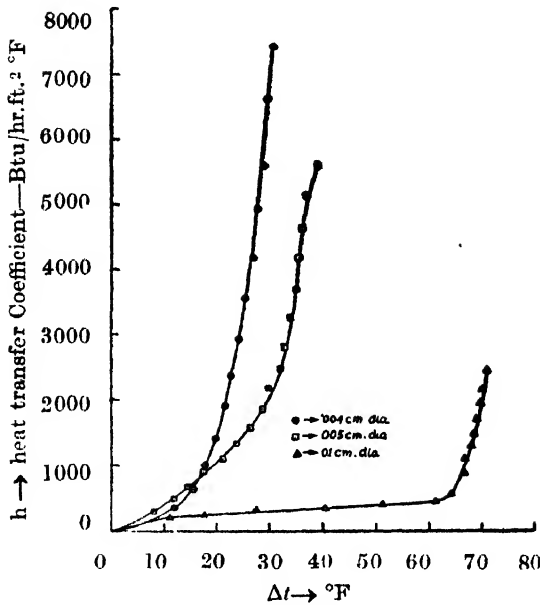


Fig. 5. h vs Δt curves.

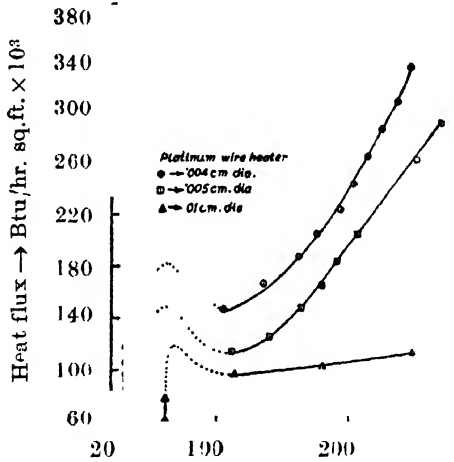


Fig. 6. q/A vs Δt curves.

Table II shows in a condensed form the different results obtained in our experiment.

DISCUSSION

From the present set of experiment it is clear that when heat flux is increased the value of ΔT at which the temperature jump occurs may be different for heater wires of different diameter but after the temperature jump to the right has occurred and stable film boiling has set in, if the heat flux is now decreased step by step gradually, then at a characteristic value of ΔT another temperature jump occurs and the operating point is shifted to left now to a point in the nucleate

TABLE I

Heat flux Btu/hr.ft ²	(T _p -T _s) °F for the heater wires of diameter		
	1.312 × 10 ⁻⁴ ft.	1.64 × 10 ⁻⁴ ft.	3.28 × 10 ⁻⁴ ft.
50 × 10 ³	0.02008	0.0251	0.0502
100 × 10 ³	0.04016	0.0502	0.1004
150 × 10 ³	0.06024	0.0753	0.1506
200 × 10 ³	0.08032	0.1004	0.2008
250 × 10 ³	0.1004	0.1255	0.2510
400 × 10 ³	0.1606	0.2008	0.4016

TABLE II

Diameter of heater ft.	Heat flux Btu/hr. ft ²	ΔT °F	Heat transfer Coeff. (h) Btu/hr. ft ² °F.
1) 1.312 × 10 ⁻⁴ (Platinum)	232.07 × 10 ³	29.36	7904.3
3) 1.64 × 10 ⁻⁴ ..	215.27 × 10 ³	38.41	5601.5
4) 3.28 × 10 ⁻⁴ ..	176.26 × 10 ³	72.70	2424.5
4) 1.562 × 10 ⁻² ..	42.1 × 10 ³	18.9	2230.0

boiling range of the boiling curve. This value of ΔT is, however, found to be almost independent of the diameter of the wire and for other boiling on horizontal platinum wires assumes almost a constant value of about 110 °F with wire diameters decreasing the boiling curve becomes more and more steep, i.e., the heat transfer coefficient has greater values with thinner wires for the same heat flux. Though in the reverse case when thicker and thicker wires are taken the heat transfer coefficient falls but after a certain value of the diameter, the coefficient appears to become independent of the diameter. The reason may be that with very thin wires the bubble diameter at detachment becomes comparable with the diameter of the wire. The reason is augmented from the experimental finding that as the wire diameter decreases the hysteresis loop also decreases in size, i.e., the wire becomes less and less superheated.

Let us consider the family of boiling curves shown in the Fig. 7. In a cooling operation in the radiation region the initial operating points of the curves in a decreasing order of heater wire diameter are *D*, *D'* etc. For curve (1) as the heat flux is decreased, the operating point gradually shifts to *C*. At this point the temperature jumps and the operating point shifts to *B*. As the heat flux is decreased further, the curve *BA* is traced. The portion *AB* is a region of stable nucleate boiling while *CD* represents stable film boiling, radiation occurring across the vapour belt. The point *C* is the point at which stable film boiling begins and

it appears from the experimental run, to be characteristic for a particular heater-liquid combination. The nature of the dotted curve BC could not, however,

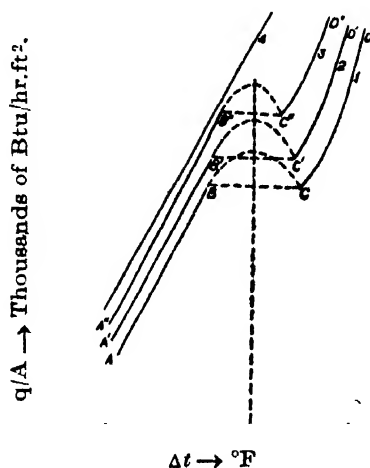


Fig. 7. Theoretical q/A vs Δt curves.

be ascertained from this particular set of experiments. The Liedenforst point should, however, lie somewhere between B and C .

From the nature of the curves it is suggested that when the wire diameter is zero, i.e., in the case of a volume-heated liquid, the unstable region shown dotted in the experimental curves should vanish. Moreover from the given experimental curves what is found is that the range B to C shortens symmetrically as the wire diameter decreases. This, however, enables one to construct the unstable dotted region as a close approximation as shown in the curves. The Liedenforst point which is characteristic of the liquid and independent of the heater wire diameters in all probability, therefore, corresponds to a value of Δt lying between B and C , B' and C' , B'' and C'' , etc. but is the same point. This in the case of di-ethyl ether is found to be 143°F .

REFERENCES

- Basu, S. P., 1964, *Indian J. Phys.*, **38**, 87-92.
 Berenson, P. J., 1962, *Int. J. Heat & Mass transfer (GB)*, **5**, 985-99.
 Drow, T. B., and Mueller, A. C., 1937, *Trans. Am. Inst. Chem. Engrs.*, **33**, 449.
 Jakob, M. and Linke, W., 1935, *Physik, Z.*, **36**, 267-280.
 Lang, C., 1888, *Trans. Inst. Engrs., Shipbuilders Scot.*, **32**, 279-295.
 Moseiki, I. and Broder, J., 1926, *Rocznichi Chem.*, **6**, 319-354.
 Nukiyama, S., 1934, *J. Soc. Mech. Engrs. Japan*, **37**, 367-374, 553-54.
 Pridgemon, L. A. and Badger, W. L., 1924, *Ind. Eng. Chem.*, **16**, 747-478.
 T. Sato, I. Michiyoshi and K. Takauchi, 1962, *Tech. Report Engg., Res. Inst., Kyoto University, Japan*, **12**, No. 8, Rep No. 98, 1-14 (Sept. 1962).

MAGNETIC STUDIES ON α -SILICON CARBIDE (α -SiC) CRYSTALS

Miss D. DAS

DEPARTMENT OF MAGNETISM

INDIAN ASSOCIATION FOR THE CULTIVATION OF SCIENCE, CALCUTTA-32

(Received December 26, 1966)

ABSTRACT. The magnetic susceptibility and anisotropy of different types of α -SiC, the wellknown high temperature semiconductor, have been measured at room temperature. The types of the samples were identified by X-rays and observation of colour and the results of measurements have been explained in the light of their crystal structures. It has been found that some of the samples are diamagnetic and others are freely ferrimagnetic. The field variation of the ferromagnetic samples have been studied both below and above saturation point and magnetic susceptibility of the paramagnetic part has been determined therefrom. The temperature variation of magnetic susceptibility and anisotropy of two varieties of diamagnetic samples have been measured from 90°K to 1000°K. Though the susceptibility increases considerably with temperature the anisotropy remains almost the same. The temperature variation of susceptibility upto a certain temperature obeys the relation

$$\chi = D(kT)^\alpha e^{-\frac{\Delta E}{2kT}} \text{ with } \alpha = -\frac{1}{2}.$$

INTRODUCTION

Silicon Carbide, the well-known high temperature semiconductor is obtained in several polymorphous modifications, one of which is cubic and is called β -SiC while the others are hexagonal or rhombohedral and are termed as α -SiC. The different modifications are obtained by the different stacking sequences of closest packed plane layers formed by silicon and carbon atoms for the three possible stacking positions, the different types being classified according to the number of layers needed to complete the stacking sequences (Azároff 1960).

These crystals which are mostly obtained commercially show different body colours arising probably from the presence of different foreign impurities like iron, aluminium, boron, magnesium, phosphorous, sulphur, fluorine, copper, nickel, zinc, antimony, nitrogen, vanadium, titanium etc (Knippenberg, 1963, Mellor). The best commercial grades are either pale green or pale yellow while the less purer grades are black or deep blue. Pure silicon carbide which is more difficult to prepare is transparent and almost colourless.

The electrical conductivity, Hall effect, Optical (1959) and other allied properties (Busch, 1946, Busch *et al.* 1946) of silicon carbide have been extensively studied over wide range of temperature (80°K to 1400°K). Results of these measurements have been utilised to ascertain its different electronic parameters.

But its magnetic properties which, it is wellknown, can furnish useful information regarding the electronic behaviours of such substances and the measurement of which are free from some major experimental difficulties encountered in electrical measurement (mainly contact difficulties) have not yet been seriously investigated. One finds only a preliminary report on some measurements on magnetic properties by Sigamony (1944) at room temperature alone, complete only for a green variety of the crystals, which obviously are inadequate for a theoretical analysis. We have therefore studied the magnetic properties of different varieties of α -silicon carbide crystals over wide range of temperatures and the present communication gives a preliminary account of such measurements with some crystals of α -SiC.

EXPERIMENTAL

The samples

Commercial variety of silicon carbide crystals were obtained in the form of blocks from Switzerland through the kindness of Prof. G. Busch of E.T.H., Zurich. These were cut into square or rectangular plates with diamond wheels avoiding contamination during cutting. Prior to any magnetic measurements the samples were tested for their structures by X-rays.

Magnetic Measurements :

The magnetic measurements consist of two parts, measurement of anisotropy and that of susceptibility.

Anisotropy

Magnetic anisotropy was measured by the method of critical torque well standardized here (Krishnan and Banerjee, 1936). For measurements at high temperatures the specimen is suspended in the tubular electric heater having non-inductive windings of nichrome wire, the pole pieces of the field magnet being protected from the heat by providing a water jacket round the heater. Interior of the experimental chamber was always evacuated to maintain the same conditions as for susceptibility measurements. The temperatures were measured with a calibrated Pt—PtRh thermocouple. Since silicon carbide normally has a weak diamagnetism, which is expected to be temperature sensitive at higher temperatures only, measurements below room temperatures were taken at some fixed points only, namely, at the boiling points of liquid nitrogen (or oxygen) and melting point of carbondioxide.

Measurement of susceptibility

The magnetic susceptibility was measured with a Jewell-pivoted micro-balance described earlier (Das, 1963). Only modification that has been made in the previous arrangements is that the optical lever method of observing the deflection of

the balance has been replaced by a photo-cell method, which has considerably increased the deflectional sensitivity of the instrument. For both high and low temperature work the balance case along with the experimental chamber was always evacuated. This evacuation was particularly necessary at high temperatures to prevent the disturbances due to convection currents. Evacuation at low temperatures was done only to maintain the uniformity of experimental conditions. The method of production of high and low temperatures and their measurements were the same as already described in the case of anisotropy measurements. The crystals were attached to the suspension system with zinc oxyphosphate cement which stands very high temperatures and at the same time feebly diamagnetic. The crystals are always suspended with the (0001) plane vertical. The procedure for measurement was the same as described in an earlier paper (Das, 1963).

RESULTS

When crystals of SiC, usually diamagnetic, are suspended with (0001) planes vertical in a uniform magnetic field, in most cases they set with (0001) plane perpendicular to the field indicating that gm. molecular susceptibility $\chi_{||}$ along the c -axis is algebraically greater than χ_{\perp} that along directions in the (0001) plane. Therefore the principal gm-molecular magnetic anisotropy of the crystal is $\Delta\chi = \chi_{||} - \chi_{\perp}$. The experimental values of $\Delta\chi$ and $\chi_{||}$ for different specimens indexed A, B, C, D, E, F, G, H and I are shown in Table I. Any deviations from observations as stated above are also indicated there. The values of field independent average susceptibility and anisotropy as found by Sigamony (1944) are given in the same table for comparison. It is observed from the table that the anisotropies are not very high and hence the correction for the effect has to be considered. When the magnetic field is perfectly homogeneous, effect of shape is negligible (Nye 1957). But due to inhomogeneity of the field, an extra couple may act on the specimen while determining the anisotropies as well as the susceptibilities. In anisotropy measurements homogeneous magnetic field was used and thus the shape effect was negligible. In case of susceptibility measurements magnetic field was intentionally made inhomogeneous but the gradient was along the vertical direction while field was horizontal. Further the shape of the crystal was such that the principal shape direction and the principal susceptibility directions were coincident. So there will be no shape effect on the values of susceptibility determined.

In contrast to other samples, the samples *D* and *G* show field dependent paramagnetism, specimens always setting with their planes along the field. Measured anisotropies showed a marked difference in values for different directions of rotation of the torsion head and also showed field dependence obviously due to ferromagnetism. These have not been included in Table I. The part of the principal

TABLE I

Sample	Colour of the sample	Crystal class of the sample	Orientation of the c-axis w.r. to the field	$\Delta\chi \times 10^6$ per gm.mol	$\chi_{\parallel} \times 10^6$ per gm.mol	Anisotropy per cent.
A	Pale green transparent.	Hexagonal 6H $a = 3.073 \text{ \AA}$ $c = 15.08 \text{ \AA}$	C-axis \parallel to field	0.91621	-10.618	8.1%
F	Light green transparent.	Hexagonal 6H $a = 3.073 \text{ \AA}$ $c = 15.08 \text{ \AA}$	C-axis \parallel to field	0.93111	-12.550	7.6%
J	Deep blue transparent.	Hexagonal 6H $a = 3.073 \text{ \AA}$ $c = 15.08 \text{ \AA}$	C-axis \parallel to field	0.87140	-10.376	7.9%
C	Black Opaque	Hexagonal 6H $a = 3.073 \text{ \AA}$ $c = 15.08 \text{ \AA}$	C-axis \parallel to field	0.90312	-7.331	11.3%
H	Deep green transparent.	Hexagonal 6H mixed with Rhombohedral 15R.	C-axis \parallel to field	0.7780	-7.321	9.9%
E	Light green transparent.	Rhombohedral 21R $a = 3.073 \text{ \AA}$ $c = 52.78 \text{ \AA}$	C-axis \parallel to field	0.93031	-5.739	14.6%
B	Black Opaque	Rhombohedral mixture of 15R and 21R.	C-axis \parallel to field	0.82279	-4.200	17.3%
D	Yellowish green transparent.	Rhombohedral 15R $a = 3.073 \text{ \AA}$ $c = 37.70 \text{ \AA}$	C-axis \perp to field	—	$\chi_{\perp} = 123.744$	—
G	Deep blue transparent.	Hexagonal 6H $a = 3.073 \text{ \AA}$ $c = 15.08 \text{ \AA}$	C-axis \perp to field	—	$\chi_{\perp} = 20.035$	—
Sigamony's green sample		—	—	Average value of $\Delta\chi$ per gm.mol. = 0.82×10^{-6}	χ_{\perp} per gm.mol. = -13.1×10^{-6}	6.4%

susceptibility which is independent of the field, have however, been calculated from the slope of the linear portion of saturation region of the intensity-field curve.

These values represent the susceptibilities for direction in the (0001) plane and may therefore be called χ_{\perp} . Temperature variation of $\Delta\chi$ and χ_{\parallel} of samples

A and B have been studied, as two typical cases from 90°K to about 1000°K and are shown graphically in figures 1 and 2. Study of temperature variation of other samples is also in progress and will be published in a future communication.

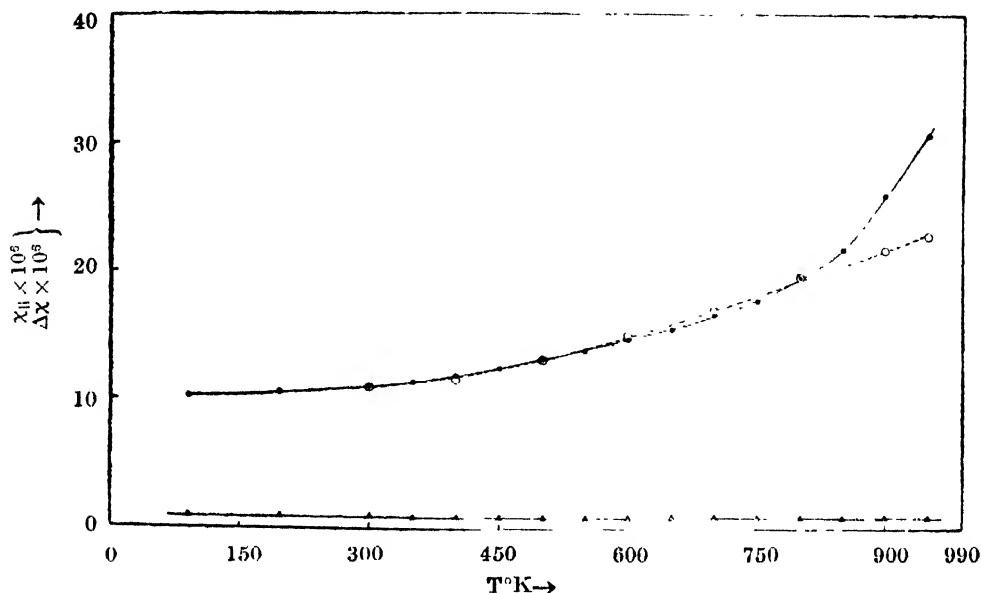


Fig. 1. Temperature variation of susceptibility ($\chi_{||}$) and anisotropy ($\Delta\chi$) of sample—A

- Experimental values of $\chi_{||} \times 10^5$
- Theoretically calculated values of $\chi_{||} \times 10^5$
- △ Anisotropy $(\chi_{||} - \chi_{\perp}) \times 10^5$

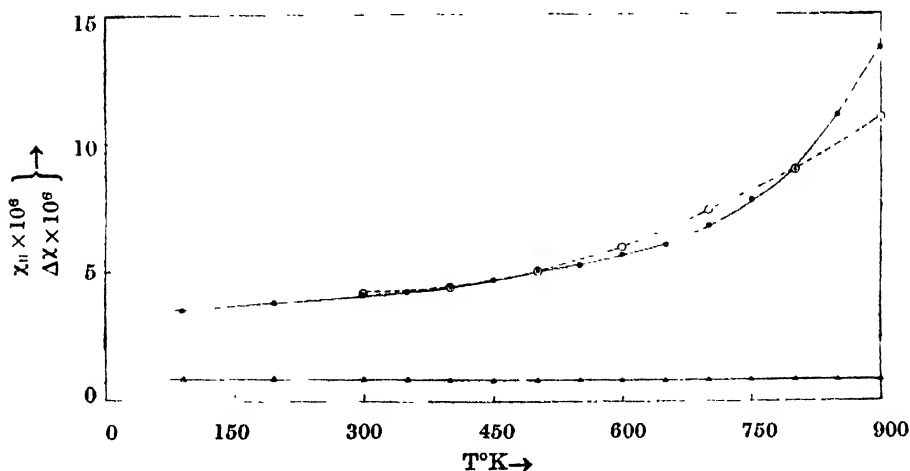


Fig. 2. Temperature variation of susceptibility ($\chi_{||}$) and anisotropy ($\Delta\chi$) of sample—B.

- Experimental values of $\chi_{||} \times 10^5$
- Theoretically calculated values of $\chi_{||} \times 10^5$
- △ Anisotropy $(\chi_{||} - \chi_{\perp}) \times 10^5$

DISCUSSION

As already stated, the present samples of SiC being of commercial variety contain different impurities and hence show various body colours (table I). In addition these may also have crystalline irregularities in them. So when discussing the properties of SiC crystals due consideration should be given to these facts.

It is evident from Table I that the values of $\Delta\chi$, the gram-molecular magnetic anisotropy of the different samples of α -SiC studied by us are small as compared to the values of graphite, molybdenite etc. ($\sim 1 \times 10^6$ C.G.S. e.m.u.) though the percentage anisotropy is pretty large ($\sim 17\%$ in some cases). These low values of $\Delta\chi$ can easily be accounted for from a consideration of the structures of different types of SiC. It is well known that the different polytypes of SiC crystal originate due to different stacking sequences of the hexagonal silicon and carbon layers (Jagodzinski *et al.* 1959). These stackings again seem to follow only such sequences that keep each silicon atom surrounded tetrahedrally by four carbon atoms and vice versa (Taylor *et al.* 1959). So the different polytypes of SiC, cubic, hexagonal or rhombohedral may be considered to be originating from the differences in the arrangements of these tetrahedra (Taylor *et al.* 1959). In hexagonal and rhombohedral forms the deviations of arrangements of the tetrahedra from the cubic variety is found to be very small, the interatomic distances being nearly the same as in the cubic variety (Choyke and Patrick, 1959). To trace the origin of anisotropy one is quite justified to think that the stacking sequence will cause a distortion in the tetrahedra (which for convenience is being considered as repeating unit) which will effect both χ_{\parallel} and χ_{\perp} and hence $\Delta\chi$. One would therefore expect the anisotropy to be small in magnetic and other properties of α -SiC crystals (hexagonal or rhombohedral). It is further evident from Table I that almost all the samples (excepting samples* D and G) are diamagnetic—the susceptibility χ_{\parallel} for different samples varying from -4.2×10^{-6} C.G.S. e.m.u. per gm. mol. to -12.6×10^{-6} C.G.S. e.m.u. per gm. mol. This variation has therefore to be attributed to the differences in the nature and amounts of impurity contents of the different samples as also to crystalline defects, in addition to the distortion in the tetrahedra mentioned above. It may be pointed out here that magnetic anisotropy of the above mentioned samples (except D and G) will remain unaffected by such foreign impurities and one should expect the same value of $\Delta\chi$ for all the samples but for differences in the distortion of the tetrahedra. Table I shows that the values of $\Delta\chi$ of all the samples are of the order 0.9×10^{-6} C.G.S. e.m.u. per gm. mol. excepting for samples B and H where admixture of different structures are found present. The percentage anisotropy shows larger variation. But it should be remembered that in percentage anisotropy the mean susceptibility is also a factor which, unlike anisotropy depends on many other

* These show field dependent paramagnetism due evidently to the nature of the impurity contents, and are excluded from present discussion.

factors as also on the distortion of the tetrahedra as stated before. This might cause the large variation in percentage anisotropy. Even then the least value of the percentage anisotropy in the table is not very small showing that the amounts of distortion produced in the tetrahedra are quite appreciable.

From figures 1 and 2 we find that $\Delta\chi$'s for samples A and B are practically independent of temperature and the values of χ_{II} 's for both the samples increase with temperature, the rate of increment being higher at higher temperatures. This indicates that χ_I will also increase with temperature nearly at the same rate as χ_{II} . This temperature dependent diamagnetism has obviously to be ascribed to the diamagnetism of thermally produced free charge carriers. But to account for the observed values of the susceptibilities, one should keep in mind the suggestion put forward at the beginning of this section, namely, the crystal contains both foreign impurities and crystalline defects. The observed susceptibilities may therefore be considered to be the combination of contributions of temperature independent diamagnetism from the crystal as well as from foreign impurities and defects, charge carrier susceptibilities due to intrinsic excitation as well as due to impurity levels and paramagnetic contribution of the impurities.

Therefore the observed susceptibility $\chi_{obs} = \chi_0 + \chi_c + \chi_c' + \chi_p$ where χ_c and χ_c' are the charge carrier susceptibilities χ_0 , the temperature independent diamagnetic susceptibility and χ_p , the paramagnetic susceptibility. The values of χ_0 and χ_p are estimated in a manner suggested by Busch *et al.* (1960). For the charge carrier susceptibilities Busch *et al.* (1963) proposed an exponential variation with temperature. We accordingly tried to explain the temperature variation of the part of the susceptibility due to charge carrier, and obtained a relation of the type $\chi = D(kT)^\alpha e^{-\frac{\Delta E}{2kT}}$ where D and α are constants and ΔE is the activation energy. The observed values of the susceptibilities can be explained with the following values of D , α and ΔE .

TABLE II

Sample	D	α	ΔE in e.volts	ΔE from electrical conductivity in e.volts (Busch, 1946)
A	2.6868	- 1/4	0.3196	0.304
B	2.8503	- 1/4	0.4557	0.270

The values of ΔE may be compared with those obtained by Busch (1946) from electrical conductivity measurements with samples having almost similar body colour and structures. It should however be noted in this connection that though the agreement between the observed and calculated values are fair at low temperatures, at higher temperatures the differences between the two sets of values

are quite appreciable (fig. 1. and 2). It may be due to the fact that the extrinsic and intrinsic contribution could not be separately estimated. In order, therefore, to explain the observed magnetic properties of these two samples as well as other samples extensive studies of the magnetic and allied properties of SiC have been undertaken and work is in progress.

ACKNOWLEDGMENTS

The author gratefully acknowledges her indebtedness to Shri A. K. Dutta for suggesting the problem and guidance during the progress of the work. She expresses her thanks to Prof. A. Bose for his kind interest in the work, to Prof. G. Busch for kindly presenting the samples, to Dr. D. R. Dasgupta for his most valuable discussions regarding the crystallographic aspects and to Shri R. Bhattacharya for general discussion.

REFERENCES

- Azaroff, Leonid, V., 1960, *Introduction to Solids*. McGraw Hill.
 Busch, G., 1946, *Helv. Phys. Acta.*, **19**, 167-199.
 Busch, G. and Labhart, H., 1946, *Helv. Phys. Acta.*, **19**, 463-92.
 Busch, G. and Mosser, E., 1953, *Helv. Phys. Acta.*, **26**, 611-656.
 Busch, G. A. and Vogt, O. R., 1960, *Proceedings of the international conference on semiconductor Physics Prague* 797-801.
 Choyke, W. J. and Patrick Lyle, 1959, *Proc. Conf. Silicon carbide, Boston*, 162-199.
 Das, D., 1963, *Indian J. Phys.*, **37**, 582-589.
 Jagodzinski, H. and Arnold, H., 1959, *Proc. Conf. Silicon Carbide, Boston*, 136-146.
 Knippenberg, W. F., 1963, *Philips. Res. Reports*, **18**, 161-174.
 Krishnan, K. S. and Banerjee, S., 1936, *Phil. Trans. Roy. Soc.*, **A235**, 343.
 Mellor, J. W., *Inorganic and Theoretical Chemistry*, vol. V, 875-883. Longman Green & Co.
 Nye, J. F., 1957, *Physical Properties of Crystals* (Oxford).
 Sigamony, A., 1944, *Proc. Indian Acad. Science*, **19A**, 377-80.
 Taylor, A. and Jones, R. M., 1959, *Proc. Conf. Silicon Carbide, Boston*, 147-154.
 —————, 1959, *Proc. Conf. Silicon Carbide, Boston*, 347-384.

NOTE ON TORSIONAL VIBRATIONS OF NON-HOMOGENEOUS SPHERICAL AND CYLINDRICAL SHELLS

R. K. BOSE

DEPARTMENT OF MATHEMATICS, R. E. COLLEGE, ROURKELA-8

(Received December 3, 1966)

ABSTRACT. This paper deals with the torsional vibration of non-homogeneous thick spherical and cylindrical shells. Non-homogeneity arises due to variable density ρ and rigidity Modulus μ . The laws of non-homogeneity are $\rho = \rho_0 r^n$ and $\mu = \mu_0 r^n$. The frequency equations are given and numerical evaluation of roots are presented for some particular cases.

INTRODUCTION

In this note some problems of elastic vibration of non-uniform and non-homogeneous thick shells are investigated. In the first case we shall consider the torsional vibration of a spherical shell in which $r = a$ and $r = b$ are internal and external radii of the shell respectively. Both inner and outer boundaries are free. In the second case we shall consider torsional vibration of a cylindrical shell with c and d as inner and outer radii. We have taken same power law variation of elastic constant and density of the material composing thick shells.

Case 1. If we suppose that the components of displacement u_r and u_θ are zero and that the azimuthal component $w (= u_\phi)$ is independent of ϕ we have components of stress in spherical polar co-ordinates as

$$\left. \begin{aligned} \Delta = 0, \quad \widehat{rr} = \widehat{\theta\theta} = \widehat{\phi\phi} = \widehat{r\theta} = 0 \quad \widehat{r\phi} = \mu \left[\frac{\partial \omega}{\partial r} - \frac{\omega}{r} \right] \\ \widehat{\theta\phi} = \frac{\mu}{r} \left[\frac{\partial \omega}{\partial \theta} - \omega \cot \theta \right] \end{aligned} \right\} \quad \dots \quad (1)$$

The stress equation of motion satisfied by w is

$$\frac{\partial}{\partial r} \widehat{r\phi} + \frac{1}{r} \frac{\partial}{\partial \theta} \widehat{\theta\phi} + \frac{3}{r} \widehat{r\phi} + 2 \frac{\partial \widehat{\theta\phi}}{r} \cot \theta = \rho \frac{\partial^2 \omega}{\partial t^2} \quad \dots \quad (2)$$

Let

$$\mu = \mu_0 r^n \quad \text{and} \quad \rho = \rho_0 r^n$$

Then

$$\widehat{r\phi} = \mu_0 r^n \left[\frac{\partial \omega}{\partial r} - \frac{\omega}{r} \right], \quad \widehat{\theta\phi} = \mu_0 r^{n-1} \left[\frac{\partial \omega}{\partial \theta} - \omega \cot \theta \right] \quad \dots \quad (3)$$

Substituting (3) in the equation (2) we get

$$\left[r^n \frac{\partial^2 \omega}{\partial r^2} + (n+2)r^{n-1} \frac{\partial \omega}{\partial r} - (n+2)r^{n-2} \omega \right] + r^{n-2} \left[\frac{\partial^2 \omega}{\partial \theta^2} + \cot \theta \frac{\partial \omega}{\partial \theta} + (1 - \cot^2 \theta) \omega \right] = \frac{\rho_0 r^n}{\mu_0} \frac{\partial^2 \omega}{\partial t^2} \quad \dots (4)$$

For rotatory vibration of the shell, we assume

$$u_r = 0 = u_\theta, \quad u_\phi = \omega = f(r) \sin \theta e^{ipt}$$

Then equation (4) reduces to

$$r^2 f''(r) + (n+2)rf'(r) + \{\lambda^2 r^2 - (n+2)\}f(r) = 0 \quad \dots (5)$$

where

$$\lambda^2 = \frac{\rho_0 p^2}{\mu_0}$$

The solution of equation (5) is

$$f(r) = r^{-\frac{n+1}{2}} \left[AJ_{\frac{n+3}{2}}(\lambda r) + BY_{\frac{n+3}{2}}(\lambda r) \right] \quad \dots (6)$$

So

$$\omega = r^{-\frac{n+1}{2}} \left[AJ_{\frac{n+3}{2}}(\lambda r) + BY_{\frac{n+3}{2}}(\lambda r) \right] \sin \theta e^{ipt}$$

Boundary condition : We assume that $\widehat{\phi r} = 0$ when $r = a$ and $r = b$... (7)

Now

$$\widehat{\phi r} = \mu_0 r^n \left[\frac{\partial \omega}{\partial r} - \frac{\omega}{r} \right] = -\mu_0 \lambda r^{(3n+5)/2} \left[AJ_{\frac{n+5}{2}}(\lambda r) + BY_{\frac{n+5}{2}}(\lambda r) \right] \sin \theta e^{ipt} \quad \dots (8)$$

From (7) and (8) we have

$$\left. \begin{aligned} AJ_{\frac{n+5}{2}}(\lambda a) + BY_{\frac{n+5}{2}}(\lambda a) &= 0 \\ AJ_{\frac{n+5}{2}}(\lambda b) + BY_{\frac{n+5}{2}}(\lambda b) &= 0 \end{aligned} \right\} \quad \dots (9)$$

Eliminating A and B from from (9) we have

$$J_{\frac{n+5}{2}}(\lambda a) Y_{\frac{n+5}{2}}(\lambda b) - J_{\frac{n+5}{2}}(\lambda b) Y_{\frac{n+5}{2}}(\lambda a) = 0 \quad \dots (10)$$

Equation (10) gives the frequency equation of torsional or rotatory vibration of the spherical shell.

Case 2. In case of thick cylindrical shell, taking the axis of the cylindrical shell as the axis of z and assuming $u = \omega = 0$ and v is independent of θ , we have stress components in cylindrical co-ordinates as

$$\widehat{rr} = \widehat{\theta\theta} = \widehat{zz} = \widehat{rz} = 0, \quad \widehat{\theta z} = \mu \frac{\partial v}{\partial z}, \quad \widehat{r\theta} = \mu r \frac{\partial}{\partial r} \left(\frac{v}{r} \right) \quad \dots (1)$$

Equations of motion in terms of displacements are

$$\left. \begin{aligned} \frac{\partial}{\partial r} \widehat{rr} + \frac{1}{r} \frac{\partial}{\partial \theta} \widehat{r\theta} + \frac{1}{r} (\widehat{rr} - \widehat{\theta\theta}) &= \rho \ddot{u} \\ \frac{\partial}{\partial r} \widehat{r\theta} + \frac{1}{r} \frac{\partial}{\partial \theta} \widehat{\theta\theta} + \frac{\partial}{\partial z} \widehat{\theta z} + \frac{2}{r} \widehat{r\theta} &= \rho \ddot{v} \\ \frac{\partial}{\partial r} \widehat{rz} + \frac{1}{r} \frac{\partial}{\partial \theta} \widehat{\theta z} + \frac{\partial}{\partial z} \widehat{zz} + \frac{1}{r} \widehat{rz} &= \rho \ddot{w} \end{aligned} \right\} \quad \dots (2)$$

If we assume $\mu = \mu_0 r^n$ and $\rho = \rho_0 r^n$ where μ_0 and ρ_0 are constants and substitute (1) in (2) we find that the first and third equation of (2) are identically satisfied and the second equation gives

$$r^n \frac{\partial^2 v}{\partial r^2} + (n+1)r^{n-1} \frac{\partial v}{\partial r} + r^n \frac{\partial^2 v}{\partial z^2} - (n+1)r^{n-2}v = \frac{\rho_0}{\mu_0} r^n \frac{\partial^2 v}{\partial t^2} \quad \dots (3)$$

Assuming $v = C \cos \gamma z V(r) e^{ipt}$ the equation (3) reduces to

$$r^2 \frac{d^2 V}{dr^2} + (n+1)r \frac{dV}{dr} + \left(\left[\frac{\rho_0 p^2}{\mu_0} - \gamma^2 \right] r^2 - (n+1) \right) V = 0 \quad (4)$$

Solution of equation (4) is

$$V(r) = r^{-\frac{n}{2}} \left[A J_{\frac{n}{2}+1}(\lambda r) + B Y_{\frac{n}{2}+1}(\lambda r) \right] \quad \dots (5)$$

where
$$\lambda^2 = \frac{\rho_0 p^2}{\mu_0} - \gamma^2$$

Therefore
$$v = C \cos \gamma z r^{-\frac{n}{2}} \left[A J_{\frac{n}{2}+1}(\lambda r) + B Y_{\frac{n}{2}+1}(\lambda r) \right] e^{ipt} \quad \dots (6)$$

The boundary conditions are

$$\left. \begin{aligned} \widehat{\theta z} &= 0 \quad \text{when } z = 0 \\ &= 0 \quad \text{when } Z = L, L \text{ being length of the cylinder} \\ \widehat{r\theta} &= 0 \quad \text{when } r = c \\ &= 0 \quad \text{when } r = d \end{aligned} \right\} \quad \dots (7)$$

First condition of (7) is satisfied. From second condition of (7) we have

$$\gamma = \frac{k\pi}{L} \quad \text{where } k \text{ is any integer} \quad \dots (8)$$

$$\widehat{r\theta} = -\mu_0 \lambda r^{\frac{3n+2}{2}} \left[A J_{\frac{n}{2}+2}(\lambda r) + B Y_{\frac{n}{2}+2}(\lambda r) \right] \cos \gamma z e^{ipt} \quad \dots (9)$$

Third and fourth conditions (7) and (9) give

$$\left. \begin{aligned} A J_{\frac{n}{2}+2}(\lambda c) + B Y_{\frac{n}{2}+2}(\lambda c) &= 0 \\ A J_{\frac{n}{2}+2}(\lambda d) + B Y_{\frac{n}{2}+2}(\lambda d) &= 0 \end{aligned} \right\} \quad \dots (10)$$

Eliminating A and B from (10) we have

$$J_{\frac{n}{2}+2}(\lambda c) Y_{\frac{n}{2}+2}(\lambda d) - J_{\frac{n}{2}+2}(\lambda d) Y_{\frac{n}{2}+2}(\lambda c) = 0 \quad \dots (11)$$

This equation gives the torsional vibration of the cylindrical shell. This equation (11) and equation (10) of case 1 are of same form.

$$\text{Putting } \lambda c = \tilde{\omega} \quad \text{and} \quad \lambda d = \eta \tilde{\omega}, \quad \frac{n}{2} + 2 = m$$

$$\text{so that} \quad \eta = \frac{d}{c}$$

(11) can be written as

$$\frac{Y_m(\eta \tilde{\omega})}{J_m(\eta \tilde{\omega})} = \frac{Y_m(\tilde{\omega})}{J_m(\tilde{\omega})} \quad \dots (12)$$

It is known (from Gray and Mathews, 1931, P261) that the s -th root in order of magnitude, of equation

$$\frac{Y_m(\tilde{\omega})}{J_m(\tilde{\omega})} = \frac{Y_m(\eta \tilde{\omega})}{J_m(\eta \tilde{\omega})} = 0, \quad \eta > 1$$

$$\text{is} \quad \tilde{\omega}^{(s)} = \partial + \frac{\alpha}{\partial} + \frac{\beta - \alpha^2}{\partial^3} + \frac{\theta' - 4\alpha\beta + 2\alpha^3}{\partial^5} + \dots$$

$$\text{where} \quad \partial = \frac{s\pi}{\eta - 1}, \quad \alpha = \frac{4m^2 - 1}{8\eta}$$

$$\beta = \frac{4(4m^2 - 1)(4m^2 - 25)(\eta^3 - 1)}{3(8\eta)^3(\eta - 1)}$$

$$\theta' = \frac{32(4m^2-1)(16m^4-456m^2+1073)(\eta^5-1)}{5(8\eta)^5(\eta-1)}$$

Roots of the equation (12) have been calculated for $n = 2$ and for different values of η i.e. for different values of the ratio α/c and are given in the following Table

TABLE

$\frac{c}{d}$.25	.5	.75
$\eta = \frac{d}{c}$	4	2	$\frac{4}{3}$
$\tilde{\omega}^{(1)}$	-0 .867	3 .708	9 .754
$\tilde{\omega}^{(2)}$	2 .453	6 .616	19 .025
$\tilde{\omega}^{(3)}$	3 .453	9 .654	28 .394

REFERENCES

- Gray and Mathews, 1931, *A Treatise on Bessel functions*, London, pp. 261.
 Love, A. E. H., 1926, *A treatise on the mathematical theory of Elasticity*, Oxford.

NUCLEAR RADIUS, PROTON CONTENT, ELECTRON SCATTERING, CHARGE DENSITY, MAGIC NUMBERS AND BORN-APPROXIMATION MODIFICATION

A. K. DUTTA

PHYSICS DEPARTMENT, CALCUTTA UNIVERSITY.

92, ACHARYA PRAFULLA CHANDRA ROAD, CALCUTTA-9.

(Received June 9, 1967)

ABSTRACT. The r.m.s radii of nuclei, with z protons are determined closely in terms of $E_n^0(A)$, the binding energy per nucleon without coulomb and asymmetry energies. Proceeding from the other side, it is observed that the form factor $F(q)$ for light or heavy nuclei, determined from experimental $\sigma(\theta)$ values for high energy electrons (Hahn et al 1956) and para-charge scattering $\sigma_M(\theta)$, is representable by a simple relation, superposed with small fluctuations. With the help of Born's approximation the $F(q)$ relation is transformed into an expression for ρ , which gives a simple relation for r.m.s radii of nuclei, consistent with that in terms of E_n^0 . The expression for ρ , so dictated by form-factor data and Born's approximation requires a normalising factor N , whose reciprocal must necessarily measure the factor to be associated with Born's approximation, when applied to nuclei. The fluctuations superposed on the basic relation for the form-factor gives rise to variations of charge density, with maxima at proton contents which are magic numbers. The relations determining basic nuclear characteristics are all expressible in terms of E_n^0 .

It has been shown (Dutta 1966) that the binding energy per nucleon $E_n^0(A)$, without coulomb and asymmetry energy corrections, determines many nuclear characteristics satisfactorily. It is considered to be a measure of the internucleonic force and is expressed as :

$$E_n^0(A) = 0.399 \ln (4.654 \times 10^4 A^4) \text{ Mev.} \quad \dots (1)$$

The optimum proton number $Z_0(A)$ in isobaric nuclei is determined by the relation,

$$Z_0/A = 0.842 \exp(-0.059 E_n^0) \quad \dots (2)$$

It may be compared with the mass-formula relation (De Benedetti, 1964),

$$Z_0/A = (1.98 + 0.015 A^{2/3})^{-1} \quad \dots (2a)$$

Similarly, the coulomb energy $U_{en}^0(Z_0, A)$ per nucleon, of strongly bounded nuclei corresponding to equivalent uniform radius, is determined by the relation,

$$U_{en}^0/E_n^0 = 1.524 \times 10^{-2} \exp(0.236 E_n^0) \quad \dots (3)$$

The expression for r.m.s. radius ' a ' as $(3/5)^{3/2} e^2 Z_0^2 / (A U_{en}^0)$, gives us, from eqns. (2) and (3),

$$'a' = 37(Z/E_n^0) \exp(-0.295 E_n^0) fm, \quad \dots (4)$$

In table I, the experimental values of Z_0 estimated from tables (Konig *et al.*, 1962) are compared with the values calculated from equations (2) and (2a). Table II compares the calculated and experimental r.m.s. radius ' a ' (Hahn, *et al.* 1956).

TABLE I
(Z_0 in isobaric nuclei)

A	13	21	31	51	73	111	139	175	197	209	235	245
$Z_0(\text{expt})$	6.4	10.1	14.6	23.0	31.9	47.5	57.1	70.3	78.4	82.4	91.7	95.6
$Z_0(\text{eqn2})$	6.7	10.3	14.7	23.0	31.9	46.6	57.1	70.3	78.3	82.6	91.9	95.4
$Z_0(\text{eq2a})$	6.3	10.0	14.6	23.5	32.6	47.7	58.3	71.5	79.2	83.3	92.1	95.5

TABLE II
(r.m.s. radius ' a ' in fm)

nucleus	He ⁴ *	O ¹²	Mg ²⁴	Si ²⁸	S ³²	Ca ⁴⁰	V ⁵¹	Cr ⁵²	In ¹¹⁵	Sb ¹²³	Au ¹⁹⁷	Pb ²⁰⁸	Bi ²⁰⁹
' a ' Hofst.	1.61	2.37	2.93	3.04	3.19	3.52	3.59	3.83	4.50	4.63	5.32	5.42	5.52
$a(\text{eqn 4})$	1.49	2.35	3.00	3.17	3.32	3.61	3.57	3.83	4.63	4.62	5.32	5.41	5.45

*He⁴ is calculated by modified relation (Dutta 1966) for small nuclei; Z_0 value is used.

Validity of eqn. (4) for all nuclei, as seen in Table II, implies a general form of expression for nuclear charge density and electron scattering. To arrive at the charge density expression search was made for a suitable expression for the form factor $F(q)$ tentatively calculated from experimental $\sigma(\theta)$. (Hahn *et al.*, 1956) by relation,

$$|F(q)|^2 = \sigma(\theta)/\sigma_M(\theta); \quad \sigma_M(\theta) = \left(\frac{Ze^2}{2E} \right)^2 \cdot \frac{\cos^2(\theta/2)}{\sin^4(\theta/2)}. \quad \dots (5)$$

It was observed that the form factor for different nuclei decrease either exponentially with q or by the relation $(\alpha + \beta q^2)^{-2}$, with an apparently periodic function, superposed on the decrease. The exponential form of $F(q)$ would require by Born's approximation, the charge density to be determined by $(\alpha + \beta r^2)^{-2}$. It would give us a divergent expression for r.m.s. radius ' a '. It is therefore, considered that the basic expression for $F(q)$ is of the form $(\alpha + \beta q^2)^{-2}$ which obtains $\rho(r)$ as an exponentially decreasing function of r . The values of $F(q)^{1/2}$ for Co, In, and Au plotted against q^2 , in Fig. 1, justifies the consideration. It is also considered that the term in addition to $(\alpha + \beta q^2)^{-2}$ to determine $F(q)$ is of the form $\phi(q)/q$. The $\phi(q)$ values are plotted in Fig. 2 and show Gaussian distribution of points at the positions of maxima and minima in Fig. 1.

The cause and nature of the superposed maxima and minima, may be correlated with the fact that some nuclei, with particular charges, which are unrelated,

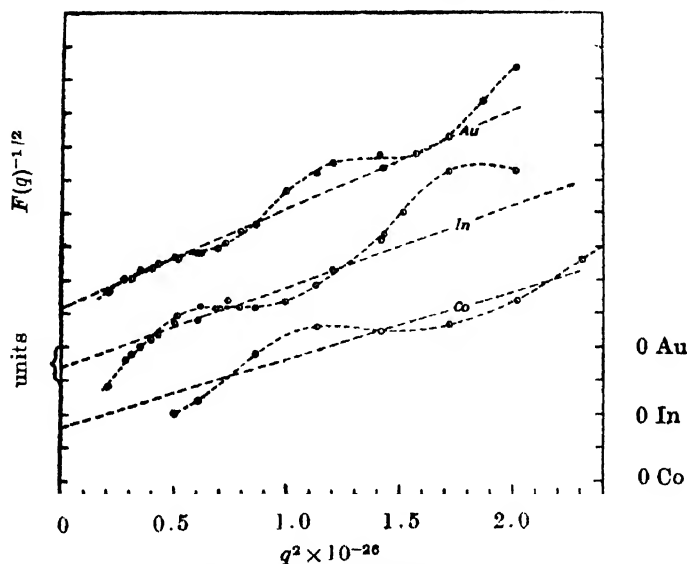


Fig. 1. $F(q)^{-1/2}$ against q^2 .

are comparatively more strongly bound. The underlying principle of the shell model is that in heavy nuclei, subcompositions with these charges are more strongly bound. By implication they should have larger charge densities at unrelated values of r . This is expected to be reflected on the general nature of the form factor expression as observed.

For correspondence with the nature of the form-factor characteristics, we use Born approximation at this stage and put the charge density expression, as

$$\begin{aligned}\rho(r) &= \rho^* \exp(-r/r_0) \pm (\rho^*/r) \sum_i k_i \pm \exp(-r^2/4r_i^2) \cdot \sin(qr_i) \quad \dots (6) \\ &= \rho^* \exp(-r/r_0) [1 + \delta(r)]. \\ &= \rho_I + \rho_{II}.\end{aligned}$$

where r_0 , r_i and $k_i \pm$ have the dimensions of $r(fm)$ and q that of $r^{-1}(fm)$. Hence

$$\langle a^2 \rangle_{(r.m.s)} = \frac{24r_0^5 \pm \sum_i 8\sqrt{\pi}(k_i \pm \cdot q_i) \cdot r_i^5 (3/2 - q_i r_i) \exp(-q_i^2 r_i^2)}{2r_0^3 \pm \sum_i 2\sqrt{\pi}(k_i \pm \cdot q_i) r_i^3 \exp(-q_i^2 r_i^2)} \quad \dots (7)$$

$$F(q) = \frac{8\pi\rho^*r_0^3}{(1+r_0^2q^2)^2} \pm \frac{2\pi^{3/2}\rho^*}{q} \cdot \sum_i k_i \pm r_i [\exp\{-r_i^2(q-q_i)^2\} - \exp\{-r_i^2(q+q_i)^2\}].$$

$$\frac{1}{(\alpha + \beta q^2)^2} \pm \frac{\pi^{1/2} \alpha^{-1/2} \beta^{-3/2}}{4q} \cdot \sum_i k_i \pm r_i \exp\{-r_i^2(q-q_i)^2\} \quad \dots (8)$$

where, $\beta/\alpha = r_0^2$; $8\pi\alpha^{1/2}\beta^{3/2}\rho^* = 1$, ρ^* is not normalised, ... (8a)
 and $\exp\{-r_i^2(q+q_i)^2\}$, is neglected in comparison with $\exp\{-r_i^2(q-q_i)^2\}$.

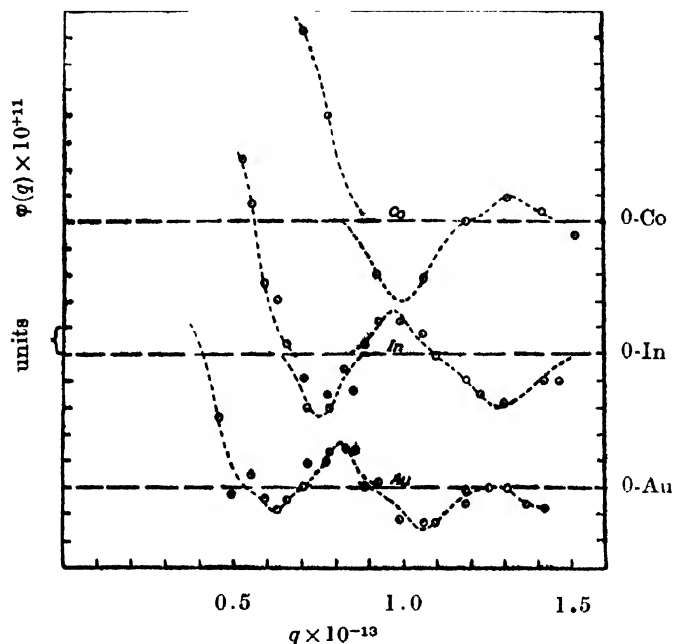


Fig. 2. $\varphi(q)$ against q .
 $\varphi(q) = \{F(q) - (\alpha + \beta p^2)^{-2}\}q$

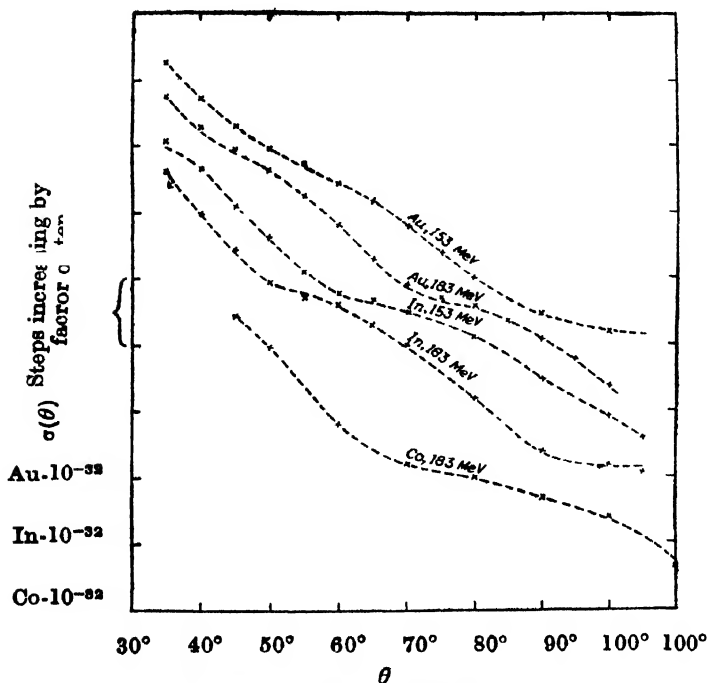


Fig. 3. $\sigma(\theta)$ against θ (Hahn et al 1956)

The parameters α and β and hence r_0 and ρ^* and the sets of parameters k_t , q_t and r_t , in table III, are determined from Figs (1) and (2). They give us, in accordance with equations (5) and (8), the $\sigma(\theta)$ values for electron scattering. The calculated values of $\sigma(\theta)$ are shown in Fig. 3 by continuous lines. The experimental points on it agree well in all cases. The evaluated parameters $k_t \pm$, q_t , r_t make the second terms in the numerator and denominator of eqn(7) for 'a²' insignificantly small. Thus, in view of equns (7) and (4)

$$'a' = \sqrt{12}r_0; \quad r_0 = 10.68 \, Z/E_n^0 \exp(-0.295E_n^0)fm.$$

TABLE III
Parameters

Co			In			Au		
$\rho^* \times 10^{-36}$	$r_0(fm)$	$a(fm)$	$\rho^* \times 10^{-36}$	$r_0(fm)$	$a(fm)$	$\rho^* \times 10^{-36}$	$r_0(fm)$	$a(fm)$
11.13	1.118	3.873	8.065	1.309	4.533	7.382	1.560	5.404
$k_t \pm \times 10^{15}$	$q_t(fm)^{-1}$	$r_t(fm)$	$k_t \pm \times 10^{15}$	$q_t(fm)^{-1}$	$r_t(fm)$	$k_t \pm \times 10^{15}$	$q_t(fm)^{-1}$	$r_t(fm)$
+8.39	0.675	7.50	+6.88	0.512	12.16	+7.155	0.372	10.38
-2.76	1.000	8.78	-1.72	0.760	15.59	-0.005	0.620	24.46
+0.71	1.324	11.43	+1.43	0.980	14.06	+1.420	0.816	14.55
			-3.21	1.312	6.94	-1.920	1.064	10.14
						-0.683	1.416	15.50

The charge densities $\rho(r)$ and $\rho_I(r)$ as also the variations from basic density $\rho_I(r)$ measured by $\delta(r)$ and $\delta_{III} \pm(r)$, a constituent of $\delta(r)$, have been calculated by equation (6) and are shown in Fig. 4. The $\delta(r)$ and $\delta_{III} \pm(r)$ values show maxima at

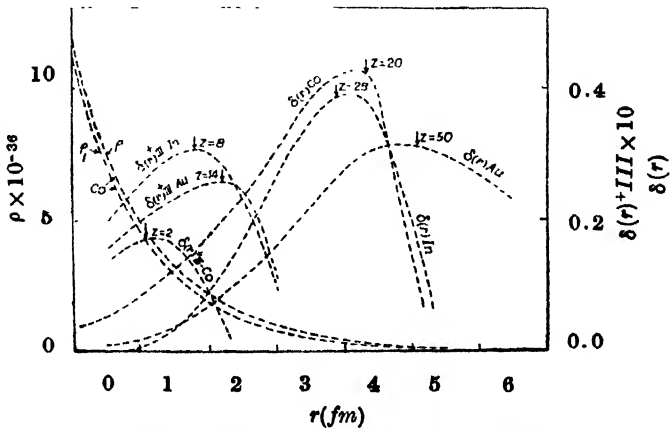


Fig. 4. $\rho(r)$, $\rho_I(r)$, $\delta(r)$, $\delta_{III} \pm(r)$ against r .

particular values of r_m for different nuclei. The expression for basic charge density $\rho_I(r)$ determines the average charge $Z(r_m)$, contained upto r_m , by the relation

$$\begin{aligned} Z(r_m)/Z &= \int_0^{r_m} r^2 \exp(-r/r_0) dr / \int_0^{\infty} r^2 \exp(-r/r_0) dr. \\ &= 1 - (1 + r_m/r_0 + r_m^2/2r_0^2) \exp(-r_m/r_0) \end{aligned} \quad \dots (10)$$

The calculated values of Z at r_m corresponding to $\delta(r)$ and $\delta_{II}^+(r)$ maxima are near 20, 28, 50 and 2,8, 14 respectively, for the nuclei Co, In and Au, indicated in Fig. 4. The charge values are mostly the magic numbers, where stronger binding was expected.

To normalise the charge density, we have

$$1 = N.4\pi \int_0^{\infty} r^2 \rho(r) dr = 8\pi N \rho^* r_0^3, \quad \dots (11)$$

since the 2nd term in equation (6) has insignificant contribution. Thus in view of equation (8a) the normalising factor $N = \alpha^2$ and the normalised charge density at $r = 0$, is

$$\rho_{0N} = N.\rho^* = \frac{1}{8\pi r_0^3} \quad \dots (12)$$

it implies that the Born approximation value of $F(q)_B$ obtained from $\rho(r)$ requires to be multiplied by a numerical factor $1/\alpha^2$ to correspond to $F(q)_e$ calculated by equation (5), where,

$$F(q)_e/F(q)_B = 1/\alpha^2 = 1.618 \times 10^{-2} \exp(0.295 E_n^0) = 0.894. A.U_{en}^0/(Z.E_n^0) \dots (13)$$

Nuclear characteristics are, thus, determined by the relations :

$$\rho(r) = \rho_{0N} [\exp(-r/r_0) \pm \sum_i (k_i \pm/r) \cdot \exp(-r^2/4r_i^2) \cdot \sin(q_i r)]$$

$$\rho_{0N} = 1/(8\pi r_0^3); \quad \alpha^2(r.m.s.) = 12.r_0^2.$$

$$F(q) = (4\pi/\alpha^2 q) \cdot \int_0^{\infty} r \cdot \rho(r) \sin(qr) dr; \quad \sigma(\theta) = \sigma_M(\theta) \cdot F(q)^2.$$

$$1/\alpha^2 = 1.618 \times 10^{-2} \cdot \exp(0.295 E_n^0) = 0.984. A.U_{en}^0/(Z.E_n^0).$$

$$r_0 = 10.68(Z/E_n^0) \exp(-0.295 E_n^0) fm.$$

$$U_{en^0}/E_n^0 = 1.524 \times 10^{-2} \exp(0.236 E_n^0).$$

$$Z/A = 0.842 \exp(-0.059 E_n^0).$$

$$E_n^0 = 0.399 \ln(4.654 \times 10^4 \cdot A^4) \text{ Mev.}$$

The irregularities determined by k_i , r_i , q_i 's are unpredictable.

REFERENCES

- DeBenedetti, S., 1964, *Nuclear Interactions*, John, Wiley & Sons, 98.
 Dutta, A. K., 1966, *Khudiram Bose and T. P. Khaitan Lectures*, Calcutta University, July.
 ———, 1966, *Indian J. Phys.* **40**, 181, 362.
 Konig, L. A., Mattauch, J. H. and Wapstra, A. H., 1962, *Nuclear Physics*, **31**, 18.
 Hahn, B, Ravenhall, D. G. and Hofstadter, R., 1956, *Phys. Ref.*, **101**, 1131.

Letters to the Editor

The Board of Editors does not hold itself responsible for opinions expressed in the letter published in this section. The notes containing short reports of original investigations communicated to this section should not contain many figures and should not exceed 500 words in length. The contributions reaching the Secretary by the 15th of any month may be expected to appear in the issue for the next month. No proof will be sent to the author.

10

AN IMPROVEMENT IN THE TECHNIQUE OF TIME MEASUREMENT

B. N. BISWAS

(Received March, 16, 1967)

It is needless to reiterate the importance of pulsed sinusoidal oscillations (Biswas *et al.*, 1966) in the measurement of time interval between two recurrent events (Chance, B., *et al.*, 1949). The common technique utilises passive resistance-capacitance network for shifting the phase of the wave and basically uses this phase-shifted pulsed sinusoid in some way or other for the aforesaid purpose. In such a case the accuracy of the measurement is impaired because of the appearance of transients at the output of the passive phase shifter. The technique described here depends on the principle of operation of a Phase Locked Pulsed Oscillator (PLPO) (Biswas *et al.*, 1967) (fig. 1) which is essentially a

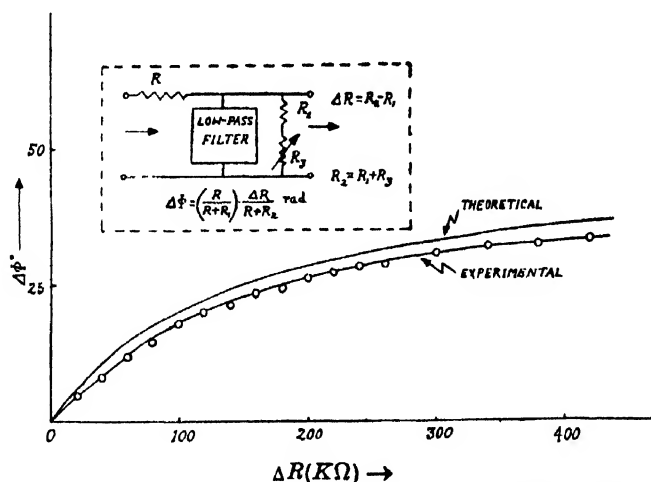


Fig. 1. Typical block diagram of a Phase Locked Pulsed Oscillator.

non-linear feedback control device. It consists of the pulsed oscillator together with a reactance modulator, a phase detector and a low-pass filter network. The use of such a feedback arrangement helps in achieving continuously variable

phase-shift of desired amount producing transientless output (waveform) and at the same time maintaining the frequency of the pulsed sinusoid at a constant value.

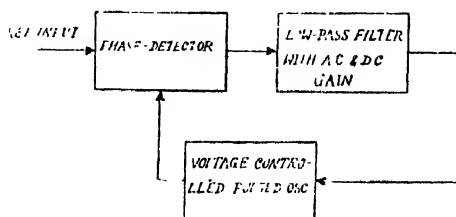


Fig. 2. Graph showing the variation of phase shift of the pulsed sinusoid with the variable load in the filter network.

To understand the mechanism of operation of the PLPO in physical terms (McAleer, 1959), let us assume, to start with, that the frequency of the local pulsed sinusoid is equal to that of the incoming reference oscillation. Then the output of the phase detector, a multiplicative device, is a d.c. voltage that depends upon the static phase difference between the reference oscillation and the local pulsed oscillation during its on-period. This d.c. voltage controls the instantaneous frequency of the local oscillation through the low-pass filter network, in general, having finite d.c. and a.c. gains. Thus any attempted change in the value of the frequency of the pulsed oscillation during its on-period will be first felt by the phase detector as a phase difference and this produces spontaneously a change in the phase detector output d.c. voltage that manages to hold the frequency of the local oscillations to a constant value. It is to be noted that during the off-period of the pulsed oscillations, the local oscillator will have a tendency to fly off from the locked frequency because of the removal of the control voltage at the output of the phase detector. But it has been seen by the authors (Biswas, 1964; Biswas *et al.*, 1967) that a proper design of the filter network can counterbalance this deleterious tendency of stepping aside of synchronism. Thus the phase transients at the output will also be negligibly small.

With such a system continuously variable phase shift lying between $+90^\circ$ and -90° between the input and output of the PLPO can easily be produced. Theoretical treatment of the subject is not given here for economising the space but the experimentally observed values and the theoretically computed values from our equations have given in fig. 2 for comparison. It is seen that they are in quite good agreement. It may be noted that the departure between the experimentally observed data and theoretically computed values is due to the mismatch between the variable load, phase detector and the reactance modulator. This can be eliminated by introducing proper balancing arrangement in the system. If one is interested in the phase following behaviour and noise squelching properties then it is suggested that a proper design of the filter network and an appropriate

choice of the gain parameter of the system can serve that desired purpose (Biswas, 1966).

REFERENCES

- Biswas, B. N., 1964, *Indian J. Phys.*, **38**, 561.
 ———— 1966, *Indian J. Phys.*, **40**, 648.
 Biswas, B. N. and Datta, G., 1966, *Indian J. Phys.*, **40**, 244.
 ———— 1967, *Indian J. Pure and Appl. Phys.*, **5** (to be published)
 Chance, B., *et al.*, 1949, "Waveforms", Radiation Laboratory Series, **19**.
 McAloer, T. W., 1959, *Proc. I.R.E.*, **47**, 1137.

11

SPACE GROUP OF O-BENZOYL BENZOIC ACID

M. L. KUNDU AND S. C. CHAKRAVORTY

DEPARTMENT OF PHYSICS BURDWAN UNIVERSITY, BURDWAN, WEST BENGAL, INDIA

(Received May 24, 1967)

The crystals of o-benzoyl benzoic acid, (chemical formula $C_6H_5COC_6H_4COOH$ and m.p. $127^\circ C$), obtained from its saturated solution both in absolute alcohol and benzene by slow evaporation, are transparent prismatic needles. Crystals from alcohol show, in general, eight faces about the needle axis, but those from benzene show six faces. The preliminary optical study of a crystal was carried out with an optical goniometer and since all the faces did not give prominent reflections, interfacial angles could only be measured approximately.

The axial lengths, $a = 7.71 \text{ \AA}$, $b = 8.28 \text{ \AA}$ and $c = 9.95 \text{ \AA}$ were determined from the rotation photographs about the proposed [100]-, [010]- and [001]- axes. The zero-level normal beam weissenberg photographs were also taken about these three axes. From the symmetry of the weissenberg photographs and other considerations it was confirmed that the crystal belongs to the triclinic system. The positive directions of a , b and c axes with the condition $a < b < c$, were chosen according to the standard practice in right handed system.

The angles between the faces (100), (010) and (001), obtained from the zero-level weissenberg photographs, are

$$\alpha^* = 76^\circ, \quad \beta^* = 96^\circ \quad \text{and} \quad \gamma^* = 92^\circ 30'$$

The values of the axial angles, calculated directly from these values with the help of standard formulae, are

$$\alpha = 103^\circ 50', \quad \beta = 84^\circ 26' \quad \text{and} \quad \gamma = 88^\circ 56'$$

The axial lengths calculated from weissenberg photograph are consistent with those obtained from rotation photographs. The calculated values are

$$a = 7.72 \text{ \AA}, \quad b = 8.27 \text{ \AA}, \quad c = 9.93 \text{ \AA}$$

The volume of the unit cell (V) was found to be 609 \AA^3 .

The density of the crystal, measured by floatation method using a mixture of carbon tetrachloride and benzyl chloride, was 1.29 gm/c.c. The number of molecular units per unit cell (Z) was found to be two and the measured density is consistent with the theoretical density obtained from the X-ray measurement on the basis that $Z = 2$ and $V = 609 \text{ \AA}^3$.

Since the crystal belongs to the triclinic system, no systematic extinctions are possible and this was also confirmed from the indices of the spots on the weissenberg photographs. Hence the space group of the crystal is either $P1$ or $P\bar{1}$. The presence of centre of symmetry in the unit cell was confirmed by the statistical tests of the intensity distributions of okl and hol reflections. For this purpose, the integrated intensities of the X-ray reflections were estimated visually by comparison with a standard graded intensity scale. The intensities were corrected for Lorentz and polarisation factors. The results of the statistical tests applied to okl and hol reflections are shown in the fig. 1.

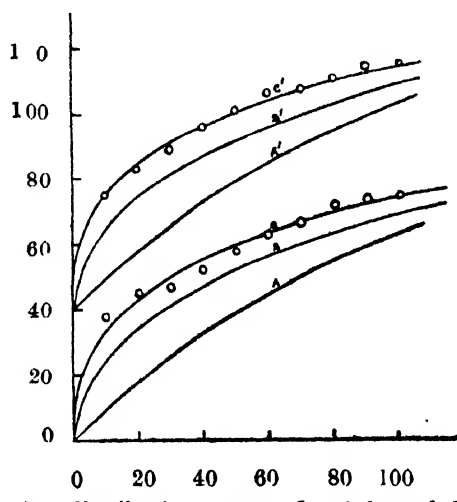


Fig. 1—Intensity distribution curves for O-benzyl benzoic acid.

A, A'—theoretical acentric, B, B'—theoretical centric,

C—experimental hypercentric for okl reflections,

C'—experimental hypercentric for hol reflections,

A', B' and C' are displaced 40% vertically.

Ordinate— $N(Z)\%$, Abscissa— $Z\%$

Results show that the experimental curves are hypercentric in nature. Further Wilson's ratios for okl and hol reflections were found to be 0.540 and 0.500 res-

pectively as against the theoretical value 0.637 for centrosymmetrical crystals. So, the space group of the crystal must be centrosymmetric i.e. $\bar{P}T$.

Hypercentric nature of the intensity distribution curves not only shows the presence of centre of symmetry in the space group but also indicates the presence of a molecular centre of symmetry in the structure (Lipson *et. al.*, 1952). But for this particular case, the presence of molecular centre of symmetry does not follow the chemical structure of the compound. Molecular centre of symmetry, in this case, may be explained on the basis that two molecular units in a unit cell form a dimer and centre of symmetry of the dimer thus coincides with that of the unit cell.

Further work is in progress.

REFERENCE

Lipson, and Woolfson H., M. M., 1952, *Acta Cryst.*, 5, 680.

12

RENNINGER EFFECT IN QUINALDIC ACID

M. Y. KHAN

DEPARTMENT OF PHYSICS, UNIVERSITY OF GORAKHPUR, GORAKHPUR, INDIA.

(Received April 26, 1967; Resubmitted July 1, 1967)

While the study of space-group of quinaldic acid was made some weak reflections different from the nature of the normal ones were observed in the position (105) and (10 $\bar{5}$). Thus their presence was a hurdle in ascertaining the space-group of the crystal. A critical study of the space-group and extinction condition was made which reveals the origin due to double reflection from a pair of strong plane (Srivastava 1957).

The forbidden reflection s (105) and (10 $\bar{5}$) was not accompanied by its usual CuK_β reflection using unfiltered CuK radiation while other reflections are accompanied with the usual CuK_β reflections. The study of the reflection conditions of the reciprocal lattice confirms the presence of Renninger's reflection (1937). The mechanism of the formation of double reflections can be understood by constructing the reciprocal lattice for this crystal. As an example we shall consider the forbidden reflection (105) in details.

The unit cell dimensions of quinaldic acid (Khan, 1967) were determined by oscillation and Weissenberg photograph by standardising the camera diameter, and from a consideration of the high angle spots (where $K_{\alpha_1\alpha_2}$ doublet is well re-

solved). These are $a = 9.77$, $b = 5.97$, $c = 28.00$ and monoclinic angle $\beta = 90^\circ 25'$.

The reciprocal lattice for the equatorial layer of [010] is shown in fig. 1. taking

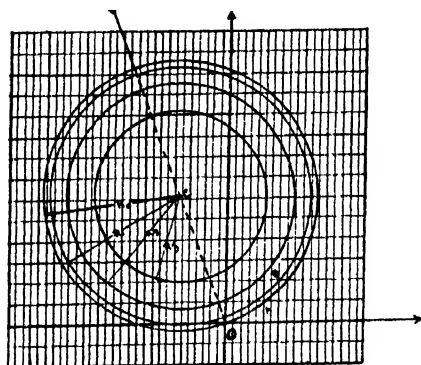


Fig. 1. Spheres of Reflection on Reciprocal Lattice.

$a^* = 0.158782$, $b^* = 0.25825$, $c^* = 0.05506$ and $\beta^* = 89^\circ 35'$, for CuK_α radiation. The circle of reflection for different layers projected on the equatorial layer were

drawn with their respective radii on transparent film with common diameter to represent the incident beam, traces of which are shown in the diagram. The radius of sphere of reflection has been taken 5 cms. One of the junctions of the diameter with the equatorial layer circle of reflection is the origin of the reciprocal lattice and the film rotated until the circle corresponding to the equatorial layer passes through the point (105). Then it is found that the second circle (Radius R_1) passes through the point B(27). Thus it appears that the reflection (105) is caused by the reflection from pair of lattice planes, one plane of the pair is (217). This graphical coincidence has been ascertained by analytical test because there are other coincidences also.

ANALYTICAL VERIFICATION

It is convenient to express the required results in polar-co-ordinates. The equatorial circle is of unit radius and always passes through the origin and it is also passing through a point $A(r, \theta)$. The co-ordinate of the centre of the circle C be $(1, \alpha)$ then the equation to the circle is

$$r/2 = \cos(\alpha - \theta) \quad (1)$$

For this,

$$\alpha = \theta + \cos^{-1}(r/2) \quad (2)$$

Let P be any point (r_1, θ_1) fig. 2, the distance of which from C is R_n . Then the radii of the circles produced by intersection of the reciprocal lattice layer with the sphere of reflection are calculated from ΔPOC .

$$R_n^2 = 1 + r_1^2 - 2r_1 \cos(\alpha - \theta_n) \quad \dots \quad (3)$$

Polar co-ordinates of the point has been calculated from the reciprocal lattice (fig. 1). For the point $A(105)$, $r = 0.31903$ and $\theta = 29^\circ 48'$. Then from Eqn. (2)

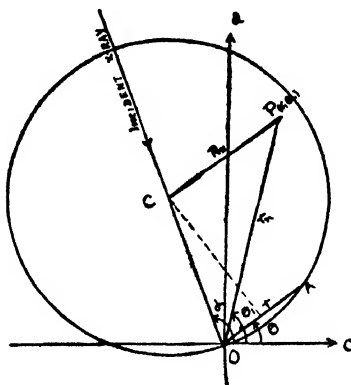


Fig. 2.

$\alpha = 110^\circ 35'$. For (217), with reciprocal lattice co-ordinates (2, 7) and polar co-ordinates $(r_1 \theta_1)$ in the plane of the first layer, we have

$$r_1 = 0.4984; \quad \theta_1 = 39^\circ 16'$$

Therefore from Eqn. (3) $R_1 = 0.9648$.

Considering this from the consideration of co-ordinates given by the relation

$$R_n = \cos v_n = \cos (\sin^{-1} \zeta_n)$$

where

$$\zeta_n = nb^*$$

Eqn. (4) gave the value of $R_1 = 0.9664$, which is in good agreement with the above.

If (hkl) are the indices of the forbidden reflection, and $(h_1 k_1 l_1)$ and $(h_2 k_2 l_2)$ those for a pair of lattice planes contributing to the formation of this reflection, then the pair can be found from the following relationship (Lipson *et al.*, 1953)

$$h = h_1 + h_2, \quad k = k_1 + k_2, \quad \text{and} \quad l = l_1 + l_2.$$

Hence the pair which contribute to the reflection (105) is (217), $(\bar{1}\bar{1}\bar{2})$. Similarly proceeding with the reflection $(10\bar{5})$ we concluded this is formed due to pair, $(21\bar{7})$ $(\bar{1}\bar{1}\bar{2})$. This interpretation has been tested analytically by calculation of ω values (Speakman 1965) for the two sets of reflections. However, intensities of these forbidden spots were found to be in reasonable agreement with the expected estimates from their contributors.

Results : The study of the indexed reflections of the Weissenberg photograph it has been found that all (hkl) reflections are present. The systematic absences

are (*hol*) with 1 odd and (*oko*), no conditions. The forbidden reflections are (105) and (105) are found due to double reflections. Hence the space-group C_{2h}^4-P2/c for quinaldic acid is established.

The author wishes to express his thanks to Prof. D. Sharma for taking interest and Dr. P. Srivastava for suggesting the problem and helpful guidance throughout. The award of CSIR fellowship is also gratefully acknowledged.

REFERENCES

- Khan, M. Y., 1967, *Z. Kristallogr.* (In press)
Lipson, H. and Cochran, W, 1953, *The crystalline state*, VII. III, pp.30.
Renninger, M. Z., 1937, *Z. Kristallogr.* **97**, 107.
Speakman, J. C., 1965, *Acta Cryst.* **18**, 570.
Srivastava, P., 1959, *Indian J. Phys.*, **33**, 123.

INDIAN JOURNAL OF PHYSICS

VOL. 41

No. 8

AND

VOL. 50

PROCEEDINGS

No. 8

OF THE

INDIAN ASSOCIATION FOR THE CULTIVATION OF SCIENCE

(Edited in collaboration with the Indian Physical Society).

AUGUST 1967

PUBLISHED BY THE
INDIAN ASSOCIATION FOR THE CULTIVATION OF SCIENCE
JADAVPUR, CALCUTTA-32

RAMAN SPECTRA OF CH_2Cl_2 , CHCl_3 AND CCl_4 AT 64°K

P. K. BISHUI, D. K. MUKHERJEE AND S. C. SIRKAR

INDIAN ASSOCIATION FOR THE CULTIVATION OF SCIENCE, CALCUTTA-32

(Received November 21, 1966)

(PLATE 6)

ABSTRACT. The Raman spectra of crystals of methylene chloride, chloroform and carbon tetrachloride at 64°K have been investigated using liquid nitrogen boiling under reduced pressure as the refrigerant and in the case of chloroform the spectrum of the crystal at -120°C has also been investigated. A comparison has been made of these spectra with those for the crystals at 93°K . In the case of methylene chloride the changes undergone by some of the Raman frequencies with the lowering of temperature to 64°K indicate slight increase in the Cl-C-Cl angle and also formation of intermolecular $\text{H}\cdots\text{Cl}$ bond. In the case of chloroform the changes indicate transformation of the phase of the crystals in the range -120°C — -180°C and also formation of similar $\text{H}\cdots\text{Cl}$ bond. In the case of carbon tetrachloride no appreciable change takes place in the Raman frequencies, but each of the lines 760 and 789 cm^{-1} seems to be sharper and to have a doublet structure at 64°K .

INTRODUCTION

The Raman spectra of chloroform and carbon tetrachloride in the solid state at about -180°C were investigated long ago by Sirkar (1936) and it was observed that some of the frequencies of chloroform undergo changes with the change of state while those of carbon tetrachloride remain unaltered. He also observed two low-frequency lines in the spectrum of solid chloroform and one such line at 85 cm^{-1} in the case of carbon tetrachloride at about -180°C . Subsequently, the Raman spectra of a large number of aromatic compounds in the frozen state at different low temperatures were studied by several workers (Ray, 1950, 1952; Biswas, 1954, 1955 and others) and some changes in the positions of the low-frequency lines with the change of temperature of the crystals were observed. More recently Sirkar *et al.* (1964) studied the Raman spectra of frozen benzene and carbon disulphide at -209°C and observed slight shifts of some of the low-frequency lines from their positions at -180°C . The lines were attributed to angular oscillations of the molecules in the crystals, the restoring forces being provided by intermolecular hydrogen bond-formation in the case of benzene and to formation of polymeric chains by the molecules in the case of crystals of carbon disulphide. Ito (1964) also studied the spectra of chloromethanes at 77°K . The behaviour of simple molecules of substituted methanes in the solid state at as low a temperature at -209°C was not known and, therefore, it was thought worthwhile to study the Raman spectra of methylene chloride, chloroform and carbon tetrachloride at -209°C in order to find out the nature of intermolecular forces acting in these crystals at such low temperatures.

EXPERIMENTAL

The experimental arrangement used earlier by Sirkar *et al.* (1964) was used in the present investigation also. Liquid nitrogen boiling under reduced pressure was used as the refrigerant to obtain a bath at -209°C . The liquids used were of chemically pure quality and they were redistilled under reduced pressure. Kodak 127 panchromatic films were used to photograph the spectra. In order to detect small changes in the positions of the Raman lines care was taken to photograph the comparison spectrum of iron arc without any lateral shift which could be detected by comparing the relative positions of the 4916A line of mercury and the 4919A line in the iron arc spectrum. The Raman spectra of the substances in the liquid state and in the solid state at -180°C were also photographed with the same spectrograph on other portions of the same roll of film in order to find out whether there was any change in the relative intensities of the lines. In the case of chloroform the Raman spectrum of the crystals at about -120°C was also photographed.

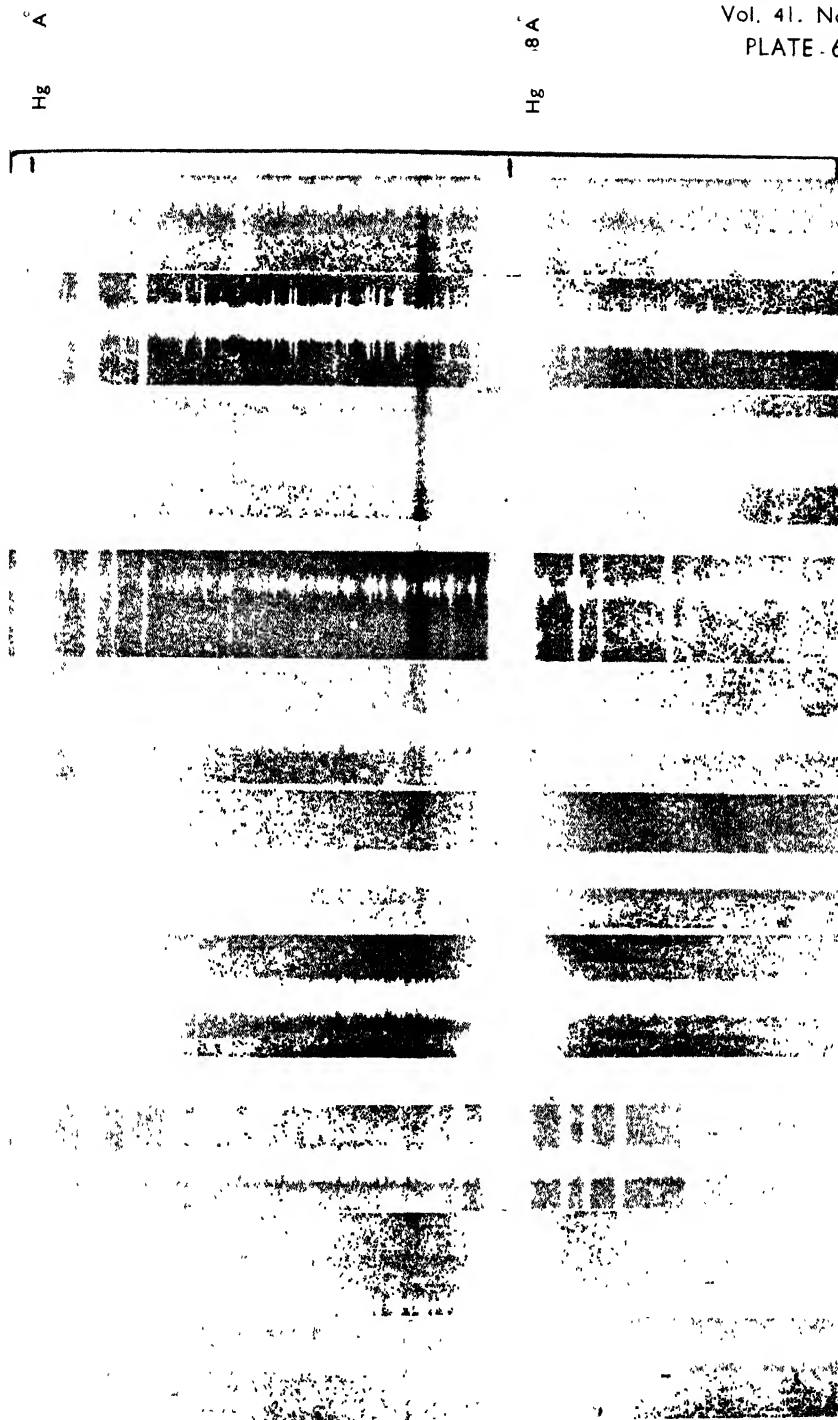
RESULTS AND DISCUSSION

The Raman lines observed are given in Tables I, II and III and some of the spectra are reproduced in Figures 1, 2 and 3, (Plate 6). The results are discussed separately for the three substances in the following sections.

Methylene chloride

The Raman spectrum of this compound at -160°C was studied previously by Mazumder (1949). He observed slight changes in the Raman frequencies. The frequencies 287 and 1158 cm^{-1} were found to increase to 293 and 1164 cm^{-1} respectively while the lines at 706 , 737 , 1424 and 2988 cm^{-1} were found to shift to 702 , 730 , 1413 and 2983 cm^{-1} respectively. Table I shows that at -180°C a new line 94 cm^{-1} is observed and except the line 745 cm^{-1} all the other lines have almost the same frequency-shifts as at -160°C . It appears that with the appearance of the new line at -180°C the line 737 cm^{-1} of the molecule in the liquid state splits up into two lines at 730 and 745 cm^{-1} respectively. When the temperature of the crystals is reduced further to -209°C the line 294 cm^{-1} appears to be broad, but on closer examination it is found to consist of two sharp components at 291 and 296 cm^{-1} respectively. Further, the frequency-shifts 745 and 1165 cm^{-1} increase respectively to 748 and 1168 cm^{-1} while the line 1415 cm^{-1} does not shift any further. Ito (1964) also observed the splitting of the line 737 cm^{-1} in the case of the crystals at 77°K , but the splitting of the line 1158 cm^{-1} observed by him is not confirmed in the present investigation.

The assignment of the lines due to the CH_2Cl_2 molecule was fully discussed by Herzberg (1945). The lines 287 , 706 and 737 cm^{-1} are due respectively to C-Cl deformation and to symmetric and asymmetric C-Cl stretching vibrations.



Raman Spectra

Fig. 1. CH_2Cl_2 at (a) 30°C
(b) -180°C
(c) -209°C

Fig. 2. CHCl_3 at (a) 30°C
(b) -120°C
(c) -180°C
(d) -209°C

Fig. 3. CCl_4 at (a) 30°C
(b) -180°C
(c) -209°C

The slight diminution of the frequencies of the symmetric stretching vibration and increase in the frequencies of both deformation and asymmetric stretching

TABLE I
Methylene chloride
 $\Delta\nu$ in cm^{-1}

Liquid	Solid		
	-160°C (Mazumder, 1949)	-180°C	-209°C
		94 (1b)	94 (1b)
287 (8)	293 (3)	294 (2)	291 (0)
			296 (1)
706 (10)	702 (5)	700 (5)	700 (5)
		730 (0)	735 (0)
737 (2)	730 (0)	745 (1)	748 (1)
1158 (1b)	1164 (1)	1165 (0)	1168 (0)
1420 (3)	1413 (2)	1415 (2)	1415 (2)
2988 (10)	2983 (5)	2983 (5)	2983 (5)
3056 (2)	3058 (2)	3056 (1)	3056 (1)

vibrations indicate that most probably the Cl-C-Cl angle increases a little in the solid state at -180°C . The Raman line 1158 cm^{-1} has been assigned to the torsional oscillation and increase in this frequency with solidification indicates probably the formation of weak Cl...H bond in the solid state. The fact that the frequency further increases to 1168 cm^{-1} at 64°K corroborates this conclusion, because such a bond becomes stronger with the contraction of the crystals at the lower temperature.

As regards the C-H oscillations, the line 1424 cm^{-1} which has been assigned to the deformation oscillation shifts to 1415 cm^{-1} in the spectrum due to the crystals at -180°C and remains almost in the same position upto 64°K . The lines 2988 cm^{-1} and 3056 cm^{-1} due to C-H stretching oscillations do not shift appreciably with the lowering of temperature of the crystals. The change in the latter two frequencies with solidification of the liquid is also negligible. Hence it appears that the H-C-H angle does not change appreciably with the solidification of the liquid. The slight lowering of the frequencies of symmetric deformation and stretching oscillations may be due to slight weakening of the C-H bond. These facts together with the increase in the frequency of torsional oscillation probably indicate that weak intermolecular H...Cl bonds are formed in a direction perpendicular to the H-C-H plane.

The new line 94 cm^{-1} is sharper at -180°C than at -209°C . The line 294 cm^{-1} also splits up into two lines at the lower temperature. These changes may be attributed to the asymmetry of the intermolecular forces in the unit cell at 64°K .

Chloroform

Table II shows that when the liquid is solidified and cooled to about -120°C the line 3019 cm^{-1} due to C-H stretching oscillation shifts to 3008 cm^{-1} and the line 1216 cm^{-1} splits up into two lines at 1208 cm^{-1} and 1224 cm^{-1} and a new line at 95 cm^{-1} appears in the spectrum. The changes in the former two lines can be explained on the assumption that weak intermolecular H...Cl bond is formed in the crystals at this temperature. When the temperature is lowered to -180°C a single line at 1232 cm^{-1} appears in place of the two lines mentioned above, the line 95 cm^{-1} splits up into two lines at 76 cm^{-1} and 97 cm^{-1} respectively

TABLE II

Chloroform

 $\Delta\nu$ in cm^{-1}

Liquid	Solid		
	-120°C	-180°C	-209°C
		76 (1b)	78 (1)
	95 (2b)	97 (1)	98 (1)
261 (10)	261 (2b)	260 (1)	260 (2)
		274 (1)	274 (2)
365 (8)	367 (4)	368 (4)	
			371 (3)
668 (8)	670 (4)	672 (5)	676 (4)
761 (4b)	760 (2b)	752 (2)	752 (2)
		766 (0)	766 (0)
	1208 (0)		
1216 (1)	1224 (0)	1232 (1)	1234 (1)
3019 (3)	3008 (4)	3016 (5)	3014 (5)

and the line 3008 cm^{-1} shifts to 3016 cm^{-1} . This latter spectrum at -180°C was discussed by one of the authors (Sirkar, 1936) long ago. The results of the present investigation, however, show that probably a change of phase of the crystal takes place when the temperature is lowered from -120°C to -180°C , because the frequency 3008 cm^{-1} , instead of diminishing slightly, increases while the two lines 1208 cm^{-1} and 1224 cm^{-1} are replaced by a line of higher frequency-shift at the lower temperature. The line 1204 cm^{-1} observed by Ito (1964) in the case of the crystals at 77°K is not observed in the spectra of the crystals either at -180°C or at -209°C in the present investigation. By studying the infrared spectra of crystals of chloroform at the temperatures 80°K and 150°K , Denariez (1965) also came to such a conclusion. She observed two bands at 1203 cm^{-1} and 1223 cm^{-1} in the spectrum of the crystals at 150°K and almost an unresolved doublet at 1219.7 cm^{-1} and 1222.2 cm^{-1} in the spectrum of the crystals at 80°K . In the Raman spectrum in the latter case the frequency-shift of the single line observed is, however, 1232 cm^{-1} and not 1221 cm^{-1} observed by her as the mean frequency. When the temperature of the crystal is lowered to 64°K no remarkable

change takes place in the spectrum, but small changes take place in some of the frequencies. The lines 672 cm^{-1} , 1232 cm^{-1} and 3016 cm^{-1} shift respectively to 676 cm^{-1} , 1234 cm^{-1} and 3014 cm^{-1} . Changes in the latter two frequencies indicate slight increase in the strength of the intermolecular $\text{H} \cdots \text{Cl}$ bond in the crystal. The frequencies 76 and 97 cm^{-1} also increase respectively to 78 and 98 cm^{-1} at 64°K for the same reason. These two frequencies are to be attributed to angular oscillations of the molecule about the two-fold axes of the tetrahedron to which the structure of the molecule would approximate if the hydrogen atom were assumed to be replaced by a chlorine atom.

Carbon tetrachloride

The Raman spectrum of carbon tetrachloride at -183°C was first investigated by one of the authors (Sirkar, 1936) and it was observed that the frequencies of the molecule do not undergo any change with the change of state and lowering of temperature, but a new line appears at 85 cm^{-1} . The Raman spectrum of this substance at 200°K was studied later by Morino *et al.* (1942) who did not observe any new low-frequency line but observed the line 789 cm^{-1} to be split up into two lines at 780.2 and 792.4 cm^{-1} respectively. Recently, the Raman spectrum of the substance at 77°K has been studied by Ito (1965) using a high resolution spectrograph and he has observed the lines 760 cm^{-1} and 789 cm^{-1} to be split up into four lines at 758.2 , 767.5 , 782.0 and 793.6 cm^{-1} respectively. Although in a note

TABLE III
Carbon tetrachloride
 $\Delta\nu$ in cm^{-1}

Liquid	Solid		
	93°K	77°K (Ito, 1965)	64°K
	88 (1b)		
219 (5)	219 (3)	219.7 (s)	96 (2b)
314 (5)	314 (4)	313.5 (w)	219 (3)
		317.1 (s)	314 (4)
459 (6)	459 (5)	456.7 (m)	459 (5)
		460.2 (vs,sh)	
		463.1 (vs,sh)	
760 (2b)	760 (1,sh)	758.2 (m)	758 (1)
		767.5 (w)	765 (0)
789 (2b)	789 (1,sh)	782.0 (w)	784 (1)
		793.6 (m)	792 (0)

published earlier (Ito, 1964) he reported a new line at 99 cm^{-1} , in the later paper this line was absent. The spectrum of the crystals at 93°K was again photographed besides that at 64°K in order to find out whether the splitting of the lines 760 cm^{-1} and 789 cm^{-1} takes place at these temperatures. A careful comparison of the spectra of the compound in the liquid state and in the solid state

at 93°K and 64°K shows that the width of each of the lines 760 cm^{-1} and 789 cm^{-1} of the liquid is about 12 cm^{-1} , but in the spectrum of the solid at 93°K this width is about 5 cm^{-1} , while at 64°K each of the lines becomes broader and seems to consist of two components touching each other as shown in Table III. The region between 760 cm^{-1} and 789 cm^{-1} in the spectrum due to the crystals at 93°K is a little darker than the general background, but as these two lines are weak the two weaker components observed by Ito (1965) are not observed in the present investigation. It appears that already in the liquid state each of these two lines has an unresolved structure and at 64°K, as the components become sharper, each line appears as a close doublet.

As regards the low-frequency region of the spectrum a broad line at 88 cm^{-1} appears in the spectrum of the crystal at 93°K and the line shifts to 89 cm^{-1} when the temperature is lowered to 64°K. With the spectrograph used in the present investigation the splitting observed by Ito (1965) of the lines 314 cm^{-1} and 459 cm^{-1} could not be observed and the total width of each of these lines in the spectrum was found to be about 5 cm^{-1} .

It appears from the results discussed above that formation of hydrogen bond is mainly responsible for the small changes of the lines of these chlorine substituted methanes in the solid state observed in the present investigation, because in the case of carbon tetrachloride no appreciable change in the vibration frequencies takes place with solidification of the liquid and lowering of temperature upto 64°K.

ACKNOWLEDGMENT

The work was done under a scheme financed by the Council of Scientific and Industrial Research and two of the authors (P.K.B. and S.C.S.) are grateful to the Council for the financial help.

REFERENCES

- Biswas, D. C., 1951, *Indian J. Phys.*, **28**, 423.
 ———, 1955, *Indian J. Phys.*, **29**, 257.
 Denariez, M. Marie, 1965, *J. Chim. Phys.*, **62**, 323.
 Herzberg, G., 1945, *Infrared and Raman Spectra* 318.
 Ito, M., 1964, *Jour. Chem. Phys.*, **40**, 3128.
 ———, 1965, *Spectrochim. Acta.*, **21**, 731.
 Mazumder, N. C., 1949, *Indian J. Phys.*, **23**, 465.
 Morino, Y., Watanabe, I. and Muzushima, S., 1942, *Sci. Pap. Inst. Phys. Chem. Res., Tokyo*, **39**, 348.
 Ray, A. K., 1950, *Indian J. Phys.*, **24**, 111, 1539.
 ———, 1951, *Indian J. Phys.*, **25**, 131.
 Sirkar, S. C., 1936, *Indian J. Phys.*, **10**, 189.
 Sirkar, S. C., Mukherjee, D. K., and Bishui, P. K., 1964, *Indian J. Phys.*, **38**, 181.

STUDY OF INTRA-MOLECULAR MOTION OF HYDROXYL GROUP BY PROTON RESONANCE METHOD

R. C. GUPTA AND V. D. AGRAWAL

DEPARTMENT OF PHYSICS, LUCKNOW UNIVERSITY

(Received December 1, 1966; Resubmitted February 8, 1967)

ABSTRACT. The occurrence of molecular or group rotation in crystalline solids has long been a subject of interest and had been investigated by various workers with their different techniques. In the present paper authors have taken a number of organic solids (Alcohols, Quinols and Naphthols) containing hydroxyl group and most of them have been investigated by one of the authors by proton resonance method from rigid lattice temperature to the melting point. It is found that second moment vs temperature curve yielded a discontinuity in the spectrum (but not yet explained) below the transition temperature i.e., before the molecular rotation. This feature in the curve is found in a large number of organic solids which contain OH group, provided OH group is not hindered by the interaction of other heavy substituent groups. The purpose of the present paper is to show that the discontinuity observed in second moment vs temperature curve or the appearance of secondary humps in nuclear magnitude resonance spectra may be due to the intramolecular motion of the hydroxyl group.

It is found that intramolecular rotation of substituent group causes the reduction in the value of rigid lattice second moment and this reduction can be estimated by the equation.

$$\langle \Delta \omega^2 \rangle_{rot} = \langle \Delta \omega^2 \rangle_{R.L.} \left[\frac{3 \cos^2 \gamma_{jk} - 1}{2} \right]^2$$

It is shown that reduction in the value of second moment is due to the production of the secondary field at the resonant nucleus. The measurement of spin-lattice relaxation times T_1 carried out at different temperature, demonstrate rotational degree of freedom. From the T_1 measurements the free energy of activation (ΔF_R^*) and enthalpy of activation (ΔH^*) have also been estimated to give support to intra-molecular motion of substituent hydroxyl groups.

INTRODUCTION

Proton magnetic studies of organic solids (Alcohols, Quinols and Naphthols) have been investigated in order to gain information concerning the intra-molecular motion of hydroxyl groups and also about the nature of the motion.

According to simple theory of N.M.R. when an external magnetic field is applied on the sample, it induces a change on a magnetic moment associated with each electron and this change which depends on electronic wave function, is in such a way that it opposes the applied field. The secondary field at any point is also contributed by neighbouring magnetic moment. Therefore, the production of secondary field causes the resonance absorption line to be broadened.

This effect on magnetic resonance absorption line has been interpreted in terms of second moment by Van Vleck (1948). Studies of temperature dependence of second moment (Kambe and Usui (1952), Pryce and Stevens (1950) and by McMillan and Opechowski (1960) show that the conclusion of Van Vleck's work are valid at all temperatures not only very near to absolute Zero. So any effect on nuclear magnetic resonance absorption spectrum can be studied by Van Vleck's theory of second moment. Clough (1963) has also indicated that any motion of an assembly of dipolar coupled nuclei has a profound effect on nuclear magnetic resonance spectrum and so also on second moment.

Authors have observed that some organic solids containing hydroxyl group show a remarkable effect on the value of second moment and on resonance spectra with rise of temperature producing secondary humps below the transition temperature. It suggests some sort of motion in the molecule (Andrew, 1950). Since it is evident that molecule itself is not in the motion, hence possibility of intramolecular motion of the substituent group within the molecule cannot be ignored. The authors have interpreted the above abnormalities obtained in the values of second moments, in second moment vs temperatures curve of Alcohols, Quinols, and Naphthols, as due to the motion of hydroxyl group, within the molecule.

The intramolecular motion within solids has been also explained with the use of spin-lattice relaxation time T_1 . With T_1 , the free energy of activation ΔE_R^* and enthalpy of activation ΔH^* have been also estimated in support of intramolecular motion.

THEORY

The motion in molecules or groups in general results from electronic interactions within the sample and from interactions between the externally applied magnetic field and the electrons in the sample (Heinert *et al.* 1959) when an external magnetic field is applied on a sample, each induced electronic magnetic dipole then gives rise to a secondary magnetic field at a nucleus in the direction of the externally applied field and is given by

$$H(\text{secondary}) = \langle \Delta\mu \rangle (1 - 3\cos^2\theta_{jk})/r_{jk}^3$$

where $\langle \Delta\mu \rangle$ is the average value of the induced moment, r_{jk} is the length of the vector joining nuclei j and k and θ_{jk} is the angle between vector and applied field axis.

The secondary field is a function of electron distribution in the free volume and of the distance of approach of neighbouring molecules. It is a time varying field and since the time average over all permitted orientations of dipole pair can be less than the steady local field for rigid system. Hence spectrum narrows when rotation sets in.

Alpert (1947, 1949) and Gutowsky and Pake (1950) studied the effect of motion in the lattice using results which were first obtained by Bloembergen *et al.* (1948). Again it has been pointed out by Andrew (1955) that any reduction in the value of second moment with rise of temperature is indicative of some sort of motion in the molecule [either rotational motion as in the case of Benzene (Andrew 1953b) or vibrational motion as in the case Naphthalene (Andrew, 1950)]. The reorientation of solids are recognised by discontinuity observed or by transition curve in second moment vs temperature curve. Hence if any discontinuity is observed, as found but not yet explained, in second moment vs temperature curve ($S-T$ curve) before the molecular rotation or below the transition temperature, it clearly suggests that any sort of intramolecular motion due to the substituent group may be present within the molecule. If such discontinuity in $S-T$ curve is not observed in substituted molecules, it indicates that motion of the concerning substituent group is hindered due to the interactions by other heavy substituent groups present within the molecule.

The effect of the groups or molecular rotation on second moment can be easily estimated. Since the secondary field is a time varying field, hence when the motion in the molecule sets in, the angle θ_{jk} (between applied field and internuclear vector) occurring in the factor $(1-3 \cos^2 \theta_{jk})$ in the second moment theory of Van Vleck, varies with the time. Since the frequency of rotation are high compared with the frequencies of interest in the resonance, it is time average of $(1-3 \cos^2 \theta_{jk})$ that effect the second moment.

$$\text{Hence } \langle (1-3 \cos^2 \theta_{jk}) \rangle_{\text{avg}} = (1-3 \cos^2 \theta^1) \cdot \frac{(3 \cos^2 \gamma_{jk} - 1)}{2}$$

Where γ_{jk} is the angle between radius vector joining j and k and rotation axis. The expression has been solved by Slichter (1963). He found a relation between the second moment at rigid lattice and the rotational second moment and is given by

$$\langle \Delta \omega^2 \rangle_{\text{rot}} = \langle \Delta \omega^2 \rangle_{\text{R.L.}} \left(\frac{3 \cos^2 \gamma_{jk} - 1}{2} \right)^2 \quad \dots (1)$$

where $\langle \Delta \omega^2 \rangle_{\text{rot}}$ is rotational second moment and $\langle \Delta \omega^2 \rangle_{\text{R.L.}}$ is second moment at rigid lattice.

The substituent groups are, however, constrained to their equilibrium position by intramolecular and intermolecular forces. Its motion from one equilibrium position to another is restricted by a potential barrier. The motion may also take place by quantum mechanical tunnelling through the hindering potential barrier. But it is suggested by Newman (1950a) that the process of mechanical tunnelling does not hold good for most of the solid studies.

In the present paper the relaxation phenomenon for the motion of groups in solid molecules have also been discussed. Here only phenomenological description has been taken without adding the details of other theories as transition state

theory (Glasstone *et al.* (1940)) and concept of free volume. If a system transforms an initial state S_1 to a final state S_2 via an activated state S^* ($S_1 \rightleftharpoons S^* \rightleftharpoons S_2$), it requires that the population of S^* should be small compared to S_1 and S_2 where S_1 and S_2 represent orientation of the substituent group in the lattice. This is a restriction which is probably satisfied for molecular motions in solids (Rice, 1958).

The correlation time τ_c for the motion can be written in terms of free activation energy ΔE_R^* which is defined as the difference in the free energy between state S_1 and S^* ;

$$\tau_c = \tau_0 \exp \left(-\frac{\Delta E_R^*}{RT} \right)$$

The N. M. R theory developed by B.P.P. which shows a relation between spin lattice relaxation time T_1 and correlation time as

$$T_1 = C \tau_c \text{ for } \omega_0 \tau_c \ll 1$$

Where C is a constant factor and $\omega_0 = 2\pi\nu_0$ where ν_0 is the resonant frequency. The enthalpy of activation ΔH^* can be obtained from the temperature variation of $\text{Log } T_1$ and given by

$$\Delta H^* = \pm (2.303)R \left(\frac{\partial \text{Log } T_1}{\partial (1/T)} \right) \quad \dots (2)$$

where R is the gas constant.

Wilson (1959) has pointed out that the theory of intramolecular rotation in molecules is still unable to account quantitatively for the factor constraining rotation, notably steric effect and properties of electronic structure. Molecular rotation by entire molecule is undoubtedly governed by the same factor, but the theory is even less understood than the theory of intramolecular rotation. There is only fragmentary information to compare the barriers to groups rotation in solids and intramolecular factors contribute strongly to these barriers. The intra-molecular restraints are determined by covalent bonding of molecules and by steric hindrances.

RESULTS AND DISCUSSIONS

Alcohols :

The second moment vs temperature curve for *Pentaerythritol* obtained by Gupta (1963) has been shown in fig. (1). For the determination of second moment for pentaerythritol he has assumed that the positions of hydroxy hydrogens agree with Hvoslef (1958) model and lie exactly in the planes defined by oxygen atoms. The direction of OH bond however deviates by 6° thus making the C-O-H angle about 110° . This feature is very important in determining the position and movement of hydroxy atoms. The portion AB shown in fig. (1) represents the second moment at rigid lattice temperature. After crossing the rigid lattice state an

anomalous shoulder CD has been observed before the transition temperature for OH group rotation and correspondingly there is an appearance of secondary

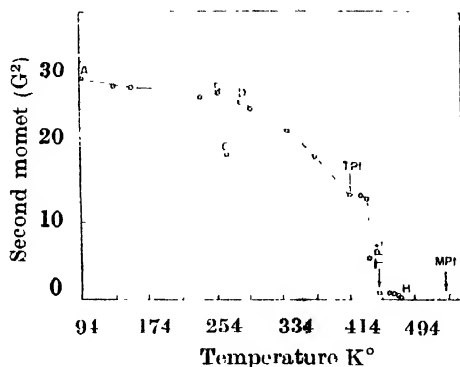


Fig. 1. Second moment versus Temperature curve for pentaerythritol.

hump at room temperature in resonance spectra shown in fig. (2). The possibility of the motion of hydroxy hydrogen has been also indicated by Ellis and Bath (1939) by their infrared studies, Nayer (1938) by his Raman studies and Hvorslef (1958) by his neutron diffraction studies.

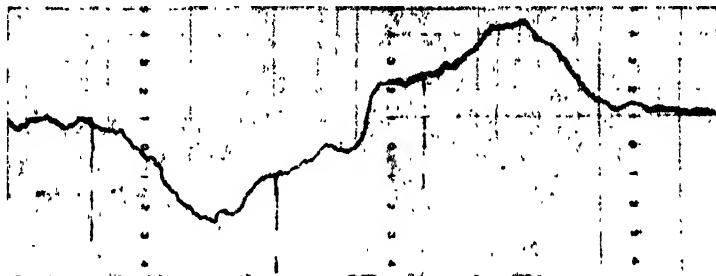


Fig. 2. N.M.R. Spectrum at room temperature showing secondary hump in pentaerythritol.

Eastermann (1929) has observed the dipolement in pentaerythritol and since it is a molecule of the space group ($1\bar{1}$) which cannot have the dipole-moment. Therefore, this dipolemoment is probably due to the intramolecular motion within the solid. Furthermore Sidgwick (1933) and Gilbert and Lansdale (1956) have also observed some sort of intramolecular motion in pentaerythritol molecule.

In pentaerythritol molecule the second moment reduces to 11.8 gauss² from its rigid lattice value 28.0 gauss². If it is assumed that hydroxyl group is rotating about C-O axis then γ_{jk} the angle of radius vector joining nuclei j and k with the rotation axis, is about 110°. Therefore, according to the equation (1), the value of the second moment should be approximately about 1/2 times of rigid lattice value. In present case the value is reduced from 28.0 gauss² to 11.8 gauss², approximately the same as required by the theory. The free activation energy ΔE_R^* for the group rotation and enthalpy of activation have been also calculated and given in Table (1).

Similar is the case with *methyl alcohol* containing C-O bond as internal rotation axis for hydroxyl group as observed by number of investigators by their Raman and Infrared spectroscopy. N.M.R. study of methyl alcohol (Gutowsky and Pake 1950, and Cook and Drain 1952), also gives approximately similar feature of the resonance spectra as is observed in the case of pentaerythritol. The spectra can be explained on the same lines as authors have discussed for pentaerythritol. Furthermore Muzushima and Kubo (1951) also agree with the present view and estimated the height of the potential barrier arguing that if the over all rotation of the molecule is small as compared with the internal rotation, the barrier height can be estimated from dispersion phenomenon by the use of the absolute reaction theory. He obtained the potential barrier to internal rotation of methyl alcohol from the difference between third law of entropy and molecular entropy.

Such a method has been adopted by Pitzer (1948), Crawford (1940) and Halford (1950). They obtained the potential barrier, for the rotation of the hydroxyl group about C-O axis, approximately about 1000 cal.

In *ethyl alcohol* the motion of the hydroxyl group has been discussed with the experimental thermodynamics quantities by Halford (1949, 1950) and Ito (1952). Gutowsky and Pake (1950) investigated ethylalcohol with N.M.R. method and their results, according to present theory, also give some indication about the motion of the hydroxyl group about C-O bond. The recent work of Barrow (1952) shows that barrier hindering the internal rotation of OH group about C-O axis is about 1000 cal.

Andrew (1950) has investigated *Lauryl alcohol* ($n\text{-C}_{10}\text{H}_{25}\text{OH}$) by proton resonance method and obtained the same discontinuity in ($S-T$) curve before the transition temperature (shown in fig. 3). But the discontinuity observed in spectrum has not been explained by Andrew. This also may be due to the motion of the hydroxyl group about C-O axis present in Lauryl alcohol. The second moment

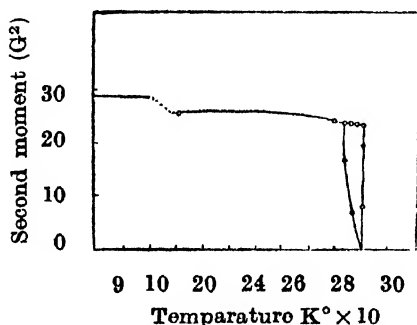


Fig. 3. Second moment versus temperature curve for Lauryl alcohol.

at rigid lattice temperature is found to be 27.77 gauss^2 . The rotational second moment is found to be 16.0 gauss^2 .

Quinols (Hydroquinones)

The ($S-T$) curve for the α -Hydroquinone obtained by Gupta (1963) has been shown in the fig. (4). In which the portion AB represents the second moment at rigid lattice temperature where all the effective motion has been frozen. A discontinuity (C) in the absorption curve has been observed at temperature 325°K . This discontinuity is also observed by Ueberitr *et al.* (1950) in their thermal studies.

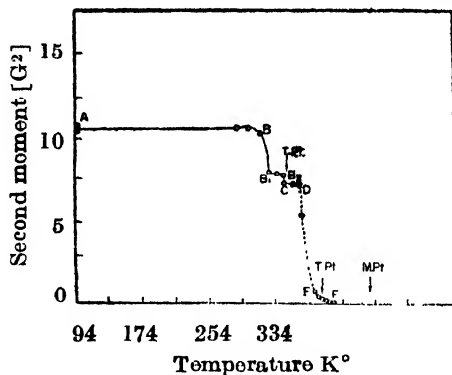


Fig. 4. Second moment versus temperature curve for α -Hydroquinone.

The interpretation of group rotation also receives support from Hidalgo (1950) who found a vibrational frequency shift of OH group in Hydroquinone approximately at about the same temperature. Furthermore high d.c. conductivity has been reported by various workers with other hydrogen bonded structure and is attributed as due to the combined proton transition and dipole rotation (Stein and Eyring, 1937).

The value of second moment of α -Hydroquinone at rigid lattice temperature is found to be about 10.7 gauss^2 and before the transition temperature for molecular rotation it reduces almost exactly one quarter of the intramolecular contribution, which satisfies the necessary criterion for rotation (Cutowsky and Pake, 1950).

In γ -Hydroquinone (Gupta 1963) the same discontinuity is found in $S-T$ curve (fig. 5). The view of group rotation receives support from Hidalgo (1960)

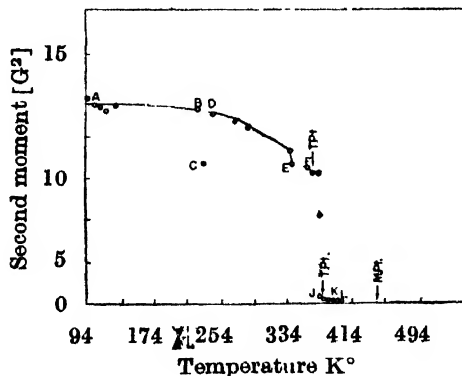


Fig. 5a. Second moment versus temperature curve for γ -Hydroquinone.

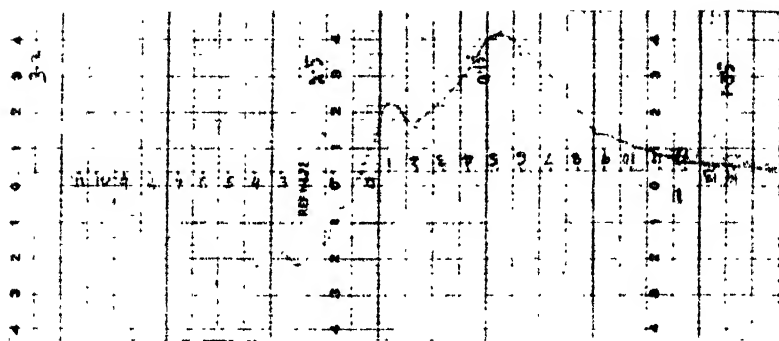


Fig. 5b. N.M.R. spectrum at 285°K showing secondary hump in γ -Hydroquinone.

who observed a vibrational frequency shift of hydroxyl group is Hydroquinone. The second moment at rigid lattice temperature is found to be about 12.0 gauss² when intramolecular motion sets in, it reduces to about 1/2 times of rigid lattice value as required by theory for rotation about C-O axis.

The spin lattice relaxation time (T_1) for α and γ -Hydroquinones have also been calculated (Gupta and Agarwal, 1967). With T_1 the value of the free activation energy ΔE_R^* and enthalpy of activation ΔH^* are estimated and given in Table I.

TABLE I

Free activation energy and enthalpy of activation (in K cal/mole)

Compounds	Free activation energy ΔE_R^*	Enthalpy of activation ΔH^*
1. Pentaerythritol	5.27	1.43
2. α Hydroquinone	3.03	3.37
3. γ -Hydroquinone	1.86	1.87
4. α -Naphthol	0.51	7.2
5. β -Naphthol	5.9	13.2

Naphthols

In α -Naphthol [Gupta, 1967, fig.6] there is some appearance of fine structure at about 312°K. Gupta has attributed this fine structure as due to the vibrational motion of the molecule, arguing that the Naphthol molecule is comparatively large and possesses no symmetry about C-O bond. But it has been pointed out by Andrew (1951) for some organic solids that there is however a decrease in the second moment below the transition temperature. He attributed that this

decrease will be partly due to the rotational oscillation of molecules, but calculation shows that this form of motion is unlikely to account for whole effect.

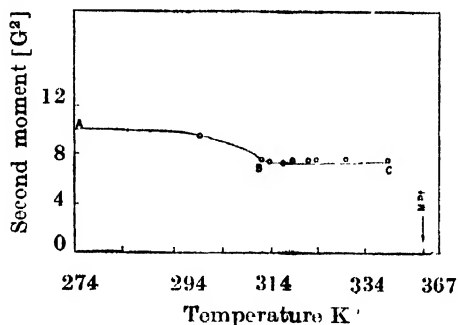


Fig. 6. Second moment versus temperature curve for α -Naphthol.

Andrew stated that it is more likely that the small portion of molecule rotating below the transition point. Therefore, according to the authors views this sort of reduction is due to the motion of hydroxyl group. It gets added support with Nagakura and Gouterman (1957) investigations in which they observed some shift in wave length due to the hydrogen bonding in α -Naphthol. Further more Aihra (1960), with the use of his sublimation pressure method, observed a transition in the crystalline state of α -Naphthol due to some sort of rotation about C-O bond. The rotational second moment is also found to be about 1/2 times of rigid lattice value supporting the theory.

In case of β -Naphthol (fig. 7), there appeared a secondary hump in resonance spectrum round about 312°K and some reduction in the value of the second moment in $S-T$ curve. Gupta has attributed this as due to the vibrational motion of the entire molecule. The secondary hump is nearly at the same temperature at which Aihra (1960) observed a transition in the crystalline state due to some sort of rotation about C-O bond. Further more it has been pointed out by Porte *et al.* (1960) for β -Naphthol that OH group forms weak hydrogen bonding with an aromatic nucleus in which the OH bond is directly along the normal to the center

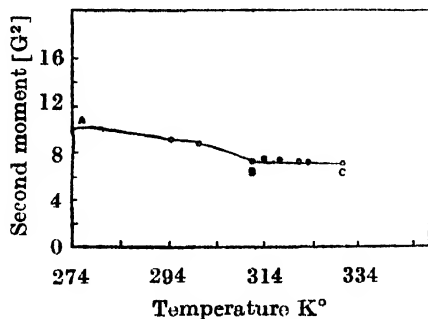


Fig. 7. Second moment versus temperature curve for β -Naphthol.

of aromatic nucleus i.e. there is a tendency for benzene molecule to pack round OH group so that OH bond points along this normal rather than to the side of the

ring. When an external field is applied the current induced in electron system in benzene exerts a secondary field of OH protons and this secondary field opposes the applied field. The result is a shifted proton resonance for OH group in β -Naphthol. Therefore Porte's investigations also suggest about the intramolecular motion of OH group about C-O bond. The value of the rotational second moment is about 1/2 times of the rigid lattice value.

The spin-lattice relaxation times (T_1) for α and β -Naphthols have also been estimated by Agrawal and Gupta (1967) and with which the free activation energy ΔE_R^* and enthalpy of activation have been computed and given in Table 1.

ACKNOWLEDGMENTS

The authors are very grateful to Prof. P. N. Sharma, D.Sc., Head of the Department, for his interest and generous help throughout the work. One of the authors (V.D.A.) is also thankful to Ministry of Education, India, for awarding research training scholarship.

REFERENCES

- Agrawal, V. D. and Gupta, R. C., 1967, *Indian Jr. of pure and applied physics*, **5**, 146.
 Ailira, A., 1960, *Bull. Chem. Soc. Japan*, **33**, 194.
 Alpert, N. L., 1947, *Phys. Rev.*, **72**, 637.
 Andrew, E. R., 1950, *J. Chem. Phys.*, **18**, 607.
 Andrew, E. R. and Eades, R. G., 1953b, *Proc. Roy. Soc., A*, 216.
 Andrew, E. R., 1955, *Nuclear Magnetic resonance*, Cambridge University Press.
 — —, 1951, *Physica*, **17**, 405.
 — —, 1949, *Phys. Rev.*, **75**, 398.
 Barrow, G. M., 1952, *J. Chem. Phys.*, **20**, 1739.
 Bloembergen, N., et al., 1948, *Phys. Rev.*, **73**, 679.
 Clough, S., 1963, *Proc. Physical Soc.*, **81**, 863.
 Crawford, B. L., 1940, *J. Chem. Phys.*, **8**, 744.
 Crook, A. H. and Drain, L. E., 1952, *J. Chem. Phys.*, **20**, 383.
 Easternman, J., 1929, *Z. Physik. Chem.*, **B2**, 287.
 Ellis, J. W. and Batn, J., 1939, *J. Chem. Phys.*, **7**, 862.
 Glasstone, K. J., 1940, *The theory of rate process*, McGraw Hill Book Company, Inc., New York.
 Gilbert, R. E. and Lonsdale, K., 1956, *Acta Crystallo*, **9**, 697.
 Gupta, R. C., 1963, *Ph.D. thesis*, University College of North Wales, Bangor, U.K.
 — — — —, 1967, *Physical Society of Japan*, **23**, 140.
 Gupta, R. C. and Agrawal, V. D., 1967, *Indian J. Phys.*, **41**, 241.
 Gutowsky, H. S. and Pake, G. E., 1950, *J. Chem. Phys.*, **18**, 162.
 Halford, J. W., 1949, *J. Chem. Phys.*, **17**, 111.
 — — — —, 1950, *J. Chem. Phys.*, **18**, 361.
 Heinert, D., et al., 1959, *J. Amer. Chem. Soc.*, **81**, 3933.
 Hidalgo, A., 1960, *Spectrochemica, Acta.*, **16**, 528.
 Hvoslof, J., 1958, *Acta crystallo*, **11**, 383.
 Ito, K., 1952, *J. Chem. Phys.*, **20**, 531.
 Kambo, K. and Usui, T., 1952, *Progr. Theor. Phys.*, **8**, 302.

- McMillan, M. and Opechowski, W., 1960, *Canad. J. Phys.*, **38**, 1168.
Muzushima, S. and Kubo, M., 1941, *J. Chem. Soc. Japan*, **62**, 502.
Nagakura, S. and Guterman, M., 1957, *J. Chem. Phys.*, **26**, 881.
Nayer, P. G. M., 1938, *Proc. Indian Acad. Sci.*, **7A**, 251.
Newman, R., 1950a, *J. Chem. Phys.*, **18**, 669.
Pitzer, K. S., 1948, *J. Amer. Chem. Soc.*, **70**, 2140.
Porte, A. L., *et al.*, 1960, *J. Amer. Chem. Soc.*, **82**, 5057.
Pryce, M. H. L. and Stevens, K. H. W. (1950), *Proc. of Physical Soc.*, **A63**, 36.
Rico, S. A., 1958, *Phys. Rev.*, **12**, 804.
Sidwick, N. V., 1933, *Covalent Link in Chemistry*, 187.
Slichter, C. P., 1953, *Principles of Magnetic resonance*, Harper & Row, New York, 62.
Stearn, A. E. and Eyring, H., 1937, *J. Chem. Phys.*, **5**, 113.
Ueberiter, K., 1950, *Z. Nature forschg.*, **56**, 101.
Van Vleck, J. H., 1948, *Phys. Rev.*, **74**, 1168.
Wilson, E. B., 1959, *Jr. Advance, Chemical Physics*, **2**, 367.

A NOTE ON INDUCED 4-DIMENSIONAL LORENTZ TRANSFORMATION

N. N. GHOSH

INDIAN ASSOCIATION FOR THE CULTIVATION OF SCIENCE, JADAVPUR, CALCUTTA-32

(Received November 19, 1966)

ABSTRACT. In the present note a set of six typical transformation schemes has been so framed that each of them leads to a representation of the 4-dimensional Lorentz transformation both proper and improper. It is shown that corresponding to a particular transformation there exists a mixed tensor of 2nd rank, which while undergoing the transformation can induce a 4-dimensional Lorentz transformation to a 4-vector associated with it yielding the connecting relations between the respective transformation coefficients. Further, under each of these transformation schemes one can set up a system of Dirac equations and construct an electromagnetic tensor whence the set of Maxwell's Equations can be formulated.

In an R_4 characterized by a set of general reversible transformation equations from coordinates x^r to x'^r with 16 covariant transformation coefficients $\partial x^r / \partial x'^p$ one can define the 6 special transformation schemes by making suitable use of the following six elementary anti-symmetric covariant tensors

$$\begin{aligned} C_{pq} & \text{ with non-vanishing components } C_{01} = C'_{23} = 1, C'_{10} = C_{32} = -1, \\ D_{pq} & \quad \quad \quad \quad \quad \quad \quad C_{02} = C_{13} = 1, C_{20} = C_{31} = -1, \quad \dots \quad (1.1) \\ E_{pq} & \quad \quad \quad \quad \quad \quad \quad C_{03} = C_{12} = 1, C_{30} = C_{21} = -1, \end{aligned}$$

and their conjugates

$$\begin{aligned} \bar{C}_{pq} & \text{ with nonvanishing components } \bar{C}_{01} = \bar{C}_{32} = -1, \bar{C}_{10} = \bar{C}_{23} = 1, \\ \bar{D}_{pq} & \quad \quad \quad \quad \quad \quad \quad \bar{C}_{02} = \bar{C}_{31} = -1, \bar{C}_{20} = \bar{C}_{13} = 1, \quad \dots \quad (1.2) \\ \bar{E}_{pq} & \quad \quad \quad \quad \quad \quad \quad \bar{C}_{03} = \bar{C}_{21} = -1, \bar{C}_{30} = \bar{C}_{12} = 1. \end{aligned}$$

To denote the contravariant tensor associated to each of the above we write the indices as superscripts.

Let us consider the first one which we call the $(C-\bar{D})$ transformation under which we postulate that C_{pq} , the primary tensor, remains invariant and \bar{D}_{pq} the secondary, goes over into $\lambda \bar{D}_{pq}$, where $\lambda = \pm 1$. The conditions which the

transformation coefficients $\partial x'/\partial x'^p$ denoted by (r_p) , must satisfy are obtained as follows :

$$\begin{bmatrix} \binom{1}{1} - \binom{0}{1} & \binom{3}{1} - \binom{2}{1} \\ -\binom{1}{0} & \binom{0}{0} - \binom{3}{0} & \binom{2}{0} \\ \binom{1}{3} - \binom{0}{3} & \binom{3}{3} - \binom{2}{3} \\ -\binom{1}{2} & \binom{0}{2} - \binom{3}{2} & \binom{2}{2} \end{bmatrix} \begin{bmatrix} \binom{0}{0} & \binom{0}{1} & \binom{0}{2} & \binom{0}{3} \\ \binom{1}{0} & \binom{1}{1} & \binom{1}{2} & \binom{1}{3} \\ \binom{2}{0} & \binom{2}{1} & \binom{2}{2} & \binom{2}{3} \\ \binom{3}{0} & \binom{3}{1} & \binom{3}{2} & \binom{3}{3} \end{bmatrix} = \begin{bmatrix} 1 & 0 & 0 & 0 \\ 0 & 1 & 0 & 0 \\ 0 & 0 & 1 & 0 \\ 0 & 0 & 0 & 1 \end{bmatrix} \quad (1.3)$$

$$\begin{bmatrix} \binom{2}{2} - \binom{3}{2} & \binom{0}{2} & \binom{1}{2} \\ -\binom{2}{3} & \binom{3}{3} & \binom{0}{3} - \binom{1}{3} \\ -\binom{2}{0} & \binom{3}{0} & \binom{0}{0} - \binom{1}{0} \\ \binom{2}{1} - \binom{3}{1} - \binom{0}{1} & \binom{1}{1} \end{bmatrix} \begin{bmatrix} \binom{0}{0} & \binom{0}{1} & \binom{0}{2} & \binom{0}{3} \\ \binom{1}{0} & \binom{1}{1} & \binom{1}{2} & \binom{1}{3} \\ \binom{2}{0} & \binom{2}{1} & \binom{2}{2} & \binom{2}{3} \\ \binom{3}{0} & \binom{3}{1} & \binom{3}{2} & \binom{3}{3} \end{bmatrix} = \begin{bmatrix} \lambda & 0 & 0 & 0 \\ 0 & \lambda & 0 & 0 \\ 0 & 0 & \lambda & 0 \\ 0 & 0 & 0 & \lambda \end{bmatrix}$$

The above are equivalent to the conditions

$$\begin{aligned} \binom{1}{1} &= \lambda \binom{2}{2}, \quad \binom{0}{1} = \lambda \binom{3}{2}, \\ \binom{1}{0} &= \lambda \binom{2}{3}, \quad \binom{0}{0} = \lambda \binom{3}{3} \\ \binom{1}{3} &= -\lambda \binom{2}{0} \quad \binom{0}{3} = -\lambda \binom{3}{0} \\ \binom{1}{2} &= -\lambda \binom{2}{1} \quad \binom{0}{2} = -\lambda \binom{3}{1} \\ \binom{01}{01} + \binom{23}{01} &= 1, \quad \binom{01}{02} + \binom{23}{02} = 0, \end{aligned} \quad \dots \quad (1.4)$$

where the symbol $\binom{p \ q}{r \ s}$ denotes $\binom{p}{r} \binom{q}{s} - \binom{p}{s} \binom{q}{r}$.

Elsewhere (Ghosh, 1965) this special $(C-\bar{D})$ transformation has been termed 'Unimodular tensor transformation' and has been discussed at length giving the

representation of an 'induced' 4-dimensional Lorentz transformation and the derivation of the corresponding Dirac equations.

Here, we shall construct the electromagnetic mixed tensor of the second rank in the $(C-\bar{D})$ field. Referring to formulae (6.2, 3, 4) of the earlier paper (Ghosh, 1965) we notice that if there exists a mixed tensor F_q^p in the $(C-\bar{D})$ field satisfying the structural relations

$$\begin{aligned} F_0^0 &= -F_1^1 = -F_2^2 = F_3^3, \\ F_2^1 &= F_0^3 = -F_1^2 = -F_3^0, \\ F_2^0 &= -F_1^3, \quad F_0^2 = -F_3^1, \\ F_1^0 &= F_2^3, \quad F_0^1 = F_3^2, \end{aligned} \quad \dots \quad (1.5)$$

with the 6 mutually independent components $F_0^0, F_2^1, F_2^0, F_0^2, F_1^0, F_0^1$ then we can correlate an antisymmetric tensor E_k^l by means of the equation

$$E_k^l = \frac{1}{4} T_{kp}^r [T_r^{lm} F_m^p - T_m^{lp} F_r^m], \quad (k, l = 0, 1, 2, 3) \quad \dots \quad (1.6)$$

where T 's are the connecting tensors characteristic for the $(C-\bar{D})$ transformation. It is easy to see that F_q^p taken in the bilinear form $A^p B_q + B^p A_q$ satisfying the structural relation

$$F_q^p C^q C_p = -F_s^s, \quad \dots \quad (1.7)$$

supplemented by the conditions $F_0^0 = -F_2^2, F_2^1 = -F_1^2, F_1^0 = F_2^3, F_0^1 = F_3^2$, is the desired mixed tensor in the $(C-\bar{D})$ field.

We shall next consider the $(C-E)$ transformation scheme under which the tensor C_{pq} remains invariant and the tensor E_{pq} goes over into λE_{pq} where $\lambda = \pm 1$. The conditions which the transformation coefficients $\begin{pmatrix} r \\ p \end{pmatrix}$ must satisfy are then given as

$$\begin{aligned} \begin{pmatrix} 1 \\ 1 \end{pmatrix} &= \lambda \begin{pmatrix} 3 \\ 3 \end{pmatrix}, & \begin{pmatrix} 0 \\ 1 \end{pmatrix} &= -\lambda \begin{pmatrix} 2 \\ 3 \end{pmatrix}, \\ \begin{pmatrix} 1 \\ 0 \end{pmatrix} &= -\lambda \begin{pmatrix} 3 \\ 2 \end{pmatrix}, & \begin{pmatrix} 0 \\ 0 \end{pmatrix} &= \lambda \begin{pmatrix} 2 \\ 2 \end{pmatrix}, \\ \begin{pmatrix} 1 \\ 3 \end{pmatrix} &= -\lambda \begin{pmatrix} 3 \\ 1 \end{pmatrix}, & \begin{pmatrix} 0 \\ 3 \end{pmatrix} &= \lambda \begin{pmatrix} 2 \\ 1 \end{pmatrix}, \\ \begin{pmatrix} 1 \\ 2 \end{pmatrix} &= \lambda \begin{pmatrix} 3 \\ 0 \end{pmatrix}, & \begin{pmatrix} 0 \\ 2 \end{pmatrix} &= -\lambda \begin{pmatrix} 2 \\ 0 \end{pmatrix}, \\ \begin{pmatrix} 01 \\ 01 \end{pmatrix} + \begin{pmatrix} 23 \\ 01 \end{pmatrix} &= 1, & \begin{pmatrix} 01 \\ 03 \end{pmatrix} + \begin{pmatrix} 23 \\ 03 \end{pmatrix} &= 0. \end{aligned} \quad \dots \quad (2.1)$$

It may be noted here that the contravariant and covariant transformation coefficients are related as in $(C-\bar{D})$ transformation and the rule of raising and lowering

of indices remain unchanged. Consider now the mixed tensor M_r^p expressed in the bilinear form $A_p B^r - B_p A^r$ satisfying the structural relation

$$M_r^p C^{rq} C_{ps} = M_s^q \quad \dots (2.2)$$

with 4 mutually independent components defined in terms of 4 quantities h_k by means of the equations

$$\begin{aligned} M_0^0 &= M_1^1 = -M_2^2 = -M_3^3 = -h_2, \\ M_2^0 &= M_1^3 = M_0^2 = M_3^1 = h_1, \\ M_2^1 &= -M_0^3 = h_0 + h_3, \quad M_1^2 = -M_3^0 = -h_0 + h_3, \\ M_1^0 &= M_0^1 = M_3^2 = M_2^3 = 0. \end{aligned} \quad \dots (2.3)$$

Introducing a set of connecting tensors $T_q^k p (k = 0, 1, 2, 3)$ defined by the nonvanishing components

$$\begin{aligned} T^{00}_0 &= 1, \quad T^{01}_2 = 1, \quad T^{02}_1 = -1, \quad T^{03}_0 = -1, \\ T^{10}_2 &= 1, \quad T^{11}_3 = 1, \quad T^{12}_0 = 1, \quad T^{13}_1 = 1, \\ T^{20}_0 &= -1, \quad T^{21}_1 = -1, \quad T^{22}_2 = 1, \quad T^{23}_3 = 1, \\ T^{30}_3 &= -1, \quad T^{31}_2 = 1, \quad T^{32}_1 = 1, \quad T^{33}_0 = -1, \end{aligned} \quad \dots (2.4)$$

the above can be expressed as

$$M_r^p = T_r^k p h_k \quad (k = 0, 1, 2, 3) \quad \dots (2.5)$$

which being inverted gives

$$h_k = \frac{1}{4} T_{kp}^r M^p_r, \quad \dots (2.6)$$

where

$$T^r_{kp} = g_{kl} T_p^{lr}.$$

g_{kl} denoting the tensor with non vanishing components

$$g_{00} = -1, \quad g_{11} = g_{22} = g_{33} = 1.$$

The set of 4 connecting tensors (2.4) is characteristic for the $(C-E)$ transformation. These in conjunction with the mixed tensor (2.3) lead to the representation of Lorentz transformation and to the derivation of Dirac equation. Under $(C-E)$ transformation scheme one can verify that the tensor F_q^p taken in the linear form $A^p B_q + B^p A_q$ supplemented by the conditions $F_0^1 = -F_2^3, F_1^0 = -F_3^2, F_0^2 = F_2^0, F_2^1 = -F_0^3, F_1^3 = F_3^1, F_3^0 = -F_1^2$, having 6 mutually independent components $F_0^0, F_2^0, F_2^1, F_1^3, F_1^0, F_0^1$ serves as electromagnetic tensor.

With D_{pq} as primary tensor we next consider the $(D-\bar{C})$ transformation scheme under which D_{pq} remains invariant and \bar{C}_{pq} goes over into $\lambda \bar{C}_{pq}$ where

$\lambda = \pm 1$. The conditions which the transformation coefficients (p^r) must satisfy are then given by

$$\begin{aligned} \begin{pmatrix} 2 \\ 2 \end{pmatrix} &= \lambda \begin{pmatrix} 1 \\ 1 \end{pmatrix}, & \begin{pmatrix} 3 \\ 2 \end{pmatrix} &= -\lambda \begin{pmatrix} 0 \\ 1 \end{pmatrix}, \\ \begin{pmatrix} 2 \\ 3 \end{pmatrix} &= -\lambda \begin{pmatrix} 1 \\ 0 \end{pmatrix}, & \begin{pmatrix} 3 \\ 3 \end{pmatrix} &= \lambda \begin{pmatrix} 0 \\ 0 \end{pmatrix}, \end{aligned} \quad (3.1)$$

$$\begin{aligned} \begin{pmatrix} 2 \\ 0 \end{pmatrix} &= \lambda \begin{pmatrix} 1 \\ 3 \end{pmatrix}, & \begin{pmatrix} 3 \\ 0 \end{pmatrix} &= -\lambda \begin{pmatrix} 0 \\ 3 \end{pmatrix}, \\ \begin{pmatrix} 2 \\ 1 \end{pmatrix} &= -\lambda \begin{pmatrix} 1 \\ 2 \end{pmatrix}, & \begin{pmatrix} 3 \\ 1 \end{pmatrix} &= \lambda \begin{pmatrix} 0 \\ 2 \end{pmatrix}, \\ \begin{pmatrix} 02 \\ 13 \end{pmatrix} + \begin{pmatrix} 13 \\ 13 \end{pmatrix} &= 1, & \begin{pmatrix} 02 \\ 01 \end{pmatrix} + \begin{pmatrix} 13 \\ 01 \end{pmatrix} &= 0. \end{aligned}$$

The contravariant and covariant transformation coefficients $\left\{ \begin{smallmatrix} q \\ s \end{smallmatrix} \right\}$, $\left(\begin{smallmatrix} r \\ p \end{smallmatrix} \right)$ are now connected by the equation

$$\left\{ \begin{smallmatrix} q \\ s \end{smallmatrix} \right\} = D_{rs} D^{pq} \left(\begin{smallmatrix} r \\ p \end{smallmatrix} \right). \quad \dots (3.2)$$

The raising and lowering of indices may be performed under the scheme

$$A^0 = A_2, \quad A^2 = -A_0, \quad A^1 = A_3, \quad A^3 = -A_1. \quad \dots (3.3)$$

We note here the relations

$$A^p A_p = 0, \quad A^p B_p + B^p A_p = 0. \quad \dots (3.4)$$

Let us now construct a mixed tensor N^p_q by means of a pair of tensors A^p , B_q taken in the bilinear form $A^p B_q - B^p A_q$ satisfying the structural equation

$$N_s^q = N_p^r D_{rs} D^{pq} \quad \dots (3.5)$$

having 4 mutually independent components expressed in terms of 4 quantities h_k by means of the equations

$$\begin{aligned} N_0^0 &= N_2^2 = -N_1^1 = -N_3^3 = -h_2, \\ N_2^1 &= -N_3^0 = N_1^2 = -N_0^3 = h_1, \\ N_0^1 &= N_2^3 = h_0 + h_3, \quad N_0^1 = N_3^2 = -h_0 + h_3, \\ N_0^2 &= N_0^3 = N_3^1 = N_1^3 = 0, \end{aligned} \quad \dots (3.6)$$

Introducing the 4 connecting tensors

$$T^0_q{}^p \text{ with non vanishing components } \left| \begin{matrix} 0 \\ 1 \end{matrix} \right| = \left| \begin{matrix} 3 \\ 2 \end{matrix} \right| = - \left| \begin{matrix} 1 \\ 0 \end{matrix} \right| = - \left| \begin{matrix} 2 \\ 3 \end{matrix} \right| = 1,$$

$$T^1_q{}^p \text{ } \left| \begin{matrix} 0 \\ 3 \end{matrix} \right| = \left| \begin{matrix} 3 \\ 0 \end{matrix} \right| = - \left| \begin{matrix} 1 \\ 2 \end{matrix} \right| = - \left| \begin{matrix} 2 \\ 1 \end{matrix} \right| = -1,$$

... (3.7)

$$T^2_q{}^p \text{ } \left| \begin{matrix} 0 \\ 0 \end{matrix} \right| = \left| \begin{matrix} 2 \\ 2 \end{matrix} \right| = - \left| \begin{matrix} 1 \\ 1 \end{matrix} \right| = - \left| \begin{matrix} 3 \\ 3 \end{matrix} \right| = -1,$$

$$T^3_q{}^p \text{ } \left| \begin{matrix} 0 \\ 1 \end{matrix} \right| = \left| \begin{matrix} 2 \\ 3 \end{matrix} \right| = \left| \begin{matrix} 1 \\ 0 \end{matrix} \right| = \left| \begin{matrix} 3 \\ 2 \end{matrix} \right| = 1.$$

we can express the above as

$$N_q{}^p = T^k_q{}^p h_k. \quad \dots (3.8)$$

Using the above connecting tensors, characteristic for the (D—C) transformation one can obtain further results in this connection.

It appears from (3.6) that we can connect h_k in a different way with the N 's so that a new transformation (D—E) is obtained. We take

$$\begin{aligned} N_0^0 &= N_2^2 = -N_1^1 = -N_3^3 = -h_2, \\ N_1^0 &= N_2^3 = N_0^1 = N_3^2 = h_1, \\ N_3^0 &= -N_2^1 = h_0 + h_3, \quad N_0^3 = -N_1^2 = -h_0 + h_3, \\ N_2^0 &= N_0^2 = N_3^1 = N_1^3 = 0. \end{aligned} \quad \dots (3.9)$$

Introducing the characteristic connecting tensors

$$T^0_q{}^p \text{ with nonvanishing components } \left| \begin{matrix} 0 \\ 3 \end{matrix} \right| = \left| \begin{matrix} 2 \\ 1 \end{matrix} \right| = - \left| \begin{matrix} 3 \\ 0 \end{matrix} \right| = - \left| \begin{matrix} 1 \\ 2 \end{matrix} \right| = 1,$$

$$T^1_q{}^p \text{ } \left| \begin{matrix} 0 \\ 1 \end{matrix} \right| = \left| \begin{matrix} 1 \\ 0 \end{matrix} \right| = \left| \begin{matrix} 2 \\ 3 \end{matrix} \right| = \left| \begin{matrix} 3 \\ 2 \end{matrix} \right| = 1,$$

... (3.10)

$$T^2_q{}^p \text{ } \left| \begin{matrix} 0 \\ 0 \end{matrix} \right| = \left| \begin{matrix} 2 \\ 2 \end{matrix} \right| = - \left| \begin{matrix} 1 \\ 1 \end{matrix} \right| = - \left| \begin{matrix} 3 \\ 3 \end{matrix} \right| = -1,$$

$$T^3_q{}^p \text{ } \left| \begin{matrix} 0 \\ 3 \end{matrix} \right| = \left| \begin{matrix} 3 \\ 0 \end{matrix} \right| = - \left| \begin{matrix} 1 \\ 2 \end{matrix} \right| = - \left| \begin{matrix} 2 \\ 1 \end{matrix} \right| = 1,$$

we can express the above as

$$N_q^p = T_q^k p h_k. \quad \dots (3.11)$$

Under $(D-E)$ transformation the tensor D_{pq} remains invariant and \bar{E}_{pq} goes over into $\lambda \bar{E}_{pq}$. The conditions which the transformation coefficients must satisfy are given by

$$\begin{aligned} \begin{pmatrix} 2 \\ 2 \end{pmatrix} &= \lambda \begin{pmatrix} 3 \\ 3 \end{pmatrix} & \begin{pmatrix} 0 \\ 2 \end{pmatrix} &= -\lambda \begin{pmatrix} 1 \\ 3 \end{pmatrix}, \\ \begin{pmatrix} 2 \\ 3 \end{pmatrix} &= -\lambda \begin{pmatrix} 3 \\ 2 \end{pmatrix} & \begin{pmatrix} 0 \\ 3 \end{pmatrix} &= \lambda \begin{pmatrix} 1 \\ 2 \end{pmatrix} \\ \dots & \dots (3.12) \\ \begin{pmatrix} 2 \\ 0 \end{pmatrix} &= -\lambda \begin{pmatrix} 3 \\ 1 \end{pmatrix} & \begin{pmatrix} 0 \\ 0 \end{pmatrix} &= \lambda \begin{pmatrix} 1 \\ 1 \end{pmatrix}, \\ \begin{pmatrix} 2 \\ 1 \end{pmatrix} &= \lambda \begin{pmatrix} 3 \\ 0 \end{pmatrix} & \begin{pmatrix} 0 \\ 1 \end{pmatrix} &= -\lambda \begin{pmatrix} 1 \\ 0 \end{pmatrix}, \\ \begin{pmatrix} 02 \\ 13 \end{pmatrix} + \begin{pmatrix} 13 \\ 13 \end{pmatrix} &= 1, & \begin{pmatrix} 02 \\ 03 \end{pmatrix} + \begin{pmatrix} 13 \\ 03 \end{pmatrix} &= 0. \end{aligned}$$

It may be noted that under $(D-E)$ transformation the formulae (3.2), (3.3) and (3.4) hold good retaining all characteristic properties.

With E_{pq} as primary tensor we can frame two transformation schemes by taking either C_{pq} as secondary or \bar{D}_{pq} as secondary. In the former the tensor E_{pq} remains invariant and C_{pq} goes over into λC_{pq} . The conditions which the transformation coefficients (r_p) must satisfy are given as

$$\begin{aligned} \begin{pmatrix} 3 \\ 3 \end{pmatrix} &= \lambda \begin{pmatrix} 1 \\ 1 \end{pmatrix} & \begin{pmatrix} 2 \\ 3 \end{pmatrix} &= -\lambda \begin{pmatrix} 0 \\ 1 \end{pmatrix}, \\ \begin{pmatrix} 3 \\ 2 \end{pmatrix} &= -\lambda \begin{pmatrix} 1 \\ 0 \end{pmatrix} & \begin{pmatrix} 2 \\ 2 \end{pmatrix} &= \lambda \begin{pmatrix} 0 \\ 0 \end{pmatrix} \\ \dots & \dots (4.1) \\ \begin{pmatrix} 3 \\ 1 \end{pmatrix} &= -\lambda \begin{pmatrix} 1 \\ 3 \end{pmatrix} & \begin{pmatrix} 2 \\ 1 \end{pmatrix} &= \lambda \begin{pmatrix} 0 \\ 3 \end{pmatrix}, \\ \begin{pmatrix} 3 \\ 0 \end{pmatrix} &= \lambda \begin{pmatrix} 1 \\ 2 \end{pmatrix} & \begin{pmatrix} 2 \\ 0 \end{pmatrix} &= -\lambda \begin{pmatrix} 0 \\ 2 \end{pmatrix} \\ \begin{pmatrix} 03 \\ 03 \end{pmatrix} + \begin{pmatrix} 12 \\ 03 \end{pmatrix} &= 1, & \begin{pmatrix} 03 \\ 01 \end{pmatrix} + \begin{pmatrix} 12 \\ 01 \end{pmatrix} &= 0. \end{aligned}$$

In the latter E_{pq} remains invariant and $\bar{D}_{\mu q}$ goes over into λD_{pq} where $\lambda = \pm 1$. The conditions which the transformation coefficients must satisfy are given as follows :

$$\begin{aligned}
 \begin{pmatrix} 3 \\ 3 \end{pmatrix} &= \lambda \begin{pmatrix} 2 \\ 2 \end{pmatrix}, & \begin{pmatrix} 1 \\ 3 \end{pmatrix} &= \lambda \begin{pmatrix} 0 \\ 2 \end{pmatrix}, \\
 \begin{pmatrix} 3 \\ 2 \end{pmatrix} &= -\lambda \begin{pmatrix} 2 \\ 3 \end{pmatrix}, & \begin{pmatrix} 1 \\ 2 \end{pmatrix} &= -\lambda \begin{pmatrix} 0 \\ 3 \end{pmatrix}, \\
 & \dots \quad (4.2) \\
 \begin{pmatrix} 3 \\ 1 \end{pmatrix} &= \lambda \begin{pmatrix} 2 \\ 0 \end{pmatrix}, & \begin{pmatrix} 1 \\ 1 \end{pmatrix} &= \lambda \begin{pmatrix} 0 \\ 0 \end{pmatrix}, \\
 \begin{pmatrix} 3 \\ 0 \end{pmatrix} &= -\lambda \begin{pmatrix} 2 \\ 1 \end{pmatrix}, & \begin{pmatrix} 1 \\ 0 \end{pmatrix} &= -\lambda \begin{pmatrix} 0 \\ 1 \end{pmatrix}, \\
 \begin{pmatrix} 03 \\ 03 \end{pmatrix} + \begin{pmatrix} 12 \\ 03 \end{pmatrix} &= 1, & \begin{pmatrix} 03 \\ 02 \end{pmatrix} + \begin{pmatrix} 12 \\ 02 \end{pmatrix} &= 0.
 \end{aligned}$$

It may be noted in both the transformation schemes that the contravariant and the covariant transformation coefficients are connected by the equation

$$\left\{ \begin{matrix} q \\ s \end{matrix} \right\} = E_{rs} E^{pq} \left(\begin{matrix} r \\ p \end{matrix} \right) \quad \dots \quad (4.3)$$

Raising and lowering of indices may be performed in both according to the rule

$$A_q E^{pq} = A^p, \quad A^p E_{pq} = A_q, \quad \dots \quad (4.4)$$

so that $A^0 = A_3, \quad A^3 = -A_0, \quad A^1 = A_2, \quad A^2 = -A_1$

and the relations $A^p A_p = 0, \quad A^p B_p + B^p A_p = 0$ hold good in both.

The characteristic connecting tensors with regard to ($E-C$) transformation are now constructed with the nonvanishing components

$$\begin{aligned}
 T^0_1{}^0 &= 1, \quad T^0_0{}^1 = -1, \quad T^0_3{}^2 = 1, \quad T^0_2{}^3 = -1, \\
 T^1_2{}^0 &= 1, \quad T^1_3{}^1 = -1, \quad T^1_0{}^2 = 1, \quad T^1_1{}^3 = -1, \\
 T^2_0{}^0 &= -1, \quad T^2_1{}^1 = 1, \quad T^2_2{}^2 = 1, \quad T^2_3{}^3 = -1 \\
 T^3_1{}^0 &= 1, \quad T^3_0{}^1 = 1, \quad T^3_3{}^2 = 1, \quad T^3_2{}^3 = 1,
 \end{aligned} \quad \dots \quad (4.5)$$

while in the ($E-\bar{D}$) transformation the characteristic connecting tensors are formed by the nonvanishing components

$$\begin{aligned}
 T^0_2{}^0 &= -1, \quad T^0_3{}^1 = 1, \quad T^0_0{}^2 = 1, \quad T^0_1{}^3 = -1, \\
 T^1_1{}^0 &= 1, \quad T^1_0{}^1 = 1, \quad T^1_3{}^2 = 1, \quad T^1_2{}^3 = 1, \\
 T^2_0{}^0 &= -1, \quad T^2_1{}^1 = 1, \quad T^2_2{}^2 = 1, \quad T^2_3{}^3 = -1, \\
 T^3_2{}^0 &= 1, \quad T^3_3{}^1 = -1, \quad T^3_0{}^2 = 1, \quad T^3_1{}^3 = -1.
 \end{aligned} \quad \dots \quad (4.6)$$

Using the standard formula in my earlier paper (Ghosh, 1965) one can get a representation of the induced 4-dimensional Lorentz transformation corresponding to each of the transformation schemes $(E-C)$ and $(E-\tilde{D})$. Proceeding as before further results in this connection will follow.

With the conjugate tensors \tilde{C}_{pq} , \tilde{D}_{pq} , \tilde{E}_{pq} a set of 6 transformation schemes can be formed having similar properties.

REFERENCE

Ghosh, N. N., 1965, *Indian J. Phys.*, **39**, 435.

STRUCTURAL EFFECTS IN NON-ELECTROLYTE SOLUTIONS

S. N. BHATTACHARYYA

DEPARTMENT OF PHYSICAL CHEMISTRY,

INDIAN ASSOCIATION FOR THE CULTIVATION OF SCIENCE, JADAVPUR, CALCUTTA-32.

(Received January 27, 1967)

ABSTRACT. Non-polar central forces and non-central forces of both weak dipolar and of structural origin have been combined into a single potential. Neglecting higher order terms the excess thermodynamic functions of a mixture of non-polar globular molecules with weakly polar globular molecules have been found to consist of four terms: pure non-polar, pure dipolar, polarisabilities and structural, g^E , h^E and v^E have been predicted for the systems fluorobenzene-carbon tetrachloride, fluorobenzene-benzene and fluorobenzene-cyclohexane for which experimental data exist. Agreement between predicted and experimental values are satisfactory for all the systems.

INTRODUCTION

Anantaraman Bhattacharyya, and Palit (1961, 1962, 1963) recently discussed the thermodynamics of liquid mixtures the molecules of both components being spherical but those of one of the components also having a point dipole at the centre. Balescu's theory [Balescu (1955), Prigogine (1957)] was modified and used to predict the excess functions with considerable success. It seemed however that the description of a molecule like chloro- or fluorobenzene as a spherical polar molecule was not quite correct; some discrepancies, particularly for the systems like fluorobenzene-benzene and fluorobenzene-carbon tetrachloride appeared to be due to the presence of another effect. It was suggested that this may have originated from the non-spherical nature of the component molecules. Carbon tetrachloride and benzene are not strictly spherical and it would be more realistic to describe a molecule like fluorobenzene as a globular molecule with a point dipole at the centre.

The object of this work is to develop a simple potential for such a molecule which will permit a calculation of the effects of the different contributions to the molecular interactions.

Various treatments of the potential have combined non-polar central forces with non-central forces. These latter have either been assumed due to weak dipoles or due to a molecular structure which lacks spherical symmetry [Rowlinson, et al (1955), Prigogine (1957)]. In this work we attempt to synthesize the two approaches and arrive at the desired potential.

According to Rowlinson et al (1955) the potential for a globular molecule is obtained from a Lennard Jones potential of spherical symmetry through the perturbation of the attractive term alone by a small non-central term.

$$\epsilon(r) = \epsilon^0[(r^0/r)^{12} - 2(r^0/r)^6\{1 + \alpha g(\theta_1, \theta_2, \theta_{12})\}] \quad (1)$$

where α is a small parameter and g is a sum of products of surface harmonics. Taking an average over the angles this gives rise to a temperature dependent parameter $\delta(T)$ which is proportional to the square of the coefficients of the non-central terms of globular origin.

$$\delta_{ij}(T) = \frac{\epsilon_{ij}\alpha_{ij}\langle g_{ij}(\omega) \rangle}{kT} \quad (2)$$

$\langle g_{ij}(\omega) \rangle$ denotes an unweighted average over all angles. The essential simplifications made by them to arrive at this simple form of potential are; (1) neglect of potentials which lead to triplet terms, (2) neglect of variation of repulsive forces, (3) assumption of $a(n, n/2)$ potential for the central forces which lead to a hypothetical potential conformal with the original unperturbed potential but which is a function of temperature. This hypothetical potential has the form

$$\begin{aligned} \epsilon(r) &= \epsilon^*[(r^*/r)^{12} - 2(r^*/r)^6] \\ &= \epsilon^0[(r^0/r)^{12}\{1 - 2\delta(T)\} - 2(r^*/r)^6] \end{aligned} \quad (3)$$

According to Prigogine (1957) such a procedure is rather arbitrary when applied to globular molecules. Non-central forces should decrease more rapidly with increasing distance than forces of spherical symmetry, a fact which does not appear in (3). g is not specified and (2) is not explicit and can only be used empirically to fit certain experimental data.

In spite of this criticism of Prigogine the hypothetical potential seems to be useful owing to its simplicity in form and the author and his colleagues have been able to predict the thermodynamic functions of mixtures of non-polar polyatomic molecules with some success. One can now take advantage of the r^{-6} dependence of the attractive part of this potential and introduce a point-dipole at the centre of such a molecule similar to what has been done by Balescu (1957) to a strictly spherical molecule. We can write down the potential as follows :

$$\epsilon(r) = \epsilon^0[(r^0/r)^{12}(1 - 2\delta) - 2(r^0/r)^6] + \bar{\epsilon}_d \quad (4)$$

where $\bar{\epsilon}_d$ is the average value of the dipolar interaction over all orientations, $\bar{\epsilon}_d$ being

$$\bar{\epsilon}_d = -\frac{1}{3kT} \cdot \frac{\mu^4}{r^6} - \frac{2\mu^2\alpha}{r^6} \quad (5)$$

For a like pair of molecules the potential now becomes

$$\begin{aligned}\epsilon(r) &= \epsilon^0 \left[(r^0/r)^{12}(1-2\delta) - 2(r^0/r)^6 \left[1 + \frac{1}{6} \frac{\bar{\mu}^4}{\bar{T}^0} + \bar{\alpha}\bar{\mu}^2 \right] \right] \\ &= \epsilon^* [(r^*/r)^{12} - 2(r^*/r)^6] \quad \dots \quad (6)\end{aligned}$$

where the reduced parameters $\bar{\mu}$, $\bar{\alpha}$ and \bar{T}^0 are defined by

$$\bar{\mu} = \frac{\mu}{(\epsilon^0 r^{03})^{\frac{1}{2}}} ; \quad \bar{\alpha} = \frac{\alpha}{r^{03}} ; \quad \bar{T}^0 = \frac{kT}{\epsilon^0}$$

Equation (6) shows that this potential is also conformal with the original unperturbed potential but dependent on temperature. The characteristic molecular parameters ϵ^* and r^* of this new potential are related to the unperturbed ϵ^0 and r^0 as below

$$\begin{aligned}\epsilon^* &= \epsilon^0 \left[1 + \frac{1}{3} \Gamma + 2\gamma + 2\delta + 2\delta \left(\frac{1}{3} \Gamma + 2\gamma \right) + \dots \right] \\ &= \epsilon^0 [1 + \psi(T)] \\ r^* &= r^0 \left[1 - \frac{1}{36} \Gamma - \frac{1}{6} \gamma - \frac{1}{3} \delta + \frac{1}{6} \delta \left(\frac{1}{3} \Gamma + 2\gamma \right) + \dots \right] \\ &= r^0 [1 + \phi(T)] \quad \dots \quad (7)\end{aligned}$$

where $\Gamma = \frac{\bar{\mu}^4}{\bar{T}^0}$, $\gamma = \bar{\alpha} \bar{\mu}^2$

The production term $2\delta(\frac{1}{3}\Gamma + 2\gamma)$ contributes very little to the total perturbation and can safely be neglected for the present analysis. According to the general ideas of average potential theory eqn. (7) can be written down as

$$\begin{aligned}\langle \epsilon_i^* \rangle &= \langle \epsilon^0 \rangle (1 + \langle \psi_i(T) \rangle) \\ \langle r_i^* \rangle &= \langle r^0 \rangle (1 + \langle \phi_i(T) \rangle) \quad \dots \quad (8)\end{aligned}$$

For the composition dependent average potential, the average perturbation $\langle \psi_i \rangle$ and $\langle \phi_i \rangle$ being exactly similar to those found out by Balescu (1957).

For a mixture of two polarisable globular molecules where the component 2 has a permanent dipole moment of magnitude μ_2 , the perturbations are now

$$\psi_{11} = 2\delta_{11} ; \quad \phi_{11} = -\frac{1}{3} \delta_{11}$$

$$\begin{aligned}\psi_{12} &= 2\delta_{12} + \gamma_{12}; \quad \phi_{12} = -\frac{1}{3}\delta_{12} - \frac{1}{12}\gamma_{12} \\ \psi_{22} &= 2\delta_{22} + \frac{1}{3}\Gamma + 2\gamma_{22}; \quad \phi_{22} = -\frac{1}{3}\delta_{22} - \frac{1}{36}\Gamma - \frac{1}{6}\gamma_{22} \quad \dots \quad (9)\end{aligned}$$

Following the procedure as outlined by Balescu with the potential (6) and perturbations (9) it is found that any excess function z^E now splits into four terms

$$z^E = z_0^E + z_d^E + z_p^E + z_s^E \quad \dots \quad (10)$$

z_0^E , z_d^E , z_p^E and z_s^E are contributions due to central forces, pure dipolar, polarisabilities and those due to non-spherical or globular nature of the molecules respectively. One may take the expressions* due to Prigogine *et al.* (1957) for z_0^E . These are

$$\begin{aligned}\frac{g_0^E}{x_1x_2} &= h_1(2\theta - 9\rho^2) + \frac{1}{2}TC_{p1}(\delta^2 - 4\theta\delta x_2 - 4\theta^2x_1x_2) - \frac{1}{2}TC_{v1}[\theta(x_1 - x_2) + \frac{1}{2}\delta]^2 \\ &\quad - \frac{3}{2}RT\rho[\theta(x_1 - x_2) + \frac{1}{2}\delta + 3\rho] \quad \dots \quad (11)\end{aligned}$$

$$\begin{aligned}\frac{h_0^E}{x_1x_2} &= (h_1 - TC_{p1})(2\theta - 9\rho^2) - \frac{1}{2}T^2\frac{dC_{p1}}{dT}(\delta^2 - 4\theta\delta x_2 - 4\theta^2x_1x_2) \\ &\quad + \frac{1}{2}T^2\frac{dC_{v1}}{dT}[\theta(x_1 - x_2) + \frac{1}{2}\delta]^2 \quad \dots \quad (12)\end{aligned}$$

$$\begin{aligned}\frac{v_0^E}{x_1x_2} &= \frac{3}{2}v_1\rho\left[\theta(x_1 - x_2) + \frac{1}{2}\delta + \frac{11}{4}\rho\right] + T\frac{dv_1}{dT}(-2\theta - \delta^2 + 4\theta\delta x_2 + 4\theta^2x_1x_2 \\ &\quad + 9\rho^2 + 3\rho\delta - 6\rho\theta x_2) + \frac{1}{2}T^2\frac{d^2v}{dT^2}(-\delta^2 - 4\theta\delta x_2 + 4\theta^2x_1x_2) \quad \dots \quad (13)\end{aligned}$$

For z_d^E the expressions due to Anantaraman () may be taken who retain θ in the expressions of dipolar excess functions.

$$\begin{aligned}\frac{g_d^E}{x_1x_2} &= \frac{1}{8}\Gamma\{-h_1(1 + \delta - 3\rho x_2) - TC_{p1}[\frac{1}{2}\delta(3 - x_1) + x_2\theta] \\ &\quad + \frac{1}{4}RT[1 - x_2(\frac{1}{2}\delta - \theta + 3\rho)]\} \quad \dots \quad (14)\end{aligned}$$

$$\frac{h_d^E}{x_1x_2} = \frac{1}{8}\Gamma(-2h_1 + TC_{p1} - \frac{1}{4}RT)[1 - x_2(\frac{1}{2}\delta - \theta + 3\rho)] \quad \dots \quad (15)$$

* Possibly several minor typographical errors occurred in the printing of equation (10.7.8) of Prigogine (1957). See also McLure *et al.* (1965).

$$\frac{v_d^E}{x_1 x_2} = \frac{1}{3} \Gamma \left\{ \left\{ \frac{1}{2} v_1 + T \frac{dv_1}{dT} \right\} \left[1 + \frac{2}{3} \rho (1 + x_1) - \frac{1}{2} x_2 (\delta - 2\theta) \right] \right. \\ \left. - \frac{5}{4} T \frac{dv_1}{dT} \delta (1 + \frac{1}{2} x_2) \right\} \quad \dots \quad (16^+)$$

From the definition of γ_{12}

$$\gamma_{12} = \frac{\alpha_1 \mu_2^2}{r_{12}^{06} \epsilon_{12}^0} \quad \dots \quad (17)$$

We may write

$$\gamma_{12} = \frac{\alpha_1}{\alpha_2} \cdot \frac{\alpha_2 \mu_2^2}{[\frac{1}{2}(r_{11}^0 + r_{22}^0)]^6 [\epsilon_{11}^0 \theta + \frac{1}{2}(\epsilon_{11}^0 + \epsilon_{22}^0)]} \quad \dots \quad (18)$$

In terms of θ , δ and ρ and a new parameter σ defined by

$$\frac{\alpha_1}{\alpha_2} = 1 + \sigma \quad \dots \quad (19)$$

and neglecting higher order terms we obtain

$$\gamma_{12} = \gamma_{22} \left\{ 1 + \sigma + 3\rho + \frac{\delta}{2} - \theta \right\} \quad \dots \quad (20)$$

The equation (20) is a fair approximation of γ_{12} when the restriction $|\sigma| < 0.3$ is obeyed.

With (20), retaining θ and neglecting higher order terms the following simplified expressions for z_p^E is obtained.

$$\frac{g_p^E}{x_1 x_2} = \gamma_{22} [h_1 (2\sigma + 9\rho) + T C_{p1} \{ \theta (1 + 2x_2) - \frac{3}{2} \delta \} - \frac{1}{4} RT (2\sigma - \theta + \frac{3}{2} \delta + 9\rho)] \quad \dots \quad (21)$$

$$\frac{h_p^E}{x_1 x_2} = \gamma_{22} \left[(h_1 - T C_{p1}) (2\sigma + 9\rho) + T^2 \frac{dC_{p1}}{dT} \{ \theta (1 + 2x_2) - \frac{3}{2} \delta \} \right] \quad \dots \quad (22)$$

$$\frac{v_p^E}{x_1 x_2} = -\gamma_{22} \left\{ \frac{1}{4} v_1 + T \frac{dv_1}{dT} \right\} (2\sigma_2 - \theta + \frac{3}{2} \delta + \frac{9}{2} \rho) \quad \dots \quad (23)$$

In the similar way the contribution z_s^E due to nonspherical shape of the molecules are found out from the perturbations (9). These are

$$\frac{g_s^E}{x_1 x_2} = h_1 [\Delta_{12} \{ 1 + \theta + (x_1 - \frac{1}{4}) \delta + (\frac{1}{4} + 3\rho)(x_1 - x_2) \} - (\delta_{11} - \delta_{22}) \\ \{ 2\theta + (1 + x_2) \delta + 6\rho \}] + T C_{p1} \delta [\Delta_{12} (x_2 - \frac{1}{4}) + (\delta_{11} - \delta_{22}) (\frac{1}{2} + x_2)] \\ + \frac{1}{2} RT [\Delta_{12} \{ 1 + \frac{1}{2} \theta + (\frac{1}{4} + 3\rho)(x_1 - x_2) \} - (\delta_{11} - \delta_{22}) \{ \frac{1}{2} \delta + 6\rho + \theta (x_1 - x_2) \}] \quad \dots \quad (24)$$

† After correcting a minor error in Anantaraman et al. (1961) for the equation (16) which unfortunately was repeated in Anantaraman et al. (1963). Caused by typographical error in the reprints of the authors.

$$\frac{h_s^E}{x_1 x_2} = (2h_1 - TC_{p1} + \frac{1}{2}RT)[\Delta_{12}\{1 + \theta/2 + (\frac{1}{4}\delta + 3\rho)(x_1 - x_2)\} - (\delta_{11} - \delta_{22})\{\frac{1}{2}\delta + 6\rho + \theta(x_1 - x_2)\}] \quad \dots (25)$$

$$\frac{v_2^E}{x_1 x_2} = -\left(\frac{1}{2}v_1 + T \frac{dv_1}{dT}\right) \{[\Delta_{12}\{1 + \theta/2 + \frac{1}{4}\delta(x_1 - x_2) - \frac{3}{4}\rho\} - (\delta_{11} - \delta_{22})\{\frac{1}{2}\delta + 3\rho(\frac{3}{2} - x_2) + \theta(x_1 - x_2)\}] + \frac{3}{2}T \frac{dv_1}{dT} \delta [\Delta_{12}(x_2 - \frac{1}{4}) + (\delta_{11} - \delta_{22})(x_2 + \frac{1}{2})]\} \quad \dots (26)$$

where $\Delta_{12} = 2(2\delta_{12} - \delta_{11} - \delta_{22})$ and other parameters have been explained elsewhere¹⁻⁴. Δ_{12} and $(\delta_{11} - \delta_{22})$ are very small and can be treated as second order quantities. Hence, if we neglect the product of θ , δ or ρ with either Δ_{12} or $(\delta_{11} - \delta_{22})$ we arrive at the simple form due to Rowlinson. i.e.,

$$\frac{g_s^E}{x_1 x_2} = (h_1 + \frac{1}{2}RT)\Delta_{12} \quad \dots (27)$$

$$\frac{h_s^E}{x_1 x_2} = (2h_1 - TC_{p1} + \frac{1}{2}RT)\Delta_{12} \quad \dots (28)$$

$$\frac{v_s^E}{x_1 x_2} = -\left(\frac{1}{2}v_1 + T \frac{dv_1}{dT}\right) \Delta_{12} \quad \dots (29)$$

It may be pointed out here that out of all the contributions to any excess function z^E only the contributions due to central forces z_0^E are very strongly dependent on θ , δ and ρ . On the other hand z_a^E and z_s^E are little affected by these parameters. For the calculation of z of any system we now encounter two unknown parameters θ and Δ_{12} in the total expression of z^E . We propose to calculate θ and Δ_{12} from the experimental values of two of the excess functions. We choose h^E and v^E for this purpose as these quantities are obtained from direct measurements and consequently are more accurate and reliable. With the values of θ and Δ_{12} thus obtained we would then try to predict g^E to test the consistency of these parameters and hence the proposed theoretical approach.

We have calculated the excess functions of the systems carbon tetrachloride-fluorobenzene, benzene-fluorobenzene and cyclohexane-fluorobenzene systems. The g^E , h^E and v^E of the systems were measured by Anantaraman *et al.* (1963a, b). The results of the calculations have been summarised in Table I. The average values \bar{z}_o^E and \bar{z}_s^E are the averages of the results obtained by taking non-polar and the polar components as reference alternatively.

Anantaraman *et al.* (1963) tried to analyse the results of these systems in light of their modified approach. They predicted the excess functions of the systems cyclohexane-fluorobenzene and benzene-fluorobenzene more or less

TABLE I

Comparison of calculated and experimental excess functions at equimolar composition and 25°C in Cal. or ml. per mole

(a) System : Carbon tetrachloride-fluorobenzene

$$\delta = 0.0058, \quad \rho = 0.0046, \quad \sigma = 0.0324 \quad \theta = -0.0138,$$

$$\Delta_{12} = 0.0159$$

Excess function -E	Calc. $z_o E$ this work	Calc. $z_o E$ †	Calc. $z_d E$ this work	Calc. $z_d E$ †	Calc. $z_s E$ this work	Calc. $z_p E$ this work	Calc. $\gamma_p E$ total this work	Calc. $z E$ total †	Expt. $z E$
$h E$	80.5	4.4	57.3	56.9	-74.3	-2.2	61.0*	61.3*	61.0
$v E$	0.25	0.01	0.18	0.19	-0.33	-0.02	0.08*	0.20	0.08
$g E$	51.7	2.8	23.1	23.0	28.5	1.3	45.6	25.8	57.0

(b) System : Benzene-fluorobenzene

$$\delta = -0.0065, \quad \rho = 0.0268, \quad \sigma = 0.0147, \quad \theta = 0.0113$$

$$\Delta_{12} = 0.0003$$

$h E$	-49.0	-56.0	58.4	58.4	-1.5	-5.0	2.1*	2.1*	2.2
$v E$	-0.08	-0.09	0.18	0.18	-0.01	-0.01	0.08*	0.09	0.08
$g E$	-31.1	-36.4	22.7	23.0	-0.6	-3.6	-12.6	-13.4	0

(c) System : Cyclohexane-fluorobenzene

$$\delta = 0.0132, \quad \rho = -0.0321, \quad \sigma = 0.0688, \quad \theta = -0.0250$$

$$\Delta_{12} = 0.0044$$

$h E$	173.8	154.5	60.4	60.1	-20.6	3.4	217.0*	214.6*	217.0
$v E$	0.65	0.61	0.19	0.18	-0.10	-0.02	0.72*	0.79	0.72
$g E$	109.6	102.5	24.5	24.6	-7.8	1.7	128.0	127.1	136.0

* Adjusted to experimental data.

† according to Bhattacharyya, *et al.* (1963a, b).

satisfactorily but their calculated excess functions of the system carbontetrachloride-fluorobenzene was in qualitative agreement only with experimental results. The most interesting feature of this system is that the experimental ratio of g^E : h^E was very nearly unity whereas they found that the calculated excess functions were almost entirely of dipolar origin and thus the system should obey Pople's relation which states that excess functions g^E_c and h^E should bear an approximate relation $g^E : h^E = 1/2$ when they are of pure dipolar origin. The calculated non-polar contributions were rather small owing to the small values of δ and ρ of the system (i.e., $\rho = 0.0046$, $\delta = 0.0058$). The value of θ of this

system was also found to be negligible and hence their result did not greatly differ from that obtained by Balescu's theory. These lead to a somewhat paradoxical situation and needs further clarification. So this system has been chosen as a test case for the present approach.

From table I it is evident that agreement between the experimental and calculated g^E for the system carbon tetrachloride-fluorobenzene by the present approach is much better and there is a substantial contribution from the structural forces which is of almost equal importance with that of central and dipolar forces. The contribution due to polarisability comes out to be very small in all cases as expected. For the systems benzene-fluorobenzene and cyclohexane-fluorobenzene the contribution due to structural forces are relatively small. This explains the success of Anantaraman *et al.* () to predict their excess functions more or less satisfactorily.

An interesting feature of the theory is that contributions of the structural forces are very similar to those of forces of dipolar origin for h^E and g^E . But though the dipolar effects are always positive for a mixture of non-polar-polar type, the structural effects may be either positive or negative. The $h_s^E : g_s^E$ ratio is also nearly equal to two for the latter. This presents the possibility that the structural forces may cancel or reduce the effect of the dipolar forces so that such a mixture may very well behave as a mixture of non-polar components. But as the $h_s^E : v_s^E$ is not same as that of $h_d^E : v_d^E$ such a simplified assumption may not adequately predict v^E . This explains the $h^E : g^E$ ratio of the system carbon tetrachloride-fluorobenzene and clears up the paradox presented by it. Theory also reveals another fact which should be mentioned. Pople's relation is meant strictly for pure dipolar effects. In an actual mixture of polyatomic molecules, interactions due to different origins remain mixed up. So in the opinion of the author no conclusion as regards the nature of the mixture can be derived simply from a inspection of the observed $h^E : g^E$.

REFERENCES

- Anantaraman, A. V., Bhattacharyya, S. N., Palit, S. R., 1961, *Trans. Farad. Soc.*, **57**, 40.
-
- _____ 1962, *Physica*, **28**, 633.
-
- _____ 1963a, *Trans. Farad. Soc.*, **59**, 1101.
-
- _____ 1963b, *Ind. Jour. Chem.*, **1**, 459.
- Balescu, R., 1955, *Acad. Roy. Belg. Cl. Sc.*, **41**, 1241.
- McLure, I. A., Bennet, J. E., Watson, A. E. P. and Benson, G. C., 1965, *J. Phys. Chem.*, **69**, 2759.
- Prigogine, I., 1957, *Molecular Theory of Solutions*, North Holland Publishing Co., Amsterdam, Chapter 14, 13, 10.
- Rowlinson, J. S., and Sutton, J. R., 1955, *Proc. Roy. Soc.*, **A229**, 271.

THE NEAR ULTRAVIOLET ABSORPTION SPECTRUM OF CYCLOHEXYL BENZENE

R. N. BAPAT

PHYSICS DEPARTMENT, COLLEGE OF SCIENCE, NAGPUR.

(Received September 3, 1966)

(Plate 7)

ABSTRACT. The near ultraviolet absorption spectrum of cyclohexyl benzene was studied at different temperatures and with different lengths of the absorbing column. The spectrum consists of about fifteen broad and diffuse bands with the 0,0 band at 37590 cm^{-1} . The maximum number of bands is obtained by using a path length of 300 cm. and 60°C. Vibrational frequencies in the excited state have values 528,940 and 1185, and combinations and overtones of these are present. Two bands have been observed on the longer wavelength side of the 0,0 band at this temperature which are not present at the room temperature. Assignments of different frequencies are discussed.

INTRODUCTION

The spectrum of Benzene and monosubstituted benzenes are well known. It has been observed that most substituent groups perturb only slightly the benzene nucleus and most of the characteristics of the benzene nucleus are maintained. The vapour spectrum of a number of complicated molecules were studied by Robertson, Music and Matsen (1950) to find the amount of modification in the benzene spectrum and the measure of the extent of perturbation by the substituent group. Phenyl cyclohexane was one of the substances studied by them in the vapour state and microphotometer tracings of the near ultraviolet absorption spectra are given by them. It was found that a large interaction moves the absorption of the monosubstituted benzene to longer wavelengths. They also state that the transition is certainly Alg-B2u. They have also given the excited state vibrational frequencies as 315, 526, 939 and 1187 for phenyl cyclohexane or cyclohexyl benzene. The spectrum was studied by these authors to find the ring strain. In the present case the near ultraviolet absorption spectrum of cyclohexyl benzene or phenyl cyclohexane has been studied in details by taking different lengths of the absorption column and different temperatures. The vibrational analysis is given.

EXPERIMENTAL

Cyclohexyl benzene is an oily liquid with boiling point 237.5°C . The liquid was distilled and the fraction of the distillate before the boiling point was reached was discarded while the liquid distilling at the temperature corresponding to the boiling point only was taken for the experimental work. Absorption length

used was 300 cms with open cell while the temperature of the absorbing column was changed from 30°C to 60°C. Increasing the temperature further did not show any improvement. Hilger's medium quartz spectrograph was used to photograph the spectra with Ilford special rapid plates. Exposure of about 15 minutes was given using Hydrogen discharge lamp. The bands were measured by means of a Hilger comparater, iron lines being used as standard lines. The wavelength of the bands were calculated by Hartman dispersion formula. The wavelength of the bands given in Table I represent the mean obtained on five different plates and are expected to be correct to $\pm 6 \text{ cm}^{-1}$ as the nature of the bands is diffuse.

RESULTS

Cyclohexyl benzene absorbs in the region 2700 to 2400A in the vapour phase. About fifteen bands were obtained in this region. At room temperature about seven bands are observed. There is no band in the longer wavelength side of the 0,0 band. As the temperature is increased from 30° to 60°C all the bands mentioned in Table I appear with maximum intensities. A reproduction of these

TABLE I
Cyclohexyl benzene bands 2700 to 2400A

λ in air A	Wave number in vacuo. cm^{-1} .	Intensity (visual)	separation from (0,0) i.e. 37590 Cm^{-1} .	Assignment
2704.7	36961	1	629	0 - 624
2670.5	37435	2	155	0 - 147
2659.5	37590	10	0	(0,0)
2640.6	37858	2	268	0 + 268
2622.7	38118	8	528	0 + 528
2594.6	38530	6	940	0 + 940
2578.2	38775	2	1185	0 + 1185
2559.8	39053	4	1463	0 + 940 + 528
2543.3	39307	1	1717	0 + 1185 + 528
2532.3	39477	1	1887	0 + 940 + 940
2516.5	39725	1	2135	0 + 940 + 1185
2499.9	39989	2	2399	0 + 940 + 940 + 528
2484.1	40243	0	2653	0 + 940 + 1185 + 528
2473.2	40421	0	2831	0 + 3 × 940
2459.7	40643	1	3053	0 + 2 × 940 + 1185

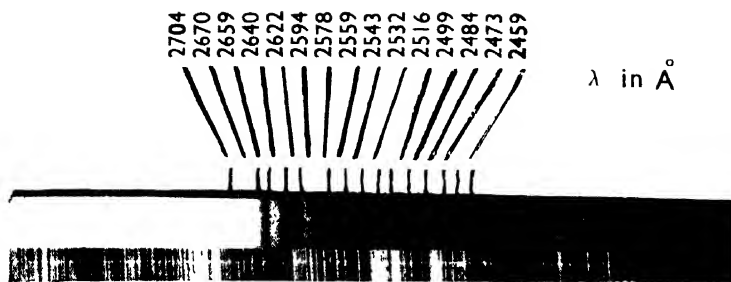


Fig. 1. Absorption Spectrum of Cyclohexylbenzene

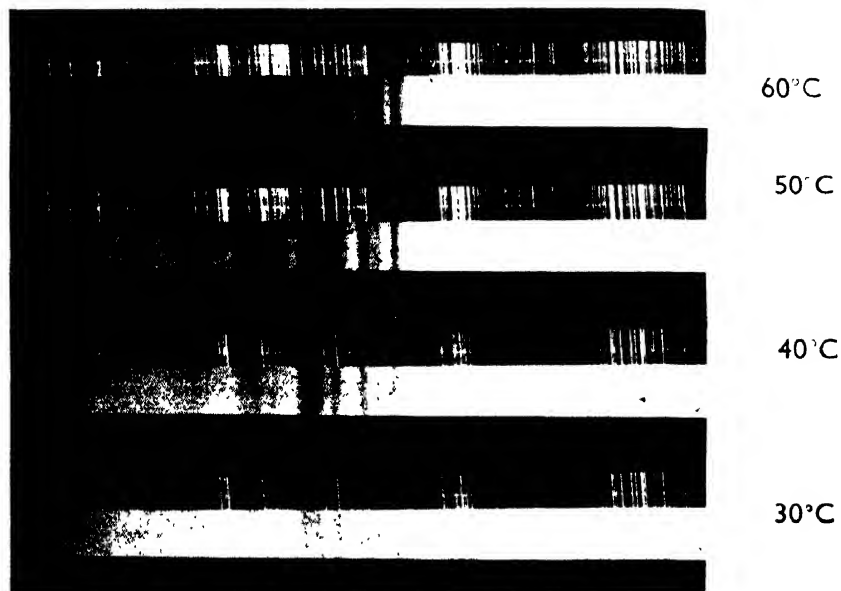


Fig. 2. Effect of Temperature on Absorption Spectrum of Cyclohexylbenzene

is given in fig.1 and Fig. 2 (Plate 7). Increasing the temperature further was found to be of no use and no new bands appear. The data on the observed bands together with the proposed assignments are given in Table I. The analysis is discussed above :

DISCUSSION

Cyclohexyl benzene may be considered as a monosubstituted benzene. The bands observed are all broad and diffuse. The principal progression with frequency of 940 is observed as in most cases of substituted benzene. This progression can be explained as due to the excited state frequency corresponding to the totally symmetric frequency near about 1000cm^{-1} in the ground state, which corresponds to the totally symmetric vibration frequency 992cm^{-1} in benzene. This excited state frequency 940cm^{-1} in case of cyclohexyl benzene corresponds to the ground state frequency 999cm^{-1} given by Raman spectrum. The second intense band at 38118cm^{-1} is separated from the 0,0 band by 528cm^{-1} . This excited state frequency is found to be in combination with other excited state frequencies and can be correlated with the ground state frequency 624cm^{-1} observed in the Raman spectrum. The third excited state frequency 1185cm^{-1} can be correlated with the ground state frequency 1203cm^{-1} observed in the Raman effect. All the observed bands could be assigned in terms of these three excited state frequencies. On the longer wavelength side when the temperature is raised two bands appear with ground state frequencies 155cm^{-1} and 629cm^{-1} . These could be assigned as due to the ground state frequencies 147cm^{-1} and 624cm^{-1} observed in the Raman spectrum. It has been observed that the monosubstituted benzenes have a very characteristic Raman band near 620cm^{-1} and this has been the case in cyclohexyl benzene also. As such the interpretation of the spectrum of cyclohexyl benzene as the spectrum of a monosubstituted benzene is justified.

REFERENCE

- Robertson, W. W., Music J. F. and Matsen F. A., 1950, *Journal American Chemical Soc.* **72**, 5260.

MAGNETIC SUSCEPTIBILITY AND LIGAND FIELD BEHAVIOUR OF PURE AND DILUTED CRYSTALS OF $\text{FeSiF}_6 \cdot 6\text{H}_2\text{O}$

MANJU MAJUMDAR AND SUNIL K. DATTA

INDIAN ASSOCIATION FOR THE CULTIVATION OF SCIENCE, CALCUTTA-32.

(Received January 28, 1967)

ABSTRACT. The magnetic anisotropy and susceptibility of $\text{FeSiF}_6 \cdot 6\text{H}_2\text{O}$ have been measured in the temperature range $300^\circ - 90^\circ\text{K}$. No phase transition has been observed in this crystal, in contrast to the case of the isomorphous cobalt and manganese salts. Measurements on crystals diluted with $\text{ZnSiF}_6 \cdot 6\text{H}_2\text{O}$ in ratios of 1 : 1 and 1 : 10 show that the dilutions do not radically modify the nature and symmetry of the ligand field at the ferrous ion, as in the latter cases. However, the experimental data may be fitted with a refined theory (which includes the effects of the trigonal field and the spin orbit interaction and the covalency factors) on the plausible assumption that the anisotropic field parameter changes with temperature, the variations being more drastic in the dilute crystals than in the pure in the temperature range studied. The available e.s.r. data have been analysed in the light of the above findings.

INTRODUCTION

Among the hexahydrated fluosilicates of the iron group of elements, the ferrous salt is one of the most extensively studied from the magnetic and optical (including e.s.r. and Mössbauer spectra), as well as structural standpoints. The neutron diffraction analysis of the crystal by Hamilton (1962) shows the space group to be $R\bar{3}m$ with one molecule in the unit cell. Each Fe^{2+} ion is surrounded by six oxygens from the ligands, the octahedron being *elongated* along the $[111]$ axis which coincides with the trigonal axis of the crystal. On the other hand, the magnetic susceptibility data of Jackson (1959) and Ohtsuka (1959) in the range $77^\circ - 1^\circ\text{K}$ show that the susceptibility along the trigonal axis, $\chi_{||}$, is smaller than that in the normal direction, χ_{\perp} , apparently indicating that the octahedron is *squat*, on the point charge model approach (see discussions).

The theory of the magnetic susceptibility of the crystal was worked out by Palumbo (1958) to explain Jackson's data, using the Spin Hamiltonian technique. However, only the lowest three levels in the ligand field and spin-orbit perturbations were taken into account on the assumption that $\Delta \gg |\lambda|$, where Δ is the trigonal field splitting parameter and λ the spin-orbit coupling coefficient.

In calculating the electric quadrupole moment of 14.4 keV state of ^{57}Fe from the Mössbauer spectra of $\text{FeSiF}_6 \cdot 6\text{H}_2\text{O}$, Eicher (1963) (see also Johnson, *et al.*, 1962; Ono and Ito, 1964) deduced expressions for fine structure energy

levels and magnetic susceptibility. He showed that the value of Δ which had been taken to be 1200 cm^{-1} , was too high and should be $\sim 750\text{ cm}^{-1}$ to fit the susceptibility as well as the electric quadrupole moment data. However, he did not consider the effects of the overlap of the 3d electron orbitals with the ligand oxygen orbitals. These effects have been taken into account by Bose and Rai (1965).

Previous investigations on other isomorphous crystals of this series, e.g., the manganese (Tsujikawa and Couture, 1955), cobalt (Majumdar and Datta, 1965) and copper salts (Thesis, Majumdar 1966, unpublished) reveal a phase transition in the region 220° – 270°K with the formation of a 'hybrid' crystal (Ubbelohde and Woodward, 1945) of a lower symmetry at low temperatures. Our magnetic data on the cobalt and copper salts indicate a drastic change in the ligand field symmetry and strength which accompanies the phase transition in these crystals. On diluting the crystals with the zinc or manganese salts the occurrence of the phase transition was found to be dependent on the nature of the diluent. It may be noted here that the neutron diffraction data (Hamilton, 1962) do not show any evidence of an order-disorder transformation in $\text{FeSiF}_6 \cdot 6\text{H}_2\text{O}$ down to 90°K .

In the present work we have investigated the magnetic behaviour of the undiluted ferrous salt, as well as those diluted with the zinc salt in different proportions with a view to studying phase transition effects if any, and to correlate the refined theory of Bose and Rai (1965) with our experimental data in the range 300° – 90°K , as also those of Jackson (1959) at 77°K and lower.

EXPERIMENT AND RESULTS

Ferrous fluosilicate was prepared by dissolving 99.9% pure iron wire in cold dilute hydrofluosilicic acid (prepared by the gradual action of powdered quartz with dilute hydrofluoric acid). The solution was concentrated in a desiccator connected to a water pump and crystallized over sulphuric acid in a nitrogen atmosphere. The pale green prismatic crystals gave an assay value of 99.5% Fe^{2+} and were almost indefinitely stable when stored in a cool and dry atmosphere. The zinc salt was prepared from reagent quality zinc carbonate and H_2SiF_6 , followed by evaporation and crystallization. Mixed crystals were prepared and analysed in the usual manner. In all cases repeated fractional crystallization was performed to achieve the highest degree of purity.

The magnetic anisotropy, $\Delta\chi$, of the crystals was measured in a torsion balance reported earlier (Majumdar and Datta, 1965). No detectable anisotropy was observed down to 90°K in the plane normal to the trigonal (*c*) axis in either the pure or the diluted crystals. Measurements in different planes containing the *c* axis gave identical anisotropy, as shown in figure 1, which includes results for two such orientations. Neither any sharp change in colour nor any abnormal thermal expansion of the crystal was observed. These facts reveal that these ferrous

salts do not undergo any change in crystallographic, and hence magnetic symmetry in the temperature range studied, in contrast to the case of the cobalt and cobalt-manganese mixed crystals.

For the measurement of magnetic susceptibility, χ_i , a Curic-type torsional balance designed by Bose *et al.*, (1964) was used. The crystal was mounted with the *c*-axis vertical and the susceptibility measured in the horizontal plane. The

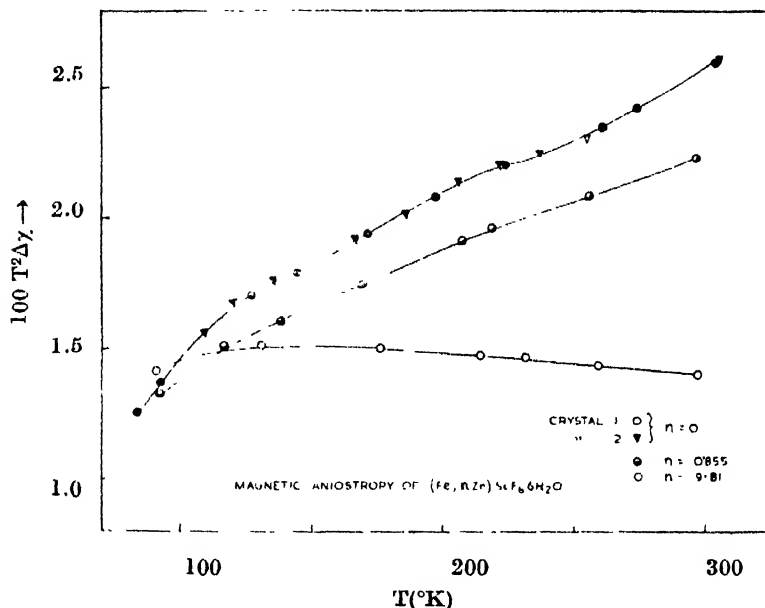


Fig. 1. Magnetic anisotropy of $(\text{Fe}, n\text{Zn}) \text{SiF}_6 \cdot 6\text{H}_2\text{O}$.

observed values of anisotropy and susceptibility, $(\Delta\chi)_{obs}$ and $(\chi_i)_{obs}$, per gm. mole of the mixed crystal were corrected for the diamagnetism of the constituents from the relationship :

$$(\chi_{\perp} - \chi_{\parallel})_p = (\chi_{\perp} - \chi_{\parallel})_{obs} - (n+1)(\chi_{\perp} - \chi_{\parallel})_{Zn} \quad (1)$$

$$(\chi_i)_p = (\chi_i)_{obs} - (n+1)\chi_{i_{Zn}}$$

where the quantities with the suffix *p* stand for the $\text{Fe}(\text{H}_2\text{O})_6^{2+}$ complex, the subscript *Zn* denotes the zinc salt and in (2) the suffix *i* stands for \parallel and \perp , *n* being the number of moles of the zinc salt per mole of the ferrous salt (evidently *n* is zero for the undiluted crystal when the residual diamagnetic term in (1) refers to the Fe^{2+} salt only), the difference in the diamagnetism of the ion cores of Fe^{2+} and Zn^{2+} being neglected in comparison with $\Delta\chi$ and χ_i . The diamagnetic susceptibilities of the zinc salt were found to be : $\chi_{\perp} = -135.8$ and $\chi_{\parallel} = -136.6$ in the usual 10^{-6} cgs em units, and were found to be temperature independent.

The anisotropy data for *n* = 0, 0.855 and 9.81 are shown in figure 1. However, the susceptibility data for only the first two are shown in figure 2, since the

relatively large dilution in the remaining crystal rendered the susceptibility values somewhat inaccurate. The interpolated values of the anisotropy and sus-

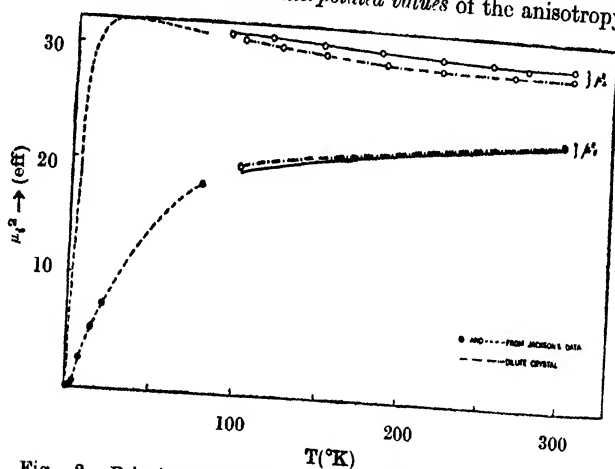


Fig. 2. Principal magnetic moments of $(\text{Fe}, n\text{Zn}) \text{SiF}_6 \cdot 6\text{H}_2\text{O}$.

ceptibilities at 20°C intervals of temperature for the pure and the 1 : 0.855 crystals are presented in tables I and II, respectively.

THEORY OF TRIGONALLY DISTORTED $\text{Fe}(\text{H}_2\text{O})_6^{2+}$ COMPLEX

The ground state $3d^6 {}^5D$ of Fe^{2+} ion is split in a field of O_h symmetry into a ground triplet, 5T_2 , and an upper doublet, 5E . Optical spectra of the pure crystal as also that containing 10% of the Fe^{2+} salt (Agnetta *et al.*, 1962) show a main vibronic band at 10.58 kK (1 kK = 10^3 cm^{-1}) which remains practically unchanged in position at 300° , 90° and 4°K , so that the difference between the mean cubic field levels may be taken to have this value. The wave functions for the 5T_2 state may be written as (labelling a state with its M_L value) :

$$T_{2g}^+ = \sqrt{\frac{2}{3}} |2\rangle - \sqrt{\frac{1}{3}} |-1\rangle$$

$$T_{2g} = |0\rangle$$

... (3)

$$T_{2g}^- = \sqrt{\frac{2}{3}} |-2\rangle + \sqrt{\frac{1}{3}} |1\rangle$$

while those for the upper 5E state are

$$E_g^+ = \sqrt{\frac{1}{3}} |2\rangle + \sqrt{\frac{2}{3}} |-1\rangle$$

$$E_g^- = \sqrt{\frac{1}{3}} |-2\rangle - \sqrt{\frac{2}{3}} |1\rangle$$

(4)

Under a trigonal distortion of the octahedral field the split components of $T_{2g} \pm$ will mix with those of $E_g \pm$ from which it is possible to calculate the admixtural coefficients $\alpha_{||}$, α_{\perp} along and normal to the trigonal field axis (Abragam and Pryce, 1951; Bose and Rai, 1965). In our present work we shall take $\alpha_{||}$, α_{\perp} to be adjustable parameters. We then make use of the fact that the set of wave functions (3) behave as atomic P -functions with an effective orbital quantum number $L' = 1$. Using the technique of Abragam and Pryce (1951) we classify the states according to the $m(=M_{L'}+M_S)$ values. The Hamiltonian for the trigonal field and spin-orbit interaction is then written as

$$H = \Delta(1-L_z'^2) + \zeta_{||}L_z'S_z + \zeta_{\perp}(L_x'S_x + L_y'S_y) \quad \dots (5)$$

where $\zeta_i (i = || \text{ or } \perp)$ is the spin orbit coupling coefficient along and normal to the trigonal axis, reduced from the free ion value and rendered anisotropic because of covalent overlap between central ion and ligand charge clouds.

The 15×15 matrix corresponding to $M_{L'} = 1, 0, -1$ and $M_S = 2, 1, 0, -1, -2$ can then be broken up into two cubic (for $m = 0, m = \pm 1$, the former further reducing to a quadratic and a linear equation), a quadratic (for $m = \pm 2$) and a linear (for $m = \pm 3$) equations. The final expressions for the nine energy values are :

(a) $m = 0$:

$$E_s = \frac{1}{2}[(\alpha_{||}\zeta_{||} + \Delta) \pm \{(\alpha_{||}\zeta_{||} - \Delta)^2 + 24\alpha_{\perp}\zeta_{\perp}^2\}^{1/2}] \quad \left. \begin{array}{l} \\ (-ve \quad \text{for } s = 0, \quad +ve \quad \text{for } s = 5) \end{array} \right\} \quad \dots (6)$$

$$E_s = \alpha_{||}\zeta_{||} \quad (\text{for } s = 4)$$

(b) $m = \pm 1$:

$$E_j = \alpha_{||}\zeta_{||}x_j \quad (j = 1, 3, 6) \text{ where } x_j\text{'s are the roots of the cubic}$$

equation

$$x^3 - (2+A)x^2 + (2A-5B^2)x + 6B^2 = 0 \quad \dots (7)$$

$$A = (\Delta/\alpha_{||}\zeta_{||}), \quad B = (\alpha_{\perp}\zeta_{\perp}/\alpha_{||}\zeta_{||})$$

(c) $m = \pm 2$:

$$E_t = \frac{1}{2}[(\Delta - \alpha_{||}\zeta_{||}) \pm \{(\Delta + \alpha_{||}\zeta_{||}) + 8\alpha_{\perp}\zeta_{\perp}^3\}^{1/2}] \quad \left. \begin{array}{l} \\ -ve \quad \text{for } t = 2, \quad +ve \quad \text{for } t = 7 \end{array} \right\} \quad \dots (8)$$

(d) $m = \pm 3$:

$$E_8 = -2\alpha_{||}\zeta_{||} \quad \dots (9)$$

Here, and in the following expressions the suffix j stands for $p = 1, 3, 6, s$ for $p = 0, 4, 5$, and t for $p = 2, 7, p = 0, 1, \dots 8$ representing the nine energy levels. The levels corresponding to E_s are singlets, while the rest are doublets.

The principal magnetic susceptibilities of the $\text{Fe}(\text{H}_2\text{O})_6^{2+}$ complex, K_{\parallel} and K_{\perp} along and normal to the trigonal axis, are then calculated from the first and second order Zeeman terms,

$$\langle \psi_{nm} | \mu | \psi_{nm} \rangle \text{ and } \sum_{n,m} | \langle \psi_{nm} | \mu | \psi_{n'm'} \rangle |^2$$

$E_n - E'_{n'}$

where the magnetic moment operator μ takes the form

$$\mu_{\parallel} = \beta(-\alpha_{\parallel}k_{\parallel}L_z' + 2S_z)$$

and

$$\mu_{\perp} = \beta[-\frac{1}{2}\alpha_{\perp}k_{\perp}(J_{+}' + J_{-}') + (S_{+} + S_{-})]$$

for the \parallel and \perp directions of the ligand field, respectively. The final expression for susceptibility is

$$K_{\eta} = \frac{N\beta^2}{kTZ} \left[\frac{1}{T} \left\{ \sum_{p=0}^8 G_{1\xi}^{(p)} \exp \left(-\frac{E_p - E_0}{kT} \right) \right\} + 2k \left\{ \sum_{p=0}^8 G_{2\xi}^{(p)} \exp \left(-\frac{E_p - E_0}{kT} \right) \right\} \right] \quad \dots \quad (10)$$

where

$$\xi = z \text{ for } \eta = \parallel$$

and

$$\xi = x = y \text{ for } \eta = \perp,$$

$G_{1\xi}^{(p)}$ and $G_{2\xi}^{(p)}$ are the first and the second order Zeeman terms defined above, Z is the partition sum $\sum_p W \exp (E_0 - E_p)/kT$, W being the degeneracy of the p -th level. In the following expressions for the G 's, q is a floating index which takes the values as indicated.

$$G_{1z}^{(j)} = 2\{\alpha_{\parallel}k_{\parallel}(c_j^2 - a_j^2) + 2b_j^2 + 4c_j^2\}^2 \quad j = 1, 3, 6$$

$$G_{1z}^{(s)} = 0$$

$$G_{1z}^{(t)} = 2[b_2^2(2 - \alpha_{\parallel}k_{\parallel}) + 4a_2^2]^2 \quad \text{for } t = 2$$

and

$$= 2[a_2^2(2 - \alpha_{\parallel}k_{\parallel}) + 4b_2^2]^2 \quad \text{for } t = 7$$

$$G_{1z}^{(8)} = 2(4 - \alpha_{\parallel}k_{\parallel})^2$$

$$G_{2z}^{(j)} = \sum_q \{2(4 + \alpha_{\parallel}k_{\parallel})c_jc_q + 2b_jb_q - \alpha_{\parallel}k_{\parallel}a_ja_q\}(E_q - E_j)$$

$$(q = 1, 3, 6; \quad q \neq j)$$

$$G_{2z}^{(t)} = 2(2 + \alpha_{\parallel}k_{\parallel})^2 a_2 b_2 (E_q - E_j) \quad (q = 2, 7; \quad q \neq t)$$

$$G_{2s}^{(s)} = \sum \{2 | \langle s | \mu_{||} | q \rangle |^2 / (E_q - E_s)$$

$$q (= 0, 4, 5; \quad q \neq s)$$

$$\begin{aligned} | \langle s | \mu_{||} | q \rangle |^2 &= 2a_0^2(2 + \alpha_{||}k_{||})^2 \quad \text{for } s, q = 0, 4 \\ &= 2b_0^2(2 + \alpha_{||}k_{||})^2 \quad \text{for } s, q = 4, 5 \\ &= 0 \quad \text{for } s, q = 5, 0 \end{aligned}$$

$$G_{2s}^{(s)} = 0$$

$$G_{1s}^{(s)} = 0$$

$$G_{2s}^{(j)} = \sum_s 2A_{sj}^2 / (E_s - E_j) + \sum_t 2B_{tj}^2 / (E_t - E_j)$$

$$G_{2s}^{(s)} = \sum_s 2A_{sj}^2 / (E_j - E_s)$$

$$G_{2s}^{(t)} = \sum_j 2B_{tj}^2 / (E_j - E_t) + 2C_t^2 / (E_t - E_s)$$

$$G_{2s}^{(s)} = \sum_t 2C_t^2 / (E_t - E_s).$$

where

$$A_{sj} = \sqrt{6} (a_0 a_j + b_0 b_j) - \frac{\alpha_1 k_1}{\sqrt{2}} (a_j b_0 + b_j a_0) + 2c_j a_0, \quad (s = 0)$$

$$A_{sj} = \sqrt{3} a_j + \frac{b_j k_1}{\sqrt{2}} - \sqrt{2} c_j, \quad (s = 4)$$

$$\begin{aligned} A_{sj} &= \sqrt{3} (b_0 a_j - 2a_0 b_j) - \frac{\alpha_1 k_1}{\sqrt{2}} (b_0 b_j - 2a_0 a_j) \\ &\quad + \sqrt{2} b_0 b_j \quad (s = 5) \end{aligned}$$

$$B_{tj} = (\sqrt{6} b_2 a_j + 2a_2 b_j) - \frac{\alpha_1 k_1}{\sqrt{2}} (b_2 b_j + a_2 c_j), \quad (t = 2)$$

$$B_{tj} = (\sqrt{6} a_2 a_j - 2b_2 b_j) - \frac{\alpha_1 k_1}{\sqrt{2}} (b_j a_2 - c_j b_2), \quad (t = 7)$$

$$C_t = \left(2b_2 - \frac{\alpha_1 k_1}{\sqrt{2}} a_2 \right), \quad (t = 2)$$

$$= \left(2a_2 + \frac{\alpha_1 k_1}{\sqrt{2}} b_2 \right), \quad (t = 7)$$

$$a_0 = \{\sqrt{3} \alpha_{\perp} \zeta_1 / (\alpha_{\parallel} \zeta_{\parallel} - E_0)\} b_0; \quad 2a_0^2 + b_0^2 = 1$$

$$a_j = \frac{\sqrt{3}(2\alpha_{\parallel} \zeta_{\parallel} - E_j)}{\sqrt{2} E_j} \quad c_j; \quad b_j = \frac{2\alpha_{\parallel} \zeta_{\parallel} - E_j}{\sqrt{2} \alpha_{\perp} \zeta_1} \quad c_j$$

$$a_j + b_j^2 + c_j^2 = 1$$

$$a_2 = \frac{\sqrt{2} \alpha_{\perp} \zeta_1}{\Delta - E_2} b_2; \quad a_2^2 + b_2^2 = 1$$

and k_i 's ($i = \parallel, \perp$) are the orbital reduction factors along and normal to the three-fold axis of the complex.

DISCUSSIONS

Our magnetic measurements show the absence of any phase change in ferrous fluosilicate, as has been observed in the manganese, cobalt and copper salts. The structure of all these salts appears to be the same at room temperature (Pauling, 1930) and is a close-packed one. The reason why phase transition occurs in only some of these crystals and not in others is not yet clear. The thermal stability of the crystals is probably more directly related to the geometry of the packing and lattice dynamical conditions than to the configurational instability of the metal-ligand complex arising from the electronic degeneracy of the central ion (Jahn Teller effect). It may be noted that both Co^{2+} and Fe^{2+} have an orbital triplet level lying lowest in a cubic field which splits leaving lowest either a singlet or a Kramers' doublet under the action of the lower symmetry field and spin orbit coupling and should, therefore, be stabilized against Jahn-Teller distortions (Van Vleck, 1960).

Because of the non-occurrence of a phase transition in either of the Fe^{2+} and Zn^{2+} salts in the temperature range studied, the effect of the latter in the mixed crystals is mainly to 'dilute' former ions in the lattice, in contrast to the case of the Co, Zn mixed crystals whose magnetic (and similar) properties are quite different from those of the cobalt salt which shows a phase transition at low temperatures (Majumdar and Datta, 1965). Thus, for instance, the $T^2 \cdot \Delta\chi$ vs. T curve for the Fe^{2+} salt and that diluted with about an equal part of Zn^{2+} are very similar (see figure 1). However, the slope of these curves decreases with increasing dilution, indicating that the strength of the anisotropic ligand field and its thermal variation is dependent upon changes in the crystal lattice brought about by dilution and their induced effects on the primary $\text{Fe}(\text{H}_2\text{O})_6^{2+}$ cluster (Van Vleck, 1939). The effect of dilution on the e.s.r. g -values is discussed later.

In calculating the energy levels from the above theory one observes that the lowest level turns out to be a singlet for negative values of Δ while it is a doublet for positive values of it. The susceptibility data of Jackson (1959)

at low temperatures, as well as our data at high temperatures can be explained only on the assumption of negative values of Δ . The resulting energy level structure and the nature of the thermal variation of susceptibility are mainly responsible for the observed fact that $\chi_{\perp} > \chi_{\parallel}$ in the temperature range studied, although the $\text{Fe}(\text{H}_2\text{O})_6$ octahedron is shown to be elongated from the neutron diffraction data (Hamilton 1962).

In correlating the theoretical expressions for the susceptibilities of the ionic complex, K_i , with the experimental values, χ_i , ($\chi_i \equiv K_i$, there being one molecule in the unit cell), we have obtained by trial and error a set of values of α_i , k_i , ζ_i ($i = \parallel, \perp$) and Δ which would give the best fit with the anisotropy and susceptibility data. We have assumed the first three parameters to be temperature independent, only Δ being assumed to vary with temperature (Bose, *et al.* 1960, *et seq.*). As mentioned earlier, Eicher (1963) chose the variable to be the Figgis parameter δ ($= \Delta/|\lambda|$). He found that δ varied with temperature in the range $1^\circ\text{--}77^\circ\text{K}$ from 6 to 9 in the perpendicular direction but remained constant at 7.5 in the axial direction. However, there seems to be absolutely no reason why δ should be different in the two directions and vary with T in only one of them while remaining constant in the other. Furthermore, as already mentioned, he did not take into consideration the covalency factors, as we have done here. In the table III we have given the values of the fixed parameters at the top and have shown how Δ has to be varied with T to give a good fit with the experimental data.

The values of the parameters $\alpha_i k_i$ and $\alpha_i \zeta_i$ chosen here are of the expected order of magnitude, since the admixture coefficients α_i are likely to be only slightly less than 1, the spin orbit coupling being small; furthermore, the orbital and spin orbit reduction factors are generally known to be between 0.8 and 0.9 for the $\text{M}(\text{H}_2\text{O})_6^{2+}$ complexes. The energy levels thus calculated have been labelled here as E_0, E_1, \dots, E_8 in order of increasing energies. It may be noted that the calculated values of the moments, μ_i , are much less sensitive to variations in $\alpha_i k_i$ and $\alpha_i \zeta_i$ than to changes in Δ in the temperature range studied. For the sake of completeness we have included the experimental data of Jackson (1959)* in the range 4.2° and 77°K in the above table and have also shown the calculated values obtained with the chosen ligand field parameters. It will then be seen that Δ has to be varied from -685 cm^{-1} at 300°K to -830 cm^{-1} at 77°K and then changed to -730 cm^{-1} at 4.2°K for the undiluted crystal. For the diluted crystal, however, the variations are much larger, Δ changing from -600 cm^{-1} at 300°K to -1065 cm^{-1} at 100°K . The substitution of Zn^{2+} for Fe^{2+} in the dilute crystal thus appreciably affects the ligand field behaviour of the $\text{Fe}(\text{H}_2\text{O})_6^{2+}$ complex.

*The values of χ_{\perp} had to be obtained by suitable transposition of his graph for χ_{\perp} vs. T , and are necessarily approximate.

TABLE I

Magnetic anisotropy and susceptibilities of $\text{FeSiF}_6 \cdot 6\text{H}_2\text{O}$
(interpolated values in 10^{-6} cgs c.m. units)

$T(^{\circ}\text{K})$	$\Delta\chi$	χ_1	χ_{II}	$\bar{\chi}$
300	2,854	12,467	9,613	11,516
280	3,121	13,325	10,204	12,285
260	3,457	14,350	10,893	13,198
240	3,906	15,587	11,681	14,285
220	4,534	17,091	12,557	15,580
200	5,230	18,900	13,670	17,157
180	6,117	21,167	15,050	19,128
160	7,313	23,938	16,625	21,501
140	9,036	27,436	18,400	24,424
120	11,424	32,183	20,759	28,375
100	14,570	38,800	24,230	32,944
90	16,457	43,122	26,665	37,633

TABLE II

Magnetic anisotropy and susceptibilities of $\text{FeSiF}_6 \cdot 6\text{H}_2\text{O}$,
 $n\text{ZnSiF}_6 \cdot 6\text{H}_2\text{O}$ (interpolated values, in 10^{-6} cgs c.m. units),
($n = 0.855$).

$T(^{\circ}\text{K})$	$\Delta\chi$	χ_1	χ_{II}	$\bar{\chi}$
300	2,484	12,144	9,660	11,316
280	2,760	13,030	10,260	12,109
260	3,108	14,023	10,915	12,987
240	3,522	15,252	11,730	14,078
220	4,060	16,680	12,620	15,327
200	4,683	18,421	13,738	16,859
180	5,518	20,593	15,075	18,754
160	6,650	23,300	16,650	21,083
140	8,245	26,835	18,590	24,087
120	10,522	31,628	21,100	28,113
100	13,850	38,625	24,775	34,008

TABLE III

Thermal variation of the anisotropic field parameter, Δ , in(a) $\text{FeSiF}_6 \cdot 6\text{H}_2\text{O}$:

$$\alpha_{\parallel} k_{\parallel} = 0.8; \alpha_{\perp} k_{\perp} = 0.8; \alpha_{\parallel} \zeta_{\parallel} = -87 \text{ cm}^{-1}; \alpha_{\perp} \zeta_{\perp} = -90 \text{ cm}^{-1}$$

$T(^{\circ}\text{K})$	$-\Delta$ cm^{-1}	μ_{\parallel}		μ_{\perp}	
		obs.	calc.	obs.	calc.
300	685	4.802	4.812	5.463	5.460
250	730	4.752	4.732	5.468	5.465
200	770	4.676	4.650	5.497	5.487
150	800	4.573	4.550	5.534	5.500
100	815	4.401	4.365	5.570	5.540
(from Jackson's data, 1959)					
77.3	830	4.247	4.227	5.50	5.53
20.4	780	2.715	2.752	5.75	5.826
4.2	730	0.758	0.782	4.44	4.51

(b) $\text{FeSiF}_6 \cdot 6\text{H}_2\text{O}$, $n\text{ZnSiF}_6 \cdot 6\text{H}_2\text{O}$: ($n = 0.855$)

$$\alpha_{\parallel} k_{\parallel} = 0.8; \alpha_{\perp} k_{\perp} = 0.8; \alpha_{\parallel} \zeta_{\parallel} = 92 \text{ cm}^{-1}; \alpha_{\perp} \zeta_{\perp} = 94 \text{ cm}^{-1}$$

300	600	4.817	4.835	5.495	5.510
250	900	4.743	4.758	5.459	5.484
200	930	4.690	4.650	5.422	5.425
150	950	4.561	4.550	5.399	5.400
100	1065	4.497	4.470	5.403	5.412

Since the lowest level in ferrous fluosilicate is nondegenerate, E_0 , and the next higher level, E_1 , lies over 10 cm^{-1} higher up, no e.s.r. spectra can be observed in this crystal with the microwave frequencies and magnetic fields ordinarily used (Abragam and Pryce, 1951). E_1 being a doublet will of course, be split by the magnetic field, and an e.s.r. signal, if observed, will correspond to a forbidden transition. Some estimates of the effective g -values were therefore made by Palumbo (1958) from the susceptibility of Jackson (1959). Using a third order perturbation technique and considering only the three lowest energy levels, he showed that good fit with the experimental data could be obtained at low temperatures on the assumption $\Delta \gg |\lambda|$, if one used a fictitious spin quantum number, $S' = 2$ in the usual Spin Hamiltonian formula. The following values were deduced : $g_{\parallel} = 2.00$; $g_{\perp} = 2.12$; $D = 10.9 \text{ cm}^{-1}$; $\Delta = 1200 \text{ cm}^{-1}$. Almost the

same values were arrived at by Ohtsuka (1959) from his own a.c. susceptibility data at low temperatures. The fit with the experimental data above 77°K is very poor, apparently because of increased population of E_3 and higher levels at high temperatures.

Rubins (1962) has reported c.s.r. data in Fe, Zn mixed fluosilicates. He deduced the $g_{||}$ -values somewhat indirectly in crystals containing 2, 10, 20 per cent of the Fe^{2+} salt as 2.38, 2.4, 2.2, while g_{\perp} in only the first crystal was estimated as 2.6. These have been ascribed to transitions between the $M_s' = \pm 1$ doublet. For the undiluted crystal $g_{||}$ was found to be ~ 9 , ascribed by him to transitions in the $M_s' = \pm 2$ doublet. These transitions, usually forbidden, were assumed to occur because of second order splitting of the Zeeman levels.

We have calculated the first order g -values for transitions within the E_1 doublet from the corresponding wave functions ψ_{\pm} using the relationship :

$$g_{||} = 2 | \langle \psi_1 | -\alpha_{||} k_{||} L_z' + 2S_z | \psi_1 \rangle | ; \quad g_{\perp} = 2 | \langle \psi_1 | -\alpha_{\perp} k_{\perp} L_x' + 2S_x | \psi_{-1} \rangle |$$

which come out as : $g_{||} = 3.88$, $g_{\perp} = 0$, which are considerably different from those reported by Rubins. This apparently arises from the extensive substitution of Zn^{2+} for Fe^{2+} in the crystal lattice which modifies the ligand field behaviour at the Fe^{2+} ion in the crystal.

We are grateful to Prof. A. Bose, D.Sc., F.N.I., for his keen interest and helpful suggestions in connection with this work.

REFERENCES

- Abragam, A. and Pryce, M. H. L., 1951, *Proc. Roy. Soc.* **A205**, 135.
 Agnetta, G., Garfano, T., Palma-Vittorelli, M. B. and Palma, M. U. 1962, *Phil. Mag.* **7**, 495.
 Bose, A., Chakravarti, A. S., and Chatterjee, R., 1960, *Proc. Roy. Soc.* **A255**, 145.
 Bose, A., Dutta Roy, S. K., Ghosh, P. and Mitra, S., 1964, *Indian. J. Phys.* **37**, 505.
 Bose, A. and Rai, R. 1965, *Indian J. Phys.* **38**, 167.
 Eicher, H. 1963, *Z. Physik.* **171**, 582.
 Hamilton, W. C. 1962, *Acta Cryst.* **15**, 353.
 Jackson, L. C. 1959, *Phil. Mag.* **4**, 269.
 Johnson, C. E., Marshall, W. and Perlow, G. J. 1962, *Phys. Rev.* **126**, 1503.
 Majumdar, M. and Datta, S. K. 1965, *Jour. Chem. Phys.* **42**, 418.
 Ohtsuka, T. 1959, *Jour. Phys. Soc. Japan*, **14**, 1245.
 Ono, K. and Ito, A. 1964, *Jour. Phys. Soc. Japan*, **19**, 899.
 Palumbo, D. 1958, *Nuovo Cimento* [10] **8**, 271.
 Rubins, R. S. 1962, *Proc. Phys. Soc.* **80**, 245.
 Tsujikawa, I. and Couture, L. 1955, *Jour. Phys. Radium* **16**, 430.
 Ubbelohde, A. R. and Woodward, I. 1945, *Nature* **155**, 170.
 Van Vleck, J. H. 1939, *Jour. Chem. Soc.* **7**, 72.
 ———— 1960, *Physica* **26**, 544.

ON THE ELECTRIC-QUADRUPOLE TRANSITIONS OF THE OCTAHEDRAL COMPLEXES OF THE TRANSITION METAL IONS

A. S. CHAKRAVARTY

SAHA INSTITUTE OF NUCLEAR PHYSICS, CALCUTTA

(Received November 16, 1966; Resubmitted March 3, 1967)

ABSTRACT. The algebraic expressions for the oscillator strengths of the electric quadrupole transitions in kd^n octahedral complexes have been derived. The oscillator strength of a particular transition has been shown to be dependent on $\langle r^2 \rangle$ and the energy separation of the two states in which the transition is taking place. A misconception regarding $\langle r^2 \rangle$ has been pointed out, though fortunately it does not effect too much the magnitudes for the oscillator strengths.

INTRODUCTION

In this paper we derive the expressions for the oscillator strengths of the electric quadrupole transitions of kd^n ($k = 3, 4, 5; n = 1, 2, \dots, 9$) octahedral complexes. It is well-known that the oscillator strength of an electric quadrupole transition is of the order of 10^{-9} and therefore much too small compared to that of electric dipole ($f \approx 10^{-3}$ to 10^{-4}) and magnetic dipole ($f \approx 10^{-5}$ to 10^{-6}) transitions. But it may become important in those cases where the electric dipole or magnetic dipole transitions vanish or are abnormally low. We have also derived the algebraic expressions for the oscillator strengths of electric and magnetic dipole transitions which will be published, shortly. The $\langle \vec{r}^2 \rangle$ have been calculated using (a) hydrogenic, (b) Slater, (c) Richardson-Watson's wave functions. There is a misconception regarding such calculations for the crystalline complexes which has been cleared up. The details of this misconception has been discussed in details in the next chapter.

THEORY

The oscillator strength for the electric quadrupole transition is given by (Griffith, 1961)

$$f = \frac{2\pi^2 \nu c}{5m\hbar} \sum_{i,j} | \langle a | \vec{r}_i \vec{p}_j + \vec{r}_j \vec{p}_i | b \rangle |^2 \quad (1)$$

where i and j are the three components of the vectors. Eqn. (1) can be reduced to the standard form by using the relation

$$(E_a - E_b) \langle a | \vec{r}_j | b \rangle = \frac{1}{m} \langle a | (-i\hbar \vec{p}_j) | b \rangle \quad (2)$$

Eqn. (2) is valid provided the eigen functions a and b are the exact solutions of the Schrodinger's equation and therefore strictly valid for a single electron in a central force field (the hydrogen atom problem). Using Eqn. (2), we get

$$\begin{aligned} \langle a | \vec{r}_i \vec{p}_j + \vec{r}_j \vec{p}_i | b \rangle &= -2\pi i m v_{ab} \langle a | \vec{r}_i \vec{r}_j - \frac{1}{3} r^2 \delta_{ij} | b \rangle \\ &= -2\pi i m v_{ab} \langle a | \vec{N}_{ij} | b \rangle \end{aligned} \quad \dots (3)$$

where \vec{N}_{ij} is the quadrupole tensor and v is the energy difference in cm^{-1} between the ground and the excited state under consideration. The quadrupole tensor \vec{N}_{ij} for a single electron has for its components xy, yz, zx and $x^2 - y^2, z^2 - 1/3r^2$. In octahedral symmetry 0_h , (xy, yz, zx) form a basis for t_{2g} and $(x^2 - y^2, z^2 - 1/3r^2)$ form a basis for e_g . The quadrupole tensor for n electrons, therefore, has off-diagonal elements which form a basis for T_{2g} and diagonal elements forming a basis for E_g . It can be easily shown that the diagonal elements vanish between the ground term and all the excited terms. We are therefore left with only T_{2g} . Thus our Eqn. (3) can be written as,

$$\langle a | \vec{r}_i \vec{p}_j + \vec{r}_j \vec{p}_i | b \rangle = -2\pi i m v_{ab} \langle a | r_i r_j | b \rangle \quad \dots (4)$$

The Hamiltonian for Eqn. (2) is given by

$$H = \sum_{k=1}^n \left(\frac{1}{2m} p_k^2 - \frac{Ze^2}{r_k} \right) + \sum_{k < \lambda} \frac{e^2}{r_{k\lambda}} \quad \dots (5)$$

where p_k is the momentum vector of the k -th electron and r_k its distance from the nucleus, m the mass of the electron, $-e$ its charge, $+Ze$ the charge on the nucleus and $r_{k\lambda}$ the distance from the k -th to the λ -th electron. It is important to note that in the above Hamiltonian there is no term representing the potential energy for the crystalline electric field of a particular symmetry.

We now test the equivalence of both sides of Eqn. (4) by using the different types of wave functions i.e., the hydrogenic, Slater's or Hartree-Fock self consistent wave functions. We, however, notice in Eqn. (4) that the R.H.S. is always non-vanishing for crystalline complexes. When an ion enters into a crystalline complex with the ligands (negatively charged dipoles) surrounding it in a particular symmetry then there will be splitting of the energy levels of the ion due to the electrostatic interaction of the crystal field produced by the ligands (Bethe, 1929). For example, when $\text{Ti}^{3+}(3d^1)$ forms an octahedral complex, the $3d$ -state of the ion splits up into E_g (doublet) and T_{2g} (Triplet). The mean energy separation of E_g and T_{2g} is written as $10 Dq$. This is our v_{ab} in Eqn. (4) which is always non-zero for crystalline complexes. The matrix element $\langle a | r_i r_j | b \rangle$ is also non-zero because this is nothing but $\langle r^2 \rangle$ over the states a and b . Thus the R.H.S. of

Eqn. (4) is non-vanishing irrespective of the form of the wave functions chosen. Now, the matrix element on the L.H.S. of Eqn. (4) can be shown to be

$$\frac{2\hbar}{i} \left(-\frac{1}{7\sqrt{3}} \right) \left[\int_0^\infty u(r)u'(r)dr + 2 \int_0^\infty ru(r) \frac{\partial u'(r)}{\partial r} dr \right] \quad (6)$$

after performing the angular integration with the wave functions

$$a(E_g \text{ type}) = \frac{u(r)}{r} Y_0^0$$

$$b(T_{2g} \text{ type}) = \frac{u'(r)}{r} \left[\frac{1}{i\sqrt{2}} (Y_2^2 - Y_2^{-2}) \right] \quad (7)$$

where

$$u(r) = rR(r) \quad \text{and} \quad u'(r) = rR'(r)$$

and the radial and angular wave functions are already normalized separately.

The reason for writing the two different radial functions for E_g and T_{2g} is that the E_g and T_{2g} wave functions interact differently with the cubic field (Watson, 1960). If, however, we assume the same radial function for both a and b (which is the usual practice), then $3d$ shell is spherical and will not interact with the cubic field. This can be easily verified by integrating the integral in Eqn. (6) by parts assuming $u(r) = u'(r)$, whence the third bracketed expression in Eqn. (6) is identically zero and this is true for all the three types of wave-functions (i.e., hydrogenic, Slater's and H-F wave functions). This means that the L.H.S. of Eqn. (4) goes to zero when the R.H.S. remains non-vanishing always. Thus it is proved that Eqn. (4) does no longer hold good for the crystalline complexes. The physical reason of such inequivalence can be understood from the following arguments. The above mentioned wave functions are true for an atom or ion but when this atom or ion forms a crystalline complex with the ligands then these wave functions are bound to be distorted due to the crystalline electric field created by the neighbouring ligands or in other words, the radial distribution of the electrons of the central ion gets somewhat altered and in any accurate calculation of the properties of such crystalline complexes we must use the accurate wave functions if they are available.

One method of constructing such wave functions would obviously be to start with the hydrogen atom problem after including in the total Hamiltonian a term containing the potential energy due to the crystal field and then try to solve the differential equation for the radial distribution which will now have different solution because of the crystal potential we have included. An analytical solution even for a single electron (the many electron solution would be enormously difficult to obtain) would be difficult to get but the numerical solution can be

obtained with the help of an electronic computer. In one case such wave functions have been obtained by Watson (1960) and this is for $\text{Mn}^{2+}(3d^5)$ in cubic field. In this case he has shown that the radial wave functions for E_g and T_{2g} would be different and he has found a very close agreement with experiment in his calculation for $10Dq$, including the sign of Dq (Kleiner, 1952). The wave functions are

$$\begin{aligned} U_{3z^2-r^2}(r) &= p_{12}N_{12}r^3 \exp(-Z_{12}r) + p_{13}N_{13}r^3 \exp(-Z_{13}r) \\ &\quad + p_{14}N_{14}r^3 \exp(-Z_{14}r) + p_{15}N_{15}r^3 \exp(-Z_{15}r) \quad \dots (8) \\ u'_{xy}(r) &= p'_{12}N_{12}r^3 \exp(-Z_{12}r) + p'_{13}N_{13}r^3 \exp(-Z_{13}r) \\ &\quad + p'_{14}N_{14}r^3 \exp(-Z_{14}r) + p'_{15}N_{15}r^3 \exp(-Z_{15}r) \end{aligned}$$

The magnitudes of p_{12} , N_{12} , Z_{12} , p'_{12} etc. are given in his paper (Watson, 1960) and we do not mention them here.

Using the above functions we have calculated both the sides of Eqn. (3) and find that the non-vanishing equivalence of Eqn. (4) is fully maintained.

Hence before calculating the oscillator strengths of the electric quadrupole transitions we must remember that we are using the correct crystal field wave functions in which case only we can proceed to calculate the R.H.S. of Eqn. (4). The matrix element $\langle \bar{r}^2 \rangle$ on the right hand side of Eqn. (4) does not vary too much (within 2%) whether we use the free ion wave functions or the cubic field wave functions. The following Table I gives the magnitudes of the radial part of the matrix element in atomic units for the different type of wave functions chosen :

TABLE I

Type of wave function	$\langle a \bar{r}_i \bar{r}_j b \rangle$ in A.U.
1. Hydrogenic or Slater	4.01780
2. Hartree-Fock	1.54803
3. Watson's Cubic Field	1.53955

It is evident from Table I that if we calculate the oscillator strengths using Hydrogenic or Slater's wave functions then the calculated values of the oscillator strengths would be about five times larger than those calculated with Hartree-Fock or Watson's cubic field wave functions.

Inserting Eqn. (4) in Eqn. (1), we get,

$$f = \frac{8\pi^4 m \nu^3 c}{5h} \sum_{i,j} |a| \eta_{ij} |b\rangle|^2 \quad (9)$$

where η is the pseudo-vector (yz, zx, xy).

Using Slater's determinantal wave functions and in the strong field approximation, the n electron matrix element is reduced ultimately to that of a single electron. The oscillator strength is then calculated in the usual way from Eqn. (9), where we use the following integrals :

$$\begin{aligned} \langle yz | \eta | z^2 \rangle &= \frac{1}{7\sqrt{3}} \langle \bar{r}^2 \rangle_{kd} & \langle zx | \eta | x^2 - y^2 \rangle &= \frac{1}{7} \langle \bar{r}^2 \rangle_{kd} \\ \langle yz | \eta | x^2 - y^2 \rangle &= -\frac{1}{7} \langle \bar{r}^2 \rangle_{kd} & \langle xy | \eta | z^2 \rangle &= -\frac{2}{7\sqrt{3}} \langle \bar{r}^2 \rangle_{kd} \\ \langle zx | \eta | z^2 \rangle &= \frac{1}{7\sqrt{3}} \langle \bar{r}^2 \rangle_{kd} & \langle xy | \eta | x^2 - y^2 \rangle &= 0 \end{aligned}$$

where

$$\langle \bar{r}^2 \rangle_{kd} = \int_0^\infty R_{kd}^2(r) r^4 dr \quad (K = 3, 4, 5) \quad \dots (10)$$

In Tables IIA, IIB and IIC, we have presented the values of $\langle \bar{r}^2 \rangle_{kd}$ for $k = 3, 4, 5$ for different values of E_{eff} in the approximations (a) and (b) calculated $\langle \bar{r}^2 \rangle_{kd}$ also in the approximation (c), since the SCF wave functions of Richardson *et al.* (Richardson 1962, 1963) are available only for $3d^n$ ions. The Table III gives the algebraic expressions for the oscillator strengths of the electric quadrupole transitions for the different configurations kd^n ($k = 3, 4, 5; n = 1$ through 9). For a particular value of k and n and for a particular complex, the oscillator strength for a particular transition can be immediately obtained from Eqn. (9) by inserting the proper values for ν , the energy difference in cm^{-1} and $\langle \bar{r}^2 \rangle_{kd}$ from the Tables IIA, IIB and IIC into Table III. Lastly in Table IV we present a few magnitudes of the oscillator strengths of the electric quadrupole transitions for aquo complexes of the $3d^n$ transition metal ions. The experimental energy separation, ν , between which the transition is taking place has been obtained mostly from Ballhausen (1962) and Jorgensen (1954, 1955) and also from current literatures. In our calculations we have taken $\langle \bar{r}^2 \rangle_{3d}$ from Table IIA obtained by using Richardson *et al.* wave functions.

From Table IV it is evident that the oscillator strengths are very small compared to those of the electric dipole ($f \sim 10^{-3} - 10^{-4}$) and magnetic dipole ($f \sim 10^{-5} - 10^{-6}$) transitions. Since there is no experimental data available on these transitions at the present we cannot compare our theoretical values.

TABLE IIA

Variation of $\langle r^2 \rangle_{3d}$ with E_{eff} using Hydrogenic or Slater and Richardson *et al.* wave function.

	Z_{eff}	$\langle r^2 \rangle_{3d}$ using hydrogenic or Slater wave function	Ions	$\langle r^2 \rangle_{3d}$ using wave function of Richardson <i>et al</i>
1.	3.5	2.880534×10^{-16}	Ti ³⁺	0.239096×10^{-16}
2.	4.0	2.205409×10^{-16}	V ³⁺	0.212284×10^{-16}
3.	5.0	1.411462×10^{-16}	V ²⁺	0.240972×10^{-16}
4.	6.5	0.835184×10^{-16}	Cr ³⁺	0.191940×10^{-16}
5.	7.5	0.627316×10^{-16}	Cr ²⁺	0.21480×10^{-16}
6.	8.5	0.488395×10^{-16}	Mn ³⁺	0.173456×10^{-16}
7.	9.5	0.390986×10^{-16}	Mn ²⁺	0.192286×10^{-16}
			Fe ³⁺	0.157285×10^{-16}
			Fe ²⁺	0.173982×10^{-16}
			Co ³⁺	0.143282×10^{-16}
			Co ²⁺	0.156598×10^{-16}
			Ni ²⁺	0.142880×10^{-16}
			Cu ²⁺	0.120423×10^{-16}

TABLE IIB

$\langle r^2 \rangle_{4d}$ Using Hydrogenic and Slater Wavefunctions with Varying Z_{eff}

	Z_{eff}	$\langle r^2 \rangle_{4d}$ Using Hydrogenic w.f.	$\langle r^2 \rangle_{4d}$ Using Slater w.f.
	4.0	8.821638×10^{-16}	4.730088×10^{-16}
	5.0	5.645848×10^{-16}	3.027256×10^{-16}
	6.0	3.920728×10^{-16}	2.102261×10^{-16}
	7.0	2.880534×10^{-16}	1.544518×10^{-16}
	8.0	2.205409×10^{-16}	1.182522×10^{-16}
	9.0	1.742545×10^{-16}	0.934338×10^{-16}
	10.0	1.411462×10^{-16}	0.756814×10^{-16}
	12.0	0.980182×10^{-16}	0.525565×10^{-16}

TABLE IIC

$\langle r^2 \rangle_{5d}$ Using Hydrogenic and Slater Wavefunctions with Varying Z_{eff}

Z_{eff}	$\langle r^2 \rangle_{5d}$ Using Hydrogenic w.f.	$\langle r^2 \rangle_{5d}$ Using Slater w.f.
4.0	$23.629387 \times 10^{-16}$	6.301170×10^{-16}
5.0	$15.122808 \times 10^{-16}$	4.032748×10^{-16}
6.0	$10.501950 \times 10^{-16}$	2.800520×10^{-16}
7.0	7.715718×10^{-16}	2.057524×10^{-16}
8.0	5.907346×10^{-16}	1.575292×10^{-16}
9.0	4.667533×10^{-16}	1.244675×10^{-16}
10.0	3.780702×10^{-16}	1.008187×10^{-16}
12.0	2.625487×10^{-16}	0.700130×10^{-16}

TABLE III

The oscillator strengths of electric-quadrupole transitions of octahedral kd^n complexes

Configuration	Transition ($g \rightarrow g$) (Ground State \rightarrow Excited St)	The Oscillator Strength f (Eqn. 9)	
kd^1	${}^2T_2 \rightarrow {}^2E$	$\frac{32}{735}$	$\frac{\pi^4 m v^3 c}{h} \langle \bar{r}^2 \rangle^2_{kd}$
kd^2	${}^3T_1 \rightarrow {}^3T_1$	$\frac{16}{245}$	$\frac{\pi^4 m v^3 c}{h} \langle \bar{r}^2 \rangle^2_{kd}$
	$\rightarrow {}^3T_2$	$\frac{16}{735}$	$\frac{\pi^4 m v^3 c}{h} \langle \bar{r}^2 \rangle^2_{kd}$
kd^3	${}^4A_2 \rightarrow {}^4T_1 \{t_{2g}^2 ({}^3T_1) e_g\}$	$\frac{32}{245}$	$\frac{\pi^4 m v^3 c}{h} \langle \bar{r}^2 \rangle^2_{kd}$
kd^4	${}^3T_1 \rightarrow {}^3A_2 \{t_{2g}^3 ({}^2E) e_g\}$	$\frac{32}{2205}$	$\frac{\pi^4 m v^3 c}{h} \langle \bar{r}^2 \rangle^2_{kd}$
	$\rightarrow {}^3E^{(1)} \{t_{2g}^3 ({}^4A_2) e_g\}$	$\frac{32}{2205}$	$\frac{\pi^4 m v^3 c}{h} \langle \bar{r}^2 \rangle^2_{kd}$
	$\rightarrow {}^3E^{(2)} \{t_{2g}^3 ({}^2E) e_g\}$	$\frac{32}{2205}$	$\frac{\pi^4 m v^3 c}{h} \langle \bar{r}^2 \rangle^2_{kd}$
	$\rightarrow {}^3T_1^{(1)} \{t_{2g}^3 ({}^2T_1) e_g\}$	$\frac{8}{735}$	$\frac{\pi^4 m v^3 c}{h} \langle \bar{r}^2 \rangle^2_{kd}$
	$\rightarrow {}^3T_1^{(2)} \{t_{2g}^3 ({}^2T_2) e_g\}$	$\frac{8}{245}$	$\frac{\pi^4 m v^3 c}{h} \langle \bar{r}^2 \rangle^2_{kd}$
	$\rightarrow {}^3T_2^{(1)} \{t_{2g}^3 ({}^2T_0) e_g\}$	$\frac{8}{245}$	$\frac{\pi^4 m v^3 c}{h} \langle \bar{r}^2 \rangle^2_{kd}$
	$\rightarrow {}^3T_2^{(2)} \{t_{2g}^3 ({}^2T_2) e_g\}$	$\frac{8}{735}$	$\frac{\pi^4 m v^3 c}{h} \langle \bar{r}^2 \rangle^2_{kd}$
	${}^5E(t_{2g}^3 ({}^4A_0) e_g) \rightarrow {}^5T_0(t_{2g}^3 ({}^3T_1) e_g ({}^3A_0))$	$\frac{16}{245}$	$\frac{\pi^4 m v^3 c}{h} \langle \bar{r}^2 \rangle^2_{kd}$
kd^5	${}^2T_2 \rightarrow {}^2A_1 \{t_{2g}^4 ({}^1E) e_g\}$	$\frac{32}{2205}$	$\frac{\pi^4 m v^3 c}{h} \langle \bar{r}^2 \rangle^2_{kd}$
	$\rightarrow {}^2E^{(1)} \{t_{2g}^4 ({}^1A_1) e_g\}$	$\frac{32}{2205}$	$\frac{\pi^4 m v^3 c}{h} \langle \bar{r}^2 \rangle^2_{kd}$

TABLE III (Continued)

Configuration	Transition ($g \rightarrow g$) (Ground State - Excited St)	The Oscillator Strength f (Eqn. 9)
	$\rightarrow {}^2E^{(2)}\{t_{2g}^4({}^1A_1)e_g\}$	$\frac{32}{2205} \frac{\pi^4 m v^3 c}{h} \langle \bar{r}^2 \rangle_{kd}^2$
	$\rightarrow {}^2T_1^{(1)}\{t_{2g}^4({}^3T_1)e_g\}$	$\frac{8}{245} \frac{\pi^4 m v^3 c}{h} \langle \bar{r}^2 \rangle_{kd}^2$
	$\rightarrow {}^2T_1^{(2)}\{t_{2g}^4({}^1T_2)e_g\}$	$\frac{8}{245} \frac{\pi^4 m v^3 c}{h} \langle \bar{r}^2 \rangle_{kd}^2$
	$\rightarrow {}^2T_2^{(1)}\{t_{2g}^4({}^3T_1)e_g\}$	$\frac{8}{245} \frac{\pi^4 m v^3 c}{h} \langle \bar{r}^2 \rangle_{kd}^2$
	$\rightarrow {}^2T_2^{(2)}\{t_{2g}^4({}^1T_2)e_g\}$	$\frac{8}{245} \frac{\pi^4 m v^3 c}{h} \langle \bar{r}^2 \rangle_{kd}^2$
kd^3	${}^1A_1 \rightarrow {}^1T_2\{t_{2g}^5({}^2T_2)e_g\}$	$\frac{64}{245} \frac{\pi^4 m v^3 c}{h} \langle \bar{r}^2 \rangle_k^2$
	${}^5T_2\{t_{2g}^4({}^3T_1)e_g^2({}^3A_2)\}$	
	$\rightarrow {}^5E\{t_{2g}^3({}^4A_2)e_g^3({}^2E)\}$	$\frac{32}{735} \frac{\pi^4 m v^3 c}{h} \langle \bar{r}^2 \rangle_k^2$
kd^7	${}^2E \rightarrow {}^2T_1^{(1)}\{t_{2g}^5({}^2T_2)e_g^2({}^1E)\}$	$\frac{8}{245} \frac{\pi^4 m v^3 c}{h} \langle \bar{r}^2 \rangle_{kd}^2$
	$\rightarrow {}^2T_1^{(2)}\{t_{2g}^5({}^2T_2)e_g^2({}^3A_2)\}$	$\frac{8}{245} \frac{\pi^4 m v^3 c}{h} \langle \bar{r}^2 \rangle_{kd}^2$
	$\rightarrow {}^2T_2^{(1)}\{t_{2g}^5({}^2T_2)e_g^2({}^1E)\}$	$\frac{8}{245} \frac{\pi^4 m v^3 c}{h} \langle \bar{r}^2 \rangle_{kd}^2$
	$\rightarrow {}^2T_2^{(2)}\{t_{2g}^5({}^2T_2)e_g^2({}^1A_1)\}$	$\frac{8}{245} \frac{\pi^4 m v^3 c}{h} \langle \bar{r}^2 \rangle_{kd}^2$
kd^7	${}^4T_1\{t_{2g}^5({}^2T_2)e_g^2({}^3A_2)\}$	
	$\rightarrow {}^4T_2\{t_{2g}^4({}^3T_1)e_g^3({}^2E)\}$	$\frac{16}{735} \frac{\pi^4 m v^3 c}{h} \langle \bar{r}^2 \rangle_{kd}^2$
	$\rightarrow {}^4T_1\{t_{2g}^4({}^3T_1)e_g^3({}^2E)\}$	$\frac{16}{245} \frac{\pi^4 m v^3 c}{h} \langle \bar{r}^2 \rangle_{kd}^2$
kd^8	${}^3A_2 \rightarrow {}^3T_1\{t_{2g}^5({}^2T_2)e_g^3({}^2E)\}$	$\frac{32}{245} \frac{\pi^4 m v^3 c}{h} \langle \bar{r}^2 \rangle_{kd}^2$
kd^9	${}^2E \rightarrow {}^2T_2$	$\frac{16}{245} \frac{\pi^4 m v^3 c}{h} \langle \bar{r}^2 \rangle_{kd}^2$

TABLE IV

The electric quadrupole oscillator strengths for the $3d^n$ transition metal ion aquo complexes

Configuration	5Ion	Complex	Transition ($g \rightarrow g$)	Energy difference (cm^{-1})	$f \times 10^9$
$3d^1$	Ti^{3+}	$\text{Ti}(\text{H}_2\text{O})_6^{3+}$	${}^2\text{T}_2 \rightarrow {}^2\text{E}$	20,300	0.0835
$3d^2$	V^{3+}	$\text{V}(\text{H}_2\text{O})_6^{3+}$	${}^3\text{T}_1 \rightarrow {}^3\text{T}_1$	25,200	0.1890
			$\rightarrow {}^3\text{T}_2$	17,100	0.0196
$3d^3$	Cr^{3+}	$\text{Cr}(\text{H}_2\text{O})_6^{3+}$	${}^4\text{A}_2 \rightarrow {}^4\text{T}_1$	24,500	0.0284
$3d^6$	Fe^{2+}	$\text{Fe}(\text{H}_2\text{O})_6^{2+}$	${}^5\text{T}_2 \rightarrow {}^5\text{E}$	10,400	0.0059
$3d^7$	Co^{2+}	$\text{Co}(\text{H}_2\text{O})_6^{2+}$	${}^4\text{T}_1 \rightarrow {}^4\text{T}_2$	8,200	0.0011
			$\rightarrow {}^4\text{T}_1$	20,000	0.0514
$3d^8$	Ni^{2+}	$\text{Ni}(\text{H}_2\text{O})_6^{2+}$	${}^3\text{A}_2 \rightarrow {}^3\text{T}_1$	14,700	0.0339
$3d^9$	Cu^{2+}	$\text{Cu}(\text{H}_2\text{O})_6^{2+}$	${}^2\text{E} \rightarrow {}^2\text{T}_2$	12,600	0.0076

ACKNOWLEDGMENT

The author wishes to express his sincere thanks to Dr. D. K. Ray of this Institute for many helpful discussions and useful comments and suggestions. Thanks are also due to Prof. A. K. Saha for his interest in the investigation.

REFERENCES

- Ballhausen, C. J., and Jorgensen, C. K., 1955, *Acta Chem. Scand.*, **9**, 397.
 Ballhausen, C. J., 1962, *Introduction to Ligand Field Theory*, McGraw-Hill Book Company, Inc., New York.
 Bothe, H. A., 1929, *Ann. Phys.*, **133**, 760.
 Griffith, J. S., 1961, *The Theory of Transition Metal Ions*, Cambridge University Press.
 Kleiner, W. H., 1952, *J. Chem. Phys.*, **20**, 1784.
 Richardson, J. W., Nieuwpoort, W. C., Powell, R. R. and Edgell, W. F., 1962, *J. Chem. Phys.*, **36**, 1057.
 Richardson, J. W., Powell, R. R., and Nieuwpoort, W. C., 1963, *J. Chem. Phys.*, **38**, 796.
 Watson, R. E., 1960, *Phys. Rev.*, **117**, 742.

NOTE ON ELECTRICAL RESPONSE IN A PIEZO-ELECTRIC PLATE TRANSDUCER WITH A PRESCRIBED INPUT

N. C. DAS

DEPARTMENT OF MATHEMATICS, JADAVPUR UNIVERSITY, CALCUTTA-32

(Received December 7, 1966)

ABSTRACT. The electrical signal produced by a transient mechanical force has been calculated for a piezoelectric plate with resistive loading at the electrical terminals.

INTRODUCTION

The investigation of responses (electrical or mechanical) in a piezoelectric transducer is doubtless, an important electromechanical problem in acoustics and ultrasonics, specially in the detection of ultrasonic waves. The mathematical treatment of the phenomena has been undertaken by Fillipczynski (1956), Redwood (1951, 1961, 1962). These papers have, in fact, contributed in a large measure to the recent studies in the topic by Sinha (1962a, 1962b, 1963, 1965) Giri (1965). As a sequel to this set of problems, the present note sets out to consider the problem of determining the electrical response in a piezoelectric plate transducer subjected to a mechanical force-input which is partly constant and partly transient.

PROBLEM, FUNDAMENTAL EQUATIONS AND BOUNDARY CONDITIONS

We consider here a piezoelectric plate transducer executing vibration in the thickness mode. Let the thickness direction of the transducer be taken in the direction of the x -axis and let its extremities be $x = 0$ and $x = X$. Our problem consists in determining the electrical response in a transducer owing to some prescribed mechanical inputs, and certain mode of displacements.

It has been shown by Redwood (1962) that under certain assumptions, ζ , the mechanical displacement in the x -direction satisfies within or without the transducer an equation of the type

$$\frac{\partial^2 \xi}{\partial t^2} = \frac{c}{\rho} \frac{\partial^2 \xi}{\partial x^2}$$

where c is the material constant and ρ is the density of the material of the transducer.

Let us seek a solution of the above equation in the form given by

$$\zeta = \phi \exp(-\omega t), \quad \omega > 0. \quad \dots (1)$$

so that ϕ satisfies
$$\frac{d^2\phi}{dx^2} - \frac{\omega^2}{v^2}\phi = 0 \quad \dots (2)$$

where
$$v^2 = \frac{c}{\rho},$$

Solving equation (2) we get,

$$\phi = A \exp\left(-\frac{\omega x}{v}\right) + B \exp\left(\frac{\omega x}{v}\right) \quad \dots (3)$$

where A, B are constants.

Following Redwood (1961) the mechanical force F exerted on an area normal to x and the electrical voltage V across the transducer are calculated as follows :

$$F + hQ = \omega Z_c \exp(-\omega t) \left\{ -A \exp\left(-\frac{\omega x}{v}\right) + B \exp\left(\frac{\omega x}{v}\right) \right\} \quad \dots (4)$$

$$V = -h\{(\xi)_x - (\xi)_0\} + \frac{Q}{C_0} \quad \dots (5)$$

where h is a piezoelectric constant of the material, Q the total charge at the surface of the transducer, C_0 the static capacitance of the transducer and Z_c the characteristic impedance of the material. Terms such as $(\xi)_x$ signify the value of ξ at $x = X$.

To ascertain the constants A and B , we must enumerate the boundary conditions of the problem. The most general type of this problem may be thought of by having a transducer of impedance Z_c situated between two systems of mechanical impedances Z_1 and Z_2 . Then the boundary conditions are that the stresses and displacements are continuous at $x = 0$ and $x = X$. We write, at $x = 0$

$$\begin{aligned} (F_1)_0 &= (F)_0 \\ (\xi_1)_0 &= (\xi)_0 \end{aligned} \quad \dots (6)$$

and at
$$x = X$$

$$\begin{aligned} (F_2)_X &= (F)_X \\ (\xi_2)_X &= (\xi)_X \end{aligned}$$

where ξ , F and V are given by the equations (1), (3), (4) and (5); and so

$$\xi = \exp(-\omega t) \left\{ A \exp\left(-\frac{\omega x}{v}\right) + B \exp\left(\frac{\omega x}{v}\right) \right\} \quad \dots \quad (7)$$

$$\xi_1 = \exp(-\omega t) \left\{ A_1 \exp\left(-\frac{\omega x}{v}\right) + B_1 \exp\left(\frac{\omega x}{v}\right) \right\} \quad \dots \quad (8)$$

$$F_1 = \omega Z_1 \exp(-\omega t) \left\{ -A_1 \exp\left(-\frac{\omega x}{v_1}\right) + B_1 \exp\left(\frac{\omega x}{v_1}\right) \right\} \quad \dots \quad (9)$$

$$\xi_2 = \exp(-\omega t) \left\{ A_2 \exp\left(-\frac{\omega x}{v_2}\right) + B_2 \exp\left(\frac{\omega x}{v_2}\right) \right\} \quad \dots \quad (10)$$

$$F_2 = \omega Z_2 \exp(-\omega t) \left\{ -A_2 \exp\left(-\frac{\omega x}{v_2}\right) + B_2 \exp\left(\frac{\omega x}{v_2}\right) \right\} \quad \dots \quad (11)$$

where the suffixes 1 and 2 denote the entities and constants of the systems of impedance Z_1 and Z_2 , respectively.

METHOD OF SOLUTION

We assume that the transducer is connected to a high-input impedance of resistance R , so that when $Z_2 \rightarrow \infty$, $(\xi)_x = 0$ and $A_2 = B_2 = 0$. From the conditions (6) the equations determining V are

$$V = -QR$$

$$A \exp\left(-\frac{\omega x}{v}\right) + B \exp\left\{\frac{\omega x}{v}\right\} = 0$$

$$A + B = A_1 + B_1 \quad \dots \quad (12)$$

$$\omega Z_1 \exp(-\omega t) \cdot (-A_1 + B_1) = \omega Z_c \exp(-\omega t) \cdot ((-A + B) - hQ).$$

$$V = h(A + B) \exp(-\omega t) - \frac{V}{C_0 R}$$

Eliminating A , B , B_1 and Q we get,

$$V \left(1 + \frac{1}{C_0 R}\right) = \frac{h \exp(-\omega t) \left\{ \exp\left(\frac{\omega X}{v}\right) - \exp\left(-\frac{\omega X}{v}\right) \right\} \left\{ 2A_1 Z_1 - \frac{hQ}{\omega} \exp(\omega t) \right\}}{(Z_c - Z_1) \exp\left(-\frac{\omega X}{v}\right) + (Z_c + Z_1) \exp\left(\frac{\omega X}{v}\right)} \quad \dots \quad (13)$$

The constant A_1 is to be determined from the applied mechanical input which is $F = F_0\{1 - \exp(-kt)\}$; $K > 0$ and F_0 is a constant. Since this is introduced at $x = 0$, we have,

$$-A_1 \omega Z_1 \exp(-\omega t) = F_0\{1 - \exp(-kt)\}.$$

so that

$$A_1 = - \frac{F_0\{1 - \exp(-kt)\}}{\omega Z_1} \exp(\omega t);$$

and equation (13) takes the form.

$$V = \frac{hc_0 R}{\omega(1+c_0 R)} \left\{ \exp\left(-\frac{\omega X}{v}\right) - \exp\left(\frac{\omega X}{v}\right) \right\} \\ \frac{2F_0\{1 - \exp(-kt) + hQ\}}{\left\{ (Z - Z_e) \exp\left(-\frac{\omega X}{v}\right) + (Z_e + Z_1) \exp\left(\frac{\omega X}{v}\right) \right\}}$$

This gives the electrical voltage i.e. the electrical response which is obviously a constant in part and transient in part.

I am thankful to Dr. D. K. Sinha, Jadavpur University for his guidance in the preparation of this paper.

REFERENCES

- Giri, R. R., 1966, *Rev. Roumaine, Tech. Scis. Serie. Mec. Applique*, **11**, 253.
 Fillipezynski, L. 1956, *Proc. Conf. Ultrasonics* Pan VI, Warsaw; 1957, 35.
 Redwood, M., 1961, *Jour. Acoust. Soc. Amer*, **33**, 527.
 ——— 1961, *Jour. Acoust. Soc. Amer.*, **33**, 1386.
 ——— 1962, *Jour. Acoust. Soc. Amer* **39**, 895.
 Sinha, D. K., 1962a, *Ind. Jour. Theor. Phys.* **10**, 21.
 ——— 1962b, *Appld. Phys. Qlly.*, **VIII**, 13.
 ——— 1963, *Ind. Jour. Theor. Phys.*, **11**, 93.
 ——— 1965, *Proc. Natl. Inst. Scis. Ind.*, **31A**, 395.

Letters to the Editor

The Board of Editors does not hold itself responsible for opinions expressed in the letter published in this section. The notes containing short reports of original investigations communicated to this section should not contain many figures and should not exceed 500 words in length. The contributions reaching the Secretary by the 15th of any month may be expected to appear in the issue for the next month. No proof will be sent to the author.

13

A NOTE ON 'HAMMER' TRACKS HAVING NO ASSOCIATED BETA-PARTICLE

G. C. DEKA

COTTON COLLEGE, GAUHATI

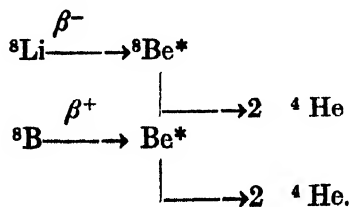
(Received March 25, 1967)

'Hammer' Tracks have been extensively investigated by many workers during recent years. And a good deal of information regarding their nature and mode of decays have been known. One thing, however, remains still obscure, e.g. in a large number of 'hammer' tracks the expected beta tracks are found to be absent. The percentage of this absence observed by various workers as listed in the following table is rather significant.

TABLE I

Reference	Beam Energy	Type of emulsions used	H.T. with no visible beta-track
Warsaw group	9 Gev/c protons	NIKFI—R	15%
-do-	24 Gev/c protons	Ilford G 5.	20%
Munir (1956)	950 Mev. protons	Ilford G 5.	22%
Deka et. al. (1961)	4.5 Gev/c π -mesons	Ilford G 5	40%
Pathak (1963)	3 Gev/c mesons	Ilford G 5	30%

It has been well known that most of the 'hammer' tracks are usually produced by the radio-active decays of ${}^8\text{Li}$ and ${}^8\text{B}$ nuclei. A few of them are believed to be due to ${}^8\text{He}$ and ${}^9\text{Li}$ also. The reactions take as follows



Each of the 'hammer' tracks produced in this way should invariably be associated with a beta particle (two beta-tracks in case of the ^6He only), the kinetic energy of these beta particles varies from a minimum to a maximum value according to the known distribution curve.

The mean ionisation potential for an emulsion nucleus is known to be 500 ev. A beta particle of energy $< 10\text{keV}$ can hardly be developed. In the early works with the less sensitive emulsions it was not possible to observe the beta tracks. But the G-5 and NIKFI R-emulsions have been very suitable to record the tracks of relativistic particles.

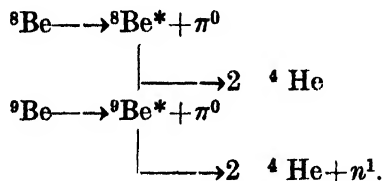
Hence, it has been rather difficult to explain the observed fact that in an appreciable number of cases the beta tracks are not seen. Two reasons seem to be obvious :—one is due to the observational bias, the other is due to the non-emission of beta particles.

The observational bias may arise due to the following causes :

1. the electrons having low energy of $\sim 15\text{keV}$ may not produce any observational tracks in the emulsions,
2. the high energy electrons which will produce a minimum ionizing track may easily be lost among the back-ground grains if the condition of the pellicles is not very good.

It is very essential that the emulsions should be fully developed and should be very clean in order to record and detect the beta tracks.

However, the contribution due to these causes should not be much higher than 7%. The real non-existence of the beta particles in some cases may be due to the decay of hyperfragments which subsequently give rise to the 'hammer' tracks. as follows :



REFERENCES

- Deka G., Evans D., Prowse D., and Baldo-ceolin, 1961, *Nuclear Physics* **24**, 657.
Gajewski, W., Pniewski, J., Pniewski, T., Sieminska, J., Soltan, M., Soltynski, K.
and Suchorzewska, J., 1961, *Warsaw Report* No. 286/vi., Dec.
Gajewski, W., Pniewski, J., Pniewski, T., Sieminska, J., Soltan, M., Soltynski, K.
and Falkowski, K., 1963, *Warsaw Report*, No. 297/vi. Feb.
Munir B. A. 1956, *Phil. Mag.* **1**, 355.
Pathak K. M., 1963, *D. Phil. thesis.*

ON THE EMISSION OF EXO ELECTRONS IN A GEIGER COUNTER

R. C. SASTRI AND S. D. CHATTERJEE

DEPARTMENT OF PHYSICS, JADAVPUR UNIVERSITY.

(Received August 29, 1967)

During the course of a study of the mechanism of Geiger counter discharge with reversed potentials it was observed that the number of cosmic ray background pulses increased substantially when the normal potential distribution was restored after operating the counter in the reversed direction for a few minutes. A closer inspection of the phenomenon soon revealed that this increase in the number of background pulses rapidly falls with time as shown in Fig. 1 which depicts a measurement of the time variation of the number of pulses. It is also evident that at a given moment the number of pulses per minute N and the time T are inversely proportional, satisfying an empirical relation of the type $N \times T = \text{constant}$. This fact is more clearly demonstrated by plotting the product of the number of pulses per minute N and time T which are shown as small circles in middle of Fig. 1.

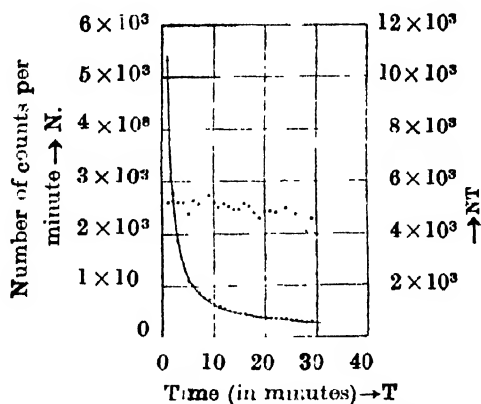


Fig. 1. Decay curve for the exo-electrons.

The observed increase in the number of pulses may be attributed to a copious emission of exo-electrons from the cylinder. This emission becomes more pronounced when the cylinder is made of colloidal graphite, a well-known semiconductor.

In a counter operating with reversed potentials, the electrons are collected by the positive cylinder. Some of these electrons are trapped by the lattice defects in the metallic cylinder which are released subsequently as exo-electrons when negative potential is restored to the cylinder. Indeed, such an emission of exo-

electrons was reported by Haxel *et al.* (1951) where the electrons trapped in lattice defects created by mechanical abrasion, were subsequently released as exo-electrons by heat treatment. Seeger (1955) also detected the emission of exo-electrons in cases where the crystal defects were created by chemical oxidation process and the after-emission was provoked by means of electron bombardment of energy of about 1000 ev. It is interesting to note that in the present study the curve shown in Fig. 1 closely resembles the time variation curve for exo-electrons obtained by Haxel *et al.*, (1951).

REFERENCES

- Haxel, O., Houtermans, F. G. and Seeger, K., 1951, *Zeit. f. Phys.* **130**, 122.
 Seeger, K., 1955, *Naturwiss.* **42**, 66.

15

CERTAIN THERMISTOR CHARACTERISTICS OF SINGLE CRYSTALS OF TUNGSTENITE (WS_2)

S. R. GUHA THAKURTA

MAGNETISM DEPARTMENT

INDIAN ASSOCIATION FOR THE CULTIVATION
 OF SCIENCE, CALCUTTA-32.

(Received August 21, 1967)

In order to further investigate the self heated thermistor property of naturally occurring tungstenite (WS_2) crystals (already reported, Guha Thakurta, 1967), its steady state current-voltage characteristics have been studied at different temperatures and pressures and for currents along both the crystallographic directions. Further, investigation has also been made under transient conditions wherein the rise of temperature with time is recorded after the sample is suddenly introduced in a high temperature enclosure. Results of these observations are graphically represented in figures 1, 2 and 3. It is to be noted here that as the behaviours are similar in both the principal directions, results of measurements in one direction only are given in the diagrams.

It is observed from figures 1 and 2, that the voltage always attains a maximum value say V_m , for a particular value of current and at a particular ambient temperature and pressure and then begins to decrease with further increase of current. This V_m together with I_m , W_m , and T_m the corresponding current, wattage absorbed by the sample and the temperature of the sample respectively are evidently important quantities in deciding the peculiarities of a particular thermistor, have been obtained from a study of fig. 1, and the values for the particular sample

corresponding to figure 1 when the ambient temperature is about 303°K and pressure 9.5×10^{-2} mm. of Hg are shown in table I. These quantities calculated theoretically following standard relation (Becker *et al* 1946, 1947) and from a knowledge of its activation energy and dissipation factor (both obtained separately) are also shown in the same table.

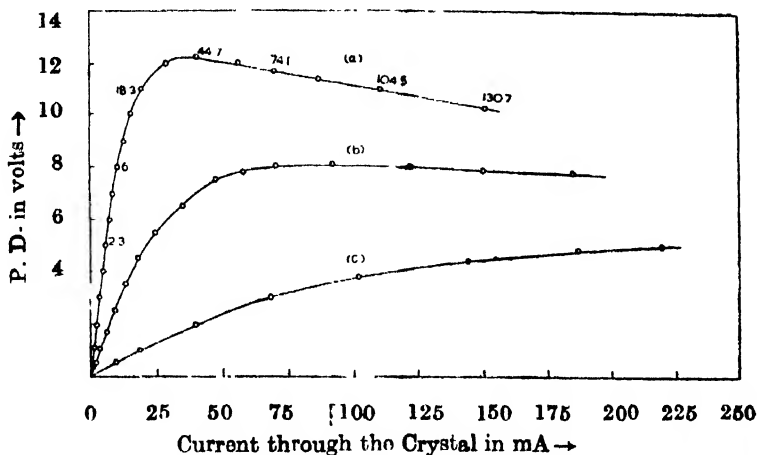


Fig. 1 Steady state current—voltage characteristics of WS_2 for currents along the C-axis at a superincumbent air pressure 9.5×10^{-2} mm of Hg., and at different ambient temperatures.

(a) Ambient temperature = 303°K .

Figures on the curve indicate the rise of temperature of the specimen in $^{\circ}\text{K}$ above the ambient.

(b) Ambient temperature = 376°K .

(c) Ambient temperature = 500°K .

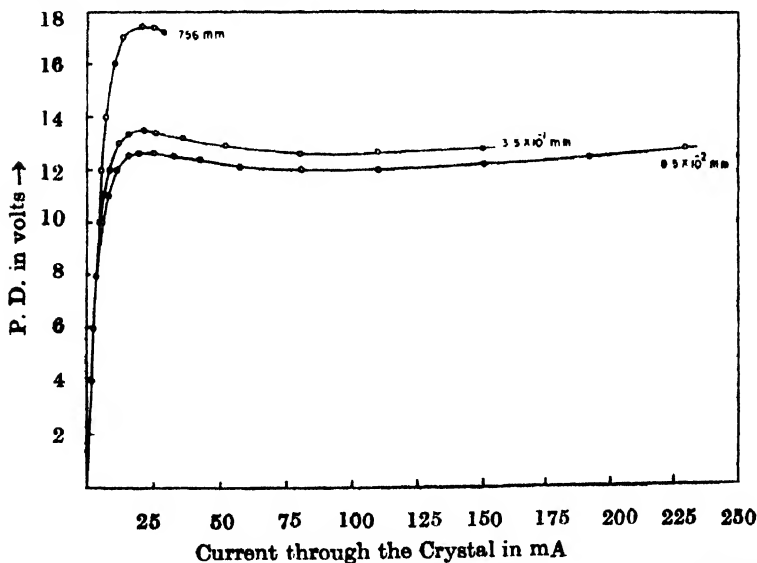


Fig. 2. Steady state current—voltage characteristics of WS_2 for current perpendicular to C-axis at an ambient temperature 333°K , and at different air pressures.

TABLE I

Activation energy = 5220°K

Resistance of the specimen at the ambient temperature 303°K and pressure 9.5×10^{-2} mm. of Hg. = 9.09×10^2 ohmsThe dissipation constant is 1.104×10^{-2} watt/°K

	Experimental	Theoretical
T_m (temperature corresponding to peak)	347°K	348°K
W_m (watts' " ")	49.53×10^{-2} watt	49.97×10^{-2} watts
R_m (resistance " ")	3.00×10^2 ohms	3.00×10^2 ohms
V_m (voltage " ")	12.20 volts	12.25 volts
I_m (current " ")	40.60 mA	40.80 mA

The steady state mentioned above is attained only after the rise in temperature of the crystal due to the passage of current through it is balanced by the dissipation of heat of the crystal to the surroundings. The dissipation constant G is related to current and voltage by the equation $G(T - T_0) = V \times I$, where T is the temperature of the crystal when a current I at a voltage V passes through the crystal and T_0 is the temperature of the surroundings. Thus from a study of watt against temperature curve, the dissipation constant G can be found out. It is needless to mention here that the dissipation constant is dependent on the superincumbent air pressure as is evident from fig. 2, where current—voltage characteristics are found to be different at different pressures (evidently due to differences in the values of G (Table II)) and this fact allows one to use the thermistor as a pressure measuring device.

TABLE II

Dependence of dissipation constant G on the surrounding air pressure (calculated from fig. 2).

Surrounding air pressure in mm. of Hg.	G in watt/°K	G per unit area
9.5×10^{-2}	2.137×10^{-3}	1.583 mw/°K
3.5×10^{-1}	2.370×10^{-3}	1.756 mw/°K
756	4.083×10^{-3}	3.025 mw/°K

In the transient condition, the rise of temperature is given by

$$T - T_0 = A_s^{1/2} \tau$$

where T is the temperature of the crystal in degrees Kelvin at time t , τ is a constant known as time constant and A is also a constant. Again $\tau = C/G$ when C is the thermal capacity and G , the dissipation constant. Thus from a study of the time-temperature curve and a knowledge of G , one can find out the value of C of the specimen at a temperature $T^\circ\text{K}$. It is, however, to be pointed out here that this relation does not hold at higher temperatures when the radiative losses become more pronounced and the thermal capacity also changes much with temperature. One such calculation with values obtained from the linear portion of the time-temperature curve (fig. 3) yields a value for C of WS_2 , within the temperature range

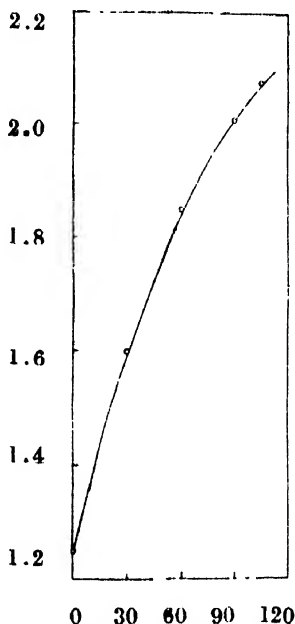


Fig. 3. Time-temperature curve for WS_2 under transient condition.

303°K — 333°K , as $0.57 \text{ joule/}^\circ\text{K}$ per gm. which compares well with $0.4 \text{ joule/}^\circ\text{K}$ per gm., the corresponding value of the specific heat of MoS_2 , the isomorphous crystal, obtained by direct measurements (there being no reported value of specific heat of WS_2 available for comparison).

The author express his best thanks to Shri A. K. Dutta for suggestion and guidance and to Prof. A. Bose for his kind interest in the work.

REFERENCES

- Guha Thakurta, S. R., 1967, *Indian J. Phys.* **41**, 99.
 Becker, J. A. ; Green, C. B. and Pearson, G. L., 1946, *Transaction of the American Institute of Electrical Engineers* **65**, 711.
 Becker, J. A. ; Green C. B. and Pearson, G. L., 1947, *Bell system Technical Journal*, **26**, 170.

ELECTRODE GLOW DURING ELECTROLYSIS

SANTI R. PALIT

INDIAN ASSOCIATION FOR THE CULTIVATION OF SCIENCE,
JADAVPUR, CALCUTTA-32.

(Received August 14, 1967)

During experiments on electrolysis (Palit 1963, 1967) we have often observed a remarkable phenomenon, and since we have been unable to find any mention of this in the literature, we report here the same.

The phenomenon in question is a glow of an electrode accompanying electrolysis. The glow is very easily produced on electrolysis with platinum wire electrodes in a simple *U*-tube or in an apparatus as shown in Fig. 1. On filling the

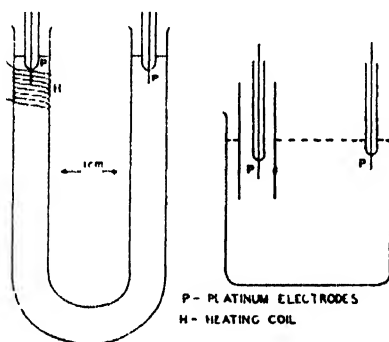


Fig. 1.

apparatus with an electrolyte solution of about 0.2N concentration and applying 220 volts D.C. (mains) a current of a few hundred milliamperes which increases with time, passes. In a short while (a few seconds to a few minutes) the current sharply drops to a lower value with slight fluctuations and one of the electrodes starts glowing brightly. This beautiful glow appears to be predominantly 'white' when viewed through an ordinary prism. The onset of glow is accompanied by formation of big bubbles on the electrode surface. Sometimes when the conditions are not quite right, these two characteristic changes (sharp drop in current strength and formation of big bubbles on the electrode) set in, but no glow is visible.

This kind of glow appears on the cathode with many electrolytes; for example, sodium chloride, sodium nitrate, potassium chloride, potassium nitrate, barium chloride, strontium chloride, calcium chloride, hydrochloric acid, nitric acid, etc. Some electrolytes show anode glow, typical examples being sodium hydroxide, sulphuric acid and many sulphates at suitable concentrations. Chlorides do not show anode glow but some nitrates under suitable conditions do. Sodium hy-

dioxide, however, shows both kinds of glow, anode glow being favoured at high concentration and cathode glow at a lower concentration. The glow (cathode) is very spectacular with barium chloride and strontium chloride solutions appearing like beautiful deep violet glow with a flame-like halo.

The factors which influence the glow are (i) nature of the electrolyte, (ii) concentration of the electrolyte, (iii) size of the electrode (iv) electrode material, (v) shape of the vessel, (vi) current density and voltage, and (vii) temperature of the electrolyte, the last factor being by far the most important. Externally heating the apparatus hastens the onset of glow so much so that if one of the electrode chambers is preheated to almost boiling by sending a regulated current through an external heating coil, the glow appears much sooner, almost as soon as the current is switched on under favourable conditions.

The following tentative explanation is offered. The cathode glow is due to the catalysed combination of hydrogen atoms (solvated or unsolvated) on the platinum surface of the electrode, i.e., $H + H = H_2$ takes place on the electrode. The narrow shape of the glowing cell not only helps to raise the local temperature but also helps to build up the local H concentration to a high enough value by preventing them from diffusing out. The anode glow is due to recombination of OH radicals to form oxygen.

If sparking and arcing are not considered, we could find reported in the literature at least two phenomena similar to the present electrode glow. One is the so-called "anode effect", i.e. a multi-star anode glow sometimes observed in the electrolysis of molten electrolytes (Mantell 1960). Another is the glow-discharge electrolysis particularly contact glow-discharge electrolysis reviewed by Hickling (1964), except that these discharges have been reported to occur at the anode and to need much higher voltage (500 volts and up). Detailed results will be published later.

Thanks are due to Sri Netai Chandra Sadhu for carrying out the major part of the work and to Sri Prithwish Kumar Basu for preliminary observations.

REFERENCES

- Hickling, A., 1964, *The Encyclopedia of Electrochemistry* edited by C. A. Hampel Reinhold Publishing Corporation P. 632.
- Mantell, C. L., 1960, *Electrochemical Engineering*, McGraw-Hill, P. 359, 369.
- Palit, S. R., 1963, *Electrochemistry, Proceedings of the First Australian Conference on Electrochemistry*, editors : J. A. Friend and F. Gutman, Pergamon Press, P. 711.
- , 1967, *Indian, J. Phys.* **41**, 309.

THE CRYSTAL AND MOLECULAR STRUCTURE OF *L*-ORNITHINE-HYDROCHLORIDE

S. GUHA, S. K. MAZUMDAR AND N. N. SAHA

CRYSTALLOGRAPHY AND MOLECULAR BIOLOGY DIVISION
SAHA INSTITUTE OF NUCLEAR PHYSICS
CALCUTTA-9.

(Received August 10, 1967)

Ornithine—a lower homologue of lysine—plays an important role in the formation of urea in the body. This communication deals with the crystal structure of a derivative of ornithine, $C_6H_{12}N_2O_2 \cdot HCl$ (Saha *et al.*, 1966). A preliminary report on this structure was presented at the symposium of the Indian Biophysical Society in April, 1967.

Ornithine hydrochloride crystallises in the monoclinic system with cell dimensions; $a = 4.99 \text{ \AA}$; $b = 8.00 \text{ \AA}$; $c = 10.00 \text{ \AA}$; $\beta = 97.0^\circ$, and space group $P2_1$. The measured density (1.420 g.cm^{-3}) corresponds to two molecules per unit cell, the calculated density being 1.416 g.cm^{-3} .

Three-dimensional intensity data collected about a and b axes by multiple film equi-inclination Weissenberg technique using CuK_α radiation were corrected for spot-size, Lorentz and polarisation factors. The relative intensity values thus obtained for different layers were brought to the same scale by using cross layer correlation method. The positions of two heavy atoms (chlorine) in the unit cell were determined from two Patterson projections, viz. (010) and (100), and a Harker section at $v = \frac{1}{2}$. The structure was solved by (a) a Buerger's minimum function derived from Cl-Cl vector in the three-dimensional Patterson map and (b) a three-dimensional Fourier synthesis based on phase angles of chlorine atoms; both calculated on IBM 1620 computer. Refinement of atomic parameters was made (five cycles) by the method of least squares using isotropic temperature factors and unit weighting factor. The final R value (including unobserved reflections) is 0.098.

The interatomic bond lengths and angles (Table II and Fig. 1) compare well with those of lysine hydrochloride (Wright *et al.*, 1962) and other amino acids (Hahn, 1957). The near equality of the two C—O bond distances (the difference being 0.012 \AA from their average value 1.254 \AA) indicates that the molecule is a zwitterion, both amino and terminal nitrogen atoms accepting a proton each. The average value of the (1.530 \AA) four C—C bond distances, though slightly higher than that of lysine hydrochloride (1.524), agrees well with the ($1.533 \pm 0.003 \text{ \AA}$) found by Bartell (1959) for medium length aliphatic carbon chains. The two

C—N⁺H₃ bond lengths are almost equal and their average (1.490 Å) compares well with that of lysine hydrochloride (1.482 ± 0.004 Å). Though the average value

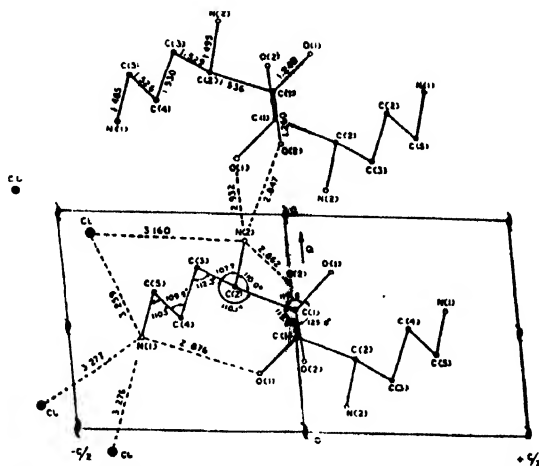


Fig. 1. The structure of L-ornithine hydrochloride viewed down the *b*-axis.

(110.7°) of three C—C—C angles in this molecule is not far from tetrahedral angle, a widening of the C(2)—C(3)—C(4) angle (112.3°) was found.

The molecules are held together by a system of hydrogen bonds. Each molecule has six hydrogen atoms available for hydrogen bond formation. Fig. 1, shows that both amino and terminal nitrogen atoms have four close neighbours each at hydrogen bond forming distances. All the C—NH...X bond angle (Table III) except C(2)—N(2)H...O_VI(1) = 166.4° and C(5)—N(1)H...Cl_{IV} = 173.5° satisfy the expected tetrahedral configuration, which indicates that these two sites are not favourable for hydrogen bond formation. The detailed paper on this structure will be published shortly.

TABLE I

Final atomic co-ordinates and temperature factors

Atom	X	Y	Z	B
Cl	0.09701	0.25000	0.41901	2.828
N(1)	0.42113	0.00143	0.64392	2.674
C(5)	0.63620	0.12784	0.67799	2.690
C(4)	0.52069	0.28208	0.74060	2.876
C(3)	0.75135	0.40285	0.78644	2.408
C(2)	0.65798	0.55106	0.86550	2.148
N(2)	0.88871	0.67100	0.88970	2.251
C(1)	0.57395	0.49112	0.00044	2.353
O(1)	0.75608	0.46503	0.09457	3.076
O(2)	0.32598	0.46701	0.00274	2.843

TABLE II
Intramolecular interatomic bond distances and angles

Bond distances		Bond angles	
N(1)—C(5)	1.485 Å	N(1)—C(5)—C(4)	110.3°
C(5)—C(4)	1.526 Å	C(5)—C(4)—C(3)	109.9°
C(4)—C(3)	1.530 Å	C(4)—C(3)—C(2)	112.3°
C(3)—C(2)	1.529 Å	C(3)—C(2)—C(1)	110.1°
C(2)—C(1)	1.536 Å	C(3)—C(2)—N(2)	107.7°
C(3)—N(2)	1.495 Å	N(2)—C(2)—C(1)	110.0°
C(1)—O(1)	1.248 Å	C(2)—C(1)—O(1)	117.8°
C(1)—O(2)	1.260 Å	C(2)—C(1)—O(2)	115.9°
		O(1)—C(1)—O(2)	125.8°

TABLE III
Intermolecular bond distances and angles

Bond distances		Bond angles	
N(1)—H...Cl _I	3.277 Å	C(5)—N(1)...Cl _I	91.5°
N(1)—H...Cl _{II}	3.259 Å	C(5)—N(1)...Cl _{II}	86.2°
N(1)—H...O _{II} (1)	2.876 Å	C(5)—N(1)...O _{II} (1)	98.9°
N(2)—H...Cl _V	3.160 Å	C(2)—N(2)...Cl _V	94.5°
N(2)—H...O _V (2)	2.862 Å	C(2)—N(2)...O _V (2)	106.0°
N(2)—H...O _{III} (2)	2.847 Å	C(2)—N(2)...O _{III} (2)	103.5°
N(1)...Cl _{VI}	3.276 Å	C(5)—N(1)...Cl _{IV} (9)	173.5°
N(2)...O _{VI} (1)	2.932 Å	C(2)—N(2)...O _{VI} (1)	166.4°

The subscripts refer to the co-ordinates of atoms in molecules I to VI. I : X, Y, Z; II : —X, Y— $\frac{1}{2}$, —Z; III : —X+1, Y— $\frac{1}{2}$, —Z; IV : —X—1, Y— $\frac{1}{2}$, —Z; V : —X, Y+ $\frac{1}{2}$, —Z; VI : —X+1, Y+ $\frac{1}{2}$, —Z.

REFERENCES

- Bartoll, L. S., 1959, *J. Am. Chem. Soc.*, **81**, 3497.
 Hahn, T., 1957, *Z. Kris.* **109**, 438.
 Saha, N. N. Majumdar, S. K., Bhattacharya, S. C., Roy, P. N., Handa, R., and Guha, S., 1966, *Indian J. Phys.* **4**, 681.
 Wright, D. A. and Marsh, R. E., 1962, *Acta Cryst.* **15**, 54.

AN X-RAY STUDY OF THE CONDENSATION PRODUCT OF DIAMINO SUCCNIC ACID AND PYRUVIC ACID $C_{10}H_{12}N_2O_8$

S. CHATTERJEE AND S. C. CHAKRABORTY

DEPARTMENT OF PHYSICS, BURDWAN UNIVERSITY,

BURDWAN, WEST BENGAL, INDIA.

(Received August 16, 1967)

Well developed transparent single crystals of the condensation product of Diaminosuccinic Acid and Pyruvic Acid, having molecular formula $C_{10}H_{12}N_2O_8$ and m.p. 226°C , were obtained from the saturated aqueous solution of the compound under controlled evaporation and repeated crystallisation. In all the crystals, excepting a few, only the axial faces were developed.

The morphological study was carried out with the help of a two circle goniometer and the measured values of α^* , β^* and γ^* were $\alpha^* = 104^\circ 37'$, $\beta^* = 98^\circ 45'$, and $\gamma^* = 114^\circ 15'$. The interfacial angles calculated from these values are $\alpha = 69^\circ 34'$, $\beta = 73^\circ 10'$ and $\gamma = 62^\circ 0'$.

The rotation photograph and normal beam zero-level Weissenberg photographs were taken about the [100]-, [010]- and [001]-axes using unfiltered CuK -radiation. The axial lengths obtained from the rotation photographs are $a = 6.53\text{\AA}$, $b = 7.10\text{\AA}$, $c = 7.53\text{\AA}$ and those calculated from the Weissenberg photographs are $a = 6.59\text{\AA}$, $b = 7.13\text{\AA}$, $c = 7.53\text{\AA}$. The approximate values of α^* , β^* and γ^* measured and calculated from Weissenberg photographs are $\alpha^* = 104^\circ 30'$, $\beta^* = 98^\circ 0'$; $\gamma^* = 114^\circ 0'$. The optical study and the summery of X-ray photographs show that the crystals belong to the triclinic system; no systematic absence of reflections is possible and this was also confirmed from the indices of reflections from the crystal under study. Thus the space group of the crystal is either P_1 or P_1 . To determine the space group uniquely statistical tests were carried out for different zonal reflections. For this the intensities were estimated visually from a calibrated set of 'master spots' and were corrected for Lorentz and Polarisation factors. The intensity distribution curves are in excellent agreement with the theoretical one for centrosymmetric case. Hence the space group was found to be $P\bar{1}$.

The volume of the unit cell calculated from the obtained parameters is 291.6\AA^3 . The density of the sample was measured by flotation method using a mixture of pyridine and carbontetrachloride and the observed value was 1.58 gm-cm^{-3} and the calculated value is 1.64 gm-cm^{-3} on the basis that the unit cell contains only one molecule.

Further work is in progress.

AN ANOMALOUS MAGNETIC BEHAVIOUR OF $K_3Cr_2(C_4O_3) \cdot 3H_2O$, STUDIED BETWEEN ROOM TEMPERATURE AND LIQUID OXYGEN TEMPERATURE

PADA RENU SAHA

DEPARTMENT OF MAGNETISM,

INDIAN ASSOCIATION FOR THE CULTIVATION OF SCIENCE

(Received August 21, 1967)

The magnetic anisotropy and susceptibility measurements of $(NH_4)_3Cr(C_2O_4)_3 \cdot 3H_2O$, assuming the salt to be monoclinic (Groth 1910), were made at room temperature and liquid oxygen temperature only by Krishnan, *et al* (1939). The $K_3Cr(C_2O_4)_3 \cdot 3H_2O$ salt supposedly isomorphous with the ammonium salt was further investigated by Datta Roy (1958) over the whole liquid oxygen range. But the X-ray data of Nickerk and Schoening (1952) show that these salts are not only not isomorphous, but the ammonium salt belongs to the triclinic space group $P\bar{1}$, with two formula units in a cell, while the potassium salt is of monoclinic space group $P2_1$ — C_{2h} ⁶, with four formula units in a cell, so that the earlier identifications of the crystallographic axes were not correct, and consequently fresh measurements should be made to reassess the magnetic behaviour of these salts. The triclinic ammonium salt being more difficult to treat (Krishnan and Mukherji 1936, 1938; Ghosh and Mitra 1964; Ghosh 1966), as a first attempt we chose the monoclinic potassium salt. As the salt under investigation has feeble anisotropy, the single crystals were cut to nearly a square horizontal cross sections, to remove anisotropy of shape, about the axes of suspension. The suspension was made with a very fine quartz fibre and the entire suspension system was made as light as possible. The measurement was carried out in a very sensitive and accurate type of magnetic anisotropy balance and gas flow type cryostat set up in this laboratory by Ghosh and Mukhopadhyay (1966).

When the crystal was suspended with *b*-axis vertical to the magnetic field, the anisotropy in the horizontal plane *i.e.* $(\chi_1 - \chi_2)$ increased as the temperature was lowered and at liquid oxygen temperature anisotropy became nearly ten times that of the room temperature value (Fig. 1a). The setting direction, *i.e.*, the angle θ between *a*- and χ_2 -axis which is 63° at room temperature was found to change by 8° over the entire liquid oxygen range.

With the *a*-axis of the crystal vertical, *b*-axis setting normal to the magnetic field, a very peculiar phenomenon was observed as the temperature was lowered. From $\sim 220^\circ K$ the crystal began to show a small change in the setting direction by a few degrees (Fig. 2c). Near $155^\circ K$ the change was found to be very rapid.

amounting to $\sim 65^\circ$ for a temperature change of a few degrees and then again gradual. Since b -axis lying in the horizontal plane for this mode of suspension

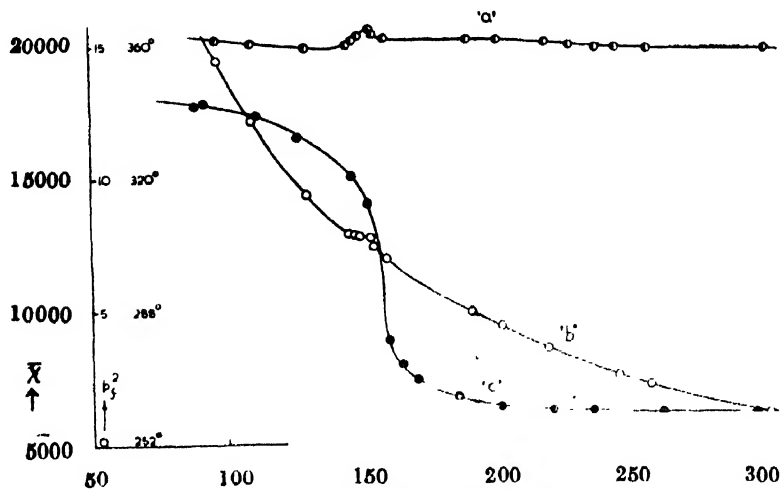


Fig. 1. half-filled circles — $(\chi_1 - \chi_2)$
hollow circles — $(\chi_1 - \chi_3)$
filled circles — $(\chi_3 - \chi_2)$

is by crystal symmetry a fixed one, this large change is quite unusual. Secondly, the anisotropy in the plane normal to a -axis was found to be decreasing with the lowering of temperature and became zero at $\sim 153^\circ\text{K}$ and then changed sign consistent with the large ($\sim 90^\circ$) change in the orientation of the original b -axis. With further lowering of temperature, the anisotropy increased again. The crystalline anisotropy $(\chi_1 - \chi_3)$ as obtained from the above mentioned measurements was found to be increasing at first with the lowering of temperature but close to 155°K the curve of $(\chi_1 - \chi_3)$ versus T showed an inflexion and then increased again smoothly (Fig. 1b). $(\chi_3 - \chi_2)$ as obtained by subtracting the two anisotropies $(\chi_1 - \chi_3)$ and $(\chi_1 - \chi_2)$ was found to be very small at room temperature, and remained almost constant with the lowering of temperature upto $\sim 150^\circ\text{K}$. With further decrease of temperature $(\chi_3 - \chi_2)$ increased slightly (Fig. 1c).

From the mean susceptibility measurement of this complex it was found that with the lowering of temperature the susceptibility increased normally but nearly at 153°K the value remained almost constant over a temperature range of $\sim 5^\circ\text{K}$ and then again increased (Fig. 2b). In the corresponding mean moment square p_j^2 curve (Fig. 2a) a hump was observed at $\sim 220^\circ\text{K}$ and a sharp maximum at $\sim 153^\circ\text{K}$, then p_j^2 value dropped nearly to the room temperature value and then increased again slightly as the oxygen temperature was reached.

Thus we may surmise that this anomalous behaviour in anisotropy and susceptibility is due to some transition in the crystal. The change in the setting direction with χ_3 -axis in the horizontal plane also supports this view. The 90°

change in the orientation of χ_3 axis within a small interval of temperature indicates that this principal magnetic axis no longer coincides with the b -axis,

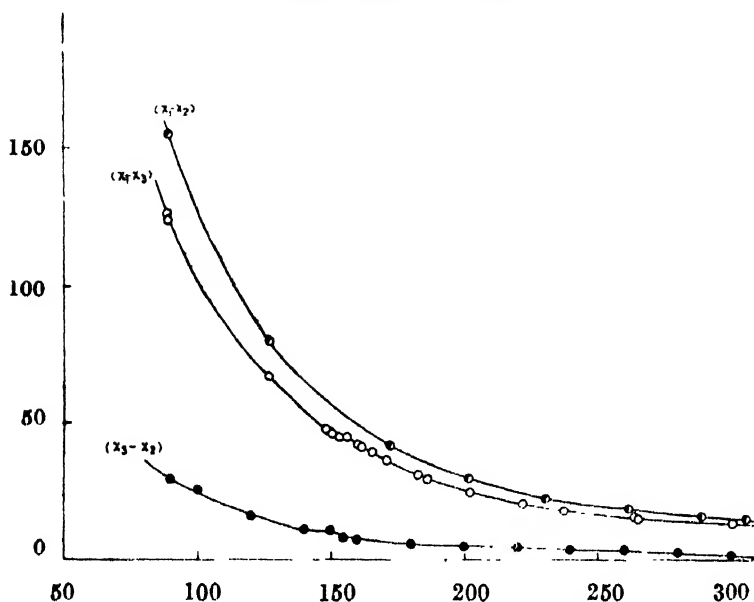


Fig. 2. half-filled circles $-p_f^2$ -curve.

hollow circles $-\bar{\chi} \times 10^{-6}$

filled circles—change of setting angle with temperature.

thus destroying the condition of uniqueness of this axis in a monoclinic crystal. Thus the transition appears to be connected with a change in the crystal system. For getting more details of the transition we have undertaken X-ray and spectroscopic measurements of the salt.

ACKNOWLEDGEMENT

The author takes this opportunity to express his gratefulness to Prof. A. Bose, D.Sc., F.N.I., and Dr. B. C. Guha D.Sc. for their guidance and help. Thanks are due to the C.S.I.R. for awarding a Junior fellowship. The author is also thankful to his colleagues Mrs. D. Ghosh and Miss. D. Mukhopadhyay for their co-operation.

REFERENCES

- Dutta Roy, S. K., 1958, *D. Phil Thesis* (Unpublished)
 Ghosh, J. K. 1966, *Indian J. Phys.* **40**, 457.
 Ghosh, U. S. and Mitra, S. 1964, *Indian J. Phys.* **38**, 19.
 Ghosh, D. and Mukhopadhyay, D. 1966, *Indian J. Phys.* **40**, 69.
 Groth, P. 1910, *Chemische Krystallographie* **3**, 166.
 Krishnan, K. S., Mukherji, A., Bose, A., 1939, *Ph. Tr. Roy. Soc.* **238**, 125.
 Krishnan, K. S. and Mukherji, A., 1936, *Phys. Rev.* **50**, 860.
 Niekerk, J. N. and Schoening, F. R. L., 1952, *Acta Crystallographica* **5**, 196, 499.

ON THE FREQUENCY SHIFT IN THOMSON SCATTERING

N. D. SEN GUPTA

TATA INSTITUTE OF FUNDAMENTAL RESEARCH
BOMBAY-5.

(Received September 5, 1967)

In a recent note Prakash (1967) while discussing the effect of radiation reaction on Thomson scattering, has reported that due to 'an instantly switched radiation' the electron gains an additional acceleration and "average" momentum depending on the initial phase of the radiation. The vector potential is taken in Prakash (1967) as

$$A(r, t) = A_0 \theta(X) \cos(wX + \chi), \quad X = t - (n.r)/c \quad \dots (1)$$

where θ is the usual step function. This form of A , with step function replaced by a suitable growth function was also considered by Kibble (1965). The physical condition that the field is switched on sharply at an instant say $t = 0$ is clearly not depicted by A as given in eq. (1). The step function is non-vanishing on the forward light-cone with origin as vertex. Perhaps, the point in taking X as the argument of θ , is that the Lorentz equation of motion (without radiation reaction) is then exactly integrable, because the field is now expressible as the function of a single parameter (1965). However, this seems superfluous, as the fact that field is switched on at $t = 0$, is incorporated in the problem as initial value (1966a,b). Apart from this the step function introduces an unwanted singularity of the electromagnetic field. It may be due to this the solution of the equation of motion (in Dirac form), as stated in Prakash (1967), does not agree with the author's solution (1966b). They cannot differ so long as the particle velocity is continuous and small in comparison to c . Moreover, the intensity effects in question are shown clearly to be non-relativistic in nature (1925).

On the other hand, the second point raised in Prakash (1967), namely the dependence of the frequency shift and other effects, on the phase of the incident radiation is quite a pertinent one. If one works with an arbitrary phase of the incident wave this is taken as zero in Sengupta (1966b) in the system in which the electron is initially at rest (Σ), then one will arrive at a frequency shift which depends on the phase. But what may be observed is an average over a system of electrons; (note that it is not time-average for a single electron in its motion). It is easy to see the consequence of this arbitrariness of the initial phase, after averaging, is to introduced a broadening of the scattered line and the mean magnitude of intensity dependent frequency shift is changed by an unimportant numerical factor from the expression as quoted in Sengupta (1966b). However,

it should be emphasized that the shift remain isotropic in (Σ) . It is quite clear that the phase of the radiation cannot change the qualitative nature of the problem because the phase may be made zero by suitable translation of space and time, and this translation will only change the initial values as initial velocity in general is not zero at the new origin.

It is not irrelevant to mention here that some of the features of the motion of electron in the field of plane electro-magnetic wave was reported by Frenkel (1925) much earlier than the author's first paper Sengupta (1965). The author regrets very much that it escaped his previous notice.

REFERENCES

- Frenkel, J., 1925, *Z. Phys.*, **32**, 27.
 Kibble, T. W. B., 1965, *Phys. Rev.* **138**, B740.
 Prakash, H., 1967, *Phys. Letters* **24A**, 492.
 Sen Gupta, N. D., Bose, S. N., 1965, *70th Birthday Commemoration*, Volume II, 55.
 ———, 1966, *Phys. Letters*, 642.
 ———, 1966b, *Z. Phys.*, **196** 385.
 ———, 1949, *Bull. Math. Soc. (Calcutta)*, **41**, 187.

INDIAN JOURNAL OF PHYSICS

VOL. 41

No. 9

AND

VOL. 50

PROCEEDINGS

No. 9

OF THE

INDIAN ASSOCIATION FOR THE CULTIVATION OF SCIENCE

(Edited in collaboration with the Indian Physical Society).

SEPTEMBER 1967

PUBLISHED BY THE
INDIAN ASSOCIATION FOR THE CULTIVATION OF SCIENCE
JADAVPUR, CALCUTTA-32

DECAY OF Tm^{176} AND LEVELS OF Yb^{176}

S. C. GUJRATHI AND S. K. MUKHERJEE

SAHA INSTITUTE OF NUCLEAR PHYSICS, CALCUTTA, INDIA.

(Received February 16, 1967)

ABSTRACT. The Tm^{176} nucleus is produced by the (n, p) reaction with 14.8-MeV neutrons on enriched (97.5%) Yb^{176} . A half-life of 1.4 ± 0.2 min is assigned to Tm^{176} . The beta and gamma ray measurements show three beta groups of end-point energies 3050 ± 100 (20%), 2000 ± 100 (40%) and 1150 ± 100 (40%) keV and eight gamma rays of energies 50 (Yb K X-ray), 91, 190, 285, 390, 870, 1050 and 1816 keV decaying with a 1.4-min activity of Tm^{176} . Coincidence and sum spectrum studies indicate that the 1150-keV beta group is in coincidence with a gamma ray energy cascade 870–1816–190–50 keV; the 2000-keV beta group is in coincidence with the 1050-keV gamma ray and a gamma ray energy cascade 1816–190–50 keV; and the 3050 keV beta group is not in coincidence. The 91-, 390-, 285-, 190- and 50-keV gamma rays form a cascade. A decay scheme of Tm^{176} is proposed and the results are discussed in the light of the Unified model. The Q_β -value for the $\text{Tm}^{176} \rightarrow \text{Yb}^{176}$ transition is 4088 \pm 100 keV. The (n, p) cross-section for Yb^{176} is found to be 1.5 \pm 0.5 mb.

INTRODUCTION

Wille and Fink (1960) bombarded enriched Yb^{176} as well as natural ytterbium with 14.5-MeV neutrons and observed a 2.0 ± 0.5 -min activity in the irradiated samples. They assumed that this activity was due to one of the three isotopes, namely Tm^{176} , Er^{173} and Yb^{177} produced by the (n, p) , (n, α) and (n, γ) reactions respectively, on Yb^{176} . Takahashi *et al* (1961) irradiated oxide powder of natural ytterbium with fast neutrons and reported a half-life of 1.5 ± 0.5 min after following the decay of beta rays in a plastic beta ray detector. In their measurement, beta rays below 3300 keV were discriminated to avoid the contributions of the activities formed by the $(n, 2n)$, (n, α) and (n, γ) reactions. They also observed a single beta group of maximum energy 4200 ± 200 keV associated with a 1.5-min activity and assigned it tentatively to Tm^{176} .

Kantele (1962) sought isotopes showing K isomerism, and bombarded enriched Yb^{176} as well as natural ytterbium metal with 14-MeV neutrons. He reported a gamma ray cascade of energies 391-293-190-52 (YbK X-ray) keV decaying with a half-life of 12 sec and assigned this activity to an isomer of Yb^{176} produced by the $(n, n'\gamma)$ reaction. The assignment was confirmed by irradiating other enriched isotopes of Yb with 14- as well as 3-MeV neutrons. Very recently Vergnes *et al* (1965) established the position of the 12-sec isomeric state of Yb^{176} at the 1038-keV level. This state was observed to decay through the 93-keV gamma transition to the 8^+ level of the ground state rotational band. They ascribed spin and parity of the 1038-keV level as 8^- and K-quantum number as 8.

We have undertaken the investigation of Tm^{176} to measure its half-life accurately and also to study the various beta and gamma transitions associated with it. Coincidence experiments were performed to find the excited levels of Yb^{176} populated in the decay of Tm^{176} .

SOURCE PREPARATION

The Tm^{176} sources were produced by the (n, p) reaction on enriched (97.5%) Yb^{176} . The energy of the neutrons was 14.8 MeV and the typical neutron flux was of the order of the 5×10^{10} neutrons/cm² sec. The strongest interfering activity of Yb^{175} (4.1d) was produced by the $(n, 2n)$ reaction on Yb^{176} . The contribution due to this activity was reduced to a large extent by irradiating the samples for a very short period. Moreover, the impurities due to all long-lived activities along with that of Yb^{175} were subtracted in the automatic subtraction process of the mult-channel analyser. Other possible contaminant activities in the source were carefully sought on the basis of the data of the isotopic and the spectrographic analysis of the supplied enriched sample as well as with the aid of suitable activity lists (Slater, 1962; Nuclear Data Sheets, 1946). The short-lived activities suspected as impurities were due to the reactions $\text{Cu}^{63} (n, 2n) \text{Cu}^{64}$ (9.5 min), $\text{Pr}^{141} (n, 2n) \text{Pr}^{140}$ (3.4 min) and $\text{Yb}^{174} (n, np) \text{Tm}^{174}$ (5.5 min) reactions. The contribution of Tm^{174} is expected to be very small since the measured (n, p) cross-section for Yb^{174} is 3.5 ± 1 mb (Gujrathi *et al.*, 1965). The amounts of impurities of Cu^{63} and Pr^{141} present in the enriched samples were insufficient to affect the main conclusions. The estimated total contribution due to all short lived impurities was less than 3% of the total decay of Tm^{176} .

For the beta ray measurements the irradiated samples of oxide powder were uniformly spread inside a bag of thin mylar. The average thickness of the source was 2mg/cm². Since the measured (n, p) cross-section for Yb^{176} was very small, a large number of irradiations on several hundred mg of enriched sample were needed to complete each measurement.

EXPERIMENTAL RESULTS

(A) Half-life measurement and the (n, p) cross-section

The enriched Yb^{176} (97.5%) was bombarded with 14.8 MeV neutrons for 5 min and immediately studied under a G.M. counter. Fig. 1(a) shows the observed half lives as 4.1d, 8.5 ± 1.5 min and 1.4 ± 0.2 min. The long-lived activity of 4.1d is due to Yb^{175} produced by the $(n, 2n)$ reaction on Yb^{176} . It can be clearly seen that even in 5-min irradiation, a large amount of $(n, 2n)$ product is produced. In another measurement the decay of beta rays was followed in an anthracene beta detector. The discriminator and the gain of the pulse height analyser were set to accept the pulses only above 500 keV which completely excluded the activity of Yb^{175} . Only two half-lives of 1.4 and 8.5 min were observed (fig. 1b). The half-lives were also studied by following the decay of 50-, 90-, 190-, 285- and 390

keV gamma rays (see Table II) in a single channel analyser. In all cases the same three activities shown in fig.1a were observed. The 1.4 ± 0.2 -min half-life was

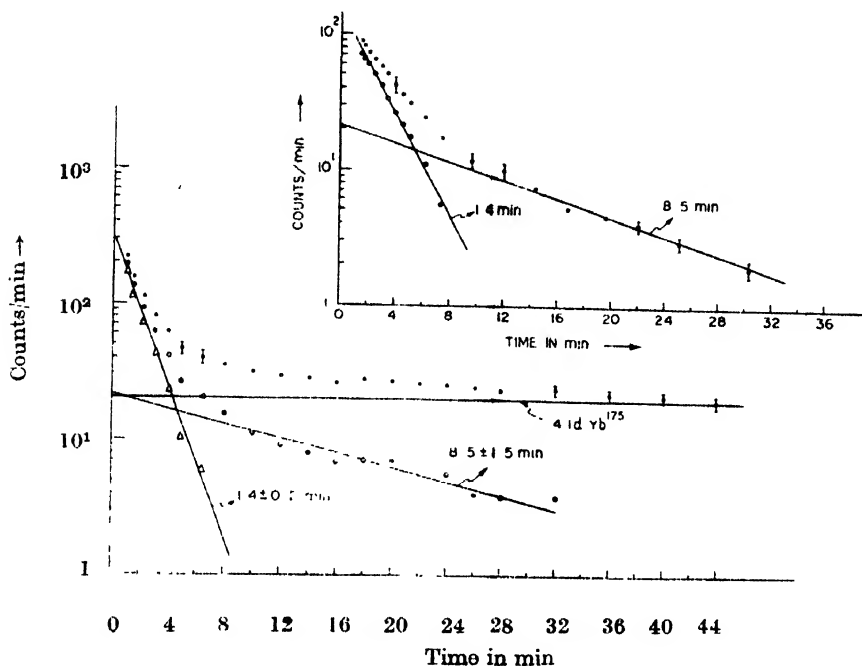


Fig. 1. Beta decay (a) in a G.M. counter,
(b) above 500 keV in an anthracene beta detector.

assigned to Tm^{176} . The 8.5 ± 105 min activity could tentatively be ascribed to Er^{173} or to an isomer of Tm^{176} . The cross section for the $Yb^{176}(n, p) Tm^{176}$ reaction was calculated by the activation technique, the experimental details of which were as reported earlier (Mukherjee *et al* 1961). The measured cross-section value was 1.5 ± 0.5 mb as compared with a value of 556mb for the $Cu^{63}(n, 2n) Cu^{63}$ reaction.

(B) Gamma and beta ray measurement

The beta ray spectrum of Tm^{176} was examined with an anthracene beta spectrometer. The detector crystal was 5.1 cm \times 1.3 cm thick and the source-to-crystal distance was 0.5 cm. The data were recorded with a 512-channel pulse-height analyser. To study the beta ray energy groups decaying with a 1.4 min half-life, the following procedure was adopted. The enriched Yb^{176} was irradiated for 2 min and the measurement was started 50 sec after the end of the bombardment. After recording the counts for 3 min the second measurement was started at 4th min after the end of the irradiation. The period of data accumulation was again 3 min. A difference spectrum was obtained from the above two measurements. By waiting for 50 sec, short-lived contaminant activities such as N^{16} (7.4 sec), Yb^{177m} (6.4 sec) and Yb^{178m} (12 sec) were eliminated. The difference spectrum was free from long-lived activities except that it contained a small

contribution of the 8.5 min activity. A third spectrum was taken 8 min after the end of the irradiation for 15 min. The background and long-lived activities were subtracted for the same period of accumulation, which gave the spectrum of the 8.5 min activity. A time-corrected contribution of the 8.5 min activity, which was present in a very small amount, was subtracted from the difference spectrum obtained from the first two measurements. Fig. 2 shows such a corrected beta spectrum and the Fermi-Kurie analysis of the same. Three beta groups of

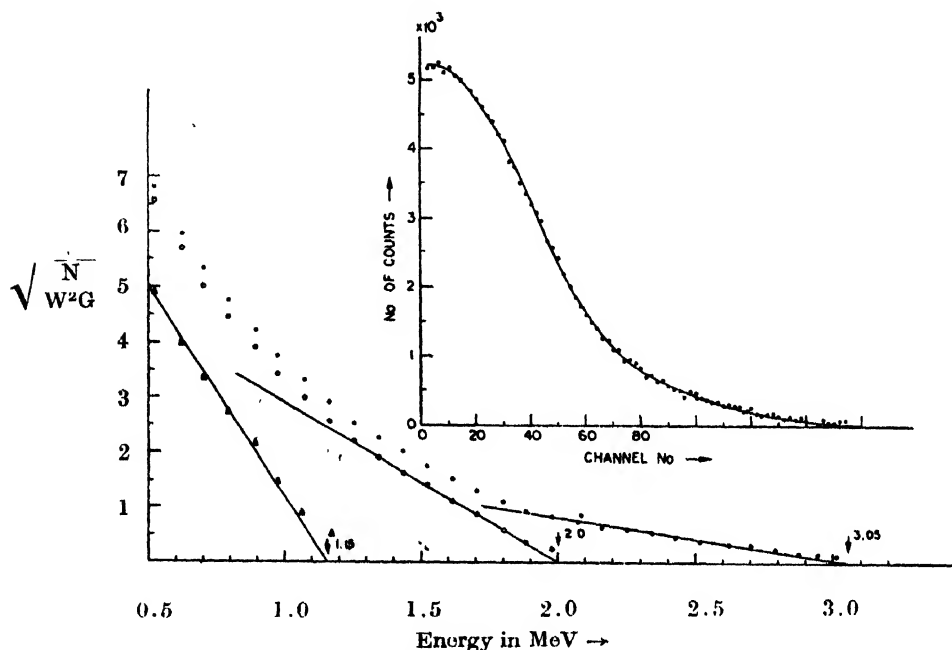


Fig. 2. Beta spectrum and the Fermi-Kurie plot of the 1.4-min activity of Tm^{176} .

maximum energies 3050 ± 100 (20%), 2000 ± 100 (40%) and 1150 ± 100 (40%) keV are observed which decay with a 1.4 min activity. It must be mentioned here that we did not observe the 4200 ± 200 keV beta group decaying with a half-life of 1.5 ± 0.5 min as reported by Takahashi *et al* (1961). The energies intensities and log ft values for the various beta groups decaying with a 1.4 min activity are given in table I.

A beta group of 2500 ± 300 keV was found to decay with 8.5 min activity.

TABLE I

The energies intensities and log ft values of the beta ray groups of Tm^{176}

Beta ray end-point energy (keV)	Intensity %	log ft. value
3050 ± 100	20	6.4
2000 ± 100	40	5.4
1150 ± 100	40	4.5

The gamma spectra were studied by a 7.6 cm \times 7.6 cm of NaI(Tl) crystal and a 512 channel analyser. The detector was covered with a 1 cm thick lucite plate to absorb beta rays. To eliminate the undesired activities the same procedure as followed in beta ray measurement was adopted. Fig. 3 shows the gamma spectrum associated with the 1.4 min activity of Tm^{176} . In the measurement,

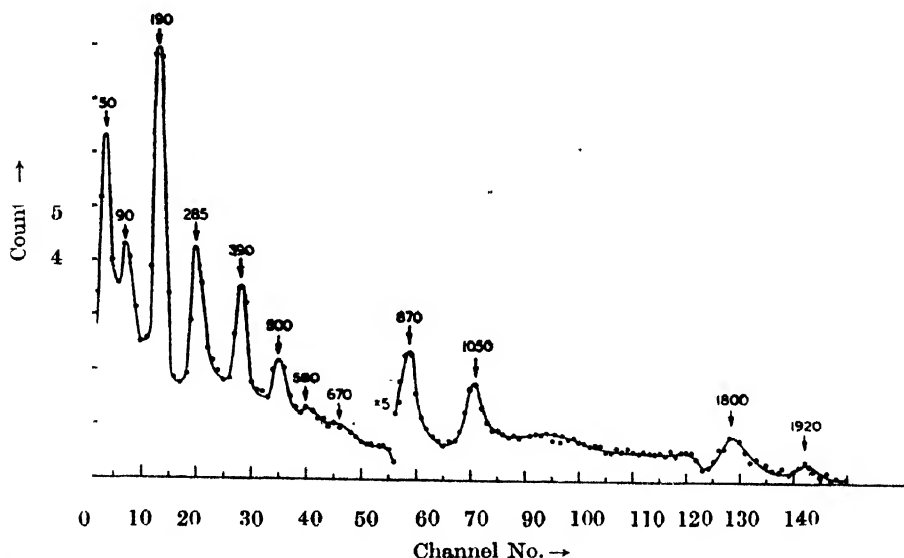


Fig. 3. Gamma spectrum of Tm^{176} with a 7.6 cm \times 7.6 cm NaI(Tl) crystal. The source-to-crystal distance was 1 cm.

the source-to-crystal distance was 1 cm. Photopeaks are evident at energies 50, 90, 190, 285, 390, 500, 580, 670, 870, 1050, 1800 and 1920 keV. The energy of the photopeak at 50 ± 5 keV is comparable with the ytterbium K X-ray energy, which is 52.3 keV. To test the cascade nature and the summing effects of the gamma rays a spectrum was taken by keeping the source at a distance of 8 cm. The gamma spectra were also studied by introducing systematically 0.01 cm to 1 cm thick lead absorbers between the source and the detector. It was found that the 500 (190+285+Yb X-rays and 91+390+Yb X-rays)-, 580(190+390)-, 670 (285+390)- and 1920(870+1050)-keV gamma rays, shown in fig. 3, were sum peaks.

To test the decay characteristics of the various gamma rays, the enriched sample of Yb^{176} was bombarded for 3 min and four spectra were taken at 0.5, 2, 3.5 and 5 min after the end of the irradiation. It was found that all the prominent gamma rays shown in fig. 3 decayed with a half-life of 1.5 ± 0.5 min. Since the low energy gamma rays decaying with a 1.4 min activity have very nearly the same energy as those of Yb^{176} , a large error in their calculated intensities was involved due to the repeated subtraction process.

A gamma ray of 500 ± 20 keV was found to decay with an 8.5 min activity. Other low energy weak gamma rays associated with this activity could not be distinguished from those of Yb^{175} which were relatively much more intense.

The gamma ray energies, their relative intensities calculated from single crystal as well as from some of the coincidence measurements and the gamma-gamma coincidence results associated with the 1.4 min activity of Tm^{176} are summarised in Table II.

TABLE II

Gamma ray energies, their relative intensities neglecting the conversions and and the gamma-gamma coincidence results in Tm^{176}

Energy of the photo peak (keV)	Unconverted gamma ray relative intensity	In coincidence with (keV)
50 ± 5 (Yb K X-ray)	60 ± 30	90, 190, 285, 390, 870, 1800
90 ± 10	15 ± 5	50, 190, 285, 390
190 ± 5	100	50, 90, 285, 390, 870, 1800
285 ± 5	72 ± 20	50, 90, 190, 390
390 ± 5	78 ± 20	50, 90, 190, 285
870 ± 10	38 ± 8	50, 190, 1050, 1800
1050 ± 10	45 ± 10	870
1800 ± 20	32 ± 8	50, 190, 870

(C) *Coincidence measurements.*

In the beta-gamma coincidence arrangements the gating gamma ray was selected with a $5.1 \text{ cm} \times 5.1 \text{ cm}$ NaI(Tl) detector and the gated beta spectrum was studied with a $5.1 \text{ cm} \times 1.4 \text{ cm}$ thick anthracene detector. In few experiments a certain portion of the beta spectrum was selected in a gate and the coincident gamma spectrum was analysed by a $7.6 \text{ cm} \times 7.6 \text{ cm}$ NaI(Tl) detector. The two scintillation detectors were positioned 1.5 cm apart facing each other with a source between them. The resolving time (2τ) of the coincidence system was $2\mu\text{s}$. A lucite beta absorber of 1 cm thickness was introduced between a source and the gamma detector. To study the coincidence results associated with the 1.4 min activity the same method of accumulation as followed in beta and gamma ray measurements was adopted.

With the integral gamma spectrum taken in the gate only two beta groups of maximum energies 2040 ± 100 and 1160 ± 100 keV appeared in coincidence (fig. 4).

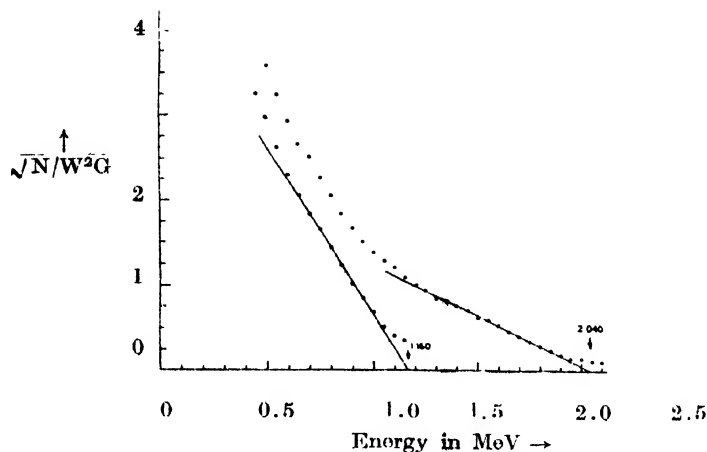


Fig. 4. Fermi-Kurie plot of the beta spectrum in coincidence with the integral gamma rays.

The gamma spectra observed in prompt coincidence with those pulses produced by the portions of the beta ray spectrum between 500 to 3050 keV and 1000 to 3050 keV, are shown in fig. 5 as curves (a) and (b), respectively. The gamma rays of energies 50, 190, 870, 1050 and 1815 keV are shown in curve (a), the same photo

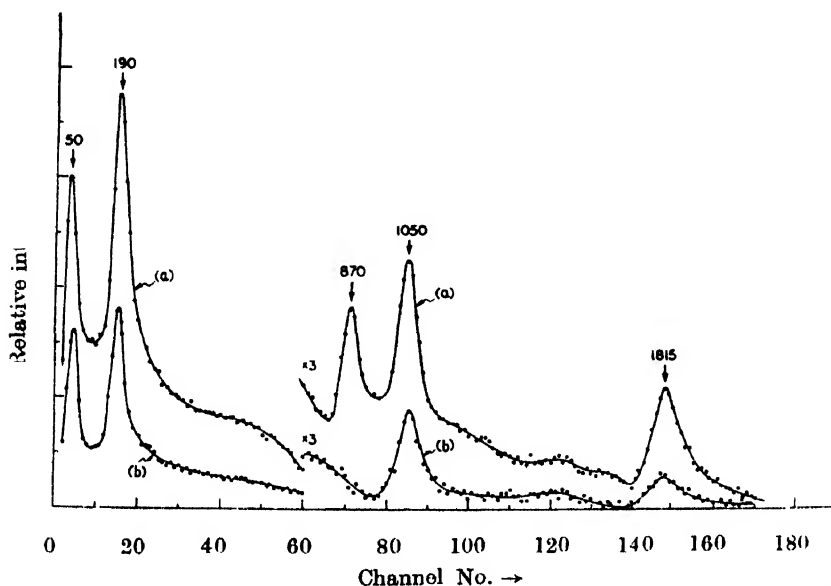


Fig. 5. Gamma spectra in coincidence with the (a) the 500 to 3050 keV and (b) 1000 to 3050 keV portions of the beta spectrum taken in gate.

peaks are present in curve (b), except the 870 keV. The spectra were corrected for the gamma ray detection efficiency of the anthracene detector. The beta

spectrum in coincidence with the 870 keV gamma ray showed only one beta group of maximum energy 1150 keV (fig. 6). The 1050 keV gamma ray was found in coincidence with the two beta groups of end-point energies 2030 ± 100 and 1140 ± 100 keV. These two beta groups were also observed in the coincidence results obtained by gating with the 50-, 190- and 1800 keV gamma rays.

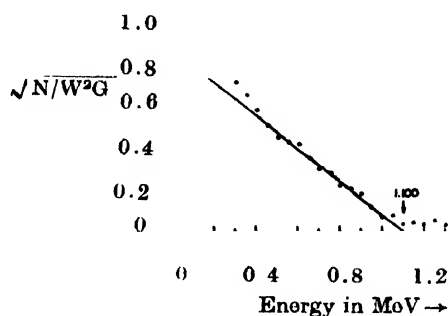


Fig. 6. Fermi-Kurie plot of the beta spectrum in coincidence with the 870-keV gamma ray.

For the gamma-gamma coincidence studies 5.1 cm \times 5.1 cm NaI(Tl) crystal was used to select the gating gamma ray and the gated spectrum was obtained with a 7.6 cm \times 7.6 cm NaI(Tl) detector along with a 512 channel analyser. Two detectors were placed at 3 cm apart facing each other with a source between them. The detectors were shielded from each other with a suitable anti-Compton-shield to reduce the effect of Compton-scattered photons. When the integral gamma spectrum was taken in the gate the coincident gamma spectrum was very similar to the one shown in fig. 3. With the integral gamma spectrum above 500 keV taken in the gate, which completely excluded the contribution of

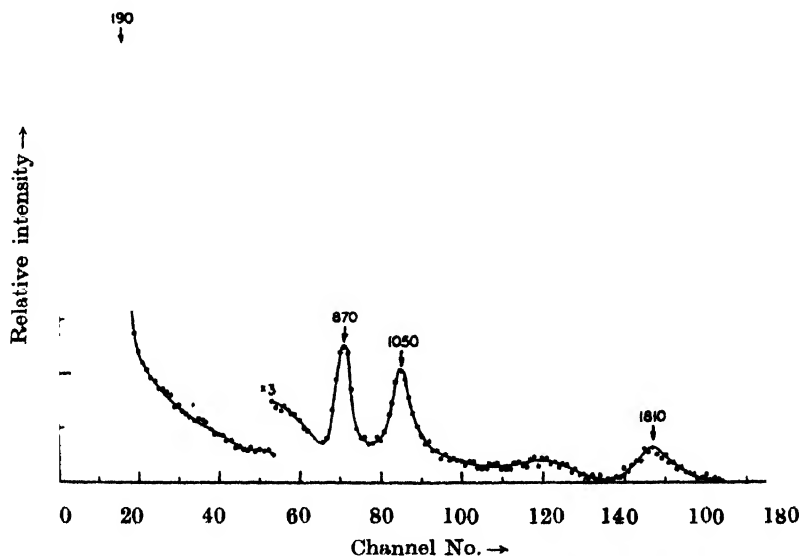


Fig. 7. Gamma spectra in coincidence with the integral gamma rays above 500 keV.

Yb^{175} the coincident gamma spectrum showed the photopeaks at energies 50, 190, 870, 1050 and 1800 keV (fig. 7). The 870 keV gamma ray was in coincidence with the 50, 190, 1050 and 1800 keV gamma rays while 1050 keV gamma ray was found in coincidence with a single gamma ray of 870 keV energy. When the 1800 keV gamma ray was taken in the gate, the coincidence spectrum showed the 50, 190- and 870 keV gamma rays. With the 390 keV gamma ray taken in the gate the 50, 90-, 190- and 285-keV gamma rays appeared in coincidence (fig. 8). The

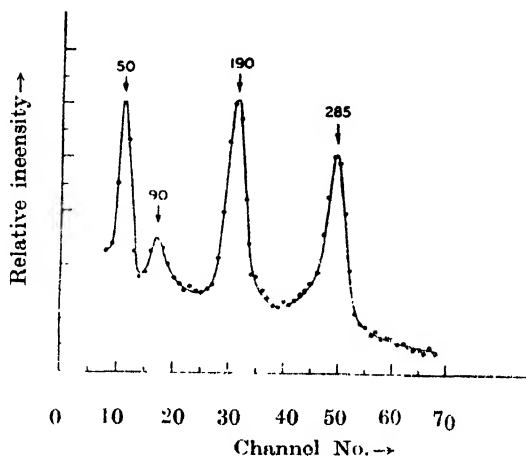


Fig. 8. Gamma spectrum in coincidence with the 390-keV gamma ray.

coincidence experiments with 50-, 190- and 285-keV gamma rays showed that there existed a gamma ray cascade of energies 90-290-285-190-50 keV. All the gamma-gamma coincidence results are given in Table II.

DECAY SCHEME AND DISCUSSION

For the isotope identification a radiochemical separation was not attempted since the measured cross-section for the $Yb^{176}(n, p)Tm^{176}$ reaction is very small. The assignment of the 1.4 min activity to Tm^{176} was based on the following arguments. This activity must be due to either Tm^{176} or Er^{173} produced by the (n, p) or (n, α) reactions, respectively since other possible reaction products of Yb^{176} are well studied (Nuclear Data Sheets, 1965) and none is associated with the above activity. From the studies of Coulomb excitation (De Boer *et al*, 1963) and also from the (α, xn) reaction (Morinaga, 1966) it is known that in Yb^{176} the gamma rays of energies 391, 293, 190 and 82 keV form a cascade of ground state rotational band $K = 0$ and give the levels at 0, 82, 272, 565 and 966 keV with spins 0^+ , 2^+ , 4^+ , 6^+ and 8^+ , respectively. The similarity of the low energy gamma rays and their cascade relationship (see Table II) observed in the decay of the 1.4 min activity with those of Yb^{176} suggests that the activity should be of Tm^{176} . It is to be noted that the gamma ray cascade of energies 90-390-285-190-50 keV decaying with a 1.4 min activity is also known from the studies (Kantele, 1964) of the

12-sec isomeric state of Yb^{176} . From the systematics for the beta decay energy (Yamada *et al*, 1961), the mass differences $\text{Tm}^{176}-\text{Yb}^{176}$ and $\text{Er}^{173}-\text{Tm}^{173}$ are 4200 and 2600 keV, respectively. The observed total beta decay energy Q_{β} -for the 1.4 min activity is 4088 ± 100 keV, in close agreement with the Q_{β} -for Tm^{176} . This also supports that the activity should be of Tm^{176} and not of Er^{173} .

A decay scheme of 1.4 min Tm^{176} which accounts for all the observed results is shown in fig 9. It should be noted that the 82-keV E2 gamma transition shown in the decay scheme was not resolved from the 91-keV gamma ray in most of the

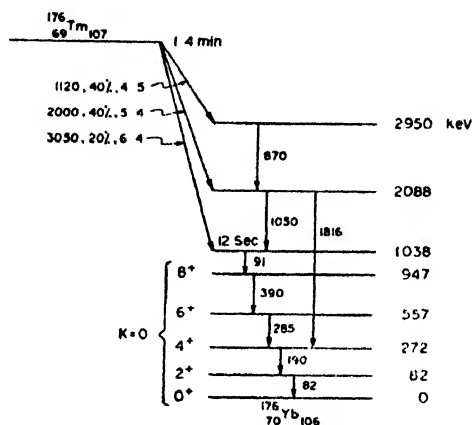


Fig. 9. Proposed decay scheme of Tm^{176} .

gamma spectra. The appearance of 50 ± 5 keV Yb K X-ray in observed gamma spectra was as expected since the theoretically calculated K internal conversion coefficient of the 82-keV E2 gamma transition is very high ($\alpha_k = 1.40$). The beta spectrum in coincidence with the integral gamma spectrum showed only two beta groups of end-point energies 2000 and 1150 keV (fig. 4). This might seem to suggest that the third beta group of 3050 keV end-point energy decays to the ground state of Yb^{176} . However, such a situation would be very unlikely because the 1800 keV gamma ray is in coincidence with two beta groups of maximum energies 2000 and 1150 keV and this fact indicates that the total decay energy is definitely greater than 3800 keV. Consequently, the 3050-keV beta group is shown to feed the 12-sec isomeric state.

The gamma spectra obtained by gating with the 500-3050 and 1000-3050 keV portions of the beta ray spectrum (fig. 5) show that the 870 keV gamma ray should be in coincidence with the 1150 keV beta group which is also confirmed by studying beta spectrum in coincidence with the 870 keV gamma ray (fig. 6). This gives the highest level in Yb^{176} at 2958 keV populated in the decay of Tm^{176} . The 1050 keV gamma ray which is in coincidence with two beta groups of end-point energies 2030 and 1140 keV and also with the 870 keV gamma ray gives the transition between the 2088 and 1038 keV levels of Yb^{176} .

In a study of the 12-sec isomeric state, Vergnes *et al.* (1965) assigned 8^- spin value to it from the consideration of the measured K-internal conversion coefficient (α_k) and total internal conversion coefficient (α_T) of the 93-keV gamma transition. α_k and α_T were obtained from the measured intensities of the 93, 190, 290 keV gamma rays and of the 50-keV X-ray, in the gamma spectrum resulted by gating with the 390-keV gamma ray. We have also estimated α_k and α_T for the 91-keV gamma transition from fig. 8 by following the same method. The intensity of the Yb K X-ray was corrected for the α_k values of the 82-, 190- and 290 keV E2 gamma transitions and also for the known K-fluorescence yield, $W_K = 0.937$. The intensity of the 91-keV photopeak was corrected for the contribution coming from the 82 keV E2 gamma transition. The experimentally measured values and the theoretical estimates (Sliv and Band, 1956, 1958) for different multipolarities of 91 keV gamma ray transition are given in Table III. Comparison shows that 91 keV gamma ray is either predominantly E2 or is a mixed E1+M2 transition.

TABLE III

Theoretical and experimental internal conversion coefficients of the 91 keV gamma transition in Yb^{176}

Calculated (Sliv and Band, 1956, 1958)				Experimentally measured value	Ref.
E1	E2	M1	M2		
0.35	1.15	3.45	28	1.1 ± 0.5	Present work
				0.9 ± 0.5	(Vergnes <i>et al.</i> , 1965)
0.42	4.45	4.20	41	4.0 ± 1.0	Present work.
				1.9 ± 0.8	(Vergnes <i>et al.</i> , 1965)

Comparison shows that it is either predominantly E2 or is a mixed E1+M2 transition.

The first possibility which gives E2-multipolarity for the 91 keV gamma transition suggests a spin as 6^+ or 10^+ for the 12-sec isomeric state. Since no reasonable combinations of the neutron and proton orbitals, which give rise to the low-lying states in Yb^{176} can have a spin value 10^+ it is plausible that the 6^+ assignment is more probable. With this spin value the 91-keV E2 gamma transition would be retarded by a factor $\approx 10^8$ from the Moszkowski single particle estimate (Moszkowski, 1965). This retardation is typical of a transition being hindered by 4 units of K-forbiddenness as it is known (Goldhaber *et al.*, 1965) that each unit of K-forbiddenness introduces a hindrance factor of $\approx 10^2$. Thus one gets a quantum number $K = 6$ for the 12-sec isomer. The observed beta transition from the 1.4 min state of Tm^{176} to an isomeric state can be classified as an allowed hindered or as a first forbidden unhindered type (Mottelson *et al.*, 1959; Gallagher

et al, 1962); this suggests a spin of Tm^{176} as 4^+ or 5^+ or 6^+ . Examination of the Nilsson diagram reveals that nuclides with 69 protons should have orbitals $1/2^+[411\downarrow]$ as their lowest configuration over a wide range of deformation. Similarly, for 107th neutron in Yb^{177} , Lu^{178} , Hf^{179} , Ta^{180} , W^{181} , Re^{182} and Os^{183} , the ground state configuration is $9/2^+[624\uparrow]$ (Mottelson *et al*, 1959; Gallagher *et al*, 1962). The coupling of $1/2^+$ with $9/2^+$ in strong coupling limit gives the possible spin values of Tm^{176} as 4^+ or 5^+ . The 4^+ spin state should be the lower one according to the rule of Gallagher and Moszkowski (1958). The 5^+ spin assignment to the ground state of Tm^{176} is in agreement with the observed log ft value for the beta transition to the 6^+ 12-sec isomeric state. The observed log ft values for the remaining two beta groups which come under the hindered or unhindered allowed type beta transitions suggest that the spin and parity of 2088 and 2950 keV levels should be either 4^+ or 5^+ or 6^+ .

The second possibility that the 91-keV gamma transition should be of E1 type with a feeble mixture of M2 indicates that the parity of the isomeric level is negative and its spin should be either 7 or 8 or 9. The value 7^- can be eliminated as it will permit strong E1 transition of 482 keV energy to the rotational 6^+ level which is not actually observed. Out of 8^- and 9^- the former one is preferable on the following arguments : (1) From the systematics study one finds that Hf^{178} and Hf^{180} decay to 8^+ level of their respective rotational bands through the E1-gamma transitions and have spins as 8^- (Nuclear Data Sheets, 1965). (2) the calculations on the two quasi-particle excited states in strongly deformed nuclei (Pyatov *et al*, 1964) give a first excited two-quasi-particle level for Yb^{176} as 8^- with the energy 1100 keV. This is in good agreement with the observed isomeric state at 1038 keV. (3) The two-quasi-particle 9^- state in Yb^{176} should lie at much higher excitations (Pyatov *et al*, 1964).

The 91 keV E1 transition would be retarded by a factor of 10^{14} giving 7 units of K-forbiddenness. This is in agreement with the quantum number $K = 8$ for the isomeric state. The observed beta transition feeding this level indicates a spin value of 8 or 8 ∓ 1 with either parity to the 1.4 min state of Tm^{176} . This also suggests that probably the 1.4 min state should be an isomeric state of Tm^{176} arising from the coupling of the neutron and proton orbitals near by 69th and 107th orbitals, respectively. In fact, one can get the spin values of 8^- and 7^+ by coupling a proton orbital $7/2-[523\uparrow]$ with the neutron orbitals $9/2^+[624\uparrow]$ and $7/2-[514\downarrow]$, respectively. In this situation the other excited states in Yb^{176} can have different possible high spin values. The present information is not sufficient to give conclusive assignments to them.

ACKNOWLEDGMENTS

The authors wish to express their gratitude to Professor B. D. Nagchaudhuri and Professor D. N. Kundu for their kind interest. They are also indebted to

Mr. B. Sethi for the helpful discussions and to the technical staff of the Neutron Physics Section for sample irradiations.

REFERENCES

- De Boer, J., Goldring, G. and Winkler, H., 1963, *Proc. Third Conf. on Reactions between Complex Nuclei*, Asilomom, Calif., 317.
- Gallagher Jr., C. J. and Moszkowski, S. A., 1958, *Phys. Rev.*, **111**, 1082.
- Gallagher Jr., C. J. and Soloviev, V. G., 1962, *Mat. Fys. Skr. Dan. Vid. Selsk.*, **2**, No. 2.
- Goldhaber, M. and Sunyar, A. W., 1965, *Alpha- beta- and gamma-ray spectroscopy*, North-Holland Publ. Co., Amsterdam, Vol. **2**, 945.
- Gujrathi, S. C. and Mukherjee, S. K., 1965, *unpublished*.
- Kantole, J., 1962, *Phys. Lett.*, **11**, 59.
- Morinaga, H., 1966, *Nuclear Phys.*, **75**, 385.
- Moszkowski, S. A., 1965, *Alpha-, beta- and gamma-ray spectroscopy*, North-Holland Publ. Co., Amsterdam, Vol. **2**, 871.
- Mottelson, B. R. and Nilsson, S. G., 1959, *Mat. Fys. Skr. Dan. Vid. Selsk.*, **1**, No. 8.
- Mukherjee, S. K., Ganguly, A. K. and Majumdar, N. K., 1961, *Prof. Phys. Soc. (London)*, **77**, 508.
- Nuclear Data Sheets, 1965, *National Academy of Sciences*. National Research Council, Washington, D.C.
- Pyatov, N. I. and Soloviev, V. G., 1964, *Priprint*, Joint Institute for Nuclear Research, Dubna.
- Slater, D. N., 1962, *Gamma rays of radio-nuclides in order of increasing energies*, Butterworths Scientific Publications, London.
- Sliv, L. A. and Band, M. I., 1956-58, *Tables of internal conversion coefficients of gamma rays*, Academy of Sciences, Press USSR, Moscow-Leningrad.
- Takahashi, K. Kuroyangi, H. Y., Kotajima, K., Nagatani, K. and Morinaga, H. 1961, *J. Phys. Soc. (Japan)*, 1965, **16**, 1664.
- Vergnes, M., Rotbard, G., Ronsin, G. and Kalifa, J., 1965, *Phys. Lett.*, **18**, 325.
- Wille, R. G. and Fink, R. W., 1960, *Phys. Rev.*, **118**, 242.
- Yamada, M. and Matumoto Z., 1961, *J. Phys. Soc. (Japan)*, **16**, 1497.

THERMAL DIFFUSION AND INTERMOLECULAR FORCES IN BINARY INERT GAS MIXTURES

S. K. DEB AND A. K. BARUA

INDIAN ASSOCIATION FOR THE CULTIVATION OF SCIENCE, CALCUTTA-32. INDIA

(Received March 7, 1967)

ABSTRACT. Thermal diffusion factors of the binary inert gas mixtures He-Ne, Ne-Kr and He-Kr have been measured by the two-bulb method. Some improvements over the previous methods of measurements have been made. The data have been utilised to obtain several significant results on the unlike interactions between these gas pairs.

INTRODUCTION

It is wellknown that of all the transport properties, thermal diffusion is most sensitive to the form of the intermolecular potential. The effect of inelastic collisions on thermal diffusion in polyatomic gases cannot as yet be predicted satisfactorily (Monchick *et al*, 1963). Consequently, for the determination of intermolecular potential from thermal diffusion data only mixtures of monatomic gases are suitable. The existing data on thermal diffusion in binary mixtures have recently been reviewed by Saxena and Mathur (1965). Even for monatomic gas mixtures, the existing data are not very consistent amongst themselves. The earlier measurements on thermal diffusion factor α in monatomic gases are those of Grew *et al* (1947, 1954) who have considered the temperature dependence of α , whereas, Atkins *et al* (1939) have considered the composition dependence. More recently Heymann and Kistemaker (1959), Grew and Mundy (1961) and Ghazlan (1963) have measured thermal diffusion factors in several binary gas mixtures by using tracer technique. In the measurements of Grew *et al* (1947, 1954) and Atkins *et al* (1939) thermal conductivity analyser was used for the purpose of gas analysis which is not capable of yielding very accurate data. Another difficulty which is also common to the more recent measurements using tracer technique is the large difference between the temperature of the lower and the upper bulbs which makes the temperature assignment somewhat uncertain. Saxena and Mathur (1965) have pointed out the inadequacy of the existing data and have also suggested that at least for systems containing He, the main source of discrepancy between experimental and the calculated values of α is the choice of the potential. Consequently, we have thought it desirable to measure thermal diffusion in some selected inert gas mixtures by making improvements in the method of measurements.

In this paper we have reported the measurement of α of He-Ne, Ne-Kr and He-Kr systems by a two-bulb method in the temperature range 340°-540°K. The

temperature dependence of α of these systems has been studied only by Grew *et al.*, (1947, 1954). For the systems He-Ne the ionization potentials of the components are not very different as distinct from the system He-Kr. The usual combination rules are based on equality of the ionization potential of the interacting molecules (Hirschfelder *et al.*, 1954). These studies are, therefore, expected to show whether the discrepancy between the experimental and the calculated values of α is mainly due to inadequacy of the combination rules for unlike interactions or due to the choice of the potential model.

EXPERIMENTAL

The apparatus consisted of two copper bulbs joined by a brass tube of 0.6 cm. diameter and a metal stopcock having a bore of the same dimension. The volume of the upper bulb was 943 cc and that of the lower bulb 65 cc. The use of copper bulbs ensures better temperature equilibration of the gases inside with the temperature of the surrounding medium. The bulbs were kept in two furnaces the temperature of which were controlled by electronic regulators. The temperature control of both the furnaces was within 1% of the temperature. The actual temperatures of the bulbs were measured by thermocouples. For analysis the bulbs were connected to suitable glass circuits and the analyses were made by a mass spectrometer (Associated Electrical Industries, MS3 model). The gases were supplied by Messrs British Oxygen Co., England. He and Ne were spectroscopically pure and Kr contained small amount of Xe as impurity.

The temperature assignment was made by the following usual formula

$$\bar{T} = \frac{T_H T_C}{T_H - T_C} \ln \frac{T_H}{T_C} \quad \dots (1)$$

where T_H and T_C are the temperatures of the upper and the lower bulb respectively. As an improvement over the previous methods we have varied both T_H and T_C so that the difference between them is not more than 100°C. This ensures that the formula for calculating \bar{T} should hold reasonably well. The relaxation time for the binary system was calculated from the equation (Saxena *et al.*, 1962).

$$\tau = \frac{L}{A} \left(\frac{T_1}{V_1} + \frac{T_2}{V_2} \right)^{-1} \left[\frac{T}{D} \right]_{AV} \quad \dots (2)$$

$$\left[\frac{T}{D} \right]_{AV} = \frac{1}{L} \int_0^L \frac{T}{D} \cdot dz$$

where L is the effective length of the tube, A is the cross-sectional area of the connecting tube, T_1 and T_2 the temperatures of the bulbs in °K and V_1 , V_2 the

corresponding volumes, T is some average temperature between T_1 and T_2 and D is the mutual diffusion coefficient at temperature T .

From the calculated relaxation times the time needed for attaining steady state for each system was estimated. After sufficient time was allowed for the steady state, the metal stop-cock was closed and samples were taken from the top and the bottom bulbs several times and the average of those were taken as the correct composition. The fact that gases in both the top and the bottom bulbs can be analysed in a mass spectrometer is an added advantage over the tracer technique where the counting probe is placed at the lower bulb only.

Thermal diffusion factor was then calculated from the equation,

$$\alpha = \frac{\ln q}{\ln T_H/T_C} \quad \dots (3)$$

where q is the separation factor given by,

$$q = \frac{(x_1/x_2)_{Top}}{(x_1/x_2)_{Bottom}} \quad \dots (4)$$

x_1, x_2 being the concentrations of the lighter and the heavier component respectively. The experimental values of α are shown in Table I. The average deviation

TABLE I
Experimental thermal diffusion factors and unlike interaction parameters

System	T	α	Unlike interaction parameters on L-J (12 : 6) potential			
			From experimental α		from combination rules	
			σ_{12} Å	ϵ_{12}/k °K	σ_{12} Å	ϵ_{12}/k °K
He-Kr (He = 92.5%)	380	.685				
	420	.750				
	450	.785	3.180	125.0	3.117	41.31
	490	.810				
	540	.830				
Ne-Kr (Ne = 95%)	339	.380				
	378	.440				
	414	.465	3.230	130.0	3.214	77.09
	454	.485				
	492	.500				
He-Ne (He = 21%)	532	.505				
	339	.260				
	391	.285				
	426	.290	—	—	2.652	19.07
	462	.290				
	496	.300				
	540	.310				

of q values was within 1%. Depending on the sensitivity of the logarithmic table the error in α values can be much larger. However, from the scatter of α values it appears that the error in our measured values should be within 5% and for the smoothed out values it should be much less. The thermal diffusion factors obtained by us are given in Table I.

As the compositions of our mixtures are quite different from those of Grew *et al* (1947, 1954) no direct comparison of our data is possible. For the system He-Kr it is possible to convert our data (7% of Kr) so that a comparison with data of Ghozlan (1963) (using Kr⁸⁵ as trace) is possible. Our α values are found to be systematically lower than those of Ghozlan (1963). It is relevant here to mention that Mason, Islam and Weissman (1964) observed a similar discrepancy with the data of Ghozlan (1963) for the H₂-Kr system. Consequently, it is likely that there is a systematic error in the measurements of Ghozlan.

COMPARISON WITH THEORY

In order to test whether the usually observed discrepancy between experimental and calculated values of α is due to the choice of the potential model we have considered the most commonly used potential energy functions viz (1) Lennard-Jones (12 : 6), (2) exp-6 and (3) core potential. These potentials can be written as follows :

1. Lennard-Jones (12:6) potential,

$$\phi(r) = 4\epsilon \left[\left(\frac{\sigma}{r} \right)^{12} - \left(\frac{\sigma}{r} \right)^6 \right] \quad \dots (5)$$

where r is the distance between the molecules, ϵ the depth of the potential well and σ is the value of r for which $\phi(r) = 0$.

2. Exp-6 potential :

$$\begin{aligned} \phi(r) &= \frac{\epsilon}{1 - \frac{6}{\alpha}} \left[\frac{6}{\alpha} \exp \left\{ \alpha - \left(1 - \frac{r}{r_m} \right) \right\} - \left(\frac{r_m}{r} \right)^6 \right] \quad r \geq r_{max} \\ &= \infty \quad r \leq r_{max} \end{aligned} \quad \dots (6)$$

where r_m is the value of r for which $\phi(r)$ is minimum and α is a parameter.

3. Core potential :

$$\begin{aligned} \phi(r) &= 4\epsilon \left[\left(\frac{\sigma - 2a}{r - 2a} \right)^{12} - \left(\frac{\sigma - 2a}{r - 2a} \right)^6 \right] \quad r > 2a \\ &= \infty \quad r \leq 2a. \end{aligned} \quad \dots (7)$$

where

σ is the value of r for which $\phi(r) = 0$.

ϵ is the depth of the potential well.

$2a$ is diameter of the spherical core.

Also

$$a^* = \frac{2a}{\sigma - 2a} \quad \text{and} \quad \frac{1}{\sigma - 2a} = 1 + \frac{1}{\sigma - 2a}$$

The force parameters for the different potential models used to calculate α are shown in Table II. For the Lennard-Jones (12:6) and exp-6 potentials the unlike interactions were approximated by the usual combination rules. For the

TABLE II

Force constants used for $L-J$ (12:6), exp-6. Kihara-core potential

	*L-J (12:6)		*Exp-6			**Kihara-core potential		
	$\sigma \text{\AA}$	$\epsilon/k^\circ\text{K}$	$r_m \text{\AA}$	$\epsilon/k^\circ\text{K}$	α	$\sigma \text{\AA}$	$\epsilon/k^\circ\text{K}$	γ
He	2.556	10.22	3.135	9.16	12.4	2.313	41.3	0
Ne	2.749	35.60	3.147	38.0	14.5	2.673	52.5	0.05
Kr	3.679	167.00	4.956	158.3	12.3	3.570	204.0	0.11

* from Saxena *et al* (1965) **from Roy *et al* (1966)

core potential σ_{12} and ϵ_{12} were calculated by the combination rules used for the Lennard-Jones (12 : 6) potential and a_{12}^* were obtained from the relation,

$$(1 - a_{12}^*)^6 = [(1 - a_1^*)^6 \sigma_1^6 \times (1 - a_2^*)^6 \sigma_2^6]^{\frac{1}{2}} \quad (8)$$

The system He-Kr (with small percentage of Kr) may be considered as quasi-Lorentzian mixture and the Kihara approximation was used to calculate α (Hirschfelder *et al*, 1954). For the other two systems the Chapman-Cowling first approximation was used (Hirschfelder *et al*, 1954). The experimental and the calculated values of α for the different potentials are shown in Figs. 1-3. The collision integrals required for calculating α were obtained from MTGL by Hirschfelder *et al*. (1954) and those tabulated for the core potential by Barker (1964). As for He and Ne the core should be very small we have not calculated for the He-Ne system on the core potential. For the system He-Ne the agreement between the experimental and the calculated values of α is reasonably good. For the system Ne-Kr the agreement between the experimental and the calculated values is nearly the same for the Lennard-Jones (12 : 6) and the core potential but much worse for the exp-6 potential. It may also be seen that the slope of the experimental curve is steeper than that of the calculated curves. Regarding the system He-Kr

the same conclusions are similar to those for Ne-Kr although the difference between the experimental and the calculated values of α is more pronounced. It may also be seen that for this system core potential is slightly better than the Lennard-

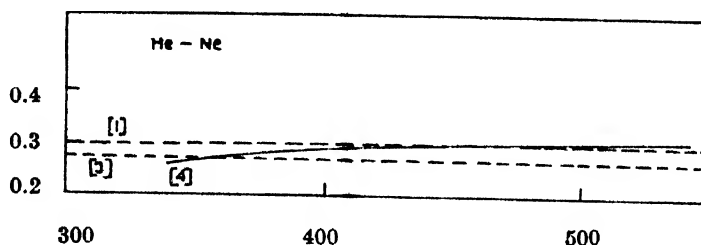


Fig. 1. Theoretical and Experimental curves for the thermal diffusion factor α of the system He-Ne.

- 1 Lennard-Jones (12 : 6)
- 3 Exp-six
- 4 Experimental.

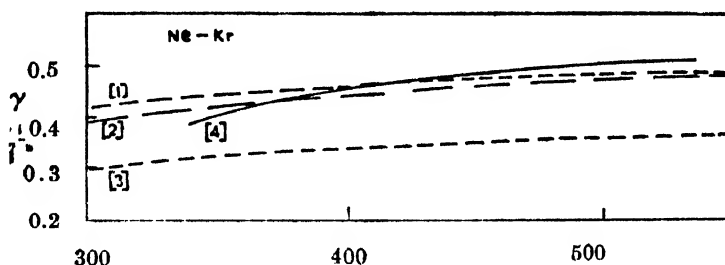


Fig. 2. Theoretical and experimental curves for the thermal diffusion factor α of the system Ne-Kr.

- 1 Lennard-Jones (12 : 6)
- 2 Kihara core.
- 3 Exp-six.
- 4 Experimental.

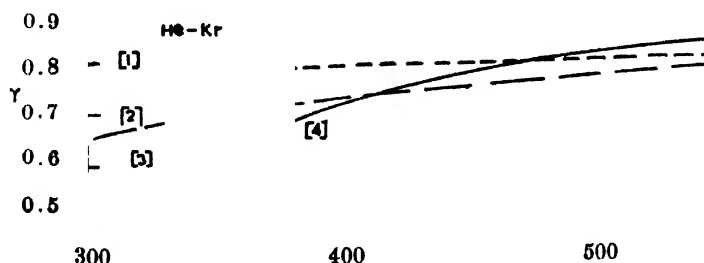


Fig. 3. Theoretical and experimental curves for the thermal diffusion factor α of the system He-Kr.

- 1 Lennard-Jones (12 : 6)
- 2 Kihara core.
- 3 Exp-six.
- 4 Experimental.

Jones (12 : 6) potential. One important result which comes out from these is that more different the constituents of the binary systems are the worse is the agreement between the experimental and the calculated values. It may be pointed out that the combination rule for ϵ (which is most important for calculating the temperature dependence of α) is based on the equality of the ionization potential for the interacting molecules (Hirschfelder *et al*, 1954). Consequently for dissimilar molecules the combination rule is likely to give erroneous results. It may also be seen that in contradiction to the suggestion of Saxena and Mathur (1965) the exp-6 potential fares worse than the Lennard-Jones (12: 6) potential for the He-Ne and very prominently for the He-Kr system.

DETERMINATION OF UNLIKE INTERACTIONS

It has been discussed above that the main source of discrepancy between the experimental and the calculated values of α probably lies in the combination rules. Consequently, we have thought it sufficient to determine the parameters for the Lennard-Jones (12: 6) potential only. Since for the system He-Ne the agreement with the calculated values is good we considered only the systems He-Kr and Ne-Kr.

The thermal diffusion factor to the first approximation can be written as (Hirschfelder *et al*, 1954).

$$\alpha_1 = A(6C_{12}^* - 5) \quad \dots (9)$$

where A is dependent on mole-fractions and potential parameters and C_{12}^* is a ratio of collision integrals which has been tabulated. A is a very slowly varying function of temperature. The second approximation to α can be written as,

$$\alpha_2 = A(6C_{12}^* - 5)(1 + k) \quad (10)$$

where k is a correction term. For α values at two temperatures, T_1 and T_2 we have,

$$\frac{[\alpha_2]_{T_1}}{[\alpha_2]_{T_2}} = \frac{A_{T_1}}{A_{T_2}} \cdot \frac{\{6C_{12}^*(T_1) - 5\}}{\{6C_{12}^*(T_2) - 5\}} \cdot \frac{(1 + k_{T_1})}{(1 + k_{T_2})} \quad (11)$$

The variation of the correction term with temperature is very small so that we may write

$$\frac{[\alpha_2]_{T_1}}{[\alpha_2]_{T_2}} = \frac{A_{T_1}}{A_{T_2}} \cdot \frac{[6C_{12}^*(T_1) - 5]}{[6C_{12}^*(T_2) - 5]} \quad (12)$$

Since A is also a slowly varying function of temperature we have calculated A_{T_1} and A_{T_2} by the usual combination rules. Then from any pair of α values at two temperatures it is possible to calculate $\epsilon_{12/k}$ values from Eq. (12). Then as a second approximation this value of $\epsilon_{12/k}$ was used to calculate A_{T_1} and A_{T_2} .

and ϵ_{12}/k was determined again. Generally the difference between those values of ϵ_{12}/k was quite small. The average ϵ_{12}/k as determined from different pairs of α was taken as the correct value.

Once ϵ_{12}/k is known, σ_{12} can be obtained from the relation,

$$\alpha_2 = \alpha_1(1+k),$$

k may be written approximately as, (Weissman *et al*, 1960)

$$k = \frac{1}{42} (8E_{22}^* - 7)^2 + \frac{2}{21} \left(1 - \frac{M_2}{M_1}\right) (8E_{22}^* - 7) \left[1 - \frac{3}{4}(5 - 4B_{12}^*)(6C_{12}^* - 5)^{-1}\right] \quad (13)$$

where

$$B_{12}^* = \frac{5\Omega_{12}^{(1,2)*} - 4\Omega_{12}^{(1,1)*}}{\Omega_{12}^{(1,1)*}}$$

and

$$E_{22}^* = \frac{\Omega_{22}^{(3,3)*}}{\Omega_{22}^{(2,2)*}}$$

the subscript 1 refers to the heavier species. From Eq. (10) it is possible to find the value of σ_{12} which represents α_2 correctly. The average of σ_{12} as determined from α values at different temperatures was taken as the correct value. The parameters thus obtained are shown in Table I together with those calculated from the combination rules.

It may be seen from the Table I that the depth of the potential well for the unlike interactions is much deeper than that given by the combination rule. It appears that the heavier molecule predominates in the interaction and equal weight cannot be placed on two dissimilar molecules to calculate the unlike interaction parameters.

ACKNOWLEDGMENT

The authors are grateful to Prof. B. N. Srivastava for his kind interest in the work.

REFERENCES

- Atkins, B. E., Bastick, R. E., and Ibbs, T. L., 1939, *Proc. Roy. Soc.*, **172**, 142.
 Barker, J. A., Fock, W., and Smith, F., 1964, *Phys. Fluids*, **7**, 897.
 Ghozlan, A. I., 1963, *Doctoral Thesis* (Amsterdam).
 Grew, K. E., 1947, *Proc. Roy. Soc.*, **189**, 402.
 Grew, K. E., Johnson, F. A., and Neal, W. E. J., 1954, *Proc. Roy. Soc.*, **22A**, 513.
 Grew, K. E., and Mundy, J. N., 1961, *Phys. Fluids*, **4**, 1325.
 Heymann, D., and Kistemaker, J., 1959, *Physica*, **25**, 556.

- Hirschfelder, J. O., Curtiss, C. F., and Bird, R. B., 1954, *Molecular Theory of Gases and Liquids*. John Wiley & Sons, Inc., New York.
- Mason, E. A., Islam, M., and Weissmann, S., 1964, *Phys. Fluids*, **7**, 174.
- Monchick, L., Yun, K. S., and Mason, E. A., 1963, *J. Chem. Phys.*, **39**, 654.
- Roy, A. N., and Deb, S. K., 1966, *Indian J. Phys.*, **40**, 12.
- Saxena, S. C., and Mason, E. A., 1962, *Mol. Phys.*, **2**, 264.
- Saxena, S. C., and Mathur, B. P., 1965, *Rev. Mod. Phys.*, **37**, 316.
- Weissman, S., Saxena, S. C., and Mason, E. A., 1960, *Phys. Fluids*, **3**, 510.

SECOND HARMONIC GENERATION IN TWO LEVEL SYSTEMS

B. K. MOHANTY

DEPARTMENT OF PHYSICS, INDIAN INSTITUTE OF TECHNOLOGY, KHARAGPUR, INDIA.

(Received January 30, 1967; Resubmitted June 2, 1967)

ABSTRACT. Interaction of strong electromagnetic field with a two energy level system is considered, with special reference to crystals. Second harmonic generation due to the field dependence of the dipole moment operator is found out. The frequency dependence of the dipole moment expectation value and the field saturation effect have been derived. The detailed relation between the field and the dipole moment, and the d.c. effect have been briefly discussed.

INTRODUCTION

A revival of interest in the study of propagation of electromagnetic waves through crystals, accomodating the nonlinear effects like multiple harmonic generation, has been noticed recently (Briss 1964). This has followed naturally after the observation of second harmonic generation (SHG) in quartz crystal, using a ruby laser source by Franken and others (Franken, et al 1961) and allied effects in other crystals by several other workers (Franken *et al*, 1963). All these effects need highly intense sources (Bonch-Bruевич *et al*, 1965) and for second harmonic generation it is found that the lack of an inversion centre in the crystal is a necessity. These processes can be described by a higher than first order perturbation calculation (Ward 1965), which means that more than two energy levels take part in the interaction. But it is quite possible that second harmonic generation can be observed in systems where only two energy levels are involved in the interaction (Bonch-Bruевич *et al*, 1965). In a previous paper (Mohanty 1967) the author has pointed out two separate conditions which are necessary to generate multiple harmonics of the applied field frequency in a two level system : The presence of a premanent dipole moment in the material system interacting with the field, or, as in the case of crystals, the dependence of the dipole moment operator on the applied field which gives a nonlinear dipole interaction operator in terms of the field. The first condition has already been discussed in the above mentioned paper (Mohanty 1967). The primary aim of this article is to discuss the second condition. Further, considering that only coherent radiation from a laser source is necessary for the process, we will directly find out the expectation value of the dipole moment for a single particle instead of trying to find the probability coefficients and then the transition probability.

DESCRIPTION OF THE MODEL

As our interests primarily lie in the processes where only two energy levels of the material system take part, the technique to be used in this discussion is the geometrical representation of the Schrodinger equation due to Feynman, Vernon and Hellworth (Feynman, *et al.* 1957). This representation involves only two energy levels of the material system, and is quite adequate as a monochromatic incident field is expected to induce a transition primarily between two levels whose transition frequency is nearly equal to the frequency of the field itself. The representation has the added advantage of giving directly the expectation value of the dipole moment operator. The technique is indicated in the previous paper by the author (Mohanty 1967).

The geometrical form of the Schrodinger equation

$$(H_0 + V)\psi = i\hbar \frac{d\psi}{dt} \quad \dots (2.1)$$

for a two level system, where H_0 is the unperturbed hamiltonian and V the interaction operator, is of the form of the equation of motion of a classical gyroscope, as explained by Mohanty (1967).

$$\frac{d\vec{r}}{dt} = \vec{\omega} \times \vec{r} \quad \dots (2.2)$$

\vec{r} and $\vec{\omega}$ are defined in the previous paper (Mohanty, 1967).

The physical significance of r_i 's are immediately found out by taking the expectation values of the dipole moment operator μ and H_0 .

$$\begin{aligned} \langle \mu \rangle &= \int \psi^* \mu \psi dv = \mu_{12} r_1 \\ \langle H_0 \rangle &= \frac{\hbar \omega_{12}}{2} r_3 \end{aligned} \quad \dots (2.3)$$

where μ_{11} are neglected in comparison with μ_{12} .

THE DIPOLE INTERACTION

The interaction V , between the field and the material system, is assumed to be of electric dipole type and is expressed by :

$$\vec{V} = -\vec{\mu} \cdot \vec{E} \quad \dots (3.1)$$

$\vec{\mu}$ being the electric dipole moment operator and \vec{E} is the electric field inducing the transition between the levels. The semiclassical form of V is sufficiently accurate for the present discussion compared to the fully quantum theoretical treatment (Mandel *et al* 1963; Sudarshan 1963). This interaction term is linear in terms of the applied field as long as μ is independent of the field.

But for the intense field which is a necessity in the present case, it is no longer possible to write μ as a single field independent term, as is done in finding out the expectation value of dipole moment which is linear in terms of the applied field. The precise relationship between μ and E is now assumed to be of a tensorial nature, but one can write it in the form (Franken *et al.* 1963);

$$\mu = \mu_0 + \mu_1 E + \mu_2 E^2 + \dots \quad (3.2)$$

This schematic relationship, in the form of a power series in E , is sufficient for the present discussion and, as can be seen presently, the full tensorial form in no way changes the result as the same time dependence for all components is assumed in these discussions. The value of successive coefficients μ_1 are in rapidly decreasing order (Franken *et al.* 1963) and so only the first two terms are preserved. As mentioned, the use of the first term only gives the linear component or the expectation value of the dipole moment through the linear component of the dipole interaction operator. The second term, however, gives a nonlinear component to the interaction operator, with frequencies 0 and 2ω . This term is expected to contribute to the nonlinear expectation value of μ .

Writing the interaction term V :

$$\begin{aligned} V &= -\mu_0 E - (\mu_1 E) E \\ &= \sum_{n=0}^2 I_n \cos n\omega t = \text{Re.} \sum_{n=0}^2 I_n e^{-in\omega t} \quad \dots \quad (3.3) \end{aligned}$$

where

$$I_0 = I_2 = -\frac{\mu_1 E_0^2}{2} ; \quad I_1 = -\mu_0 E_0$$

the nonlinearity of the dipole interaction operator is now clearly demonstrated.

So,

$$\begin{aligned} \omega_1 &= \sum_n \frac{2(I_n)_{12}}{\hbar} \cos n\omega t \\ \omega_2 &= \sum_n \frac{2(I_n)_{12}}{\hbar} \sin n\omega t \quad \dots \quad (3.4) \end{aligned}$$

As ω_1 and ω_2 contain sinusoidal terms of three frequencies, 0, ω and 2ω , the values of the \vec{r} components are now expected to contain all these, as well as the higher harmonics of ω . The second harmonic component of $\langle \mu \rangle$ then emerges as the sum of the product of $\mu_1 E$ in eqn. (3.2) and the linear frequency component of r_1 , and the product of μ_0 in eqn. (3.2) and the second harmonic

component of r_1 . One then writes for the second harmonic value of $\langle \mu \rangle$, using (2.3) and (3.2);

$$\begin{aligned}\langle \mu \rangle_{2\omega} &= (\mu_{12} r_1)_{2\omega} \\ &= (\mu_0)_{12}(r_1)_{2\omega} + (\mu_1 E)_{12}(r_1)_a\end{aligned}\quad \dots (3.5)$$

To solve the eqn. (2.2) one can now subject all the r' components to the rotating coordinate transformation given in 1, which gives the changed equation :

$$\frac{dr'}{dt} = \vec{\omega}' \times r'$$

with

$$\omega'_1 = (K_1 + K_2 \cos \omega t)$$

$$\omega'_2 = 0$$

$$\omega'_3 = \omega_{12} - \omega; \quad K_n = \frac{2(J_n)_{12}}{h}$$

where the V_{11} and V_{22} terms in ω'_3 are neglected in comparison with ω_{12}

The explicit form of the above equation is :

$$\frac{dr'_1}{dt} = -\Delta r'_2$$

$$\frac{dr'_2}{dt} = \Delta r'_1 - [K_1 + K_2 \cos \omega t] r'_3 \quad \dots (3.7)$$

$$\frac{dr'_3}{dt} = [K_1 + K_2 \cos \omega t] r'_2$$

where

$$\Delta = \omega_{12} - \omega.$$

THE VALUE OF $(r_1)_\omega$ AND $(r_1)_{2\omega}$

A solution of the type

$$r'_i = \sum r_{i, (n)} e^{-in\omega t} \quad \dots (4.1)$$

is assumed to solve the set of equations (3.7). $r_{1, (0)}$ and $r_{2, (0)}$ are the linear solutions and $r_{1, (1)}$ and $r_{2, (1)}$ are the second harmonic part.

After performing the necessary differentiation and collecting the coefficients of $e^{-in\omega t}$ one gets :

$$\begin{aligned} -in\omega r_{1,(n)} &= -\Delta r_{2,(n)} \\ -in\omega r_{2,(n)} &= \Delta r_{1,(n)} - K_1 r_{3,(n)} - \frac{K_1}{2} [r_{3,(n-1)} + r_{3,(n+1)}] \\ &\dots (4.2) \\ -in\omega r_{3,(n)} &= K_1 r_{2,(n)} + \frac{K_2}{2} [r_{2,(n+1)} + r_{2,(n-1)}] \end{aligned}$$

One must consider also the symmetry properties of $r_{l,(n)}$:

$$r_{l,(n)} \left(-\frac{K_2}{2K_1} \right) = (-1)^n r_{l,(n)} \left(\frac{K_2}{2K_1} \right) \quad \dots (4.3)$$

Now putting $\frac{K_2}{2K_1} = Q$; $\frac{\Delta}{K_1} = D$ and $\frac{i\omega}{K_1} = N$;

and expanding $r_{l,(n)}(Q)$ in terms of Q :

$$r_{l,(n)}(Q) = \sum_{j=0}^{\infty} r_{l,(n),j} Q^j \quad \dots (4.4)$$

one sees, using eqn.(4.3), that only even combinations of n and j can exist in the expansion of $r_{l,(n)}(Q)$ in eqn. (3.4).

Using equations (4.2) and (4.4) and collecting the coefficients of Q^j , one gets :

$$\begin{aligned} nNr_{1,(n),j} &= Dr_{2,(n),j} \\ -nNr_{2,(n),j} &= Dr_{1,(n),j} - r_{3,(n),j} - r_{3,(n+1),(j-1)} - r_{3,(n-1),(j-1)} \\ -nNr_{3,(n),j} &= r_{2,(n),j} + r_{2,(n+1),(j-1)} + r_{2,(n-1),(j-1)} \end{aligned} \quad \dots (4.5)$$

It is quite easy to seem that for $j = 0$; $r_{l,(n),0}$ is independent of Q (eqn. 4.4) and as this solution may be assumed to be an exact one with only a frequency ω for r_1 , and r_2 no higher order solution exists. (Mohanty 1967; for a similar comment, also see Sengupta 1967)

So,

$$r_{l,(n),0} = d_{n0} r_{l,(n),0} \quad \dots (4.6)$$

Then the zeroeth order ($n = 0$) solution, giving the value of $(r_1)_\omega$ is :

$$\begin{aligned} r_{2,(0),0} &= 0 \\ r_{1,(0),0} &= \frac{1}{D} r_{3,(0),0} \end{aligned} \quad \dots (4.7)$$

The first order ($n = 1$) equation is :

$$\begin{aligned}Nr_{1,(1),1} &= Dr_{2,(1),1} \\ -Nr_{2,(1),1} &= Dr_{1,(1),1} - r_{3,(1),1} - r_{3,(0),0} \\ -Nr_{3,(1),1} &= r_{2,(1),1}\end{aligned}\quad (4.8)$$

One then has,

$$\begin{aligned}r_{1,(0),0} &= \frac{K_1}{\Delta^2 - \omega^2 + K_1^2} r_{3,(0),0} \\ r_{1,(1),1} &= \frac{\Delta K_1}{\Delta^2 - \omega^2 + K_1^2} r_{3,(0),0} \\ r_{2,(1),1} &= \frac{i\omega K_1}{\Delta^2 - \omega^2 + K_1^2} r_{3,(0),0}\end{aligned}\quad (4.9)$$

Effecting the inverse transformation given in (Mohanty 1967) and collecting the relevant terms :

$$\begin{aligned}r_1(\omega) &= \frac{K_1}{\omega_{12} - \omega} r_{3,(0),0} \cos \omega t \\ r_1(0) &= \frac{1}{4} \frac{K_2(\omega_{12} - 2\omega)}{\omega_{12}(\omega_{12} - 2\omega) + K_1^2} r_{3,(0),0} \\ r_1(2\omega) &= \frac{1}{4} \frac{K_2\omega_{12}}{\omega_{12}(\omega_{12} - 2\omega) + K_1^2} r_{3,(0),0} \cos 2\omega t\end{aligned}\quad (4.10)$$

From these values, making use of eqn. (2.3) we have,

$$\langle \mu \rangle_{2\omega} = (2\hbar)^{-1} r_{3,(0),0} \left[\frac{(\mu_0)_{12}(\mu_0 E_0^2)_{12}}{2(\omega_{12} - 2\omega) + 2K_1^2/\omega_{12}} + \frac{2(\mu_1 E_0)_{13}(\mu_0 E_0)_{12}}{(\omega_{12} - \omega)} \right] \cos 2\omega t \quad \dots (4.11a)$$

$$\langle \mu \rangle_0 = (2\hbar)^{-1} r_{3,(0),0} \left[\frac{2(\mu_1 E_0)_{12}(\mu_0 E_0)_{12}}{(\omega_{12} - \omega)} + \frac{1(\mu_0)_{12}(\mu_1 E_0^2)_{12}(\omega_{12} - 2\omega)}{2(\omega_{12} - 2\omega)\omega_{12} + K_1^2} \right] \quad (4.11b)$$

DISCUSSION

We shall now discuss the exact tensorial nature of μ . The schematic dependence of polarisation P (dipole moment per unit volume) and the field E is written down as (Bonch-Bruевич *et al.* 1965);

$$P = \chi_0 E + \chi E^2 + \dots \quad (5.1)$$

The process of second harmonic generation is described by χ , and it is evident that this is related to $\langle \mu \rangle_{0,2\omega}$ of the eqn. (4.11). For the generation of second

harmonic an essential condition is the lack of a symmetry centre in the crystal, otherwise a strong, static electric field must be applied to enhance the nonlinearity of the relation between the crystal polarisation and the applied field. In general, for such a case the quadratic part of P is written down as

$$P_i^{(2)} = \Sigma \Sigma \chi_{ijk} E_j E_k \quad (5.2)$$

Consideration of the fact that the order of writing down the fields E_j and E_k is immaterial and that this tensor is formally similar to the piezo-electric tensor (Franken *et al.* 1961) enables us to write down a contracted form by replacing the suffixes i, j by only one suffix m . A further symmetry restriction proposed by Kleinman (1962) allows the inter-change of i and j , which has the advantage of reducing the number of independent tensor elements. χ is a 3×6 tensor, and particularly, for quartz,

$$P^{(2)} = \begin{pmatrix} \chi_{11} & -\chi_{11} & 0 & \chi_{14} & 0 & 0 \\ 0 & 0 & 0 & 0 & -\chi_{14} & -\chi_{14} \\ 0 & 0 & 0 & 0 & 0 & 0 \end{pmatrix} \begin{pmatrix} E_x^2 \\ E_y^2 \\ E_z^2 \\ 2E_y E_x \\ 2E_x E_z \\ 2E_x E_y \end{pmatrix} \dots \quad (5.3)$$

By suitable experimental arrangements the contribution from some elements can be reduced and one can check the additional symmetry requirements (Miller 1963). Under this condition eqn. (5.3) gives :

$$P^{(2)} = \hat{i}\chi_{11}E_x^2 - \hat{j}2\chi_{14}E_xE_z \quad (5.4)$$

A comparison of the contributions from χ_{11} and χ_{14} shows that $\chi_{11} \gg \chi_{14}$ for a ruby laser. This demonstrates the possibility of reducing the number of elements of the tensor by suitable arrangements.

Finally a few words about the generation of a frequency independent part of $\langle \mu \rangle$, otherwise known as the d.c. effect are in order. An inspection of the value of $\langle \mu \rangle_0$ in eqn. (4.11b) shows the inherent difficulties in the experimental detection of this effect. At $\omega_{12} = \omega$, as the fundamental harmonic part of $\langle \mu \rangle = \langle \mu \rangle_\omega$ predominates; and also at $\omega_{12} = 2\omega$, as there is negligible power transfer at or near this frequency in the case of $\langle \mu \rangle_0$, it is a difficult effect to detect. This may explain the inconveniences originally encountered in the observation of this effect.

ACKNOWLEDGMENT

The author wishes to express his thanks to Prof. H. G. Venkates for his guidance and Prof. H. N. Bose for his kind encouragement in carrying out this piece of research. The author is also indebted to Prof. N. D. Sengupta for some stimulating discussions.

REFERENCES

- Bonch-Bruевич and Khodovoi, 1965, *Soviet Phys. USPEKHI*, **8**, 1.
 Briss, R. R., 1964, *Symmetry and Magnetism*, North Holland Publishing Co., p. 240.
 Feynman, R. P., Vernon, F. L., and Hellworth, R. W., 1957, *J. Appl. Phys.* **28**, 49.
 Franken, Hill, Peters and Weinreich, 1961, *Phys. Rev. Letts.*, ; **7**, 118.
 Franken, P. A. and Ward, J. F., 1963, *Revs. of Mod. Phys.* ; **35**, 23.
 Kleinman, D. A., 1962, *Phys. Rev.*, **126**, 1977.
 Mandel, L. and Wolf, E., 1963, *Phys. Rev. Letts.*, **10**, 276.
 Miller, R. C., 1963, *Phys. Rev.*, **131**, 95.
 Mohanty, B. K., 1967, *Indian J. Phys.*, **41**, 60.
 Sengupta, N. D., 1967, *Z. Physik.*, **200**, 13.
 Sudarshan, E. C. G., 1963, *Phys. Rev. Letts.* **10**, 77.
 Ward, J. F., 1965, *Revs. of Mod. Phys.*, **37**, 1,

THE LIFETIME OF METASTABLY BOUND POLAR MOLECULES

A. K. GHOSH

INDIAN ASSOCIATION FOR THE CULTIVATION OF SCIENCE, CALCUTTA-32.

(Received March 7, 1967)

ABSTRACT. Lifetime of metastably bound double molecules in polar gases has been considered. The method applied is similar to the one-body theory of α -radioactivity. The results show that the metastable systems have usually a life-time which is long compared to the mean time between collisions. Consequently, metastably bound molecules have to be treated as stable bound molecules.

INTRODUCTION

The bound double molecules may be defined as two molecule systems for which the total energy is less than the energy of the separated molecules (Stogryn *et al*, 1959). However, depending on the energy of the system, there are bound systems which from the standpoint of quantum mechanics can dissociate only by leakage through the potential barrier. These systems are known as metastably bound double molecules. The consideration of dimers is necessary for a proper understanding of the equation of state in gases and also to interpret transport properties of dense gases. An important property of the metastable systems is its half-life for dissociation. If the collision time is short compared to half-life, then the metastable molecules behave like bound molecules and if the reverse is true they are to be treated as free molecules. For non-polar gases, Stogryn and Hirschfelder (1959) have considered the half-life of metastably bound molecules. As the intermolecular potential of polar molecules differs widely from that of non-polar ones due to the presence of long-range dipole forces, it is necessary to consider separately the half-life of metastably bound double molecules in polar gases. In this paper, a calculation of the half-life has been made for H_2S which is a typical polar molecule.

THEORETICAL FORMULATION AND CALCULATION

It is possible to calculate the half-life of metastable molecules by using the WKB approximation, the theory being very similar to the one body model theory of α -radioactivity (Bethe, 1937, Kemble, 1937, and Bohm, 1951). Following this procedure, the time period of vibration t can be written as (Stogryn *et al*, 1959),

$$t = 2 \int_{r_1}^{r_2} \frac{dr}{\sqrt{2\mu(K - \phi_{eff})}} \quad \dots (1)$$

where K is the initial relative kinetic energy or the total kinetic energy in the centre of mass coordinate system, μ the reduced mass of the molecules, r_1 , r_2 the two turning points for a fixed value of K and Kb^2 , and $\phi_{eff} = \phi(r) + Kb^2/r^2$, b being the impact parameter. Thus, the probability of dissociation per second, P , is given by,

$$P = \theta/t \quad \dots (2)$$

where θ is the probability of transmission through the barrier and the mean life time τ is

$$\tau = \frac{1}{P} = t/\theta \quad \dots (3)$$

Following the WKB method, the transmission coefficient, θ is given by,

$$\theta = e^{-2G}$$

where

$$G = \frac{1}{\hbar} \int_{r_1}^{r_2} \sqrt{2\mu(\phi_{eff} - K)} dr, \quad (4)$$

r_1 and r_2 being the turning points inside and outside the potential well respectively. The WKB approximation is valid for $G > 1$.

For polar molecules the potential energy of interaction can be written as (Hirschfelder, *et al*, 1954),

$$\phi(r) = 4\epsilon[(\sigma/r)^{12} - (\sigma/r)^6] - \frac{\mu^2}{r^3} g(\theta_1, \theta_2, \phi) \quad (5)$$

$$g(\theta_1, \theta_2, \phi) = 2 \cos \theta_1 \cos \theta_2 - \sin \theta_1 \sin \theta_2 \cos \phi$$

where θ_1, θ_2 are the angles of inclination of dipoles (dipole moment μ) to the line joining the centres of the molecules and ϕ is the azimuthal angle. For $\mu \rightarrow 0$, Eq. (5) reduces to the well known Lennard-Jones (12:6) potential for non-polar gases. For any particular relative orientation of the dipoles a numerical value can be assigned to $g(\theta_1, \theta_2, \phi)$ i.e. eq. (5) becomes,

$$\phi(r) = 4\epsilon[(\sigma/r)^{12} - (\sigma/r)^6] - \frac{A\mu^2}{r^3} \quad (6)$$

Let us define the following reduced quantities,

$$\phi^* = \phi/\epsilon, \quad K^* = K/\epsilon \quad \text{and} \quad b^* = b/\sigma$$

Then we have,

$$\phi_{eff}^* = 4y^6 - 4y^3 - 4A^*y^{3/2} + K^*b^{*2}y, \quad (7)$$

where $y = r^{*-2}$ and $A^* = \frac{A\mu^2}{4\epsilon\sigma^3}$

Consequently,

$$t = \frac{h}{2\epsilon\Lambda^*} \int_{y_2}^{y_1} dy / [y^{3/2}(K^* - 4y^6 + 4y^3 + 4A^*y^{3/2} - K^*b^{*2}y)^{\frac{1}{2}}] \quad \dots \quad (8)$$

and

$$G = \pi/\Lambda^* \int_{y_3}^{y_2} \frac{(4y^6 - 4y^3 - 4A^*y^{3/2} + K^*b^{*2}y - K^*)^{\frac{1}{2}}}{y^{3/2}} dy \quad (9)$$

where Λ^* is the reduced de Broglie wavelength of the molecules given by $\Lambda^* = h/\sigma\sqrt{m\epsilon}$ with σ , ϵ having usual significance.

The hyper-elliptic integrals in the right hand side of eqs. (8) and (9) were evaluated numerically. The limits of the integrals and the values of the integrals at the limiting points were obtained by the method described by Stogryn and Hirschfelder (1959).

TABLE I
Lifetime for metastably bound double molecules of H_2S

K^*b^{*2}	K^*	Λ^*G/π	$2\epsilon\Lambda^*t/h$	τ_{H_2S} (sec)
1.5734	0.03	1.455	9.19	2.47×10^8
	0.06	0.615	13.47	6.21×10^{-3}
	0.09	0.130	26.45	2.29×10^{-9}
3.1486	0.10	2.810	1.40	1.60×10^{27}
	0.20	1.581	1.63	1.79×10^{10}
	0.30	0.903	2.14	9.48
	0.40	0.404	2.45	1.31×10^{-9}
	0.98	0.137	1.18	1.30×10^{-10}
4.4382	1.00	0.081	2.32	4.22×10^{-10}
	1.02*	0.033	6.79	2.70×10^{-11}

G value for $K^ = 1.02$ is less than 1. Thus, WBK method does not hold for it.

In order to make sample calculation for H_2S it was assumed that the dipoles were in the head-to-tail position which corresponds to $A^* = 0.529$. For this potential the force constants have been obtained by Itean *et al*, (1961) and they are : $\sigma = 4.034 \text{ \AA}$; $\epsilon/k = 88.4^\circ\text{K}$ and $\Lambda^* = 0.197$. The integrals were evaluated for three fixed values of K^*b^{*2} and several values of K^* . The potential energy curves corresponding to K^*b^{*2} values are shown in Fig. 1. The values of τ thus obtained for H_2S are given in Table I.

The mean time between collisions is of the order of 10^{-9} or 10^{-10} secs. at N.T.P. A comparison with the results obtained for Argon by Stogryn and Hirschfelder

(1959) shows that the lifetime for metastably bound double molecules for a polar gas is much larger than for a non-polar gas. This result is expected due to the presence of long-range dipole-dipole force in polar gases which is generally attrac-

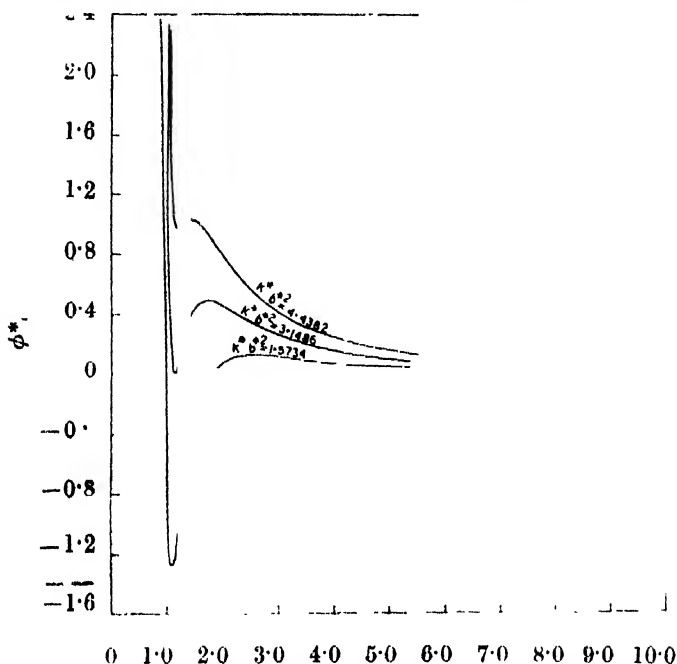


Fig. 1. Effective potential energy curves for H_2S .

tive. Thus except at very high energies the metastably bound molecules behave as stable molecules for polar gases. Consequently, the effect of metastable systems will be more in polar gases than in non-polar gases.

ACKNOWLEDGMENT

The author is grateful to Dr. A. K. Barua for his guidance and to Prof. B. N. Srivastava for his kind interest.

REFERENCES

- Bethe, H. A., 1937, *Rev. Mod. Phys.*, **9**, 69.
- Bohm, D., 1951, *Quantum Theory* Prentice-Hall, Inc., Englewood Cliffs, Chap. 12.
- Hirschfelder, J. O., Curtiss, C. F., and Bird, R. B., 1954, *Molecular Theory of Liquids and Gases*, John Wiley & Sons, Inc., New York.
- Itean, E. C., Glueck, A. R., and Svehla, R. A., 1961, *Nasa Technical Note*, D-481.
- Kemble, E. C., 1937, *The Fundamental Principles of Quantum Mechanics*, McGraw Hill Book Company, Inc., New York, Sec. 31.
- Stogryn, D. E., and Hirschfelder, J. O., 1959, *J. Chem. Phys.*, **31**, 1531.

DECAY OF Tm^{174}

S. C. GUJRATHI AND S. K. MUKHERJEE

SAHA INSTITUTE OF NUCLEAR PHYSICS, CALCUTTA, INDIA.

(Received February 16, 1967)

ABSTRACT. The Tm^{174} nucleus is produced by $\text{Yb}^{174} (n, p) \text{Tm}^{174}$ reaction with 14.8-MeV neutrons on enriched (99%) Yb isotope and is studied by means of beta-gamma scintillation counter techniques. The beta and gamma measurements show beta groups of end-point energies 1200 ± 50 (82%) and 700 ± 50 (18%) keV and gamma rays of energies 50 (Yb K X-ray), 75, 175, 275, 350, 370, 500, 630, 870, 990, 1260 and 1350 keV decaying with a 5.5 ± 0.5 -min activity of Tm^{174} . The gamma-gamma coincidence studies confirm previously reported gamma-ray cascades along with a new cascade of 500-1350-275-75 keV. The gamma spectrum in coincidence with the beta rays above 300 keV shows the existence of the previously unreported 1350-keV gamma transition in the new cascade and also gives the 870-keV gamma transition between the 2380-keV level and the 1510-keV isomeric state of Yb^{174} . A decay scheme of Tm^{174} is proposed and the results are compared and discussed in the light of the unified model and the pairing correlation model. The (n, p) cross-section for Yb^{174} is found to be 3.5 ± 1 mb.

INTRODUCTION

Wille and Fink (1960) reported for the first time the production of the nuclide Tm^{174} by neutron irradiations of enriched Yb^{174} and assigned a 5.5-min half-life to it. Takahashi *et al* (1961) observed a 5-min activity in the products formed by the fast neutron bombardment on natural ytterbium oxide. Kantele *et al* (1964) made a study of the Tm^{174} isotope and reported its half-life as 5.2 ± 0.3 min after following the decay of the 1000-keV gamma ray in a single-channel analyser. They also reported a decay scheme of Tm^{174} based on the results of sum and sum-peak spectra along with the knowledge of the 850- μs isomeric state (Kantele, 1964) at 1520 keV in Yb^{174} . According to the decay scheme of Kantele *et al.* (1964), the Tm^{174} nucleus decays by two beta groups of maximum energies 1200 ± 100 ($\approx 80\%$) and 0.700 keV ($\approx 20\%$) to the excited levels of Yb^{174} at 1886 and 2386 keV, respectively. The 2385-keV level decays by the 497-keV gamma transition to the 1886-keV level, which in turn populates the 850- μs isomeric state at 1520 keV. The isomeric state apparently depopulates by a multipole cascade of the 995-275-175-76 keV gamma rays. They have also tentatively suggested other weak modes of decay of the isomeric state through the cascades 1270-175-76 keV and 630-366-275-76 keV. It is known (Orth, 1964) from the decay of the 165-d isomer of Lu^{174} that the isomeric state at 1520-keV in Yb^{174} decays to 4^+ , 6^+ , and 8^+ members of the ground state rotational band with relative intensities ≈ 0.1 , 1.0 and ≈ 0.01 . Very recently Funke *et al* (1965) in their study of Lu^{174m} reported the decay of the 1526-keV isomeric state

of Yb^{174} in two cascades 995-280-175-76.5 and 630-365-280-175-76.5 keV having the intensity ratio 41 ± 5 . They have not observed the third cascade 1270-175-76.5 keV reported by previous authors (Kantele, 1964; Orth, 1964).

The present investigation was undertaken to study the decay of Tm^{174} in more detail with an intention of studying the weak gamma transitions assigned tentatively by Kantele *et al.*, (1964) and also to resolve the discrepancies regarding the number of cascades and their relative intensities observed in the de-excitation of the isomeric state of Yb^{174} .

SOURCE PREPARATION

The Tm^{174} isotope was produced by the (n, p) reaction on Yb^{174} enriched to 99%. The incident neutron energy was 14.8 MeV, and the typical neutron flux of the order of 4×10^{10} n/cm² sec was maintained at this level in all the irradiations. The possible contaminant activities in the source were carefully looked for on the basis of the data of isotopic and spectrographic analysis of the supplied enriched sample as well as with the aid of suitable activity lists (Slater, 1962; Nuclear Data Sheets, 1964). A long-lived activity noticed as an impurity in a very small amount was due to Yb^{175} (4.1 d). This was produced by the $(n, 2n)$ reaction on Yb^{176} which was present as much as 0.4% in the enriched isotope. The contribution due to this activity was subtracted out in all the measurements. The other short-lived activities, suspected as impurities, were due to the reactions $\text{Cu}^{63} (n, 2n) \text{Cu}^{62}$ (9.5 min); $\text{Pr}^{141} (n, 2n) \text{Pr}^{140}$ (3.4 min) and $\text{Yb}^{176} (n, p) \text{Tm}^{176}$ (1.4 min). The contribution of Tm^{176} is expected to be very small since the measured (n, p) cross-section for Yb^{176} is 1.5 ± 0.5 mb (Gujrathi *et al.*, 1965). The impurities of Cu^{63} and Pr^{141} present in the enriched sample were insufficient to alter the main conclusions. The estimated total contribution due to all these impurities was less than 3% of the total decay of Tm^{174} .

For the beta ray measurements the irradiated enriched ytterbium in the form of oxide powder was uniformly spread inside a bag of thin mylar. The average thickness of the source was 1 mg/cm². Since the measured (n, p) cross-section for Yb^{174} is small, a large number of irradiations on several hundred milligrams of enriched isotopes were needed to complete each measurement.

EXPERIMENTAL RESULTS

(A) Half-life measurement and the (n, p) cross-section

The half-life of Tm^{174} was measured as 5.5 ± 0.3 min in close agreement with previous reports. The half-life was also studied by following the decay of 50, 175, 275, 370 and 990-keV gamma rays (see Table 1) in a single-channel analyser. In all cases a clear half-life of 5 ± 1 min was observed. The cross-section for the $\text{Yb}^{174} (n, p) \text{Tm}^{174}$ reaction was calculated by the activation technique, the

Decay of Tm^{174}

experimental details of which were as reported earlier (Mukherjee *et al.*, 1961). The measured value of the cross-section was 3.5 ± 1 mb as compared with the value of 556 mb for the $Cu^{63}(n, 2n) Cu^{62}$ reaction.

(B) Gamma and beta ray measurements

The experiments were performed to study the gross features of the gamma ray spectra of Tm^{174} produced by bombarding enriched Yb^{174} . The gamma spectra were measured with a $7.6\text{ cm} \times 7.6\text{ cm}$ NaI(Tl) crystal optically coupled to a RCA-8054 photomultiplier and a 512-channel analyser. Fig. 1 shows a typical gamma ray spectrum in which the source was placed at a distance of 3 cm from the crystal on a 0.5 cm thick lucite plate to cut off the beta particles. Photo peaks are observed at energies 50, 75, 175, 275, 370, 490, 630, 870, 990, 1260 and 1340 keV. Due to the summing of the cascade gamma rays some of the peaks have been slightly broadened. This effect is clearly seen in the 490 and 990-keV gamma rays. The gamma spectra were also studied by systematically introducing 0.1 to 1 cm thick lead absorbers between the source and the detector to reduce the summing of X-rays and the low energy gamma rays. The broadenings at 550 keV and 1040 keV shown in fig. 1, were found to be due to the Yb K X-ray or the low-energy gamma ray summing with the 490 and 990 keV gamma rays. To study the decay characteristics of the photopeaks observed in the single-crystal measurements, another experiment was performed in which three gamma spectra were taken in succession at 1 min, 5 min and 11 min after the end of the

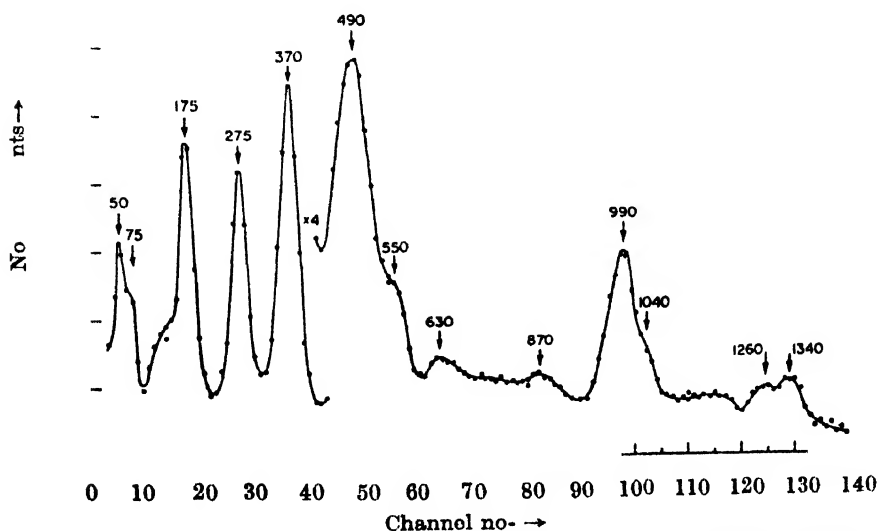


Fig. 1. Gamma spectrum of Tm^{174} taken with a $7.6\text{ cm} \times 7.6\text{ cm}$ NaI(Tl) detector. Source-to-crystal distance was 3 cm.

bombardment. Fig. 2 shows that all the prominent gamma rays are decaying with a half-life of 5 ± 1 min.

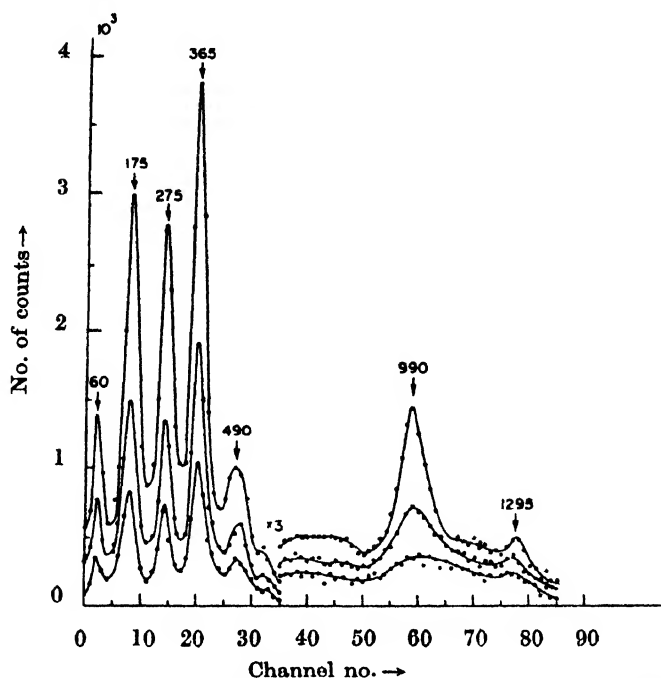


Fig. 2. Gamma spectra of Tm^{174} taken at 1 min. 6 min. and 11 min. after the end of the irradiation of enriched Yb^{174} shown as curves (a), (b) and (c), respectively.

The gamma ray energies, their relative intensities calculated from single crystal as well as from some of the coincidence measurements and the gamma-gamma coincidence results are given in table 1.

TABLE 1

Gamma ray energies, their relative intensities neglecting the conversions and the gamma-gamma coincidence results.

Energy of the photo peak (keV)	Unconverted gamma-ray relative intensity	In coincidence with (keV)
50 ± 5 (Yb K X-ray)	30 ± 10	175, 275, 350, 500, 630, 990, 1260, 1350
75 ± 5	10 ± 3	
175 ± 5	72 ± 15	50, 275, 350, 500, 630, 990, 1260, 1350
275 ± 5	90 ± 15	50, 175, 350, 500, 630, 990, 1350
350 ± 10	7 ± 2	50, 175, 275, 500, 630
370 ± 10	100	
500 ± 10	15 ± 4	370
630 ± 10	5 ± 2	
870 ± 10	5 ± 2	
990 ± 10	75 ± 15	50, 175, 275
1260 ± 15	6 ± 2	50, 175
1350 ± 15	7 ± 2	50, 175, 275

The beta measurements were performed with a $5.1 \text{ cm} \times 1.3 \text{ cm}$ thick anthracene crystal mounted on a RCA-6810A photomultiplier and a 512-channel analyser. The source to crystal distance was 0.5 cm. Fig. 3 shows the Fermi-Kurie analysis of the beta spectrum of Tm^{174} . Two beta groups with maximum energies of 1200 ± 50 (82%) and 700 ± 50 (18%) keV are found associated with the decay of Tm^{174} . The energies, intensities and the log ft values of the two

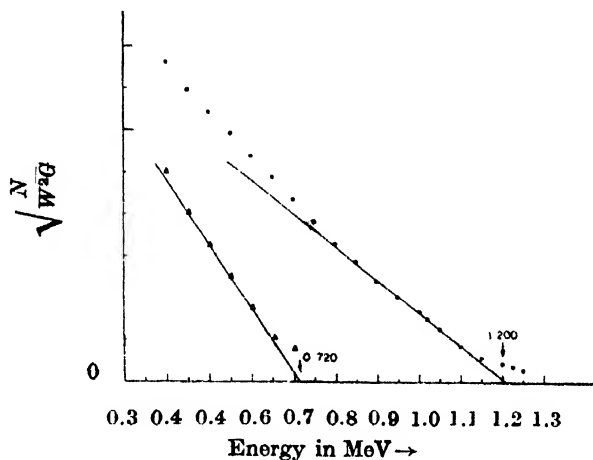


Fig. 3. Fermi-Kurie plot of the beta spectrum of Tm^{174} . The detector was a $5.1 \text{ cm} \times 1.3 \text{ cm}$ thick anthracene crystal. Source-to-detector distance was 0.5 cm.

beta groups are given in table 2. In the measurement a very weak beta group of 2500 ± 400 keV (2-3%) was observed to decay with 6 ± 2 min-activity. This group was not assigned to Tm^{174} as it was found in coincidence with the 510-keV annihilation gamma rays. It might be due to the suspected impurities of Cu^{62} (9.5 min) and Pr^{140} (3.5 min) present in very small amounts in the Tm^{174} sources

TABLE 2

Energies, intensities and log ft values of the beta ray groups.

Beta ray end-point energy (keV)	Intensity (%)	log ft. value
1200 ± 50	82	4.8
700 ± 50	18	4.6

DISCUSSION

(C) Coincidence results

To study the cascade nature of the various gamma rays and beta-gamma relationships, coincidence studies were made. In the gamma-gamma coincidence studies, a $5.1 \text{ cm} \times 5.1 \text{ cm}$ NaI(Tl) crystal spectrometer was used to select the

gating gamma ray and the gated spectrum was taken with another 7.6 cm \times 7.6 cm NaI(Tl) crystal. For the beta-gamma coincidence measurements the 7.6 cm \times 7.6 cm NaI(Tl) in the above arrangement was replaced by a 5.1 cm \times 1.3 cm thick anthracene crystal. The resolving time (2τ) of the coincidence system was 2 μ s.

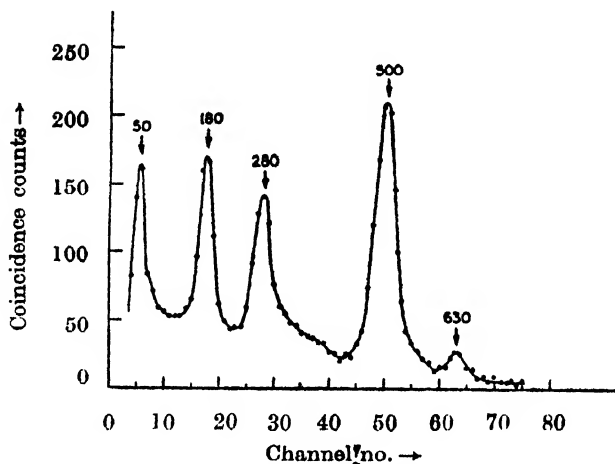


Fig. 4. Gamma spectrum in coincidence with the 370-keV gamma ray.

Most of the prominent gamma rays observed in the single-crystal spectrum were taken in the gate, and the coincidence gamma spectra were studied. The spectrum in coincidence with the Yb K X-ray showed clear photo peaks at 175, 275, 350, 500, 630, 990, 1260 and 1350 keV. The existence of the fourfold cascade of an X-ray and 175, 275 and 990-keV gamma rays reported by Kantele *et al.*, was confirmed. With the 370-keV gamma ray in the gate the 500-keV gamma ray was observed in coincidence with the other photopeaks at 50, 180, 280 and 630 keV as shown in fig. 4. With the 275-keV gamma ray in the gate, the coincidence spectrum showed the 55, 75, 175, 275, 350, 500, 635, 990 and 1350-keV gamma rays (fig. 5); while with the 175-keV gamma ray all these gamma rays with an addition of the 1260-keV gamma ray appeared in coincidence. In fig. 6, curve (a) shows the result obtained by gating with the 1200-1400-keV portion of the gamma-ray spectrum, which includes both the photopeaks of energies 1260 and 1340 keV and curve (b) shows the results on gating with the 1200-1260-keV portion of the gamma spectrum which includes mostly the 1260-keV photopeak. It can be seen from fig. 6 that the intensities of the 275 and 500-keV photopeaks are decreased in curve (b) relative to the intensities of the 50 and 175-keV gamma rays. All the gamma-gamma coincidence results are summarised in table 1.

The beta spectrum in coincidence with the 370-keV gamma ray showed two beta groups of end point energies 1200 ± 50 and 700 ± 50 keV with the same intensities as observed in the single-crystal measurement. When the beta spec-

spectrum was gated with the 500-keV gamma ray, a single beta group of 700 ± 50 keV was observed in coincidence. With the 990-keV gamma rays no beta particles

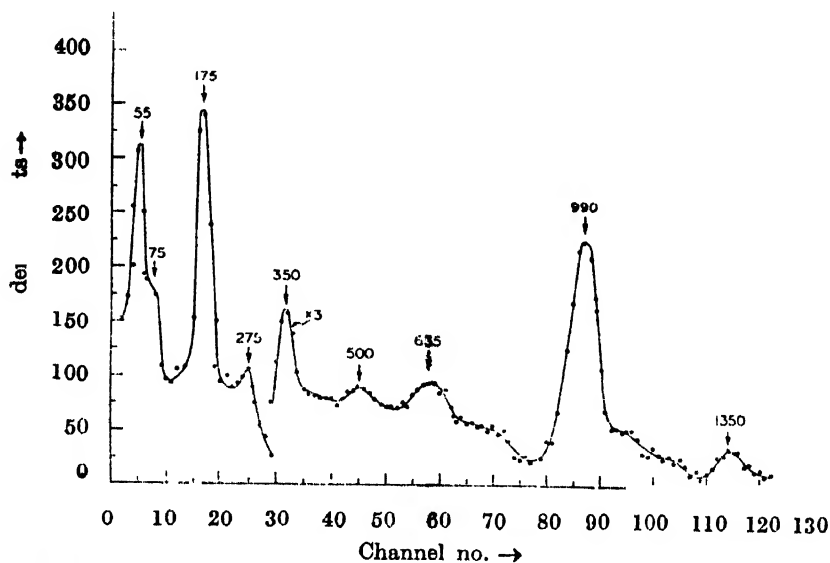


Fig. 5. Gamma spectrum in coincidence with the 275-keV gamma ray.

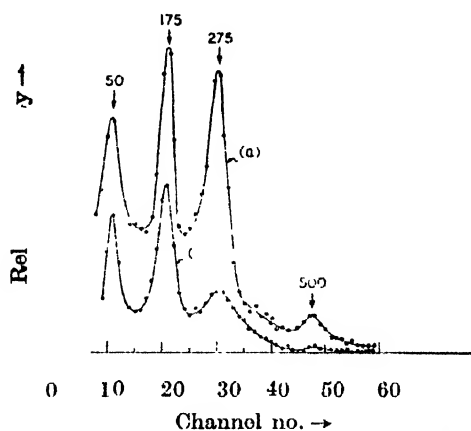


Fig. 6. Gamma spectra obtained in coincidence when the gating window was set at the 1200–1400 and 1200–1260-keV portions of the gamma spectrum, shown as curves (a) and (b), respectively.

were observed in prompt coincidence. The coincidence spectra were also studied by gating with the 275 and 175-keV gamma rays which showed an indication of the 1200-keV beta group. The results were not conclusive as it was difficult to estimate the contributions due to the spectra obtained by beta particles and the Compton scattered electrons from the coincident high-energy gamma rays. To cross-check this result and also to find gamma rays in coincidence with the beta particles, a gamma spectrum in coincidence with the beta rays was studied.

The gated beta spectrum was biased up to 300 keV to avoid the contribution of high energy gamma rays arising due to gamma-gamma coincidences with the low-energy ones. Fig. 7 shows this coincidence result with the evidence for the existence of the photo peaks at 50, 175, 275, 370, 500, 870 and 1350 keV.

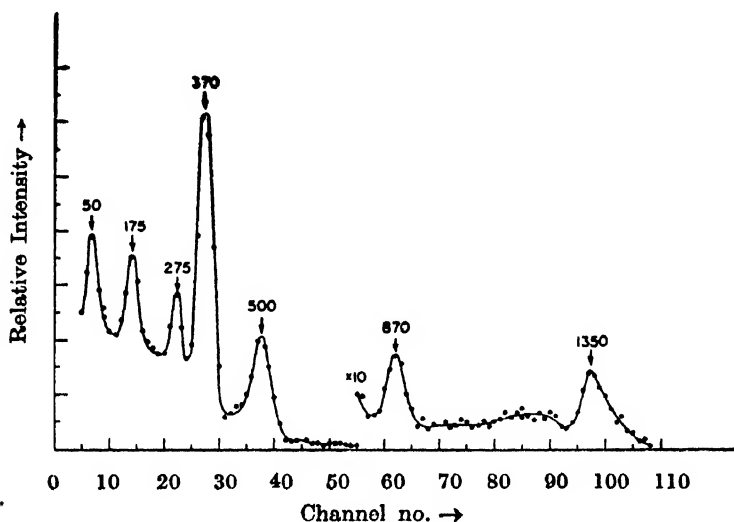


Fig. 7. Gamma spectrum in coincidence with the beta rays greater than 300 keV.

In the spectrum the intensities of the low-energy gamma rays of energies 50, 175 and 275 keV is slightly higher due to the coincidences between these gamma rays and the high energy coincident gamma rays detected in anthracene crystal.

DISCUSSION

The (n, p) cross-section value for Yb^{174} is 3.5 ± 1 mb and is comparable with the observed (n, p) cross sections in this mass region of rare earth (Wille *et al.* 1960; Gardner, 1962; Chatterjee, 1964). This value is higher than the one predicted by Gardner (1962) which is 2 mb. It also fits quite satisfactorily with the trends of (n, p) reaction cross-sections at 14-MeV neutrons (Chatterjee, 1964).

A proposed decay scheme of Tm^{174} which contains all the prominent features of the observations is shown in fig. 8. This agrees in many respects with the one given by Kantele *et al.* (1964). It should be noted that the 75-keV gamma transition is known (Sliv *et al.* 1956-58) to be highly converted ($\alpha_T = 10.24$) and therefore in most of the experiments it was not observed. Instead a 50-keV Yb K X-ray appeared. In the decay scheme the gamma transitions of 350, 630, 870 and 1260 keV were assigned tentatively by Kantele *et al.* (1964). They are confirmed by coincidence measurements in our studies. The new gamma ray of 1350 keV is due to the transition from the 1880-keV level to the 525-keV level of the ground state rotational band in Yb^{174} . This is concluded from the coincidence results obtained by gating with the 50, 175 and 275-keV gamma

rays, with the 1200-1260 and 1200-1400-keV portions of the gamma spectrum (figs. 5 and 6) and also from the observed gamma spectrum in coincidence with the beta rays greater than 300 keV (fig. 7). From the studies of the Coulomb excitation of the rotational levels in Yb^{174} , it is known (De Boer *et al*, 1963) that the gamma cascade of energies 350-275-175-75 keV corresponds to the ground state rotational band $K = 0$. Assuming the 275, 175 and 75-keV as $E2$ gamma transitions, the theoretically calculated total internal-conversion coefficients, (α_T) are 0.900, 0.424 and 10.24, respectively (Sliv and Band, 1956-58). By taking account of the α_T values for these gamma transitions one obtains the following total intensities: 99 ± 15 , 103 ± 16 and 112 ± 31 , respectively, which are consistent with the decay scheme.

The ground state spin of the Tm^{174} can be assigned from the orbital systematics using Nilsson diagram. The 69th proton orbital $1/2^+ [411 \downarrow]$ consistently appears in the ground state of Tm isotopes with mass numbers 165 to 173. Similarly, the 105th neutron orbital $7/2^- [514 \downarrow]$ consistently appears in the ground state of ${}_{70}\text{Yb}^{175}$, ${}_{71}\text{Lu}^{176}$, ${}_{72}\text{Hf}^{177}$, ${}_{73}\text{Ta}^{178}$, and ${}_{74}\text{W}^{179}$. Therefore one can reasonably assume that the ground state of ${}_{69}\text{Tm}^{174}_{105}$ consists of these two configurations, and according to the coupling rules of Gallagher and Moszkowski (1958) the expected ground state spin of it should be 4^- . The observed log ft values for the beta transitions from Tm^{174} are the allowed unhindered type and suggest that the spins of the 2380 and 1880-keV levels of Yb^{174} should be 5^- or 4^- or 3^- . The

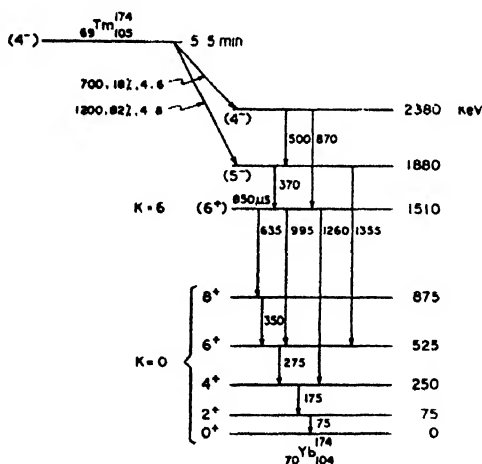


Fig. 8. Proposed decay scheme of Tm^{174} .

assignment of 6^+ (Katele, 1964) or probably 7^- (Funke, *et al*, 1965) spin value to the 850- μs isomeric state at 1510 keV and the observed gamma transitions from the levels at 2380 and 1880 keV to the 1510-keV state rule out the possibility of 3^- . As suggested by Katele *et al*, (1964) the pairing model calculations of Gallagher and Soloviev (1962) give the levels at 2300, 1800 and 1600 keV with the spins as 4^- , 5^- and 6^+ which can fit with the observed levels at 2380, 1880

and 1510 keV, respectively. The 4^- and 5^- levels are the proton two-quasi-particle excitations having the configurations $7/2 [523 \uparrow]$, $1/2^+ [411 \downarrow]$ and $1/2^+ [411 \downarrow]$, $9/2^- [514 \uparrow]$, respectively and the 6^+ level is due to the neutron two-quasi particle configuration $5/2^- [512 \uparrow]$ and $7/2^- [514 \downarrow]$.

We have calculated the hindrance factors for the 1260, 990 and 630-keV gamma transitions from the observed intensities for different multipolarities obtained by assuming 6^+ and 7^- spins for the 850- μ s isomeric state. It is found that 6^+ assignment to the 1510-keV isomeric state in Yb^{174} is more consistent with our observations instead of 7^- arising due to the neutron two-quasi particle configurations $9/2^+ [624 \uparrow]$, $5/2^- [512 \uparrow]$. From the $(\text{O}^{16}; \text{O}^{16}\gamma)$ reaction on Yb^{174} , the levels at 75, 250, 525 and 875 keV which form a group of the ground state rotational band $K = 0$ are assigned the spins as 2^+ , 4^+ , 6^+ and 8^+ , respectively (De Boer *et al.*, 1963).

ACKNOWLEDGMENTS

The authors wish to express their gratitude to Professor B. D. Nagechaudhuri and Professor D. N. Kundu for their kind interest. They are also indebted to Dr. H. Bakhru and Mr. B. Sethi for the helpful discussions and to the technical staff of the Neutron Physics Section for sample irradiations.

REFERENCES

- Chatterjee, A., 1964, *Nuclear Phys.*, **60**, 273.
 De Boer, J., Goldring, G. and Winkler, H., 1963, *Proc. Third Conf. on Reactions between Complex Nuclei*, Asilomar, Calif., 317.
 Funke, L., Graber, H., Kaun, K. H., Sodan, H., and Weruer, L. 1965, *Nuclear Phys.*, **61**, 465.
 Gallagher, Jr., C. J. and Moszkowski, S. A., 1958, *Phys. Rev.*, **111**, 1082.
 Gallagher, Jr., C. J. and Soloviev, V. G., 1962, *Mat. Fys. Skr. Dan. Vid. Selsk.*, **2**, No. 2.
 Gardner, D. G., 1962, *Nuclear Phys.*, **29**, 373.
 Gujrathi, S. C. and Mukherjee, S. K., 1965, (to be published).
 Kantele, J., Broom, K. M. and Chittenden II, D. M., 1964, *Ann. Acad. Fenni. Series A* VI, No. 162.
 Kantele, J., 1964, *Phys. Lett.*, **11**, 59.
 Mukherjee, S. K., Ganguli, A. K. and Majumdar, N. K., 1961, *Proc. Phys. Soc. (London)*, **77**, 508.
 Nuclear Data Sheets, 1964, *National Academy of Sciences*, National Research Council, Washington, D.C.
 Orth, C. J., 1964, *Bull. Am. Phys. Soc.*, **9**, 498.
 Slater, D. N., 1962, *Gamma rays of radio-nuclides in order of increasing energies*, Butterworths Scientific Publications (London).
 Sliv, L. A. and Band, M. I., 1956-58, *Tables of internal conversion coefficients, of gamma rays*, Academy of Sciences, Press USSR, Moscow-Leningrad.
 Takahasi, K. Kuroyangi, H. Y., Kotajima, K., Nagatani, K., and Morinaga, H., 1961, *J. Phys. Soc. (Japan)*, **16**, 1664.
 Wille, R. G. and Fink, R. W., 1960, *Phys. Rev.*, **118**, 242.

STUDY OF THE TRANSVERSE VIBRATION OF THE ELASTIC-PLASTIC STRING UNDER DIFFERENT PLASTICITY CONDITIONS

S. K. GHOSH AND SUNIL KUMAR BANERJEE

DEPARTMENT OF PHYSICS, JADAVPUR UNIVERSITY, CALCUTTA-32, INDIA

(Received February 27, 1967)

ABSTRACT. Theoretical work on the wave propagation in an elastic-plastic string struck transversely at its middle point is discussed in this paper graphically. The only basic assumption is that the tension of the string is some known non-linear function of strain. This means that the phase velocity of the transverse wave changes from point to point as the pulse is propagated through such a string which ultimately becomes asymmetrical in shape. The main object of this paper is to explain graphically :

- (i) variations in displacements with time,
- (ii) variations in pressure with time,
- (iii) time of collision under different plasticity conditions, into three different sections.

INTRODUCTION

Before the discussion of the problem under consideration something must be said about the elastic-plastic behaviour of the string employed in the present issue. The foundation of the theory of plasticity has not yet been firmly established and the various survey papers about the subject differ from one another not only in scope but also in the points of view of their respective authors. In the case of a perfectly elastic string vibrating under transverse impact the stress-strain law is provided by a linear relation which is independent of time. It may be noted in this connection that any deviation of the assumption about this linearly in the stress to strain relation will introduce plasticity in the material of the string. In the present theory strain is neither linearly dependent on strain nor does it depend upon the strain-rate but unlike the case of a perfectly flexible string the tension is assumed to be a known non-linear function of strain. The important contribution of this assumption is that the phase velocity of the string due to transverse impact does not remain constant as the pulse is propagated along the string, but depends upon strain and changes from point to point of it. Thus the velocities at different points are different functions of strain. Naturally the velocity gradients at different points of the string are also different functions of strain and the measure of the change in velocity gradient at the struck point is evidently a measure of the plasticity of the string.

For the purpose of a thorough and a much better investigation of the above theory some theoretical graphs are drawn and the various interesting results

coming out of them are found to agree well with the earlier theories of the subject matter under discussion. In this paper special attention is given to the discussion of the graphical results as stated in the abstract in three different sections:

EXPLANATIONS OF THE SYMBOLS USED

l = Length of the string = $a + b$.

a = Shorter segment of the string.

b = Longer segment of the string.

s = Variable measured along length of the string fixed at $s = 0$ and $s = l$.

t = Variable time.

y_a = Displacement of the struck point.

ρ = linear density of the string.

m = Mass of the hammer.

ϵ = Variable strain at any point of the string.

$c_1(\epsilon)$ = Velocity of the transverse wave motion of the string in the portion $0 < s < a$.

$c_2(\epsilon)$ = Velocity of transverse wave motion of the string in the portion $a < s < l$.

$c_a(\epsilon)$ = Velocity of transverse wave motion at the struck point.

v_0 = Velocity of impact.

P = Pressure exerted by the hammer.

$$\psi(\epsilon) = \left[\left(\frac{dc_2}{ds} \right)_{s=a} - \left(\frac{dc_2}{ds} \right)_{s=a} \right]$$

$$q = \frac{2\rho c_a}{m}.$$

$$r = 9\psi(\epsilon)$$

$$\theta_a = \frac{2a}{c_a}.$$

It has already been stated in the abstract that the paper proposes to find out displacement and pressure fluctuations at the struck point of the string. In doing so computations are made with the help of some numerical datas as :

$$l = 96 \text{ cm}, \quad m = 25 \text{ gms}, \quad \rho = 1 \text{ gm/cm}, \quad c_a = 3000 \text{ cm/sec.}$$

$$v_a = 40 \text{ cm/sec}, \quad \theta = \frac{2l}{c_a} = .064 \text{ sec}, \quad q = \frac{2\rho c_a}{m} = 300.$$

and

$$\sqrt{q^2 - 4r} = 10\sqrt{900 - 12\psi(\epsilon)}$$

TIME DISPLACEMENT VARIATIONS AT THE
STRUCK POINT

The expression for the displacement at the struck point as obtained by Ghose *et al* (1965) in an earlier publication during the 1st epoch is,

$$y_a = \frac{v_0 A}{\beta + \alpha} [e^{-\alpha t} - e^{-\beta t}]$$

where (α, β) are given by

$$[\alpha, \beta] = 150 \pm 5 \sqrt{900 - 12\psi(\epsilon)}$$

It can be easily seen that the nature of the values of (α, β) depend upon the discriminant of (2) i.e., $\sqrt{900 - 12\psi(\epsilon)}$. Thus the values of (α, β) will be either all real distinct or real equal or else imaginary depending upon the values of $\psi(\epsilon)$. The discussion is therefore restricted to these three different cases that may arise. When $q^2 > 4r$ i.e., when $\psi(\epsilon) < 75$

$$y_a = \frac{2v_0}{\sqrt{q^2 - 4r}} e^{-\frac{1}{2}qt} \sinh \left\{ \frac{1}{2} \sqrt{q^2 - 4r} \right\} t$$

when $q^2 = 4r$, i.e., when $\psi(\epsilon) = 75$,

$$y_a = v_0 t e^{-\frac{1}{2}qt}$$

when $q^2 < 4r$ i.e., when $\psi(\epsilon) > 75$,

$$y_a = \frac{2v_0}{\sqrt{4r - q^2}} e^{-\frac{1}{2}qt} \sin \left\{ \frac{1}{2} \sqrt{4r - q^2} \right\} t$$

Fig. 1 represents the complete behaviour of time displacement variations for the case $\psi(\epsilon) \leq 75$.

The curve for $\psi(\epsilon) = 0$, i.e. when the string is elastic shows that the displacement increases with time exponentially and ultimately becomes steady at a finite value.

Curves for $0 < \psi(\epsilon) \leq 75$ which is the critical value of $\psi(\epsilon)$ [$\psi(\epsilon) \geq 75$] show a distinct feature analogous to the damped vibration in string. Here the maxima of the displacements decrease as $\psi(\epsilon)$ increases. But the rate of fall of displacement increases progressively with $\psi(\epsilon)$. This is clearly due to increased damping associated with the increased plasticity of the material

The case for $\psi(\epsilon) > 75$ makes the time-displacement curve damped oscillatory. The amplitude of vibration of this curve though at first increasing is much

less pronounced in this case than in other cases of $\psi(\epsilon)$. It then remains almost constant during the first epoch as it is clear from the graph itself. This shows

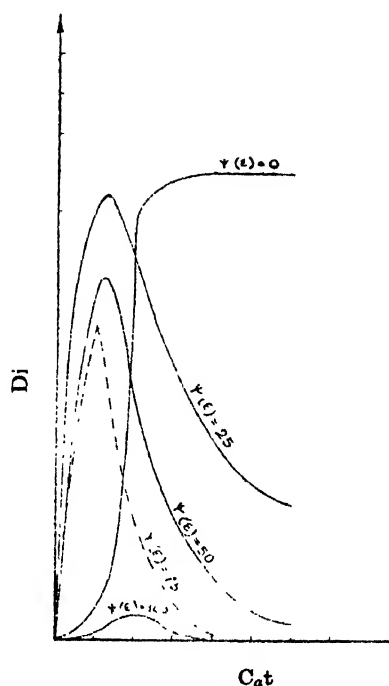


Fig. 1.

that immediately after impact the pulse propagates along the string with more or less a constant velocity. The fall of displacement is however much more slow in this case due to increased plasticity of the string as the case should be. At large value of plasticity it is associated with large damping. The amplitude is therefore very small and the curve resembles a highly damped motion.

The theoretical time-displacement graphs obtained by the present author reveals the fact that the displacements gradually diminish due to increased plasticity of the string, a conclusion quite analogous to that derived by Kolsky (1960) in the case of thin bars which are visco-elastic in nature.

PRESSURE-TIME VARIATION AT THE STRUCK POINT

The expressions for pressure at different epochs exerted by the hammer on the string as derived by the author in an earlier publication (Ghosh, 1965) are as follows :

During the interval, $0 < t < \theta_\alpha$

$$P_1 = \frac{mv_n}{(q^2 - 4r)^{\frac{1}{2}}} [\alpha^2 e^{-\alpha t} - \beta^2 e^{-\beta t}] \quad (1)$$

During, $\theta_a < t < 2\theta_a$,

$$P_2 = P_1 + \frac{2m\nu_0 q}{q^2 - 4r} [\alpha^2(2+A-\alpha t_1)e^{-\alpha t_1} + \beta^2(2-A-\beta t_1)e^{-\beta t_1}] \quad (2)$$

where,

$$[\alpha, \beta] = \frac{1}{2} [q \pm \sqrt{q^2 - 4q\psi(\epsilon)}] \quad (3)$$

It may be observed that the r.h.s. of (3) actually explains the nature of the roots (α, β) . The only undefined quantity on the r.h.s. of (3) is $\psi(\epsilon)$ which is termed as the 'representative of plasticity' in the string and capable of assuming any arbitrary value. Naturally the values of (α, β) may be either real unequal or real equal, or else imaginary subject to the 3 conditions $q^2 \geq 4q\psi(\epsilon)$ i.e., $\psi(\epsilon) \leq 75$.

The main object of this section is to study the pressure-time variations under different plasticity conditions i.e., corresponding to different values of $\psi(\epsilon)$. It is therefore necessary to define the expressions for pressure at different epochs suitably relative to various values for $\psi(\epsilon)$.

Thus for values of $q^2 \geq 4q\psi(\epsilon)$ i.e., $\psi(\epsilon) \leq 75$ the pressure expression during the different epochs are given,

During, $0 < t < \theta_a$, when $q^2 > 4q\psi(\epsilon)$ i.e., when $\psi(\epsilon) < 75$

$$P_1 = \frac{m\nu_0 e^{-\frac{1}{2}qt}}{(q^2 - 4r)^{\frac{1}{2}}} \left[(q^2 - 2r) \sinh \frac{(q^2 - 4r)^{\frac{1}{2}}}{2} t - q(q^2 - 4r)^{\frac{1}{2}} \cosh \frac{(q^2 - 4r)^{\frac{1}{2}}}{2} t \right]$$

Similarly when, $q^2 = 4r$, i.e., $\psi(\epsilon) = 75$.

$$P_1 = m\nu_0 q \psi(\epsilon) t e^{-\frac{1}{2}qt}$$

Similarly when, $q^2 < 4q\psi(\epsilon)$ i.e., $\psi(\epsilon) > 75$

$$P_1 = \frac{2m\nu_0 q}{(4r - q^2)^{\frac{1}{2}}} \psi(\epsilon) e^{-\frac{1}{2}qt} \sin \left\{ \frac{1}{2} (4r - q^2)^{\frac{1}{2}} t + \tan^{-1} \frac{q(4r - q^2)^{\frac{1}{2}}}{2r - q^2} \right\}$$

It will be observed later that pressure falls to zero during the 1st epoch in all the cases excepting the critical one and so the expressions for pressure in higher epochs are not written here.

With these expressions for pressure as a function of time a few graphs are drawn under various plasticity conditions and the different interesting conclusions derived from them agree well with the earlier theoretical results about the matter.

Figs. 2 and 3 correspond to the pressure time variations under different values of $\psi(\epsilon)$.

Time
Fig. 2

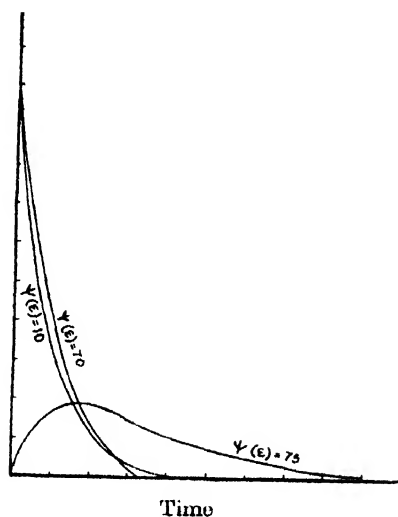


Fig. 3

Fig. 2 represents the pressure-time curve for $\psi(s) = 0$. The case corresponds to that of perfectly elastic string. Here the pressure which is very large at the beginning falls to a minimum, becomes high as a fresh new wave is generated at the beginning of the 2nd epoch. The behaviour of the string in this case is quite similar to that derived by Ghose (1952) in the case of a perfectly flexible string. Fig. 3 is a complete picture of the pressure-time variations due to the increased plasticity of the string.

By studying the pressure time curves for various values of $\psi(\epsilon)$ it is found that for values $\psi(\epsilon) < 75$ i.e., $q < 4r$, the pressure suddenly jumps to a value kv_0c at $t = 0$ and then falls exponentially to zero within the first epoch with

comparatively little change in nature. But the duration of contact diminishes as $\psi(\epsilon)$, the representative of plasticity, increases. This means that the medium becomes more and more dispersive as well as dissipative in nature. The above remarks receive a strong support from the experimental results of Ghosh *et al* (1965) who, in the case of a thin bar, has shown that the pressure terminates during the first epoch when it is struck by a light and soft (or plastic) load.

The curve for $\psi(\epsilon) = 75$ i.e., for $q^2 = 4r$ is critical. By studying the pressure time variation in this case it is found that the amplitude of the stress pulse is much diminished showing that the response of this critical plasticity condition on the pressure pulse is so marked that the shape of the pressure curve is changed altogether. The progressive rise of the pressure pulse is rather smooth and the rate of fall is more slow showing no tendency of the pressure being terminated within the first epoch.

The curve for $\psi(\epsilon) > 75$ i.e., shows that when the material of string is more plastic, stress is not generated in the string by impact shown by the negative values of pressure. The energy of impact is dispersed so quickly that the string undergoes very small displacement at the struck point as shown by the time displacement curve for $\psi(\epsilon) = 100$.

Phase angle versus $\psi(\epsilon)$:

It has been observed that when $q^2 < 4r$, the pressure equation becomes damped oscillatory. This result is in agreement with the case of a light and soft load striking a flexible string transversely. The values of $\psi(\epsilon) > 75$ i.e., large values of plasticity are responsible for the initiation of a type of waves through the material that the stress developed in the specimen due to the propagation of pulse is no longer in phase with it. The stress becomes more and more out of phase with the pulse as the value of $\psi(\epsilon)$ increases. This feature is depicted in fig. 4, in which the variation of δ with $\psi(\epsilon)$ is shown. For large values of $\psi(\epsilon)$,

gle
Loss

$\psi(\epsilon)$
Fig. 4

ad. inf.

Time of

$\psi(\epsilon)$
Fig. 5

δ is necessarily large which means that the stress needs a longer time to rise. Here,

$$\delta = \tan^{-1} \frac{q(4r - q^2)^{\frac{1}{2}}}{2r - q^2}$$

TIME OF COLLISION UNDER DIFFERENT PLASTICITY CONDITIONS

When the impacting load strikes the string, it first moves in the forward direction, then momentarily comes to rest and then begins to move in the opposite direction. The duration for which the string remains in contact with the moving load is defined to be the time of collision.

The time of collision plays a very important part which explains the actual acoustical behaviour of the string vibrating in any mode. The amplitude of vibration at different harmonics depends upon the pressure imparted to the string, as well as, on the time of collision for which the pressure acts from the beginning. The expression for pressure at the struck point has already been derived by the author in a previous publication. The purpose of this section is to examine graphically the time of collision under different plasticity conditions, i.e., $\psi(c)$, the representative of plasticity, assuming different arbitrary values.

The time of collision for any particular epoch can be found algebraically to be the lowest positive root obtained by solving the pressure equation at the struck point to zero i.e., $P_n(t) = 0$. This method is employed when it becomes difficult to obtain time of collision graphically, usually at higher epochs.

Fig. 5 represents graphically how the nature of the times of collision between the load and string changes as the plasticity increases more and more.

The time of collision is comparatively large in the case of an elastic string i.e., corresponding to value of $\psi(c) = 0$. It then falls suddenly and then attains almost a steady state for values of $0 < \psi(c) < 75$. The portion of the graph for this range of values of $\psi(c)$ is almost a straight line whose slope gradually diminishes until the critical stage is reached. When the critical value is attained by $\psi(c)$ i.e., when $\psi(c) = 75$ the time of collision jumps to infinity showing thereby that the load remains in contact with the string and moves with it.

The discussions made in the above three sections depict the actual dynamical conditions of the string struck transversely at its middle point. The corresponding conditions when it is struck near one end will be published in a subsequent issue of the journal.

REFERENCES

- Ghosh, M. and Ghosh, S. K., 1952, *Indian J. Phys.*, **26**, 463.
 Ghosh, S. K. and Banerjee, Sunil Kumar, 1965, *Indian J. Phys.*, **39**, 580.
 Kolsky, H., 1960, *International Symposium on Stress Wave Propagation in Materials*. pp. 84.

EFFECTS OF ANHARMONICITY ON THE INTER-MOLECULAR POTENTIALS DERIVED FROM CRYSTAL PROPERTIES

YASHWANT SINGH AND A. K. BARUA

INDIAN ASSOCIATION FOR THE CULTIVATION OF SCIENCE, CALCUTTA-32, INDIA.

(Received March 7, 1967)

ABSTRACT. The effect of anharmonicity on the intermolecular potentials derived from crystal properties (using Einstein approximation) has been considered for an elaborate six-parameter potential. The results obtained in this paper show that crystal properties cannot be used for an accurate determination of the pair-wise additive intermolecular potential.

INTRODUCTION

The effect of anharmonicity on the intermolecular potentials derived from crystal properties on the Einstein approximation has not yet been determined satisfactorily. Calculations performed by Zucker (1958) for the Lennard-Jones (12:6) potential show that the effect of anharmonicity cannot be neglected. On the other hand, Guggenheim and McGlashan (1960), have used mainly crystal properties to determine the intermolecular potential of argon on an elaborate six-parameter model. Guggenheim and McGlashan (1960) could not assess the effect of anharmonicity and they assumed it to be negligibly small. They argued that due to the limitations of the Lennard-Jones (12:6) potential the conclusion reached by Zucker (1958) regarding the effect of anharmonicity is uncertain. Consequently, it is very desirable to obtain an estimate of the effect of anharmonicity on the crystal properties for the six-parameter potential itself.

Another factor which should play a significant part (Jansen, 1963; Barker, 1964) in the determination of intermolecular potentials from crystal properties is the contribution of many-body interaction, i.e. the intermolecular potential can no longer be considered as pair-wise additive. In principle, bulk properties of scalar character are not particularly suitable for obtaining information on non-additive forces as their functional dependence on these forces is too implicit (Jansen, 1963). However, some information on the non-additive interactions can be obtained by an accurate analysis of the gaseous and the solid state properties of the same substance.

Recently, Barker (1964) has obtained the intermolecular potential of argon on the core potential by utilising only low-pressure gaseous properties in which effects of many-body interactions and anharmonicity may be neglected. The potential energy curve thus obtained is much closer to six-parameter potential

than to the Lennard-Jones (12:6) potential. The force parameters for argon as obtained by us in this paper from crystal properties at 0°K are quite different from those obtained from gaseous data (Barker, 1964). This probably shows that the core potential is sensitive and flexible enough to show the effects of anharmonicity and many-body interactions if they are of significant magnitude. We have used the core potential to calculate the entropy of solid argon at different temperatures.

CALCULATIONS AND RESULTS

The core potential with a spherical core of diameter γ may be written as,

$$\Phi(r) = 4\epsilon \left[\left(\frac{1-\gamma^*}{r^*- \gamma^*} \right)^{12} - \left(\frac{1-\gamma^*}{r^*- \gamma^*} \right)^6 \right] \quad \dots (1)$$

where r is the internuclear distance, ϵ the depth of the potential $r^* = r/\sigma$ and $\gamma^* = \gamma/\sigma$. σ is the value of r for which $\Phi(r) = 0$. At 0 K anharmonicity effect is present only in zero-point energy and we shall neglect it. We have used the heat sublimation L_0 and the lattice distance at 0°K for calculating the force constants of argon for the core potential. The equations used are the following

$$L_0 = 2N\epsilon \left[C_{12} \left(\frac{1-\gamma^*}{r^*- \gamma^*} \right)^{12} - C_6 \left(\frac{1-\gamma^*}{r^*- \gamma^*} \right)^6 \right] \quad \dots (2)$$

and

$$C_6 = 2C_{12} \left(\frac{1-\gamma^*}{r^*- \gamma^*} \right)^6 + \left[\frac{\hbar^2}{8\pi^2 m \sigma^2 \epsilon (1-\gamma^*)^2} \right. \\ \left. - 77C_8 \left(\frac{1-\gamma^*}{r^*- \gamma^*} \right)^8 - 10C_{10} \left(\frac{1-\gamma^*}{r^*- \gamma^*} \right)^{10} \right. \\ \left. - 22C_{14} \left(\frac{1-\gamma^*}{r^*- \gamma^*} \right)^{14} - 5C_{18} \left(\frac{1-\gamma^*}{r^*- \gamma^*} \right)^{18} \right] \quad \dots (3)$$

C_6, C_8, \dots etc. are crystal constants which depend on the lattice (Hirschfelder *et al.*, 1954).

In the calculation of σ and ϵ from eqs. (2) and (3) we have assumed γ^* to have the same value as determined by Barker (1964). The results obtained are shown in table I together with the values for the Lennard-Jones (12:6) potential. It may be seen that unlike the Lennard-Jones (12:6) potential the two sets of constants for the core potential as determined from the gaseous and crystal data differ considerably from each other.

TABLE 1
Constants for the core potential and Lennard-Jones (12:6) potential

	Constants determined from					
	Crystal Properties			Gaseous Properties		
	γ^*	$\sigma^\circ\text{A}$	$\epsilon/k^\circ\text{K}$	γ^*	$\sigma^\circ\text{A}$	$\epsilon/k^\circ\text{K}$
Core potential	0.1	0.348	117.25	0.1	3.363	142.9 ⁽¹⁾
Lennard-Jones (12 : 6)	0.0	3.403	122.46 ⁽²⁾	0.0	3.409	119.49 ⁽³⁾

(1) Barker, *et al* (1964).

(2) Zucker, (1956).

(3) Whalley *et al* (1955).

For the core potential, the frequency of vibration on the Einstein approximation is given by,

$$\nu = \frac{2\epsilon}{\pi^2 m \sigma^2 (1 - \gamma^*)^2} \left[22C_{14} \left(\frac{1 - \gamma^*}{r^* - \gamma^*} \right)^{14} - C_8 \left(\frac{1 - \gamma^*}{r^* - \gamma^*} \right)^8 \right] \quad \dots \quad (4)$$

In order to check the reliability of the force parameters calculated by us we have calculated the Debye temperature at 0°K from the relation

$$\theta_0 = (5/3)^{1/2} \frac{h\nu}{k} \quad \dots \quad (5)$$

The frequency ν being obtained from eq. (4). The experimental value of θ_0 is 93.3°K and those calculated by using the force constants determined from crystal data and gaseous data are 94.1°K and 77.5°K respectively. The excellent agreement between the experimental value of θ_0 and the value calculated from the crystal properties at 0°K show that this set of constants should reproduce satisfactorily other crystal properties at higher temperatures minus anharmonicity effects. Since the force parameters for the core potential have been determined by fitting with solid state data at 0°K, they should adjust themselves to take into account the many-body interactions.

The molar entropy of the crystal can be expressed as,

$$S/R = \frac{3}{2} x \coth \frac{x}{2} - 3 \ln \left(2 \sinh \frac{x}{2} \right) \quad \dots \quad (6)$$

where

$$x = \frac{h\nu}{kT} \quad \dots \quad (7)$$

The entropy values at different temperatures have been calculated on the core potential from both the sets of constants using eqs. (4)–(6). The results together

with the experimental values are shown in table II. The quantities $(S_G - S_C)/R$ and $(S_E - S_C)/R$ represent approximately the effect of many body interactions and anharmonicity respectively.

TABLE II
Entropy values calculated for the core potential, at $p \rightarrow 0$

T°K	From gaseous properties data (S/R) _G	From crystal properties data (S/R) _C	Experimental (S/R) _E ^(a)	$1 - y \operatorname{cosech}^2 x/2$
20	0.642	0.380	0.754	1.0655
30	1.458	1.038	1.524	
40	2.223	1.713	2.231	1.1403
50	3.099	2.399	2.854	
60	3.731	3.106	3.417	1.0953
70	4.247	3.653	3.938	
80	4.638	4.199	4.431	1.0745

¹ Guggenheim *et al* (1960).

We shall now utilise the results obtained above to see if the consideration of anharmonicity improve the agreement between experiment and theory on the six-parameter potential. The six parameter potential in the neighbourhood of its minimum may be written as (Guggenheim *et al*, 1960).

$$\phi(r) = -\epsilon + k \left(\frac{r-r_m}{r_m} \right)^2 - \alpha \left(\frac{r-r_m}{r_m} \right)^3 + \beta \left(\frac{r-r_m}{r_m} \right)^4 \quad (7)$$

where ϵ is the depth of the potential well at $r = r_m$. when r is very large $\phi(r)$ vaies primarily as r^{-6} and may be written as

$$\phi(r) = -\lambda \left(\frac{r_m}{r} \right)^6 \quad \dots \quad (8)$$

On the Einstein approximation for the acoustic modes of vibration of the frequency ν is given by

$$\frac{2\pi^2 m \nu^2 r_m}{12} = \frac{1}{3} k (1+\Delta)^{-1} (1+3\Delta) - \alpha \Delta (1+\Delta)^{-1} (1+2\Delta) + 2\beta \Delta^2 (1+\Delta) (1+\Delta)^{-1} \\ (1+\frac{5}{3}\Delta) - 5 \frac{C_8 - 12}{12} \lambda (1+\Delta)^{-8} \quad \dots \quad (9)$$

where

$$= \left(\frac{r-r_m}{r_m} \right)$$

The molar total energy U can be expressed as

$$U/RT = \frac{12}{2kT} \left[-\epsilon + k\Delta^2 - \alpha\Delta^3 + \beta\Delta^4 - \frac{C_6-12}{12} \lambda(1+\Delta)^{-6} + \frac{3}{2} x \coth \frac{x}{2} \right] \dots \quad (10)$$

being taken as zero for infinitely dispersed atoms at rest. The expression for S/R on the six-parameter potential remains the same as that given by eq. (5). We have also the relation,

$$\begin{aligned} pV/RT = - \frac{2}{kT} & \left[2k\Delta(1+\Delta) - 3\alpha\Delta^2(1+\Delta) + 4\beta\Delta^3(1+\Delta) + 6 \frac{C_6-12}{12} \lambda(1+\Delta)^{-6} \right] \\ & \frac{3}{\pi^2 m \bar{v}^2 r_m^2} \frac{1}{2} x \coth \frac{x}{2} \left[\frac{2}{3} k(1+\Delta)^{-1} - \alpha(1+\Delta)^{-1}(1+4\Delta+2\Delta^2) \right. \\ & \left. + 4\beta\Delta(1+\Delta)^{-1} \left(1+3\Delta + \frac{5}{3} \Delta^2 \right) + 40 \frac{C_6-12}{12} \lambda(1+\Delta)^{-8} \right] \end{aligned} \quad (11)$$

where p is the pressure and V the molar volume.

Initially we have neglected anharmonicity and taken $\beta = 0$ and for λ/k the quantum mechanically calculated value 150°K was chosen. By using the experimental values of the lattice distance and entropy values (given in column 3 of table II) at 80°K and 40°K and following the method described by Guggenheim and McGlashan (1960) we have calculated the constants α , k and r_m .

When the atom is displaced from its lattice site by a distance with components ξ , η , ζ along the principal axes of the crystal the increase in energy is given by

$$\begin{aligned} (\xi^2 + \eta^2 + \zeta^2) \frac{12}{r_m^2} & \left[\frac{1}{3} k(1+\Delta)^{-1}(1+3\Delta) - \alpha\Delta(1+\Delta)^{-1}(1+2\Delta) + 2\beta\Delta^2(1+\Delta)^{-1} \right. \\ & \left. \left(1 + \frac{5}{3} \Delta \right) - 5 \frac{C_6-12}{12} \lambda(1+\Delta)^{-8} \right] + (\xi^4 + \eta^4 + \zeta^4) \frac{12}{r_m^4} \times \frac{5}{3} \left[-\frac{1}{5} \alpha(1+\Delta)^{-1} \right. \\ & \left. + \frac{1}{5} \beta(1+\Delta)^{-1}(1+5\Delta) - 14 \frac{C_{10}-12}{12} \lambda(1+\Delta)^{-10} \right] + O(\rho^6) \end{aligned} \quad \dots \quad (12)$$

higher order in ρ being neglected. When anharmonic terms in eq. (12) are considered, the energy level along any of the perpendicular axes is given by

$$(n + \frac{1}{2})x + (n^2 + n + \frac{1}{2})y \quad \dots \quad (13)$$

y is defined as,

$$y = - \frac{3h^2}{8\pi^4 m^2 r_m^4 v^2 kT} \left[\alpha(1+\Delta)^{-1} - \beta(1+\Delta)^{-1}(1+5\Delta) + 70 \frac{C_{10}-12}{12} \lambda(1+\Delta)^{-10} \right] \quad \dots \quad (14)$$

We have also (taking $\beta = 0$ in the harmonic approximation)

$$U/RT = \frac{12}{2kT} \left[-\epsilon + k\Delta^2 - \alpha\Delta^3 + \beta\Delta^4 - \frac{C_6 - 12}{12} \lambda(1+\Delta)^{-6} \right] \\ + \frac{3}{2} x \coth \frac{x}{2} \left[1 - y \left(\operatorname{cosech}^2 \frac{x}{2} - \frac{\coth x/2}{x} \right) \right] \quad (15)$$

$$S/RT = \frac{3}{2} x \coth \frac{x}{2} \left[1 - y \operatorname{cosech}^2 \frac{x}{2} \right] - 3 \ln (2 \sinh x/2) \quad (16)$$

$$pV/kT = - \frac{2}{kT} \left[2k\Delta(1+\Delta) - 3\alpha\Delta^2(1+\Delta) + 4\beta\Delta^3(1+\Delta) + 6 \frac{C_6 - 12}{12} \lambda(1+\Delta)^{-6} \right] \\ - \frac{3}{\pi^2 m v r_m^2} \frac{1}{2} x \coth \frac{x}{2} \left[1 - y \operatorname{cosech}^2 \frac{x}{2} + \frac{dy/dr}{dx/dr} \coth x/2 \right] \times \\ \left[\frac{2}{3} K(1+\Delta)^{-1} - \alpha(1+4\Delta+2\Delta^2) + 4\beta\Delta(1+\Delta)^{-1} \left(1 + 3\Delta + \frac{5}{3} \Delta^2 \right) \right. \\ \left. - 40 \frac{C_6 - 12}{12} \lambda(1+\Delta)^{-6} \right] \quad \dots \quad (17)$$

TABLE III

Force constants of argon for six-parameter model

Set No.	$\lambda/k^\circ\text{K}$	$r_m \text{ \AA}$	$\epsilon/k^\circ\text{K}$	$10^{-2} k/k^\circ\text{K}$	$10^{-3} g/k^\circ\text{K}$	$10^{-4} \beta/k^\circ\text{K}$	Ref.
1	150	3.805	139.11	60.0	24.5	0	This work
2	150	3.818	139.5	44.3	18.3	0	Ref. 4.
3	150	3.812	137.5	44.9	19.6	1.96	

TABLE IV

Experimental and the calculated values of the molar enthalpy for $p \rightarrow 0$

TeK	H/R (Calculated) from Set 1	H/R (Experimental) ^a
20	-924.4	-922.0
40	-872.1	-878.0
60	-811.7	-819.0
80	-748.1	-748.1

(1) Guggenheim *et al.*, (1960).

In order to ascertain the effect of anharmonicity the values of y were obtained from eq. (16) by using the experimental value of entropy and the values of α , k , r_m as obtained earlier. The values of the term $(1-y \operatorname{cosech}^2 x/2)$ at different temperatures are shown in column 5 of table II. Once the factor y is known, ϵ/k can be calculated from eq. (15) by using the experimental value of U . The values of the constants obtained for the six-parameter potential are shown in table III. In order to calculate pV/RT it is necessary to obtain dy/dr and dx/dr . From the values of y the corresponding β values may be calculated from eq. (14) and eq. (16) gives

$$r dy/dr = \frac{3h^2}{8\pi^4 m^2 r_m^4 \sqrt{2} kT} \left[\alpha(1+\Delta)^{-1} + 4\beta(1+\Delta)^{-1} + 700 \frac{C_{10}-12}{12} \lambda(1+\Delta)^{-10} \right] \quad (18)$$

From Eqs. (6) and (9)

$$r dx/dr = \frac{3x}{\pi^2 m r_m^2 \sqrt{2}} \left[\frac{2}{3} (1+\Delta)^{-1} \cdot \alpha(1+\Delta)^{-1} (1+4\Delta+2\Delta^2) \right. \\ \left. + 4\beta\Delta(1+\Delta)^{-1} \left(1-3\Delta + \frac{9}{3} \Delta^2 \right) + 40 \frac{C_8-12}{12} \lambda(1+\Delta)^{-8} \right] \dots \quad (19)$$

COMPARISON WITH EXPERIMENT

Since experimental entropy values have been utilised for the determination of the potential parameters, these cannot be used for the comparison between the theory and the experiment. From table IV it may be seen that by considering anharmonicity effects the agreement between the experimental and the calculated values of molar enthalpy is well within 1% at all temperatures. The experimental and the calculated values of the lattice parameter and the lattice volume at $p=0$ are shown in table V. It may be seen that the agreement between experiment and theory is slightly better when anharmonicity is taken into account. In the calculated values from set no. 3 the anharmonicity is considered but it is assumed too small. However, the most sensitive test for anharmonicity effects is the pressure variation of the quantity pV/RT . A convenient way of expressing this is the quantity $V(o)-V(p)$, $V(o)$, $V(p)$ being the molar volumes at zero pressure and p at m ; respectively. The quantity $V(p)$ was calculated from eq. (11) by using all the sets of constants given in table II (the anharmonic terms being omitted for sets 2 and 3). The experimental and the calculated values of the quantity $V(o)-V(p)$ are shown in table VI,

TABLE V

Experimental and the calculated values of the lattice distance and the molar volume $V(o)$ at $p \rightarrow 0$

TeK	Calculated from				Experimental ^a	
	Set No. 1		Set No. 3		$r_m^* \text{\AA}$	$V \text{ cm}^3/\text{mol}$
	$r_m^* \text{\AA}$	$V \text{ cm}^3/\text{mol}$	$r_m^* \text{\AA}$	$V \text{ cm}^3/\text{mol}$		
20	3.767	22.770	3.768	22.820	3.760	22.650
40	3.778	22.974	3.784	23.080	3.780	23.005
60	3.827	33.875	3.810	23.557	3.818	23.706
80	3.869	24.674	3.850	24.307	3.860	24.500

^a Pollack, (1964).

$r_m^* = r/\sqrt{2}$, r being the lattice distance.

TABLE VI

Experimental and the calculated values of the quantity $V(o) - V(p)$ at various pressure and $T = 65^\circ\text{K}$

Pressure p (atm.)	Calculated from			Experimental
	Set 1	Set 2	Set 3	
193.6	0.23	0.32	0.31	0.26
387.1	0.45	0.63	0.57	0.50
483.1	0.54	0.78	0.72	0.59
580.7	0.63	0.97	0.82	0.71
967.8	0.97	1.33	1.25	1.09

DISCUSSION OF RESULTS

It may be seen from table VI that the agreement between experimental and calculated values is much better if anharmonicity is considered (set 1). For set 3 the agreement is slightly better than set 2, which is probably due to the reason that anharmonicity is very slightly taken into account in set 3. Since $V(o) - V(p)$ is most sensitive to the effect of anharmonicity, results show that anharmonicity does play a significant role in determining the crystal properties. The term $(1 - y \operatorname{cosec} h^2 x/2)$ which is a measure of the effect of anharmonicity

show a maximum value around 40°K which is in agreement with the temperature variation of the Gruneisen parameter γ' for argon (Pollack, 1964). The calculated values of the quantity $V(o) - V(p)$ is slightly lower than the experimental values when anharmonicity is considered whereas if this is neglected the calculated values are higher than the experimental values. One reason for the over correction for anharmonicity is the approximate equations used for considering anharmonicity and the other reason may be that we have used the experimental values of the lattice distance in our calculation which means that anharmonicity has already been taken into account partially.

It is relevant here to consider the uncertainty in the anharmonicity effect found by us due to the use of the Einstein approximation which does not consider the coupling between the harmonic oscillators. However, it has been shown by Zucker (1958) that the Hankel's modification of the Einstein model (which does not include harmonic coupling) gives much better agreement between experiment and theory than the Debye approximation (which considers inter-dependence of the oscillators, but does not include anharmonic effect). Near 0°K the two methods are in very good agreement and difference between them increases as the temperature increases (Zucker, 1958). This probably proves that if the constants for the intermolecular potential fitted to data at 0°K then only the consideration of anharmonicity effects can explain the experimental data satisfactorily. In the present paper we have followed a similar procedure and the most of the effects obtained by us must be due to anharmonicity.

Regarding the effect of many body interactions several observations are relevant. In agreement with the calculations performed by Jansen (1963a, 1963b), Barker (1964) has observed that for argon non-additive interaction contributes about 30% to the heat of sublimation L_0 at 0°K. The effect of non-additive interaction on entropy is shown by the term $(S_C - S_G)/R$ in table II. It must be pointed out that $(S_C - S_G)/R$ gives only qualitative magnitude of the many body effect on entropy. Since it is not possible to obtain the effect of non-additive interactions accurately from theory it is not justified to use solid state properties even in conjunction with gaseous properties for the determination of intermolecular potentials.

ACKNOWLEDGMENT

The authors are grateful to Prof. B. N. Srivastava, D.Sc., F.N.I., for his kind interest and encouragement.

REFERENCES

- Axilrod, B. M., 1951, *J. Chem. Phys.*, 19, 719, 724.
Barker, J. A., Fock, W., and Smith, F., 1964, *Phys. Fluids*, 7, 897.

- Guggenheim, E. A., McGlashan, M. L., 1960, *Proc. Roy. Soc. (Lond.)*, **A225**, 456.
- Hirschfelder, J. O., Curtiss, C. F., and Bird, R. B., 1954, *Molecular Theory of Gases and Liquids*, John Wiley Sons, Inc., New York.
- Jansen, L., 1963, *Phys. Letters*, **4**, 91.
- Jansen, L., and Zimring, S., 1963, *Phys. Letters*, **4**, 95.
- Pollock, G. L., 1964, *Rev. Mod. Phys.*, **36**, 748.
- Whalley, E., and Schneider, W. G., 1955, *J. Chem. Phys.*, **23**, 1644.
- Zucker, I. J., 1958, *Phil. Mag.*, **3**, 987.
- J., 1956, *J. Chem. Phys.*, **25**, 915.

FIELD EFFECT MEASUREMENTS ON GaAs

D. N. BOSE

DEPARTMENT OF PHYSICS, JADAVPUR UNIVERSITY, CALCUTTA-32, INDIA

(Received March 7, 1967)

ABSTRACT. Field-effect measurements were performed on $1.5\Omega\text{cm}$. n type GaAs between 150°K and 298°K . The 50 c/s field-effect mobility μ_{fe} was found to be $250\text{ cm}^2/\text{volt-sec}$. at 298°K and varied as $1/T$ with temperature with hysteresis effects occurring at low temperatures. D. C. field-effect relaxations could be observed at low temperatures only and showed pronounced asymmetry. The conductance minimum could not be observed but the presence of depletion could be inferred. No ambient dependence of the field-effect was found suggesting the presence of trapping states within the space charge region. Electron-irradiated specimens were found to have $\mu_{fe} = 3500\text{ cm}^2/\text{volt-sec}$, almost equal to the bulk mobility.

Although there have been a considerable number of investigations on the surface properties of group IV semiconductors germanium and silicon, the III-V compounds which have similar bulk properties have been given comparatively little attention.

Eaton *et al* (1962) reported measurements on p type InSb and found these surfaces to be p type. The first measurements on GaAs were carried out by Gerlich (1962) on n type material. He was unable to observe the minimum of the conductance in the field-effect curve but from the direction of the change of conductance concluded that an accumulation layer existed on the surface. He estimated a fast state density of $3.10^{11}/\text{cm}^2$.

Pilkun (1964) was able to observe the conductance minimum at low frequencies $0.6\text{--}1.0\text{c/s}$ but not at higher frequencies. The conductance changes were very small at the low frequencies corresponding to a field-effect mobility of $3.5\text{ cm}^2/\text{volt-sec}$ compared to a value of $1400\text{ cm}^2/\text{volt-sec}$ at 8kc/s . At low frequencies the surface appeared to be very close to the conductance minimum and on the majority carrier n type side. Hence a depletion layer condition was considered to exist. As the surfaces of n type material were found to be insensitive to ambient changes the low field-effect mobilities at low frequencies were attributed to acceptor states not on the surface but within the space-charge region trapping the induced charge. P type specimens were found to be essentially different in that they were influenced by ambient and there was an absence of slow trapping.

Flinn and Emmony (1963) and Flinn and Briggs (1964) also found evidence for depletion or inversion layer conditions on n type material. The surface-conductance minimum could not be located by surface potential and was estimated

from measurements of surface photo-voltage. The surfaces were found to be sensitive to ambient changes.

In the experiments reported here the field-effect mobility was measured at 50 c/s from room temperature, 298°K, down to 150°K. The effect of d.c. and pulsed fields as well as ambient changes were investigated. Finally some experiments were carried out on electron-irradiated specimens which had additional bulk defect levels introduced.

EXPERIMENTAL TECHNIQUES

Samples used were prepared from *n* type material having bulk resistivities of 1-5Ω cm at 300°K corresponding to carrier concentrations of $12.5\text{--}2.5 \times 10^{14}/\text{cm}^2$. Difficulty was encountered in making suitable electrical contacts to the specimens, best results being obtained using indium pellets etched in H_2SO_4 which were diffused into the GaAs by heating in vacuum at 250° for 2-3 hours. The surfaces were polished with Aloxite and etched in a standard peroxide etch containing 1 part by volume of H_2O_2 , 3 parts H_2SO_4 and 1 part H_2O .

Specimens were placed in a cryostat which could be cooled to 150°K. A field-electrode of conducting glass was placed above the upper surface of the specimen separated from it by a 30μ mylar spacer and provision was made for the application of 50 c/s, d.c. and pulsed voltages to the electrode. The field-effect circuit used was described by (1955) Low and is shown in fig. 1. Modulation of the

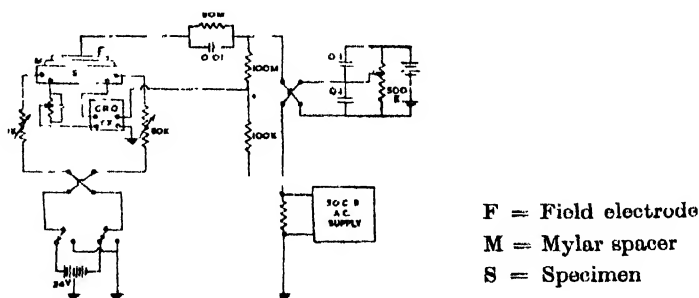


Fig. 1. Field-effect circuit

specimen conductance by the applied field, when a constant specimen current is passed, gives rise to an output signal voltage which is fed to the vertical plates of a high-gain differential input oscilloscope. The horizontal plates are supplied by a signal derived from the field voltage and the horizontal deflection is thus proportional to the induced charge on the specimen surface. The slope of the field effect curve is therefore proportional to the field-effect mobility :

$$\mu_{fs} = \frac{\Delta G_s}{\Delta \sigma}$$

where ΔG is the change in surface conductance in $mhos/\square$ and $\Delta\sigma$ is the induced charge in $coulombs/cm^2$.

RESULTS

At 298°K the field-effect curve using 50 c/s was a closed line and $\mu_{fe} = 250$ $cm^2/volt\text{-}sec$ at the field-free point, compared with a value of 550 $cm^2/volt\text{-}sec$. found by Flinn and Briggles (1964) from 50 c/s to 30 ke/s. From the sign of the slope of the field effect curve the surface was found to be n type on all the four specimens examined, there being no indication of a conductance minimum. Hence evaluation of surface potential as for germanium was not possible. No change in conductance due to d.c. voltages of 1.2 kv. could be detected at 300°K suggesting the presence of a high density of slow surface states, greater than the maximum induced charge density of $10^{12}/cm^2$. In contrast with germanium, no ambient dependence of the 50c/s field-effect could be detected using water vapour and ozone. This suggested that the states responsible for the slow trapping were not situated at the interface, but may be bulk trapping states within the surface space-charge region as postulated by Pilkuhn.

As the temperature was lowered the 50c/s field-effect curve developed hysteresis loops as shown in fig. 2a. and the field-effect mobility as measured by the slope at the field-free point was found to increase as shown in fig. 2b. The increase followed the $1/T$ law proposed by Ehrenreich for changes in bulk mobility

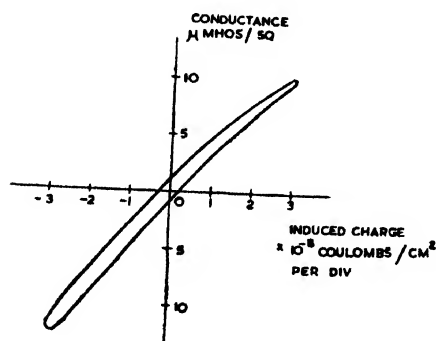


Fig. 2a. 50 c/s field-effect at 300°K

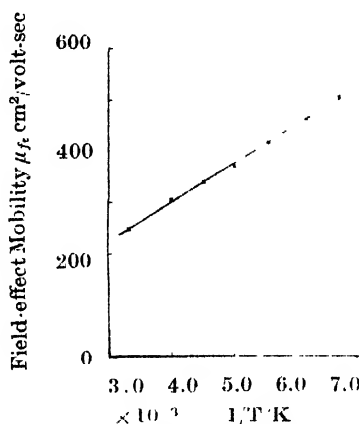


Fig. 2b. Variation of μ_{fe} with temperature

with temperature and could hereby be explained. At 150°K changes in conductance due to applied d.c. fields were evident indicating an increase in the trapping time of the slow states. The conductance changes due to d.c. fields exhibited asymmetry as shown in fig. 3. With positive voltages attracting electrons to the surface, the change in conductance was relatively small and the time-constant was 50 msec; with negative voltages repelling electrons from the surface the conductance change was large and of time-constant 500 msec.

Pulsed fields were next applied in order to obtain more information about the time-constants of the trapping states. A time-constant of 500 msec. at 150°K was found to be present, but a more detailed investigation was not possible due to the small magnitude of the signals available.

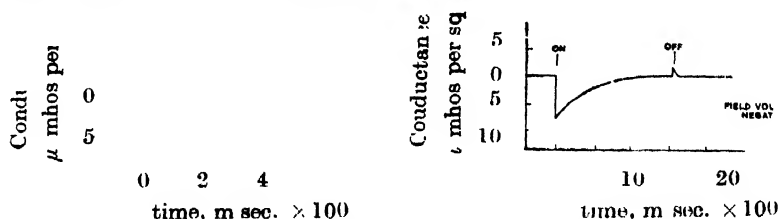


Fig. 3. D. C. field-effect.

Because of the unavailability of material with low carrier concentrations which would provide larger field-effect signals, some additional experiments were carried out on electron-irradiated GaAs. While studying radiation damage in GaAs, Grimshaw and Banbury (1964) had noticed changes in surface conductance in addition to bulk changes caused by the introduction of acceptor levels. In the present experiment specimens with initial carrier concentration of $3.10^{16}/\text{cm}^3$ at 300°K showing no measurable field modulation of conductance were irradiated with 1.0 Mev electrons thus introducing bulk acceptor levels 0.2 eV below the conduction band as found from optical absorption measurements by Pegler and Banbury. The free electron concentration was thus decreased to $6.10^{15}/\text{cm}^3$. Hall effect mobilities before and after irradiation were measured and found to be 4040 and 3260 $\text{cm}^2/\text{volt-sec}$ respectively, the decrease being due to increased scattering by the acceptor levels introduced. The specimens were irradiated alternately from each side to achieve a more uniform distribution of damage. A calculation of damage rate vs. depth shows that appreciable non-uniformity will remain however as the sample thicknesses were 0.3-0.4 mm. The defect concentration will therefore increase towards the surface and this is liable to invalidate barrier calculations. The surfaces examined after irradiation were again found to be *n* type with no indication of a conductance minimum present, but the field-effect mobility at room temperature was found to be 3200 $\text{cm}^2/\text{volt-sec}$. an order of magnitude higher than on unirradiated specimens, and almost equal to the bulk mobility.

DISCUSSION

GaAs differs from germanium and silicon in that the intrinsic carrier concentration at room temperature is very small, $10^7/\text{cm}^3$. Since the impurity concentration is generally $<10^{14}/\text{cm}^3$, minority carriers are virtually nonexistent in the bulk. The absence of the conductance minimum in the field-effect may therefore be due either to the surface being far from an inversion layer condition or due to an inadequate generation of minority carriers as the surface is swept through the

minimum by the induced field. As the diffusion length of minority carriers in GaAs is also very small the diffusion of carriers from the bulk to the surface would be insufficient to maintain equilibrium. Thus for a rate of inducing positive charge large compared to the minority carrier generation rate the effective field-effect mobility would be determined by the majority carrier and no conductance minimum would be apparent. At a sufficiently low frequency of inducing field minority carriers may be generated to maintain equilibrium and the conductance minimum would be observable. This would explain the hysteresis effects observed in the field-effect curve at low temperature and Pilkuhn's results qualitatively.

Pilkuhn did not attempt a more quantitative analysis of his results. The importance of the generation of minority carriers through localised centres can be estimated from the following analysis. Neglecting recombination through traps and considering band-band transitions alone, it is possible to calculate the generation rate of carriers at room temperature. For a carrier concentration $n = 2.10^{15}/\text{cm}^3$ Hilsum and Holeman (1960) found a minority carrier lifetime of 10^{-9} secs. From this the generation rate of minority carriers is found to be $10^7/\text{cm}^3$ sec. at room temperature. The rate required to maintain equilibrium in Pilkuhn's experiment at 0.6 c/s as calculated from his field-effect curves is much larger $10^{11}/\text{cm}^3/\text{sec}$. The large difference shows that generation of minority carriers proceeds mainly through localised centres and not by band-band transitions. The asymmetrical d.c. field-effect characteristic can likewise be attributed to inadequate minority carrier generation. When a negative voltage is applied, electrons are repelled from the surface and the generation time of holes determines the relaxation time-constant. With a positive voltage applied, the electrons required are supplied from the bulk at a much faster rate. Thus although the field-effect curve shows a n type surface with no sign of the minimum, the hysteresis effects at low temperature and the d.c. field-effect are characteristic of a two-carrier process supporting the idea that the surface is not in an accumulation layer but in a depletion layer condition.

The large difference between the field-effect mobility on irradiated and un-irradiated specimens is difficult to explain but may be due to loss of negative charge from surface states as found by Spear (1958) on germanium surfaces irradiated by 5Kev-4.5Mev electrons. An increase in the electron concentration in the space charge region would thus occur, which might convert the depletion layer initially present into an accumulation layer. As the field-effect mobility approaches the bulk mobility, a very small density of screening states would have to be postulated at the new value of surface potential. In view of the difficulty in identifying surface states on germanium with states within the space charge region postulated in GaAs, it is not possible to go further without more direct measurements.

ACKNOWLEDGMENTS

The author is indebted to Dr. P. C. Banbury for helpful discussions, to Prof. R. W. Ditchburn for the provision of laboratory facilities and to I.C.I. (India) Private Ltd., for the grant of a Technical Scholarship. •

REFERENCES

- Eaton, G. K., King, R. E. J., Morten, F. D., Partridge, A. T., and Smith, J. G., 1962, *J. Phys. Chem. Solids* **15**, 117.
Flinn, I., and Briggs, A., 1964, *Proc. Int. Conf. on Phys. and Chem. of Solid Surfaces*, Brown University, 136.
Flinn, I. and Emmony, D. C., 1963, *Phys. Letters* **6**, 133.
Gerlich, D. 1962, *J. Appl. Phys.* **33**, 1815.
Grimshaw, J. A. and Banbury, P. C., 1964, *Proc. Phys. Soc.* **84**, 151.
Pilkuhn, M. H., 1963, *J. Phys. Chem. Solids* **25**, 141.
Spear, W. E., 1958, *Phys. Rev.* **112**, 362.
Hilsun, C., and Holoman, B., 1960, *Proc. Int. Conf. on Semiconductor Physics*, Prague,
Low, G. G. E., 1955, *Proc. Phys. Soc. (London)*, **B680**, 10 1154.

IONOSPHERIC ABSORPTION IN THE VLF BAND

H. BHATTACHARYA

PHYSICS DEPARTMENT, BOSE INSTITUTE, CALCUTTA-9, INDIA

(Received March 8, 1967)

ABSTRACT. Experiments on the propagation of VLF waves at great distances reveal that there is an absorption band for frequencies in the range of 3 kc/s. In the present paper an attempt has been made to account for this absorption theoretically. From the expression of the reflection coefficient of the ionosphere at VLF, the absorption in dB has been computed. The plots of absorption as a function of frequency for different values of the angle of incidence at the Ionosphere show that when the incident angle is 80° , there is a dip in the absorption curve in the 3 kc/s range. This explains the absorption band that is observed in this frequency range.

INTRODUCTION

Radio wave propagation at very low frequencies (from 3 to 30 k/s) is characterized by the fact that the ground attenuation is very low and the sky waves are almost totally reflected from the ionosphere which has a height of the order of 60 to 80 km. In fact, the VLF waves which have travelled considerable distances act as if they were propagated through a wave-guide formed by the earth and the lower edge of the ionosphere. The attenuation under such conditions is that caused by spreading and absorption of the energy by the ground and the ionosphere. Taylor (1960) studied the attenuation rates for VLF waves and found that for 6 kc/s the attenuation was about 7 to 9 db/1000 km and decreased to about 1 to 3 db/1000 km at frequencies above 10 kc/s. Wait and Spies (1960) could account for these observed results theoretically from the point of view of modal propagation.

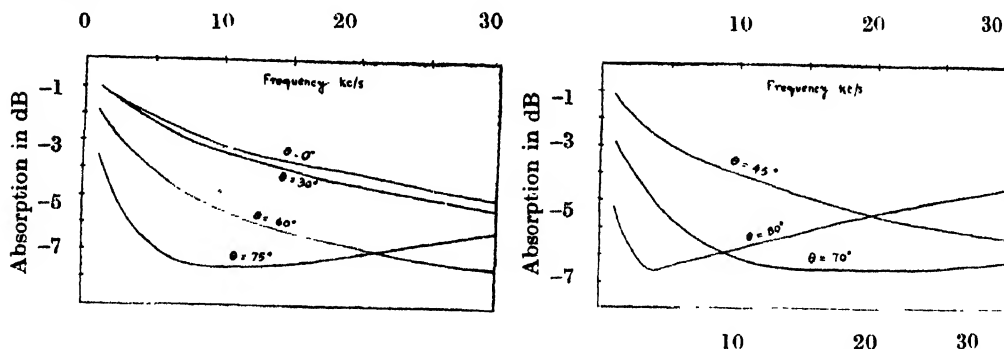
Despite the fact that the VLF waves propagate to great distances with small attenuation their use has been neglected for many years. Recently, however, with the pressing need for long-range navigational systems, world-wide communication systems and tracking of atmospheric storms and hurricanes, the desirable transmission properties of VLF are again being utilized. In view of the gaining importance of VLF in long-range communication, systematic experiments are being carried out at Boulder (USA), Slough (UK) and Toyokawa (Japan) with a network of receiving stations distributed through respective countries to study in detail the propagational characteristics of these waves. The results of these experiments show the presence of an absorption band for frequencies of the order of 3 kc/s for long-range propagation. In the present paper an attempt is made to explain this absorption band in a very simple way.

RESULTS AND DISCUSSION

For the reflection coefficient of the ionosphere at VLF we write (Bhattacharya *et al.*, 1964)

$$|R(\omega, \theta)| \cong \frac{[1 + (\omega_r/\omega)^2 \cos^4 \theta]^{\frac{1}{2}}}{1 + (\omega_r/\omega) \cos^2 \theta + (2\omega_r/\omega)^{\frac{1}{2}} \cos \theta} \quad (1)$$

where θ is the angle of incidence at the ionosphere and $\omega_r = 4\pi Ne^2/m\nu$, N being the electron number density, e the electronic charge in esu, m the electronic mass in grams, ν the electron collisional frequency and ω the angular frequency of the exploring wave in the VLF band. Our laboratory experiments show the average ionospheric reflection height at 86 km. Substituting the value of N ($\sim 10^3$), ν ($\sim 3.16 \times 10^6$), (Ratcliffe, 1960) at this height and also e ($= 4.8 \times 10^{-10}$ esu) and e/m ($= 5.2 \times 10^{17}$) we get $\omega_r \cong 10^8$. From (1) we have $20 \log_{10} |R(\omega, \theta)|$ for the ionospheric absorption in decibels for VLF waves. The plots of this expression as a function of $\omega/2\pi$ for different angles of incidence are given in figs. 1(a) and 1(b). We observe that for $\theta = 80^\circ$, that is, for long-range propagation there is a dip in the absorption curve in the range of 3 kc/s, corresponding to maximum absorption. This is in complete accord with the experimental observation.



Figs. 1.(a) and (b) Comes showing absorption *vs.* frequency for different angles of incidence.

In developing (1) we have applied the Fresnel's reflection coefficient to the ionosphere, thereby limiting the ionosphere to a sharply bounded continuum. In fact the reflection coefficient is in the form of a series (Wait, 1962) of which the first term is a Fresnel type and the succeeding terms account for the finite thickness of the ionospheric layer. But, in view of the fact that there is a very sharp gradient in electron density in the region at a height 60–80 km and also that the wavelengths of the VLF waves are much larger than the scale of horizontal irregularities, our present consideration of ionosphere as a sharply bounded continuum is not unjustified. Further, the effect of the earth's magnetic field can also be neglected in view of the obliqueness of the incident rays at the ionosphere.

It may be pointed out that from (1) we have no knowledge how reflection coefficient varies as a function of frequency at grazing incidence. Moreover, it

fails to account for the effect of the earth's curvature which is prominent at grazing and near-grazing incidence.

ACKNOWLEDGMENTS

The author wishes to thank Prof. S. R. Khastgir for his interest in the problem. He is thankful to the Govts. of India and USA for sponsoring the PL-480 Scheme of which the present study forms a part of the programme.

REFERENCES

- Bhattacharya, H. and Rao, M., 1964, *J. Atmosph. Terr. Phys.*, **26**, 263.
Ratcliffe, J. A., 1960, *Physics of the Upper Atmosphere*, Academic Press (Lond.), p. 106.
108, 442.
Taylor, W. L., 1960, *J. Geophys. Res.*, **65**, 1933.
Wait, J. R., 1962, *J. Res. NBS*, 66D, **53**, 453.
Wait, J. R. and Spies, K., 1960, *J. Geophys. Res.*, **65**, 2325.

SEMIEMPERICAL ONE CENTRE AND TWO CENTRE ELECTRON REPULSION INTEGRALS

S. PAHARI AND A. K. KAR

DEPARTMENT OF APPLIED CHEMISTRY, INDIAN INSTITUTE OF TECHNOLOGY, KHARAGPUR

(Received January, 21, 1967)

ABSTRACT. One centre and Two centre electron repulsion integrals were calculated for the π -electrons in C-C, O-O C-O, N-N, C-N, N-O, C-Cl, Cl-Cl etc with the help of several equations and the corresponding integrals for ethylene, benzene and formaldehyde were reported. Fisher-Hjalma's equation (1964) for two centre and the equation $(0.86E/R + 7.86)$ e.v, where E is the electronegativity of the atom in electron volt in Pauling's scale and R is the Slater's atomic radius, for one centre electron repulsion integral seems to be the best choice.

In the last few years semiempirical M.O. theory has achieved considerable success, particularly the method of Pariser and Parr (1953) for the calculation of electronic spectre of conjugated systems and that of Pople (1953) for the calculation of ionization potential and bond distance etc., of the same type of molecules. Several simple modifications of the methods were proposed later with a view to better correlating the data.

Any such method require the evaluation of a number of electrons repulsion integrals e.g.,

$$\int \int x_p^*(1) x_q^*(1) \frac{e^2}{r_{12}} x_R(2)x_S(2) \delta T_1 \delta T_2 = (p|qrs) \quad (1)$$

where x_p etc. are atomic orbitals.

Extract evaluation using Slaters, a , o 's were carried out (Parr *et. al*, 1950), but the results in predicting molecular parameters were not encouraging, leaving apart the tedious calculations. That is the reason of use semi-empirical parameters and introducing the idea of zero differential overlap, the required integrals are reduced to the evaluation of $(pp|pp)$ [2 electron 1 centre] and $(pp|qq)$ [2 electron 2 centre] only.

Here we have defined as usual :

$$(pp|pp) = I_p - E_p \quad \dots \quad (2)$$

where I_p and E_p are valence state ionization potential and electron affinity of an atom respectively. The data of Pritchard and Skinner (1954-55) and L. Oleari

et al (1966) are used. For many atoms I_p and E_p data are not available, so from a plot of (fig. 1), $(pp|pp)$ vs E/r a linear relation is obtained (where E is the electronegativity in Paulings scale and r is the Slaters atomic radius (Slater 1953) :

$$(pp|pp) = 0.8642 E/r + 7.86 \quad \dots (3)$$

which can be used to calculate $(pp|pp)$ of any atom.

$(pp|qq)$ is calculated in one set for $r \geq 2.80 a^\circ$ (hard sphere model of Parr, 1952) by :

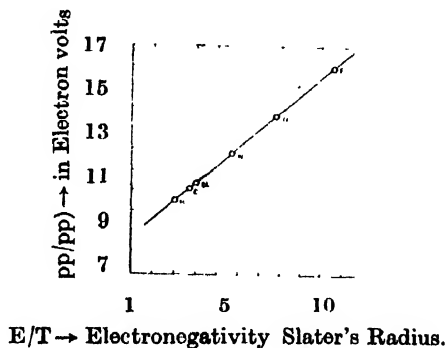


Fig. 1.

$$(pp|qq) = \frac{7.1975}{r} \left\{ \left[1 + \left(\frac{R_p + R_q}{2r} \right)^2 \right]^{\frac{1}{2}} + \left[1 + \left(\frac{R_p - R_q}{2r} \right)^2 \right]^{\frac{1}{2}} \right\} \quad \dots (4)$$

where $R_p = \frac{4.597}{Z_p} \times 10^{-8}$ cm and Z_p = Slater's effective nuclear charge ... (5)

For the distances less than $2.80a^\circ$ $(pp|qq)$ is expressed as

$$ar + br^2 = \frac{1}{2} [(pp|pp) + (qq|qq)] - (pp|qq) \quad \dots (6)$$

a and b are evaluated for a set by solving equation (6) for $r = 2.80 a^\circ$ and $3.70 a^\circ$. In this way $(pp|qq)$ integrals are evaluated for C-C, C-O, O-O, N-N, C-N, N-O etc. and are expressed as a function of r (table 1).

$(pp|qq)$ are also evaluated in another set by using an equation almost like Fisher-Hjalmar (1965) where $(pp|qq)$ is defined by equation (4) for $r \geq 2.794 a^\circ$ and for $r \leq 2.794 a^\circ$.

$$(pp|qq) = \frac{1}{2} [(pp|pp) + (qq|qq)] + ar^2 + br^3 + cr^4 \quad \dots (7)$$

a , b , and c are evaluated for C-C, C-O, C-N, C-Cl etc. from equation (4) for $r = 2.794, 3.7$ and $3.4 a^\circ$. The results are listed in table 1.

The corresponding values by the two methods are calculated for ethylene, for-maldehyde, benzene and are shown in table II.

Fisher-Hjalmar's equation (1964) for $(pp|qq)$:

$$(pp|qq) = \frac{1}{2}(\mu_p + \mu_q)[8.7542 - 1.4005\rho + 0.16724\rho^2 - 0.00961\rho^3] \quad (8)$$

where

$$\rho = \frac{\mu_p + \mu_q}{2} R$$

is a very general one and integrals for the distances in benzene, ethylene and formaldehyde are also calculated with the help of this equation and are listed for comparison.

TABLE I

$(pp|qq)$ for $r \leq 2.80$ and 2.794 \AA°

Column A represents a and b of eqn. (6) for $r \leq 2.80 \text{ \AA}^\circ$ and column B represents a , b and c of eqn. (7) (modified Fisher-Hjalmar's eqn.) for $r \leq 2.794 \text{ \AA}^\circ$. For r greater than these distances $(pp|qq)$ is given by eqn. (4).

$pp qq$ for bond	$\frac{1}{2}[(pp qq) + (pp qq)]_{e.v.}$	Column A		Column B		
		a	b	a	b	c
C — C	11.08 ¹	0.1167	-2.337	-1.734	0.4669	-0.03716
O — O	14.52 ¹	0.486	-4.63	-3.8249	1.3221	-0.1343
C — O	12.80 ¹	0.2982	-3.486	-2.047	+0.4358	-0.01529
N — N	$\begin{cases} 12.98^1 \\ 12.74^2 \end{cases}$	$\begin{cases} +0.3203 \\ 0.2972 \end{cases}$	$\begin{cases} -3.6142 \\ -3.464 \end{cases}$	$\begin{cases} -2.8617 \\ - \end{cases}$	$\begin{cases} 0.9225 \\ - \end{cases}$	$\begin{cases} -0.08825 \\ - \end{cases}$
C — N	$\begin{cases} 12.02^1 \\ 11.91^2 \end{cases}$	$\begin{cases} 0.2172 \\ 0.2065 \end{cases}$	$\begin{cases} -2.9687 \\ -2.8991 \end{cases}$	$\begin{cases} -2.2929 \\ - \end{cases}$	$\begin{cases} 0.6926 \\ - \end{cases}$	$\begin{cases} -0.06257 \\ - \end{cases}$
N — O	$\begin{cases} 13.75^1 \\ 13.58^2 \end{cases}$	$\begin{cases} 0.4041 \\ 0.3876 \end{cases}$	$\begin{cases} -4.1363 \\ -4.0294 \end{cases}$	$\begin{cases} -3.3424 \\ - \end{cases}$	$\begin{cases} 1.1218 \\ - \end{cases}$	$\begin{cases} -0.1112 \\ - \end{cases}$
Cl — Cl	$\begin{cases} 11.30^1 \\ 11.27^2 \end{cases}$	$\begin{cases} 0.1998 \\ 0.1919 \end{cases}$	$\begin{cases} -2.7264 \\ -2.7076 \end{cases}$	$\begin{cases} - \\ - \end{cases}$	$\begin{cases} - \\ - \end{cases}$	$\begin{cases} - \\ - \end{cases}$
C — Cl	$\begin{cases} 11.19^1 \\ 11.75^2 \end{cases}$	$\begin{cases} 0.1399 \\ 0.1384 \end{cases}$	$\begin{cases} -2.4666 \\ -2.4561 \end{cases}$	$\begin{cases} -1.8512 \\ - \end{cases}$	$\begin{cases} 0.5097 \\ - \end{cases}$	$\begin{cases} -0.041005 \\ - \end{cases}$
F — F	$\begin{cases} 16.70^1 \\ 17.33^2 \end{cases}$	$\begin{cases} 0.7037 \\ 0.7653 \end{cases}$	$\begin{cases} -6.0474 \\ -6.4473 \end{cases}$	$\begin{cases} - \\ - \end{cases}$	$\begin{cases} - \\ - \end{cases}$	$\begin{cases} - \\ - \end{cases}$
C — F	$\begin{cases} 13.89^1 \\ 14.205^2 \end{cases}$	$\begin{cases} 0.4102 \\ 0.4406 \end{cases}$	$\begin{cases} -4.1941 \\ -4.3917 \end{cases}$	$\begin{cases} -1.7279 \\ - \end{cases}$	$\begin{cases} 0.8243 \\ - \end{cases}$	$\begin{cases} -0.1134 \\ - \end{cases}$
S — S	10.81 ¹	0.1408	-2.377	-	-	-
C — S	10.945 ¹	0.1291	-2.355	-1.7230	0.4618	-0.036
S — O	12.665 ¹	0.3145	-3.519	-	-	-

¹ Data of L. Oleari *et al.*, (1966).

² Data of Pritchard and Skinner (1953).

TABLE II

Subs.	Integrals		Distance in a°	Using eqn. 6	Using eqn. 7	Using eqn. 8 ⁺
C ₂ H ₄	(11/11)	ev	0	11.08	11.08	11.08
	(11/22)	ev	1.337	8.1636	8.9775	7.1926
CH ₂ O	(11/11)C	ev	0	11.08	11.08	11.08
	(11/11)O	ev	0	14.52	14.52	14.52
	(11/22)C=O	ev	1.210	8.1452	9.6823	9.7149
Benzene	(11/11)	ev	0	11.08	11.08	11.08
	(11/22)	ev	1.397	8.043	8.8273	7.9377
	(11/33)	ev	2.42	6.088	6.26078	5.61760
	(11/44)	ev	2.794	5.462	5.4236	4.5152

⁺ μ Values are taken from Mulliken, *et al.*, (1949).

As it is evident from Table-II, the values for (pp/qq) obtained by equation (7) are comparatively higher, while those obtained by the use of equation (8) are comparatively lower for hydrocarbons. However, the reverse is the case for heteromolecules with equation (8) in comparison to those of equation (6) or equation (7). Thus although the results obtained by equation (8) are not exactly identical, but are in the expected order as seen from Parriser and Parr (Loc.cit).

Therefore, apparently equation (3) for (pp/qq) and equation (8) for (pp/qq) seems to be the simplest and the best choice.

The authors are grateful to Prof. S. K. Bhattacharyya, Head of the Department of Applied Chemistry, I.I.T., Kharagpur for his constant encouragement throughout the course of the work and are highly thankful to Miss J. Ghosh and Miss P. Mahanty of the same Department for their kind cooperation.

REFERENCES

- Inga Fisher-Hjalmars, 1964, *Molecular Orbitals in Chemistry, Physics and Biology, A tribute to R. S. Mulliken*, edited by P. O. Lowden and B. Pullman, Academic Press, pp. 361.
- , 1965, *Tetrahedron*, **19**, 1805.
- Mulliken, R. S., Rieke, C. M., Orloff, O., and Orloff, H., 1949, *J. Chem. Phys.*, **17**, 1248.
- Oleari, L., Sipio, L. D. and Michelis, G. P., 1966, *Molecular Physics*, **10**, 97.
- Pariser, R. and Parr, T. G., 1953, *J. Chem. Phys.*, **21**, 466, 767.
- Parr, R. G., Craig, D. P. and Ross, I. G., 1950, *J. Chem. Phys.*, **18**, 1561.
- Pople, J. A., 1953, *Trans. Faraday. Soc.*, **49**, 1375.
- Pritchard, H. O. and Skinner, H. A., 1953, *Trans. Faraday. Soc.*, **49**, 1254.
- , 1955, *Chem. Rev.*, **55**, 748.
- Slater, J. G., 1953, *Quantum Theory of Matter*, McGraw Hill, Table 6-42, p. 146.

Letters to the Editor

The Board of Editors does not hold itself responsible for opinions expressed in the letter published in this section. The notes containing short reports of original investigations communicated to this section should not contain many figures and should not exceed 500 words in length. The contributions reaching the Secretary by the 15th of any month may be expected to appear in the issue for the next month. No proof will be sent to the author.

21

H.M.O. CALCULATIONS ON TETRABENZONAPHTHALENE

A. B. SANNIGRAHIK,* A. K. KAR AND S. PAHARI

DEPARTMENT OF APPLIED CHEMISTRY,
INDIAN INSTITUTE OF TECHNOLOGY,
KHARAGPUR, INDIA.

(Received September 19, 1966 ;

Resubmitted April 26, 1967)

Tetrabenzonaphthalene (fig. 1) has been reported (Lang, *et al.*, 1961) to be a product of pyrolysis of fluorene. Recently it (Lewis, *et al.*, 1963) has been identified as one of the rearrangement products of 9—9' bifluorenylidene at 460°C. This compound is thermally stable, alternant hydrocarbon. The ultraviolet spectra of this compound was observed (Lewis *et al.*, 1963) at 350m μ for the longest wave length $\pi \rightarrow \pi$ transition.

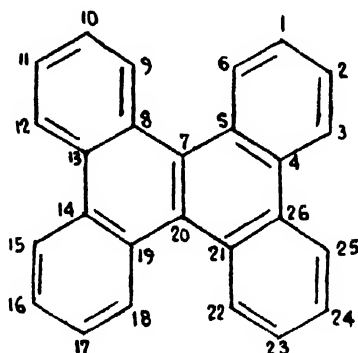


Fig. 1

The object of the present investigation is to make M.O. calculations on this molecule to see what information can be obtained about this molecule theoretically.

The method of calculation is well-known (Basu, 1954). Tetrabenzonaphthalene I belongs to the point group D_{2h} . Eliminating the plane of molecules which

*Present address : Deptt. of Chemistry, Tokyo Institute of Technology, Tokyo, Japan.

transforms all the p_z atomic orbitals in the same way, it is sufficient to consider the symmetry group C_2 for molecule. The various M.O. species corresponding to different representations has been point out.

The secular equations obtained after expanding the secular determinants corresponding to different M.O. species were solved for the energy values by IBM 1620. The charge densities q bond order p and free valence index F were calculated from the coefficients and is given in table I.

The $\pi \rightarrow \pi$ longest wave length transition is calculated from the difference of energy between highest occupied level to lowest unoccupied level. The above transition is from A_1 to B_2 involving energy of the amount 1.0229β .

TABLE I

Charge densities, bond order and free valence index at different positions.

Charge densities q_i	Bond order P_{rs}	Free valence index F_r
$q_1 = .99993$	$p_{12} = .62909$	$F_1 = .40290$
$q_2 = .99924$	$p_{13} = .69401$	$F_2 = .40895$
$q_3 = 1.00001$	$p_{34} = .59666$	$F_3 = .44138$
$q_4 = 1.00003$	$p_{45} = .550787$	$F_4 = .14087$
$q_5 = 1.00000$	$p_{56} = .58972$	$F_5 = .13281$
$q_6 = 1.00002$	$p_{16} = .70006$	$F_6 = .44227$
$q_7 = 1.00008$	$p_{67} = .458745$	$F_7 = .18383$
	$p_{44} = .44375$	
	$p_{77} = .63074$	

Using the equation (Streitwieser, 1961)

$$\nu(c_m^{-1}) = (19020 - 330)\Delta m + (10520 - 340) \quad \dots (7)$$

where $\Delta m = 1.0229$, the calculated value of λ_{max} for p band is found to be $341m\mu$. The observed value is $350m\mu$.

Symmetrical fusion of 4 benzene rings to the naphthalene nucleus offers some interesting modifications in the bond length of the parent hydrocarbon. In the resulting hydrocarbon the original 9-10 bond of the naphthalene has shortened further owing to the fusion of benzene rings as it is evident from the following M.O. diagram (fig. 2) of naphthalene (Coulson *et al*, 1965).

$$\begin{array}{lll} p_{12} = .72456 & p_{9-10} = .51823 & F_1 = .45279 \\ p_{23} = .60317 & & F_2 = .40432 \\ p_{10} = .5547 & & F_{10} = .10442 \end{array}$$

In case of naphthalene, F_r is the highest in position 1 and for tetrabenzonaphthalene it is in position (6) and (3). It has been pointed out that self atom polarizability values π_{rr} runs almost parallel to the F_r value (although no linear

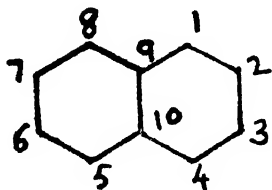


Fig. 2

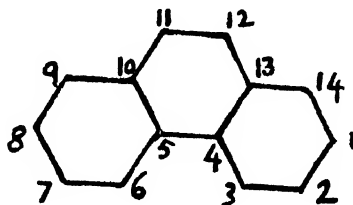


Fig. 3

relationship between them exists). The position of highest F_r is thus the most reactive position for the substitution reaction (nucleophilic or electrophilic attack). Thus position (6) is the most reactive position in tetrabenzonaphthalene.

In phenanthrene the positions of highest reactivity are positions 11 and 12

$$P_{11-12} = 0.63074$$

in this sense ($F_r = 0.45147$). The next reactive position is 14 ($F_r = 0.45011$) and next to it is position 3 ($F_r = .44052$). Tetrabenzonaphthalene results by the fusion of two phenanthrene rings. Naturally no substitution can take place in 11 and 12 positions. But the order of reactivity in other positions remain the same.

If HX or X_2 , where X is a monovalent radical, addition takes place, the bond with highest bond order is expected to be attacked first. Here it is 1 to 6 bond in tetrabenzonaphthalene. Comparing other cases also it may be said that in one of the two bonds near the atom of highest F_r , the ease of addition will be maximum.

The total π -energy of the system Tetrabenzonaphthalene is 36.7891β . Hence, 10.7891β is the delocalisation energy of the π -electrons in this net work. Thus the annealation energy (Brown, 1950) A of this system formed by fusing symmetrically 4-benzene rings into a naphthalene ring is $(11.683 - 10.789)\beta = .8937\beta$. Using the equation—

$$A = (2.1533\sqrt{P_a P_b} - 1.73251)\beta \quad \dots (9)$$

where A = annealation energy and P_a and P_b are the bond orders at the position of fusions, and taking P_a for benzene to be .667 and P_b for 1-2 bond in naphthalene to be .725 we get $A = .9436\beta$. The agreement is quite satisfactory. The equation was first proposed to consider the fusion of two systems. But, however, if Tetrabenzonaphthalene is formed by fusion of 2-phenanthrene rings, A from the equation comes to be .0645 β whereas from difference of theoretical D.E. it is .1075 β .

The authors' thanks are due to Prof. S. K. Bhattacharyya for his encouragement and to Sri A. K. Maiti for help in computational work.

R E F E R E N C E S

- Basu, S, 1954., *Indian J. Phys.*, **28**, 511.
Brown, R. D., 1950, *Trans. Farad. Soc.*, **46**, 1013.
Coulson, C. A. and Streitweiser, 1965, *Supplementary Tables of M.O. Calculations*, Vol.2, Pergamon Press.
Lang, K. ; Hufflebs H. and Kalonay J., 1961, *Chem. Ber*, **94**, 523.
Lewis, I. C. and Edstorm, T., 1963, *J. Org. Chem.*, **28**, 2250.
Steritweiser, A. (Jr.), 1961, *M.O. Theory of Org. Chemists*, John. Wiley & Sons, New York, pp. 217.

BOOK REVIEWS

SELECTED READINGS IN PHYSICS : THE CONTRIBUTIONS OF FARADAY AND MAXWELL TO ELECTRICAL SCIENCE, by R. A. R. Tricker, pp. 289, price 25 sh. net. Pergamon Press.

As will be evident from the title of the book, its scope is limited only to collateral contributions of Faraday and Maxwell towards the development of the theory of electro-magnetism. Naturally, we get only a one-sided view of the great experimental genius of Faraday and finish somewhat discontented. The treatment, with the introductory comments by the author explaining where Faraday ended by laying the foundations and Maxwell took up completing the grand mathematical superstructure, of the electromagnetic theory, is, however so refreshing that one may soon forgive the author for not writing more extensively on Faraday alone. Since the original works of Faraday and Maxwell are available to so few of us, the present book will be invaluable in getting first hand information on these; while the critical estimates by the author of the limitations of the theory involving the concept of an electro-magnetic ether, is no less valuable to the students.

A.B.

WAVES AND OSCILLATIONS—by R. A. Waldron. D. Van Nostrand Co., Inc., 1964. pp. vii+135.

The book is an interesting introduction to the phenomena of waves and oscillations. The author touches upon the elementary concepts at the outset and moves on to discuss the following topics : reflection and refraction, resonance, interference and diffraction, guided waves and topics in network theory.

The book presents, in a lucid manner, the basic properties of waves and their propagation characteristics. However, the subject of wave propagation in a magnetoactive medium has unfortunately been omitted. The book incorporates quite a few equations of wave mathematics, but Maxwell's equations are conspicuous by their absence.

Although the major emphasis is on the basic physics, some of the suitable points involved have also been well elucidated in a semi-sophisticated way; for example, the behaviour of metals to different waves (pp. 28–31), the formation of a backward wave in a periodic structure (p. 90), the principle of operation of a helix guide and the problems of microwave communication (pp. 95–96).

The most interesting feature in the book is the exposition of the underlying similarity between certain phenomena associated with different types of waves. One may point out here the analogy drawn between the Fabry-Perot interferometer and a high-Q cavity resonator (p. 71) and that between the diffraction by a slit and the response of a network via the Fourier transform (p. 117). The reference to the mammalian ear (pp. 108–109) and the human retinal cone (pp. 109–111) in connection with the matching of transmission lines and guided-wave type of propagation is worth mentioning.

Ad added attraction of the book is the information it carries on a few themes of current interest, such as 'the longest electromagnetic waves' (p. 21), 'infrared and optical masers' (p. 62), 'optical waveguides' (p. 107) and 'mechanical filters' (p. 124).

The book may be recommended to college and university students as well as new research workers in physics, who will find in it a stimulus for further study.

J.B.

INDIAN JOURNAL OF PHYSICS

VOL. 41

No. 10

AND

VOL. 50

PROCEEDINGS

No. 10

OF THE

INDIAN ASSOCIATION FOR THE CULTIVATION OF SCIENCE

(Edited in collaboration with the Indian Physical Society).

OCTOBER 1967

PUBLISHED BY THE
INDIAN ASSOCIATION FOR THE CULTIVATION OF SCIENCE
JADAVPUR, CALCUTTA-32

VISCOSITY OF POLAR-NONPOLAR GAS MIXTURES

ARUN K. PAL AND A. K. BARUA

INDIAN ASSOCIATION FOR THE CULTIVATION OF SCIENCE, CALCUTTA-32, INDIA

(Received May 31, 1967)

ABSTRACT. Viscosity of ammonia-nitrogen and sulphur dioxide-hydrogen gas mixtures has been measured over a temperature range from 30° to 200°C and at pressures below 10 cm. Hg. by using a precision oscillating disc viscometer. The results have been utilised to obtain informations on unlike interactions and also to generate inter-diffusion coefficients of these systems.

INTRODUCTION

It has been shown by a number of workers (Weissman *et al.* 1962; Weissman, 1964; Srivastava, 1961 and Hirschfelder *et al.* 1960) that on the basis of the Chapman-Enskog theory it is possible to determine unlike interactions from viscosity of gas mixtures. The combination rules generally used to calculate unlike interactions (Hirschfelder *et al.* 1954) being uncertain, only information obtained from experimental data are reliable. Viscosity, to the first approximation, is not affected significantly by inelastic collisions (Monchick *et al.* 1963). Thus, this property can be used with confidence for obtaining information on the spherical part of the intermolecular potential of polyatomic gases as well.

In this paper we have reported the results of our measurements of the viscosity of the polar-nonpolar gas mixtures, ammonia-nitrogen and sulphur dioxide-hydrogen over a temperature range from 30°–200°C and at pressures below 10 cm. Hg. Attempts have been made to derive information on unlike interactions from these data.

EXPERIMENTAL

The precision all-metal oscillating-disc viscometer together with its accessories used in our measurements has been described in detail in earlier papers (Kestin *et al.* 1959; Kestin *et al.* 1963; Pal *et al.* 1967a and Pal *et al.* 1967b). The working formulae and method of preparation of gas mixtures have also been described (Pal *et al.* 1967a, 1967b).

The gases ammonia and sulphur dioxide were prepared by standard laboratory procedures (Pal *et al.* 1967a). Hydrogen and Nitrogen used for calibration were supplied by the Indian Oxygen Co., Ltd. (purity 99.95%). The overall accuracy of our viscosity data for the mixtures should be within 1%. The viscosity data obtained by us are given in tables I and II. It may be mentioned here that for pure ammonia the viscosity values obtained by us are on the average 2%

lower than those reported earlier (Pal *et al*, 1967a). Mass spectrometric analysis showed that the previously used ammonia gas contained small percentage of air as impurity which can easily explain the discrepancy. However, the general conclusions drawn (Pal *et al*, 1967a) regarding ammonia remain unaltered. With the present data for ammonia the agreement with the earlier data (Carmichael *et al*, 1963 and Iwasaki *et al*, 1964) become excellent (within 1%) over the whole temperature range.

The only previous data for the systems ammonia-nitrogen and sulphur dioxide-hydrogen are those of Trautz *et al*, (1931). As the experimental temperatures are different it is not possible to compare our experimental data with the earlier ones. However, in the range where comparison is possible by interpolation the agreement of our data with those of Trautz *et al*, (1931) is within 2% which should be considered as satisfactory in view of the uncertainties in the earlier experimental methods

COMPARISON WITH THEORY

The viscosity of a binary gas mixture can be expressed as (Hirschfelder *et al*, 1954),

$$[\eta_{mix}]_1 = \frac{1 + Z_\eta}{X_\eta + Y_\eta} \quad \dots (1)$$

where

$$X_\eta = \frac{x_1^3}{\eta_1} + \frac{2x_1x_2}{\eta_{12}} + \frac{x_2^3}{\eta_2}$$

$$Y_\eta = \frac{3}{5}A^*_{12} \left\{ \frac{x_1^3}{\eta_1} \left(\frac{M_1}{M_2} \right) + \frac{2x_1x_2}{\eta_2} \left(\frac{(M_1 + M_2)^2}{4M_1M_2} \right) \left(\frac{\eta_{12}^3}{\eta_1\eta_2} \right) + \frac{x_2^3}{\eta_2} \left(\frac{M_2}{M_1} \right) \right\}$$

$$Z_\eta = \frac{3}{5}A^*_{12} \left\{ x_1^2 \left(\frac{M_1}{M_2} \right) + 2x_1x_2 \left[\left(\frac{(M_1 + M_2)^2}{4M_1M_2} \right) \left(\frac{\eta_{12} + \eta_{12}}{\eta_1 + \eta_2} \right) - 1 \right] + x_2^2 \left(\frac{M_2}{M_1} \right) \right\}$$

where x_1 , x_2 are the mole fractions of the components 1 and 2, M_1 , M_2 being the corresponding masses. η_{12} is the viscosity of a hypothetical gas of mass $\frac{2M_1M_2}{M_1 + M_2}$ and A^*_{12} is a ratio of collision integrals which is a very slowly varying function of temperature.

It is possible to represent polar-nonpolar interaction as interaction between two nonpolar molecules. Consequently, we have used Lennard-Jones (12:6)

potential for our calculations. The combination rules for polar-nonpolar interactions can be written as (Hirschfelder *et al.*, 1954),

$$\sigma_{np} = \frac{1}{2}(\sigma_n + \sigma_p) \xi^{-1/6} \quad \dots (2a)$$

$$\epsilon_{np} = \sqrt{\epsilon_n \epsilon_p} \xi^2 \quad \dots (2b)$$

where the subscript n and p stand for nonpolar and polar component respectively. ξ is given by

$$\xi = \left[1 + \frac{1}{4} \frac{\alpha_n \mu_p^{*2}}{\sigma_n^3} \sqrt{\epsilon_p / \epsilon_n} \right] \quad \dots (3)$$

where α_n is the polarizability of the nonpolar molecule in cubic angstroms. The force parameters for the nonpolar gases were taken as those determined from viscosity data (Hirschfelder *et al.*, 1954) and for the polar components the values of σ_p and ϵ_p as obtained on the 12-6-3 model (Monchick *et al.*, 1961) were used. The values of η_{mix} at different temperatures as obtained from eqn. (1) are shown in column 4 of Tables I and II. It may be seen that the agreement between the experimental and the calculated values of η_{mix} is excellent (within 1%).

Recently, Chakraborty and Gray (1965) have measured the viscosity of a number of polar-nonpolar gas mixtures over the temperature range from 25°C to 80°C. They found that for those systems generally the agreement between the experimental and the calculated values of η_{mix} to be not quite satisfactory. It is difficult to say whether this discrepancy is due to some particular feature of the systems studied or due to experimental uncertainties.

UNLIKE INTERACTION FROM MIXTURE VISCOSITY DATA

It has been shown by a number of workers (Weissman *et al.*, 1962; Weissman 1964, and Srivastava, 1961) that it is possible to determine unlike interactions from viscosity of gas mixtures. Eqn. (1) can be solved for η_{12} in the following manner (Srivastava, 1961)

$$\eta_{12} = \frac{-b \pm \sqrt{b^2 - 4ac}}{2a} \quad \dots (4)$$

where

$$a = \frac{6}{5} A^*_{12} \left(\frac{x_1 x_2}{\eta_1 \eta_2} \right) \left(\frac{(M_1 + M_2)^2}{4M_1 M_2} \right) (\eta_{mix} - \eta_1 - \eta_2)$$

TABLE I

Viscosity and inter-diffusion coefficient of $\text{NH}_3\text{-N}_2$ gas mixtures at different temperatures

T°C	mole fraction of NH_3	$\eta \times 10^7$ ($\text{gcm}^{-1}\text{sec}^{-1}$)	$\eta_{mix} \times 10^7$ ($\text{g.cm}^{-1}\text{sec}^{-1}$)	$({}_pD_{12})$ ($\text{cm}^2\text{sec}^{-1}$)	$({}_p d_{12})$ ($\text{cm}^2\text{sec}^{-1}$)
24	1.0000	102.81	—		
	0.7964	119.44	120.46		
	0.5709	136.17			
	0.5027	141.60	142.21	0.210	0.217
	0.4020	148.61	—		
	0.2007	167.85	165.21		
	0.0000	175.05	—		
54	1.0000	113.72	—		
	0.7700	136.40	134.89		
	0.5876	151.71	—		
	0.5021	158.05	157.61	0.267	0.269
	0.4003	167.03	—		
	0.2007	179.37	179.42		
	0.0000	191.30	—		
100	1.0000	130.75	—		
	0.7700	154.95	154.52		
	0.5876	170.10	—		
	0.5021	177.34	177.25	0.332	0.332
	0.4003	185.08	—		
	0.2007	198.92	198.81		
	0.0000	210.10	—		
150	1.0000	149.28	—		
	0.7603	176.11	175.02		
	0.5920	190.03	—		
	0.4928	179.01	198.21	0.412	0.418
	0.3985	203.75	—		
	0.2252	216.72	217.80		
	0.0000	230.5	—		
200	1.0000	167.98	—		
	0.7603	195.72	197.70		
	0.5920	207.85	—		
	0.4928	215.20	217.91	0.507	0.510
	0.3985	222.11	—		
	0.2252	236.25	238.52		
	0.0000	252.25	—		

TABLE II

Viscosity and inter-diffusion data of SO₂-H₂ gas mixture at different temperatures

T°C	mole frac- tion of SO ₂	$\eta \times 10^7$ (gm.cm ⁻¹ sec ⁻¹)	$\eta_{mix} \times 10^7$ (gm.cm ⁻¹ sec ⁻¹)	(pD_{12}) (cm ² .sec ⁻¹)	(pD_{12}) (cm ² .sec ⁻¹)
30	1.0000	133.01	—		
	0.8219	134.45	136.40		
	0.5957	135.01	—		
	0.4919	136.75	140.71	0.600	0.610
	0.4059	137.01	—		
	0.2005	136.41	139.33	—	
	0.0000	90.00			
55	1.0000	144.02	—		
	0.7866	145.46	148.42		
	0.5975	147.21	—		
	0.4863	148.46	150.05	0.705	0.701
	0.4000	148.01	—		
	0.2005	147.12	149.76		
	0.0000	95.60	—		
100	1.0000	168.90	—		
	0.7866	168.06	172.62		
	0.5975	167.95	—		
	0.4863	166.91	174.83	0.884	0.876
	0.4000	165.95	—		
	0.2005	162.89	167.31		
	0.0000	104.70	—		
150	1.0000	192.20	—		
	0.8110	192.03	195.24		
	0.6024	192.50	—		
	0.5023	192.52	198.48	1.105	1.086
	0.4018	192.53	—		
	0.2000	177.88	186.00		
	0.0000	115.50	—		
200	1.0000	211.50	—		
	0.8110	214.11	214.23		
	0.6024	214.99	—		
	0.5023	215.40	216.21	1.330	1.306
	0.4018	213.37	—		
	0.2000	194.72	200.30		
	0.0000	122.60	—		

$$b = \frac{3}{5} A^*_{12} \left[2x_1x_2 + x_1^2 \left(\frac{M_1}{M_2} \right) \left(\frac{\eta_{m1x}}{1} \right) + x_2^2 \left(\frac{M_2}{M_1} \right) \left(\frac{\eta_{m2x}}{\eta_2} \right) - x_1^2 \left(\frac{M_1}{M_2} \right) - x_2^2 \left(\frac{M_2}{M_1} \right) \right] + \eta_{m1x} \left(\frac{x_1^2}{\eta_1} + \frac{x_2^2}{\eta_2} \right) - 1$$

$$c = 2x_1x_2 \eta_{m1x}$$

It is possible to determine the unlike interaction parameters, σ_{12} and ϵ_{12} from the temperature dependence of η_{12} . η_{12} can also be used to generate pD_{12} from the relation (Hirschfelder *et al.*, 1954),

$$pD_{12} = \eta_{12} \frac{3}{5} \frac{(M_1 + M_2)}{M_1 M_2} \cdot A^*_{12} RT. \quad (5)$$

p being the pressure in atmosphere. By substituting the values of A^* as obtained by using force parameters calculated from the combination rules pD_{12} values can be obtained. It may be pointed out that this calculation of pD_{12} is equivalent to obtaining unlike interaction parameters. It is possible to measure the viscosity of gas mixtures much more precisely than the diffusion coefficients. Consequently, this method of obtaining D_{12} from the mixture viscosity data should be more reliable than the actual measurements of this property by the existing techniques.

In column 6 of tables I and II are also shown the calculated values of D_{12} on the Chapman-Enskog theory by using the combination rules given in eqns. (2a) and (2b). It may be seen that the agreement between the values of D_{12} thus obtained with those calculated from the mixture viscosity data is excellent. This probably shows the usefulness of the combination rules inspite of their semi-empirical nature.

ACKNOWLEDGMENT

The authors are grateful to Prof. B. N. Srivastava for his kind interest.

REFERENCES

- Carmichael, L. T., Reamer, H. H., and Sage, B. H., 1963, *J. Chem. Eng. Data*, **8**, 400.
 Chakraborty, P. K., and Gray, P., 1965, *Trans. Faraday Soc.*, **61**, 2422.
 Hirschfelder, J. O., Taylor, M. H. and Kihara, T., 1960, *Report WIS-OOR-29*.
 Hirschfelder, J. O., Curtiss, C. F., and Bird, R. B., 1954, *Molecular Theory of Gases and Liquids*, John Wiley & Sons, Inc., New York.
 Iwasaki, H., Kestin, J. and Nagashima, A., 1964, *J. Chem. Phys.*, **40**, 2988.
 Kestin, J. and Leidenforst, W., 1959, *Physica*, **25**, 1033.
 Kestin, J. and Mason, E. A., 1961, *J. Chem. Phys.*, **35**, 1676.
 Monchick, L., and Mason, E. A., 1961, *J. Chem. Phys.*, **35**, 1676.
 Monchick, L., Yun, K. S. and Mason, E. A., 1963, *J. Chem. Phys.*, **39**, 654.
 Pal, A. K. and Barua, A. K., 1967a, *Trans. Faraday Soc.*, **63**, 341.
 ———, 1967b, *J. Chem. Phys.*, **47**, 216.
 Srivastava, I. B., 1961, *Indian J. Phys.*, **35**, 86.
 Trautz, M., and Heberling, R., 1931, *Ann. Physik*, **10**, 155.
 Weissman, S., 1964, *J. Chem. Phys.*, **40**, 3397.
 Weissman, S. and Mason, E. A., 1962, *J. Chem. Phys.*, **37**, 1289.

THERMAL DIFFUSION IN MONATOMIC-POLYATOMIC GAS MIXTURES

S. K. DEB

INDIAN ASSOCIATION FOR THE CULTIVATION OF SCIENCE, CALCUTTA-32

(Received May 31, 1967)

ABSTRACT. Thermal diffusion factors of the systems H_2 -Xe, CO_2 -Kr and CO_2 -Xe have been measured by the two-bulb method over the temperature range from 330°-600°K. The results have been interpreted in terms of the Chapman-Enskog theory as well as the recent theory taking into consideration the effect of inelastic collisions on thermal diffusion phenomena.

INTRODUCTION

Recent theoretical work shows the necessity of considering the effect of inelastic collisions on thermal diffusion factor in polyatomic gases. The Chapman-Enskog theory (Chapman *et al.*, 1952) takes into consideration only the spherical part of the intermolecular potential and can be applied to polyatomic gases for properties which are not significantly affected by inelastic collisions. Schirdewahn, Klemm and Waldmann (1961) suggested a semi-empirical method for obtaining the effects of rotational degrees of freedom on thermal diffusion which is only applicable to isotopes. Subsequently, a more generalised approach to the problem has been given by Monchick, Yun and Mason (1963) and Monchick, Munn and Mason (1966). These theoretical treatments have been found not to be quite successful in interpreting existing thermal diffusion data on polyatomic gases. Another major factor which is hindering a proper explanation of thermal diffusion factors in polyatomic gases is the scarcity of reliable experimental data. Consequently, it is essential to have precise measurements of thermal diffusion factors in polyatomic gas mixtures. As a starting point it is preferable to study binary systems having one component as polyatomic. With this end in view, we have measured the temperature dependence of thermal diffusion factor of the systems H_2 -Xe, CO_2 -Kr and CO_2 -Xe in the range from 330°K to 600°K by the two bulb method. The systems have the interesting feature that carbon dioxide in contrast to hydrogen is expected to show the effect of inelastic collisions on thermal diffusion quite prominently.

EXPERIMENTAL

The all-metal two-bulb apparatus together with the accessories for the measurement of thermal diffusion factor has been described in detail by Deb and Barua (1967). The monatomic gases were supplied by the British Oxygen

Co., Ltd., and hydrogen gas (purity 99.95%) by Indian Oxygen Co., Ltd.. Carbon dioxide was prepared by heating BaCO_3 with PbCl_2 and the purity of the gas was tested in a mass spectrometer (Associated Electrical Industries, MS3 model). The temperature was assigned according to the following formula, (Brown, 1940).

$$\bar{T} = \frac{T_H T_C}{T_H - T_C} \cdot \ln \frac{T_H}{T_C} \quad \dots (1)$$

where T_H and T_C are the temperatures of the upper and the lower bulb respectively.

The separation factor q can be calculated from the relation,

$$q = \frac{(x_1/x_2)_{Top}}{(x_1/x_2)_{Bottom}} \quad \dots (2)$$

where x_1 and x_2 are the compositions of the lighter and the heavier molecules respectively. Thermal diffusion factor α can be calculated from the relation,

$$\alpha = \frac{\ln q}{\ln T_H/T_C} \quad (3)$$

The experimental procedure has already been described in an earlier paper (Deb *et al.*, 1967). The analysis of the samples after steady state has been reached was done by a mass spectrometer. The results of our measurements are shown in table I and figs. 1-3.

COMPARISON WITH EARLIER DATA

Heymann and Kistemaker (1959) obtained the thermal diffusion factor for the system H_2 -Xe by the two bulb method with Xe in trace. Their experimental values were higher than the theoretical thermal diffusion factor by 5 to 10%. Since in our experiment, the composition of Xe is far from trace, no direct comparison with their data is possible. However, our experimental values are also higher than the predicted values.

Cozens and Grew (1964) obtained the thermal diffusion factor for the mixture CO_2 -Kr and CO_2 -Xe in the temperature range 150°K to 1000°K, using one of the components in trace concentration. However, for these mixtures also, the compositions of the components in our experiments do not correspond to those of Cozens and Grew and hence no direct comparison is possible. Our experimental values are higher than those calculated on the L-J (12:6) model. One of the possible explanations should be the fact that the first approximation to the theoretical thermal diffusion factor may be considerably lower than the exact value. As had been pointed out by Mason (1957), error in the first approximation of thermal diffusion factor is much greater than for the other transport coefficients. The

general formulae given for higher approximations are very complicated and have been calculated by Mason (1957) and Saxena *et al*, (1958) only for mixtures containing one component in trace.

INTERPRETATION OF THE DATA

The thermal diffusion factor α can be represented on the Chapman-Cowling first approximation as (Hirschfelder, *et al*, 1964),

$$\alpha = A(6C_{12}^* - 5) \quad (4)$$

where C_{12}^* is a ratio of collision integrals and A is a function of masses, molefractions and potential parameters. For polyatomic gas mixtures the convergence of α is not known satisfactorily. Consequently, we shall confine our calculation of α to the first approximation. For the calculation of α the Lennard-Jones (12:6) potential has been used. The force constants taken were those determined from experimental viscosity data and the unlike interactions were approximated by the usual combination rules. The calculated values of α thus obtained from eq. (4) are shown in figs. 1-3 together with the experimental values of α .

TABLE I

Experimental values of thermal diffusion factors

H ₂ -Xe(H ₂ = 18.0%)		CO ₂ -Kr(CO ₂ = 37.5%)		CO ₂ -Xe(CO ₂ = 47.0%)	
T	α	T	α	T	α
337	0.31	350	0.17	383	0.23
397	0.34	390	0.18	421	0.24
468	0.36	438	0.19	469	0.27
534	0.38	471	0.20	520	0.30
		529	0.21	566	0.33
		572	0.21	601	0.36
		611	0.21		

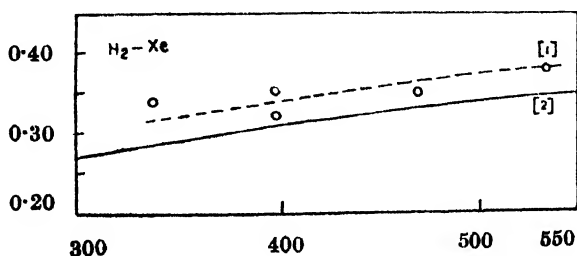


Fig. 1. Experimental and theoretical curves for the thermal diffusion factor α of the system H₂-Xe.

- [1] Experimental
- [2] Lennard-Jones (12 : 6)
- o Experimental points

As discussed earlier eq. (4) does not include the effect of inelastic collisions. In order to take this factor into account Monchick, Munn and Mason (1966) have recently given a treatment by solving the generalised Maxwell-Stefan equation. This theory has been found not to be quite successful in interpreting the existing thermal diffusion factor data for polyatomic gas mixtures (Monchick *et al.*, 1966 and Ghosh *et al.*, 1967). Consequently, we have tested this theory only for the CO₂-Xe system for which deviation from the Chapman-Enskog theory is maximum. According to this method the thermal diffusion factor can be written to the first approximation as,

$$\alpha_{ij} = \frac{1}{5k} \frac{\mu_{ij}(6C_{ij}^* - 5)}{n[D_{ij}]_1} \cdot \left(\frac{\lambda_j}{x_j M_j} - \frac{\lambda_i}{x_i M_i} \right) \quad (5)$$

where μ_{ij} is the reduced mass of the system. D_{ij} the diffusion coefficient, λ 's represent the thermal conductivities and x 's the mole fractions. By making some approximations λ can be expressed as (Monchick *et al.*, 1966),

$$\lambda_i \approx 4x_i \sum_{\alpha=1}^N \Lambda_{i\alpha} \left\{ x_\alpha + \sum_{\beta=1}^N \left[(\Delta\alpha_{\alpha\beta}^{10,10}) \left(\sum_{\gamma=1}^N \Lambda_{\beta\gamma} x_\gamma \right) - \left(\frac{x_\beta}{\mathcal{L}_{\beta\beta}^{01,01}} \right) (\Delta\mathcal{L}_{\alpha\beta}^{10,01}) \right] \right\} \dots (6)$$

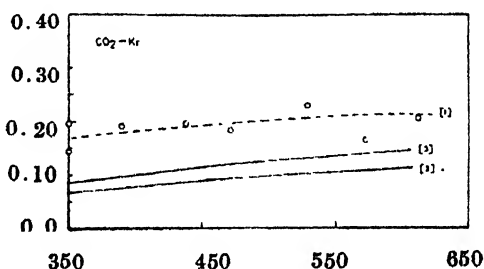


Fig. 2. Experimental and theoretical curves for the thermal diffusion factor α of the system CO₂-Kr.

[1] Experimental

[2] Lennard-Jones (12:6)

[3] Lennard-Jones (12:6) using experimental thermal conductivity values of CO₂

0 Experimental points

where

$$\Lambda_{\alpha\beta} = \left| \frac{\mathcal{L}_{\alpha\alpha'}^{10,10}}{\delta_{\beta\alpha'}} \right| \left| \frac{\delta_{\alpha\alpha}}{0} \right| \left| \mathcal{L}_{\alpha\alpha'}^{10,10} \right|^{-1} \dots (7)$$

The expressions for $\mathcal{L}_{\alpha\alpha'}^{rs,t's'}$ and $\Delta\mathcal{L}_{\alpha\alpha'}^{rs,r's'}$ have been given in detail by Monchick *et al.*, (1965). The terms $\mathcal{L}_{\alpha\alpha'}^{rs,r's'}$ involve cross-relaxation times. The molecular parameters required for the calculation of λ were chosen in the manner

similar to that described by Monchick *et al.* (1966). The result thus obtained is shown in fig. 3.

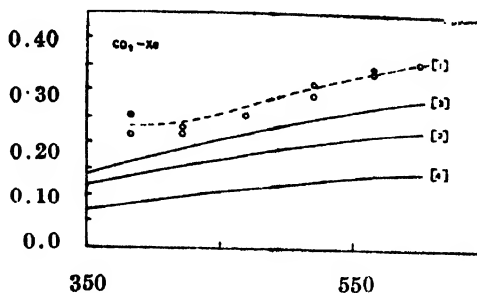


Fig. 3. Experimental and theoretical curves for the thermal diffusion factor α of the system $\text{CO}_2\text{-Xe}$.

- [1] Experimental
- [2] Lennard-Jones (12:6)
- [3] Lennard-Jones (12:6) using experimental thermal conductivity values of CO_2 .
- [4] Theoretical values calculated according to the formula of Monchick, (1966)
- 0 Experimental points

It may be seen that the consideration of the inelastic effects by the method of Monchick *et al.* (1966) makes the agreement between theory and experiment worse than that obtained by using Chapman-Enskog theory. At present it is difficult to ascribe definitely the reason for this apparently anomalous result. It may, however, be due to the basic limitation of the Maxwell-Stefan equation or due to the number of approximations made in the evaluation of α from eq. (5).

It is also possible to express α on the Chapman-Enskog theory in terms of thermal conductivity. Thermal diffusion is dependent on the thermal conductivity of the components, which is also affected significantly by inelastic collisions. Therefore a tentative way of taking into accounts effects of inelastic collisions (at least partially) on thermal diffusion is to use experimental thermal conductivities in eq. (1) to calculate α . The results thus obtained for $\text{CO}_2\text{-Kr}$ and $\text{CO}_2\text{-Xe}$ systems by using experimental thermal conductivity data for CO_2 are shown in figs. 2 and 3. It may be seen that the agreement thus obtained is better than that obtained by all other methods.

The results obtained above show the inadequacy of our present knowledge of thermal diffusion phenomena in polyatomic gas mixtures. A more sophisticated theory to take into account effects of inelastic collisions on thermal diffusion is necessary.

ACKNOWLEDGMENT

The author wishes to thank Dr A. K. Barua for suggesting the problem and helpful guidance and to Prof. B. N. Srivastava, D.Sc., F.N.I., for his kind encouragement and interest in the work.

REFERENCES

- Brown, H., 1940, *Phys. Rev.*, **58**, 661.
- Chapman, S., and Cowling, T. G., 1952, *The Mathematical Theory of Non-Uniform Gases*. Cambridge University Press.
- Cozens, J. R. and Grew, K. E., 1964, *Phys. Fluids.*, **7**, 1395.
- Deb, S. K. and Barua, A. K., 1967, *Indian J. Phys.* **41**, 646.
- Ghosh, A. K., Batabyal, A. K. and Barua, A. K., 1966, *J. Chem. Phys.* **47**, 452.
- Heymann, D., and Kistemaker, J., 1959, *Physica*, **25**, 556.
- Hirschfelder, J. O., Curtiss, C. F. and Bird, R. B., 1964, *Molecular Theory of Gases and Liquids*, John Wiley and Sons, N. Y.).
- Mason, E. A., 1957, *J. Chem. Phys.*, **27**, 75, 782.
- Monchick, L., Munn, R. J., and Mason, E. A., 1966, *J. Chem. Phys.*, **45**, 3051.
- Monchick, L., Pereira, A. N. G. and Mason, E. A., 1965, *J. Chem. Phys.*, **42**, 3241.
- Monchick, L., Yun, K. S. and Mason, E. A., 1963, *J. Chem. Phys.*, **39**, 654.
- Saxena, S. C. and Mason, E. A., 1958, *J. Chem. Phys.*, **28**, 623.
- Schirdewahn, J., Klemm, A., and Waldmann, L., 1961, *Z. Naturforsch.* **16a**, 133.

DIELECTRIC ABSORPTION OF AND INTERNAL ROTATION IN ANISOLES AND SUBSTITUTED ANISOLES IN SOLUTIONS IN NON-POLAR SOLVENTS

G. S. KASTHA, B. DUTTA (nee SINHA) AND S. B. ROY

OPTICS DEPARTMENT, INDIAN ASSOCIATION FOR THE CULTIVATION OF SCIENCE
CALCUTTA-32 INDIA

(Received May 12, 1967)

ABSTRACT. The dielectric loss due to absorption of microwaves of frequency 38.8 KMc/s in dilute solutions of anisoles and some substituted anisoles in a number of non-polar solvents at different temperatures (T) have been investigated. It has been found that under the assumption of a single relaxation time (τ) the plots of $\log(\tau T)$ against $1/T$ for the solutions of *o*-chloro-, *o*-bromo-, *o*-nitro- and *p*-chloroanisoles in paraffin, *n*-hexane, CCl_4 and benzene, are linear while in the case of anisole solutions, such plots are *s*-shaped curves, showing thereby existence of more than one relaxation time. The observed results in this case have been analysed under the assumption of two relaxation times τ_1 and τ_2 the former due to rotation of the molecule as a whole and the latter due to rotation of the methoxy group. The analysis shows that the percentage contribution to the overall loss due to the rotation of the methoxy group is about 10% in paraffin solution and about 30% in hexane solution. This percentage is still higher in benzene and CCl_4 solutions. The value of τ_2 in paraffin and hexane solutions at about 275°K is about 4×10^{-12} sec with a potential barrier of 4.3 K.Cal/mole. This value of τ_2 in benzene and CCl_4 occurring at about 295°K seems to be consistent with experimental results. The values of τ_1 due to rotation of the molecule as a whole in the case of anisole in all these cases are compatible with those observed for rigid dipolar molecules of similar size under similar circumstances.

INTRODUCTION

The phenomenon of dielectric relaxation of polar molecules in the liquid state and in solutions in non-polar solvents has been extensively studied both theoretically and experimentally. The agreement between the two has been found to be fairly satisfactory in the case of polar molecules with rigid dipoles but in the case of molecules with polar groups, having the possibility of rotational motions the agreement is not satisfactory.

From considerations of rotational Brownian motion of the different polar groups attached to the polar molecule, Budo (1938), following Debye, showed that in general a number of different relaxation times characteristic of the different polar groups and of the whole molecule are to be expected, in contrast to a single relaxation time observed in the case of rigid dipolar molecules. He also showed that the relative contributions by various polar groups to the overall dielectric loss will be proportional to the square of the ratios of the partial moments of the

respective groups to the moment of the whole molecule. Many workers have experimentally investigated the dielectric loss of such molecules but their experimental findings differ widely amongst each other. As, for example, in the case of solution of methoxy benzene in benzene at 20°C, the time of relaxation of the OCH_3 group have been reported as varying from 7×10^{-12} sec to 0.8×10^{-12} sec., while the percentage contribution to the overall loss due to the methoxy group varies from 80% to about 20% (Hase, 1953; Fisher, 1954; Klages, 1954; Grubb *et al*, 1961; Klages *et al*, 1961; Forest *et al*, 1964).

Because of this wide divergence in the results reported by various workers, an investigation of the dielectric behaviour of anisole and some substituted anisoles dissolved in some non-polar solvents at different temperatures was undertaken. An analysis of the results of the investigation has been presented in this paper.

EXPERIMENTAL

Anisole, *o*-chloro-, *o*-bromo-, *o*-nitro- and parachloro anisoles studied in the present investigation were of chemically pure quality. These were fractionated and the proper fractions were distilled under reduced pressure and dried before being used in the investigations. The solvents carbon tetrachloride, benzene, *n*-hexane and medicinal paraffin were dried by usual method. The dried solvents showed slight losses in the 38.8 Kmc/s frequency region, which were properly taken into account in determining the overall losses due to the various solutions. The experimental arrangement and method of calculation of loss tangent ($\tan \delta$) were the same as described earlier (Bhattacharjee *et al*, 1964).

THEORY OF THE METHOD

Following Budo (1938), the average dipole moment of anisole or the para substituted anisole in a high frequency electric field of angular frequency ω is given by

$$(\mu)_{av} = \left\{ \frac{\mu_1^2}{1+j\omega\tau_1} + \frac{\mu_2^2}{1+j\omega\tau_2} \right\} \frac{E_0 e^{j\omega t}}{3kT} \quad \dots (1)$$

where μ_1 is the dipole moment along the C-O bond, the axis of rotation of the methoxy group and τ_1 is the relaxation time for the orientation of the whole molecule, μ_2 is the moment component perpendicular to the axis of rotation and τ_2 is the relaxation time associated with it. If the moment μ_g of the methoxy group is inclined at an angle ϵ to the axis of rotation then $\mu_2 = \mu_g \sin \epsilon$ and μ_1 is composed of the moments $\mu_g \cos \epsilon$, μ_s , the moment of the atom in the para position and some contribution from the mesomeric structures (Grubb *et al*, 1961). This will be the average moment if in all the molecules the methoxy group is free to rotate. However, if only the fraction t is capable of rotation

(Fischer, 1964; Klages *et al*, 1961) the fraction $(1-t)$ will relax in the field as rigid molecules and the average moment will be modified as

$$\begin{aligned}
 (\mu')_{av} &= \left\{ \frac{(1-t)\mu^2}{1+j\omega\tau_1} + t \left(\frac{\mu_1^2}{1+j\omega\tau_1} + \frac{\mu_2^2}{1+j\omega\tau_2} \right) \right\} \frac{E_0 e^{j\omega t}}{3kT} \\
 &= \left\{ \frac{\mu^2 - t(\mu^2 - \mu_1^2)}{1+j\omega\tau_1} + \frac{t\mu_2^2}{1+j\omega\tau_2} \right\} \frac{E_0 e^{j\omega t}}{3kT} \quad \dots (2)
 \end{aligned}$$

Remembering that the observed dipole moment μ is given by $\mu^2 = \mu_1^2 + \mu_2^2$ equation (2) gives

$$\begin{aligned}
 (\mu')_{av} &= \left(\frac{\mu^2 - t\mu_2^2}{1+j\omega\tau_1} + \frac{t\mu_2^2}{1+j\omega\tau_2} \right) \cdot \frac{E_0 e^{j\omega t}}{3kT} \\
 &= \left(\frac{C_1\mu^2}{1+j\omega\tau_1} + \frac{C_2\mu^2}{1+j\omega\tau_2} \right) \frac{E_0 e^{j\omega t}}{3kT} \quad \dots (3)
 \end{aligned}$$

where $C_1 = 1 - \frac{t\mu_2^2}{\mu^2}$, $C_2 = \frac{t\mu_2^2}{\mu^2}$ and $C_1 + C_2 = 1$... (3a)

Combining this expression with Debye expression for $\tan \delta$ in the case of very dilute solutions in non-polar solvents, we obtain

$$\tan \delta = \frac{(\epsilon' + 2)^2}{\epsilon'} \cdot \frac{4\pi N \mu^2 c}{27kT} \left(\frac{C_1 \omega \tau_1}{1 + \omega^2 \tau_1^2} + \frac{C_2 \omega \tau_2}{1 + \omega^2 \tau_2^2} \right) \quad \dots (4)$$

ϵ' is dielectric constant of the solution at the frequency of the applied field and all other constants having their usual significance. When the concentration c is small $\epsilon' \rightarrow \epsilon_0$ the static dielectric constant of the solvent. Eqn. (4) then gives

$$\frac{T \tan \delta}{c} \left| \frac{4\pi N \mu^2}{27k} \frac{(\epsilon_0 + 2)^2}{\epsilon_0} \right| = \xi(T) = \frac{C_1 \omega \tau_1}{1 + \omega^2 \tau_1^2} + \frac{C_2 \omega \tau_2}{1 + \omega^2 \tau_2^2} \quad \dots (5)$$

with $\omega\tau_1 = x_1$ and $\omega\tau_2 = x_2$

$$\xi(T) = C_1 \frac{x_1}{1+x_1^2} + C_2 \frac{x_2}{1+x_2^2} = C_1 f(x_1) + C_2 f(x_2) \quad \dots (6)$$

where

$$f(x) = \frac{x}{1+x^2}$$

RESULTS

The experimental values of $\tan \delta$ at different temperature (T) for the different solutions of anisole are given in table I. In the case of solutions of anisole in hexane, benzene and carbon tetrachloride when the curves $\frac{T \tan \delta}{C}$ vs T showed maxima, the dipole moments were calculated as usual (Sinha *et al*, 1966) under the assumption of single relaxation time. In all the other cases the values of dipole moments reported in literatures were used for the evaluation of τ values which are included in the tables. Table I also includes the values of $\xi(T)$ calculated from the eqn. (5) in which the observed value of 1.25D was used for μ , the dipole moment of anisole.

DISCUSSION

(a) Existence of two relaxation times :

With the help of the τ -values calculated under the assumption of a single relaxation time, graphs of $\log(\tau T)$ against $1/T$ have been drawn for anisole and substituted anisoles. These graphs are shown in figures (1-5). It is seen that the graphs are almost straight lines in the case of all the substituted anisoles, and similar to those observed in the case of molecules with rigid dipole moments (Sinha *et al*, 1965; 1966). But in the case of solutions of anisole in paraffin, hexane, benzene and CCl_4 (figs. 5a-5d) the graphs are s-shaped curves. This non-linearity shows that the results are not explicable under the assumption of a single relaxation time for anisole.

From table I it is seen that the values of $\xi(T)$ in the case of solutions in hexane, benzene and CCl_4 at first increase with increase of temperature, then attain a

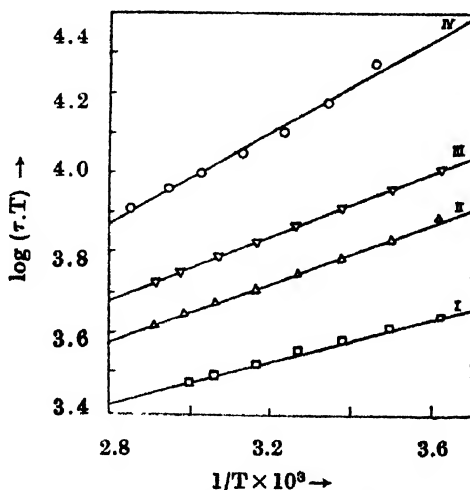


Fig. 1. Plots of $\log(\tau T)$ vs $1/T$ for solutions of *o*-nitro-anisole in different solvents. (τ -in pico-secs) I-hexane, II-Benzene, III-Carbondetrachloride IV-Paraffin.

TABLE I
Anisole

2.73 × 10 ⁻⁴ moles/cc in hexane				2.73 × 10 ⁻⁴ moles/cc in benzene				2.73 × 10 ⁻⁴ moles/cc in CCl ₄				3.64 × 10 ⁻⁴ moles/cc in paraffin			
Temp. °K	tan δ × 10	τ* × 10 ¹² sec.	ξ(T)**	Temp. °K	tan δ × 10	τ* × 10 ¹² sec.	ξ(T)**	Temp. °K	tan δ × 10	τ* × 10 ¹² sec.	ξ(T)**	Temp. °K	tan δ × 10	τ* × 10 ¹² sec.	ξ(T)**
276	0.999	5.12	0.404	275	.0761	8.58	0.307	275	.0705	9.40	0.284	297	.0647	14.09	0.211
286	0.977	4.77	0.410	285	.0782	7.71	0.327	285	.0747	8.13	0.311	307	.0688	12.55	0.232
296	0.955	4.10	0.414	295	.0803	6.86	0.347	295	.0767	7.28	0.332	317	.0730	11.18	0.254
306	0.910	3.46	0.408	305	.0823	5.96	0.368	305	.0788	6.40	0.360	329	.0771	9.85	0.279
316	0.868	3.18	0.400	311	.0864	4.10	0.380	311	.0809	5.25	0.378	337	.0792	9.16	0.294
326	0.822	2.94	0.393	319	.0823	3.30	0.385	319	.0830	4.10	0.388	347	.0813	8.41	0.311
336	0.777	2.74	0.383	329	.0782	3.04	0.377	329	.0788	3.35	0.380	355	.0834	7.74	0.325
				339	.0741	2.82	0.368	339	.0747	3.19	0.371				

*Calculated with $\mu = 1.13D$ *Calculated with $\mu = 1.10D$ *Calculated with $\mu = 1.09D$ *Calculated with $\mu = 1.10D$ from the graph $T \tan \delta/c$ vs $1/T$.**Calculated with $\mu = 1.25D$

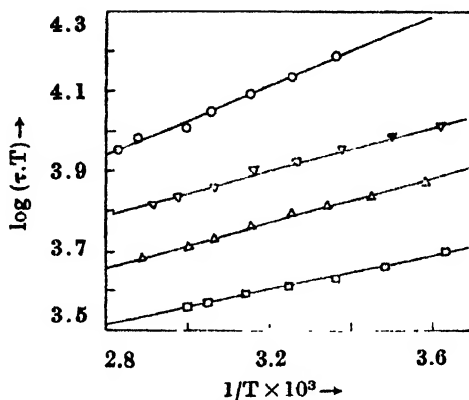


Fig. 2. Plots of $\log(\tau.T)$ vs $1/T$ for solutions of *p*-chloro-anisole in different solvents. (τ -in pico-secs). I-*n*-hexane, II-Benzene, III-Carbon tetrachloride, IV-Paraffin.

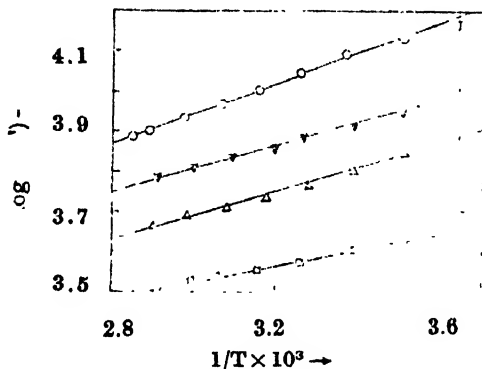


Fig. 3. Plots of $\log(\tau.T)$ vs $1/T$ for solutions of *o*-chloro-anisole in different solvents. (τ -in pico-secs). I-*n*-hexane, II-Benzene, III-Carbontetrachloride, IV-Paraffin.

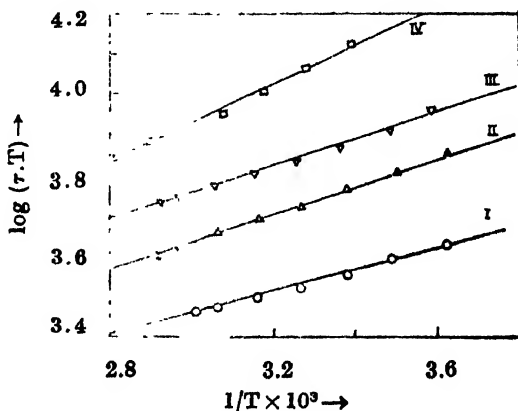


Fig. 4. Plots of $\log(\tau.T)$ vs $1/T$ for solutions of *o*-bromoanisole in different solvents. (τ -in pico-secs). I-*n*-hexane, II-Benzene, III-Carbontetrachloride, IV-Paraffin.

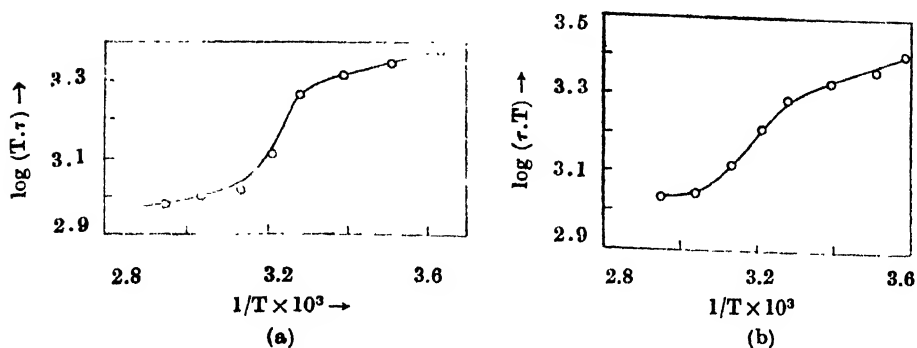


Fig. 5. Plots of $\log(\tau T)$ vs $1/T$ for solutions of anisole in different solvents. (τ in pico-secs).
(a) Benzene, (b) Carbondotetrachloride

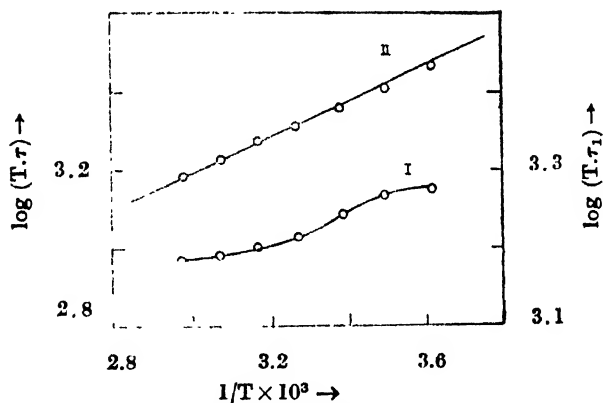


Fig. 5c. Curve I plot of $\log(\tau T)$ vs $1/T$ for solution of anisole in hexane
Curve II. „ $\log(\tau_1 T)$ vs $1/T$ „ „ „ (τ and τ_1 in pico-secs)

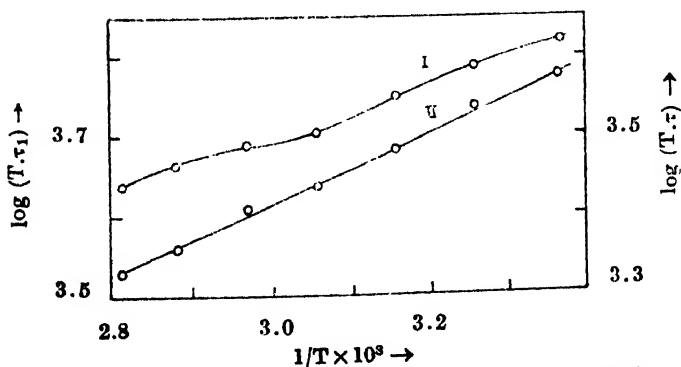
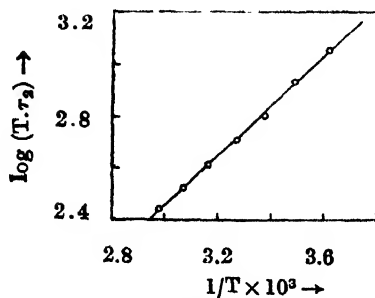


Fig. 5d Curve I. plot of $\log(\tau_1 T)$ vs $1/T$ for solution of anisole in paraffin
Curve II. „ $\log(\tau T)$ vs $1/T$ „ „ (τ and τ_1 in pico-secs)

Fig. 5a. Plot of $\log(\tau_2 T)$ vs $1/T$ (τ_2 in pico-secs)

maximum value and finally gradually decrease. The rate of increase of $\xi(T)$ in benzene and CCl_4 solutions is higher than in hexane solution, the rate of decrease being almost the same, in all solutions. In the case of paraffin solution $\xi(T)$ increases monotonously with increase of temperature. All these are shown in fig. 6.

From equation (6) we have

$$\frac{d\xi}{dT} = c_1 \frac{\partial f(x_1)}{\partial T} + C_2 \frac{\partial f(x_2)}{\partial T} \quad \dots (7)$$

With $x_1 = \frac{A_1}{T} \exp\left(-\frac{V_1}{RT}\right)$ and $x_2 = \frac{A_2}{T} \exp\left(-\frac{V_2}{RT}\right)$ (A_1 , A_2 are constants, V_1 and V_2 the activation energies per mole for dielectric relaxation of the whole molecule and the methoxy group respectively), eqn. (7) becomes

$$-\frac{d\xi}{dT} = \frac{C_1}{T} \left(1 + \frac{V_1}{TR}\right) \frac{x_1(x_1^2 - 1)}{(x_1^2 + 1)^2} - \frac{C_2}{T} \left(1 + \frac{V_2}{TR}\right) \frac{x_2(1 - x_2^2)}{(1 + x_2^2)^2} \quad \dots (7a)$$

At the temperature where $\xi(T)$ is maximum $\frac{d\xi}{dT} = 0$ if the condition $x_1 = 1$ and $x_2 = 1$ holds simultaneously.

In that case $\xi(T)_{max} = \frac{1}{2}(C_1 + C_2) = 0.5$

Actually the maximum value of $\xi(T)$ in the case of these solutions (fig. 6) are all less than 0.5 which indicates the presence of more than one relaxation time.

b) Limits for τ_1 and τ_2 .

Since the condition $x_1 = x_2 = 1$ is not satisfied at the temperature when $\xi(T)$ is maximum it is seen from eqn. (7a) that $\frac{d\xi}{dT}$ at this temperature may be

zero for suitable values of $x_1 > 1$ and $x_2 < 1$ or vice versa. We have assumed the relaxation time for the whole molecule to be greater than τ_2 the relaxa-

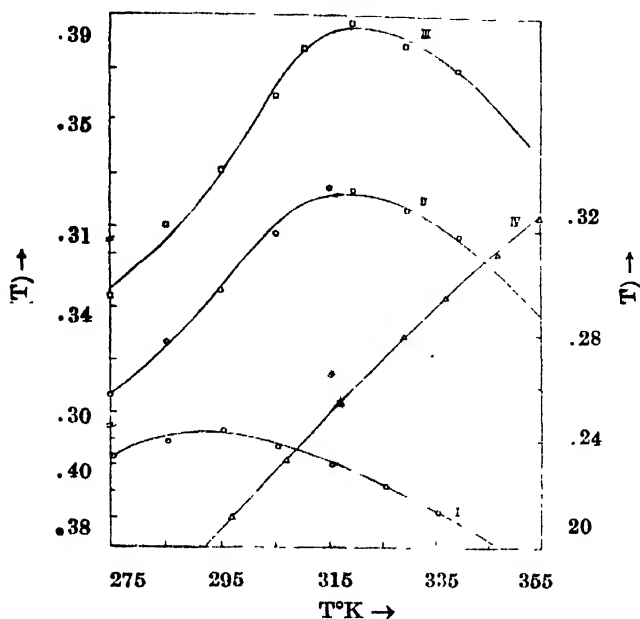


Fig. 6. Plots of $\xi(T)$ vs T for solutions of anisole in different solvents.

I-*n*-hexane, II-Benzene, III-Carbontetrachloride (left-hand side ordinate values)

IV-Paraffin (Righthand side ordinate values)

For curves I, II and III the appropriate ranges for $\xi(T)$ are shown by the broken intervals.

tion time for methoxy group and since $x_1 = \omega\tau_1$ and $x_2 = \omega\tau_2$, $x_1 > x_2$. With $\omega = 2.44 \times 10^{11}$ rad/sec $x_1 > x_2$ means $\tau_1 > 4.1 \times 10^{-12}$ sec and $\tau_2 < 4.1 \times 10^{-12}$ sec.

c) Determination of the values of τ_1 and τ_2 .

For the determination of the values of τ_1 and τ_2 the analysis of the experimental data of the solutions of anisole has been made on the following considerations :

i) In the same solvent and at the same temperature the value of τ_1 of anisole is very nearly the same as that of a rigid molecule of similar size.

ii) The value of τ_2 (of the methoxy group) is less than 4×10^{-12} sec. for temperatures 296°K and above and becomes equal to 4×10^{-12} sec. at temperatures in between 275°K and 296°K.

Using the value of $\xi(T)$ for hexane solution from table I along with eqn. (6) the following relations are obtained :

$$\xi(276) = C_1 f(x_1) + C_2 f(x_2) = 0.404 \quad (8)$$

$$\xi(296) = C_1 f(x_1) + C_2 f(x_2) = 0.414$$

with

$$C_1 + C_2 = 1$$

For bromobenzene, a molecule having the same size as anisole the values of the relaxation time in hexane solution at temperatures 276°K and 296°K are respectively about 9×10^{-12} and 7×10^{-12} secs. (Sinha *et al*, 1966). The corresponding values of $f(x_1)$ are about 0.37 and 0.42. Assuming that these values also hold for anisole and that the value of τ_2 at 276°K is $\sim 4 \times 10^{-12}$ sec i.e. $f(x_2) \approx 0.5$ the insertion of these values in the first expression of equation (8) gives $.37C_1 + .5C_2 = .403$ whence $C_1 \sim 0.7$ and $C_2 \sim 0.3$. Using these values of C_1 and C_2 in the second relation of equation (8) the value of $f(x_2)$ at 296°K comes out to be 0.4 approximately i.e. $\tau_2 \sim 2 \times 10^{-12}$ sec. In this way the values of τ_1 and τ_2 at all temperatures have been determined approximately. Afterwards, the values of C_1 , C_2 , τ_1 and τ_2 have been slightly adjusted so that the calculated $\xi(T)$ values are in satisfactory agreement with the experimental values of $\xi(T)$ at the corresponding temperatures and the plots of $\log(\tau_1 T)$ vs $1/T$ and $\log(\tau_2 T)$ vs $1/T$ yield good straight line graphs. The τ_1 - and τ_2 -values are given in table II and the graphs are shown in figs 5(c) and 5(e). The hindering potential energies V_1 and V_2 calculated from the graphs in the usual way are given at the foot of the Table. Once the values of τ_2 at different temperatures have been determined, the calculation of τ_1 -values in paraffin solution become much simplified. The final values of τ_1 calculated with $C_1 = 0.9$ and $C_2 = 0.1$ are given in table III and the graph of $\log(\tau_1 T)$ vs $1/T$ is shown in fig. 5(d). The value of the potential barrier V_1 obtained from the graph is given along with the Table.

Solution	C_2	$t\%$
Hexane	0.3	38.7
Paraffin	0.1	12.9

In tables II and III the values of the time of relaxation of bromobenzene at different temperatures in hexane and paraffin solutions respectively have been included for comparison. It is seen that in each case the τ_1 -values of anisole are comparable with those of bromobenzene, a molecule having the same size as that of anisole.

Now an estimate of the percentage of molecules capable of relaxation by the processes of rotation of the molecule as a whole of the methoxy group is made by using the relation $C_2 = t(\mu_2/\mu)^2$. Putting $\mu = 1.25\text{D}$ and $\mu_2 = 1.10\text{D}$ (Hase, 1953; Fisher, 1954) the following values of t are obtained :

The small value of $C_2 = 0.1$ in paraffin solution indicates that in this case most of the anisole molecules relax by the process of the rigid rotation of the whole molecule and consequently, the plot of $\log(\tau_1 T)$ vs $1/T$ (obtained by using the τ -values calculated under the assumption of a single relaxation time) shows only small departure from linearity fig 5b.

TABLE II
Anisole in hexane
 $C_1 = 0.7$ $C_2 = 0.3$

Temperature	$\tau_2 \times 10^{12}$ sec	$\tau_1 \times 10^{12}$ sec	$\tau \times 10^{12}$ sec Bromobenzene
276	4.06	9.80	8.50
286	2.99	8.94	7.60
296	2.16	8.04	6.96
306	1.68	7.42	6.25
316	1.31	6.85	5.45
326	1.03	6.27	
336	0.82	5.82	

$V_2 = 4.33\text{K.Cal/Mole}$, $V_1 = 1.00\text{K.Cal/Mole}$

TABLE III
Anisole in Paraffin
 $C_1 = 0.9$ $C_2 = 0.1$

Temperature	$\tau_1 \times 10^{12}$ sec	$\tau \times 10^{12}$ sec Bromobenzene
297	20.1	19.96
307	17.8	17.14
317	15.2	15.09
329	13.3	13.33
337	12.1	11.79
347	10.5	10.67
355	9.6	

$V_1 = 2.2\text{K.Cal/Mole}$

In the case of hexane solution $C_2 = 0.3$ and the plot of $\log(\tau T)$ vs $1/T$ (fig. 5c) shows greater deviation from linearity. Such deviations are still more pronounced in the case of solutions in benzene and in CCl_4 and may therefore indicate greater values of C_2 in the two cases.

Analysis of the data (in terms of the τ_2 -values so determined) in the case of solutions in benzene and CCl_4 has not been very successful. However, it may be noted that the maximum value of $f(x_2) = 0.5$ in the case of benzene and CCl_4 solutions should occur at temperatures well beyond the temperatures at which $\xi(T)$ is maximum in the respective cases i.e. between 275°K and 305°K . If we assume that in the case of solution in benzene $f(x_2)$ is max. at about 295°K , the value of τ_2 at this temperature will be $4 \times 10^{-12}\text{sec.}$ which agrees well with the values of $4.4 \times 10^{-12}\text{sec.}$ in benzene solution at 25°C (Fisher, 1954) and $4.6 \times 10^{-12}\text{sec.}$ reported by Hase (1953) at 25°C in other solvents. Further experiments are being

conducted to obtain complete information about τ_2 , the relaxation time of the methoxy group in anisole in different environments.

d) *Substituted anisoles*

It can be seen from figs. 1-4 that the graphs of $\log(\tau.T)$ vs $1/T$ in the case of the solutions of *o*-chloro-, *o*-bromo-, *o*-nitro- and *p*-chloroanisoles in all the solvents are all straight lines similar to those observed in the case of molecules with rigid dipoles and having a single relaxation time (Sinha *et al.*, 1966). It, therefore, suggests that the molecules of these substituted anisoles relax predominantly by the process of rotation of the molecule as a whole. Considerations of the expected values of C_2 for these compounds also lend support to this idea. For, if the value of t for the different compounds in less viscous solvents is taken to be 40% then from the relation $C_2 = t \cdot (\mu_2/\mu)^2$ it is seen that as the value of μ of the substituted anisoles varies from 2.5D for the halo substituted anisoles to 4.8D for ortho nitroanisole, the values of C_2 come out to be about 0.1 for the former compounds and .025 in the latter compound. It may, therefore, be concluded that, the contributions to the dielectric loss in these cases are mainly due to the rotation of the molecule as a whole.

It may be noted here that in the case of solution of *p*-chloroanisole in Nujol Grubb and Smyth (1961) reported very high values of τ_1 for the rotation of the molecule as a whole. The τ_1 -values are very large compared with those for molecules of similar sizes and may have resulted from an attempt to interpret the observed results in terms of two relaxation times.

REFERENCES

- Bhattacharyya, J., Sinha, B., Roy, S. B. and Kastha, G. S., 1964, *Indian J. Phys.*, **38**, 413.
 Budo, A., 1938, *Phys. Zeit.*, **39**, 706.
 Fisher, E., 1954, *Z. Naturf.*, **9a**, 909.
 Forest, E. and Smyth, C. P., 1964, *J. Am. Chem. Soc.*, **86**, 3475.
 Grubb, E. L. and Smyth, C. P., 1961, *J. Am. Chem. Soc.*, **83**, 4873.
 Hase, H., 1953, *Z. Naturf.*, **8a**, 695.
 Klages, G., 1954, *Z. Naturf.*, **9a**, 336.
 Klages, G. and Zentek, A., 1961, *Z. Naturf.*, **16a**, 1016.
 Sinha, B., Roy, S. B. and Kastha, G. S., 1965, *Indian J. Phys.*, **39**, 328.
 ————, 1966, *Indian J. Phys.*, **40**, 101.

INELASTIC INTERACTIONS OF GAMMA RAYS WITH K-SHELL ELECTRONS

B. S. GHUMMAN AND B. S. SOOD

PHYSICS DEPARTMENT, PUNJABI UNIVERSITY, PATIALA-4, INDIA

(Received June 14, 1967; Re-submitted August 3, 1967)

ABSTRACT. The technique of the absolute intensity measurement of *K*-shell fluorescent radiation by a NaI(Tl) crystal has been employed to measure the cross-sections of the inelastic interactions of 280, 662 and 1250 keV gamma rays with *K*-shell electrons in lead and gold. The *X*-rays efficiency of the detector has been measured experimentally by comparing the ratio of gamma rays and *X*-rays following internal conversion from Au^{198} and Hg^{203} sources. For 280 keV gamma rays the measured cross-sections agree with the known photo-electric cross-sections showing that the *X*-rays are produced essentially through the photo-electric interaction. For 662 and 1250 keV the measured cross-sections are somewhat higher than those of photo-electric interaction indicating the contribution of the Compton scattering from *K*-shell electrons, the integrated cross-section of which is estimated to be equal to that from free and stationary electrons.

INTRODUCTION

The inelastic interactions of gamma rays with *K*-shell electrons of the target atoms result in *K*-vacancies which emit fluorescent *X*-rays or eject Auger electrons. The processes of interactions are, (i) Photoelectric effect and (ii) Compton scattering from bound electrons. The number of *K*-vacancies created, which is equal to the *K*-shell *X*-rays emitted divided by the *K*-shell fluorescence yield, is a measure of the cross-sections of these interactions. The measurement of the number of *X*-rays emitted when a target is irradiated with a known flux of gamma rays thus provides a method to obtain information about the cross-sections of these processes.

The experiments performed to determine the cross-sections of inelastic interactions of 280, 662 and 1250 keV gamma rays with *K*-shell electrons in Pb and Au by measuring the absolute yield of the *K*-shell fluorescent *X*-rays are described and an effort has been made to interpret the results in terms of the cross-sections of the above mentioned processes.

EXPERIMENTAL ARRANGEMENT AND PROCEDURE

The experimental set-up used is shown in fig. 1. Gamma rays of energies 280, 662 and 1250 keV were obtained from radioactive sources of Hg^{203} , Cs^{137} and Co^{60} respectively. The targets of the gold and lead in the form of circular foils (2.5 cm dia) were used. The thickness of the target could be varied by changing

the number of foils. With one element measurements were made by using targets of thicknesses t , $2t$, $4t$ etc. The fluorescent X -rays emitted from the target were counted with a single channel spectrometer with a $2.5\text{ cm dia} \times 2.5\text{ cm height}$ NaI(Tl) crystal. Direct radiation from the source was prevented from

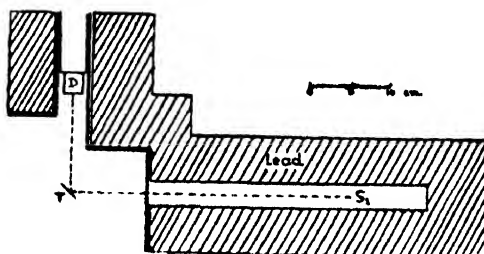


Figure 1. Experimental arrangement.

reaching the counter by graded shielding consisting of lead, tin, copper and aluminium. Source and detector were also shielded by graded absorbers to prevent scattering from walls and surroundings to the detector. The graded shielding had to be used for preferential absorption of fluorescent X -rays produced in the lead shielding. The energy spectrum of radiation emitted from the lead target in the fluorescent X -rays region is shown in fig. 2. It contains a prominent K -

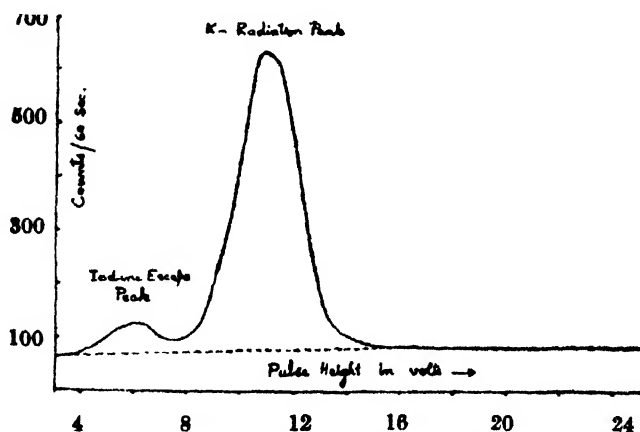


Figure 2. Spectrum of K -radiation when lead is irradiated with 280 keV gamma rays. Dotted curve is the spectrum taken with an equivalent aluminium.

shell X -rays peak. The spectrum taken with an equivalent aluminium target is also shown. The spectrum without any target in position showed a general background lower than that with Al target indicating that only those fluorescent X -rays which are emitted from the target and are of interest in the present investigations are recorded in the counter.

The measurement of the cross-section for the creation of K -vacancies consisted of determining the number of K -shell fluorescent X -rays emitted from the

target, the source strength, the number of atoms per cc. of the target, the scatterer-detector and source-scatterer solid angles. The number of X -rays emitted from the target was calculated by measuring the area under the photo-peak of the X -rays spectrum and taking into account (i) the effective detection efficiency of the X -rays under the photo-peak in the experimental set-up used and (ii) the absorption of the incident gamma rays and the emitted X -rays in the target. Both these factors were determined experimentally as discussed later. The effective efficiency accounts for (i) the absorption of X -rays in the air between the target and the detector (ii) the absorption of X -rays in the crystal package, (iii) the iodine escape peak in crystal (Crouthamel, 1960) and (iv) photo-peak efficiency, corresponding to the fraction of X -rays which lose their full energy in the crystal. The source strength was determined in terms of the area under the photo-peak of the gamma rays under investigation, the absolute strength being not needed. The source-target solid angle was calculated from the known geometry, while the scatterer-detector solid angle was determined experimentally by replacing the scatterer with a weak source of the energy under investigation and comparing this weak source with the actual source used in the main experiment. Assuming isotropic distribution of X -rays, the cross-section for the creation of K -vacancies is given by

$$\sigma = \frac{N_1}{N_2} \cdot \frac{S_2}{S_1} \cdot \frac{\epsilon_\gamma}{\epsilon_K \omega_K} \cdot \frac{4\pi}{\omega_1 \rho t \beta} \quad \dots (1)$$

where N_1/N_2 is the ratio of the counting rates due to the K -shell X -rays and the small source placed at the position of the target, S_2/S_1 is the ratio of the strengths of the weak and actual source, ϵ_γ is the photo-peak efficiency of the detector for gamma rays, ϵ_K is the effective detection efficiency of X -rays as defined above, ω_1 is the source-scatterer solid angle, ρ is the number of atoms per cc. of the target, t is the thickness of the target, β is the correction that accounts for the absorption of the incident gamma rays and emitted X -rays and ω_K is the K -shell fluorescence yield. S_2/S_1 was measured with an accuracy of 2 per cent by comparing the counts in the gamma ray photo-peaks of the two sources. Two sources of intermediate strength were used to avoid corrections due to source-detector geometry. The value of ϵ_γ , the gamma ray photo-peak efficiency, was taken from the tables of Crouthamel (1960) and graphs of Leutz *et al* (1965). The sequence of taking observations was arranged so as to minimize the effects of drifts in electronics and source decays.

DETERMINATION OF EFFECTIVE EFFICIENCY OF THE DETECTOR

Au^{198} decays by β emission to 412 keV level in Hg^{198} which de-excites by gamma ray emission or electron conversion. The K -shell conversion results in

K-vacancies in Hg and emit X-rays or Auger electrons. The *K*-conversion coefficient is defined as

$$\alpha_K = \frac{N_K \epsilon_\gamma}{N_\gamma \epsilon_K} \frac{1}{\omega_K}$$

where N_γ and N_K are the counting rates due to gamma rays and *K*-shell X-rays respectively and the other terms have been defined earlier. Knowing the value of $\alpha_K = 0.0302 \pm 0.0004$ (Suba Rao, 1966), $\epsilon_\gamma = 0.231$ (Crouthamel, 1960; Leutz *et al*, 1966) and measuring N_K and N_γ from the spectrum obtained by placing an Au^{198} source at the position of the target, the value of $\epsilon_K \omega_K$ was calculated to be 0.85 ± 0.04 for the 70.8 keV Hg X-rays in the present experimental arrangement. The analysis of the Au^{198} spectrum to determine N_γ and N_K is shown in fig. 3.

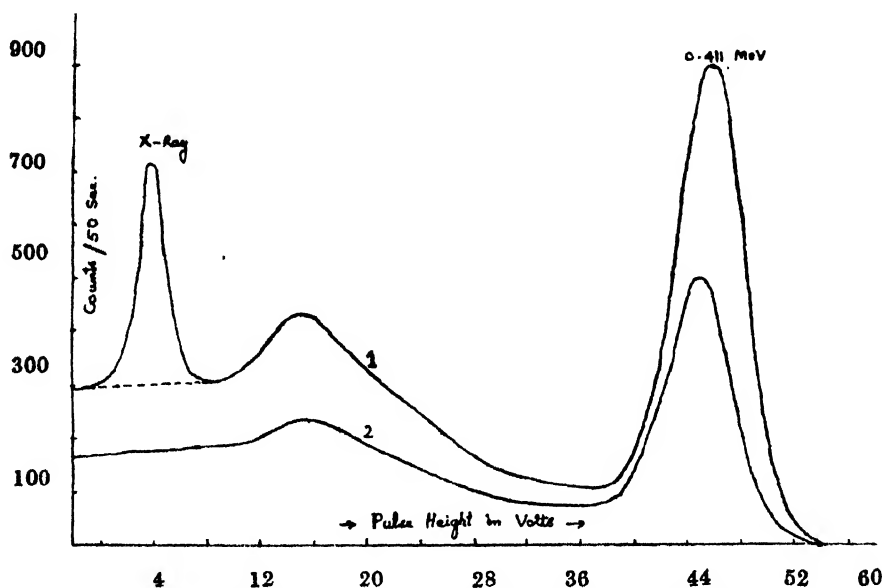


Figure 3. Pulse height distribution of Au^{198} spectrum. Curve 1 direct spectrum and curve 2 with graded absorber to absorb X-rays.

Similar measurements were also made for Tl X-rays using a Hg^{203} source which decays to 280 keV level in Tl and a value of 0.82 ± 0.04 was found for $\epsilon_K \omega_K$. The value of $\epsilon_K \omega_K$ was also determined by measuring the coincidence rate between β rays feeding 412 keV level and X-rays following internal conversion in Hg^{198} . The ratio of the β -X coincidence rate and β count rate is given by

$$N_{\beta X}/N_\beta = \omega_K \epsilon_K \omega_\beta \quad (2)$$

The target was replaced by the small Au^{198} source in the main experimental arrangement and a plastic scintillator was used for counting β rays. The β -ray counter was biased at 500 keV so that the internal conversion electrons are not

counted. Coincidence count rate was again measured by placing a graded X -rays absorber before the NaI(Tl) crystal. This counting rate corresponds to 412 keV gamma rays which are counted in X -rays channel. Subtraction of this normalized counting rate from the first gave the true counting rate. Solid angle ω_2 was measured from the geometry of experimental set-up. The value of $\epsilon_K \omega_K$ as determined above came out to be $82 \pm .06$.

The value of ϵ_K for gold and lead X -rays is expected to be the same as that for Hg and Tl and ω_K also does not vary more than 0.05 per cent in the Z range for 79 to 82. Therefore a mean value of 0.83 ± 0.04 is used in eq. (1) for $\epsilon_K \omega_K$.

ABSORPTION OF INCIDENT GAMMA RAYS AND EMITTED X-RAYS IN THE TARGET

It can be shown (Shute *et al*, 1960) that the effective thickness of a target of real thickness t when the absorption of the incident gamma rays and emitted X -rays is taken into account is given by

$$t_{eff} = \frac{1 - \exp [-(\mu_K + \mu_\gamma)t / \cos \theta]}{\mu_K + \mu_\gamma} \quad \dots (3)$$

where θ is the angle that the incident gamma rays and emitted X -rays make with the target and μ_γ and μ_K are the linear absorption coefficients for gamma rays and X -rays. The value of $\mu_\gamma + \mu_K$ was determined experimentally by measuring the ratio of the counting rates under the photo-peak with target of thickness t and $2t$ respectively. The ratio is given by

$$R = 1 + \exp [-(\mu_K + \mu_\gamma)t / \cos \theta] \quad \dots (4)$$

The value of R was determined with an accuracy of 0.5 per cent and $\mu_\gamma + \mu_K$ was determined to be 2.85, 2.45 and 2.41 for 280, 662 and 1250 keV gamma rays respectively for lead and 2.88, 2.63 and 2.59 for gold.

RESULT AND DISCUSSIONS

About ten independent runs were made with each target at one gamma ray energy and the results are shown in column 3 of table 1. The errors given are due to the statistics of the counting rate and the uncertainties involved in the comparison of source strengths, the determination of $\epsilon_K \omega_K$ and estimation of other corrections. The calculated (Grodstein, 1957) K -shell photo-electric cross-sections are given in column 4. Column 5 gives the difference between the measured inelastic cross-sections and the calculated K -shell photo-electric cross-sections and should give the contributions of K -shell electron Compton scattering and the secondary processes, e.g. K -shell excitation or ionization of the target atoms by photo- and Compton electrons. Column 6 gives the calculated Compton scattering cross-section for two electrons if assumed free and at rest after the

formula given by Klein and Nishina. It is seen from the table that at 280 keV the measured cross-section agrees fairly well with the calculated *K*-shell photo-electric cross-section showing that for low energy gamma rays and high-*Z* elements the *K*-shell fluorescent *X*-rays are produced essentially through photo-electric interaction and this method can be used to measure the *K*-shell photo-electric cross-sections of low energy radiation in high-*Z* elements.

TABLE 1

K-shell interaction cross-sections of 280, 662 and 1250 keV gamma rays with gold and lead.

Gamma ray energy in MeV	Element	$\sigma(\text{exp.})$ in barns	$\sigma(\text{NBS})$ in barns	$\sigma(\text{exp.}) - \sigma(\text{NBS})$ in barns	σ_c in barns
0.280	Au	82.6 ± 5.5	83.4	—	0.73
	Pb	95.1 ± 6.0	95.5	—	0.73
0.662	Au	11.4 ± 0.9	10.6	0.8 ± 0.9	0.51
	Pb	13.4 ± 1.0	12.4	1.0 ± 1.0	0.51
1.25	Au	3.7 ± 0.5	2.9	0.8 ± 0.5	0.38
	Pb	4.2 ± 0.5	3.7	0.6 ± 0.5	0.38

The contribution of *K*-shell Compton scattering cross-section as given in column 5 increases with gamma ray energy and at 1.25 MeV it is about 20 per cent if the contributions of secondary processes being second order effects are neglected. The data available on Compton scattering of gamma rays from bound electrons (Motz *et al.*, 1961; Verma *et al.*, 1962) are quite scanty. Our earlier experiments (Anand *et al.*, 1964) on small angle scattering of low energy gamma rays have shown that for small values of momentum transfer involved in scattering, the Compton scattering cross-section from bound and moving electrons is less than that from free and stationary electrons. The experiments on large angle scattering (Motz *et al.*, 1961; Verma *et al.*, 1962) of high energy gamma rays, however, show that the situation is reversed at large values of momentum transfer and the Compton scattering from bound electrons becomes more intense than that from free electrons. No information is yet available about the integrated Compton cross-section from bound electrons where the momentum transfer may vary from zero to some maximum value depending upon the energy of the gamma rays. From the data so far available it may be guessed that the integrated Compton scattering cross-section from the bound electrons may be either less than, or equal to, or greater than that from free electrons depending upon the maximum value of the momentum transfer which in turn depends upon the energy of gamma rays. At 662 and 1250 keV the integrated Compton scattering

cross-section from K-shell electrons as shown in column 5 of table 1, may be taken to be equal to that from free and stationary electrons. Large uncertainties present in these values do not allow us to draw any precise conclusion. However, at still higher energies where the photo-electric cross-sections become comparable with the Compton scattering cross-section from K-shell electrons it may be of interest to perform similar experiments to see if for still larger values of momentum transfer the overall Compton scattering cross-sections for bound electrons is more than that from free electrons.

REFERENCES

- Anand, S., Singh, M. and Sood, B. S., 1964, *Curr. Sci.*, **33**, 139.
Crouthamel, C. E., 1960, *Applied Gamma Ray Spectroscopy*, Pergamon Press, 108.
Grodstein, G. W., 1957, *X-ray Attenuation Coefficients from 10 KeV to 100 MeV*, NBS Circular, 583.
Leutz, H., Schulz, G. and Van Gelderen, L., 1966, *Nuc. Instr. Method*, **40**, 257.
Motz, J. W. and Missoni, G., 1961, *Phys. Rev.*, **124**, 1458.
Shute, G. G. and Sood, B. S., 1960, *Proc. Roy. Soc.*, **A257**, 52.
Suba Rao, B. N., 1966, *Nuc. Instr. Method*, **45**, 22.
Varma, J. and Eswaran, A., 1962, *Phys. Rev.*, **127**, 1197.

A CONVENIENT AND SENSITIVE BALANCE FOR MEASURING MAGNETIC ANISOTROPIES OF SINGLE CRYSTALS

D. NEOGY*, S. BANERJI, P. KUMAR AND A. MAHALANABIS

PHYSICAL LABORATORIES, UNIVERSITY OF BURDWAN, BURDWAN, WEST BENGAL, INDIA.

(Received April 10, 1967)

ABSTRACT. For measuring magnetic anisotropies of single crystals a new sensitive balance has been described. The instrument incorporates electrodynamic method of balancing the couple experienced by a crystal and is operated electrically from a distance. Elimination of manual handling of the balance ensures high reproducibility and operational convenience. It is well adapted for low temperature work. The performance of the balance is thoroughly tested and discussed.

INTRODUCTION

The past few decades have witnessed a sharp rise in interest in the magnetic properties of single crystals. Studies on the diamagnetic organic crystals by Krishnan and Banerji (1935, 1938), Banerji (1938) and recently by Mookherji *et al* (1959, 1961) show the close correlation between the magnetic anisotropy and the molecular and crystal structure. In understanding the nature of the ligand fields in the single crystals of the transition metal ions, the magnetic anisotropy and its variation with temperature play a very fundamental role. Extensive investigation on the crystals of the iron group elements undertaken by Bose and co-workers (1961, 1963) points to the sensitive field dependence of the magnetic anisotropy and its thermal variation. Also, in the case of the rare-earth ions where the electrons responsible for giving rise to paramagnetism, are partially shielded by closed shell of outer electrons, the studies of Neogy (1963), Neogy and Mookherji (1965) show the significance of anisotropy for correct determination of the crystal field parameters. Because of this pivotal importance of the magnetic anisotropy we are faced with the problem of collecting a large amount of data of fairly high standard on this physical property. To ensure a fast process for doing the same, it is very necessary, that a simple and very sensitive method be evolved to take the drudgery out of the existing methods for measuring anisotropy.

A quick survey of the present methods of measuring magnetic anisotropy shows that there are only three of them to be taken notice of. Out of these, the oscillation method has long been discarded as being rather crude. The only

* CSIR Pool Officer.

two widely used techniques are the well-known Krishnan and Banerji's spin method and later developed Stout and Griefel's (1950) null method. The details of these two methods are available in the original literature and it will suffice to point out here that both the procedures require manual handling of the delicate suspension system which is rather inconvenient and puts undue physical strain on the worker. Furthermore, the spin method involves determination of torsional constants of the quartz fibres which is not very easy to handle and at low temperature when the anisotropies of paramagnetic crystals increase manyfold their room temperature value, the sudden violent spinning often becomes a problem. In the Stout and Griefel method if torsional constant of the fibre is small, there may be appreciable error in fixing the zero position after the crystal is rotated through 45° or any other angle due to the small residual magnetic field. This error may, however, be avoided if the magnet is rotated through the fixed angle instead of the crystal and this incidentally does away with the necessity of using a hexagonal mirror. The accuracy of these methods can obviously be increased by the use of large well-calibrated torsion head as is often done, (Guha Thakurta *et al.*, 1966). A highly suitable yet very simple way to get around the difficulties, is the electrodynamic method of balancing the couple experienced by the crystal in the Stout and Griefel method. This eliminates all kinds of direct manual operation on the suspension system and also, since the restoring couple is not furnished by the application of torsion to the suspension fibre, it is no longer necessary to use delicate fibres for this purpose. The description of the balance is given in the next section. The linearity of values obtained for crystals of different masses and also for different $\sin 2\theta$ values, where θ 's are the angles of rotation of the magnet, is examined. Some crystals which are usually held as standard for magnetic field calibration work are also measured using $\text{CuSO}_4 \cdot 5\text{H}_2\text{O}$ as standard and the values are compared with those of previous workers.

DESCRIPTION OF THE BALANCE

A schematic diagram of the balance is shown in fig. 1. Essentially, it may be looked upon as a modified form of a suspended coil galvanometer. The balance coil (5) is wound upon a light rectangular aluminium frame attached to a thin glass rod (20) carrying a small plane mirror (19). The coil is suspended by means of a pyrex fibre (2) from a small torsion head (1) and is free to move in the radial field of the local magnet (6). The two leads of the coil are brought out by means of two phosphorbronze spirals (4) attached to the coil. The spirals are wound in opposite directions to nullify any rotational effect on the suspension system due to the thermal expansion of the spirals, owing to temperature fluctuations during the course of measurement. A sufficiently long glass rod (9) is rigidly attached to the lower end of the glass rod carrying the coil. A small glass hook (11) is fixed to the free end of the long glass rod. The crystal (13) to be studied is attached to

another very thin glass rod (12) with a hook at one end; the length of the rod is so adjusted that when it is suspended from the upper hook, the crystal comes just at the centre of the pole gap of the rotatable electromagnet (14). A heavy glass bead (10) is fixed to the rod (9) to increase the stability of the system against

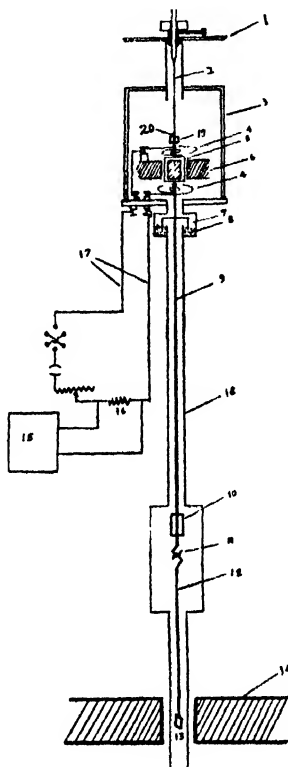


Fig 1

Figure (1)—(1) Torsion head. (2) Pyrex fibre. (3) Perspex case. (4) Phosphorbronze spirals. (5) Aluminium frame. (6) Permanent Magnet. (7) Oil-sealing glass cup. (8) Watch oil. (9) Glass rod. (10) Glass bead. (11) Glass hooks. (12) Very thin glass rod for crystal suspension. (13) Crystal. (14) Pole-pieces of rotatable electromagnet. (15) Potentiometer. (16) Standard resistance. (17) Coil leads. (18) Outer casing. (19) Plane Mirror. (20) Glass rod.

disturbances during the process of changing specimens to be measured. The light spot deflected by the mirror is detected by a differential phototube arrangement.

The balance may easily be adapted for low temperature work with the introduction of an oil-sealing mechanism '7' and '8' which hermetically separates the crystal chamber from the upper part of the balance and thus prevents the humidity from entering the balance box.

MEASUREMENT OF CURRENT

As the couple experienced by the crystal is proportional to the square of the magnetic field it is essential that the latter should be maintained strictly constant.

The change in the magnetic field due to small variation in the coil current is avoided by using an electronically regulated power supply capable of maintaining the current within 0.05% of the desired value up to 5 amperes. For fine adjustment of the current a screw motion rheostat is connected in series with the magnet. The constancy of the current is checked by means of the arrangement showing in fig. 2 wherein the voltage drop across a standard resistance (1) is balanced by the potentiometric arrangement shown. It is not necessary to measure the actual voltage drop across (1) : the constancy of this voltage drop is essential. The absence of any deflection in the galvanometer (3) ensures this constancy. The current in the potentiometer circuit is checked from time to time by means of the standard cell (2). This arrangement is sensitive enough to give a deflection of 10 cm, in the 'Multiflex' galvanometer for 1 mA change in the coil current.

OPERATION

The procedure adopted to align the direction of the maximum susceptibility of the crystal in the horizontal plane with the magnetic field direction, is similar to that of Stout and Griefel, the only difference lying in the fact that the magnet is rotated instead of the torsion head. The exciting coils of the electromagnet are energised and if the crystal is not at the zero position a deflection of the suspension system is observed. The magnet is rotated until there is no deflection on make and break of the current. This gives the 'zero position' of the balance and the corresponding position of the magnet is noted. From this position the magnet is rotated through any angle. This angle of rotation should be less than 45° and preferably greater than 30° . When the magnetic field is switched on the crystal will experience a couple and will try to align in the direction of the magnetic field. The crystal is restored to its original position by passing a current through the balancing coil. In order that the deflection from the 'zero-position' be less both the currents viz. the current through the electromagnet and that through the balancing coil should be increased or decreased simultaneously. Because the upper permanent magnet is placed high above the lower electromagnet and has no interaction with it, the torque acting on the coil is directly proportional to the current in it. This current is determined by measuring the potential drop across

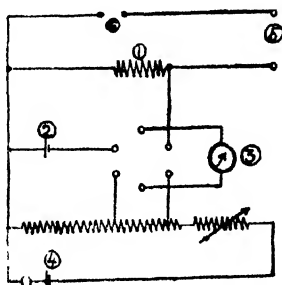


Figure 2—(1) Standard resistance. (2) Standard cell. (3) Multiflex Galvanometer. (4) Driving cell. (5) To current regulated power supply. (6) Magnet.

a standard resistance with the help of a precision potentiometer capable of measuring upto microvolt.

For calibrating the balance the current I_s required for balancing the couple due to a standard specimen is found out in the abovementioned way. For measuring anisotropy of any substance the standard sample is replaced by it and the coil brought to the original position by rotating the torsion head, if required. We have seen during measurement that if the hook-joint is made rigid by a drop of wax and opened by melting the wax in the joint with a hot brass rod carefully, the position of the coil is not at all altered on changing the crystal. Now, the current I_u required for balancing the couple for the unknown specimen is determined.

The couple experienced by the standard sample

$$\Gamma_s \propto I_s = \frac{A(\Delta\chi)_s m_s}{M_s} \sin 2\theta. \quad \dots (1)$$

and that by the test sample

$$\Gamma_u \propto I_u = \frac{A(\Delta\chi)_u m_u}{M_u} \sin 2\theta \quad \dots (2)$$

where A is the constant of proportionality and $\Delta\chi$, m , M correspond to magnetic anisotropy, mass and molecular weight of the crystal. θ denotes the angle through which the magnet has been rotated in both cases. The subscripts s and u stand respectively for the standard and test sample.

If the angle of rotation θ is the same for both the cases then

$$\Delta\chi_u = \Delta\chi_s \frac{I_u}{I_s} \cdot \frac{m_s}{m_u} \cdot \frac{M_u}{M_s} \quad \dots (3)$$

RESULTS

The performance of the balance was examined by measuring the current required to balance the couple acting on the crystal for different angular positions of the crystal with respect to the field direction. According to the relation (1) or (2) the ratio of sine 2θ and that of the couple should be constant. We measured the couples acting on the $\text{CuSO}_4 \cdot 5\text{H}_2\text{O}$ crystal by rotating the magnet through 30° , 35° , 40° and 44° from its zero position and the linearity is observed to be within 0.05% which demonstrates the excellent response of the balance. The graph in fig. 3 shows the linearity between $\sin 2\theta$'s and the corresponding balancing e.m.f.'s as the measure of the couples. It may be pointed out here that this check should be taken as the true test of the reproducibility of the balance itself since in these measurements only the couple acting on the crystal is changed by rotating the magnet keeping all other factors constant. However, the overall accuracy in

measurement of anisotropy depends on various factors, e.g., perfection of the crystal, the correct mode of suspension of the crystal and the homogeneity of the magnetic field over the region. The reproducibility and accuracy of our balance is also checked by measuring the balancing currents for crystals of different masses

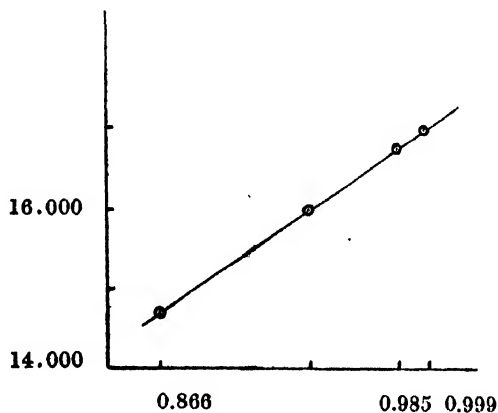


FIG. 3—The linearity in the variation of e.m.f. with values of $\sin 2\theta$.

Abscissae—Values of $\sin 2\theta$. Ordinate—e.m.f. in μV .

of the specimen in the same magnetic field. It is evident from the expression of the anisotropy that the variation of e.m.f. with mass should be linear. Using different crystals of $\text{CuSO}_4 \cdot 5\text{H}_2\text{O}$ we find that the linearity is within 0.2%. The higher error in this case is obviously more due to lack of perfection in the crystals and mode of suspension and inhomogeneity of the fields rather than the reproducibility of balance. A graph between different masses of $\text{CuSO}_4 \cdot 5\text{H}_2\text{O}$ crystal with the corresponding e.m.f.'s is shown in fig. 4.

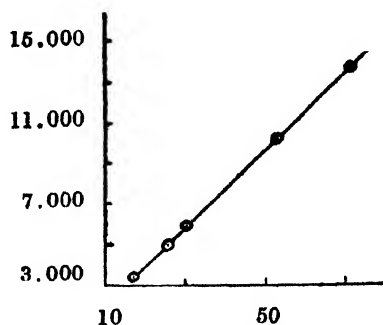


FIG. (4)—The linearity in the variation of e.m.f. with mass of the crystal.

Abscissae—Mass in mg. Ordinate—e.m.f. in μV .

The magnetic anisotropy of three different crystals belonging to the monoclinic system were measured with the balance. For this purpose the field was calibrated first with $\text{CuSO}_4 \cdot 5\text{H}_2\text{O}$ crystal (with c-axis vertical). Measurement

was done by suspending the sample with *b*-axis vertical. The results are given in table 1. The overall accuracy of these values was estimated as less than 0.5%.

As is obvious from the description and operation of the balance it is extremely simple in construction and easy to operate. The changing of samples is also effected very quickly. If the phototube null detecting system is made enough sensitive the same balance is capable of giving highly accurate values both for

TABLE 1

Crystal	$(\chi_1 - \chi_2) \times 10^6$		Temperature
	Present value	Previous workers' value	
$\text{CuK}_2(\text{SO}_4)_2$	327.7	322.3*	300°K
$\text{NiK}_2(\text{SO}_4)_2$	133.8	131.2*	
$\text{CoK}_2(\text{SO}_4)_2$	2530	2540**	

* Dutta (1954).

** Guha Thakurta *et al* (1966).

DISCUSSION

crystals of low and high anisotropy since it only involves measurement of e.m.f. which can be done pretty accurately by a good potentiometer with a sensitive galvanometer.

A few points of caution may, however, be mentioned at this point. During the course of measurement it was discovered that the error due to the anisotropy of the pyrex suspension rod which lies between the pole gap may cause appreciable error. Hence it is absolutely necessary to use as thin rod as possible and check each of them before use. Another factor which needs special attention for ensuring satisfactory working of the balance is the elimination of zero shift. Various factors are responsible for such shift in these sensitive instruments. If, however, particular care is bestowed on the neatness in constructing the balance this can be reduced to negligible proportions. The suspension fibre and phosphorbronze spirals should be scrupulously cleaned; the soldered joints should be as neat as possible and one should avoid any sharp bend in the bronze spirals: finally one should avoid any drastic temperature change during the course of the experiment as far as possible.

The distance between the coil and the electromagnet should be made large enough to avoid any appreciable stray field at the position of the coil compared to the field due to the local magnet. This is necessary since the angular position of the magnet has to be changed in course of measurement and this would entail a corresponding change in the effective field on the coil. The comparative strength

of the stray field could be detected by keeping a small current running through the coil and noting whether there is any change in the deflected position of the mirror by rotating the electromagnet.

The figures 3 and 4 display the fine performance of the balance. High linearity of c.m.f. with the mass and $\sin 2\theta$ shows the high reproducibility of the instrument. The UNICO electromagnet, probably the only Indian product in this category, was used in the measurement. It was found that the homogeneity of the field with a pole gap of 4 cm was restricted within 1.2 cm around the centre of the pole gap.

ACKNOWLEDGMENTS

We take great pleasure in thanking Prof. A. Mukherji for constant encouragement during the progress of the work. Thanks are also due to Dr. T. Mookherji and S. P. Chachra for helpful discussions.

REFERENCES

- Banerjee, S., 1938, *Z. Kristallogr.*, **A100**, 316.
 Bose, A., Chakraborty, A. S. and Chatterjee, R., 1961, *Proc. Roy. Soc.*, **A261**, 43, 207.
 Bose, A., Dutta Roy, S. K., Ghosh, P. K. and Mitra, S., 1963, *Indian J. Phys.*, **37**, 505.
 Dutta, S. K., 1954, *Indian J. Phys.*, **28**, 239.
 Guha Thakurta, D. and Mukhopadhyay, D., 1966, *Indian J. Phys.*, **40**, 69.
 Krishnan, K. S. and Banerjee, S., 1935, *Phil. Trans.*, **A245**, 265.
 —————, 1938, *Z. Kristallogr.*, **A99**, 499.
 Neogy, D. and Mookerji, A., 1965, *J. Phys. Soc. (Japan)*, **20**, 1332.
 —————, 1965, *Physica*, **31**, 1325.
 Neogy, D., 1963, *Physica*, **29**, 974.
 Mookerji, A., Mookherjee, S. N. and Neogy, D., 1961, *Bull. Chem. Soc. (Japan)*, **34**, 233.
 Mookerji, A., Mittal, R. L. and Neogy, D., 1959, *Bull. Nat. Inst. Sci. (India)*, **14**, 54.
 Stout, J. W. and Griefel, M., 1950, *J. Chem. Phys.*, **18**, 1449.

THE $(n, 2n)$ REACTION CROSS SECTION OF P^{31} , Zn^{64} , Ga^{69} AND Ag^{107} FOR 14.8 MeV NEUTRONS

B. MITRA

BOSE INSTITUTE, CALCUTTA, INDIA,

(Received May 10, 1967)

ABSTRACT. The $(n, 2n)$ cross sections of 14.8 MeV neutrons have been measured for four nuclei by activation analysis method, in a relative way. The results have been compared with calculated values from evaporation model of compound nucleus. Significant disagreement of values of nuclear temperature was obtained in some cases.

INTRODUCTION

The $(n, 2n)$ cross section of 14.8 MeV neutrons have been measured by activation analysis method, for nuclei P^{31} , Zn^{64} , Ga^{69} , Ag^{107} , relative to $(n, 2n)$ cross section of Cu^{63} .

There exists a number of cross section data for these nuclei. But there are large spread in the values presented in the literature for any of the reactions and therefore it was thought necessary to re-investigate them with a good degree of accuracy.

It is generally held that the $(n, 2n)$ represents the reaction whose cross section can be quantitatively predicted from the evaporation theory. It was thought worthwhile to study mostly the low- Z nuclei and compare the results with this theory.

All the above nuclei become positron-active after $(n, 2n)$ reaction. Hence activation analysis was done by using a gamma-scintillation spectrometer for the study of the annihilation radiation. In the case of P^{31} , a new variation of method other than straightforward gamma counting has been used and the details have been reported elsewhere (Mitra *et al.*, 1965).

EXPERIMENTAL PROCEDURE

Neutrons were obtained from the Bose Institute's Cockcroft-Walton generator where (t, d) neutrons were generated using a low deuteron energy equal to 120 KeV. Irradiations were done in the direct neutron beam, in the forward direction. Activation analysis were performed as detailed below.

Method of Irradiation :

The irradiation procedure has been described in a previous paper on (n, p) cross sections (Mitra *et al.*, 1966). Except in the case of phosphorus, samples in

the form of either powder or foil, were irradiated, being contained in graphite holders, where the holders were pots of diameter 2.5 cms and had a rim-height of 2 mm. These were of nearly uniform weight of about 1 gm each. Sample distance from tritium target was 5.5 cms. Neutron flux during irradiation was kept constant with a variation limit of $\pm 5\%$. This was checked by employing a monitor composed of a heavily biased plastic scintillation counter. Irradiation in every case was for a time period sufficiently long to ensure saturation of product.

Counting the irradiation products

The irradiated samples, all positron-active, were counted for annihilation gamma rays. This was performed by standard scintillation detectors. When a single counter was used (in case of phosphorus) a 5.1 cm, 1.9 cm NaI(Tl) phosphor was used and in case of other samples, counting was done by two counters, where the samples were sandwiched in between these two, and in these cases two 2.5×2.5 cm NaI(Tl) Harshaw crystals were used. In the single spectrometer Dumont 6292 phototube was used and when two spectrometers were used, RCA 6199 phototubes were used. Conventional electronics composed of linear amplifiers and single-channel pulse-height analysers were used.

To convert all the positrons to annihilation quanta, two 0.75 cm thick aluminium discs were used to sandwich the thin sample-pot. It was a calculated thickness to convert all the different energy β^+ that were expected from the daughters. The counters were individually calibrated by a known Na^{22} small positron source. For the cases other than phosphorus, the pulse height analysers were differentially adjusted to receive only the half width of the annihilation peaks individually. A different method was used in the case of P^{31} study, where nearly the same life-time contributions from 1.78 MeV γ -photons from Al^{26} obtained by (n, α) reaction in P^{31} , makes the measurement of annihilation quanta only from P^{30} difficult. The details of this method have been published elsewhere (Mitra *et al*, 1965).

The Standard Cross Section

The measurements reported are relative ones. The standard cross section taken was the $(n, 2n)$ cross section of Cu^{63} at 14.8 MeV. In all the cases of nuclei reported here, this appeared to be a good standard since Cu^{62} is a pure positron emitter and the absolute cross section is fairly accurately known. From a curve represented by Glover and Weigold (1962) depicting a variation of this cross section with energy, where data of Fergusson and Thompson (1960) were considered, the relevant cross section at 14.8 ± 0.1 MeV was found to be given by 530 ± 25 mb absolute. Excitation function measurement of this reaction made later by Csikai (1966) also yielded a value 541 mb, which is covered by the spread in the used cross section.

The Errors

All the errors associated with such activation measurements have been analysed in the previous paper (Mitra *et al*, 1966). An important one was caused due to different geometrical dispositions towards the target of the sample and the standard foil. This error was resolved by determining a correction factor by measuring the apparent value of the $(n, 2n)$ cross section in Cu^{63} by using copper powder as sample and copper foils as usual monitor. Standard foils were placed on the top of the samples. The usual procedure of sandwiching the sample between two monitor foils and reading the two foils by holding them together has been dispensed with.

RESULTS

The $(n, 2n)$ reaction cross sections have been determined for the four nuclei P^{31} , Zn^{64} , Ga^{69} and Ag^{107} relative to $\text{Cu}^{63}(n, 2n) = 530 \pm 25$ mb. The details, viz. neutron energy, chemical form, value of cross section obtained and comparable values obtained by other workers are presented in the following table.

TABLE 1

Nucleus	Chemical form	En in MeV	$\sigma(n, 2n)$ in mb	Author (Reference)
P^{31}	Red phosphorus and $\text{Ca}_3(\text{PO}_4)_2$	14.74	8.7 ± 2.7	Fergusson <i>et al</i> , 1960
		14.4 ± 0.3	10.9 ± 0.85	Rayburn, 1961
		14.13 ± 0.1	5.1 ± 0.45	Cevolani <i>et al</i> , 1962
		14.8 ± 0.1	8.5 ± 1.2	Grimeland <i>et al</i> , 1964
		14.8 ± 0.1	16.0 ± 1.6	Present investigation
Zn^{64}	Metal	14.4	167 ± 1.6	Rayburn, 1961
		14.1	105 ± 7	Cevolani <i>et al</i> , 1962
		14.6 ± 0.1	201 ± 13	Csikai, 1966
		14.8 ± 0.1	102 ± 10	Present investigation
Ga^{69}	Ga_2O_3	14.4	923 ± 7.6	Rayburn, 1961
		14.1	735 ± 44	Cevolani <i>et al</i> , 1962
		14.8	983 ± 150	Present investigation
Ag^{107}	Metal foil	14.14 ± 0.18	458 $\pm 11\%$	Yasumi, 1957
		14.1	734 ± 44	Cevolani <i>et al</i> , 1962
		14.4	889 ± 7.4	Rayburn, 1961
		14.8 ± 0.1	601 ± 90	Present investigation

DISCUSSION AND COMPARISON WITH THEORY

The $(n, 2n)$ cross section was always thought to be well predicted from statistical theory and hence this particular reaction has been considered to be

represented as evaporative process "par excellence". From evaporation consideration, the cross section has been given by Blatt *et al.*, (1955) :

$$\sigma(n, 2n) = \sigma(n, n) \left[1 - \left(1 + \frac{E_c}{\theta} \right) \exp \left(-\frac{E_c}{\theta} \right) \right] \quad \dots (1)$$

where $\sigma(n, n)$ is the cross section for the emission of a neutron, the factor in the square bracket is the probability that a second neutron is emitted after the first. $E_c = (E_n - E_{binding})$, i.e. it is the excess energy available for the emission of the second neutron. θ is the nuclear temperature of the first residual nucleus. To the first approximation $\sigma(n, n)$ may be equated to $\sigma_c(n)$, which is the compound nucleus formation cross section. From very approximate consideration, nuclear temperature is given by Blatt *et al.*, 1955 :

$$\theta = \left(\frac{E_n}{a} \right)^{1/2} \quad (2)$$

where $E_n = 14.8$ MeV and a may be computed from the relation $a = 0.115A$, based on Fermi gas model (Ericson, 1960). We have approximated $\sigma(n, n)$ by $[\sigma_{non\ el.} - \sum_i \sigma_i]$, where i represents all measured cross sections, viz., $\sigma(n, \alpha)$, $\sigma(n, p)$ etc., except $\sigma(n, 2n)$. Measured data of $\sigma_{non\ el.}$ i.e. non-elastic cross section for 14.8 MeV neutrons, exist for many nuclei (McGregor *et al.*, 1957). We have taken these measured values and for those nuclei where there are no measured values, these were computed from $A^{1/3}$ -dependence curve given from optical model calculations (McGregor *et al.*, 1957; Perey *et al.*, 1962).

For partial cross sections like $\sigma(n, p)$, $\sigma(n, \alpha)$ etc. we have selected values from reported experimental data. The table 2 shows the results of comparison of our data with statistical theory. In the table, the second column represents the threshold energy for $(n, 2n)$ reactions which have been calculated from values given in Wapstra table (Everling *et al.*, 1960) from which E_c i.e. excitation energy left after first neutron emission is calculated. In column 4, $\sigma_{nonel.}$ values are tabulated. The sources of these experimental (or computed, in some cases) values are presented as legend. The procedure is similar for all other partial cross section values presented in other columns. Column 10 indicates the values of θ , computed from equation (2) obtained by approximation from Maxwellian spectra. In column 9 are presented our experimental values of $\sigma(n, 2n)$. The last column presents calculated values of nuclear temperature obtained from equation (1), using our experimental values.

The equation (1) is known to over-estimate the cross section (Strohal, 1962) since it is assumed in it that (i) $\sigma(n, n)$ can be replaced by $\sigma_c(n)$ and (ii) that it is always possible for a second neutron to be emitted wherever excitation is left for that after first neutron emission. However, direct comparison with

TABLE 2
Comparison of $\sigma(n, 2n)$ with statistical theory

Nucleus	E_{th} (MeV)	E_c (MeV)	σ (non- $stat.$) barns	σ (n, p) barns	σ (n, α) barns	$[\sigma(n, np) + \sigma(n, pn) + \sigma(nd)]$ barns	measured $\sigma(n, 2n)$ barns	θ (MeV) Calc. from (2)	θ (MeV) Calc. from (1)
P ³¹	12.72	2.08	$1.13 \pm 0.03^{(1)}$	$0.85 \pm 0.03^{(2)}$	$0.105 \pm 0.010^{(3)}$	$0.025^{(2)}$	0.016 ± 0.002	2.04	10.41
Zn ⁶⁴	11.973	2.827	$1.52^{(3)}$	$0.155 \pm 0.012^{(4)}$	$0.008^{(5)}$	$0.281 \pm 0.018^{(1)}$	0.102 ± 0.01	2.01	3.12
Ga ⁶⁹	10.331	4.470	$1.54^{(3)}$	$0.042^{(6)}$	$0.020^{(3)}$	—	0.983 ± 0.15	1.38	1.96
Ag ¹⁰⁷	9.446	5.337	$1.89^{(3)}$	$< 0.010^{(7)}$	$0.010^{(5)}$	—	0.601 ± 0.09	1.20	4.62

(1) Allen, 1961;

(2) Normalized from differential value, Chatterjee (1965);

(3) Computation from optical model calculation (Perey *et al.*, 1962);(4) Weigold *et al.*, 1962;

(5) Howerton, UCRL 5226 (Revised)

(6) Bornmann, 1962;

(7) Assessed from the average curve in Chatterjee (1964);

(8) Grimeland *et al.*, 1965;

(9) Experimental value, author, dissertation, 1965.

evaporation model has been made by comparing θ calculated by equation (1) using experimental values of $\sigma(n, 2n)$ with θ obtained from the equation 2.

From table 2 it will be seen that only in the cases of Zn^{64} and Ga^{69} , the obtained temperatures somewhat agree with the evaporation model. In the case of P^{31} , θ is appreciably larger, and it is also high in case of Ag^{107} (a middle-Z-nucleus). Our case represents an "average" cross section in a broad energy variation of ± 100 KeV. Hence it is difficult to find an explanation for large departure of θ from the results obtained from the evaporation model. In case of Ag^{107} , measured values of $\sigma(n, np)$, $\sigma(n, pn)$, $\sigma(n, d)$ with any degree of accuracy are not known to exist. If these are considerably large, the θ value will be modified.

In the case of P^{31} , the θ value is more than 10 MeV. The experimental cross section in this near-threshold energy is small, but larger by a factor of two than the value obtained by Grimeland *et al.*, (1964) in exactly the same energy. Our cross section agrees fairly well with Rayburn's value (Fergusson *et al.* 1960) normalized to 14.8 MeV.

CONCLUSION

In these nuclei, if pronounced direct effects are present, experimental cross sections must appear smaller, because the first neutron takes away larger energy from total excitation. But it is difficult to state, with certainty, that in these cases actually the direct reactions are responsible for low cross section : because cross sections of processes like $(n, \alpha n)$ or (n, nx) are believed to be considerable in some cases.

Although this method has been followed by Fergusson and Thomson (1960), such crude comparison, without considering structure effects may not yield conclusive results about the presence of direct effects. Of course the apparent large departure from these estimated values from the experimental ones is tempting enough to conclude about their presence. It is indicated that actual measurement of processes where neutron emission is possible along with other charged particle emission should scrupulously be made, by using particle discrimination methods. Also spectroscopy of emitted neutrons is necessary to assess the high energy limit of first neutron, so that the second neutron emission is correlated to quantitatively assess the $(n, 2n)$ process only.

ACKNOWLEDGEMENT

The author is deeply indebted to Dr. D. M. Bose, Director Bose Institute, for his kind interest and encouragement in the work. He is grateful to Dr. S. R. Khastgir, Head of the Dept. of Physics, for his keen interest in the work.

REFERENCES

- Allan, D. L., 1961, *Nuclear Phys.*, **24**, 274.
Blatt, J. M., and Weisskopf, V. F., 1955, *Theoretical Nuclear Physics*, John Wiley, N. Y.
Bormann, M., 1962, *Z. Physik*, **166**, 477.
Covolani, M. and Petralia, S., 1962, *Nuov. Cim.*, **26**, 1328.
Chatterjee, A., 1964, *Nuclear Phys.* **60**, 273.
———, 1965, *Nucleonics*, (Aug).
Csikai, J., 1966, *Atomki Kozlemenység (Report)*, 8 Kotet/66179, Debrecen
Ericson, T., 1960, *Advances in Physics*, **9**, 425.
Everling, F., König, L. A., Mattauch, J. H. E. and Wapstra, A. H., 1960, *Nuclear Phys.*, **18**, 529.
Fergusson, J. M. and Thompson, W. E., 1960, *Phys. Rev.*, **118**, 228.
Forbes, S. G., 1952, *Phys. Rev.*, **88**, 1309.
Glover, R. N. and Weigold, E., 1962, *Nuclear Phys.*, **29**, 309.
Grimeland, B. and Opsahl-Anderson, P., 1964, *Nuclear Phys.* **51**, 302.
Grimelandi, B., Kjellsby and Vines, J., 1965, *Phys. Rev.*, **137**, B878.
Kantele, J. and Gardner, D. G., 1962, *Nuclear Phys.*, **35** 354.
McGregor, M. H., Ball, W. P. and Booth, R., 1957, *Phys. Rev.*, **108**, 726.
Mitra, B. and Ghose, A. M., 1966, *Nuclear Phys.*, **83**, 157.
Mitra, B., Chatterjee, A and Ghose, A. M., 1965, *Proc. Nucl. Phys. Symp. Calcutta*.
Perey, F. G. J. and Buck, B., 1962, *Nuclear Phys.*, **32**, 352.
Rayburn, L. A., 1961, *Phys. Rev.*, **122**, 168.
Strohal, P., Cindro, N. and Eman, B., 1962, *Nuclear Phys.*, **30**, 49.
Weigold, E., 1962, *Nuclear Phys.*, **32**, 106.
Yasumi, S., 1957, *J. Phys. Soc. Jap.*, **12**, 443.

ON THE ASSIGNMENTS OF THE VIBRATIONAL FREQUENCIES OF SOME BENZYL COMPOUNDS

S. CHATTOPADHYAY

OPTICS DEPARTMENT,

INDIAN ASSOCIATION FOR THE CULTIVATION OF SCIENCE, CALCUTTA-32. INDIA

(Received April 26, 1967)

ABSTRACT. The Raman and infrared spectra of the molecules of benzyl chloride, benzyl bromide, benzyl cyanide and benzyl amine have been thoroughly investigated and a reasonably complete assignment of the vibrational frequencies in each case has been made.

INTRODUCTION

Assignments of the vibrational frequencies of benzene derivatives when the substituent is a single atom or a simple group of atoms have been made by numerous workers and as a result certain characteristic features of the vibrational spectra of such molecules are now easily recognised. However, when the substituent group is rather complicated the analysis of the vibrational spectrum of the whole molecule becomes difficult and reliable assignments of the vibrational frequencies have been made only in few cases. In a recent paper (Chattopadhyay *et al*, 1966) the assignment of the vibrational frequencies of benzyl acetate has been made and it has been pointed out that the assignment of the frequencies of vibration of the two constituent parts of the molecule could be made approximately independently. In the same paper it was also proposed to undertake the analysis of the vibrational spectra of other benzyl compounds.

The Raman spectra of a number of benzyl derivatives have been investigated by previous workers (Reitz *et al*, 1935; Sirkar *et al*, 1946; Ray, 1951-1952; Deb, 1961) and partial assignments of the vibrational frequencies of some of the molecules are given in Landolt and Börnstein Table (1951). The assignment of a number of infrared absorption bands of benzyl amine has been made by Leysen and Rysselberge (1963). In order to make assignments of the vibrational frequencies, the Raman and Infrared spectra of the benzyl chloride, bromide, cyanide and amine have been thoroughly investigated and assignments of the observed vibrational frequencies have been discussed in the present paper.

EXPERIMENTAL

Chemically pure samples of benzyl chloride, benzyl bromide, benzyl cyanide and benzyl amine obtained from B.D.H., Eastman Organic Chemicals and Ward Blenkinsop and Co. Ltd. were first fractionated and the proper fractions were

repeatedly distilled under reduced pressure before use. The Raman spectra of the compounds and the character of polarisation of the Raman lines were studied in the manner described in a previous paper (Chattopadhyay *et al.*, 1966) with a Fuess glass spectrograph having dispersions of $13\text{\AA}/\text{mm}$ and $19\text{\AA}/\text{mm}$ in the Hg 4047\AA and 4358\AA regions respectively. The Raman spectrograms were obtained with different times of exposure and with appropriate filters in order to identify as many Raman lines as possible. The infrared spectra of the compounds in dilute solutions in different solvents and of the pure liquids were recorded on a Perkin Elmer Model 21 double beam infrared spectrophotometer with NaCl optics. The absorption spectra due to pure liquids were obtained with very thin films of the liquid formed between two NaCl discs and also in a cell of thickness .025mm, so that the existence of very weak absorption bands could be definitely ascertained.

RESULT

The frequency shifts of the Raman lines ($\Delta\nu$ in cm^{-1}) of benzyl chloride, bromide, cyanide and amine and the frequencies (ν in cm^{-1}) of the infrared absorption maxima of these compounds are given in Tables I-IV. The visually estimated intensities of the Raman lines are given in parentheses following the frequency-shift values and the states of polarisation are denoted by the letters P and D as usual. The Raman frequency-shifts reported by other workers together with the intensity values and nature of polarisation whenever available have been included in the appropriate Tables. The intensity and nature of the infrared absorption bands are denoted by the letters *s*-strong; *m*-medium; *w*-weak; *b*-broad; *sh*-shoulder and *v*-very. In the case of benzyl amine the table also includes the frequencies of the infrared absorption bands observed by Leysen and Rysselberge (1963).

The frequencies of vibration of all the molecules studied in the present investigation together with the proposed assignment are given in Table V. This Table also contains the assignments of some of the vibrational frequencies of these compounds according to Kohlrausch as given in Landolt Börnstein table (1951).

DISCUSSION

All the molecules of the benzyl compounds studied in this work, do not possess in the strictest sense any symmetry element other than the element of identity. However, under certain special configuration the molecules will have the symmetry of the point group C_6 . In any case each of the molecules of benzyl chloride and benzyl bromide will have 39, benzyl cyanide 42 and benzyl amine 45 frequencies of vibration.

If the substituent group be treated as a single unit all the molecules will have approximately the symmetry of the point group C_{2v} and in that case there will

be thirty frequencies of vibration characteristic of the phenyl ring divided among the appropriate symmetry classes. On the other hand if the phenyl ring (denoted by ϕ) is treated as a single unit then the group $\phi\text{CH}_2\text{X}$ will give rise to a characteristic vibrational modes whose number is 9 when $\text{X} = \text{Cl}$, or Br , 12 when $\text{X} = \text{CN}$ and 15 if X represent the NH_2 group.

The assignments discussed in the following paragraphs have been made on the basis of the intensities in Raman scattering and infrared absorption, the character of polarisation of the Raman lines and the assignments made in the case of monohalobenzenes (Whiffen, 1956) and dihalomethanes (Herzberg, 1956; Landolt and Börnstein, 1951).

a) *Vibrational frequencies of the phenyl ring :*

The frequencies of vibrations corresponding to the modes 6A , $6\text{B}(e_g^+)$; 8A , $8\text{B}(e_g^+)$; 9A , $9\text{B}(e_g^+)$; $18\text{A}(e_u^-)$ and 19A , $19\text{B}(e_u^-)$ of benzene are easily recognised in the vibrational spectra of the benzyl compounds and these are shown in Table V. The frequencies of the modes $10\text{A}(e_g^-)$, $16\text{A}(e_u^+)$ and $17\text{A}(e_u^+)$ in benzene are not expected to change much in monosubstituted benzenes and accordingly the weak Raman lines in the spectra of the benzyl compounds at about 405 cm^{-1} and 845 cm^{-1} have respectively been assigned to the modes 16A and 10A while the infrared bands in the region $940\text{-}970\text{ cm}^{-1}$ observed with the different benzyl compounds have been identified with the mode 17A .

All the benzyl compounds show very strong and well polarised Raman lines at about 1000 cm^{-1} and this frequency also appears as very weak absorption bands in the infrared spectra of these molecules. This band has been assigned to the mode $1a_{1g}$ of benzene.

The mode $12b_{1u}$ of benzene is mainly a in plane C-C-C angle deformation vibration with some stretching of the $\text{C}=\text{C}$ bonds. Since the frequency of vibration of C-C-C angle deformation mode ($6\text{A}e_g^+$) is considerably lowered on substitution, it is expected that the frequency of the mode $12b_{1u}$, would decrease when one of the H atom is replaced by a different atom or a group of atoms. Thus in fluoro- and chlorobenzene the strong polarised Raman lines at 806 cm^{-1} and 786 cm^{-1} have been assigned to this mode (Whiffen, 1956) while in toluene and ethyl benzene, which may be regarded as benzyl compounds, the frequencies corresponding to this mode are represented respectively by the well polarised Raman lines at 786 and 763 cm^{-1} . In the spectra of the various benzyl derivatives there are strong polarised Raman lines in the frequency region $760\text{-}796\text{ cm}^{-1}$ and in the infrared spectra these frequencies appear as absorption bands of medium to strong intensity. These frequencies have been assigned to the mode $12b_{1u}$ of benzene.

In the Raman spectra of all the benzyl compounds there are well polarised and moderately strong lines in the frequency region $1200\text{-}1210\text{ cm}^{-1}$. In infrared

absorption these frequencies in certain cases appear as strong bands. This frequency according to Whiffen (1956) is attributable to a trigonal mode involving considerable stretching of the C-X bond.

While this suggestion seems justified, it is difficult to determine the corresponding mode of vibration in benzene. However, it is evident that one of the C-H stretching vibrational modes of benzene is appropriately modified to give rise to this frequency in many monosubstituted benzenes. It is suggested that in this mode of vibration, the five CH groups in the phenyl ring move out as in mode I and for the remaining C-X group while the C atom moves out the atom X moves in, thereby compressing the C-X bond. Thus the frequency is due to a mode involving the stretching of the C - C bonds and compression of the C-X bond.

The assignments of the remaining frequencies of the phenyl ring is made following Whiffen (1956). Thus the frequencies in the regions $1315\text{-}1330\text{ cm}^{-1}$ and $1376\text{-}1390\text{ cm}^{-1}$ which appear some times as weak Raman lines or weak infrared absorption bands in the spectra of the various benzyl compounds have respectively been assigned to the modes $3a_{2g}$ and $14b_{2u}$ of benzene. The mode $15b_{2u}$ of benzene is represented by the strong to moderately strong infrared bands in the region $1058\text{-}1072\text{ cm}^{-1}$ in the spectra of the molecules of the benzyl derivatives while the weak Raman line at about 990 cm^{-1} is assigned to the mode $5b_{2g}$.

In the case of monohalobenzenes Whiffen (1956) assigned the frequencies at about 680 and 740 cm^{-1} respectively to the modes $4b_{2g}$ and $11a_{2u}$ of benzene. However, from a consideration of the intensity in infrared absorption it appears justifiable that the very strong band at 695 cm^{-1} observed with all the compounds studied should correspond to the mode $11a_{2u}$ while the Raman band at about 750 cm^{-1} to the mode $4b_{2g}$.

Of the modes $10B(e_g^-)$, $16B(e_u^+)$, $17B(e_u^+)$ and $18B(e_u^-)$ of benzene the strong, depolarised Raman line of lowest frequency shift in the spectrum of the benzyl molecules is assigned to the mode $10B$ while the weak depolarised Raman line at 320 cm^{-1} may correspond to the mode $16B$. The infrared active modes $17B$ and $18B$ have tentatively been identified with the infrared bands in the region $870\text{-}890\text{ cm}^{-1}$ and $910\text{-}920\text{ cm}^{-1}$ respectively.

As with other monosubstituted benzenes, the benzyl derivatives will have five C-H stretching vibrational frequencies derived from any five of the modes $2a_{1g}$; $7A$, $7B(e_g^+)$; $13b_{1u}$ and $20A$, $20B(e_u^-)$ of benzene. One of these modes is converted into a C-X stretching mode of vibration while the other modes give rise to C-H stretching vibrational frequencies which are very nearly the same. Because of the inadequate dispersion of the spectrograph used and the limitations of the NaCl optics of infrared spectro-photometer it has not been possible to definitely ascertain all these vibrational frequencies. In the Raman spectra of all the

benzyl compounds there are broad polarised and moderately strong lines in the region $3050\text{--}3065\text{ cm}^{-1}$. These frequencies in all probability arise from the mode $2(a_{1g})$ of benzene. The broadness of the lines may be due to the fact that Raman lines arising from the modes 7B and 13 of benzene have been superposed. The very strong and broad infrared band at 3065 cm^{-1} in benzyl chloride and at 3100 cm^{-1} in benzyl amine may similarly arise in each case from the superposition of the bands due to the modes 20A and 20B of benzene.

Besides the above vibrational frequencies most of the benzyl compounds show weak to moderately strong and some times depolarised Raman lines in the frequency range $550\text{--}585\text{ cm}^{-1}$ and in many cases polarised and moderately strong lines at about 810 cm^{-1} which are absent in the spectra of monohalogenated benzenes. Also in benzyl chloride, ethyl benzene and benzyl mercaptan strong Raman lines are observed at 679 , 672 and 673 cm^{-1} respectively corresponding to which no Raman lines are found in the spectra of the monohalobenzenes. These frequencies in all probability arise from the vibration of the $\phi\text{CH}_2\text{X}$ group of the molecules.

(b) *Vibrational frequencies of $\phi\text{CH}_2\text{X}$ group*

The most important vibrational frequencies of this group arise from the motion of the CH_2 group. This group gives rise to five distinct frequencies corresponding to one twisting mode, two rocking modes, one scissoring mode and two stretching modes of vibration. From a careful study of the assignments of the vibrational frequencies in dihalomethanes (Herzberg, 1956; Landolt and Börnstein, 1951) the frequencies of vibration which correspond to these modes in the benzyl compounds are easily identified. Thus the Raman lines in the various molecules appearing in the region $1400\text{--}1440\text{ cm}^{-1}$ are attributed to the scissoring mode while one of the rocking modes gives rise to the Raman lines and infrared bands in the region $1220\text{--}1270\text{ cm}^{-1}$. The other rocking mode of vibration in all probability is represented by the Raman lines of moderate intensity at about 810 cm^{-1} which also appear strongly in infrared absorption. The frequency of the CH_2 -torsional motion in dihalomethanes is about 1150 cm^{-1} which changes only slightly if the mass of any of the halogen atoms is increased. This vibrational mode in the case of benzyl derivatives will have almost the same frequency as that of the modes 9B of the phenyl ring and thus has not been detected. The polarised Raman line of medium intensity at about 2970 cm^{-1} in the spectra of benzyl chloride and bromide and at about 2920 cm^{-1} in other benzyl compounds represents the symmetric C-H stretching vibration of the CH_2 group. The asymmetric C-H stretching vibration in the dihalomethanes is about 3050 cm^{-1} . This frequency is not sensitive to the mass and nature of the halogen atoms and in the benzyl compounds would be expected to have almost the same frequency. But unfortunately this frequency is very close to the aromatic C-H stretching frequency in the phenyl ring and has

TABLE I
Benzyl chloride

Raman shifts ($\Delta\nu$ cm ⁻¹)		Infrared bands (ν cm ⁻¹)				
Landolt Börnstein (1951)	Present author	Pure Liquids		Solution		
		Thick film	Thin film	Carbon tetra chloride	Chloroform	Cyclo hexane
130(8sb)	137(5b)D					
269(3).61	267(3)P?					
330(2).89?	332(2)P					
470(5).28	472(4)P					
560(3).91	558(3)					
616(6).91	620(5)D					
679(10b)	673(6b)P		678 s			
700(3).25	700(1)?	695 vs	695 vs	695 vs	685 s	695 vs
766(6).61	764(4)P?		760 m			760 m
806(2)	813(3)D	810 vs	812 m		812 m	812 m
816(4).35						
	876(1)				890 sh	
		920 mb		930 vwb	930 sh	
		965 sh		952 sh	950 sh	955 vvw
		982 sh				985 vvw
1003(10).08	1000(10)P	1002 w		995 wb	1005 vvw	
1030(6).12	1030(4)P	1026 s	1028 w		1028 vvw	1025 vvw
		1071 vs	1072 m	1065 wb	1072 m	1070 mb
1165(5)	1162(2)	1160 s	1155 vwb	1152 sh		
1182(2).74	1185(1)					
1209(7).20	1205(5)P	1210 mb	1210 wb	1210 mb	1210 sh	1208 m
1264(6).43	1258(5)D	1264 vs	1268 s	1265 vs	1268 vs	1262 vs
		1323 mb	1320 sh			
1382(0)		1390 wb				
1438(3)	1439(2)					
1452(1).97		1450 vs	1458 s	1458 m	1460 s	
	1497(2)	1498 s	1500 m	1500 m	1500 m	1495 s
1586(2)		1590 m				
1603(8).69	1607(5)D	1604 mb			1606 vvw	1606 vvw
2964(1b)	2960(3)P	2983 sb	2990 mb			
	3024(1)	3030 sh		3020 sh		
3057(2b)	3057(6b)P		3058 mb	3050 wb		3052 mb
		3065 vsb				

TABLE II
Benzyl Bromide

Raman shifts ($\Delta\nu$ cm ⁻¹)			Infrared bands (ν cm ⁻¹)			
Reitz and Stockmair (1935)	Ray (1952)	Present author	Pure liquid		Solution in	
			Thick film	Thin film	Carbon tetrachloride	carbon disulphide
133 (10b)	103 (4)D	121 (6b)D				
236 (3)	239 (2)P	243 (4)P				
320 (4)		314 (1)				
452 (4)	448 (5b)P	459 (5)P				
548 (2)	544 (2)D	551 (5)D				
605 (10b)	601 (7b)P	613 (6b)D				
690 (0)			690 vs	688 vs	690 s	691 vs
755 (2)	749 (0)D	763 (3)D	751 s	750 vs	769 vsb	750 m
804 (2)	803 (1b)D	807 (3)D	800 wb	798 s	810 sh	805 vw
			888 sh	888 sh		
				910 vw	920 m	
				960 sh	970 wb	
1000 (6)	996 (5)P	1001 (10)P		1000 vw	1002 sh	
1027 (2)	1015 (0)P	1031 (4)P	1026 w	1026 w		1028 vvw
			1065 m	1065 s	1065 vwb	1061 vw
1114 (1)						
1163 (2b)	1162 (0)D	1165 (3)				
		1183 (2)				
		1205 (2)	1200 s	1200 vs	1202 m	
1222 (10b)	1221 (6b)P	1229 (6b)D	1224 s	1223 vs	1228 s	1222 s
		1315 (2)				
			1376 m			1380 sh
1438 (1)		1438 (2)	1440 sh	1444 wb	1440 sh	1421 sb
			1452 vs		1454 w	
1497 (1)		1494 (2)	1494 s	1494 vw		
		1537 (2)			1522 mb	
			1585 wb			1589 sh
1598 (6)	1595 (5b)D	1608 (6)D	1600 wb		1610 sh	1610 sh
	2949 (0)D					
	2970 (2)P	2969 (2)P				
	3054 (4b)P	3053 (4b)P	3040 sb	3052 sh	3053 mb	3048 mb

TABLE III
Benzyl cyanide

Raman shifts ($\Delta\nu$ cm ⁻¹)		Infrared bands (ν cm ⁻¹)				
Landolt Börnstein (1951)	Present author	Pure Liquid		Solution in		
		Thick film	Thin film	Carbon tetra- chloride	Chloroform	Carbon disul- phide
126 (b)	135 (4)D					
216 (2sb)	216 (1)					
235 (3b)	236 (2)P					
322 (4)	323 (2)D					
358 (5)	360 (3)D					
428 (3b)	424 (3)P					
468 (1b)	470 (0)					
618 (7)	619 (5)D					
		696 vs	695 vs	692 vs	690 s	691 vs
		734 vs	734 vs			726 vs
744 (2)						
	751 (0)					
798 (6)	796 (4)P	780 vw	780 vvw			792 sh
812 (6b)	812 (4)P	805 vw				
849 (1)		882 vw	878 sh			
			925 mb			
					934 m	920 wb
		940 m				
		960 vvw				
991 (1)						
1003 (10)	1001 (10)P	1004 w	1004 vw	1002 sh		1000 sh
1031 (8)	1030 (4)P	1033 s	1030 m	1029 w	1028 w	1028 w
		1080 s	1076 mb		1080 w	1070 w
1157 (4)	1153 (3)P	1151 sh	1155 vw			1165 wb
1188 (4)	1189 (4)P	1190 w	1182 vw			
1192 (7)						
				1230 vwb?		
		1332 vvw	1331 vvw		1325 sh	
		1378 w	1388 sh			
1414 (5)	1413 (3)P	1421 vs	1420 sh	1418 m	1420 w	1414 s
		1458 s	1458 s	1454 m	1455 vs	
1499 (0)	1495 (2)D	1500 s	1500 s	1498 m	1499 s	
1586 (5)	1590 (1)	1590 sh	1586 sh		1584 s	
1602 (6)	1605 (4)D	1606 m	1604 m	1602 vvw	1604 m	1604 vvw
2252 (6)	2250 (4)P	2265 m	2262 sh	2268 w	2215 s	2260 w
2914 (5b)	2920 (4)P	2950 m	2924 w	2906 w		
2984 (3)						
3011 (3)						
3046 (3)						
3059 (9)		3050 m	3048 mb	3052 mb		3050 m
3085 (8b)	3069 (6b)P					

TABLE IV
Benzyl amine

Raman shift ($\Delta\nu$ cm ⁻¹)			Infrared bands (ν cm ⁻¹)	
Landolt Börnstein (1951)	Sirkar and Bishui (1946)	Present author	Pure Liquid Thin Film	Leysen and Rysseberge (1963)
168 (4b)	175 (2b)D	157 (4b)D		
404 (1)	412 (0b)	412 (2b)		
482 (2)	483 (0b)P	480 (2b)		
579 (1)		580 (1)		
620 (8)	628 (2)D	622 ₂ (5)D		
645 (0)			695 vs	696
	740 (0)		734 vsb	
750 (1)		751 (1)		
			770 (s)	
782 (5b)	786 (2)P	783 (4)P		
			810 s	797
846 (1)	834 (0)	846 (1)	836 vs sh	
			870 vsb	
			910 vs	
989 (1)			990 m	
1001 (10)	1007 (5)P	1002 (10)P	996 m	1000
1028 (6)	1030 (2)P	1024 (4)P	1024 m	1026
1058 (1)			1052 m	1058
1157 (5)	1160 (2)P	1156 (4)D	1150 vw	1153
1179 (2)		1175 (2)		
1202 (5)	1207 (4)P	1206 (4)P	1200 vw	
			1290 w	1290
			1320 w	
			1384 m	1383
1390 (1)				
	1402 (0)	1401 (1)		
1452 (2b)	1458 (3)D	1459 (2b)	1455 vs	1453
1491 (0)			1498 vs	1497
1582 (4)	1590 (1)D	1589 (2)	1598 vsb	
1604 (8)	1605 (8)D	1603 (5)D		1608
2859 (1)	2872 (2)P	2865 (2)	2865 s	
2946 (2)	2935 (3)P	2920 (2)	2925 s	
3006 (2)				
3035 (2)				
3054 (8)		3057 (5)P		
3062 (8)	3063 (10d)P		3100 vs	
3314 (2)	3316 (2)P	3312 (2)P		3289
3380 (0)				3378

TABLE V
Frequencies of vibration in Benzyl compounds

Present Author					Assignment due to Kohlrausch
Benzyl Chloride	Benzyl Bromide	Benzyl Cyanide	Benzyl Amine	Assignment and corresponding mode in Benzene	
137	121	135	157	10B e_g^-	
		216		CH ₂ X	
267	243	236		CH ₂ X	
332	314	323		16B e_u^+	
		360		CH ₂ X	
			412	16A e_u^+	
472	459	424	480	6A e_g^+	
		470		CH ₂ X	
558	551		580	CH ₂ X	
620	613	619	622	6B e_g^+	17 A & B e_u^+
673				CH ₂ X ?	
700 ?	690	696	695	11 a_2u	
	751	751	751	4 b_{2g}	5 b_{2g}
764	763	796	783	12 b_1u	
813	807	812	810	CH ₂ Rock	
		849	846	10A e_g^-	10B & A e_g^-
876	888	882	870	17B e_u^+	
920	910	920	910	18B e_u^-	
965	970	940		17A e_u^+	
982		991	990	5 b_{2g}	
1000	1001	1001	1002	1 a_{1g}	
1030	1031	1030	1024	18A e_u^-	18A e_u^-
1071	1065	1076	1052	15 b_2u	
1162	1165	1153	1156	{ 9B e_g^+ CH ₂ twist	9B e_g^+
1185	1183	1189	1175	9A e_g^+	9A e_g^+
1205	1205	1192	1206	ν (CH ₂ -X)	
1258	1229	1230		CH ₂ -Rock	

TABLE V (contd.)

Benzyl Chloride	Benzyl Bromide	Present Autohr			Assignment due to Kohlrausch
		Benzyl Cyanide	Benzyl Amine	Assignment and corresponding mode in Benzene	
			1290	?	
1323	1315	1331	1320	3 a_{2g}	3 a_{2g}
1390	1376	1378	1364	14 b_{2u}	15 b_{2u}
1439	1438	1418	1401	CH ₂ -Scissor	
1450	1452	1455	1449	19B e_u^-	
1497	1494	1495	1498	19A e_u^-	
1590	1585	1590	1589	8A e_g^+	
1607	1608	1605	1603	8B e_g^+	
		2250		ν (C \equiv N)	
			2865	?	
2960	2969	2920	2920	ν (CH) ₃ of CH ₂ X	
3024		3046	3035		
		3059			
3057	3053	3069	3057	$\left\{ \begin{array}{l} 2 \ a_{1g} \\ 7B \ e_g^+ \\ 13 \ b_{1u} \end{array} \right.$	
			3062		
3065			3100	$\left\{ \begin{array}{l} 20A \ e_u^- \\ 20B \ e_u^- \end{array} \right.$	
			3312		ν (NH) ₃
			3378	ν (NH) ₃	

not been identified. In the Raman spectra of benzyl chloride, benzyl bromide and benzyl cyanide there are polarised Raman lines of medium intensity at 267, 243 and 236 cm^{-1} respectively. These frequencies might arise from a mode of vibration similar to that giving rise to a strong polarised Raman line at 283 cm^{-1} in dichloromethane (Herzberg, 1956). All the proposed assignments are given in table V.

Besides the frequencies arising out of the vibrations of CH₂ group there are certain characteristic group frequencies which are easily recognised. The strong polarised Raman line at 2250 cm^{-1} in benzyl cyanide arises from the stretching vibration of the C \equiv N bond. The intensity and position of the nitrile band in the infrared absorption spectra due to solutions in different solvents are found to alter considerably.

In the case of benzyl amine a weak polarised Raman line at 3312 cm^{-1} has been observed. Reitz and Stockmair (1935) have reported two bands at 3307 and 3385 cm^{-1} of which the latter is very weak. Leysen and Rysselberge (1963) have observed two bands at 3289 and 3378 cm^{-1} in the infrared spectrum of benzyl amine. These two bands are easily assigned respectively to the symmetric and asymmetric N-H stretching vibrational frequencies of the NH_2 group. In addition to the frequencies of vibration whose assignments have been discussed above there are certain other frequencies in the spectra of the benzyl compounds which in all probability arise from the vibration of the $\phi\text{CH}_2\text{X}$ group. These frequencies are marked in table V but no attempt has been made to propose any definite assignment of these frequencies.

ACKNOWLEDGMENT

The author is grateful to Professor G. S. Kastha, D.Sc. for his continued guidance throughout the progress of the work.

REFERENCE

- Chattopadhyay, S. and Mukherjee, D. K., 1966, *Indian J. Phys.*, **40**, 409.
Deb, K. K., 1961, *Indian J. Phys.*, **35**, 16.
Herzberg, G., 1956, *Infrared and Raman spectra of Polyatomic molecules*, D. Van Nostrand Co., Inc., N.J.
Landolt and Börnstein Tables, 1951, *Auft* 6, Band I, Teil 2.
Leysen, R. and Rysselberge, J. Van., 1963, *Spectrochim Acta*, **19**, 243.
Ray, A. K., 1951, *Indian J. Phys.*, **25**, 131.
———, 1952, *Indian J. Phys.*, **26**, 226.
Reitz, A. and Stockmair, W., 1935, *Mathem-naturw. Klasse, Abt.*, IIb, Band 144, Heft. 10, 666.
Sirkar, S. C. and Bishui, B. M., 1946, *Indian J. Phys.*, **20**, 111.
Whiffen, D. H., 1956, *J. Chem. Soc.*, 1350.

THE CRYSTAL STRUCTURE OF GLYCOCYAMINE HYDROBROMIDE

P. N. ROY, S. K. MAJUMDAR AND N. N. SAHA

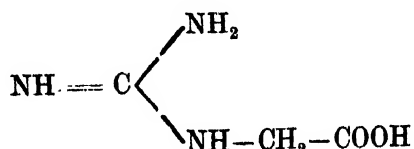
CRYSTALLOGRAPHY AND MOLECULAR BIOLOGY DIVISION, SAHA INSTITUTE OF NUCLEAR PHYSICS, CALCUTTA-9, INDIA.

(Received December 20, 1967)

ABSTRACT. Crystals of glycocyamine hydrobromide, $C_3H_7O_2N_3 \cdot HBr$, belong to the monoclinic space group $P2_1/c$ with cell dimensions $a = 5.53 \text{ \AA}$, $b = 13.52 \text{ \AA}$, $c = 9.20 \text{ \AA}$ and $\beta = 92^\circ$. There are four molecules per unit cell. The structure has been solved by three dimensional Patterson and heavy atom (bromine) phased Fourier syntheses. The coordinates of the atoms (hydrogen atoms excluded) with their isotropic temperature factors have been refined by two-dimensional least-squares method. The molecule of glycocyamine is characterised by two planar groups, e.g. the carboxyl group and the guanidyl group. The molecule is not a zwitterion, the two C—O bond lengths in the carboxyl group being 1.28 \AA and 1.34 \AA . The molecules in the crystal are held together by a three-dimensional network of hydrogen bonds of the types $N-H \cdots O$, $N-H \cdots Br$ and $O-H \cdots Br$.

INTRODUCTION

Glycocyamine or guanidoacetic acid has the following chemical formula :



Though not included in the list of standard amino acids, guanidoacetic acid, like amino acetic acid (glycine), plays an important biological role so far as the formation of creatine, a metabolic product of great interest, in the living system is concerned. Glycocyamine forms a part of our general program of study of the influence of various substituted groups in the α -amino or the side chain groups of different amino acids on their crystal structure, configuration and electronic charge distribution. The study of the structure of glycocyamine in the form of its different hydrohalides and metal complexes is in progress in our laboratory. This short communication deals with the crystal structure of glycocyamine hydrobromide.

UNIT CELL AND SPACE GROUP

Single crystals of glycocyamine hydrobromide were grown in the form of colourless plates by slow evaporation of an aqueous solution of this compound

at room temperature. Due to long exposure to ordinary atmospheric conditions, the sample was found to lose its single crystal characteristics. The crystal was, therefore, coated with durofix and kept in a sealed thin walled glass capillary for taking X-ray photographs. The unit cell dimensions as determined from rotation and Weissenberg photographs are :

$$a = 5.53 \text{ \AA}, \quad b = 13.52 \text{ \AA}, \quad c = 9.20 \text{ \AA}, \quad \beta = 92^\circ.$$

The systematic absences of *hol* reflections with *l* odd and *oko* with *k* odd indicate that the space group is $P2_{1/c}$. The density of the crystal as determined by the method of floatation is 1.85 g cm^{-3} , while the calculated value assuming four formula units of $\text{C}_3\text{H}_7\text{O}_2\text{N}_3\cdot\text{HBr}$ is 1.89 g cm^{-3} .

Three dimensional intensity data were collected about *a* and *c* axes by multiple film equi-inclination Weissenberg technique using $\text{CuK}\alpha$ radiation. The intensities were estimated visually and corrected for spot size, Lorentz and polarisation factors. The linear absorption co-efficient of the crystal for $\text{CuK}\alpha$ radiation was 82 cm^{-1} . No correction for absorption was, however, made at the initial stage but due to slow convergence of refinement it was found necessary to make the absorption correction at a later stage of refinement. The intensity data obtained from different layers were put on the same relative scale by cross layer correlation method and were put on the absolute scale by Wilson's method.

STRUCTURE DETERMINATION

The positions of the four heavy atoms (Bromine) in the unit cell were determined from two Patterson projections on (100) and (001) shown in Fig. 1 and Fig. 2. An attempt to derive the structure from these two sets of intensity data, i.e. *okl* and *hko* reflections, was not successful. Consequently, three dimensional intensity data were used for the determination of the structure. A three dimensional Fourier synthesis was calculated using observed structure amplitudes to which phases were assigned from four bromine atoms. The computation for Fourier summation was done on the C.D.C. 3600 computer using Fourier program written and kindly supplied to us by Dr. Blount. The Fourier synthesis revealed the structure completely. Structure factors for all reflections were then calculated using the co-ordinates of all the atoms in the molecule and the disagreement factor $R = \Sigma (|F_o| - |F_c|) / \Sigma |F_o|$ was found to be 32%.

The atomic parameters have been refined by the least squares method on IBM 1620 using G. A. Mair's program. The *R* value at this stage came down to 16.6% and 18.6% for *okl* and *hko* reflections respectively. The atomic parameters at this stage of 2D-refinement are given in table I. Intramolecular and

intermolecular bond lengths and angles are given in table II and III and diagrammatically shown in fig. 3 and fig. 4 respectively.

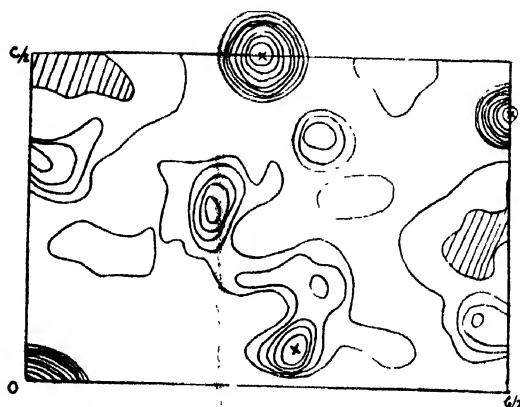


Fig. 1. Patterson synthesis of glycocyanine hydrobromide projected on (100). The Br—Br peaks are indicated by crosses.

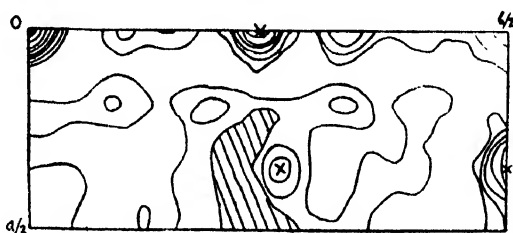


Fig. 2. Patterson synthesis of glycocyanine hydrobromide projected on (001). The Br—Br peaks are indicated by crosses.

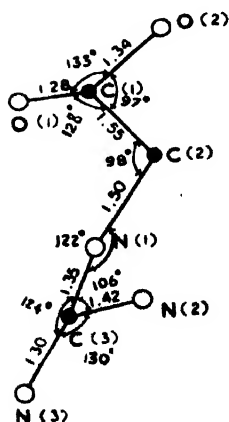


Fig. 3. Bond lengths and bond angles of glycocyanine hydrobromide.

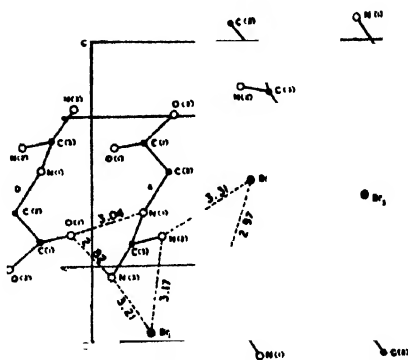


Fig. 4. Projection of the structure along the *a* axis. The dashed lines indicated the hydrogen bonds.

DISCUSSION OF THE STRUCTURE

The two C—O bond distances in the carboxyl group of glycoeyamine hydrobromide have been found to be C(1)—O(1) = 1.28 Å and C(1)—O(2) = 1.34 Å. This indicates that the hydrogen atom is bound to the carboxyl oxygen O(2). The bond distances C(2)—C(1) = 1.55 Å and C(2)—N(1) = 1.50 Å (table I and fig. 3) agree well with the average values 1.35 Å and 1.50 Å respectively for these bonds, as deduced by Hahn (1957) from other amino acids. The three C—N bond distances in the guanidly group of glycoeyamine hydrobromide i.e. C(3)—N(3) = 1.30 Å, C(3)—N(2) = 1.42 Å and C(3)—N(1) = 1.35 Å compare well with those of Arginine hydrobromide (Wyckoff, 1966) but are slightly different from those of arginine dihydrate (Karle *et al.*, 1964).

TABLE I

Glycoeyamine hydrobromide : Atomic co-ordinates and temperature factor

Atom	<i>x/a</i>	<i>y/b</i>	<i>z/c</i>	<i>B</i> (Å ²)
Br.	.1695	.1340	.0301	1.71
N(1)	.7265	.1249	.4397	3.00
N(2)	.3649	.1687	.3528	1.00
N(3)	.5986	.0404	.2295	1.00
C(1)	.8363	.1235	.6802	2.74
C(2)	.6610	.1790	.5737	4.00
C(3)	.5619	.1033	.3332	0.81
O(1)	.9889	.0560	.6508	2.18
O(2)	.8134	.1840	.7938	3.11

TABLE II

Glycoeyamine hydrobromide : Intramolecular bond lengths and bond angles

Bond length	Å	Bond angle	
C(1)—O(1)	1.28	O(1)—C(1)—O(2)	133°
C(1)—O(2)	1.34	O(1)—C(1)—C(2)	128°
C(1)—C(2)	1.55	O(2)—C(1)—C(2)	97°
C(2)—N(1)	1.50	C(1)—C(2)—N(1)	98°
N(1)—C(3)	1.35	C(2)—N(1)—C(3)	122°
C(3)—N(2)	1.42	N(1)—C(3)—N(2)	106°
C(3)—N(3)	1.30	N(1)—C(3)—N(3)	124°
		N(3)—C(3)—N(2)	130°

TABLE III
Intermolecular bond distances and angles

Hydrogen bond lengths	Å	Hydrogen bond angles	
N(1)—H O(1)	3.04	C(1)—O(2) Br	111°
N(3)—H Br	3.21	C(2)—N(1) O(1)	140°
N(2)—H Br	3.17	C(3)—N(1) O(1)	88°
N(2)—H Br	3.31	C(3)—N(3) O(1)	85°
N(3)—H O(1)	2.82	C(3)—N(C) Br	92°
O(2)—H Br	2.97	C(3)—N(2) Br	146°
		C(3)—N(2) .. . Br	91°

The molecular packing of glycoeyamine hydrobromide molecules in the crystal viewed along a axis is shown in Figb.4. There are six hydrogen atoms in each molecule of glycoeyamine hydrobromide available for hydrogen bond formation, one from the carboxyl group—COOH and five from the guanidyl ion $N^+H_2 - C(NH_2) - NH -$. The guanidyl ion makes three hydrogen bonds with bromine ions and two with carboxyl oxygens. The hydrogen atom attached to the carboxyl oxygen O(2) makes hydrogen bond with bromine ion. Thus all the hydrogen atoms available for hydrogen bond formation or in the other words all the available sites for hydrogen bond formation have been satisfactorily accounted for.

Further structural details and conformation will be published elsewhere in due course.

REFERENCES

- Hahn, T., 1957, *Zeit. fur. Krist.*, **109**, 438.
 Karle, I. L. and Karle, J., 1964, *Acta Cryst.*, **17**, 835.
 Wyckoff, R. W. G., 1966, *Crystal Structures*, **5**, 701.

Letters to the Editor

The Board of Editors does not hold itself responsible for opinions expressed in the letter published in this section. The notes containing short reports of original investigations communicated to this section should not contain many figures and should not exceed 500 words in length. The contributions reaching the Secretary by the 15th of any month may be expected to appear in the issue for the next month. No proof will be sent to the author.

22

SPACE GROUP AND UNIT CELL DIMENSIONS OF COPPER MONOCHLOROACETATE 2.5 HYDRATE

INDRANI MUKHERJEE (née DASGUPTA)

MAGNETISM DEPARTMENT,

INDIAN ASSOCIATION FOR THE CULTIVATION OF SCIENCE,

JADAVPUR, CALCUTTA-32, INDIA.

(Received November 10, 1967)

The measurement of the magnetic susceptibility of copper acetate monohydrate within the range of 300°K to 90°K , has shown that close down to $262^{\circ}\text{K} \pm 1^{\circ}\text{K}$, the susceptibility follows roughly Curie Law, it rises to a maximum at that temperature and falls rapidly thereafter (Guha, 1951). The study of the electron paramagnetic resonance of the salt, predicted the existence of isolated pairs of copper ions coupled by exchange interaction forces, with effective $S = 1$, and that each copper ion is bonded by four oxygen atoms in a plane (Bleaney *et al.*, 1952). The presence of this type of pairs of copper ions which are known as dimers was corroborated in the structure analysis of the salt (Nieckerk *et al.*, 1963). Since then, such occurrences have been predicted in quite a number of copper salts like copper propionate monohydrate (Mitra *et al.*, 1964), copper monochloroacetate monohydrate (Abe, *et al.*, 1961), Copper monochloroacetate, 2.5 hydrate (Ablov *et al.*, 1961) etc. In the present note, preliminary data on the structure of $2 [\text{Cu}(\text{CH}_2\text{Cl COO})_2] \cdot 5\text{H}_2\text{O}$, are reported.

The crystals of $2 [\text{Cu}(\text{CH}_2\text{Cl COO})_2] \cdot 5\text{H}_2\text{O}$ were crystallised by the slow evaporation of an aqueous solution of the substance. These are prismatic monoclinic crystals with bright bluish green colour.

The unit cell dimensions were obtained from rotation and Weissenberg photographs. The dimensions are given below :

$$a = 16.85\text{\AA} \quad b = 13.73\text{\AA} \quad c = 17.24\text{\AA} \quad \beta = 90^{\circ}$$

Zero and first layer Weissenberg photographs along b axis were taken and the systematic extinctions were observed. These are as follows :

hkl	no condition
$h0l$	$h+l = 2n$ absent
$0k0$	$k = 2n+1$ absent

The above conditions assign the space group as $P2_1/n$.

The density as determined by floatation method by using a mixture of bromoform and benzene, is $\rho = 1.91 \text{ gm cm}^{-3}$.

The density calculated by considering eight molecules per unit cell is $\rho = 1.95 \text{ gm cm}^{-3}$.

Further work on the determination of the complete structure of the crystal is in progress.

The author expresses her sincerest gratitude to Mr. S. Ray, Research Officer, Department of Magnetism, for suggesting the problem and for constant help and guidance throughout the work, and to Prof. A. Bose, D.Sc., F.N.I. for the kind interest taken by him. Thanks are also due to the C.S.I.R. for financial assistance.

REFERENCES

- Abe, H., and Shirai, H., 1961, *J. Phys. Soc. Japan*, **16**, 118.
 Ablov, A. V., Yablokov, Y. V. and Zohru, I. I., 1916, *Proc. Ac. Sc. U.S.S.R.*, **141**, 1116.
 Bleaney, B. and Bowers, K. D., 1952, *Proc. Roy. Soc.*, **A214**, 451.
 Guha, B. C., 1951, *Proc. Roy. Soc.*, **A206**, 353.
 Mitra, S. and Sengupta, P., 1965, *Physica*, **31**, 362.
 Niekerk, J. N. Van and Schoening, F. K. L., 1953, *Acta Cryst.*, **6**, 227.

23

X-RAY STUDY OF THE MONOCLINIC MODIFICATION OF PARA ACETOTOLUIDIDE CRYSTALS

B. KHASWAS*

INDIAN SCHOOL OF MINES, DHANBAD, INDIA.

(Received March 13, 1967)

Acetyl-para-Toluidin i.e. Para Acetotoluidide ($\text{CH}_3\text{C}_6\text{H}_4\text{CONHCH}_3$) crystallises in two modifications Beilstein—one stable as platy monoclinic crystals and another metastable as rhombic needle like crystals respectively on slower and

*Present address : Physics Division, Indian Agricultural Research Institute, New Delhi.

quicker evaporation from its saturated solution in alcohol at room temperature. The melting point is however the same for both the modifications.

The appearance of the two modifications of crystals which are obtained from the alcoholic solution of the substance at room temperature and have the same melting point but belong to two different crystal systems is rather uncommon. The explanation is presumably to be sought in the internal disposition of the atoms of the molecules in the unit cells of the crystals. With this end in view an X-ray study of the stable modification was undertaken.

The six sided platy flake crystals were examined with the help of a Fuess Horizontal Circle goniometer. The interfacial angles measured were found to be the same as those recorded in Groth (1917). Oscillation and Weissenberg photographs of these crystals along [010] and [001] using CvK radiation gave the following unit cell parameters :

$$a = 11.690 \text{ \AA} \quad b = 9.689 \text{ \AA} \quad c = 7.599 \text{ \AA} \quad \beta = 106.0^\circ$$

The axial ratio thus calculated as 1.2069 : 1 : 0.7841 is in good agreement with that of 1.2176 : 1 : 0.7868 given by Groth (1917).

The normal beam zero, 1st. and 2nd. layer Weissenberg photographs along *b* and *c* axes gave the following conditions limiting possible reflections :

hkl : no condition.

hol : ($l = 2n$),

oko : no condition

The crystals are thus assigned to the space-group C_2^4P2/c . The density as obtained by flotation method in a solution of $ZnSO_4$ in water was found to be 1.19 gm/c.c. The calculated density for four molecules per unit cell is 1.21 gm/c.c. Further work is in progress.

The author expresses his sincerest gratitude to Dr. J. Dhar, Professor of Physics, Indian School of Mines, Dhanbad for his valuable guidance during the progress of the work.

REFERENCES

- "Beilsteins Handbuch Der, Organischen Chemie" Velay von Jubies Springer, Berlin, 1929, p. 920.
- Groth P. 1917, *Chemische Krystallographic*. Vol 4, p. 399.
- "The Condensed Dictionary"—Reinhold Publishing Corporation 1942, third edition, p. 46.

EXCITATION SPECTRA OF EVEN-EVEN NUCLEI OF NON-DEFORMED REGION

R. V. RAMAMOHAN

DEPARTMENT OF PHYSICS, UNIVERSITY OF AGRICULTURAL SCIENCES, BANGALORE, INDIA,

(Received August 29, 1967)

Angular correlation studies of three even-even radioactive nuclei, namely Fe^{58} , Te^{124} and Ba^{134} , which come under the non-deformed region of mass $40 \leq A \leq 154$ where undertaken by Rama Mohan *et al* (1965 and 1967). in order to assign the spins of the excited states and the characteristics of transitions, by using a slow-fast triple coincidence scintillation spectrometer. These experimental results are now analysed with those predicted theoretically on the basis of various existing models by Bohr and Mottelson (1953), Davydov and Fillipov (1958, 1960), Mallaman (1961), Raz(1959), Scharff *G*-Goldhaber *et al* (1958) and Wilets and Jean (1956).

The general characteristics observed by the experimental studies of Ramamohan *et al*, are 0^+ , 2^+ spins for the ground and first excited (1965, 1967) states for all the three even-even nuclei, with quadrupole multipolarities in the transition from the first excited state to the ground state.

The spin of the second excited state of Te^{124} is characterised by spin 4 where as those of the remaining two nuclei by the spin 2. These characteristics of Te^{124} confirm the Bohr-Mottelson's model, for even-even nuclei with the ground state rotational bands with 0^+ , 2^+ , 4^+ values. There is, however, an exception to the regularities observed in the even-even nuclei in the region $40 \leq A \leq 154$. The ground state rotational band in even-even nuclei are characterised by consecutive states with ΔI being 2 and the transition proceeds by a cascade of pure $E2$.

According to Scharff- Goldhaber and Weneser, the following characteristics are observed in the region of $66 \leq A \leq 154$. The ratio of the energy of the second excited state to that of the first excited state ranges between 2 and 2.5. The low lying states usually have the spin sequence 0^+ , 2^+ and 2^+ and the $E2$ cross over transition occurs with greater probability than the upper transition. The cross over transition $2^+ \rightarrow 0^+$ proceeds by $E2$ while the upper transition is predominantly $E2$ with a small admixture of $M1$. Coulomb excitation data also indicate that the probability for a transition from the first excited state to the ground state is higher than that which would be expected on the basis of a single particle model. This fact reveals that the large $E2$ transition probabilities in case of lighter elements are due to collective excitations of individual nucleons. Besides, it is also noted that the energy of the first excited state increases as the number of

neutrons or protons approaches to the completion of the shell and shows a prominent peak at the filled shell. These facts predicted theoretically by nuclear models are noticed in the level characteristics of Fe^{58} and Ba^{134} arrived by the experimental investigations of Ramamohan *et al.*, (1965, 1967).

The spin sequence of the ground, first and second excited states of Fe^{58} and Ba^{134} are obtained as 0, 2 and 2. The ratio between the energies of the second excited state to the first one is respectively 2 and 1.93. Further the transition from the second to the first excited state is characterised by E2+M1 multipolarities. This result confirms the validity of the theoretical predictions of Mallaman (1961). The 0^+ , 2^+ and 2^+ pattern in the low lying excited states is mainly due to collective vibrations of individual nucleons.

The slight decrease in the value of the ratio between the energies of the second excited state to that of the first for Ba^{134} is due to the fact that the neutron number 78 of that isotope is in the vicinity of the magic number 82.

The harmonic pattern of energy levels of Ba^{134} at energies 605 keV, 1168 KeV and 1845 keV with the spins 0, 2 and 4 and with the dipole radiation in $4 \rightarrow 2$ transition is in agreement with the Bohr-Mottelson's predictions of weak to moderate coupling model.

The 0, 2 and 2 spin levels with energies 0 keV, 800 keV and 1600 keV, observed in the studies of Fe^{58} by the same investigators Ramamohan *et al.*, form the harmonic pattern supporting the theoretical predictions of Bohr-Mottelson model in the region of strong coupling with unstable potential.

Hence, it is concluded that the nuclear excitation spectra arrived by experimental studies is in good agreement with that predicted by theoretical methods, using the various nuclear models.

REFERENCES

- Bohr, A. and Mottelson, B., 1953, *Mat. Fys. Medd. Dan. Vid. Selsk.*, **27**, No. 16.
 Davydov., A. and Fillipov. G., 1958, *Nucl. Phys.*, **8**, 237.
 ———, 1960, *Nucl. Phys.*, **20**, 499.
 Mallaman, G., 1961, *Nucl. Phys.*, **24**, 535.
 Ramamohan, R. V., Venkata Reddy. K., Venkatapathi Raju and S. Jnanananda, 1966.
 Ind. Jr. Pure and App. Phys., **4**, 420.
 ———, 1965, *Indian J. Phys.*, **39**, 521.
 ———, 1967, *Indian J. Phys.*, **41**, 30.
 Raz, B., 1959, *Phys. Rev.*, **114**, 1116.
 Scharff. G-Goldhaber and Weneser, 1958, *Phys. Rev.*, **98**, 212.
 Wilets, L. and Jean, M., 1956, *Phys. Rev.*, **102**, 788.

THE MAGNETIC PROPERTIES OF SPECULAR HEMATITE

A. K. MUKERJEE

DEPARTMENT OF MAGNETISM, INDIAN ASSOCIATION FOR THE CULTIVATION OF SCIENCE,
CALCUTTA-32, INDIA

(Received November 11, 1967)

The temperature variation of magnetisation and susceptibility of specular hematite ($\sim 99.1\%$ α - Fe_2O_3 , origin Mt. Popa, Burma; obtained from the collections in the laboratory) has been studied in the range of 100°K to 1000°K for fresh as well as samples heat treated to a temperature of 1000°K. The results are shown in fig. 1.

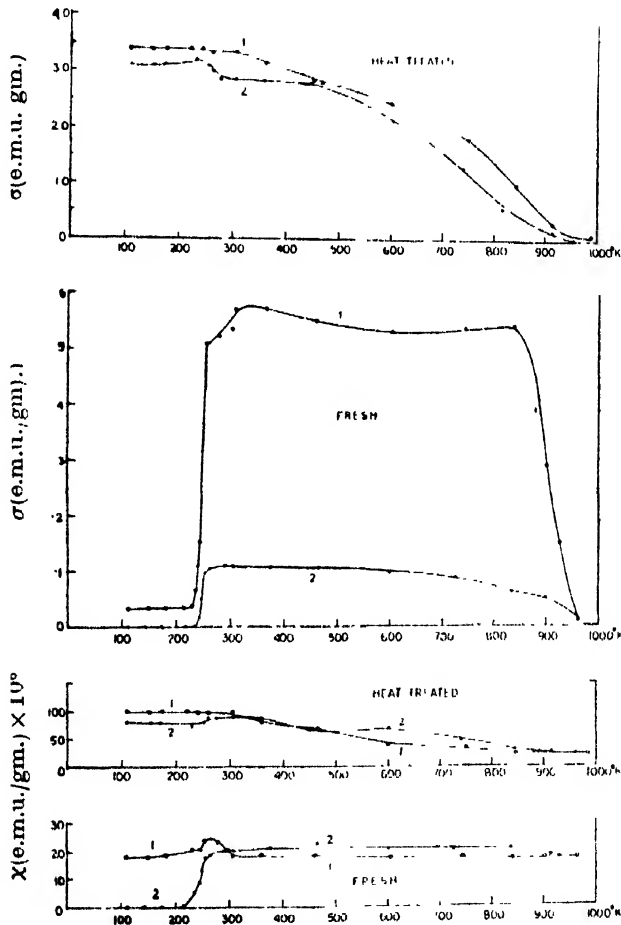


Fig. 1. Magnetisation (σ) and susceptibility (χ) at different temperatures of single crystals of hematite for fresh and heat treated samples. (1) along the basal plane (2) along the trigonal axis.

For fresh samples the temperature variation of field independent susceptibilities both along the *c*-axis and in the basal plane agree well with the findings of Tasaki and Iida (1963) on synthetic hematite, but there the ferromagnetism, unlike ours, appears only along the plane above Morin temperature ($\sim 250^\circ\text{K}$) and at lower temperatures no ferromagnetism exists at all in either of the directions. In respect of the temperature variations of both the susceptibilities and the ferromagnetism in the plane, the present observations resemble those of Néel *et al* (1952) and Lin (1959), on very pure natural crystals, but differ with their observations of ferromagnetism along the *c*-axis. Lin (1959) observed considerable ferromagnetism along the axis below the Morin temperature ($\sim 250^\circ\text{K}$) which falls sharply to a low value at higher temperatures. Néel *et al.*, (1952) no doubt observed considerable ferromagnetism at lower temperatures (below $\sim 250^\circ\text{K}$) but its temperature variation unlike the observation of Lin (1959) was rather slow. In our case on the contrary the ferromagnetism along the *c*-axis vanishes below $\sim 250^\circ\text{K}$ and appears rather sharply above this temperature.

The measurements on heat treated samples agree closely with those of Mukerjee (1967), the magnitude of magnetisation and susceptibility increasing considerably and the sharp changes at $\sim 250^\circ\text{K}$ vanishing altogether.

The author is thankful to Shri A. K. Dutta for his constant guidance and Professor A. Bose for his kind interest in the work.

REFERENCES

- Lin, S. T., 1959, *Phys. Rev.*, **116**, 1447.
 Mukerjee, A. K., 1967, *Indian J. Phys.*, **41**, 465.
 Néel, L. and Pauthenet, R., 1952, *Compt. Rend.* **234**, 2172.
 Tasaki, A. and Iida, S., 1963 *J. Phys. Soc. Japan*, **18**, 1148.

26

A SIMPLE EXPERIMENTAL DEMONSTRATION OF THE BREAKDOWN OF FARADAY'S LAW OF ELECTROLYSIS

SANTI R. PALIT

DEPARTMENT OF PHYSICAL CHEMISTRY, INDIAN ASSOCIATION FOR THE CULTIVATION
OF SCIENCE, JADAVPUR, CALCUTTA-32, INDIA.

The author adduced experimental evidence (Palit, 1967) indicating wide deviation from Faraday's law in the electrolysis of weakly conducting solutions, particularly conductivity water. Since this fact runs counter to a long accepted idea, the author presents here a simple experimental device which conclusively demonstrates the failure of Faraday's law.

Experimental—The experimental arrangement is shown in fig. 1. Of the two conical flasks one contains a 0.5N potassium sulphate solution which is highly

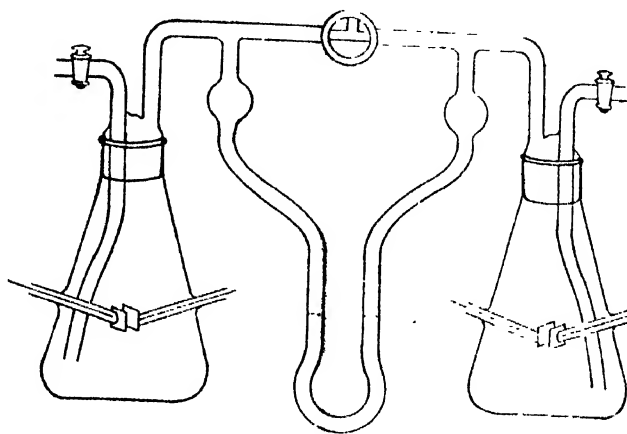


Fig. 1.

recommended as a coulometric solution by Lingane (1945); the other contains conductivity water. Each flask is provided with two platinum electrodes (1 cm \times 0.5 cm) and the two flasks are connected in series. With the three-way stopcock open to the atmosphere, a current of about one to two milliamperes is passed by applying the D.C. mains voltage (230 volts). This is continued for a few hours until the two solutions become saturated with electrolytic gas. The stopcock is then closed so that the gases do not escape to the atmosphere but collect on the opposite sides of the manometer. If Faraday's law is valid, equal quantities of gas would get collected on both sides. Since the two empty spaces are approximately of equal volume, the manometer would therefore show hardly any difference of pressure with progress of electrolysis. However, if the author's idea that Faraday's law is not valid and predominantly non-electrolytic conduction takes place in the electrolysis of water, is correct, the manometer would indicate increasing pressure in the coulometer (potassium sulphate solution) side with progress of electrolysis.

Experimentally, using a small empty space in each flask it is observed that a difference of level is increasingly produced with progress of electrolysis, the coulometer side building up the higher pressure. This convincingly demonstrates the breakdown of Faraday's law in the electrolysis of water. The demonstration can be repeated again and again by releasing and equalising the pressures on both sides of the manometer by proper turning of the three-way stopcock followed by closing the stopcock. With our set-up the rate of production of level difference is observed to be about thirty mm per hour for 2 milliampere current. This on conversion to volume taking into account the dimension of the apparatus means that barely one-third of the Faradaic value of the electrolytic gas is liberated

on electrolysis of pure water. The fact that an appreciable difference in level can be demonstrated in less than half an hour makes this simple experiment a great success as a lecture demonstration. In addition to the above differential measurement which very convincingly demonstrates the failure of Faraday's law this apparatus is also very suitable by connecting one side of the manometer to the atmosphere for measuring the rate of gas evolution singly in any one of the cells.

Our above observations confirm our previous finding that Faraday's law falls short considerably in the electrolysis of water. Such wide discrepancy is difficult to be explained by assuming side reactions, for example, by assuming H_2O_2 formation at anode and reduction of the same at cathode, as suggested by Page and Lingane (1957) to be responsible for small observed deficit in hydrogen oxygen gas coulometer. It appears that with decrease of ionic concentration and current strength, and increase of voltage, the current tends to be carried by a mechanism different from that envisaged by Faraday's law. As to the mechanism of this non-electrolytic conduction, it is recalled that in some crystals as also in solutions of sodium in liquid ammonia partly ionic and partly electronic conduction simultaneously takes place. In water medium the electronic conduction is more likely to be through the intermediacy of charged water molecules, $H_2O^-_{aq}$ and $H_2O^+_{aq}$, particularly as hydrated electron has been shown to exist during electrolysis of sodium sulphate solution by Walker (1966, 1967). However, we prefer to keep the question of detailed mechanism open until more definite evidence is forthcoming. Detailed results with this apparatus will be published later.

Thanks are due to Sri Prithwish Kumar Basu for experimental assistance.

REFERENCES

- Lingane, J. J., 1945, *J. Amer. Chem. Soc.*, **67**, 1916.
Page, J. A. and Lingane, J. J., 1957, *Anal. Chem. Acta*, **16**, 175.
Palit, S. R., 1967, *Indian J. Phys.*, **41**, 309.
Walker, D. C., 1966, *Canad. J. Chem.*, **44**, 2226.
———, 1967, *Quart. Rev.*, **21**, 83.

27

A NOTE ON LONGITUDINAL DISTURBANCES IN A SEMI-INFINITE PIEZOELECTRIC ROD IN A MAGNETIC FIELD

D. K. SINHA

DEPARTMENT OF MATHEMATICS, JADAVPUR UNIVERSITY, CALCUTTA-32, INDIA.

(Received December 6, 1967)

The piezoelectric problems constitute an important branch of study in view of their applications in ultrasonics and acoustics and these problems have been

considered by Sinha (1962, 1963, 1965a, 1965b, 1968a, 1968b) and Das (1967), but these do not take into account the influence of a magnetic field.

The effect of a magnetic field on the disturbances in a piezoelectric material has been, perhaps, studied first by Benes and Soska (1964). The present note is an effort towards to this end and it seeks to investigate the disturbances when a piezoelectric bar is acted upon by a magnetic field. The Laplace transform serves as an important tool for the solution of the problem.

A semi-infinite piezoelectric bar is acted upon by a magnetic field represented by the magnetic induction B in a direction perpendicular to the direction of the bar. To the finite end, taken to be $x = 0$, a time-dependent displacement is applied. Our object is to determine the longitudinal disturbances in the bar that stem from the interplay of mechanical and electromagnetic fields. The fundamental equations are, therefore, given by, vide, Benes and Soska (1964)

$$C_{ijkl} \frac{\partial u_{kl}}{\partial x_j} + \epsilon_{ijk} \left[e_{jrs} \left(\frac{\partial u_{rs}}{\partial t} + \frac{\partial u_{rs}}{\partial x_m} \cdot \frac{\partial u_m}{\partial t} \right) + \epsilon_0 k_{jm} \frac{\partial E_m}{\partial t} \right] = \rho \frac{\partial^2 u_i}{\partial t^2} \quad \dots (1)$$

$$2u_{kl} = \frac{\partial u_k}{\partial x_l} + \frac{\partial u_l}{\partial x_k} \quad \dots (2)$$

where the notations have their usual meanings as in Benes *et al* (1964). For longitudinal disturbances in the direction along the x -axis, with no electric field, the above equations give

$$C_{22} \frac{\partial^2 u}{\partial x^2} - e_{1,2} B \frac{\partial^2 u}{\partial x \partial t} = \rho \frac{\partial^2 u}{\partial t^2} \quad \dots (3)$$

The boundary conditions give $u \rightarrow 0$ as $x \rightarrow \infty$, ... (4)

$$u = P_0 H(t) \text{ at } x = 0 \quad \dots (5)$$

where P_0 is a constant and $H(t)$ is a step function of force, equal to unity when $t > 0$ and equal to zero when $t < 0$.

To solve the problem, let us use the Laplace transform $\bar{f}(p)$ of a function $f(t)$,² of parameter p , given by

$$\bar{f}(p) = \int_0^\infty f(t) e^{-pt} dt \quad (\text{Re}(p) > 0) \quad \dots (6)$$

Taking the Laplace transform of (3), we have

$$C_{22} \frac{\partial^2 \bar{u}}{\partial x^2} - e_{1,2} B p \frac{\partial \bar{u}}{\partial x} - \rho p^2 \bar{u} = 0.$$

The solution of this equation is given by

$$\bar{u} = C_1 e^{+m_1 x} + C_2 e^{+m_2 x} \quad \dots (7)$$

where m_1, m_2 are the roots of the equation

$$C_{22}m^2 - e_{1,2}p B_m - \rho p^2 = 0 \quad \dots (8)$$

The conditions (4) and (5), give $\bar{u} \rightarrow 0$ as $x \rightarrow \infty$... (9)

$$\bar{u} = \frac{P_0}{p} \text{ at } x = 0 \quad \dots (10)$$

Hence (7) yields, on using, (9), $e_1 = 0$

We can write

$$\bar{u} = C_2 e^{-m_2 x}$$

$$m_2 = p \sqrt{e_{1,2}^2 B^2 + 4\rho C_{22}} \text{ where}$$

Using (10), we have

$$\frac{P_0}{p} = C_2$$

Therefore,

$$\bar{u} = \frac{P_0}{p} e^{-p \sqrt{e_{1,2}^2 B^2 + 4\rho C_{22}}}$$

Inverting this transform we have

$$\begin{aligned} u &= 0, \quad 0 < t < \sqrt{e_{1,2}^2 B^2 + \rho C_{22}} \\ &= P_0, \quad t > \sqrt{e_{1,2}^2 B^2 + \rho C_{22}} \end{aligned}$$

which gives the displacement.

REFERENCES

- Benes, F. and Soska, F., 1964, *Czech. Jour. Phys.*, **14**, 188
 Das, N. C., 1967, *Indian J. Phys.*, **41**, 611.
 Sinha, D. K., 1962, *Jour. Acoust. Soc. Amer.*, **34**, 1093.
 ———, 1963, *Ind. Jour. Theor. Phys.*, **11**, 93-99.
 ———, 1965a, *Zeits. Ang. Math. Phys.*, **1**, 411.
 ———, 1965b, *Proc. Natl. Inst. Sci.*, **31**, 395.
 ———, 1968a, *Ind. Jour. Pure. Appld. Phys.*, **5**, 611.
 ———, 1968b, *Czech. Jour. Phys.*, (in Press).

THE CRYSTAL STRUCTURE OF POTASSIUM HYDROGEN FUMARATE, $\text{KC}_4\text{H}_3\text{O}_4$

M. P. GUPTA AND P. K. ROY

DEPARTMENT OF PHYSICS, UNIVERSITY OF RANCHI.

(Received January 3, 1968)

The potassium salts of fumaric acid have been studied by Gupta (1956), Gupta and Barnes (1961). The present work reports the preliminary results of X-ray crystal structure analysis of potassium hydrogen fumarate, $\text{KC}_4\text{H}_3\text{O}_4$. The crystallographic data for the substance are given below and are the same as reported by Gupta and Barnes (*ibid*)

$$a = 6.952 \text{ \AA}, \quad b = 7.483 \text{ \AA}, \quad c = 6.24 \text{ \AA}, \quad \alpha = 107^\circ 05', \quad \beta = 117^\circ 00'$$

$$\gamma = 96^\circ 04', \quad V = 265.5 \text{ \AA}^3, \quad \rho = 1.936 \text{ gm/cm}^3$$

$$Z = 2; \text{ Sp.gr. } P\bar{1}; \quad \mu \text{ linear absorption co-efficient for CuK}\alpha = 82.0 \text{ cm}^{-1}$$

Reflexions of the type okl , hol , hko , $h\bar{l}\bar{l}$ and $hk\bar{h}$ were collected using small single crystals and Weissenberg normal beam zero layer photography around appropriate crystallographic axes. Intensities were estimated visually. There was some difficulty initially in locating the potassium atoms from the Patterson projections but once they were located, the heavy atom technique was adopted and after normal Fourier methods had been exhausted, least squares refinement of the experimental data was undertaken, using only an overall isotropic temperature factor and unit weights. Figure below gives a view of the structure as looking down the $[100]$ axis.

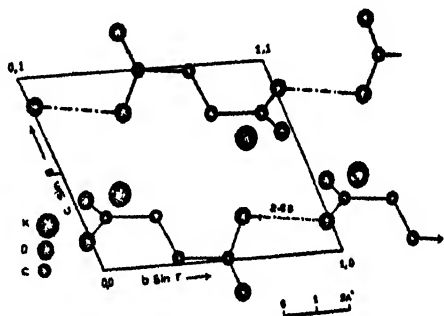


Fig. 1

R factors after several cycles of least squares refinements are

$$R(okl) \ 14.5; \ R(hol) \ 14.0; \ R(hko) \ 16.5; \ R(h\bar{l}\bar{l}) \ 16.2;$$

The bond lengths and angles of the fumarate group are similar to those reported for fumaric acid (Brown 1966, Post *et al*, 1966). The interesting features of the structure, however, are as follows :

(1) The fumarate group, unlike in the fumaric acid structure, is non-planar, one of the two carboxyl groups being twisted by as much as 35° out of the plane of the rest of the atoms.

(2) Hydrogen bonding of 2.63\AA between two adjacent molecules, forming an extensive chain of molecules inside the crystal. The hydrogen bonds, moreover, are between two oxygen atoms, both of which are of the type $\text{OH}\dots\text{OH}$ (i.e. longer of the two C-O bonds in a COOH group) and this situation is similar to that observed in the structure of bisphenylacetate, $(\text{C}_6\text{H}_5\text{CH}_2\text{COO})_2\text{HK}$, (Speakman 1949, Bacon and Curry 1957).

(3) A five-fold co-ordination of oxygen atoms around the metal ion with K^+-O distances ranging from 2.74\AA to 3.03\AA . The surrounding of the metal ions by the oxygen atoms provides for combinations of distorted octahedra and tetrahedra.

As the result (1) and (2) above have interesting points of stereochemistry and packing to settle, further work is being done to refine the structure using complete three dimensional data. As this may take some time, we are publishing here the essential features of this crystal structure and we believe that these results are not likely to be modified to any marked extent even after a full three dimensional analysis.

REFERENCES

- Bacon, G. E. and Curry, N. A., 1957, *Acta. Cryst.*, **10**, 524.
 Bednowitz, A. L. and Post, B., 1966, *Acta. Cryst.*, **21**, 566.
 Brown, C. J., 1966, *Acta. Cryst.*, **21**, 1.
 Gupta, M. P., 1956, *Acta. Cryst.*, **9**, 263.
 Gupta, M. P. and Barnes, W. H., 1961, *Canad. J. of Chem.*, **39**, 1739.
 Speakman, J. C., 1949, *J. Chem. Soc.*, 3357.

29

COSMIC RAY FLUXES AT DIFFERENT ZENITH ANGLES

SAMIR GHOSH AND SIMA SENGUPTA

PHYSICAL LABORATORY, PRESIDENCY COLLEGE, CALCUTTA, INDIA.

(Received July 14, 1967 ; Resubmitted October 6, 1967).

An experiment has been performed to find out the variation of integral cosmic-ray fluxes with zenith angles. The geographical co-ordinates at the place of measurement are Lat. $22^\circ 34'\text{N}$, Long. $88^\circ 24'\text{E}$ and height from sea-level is 20 ft.

A four-fold Geiger-Müller counter telescope has been utilized for this purpose and the fluxes have been recorded by a four-fold coincidence circuit. The counter telescope has been placed under a thin Aluminium foil of 0.06 mm thickness.

The telescope has been given a rotation of 180° degrees from East to West at small steps of zenith angles. The probabilities of fluxes at different zenith angles have been plotted in fig. 1.

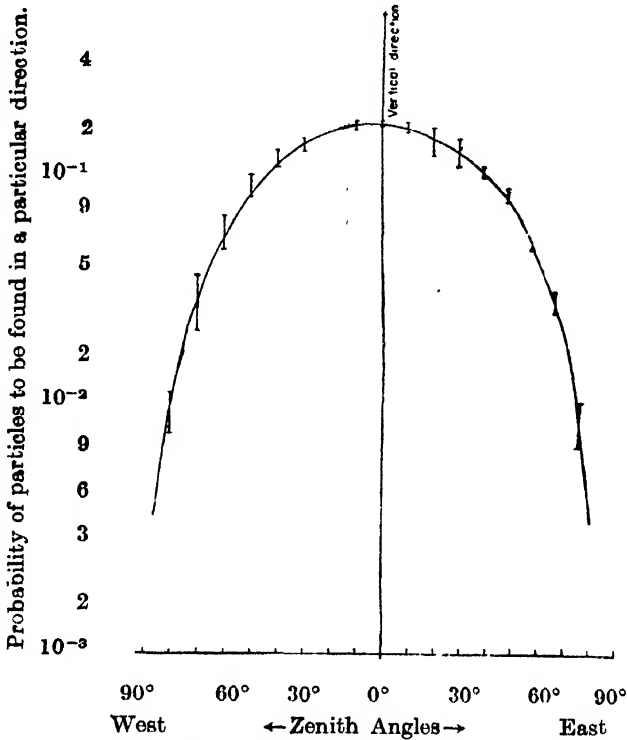


Fig. 1. Probabilities of fluxes against zenith angles.

The data presented by Allen and Apostolakis (Allen, 1961) on the variation of cosmic-ray fluxes with zenith angles in between 65° and 85° corresponds to our experimental data for the same region. They have measured particles of the momentum region 1 GeV/c to 100 GeV/c. But in our case the momenta of the particles recorded are 25 MeV/c and above. This shows that the variation of cosmic-ray fluxes with zenith angles does not differ for the momentum region 25 MeV/c to 1 GeV/c and 1 GeV/c to 100 GeV/c. The experimental data shows that nearly 80% of the cosmic-ray particles research the sea-level at the directions lying in between 0° and 40° degrees zenithal angles. Above 40° degrees the flux drops down very fast with increase of angles.

On the basis of the above experimental data the vertical, as well as, different directional components of cosmic-rays can be obtained from the total count by a single counter used in some experiments. The total solid angle covered by the counter is to be found out for obtaining the directional fluxes.

We offer our sincere thanks to Prof. Dr. R. L. Sen Gupta for his encouragement.

REFERENCE

Allen, J. E. and Apostolakis, A. J., 1961, *Proc. Royal Soc., A*, VI, 365, 117-132.

BOOK REVIEWS

MECHANICS OF MATERIALS—by Prof. Seibert Fairman and Prof. Chester S. Cutshell, John Wiley & Sons, Inc., New York. Price \$ 14.95.

The book was first published in the year 1953 and the fourth reprint, which was given for review, came out in the year 1963.

The basic elements of the subject have been carefully selected and incorporated in the book giving complete first course in Strength of Materials.

The book will be very helpful to the students. Many worked out typical problems, to explain the theory, have been included to make it more interesting to the students.

The book deals very lucidly the chapter on deflection of beams, specially the area moment method, and the statically indeterminate beams. The chapter of combined stresses given at the end gives a better understanding of the subject matter to the students.

It is a well planned and well written text book. The unit used in the book is F.P.S. system.

G.C.S.

THE STATISTICAL THEORY OF NON-EQUILIBRIUM PROCESS IN A PLASMA—by Yu. L. Klimontovich, Pergamon Press, 1967. Pp. xv+284. Price 70sh net.

This is an English edition of the original Russian text by Dr. Klimontovich, published by Moscow State University in 1964. The major portion of the material in the book was presented earlier in lectures at the Mechanics and Mathematics Faculty of the University. It should, however, be noted that the present translation by H. S. H. Massey and O. M. Blunn under the editorship of D. Ter Haar incorporates, to its credit, corrections and revisions supplied by the author in 1966.

The book treats the statistical theory of processes in a plasma in terms of equations relating to the microscopic phase densities of each component of the plasma and the microscopic strengths of the electric and magnetic fields. The author starts with a closed system of equations for the random functions of the microscopic quantities, and the problem boils down to determining the moments of the functions. The approximation of the first two moments is mainly dealt with.

The author's approach leads to considerable simplification of the solution of a number of problems in as much as the resulting system of equations in this method is much simpler than the system of very complex equations for the distribution functions of the co-ordinates and momenta of both the particle and the field oscillator.

The book has, under its purview, kinetic equations in the self-consistent field approximation as well as correlation and spectral functions for a spatially uniform or non-uniform plasma. A chapter is devoted to kinetic equations and spectral functions, taking into account the radiation by plasma waves. The first chapter which is of a subsidiary nature presents Maxwell's equations for slow and fast processes while the last chapter gives a hydrodynamic description of processes in a plasma.

Although the treatment, as mentioned by the author in the Introduction, is not exhaustive, it covers quite a wide range of topics in plasma theory by a unified method. The book

can be recommended to students specialising in plasma physics; it is a must for those who intend to work on statistical theories of a plasma.

J.B.

MAGNETOHYDRODYNAMICS—By Andrey Gennadievich Kulikovskiy and Grigoriy Aleksandrovich Lyubimov. Translated from the Russian by Scripta Technica, Inc. (Technical Editor: Ludwig Oster, Yale University, New Haven).

The competent book on the newly developing subject of Magnetohydrodynamics is a valuable addition to the existing texts on the subject. The book presents in a well organised manner the subject of Magnetohydrodynamics. The authors deal with the basic principles of electrodynamics in an elegant manner and proceed ahead introducing the basic equation of fluid dynamics. The conservation laws in writing the equation are emphasised. The authors have given good application of the equation and presented the solution of some solvable problems. It is very instructive to learn the techniques and the way of handling the equation of Magnetofluid-dynamics. The chapters on shock waves in Magnetohydrodynamics and further treatment of propagation of weak shock waves and the structure of shock waves give a clear description of the subject. The book can serve a good text for a student entering in this field for the first time.

The Scripta Technica and its technical Editor are to be thanked for making a valuable book like this available to English knowing workers in the field.

A.C.B.

PLASMA DYNAMICS—edited by F. H. Clauser, 1960. Addison-Wesley Publishing Company, Inc. Pp. ix+369. List Price 12.50 dollars.

The book is an edited version of the proceedings of an international symposium on plasma dynamics, held at Massachusetts, USA in June 1958. The symposium, in which quite a few renowned scientists took part, covered the many-sidedness of plasma dynamics, as reflected in the fields of thermonuclear physics, gas discharges, electron beam dynamics, statistical mechanics, fluid mechanics, aerodynamics and astrophysics; all the aspects have, naturally been reproduced in the symposium volume, which thus presents plasma dynamics in a very broad and integrated manner.

Each chapter of the volume is based on an introductory speech, followed by discussions, discourses and comments. That plasma dynamics is a living and intriguing subject is aptly borne out by a number of contradictory views.

As the symposium was meant for experts, the volume might appear, to a non-specialist, somewhat sketchy, lacking in details. However, by way of compensation, the interested reader would find a long list of references in the bibliography, which is of particular help because of its topicwise arrangement.

J.B.

GAMMA-RAYS OF NUCLIDES IN ORDER OF INCREASING ENERGY—By D. N. Slater. Published by Butterworths, London, 1962. Price 45sh.

During the last decade identification and description of the members of gamma-ray emitting nuclides have proceeded at an enormous pace. Knowledge of their individual characteristics have been classified and reported in several journals and Nuclear data tables. However a periodic census is necessary to keep the active research workers abreast of the new developments in the field. The compilation of the present volume is such a census. It provides a list of energies of gamma-rays emitted by radio-nuclides, arranged in order of

increasing magnitude. It has been prepared particularly to assist in the identification and elucidation of the gamma-scintillation spectra. The author has based his compilation upon some predecessors^{1,2,3,4}. He has also selected "preferred values" of gamma-ray energies (in Mev) from the Table of Isotopes of Strominger *et al*¹. This has simplified the compilation to a remarkable extent. On the other hand if he had emphasized the discrepancies they might have served as a stimulus for new work.

The classification of entries in the table are the following :

- (a) Photon-energy (Mev), arranged in order of increasing magnitude.
- (b) Nuclides (including metastable existed states).
- (c) Half-life.
- (d) Modes of formation.
- (e) Percent abundance of relevant stable isotope.
- (f) Thermal neutron activation cross-section (Barns) or Fission yield.
- (g) Per cent abundance of gamma-radiation.
- (h) Genetic relationship.

The book would be a very useful manual for the gamma-ray spectroscopists in particular. The printing and get up of the volume are excellent.

S.D.C.

1. Strominger, D., Hollander, J. M. and Seaborg, G. T., *Revs. Modern Phys.*, **30**, No. 2, Part 2, April, 1958.
2. Crouthanel, C. E. *Applied Gamma-ray Spectrometry*. Pergamon Press, 1960.
3. Hollander, J. M., Perimen, I. and Seaborg, G. T., *Revs. Modern Phys.*, **25**, 1953, 469.
4. Bainbridge, K. T. and Nier, A. O., *Nat. Res. Coun. Nuclear Energy Ser.*, Prelim. Rep. No. 9, Dec., 1950.

INDIAN JOURNAL OF PHYSICS

VOL. 41

No. 11

AND

VOL. 50

PROCEEDINGS

No. 11

OF THE

INDIAN ASSOCIATION FOR THE CULTIVATION OF SCIENCE

(Edited in collaboration with the Indian Physical Society).

NOVEMBER 1967

PUBLISHED BY THE
INDIAN ASSOCIATION FOR THE CULTIVATION OF SCIENCE
JADAVPUR, CALCUTTA-32

INVESTIGATION OF THERMIONIC EMISSION AT LOW INTENSITY WITH A GEIGER COUNTER

R. C. SASTRI AND S. D. CHATTERJEE

DEPARTMENT OF PHYSICS, JADAVPUR UNIVERSITY, CALCUTTA-32, INDIA.

(Received April 10, 1967)

ABSTRACT. An attempt has been made to investigate thermionic emission at low intensities by counting the individual electrons with a Geiger counter. In the first case, a Geiger counter with its axial anode wire is heated to serve as an electron emitter. Subsequently, a heated offset wire parallel to the axial wire anode is operated as an electron emitter. In either case, Richardson's thermionic emission equation is verified while the lowest figure of the thermionic current density measured is 3 electrons/cm². sec.

INTRODUCTION

All the methods of investigating thermionic emission reported before have been based on measurements of integral emission current. The lowest limit of thermionic current density measured is that due to Germer (1925). Working between the temperature range of 1440°K and 2475°K, he measured a variation of current from 10^{-15} amp. to 10^{-4} amp. A current of 10^{-15} amp. is equivalent to an emission of approximately 6×10^3 electrons/cm².sec. Furthermore, with most substances the current cannot be measured on a sensitive galvanometer at temperatures below 1000°C. In order to explore thermionic emission phenomena in the region of comparatively low temperatures it is imperative that individual electrons should be counted. The simplest equipment for such an exigency is the Geiger counter. Since the Geiger counter is a gas filled device the effect of gaseous atmosphere on thermionic emission from a filament, of say tungsten, becomes important. Langmuir (1913, 1914) investigated the effect of different gases on the emission of tungsten at about 2000°C. The gases experimented with, included hydrogen, water vapour, oxygen, nitrogen and argon. His investigations revealed that the presence of argon did not alter appreciably the values of the Richardson constants of the emitter. The only effect of argon when present in a small quantity is to facilitate the attainment of saturation through the action of positive ions, formed by impact ionization, in reducing the effect of mutual repulsion of electrons. No doubt when the pressure of the argon is appreciable the current will be magnified owing to the ionization by collisions, but the effect would be of importance in the detection of individual electrons. It is natural, therefore, to expect that the behaviour of other inert gases would be analogous to that of argon. Consequently, there is a reasonable prospect of studying thermionic emission with the help of a non-selfquenching Geiger counter filled with an inert gas at an appropriate pressure. The self-quenching counters, however,

with a mixture of argon and organic vapour, would change the values of the thermionic emission constants. Such an effect has indeed been observed by Ettinger and Móscicki (1962). Nevertheless, either types of counters may be used for the study of low temperature emission of electrons.

This paper describes the detection of thermal electrons from a hot tungsten wire anode in a Geiger counter. A further modification in which a heated offset wire parallel to the axial wire anode served as an electron emitter is also reported. In both these cases Richardson's thermionic emission equation is verified. An attempt was also made to operate a Geiger counter with reversed potentials, viz., by using the axial wire as a cathode. An account of this investigation will form the subject matter of a subsequent communication.

THERMIONIC EMISSION FROM A HOT TUNGSTEN WIRE ANODE

It is well known that a Geiger counter can detect an ionizing event if it can release a single electron anywhere within the sensitive volume of the counter. Thus, a Geiger counter should be able to detect thermal electrons if they are produced within the sensitive volume of the counter.

In a thermionic vacuum tube of cylindrical geometry, the heating current of the axial wire generates a magnetic field of heating current which may, as Richardson (1914) suggested, play an important role, sometimes effectively preventing electrons from reaching the anode, even with a high potential. Hull (1926) found that electrons are deflected in the direction of the electron current in the wire and describe elongated cycloidal paths. However, the effect is small with filaments of ordinary size, and is masked by the relatively enormous effect of the accelerating radial voltage gradient.

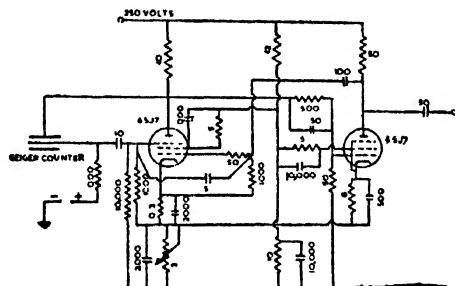
With applied potentials reversed the radial voltage gradient exerts a retarding force on the electrons, preventing them from reaching the cylindrical anode. Thus, a Geiger counter, with a heated axial filament, may be likened to a unidirectional gas filled device. Nevertheless, it does respond to the emission of individual electrons from the heated filament. This is so, because the cycloidal return path traversed by the emitted electron in the vicinity of the wire produces a Townsend avalanche culminating in a Geiger pulse.

EXPERIMENTAL CONSIDERATIONS AND RESULTS

The experimental arrangement adopted for the study of thermionic emission with a Geiger counter, the hot tungsten anode wire serving as the thermal electron emitter is shown in block diagram in fig. 1. It consisted of a Geiger counter, an insulated battery to heat electrically the axial anode wire, Maier-Leibnitz's quenching circuit and a scaler. The Geiger counter consisted of a copper cathode having a diameter 1.5 cms. and length 6 cms. A fine wire of tungsten having a diameter of 4 mil served as the axial anode which was heated to produce thermal

The diagram illustrates the electronic circuit components and their interconnections. An insulated battery provides power to the O.M. counter and the H.L. gyrovacuum circuit. The O.M. counter is also connected to an H.T. supply and a variable resistor R. The H.L. gyrovacuum circuit is connected to a scaler.

counter voltage was supplied from an electronically stabilised H.T. supply unit. Fig. 2 shows details of Maier-Leibnitz's quenching circuit which was used for quenching the Geiger counter. This circuit works on the multivibrator principles but uses two different grids of input tube for the signal and the regenerative feed back. The discharge pulse of the counter excites the quenching circuit to one



oscillation during which the counting voltage is kept below the threshold and the counter has time to recover. At the end of the oscillation (after about 0.2 millisecond) the counter voltage and all other voltages of the circuit are restored rapidly to their initial values. Thus, the next count can take place under exactly the same conditions as the first. The output pulses of the quenching unit are all equal and no discharge occurs in the Geiger counter while the quenching circuit is unable to quench them. The output pulses from the M.L. quenching unit, were fed to a scaler for registration of the pulses. The temperature of the heated anode wire was determined by the resistance measurement of the anode wire with the help of a potentiometer which was calibrated against a standard cell (Weston type D-550-B).

As the temperature of the axial wire was gradually increased there was a progressive increase in pulse size till the counter stepped into the region of stabilized corona.

To arrive at a reasonable understanding of what happens within the volume of the Geiger counter when the thin axial wire is being heated it may be assumed that the radiation and convection effects are negligible and the radial temperature distribution may be determined by the steady state conduction process alone. In the steady state we have $\nabla T = 0$ and for a radial distribution of temperature

$$\frac{1}{r} \frac{d}{dr} \left(r \frac{dT}{dr} \right) = 0 \quad \dots (1)$$

solving for T , we get

$$T = C \log_e r + B \quad \dots (2)$$

where C and B are constants.

Assuming that the cylinder remains, more or less, at the room temperature, so that $T = T_0$ at $r = b$ (the radius of the cylinder) and $T = T_1$, at $r = a$ (the radius of the axial wire), the temperature at any point r , from the axis of the cylinder is, therefore, given by

$$T(r) = \alpha \log_e r + \beta \quad \dots (3)$$

where, α and β are determinable constants.

There is also slight increase in pressure of the gas within the counter volume. The pressure is independent of r . But the gas density $n(r)$ is given by

$$n(r) = P/T(r) \quad \dots (4)$$

Around the axial wire in the Townsend avalanche region which is of the order of 5 wire radii there is a considerable attenuation of the gas density. This lowers the threshold potential of the counter which manifests itself as an increase in overvoltage of the counter for the existing potential distribution.

An explanation for the enhancement of the overvoltage due to the attenuation of the density of the gaseous mixture in the neighbourhood of wire may be sought in the fact that Paschen's law governs at least roughly all spark-breakdown phenomena. Thus V_c , the starting potential of corona or glow may be taken as governed by Paschen's law which may be given by the function equation

$$f \left(\frac{V_c}{P\delta} \right) = \frac{1}{P\delta} \log \frac{1}{\phi(V_c/P\delta)} \quad \dots (5)$$

It may be seen that on the basis of the above equation V_c the starting potential is a function of P

$$\text{i.e. } V_c = F(P\delta) \quad \dots (6)$$

This has been found experimentally to be true. It was indeed discovered experimentally by Paschen (1889), and was proved theoretically by Townsend (1915), Schumann (1923) and Thomson (1933) on general considerations irrespective of

the mechanism assumed. It is obvious that it holds for uniform or non-uniform fields caused by gap geometry.

The physical interpretation of this law is relatively simple. The product $P\delta$ represents in essence the number of molecules to be encountered by an ion or an electron crossing the gap. This number, as with all applications of Avagadro's law depends primarily on gas density and not on pressure alone. Hence one can really insert $\rho\delta$ for $P\delta$ in the Paschen's law equation, where ρ is the gas density. Hence, where temperature is varied in the vicinity of the wire by electrically heating the same the value of V_c becomes a function of $\rho\delta$. Since the electric field remains, more or less constant, the attenuation of ρ in the vicinity of the axial wire, lowers the value of V_c , which is the starting potential for stabilized corona. In other words, the entire Geiger region is shifted towards the lower voltage side and the threshold potential for Geiger action is correspondingly lowered. Such a situation implies that the Geiger counter is being operated at higher overvoltage than previously. Thus the operation of lowering the density of the enclosed gas in the vicinity of the wire is really equivalent to the enhancement of the operating voltage under normal conditions

It is, therefore, required that the potential across the counter had sometimes to be lowered to confine its range of operation within the Geiger region as the temperature of axial anode wire was gradually raised to produce an adequate

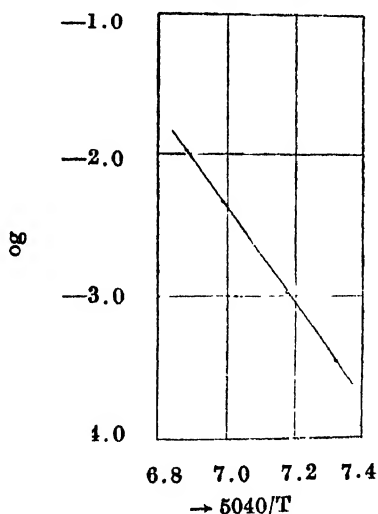


Fig. 3. Richardson's plot for the hot tungsten wire anode in a self quenching Geiger counter.

number of thermal electrons. It was further noted that the plateau of Geiger counter was consistently shortened as a result of the attenuation of the density of the enclosed gas in the vicinity of the wire. A probable deterioration of the plateau on account of an axial thermal gradient was indeed pointed out by McCutchen (1956) on theoretical considerations. The preliminary experiments on thermionic emission were performed simultaneously with a self-quenching counter and

with a pure gas (argon) filled counter. The results obtained are shown in tables 1 and 2.

TABLE 1

Thermionic emission from a Tungsten wire with a self-quenching counter

T (in °K)	N (Number of counts per minute)	$5040/T$	N/T^2	ϕ (in eV)	A (amp./cm ² . degree ²)	Remarks
688	166	7.324	3.506×10^{-4}	3.39	50.2	Area of the emitting surface not well de- fined.
702	533	7.180	1.081×10^{-3}			
721	2454	6.990	4.722×10^{-3}	3.39	50.2	Area of the emitting surface not well de- fined.
732	5795	6.885	1.081×10^{-2}			

Note : (1) $5040/T = 1 \text{ eV}/kT \log_{10}$ where k is the Boltzmann constant.

(2) The results have been confined to low temperature measurements of thermionic emission because of deadtime difficulties encountered at higher temperatures.

TABLE 2

Thermionic emission from a tungsten wire with a non-selfquenching counter

T (in °K)	N (Number of counts per minute)	$5040/T$	N/T^2	ϕ (in eV)	A (amp./cm ² . degree ²)	Remarks
915	101	5.508	1.179×10^{-4}	4.62	71.8	Area of the emitting surface not well de- fined.
931	286	5.414	3.301×10^{-4}			
953	1142	5.287	1.257×10^{-3}			
965	2336	5.223	2.509×10^{-3}			

Note : (1) $5040/T = 1 \text{ eV}/kT \log_{10}$ where k is the Boltzmann constant.

(2) The results have been confined to low temperature measurements of thermionic emission because of deadtime difficulties encountered at higher temperatures.

A plot of $\log_{10} N/T^2$ versus $5040/T$, where N/T^2 is the number of counts per minute per degree squared and T the corresponding temperature of the axial anode wire in degrees absolute yielded a straight line satisfying the Richardson's thermionic emission equation. The work function for tungsten as calculated from the slope of the plots (figs 3 and 4) was 3.39 eV in a selfquenching counter and 4.62 eV in an argon filled counter.

Looking at the results it seems likely that in the first case the unexpected lowering of the normal work function in a retarding field may be due to the presence of adsorbed layers of the selfquenching vapour on the surface of the axial anode wire. However, in the case of pure argon filled non-selfquenching counter, the work function of tungsten anode is higher. The higher value may be consistent with Schottky's mirror image theory.

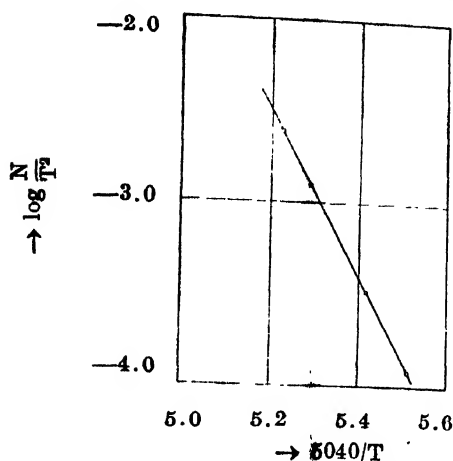


Fig. 4. Richardson's plot for the hot tungsten wire anode in a non-selfquenching Geiger counter.

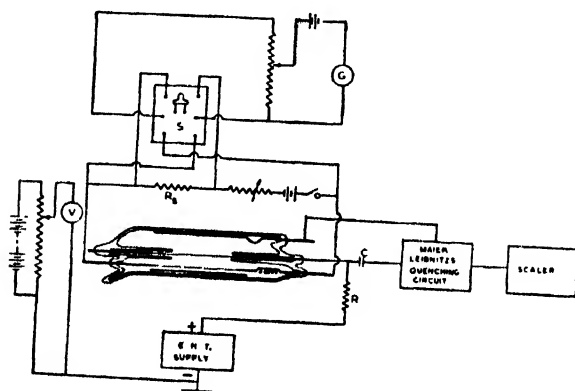


Fig. 5. Schematic diagram of the experimental arrangement for the study of thermionic emission (using an offset wire as thermal electron emitter).

THERMIONIC EMISSION FROM A HEATED OFFSET WIRE IN A GEIGER COUNTER

An analysis of the experimental results presented above indicates that a normal Geiger counter, with a heated anode wire is not well suited for a study of thermionic emission for the following reasons.

(1) the emitted electrons cannot escape against a retarding field; they return back to the heated anode.

(2) the radial thermal gradient surrounding the axial anode attenuates the density of the filling gas in its vicinity resulting in the enhancement of the neighbouring field gradient and proneness to continuous discharge.

In order to circumvent these difficulties a new counter was fabricated with an extra offset wire parallel to the axial wire anode. The offset wire was electrically heated to serve as electron emitter. It was usually maintained at a

potential, appropriate for its location within the existing field distribution, by means of an auxiliary battery. However, it did not make much difference in measurement when the offset wire was kept floating while being heated by an independent battery.

EXPERIMENTAL ARRANGEMENT AND RESULTS

Fig. 5 depicts schematically the experimental arrangement adopted for the study of thermionic emission using an offset wire in a Geiger counter as the thermal electron emitter. The offset wire was heated electrically by an insulated storage battery. The other components of the circuit consisted of a standard resistor (1ohm), a potentiometer, an adjustable voltage source, an E.H.T. supply for the Geiger counter, Maier-Leibnitz's quenching circuit and a scaler. The modified Geiger counter consisted of a pyrex glass tube envelope of diameter 3.8 cms. whose inner surface was coated with aquadag to form the cylindrical cathode of length 8 cms. The axial tungsten wire had a diameter of 0.1 mm. spotwelded on either side to thick tungsten leads, which in turn were sealed into protecting glass tubes and were available for electrical connections. The offset wire for producing thermal electrons had a diameter of 0.15 mm. and was stretched parallel to the axial anode wire. One end of the offset wire was spotwelded to a tungsten rod while the other end was spotwelded to another tungsten rod via a small tungsten spring to keep the offset wire taut while being heated.

The necessity of keeping the diameter of the offset wire somewhat thicker than the axial wire was dictated by circumstances which led to the simultaneous appearance of an image inverted pulse superimposed on a normal Geiger pulse at the axial wire terminal, as reported earlier by the authors (Sastri *et al*, 1967).

The counting portion of the counter for thermal electrons was confined to a length of 4.5 cms. by providing suitable glass tubes at the end of the axial anode wire. Both the offset wire and the axial anode wire were flashed in high vacuum while the counter was being evacuated, in order to smoothen the asperities on the surface. The counter was filled at 11cms. Hg pressure with 10 cms. argon stated to be "spectroscopically pure" and 1 cm. of hydrogen. The gaseous mixture was introduced into the counter after passing through traps immersed in liquid nitrogen. Maier-Leibnitz's quenching circuit (fig. 2) was used for quenching the Geiger counter. The output pulses from the M.L. quenching unit were fed to a scaler for registration of pulses. From an auxiliary voltage source, polarisation potential adjusted to the free wire potential in the electrostatic field of the counter, was applied to the offset wire with the help of a voltmeter. The temperature of the offset wire was determined by the resistance measurement as mentioned above.

Measurements were taken in the temperature range of 841°K to 934°K. The results obtained are presented in the table 3. It may be seen from this table that the counts due to thermal electrons varied from 40 per minute at 841°K

to 18,880 per minute at 934°K. The former count gives the lowest figure of the thermionic current density measured as equivalent to 3 electrons/cm².sec. at a temperature of 841°K.

Fig. 6 shows the Richardson's plot $\log_{10} N/T^2$ versus $5040/T$, where N/T^2 is the number of counts per minute per degree squared and T the corresponding

TABLE 3
Thermionic emission from a heated offset wire in Geiger counter

Temp. (in °K)	N (Number of counts per minute)	$5040/T$	N/T^2	ϕ (in eV)	A (amp./cm ² . degree ²)	Remarks
841	40	5.992	5.656×10^{-5}			
852	88	5.916	1.213×10^{-4}			
864	210	5.833	2.813×10^{-4}			
882	700	5.714	8.997×10^{-4}	4.33	62.2	Area of the emitting surface not well de- fined.
904	2945	5.575	3.602×10^{-3}			
921	8670	5.471	1.022×10^{-2}			
934	18880	5.396	2.165×10^{-2}			

temperature of the offset wire in degree absolute. The work function for tungsten as calculated from the slope of the plot is 4.33 eV, which compares not unfavourably

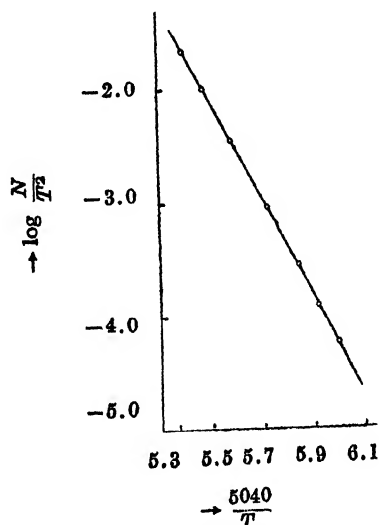


Fig. 6. Richardson's plot for the emission of electrons from a heated offset wire of tungsten. with the accepted value of 4.54 eV. The slight diminution of work function may perhaps be attributed to the presence of hydrogen in the gaseous mixture.

For instance, Weissler and Wilson (1953) have reported a diminution in work function of the order of 0.5 eV in hydrogen or nitrogen atmosphere whereas the inert gases produced no change at all employing Oatley's contact potential method of measurement.

Although the present investigation is more or less of a qualitative and introductory character, it is expected that further refinement in measurement and technique, employing an anti-coincidence method for the elimination of the cosmic ray background, would improve the accuracy of measurement at lower temperature by at least one order of magnitude.

Further investigations have been carried out on the energy distribution of thermionically emitted electrons with the modified form of the counter operating in the proportional region. The results will be reported in a future communication.

REFERENCES

- Ettinger, K. W. and Mscicki, W., 1962, *Acta Phys. Polon. (Poland)*, **22**, 129.
Germer, L. H., 1925, *Phys. Rev.*, **25**, 795.
Hull, A. W., 1925, *Phys. Rev.*, **25**, 645.
Langmuir, I., 1913, *Phys. Rev.*, **2**, 450.
1914, *Phys. Zeits.*, **15**, 518.
McCutchen, C. W., 1956, *Rev. Sci. Inst.*, **27**, 106.
Paschen, F., 1889, *Wied. Ann.*, **37**, 69.
Richardson, O. W., 1914, *Proc. Roy. Soc. Sec., A*, **90**, 174.
Sastri, R. C. and Chatterjee, S. D., 1967, *Indian J. Phys.*, **41**, 147.
Schumann, W. O., 1923, *Durchbruchfeldstärke von Gasen*, Springer Verlag, Berlin, p. 51 and 114.
Thomson, J. J., 1933, *Conduction of Electricity through gases*, vol. 2, Cambridge, p. 486.
Townsend, J. S., 1915, *Electricity in gases*, Oxford, p. 327 and 380.
Weissler, G. L. and Wilson, T. N., 1953, *J. Appl. Phys.*, **24**, 472.

ELECTRICAL AND THERMAL PROPERTIES OF PbTe DOPED WITH MAGNETIC IMPURITIES*

K. S. V. L. NARASIMHAN AND K. P. SINHA

NATIONAL CHEMICAL LABORATORY, POONA 8, INDIA.

(Received April 8, 1967)

ABSTRACT. Thermoelectric power, thermal conductivity and electrical resistivity of p -type PbTe doped with iron, manganese, tellurium and n -type PbTe doped with gadolinium and manganese are reported. Iron acts as donor or acceptor depending on the impurity concentration. Manganese was found to be a donor dopant. The variation of these parameters with temperature is discussed. The resistance was found to behave in an anomalous manner both in the pure as well as doped p -type specimens. The possible causes of the observed behaviour in these systems are discussed.

INTRODUCTION

There has been considerable interest in the thermoelectric properties of PbTe , because of its value in power generation. Present day interest in thermoelectricity is to obtain a high figure of merit by incorporating suitable impurities. The studies have been hitherto confined to non-magnetic impurities. The presence of paramagnetic impurities may, however, drastically alter carrier concentration and influence other physical properties such as thermal conductivity, thermoelectric power and electrical resistivity (Narasimhan *et al*, 1965).

In the present paper we report the thermoelectric properties of p - and n -type PbTe doped with paramagnetic and neutral impurities. The possible causes of the observed anomalous resistance of p -type PbTe are also discussed.

METHOD OF PREPARATION OF SPECIMEN AND MEASUREMENT

Lead (A. E. C. Trombay), tellurium, iron, manganese and gadolinium were all spectroscopically pure (as supplied by Johnson and Mathey). The elements were taken in their proper proportions and heated at a temperature of 1000°C for 24 hours in an evacuated silica tube and quenched at 800°C . The homogeneous regions tested by thermoelectric probing were cut off and pressed to form cylindrical pellets. The pellets so prepared (usually of length 12 mm and diameter 10 mm) were sintered in vacuum at a temperature of 650°C for 24 hours. These sintered blocks were nickel plated at the two ends and used for measurement.

Communications Nos. 1024 and 1056 from the National Chemical Laboratory, Poona 8, India.

For preparing the doped samples the required quantity of the dopant was added to PbTe and the compound remelted. The same treatment as mentioned for the undoped compound was given.

The measurements of thermoelectric power, electrical conductivity and thermal conductivity were carried out by means of z meter technique (Harman 1958, Harman *et al* 1959). The details of the apparatus and measurement are discussed elsewhere (Narasimhan 1967).

RESULTS AND DISCUSSION

The results of each system are discussed separately.

PbTe doped with iron

The variations of thermoelectric power, thermal conductivity and resistivity with temperature are shown in table 1.

When p -type PbTe was doped with iron the conductivity changed from p -type to n -type depending on the concentration of the dopant. When 0.1 at. % iron is added to p -type PbTe the thermoelectric power (α) changed its sign relative to that for the pure system. On increasing the concentration of iron to 0.5 at % thermoelectric power increases to a large value while the sample remained n -type.

The change in the sign of thermoelectric power on adding iron may be due to donor action of iron. Iron atoms go into the solution as iron telluride (probably as FeTe_2). These iron telluride molecules substitute for the PbTe molecules thereby vacant sites are created. Atoms from lead excess occupy these vacant sites and as the valence electrons of the lead atoms are not involved in chemical bonding they are easily ionized to the conduction band. This mechanism by which impurity atoms dope is responsible for the n -type conductivity. Increasing the concentration of lead leads to substitution of more and more PbTe molecules and increase of electron concentration. On the other hand large increase of added dopant leads to p -type conductivity. This may be explained in the following way. In a crystal there are always certain number of lead and tellurium ion vacancies. On adding small concentration of iron, the lead vacancies created are filled up by the excess lead atoms, thereby maintaining in equilibrium the concentration of lead vacancies. If the vacancies created by the iron atoms is large compared to the excess lead atoms present then the number of lead vacancies are more than the tellurium vacancies. The tellurium atoms surrounding these lead vacancies have two electrons less which they take up from the environment and thus the holes are created (Kobayashi *et al* 1964). Somewhat similar situation exists in Bi_2Te_3 also (Ainsworth 1956). Excess bismuth atom gives n -type conduction, whereas, limited excess concentration leads to hole conductivity.

Fritts (1960) observed that iron acts like a neutral impurity in PbTe. Brebrick *et al* (1962), on the other hand, found that iron acts like a low lying donor from his measurements on Te saturated PbTe doped with iron. However, the thermoelectric properties of these doped compounds have not been reported.

The thermoelectric power decreases on adding 0.1 at. % iron but increases to a large value at 0.5 at % iron additions. At higher concentrations the number of electrons also increases because originally we have a *p*-type semiconductor and we are adding *n*-type impurity. This results in the compensation of acceptors and when the donor concentration is large we have enough donors to give sufficient electrons to observe a high thermoelectric power. At 2 at. % iron concentrations, as discussed above, iron acts like an acceptor and hence increase in the concentration of holes and large thermopowers.

Thermal conductivity (*K*) decreases on adding iron. This decrease is perhaps due to the scattering of phonons by the added impurities. We can calculate the scattering crosssection for the impurity atom by using Ioffe's formula (Ioffe *et al* 1960). According to this

$$\frac{K_{L(0)}}{K_L} = 1 + \frac{N}{N_0} \cdot \theta \cdot \frac{l_{T(0)}}{a}$$

where *N* is the addition concentration, *N*₀ is the total atomic concentration, *a* is the distance between two neighbouring atoms in the lattice, *l*_{*T*(0)} is the mean free path of the phonon in the undoped specimen, *θ* is the factor in the expression *S* = *θa*² where *S* is the scattering cross section. *K*_{*L*} and *K*_{*L*(0)} are the lattice thermal conductivity with and without addition of second component. *l*_{*T*(0)} can be calculated by using the kinetic formula

$$K_L = \frac{1}{3} C_V \bar{V} l_{T(0)}$$

where *C_V* is the specific heat per unit volume and *V̄* is group velocity of phonon. The value of *C_V*, *a* and *V̄* were taken from the table of Ioffe *et al* (1960). *K_L* was calculated by subtracting the electronic component of thermal conductivity from the measured thermal conductivity by utilizing the Weidemann-Franz ratio. The values of *θ* so calculated are shown in table 2. The value of the scattering cross section is higher at 273.1°K than at room temperature.

The resistivity of all the *p*-type samples and one of the *n*-type sample viz., PbTe doped with 0.1 at. % iron showed increase of resistivity with decrease of temperature. Putley (1955) observed this type of behaviour in his *p*-type samples and suggested that these may be due to the presence of impurity levels situated at 0.1 eV above the valence band. He observed this behaviour in five of the *p*-type samples and in one of his *n*-type samples S21C also. In *n*-type PbTe the impurity level is considered to be situated at 0.1 eV from the conduction band.

Shogenji *et al* (1957) reported that a sample of *p*-type PbTe heat treated with copper showed the anomalous resistivity behaviour. Kanai *et al* (1957) have also reported that a sample of *p*-type PbTe exhibited this anomalous behaviour. In all these cases the Seebeck coefficient was not reported. In the present measurements the type of conductivity was judged only by the Seebeck coefficient measurement. There was no change of sign observed throughout the temperature range investigated. It is most likely that Hall coefficient will also behave in a similar way.

The possibility of spurious voltage was tested. The solder was scrapped off and the sample resoldered and the measurements repeated. No changes in the original behaviour were observed. After cooling to liquid air temperature the sample was brought to room temperature. The resistivity was showing the initial value. Hence these observed anomalies are not due to any spurious voltages.

Scanlon (1959) found that a sample of PbS coated with sulphur vapour showed Hall coefficient reversal similar to those of Putley (1955) and Shogenji *et al* (1957). This second sign reversal was observed in the extrinsic region. Scanlon (1959) attributed these to *p*—*n* junction, in which an *n*-type sample is covered on all the surface with a *p*-type layer. In the present measurements, however, no heat treatment was given to form *p*—*n* junction. It is interesting to note that only in *p*-type PbTe such a behaviour was observed. When *p*-type PbTe was doped sufficiently with a donor to make it *n*-type, the anomaly was lost and the resistivity decreased with decrease of temperature. Also, *n*-type lead telluride prepared by taking 0.2 at. % excess lead did not show the resistance anomaly. Moreover, the treatment given to *p*-type PbTe and *n*-type PbTe was identical and it seems unlikely that the anomaly observed in *p*-type PbTe is due to the presence of *p*—*n* layers. A conclusive test was carried out to find out the presence of *p*—*n* layers. The samples exhibiting the anomaly were scraped on both the lateral sides to remove some layers. The thermoelectric probe was moved throughout the surface to find out *p*—*n* layers. The experiment was repeated for each mm layer removed on both the end as well as lateral sides. There was no change of sign of the cold end terminal. The hot probe has to be connected to the $-ve$ terminal and the cold end to the $+ve$ terminal for current to flow. This proved conclusively that there are no *p*—*n* layers.

This suggests that there are impurity levels situated in the forbidden gap and the scattering of carriers by the impurity atoms is important. The appearance of anomaly in *p*-type PbTe shows that impurity levels are near the valence band and form acceptor levels. From the slopes of log resistivity against temperature the energy levels of the impurity atom is calculated. We assume that the increase of resistivity with decrease of temperature is due to the electrons falling back into the valence band thereby reducing the concentration of holes. The impurity levels in general are situated at 0.1 eV. The value of energy gap_A was found to

be 0.1 eV as derived on the assumption that there is no compensation and the concentration of donor atoms is very small. The reason as to why n -type PbTe do not exhibit the resistance anomaly is that the acceptor levels are all compensated by the donors and with decrease of temperature the resistance decreases because of the interaction of carriers with phonons becoming small.

p-type PbTe-Te

The variations of thermoelectric properties as a function of excess tellurium were studied with a view to finding an optimum composition which gives high figure of merit. The doping was carried upto 5 at. % excess tellurium. Thermoelectric power remains nearly the same with increasing concentration of tellurium. Excess tellurium atoms occupy the tellurium vacancies and accept the electrons from the neighbouring atoms and thus induce p -type conductivity. Fairly high concentration of excess tellurium may be introduced into PbTe depending on the heat treatment. The solubility of excess Pb or Te in PbTe is not more than one hundredth of one percent in pure samples. By quenching at elevated temperatures it should, however, be possible to introduce large excess. Since all the samples in the present measurements are quenched at 800°C it is likely that large excess could be incorporated. Fritts (1960) observed that any precipitation of excess phase will lead to increase in resistivity at room temperature. For the highly doped sample i.e. 5 at. % excess tellurium an increase in the resistivity was observed at room temperature (fig. 1). It is likely that in this sample some tellurium has precipitated out and these rejected tellurium atoms have collected at dislocations during freezing.

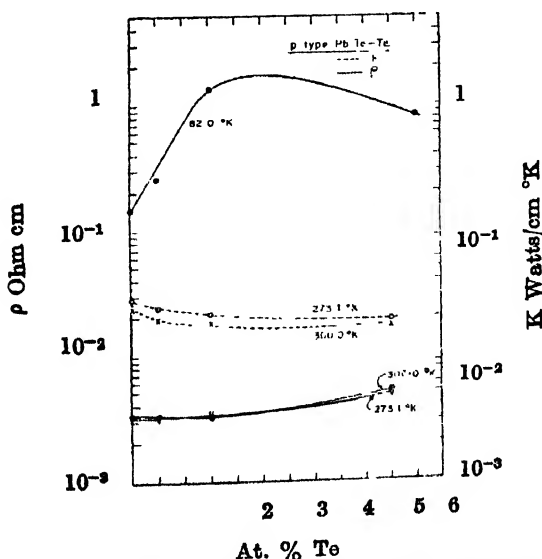


Fig. 1. Variation of electrical resistivity (ρ) and thermal conductivity (K) for various concentrations of tellurium doped on p -type PbTe.

Thermal conductivity decreases (fig. 1) with increasing concentration of excess tellurium due to the scattering of phonons by tellurium impurities. The value of scattering cross section is shown in table 2. The figure of merit is highest for the sample doped with 0.5 at. % Te showing thereby that at this concentration we have effected a decrease in thermal conductivity without affecting the resistivity.

p-type PbTe-Mn

Manganese is a donor dopant in PbTe. Owing to this, thermoelectric power changes sign and becomes negative.

The low values of thermoelectric power (table 3) suggest the onset of degeneracy and the resistivity increase observed is due to impurity scattering of carriers. In view of the high concentration of manganese added X-ray powder pattern was analysed to find out the presence of second phase. The specimen was found to be quite homogeneous and no extra lines from the impurity atom could be found.

n-type PbTe-Gd

n-type PbTe was prepared by taking 0.1 at % excess lead over the stoichiometric composition. To this various amounts of gadolinium were added. The results of the measurement are shown in the figures. Figs. 2, 3 and 4 show the variation of thermoelectric power, thermal conductivity and electrical resistivity as a function of impurity additions at various temperatures.

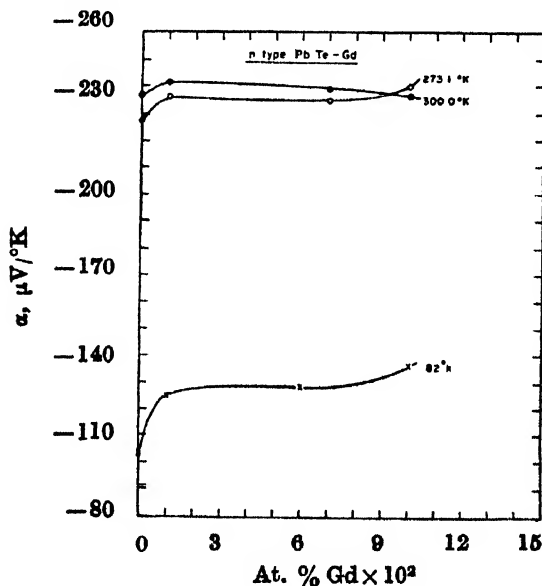


Fig. 2. Variation of thermoelectric power of *n*-type PbTe doped with various concentrations of Gd at different temperatures.

In the undoped specimen thermoelectric power decreases with decrease of temperature as is expected from the theory. The increase in the value of thermoelectric power at low temperatures with increasing gadolinium concentration may

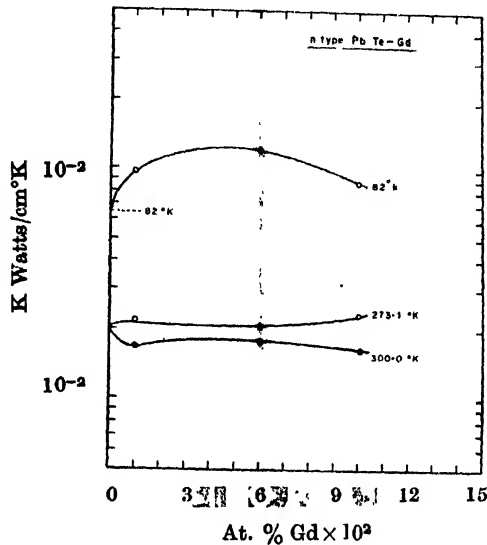


Fig. 3. Variation of thermal conductivity of *n*-type PbTe doped with various concentrations of added Gd at different temperatures.

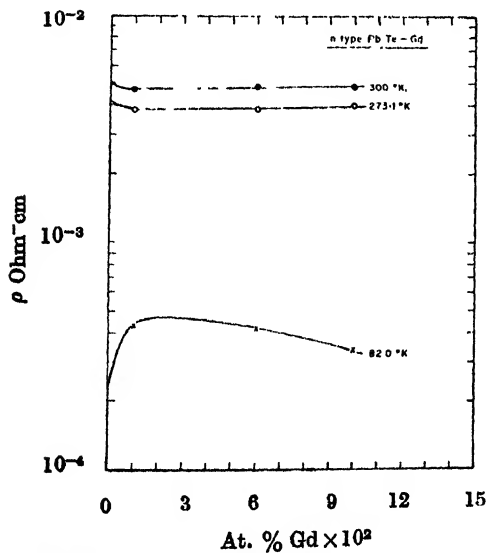


Fig. 4. Variation of resistivity of *n*-type PbTe doped with various concentrations of gadolinium at different temperatures.

be due to the increase in the value of r in the expression for thermoelectric power (α)

$$\alpha = \pm \frac{k_B}{e} \left(A + \ln \frac{2(2\pi m k_B T)^{3/2}}{h^3 n} \right) \quad \dots (1)$$

where k_B is Boltzmann constant, $A = r+2$; r depends on electron scattering mechanism. With increasing concentration of gadolinium, the scattering of electrons increases. Alternatively, gadolinium acts like a trapping centre for holes leading to the increase in the thermoelectric power of electrons.

The undoped specimen has a $T^{-2.5}$ dependence on mobility. If we consider the acoustic mode lattice scattering then the mobility should have a $T^{-3/2}$ dependence. Perhaps this deviation could be explained if we considered a mixture of acoustic and optic mode scattering and interband transition of charge carriers, effected by these. Based on these assumptions Krishnamurthy *et al.* (1965) arrived at an expression

$$\mu = \mu_{(0)}^{(0)} T^{-5/2} \quad \dots (2)$$

where $\mu_{(0)}^{(0)}$ is the temperature independent factor. In this formulation two phonon processes involving one acoustic and one optical phonon and two optical phonons were considered. The agreement with the experimental result suggests that interband transition and both acoustic and optic mode scattering effects are important for the scattering mechanism in PbTe and other compound semiconductors.

For the doped samples, the mobility has a $T^{-1.0}$ and $T^{-2.0}$ dependence which may be due to the onset of impurity effects. In another paper Krishnamurthy *et al.*, (1966) have given a general expression incorporating two-phonon processes and one phonon impurity induced processes. The total mobility has the form

$$\mu_t = \frac{\mu_0^{(s)} \mu_0^{(0)} T^{-5/2}}{\mu_0^{(0)} T^{-1} + \mu_0^{(s)}} \quad \dots (3)$$

Thus for $\mu_0^{(0)} T^{-1} \gg \mu_0^{(s)}$, the mobility $\mu_t = \mu_0^{(0)} T^{-3/2}$ and for reverse condition $\mu_t = \mu_0^{(s)} T^{-5/2}$. It is clear that in the intermediate regions the exponents on temperature will have values ranging from -1.5 to -2.5 depending on the relative magnitudes of the terms in the denominator.

Thermal conductivity shows an increase with increasing gadolinium additions at 82°K (fig. 3). For the same reason the temperature variation of thermal conductivity in the case of doped samples have much stronger temperature

Table 1
Variation of thermal conductivity, thermoelectric power and electrical resistivity of p-type PbTe doped with iron

Sample No.	Composition	Thermal conductivity			Resistivity ohm cm			Thermoelectric power $\mu\text{V}/^\circ\text{K}$		
		300°K	273.1°K	82°K	300°K	273.1°K	82°K	300°K	273.1°K	82°K
17	Undoped PbTe	2.35×10^{-2}	2.89×10^{-2}	—	(see Table III)			171	185	53
54	0.1 at. % iron	—	—	—	9.64×10^{-2}	1.25×10^{-1}	9.92×10^{-1}	—53	—65	—63
53	0.5 at. % iron	1.71×10^{-2}	1.86×10^{-2}	7.05×10^{-2}	1.04×10^{-2}	8.5×10^{-2}	1.3×10^{-3}	—308	—311	—145
52	1 at. % iron	2.09×10^{-2}	3.17×10^{-2}	—	3.3×10^{-3}	2.3×10^1	1.39×10^{-3}	205	192	86
44	2 at % iron	1.84×10^{-2}	1.96×10^{-2}	—	4.11×10^{-2}	5.19×10^{-2}	4.29	296	326	121

dependence. The undoped specimen has a T^{-1} dependence in agreement with theory (Peierls 1929).

n-type PbTe-Mn

The variations of thermoelectric power and electrical resistivity are shown in figs. 5 and 6. The resistivity increases with impurity concentration with their atoms causing electron scattering leading to a decrease in mobility. But beyond

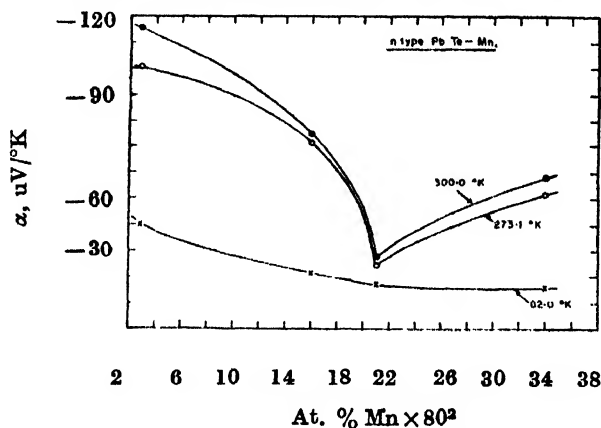


Fig. 5. Variation of thermoelectric power of *n*-type PbTe doped with various concentrations of Mn at different temperatures.

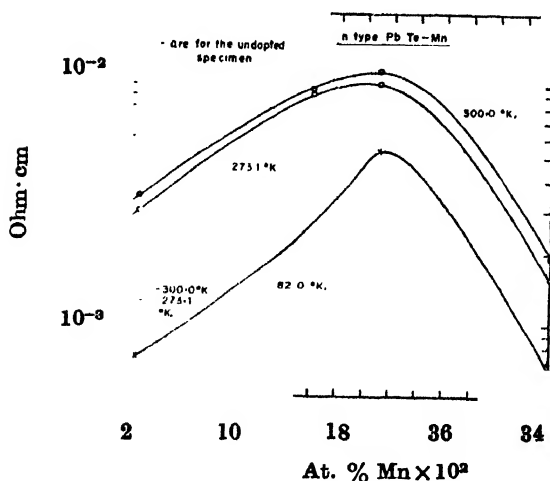


Fig. 6. Variation of electrical resistivity of *n*-type PbTe doped with various concentrations of Mn at different temperatures.

(at 82°K pure *n*-type PbTe has a ρ value 1.34×10^{-4} ohm cm.)

a particular concentration the donor electrons from the impurity atoms lead to increase in electronic conductivity. Thermoelectric power variation with temperature in the case of highly doped sample shows the onset of degeneracy.

The slope of temperature dependence of conductivity decreases in magnitude as the concentration is increased. The experimental curves in most of the cases have T^{-1} dependence. This is perhaps due to the combined effect of impurity and phonon (optical and acoustical) scattering effects.

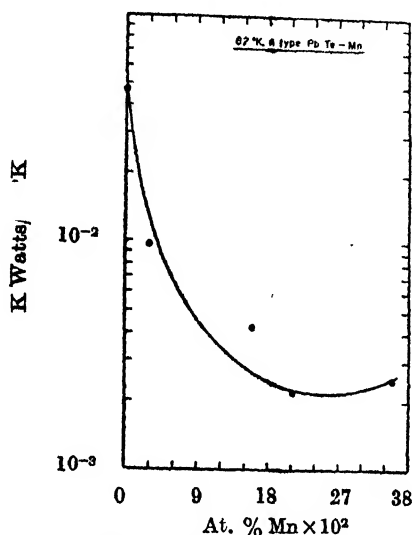


Fig. 7. Variation of thermal conductivity of *p*-type PbTe for various concentrations of Mn at 82°K.

Table 2

Values of the parameter θ and energy gap for various doped samples of *p*-type PbTe.

Sample No.	300°K (θ)	273.1°K (θ)	Energy gap from a plot of $\ln\rho^*$ vs $1/T$
Undoped PbTe	—	—	0.08 eV
53 0.5 at. % iron	9.2	11.0	—
52 1 at. % iron	1.9	—	0.09 eV
44 2 at. % iron	1.4	2.1	0.09 eV
16 10 at. % manganese	6.6	23.8	—
48 0.5 at. % excess Te	6.0	4.6	0.01 eV
50 1.5 at. % excess Te	2.8	3.2	0.13 eV
51 5 at. % excess Te	0.9	1.1	0.13 eV

* ρ is the electrical resistivity.

Large reduction in the value of thermal conductivity (fig. 7) at 82°K suggests large scattering cross section for the impurity atom. This may be due

Table 3
Resistivity and thermoelectric power of p-type PbTe doped with tellurium and manganese

Sample No.	Composition	Resistivity ohm cm.			Thermoelectric power $\mu\text{V}/^\circ\text{K}$		
		300°K	273.1°K	82°K	300°K	273.1°K	82°K
17	PbTe (undoped)	3.3×10^{-3}	3.3×10^{-3}	1.49×10^{-1}	171	185	53
48	0.5 at. % excess tellurium	3.3×10^{-3}	3.2×10^{-3}	2.58×10^{-1}	189	189	86
50	1.5 at. % excess tellurium	3.3×10^{-3}	3.4×10^{-3}	1.324	175	164	62
51	5 at. % excess tellurium	5.1×10^{-3}	4.9×10^{-3}	8.23×10^{-1}	197	184	61
16	10 at. % manganese	1.26×10^{-1}	1.19×10^{-1}	4.59×10^{-2}	-2	-3	-5

Ainsworth, L., 1956, *Proc. Phys. Soc.*, **B** 9, 606.
 Brebrick, R. F. and Grubner, I., 1962, *J. Chem. Phys.*, **3**, 1283.
 Fritts, R. W., 1960, *Thermoelectric Materials and Devices*, Ed. Cadoff and Miller.
 Harman, T. C., 1958, *J. Appl. Phys.*, **29**, 1373.
 Harman, T. C., Cahn, J. H. and Logan, M. J., 1959, *J. Appl. Phys.*, **30**, 1351.
 Ioffe, A. V. and Ioffe, A. F., 1960, *Sovt. Phys. Solid State*, **2**, 719.
 Kanai, Y. and Nii, R., 1957, *J. Phys. Soc. Japan*, **12**, 441.
 Klemmens, P. G., 1957, *Proc. Roy. Soc.*, **208**, 108.
 Kobayashi, A., Sato, Y. and Fujimoto, M., 1964, *Proc. Inter. Conf. on Semiconductors*,
 Paris, p. 1257.
 Krishnamurthy, B. S. and Sinha, K. P., 1965, *J. Phys. Chem., Solids*, **2**, 1949.
 , 1966, *J. Phys. Chem. Solids*, **27**, 629.
 Narasimhan, K. S. V. L. and Sinha, K. P., 1965, *Ind. J. Pure and Appl. Phys.*, **3**, 221.
 Narasimha, K. S. V. L., 1967, *Ind. J. Pure and Appl. Phys.*, **5**, 281.
 Peierls, R., 1929, *Ann. Physik*, **3**, 1055.
 Putley, E. H., 1955, *Proc. Phys. Soc.*, **B** 8, 22.
 Scanlon, W. W., 1959, *Solid State Physics*, Vol. 9, Academic Press, New York.
 Shogenji, K. and Uchiyama, 1957, *J. Phys. Soc. Japan*, **12**, 431.

S-WAVE NEUTRON STRENGTH FUNCTION, POTENTIAL SCATTERING RADIUS AND THE OPTICAL MODEL

CHHAYA GANGULY AND N. C. SIL,

DEPARTMENT OF THEORETICAL PHYSICS, INDIAN ASSOCIATION FOR THE CULTIVATION OF SCIENCE, JADAVPUR, CALCUTTA-32, INDIA.

(Received March 30, 1967)

ABSTRACT. The S -wave neutron strength function $\frac{\bar{\Gamma}_n^0}{D}$ and the potential scattering radius R' have been studied using spherical optical model potential with (i) pure surface absorption and (ii) combined volume and surface absorption. The numerical results have been plotted against mass numbers over the region $A = 40$ to $A = 200$ and have been compared with the experimental data.

INTRODUCTION

The nuclear optical model has been found to give satisfactory explanation in predicting the resonance behaviour of S -wave neutron strength function $\frac{\bar{\Gamma}_n^0}{D}$, the average ratio of neutron width to average level spacing, with respect to atomic mass at low energies. The neutron strength function is a measure of the average cross section for formation of the compound nucleus in the low energy phenomena. The earliest calculations (Feshbach *et al*, 1954) have been carried out with spherically symmetric complex potential of the simple square well form and the ratio shows enhanced rises near mass numbers $A \sim 55$ and $A \sim 155$ and a minimum around $A \sim 100$. Though a qualitative agreement has been obtained between the theoretical prediction and the actual measured values but the agreement unsatisfactory quantitatively since the theoretical results give more sharp and narrow resonances and more pronounced dip of $\frac{\bar{\Gamma}_n^0}{D}$ with the variation of mass numbers when compared with the experimental findings. However, later investigations (Feshbach, 1958) with realistic, diffused potentials of Woods-Saxon type (1954), with the same form of uniform radial distribution of the real and imaginary part, have reproduced the giant resonances fairly well showing better agreement with experiment. But there still remain two major discrepancies to be explained. One of these concerns the peak near $A \sim 155$ where the experimental curve seems to be much broader, lower and more irregular than the theoretical curve and indicates the existence of two small peaks. The other discrepancy has been noticed close to the valley between the resonances where the values of the strength

function predicted by theory are considerably high in comparison with the observed data.

As regards the first difficulty it has been suggested that the non-spherical shape of target nuclei in the region $140 < A < 190$ should be taken into account in order to avoid the marked disagreement with experimental observations. Investigations by many authors (Margolis *et al* 1957; Chase *et al*, 1958 and Jain 1964) have shown successfully that the aspherical nature of nuclear structure has a tendency to break the giant resonance into a number of resonances, thereby improving the agreement with experiment.

To eliminate the second difficulty the interesting suggestion to introduce enhanced surface absorption in place of volume absorption has already been put forward and several attempts have been made to clarify the point. For low incident energies the absorption may be taken to be concentrated mainly in nuclear surface rather than distributed uniformly over the entire nucleus because of the weakened effect of Pauli exclusion principle in the surface region and this is represented by the surface peaked radial distribution of the imaginary potential (Harada *et al*; 1959)

In the present work we have investigated the detailed structure of $\frac{\bar{\Gamma}_n^0}{D}$ and potential scattering length R' taking into account (i) pure surface absorption and (ii) combined volume and surface absorption. The numerical results of our theoretical calculations which are based on the analytical expressions of $\frac{\bar{\Gamma}_n^0}{D}$ (normalised to 1 ev) and R' given in our previous note (Ganguly *et al*, 1966) are plotted against mass numbers over the region $A = 40$ to $A = 200$ for comparison with experimental data.

Our results are in agreement with the calculation of Khanna and Tang (1959), Fiedeldey and Frahn (1961) and Jain (1964) and support the argument that surface concentration of the imaginary potential lowers the value of the strength function in the region $90 < A < 130$ thereby bringing the results in closer agreement with experiment. We disagree with the conclusions of Elagin *et al* (1962) who failed to reproduce any new effect due to surface absorbing potential beyond that for pure volume absorption.

THEORY

The radial wave equation for the scattering of S-wave neutrons is given by

$$\frac{d^2 u_0}{dr^2} + \left[k^2 - \frac{2m}{\hbar^2} V(r) \right] u_0(r) = 0 \quad \dots (1)$$

where $V(r)$ is the interaction potential and $k^2 = \frac{2mE_n}{\hbar^2}$, m and E_n being respec-

tively the mass and energy of the incident neutron. The wave function $u = r\psi$ satisfies the necessary boundary conditions for the scattering problem at $r = 0$ and $r \rightarrow \infty$. In the asymptotic region, $r \rightarrow \infty$ the radial solution as a combination of incoming and outgoing waves is given for $l = 0$

$$u_0(r) = G[u_0^{(-)}(r) - S_0 u_0^{(+)}(r)] \quad \dots (2)$$

where G is a constant.

At sufficient low neutron energies the scattering amplitude S_0 averaged over resonances according to Feshbach, Porter and Weisskopf (1954) has the value

$$S_0 = e^{-2ikR'} \left(1 - \frac{\pi \bar{\Gamma}_n}{D} \right) \quad \dots (3)$$

where R' is a length of the order of magnitude of the nuclear radius and is a slowly varying function of the energy.

Hence for

$$kR' \ll 1$$

$$\frac{\bar{\Gamma}_n^0}{D} = \frac{1}{\pi} \operatorname{Re} (1 - S_0) \quad \dots (4)$$

$$kR' = \frac{1}{2} \operatorname{Im} (1 - S_0) \quad \dots (5)$$

The averaged cross sections of scattering and absorption are related to $\frac{\bar{\Gamma}_n^0}{D}$ and R' as follow :

$$\sigma_{sc} = \frac{\pi}{k^2} |1 - S_0|^2 \approx 4\pi R'^2 \quad (6a)$$

$$\sigma_a = \frac{\pi}{k^2} \left(1 - |S_0|^2 \right) \approx \frac{2\pi^2}{k^2} \frac{\bar{\Gamma}_n}{D} \quad \dots (6b)$$

We choose the neutron-nucleus potential to be of the form

$$V(r) = - \left[(V_0 + iW_0) \frac{1}{1 + e^{\frac{(r-R)}{a}}} + 4iW_1 \frac{e^{\frac{(r-R)}{a}}}{[1 + e^{\frac{(r-R)}{a}}]^2} \right] \quad \dots (7)$$

where a is the diffusivity parameter and the radius parameter R' is assumed as $R = 1.25A^{1/3}$. Corresponding to this form of nuclear potential which takes care of both volume and surface absorption we have derived (1966) the following expression for S -wave neutron strength function normalised to 1 ev and potential scattering radius R'

$$\frac{\bar{\Gamma}_n^0}{D} = - \frac{2k_0 a}{\pi} \operatorname{Im} (Q) \quad \dots (8)$$

$$R' = R + 2\gamma a + a \operatorname{Re} (Q) \quad \dots (9)$$

where γ is Euler's constant and the complex quantity Q is given by

$$Q = [\psi(\lambda_0 + \mu) + \psi(-\lambda_0 + \mu)] + \pi.$$

$$\left[\left(\frac{b}{1+b} \right)^{\lambda_0} F\left(\lambda_0 + \mu, 1 + \lambda_0 - \mu, 1 + 2\lambda_0; \frac{b}{1+b}\right) \frac{\Gamma(1-2\lambda_0)}{\Gamma(1-\lambda_0-\mu)\Gamma(-\lambda_0+\mu)} \right.$$

$$\cot. \{\pi(\lambda_0 + \mu)\} - \left(\frac{b}{1+b} \right)^{-\lambda_0} F\left(-\lambda_0 + \mu, 1 - \lambda_0 - \mu, 1 - 2\lambda_0; \frac{b}{1+b}\right)$$

$$\frac{\Gamma(1+2\lambda_0)}{\Gamma(1+\lambda_0-\mu)\Gamma(\lambda_0+\mu)} \cot. \{\pi(-\lambda_0 + \mu)\}$$

$$\left[\left(\frac{b}{1+b} \right)^{\lambda_0} F\left(\lambda_0 + \mu, 1 + \lambda_0 - \mu, 1 + 2\lambda_0; \frac{b}{1+b}\right) \frac{\Gamma(1-2\lambda_0)}{\Gamma(1-\lambda_0-\mu)\Gamma(-\lambda_0+\mu)} \right.$$

$$\left. - \left(\frac{b}{1+b} \right)^{-\lambda_0} F\left(-\lambda_0 + \mu, 1 - \lambda_0 - \mu, 1 - 2\lambda_0; \frac{b}{1+b}\right) \frac{\Gamma(1+2\lambda_0)}{\Gamma(1+\lambda_0-\mu)\Gamma(\lambda_0+\mu)} \right]$$

in which $\lambda = \pm[-a^2(k^2 + p^2)]^{\frac{1}{2}}$, $\mu = \frac{1}{2} \pm \frac{1}{2}[1 + 4a^2q^2]^{\frac{1}{2}}$

$$p^2 = \frac{2m}{\hbar^2}(V_0 + iW_0), q^2 = \frac{2m}{\hbar^2}(iW_1), b = \exp(-R/a) \text{ and}$$

λ_0 is the value of λ at $k = 0$ F denoting hypergeometric functions.

For numerical computation we note that $b \ll 1$ in the range of mass numbers we are interested so that the hypergeometric functions reduce to 1 and

$$\left(\frac{b}{1+b} \right)^{\pm\lambda_0} \approx e^{\mp i p R}$$

RESULTS AND DISCUSSION

Fig. 1 and 2 give the calculated values of $\frac{\bar{\Gamma}_n^0}{D}$ and R' respectively plotted against

mass numbers in the region $A = 40$ to $A = 200$ for different shapes of the imaginary potential, for comparison the corresponding experimental data (as given in the paper of Perey *et al.*, 1962) are also shown. The values of our parameters are the same as given by Jain (1964) viz.

$$V_0 = 52 \text{ Mev}, a = 0.52 \text{ fm and } R = 1.25A^{1/3} \text{ fm.}$$

W has been suitably chosen by us as $W = 3.5$ Mev for pure surface absorption and $W_0 = W_1 = 2.30$ Mev for volume plus surface absorption. We have taken the same diffusivity parameter for both the real and imaginary parts of the potential.

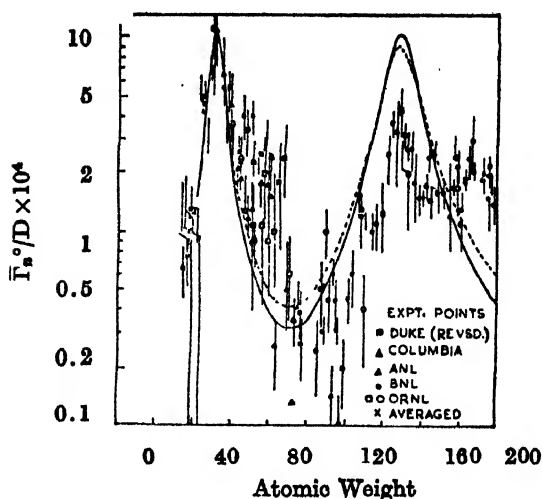


Fig. 1. Calculated values of S -wave neutron strength function, $\bar{\Gamma}_s^0/D$ as a function of mass number, compared with experimental data. The solid curve is for pure surface absorption and the dotted curve corresponds to combined volume and surface absorption.

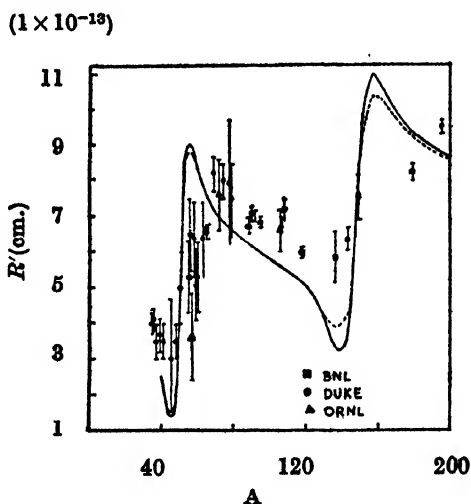


Fig. 2. Calculated potential scattering radius R' as a function of mass number compared with experiment. The solid curve and dotted curve correspond to pure surface absorption and combined volume and surface absorption respectively.

In order to show the effect of surface absorption on the strength function we compare cases of pure surface absorption and combined volume and surface absorption, the real part of the potential being taken to be of Woods—Saxon type with the same parameters for all the calculations. Neutron strength function in the case of pure volume absorption with uniform radial distribution of Woods-Saxon type has been investigated by many authors (Feshbach, 1958 : Ghosh

et al, 1961) and found to be in fair agreement with experimental data near the giant resonance $A \sim 50$ while at the minimum the theoretical values are significantly higher than the measured values.

In fig. 1, we have kept the peak heights at $A \sim 50$ almost the same in both the cases of pure surface absorption and volume plus surface absorption by adjusting the strength of the imaginary potential while all other potential parameters left unchanged. We have found that the diminution of the strength of the imaginary potential lowers the value of minima and raises the heights of the peaks simultaneously while the opposite results are obtained when the strength is increased. The main effect of surface absorption has been shown in the vicinity of the minimum at $A \sim 91$ where the calculated values of $\frac{\bar{\Gamma}_n^0}{D}$ are smaller in the case of pure surface absorption compared with that in the case of combined volume and surface absorption. The two maxima of $\frac{\bar{\Gamma}_n^0}{D}$ in the case of pure surface absorption are equal in height on account of the periodicity of our expression for $\frac{\bar{\Gamma}_n^0}{D}$ in R unlike the case for volume plus surface absorption (also for pure volume absorption). As regards the second maximum at $A \sim 148$ we notice that unlike the theoretical curve the experimental curve indicates the existence of two small peaks rather than a smooth peak and the measured points are more irregular, lower and scattered. This disagreement may be explained by taking into account the deformed structure of nuclei in that region.

The fig. 2 gives the results of theoretical calculations for R' , the potential scattering radius, compared with the experimental data (as quoted by Perey *et al*, 1962). We see that the theoretical curve for pure surface absorption gives deeper minima and higher maxima than that for combined volume and surface absorption. The agreement with experiment is fairly good in the region $A = 40$ to 150. The results of calculations with combined volume and surface absorption give somewhat better agreement with experiment than those with pure surface absorption. Above $A = 150$ the theoretical curves deviate much from experimental findings, the discrepancy may be due to aspherical shape of nuclei in that region.

We wish to thank Professor D. Basu for his many helpful discussions.

REFERENCES

- Chase, D. M., Wilets, L. and Edmonds, A., 1958, *Phys. Rev.*, **110**, 1080.
 Elagin, Yu. P., Lyulka, V. A. and Nemirovskii, P. E., 1962, *Soviet Phys. JETP*, **14** 682.
 Feahbach, H., Porter, C. and Weisskopf, V. F., 1954, *Phys. Rev.*, **9**, 448.

- Feshbach, H., 1958, *Annual Rev. of Nuclear Science*, **8**, 88.
Fiedeldey, H. and Frahn, W. E., 1962, *Nucl. Phys.*, **38**, 686.
Ganguly, C. and Sil, N. C., 1966, *Indian J. Phys.*, **40**, 623.
Ghosh, A. and Dutta, S. K., 1961, *Indian J. Phys.*, **35**, 550.
Harada, K. and Oda, N., 1959, *Progr. Theor. Phys.*, **21**, 260.
Jain, A. P., 1964, *Nucl. Phys.*, **50**, 157.
Khanna, F. C. and Tang, Y. C., 1959, *Nucl. Phys.*, **15**, 337.
Margolis, B. and Troubetzkoy, E. S., 1957, *Phys. Rev.*, **106**, 105.
Perey, F. and Buck, B., 1962, *Nucl. Phys.*, **32**, 353.
Woods, R. D. and Saxon, D. S., 1954, *Phys. Rev.*, **95**, 577.

INTERMOLECULAR FORCES AND VISCOSITY OF SOME POLAR ORGANIC VAPOURS

ARUN K. PAL

INDIAN ASSOCIATION FOR THE CULTIVATION OF SCIENCE, CALCUTTA-32.

(Received March 23, 1967)

ABSTRACT. Viscosity of several polar organic vapours has been measured by a precision all-metal oscillating-disc viscometer, over the temperature range 30°–200°C and below a pressure of 10 cm Hg. The results have been utilised to obtain some significant information on inter-molecular forces in these substances.

INTRODUCTION

Amongst transport properties like thermal conductivity and thermal diffusion, viscosity is not significantly affected by inelastic collisions. This property, with the recent improvements in the techniques (Kestin *et al*, 1959; Flynn *et al*, 1963) can be measured very accurately. Consequently, temperature dependence of viscosity is one of the most important sources of information regarding inter-molecular forces in polyatomic gases. For polar gases a further complication in the intermolecular forces is the angle-dependent dipole-dipole interaction. In order to have precise knowledge of intermolecular forces in polar gases we have taken up a programme for the measurement of viscosity of these gases over a range of temperatures. In this paper we have reported the viscosity data for three polar organic vapours, viz. diethyl ether, ethyl acetate and *ter*-butyl alcohol over the temperature range 30°–200°C.

EXPERIMENTAL

The viscosity was measured by an all-metal oscillating-disc viscometer similar in design to that of Kestin and Leidenfrost (1959). The apparatus together with its accessories have been described in detail by Pal *et al* (1967). At low densities it is possible to calculate viscosity from the following simple expression, (Clifton, 1963),

$$\eta = C^{-1}[(\lambda/\tau) - (\lambda_0/\tau_0)], \quad \dots (1)$$

where η is the viscosity of the gas, λ , λ_0 and τ , τ_0 are the logarithmic decrements and time periods of oscillation in the gas and vacuum respectively and C is a constant of the apparatus. In order to determine the constant C , H_2 and N_2 were taken as the calibrating gases (purity better than 99.95%). The viscosity data for these gases were taken from the best available sources (Barua *et al*, 1964, Kestin

et al, 1963). Diethyl ether, ethyl acetate and ter-butyl alcohol were of analytical reagent standard and were distilled and dried by specific drying agents. The reproducibility of dampings were within 0.1% and the overall accuracy of our measurements should be well within 1%.

The viscosity values for these polar gases have been recorded in table 1. Previous viscosity data are available only for diethyl ether. For this substance the present data are 7-8% lower than those reported by Titani (1933) in the higher temperature range. In the lower temperature range as well (upto 77.8°C) our values are 4-5% lower than those reported by Craven *et al* (1951). The possible causes have been discussed in detail in a previous paper (Pal *et al*, 1967).

INTERMOLECULAR POTENTIALS

The intermolecular potential for polar gases is usually represented by the Stockmayer or 12-6-3 potential which can be written as,

$$\phi(r) = 4\epsilon[(\sigma/r)^{12} - (\sigma/r)^6 + \delta(\sigma/r)^3], \quad (2)$$

$$\delta = \frac{1}{4} \mu^{*2} g(\theta_1, \theta_2, \varphi); \quad \mu^* = \mu/(\epsilon\sigma^3)^{1/2}, \quad (2a)$$

$$g(\theta_1, \theta_2, \varphi) = 2 \cos \theta_1 \cos \theta_2 - \sin \theta_1 \sin \theta_2 \cos \varphi \quad \dots \quad (2b)$$

where μ_1, μ_2 are the dipole moments of the interacting molecules, θ_1, θ_2 are angles of inclination of the dipoles to the line joining the centres of the molecules, φ is the azimuthal angle. For μ_1 , or $\mu_2 \rightarrow 0$, eq. (2) reduces to the well-known Lennard-Jones (12:6) potential for non-polar molecules (Hirschfelder *et al*, 1954). Monchick *et al* (1961) have calculated the collision integrals for the 12-6-3 potential by assuming equal probability for all the relative orientations of the interacting dipoles. In order to fit the viscosity data to the 12-6-3 potential we have followed the procedure of Monchick *et al* (1961) according to which we have the following equations :

$$\begin{aligned} \log [\eta \times 10^7 / M^{1/2} T^{7/6}] &= \log [T^{*2/3} < \Omega^{(2,2)*}(T^*) >]^{-1} + 0.05377 - \frac{1}{3} \log \mu \\ &\quad + \frac{2}{3} \log \delta_{max}, \quad (3) \\ \log T &= \log T^* + \log (\epsilon/k), \quad (4) \end{aligned}$$

where η is in g/cm. sec, M the molecular weight in gm/mole, T is in °K and μ in debyes (1 debye = 10^{-18} esu). If the model is capable of representing the data, a plot of the experimental quantities $\log [10^7 \eta / M^{1/2} T^{7/6}]$ vs. $\log T$ should be superposable by translation of axes on a plot of $\log [T^{*2/3} < \Omega^{(2,2)*}(T^*) >]^{-1}$ vs. $\log T^*$ ($< \Omega^{(2,2)*} >$ being the averaged collision integrals). The amount of translation

along the abscissa determines ϵ/k and that along the ordinate gives δ_{max} which is given by the relation

$$4\epsilon\sigma_0\delta_{max} = 2\mu^2 \quad \dots (5)$$

It has, however, been observed that the viscosity data cannot be fitted satisfactorily to the 12-6-3 potential by the method described above. The discrepancy is more pronounced in the lower temperature region. As a typical example, the experimental and the theoretical plots from eqs. (3) and (4) are shown in figs. 1 and 2 for diethyl ether. It is clear from a look at figs. 1 and 2 that the two curves are not at all superposable at lower temperatures. At higher temperatures the

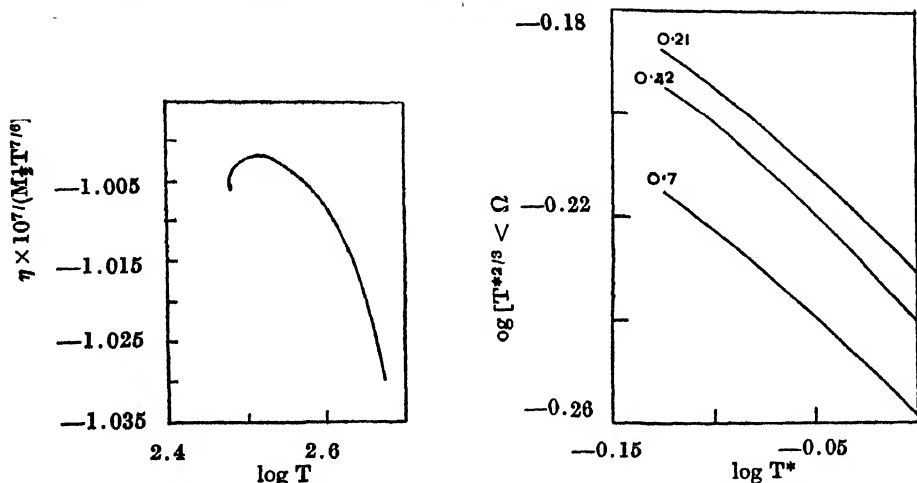


Figure 1. Plot of $\log [\eta \times 10^7 / (M^{1/2} T^{7/6})]$ vs. $\log T$. Figure 2. Plot of $\log [T^{2/3} / \Omega^{(2,2)} T^*]$ vs. $\log T^*$.

plots are almost straight lines and are superposable. This feature is quite understandable from physical considerations. The assumption of equal probability for all the relative orientations of the interacting dipoles will hold when the time of interaction is large compared to the time between collisions. This condition is likely to be satisfied better at higher temperatures. It also appears that particularly at lower temperatures viscosity is affected significantly by the dipole-dipole forces. Thus the suggestion of Monchick *et al* (1961) that the viscosity is insensitive to the dipole-dipole forces probably holds only at high temperatures.

At lower temperatures when the collision time increases, the dipoles may get a chance to reorient during an encounter. Different pairs of molecules will thus interact with different relative orientations and it is possible to assume an 'effective' relative orientation for all the molecules which will be a function of temperature. This idea can easily be tested by taking δ to be an independent parameter (Itean *et al* 1961). Under this condition we have the following equations

$$\log [\eta \times 10^7 / (MT)^{1/2}] = \log [\Omega^{(2,2)} (T^*, \delta)]^{-1} + \log 266.93 - 2 \log \sigma \quad \dots (6)$$

$$\log T = \log T^* + \log (\epsilon/k) \quad \dots (7)$$

where $\Omega^{(2,2)*}(\delta, T^*)$ is the unaveraged collision integrals which have been evaluated by Itean *et al* (1961) and also by Monchick *et al* (1961).

Table 1

Viscosity of diethyl ether, ethyl acetate and ter-butyl alcohol at different temperatures and force constants for the 12-6-3 model by assuming an effective relative orientation of the dipole

Substance	T°C	$\eta \times 10^8$ (g.cm ⁻¹ .sec. ⁻¹)	Potential parameters		
			$\sigma(\text{\AA})$	$\epsilon/k(^{\circ}\text{K})$	δ
Diethyl ether	30.0	66.56	5.684	476.4	0.63
	55.2	73.87			
	100.0	85.20			
	150.5	96.96			
	200.0	106.50			
Ethyl acetate	30.5	68.12	5.711	475.8	0.64
	54.5	75.29			
	99.2	86.56			
	150.2	98.78			
	200.1	109.50			
ter-Butyl alcohol	30.0	67.41	5.699	457.1	0.63
	55.6	74.34			
	100.0	85.10			
	149.7	95.73			
	200.0	105.25			

A series of plots of $\log [\Omega^{(2,2)*}(T^*)]^{-1}$ vs. $\log T^*$ for different δ values were made. On these plots another plot of $\log \left[\frac{\eta \times 10^7}{M^{\frac{1}{2}} T^{\frac{1}{2}}} \right]$ vs $\log T$ was superposed by the translation of axes. The value of δ was determined from the curve which gave the best fit and ϵ/k were obtained from the amount of translations along the ordinate and abscissa respectively. The effective value of g was obtained from the relation

$$g_{eff} = \frac{\sigma_0^3 \cdot \delta \cdot (\epsilon/k)}{1811\mu^2} \quad \dots (8)$$

where σ is in \AA , ϵ/k is in $^{\circ}\text{K}$ and μ is expressed in debye. However, it may be seen that δ as obtained by us are positive which correspond

to repulsive orientation of the dipole and are physically less probable. This may be due to the offcentre nature of the dipoles. Some progress in this direction has been made for equilibrium properties by Lawley *et al* (1963).

ACKNOWLEDGMENTS

The author is grateful to Dr. A. K. Barua for his guidance and to Prof. B. N. Srivastava for his kind interest in the work.

REFERENCES

- Barua, A. K., Afzal, M., Flynn, G. P. and Ross, J., 1964, *J. Chem. Phys.*, **41**, 374.
 Clifton, D. G., 1963, *J. Chem. Phys.*, **38**, 1123.
 Craven, P. M., and Lambert, J. D., 1951, *Proc. Roy. Soc. (London)*, **A205**, 439.
 Flynn, G. P.; Hanks, R. V., Lemaire, N. A. and Ross, J. F., 1963, *J. Chem. Phys.*, **38**, 154.
 Hirschfelder, J. O.; Curtiss, C. F. and Bird, R. B., 1954, *Molecular Theory of Gases and Liquids*, John Wiley & Sons, Inc., New York.
 Itean, E. C.; Glueck, A. R. and Svehla, R. A., 1961, *NASA Technical Note*, D-481.
 Kestin, J. and Leidenfrost, W., 1959, *Physica*, **25**, 1033.
 Kestin, J., and Whitelaw, J. H., 1963, *Physica*, **29**, 335.
 Lawley, K. P. and Smith, E. B., 1963, *Trans. Faraday. Soc.*, **59**, 301.
 Monchick, L. and Mason, E. A., 1961, *J. Chem. Phys.*, **35**, 1676.
 Newell, G. F., 1959, *Z. angew., Math. Phys.*, **10**, 160.
 Pal, A. K. and Barua, A. K., 1967, *Trans. Faraday. Soc.*, **63**, 341.
 , 1967, *Brit. J. Appl. Phys.*, (In press).
 Titani, T., 1933, *Bull. Chem. Soc., Japan*, **8**, 255.

DEBYE TEMPERATURE OF IONIC CRYSTALS

S. P. SRIVASTAVA, S. KUMAR AND M. P. MADAN

DEPARTMENT OF PHYSICS, UNIVERSITY OF LUCKNOW, INDIA.

(Received March 21, 1967)

ABSTRACT. Relations have been derived connecting the Debye characteristic temperature Θ with some of the lattice properties of the ionic crystals using the interaction potential approach. The relations are independent of the particular shape of the potential functions and also consider the polarization of ions arising from the electric field due to the displacement of the ions. Computed values of Θ agree very well with the Θ values obtained from specific heat and the elastic constant data.

INTRODUCTION

It is well known that the Debye characteristic temperature Θ is an important indicator of a number of physical properties of a solid. The most reliable method of evaluating Θ is from the specific heat of solids. However, when such calorimetric values of Θ are scarce, one has to look for other methods of determining it. Estimates of Θ can be obtained from the elastic constant data (De Launay 1956, Quimby *et al.*, 1953, Betts *et al.*, 1956a, b, Horton *et al.*, 1959, Horton 1959) by finding the sum of the inverse cubes of the three phase velocities of propagation of the elastic waves averaged over all directions. In general, particularly for anisotropic media, the evaluation of this sum is a complicated and tedious problem. Another method which is significantly simple is the computation of Θ utilizing the observed lattice properties of a solid. In the present paper we discuss this approach for ionic crystals of the alkali halide type.

Blackman (1955) from the lattice theory of specific heat obtained a relation between Θ and the compressibility β of a lattice for crystals of the rocksalt type as

$$\Theta = \frac{2}{k} \cdot \frac{1}{2\pi} \left(\frac{5R_0}{m\beta} \right)^{\frac{1}{3}} \quad (1)$$

where h is Planck's constant, k is the Boltzmann's constant, R_0 is the equilibrium interionic distance and m is the reduced mass. Using a Born-Mayer type of ionic potential Mitra *et al.* (1960a) also derived a similar relation. This relation was obtained by considering a specific form of the potential energy of the crystal and the expressions for its first and second derivatives for the static lattices. The characteristic frequency ν was obtained from the relation

$$\nu = \frac{1}{2\pi} \sqrt{\frac{f}{m}} \quad \dots (2)$$

where f is the coefficient of displacement of one lattice relative to the other when the potential energy due to such a relative displacement is expressed as a power series (Huggins 1937). This method ignores the ionic polarization produced by the relative displacement of the two lattices which, however, has a considerable effect on the frequency (Born *et al* 1954). Further, this relation is strictly applicable only if the compressibility and the lattice constants for static lattices are used, which unfortunately are not directly observable. In order to be able to use the room temperature data the relation should be modified. In what follows, relations are derived for ionic crystals connecting the Debye characteristic temperature Θ with the compressibility and other lattice properties but without assuming a specific form of the potential energy function. The electronic polarizability of the ions has also been considered. The relations are further modified to permit the use of the room temperature input data. In addition to the above modifications the present work also differs in the use of more recent experimental data (Cubicciotti 1959) for the compressibility and the interionic distance.

DETERMINATION OF Θ

The potential energy ψ of the crystal per pair of ions can be written in the form

$$\psi = \phi_C + \phi_R \quad \dots (3)$$

where ϕ_C is the Coulomb potential and is of the form $\alpha'e^2/R$ where α' is the Madelung's constant. ϕ_R contains the energy contributions other than the electrostatic energy and includes the repulsive energies, the Van der Waals attractive energies and may include the zero-point energy. An expression for the force constant f can be obtained following Born *et al* (1954), Szigeti (1951) and Krishnan *et al* (1951) as

$$f = \frac{1}{3} \left[\phi''_R + \frac{2}{R_0} \phi'_R \right] \quad \dots (4)$$

For static lattices, using the two well known conditions for the first and second derivatives of the potential energy one obtains (Born *et al*, 1954, Szigeti 1951)

$$f = \frac{3cR_0}{\beta} \quad \dots (5)$$

where c is the packing factor ($c = 2$ for NaCl type crystals and $c = 1.54$ for CsCl type crystals). In general, using the expressions given by Hildebrand (1931)

$$\left(\frac{d\psi}{dR} \right)_{R=R_0} = \frac{3vT\alpha}{\beta R_0} \quad \dots (6)$$

and

$$\left(\frac{d^2\psi}{dR^2} \right)_{R=R_0} = \frac{9v}{\beta R_0^2} F_{TP} \quad \dots (7)$$

where α is the thermal expansion coefficient and F_{TP} is a temperature dependent factor which is very nearly equal to unity (Cubicciotti 1959), we derive for f the expression

$$f = \frac{3cR_0}{\beta} \left[F_{TP} + \frac{2}{3} T\alpha \right] \quad (8)$$

The electronic polarizability is considered by taking into account the contribution to the potential energy from the polarization field of the medium (Born *et al.*, 1954) and the expression for ν is obtained as

$$\nu = \frac{1}{2\pi} \left(\frac{\epsilon_\infty + 2}{\epsilon + 2} \right)^{\frac{1}{3}} \left(\frac{f}{m} \right)^{\frac{1}{3}} \quad \dots \quad (9)$$

where ϵ and ϵ_∞ are the static and high frequency dielectric constants. In addition, one can also take into account the deformation of the charge distribution resulting from overlap. Lyddane *et al.*, (1941) and Szigeti (1951) treat this problem by introducing the idea of an effective charge and obtain another expression connecting the compressibility and the frequency. However as equation (5) is independent of the electronic charge and gives a better agreement with the experiment (Hardy 1961, Hass 1960), it is preferred. Using equations (8) and (9) one can readily obtain

$$\Theta = \frac{F'}{2\pi} \left(\frac{3cR_0}{m\beta} \right)^{\frac{1}{3}} \quad \dots \quad (10)$$

where

$$F' = \left[\left(F_{TP} + \frac{2}{3} T\alpha \right) \left(\frac{\epsilon_\infty + 2}{\epsilon + 2} \right) \right]^{\frac{1}{3}} \quad (11)$$

For the simple case when $T = 0$ and the polarization of the medium is ignored one obtains from equation (10), for NaCl type lattices,

$$\Theta = \frac{h}{k} \cdot \frac{1}{2\pi} \left(\frac{6R_0}{m\beta} \right)^{\frac{1}{3}} \quad \dots \quad (12)$$

which is the same relation as that obtained by Mitra and Joshi (1960a).

RESULTS AND DISCUSSION

Θ calculated from equation (10) using the experimental data for R_0 , β (Cubicciotti 1959) and α (Weyl 1955, Kumar 1959, 1960) are given in table 1 (column 2) together with Θ values (column 5) estimated from experimental infrared absorption frequencies (Barnes 1932, Jones *et al.*, 1961, Hass 1960). For comparison Θ of Blackman (1955) and θ_D from specific heat data are also given. It is well known now that the Θ values derived from different properties are not

necessarily equal. Θ varies considerably with temperature and as such different Θ values should be compared only if they are evaluated for the same temperature

Table
Values of Debye Temperatures $\Theta^\circ\text{K}$

Crystals	Eq. (10)	Exptl. (Blackman 1955)	Exptl. (A.I.P.* 1963)	Exptl. freq.	Elastic constant	(Mitra and Joshi 1960a)	(Black- man 1955)
LiF	399	607—750	732	440 ^a	676 ^d	834	686
NaF	296	—	—	355 ^a	—	469	—
NaCl	250	275—300	321	235 ^a , 235 ^b	295 ^d	322	292
NaBr	205	—	—	195 ^c	202 ^d	262	—
NaI	181	—	164	168 ^c	156 ^e	222	—
KCl	198	218—235	235	205 ^b , 207 ^c	230 ^d	270	233
KBr	164	152—183	174	167 ^c	167 ^d	198	185
KI	144	115—200	132	146 ^c	124 ^d	170	162
RbCl	168	—	—	171 ^c	—	203	—
RbBr	125	120—135	—	129 ^c	129 ^e	148	136
RbI	111	100—118	—	109 ^c	102 ^e	125	119
CsCl	139	—	—	143 ^c	—	166 ^f	—
CsBr	103	—	—	106 ^c	136 ^e	120 ^f	—

a Using experimental frequency from Barnes (1932).

b Using experimental frequency from Hass (1960).

c Using experimental frequency from Jones *et al.*, (1961).

d Reddy (1963).

e Joshi *et al.*, (1960).

f Mitra *et al.*, (1960b).

*American Institute of Physics Handbook, 1963.

range. The theory shows that Blackman's relation as well as our relation will not agree with the representative Θ which is obtained from calorimetric measurements in the liquid helium range or lower (column 4). By using the lattice property data at room temperature one expects to get the values of Θ near this temperature. It can be seen from the table that Θ values calculated from equation (10) (column 2) compare well with the Θ values obtained from the room temperature elastic constant data (column 6) and with the Θ values from experimental values of frequencies (column 5) and exhibit a significant improvement over the earlier computed values (columns 7 and 8) using equations similar to ours. When a reference is made to the θ_D - T plots for alkali halides (Blackman 1955) it is to be noted that our values are lower than the average values of θ_D for LiF and NaCl. For KCl the curve indicates a trend to lower values when approaching temperatures of the order of 275°K and as such our value exhibits a reasonable agreement.

It also applies to KBr. For KI, even though our value compares well with the average θ_D , it does not agree with the general tendency of θ_D value to increase with increasing temperature. Blackman also points out that the case of KI is anomalous and further investigation of this crystal is desirable. For RbBr and RbI our values agree well with the average θ_D values. For CsCl and CsBr only indirect experimental values of Θ from frequency are available and with these our values show an excellent agreement. In general for most of the ionic crystals our equation (10) seems to be definitely superior.

ACKNOWLEDGMENT

It is a pleasure to thank Professor P. N. Sharma for his interest.

REFERENCES

- American Institute of Physics Handbook*, 1963, New York : McGraw Hill Book Co., Inc.
- Barnes, R. B., 1932, *Z. Physik*, **75**, 723.
- Betts, D. D., Bhatia, A. B. and Horton, G. K., 1956a, *Phys. Rev.*, **104**, 43.
- Betts, D. D., Bhatia, A. B., and Wyman, M., 1956b, *Phys. Rev.*, **104**, 37.
- Blackman, M., 1955, *Handbuch der Physik*, VII/1, 325.
- Born, M., and Huang, K., 1954, *Dynamical Theory of Crystal Lattices*, Oxford : Clarendon Press.
- Cubiciotti, D., 1959, *J. Chem. Phys.*, **31**, 1646.
- De Launay, J., 1956, *Solid State Physics*, Vol. 2, New York : Academic Press, p. 286.
- Hardy, J. R., 1961, *Phil. Mag.*, **6**, 27.
- Hass, M., 1960, *Phys. Rev.*, **119**, 633.
- Hildebrand, J. H., 1931, *Z. Physik*, **67**, 127.
- Horton, G. K. and Schiff, H., 1959, *Proc. Roy. Soc. (London)*, **A250**, 248.
- Horton, G. K., 1959, *Proc. Roy. Soc. (London)*, **A252**, 551.
- Huggins, M. L., 1937, *J. Chem. Phys.*, **5**, 143.
- Jones, G. O., Martin, D. H., Mawer, P. A. and Perry, C. H., 1961, *Proc. Roy. Soc. (London)*, **A261**, 10.
- Joshi, S. K. and Mitra, S. S., 1960, *Proc. Phys. Soc. (London)* **76**, 295.
- Krishnan, K. S. and Roy, S. K., 1951, *Proc. Roy. Soc. (London)*, **A207**, 447.
- Kumar, S., 1959, *Proc. Nat. Inst. Sci. India*, **25A**, 364.
- 1960, *Central Glass Ceramic Res. Inst. Bull.*, **7**, 58.
- Lyddane, R. H., Sachs, R. G., and Teller, E., 1941, *Phys. Rev.*, **59**, 673.
- Mitra, S. S., and Joshi, S. K., 1960a, b, *Physica*, **26**, 284, 825.
- Quimby, S. L. and Sutton, P. M., 1953, *Phys. Rev.*, **91**, 1122.
- Reddy, P. J., 1963, *Physica*, **29**, 63.
- Szigeti, B., 1951, *Proc. Roy. Soc. (London)*, **A204**, 51.
- Weyl, W. A., 1955, *Naval Res. Techn. Reports Nos. 64, 65, 66*, Pen. State University.

INFRARED ABSORPTION FREQUENCY OF IONIC CRYSTALS

S. P. SRIVASTAVA, S. KUMAR AND M. P. MADAN

DEPARTMENT OF PHYSICS, UNIVERSITY OF LUCKNOW, INDIA.

(Received March 21, 1967)

ABSTRACT. Relations are derived for the absorption frequency of ionic crystals in terms of various lattice properties following a simple and direct approach through the assumption of a few realistic interaction potential functions, in particular an exp : exp type of potential. The derived relations permit the use of room temperature input data and also consider the electronic polarizability which is neglected in the rigid ion approximation. The absorption frequencies have been computed utilizing recent data for various lattice properties. A very satisfactory agreement has been found with the measured values of the frequency as well as with the frequency computed from the frequency versus wave vector dispersion curves.

INTRODUCTION

Born and his collaborators (1954) using a simple interionic force model correlated the cohesive energies with the lattice constants and the compressibility and obtained a reasonable degree of success. Szigeti (1949, 1951) and independently Odelevski (1950), using the simple Born model derived relations for the absorption frequency in connection with the theory of dielectric constants but found the results at variance with the experiment. The disagreement with the experiment was also noticed with regard to lattice vibration calculations based on simple Born model, in particular, when the frequency versus wave vector dispersion curves were compared with those determined experimentally by inelastic neutron scattering (Woods *et al.* 1960, 1963, Cowley *et al.* 1963). Szigeti (1951) pointed out that the failure of his relations indicated the distortion polarization of ions displaced relative to one another. Attempts to explain part of the deviations have been made by Born *et al.* (1954), Tolpygo (1950), Lundqvist (1955, 1957) and in terms of a more complicated model of dielectric polarization by Dick *et al.* (1958) and by Hanlon *et al.* (1959). Yamashita (1955) in their treatment of the dielectric constants of ionic crystals have also considered the connection between polarization of ions and the repulsive force between them. Woods *et al.* (1960, 1963) and Cowley *et al.* (1963) used a shell model originally developed by Dick *et al.* (1958) for the interpretation of their results from inelastic neutron scattering. Somewhat similar attempts to explain the experimentally observed dispersion curves have been made by Hardy (1959, 1961, 1962) and Hardy *et al.* Karo (1960).

Szigeti (1951) obtained two relations, the first connecting the absorption frequency ω_0 with the static and high frequency dielectric constants ϵ and ϵ_∞ , respectively, as

$$\epsilon - \epsilon_\infty = (\epsilon_\infty + 2)^2 \frac{4\pi N(ze^*)^2}{9m\omega_0^2} \quad \dots (1)$$

where m is the reduced mass of an ion pair and N the Avogadro Number, and the second connecting the absorption frequency with the compressibility β as

$$m\omega_0^2 \left(\frac{\epsilon + 2}{\epsilon_\infty + 2} \right) = \frac{3v}{\beta R_0^2} \quad \dots (2)$$

where v is the volume of the lattice cell and R_0 the equilibrium interionic distance. Szigeti (1951) introduces the idea of an effective charge e^* to account for the distortion of ions by overlap forces. Attempts to compute the magnitude of e^*/e have been made among others by Szigeti (1951), Lundqvist (1955, 1957), Dick *et al* (1958) and Havinga (1961). Lundqvist has also investigated the effect of the second neighbour interactions neglected in the simple theory, by assuming a more complicated model involving three body as well as two body interactions. Three body interactions have also been discussed by Szigeti (1960, 1961), Karo *et al* (1963) and Hardy *et al* (1965). It should be pointed out that Szigeti relation (2) connecting the absorption frequency with the compressibility does not involve e^* and should still be correct in the approximation when ionic distortion is treated in terms of distortion dipoles determined by the nearest neighbour ionic separation. The deviation of the results of this equation from the experiment therefore should not be attributed to distortion moments and one must look for the explanation of discrepancies elsewhere.

Information about infrared absorption frequency ω_0 can also be obtained from the frequency ω versus wave vector q dispersion curves (Woods *et al*, 1960, 1963, Cowley *et al*, 1963, Karo *et al*, 1963, Hardy *et al*, 1965, Kellermann 1940, 1941) and finding the transverse optical frequency at $q = 0$, which incidentally is a laborious procedure and provides an indirect description of the interionic forces. Szigeti's expressions as well as the frequency versus wave vector dispersion curves based on simple Born model or other complicated models of dielectric polarization (Woods *et al*, 1960, 1963, Cowley, *et al*, 1963, Dick *et al* 1958, Karo *et al* 1963, Hardy *et al* Karo 1965) are independent of the particular shape of the potential function or the potential parameters. In addition these expressions require the condition for the stability of a static lattice. They are strictly applicable only at very low temperatures and also if zero point vibrations are neglected. Deviations (Hass 1960) are found to occur when room temperature values are inserted in these relations.

Another approach which is simple and direct is through the assumption of a central pairwise potential function and the consideration of electronic polarizability which is neglected in the rigid ion approximation. Relations can then be derived for the absorption frequency in terms of various lattice properties. Further, as the various lattice properties are not directly observable for static lattices the relations can be modified so that they permit the use of room temperature values. In what follows, the determination of the absorption frequencies on the basis of more realistic potential forms in conjunction with various lattice properties has been made. The derived relations allow the use of room temperature data for the compressibility β , the interionic distance R_0 and other lattice properties. Moreover, the values of R_0 and β as well as of the Madelung term occurring in the potential function and as reported in Born *et al* (1954) and Huggins (1937) have undergone a rather important change. Since then a redetermination of these quantities has been made and a more reliable data is available (Cubicciotti 1959, Spangenberg 1956, Spangenberg *et al* 1957) which has been used in the present work.

INTERACTION POTENTIALS

A knowledge of the accurate potential energy function is very necessary for investigating the interaction potential approach which lays emphasis on the particular shape of the potential function. The potential energy ψ of the crystal per pair of ions can be written in the form

$$\psi = \phi_C + \phi_R \quad \dots (3)$$

where ϕ_C is the Coulomb potential and is of the form $\alpha'e^2/R$ where α' is the Madelung's constant and e the electronic charge. ϕ_R contains the energy contributions other than the electrostatic energy and includes the repulsive energies, the Van der Waals attractive energies and may include the zero-point energy. The forces included in ϕ_R are of great importance for the absorption frequency, the compressibility and the other lattice properties. It is a reasonable approximation to take into account the forces between nearest neighbours only. If zero-point energy is included as a part of the lattice energy, the cohesive energy U per mole is given by

$$U = -[N\psi + \epsilon_0] \quad \dots (4)$$

where ϵ_0 is the zero-point energy per mole. ϕ_R can be expected to be of the form

$$\phi_R = B \exp(-R/\rho) \quad \dots (5)$$

or may be taken to be of the type

$$\phi_R = B \exp(-R/\rho) - CR^{-6} \quad \dots (6)$$

when Van der Waals forces are also considered, where, B , C and ρ are the potential parameters. The interatomic potential between two inert gas atoms has been studied intensively using the familiar Lennard-Jones 12:6 potential form as well

as by the other potential forms such as the Buckingham-Corner, the exp : six and more recently by the exp:exp potential form. Alkali halides are the closest to the theoretical model for ionic crystals having rare gas structures. In view of the apparent success of these potentials in explaining the behaviour of inert gas atomic structures, ϕ_R can also be given a form based on these potentials provided the potential parameters are determined independently and directly using the observed lattice properties. This restriction is important because it has been shown by Rittner (1951) that the earlier attempts to calculate the binding energies and other properties of alkali halide gas molecules from Born lattice theory assuming that the repulsion constants are the same for gas molecules as for the crystals are certainly not valid. A few of the properties of some ionic crystals using simple inverse forms that is BR^{-12} for the repulsive energy and CR^{-6} for the attractive energy (Lennard-Jones potential) were studied by Sharma and Madan (1961, 1964). However, the expressions for the Van der Waals terms ($-CR^{-6}$, $-DR^{-8}$, etc.) are not very satisfactory for closely situated atoms when the overlap is predominant, though the dipole-dipole potential probably reproduces the correct order of magnitude. A more realistic form is perhaps desirable to express this attractive contribution to the total lattice energy. As such, of particular interest is the exp : exp form for the interaction energy. This potential was used initially to explain the vibrational spectra of diatomic molecules, but has not been tried for ionic crystal lattices. Here we have considered this potential to examine the characteristic frequencies and other lattice properties. In order to test its suitability as an ionic potential we have also investigated, for comparison, the potentials given by equations (5) and (6) as well as the Lennard-Jones potential. Using an exp : exp form, the equation for ϕ_R is written in a simplified form as

$$\phi_R = Be^{-2R/\rho} - Ce^{-R/\rho} \quad \dots (7)$$

where B , C and ρ are the potential parameters.

ESTIMATION OF LATTICE FREQUENCIES

Many of the macroscopic properties of crystals can be obtained from the dynamic motions of their lattice particles. The statistical mechanics of such motions gives the expressions for the free energy of the system which in turn can be related with the total internal energy E and the entropy by the thermodynamical relations (Born *et al*, 1954) such that we can write

$$E = U + E_{vib} \quad (8)$$

Here U , the lattice energy is a function only of the interatomic distances or of volume in the adiabatic approximation (Dobbs *et al* 1957). E_{vib} represents the thermal energy excluding the zero-point energy. The zero-point energy which is also dependent only on volume, is included in U (see equation (4)). The ions in the crystal are held in their respective positions by the forces included in the

representation of U . Usually the derivatives of U are evaluated at absolute zero and in the absence of zero-point energy. In order to be able to use the room temperature values of lattice properties, the derivatives should be evaluated at the mean positions which the atoms actually occupy at the temperature T . For this purpose one can use the expressions given by Hildebrand (1931), obtained from equation (8) as (using ψ instead of U for convenience)

$$\left(\frac{d\psi}{dR} \right)_{R=R_0} = \frac{3vT\alpha}{\beta R_0} \quad \dots (9)$$

and

$$\left(\frac{d^2\psi}{dR^2} \right)_{R=R_0} = \frac{9v^2}{\beta R_0^2} F_{TP} \quad \dots (10)$$

where α is the thermal expansion coefficient and F_{TP} is a temperature dependent factor which is very nearly equal to unity. The expression for this is given in Cubicciotti (1959). When there is a small displacement of the lattice of positive ions relative to the lattice of negative ions, there is a change in the internal energy of the crystal. The contributing effect is mainly contained in the change $\delta\phi_R$ (Szigeti 1951, Krishnan *et al*, 1951). The energy change is

$$\delta\phi_R = \frac{1}{2} m \omega_r^2 r^2 \quad \dots (11)$$

where r is the displacement of the two kinds of ions relative to each other, and $m\omega_r^2 = f$, the force constant. Neglecting anharmonicity the frequency ω_r is given as

$$\omega_r = \sqrt{\frac{f}{m}} \quad \dots (12)$$

To evaluate f , one has to add up the interactions of one of the ions with its nearest neighbours. Starting with the appropriate equation for the interaction potential, the force constant could be estimated as a coefficient of r in the expansion of $d\psi/dR$ as a power series in r . The potential parameters are then evaluated with the help of the relations (9) and (10). Thus for a crystal of NaCl type, using the exp:exp potential (equation (7)) we obtain

$$f = \frac{1}{3} \left[\frac{1}{\rho R_0} \left(\frac{\alpha' e^2}{R_0^2} - \frac{3vT\alpha}{\beta R_0} \right) (3R_0 - 2\rho) - \frac{2}{\rho^2} \left(\frac{\alpha' e^2}{R_0} - E' \right) \right] \quad \dots (13)$$

where E' are the energy values which are derived from the experimental energy values listed by Seitz (1940) considering the zero-point energies (Cubicciotti 1959). Alternatively, one could proceed following Krishnan *et al* (1951) and Born

et al (1954) and obtain f in terms of the first and second derivatives of ϕ_R as

$$f = \frac{1}{3} \left[\phi_R'' + \frac{2}{R_0} \phi_R' \right] \quad (14)$$

It can be verified easily that equations (13) and (14) are essentially equivalent. Equation (14) is more convenient for computational purposes. Similarly using the potential forms represented by equations (5) and (6) we obtain for the force constant f as

$$f_{eq.(5)} = \frac{1}{3\rho R_0} \left[\frac{\alpha' e^2}{R_0} - E' \right] \left(\frac{R_0}{\rho} - 2 \right) \quad (15)$$

and

$$f_{eq.(6)} = \frac{1}{3} \left[\frac{1}{\rho R_0} \left(\frac{\alpha' e^2}{R_0} - E' + \frac{C}{R_0^6} \right) \left(\frac{R_0}{\rho} - 2 \right) - \frac{30C}{R_0^8} \right] \quad (16)$$

whereas for the Lennard-Jones 12:6 potential f has the value

$$f_{L-J} = \frac{1}{3R_0^2} \left[17R_0 \left(\frac{\alpha' e^2}{R_0^2} - \frac{3vT\alpha}{\beta R_0} \right) - 7 \left(\frac{\alpha' e^2}{R_0} - E' \right) \right] \quad (17)$$

The values of the force constants thus determined are given in table 1, where they have been compared with each other. The force constant f is entirely

Table 1
Values of force constants $f \times 10^{-4}$

Crystals	(Eq. 13)	(Eq. 17)	(Eq. 16)	(Eq. 15)
LiF	6.60	8.10	6.84	6.75
LiCl	4.31	5.94	4.41	4.26
LiBr	3.83	5.59	3.87	3.37
LiI	3.25	4.90	3.33	2.21
NaF	5.55	6.22	6.34	6.25
NaCl	4.31	4.81	5.30	5.12
NaBr	3.63	4.10	4.28	4.09
NaI	3.08	4.05	2.98	2.65
KCl	3.12	3.49	4.10	3.95
KBr	2.40	2.85	4.33	4.18
KI	2.22	2.50	3.84	3.28
RbCl	3.35	3.50	4.59	3.71
RbBr	2.94	3.02	4.32	3.38
RbI	2.65	3.06	2.71	2.08
CsCl	3.07	3.25	3.43	2.57
CsBr	2.74	2.57	3.07	2.89
CsI	2.44	2.87	2.06	—

determined from a knowledge of ϕ_R and is for the type of displacement in which the electronic polarizability in the crystal is ignored. The electronic polarizability is considered by taking into account the polarization of the medium (Born *et al* 1954, Szigeti 1951, Lyddane *et al* 1941) and an expression for the force constant can be obtained (Born *et al* 1954) as

$$\frac{f}{m} = \frac{\epsilon+2}{\epsilon_{\infty}+2} \omega_0^2 \quad \dots (18)$$

Equation (18) is derived by considering a lattice of polarizable ions, which contribute to the local polarization, firstly, a moment due to their displacement from lattice sites and secondly, the moments induced in the ions by the effective field representing the Coulomb interaction. In addition, one can also consider the electronic dipole moment created by local distortions when a positive ion approaches a more polarizable negative ion and which affects the field in the overlapping regions (Szigeti 1951, Mott *et al* 1948). Following Szigeti's idea of an effective charge e^* one can derive an expression for the force constant f in terms of the dielectric constants and the distance R_0 . The result is

$$f = \frac{2\pi(e^*)^2}{9R_0^3} \cdot \frac{(\epsilon_{\infty}+2)(\epsilon+2)}{(c-\epsilon_{\infty})} \quad \dots (19)$$

It can be seen from equation (18) that a knowledge of ω_0 is necessary for the determination of f , whereas, for equation (19) we need in addition to the experimental data on dielectric constants, the values of e^* and R_0 . The effect of local distortions due to the neighbouring ions is eliminated in equation (18) and as such it is preferred. Hardy (1961) also indicates that equation (18) is obeyed better than equation (19) particularly for crystals containing light ions. Equations (13) and (15) to (17) in conjunction with equation (18) may now be subjected to test in computing the infrared absorption frequencies. These are tabulated in table 2. The experimental frequencies reported are those given by Barnes (1932) and Jones *et al* (1961). As mentioned earlier, the parameters occurring in various relations for interaction potentials as well as for f are determined using relations (9) and (10). C , the Van der Waals constant, in expression (6) can be evaluated from the above conditions or its value as given by Huggins (1937) from a careful analysis of optical data can be used. β and other terms used were those reported by Cubicciotti (1959) except the α values which are those listed by Weyl (1955) and Kumar (1959, 1960). It can be seen from the table that for crystals containing lighter ions, the exp:exp potential is definitely better than the Lennard-Jones potential. Exp. model or modified exp. model gives satisfactory results only for a few crystals. As we proceed down the table, we see that Lennard-Jones potential gives quite good results for crystals containing heavier ions. This is in confirmation with our earlier findings (Sharma *et al* 1961). However, one

cannot fail to notice that the exp:exp potential also yields equally good results for these crystals leading to the conclusion that this potential is definitely better

Table 2
Values of absorption frequencies
 $\omega_0(10^{13}\text{sec.}^{-1})$

Crystals	Exptl. (Barnes 1932)	Exptl. (Jones <i>et al.</i> , 1961)	exp : exp	Lennard- Jones 12 : 6	Modified exp.	exp.
LiF	5.78	—	5.22	5.78	5.32	5.28
LiCl	—	—	4.04	4.74	4.09	4.02
LiBr	—	—	3.79	4.58	3.81	3.56
LiI	—	—	3.68	4.47	3.68	3.00
NaF	4.64	—	3.87	4.10	4.14	4.11
NaCl	3.09, 3.09*	—	3.22	3.41	3.58	3.49
NaBr	2.52	2.55	2.66	2.83	2.89	3.83
NaI	2.20	2.20	2.34	2.68	2.30	2.17
KCl	2.67, 2.68*	2.71	2.51	2.64	2.87	2.82
KBr	2.13	2.18	1.88	2.05	2.52	2.48
KI	1.85	1.91	1.74	1.85	2.29	2.12
RbCl	2.22	2.24	2.20	2.24	2.57	2.31
RbBr	1.65	1.69	1.62	1.65	1.98	1.79
RbI	1.45	1.42	1.45	1.55	1.45	1.28
CsCl	1.85	1.87	1.81	1.87	1.92	1.66
CsBr	1.41	1.39	1.49	1.45	1.58	1.54

* Hass (1960).

than the other ionic interaction models for the whole family of alkali halides considered here and should be preferred for the calculation of lattice properties. The present computed values of the absorption frequency of those alkali halides which have been considered by Karo *et al* (1963), Hardy *et al* (1965), Woods *et al*, (1960, 1963) and Cowley *et al* (1963) can be compared with the values obtained from frequency versus wave vector dispersion curves for $q = 0$ by them. It is seen in general (from their curves) that the agreement is very reasonable and the deviations observed by us from the experimental measurements using the f values from exp:exp model or Lennard-Jones 12:6 model appear to be roughly of the same nature and magnitude as that noticed by them. We did not hope to produce as good an agreement between the theory and experiment as that found by using the dispersion curve approach, nevertheless in view of the present simple and direct approach it is significant that we appear to confirm their results within a few percent. We consider that the agreement verifies that the general

picture and main features of our approach are correct and our theory leads to results which are in general in reasonable agreement with the experimental data that exist, and also with the values obtained from dispersion curves.

Using the experimental values of the absorption frequency ω_0 , Szigeti (1951) calculated the compressibilities employing equation (2) using however, the room temperature data. The equation (2) is obtained with the aid of equation (18) and the relation

$$\frac{1}{\beta} = \frac{R_0^2 f}{3v} \quad \dots (20)$$

Odelevski (1950), Dick *et al* (1958), Hanlon *et. al* (1959) and Lundqvist (1955, 1957) have proposed generalisations of the Szigeti formula (2) to take into account different aspects of dielectric polarization. Hass (1960) using these different proposed formulae finds that his experimental data is in good agreement with frequencies calculated using the Szigeti formula (2). The formulae of Odelevski and Lundqvist when combined also give comparable results, though its appropriateness for all the alkali halides is doubtful. Thus it is prefer-

Table 3
Values of compressibilities

Crystals	$\frac{\beta_{\text{calc.}}}{\beta_{\text{obs.}}}$ (a)	$\frac{\beta_{\text{calc.}}}{\beta_{\text{obs.}}}$ (b)	$\frac{\beta_{\text{calc.}}}{\beta_{\text{obs.}}}$ (c)	$\frac{\beta_{\text{calc.}}}{\beta_{\text{obs.}}}$ (d)
LiF	0.82*	1.05*	1.00	1.00
NaF	0.70*	0.85*	0.83	1.01
NaCl	1.13*(1.12)	1.08*(1.08)	0.99	1.03
NaBr	1.03	1.14	1.13	1.01
NaI	1.16	1.14	1.05	1.03
KCl	0.91(0.93)	0.94(0.96)	0.96	1.07
KBr	0.97	0.95	0.95	1.30
KI	0.98	0.98	0.99	1.18
RbCl	0.96	0.92	0.89	1.00
RbBr	0.94	0.89	0.83	0.99
RbI	1.04	0.95	0.66	1.02
CsCl	0.94	0.91	0.87	1.00
CsBr	0.94	0.96	0.87	0.98

(a) Using equation (21) with experimental values of frequency (Jones *et al.*, 1961).

(b) Using Szigeti equation but recent data.

(c) Szigeti (1951).

(d) Calculated from equation (21) using the exp:exp potential.

Values marked * and in parentheses are those for which the experimental frequencies have been taken from Barnes (1932) and Hass (1960), respectively.

able to use the Szigeti relation (2). However, this relation was derived without considering the specific form of the potential. A relation similar to equation (20) connecting the compressibility and the force constant (and hence the absorption frequency) but permitting the use of room temperature values of R_0 and β can also be derived. Such a relation is useful but cannot be used to test the appropriateness of a particular ionic potential. Using equation (14) and equations (9) and (10) it can be shown that

$$\frac{1}{\beta} = \frac{R_0^3 f}{3v(F_{TP} + \frac{2}{3}T\alpha)} \quad \dots (21)$$

The values of the compressibilities thus calculated are given in table 3. In this table are also given the values of $(\beta_{calc.}/\beta_{obs.})$ following Szigeti when recent data for absorption frequency (Barnes 1932, Jones *et al* 1961), R_0 and β (Cubieciotti 1959) are considered. For comparison old values of Szigeti (1951) are also listed in column 4. We have also listed in this table the values of the ratio, taking $\beta_{calc.}$ by using the f values obtained from the interionic potential (column 2, table 1). Even though $\beta_{obs.}$ were one of the experimental data in addition to the experimental E' , R_0 and α values used for the determination of potential parameters, it is of some use to obtain these values to see how well the force constants obtained from different lattice properties taken together reproduce a single lattice property. When a comparison is made between columns 2 and 3 it is seen that the values of compressibility using modified equation (21) agree more with the experimental values for most of the crystals. The agreement is slightly inferior to value calculated using Szigeti relation for only a few crystals such as LiF and NaF. This is mainly due to the large deviation from unity of the factor F_{TP} for these crystals. It may be remarked that these new redetermined values computed using recent data show a better agreement with experiment over the old values of Szigeti.

ACKNOWLEDGMENTS

It is a pleasure to thank Professor P. N. Sharma for his interest. S.P.S. and S.K. express their gratefulness to the Government of India for the award of Research Training Scholarships.

REFERENCES

- Barnes, R. B., 1932, *Z. Physik*, **75**, 723.
 Born, M. and Huang, K., 1954, *Dynamical Theory of Crystal Lattices*, Oxford: Clarendon Press.
 Cowley, R. A., Cochran, W., Brockhouse, B. N. and Woods, A. D. B., 1963, *Phys. Rev.*, **131**, 1030.
 Cubieciotti, D., 1959, *J. Chem. Phys.*, **31**, 1646.
 Dick, B. G. and Overhauser, A. W., 1958, *Phys. Rev.*, **112**, 90.

- Dobbs, E. R. and Jones, G. O., 1957, *Reports on Progress in Physics*, **20**, 516.
- Hanlon, J. E. and Lawson, A. W., 1959, *Phys. Rev.*, **113**, 472.
- Hardy, J. R., 1959, *Phil. Mag.*, **4**, 1278.
 1961, *Phil. Mag.*, **27**.
 1962, *Phil. Mag.*, **7**, 315.
- Hardy, J. R. and Karo, A. M., 1960, *Phil. Mag.*, **5**, 859.
 1965, *Lattice Dynamics*, Edited by Wallis, R. F., Oxford : Pergamon Press, p. 195.
- Hass, M., 1960, *Phys. Rev.*, **119**, 633.
- Havinga, E. E., 1961, *J. Phys. Chem. Solids*, **18**, 253.
- Hildebrand, J. H., 1931, *Z. Physik*, **67**, 127.
- Huggins, M. L., 1937, *J. Chem. Phys.*, **55**, 143.
- Jones, G. O., Martin, D. H., Mawer, P. A. and Perry, C. H., 1961, *Proc. Roy. Soc. (London)*, **A261**, 10.
- Karo, A. M. and Hardy, J. R., 1963, *Phys. Rev.*, **129**, 2024.
- Kellermann, E. W., 1940, *Phil. Trans. Roy. Soc. (London)*, **A238**, 513.
 1941, *Proc. Roy. Soc. (London)*, **A178**, 17.
- Krishnan, K. S. and Roy, S. K., 1951, *Proc. Roy. Soc. (London)*, **A207**, 447.
- Kumar, S., 1959, *Proc. Nat. Inst. Sci. India*, **25A**, 364.
 1960, *Central Glass Ceramic Res. Inst. Bull.*, **7**, 58.
- Lundqvist, S. O., 1955, *Ark. Fys.*, **9**, 435.
 1957, *Ark. Fys.*, **12**, 263.
- Lyddane, R. H., Sachs, R. G. and Teller, E., 1941, *Phys. Rev.*, **59**, 673.
- Mott, N. F., and Gurney, R. W., 1948, *Electronic Processes in Ionic Crystals*, Oxford : Clarendon Press.
- Odelevski, V. I., 1950, *Izv. Akad. Nauk. Ser. Fiz. S.S.S.R.*, **14**, 232.
- Rittner, E. S., 1951, *J. Chem. Phys.*, **19**, 1030.
- Seitz, F., 1940, *Modern Theory of Solids*, New York. McGraw Hill Book Co., Inc.
- Sharma, M. N., and Madan, M. P., 1961, *Indian J. Phys.*, **35**, 596.
 1964, *Indian J. Phys.*, **38**, 231.
- Spangenberg, K., 1965, *Naturwiss*, **43**, 394.
- Spangenberg, K. and Haussuhl, S., 1957, *Z. Krist.*, **109**, 422.
- Szigeti, B., 1949, *Trans. Faraday Soc.*, **45**, 155.
 1951, *Proc. Roy. Soc. (London)*, **A204**, 51.
 1960, *Proc. Roy. Soc. (London)*, **A253**, 377.
 1961, *Proc. Roy. Soc. (London)*, **A261**, 274.
- Tolpygo, K. B., 1950, *Zh. Eksp. Teor. Fiz.*, **20**, 497.
- Weyl, W. A., 1955, *Naval Res. Techn. Reports Nos. 64, 65, 66*, Pennsylvania. State University.
- Woods, A. D. B., Cochran, W. and Brockhouse, B. N., 1960, *Phys. Rev.*, **119**, 980.
- Woods, A. D. B., Brockhouse, B. N., Cowley, R. A., and Cochran, W., 1963, *Phys. Rev.*, **131**, 1025.
- Yamashita, J. and Kurosawa, J., 1955, *J. Phys. Soc. Japan*, **10**, 610.

ATTENUATION CHARACTERISTICS OF VLF WAVES FROM THE WAVEFORMS OF ATMOSPHERICS

MANORANJAN RAO

BOSE INSTITUTE, CALCUTTA, INDIA.

(Received April 26, 1967)

ABSTRACT. In this paper a reevaluation of the data published earlier by Khastgir *et al* (1960) and Bhattacharya *et al* (1964) has been made to obtain the attenuation coefficients of VLF radio waves. The wave-guide mode-equation deduced by Wait (1957, 1958) has been used and the results obtained are compared with those of Taylor and Lange (1958). Attempt is made to explain the discrepancies between the results of the different authors.

INTRODUCTION

Ever since it had been established that lightning discharges radiated electromagnetic energy mainly in the VLF-band of frequencies, increasing attention of the various investigators in this field has been directed to the utilization of the naturally occurring VLF emissions for the study of the propagation characteristics of frequencies in the VLF-band. The main idea was to study how the spectra radiated by the lightning discharges varied with distance. Different workers adopted different techniques in recording and analysing the atmospherics or their waveforms for obtaining maximum information about the VLF-propagation with minimum possible assumptions. For example, Gardner (1950) recorded only the integrated levels of atmospheric noise on some chosen frequencies and studied how these levels changed with the time of the day. Bowe (1951), on the other hand, recorded tuned amplifier responses to individual sferics on certain chosen frequencies and determined how the radiation field on any frequency with respect to that on some reference frequency varied with distance. Similarly Chapman *et al* (1953), Taylor *et al* (1958), Taylor (1960), Hepburn (1959, 1960) Obayashi *et al.* (1959, 1956), and Croom (1964) also studied the change in the radiated spectra of atmospherics with distance and obtained reasonably accurate values for the attenuation coefficients for the VLF-frequencies. Khastgir *et al* (1960) and Bhattacharyya *et al* (1964) also made similar studies and following the method given by Bowe (1951) deduced how the ratio of field components on two frequencies varied with distance. In present paper an attempt is made to obtain the absolute values of the attenuation coefficients from the data published by Khastgir *et al* (1960) and Bhattacharya *et al* (1964).

THE METHOD OF ANALYSIS

While Khastgir *et al* (1960) recorded the tuned amplifier responses on some selected frequencies only (usually four in number), Bhattacharya *et al* (1964) subjected the recorded waveform to Fourier transformation by laborious numerical integration and obtained more or less continuous spectra within the range of 3-15 kc/s. These authors adopted the method given by Bowe (1951) which can be briefly summarised as follows :

The radiation field on any frequency f at a distance d can be written as

$$E(f, d) = \frac{A(f)}{d} \cdot \rho(f, d) \quad (1)$$

where $A(f)$ describes the source spectrum and $\rho(f, d)$ represents the attenuation suffered by the component frequency f and is a function of distance d . Obviously the distance occurring in the denominator accounts for the free-space decrement. If the amplitude at any frequency f_n is measured relative to that at some reference frequency f_0 we can write,

$$\frac{E(f_n, d)}{E(f_0, d)} = \frac{A(f_n)}{A(f_0)} \cdot \frac{\rho(f_n, d)}{\rho(f_0, d)} \quad \dots (2)$$

Now if we assume that $A(f_n)/A(f_0)$ is statistically invariant, and if measurements are made on several lightning sources at different distances, then the ratio $E(f_n, d)/E(f_0, d)$ when plotted against d would indicate how $\rho(f_n, d)/\rho(f_0, d)$ behaves as a function of d . Following this argument of Bowe (1951) Khastgir *et al* (1960) and Bhattacharya *et al* (1964) gave plots of $E(f_n, d)/E(f_0, d)$ against d , for several values of f_n .

It has now been established that the VLF-waves when propagated to great distances over earth behave as if they are propagated through the waveguide formed by the lower boundary of the ionosphere and the earth. Extensive theoretical work has been done by several workers on this aspect of the problem viz. Budden (1961), Wait (1962). The expression deduced by Wait (1957, 1958) has been used by Taylor *et al* (1958) and Croom (1964) with consistent results. The expression deduced by Wait is given by :

$$E(f, d) = \frac{A(f)}{(a \ln d/a)^{\frac{1}{2}}} \cdot \exp [-\alpha(f)d] \quad \dots (3)$$

where $E(f, d)$ and $A(f)$ have the same meaning as in (1) and $\alpha(f)$ is the attenuation

coefficient in nepers and a is the radius of the earth. In view of (3), the left hand side of (2) can be written as

$$\frac{E(f_n, d)}{E(f_0, d)} = \frac{A(f_n)}{A(f_0)} \exp [\alpha(f_0) - \alpha(f_n)]d \quad (4)$$

Taking logarithms we write :

$$\ln \frac{E(f_n, d)}{E(f_0, d)} = \ln \frac{A(f_n)}{A(f_0)} + [\alpha(f_0) - \alpha(f_n)]d. \quad (5)$$

Thus if the assumption is made that $A(f_n)/A(f_0)$ is a statistical constant of the source, the plots of $\ln \frac{E(f_n, d)}{E(f_0, d)}$ against d would give a straight line with a slope equal to the relative attenuation coefficient $[\alpha(f_0) - \alpha(f_n)]$.

RESULTS AND DISCUSSION

The data given by Bhattacharya *et al* (1964) for the ratio $E(f_n, d)/E(f_0, d)$ for different distances are replotted satisfying the equation (5) in fig. 1. The

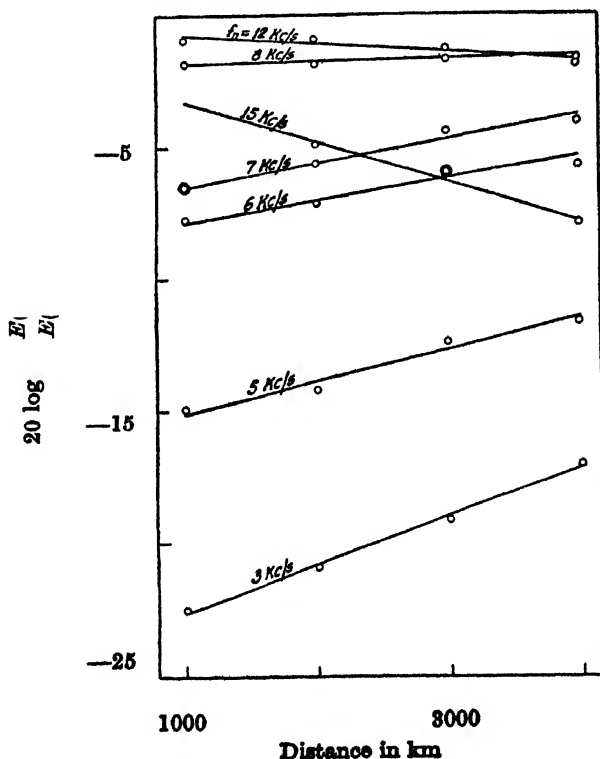


Fig. 1. Variation of $20 \log \frac{E(f_n, d)}{E(f_0, d)}$ with distance d for frequencies $f_n = 3, 5, 6, 7, 8, 12$ and 15 kc/s. (The reference frequency $f_0 = 10$ kc/s.)

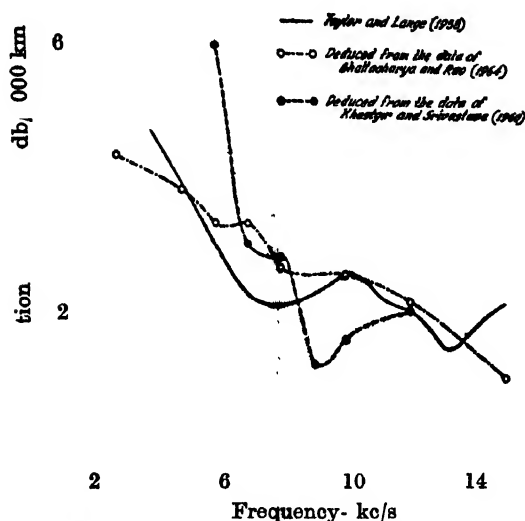


Fig. 2. Attenuation Coefficients in db/1000 km for frequencies in the range 3-15 kc/s
—Comparison with the results of other workers.

ordinates are expressed in *db* and straight line approximation holds good at almost all the frequencies of 3, 5, 6, 7, 8, 12 and 15 kc/s. The reference frequency chosen by the authors was 10 kc/s and so the slopes of the straight lines in the figure correspond to the attenuation coefficients at the particular frequencies relative to that at 10 kc/s.

A similar calculation has been done for the data of Khastgir *et al* (1960), and the relative attenuation coefficients have been determined. It has been found in this case that the plots showing $E(f_n, d)/E(f_0, d)$ against d are too scattered to yield a straight line. This is due to the fact that the distances reported by Khastgir *et al* are rather small (the maximum distance being 1600 km). Since equation (3) takes into account only the dominant mode in the series representation of the field component, it is valid only when the distance from the source is very great. Nevertheless, mean straight lines are drawn through the scatter of points representing the data of Khastgir *et al* and the relative attenuation coefficients have been determined (these mean curves are not shown). The reference frequency chosen by Khastgir *et al* is 12 kc/s. In order to effect a comparison between the results thus obtained and those given by others, the values of α at 10 and 12 kc/s have been taken from Taylor *et al* (1958) and the relative attenuation coefficients have been converted into absolute units. The final results are given table 1 and are illustrated in fig. 2.

It can be seen from fig. 2 that the results of Bhattacharya *et al* show a better general agreement with those of Taylor *et al* than the results of Khastgir *et al*. The main reason for this is, as already mentioned, the relatively

Table 1

Attenuation coefficients of VLF-waves for frequencies 3-15 kc/s

f Frequency in kc/s.	Attenuation coefficient α in db/1000 Km.		
	Taylor and Lange*	Bhattacharya and Rao	Khastgir and Srivastava
3	×	4.35	×
4	4.75	×	×
5	3.88	3.85	×
6	3.05	3.35	6.00
7	2.25	3.35	3.00
8	2.10	2.65	2.80
9	2.25	×	1.20
10	2.55	(2.55)	1.60
11	2.25	×	×
12	2.00	2.15	(2.00)
13	1.50	×	×
14	1.75	×	×
15	2.10	1.00	×

* These values are obtained approximately from the curves given by Taylor and Lange. The figures in brackets are taken from the data of Taylor and Lange for comparison (see text).

smaller distances of the lightning sources in the observations of Khastgir *et al.* Even between the curves corresponding to the data of Bhattacharya *et al* and to those of Taylor *et al* the discrepancies are quite apparant. The main source for these discrepancies is the assumption made by Bhattacharya *et al* regarding the constancy of spectral content of the source. Taylor *et al* (1958) overcame this unrealistic assumption by recording the same sferic at more than one station and by taking the ratio of the spectra at these stations. Also, while the data of Bhattacharya *et al* represent averages over a large number of sferics irrespective of the direction of travel, the terrain, etc, those of Taylor *et al* correspond to a few sferics originating from a particular storm.

ACKNOWLEDGEMENTS

The author expresses his thanks to Prof. S. R. Khastgir, D. S.c, F.N.I., for his interest in the problem. He is also grateful to the Govt. of India and the U.S.A. for sponsoring a research scheme under the PL-480 AID program.

REFERENCES

- Bhattacharya, H. and Manoranjan Rao, 1964, *J. Atmosph. Terr. Phys.*, **26**, 263.
- Bowe, P. W. A., 1951, *Phil. Mag.*, **42**, 121.
- Budden, K. G. 1961, *The wave-guide mode theory of wave propagation*, Logos Press, London.
- Chapman, F. W. and Mathews, W. D. 1953, *Nature, Lond.*, **172**, 495.
- Chapman, F. W. and Macario, R. C. V. 1956, *Nature, Lond.*, **177**, 930.
- Croom, D. L. 1964, *J. Atmosph. Terr. Phys.*, **26**, 1015.
- Gardner, F. F. 1950, *Phil. Mag.*, **41**, 1259.
- Hepburn, F. 1959, *Ph.D. Thesis*, University of Nottingham.
- 1960, *J. Atmosph. Terr. Phys.*, **19**, 37.
- Khastgir, S. R. and Srivastava, R. S. 1960, *Proc. Nat. Inst. Sci. (India)*, **26**, (Suppl. II), 58.
- Obayashi, T., Fujii, S. and Kidokoro, T. K. 1959, *J. Geomag. and Geoelect.*, **10**, 47.
- Taylor, W. L. and Lange, L. J. 1958, *Recent Advances in Atmospheric Electricity*, (Ed. Smith), Pergamon Press, London, p. 609.
- Taylor, W. L. 1960, *Journal of Research, NBS (Radio Propagation)*, **64 D**, 349.
- Wait, J. R. 1957, *Geofis. Pur. Appl.*, **37**, 103.
- 1958, *J. Geophys. Res.*, **63**, 125.
- 1962, *Electromagnetic Waves in Stratified Media*, Pergamon Press, N.Y.

THE CRYSTAL STRUCTURE OF SARCOSINE HYDROCHLORIDE]

S. C. BHATTACHARYYA, S. K. MAZUMDAR AND N. N. SAHA

CRYSTALLOGRAPHY AND MOLECULAR BIOLOGY DIVISION, SAHA INSTITUTE OF NUCLEAR
PHYSICS, CALCUTTA-9, INDIA.

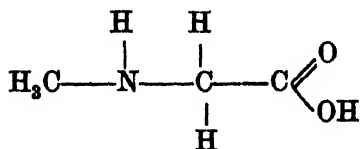
(Received December 20, 1967)

ABSTRACT. Crystals of sarcosine hydrochloride, $C_3H_7O_2N.HCl$, belong to the monoclinic space group $P2_1$ with cell dimensions $a=9.00 \text{ \AA}$, $b=5.93 \text{ \AA}$, $c=5.41 \text{ \AA}$ and $\beta=96^\circ$. The number of molecules per unit cell is two. The crystal structure has been solved by two dimensional Patterson and heavy atom Fourier synthesis. The positional co-ordinates of atoms (hydrogen atoms excluded), together with their isotropic temperature factors, have been refined by the method of least-squares, R value at this stage of refinement being 0.18.

The sarcosine molecule is not a zwitterion, the two C—O distances being $C(1)—O(1) = 1.19 \text{ \AA}$ and $C(1)—O(2)H = 1.35 \text{ \AA}$. The molecules in the crystal are held together by a three-dimensional network of hydrogen bonds of the types $N-H\cdots O$ and $O-H\cdots O$. The protonated α -amino nitrogen of the $C(2)—N^+H_2—C(3)$ group makes two hydrogen bonds with the two chlorine ions and assume a tetrahedral configuration.

INTRODUCTION

Sarcosine—a methyl derivative of glycine—belongs to a group of biologically important compounds containing 1-carbon pool participating in transmethylation reaction and its chemical formula is,



One of the objects of the study of this compound is to derive information about the influence of the substitution of a methyl group in the amino group of glycine on molecular structure and biological properties. Sarcosine in the form of different hydrohalides and metal complexes is being studied in our laboratory. The present communication deals with the crystal structure of sarcosine hydrochloride.

The needle shaped single crystals of sarcosine hydrochloride were prepared by slow evaporation of an aqueous solution of this compound at room temperature. The unit cell dimensions, as determined from rotation, oscillation and Weissenberg photographs, are :

$$a = 9.00 \text{ \AA}, \quad b = 5.93 \text{ \AA}, \quad c = 5.41 \text{ \AA} \text{ and } \beta = 96^\circ$$

Systematic absence of okl reflections for k odd and other considerations clearly indicate that the space group of sarcosine hydrochloride is $P2_1$. The density of crystal, as determined by the method of floatation is 1.56g.cm^{-3} while that calculated for two formula units of $(\text{C}_3\text{H}_7\text{O}_2\text{N.HCl})$ in the unit cell is 1.46g.cm^{-3} .

Three dimensional intensity data were collected about b and c axes by multiple film equi-inclination Weissenberg technique. The dimension of the crystals used was so small that the absorption correction was thought unnecessary (the linear absorption co-efficient for CuK_α being 55 cm^{-1}). The intensities were, however, corrected for spot shape, Lorentz and polarisation factors and put on absolute scale by Wilson's method.

STRUCTURE DETERMINATION

The positions of the two heavy atoms (i.e. chlorine) in the unit cell were located from two Patterson projections along b and c axes. The (010) projection being centrosymmetric, the structure analysis was first attempted with hol reflections only. A minimum function was drawn graphically using a single Cl-Cl peak in the Patterson synthesis projected on (010) . Though the minimum function could not reveal the structure satisfactorily, it provided some clue to the structure. At this stage a Fourier synthesis projected on (010) was calculated using about 50% of the observed $|F_o|$ values and the phases of the heavy atoms i.e. two chlorine atoms.

The Fourier synthesis was computed on IBM 1620 using the program written by us here in our laboratory. A tentative model of the structure was derived from the (010) Fourier projection and the minimum function. The x and z parameters

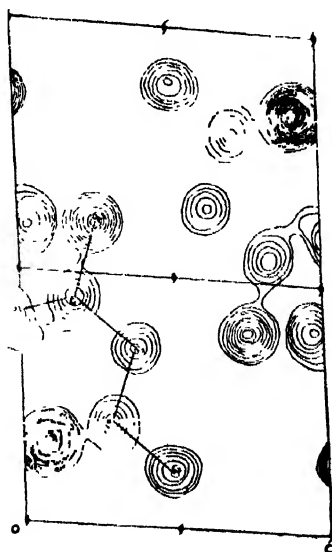


Fig. 1. Sarcosine hydrochloride: Fourier synthesis projected on (010) .

of the atoms obtained from the tentative model were used in the calculation of structure factors and the value of the disagreement factor (R) for *hol* reflections only was found to be 36.9%. The atomic parameters were first refined by a difference Fourier synthesis and later by least-squares method. After a few cycles of refinement the R value dropped to 19.8%. A unit weighting scheme was used throughout the refinement. A Fourier synthesis projected on (010) was calculated at this stage of refinement and is shown in fig. 1.

In order to determine the y co-ordinates of the atoms a chlorine-phased Fourier synthesis projected along c axis was calculated. Due to considerable overlapping of electron density peaks, as was observed on this projection and a spurious mirror plane of symmetry normal to b axis, as inherent in such structure, the determination of y co-ordinates of the atoms from $\rho(xy)$ projection became rather difficult. It was, therefore, thought worthwhile to take full advantage of the knowledge of the tentative model derived from the b -axis projection to interpret the Fourier map. Fortunately, this worked all right. The x and y co-ordinates of atoms thus obtained were refined by least-squares method using hko data alone. After four cycles of refinement the R value for hko reflections was 15.9%. At this stage, three-dimensional refinement of all the atomic parameters was started by least-squares method and after a few cycles of refinement the R value was found to be 18%. The atomic parameters as obtained at this stage of refinement are given in table 1. The intramolecular and intermolecular bond lengths and bond angles are given in tables 2 and 3, respectively, and diagrammatically shown in fig. 2.

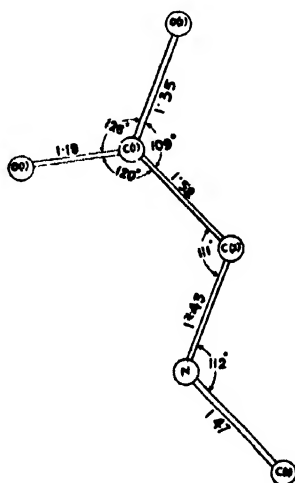


Fig. 2. Sarcosine hydrochloride: Bond lengths and bond angles.

DISCUSSION OF THE STRUCTURE

The two C—O bond lengths $C(1) - O(1) = 1.19 \text{ \AA}$ and $C(1) - O(2) = 1.35 \text{ \AA}$ in the carboxyl group of sarcosine hydrochloride (table 2) indicate that the hydrogen

atom is bound to O(2) and the molecule is not a zwitterion. The C = O double bond length (1.19 Å) agrees fairly well with the average value for this bond (1.205 Å) deduced by Hahn (1957) from other amino acids. The C—O single bond distance (1.35 Å), though shorter than standard C—O bond length (1.41 Å) quoted by Pauling (1960), is in good agreement with the average value (1.365 Å) cited by Hahn (1957). The C(2)—N⁺H₂ bond length (1.43 Å) of sarcosine hydrochloride has been found to be much shorter than the average value (1.502 Å) of this bond for other amino acids, but it compares well with that in N-acetylglycine (Donohue, *et al* 1962). The bond length C(1)—C(2) = 1.52 Å is in good agreement with that for the same bond in other amino acids. The bond distance C(3)—N(1) = 1.47 Å between terminal methyl carbon and the amino nitrogen agrees well with the standard C—N bond distance (Pauling, 1960). Of the three angles around the

Table 1

Sarcosine hydrochloride : atomic coordinates and isotropic temperature factors

Atom	<i>x/a</i>	<i>y/b</i>	<i>z/c</i>	<i>B</i> (Å ²)
Cl	.1602	.2548	.0760	1.28
O(1)	.4066	.7888	— .0483	1.59
O(2)	.6009	.7341	.2558	1.55
N(1)	.2087	.7604	.2804	2.19
C(1)	.4612	.7923	.1613	1.00
C(2)	.3617	.7981	.3704	0.52
C(3)	.1142	.7360	.4842	1.67

Table 2

Sarcosine hydrochloride : intermolecular bond lengths and bond angles

Bond length in Å		Bond angle in degrees	
C(1)—O(1)	1.19	O(1)—C(1)—O(2)	126°
C(1)—O(2)	1.35	O(1)—C(1)—C(2)	120°
C(1)—C(2)	1.52	O(2)—C(1)—C(2)	109°
C(2)—N(1)	1.43	C(1)—C(2)—N(1)	111°
N(1)—C(3)	1.47	C(2)—N(1)—C(3)	112°

Table 3

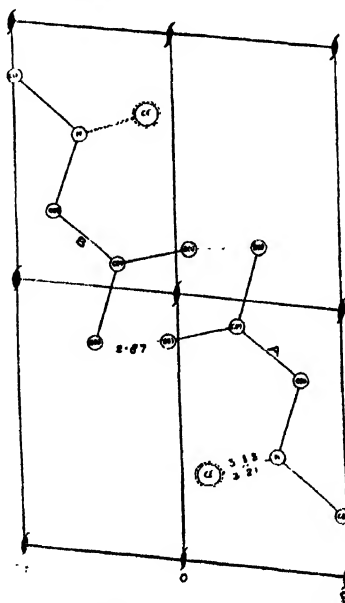
Sarcosine hydrochloride : intermolecular bond lengths and bond angles

Hydrogen bond distance (Å)		Hydrogen bond angles	
O(2)—H—O(1)	2.87	C(1)—O(2)—O(1)	108°54'
N(1)—H—Cl _I	3.15	C(2)—N(1)—Cl _{II}	93°10'
N(1)—H—Cl _{II}	3.21	C(2)—N(1)—Cl _{II}	110°12'
		C(3)—N(1)—Cl _I	95°22'
		C(3)—N(1)—Cl _{II}	106°23'

Cl_I and Cl_{II} are related by a unit translation along *b* axis.

carboxyl carbon C(1), the two on the either side of the C(1) = O(1) double bond, i.e. O(1)—C(1)—O(2) = 126° and O(1)—C(1)—C(2) = 120° are, as expected, greater than the remaining angle O(2)—C(1)—C(2) = 109°. As in other amino-acids the bond angle C(1)—C(2)—N in sarcosine hydrochloride is almost tetrahedral within the range of experimental error. The bond angle C(2)—N—C(3) which is expected to be 120°, as in N-acetylglycine, has been found to be 112°. It appears that the amino nitrogen in this case has assumed more or less a tetrahedral configuration.

The molecular arrangement of sarcosine hydrochloride projected on (010) is shown in fig. 3. There are altogether three hydrogen atoms in the molecule

Fig. 3. Sarcosine hydrochloride : Molecular packing viewed along *b* axis.

available for hydrogen bond formation, one from the carboxyl oxygen and two from amino nitrogen of C—N⁺H₂ group. The carboxyl oxygen O(2) of one mole-

cule forms a hydrogen bond with the carboxyl oxygen O(1) of the other symmetry related molecule. The O(2)—H---O(1) hydrogen bond distance is 2.87 Å (Table 3). The protonated amino nitrogen of the C(2)—N⁺H₂-CH₃ group forms two hydrogen bonds with two chlorine ions and assumes a tetrahedral configuration. The two N—H...Cl⁻ distances are 3.15 Å and 3.21 Å (table 3).

Three dimensional refinement of the structure on a fast computer is in progress. An elaborate account of the structural details and conformation will be published elsewhere shortly.

REFERENCES

- Donohue, J. and Marsh, R. E., 1962, *Acta Cryst.*, 15, 941.
Hahn, T., 1967, *Zeit. fur. Krist.*, 109, 438.
Pauling, L., 1960, *The Nature of the Chemical Bond*, Cornell University Press, p. 275.

E.P.R. INVESTIGATION ON ORTHORHOMBIC g -TENSORS IN COPPER RUBIDIUM SULPHATE HEXAHYDRATE, COPPER CESIUM SULPHATE HEXAHYDRATE AND COPPER THALLIUM SULPHATE HEXAHYDRATE

A. K. PAL, R. N. BAGCHI, P. R. SAHA AND R. K. SHAHA

MAGNETISM DEPARTMENT

INDIAN ASSOCIATION FOR THE CULTIVATION OF SCIENCE,
JADAVPUR, CALCUTTA-32. INDIA

(Received May 30, 1967)

ABSTRACT. Electron paramagnetic resonance technique has been employed to determine precisely the orthorhombic g -tensors and their orientations in the unit cell in three copper tutton salts, namely, copper rubidium sulphate hexahydrate, copper cesium sulphate hexahydrate and copper thallium sulphate hexahydrate. The results have been compared with those of other Tutton salts reported earlier (Bose *et al.*, 1964 ; Ghosh *et al.*, 1965). The comparison brings out clearly appreciable variation in the nature of the ligand field from salt to salt, presumably due to the long range effect arising from distant neighbours outside the primary ligand cluster.

INTRODUCTION

In previous communications (Bose *et al.*, 1964; Ghosh *et al.*, 1965) it has been shown that the e.p.r. method can be conveniently utilized in probing the three orthorhombic axes of the magnetic complex and finding the three principal ionic g -values in the single crystals of copper tutton salts. The results of application of the method to the case of copper potassium sulphate hexahydrate, copper ammonium sulphate hexahydrate, copper potassium selenate hexahydrate and copper ammonium selenate hexahydrate have been reported in that connection. The same method has been adopted to three other tutton salts, copper rubidium sulphate hexahydrate, copper cesium sulphate hexahydrate and copper thallium sulphate hexahydrate; and the results are discussed in the present paper.

METHOD OF MEASUREMENT

In all these salts variation of g -values was studied at room temperature in four natural planes of the crystals, namely $c(001)$ plane, $b(010)$ plane, $q(011$ or $0\bar{1}1)$ plane and $p(110$ or $1\bar{1}0)$ plane with the help of 1.2cm transmission type e.p.r. spectrometer (Ghosh *et al.*, 1963). Actually measurements in three planes are sufficient for determining the G_i 's denoting the principal ionic g -values and their orientations, but the measurement in an additional plane has been used to make a check on the final results.

As already described in the previous papers (Bose *et al.*, 1964; Ghosh *et al.*, 1965) for any setting of the crystal two values of g in a general plane containing the r.f. and the static magnetic field for two inequivalent ions in the unit cell are obtained at correspondingly different magnetic fields. The crystal is rotated in a given plane at intervals of 10° (sometimes 5°) and the g^2 -values have been plotted against the angular rotations. The general equation of the g^2 -ellipsoid as shown earlier (Bose *et al.*, 1964) is

$$\zeta_{11}X^2 + \zeta_{22}Y^2 + \zeta_{33}Z^2 + 2\zeta_{12}XY + 2\zeta_{23}YZ + 2\zeta_{13}XZ = 1,$$

where $\zeta_{11} = \sum_{i=1}^3 G_i^2 \alpha_i^2$, $\zeta_{22} = \sum_{i=1}^3 G_i^2 \beta_i^2$, $\zeta_{33} = \sum_{i=1}^3 G_i^2 \gamma_i^2$

$$\zeta_{12} = \sum_{i=1}^3 G_i^2 \alpha_i \beta_i, \quad \zeta_{13} = \sum_{i=1}^3 G_i^2 \alpha_i \gamma_i, \quad \zeta_{23} = \sum_{i=1}^3 G_i^2 \beta_i \gamma_i.$$

in which α_i , β_i , γ_i represent the direction cosines of G_i relative to the orthogonal $X(a)$, $Y(b)$ and $Z(c')$ axes of the crystal respectively.

RESULTS AND DISCUSSION

From the above measurements the six independent coefficients ζ_{ij} s defining the g^2 -ellipsoid have been determined. These are given in table 1.

Table 1

	ζ_{11}	ζ_{22}	ζ_{33}	ζ_{12}	ζ_{13}	ζ_{23}
$\text{Cu}(\text{RbSO}_4)_2 \cdot 6\text{H}_2\text{O}$	5.217	4.995	4.210	0.600	0	-0.125
$\text{Cu}(\text{CsSO}_4)_2 \cdot 6\text{H}_2\text{O}$	5.215	5.016	4.487	0.655	0.209	-0.029
$\text{Cu}(\text{TlSO}_4)_2 \cdot 6\text{H}_2\text{O}$	5.211	5.002	4.407	0.682	0.234	-0.193

By the method of matrix diagonalisation, from these six coefficients in each of these salts the principal g -values and their orientations have been obtained. The principal g -values and their orientations are shown in table 2 and table 3 respectively. The experimental data for other tutton salts reported elsewhere (Bose *et al.*, 1964; Ghosh *et al.*, 1965) are also included in tables 2 and 3 for comparison.

It will be seen from table 2 that the g^2 -ellipsoids in all these salts are of definitely orthorhombic symmetry. It will be seen by examining table 3 that the angle, the G_3 -axis makes with the symmetry axis of the monoclinic crystal (i.e. b -axis) is nearly the same for all the salts. On the other hand, all other angles vary appreciably for the different salts. This is perhaps due to the fact that in all the salts G_3 axis coincides with the approximate tetragonal axis of the paramagnetic complex and the difference in orientations in the different salts arise from a distribution of alkali atoms or acid radicals, which vary from salt to salt,

Table 2

	G_1	G_2	G_3
$\text{Cu}(\text{KSO}_4)_2 \cdot 6\text{H}_2\text{O}^*$	2.05 ₅	2.15 ₇	2.38 ₄
$\text{Cu}(\text{NH}_4\text{SO}_4)_2 \cdot 6\text{H}_2\text{O}^*$	2.05 ₈	2.20 ₈	2.35 ₈
$\text{Cu}(\text{Rb SO}_4)_2 \cdot 6\text{H}_2\text{O}$	2.04 ₃	2.12 ₇	2.39 ₂
$\text{Cu}(\text{Cs SO}_4)_2 \cdot 6\text{H}_2\text{O}$	2.07 ₅	2.14 ₉	2.40 ₇
$\text{Cu}(\text{Tl SO}_4)_2 \cdot 6\text{H}_2\text{O}$	2.02 ₇	2.17 ₀	2.40 ₈
$\text{Cu}(\text{KSeO}_4)_2 \cdot 6\text{H}_2\text{O}^\dagger$	2.07 ₅	2.16 ₄	2.35 ₇
$\text{Cu}(\text{NH}_4\text{SeO}_4)_2 \cdot 6\text{H}_2\text{O}^\dagger$	2.05 ₂	2.12 ₃	2.39 ₆

*Bose *et al.*, 1964, \dagger Ghosh *et al.*, 1965.

Table 3

	$\text{Cos}^{-1}\alpha_1$	$\text{Cos}^{-1}\beta_1$	$\text{Cos}^{-1}\gamma_1$	$\text{Cos}^{-1}\alpha_2$	$\text{Cos}^{-1}\beta_2$	$\text{Cos}^{-1}\gamma_2$	$\text{Cos}^{-1}\alpha_3$	$\text{Cos}^{-1}\beta_3$	$\text{Cos}^{-1}\gamma_3$
$\text{Cu}(\text{KSO}_4)_2 \cdot 6\text{H}_2\text{O}$	72°.8	106°.9	24°.5	54°.1	134°.1	114°.4	41°.1	49° (48°.6)*	92°
$\text{Cu}(\text{NH}_4\text{SO}_4)_2 \cdot 6\text{H}_2\text{O}$	109°.9	115°.7	33°.5	41°.9	131°.8	92°.2	54°.9	52°.7 (49°.6)*	56°.6
$\text{Cu}(\text{KSeO}_4)_2 \cdot 6\text{H}_2\text{O}$	108°.9	104°.5	23°.6	49°	139°	89°.4	46°.5	52°.6 (50°.7)*	66°.5
$\text{Cu}(\text{NH}_4\text{SeO}_4)_2 \cdot 6\text{H}_2\text{O}$	92°.2	128°	38°.1	36°.6	119°.3	109°.9	53°.5	51°.9 (51°.)*	59°
$\text{Cu}(\text{RbSO}_4)_2 \cdot 6\text{H}_2\text{O}$	98°.5	75°.1	17°.3	51°.2	136°.3	73°	40°.1	50°.1 (49°.8)*	93°.1
$\text{Cu}(\text{CsSO}_4)_2 \cdot 6\text{H}_2\text{O}$	121°.5	59°.4	46°.8	67°.5	125°.3	43°.8	40°.3	50°.3 (50°.9)*	83°.8
$\text{Cu}(\text{TlSO}_4)_2 \cdot 6\text{H}_2\text{O}$	118°.2	58°.9	44°.5	63°.9	124°.3	45°.6	40°.2	49°.9 (49°.7)*	87°.8

*Angular values within parentheses are the angles obtained from magnetic anisotropy experiments (Bose *et al.*, 1957) on the assumption of approximate tetragonal symmetry about the G_3 axis.

packed about the equatorial plane of the complex without affecting appreciably the relative orientations of the symmetry axis. The orientation angles do not appear to bear any strict sequence to the ionic radii of the alkali atoms or the acid radicals. It appears that the NH_4 and Tl sulphate salts which do not strictly belong to those of the alkali metal series K, Rb and Cs, have decidedly a more pronounced orthorhombicity of the ligand field. Their angular orientations except

$\cos^{-1} \beta_s$ also do not fit in the sequence of the other three sulphate salts. In the selenate salts, however, this larger orthorhombicity appears to be largely compensated by the presence of SeO_4^{-2} ion.

Variation in the g -tensor in the isomorphous Tutton salts indicates very clearly that the ligand field, especially its anisotropic part, is not only dependent on the primary ligand cluster but also upon what are the more distant neighbours and how they are situated, in short what is their effect upon the Cu^{2+} ion directly or indirectly through the immediately neighbouring water dipoles, since in the isomorphous series of salts it is only some of these distant neighbours which are different. The information, however, is as yet far from complete and situation is too complex to render an accurate explanation of the said difference in anisotropy behaviour.

ACKNOWLEDGMENT

The authors are indebted to Prof. A. Bose, D.Sc., F.N.I. for valuable suggestions and advice.

REFERENCES

- Bose, A., Ghosh, U. S., Bagchi, R. N. and Pal, A. K., 1964, *Indian J. Phys.*, **38**, 381.
Bose, A., Mitra S. C. and Sunil K. Dutta, 1957, *Proc. Roy. Soc.*, **A239**, 165.
Ghosh, U. S., Bagchi, R. N. and Pal, A. K., 1963, *Indian J. Phys.* **37**, 555.
Ghosh, U. S., Pal, A. K. and Bagchi, R. N., 1965, *J. Phys. Chem. Solids*, **26**, 2041.

Letters to the Editor

The Board of Editors does not hold itself responsible for opinions expressed in the letter published in this section. The notes containing short reports of original investigations communicated to this section should not contain many figures and should not exceed 500 words in length. The contributions reaching the Secretary by the 15th of any month may be expected to appear in the issue for the next month. No proof will be sent to the author.

30

ELECTRODE GLOW DURING ELECTROLYSIS AND LIBERATION OF HYDROGEN AND OXYGEN TOGETHER ON THE ELECTRODES

SANTI R. PALIT

DEPARTMENT OF PHYSICAL CHEMISTRY,
INDIAN ASSOCIATION FOR THE CULTIVATION OF SCIENCE,
JADAVPUR, CALCUTTA-32, INDIA.

(Received December, 30, 1967)

In a preliminary note (Palit, 1967) the author has reported that on applying a D.C. voltage of about 200 volts, one of the electrodes usually the cathode starts glowing after an initial incubation period. This is accompanied by a sharp drop in current strength, and by the discharge of big bubbles in place of the usual stream of fine bubbles of gas on the glowing electrode as also to some extent on the other electrode. However, the gas liberated on the electrodes on analysis showed results which are novel, unexpected and hitherto unknown, and the present note makes a preliminary report of the same.

Analysis of the Gas—The gas liberated on the cathode on analysis was found to contain both hydrogen and oxygen. However, the oxygen content was not constant. Sometimes the gas collected over the cathode could be exploded leaving a small residue and at other times the gas could not be exploded by electric spark. The gas collected over various electrolytes (0.2N solutions of hydrochloric acid, ammonium sulphate, barium chloride and potassium chloride) was found to contain on analysis in a Hempel pipette a considerable quantity of oxygen (15 to 50 percent by volume). This is probably the first time that oxygen is reported to be liberated in considerable quantity at the cathode side. We also checked up the composition of the gas liberated on the non-glowing anode. It was observed that as long as the glow does not start on the cathode, the anodic gas is composed of oxygen only. However, when the cathode starts glowing the gas liberated on

the anode is a mixture of oxygen with a large percentage of hydrogen. Similar things (i.e. the presence of oxygen in the cathodic gas and hydrogen in the anodic gas) are observed even under incipient glow condition, i.e. when there is no glow but big bubbles start forming on the respective electrode in place of the usual fine bubbles.

Faraday's Law—We checked up to see the relationship between the extent of electrodecomposition and Faraday's law. A number of electrolytes were examined and the results were quite surprising. The volume and composition of the gas liberated by electrodecomposition with the same quantity of electricity was found to be highly variable with the nature of the electrolyte and was usually in excess of that given by Faraday's law. However, the reproducibility was poor, there being large variation in yield from experiment to experiment under apparently the same conditions. Evidently, Faraday's law has nothing to do with this reported phenomenon and the mechanism must be different from normal ionic conduction mechanism.

Mechanism—It is difficult from such preliminary information to venture a suggestion about the mechanism of the observation in question. It was first thought that along with usual electrolysis another concurrent decomposition of water was taking place either due to the catalytic decomposition of water vapour on the glowing electrode, or due to localised high potential gradient owing to micro-cavity formation, or due to some local action. This idea agreed quite well with observations on barium chloride solution which gives this glow very well and where the volume of oxygen liberated at the cathode side is below 20 per cent. However, in some other cases (HCl, NaOH and KCl) this idea is untenable as the oxygen content of the cathodic gas is between 40 to 50 per cent. Plain decomposition of water can not account for more than one-third volume of oxygen. Besides, the idea of catalytic thermal decomposition of water can not be supported on thermodynamic grounds. The sudden drop of current along with disappearance of turbulence at the onset or near-onset of glow is very significant and is analogous to somedischARGE and glow phenomena in gases. Probably some kind of explanation from that field has to be invoked. However, it appears that some ion radicals (probably charged molecular aggregates of water) are involved. This is inferred from the fact that the intensity of glow as well as current strength decreases on applying a magnetic field at right angles to the flow of current. Further experiments are in progress and detailed results will be published later.

Thanks are due to Prithwis Kumar Basu for experimental assistance.

REFERENCE

Palit, S. R., 1967, *Indian J. Phys.* **41** 309.

N¹⁴ QUADRUPOLE RESONANCE IN BENZENE SULPHONAMIDE

KARTAR SINGH AND SANTOKH SINGH

MINISTRY DEFENCE, RESEARCH AND DEVELOPMENT ORGANIZATION,
DEFENCE SCIENCE LABORATORY, METCAFE HOUSE, DELHI-6, INDIA.

(Received November 9, 1967; Resubmitted January 25, 1968)

Nuclear quadrupole resonance in nitrogen compounds such as hexamethylene tetramine (Watkins *et al*, 1952), amino and amido compounds (Kojima *et al*, 1959), cyanogen compounds (Casabella *et al*, 1958), nitriles (Nigita *et al*, 1960), urea (Chiba, 1958), thiourea (Guibe, 1961), ammonia (Smith *et al*, 1964), nitrogen Schott (1962) (α phase) has been reported recently. Most of these compounds involve N—C, N \equiv N or N—H bonds. The resonant frequency in these compounds lies in the range 2Mc/s-5Mc/s. In this note N¹⁴ resonance in benzene sulphonamide (C₆H₅SO₂NH₂) is reported.

The resonance was studied by means of Pound-Watkins spectrometer (Pound, 1952; Pound *et al*, 1950) using frequency modulation. The incidental amplitude modulation was eliminated to a great extent by introducing a compensating modulation signal of suitable phase and amplitude (Dutcher *et al*, 1961). The resonant signal was amplified by a narrow band amplifier and rectified by a schuster-type detector (Schuster, 1951).

The compound benzene sulphonamide is slightly piezoelectric in nature and gives rise to a number of signals which are similar in shape to quadrupole resonance signal. This disturbance has been avoided by grinding the material to a fine powder which raises accoustical resonance of the crystallites but does not effect the quadrupole resonance. The whole of the frequency spectrum from about 1.5Mc/s to 7.0Mc/s has been scanned. Only one resonance line has been found at the liquid oxygen temperature. The resonance frequency lies at $f = 3.172 \text{ Mc/s} \pm .001 \text{ Mc/s}$ and the corresponding quadrupole coupling constant $e^2qQ/h = 4.229 \text{ Mc/s}$ assuming asymmetry parameter η to be zero. If there is a free internal rotation of NH₂ at this temperature or hydrogen bonding involving lone pair of electrons on nitrogen the asymmetry in field gradient may be removed. The line width between points of maximum slope is 1.1 Kc/s. A comparison of results for benzene sulphonamide and hexamethylene tetramine is given in table 1.

Table 1

Compound	ν_0 mc/s	$\Delta\nu_{12}$ kc/s	Reported
$C_6H_5SO_2NH_2$	3 172	1.1	—
$(CH_6) N_4$	3.402	1.1	1.08kc/s

The derivative of the absorption line is shown in fig. 1a. For comparison the shape of the resonance curve due to hexamethylene tetramine is given in fig. 1b.

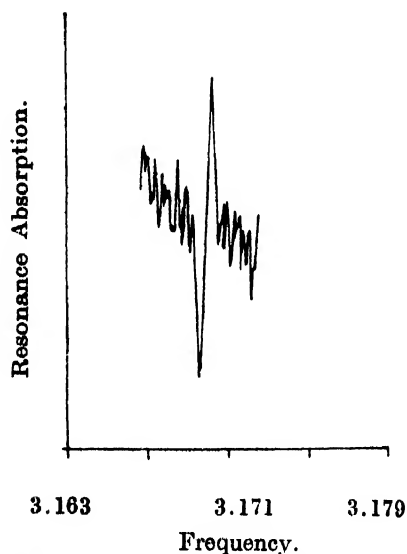


Fig. 1a. Resonance peak for benzeno sulphonamide.

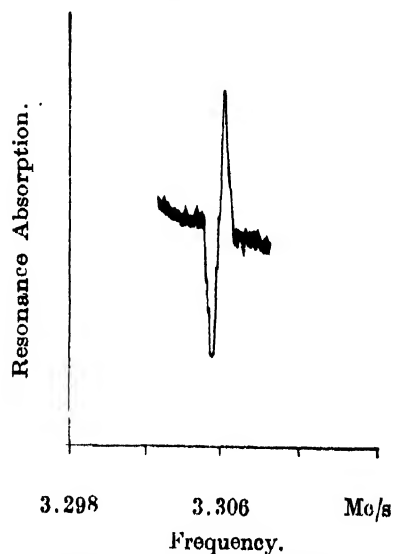


Fig. 1b. Resonance peak for the hexamino.

REFERENCES

- Casabella, P. Bray, P. J., 1958, *J. Chem. Phys.* **29**, 1105.
 Chiba, T. 1958, *J. Phys. Soc. Japan* **13**, 869.
 Dutcher, C. H. and Scott, T. A. 1961, *Rev. Sci. Instr.* **32**, 457.
 Guibe, L. 1960, *Arch. Sci. Switzerland*, **13**, 657.
 Kojima, S. et al, 1959, *J. Chem. Phys.* **31**, 271.
 Nogita, H., and Bray, P. J., 1960, *J. Chem. Phys.* **33**, 1876.
 Pound, R. V. and Knight, W. D. 1950, *Rev. Sci. Instr.* **21**, 219.
 Pound, R. V. 1952, *Prog. Nucl. Phys.*, **2**, 21.
 Schuster, N. A. 1951, *Rev. Sci. Instr.* **22**, 254.
 Scott, T. 1962, *J. Chem. Phys.* **36**, 1459.
 Smith, D. H. and Cotts, R. M. 1964, *J. Chem. Phys.* **41**, 2403.
 Watkins, G. and Pound, R. V. 1952, *Phys. Rev.* **85**, 1062.

SPACE GROUP AND UNIT CELL DIMENSIONS OF COMPLEX SILVER LUTIDINE NITRATE

T. RATHO AND MRS. M. KRISHNASWAMY

REGIONAL ENGINEERING COLLEGE, ROURKELA-8, INDIA.

(Received January 24, 1967).

Complex silver lutidine nitrate crystals are obtained by slow evaporation from an aqueous solution of the substance in acetone.

The crystals belong to the orthorhombic system. The unit cell dimensions are obtained from rotation and Weissenberg photographs along [001]. The dimensions of the unit cell are as follows :

$$a = 13.39\text{\AA}, \quad b = 16.93\text{\AA}, \quad c = 6.88\text{\AA}$$

zero and first layer Weissenberg photographs along [001] were taken and the following systematic extinction were obtained.

hoo—even present; *oko* —even present; *ool*—even present; *hko*—no condition; *okl*—*k*+1 even *hol*—*h* even

From the above conditions the space group is assigned as $P_{na}21$

The density was determined by flotation method and was found to be 1.564gm/cc

The density calculated by considering 4 molecules per unit cell is 1.636gm/cc.

Further work on the determination of the complete structure of the substance is in progress.

REFERENCES

Lipson, H., 1949, *Act. Cryst.* 2, 43.

Azroff, L. V. and Buerger, M. J. 1958, *The Powder Method*, 150.

A THEORY OF CLASSICAL LIQUIDS

S. C. MISRA

S. C. S. COLLEGE PURI, ORISSA, INDIA

(Received January 11, 1968)

In case of liquid the configuration changes continuously with time. Taking the time average of these different configurations, we would plot the average

number of nuclei as a function of the distance from the atom at the origin. We would now get a continuous curve with peaks at different distances, the heights of these peaks decreasing as the distance from the atom at the origin increases. After some distance this curve fails to show any structure. With rise of temperature the heights of these peaks and the number of distinct peaks decrease.

The continuous curve with peaks and flat regions in case of liquids can be explained by the assumption that a liquid consists of a large number of randomly oriented crystals of submicroscopic size, each containing quite a few atoms, and are connected with each other by layers of a wholly amorphous phase. The Submicroscopic crystals, again are formed and are broken down within a short time giving rise to new crystals which again break down and so on. These groups are named by Stewart (1930, 1931) as "cybotactic groups" (or regions).

It is of interest to note that the average number of nearest neighbours of the atom at the origin is approximately same as it is in the solid. So this atom in the above plot will vibrate as in a solid. Since this atom is chosen at random, we conclude that all the atoms in a liquid will vibrate and for simplicity we may assume that the amplitude of vibration of the atoms in the liquid state is constant and is the same as the amplitude at the melting point.

In addition to this vibration the atoms in the amorphous phase may have the motion of translation like the atoms in a perfect gas. To find the number of such atoms, we will assume after Silverman (1933) that the groups or clusters break down due to the impact of the simple atoms in the amorphous phase. When these simple atoms collided against a cluster, some of them are captured in the cluster and some atoms from the cluster are thrown out. Thus the old ones breaks down giving rise to new ones, We may take the possibility of emission to be proportional to the possibility of capture.

$\pi\lambda^2$ is the area of cross section of the incoming atom, where λ is the wavelength associated with it. If v is its velocity then $\pi\lambda^2v$ is the volume of the cylinder swept by the atom in unit time. If n is the number density, then $\pi\lambda^2vn$ is the number of encounters with this atom in unit time. Thus the possibility of capture and hence the possibility of emission may be taken to be proportional to the number of such encounters. The number density n can be taken as $Lf(v)$ where L is the total number of atoms present in the total volume V of which $f(V)$ is a function. Since $\lambda \propto \frac{1}{v}$ and $v \propto T^{\frac{1}{2}}$, the possibility of emission may be given by $\theta T^{-\frac{1}{2}}$ where θ is a constant.

Thus the number of atoms emitted by the clusters may be given by $\theta T^{-\frac{1}{2}}N$ where N is the number of atoms in the clusters. When temperature rises, this measures the temperature rate of decrease of the number of atoms in the clusters at the temperature. So we write

$$dN = -\theta T^{-\frac{1}{2}}NdT$$

from this we get

$$N = Le^{-2\theta(T - T_m)}$$

imposing the condition that at temperature T_m the solidification point all the L atoms lose the motion of translation i.e. at $T = T_m$, $N = L$. So the number of atoms in the amorphous phase is given by

$$L - N = L[1 - e^{-2\theta(T - T_m)}]$$

Using this expression we are explaining the equation of state, specific heat, surface tension, viscosity and diffusion of liquids in other papers.

REFERENCES

- Silverman, D. 1933, *Trans. Faraday Soc.* **29**, 1285
 Stewart, G. W. 1930, *Phys. Review*, **35**, 726
 1931, *Phys. Review*, **38**, 1575

BOOK REVIEWS

QUANTUM THEORY OF SOLIDS—C. Kittel. Published by John Wiley & Sons, Inc. 1963, pp. 453, Price \$ 13.50.

Professor C. Kittel's earlier contribution "Introduction to Solid State Physics" is well known to students and teachers of solid Physics, and has been widely accepted as a general text book for an introductory course in this developing branch of physics. The present contribution is intended for more advanced studies purely on the theoretical aspects of solid state physics, and may be considered as a natural extension of his earlier one, although a gap seems still to exist between the two contributions.

The book starts with a brief mathematical introduction stating the useful formulae of crystal physics and quantum mechanics necessary for calculations of solid state theory. The various excitations in solids have been dealt with very thoroughly in the first few chapters. The advanced theoretical treatment of field particles, phonon, magnon, plasmons, polarons, excitons etc. will interest the students of not only solid state physics but also quantum field theory and particle physics. The book covers the theoretical aspects of almost all essential topics of solid state physics including theories of energy bands, Brillouin zones, Fermi surface, metals and alloys, superconductivity, semiconductor properties, magneto-resistance, magnetodynamics in solids etc. The reviewer is particularly happy to find a separate chapter entirely devoted to Green's function technique which is often used very profitably in solving many problems of solid state theory. The main text in each chapter has been followed by a set of illuminating problems, left to the students as exercise.

The method of second quantization has been necessarily and frequently used in the first part of the book, and it would have been more appropriate if an introductory note on second quantization technique were included in the very first chapter on "Mathematical Introduction". The reviewer would have been happier if he could find a more elaborate treatment on the calculation of band structure in solids with specific examples and a separate chapter on the theories of various relaxation processes in solids.

The author has stated in the "Preface" that the present contribution is intended for use in a one year graduate course and the object of this text book is to present the central principles of quantum theory of solids to theoretical physicists generally and to those experimental solid state physicists who have had a one year course in quantum mechanics. In view of the very sophisticated nature of theoretical treatment of the most modern topics using advanced quantum mechanical techniques it is doubtful whether this new contribution may be regarded as a text book for graduate course at the present state of academic curriculum, usually followed by the universities. Moreover, the experimentalists, even after going through one year quantum mechanics course, are likely to find the presentation difficult. In the opinion of the reviewer this new contribution will be undoubtedly welcomed by the theoretical physicists working on solid state physics and quantum field theory. They will find to their satisfaction that most of the basic materials of their interest are well knit in a compact form and thus save much labour in searching huge volumes of scattered literature.

U. S. G.

ADVANCED QUANTUM THEORY—by P. Roman. Published by Addison-Wesley publishing Co. Inc, 1965, pp. 735, price \$ 17.50.

There is a growing feeling that the course of quantum mechanics should be divided into two parts, elementary and advanced. In fact, many universities now-a-days offer two courses

on quantum mechanics. But the topics covered in the courses vary from school to school. Here is a highly valuable contribution by Professor P. Roman which can serve as a proper text book and resolve the difficulty often encountered by the academic experts regarding the contents of a unified course of quantum mechanics, split into two parts.

The present contribution is entirely devoted to the advanced course, though the author with a high degree of skill in presentation starts from the basic postulates of quantum mechanics. The whole advanced course is so clearly and lucidly exposed that it needs very little preliminary knowledge of the elementary quantum mechanics. The contents are broadly divided into three parts. Part I deals with the framework of quantum theory including topics like second quantization, density matrix, time-development of quantized states, relativistic quantum mechanics etc. Part II mainly deals with collision theory and scattering, and contains topics like method of partial waves, dispersion relation, time-dependent approach to scattering theory, S-matrix, T-matrix, application of the collision theory to many-body problems etc. The reviewer is particularly happy to find the contents of Part III which is entirely devoted to symmetry properties of quantized systems and application of group theory to quantum mechanics. Concepts of symmetry and group theory are not only helpful in simplifying the procedures of quantum mechanical calculation but also highly valuable for a clear understanding of its principle. The author has rightly included it in the advanced course on quantum mechanics. Part I and II thus provide the knowledge of fundamental principles necessary for tackling the various problems of atomic, molecular, solid state physics and nuclear physics, field theory, particle physics, respectively, while part III is meant for strengthening the conceptual basis and general background of quantum mechanics. Each chapter ends with a brief summary and a number of systematically arranged illuminating problems, left to the students as exercise, where they will find the application of the basic principles developed in the text. The academic value of the book has been further enhanced by the inclusion of four important appendices on linear algebra and Hilbert space, group theory, Dirac equation and Green's function technique.

In the preface of the book the author has been outspoken in pointing out the misinterpretation of the oft-repeated argument that things are learned through their application. He writes "Physics, unlike agriculture, plumbing or even engineering at its very best is not merely a professional activity. In bygone days physics was often referred to as natural philosophy. Physics has been the product of ever searching, restlessly enquiring, wondering human mind, the outcome of a longing for understanding and appreciating the world we live in. It is this aspect of Physics which in this book, I tried to stress most." Indeed, the author has been very cautious in confining the students most to the conceptual area and logic of quantum mechanics. He is against any premature rush into applications before completing a systematic survey of the field and an adequate assimilation of the fundamental ideas and methodology. Often such premature rush leads to confusion and wrong conclusion. The reviewer is probably one of the few persons who entirely agree with the author. However, application and conceptual basis can always be made complementary, and the author would not have gone against his own principle if a few applications were included in the text with an eye to enhancing the conceptual basis and clarifying abstract logic.

U. S. G.

THE THEORY AND PRACTICE OF SCINTILLATION COUNTING—by J. B. Birks,
Published by Pergamon Press.

This book is a good replacement of an early book "Scintillation Counters" published in 1953 written by the same author. As the title indicates the book treats the theory of the scintillation mechanism and application of the scintillation counter. It is a good collection

of the development in the theoretical and practical aspects of scintillation counting. There is no other book in this line which is not already outdated and as such is useful for those who are developing new scintillators and for those who are using the scintillation counting arrangement. A major portion in the book is devoted to the scintillation process in organic, inorganic and other phosphors and acts as a guide and starting point for further research in developing new phosphors. Though the different components comprising the scintillation counter is discussed, its uses are so numerous that full description of all its applications is not possible even in this large volume and the author has very ably outlined the different applications with a good bibliography for any one interested in a particular application to find the early work quite easily. It is a good book in any library open to users in this field.

A. P. P.

ELEMENTARY PARTICLES & COSMIC RAYS By Alladi Ramakrishnan Published by Pergamon Press, London.

This is a comprehensive text-book on the theory of elementary particles, their interactions being described through quantum electrodynamics and through cosmic ray phenomena. Throughout, a physical approach has been made to the problems involving and characterized by complex, formal mathematical methods.

The book is divided into two parts. Part I covers the major portion of the book and is devoted to the theory of elementary particles and gives an integrated account of the quantum mechanical collision processes, meson physics and strange particles. The first two chapters give a detailed description of strange particle interactions. A systematic account is given of free particle wave functions of various elementary particles with the corresponding attributes embedded suitably in the wave function subject to the constraints of relativity. Particle interaction is then described through perturbation theory for a non-relativistic system. The kernel function formalism of Feynman and its relation to field theory have been described by introducing the concept of negative energy.

The author has used probabilistic approach extensively to the theory of scattering and perturbation expansions as well as in the theory of cascades in Part II. The stochastic processes in cascade theory is very well covered, thanks to the author's own original researches in this subject. Part II deals with the cosmic ray phenomena. Chapter X deals with the primary cosmic radiation and time variations. Unfortunately, this chapter on one of the most active fields of present-day cosmic-ray research has been scantily covered. Modulation effects barely get a page and the several theoretical models suggested for the diurnal and other modulation effects are insufficiently described. However, the "Interaction of Cosmic Rays with Matter" has been well taken up in Chapter XII. The theories on multiple production by Heisenberg, Fermi, Bhabha and others have been presented clearly and in sufficient detail.

The book, on the whole, is an excellent attempt to give an integrated presentation of some of the major fields in modern physics. It is a required reference book for all research workers in cosmic rays and theoretical physics. Also, this book is a "pedagogic necessity" in countries like India to meet the needs of the revived interest in theoretical physics and mathematical sciences.

S. D. O.

COLLECTED PAPERS OF KAPITZA VOL. 3. by D. ter Haar, pp. 224, Price 84/-sh, 1967. Pergamon Press.

This volume comprises a miscellany of papers, reviews, lectures, biographical memoirs, and philosophical articles representing a good cross section of the many sided activities of Professor Kapitza's mind.

The first published paper of Kapitza on cod liver oil is as far apart from his later works on ultra-magnetic fields or liquid helium machine or future of science, as is heaven from earth, but nevertheless gives interesting details of the primitive method of catching cod and extracting its liver oil in Russia.

Since Kapitza's review on the now obsolete book on Magnetism and Atomic structure by Stoner was published, the science of Magnetism has taken over entirely the new garb of Quantum Mechanics and assumed all the importance in revealing secrets of atomic and molecular structure, as well as in giving man control over electronic and even nuclear motions as predicted by Kapitza. Momentary high fields exceeding by one order, from those produced by Kapitza, have been generated leading to interesting revelations of atomic and nuclear binding energies. On the one hand, research on supraconductors has made feasible a supraconducting magnet giving a steady field of about 150 kilooersteds, on the other hand electronic devices have overcome the problem of breaking a power of the order of 10^5 kw through a small coil to give pulse fields of $\sim 10^6$ oersteds for a few milliseconds.

In reading through the article on the Institute of Physical Problems, which the present reviewer had the good fortune of visiting personally in 1956, it is felt that the remarks on the sophistication in equipments and the difficulties in procurement of such, apply with equal force today in most of the Indian research laboratories.

Four of the articles are aptly devoted to the memories of Rutherford, foremost of the pathfinders of the modern nuclear age, one of whose most renowned "boys" was Kapitza.

Without going into a detail of the other articles it suffices to say, wherever one opens the volume some originally interesting aspect catches the eye and fixes it until the article is finished and then one craves for more. One is, however, apt to be critical of Kapitza's attitude towards the German scientists in the article "We fight for freedom." In spite of what U.S.S.R. and other countries suffered in their fight with Kaiser's or Hitler's ideological Germany, it would be puerile to shut ones eyes to the achievements of German scientists, philosophers, literatures, poets, artists and composers.

A. B.

INDIAN JOURNAL OF PHYSICS. VOL. 41, 1967

Statement about ownership and other particulars about Indian Journal of Physics Vol. 41, 1967

FORM IV

(See Rule 8)

- | | | |
|---|----|---|
| 1. Place of publication | .. | 2 and 3, Raja Subodh Mallick Road, Calcutta-32. |
| 2. Periodicity of its publication | .. | Monthly |
| 3. Printer's Name | .. | Sri Kalipada Mukherjee |
| Nationality | .. | Indian |
| Address | .. | 204/1, B. T. Road, Calcutta-35. |
| 4. Publisher's Name | .. | Sri Samarandranath Sen |
| Nationality | .. | Indian |
| Address | .. | Registrar, I.A.C.S. Cal-32 |
| 5. Editor's Name | .. | (A List of Board of Editors is given below) |
| Nationality | .. | |
| Address | .. | |
| 6. Names and addresses of individuals who own the newspaper and partners or shareholders holding more than one per cent of the total capital. | | |

I, Samarandranath Sen, hereby declare that the particulars given above, are true to the best of my knowledge and belief.

- | | |
|---|---|
| 1. Prof. K. Banerjee, Indian, Noapara P.O. Barasat, 24-Parganas. | 8. Prof. S. R. Khastgir, Indian, Head of the Dept. of Physics, Bose Institute, 93/1, Acharya Prafulla Ch. Road Calcutta-9. |
| 2. Dr. G. N. Bhattacharyya, Indian, Department of Applied Physics University College of Technology 92, Acharya Prafulla Ch. Road, Calcutta-9. | 9. Prof. D. S. Kothari, Indian, Department of Physics, University of Delhi, Delhi. |
| 3. Prof. D. M. Bose, Indian, Director, Bose Institute 93/1, Acharya Prafulla Ch. Road, Calcutta-9. | 10. Prof. B. D. Nag Choudhuri Indian, Director, Saha Institute of Nuclear Physics 92, Acharya Prafulla Ch. Road, Calcutta-9. |
| 4. Prof. S. N. Bose, Indian, National Professor, 22, Iswar Mill Lane, Calcutta-6. | 11. Prof. K. R. Rao, Indian, Head of the Dept. of Physics, Andhra University, Waltair. |
| 5. Prof. S. D. Chatterjee, Indian, Head of the Dept. of Physics Jadavpur University Jadavpur, Calcutta-32. | 12. Dr. D. B. Sinha, Indian, Reader, Dept. of Applied Physics University College of Technology 92, Acharya Prafulla Ch. Road, Calcutta-9. |
| 6. Prof. P. S. Gill Indian, Director, Central Scientific Instruments Organisation, Chandigarh, Punjab. | 13. Prof. S. C. Sirkar, Indian Emeritus Professor, I.A.C.S. Calcutta-32. |
| 7. Prof. B. N. Srivastava, Indian, Acting Director, I.A.C.S. Jadavpur, Calcutta-32. | 14. Dr. R. Ramanna Indian Director, Physics Group, Bhabha Atomic Research, Centre, Apollo Pier Road, Bombay. |
| | 15. Prof. A. Bose, (Secretary), Indian, Department of Magnetism, I.A.C.S., Calcutta-32. |

Date 12.2.68

(Sd) Samarendra Nath Sen.

INDIAN JOURNAL OF PHYSICS

VOL. 41

No. 12

AND

VOL. 50

PROCEEDINGS

No. 12

OF THE

INDIAN ASSOCIATION FOR THE CULTIVATION OF SCIENCE

(Edited in collaboration with the Indian Physical Society).

DECEMBER 1967

PUBLISHED BY THE
INDIAN ASSOCIATION FOR THE CULTIVATION OF SCIENCE
JADAVPUR, CALCUTTA-32

ON THE DETERMINATION OF UNIT CELL DIMENSIONS FROM POWDER DIFFRACTION DATA OF COMPLEX SILVER LUTIDINE NITRATE

T. RATHO AND Mrs. M. KRISHNASWAMY

REGIONAL ENGINEERING COLLEGE ROURKELLA-8.

INDIA.

(Received May 25, 1967; Resubmitted December 26, 1967).

ABSTRACT. Debye Scherrer pattern of Silver Lutidine Nitrate has been photographed using a Rigaku camera at room temperature. The analysis showed that the crystal belongs to the orthorhombic system with $a = 13.7 \text{ \AA}$; $b = 16.8 \text{ \AA}$ and $C = 7.12 \text{ \AA}$; The unit cell contained four molecules. The space group $P222$ or $Pmm2$ can be assigned to the crystal.

INTRODUCTION

Silver Lutidine Nitrate, $\text{Ag}(\text{C}_7\text{H}_9\text{N})_2\text{NO}_3$ is a white microcrystalline substance whose dia-magnetic properties are of special interest. The crystallographic data was obtained from powder diffraction data.

EXPERIMENTAL

A Machlett A-2 X-ray diffraction tube with copper target running at 30 K.V. and 20 m.A. supplied the X-rays. The radiation was made monochromatic by using a Ni filter. The specimen, finely powdered, was contained in a Lindemann glass capillary tube of 0.5 mm diameter and of 0.01mm wall thickness. The Debye Scherrer pattern was obtained in four hours over a photographic film in a Rigaku camera of 9 cm diameter.

The interplanar distances were calculated accurately after measurements on the diffraction pattern and attempts were made to index the powder lines in terms of cubic, tetragonal and hexagonal systems. Since the data did not fit in with any of these systems, Lipson's method (Lipson, 1949) was tried.

The values of $\text{Sin}^2\theta$ for the rings in the powder pattern are given in the table. With these values the difference diagram was drawn according to Lipson's method. The frequently occurring values 0.00315, 0.00206 and 0.01175 were taken as the constants A , B and C respectively.

$$\left(A = \frac{\lambda^2}{4a^2}; \quad B = \frac{\lambda^2}{4b^2}; \quad C = \frac{\lambda^2}{4c^2} \right)$$

Using the equation $\text{Sin}^2\theta = Ah^2 + Bk^2 + Cl^2$ and the above values of A , B and C , all the rings were indexed quite satisfactorily.

The axial lengths calculated from the values of A , B , C are $a = 13.7\text{\AA}$, $b = 16.8\text{\AA}$, $c = 7.12\text{\AA}$.

The values of $\text{Sin}^2\theta$, calculated with these axial lengths, the intensities of the lines on the Debye Scherrer pattern and the corresponding d spacing values are given in the table.

As there have been no systematic absences the space group $P222$ or $Pmm2$ can be assigned to the crystal. It contains four molecules per unit cell. The observed density 1.5645gms./c.c. is in good agreement with the calculated density of 1.5535gms/c.c.

TABLE I

No. of lines	Intensity	$d\text{\AA}$ observed	Values of $\text{Sin}^2\theta$		Indices
			Observed	Calculated	
1.	w	14.188	0.00295	0.00315	100
2.	s	7.384	0.01090	0.01139	120
3.	s	7.018	0.01207	0.01175	001
				0.01260	200
4.	s	6.510	0.01402	0.01381	011
5.	vs	6.010	0.01645	0.01696	111
6.	vvw	5.409	0.02031	0.01999	021
				0.02084	220
7.	w	4.273	0.03255	0.03259	221
				0.03296	040
8.	m	4.088	0.03556	0.03611	140
9.	w	4.004	0.03709	0.03659	320
10.	ms	3.806	0.03998	0.04010	301
11.	s	3.702	0.04334	0.04289	231
12.	vs	3.537	0.04749	0.04700	002
				0.04786	141
				0.04689	330
13.	w	3.387	0.05174	0.05150	050
				0.05221	112
14.	vw	3.222	0.05725	0.05731	241
15.	vw	3.083	0.06253	0.06215	401
16.	vw	2.969	0.06742	0.06784	222
17.	vw	2.896	0.07086	0.07039	421
18.	w	2.744	0.07817	0.07875	500
				0.07741	312
				0.07814	232

TABLE I—(contd).

No. of lines	Intensity	$d\text{\AA}$ observed	Values of $\sin^2\theta$		Indices
			Observed	Calculated	
19.	s	2.705	0.08124	0.08081	510
				0.08069	431
20.	s	2.645	0.08570	0.08591	061
21.	s	2.581	0.08922	0.08906	161
22.	ms	2.461	0.09813	0.09850	052
				0.09851	261
				0.09874	521
23.	ms	2.347	0.1079	0.10781	013
				0.1083	342
24.	w	2.254	0.1170	0.11714	123
25.	ms	2.182	0.1248	0.12456	460
				0.12415	601
				0.12429	033
				0.12431	162
26.	w	2.091	0.1359	0.1363	461
				0.1362	313
27.	vw	2.042	0.1425	0.1420	551
				0.1423	323
28.	w	2.001	0.1484	0.1489	452
29.	w	1.913	0.1625	0.1625	612
30.	vw	1.867	0.1704	0.1699	253
31.	vw	1.823	0.1785	0.1789	632
32.	w	1.790	0.1854	0.1856	353
33.	vw	1.750	0.1939	0.1934	642
34.	vw	1.724	0.2000	0.2006	204
				0.1999	562
35.	vvw	1.7098	0.2033	0.2030	533
36.	vw	1.658	0.2161	0.2164	304
37.	w	1.618	0.2269	0.2274	623
38.	vw	1.584	0.2363	0.2360	553
39.	vw	1.564	0.2431	0.2427	154
40.	vw	1.540	0.2516	0.2521	254
				0.2521	643
				0.2622	064
41.	vvw	1.507	0.2618	0.2750	524
42.	vw	1.469	0.2755	0.2853	534
43.	vw	1.444	0.2849	0.2905	364
44.	vw	1.429	0.2909	0.3051	125
45.	vvw	1.396	0.3047	0.3242	315
46.	vw	1.355	0.3238	0.3344	644
47.	vw	1.332	0.3349	0.3484	155
48.	vvw	1.307	0.3480	0.3579	255
49.	vvw	1.288	0.3583		

ACKNOWLEDGMENTS

The authors wish to express their sincere thanks to the Education Ministry, Government of India for awarding a Research Scholarship to one of them (Mrs. M. Krishnaswamy). Their thanks are also due to Dr. D. V. Ramana Rao and Mr. R. N. Patel of the department of Chemistry for making the pure substance available to them.

REFERENCES

Lipson, H. 1949, *Act. Cryst.* **2**, 43.

Azroff and Buerger—*The Powder Method*.

ELASTIC SCATTERING OF ELECTRONS BY ATOMIC HYDROGEN

R. JHA AND N. C. SIL

DEPARTMENT OF THEORETICAL PHYSICS,

INDIAN ASSOCIATION FOR THE CULTIVATION OF SCIENCE,

JADAVPUR, CALCUTTA-32. INDIA

(Received June 14, 1967)

ABSTRACT. Variational method of Hulthén (1944) has been used to calculate the S -wave phase-shifts in elastic scattering of electrons by atomic hydrogen in the energy range of 0 to 13.6 eV, by solving the integro-differential equation of Temkin and Lamkin (1961) in the adiabatic exchange approximation. Calculations have also been performed for the polarisation potential of Obédkov (1963).

INTRODUCTION

We know that in the low energy collision of electron with hydrogen atom, both the exchange and polarisation effects have appreciable influence on the scattering process. The exchange effect arising out of the indistinguishability of the incident and bound electrons decreases with increase in energy. The polarisation effect which is due to the distortion of the atomic charge cloud under the influence of the incoming electron also falls with increase in energy but less rapidly compared to the exchange effect.

Variational calculations of the S -wave phase-shifts in elastic e - H scattering have been carried out by Massey and Moiseiwitsch (1951), and Staver (1951) and in the low energy limit by Seaton (1957), and by Borowitz and Greenberg (1957). All these calculations show that phase-shifts obtained in the exchange approximation differ markedly at low energies from those obtained in the central field approximation, which takes no account of the exchange effect. It may be mentioned that Massey and Moiseiwitsch (1951) took account of polarisation effect partially, by using the correlation term in the variational trial wave function. Bederson *et al.* (1958) have also carried out variational calculation of the problem taking into account exchange and polarisation. The polarisation potential has been taken from the works of Dalgarno and Lynn (1957). Malik and Trefftz (1960) have carried out numerical computation of the S , P and D wave phase-shifts in low energy elastic scattering of electrons by atomic hydrogen, with the inclusion of exchange and polarisation effects, represented by the polarisation

potential $V_p(r) = \frac{-\alpha}{2(25+r^4)}$ where α is the polarisability of hydrogen atom.

Temkin and Lamkin (1959, 1961) have introduced the polarised orbital method, similar in principle to perturbed stationary states method. In this method, Temkin and Lamkin (1961) have considered only the dipole polarisation potential, by making allowance for the dipole term in the first order perturbed hydrogen atom wave function derived by Dalgarno and Lewis (1955).

Here in the present work we have solved the integro-differential equation of Temkin and Lamkin (1961) by the variational method of Hulthén (1944) and have computed the S -wave phase-shifts in the low energy region. For comparison, we have further calculated the S -wave phase-shifts in the exchange approximation using another adiabatic dipole polarisation potential deduced by Ob'edkov (1963) the resulting integro-differential equation has been solved by the same variational method. For convenience, our calculations for the case of polarisation potentials of Temkin and Lamkin (1961) and those of Ob'edkov (1963) will be referred to as I and II respectively.

THEORY

The Schrödinger wave equation for the system of electron and hydrogen atom is

$$(H-E)\psi(r_1, r_2) = 0 \quad \dots (1)$$

$$H = -\frac{\hbar^2}{2m} \nabla_1^2 - \frac{\hbar^2}{2m} \nabla_2^2 - \frac{e^2}{r_1} - \frac{e^2}{r_2} + \frac{e^2}{r_{12}}, \text{ being the Hamiltonian of the}$$

system and E , the total energy of the system is $\frac{\hbar^2 k^2}{2m} + E_0$, r_1 and r_2 are the distances of the electrons from the nucleus and other symbols have their usual meanings.

To take into account the exchange effect we approximate ψ as follow:

$$\psi^\pm(r_1, r_2) = \frac{1}{\sqrt{2}} [F(r_1) \psi_0(r_2) \pm F(r_2) \psi_0(r_1)] \quad \dots (2)$$

where $\psi_0(r)$ is the wave function of the ground state of hydrogen atom, $F(r)$ is the wave function of the scattered electron, and $+v_s$ and $-v_s$ signs refer to the singlet and triplet cases respectively, the scattered electron wave function $F(r)$ have the asymptotic form

$$F(r) \rightarrow e^{ik \cdot r} + \frac{e^{ikr}}{r} f(\theta) \\ r \rightarrow \infty$$

$F(r)$ can be expanded as $F(r) = \sum_{l=0}^{\infty} \frac{f_l(r)}{r} Y_l^0(\Omega)$, $f_l(r)$ satisfying the boundary

condition

$$f_l(r) \rightarrow \sin \left(kr - \frac{l\pi}{2} + \eta_l \right);$$

$$r \rightarrow \infty$$

$f_s(r) \rightarrow 0$ where η_0 being the phase-shift.
 $r \rightarrow 0$

Following Massey and Moiseiwitsch (1951) we arrive at the following integro-differential equation (using atomic units)

$$\left[\frac{d^2}{dr_2^2} - \frac{l(l+1)}{r_2^2} + 2 \left(1 + \frac{1}{r_2} \right) e^{-2r_2} + k^2 \right] f_s(r_2)$$

$$= \pm \left(\frac{4}{2l+1} \right) \frac{e^{-r_2}}{r_2} \left[\frac{1}{r_2} \int_0^\infty f_s(r_1) \frac{2e^{-r_1}}{r_1} \times \frac{r_{<}^l}{r_{>+1}} dr_1 \right.$$

$$\left. - \left(\frac{k^2+1}{2} \right) \delta_{l0} \int_0^\infty f_l(r_1) \frac{2e^{-r_1}}{r_1} dr_1 \right] \quad \dots (3)$$

In the above derivation, no allowance has been made for the polarisation effect. We should take into consideration the fact that the bound electron wave function will be perturbed by the scattered electron. The polarised atom acts as a dipole yielding an additional attraction for the scattered electron which can be represented by a polarisation potential $V_p(r)$. It appears as a potential term in the scattering equation, in addition to the already existing static potential part. Thus, in exchange-adiabatic approximation, we get

$$\left[\frac{d^2}{dr_2^2} - \frac{l(l+1)}{r_2^2} + k^2 + 2 \left(1 + \frac{1}{r_2} \right) e^{-2r_2} - 2V_p(r_2) \right] f_l(r_2)$$

$$= \pm \left(\frac{4}{2l+1} \right) \frac{e^{-r_2}}{r_2} \left[\frac{1}{r_2} \int_0^\infty \frac{2e^{-r_1}}{r_1} f_l(r_1) \frac{r_{<}^l}{r_{>+1}} dr_1 \right.$$

$$\left. - \left(\frac{k^2+1}{2} \right) \delta_{l0} \int_0^\infty \frac{2e^{-r_1}}{r_1} f_l(r_1) dr_1 \right] \quad \dots (4)$$

Ob'edkov (1963) has arrived at the following expression for $V_p(r)$

$$V_p(r) = - \left(\frac{2}{3} \right)^6 \left[\frac{64}{9r^2} - \left(3r + 8 + \frac{32}{3r} + \frac{64}{9r^2} \right) e^{-1.5r} \right]^2 \quad \dots (5)$$

It has the asymptotic form $\frac{-\alpha}{r^4}$ where α is the polarisability of the atom.

The method of polarised orbitals of Temkin and Lamkin (1961) employs a trial wave function having the form

$$\psi^{\pm}(r_1, r_2) = F(r_1)[\psi_0(r_2) + \psi_{pol}(r_1, r_2)] \pm F(r_2)[\psi_0(r_1) + \psi_{pol}(r_2, r_1)]$$

$$\text{where } \psi_{pol}(r_1, r_2) = -\epsilon(r_1, r_2) \psi_0(r_2) \frac{1}{r_1^3} \left(\frac{r_2^3}{2} + r_2 \right) \cos \theta_{12}$$

$$\begin{aligned} \text{and } \epsilon(r_1, r_2) &= 1 \text{ for } r_1 > r_2 \\ &= 0 \text{ for } r_1 < r_2 \end{aligned}$$

According to Temkin and Lamkin

$$\iint Y_l^{0*}(\Omega_1) \psi_0^*(r_2) \left[\nabla_1^2 + \nabla_2^2 + \frac{2}{r_1} + \frac{2}{r_2} - \frac{2}{r_{12}} + k^2 - 1 \right] \psi^{\pm}(r_1, r_2) dr_2 d\Omega_1 = 0$$

which they have regarded as consistent with the first order determination of the perturbed function. They have arrived at the following radial equation for S -wave scattering in polarised orbital approximation.

$$\begin{aligned} & \left[-\frac{d^2}{dr_1^2} - 2e^{-2r_1} \left(1 + \frac{1}{r_1} \right) - \frac{\alpha_1(r_1)}{r_1^4} - k^2 \right] u(r_1) \\ & \pm \left[8r_1 e^{-r_1} \left\{ c_1 + \frac{1}{r_1} \int_0^{r_1} r_2 e^{-r_2} u(r_2) dr_2 - \int_0^{r_1} e^{-r_2} u(r_2) dr_2 \right\} \right. \\ & \quad \left. - \frac{8}{3} r_1 e^{-r_1} \left(\frac{r_1^3}{2} + r_1^2 \right) \times \left\{ c_2 - \int_0^{r_1} \frac{e^{-r_2}}{r_2^3} u(r_2) dr_2 \right\} \right] = 0 \quad \dots (6) \end{aligned}$$

$$\text{where } C_1 = \int_0^{\infty} \left\{ 1 - \left(\frac{1+k^2}{2} \right) r_2 \right\} e^{-r_2} u(r_2) dr_2$$

$$\text{and } C_2 = \int_0^{\infty} \frac{e^{-r_2}}{r_2^3} u(r_2) dr_2$$

The trial function $u(r) = \sin kr + (a + be^{-r})(1 - e^{-r}) \cos kr$ and the polarisation potential $V_p(r)$ is given by $\frac{\alpha_1(r)}{2r^4}$

where

$$\alpha_1(r) = \frac{2}{3} - \frac{2}{3} e^{-2r} (r^5 + \frac{2}{3} r^4 + 9r^3 + \frac{27}{5} r^2 + \frac{27}{3} r + \frac{27}{2})$$

(c.f. Temkin and Lamkin 1961). In the exchange-adiabatic approximation, the last term on the right-hand side is neglected. Moreover, certain new non-local terms on the right hand side have been omitted by Temkin and Lamkin (1961), their importance for p -wave scattering has been pointed out by Sloan (1964). The coupled-integro differential equation (6) has been solved by the same variation method with the polarisation potential

$$V_p(r) = -\frac{\alpha_1(r)}{2r^4}$$

We have solved the above equation (4) in the exchange-adiabatic approximation, by Hulthén's variational method and have computed the S -wave phase shifts, by the trial function

$$f(r) = \frac{\sin kr}{kr} + (a + be^{-r})(1 - e^{-r}) \frac{\cos kr}{kr} \text{ with } V_p(r) \text{ as given by (5).}$$

Here a is the phase-parameter and b is the adjustable variational parameter.

RESULTS AND DISCUSSIONS

We have obtained the scattering lengths $A \pm$ from our S -wave phase shifts (singlet and triplet) using modified effective range formula (O'Malley *et al*, 1962)

$$k \cot \eta_0(k^2) = -\frac{1}{A} + \frac{\pi \alpha k}{3} + \frac{4\alpha k^2}{3} \log(1.23\alpha^{\frac{1}{2}}k) \\ + \left(\frac{1}{2}r_0 + \frac{\pi \alpha^{\frac{1}{2}}}{3} - \frac{\pi \alpha^{3/2}}{3A^2} - \frac{\pi^2 \alpha^2}{9A^3} \right) k^2 + \dots$$

with the phase shift values $\eta_0(.0001)$ and $\eta_0(.000025)$. We have obtained the scattering lengths

$$A^+(\text{singlet}) = 6.767, 5.136$$

$$A^-(\text{triplet}) = 1.965, 1.776$$

in units of a_0 , for cases I and II respectively. These may be compared with Temkin and Lamkin values $A^+ = 5.6 a_0$ and $A^- = 1.9 a_0$. We have obtained the zero energy cross sections for the two cases (I and II) $57.37\pi a_0^2$ and $35.841\pi a_0^2$ respectively. In the adjoining table, we have given a list of our calculated S -wave phase-shift values and scattering lengths for the two cases along with those of Temkin and Lamkin (1961) for comparison.

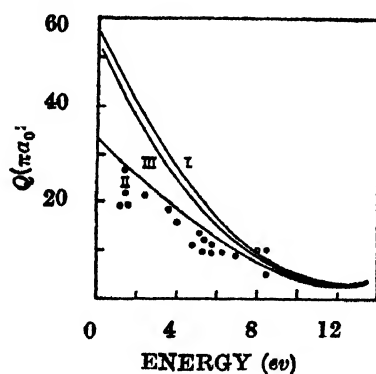
TABLE 1
S-wave phase shifts in radians

K	I		II		III	
	Singlet ()	Triplet (-)	Singlet ()	Triplet (-)	Singlet ()	Triplet (-)
.01	3.077	3.123	3.074	3.125	3.086	3.136
.1	2.522	2.949	2.495	2.927	2.701	2.962
.2	2.025	2.737	1.999	2.738	2.131	2.814
.5	1.157	2.146	1.250	2.189	1.272	2.245
1	.666	1.480	.742	1.490	.753	1.702

TABLE 2

	A (Singlet)	A ⁻ (Triplet)
I	6.5	1.9
II	6.767	1.965
III	5.136	1.776

In the figure we have plotted our S-wave elastic cross sections against energy for the two cases and have compared the results of S-wave elastic cross section of Temkin and Lamkin (1961) and the experimental data of Brackman *et al.* (1958).



The S-wave cross section (in πa_0^2) plotted against energy (in eV) of the incident electron.
 Curve I—Present calculations with polarisation potential of Temkin and Lamkin (1961)
 Curve II—Present calculations with polarisation potential of Obedkov (1963).
 Curve III—S-wave elastic cross section (in adiabatic exchange approximation) by Temkin and Lamkin (1961)
 Circle—Experimental points of Brackman *et al.* (1958).

We find that the agreement of Case II with experiment is better than with Case I. Again the results of our variational calculation in Case I is in close agreement with the corresponding results of numerical solution by Temkin and Lamkin (1961). Hence with a suitable choice of trial wave function it is possible to obtain results of comparable accuracy with those of numerical methods. The disagreement with experiment still left may be mainly due to the adiabatic assumption made in the polarisation potential and the neglect of higher order terms in it, especially the quadrupole one.

ACKNOWLEDGMENT

The authors are thankful to Prof. D. Basu for many valuable discussions. Thanks are also due to the authorities of C.M.E.R.I., Durgapur, for extending the facility of using I.B.M. 1620 Computer.

REFERENCES

- Borowitz, S., and Greenberg, H., 1957, *Bull. Amer. Phys. Soc.*, **2**, 172.
Bruckmann, R. T., W. L. Fite and Neynaber, R. H., 1958, *Phys. Rev.*, **122**, 1157.
Bransden, B. H., Dalgarno, A., John, T. L. and Souton, M. J., 1958, *Proc. Phys. Soc.*, **71**, 877.
Dalgarno, A. and Lewis, J. T., 1955, *Proc. Roy. Soc.*, **233**, 70.
Dalgarno, A. and Lynn, N., 1957, *Proc. Phys. Soc.*, **70**, 223.
Hulthén, L., 1944, *Kgl. Fysiograf. Salskap Lund Fork* **14**, No. 21.
Malik, F. B. and Trefftz, E., 1960, *Z. Astrophys.*, **50**, 96.
Massey, H. S. W. and Moiseiwitsch, B. L., 1951, *Proc. Roy. Soc.* **205**, 483.
Ob'edkov, V. D., 1963, *Vestn. Leningr. Univ. Ser. Fiz. Khim.* **22**, 23.
O'Malley, T. F., Rosenberg, L., and Spruch, L., 1962, *Phys. Rev.*, **125**, 1300.
Seaton, M. J., 1957, *Proc. Roy. Soc.*, **241**, 522.
Sloan, I. H., 1964, *Proc. Roy. Soc.*, **281**, 151.
Staver, T. B., 1951, *Arch. Math. Naturw. B*, **51**, 29.
Temkin, A. and Lamkin, J. C., 1961, *Phys. Rev.*, **121**, 788.

AMPLITUDE PARITY AND X^0 -MESON

S. K. KUNDU

REGIONAL COLLEGE OF EDUCATION, BHUBANESWAR, ORISSA, INDIA.

(Received June 30, 1967).

ABSTRACT. The A -invariance of Bronzan and Low is discussed and its relevance to X^0 -decay processes is examined for the spin parity alternatives $J^P = 0^-$ or 1^+ . It is shown that $A = 1$ favours the present experimental observations.

INTRODUCTION

The abundance of $\rho^0\gamma$ decays relative to $\omega^0\gamma$ decays for the X^0 -meson is explained by assigning to it a positive value of A -parity (Bronzan *et al*, 1964). This assignment makes $\eta\pi^+\pi^-$ an A -forbidden mode since an A -allowed $\eta\pi^+\pi^-$ channel would be irreconcilable with the narrowness of the X^0 resonance. If X^0 is assigned its usually accepted spin-parity $J^P = 0^-$, then $A = 1$ for the X^0 makes $X^0 \rightarrow 2\gamma$ an A -allowed process. An estimate of the decay rate of $X^0 \rightarrow 2\gamma$ suggests that this should be an observable mode. On the other hand $J^P = 1^+$ would forbid $X^0 \rightarrow 2\gamma$ absolutely. Estimates of $X^0 \rightarrow \pi^+\pi^-\gamma$ are made for both spin-parity assignments and $J^P = 1^+$ is found to give better agreement for the branching ratios as well as account for the failure to see $X^0 \rightarrow 2\gamma$. Further remarks are also made about the $\pi^+\pi^-\gamma$ mode and it is shown how the angular distribution for the $J^P = 1^+$ case could simulate the unique $J^P = 0^-$ distribution.

ANALYSIS AND CONCLUSIONS

The decay modes for the observed resonance at 960 MeV (X^0 -meson) suggests that $G = C = 1$ and hence $I = 0$. Further investigations (Goldberg *et al*, 1964; Kalbfleisch *et al*, 1964) show that $X^0 \rightarrow \gamma + \rho^0$ is a prominent decay mode while $X^0 \rightarrow \gamma + \omega^0$ is not. Both the transitions are C -allowed, but $A = 1$ for ρ^0 and $A = -1$ for ω^0 . This later consideration immediately suggests the applicability of an A -selection rule. The three boson decay such as $\eta \rightarrow \pi^0 + \pi^+ + \pi^-$ yields for its decay width the value 0.3 MeV corresponding to $G^2 = 1$ (Brown *et al* 1964). If X^0 has values $J^P = 0^-$ and $A = 1$ then $X^0 \rightarrow \eta + \pi^+ + \pi^-$ is A -forbidden and using the same technique (Brown *et al*, 1964) one gets

$$\Gamma(X^0 \rightarrow \eta + \pi^+ + \pi^-) \approx (n/\alpha)^2 (m_\eta/m_\pi)(Q_\pi/Q_\eta) a \Gamma(\eta \rightarrow 3\pi) \quad \dots (1)$$

where the term $(n/\alpha)^2$ corresponds to the G^- forbiddenness of $\eta \rightarrow 3\pi$ and Q is a phase space factor. The average $\delta m/m$ values for baryons is used to compute n .

For the case $J^P = 1^+$, we compare the kinematic factors with decay as follows

$$\Gamma(\omega^0 \rightarrow 3\pi) \approx 3\Gamma_0(m_0/m_\omega)(E_\omega/m_0)^4(3\pi/128) \quad \dots \quad (2)$$

$$\Gamma(X^0 \rightarrow 3\pi) \approx \Gamma_0(m_0/m_x)(m_x/m_\pi)^4(E_x/m_0)^2(\pi/16)a \quad \dots \quad (3)$$

where Γ_0 is a set of standard factors, $E_\omega = m_\omega - 3m_\pi$ and $E_x = m_x - 2m_\pi - m_\eta$, the factors $(3\pi/128)$ and $(\pi/16)$ are phase space integrals, and the factor 3 in $\Gamma(\omega^0 \rightarrow 3\pi)$ comes from the symmetry of the final state. Inserting numerical values and taking $\Gamma(\eta \rightarrow 3\pi) \approx 300$ eV and $\Gamma(\omega^0 \rightarrow 3\pi) \approx 9.5$ MeV (Gelfand *et al.*, 1963), one finds

$$\Gamma(X^0 \rightarrow \eta + \pi^+ + \pi^-) \approx 0.3 \text{ MeV} \quad \dots \quad (4)$$

and it is same for both the J^P values 0^- and 1^+ . The total decay width of the X^0 -meson, without A -forbiddenness factor however, would be of the order of 20 MeV with allowance for the $\eta\pi^0\pi^0$ mode, and hence contradicts observation*. Thus we conclude that $A = 1$ for X^0 -meson favours the proceeding analysis relating to the spin-parity assignments $J^P = 0^-$ or 1^+ . This further suggests that $X^0 \rightarrow 2\gamma$ is A -allowed in contrast to $\pi \rightarrow 2\gamma$ or $\eta \rightarrow 2\gamma$ for which we use $a = 1/40$ the A -forbiddenness factor (Bronzan *et al.*, 1964). If $J^P = 0^-$ for the X^0 -meson, we can scale as (energy)³ from the measurement $\Gamma(\pi \rightarrow 2\gamma) \approx 6$ eV,

$$\begin{aligned} \Gamma(X^0 \rightarrow 2\gamma) &\approx (m_x/m_\pi)^3 a^{-1} \Gamma(\pi \rightarrow 2\gamma) \\ &\approx 0.1 \text{ MeV} \end{aligned} \quad \dots \quad (5)$$

Since the total width for the X^0 -meson is less than 4 MeV, $X^0 \rightarrow 2\gamma$ should be an observable mode. The next possible assignment will be $J^P = 1^+$, for which 2γ decay for X^0 -meson is absolutely forbidden. In the following we make numerical estimate for the X^0 -decay ratios for its two J^P values. The $\gamma\pi^+\pi^-$ decay is assumed to pass through ρ^0 as an intermediate state (Kalbfleisch *et al.*, 1964) with a decay width given by

$$\Gamma(X^0 \rightarrow \gamma + \rho^0) \approx 2\alpha\mu^2 q(q/m_0)^{2\lambda} \left\{ \frac{1}{a} \right\} \quad \dots \quad (6)$$

where q is the γ -energy, λ the multipole order, $m_0 \approx 1$ BeV as the average baryon mass and μ measures the anomalous magnetic moments. We take $\mu \approx 1$ for electrical transitions, hence

$$\Gamma(X^0 \rightarrow \gamma + \rho^0) \approx 0.1 \text{ MeV} \quad \dots \quad (7)$$

* This result also prompted the independent remark that $X^0 \rightarrow \eta + \pi^+ + \pi^-$ should be A -forbidden to make the electromagnetic decay competitive (Baider *et al.*, 1965).

For magnetic transitions we use $\mu \approx 3$ and get

$$\Gamma(X^0 \rightarrow \gamma + \rho^0) \approx 1.0 \text{ MeV for } M1 \quad \dots (8)$$

$$\approx 0.04 \text{ MeV for } M2 \quad \dots (9)$$

where the transitions are A -allowed.

The effectiveness of the preceeding calculations is checked by considering the process $\eta \rightarrow \gamma + \rho^0$. The only difference should be that ρ^0 is virtual. We multiply (7), (8) and (9) by $(2\pi)^{-1} \Gamma(\eta \rightarrow \gamma + \rho^0) dE / (E - E_0)^2$ and integrate over all values of E , where $E = (m_\eta - 2m_\pi - q)$ with $E_0 = m_\rho - 2m_\pi$. Also $\Gamma(\eta \rightarrow \gamma + \rho^0) = \Gamma_0 (E/E_0)^{3/2}$ and $\Gamma_0 \approx 100 \text{ MeV}$. This gives on using $a = (1/40)$, the value

$$\Gamma(\eta \rightarrow \gamma + \rho^0) \approx 60 \text{ eV} \quad (10)$$

All the results are tabulated as follows :

J^P	$\Gamma(X^0 \rightarrow \text{all decay modes}) \text{ MeV}$	$\Gamma(X^0 \rightarrow \eta + \pi^+ + \pi^-) \text{ MeV}$	$\Gamma(X^0 \rightarrow \gamma + \pi^+ + \pi^-) \text{ MeV}$	$\Gamma(X^0 \rightarrow 2\gamma) \text{ MeV}$
0^-	1.60	0.30	1.00	0.10
1^+	0.60	0.30	0.14	0.00

The decay ratios are in better agreement with observations for $J^P = 1^+$. However the detection of $X^0 \rightarrow 2\gamma$ would exlude $J^P = 1^+$, this mode should be present to order 5-10% for $J^P = 0^-$. It is interesting to note that in the decay process $X^0 \rightarrow \gamma + \pi^+ + \pi^-$ the spin 1 of the intermediate ρ^0 state assures that the angular distribution is $1 + b \cos^2 \theta$. The parameter b is strongly dependent on $E1$ - $M2$ interference for $J^P = 1^+$, being $b = \frac{(r-3)^2 - 8}{(r+1)^2}$, where r is the amplitude ratio ($M2/E1$). Following the suggestions in equation (7), (8) and (9) that $r = 0.6$, one has $b = -(7/8)$, a good approximation to the value $b = -1$ characteristic of $J^P = 0^-$. Angular correlation between the X^0 production and decay planes would exlude $J^P = 0^-$ but the absence of such correlation might only reflect lack of X^0 -polarization.

ACKNOWLEDGMENT

The author wishes to thank Professor Abdus Salam, F.R.S. for useful comments

REFERENCES

- Badier, J. *et al.*, 1965, *Phys. Rev. Letters*, **17**, 337.
Bronzan, J. B. and Low, F. E., 1964, *Phys. Rev. Letters*, **12**, 522.
Brown, L. M. and Faier, H., 1964, *Phys. Rev. Letters*, **13**, 73.
Brown, L. M. and Singer, P., 1964, *Phys. Rev.*, **133**, B812.
Gelfand, N. *et al.*, 1963, *Phys. Rev. Letters*, **11**, 436.
Goldberg, M. *et al.*, 1964, *Phys. Rev. Letters*, **12**, 546.
Goldberg, M. *et al.*, 1964, *Phys. Rev. Letters*, **13**, 249.
Kalbfleisch, G. R. *et al.*, 1964, *Phys. Rev. Letters*, **12**, 527.
Kalbfleisch, G. R. *et al.*, 1964, *Phys. Rev. Letters*, **13**, 349.

NOTE ON FORCED VIBRATION OF A THIN NON-HOMOGENEOUS CIRCULAR PLATE WITH A CENTRAL HOLE

R. K. BOSE

DEPARTMENT OF MATHEMATICS, R. E. COLLEGE, ROURKELA-8, INDIA.

(Received July 26, 1967 ; Resubmitted January 30, 1968).

ABSTRACT. In this paper we have considered the vibration produced in a thin non-homogeneous circular plate with a central hole by an application of a periodic force acting on the internal boundary. Young's modulus and density are supposed to vary linearly with the radius vector.

We have determined the displacement produced due to the elastic vibrations produced in a thin circular non-homogeneous plate by an application of an internal pressure which varies with time. Here Young's modulus E and density ρ are taken as $E = E_0 r$ and $\rho = \rho_0 r$, where r is the radius vector and E_0 and ρ_0 are constants. The stress distribution is chosen symmetrical with respect to the axis through the centre of the plate and perpendicular to the plane (xy -plane) of it. By symmetry it follows that shearing stress $\sigma_{r\theta}$ vanishes.

The equation of motion is

$$\frac{\partial \sigma_{rr}}{\partial r} + \frac{\sigma_{rr} - \sigma_{\theta\theta}}{r} = \rho \frac{\partial^2 u}{\partial t^2} \quad \dots \quad (1)$$

The stress strain relation are

$$\left. \begin{aligned} E \cdot e_{rr} &= \sigma_{rr} - \nu \sigma_{\theta\theta} \\ E \cdot e_{\theta\theta} &= \sigma_{\theta\theta} - \nu \sigma_{rr} \end{aligned} \right\} \quad \dots \quad (2)$$

The strain components are

$$e_{rr} = \frac{\partial u}{\partial r} \text{ and } e_{\theta\theta} = \frac{u}{r} \quad (3)$$

From equations (2) and (3) we have

$$\left. \begin{aligned} \sigma_{rr} &= \frac{E}{1-\nu^2} \left[\frac{\partial u}{\partial r} + \nu \frac{u}{r} \right] = \frac{E_0}{1-\nu^2} \left[r \frac{\partial u}{\partial r} + \nu u \right] \\ \sigma_{\theta\theta} &= \frac{E}{1-\nu^2} \left[\frac{u}{r} + \nu \frac{\partial u}{\partial r} \right] = \frac{E_0}{1-\nu^2} \left[u + \nu r \frac{\partial u}{\partial r} \right] \end{aligned} \right\} \quad \dots \quad (4)$$

Since we have $E = E_0 r$ and $\rho = \rho_0 r$... (5)

From equations (1) and (4) we have

$$r^2 \frac{\partial^2 u}{\partial r^2} + 2r \frac{\partial u}{\partial r} - (1-\nu)u = \frac{\rho_0}{E_0} (1-\nu^2) r^2 \frac{\partial^2 u}{\partial t^2} \quad \dots (6)$$

Boundary conditions :

$$\left. \begin{aligned} \sigma_{rr} &= -P(1-\cos \omega t) & r &= r_0, \quad t > 0 \\ \sigma_{rr} &= 0 & r &= r_1, \quad t > 0 \end{aligned} \right\} \quad \dots (7)$$

The initial conditions are that,

$$\text{at } t = 0, \quad u = \frac{\partial u}{\partial t} = 0, \quad r_0 \leq r \leq r_1$$

Multiplying both sides of the equation (6) by e^{-pt} and integrating with respect to t from 0 to ∞ , we obtain the ordinary differential equation

$$r^2 \frac{d^2 \bar{u}}{dr^2} + 2r \frac{d\bar{u}}{dr} + [-(1-\nu) - a^2 r^2 p^2] \bar{u} = 0 \quad \dots (8)$$

where $a^2 = \frac{\rho_0}{E_0} (1-\nu^2)$ and $\bar{u} = \int_0^\infty u e^{-pt} dt.$

Solving equation (8) we have

$$\bar{u} = r^{-1} [AI_k(\text{apr}) + BK_k(\text{apr})] \quad \dots (9)$$

where $k = \frac{\sqrt{5-4\nu}}{2}$

Taking the value of the Poisson's ratio $\nu = 0.25$ Equation (9) becomes

$$\bar{u} = r^{-1} [AI_1(\text{par}) + BK_1(\text{par})] \quad \dots (10)$$

where $a^2 = \frac{\rho_0}{E_0} \cdot \frac{15}{16}$

Taking Laplace transform of equation (7) we have

$$\left. \begin{aligned} \sigma_{rr} &= \frac{E_0}{1-\nu^2} \left[r \frac{\partial \bar{u}}{\partial r} + \nu \bar{u} \right] = \frac{-P\omega^2}{p(p^2 + \omega^2)} & r &= r_0 \\ \sigma_{rr} &= \frac{E_0}{1-\nu^2} \left[r \frac{\partial \bar{u}}{\partial r} + \nu \bar{u} \right] = 0 & r &= r_1 \end{aligned} \right\} \quad \dots (11)$$

Substituting equation (10) in Eq. (11) we have

$$\left. \begin{aligned} & A \left[I_1(apr_0) - \frac{4}{5} r_0 ap I_0(apr_0) \right] \\ & \quad + B \left[K_1(apr_0) + \frac{4}{5} ar_0 p K_0(apr_0) \right] = \frac{4}{5} r_0^{\frac{1}{2}} \frac{P \omega^2}{p(p^2 + \omega^2)} \\ & \quad \vdots \\ & A \left[I_1(apr_1) - \frac{4}{5} ar_1 p I_0(apr_1) \right] + B \left[K_1(apr_1) + \frac{4}{5} ar_1 p K_0(apr_1) \right] = 0 \end{aligned} \right\} \dots \quad (12)$$

If we write the equation (12) in the form

$$AL_0 + BM_0 - Q = 0$$

$$AL_1 + BM_1 + 0 = 0$$

where

$$\left. \begin{aligned} L_{0,1} &= I_1(apr_{0,1}) - \frac{4}{5} r_{0,1} ap I_0(apr_1) \\ M_{0,1} &= K_1(apr_{0,1}) + \frac{4}{5} r_{0,1} ap K_0(apr_{0,1}) \\ Q &= \frac{4}{5} r_0^{\frac{1}{2}} \frac{P \omega^2}{p(p^2 + \omega^2)} \end{aligned} \right\} \dots \quad (13)$$

and

$$Q = \frac{4}{5} r_0^{\frac{1}{2}} \frac{P \omega^2}{p(p^2 + \omega^2)}$$

Solving for A and B we have

$$A = \frac{M_1 Q}{L_0 M_1 - M_0 L_1} \quad \text{and} \quad B = \frac{-L_1 Q}{L_0 M_1 - M_0 L_1} \quad \dots \quad (14)$$

By (13) and (14), equation (10) becomes

$$\left. \begin{aligned} \bar{u} &= r^{-1} \cdot Q \cdot \frac{[M_1 I_1(arp) - L_1 K_1(arp)]}{L_0 M_1 - M_0 L_1} \\ &= r^{-1} \cdot \frac{4}{5} r_0^{\frac{1}{2}} \cdot \frac{P \cdot \omega^2}{p(p^2 + \omega^2)} \cdot \frac{F(p)}{G(p)} \\ \text{where} \quad F(p) &= \left[K_1(apr_1) + \frac{4}{5} ar_1 p K_0(apr_1) \right] I_1(arp) \\ &\quad - \left[I_1(apr_1) - \frac{4}{5} apr_1 I_0(apr_1) \right] K_1(arp) \end{aligned} \right\} \dots \quad (15)$$

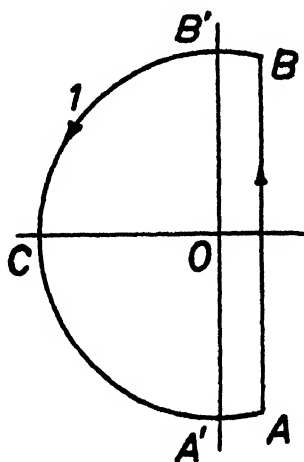
and

$$G(p) = \left[I_1(apr_0) - \frac{4}{5} r_0 a p I_0(apr_0) \right] \left[K_1(apr_1) + \frac{4}{5} ar_1 p K_0(apr_1) \right] \\ - \left[K_1(apr_0) + \frac{4}{5} ar_0 p K_0(apr_0) \right] \left[I_1(apr_1) - \frac{4}{5} apr_1 I_0(apr_1) \right]$$

Applying Laplace's Inversion Theorem we have for the displacement

$$\frac{5}{4} \frac{r_0 - r_1}{Pw^2} u = \int_{c-i\infty}^{c+i\infty} \frac{F(p)}{p(p^2 + w^2)G(p)} e^{pt} dp \quad \dots (16)$$

To evaluate the integral on the right-hand side of the above equation, consider the integral taken round the closed contour consisting of a line at a distance c from the imaginary axis and the portion (lying to the left) of a circle whose centre is the origin and whose radius is $R = \frac{(n + \frac{1}{2})\pi}{(r_1 - r_0)a}$ — chosen so that the contour avoids all poles of the integrand. It can be shown that the limit of the integral around this circular arc tends to zero as n tends to infinity so that Cauchy's theorem enables us to replace, the line integral in equation (16) by the sum of the residues of the function $\frac{p(p^2 + w^2)G(p)}{F(p)e^{pt}}$ lying to the left of the line $R(p) = c$



The contour used in the evaluation of the integral.
(16)

The poles of this are at the points $p = 0$, $p = \pm iw$ and at the roots of the transcendental equation $G(p) = 0$, which have been shown by Tranter (1942) to be simple and purely imaginary. They will be written in the form $p = \pm i\alpha$.

If $w \neq \alpha_s$ for any value of s , the sum of the residues of the function at $p = \pm iw$ is easily seen to be.

$$\frac{-F(iw) \cos wt}{w^2 G(iw)} \text{ and that at } p = 0 \text{ is } \frac{F(0)}{w^2 G(0)} \quad \dots (17)$$

The sum of the residues of the integrand at the remaining poles is

$$\sum_{s=1}^{\infty} \frac{1}{w^2 - \alpha_s^2} \left[\frac{e^{i\alpha_s t} F(i\alpha_s)}{\left(\alpha \frac{dG}{d\alpha} \right)_{\alpha=\alpha_s}} + \frac{e^{-i\alpha_s t} F(-i\alpha_s)}{\left(\alpha \frac{dG}{d\alpha} \right)_{\alpha=-\alpha_s}} \right] \quad \dots (18)$$

After little reduction we can show that

$$\begin{aligned} \left(\alpha \frac{dG}{d\alpha} \right)_{\alpha=\alpha_s} &= \left(\alpha \frac{dG}{d\alpha} \right)_{\alpha=-\alpha_s} \\ &= \xi (\gamma^2 \alpha_s^2 r_0^2 a^2 - 2\gamma + 1) - \frac{1}{\xi} (\gamma^2 \alpha_s^2 r_1^2 a^2 - 2\gamma + 1) \end{aligned}$$

where $\gamma = \frac{4}{5}$ and $\xi = \frac{J_1(\alpha_s r_1 a) - (\gamma \alpha_s r_1 a) J_0(\alpha_s r_1 a)}{J_1(\alpha_s r_0 a) - (\gamma \alpha_s r_0 a) J_0(\alpha_s r_0 a)}$

$$= \frac{j(r_1)}{j(r_0)} \quad \text{say}$$

and that

$$F(i\alpha_s) = F(-i\alpha_s) = -\frac{1}{2} \pi \{ [Y_1(\alpha_s r_1 a) - \gamma \alpha_s r_1 a Y_0(\alpha_s r_1 a)] J_1(\alpha_s r_0 a) - j(r_1) Y_1(\alpha_s r_0 a) \}$$

Substituting these results in equation (17) and (18) we obtain finally

$$\begin{aligned} \frac{5}{4} \frac{u}{Pr_0^4} &= r^{-1} \left[\frac{r_0}{r} \left\{ \frac{r^2 + (2\gamma - 1)r_1^2}{(2\gamma - 1)(r_1^2 - r_0^2)} \right\} - \frac{F(iw)}{G(iw)} \cos wt \right. \\ &\quad \left. + 2w^2 \sum_{s=1}^{\infty} \frac{F(i\alpha_s)(w^2 - \alpha_s^2)^{-1} j(r_0) j(r_1) \cos(\alpha_s t)}{(\gamma^2 \alpha_s^2 r_0^2 a^2 - 2\gamma + 1) j(r_1) - \gamma^2 \alpha_s^2 r_1^2 a^2 - 2\gamma + 1) j(r_0)} \right] \quad \dots (19) \end{aligned}$$

Here summation is taken over all positive roots of the equation $G(i\alpha_s) = 0$. From equation (19) stresses can be calculated.

My sincere thanks are due to Dr. A. K. Das for suggesting the problem.

REFERENCES

- Love, A. E. H. *Mathematical Theory of Elasticity* (Reprinted) New York, Dover Publication, 1944.
 Sneddon, Ian, N., 1951, *Fourier Transforms*, 155.
 Tranter, C. J., 1942, *Phil. Mag.*, 33, 614.

ELASTIC SCATTERING OF ELECTRONS BY HELIUM ATOM

R. JHA, S. N. BANERJEE AND N. C. SIL

DEPARTMENT OF THEORETICAL PHYSICS,

INDIAN ASSOCIATION FOR THE CULTIVATION OF SCIENCE,

JADAVPUR, CALCUTTA-32.

(Received June 19, 1967)

ABSTRACT. The S -wave phase-shifts (η_0) in the elastic \bar{e} -He collision problem have been computed by Hulthén's variational method in the energy range of 5 eV to 54.4 eV. The total wave function of the helium atom and electron system has been expanded in such a way as to include virtual excitation to 2^1S and 2^3S states. Our results for S -wave partial cross-sections have been compared with the theoretical findings of Marriott (1963), LaBahn and Callaway (1964), Moiseiwitsch (1953), and Zhikhareva (1965) and with the experimental results of Golden and Bandel (1965) and Ramsauer and Kollath (1929, 1932).

INTRODUCTION

The exchange and polarisation effects play important role in the scattering of electrons by atoms. These effects are especially important in the low-energy region. Marriott (1963) has employed a numerical method for the calculation of all significant partial cross-sections for elastic and inelastic collisions of electrons with helium atom. Explicit allowance has been made by him for electron exchange and all coupling terms between 1^1S , 2^1S and 2^3S states have been retained. LaBahn and Callaway (1964) have taken a complete antisymmetrized wave function to include exchange effect. Further, the formalism used by them was obtained from an extension of Hartree-Fock theory where the atomic distortion is approximated by a polarization potential. They have computed cross-sections for elastic scattering of electrons from helium atoms and have also given a tabulated values of partial wave phase shifts in the energy range of 0 to 54.4 eV. Zhikhareva (1965) has calculated the cross-sections for S -wave elastic scattering in \bar{e} -He collision assuming coupling of the 1^1S , 2^1S and 2^3S states of the helium atom. He has found two resonances (9.52 eV and 16.9 eV) in the S -wave cross-section of elastic scattering of electron by helium atom.

In our previous work (1966) we have investigated the problem of \bar{e} -He collision, taking into consideration the virtual excitation to 2^1S state only, but neglecting the exchange effect. In the present work, however, we have considered the exchange effect and have also made allowance for the distortion induced in the atom by the scattering electron in the form of the virtual excitations to 2^1S and 2^3S

states in addition to the original ground state (1^1S). The virtual excitation to 2^1S and 2^3S states includes the coupling between the 1^1S , 2^1S and 2^3S states. Following Geltman (1965), we have formulated the problem such that the virtual excitation vanishes at the scattering centre and in the asymptotic region.

We have carried out calculations for S -wave phase-shifts by Hulthén's variational method in the energy range of 5 ev to 54.4 ev. Numerical computations have been performed by taking very small intervals in the energy region of 19 ev to 30 ev so as to get any resonance level in that region. Experiments by Schulz (1963), Simpson and Fano (1963), Kuyatt *et al* (1965) have indicated resonance level at 19.3 ev in the said energy region. Investigations have also been carried out with a wide energy interval in the rest of the energy region of 30 ev to 54.4 ev. The calculated values of S -wave elastic cross-sections have been compared with the theoretical results of Marriott (1963), LaBahn and Callaway (1964), Moiseiwitsch (1953) and Zhikhareva (1965). The experimental findings of Ramsauer and Kollath (1929, 1932) and Golden and Bandel (1965) have also been shown for comparison.

THEORY

The Schrödinger wave-equation for the electron and helium atom system is

$$(H-E)\psi(r_1, r_2, r_3) = 0 \quad \dots (1)$$

with
$$H = -\frac{\hbar^2}{2m} (\Delta_1^2 + \Delta_2^2 + \Delta_3^2) - 2e^2 \left(\frac{1}{r_1} + \frac{1}{r_2} + \frac{1}{r_3} \right) + e^2 \left(\frac{1}{r_{12}} + \frac{1}{r_{13}} + \frac{e^2}{r_{23}} \right); E, \text{ the total}$$

energy of the system is given by $E = \frac{\hbar^2 k^2}{2m} + E_0$ where E_0 = ground state energy of the helium atom and k = wave-number of the scattered electron, other symbols have their usual meanings. The co-ordinate wave function of the helium atom and electron system, considering the 1^1S — 2^1S — 2^3S states of the atom, may be written in the form (cf. Drukarev, 1965)

$$\begin{aligned} \psi(r_1, r_2, r_3) = & \frac{1}{\sqrt{2}} [\psi_1^1 S(r_1, r_2) F_1(r_3) - \psi_1^1(r_1, r_2) F_1(r_3)] \\ & + \frac{1}{\sqrt{6}} [\psi_2^1 S(r_1, r_2) F_2(r_3) - \psi_2^3 S(r_1, r_2) F_2(r_2) + 2\psi_2^3(r_2, r_3) F_2(r_1)] \\ & + \frac{1}{\sqrt{2}} [\psi_3^1 S(r_1, r_2) F_3(r_3) - \psi_3^1 S(r_1, r_3) F_3(r_2)] \quad \dots (2) \end{aligned}$$

For the singlet state (1^1S) we take the Hylleraas (1929) wave function $\psi_{1^1S}(r_1, r_2) = \left(\frac{Z^3}{\pi}\right) e^{-Z(r_1+r_2)}$ where $Z = \frac{27}{16}$. We have used 2^1S wave function as given by Marriott and Seaton (1957) and 2^3S state wave function by Morse *et al.* (1935). These wave functions are as follow :

$$\psi_{2^1S}(r_1, r_2) = \frac{.478 \times 2^{1/4}}{\pi} \left\{ \begin{aligned} &e^{-2r_1}(e^{-1.136r_2} - .317r_2 e^{-.446r_2}) \\ &+ e^{-2r_2}(e^{-1.136r_1} - .317r_1 e^{-.464r_1}) \end{aligned} \right\}$$

$$\psi_{2^3S}(r_1, r_2) = \frac{.882 \times 2^{1/4}}{\pi} \left\{ \begin{aligned} &e^{-2r_1}(e^{-1.57r_2} - .34r_2 e^{-.61r_2}) \\ &- e^{-2r_2}(e^{-1.57r_1} - .34r_1 e^{-.61r_1}) \end{aligned} \right\}$$

The functions $F(r)$ describe the state of the scattered electron. To take into consideration the virtual excitation of the atom to 2^1S and 2^3S states, we approximate the wave function of the total system of the electron and helium atom in the following form :

$$\begin{aligned} \psi(r_1, r_2, r_3) = & \frac{1}{\sqrt{2}} \left[\psi_{1^1S}(r_1, r_2) F_0(r_3) - \psi_{1^1S}(r_1, r_3) F_0(r_2) \right] \\ & + \frac{1}{\sqrt{2}} \left[\psi_{1^1S}(r_1, r_3) F_1(r_2) - \psi_{1^1S}(r_1, r_2) F_1(r_3) \right] \\ & + \frac{1}{\sqrt{6}} \left[\psi_{2^3S}(r_1, r_2) F_2(r_3) - \psi_{2^3S}(r_1, r_3) F_2(r_2) + 2\psi_{2^3S}(r_3, r_2) F_2(r_1) \right] \\ & + \frac{1}{\sqrt{2}} \left[\psi_{2^3S}(r_1, r_3) F_3(r_2) - \psi_{2^3S}(r_1, r_2) F_3(r_3) \right] \quad \dots \quad (3) \end{aligned}$$

where
$$F_0(r) = \frac{\sin kr}{kr} + a(1 - e^{-\alpha r}) \frac{\cos kr}{kr}$$

$$F_1(r) = (c_1 r + c_2 r^2) e^{-\alpha r}$$

$$F_2(r) = (c_3 r + c_4 r^2) e^{-\alpha r}$$

$$F_3(r) = (c_5 r + c_6 r^2) e^{-\alpha r}$$

Here ' α ' is the usual phase parameter $\tan \eta_0$ whereas, c_i ($i = 1, \dots, 6$) are adjustable variational parameters.

To calculate η_0 by Hulthén's variational method, we define the variational integral in the usual way as $L = \int \psi^* (H - E) \psi dr_1 dr_2 dr_3$ and impose the condition.

$$L(a, c_i) = 0; \quad (i = 1, \dots, 6) \quad \dots (4)$$

$$\frac{\partial L}{\partial c_i} = 0; \quad (i = 1, \dots, 6) \quad \dots (5)$$

The co-efficients of c_i are evaluated for a particular energy. The six variables $c_i (i = 1, \dots, 6)$ appearing in the six linear equations (5) are evaluated in terms of a by the method of matrix inversion for a particular energy. Substituting these values in (4), we get a quadratic equation in ' a ' which yields the phase shift for the particular energy. The S -wave partial cross-section is then calculated by the formula $Q_{00} = \frac{4\pi}{k^2} \sin^2 \eta_0$.

RESULTS AND DISCUSSIONS

In the following table we have given our calculated S -wave partial cross-sections in the energy range of 20.606 ev to 27.365 ev. and have compared with the corresponding results of Marriott (1963). Our results compare favourably with those of Marriott (1963).

TABLE 1

Energy	S-wave cross-section R. Marriott	S-wave cross-section Present calculation
20.606	2.62	2.64
21.010	2.57	2.58
21.400	2.49	2.54
21.790	2.47	2.51
24.580	2.19	2.28
27.365	1.97	2.05

In fig. 1, the calculated values of scattering cross-sections have been plotted against energy and have been compared with theoretical results of Moiseiwitsch (1953), Zhikhareva (1965). The experimental findings of Ramsauer and Kollath (1929, 1932) have been shown for comparison. In fig. 2, we have plotted our calculated values of S -wave cross-sections against energy. A comparison has been made with the theoretical S -wave cross-sections calculated from the tabulated S -wave phase-shift values given by LaBahn and Callaway (1964), and experimental data of Golden and Bandel (1965). Perhaps a better choice of trial wave functions

containing a large number of adjustable linear as well as non-linear variational parameters might have led to the occurrence of resonance level in the energy region we have investigated.

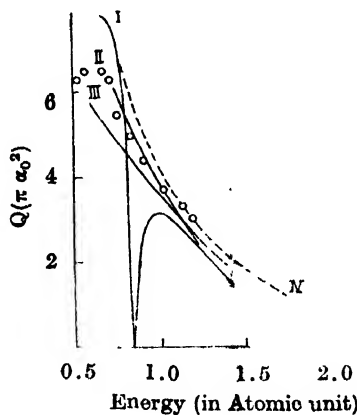


Fig. 1. The S-wave cross-section (in πa_0^2) plotted against energy (in atomic units) of the incident electron.

- Curve I Curve obtained from Zhikhareva (1965)
- Curve II Curve for broken bonds obtained from Zhikhareva (1965)
- Curve III Curve from calculations of Moiseiwitsch (1953)
- Curve IV Present calculations.
- Circle Experimental values of Ramsauer *et al.*, (1929, 1932)

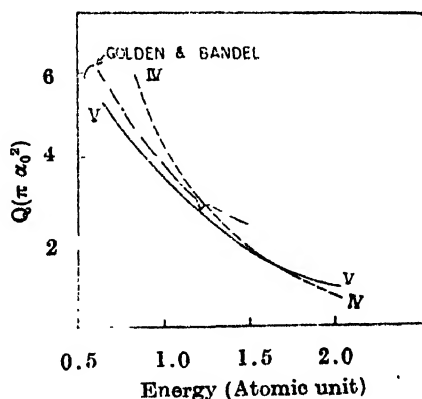


Fig. 2. The S-wave cross-section (in πa_0^2) plotted against energy (in atomic units) of the incident electron.

- Curve IV Present calculations.
- Curve V Cross section obtained from the tabulated S-wave phase shift values given by LaBahn *et al.*, (1964).
- · — Experimental curve of Golden *et al.* (1965).

ACKNOWLEDGEMENT

The authors are thankful to Prof. D. Basu for his valuable comments and helpful discussions. Thanks are also due to the authorities of C.M.E.R.I., Durgapur, for their help in computation of the numerical results on I.B.M. 1620.

REFERENCES

- Drukarev, G. F., 1965, *The Theory of Electron-Atom Collisions*—Academic Press, London, New York.
- Geltman, S., 1965, *Astrophys. J.*, **141**, 376.
- Golden, D. E., and Bandel, H. W., 1965, *Phys. Rev.*, **138**, 14A.
- Hylleraas, E. A., 1929, *Z. Phys.*, **54**, 347.
- Jha, R., Banerjee, S. N. and Sil, N. C., 1966, *Indian J. Phys.*, **40**, 543.
- Kuyatt, C. E., Simpson, J. A., and Mielczarek, S. R., 1965, *Phys. Rev.*, **138**, 385.
- LaBahn, R. W., Callaway, J., 1964, *Phys. Rev.*, **135A**, 1539.
- Marriott, R., 1963, *Atomic Collision processes*, edited by M. R. C. McDowell, North Holland Publishing Company, Amsterdam.
- Marriott, R. and Seaton, M. J., 1957, *Proc. Phys. Soc.*, **70**, 296.
- Moiseiwitsch, B. L., 1953, *Proc. Roy. Soc.*, (A) **219**, 102.
- Morse, P. M., Young, L. A. and Hauritz., E. S., 1935, *Phy. Rev.*, **48**, 948.
- Ramsauer, C. and Kollath, R., 1929, *Ann. Physik*, **3**, 536.
- 1932, *Ann Physik*, **12**, 529.
- Schulz, G. J., 1963, *Phy. Rev. Letters*, **10**, 104.
- Simpson, J. A. and Fano, U., 1963, *Phy. Rev. Letters*, **11**, 158.
- Zhikhareva, T. V., 1965, *Optics and Spectroscopy*, **19**, 474.

EFFECT OF CHEMICAL COMBINATION ON THE ASYMMETRY OF THE $K\alpha$ LINES OF COBALT

CHINTAMANI MANDE*, A. S. NIGAVEKAR AND
(Miss) PUSHPA CHIVATE

DEPARTMENT OF PHYSICS, UNIVERSITY OF POONA, POONA-7, INDIA.

(Received August 1, 1967).

ABSTRACT. The asymmetry indices of the $Co K\alpha_1$ and $K\alpha_2$ lines have been determined for cobalt metal and some of its divalent and trivalent compounds and complexes. The X-ray lines were excited by the fluorescence technique and were registered using a 40 cm bent crystal spectrograph. It has been observed that the indices of asymmetry for both the lines are progressively reduced as one goes from cobalt metal to $Co(II)$ and $Co(III)$ compounds. It has been shown that the asymmetry index depends upon the number of $3d$ electrons in any substance. The surroundings of the central atom, on the other hand, do not seem to play any significant role in the change of the asymmetry index. X-ray fluorescence spectroscopy can therefore be used to determine unknown valencies in complexes of transition metals. The change in the asymmetry of these lines has been attributed to exchange polarisation effect.

INTRODUCTION

The effect of chemical combination on the width and the asymmetry of the $K\alpha_1$, α_2 , lines has been studied in the thirties by many workers (Bearden and Shaw, 1935; Roschberry and Bearden, 1936; Orbert and Bearden, 1938). Recently Meisel and his coworkers (1961, 1962, 1962, 1965, 1965) have shown fresh interest in this problem and have studied in detail the shape of the $K\alpha$ lines of some transition metals of the first series in a large number of compounds and complexes. We thought it worthwhile to study the asymmetry of these lines from two points of view, namely, (1) the effect of valency and (2) the effect of surroundings of the central metal atom emitting the radiation. In this paper we report the results of our investigations carried out with this view on the K lines of some compounds and complexes of cobalt.

EXPERIMENTAL

It is well known that the chemical composition of a substance changes during excitation by direct electron bombardment in an X-ray tube. We have, therefore, employed in this work the technique of fluorescence for exciting the X-ray lines. The general experimental arrangement is shown schematically in fig. 1.

* Present address: Dept. of Physics, Nagpur University, Nagpur.

A Philips sealed X-ray tube with tungsten target was employed for the generation of the primary X-rays. It was operated at 25 KV and 15 ma. The spectra were registered on a 40 cm bent crystal spectrograph, designed and constructed in the Poona University Central Workshop. The (100) planes of a well tested mica crystal were used to record the spectra, which were photographed on Agfa ultra-violet plates. By giving exposures between 90 to 100 hours it was possible to obtain the spectral lines with photodensities satisfying the necessary condition for linear relationship between S , the photodensity and the intensity I . Microphotometer records of the plates were obtained with magnification 50 on a Moll microphotometer.

The fluorescent targets for solid substances were made by pressing their fine powders into a rectangular cavity in a perspex sheet. The samples were then covered by cellophane tape for protection from moisture.

The preparation of cells for obtaining fluorescence spectra of substances in the liquid state presents considerable difficulty. It is necessary to use a cell which will not be attacked by the solution and whose walls will not appreciably absorb the primary and the fluorescent radiations. The cells in this work were prepared by putting the solution between two thin films of celluloid separated by a U shaped perspex sheet.

The fluorescent targets thus prepared were mounted on a metallic attachment which was screwed on the shield of the X-ray tube as shown in fig. 1. With this

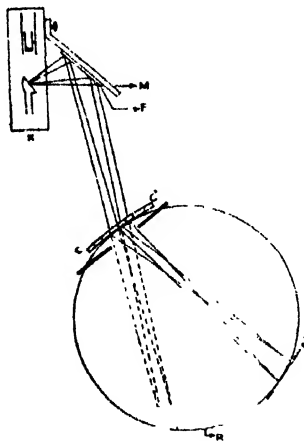


Fig. 1

arrangement it is possible to keep the fluorescent targets very close to the X-ray tube which is necessary because the intensity of the fluorescent radiation is very weak.

RESULTS AND DISCUSSION

It is well known that microphotometer traces do not give, in general, the true intensities directly. It is, therefore, necessary to convert the microphotometer curves into true intensity curves, which was carried out by adopting the usual procedure of determining the photodensities (Blokhin, 1962). The apparent intensities of a large number of points, situated at a distance of 1 mm from each other on every microphotometer trace, were first converted into true intensities and were subsequently plotted on graph papers. One of the typical curves obtained by this method for cobalt metal is shown in fig. 2. This curve (as well as all the others for the compounds and complexes) has not been corrected for the

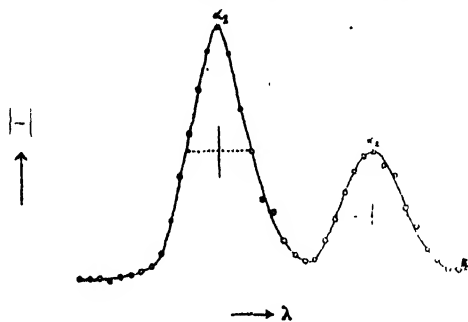


Fig. 2

finite resolving power of the X-ray spectrograph. However, it can be safely assumed that instrumental broadening would not appreciably affect the asymmetry indices in which we are primarily interested in this work, since this broadening effect would occur on both sides of the line profiles.

It may be remarked here that the earlier workers have used either ionization chambers or G.M. counters for recording the X-ray lines. These detection techniques, although more sensitive and quicker, do not give the exact position of the maximum ordinate of a spectral line. In this respect, our procedure in which the position of the maximum ordinate is determined with greater certainty, is superior.

The index of asymmetry of an X-ray line has been defined (Allison, 1933) as the ratio of the part of the full width at half maximum lying to the long wavelength side of the maximum ordinate to that on the short wavelength side. In table 1 are given the results on the asymmetry of the $K\alpha_1$ and the $K\alpha_2$ lines of cobalt obtained in this investigation. The results of Parratt (1936) and Bearden and Shaw (1935) are also included in this table for comparison. Our values of the asymmetry index for both these lines for the metal agree fairly well with those given by these workers.

It will be seen from table 1 that $K\alpha_1$ and $K\alpha_2$ lines which are asymmetric in the case of cobalt metal, tend to become more or less symmetric in compounds and

complexes. This change does not depend upon the co-ordination number of cobalt in the compounds and complexes. It can therefore be concluded that the surroundings of the central atom do not play any significant role in the change of the asymmetry index.

It can also be seen in table 1 that the asymmetry index decreases progressively as one goes from cobalt metal to Co (II) and Co (III) compounds. This decrease appears to be more or less regular, except in the case of the $K\alpha_2$ line of pink cobalt chloride. The low value of the asymmetry index of this compound seems to be rather exceptional.

The observed reduction in the asymmetry index seems to be linked with the number of electrons in the $3d$ shell. In cobalt metal the d band contains 8.28 electrons per atom (Goodenough, 1963) while in Co (II) and Co (III) complexes there are 7 and 6 electrons respectively in the d shell. The average values of the asymmetry indices for the $K\alpha_1$ line are 1.380, 1.052 and 0.934 for cobalt metal and the divalent and the trivalent complexes respectively. For the $K\alpha_2$ line the average values are 1.297, 1.023 and 0.93. The observed ratios of the asymmetry indices for both the $K\alpha_1$ and $K\alpha_2$ lines agree remarkably well with the proportionality of the number of electrons in the $3d$ shell (8.28 : 7 : 6). This relationship has been established for the first time in this work.

TABLE 1
Experimental data on index of asymmetry

	Co- ordination number	Index of Asymmetry	
		$K\alpha_1$	$K\alpha_2$
1. Cobalt metal (Authors)		1.380	1.297
" " (Parratt)		1.440	1.300
" " (Bearden & Shaw)		1.360	1.290
2. Cobalt Chloride (blue)	4	1.07	1.05
3. Cobalt Chloride (pink)	6	1.05	0.75
4. Diquinolinium Cobalt (II) Chloride	4	1.07	1.02
5. Diquinolinium Cobalt Chloride (pink) (Liquid)	6	0.95	0.92
6. Cobalt (II) Oxinate (anhydrous)	4	1.02	1.01
7. Cobalt (II) Oxinate (hydrous)	6	1.05	1.01
8. Cobaltic (III) Oxide Co_2O_3	6	0.95	0.93
9. Hexammino Cobalt (III) Chloride $[\text{Co}(\text{NH}_3)_6] \text{Cl}_3$	6	0.92	0.94
10. Sodium Cobaltinitrite (III) $\text{Na}_3\text{Co}(\text{NO}_2)_6$	6	0.93	—
11. Aqua Pentaammino Cobaltic (III) Oxalate $[\text{Co}(\text{NH}_3)_5\text{H}_2\text{O}]_2(\text{C}_2\text{O}_4)_3$	6	0.92	—

The modification of the wavefunctions of the spin up and spin down $1s$ electrons owing to exchange polarization effects with the unpaired $3d$ electrons has been of considerable interest in recent years (Freeman and Watson, 1965). The present asymmetry also seems to arise from such exchange polarisation effects. Assuming that the polarisation of the p orbitals involved in the emission of the $K\alpha_1, \alpha_2$ lines is negligible, one can attribute the observed asymmetry of these lines to the polarisation of $1s$ up and $1s$ down orbitals. A detailed study of the asymmetry index of a large number of complexes in various transition metals would therefore reveal the extent to which the $1s$ shell gets polarised. Theoretical work in this direction has been undertaken by Dr. K. P. Sinha of the National Chemical Laboratory, Poona and would be reported later. X-ray spectroscopy can thus be a valuable tool for the measurement of the exchange polarisation, complementary to Mössbauer and EPR techniques.

Another important aspect of this investigation is that this method can be used to determine unknown valencies in compounds and complexes. We can cite here the example of the pink solution of diquinolinium cobalt chloride. To our knowledge the valency of cobalt in this complex has not yet been determined. From the asymmetry index, it seems that the valency of the cobalt atom in this complex is three.

ACKNOWLEDGMENTS

We are thankful to Dr. K. P. Sinha of the National Chemical Laboratory, Poona for helpful discussions. One of us (P.C.) expresses her thanks to the Council of Scientific and Industrial Research, New Delhi for the award of a Junior Research Fellowship.

REFERENCES

- Allison, S. K., 1933, *Phys. Rev.*, **44**, 63.
Bearden, J. A. and Shaw, C. H., 1935, *Phys. Rev.*, **48**, 18.
Blokhin, M. A., 1962, *X-ray Spectroscopy*, Hindustan Publishing Corporation (India).
Freeman, A. J. and Watson, R. E., 1965, *Magnetism*, Ed. Suhl and Rado, Academic Press, New York.
Goodenough, J. B., 1963, *Magnetism and Chemical Bond*, Interscience Publishers.
Meisel, A. and Nefedow, W., 1961, *Z. Chem.*, **1**, 337.
1962, *Z. Physik. Chem.*, **219**, 194.
Meisel, A. and Doring, E., 1962, *Physik Chem*, **220**, 397.
Meisel, A. and Leonhardt, G., 1965, *Z. anorg. allg. Chemie.*, **339**, 1.
Meisel, A. and Trong ba To., 1965, *J. Prakt. Chem.*, **29**, 192.
Meisel, A., 1965, *International Conference on "X-ray Spectra and Chemical Bonding"*, Leipzig, Karl Marx Universität Leipzig Publication, 212.
Obert, L. and Bearden, J. A., 1938, *Phys. Rev.*, **54**, 1000.
Parratt, L. G. 1936, *Phys. Rev.*, **50**, 1.

MASS DISTRIBUTION STUDIES IN NUCLEAR FISSION USING LEXAN DETECTOR

R. RANGARAJAN*, K. N. IYENGAR AND M. R. HIRANANDANI

TATA INSTITUTE OF FUNDAMENTAL RESEARCH, COLABA, BOMBAY 5, INDIA.

(Received August 31, 1967).

ABSTRACT. An investigation of the ranges of fission fragments from thermal fission of ^{235}U has been made using "Lexan" polycarbonate detector. A method of sandwiching the Uranium between two layers of "Lexan" enabled a simultaneous measurement on the two fragments. The average ranges of the fragments of the light and heavy groups in Lexan were found to be 20.22 ± 0.027 microns and 16.38 ± 0.021 microns respectively. It is found that from the correlated range measurements, the fragment masses can be estimated fairly accurately using an iteration procedure.

INTRODUCTION

The determination of fragment masses in fission by physical methods requires a simultaneous measurement of the kinetic energies or the velocities of the two fragments. In the past, attempts have been made to obtain the fragment mass distribution by measurement of the ranges of fragments using radiochemical methods (Aras *et al*, 1965) and employing known range-energy relationships. Ranges of fission fragments have also been measured using nuclear emulsions (Manley, 1962). In recent years, solid state track detectors are being used increasingly in the detection of fission fragments (Fleischer *et al*, 1965) especially for recording events of low probability such as in photofission. The present work was undertaken to assess the accuracy with which fragment mass distributions could be determined by measuring fragment ranges in the thermal fission of ^{235}U , with a "Lexan" polycarbonate (Fleischer *et al*, 1964) detector. "Lexan" being a primary ionisation threshold detector, records alpha particles of energy only less than 0.5 MeV (Fleischer *et al*, 1967). The study of fission events in the presence of the background of alpha particles was thus possible. Moreover, the ranges of γ fission fragments in this detector are larger than those in nuclear emulsions because the stopping power of the polycarbonate is smaller than that of nuclear emulsion. Simplicity of handling and ease of processing of these detectors are added advantages. In the present work the ranges of the two fragments are found simultaneously by using a sandwich technique and fragment masses are derived from the measured ranges by a method of iteration.

* Bhabha Atomic Research Centre, Trombay, Bombay.

EXPERIMENT

A sandwich of natural uranium was prepared by pressing a drop of 10% uranium nitrate between two layers of Lexan (density 1.25, composition $H_{18}C_{16}O_3$) joined together at one end. The layers which were held pressed between two perspex plates with screws were exposed to a beam of neutrons in the thermal column of "CIRUS" for about a day where the flux of neutrons is about 3×10^7 $n/cm^2/sec$. After exposure, the sandwich was washed and etched in a 6N solution of NaOH at $70^\circ C$ for about 30 minutes. The fragment tracks were measured by viewing the sandwich under a microscope with a magnification of $1000\times$. It was found that a drop of sandal wood oil between the layers kept the surfaces in close contact. A dye, 'Nigrosine' was introduced into the tracks to enhance the contrast characteristics. This enabled better accuracy in the measurements. A track density of between 10 and 25 per field of view was maintained. The two surfaces of the sandwich were found to have a lateral displacement of between 5 and 40 microns. The correlation could be obtained easily here from the similarity in direction because of the low track density. A total of 2000 events were scanned and the data analysis was performed on the computer CDC 3600. Measured ranges were corrected for a slight change in the length by a factor connected with the dip angle of the track (Price).

RESULTS AND ANALYSIS

(a) Range measurements of fission fragments

The range distributions of light and heavy fragments were obtained from the measurements on correlated fragments making use of the fact that in general lighter fragment has a longer range. These distributions are shown in fig. (1).

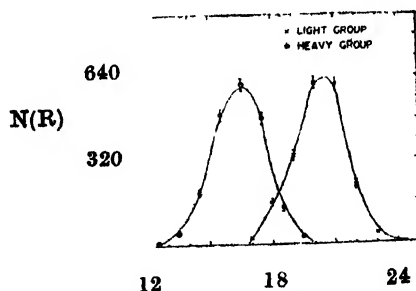


Fig. 1. Range-frequency plot of correlated fragment tracks in Lexan from thermal fission of ^{235}U .

The average ranges of the light and the heavy groups were found to be 20.22 ± 0.027 microns and 16.38 ± 0.021 microns respectively. These values are about 1.5 times larger than the corresponding ranges in nuclear emulsions (Vigneron,

1950) and about 1.1 times larger than those in the celluloid backing of normal photographic films (Gerhardt *et al*, 1966).

Fig. (2) shows the distribution in the range of one of the fragments for various fixed ranges of the complimentary fragment. It is not necessary here to associate the longer range with the lighter fragment and vice versa. The results are found to be similar to those obtained by Brunton and Hanna (1950) for the kinetic energies

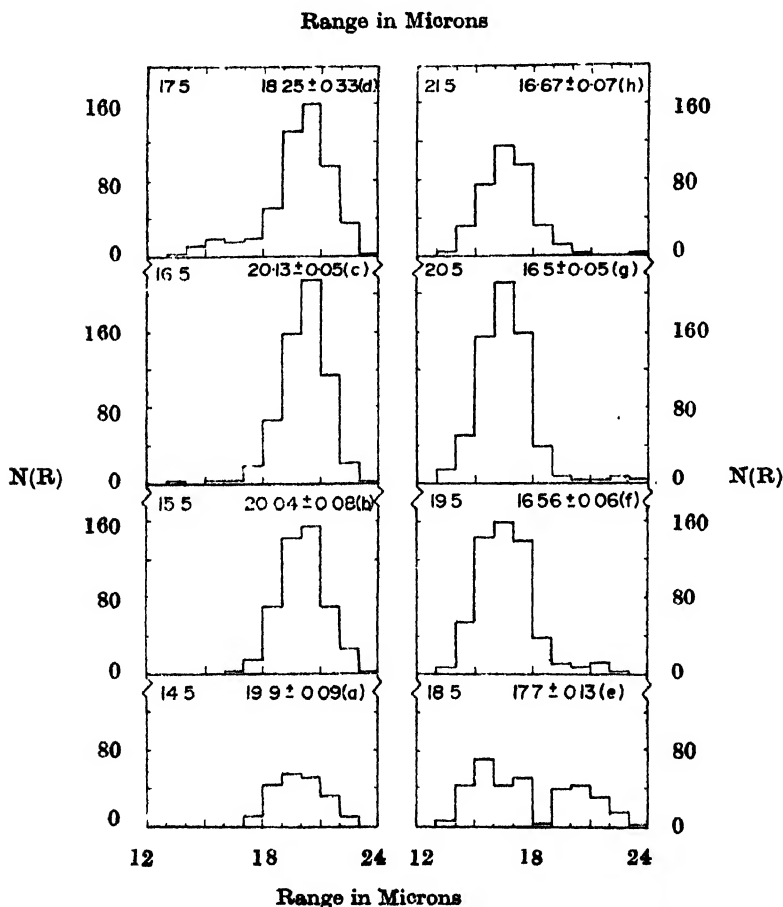


Fig. 2. The distribution in range of one fragment for various fixed ranges of the complimentary fragment. The number on the left hand top corner, of represents the range of the fixed fragment. The mean of the distribution obtained is represented on the right hand top corner. The error given is statistical.

of fission fragments. This suggests the validity of a direct correspondence between range and energy. However, since most of the contribution to the spectra of fig. (2) comes from the most probable masses, any breakdown of the direct correspondence in other mass regions may not be apparent here.

Fig. (3) shows the obtained distribution in the total range of the two fragments. The experimental points have been fitted to a Gaussian distribution by the least square method. The average value of the total range and its variance are found to be 36.62 microns and 3.23 respectively.

(b) *Determination of mass distributions from range measurements*

Lindhard *et al* (1963) have used the Thomas-Fermi model of the atom to calculate theoretically the range energy relationships for heavy ions. These calculations are based on the Bloch's relation $I = I_0 Z_0$, where I is the average ionisation potential, I_0 is the Bloch's constant and Z_0 the charge number of the medium. This relation is not strictly valid for the detector used here (Brandt, 1956). The mass distribution was obtained here using the range-energy relation given by Barkas and Berger (1964) and applying an iteration procedure as described below.

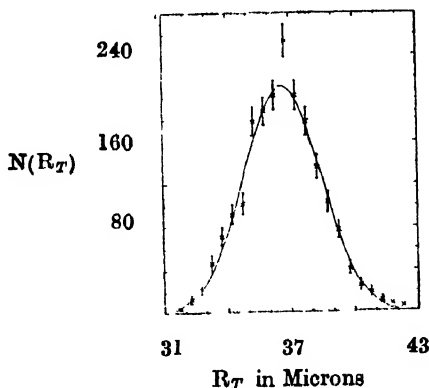


Fig. 3. The distribution in total range of the two fragments. The curve drawn is a gaussian with a mean of 36.62 microns and standard deviation 1.80 microns.

The range R of a fragment of mass M and charge Z , moving with a velocity βC is given by

$$R = \frac{M}{Z^2} (\lambda + B_z) \quad (1)$$

where λ is the range of a proton of velocity βC and the term B_z takes into account the range extension caused by the capture of electrons by a positive ion of charge Ze . For the case of "Lexan" used, the value of λ was obtained by a numerical integration of the stopping powers, of the constituent atoms as given by Whaling

(1958) and the value of B_z was evaluated according to Barkas and Berger (1964). These values of λ and B_z are given by

$$\lambda = 84.1264 \times \beta^{10/3} \text{ gms/cm}^2 \quad \dots (2)$$

$$B_z = 7.717 \times 10^{-4} \times M^{5/3} \times \beta \text{ gms/cm}^2 \quad \dots (3)$$

A constant charge density of 0.394, equal to that of the parent nucleus, was used in arriving at the value of B_z given by equation 3. Assuming a linear relation between energy and range of the fission fragment, approximate fragment masses were first calculated from the relationships

$$M_1 \cdot R_1 = M_2 \cdot R_2 \quad \dots (4)$$

and
$$M_1 + M_2 = M, \quad \dots (5)$$

where M is the mass of the fissioning nucleus. These masses M_1 and M_2 were fed back in equations 1, 2 and 3 and the values of β_1 and β_2 were estimated. Better estimates of M_1 and M_2 were then obtained using the rigorous relationship

$$M_1 \beta_1 = M_2 \beta_2 \quad \dots (6)$$

These new values of M_1 and M_2 were again fed into equations 1, 2 and 3 and three such iterations were made using the computer. In all the cases the results of the last two iterations were found to be converging to within five mass units. The resultant mass ratio distribution is shown in fig. 4. For the sake of comparison, the mass ratio distributions derived from measurements of fragment

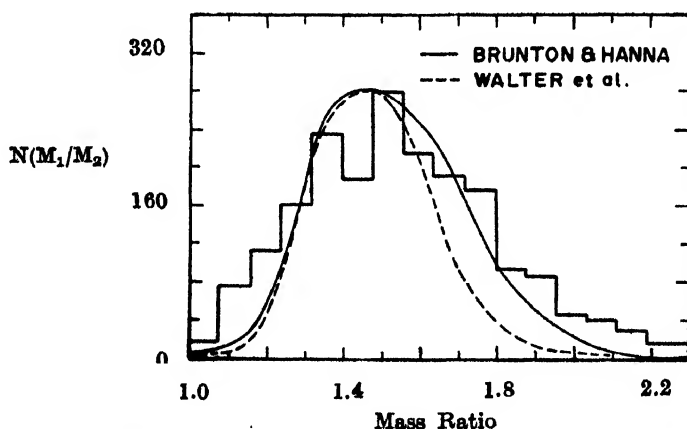


Fig. 4. Plot of mass ratio versus frequency. The histogram refers to the present experiment. The dotted curve is computed from the data of Walter *et al* (1963) and the continuous curve is from Brunton and Hanna (1950)

energies by double ionisation chamber method (Brunton *et al*, 1950) and slid-state detectors (Walter *et al*, 1963) are also shown. It is seen that the present data compare favourably with the results of Brunton and Hanna (1950) except for the region

of near symmetry. The agreement of the present results with that of Walter *et al* (1963) is not, however, very good. This discrepancy could be due to not including in our calculations the effect of nuclear stopping also termed "Ionisation defect" (Lamphere, 1960). It must be mentioned here that while Brunton and Hanna (1950) did not correct for the ionisation defect in their results, Walter *et al* (1963) have corrected for the same by an elaborate method of calibration (Schmitt *et al*, 1965) for the solid-state detectors. In any case, the present results show that the range measurements on correlated fragments can be used for approximate fragment mass ratio determinations and therefore this method can be applied to the cases where low counting rates prohibit the use of conventional methods. The method could be improved further by using a better range-energy relationship which takes into account atom-atom elastic collisions as well as experimentally observed fragment charge distributions in fission (Reisdorf *et al*, 1967).

ACKNOWLEDGEMENTS

We are thankful to Dr. R. Ramanna for his continued interest and guidance and to Dr. S. S. Kapoor and Shri D. M. Nadkarni for helpful discussions. Dr. P. B. Price was kind enough to give us the Lexan used in this experiment. Our thanks are also due to Km. K. D. Prabhu for careful microscopic work and to Messrs Imperial Chemical Industries for supplying the Nigrosine dye.

REFERENCES

- Aras, N. K., Menon, M. P., and Gordon, G. E., 1965, *Nucl. Phys.*, **69**, 337.
 Barkas, W. H. and Berger, M. J., 1964, *NASA-Report no.* SP-3013.
 Brandt, W., 1956, *Phys. Rev.*, **104**, 691.
 Brunton, D. C. and Hanna, G. C., 1950, *Can. Jr. Res.*, **28A**, 190.
 Fleischer, R. L., Price, P. B. and Walker, R. M., 1965, *Ann. Rev. Nucl. Sc.*, **15**, 1.
 Fleischer, R. L., Price, P. B., Walker, R. M. and Hubbard, E. L., 1964, *Phys. Rev.*, **133A**, 1443.
 Fleischer, R. L., Price, P. B., Walker, R. M. and Hubbard, E. L., 1967, *Phys. Rev.*, **156**, 353.
 Gerhardt, H., Gonnenswein, F., Heinrich, H. and Hipp, H., 1966, *Proc. Coll. Inter. Foto. Cosep. Firenze*. (Preprint)
 Lamphere, R. W., 1960, *Fast neutron physics*, Inter Science Publisher, New York, Vol. 1, 449.
 Lindhard, J., Scharff, M. and Schiott, H. E., 1963, *Mat. Fys. Medd. Dan. Vid. Selsk.*, **33**, no. 14.
 Manley, J. H., 1962, *Nucl. Phys.*, **33**, 70.
 Price, P. B. (*Private Communication*).
 Reisdorf, W. and Armbruster, P., 1967, *Phys. Letters*, **24B**, 501.
 Schmitt, H. W., Gibson, W. M., Neiler, J. H., Walter, F. J. and Thomas, T. D., 1965, SM-60/40, *Proceedings of the Symposium on Physics and Chemistry of Fission*, Salzburg.
 Vigneron, L., 1950, *Comp. Rendu*, **231**, 1473.
 Walter, F. J., Schmitt, H. W. and Neiler, J. H., 1963, *ANL-6797*, p. 441.
 Whaling, W., 1958, *Handbuch der Physik*, **34**, 193.

STUDIES ON THE FADING OF THE RADIO WAVES RETURNED FROM THE SPORADIC E-REGION OF THE IONOSPHERE

SUMAN GANGULY AND SISUTOSH SAMANTA

BOSE INSTITUTE, CALCUTTA.

(Received September 1, 1967).

ABSTRACT. In some of the studies with vertical pulsed transmission, the blanketing type and the q -type of E_s have been observed. The wind-type of E_s having a quickly varying top frequency has also been found. Using a horizontal dipole as the receiving aerial, the fading records of the E_s -echoes have occasionally shown a double-trace on the moving film for both the first and the second orders of reflection. On rare occasions, an additional trace has also been observed in this region. A tentative explanation of the double or triple trace has been suggested.

Using the selective aerial for the reception of one or the other of the two magneto-ionic components, the fading records of a *single* downcoming wave from the sporadic E -region have been taken on the moving film. The statistical distribution of the amplitude has shown that usually at noon hours, both the Rayleigh and the Rice types of distribution occur, whereas during morning, evening and early night hours, when the reflection is from the E_s -region, there have been other types of amplitude distribution. Of these, the most frequent type has shown usually two maxima in the amplitude distribution curve. The double-peak or the so-called M-type distribution suggests the existence of two simultaneous and independent super-imposed processes. It is likely that the double-peak is associated with the occurrence of a double-layer in the sporadic E -region.

Typical v_f -distribution curves have also been shown. The rms line-of-sight velocity of the irregularities in the E_s -region has been calculated.

INTRODUCTION

In the present paper, the results of some of the investigations with vertical pulsed transmission on the echoes from the sporadic E -region carried out at Calcutta on different frequencies has been presented. With regard to the different types of sporadic E , the blanketing type and the q -type of E_s have been observed at times. It has also been possible to observe the wind-type of E_s having a rapidly varying top frequency. A major part of the work has been devoted to the recording of random fading patterns for the downcoming radio pulses reflected from the sporadic E -region. Usually frequencies greater than the critical penetration frequency of the normal E -layer have been employed. Using a horizontal dipole as the receiving aerial, it has been occasionally found that the random fading record on the moving film has a double-trace in the sporadic E -region.

for both the first and the second orders of reflection. On a few records, an additional trace on the moving film has also been observed.

Some statistical studies of the single downcoming wave returned vertically from the sporadic *E*-region have also been incorporated in the paper. To obtain a single downcoming wave, the selective aerial system for circular polarization, first designed and employed by Ratcliffe and White (1933) for the study of the polarization of the downcoming wave, has been mostly used. For frequencies greater than the critical penetration frequency of the normal *E*-layer, the ordinary and the extraordinary components are expected to be circularly polarized. In reality, however, there is a departure from circular polarization and the suppression of one or the other component is not complete. Since the extraordinary component usually suffers in the day-time a much larger absorption in the sporadic *E*-region than the ordinary component, the use of the selective aerial system of Ratcliffe and White with the receiver would give for all practical purposes, a single ordinary component. When, however, the two magneto-ionic components are of comparable magnitude, and they are unresolved, a rhythmic or periodic fading (Appleton *et al*, 1947) under conditions of gradually increasing or decreasing electron-density in the ionosphere, has been at times observed, as expected. In the analysis of the fading records, the parts showing only random fading have been utilized. It may be noted that periodic fading can be avoided by observing *visually* the fading pattern on the CRO screen (Mitra, 1949).

The statistical studies have shown the Rayleigh (1899) and the Rice (1944) type of amplitude distribution along with other types. Of the other types, the most frequently observed type has shown two maxima in the amplitude distribution curve. This double-peak type was first observed by Das Gupta and Vij (1960) for the reflection from the *F*-layer and was called the *M*-type. Such double-peak amplitude distribution was also obtained by Kushnerevsky and Zayarnaya (1962) in the case of *F*₂-reflection. The time-analysis of the random fading records of the single downcoming wave returned from the sporadic *E*-region has also been carried out, enabling the determination of the rms line-of-sight velocity of the irregularities in the sporadic *E*-region.

Statistical analyses of random fading of a single downcoming radio wave had previously been carried out by various investigators, viz, Rice (1944, 1945), Ratcliffe (1948, 1956), Mitra (1949), McNicol (1949), Alpert (1948), Subhadramma (1955, 1958) Schwentek (1962), Yeh and Villard (1962), Rao and Rao (1964), Sen and Khastgir (1965) and others.

THEORETICAL CONSIDERATIONS

Amplitude analysis of the random fading records : A major cause of random fading of a single downcoming radio wave returned from the ionosphere is due to the random motion of the ionospheric irregularities which would scatter in a random

manner the radio waves incident on them. The resultant amplitude is considered as due to a large number of scattered components from a series of diffracting centres distributed at random, both in space and time, in the ionospheric region. Considering a large number of scattered components of random amplitude and phase, the probability of occurrence of the resultant amplitude at any instant would be obtained from the well-known expression given by Rayleigh (1899).

The Rayleigh probability distribution at any instant is given by :

$$P(r) = \frac{r}{\psi} \exp\left(-\frac{r^2}{2\psi}\right) \quad \dots (1)$$

where r is the resultant amplitude of the scattered components and ψ is a term which is half of the mean square value of the amplitudes.

If the rms value of the amplitudes of the scattered components be denoted by R , then $\psi = \frac{\bar{r}^2}{2} = \frac{R^2}{2}$.

The Rayleigh expression can then be expressed as :

$$P(r) = \frac{2r}{R^2} \exp\left(-\frac{r^2}{R^2}\right) \quad \dots (2)$$

If now the most probable amplitude (i.e., the amplitude for which $P(r)$ is maximum) be represented by r_m , then it can be shown

$$r_m^2 = \psi = \frac{R^2}{2} \quad \dots (3)$$

The Rayleigh distribution may then be written as :

$$P(r) = \frac{r}{r_m^2} \exp\left(-\frac{r^2}{2r_m^2}\right) \quad \dots (4)$$

Writing (4) in the form

$$\log \frac{P(r)}{r} = \log\left(\frac{1}{r_m^2}\right) - \frac{r^2}{2r_m^2} \quad \dots (5)$$

it is evident that the plot of $\log \frac{P(r)}{r}$ against r^2 would be a straight line, the slope

of which would give $\frac{1}{2r_m^2}$ and the intercept $\log\left(\frac{1}{r_m^2}\right)$.

If in addition to the scattered components from the irregularities in the ionospheric layer, there is a steady specularly reflected component, then it is evident that the observed probability distribution of amplitude at any instant at the receiving point would no longer be given by the Rayleigh formula. It was shown by Rice (1944, 1945) that under such condition, the probability distribution of the amplitude would be given by

$$P(r) = \frac{r}{\psi} \exp\left(-\frac{r^2 + B^2}{2\psi}\right) I_0\left(\frac{rB}{\psi}\right) \quad \dots (6)$$

Here B is the amplitude of the steady component, I_0 is the Bessel function of zero order and imaginary argument and the other symbols have the same meaning as in the Rayleigh expression.

When $r \approx B$, the most probable amplitude in the Rice distribution would be given by :

$$r_m^2 = B^2 + \frac{R^2}{2} \quad \dots (7)$$

From the curves showing the probability distribution of amplitude in an experimental record, it is possible by comparison with the curves drawn from the theoretical formulae, to estimate the ratio of the amplitude of the steady reflected component to the rms value of the resultant amplitude of the scattered components. McNicol (1949) gave a series of curves for the various values of $b = \frac{\sqrt{2}B}{R}$.

It was shown that when $b < 1$, $P(r)$ would follow approximately a Rayleigh distribution and when $b > 3$, the distribution would be almost Gaussian.

(b) *Time analysis of the random fading records.*

If we divide the time of the fading records into a series of equal intervals of time, τ , and if v_τ represents the change in amplitude during each such time-interval, then assuming that each of the ionospheric irregularities scatters equal amount of power and has the line-of-sight velocities distributed about the rms velocity according to the Gaussian law, the probability distribution of the amplitude-changes over the time-interval, τ , can be found. Following a procedure worked out by Fürth and Macdonald (1947), who analysed the radio noise which pass through a Gaussian band-pass filter, Ratcliffe showed that when τ is small, the probability distribution $P(v_\tau)$ would be given by :

$$P(v_\tau)dv_\tau = \frac{1}{\sqrt{\pi}} e^{-x^2} dx \quad \dots (8)$$

where $x = \frac{v_\tau}{2\pi\sigma\tau R}$ and σ is the standard deviation of the Gaussian velocity distri-

bution. With the help of (8), Ratcliffe showed that the rms line-of-sight velocity of the ionospheric irregularities would be :

$$v_0 = \frac{\lambda |\bar{v}_\tau|}{8\pi\tau} \quad (\text{vertical incidence}) \quad \dots (9)$$

Computing the value of the ratio, $\frac{|\bar{v}_\tau|}{\tau}$, (which has been termed the "speed of fading") from the fading records the rms line-of-sight velocity of the ionospheric irregularities can be determined with the help of (9). Following Booker, *et al* (1950), the value of v_0 can also be obtained from the auto-correlation function, $P_n(\tau)$, of the fading record. As we have not incorporated the analysis of the fading observations by the auto-correlation method, the theory of the auto-correlation method has been left out.

EXPERIMENTAL ARRANGEMENTS

The pulse-transmitter used in this investigation delivers a peak power of 8 KW and is fitted with a 833-valve in cathode-pulsed configuration. This pulse-duration can be varied from 50 to 200 microseconds and the repetition frequency is 50 c/s. The working frequency has a range from 1.5 to 12 Mc/s covered in six bands. The receiver is a modified Hammerlund, in which the band-width has been increased to 30 kc/s with sensitivity slightly improved. A ground-pulse suppressor has been incorporated as had been suggested by Mitra and Roy (1951). The response of the receiver has been made linear over a large dynamic range. The horizontal dipoles fed by co-axial cables have been used both for transmission and reception. As has already been mentioned, for suppressing one or the other of the two magneto-ionic components of the downcoming radio wave, the selective aerial system of Ratcliffe and White (1933) consisting of a pair of crossed loop has been used with the receiver. The experimental arrangement for the suppression of one or the other of the two magneto-ionic components (supposed to be circularly polarised) is shown in fig. 1. The output of the selective aerial system has been fed into the receiver by means of co-axial cables preceded by a transistorized

Loop 1. Loop 2

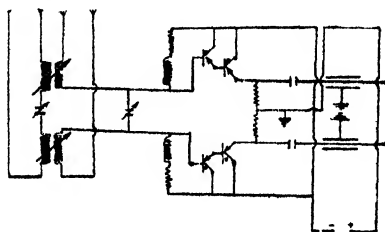


Fig. 1. Polarization arrangement with a pair of crossed loops.

impedance-matching device as shown in the figure. This arrangement has also helped to improve the signal-to-noise ratio in the receiver.

The video output from the receiver has been intensity-modulated by a suitable gate-generator locked in phase to the transmitter pulse. The gate-generator consists of three stages of mono-stable multi-vibrators arranged in cascade so that the variable time and the width of the gate-pulse have been made available over a wide range.

The recording oscilloscope was assembled in the laboratory using B16522 cathode ray tube with bluish white phosphor. The records have been taken on a moving film Cossor Camera at a film speed of 0.2 inch per second.

EXPERIMENTAL RESULTS AND THEIR DISCUSSION

The study of the sporadic *E*-region at different hours of the day and the night and at various frequencies has shown the blanketing type as well as the *q*-type *E_s*. The number of their occurrences has indicated clearly a preference for the summer and the rainy season. Though no regular routine measurements of the top frequencies or the cusp frequencies have been made, the wind-type of *E_s*, whose top frequency has been found to vary rapidly with time during the evening hours, has also been observed.

Working with an unpolarized receiver, i.e., using a horizontal dipole aerial with the receiver, a distinct double splitting of the sporadic *E*-trace on the moving film has been occasionally observed, both for the first order and the second order echoes. A few records have also shown an additional trace.

Fig. 2(a) illustrates a typical fading record showing a single unresolved trace of the *E_s*-echo, both for the first order and the second order echoes, as depicted on the upper and the lower halves of the record respectively. In fig. 2(b) is given a fading record which has shown a double trace on the moving film for both the first and the second orders. Fig. 2(c) illustrates a fading record which has shown an additional trace in the sporadic *E*-region for first and the second orders of reflection. The single trace of *E_s* in fig. 2(a) is due to the reflection of the unresolved magneto-ionic components from the sporadic *E*-region. When, however, the two magneto-ionic components are resolved and separated from each other, a double trace may be expected from the sporadic *E*-region. But such splitting may not always be possible, as the *E_s*-layer is very thin. The observed double trace shown in fig. 2(b) should therefore be attributed to the occasional existence of a double layer in that region. The partial reflection from the double layer would necessarily give rise to the double trace observed on the moving film. Of the three traces shown in fig 2(c), the undulatory trace at the top appears to indicate interference between the two unresolved magneto-ionic components under conditions of gradually changing electron-density in that region or below, giving rise to a rhythmic or periodic fading. The other two broad traces in

fig. 2(c) point to the existence of two more layers in the region on very rare occasions.

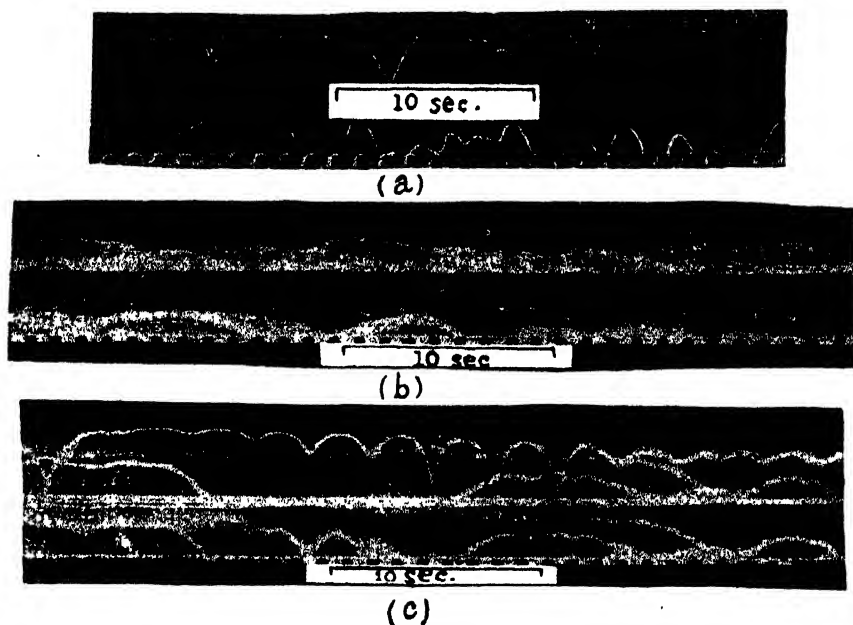


Fig. 2. (a) Fading record showing the usual single trace on the moving film for the first order and the second order echoes from the sporadic E-region on frequency 2.7 Mc/s. Date : 4-7-66, time : 2015 IST.

(b) Fading record showing the double trace on the moving film for the first order and the second order echoes from the sporadic E-region on frequency 3.2 Mc/s. Date : 22-11-65, time : 1951 IST.

(c) Fading record showing the triple trace on the moving film for the first order and the second order echoes from the sporadic E-region on frequency 3.2 Mc/s. Date : 22-11-65, time : 1833 IST.

(The first-order echoes are at the top and the second-order echoes are at the bottom of the moving film. Rhythmic or periodic fading of magneto-ionic origin can be seen in some parts.)

In this connection, it should be mentioned that the ionogram and the electron-density profile for a night flight over Ft. Churchill, Manitoba, Canada, incorporated in the paper by Seddon (1922) showed two or more electron-concentrations in the sporadic E-region of the ionosphere. The same paper also illustrated two concentrations in the electron-density profile at noon over New Mexico, U.S.A. and at night over Woomera, Australia. There is thus some experimental evidence in support of the existence of two or more electron-concentrations in this region which would cause a double (or triple) trace on the moving film.

Statistical studies of the amplitude of the single downcoming wave, obtained by using the selective aerial-system connected to the receiver, have been made

from a large number of fading records. The analysis has shown that the Rayleigh and the Rice types occur usually during the noon and the afternoon hours. During the morning, evening and early night hours, when usually reflection occurs from the sporadic E-region other types of amplitude distribution have been observed. Of the other types the most frequent type is the double-peak type or the so-called *M*-type. The types which have been less frequently observed show (i) an irregular distribution, (ii) a half-gaussian distribution and (iii) a log-normal distribution. In fig. 3(a) are shown two typical Rayleigh types of amplitude distribution for (i) $b = 0$ and (ii) $b = 0.707$. Fig. 3(b) shows a typical Rice distribution for $b = 1.4$. When $b > 3$, the distribution becomes Gaussian as is shown in fig. 3(c). The theoretical distribution is shown by the continuous line, whereas, the experimental points are indicated by black dots. The three amplitude distribution

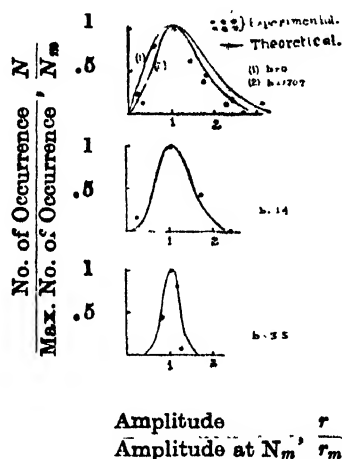


Fig. 3. (a) Rayleigh-type amplitude distribution (normalised) for $b = 0$ and $b = .707$ on 2.9 Mc/s. Date: 28-11-65, time: 0215 IST.
 (b) Rice-type amplitude distribution (normalised) for $b = 1.4$ on 2.5 Mc/s. Date: 9-8-63, time: 1830 IST.
 (c) Gaussian-type amplitude distribution (normalised) for $b = 3.5$ on 2.9 Mc/s. Date: 28-11-65, time: 0215 IST.

curves, each showing a double peak are illustrated in figs. 4(a), 4(b) and 4(c). An irregular type of amplitude distribution is shown in fig. 5(a), while a half-gaussian distribution is illustrated in fig. 5(b). The log-normal distribution of amplitude is shown in fig. 6(b) which corresponds to the actual amplitude distribution curve shown in fig. 6(a).

The number of maxima in the fading pattern per minute has been calculated and is found to vary between 2 and 5 at normal working frequencies (2.5—5 Mc/s), increasing almost linearly with the wave-frequency. Such linearity had been reported earlier by Skinner and Wright (1957).

The ν_r -distribution has been obtained for the various types of amplitude distributions. This distribution has been found to be Gaussian for the

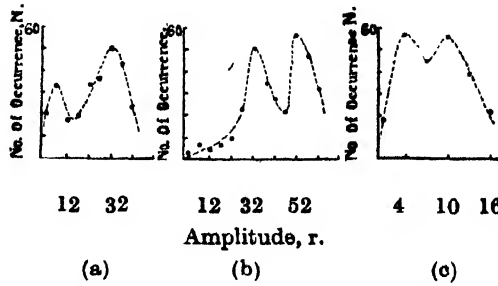


Fig. 4. (a) M-type distribution (first order) on 4.2 Mc/s. Date : 8-7-66, time : 1635 IST.
 (b) M-type distribution (first order) on 3.1 Mc/s. Date : 8-7-66, time : 1735 IST.
 (c) M-type distribution (second order) on 3.1 Mc/s. Date : 8-7-66, time : 1735 IST.
 (The amplitudes are in arbitrary units.)

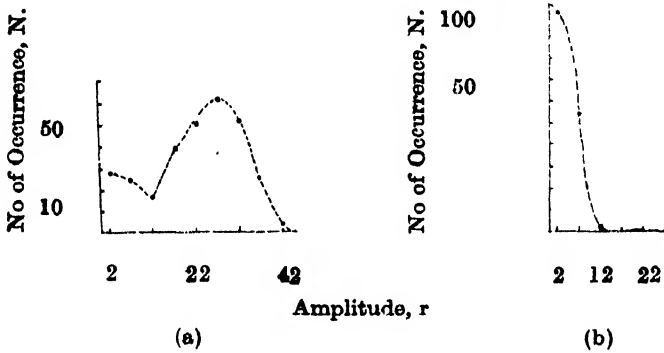


Fig. 5. (a) Irregular-type distribution (first order) on 2.9 Mc/s. Date : 3-12-66, time : 0710 IST.
 (b) Semi-Gaussian distribution (first order) on 2.5 Mc/s. Date : 9-8-63, time : 1830 IST.
 (The amplitudes are in arbitrary units.)

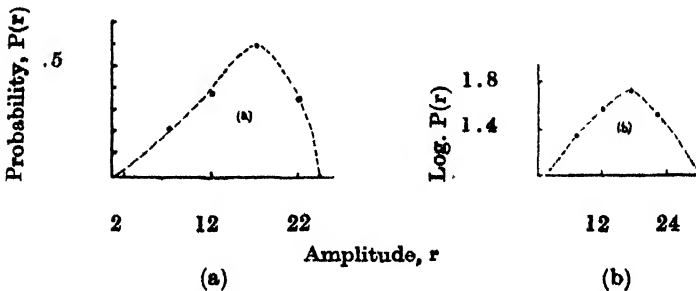


Fig. 6. Log-normal distribution shown in (b) and the corresponding amplitude distribution (first order) shown in (a) on 2.5 Mc/s. Date : 9-8-63, time : 1830 IST.
 (The amplitudes are in arbitrary units.)

Rayleigh type of amplitude distribution. For the other types of amplitude-distribution, the ν_r -distribution has been found to correspond to the Pearson type VII distribution. These are illustrated in figs. 7(a) and 7(b). The values of the rms line-of-sight velocity ν_0 of the irregularities in the sporadic E-region, as computed from the ν_r -distributions shown in figs. 7(a) and 7(b) with the help of

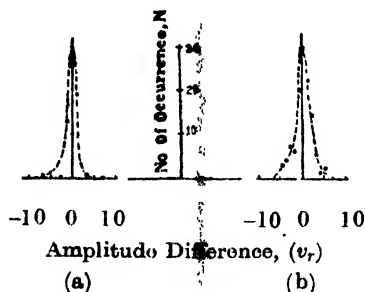


Fig. 7. (a) ν_r -distribution (first order) on 2.9 Mc/s. Date : 28-11-65, time : 0215 IST.
 (b) ν_r -distribution (second order) on 2.9 Mc/s. Date : 28-11-65, time : 0215 IST.
 (The amplitudes differences are in arbitrary units and $\tau = 0.215$ sec.)

(9) have come out to be 1.1 m/sec. and 8.6 m/sec. respectively. In computing ν_0 , the average amplitude-difference $\bar{\nu}_r$ and the average amplitude \bar{r} are expressed in the same arbitrary units. The data for determining ν_0 are given below :

$$f = 2.9 \text{ Mc/s, } \lambda = 103.45 \text{ metres, } \tau = 0.215 \text{ sec.,}$$

$$\bar{\nu}_r = 0.7 \text{ and } \bar{r} = 37.4 \text{ for the first order echo (fig. 7a)}$$

$$\bar{\nu}_r = 1.82 \text{ and } \bar{r} = 12.75 \text{ for the second order echo (fig. 7b)}$$

The interpretation of the double-peak amplitude distribution will be discussed elsewhere. This is most likely associated with the double layer observed in the sporadic E-region.

ACKNOWLEDGMENTS

Our grateful thanks are due to Prof. S. R. Khastgir for his kind interest and constant help during the course of the investigation. Our sincere thanks are also due to the Council of Scientific and Industrial Research, New Delhi, for sponsoring a research scheme on Ionospheric Absorption.

REFERENCES

- Alpert, J. L., 1958, *vide Radio wave Propagation by Ginzberg and Feinberg*.
 Appleton, E. V. and Beynon, W. J. G., 1947, *Proc. Phys. Soc. (Lond.)*, **58**, 59.
 Booker, H. J., Ratcliffe, J. A. and Shinn, O. R., 1950, *Phil. Trans, Roy. Soc. (Lond.)* **A**, **262**, 579.
 Das Gupta, P. and Vij, K. K., 1960, *J. Atmos. Terr. Phys.*, **18**, 265.
 Fürth, R. and Macdonald, D. K. C., 1947, *Proc. Phys. Soc. (Lond.)*, **59**, 388.
 Kushnerevsky, J. V. and Zayarnaya, E. S., 1962, *vide Some Ionospheric Results obtained during the International Geophysical Year*, edited by W. J. G. Beynon, p. 319.

- McNicol, R. W. E., 1949, *Proc. I.E.E.*, **96**, Part III, 517.
- Mitra, S. N., 1949, *Proc. I.E.E.*, **96**, Part III, 441.
- 1949, *Proc. I.E.E.*, **96**, Part III, 505.
- Mitra, S. N. and Roy, J. M., 1951, *Electrotechnics*, No. 23, 5.
- Rao, B. R. and Rao, P. S. K., 1964, *J. Atmos. Terr. Phys.*, **26**, 841.
- Ratcliffe, J. A., 1948, *Nature*, **162**, 9.
- 1956, *Reports on Progress in Physics*, **19**, 188.
- Ratcliffe, J. A. and White, F. W. G., 1933, *Phil. Mag.*, **16**, 423.
- Rayleigh, Lord, 1899, *Collected Works*, (Camb. University Press), **1**, 495.
- Rice, S. O., 1944, *Bell. Syst. Tech. J.*, **23**, 282.
- 1945, *Bell. Syst. Tech. J.*, **24**, 46.
- Schwentek, H., 1962, *J. Atmos. Terr. Phys.*, **23**, 68.
- Seddon, J. C., 1962, *vide Ionospheric Sporadic E*, edited by E. K. Smith and Sadami Matsushita, p. 81.
- Sen, N. N. and Khastgir, S. R., 1965, *Ind. Jour. Pure & App. Physics*, **3**, 167.
- Skinner, N. J. and Wright, R. W., 1957, *Proc. Phys. Soc. (Lond.)*, **B70**, 833.
- Subhadramma, G. V., 1955, *Jour. Sci. Res., Banaras Hindu University*, **6**, 162.
- 1959, *Ph.D. Thesis*, Banaras Hindu University,
- Yeh, K. C. and Villard, O. G., 1962, *J. Atmos. Terr. Phys.*, **20**, 137.

PRESSURE DEPENDENCE OF THE ELECTRICAL CONDUCTANCE OF PRESSED CASSITERITE POWDERS

S. C. MITRA* AND B. U. OKONJI

UNIVERSITY OF NIGERIA, NSUKKA.

(Received August 29, 1967)

ABSTRACT. Pressure dependence of the electrical conductance of cassiterite powder has been investigated at room temperature and low compression, up to pressure of 90 kg/cm^2 . The conductance is found to increase with pressure exponentially according to the equation $G = A \exp(Kp_m)$. A model based on elastic properties and surface charge layers of the grains is developed to qualitatively explain the results.

INTRODUCTION

Whilst a fairly large amount of work has been done on the pressure dependence of conductance of powdered metals, similar works on semiconducting powders have been somewhat limited.

The pioneer work of Kantorovicz (1931) on metal powders shows that the electrical conductance G varies according to eqn (1)

$$G = C_1 p_m^{\frac{1}{2}} + C_2 \quad \dots (1)$$

where p_m is the pressure and C_1 and C_2 are constants depending on the elastic properties of the metal.

Holm (1958) has given a theoretical basis of eqn (1) showing that on the basis of constriction resistances arising out of the narrow highly resistive points of contact of the grains through which the current flows, the conductivity of pressed metal powders satisfies eqn (2)

$$G = C \left(\frac{p_m}{H} \right)^{\frac{1}{2}} + f(p_m) \quad \dots (2)$$

where H is the hardness factor and C and $f(p_m)$ are functions of the elastic properties of the material; K is a constant such that ordinarily $\frac{1}{2} < K < 1$; for clean contact surface K is equal to $\frac{1}{2}$.

The earliest works on pressure dependence of resistance of semiconducting powders were on aluminium oxide and zinc oxide by Davis (1950), and by Brentanno and Davis (1951). They find that in a general way the conductance of powders

* Present address—Defence Laboratory, Jodhpur.

increases with pressure. Bridgmann (1951) measured the resistance of semiconducting powders in the high compression range up to $50,000 \text{ kg/cm}^2$ hydrostatic pressure and finds that in the case of zinc oxide the resistance decreases with increasing pressure both at 25°C and 100°C but decreases with decrease of pressure at 200°C .

The investigations of Davis were followed up by Brentanno and Goldberg (1954). They applied unidirectional stress up to $38,000 \text{ lb/in}^2$ over a range of temperatures and confirm the general findings of Davis. They, however, find that with pressure variation the conductance attains a maxima and for lower temperature the maxima is obtained at lower pressure.

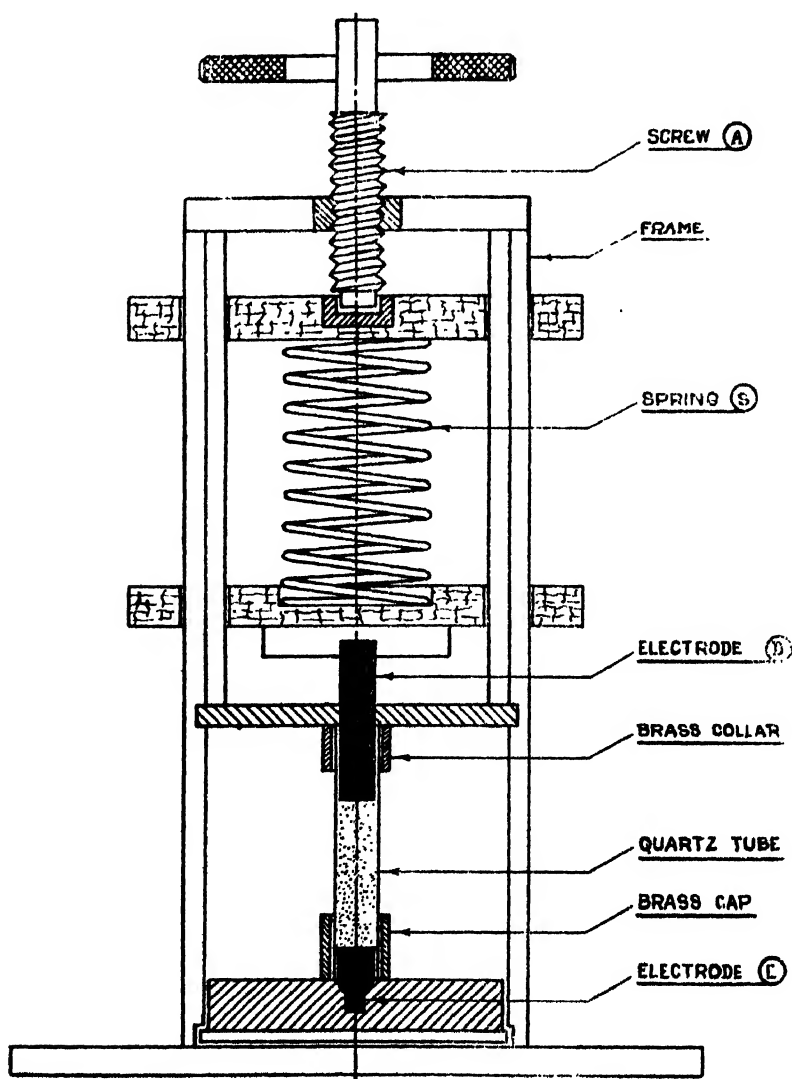


Fig. 1. Schematic Diagram of the Compressor.

Works hitherto on the conductance of semiconducting powders had been confined in interest to high compression range. The present work is a study of what happens to a semiconducting powder when subjected to low compression.

EXPERIMENTAL

Electrical resistance of pressed cassiterite powder at different unidirectional pressure was measured in an ambient of air at room temperature. The apparatus used is shown in fig. 1.

The powder is contained in a quartz tube mounted vertically on a brass cap containing the lower electrode *E*. Pressure is applied by means of a screw *A*, acting through the intermediary of a calibrated spring *S* to the second electrode *D*. Resistance was measured by conventional method.

Readings of conductance were taken at an interval of 17.7 kgm/cm² up to 88.4 kgm/cm² during increase and decrease of pressure.

RESULTS

Measurements have been made on three samples *S*₁, *S*₂ and *S*₃ of lengths 3.37, 4.6, and 4.7 cms respectively and 2.83 sq. cm. cross sectional area.

Pressure dependence of conductance is plotted as logarithm of conductance Vs pressure (fig. 2). The curve is linear and satisfies equation

$$G = A \exp(Kp_m) \quad \dots (3)$$

where *G* = Conductance and *p* = pressure at the electrode.

A and *K* are constants which varies slightly from specimen to specimen

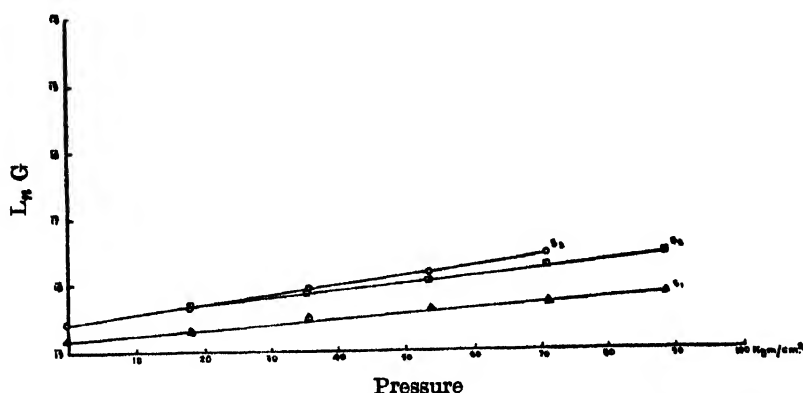


Fig. 2. Pressure variation of conductance of cassiterite powder.

INTERPRETATION OF EXPERIMENTAL RESULTS

Powdered materials consist of an agglomeration of grains with interstices and grain boundaries. In the case of powdered metal the flow of current is

channelised only through microscopic contact spots which accounts for the high resistance of metal powders (Holm 1958). The contact areas may be fully or partially conducting, in the latter case due to overlying multimolecular gas films. With increased pressure the conducting contact areas enlarge, due to elastic or plastic deformations of the grains as well as due to the elimination of the disturbing films. The electrical conductance of metal powder is thus a function of pressure, as well as of the geometrical and mechanical properties of the grains and resistivity of the material.

In semiconducting powders the above picture is modified due to the presence of surface charge on the grains (Hannay 1960). The individual crystallites are generally covered by a layer of charge at the surface. The electrical properties of the surface layers are significantly different from those of the interior. The surface layer may be either the exhaustion or enriched type. In the former case, the surface has reduced conductivity than the bulk and in the latter case opposite. Under pressure, at the points of contacts of the grains, some quasi-sintering will take place as a result of which the grains will be inter-connected by necks, whose diameters are comparable with the depth of the space charge layer. The carrier concentration at the neck will be different from that of the bulk. Consequently, the position of the Fermi level at and away from the neck will be different, thereby modifying the energy band structure. The conductance of the necks will be predominant in the overall conductance of the samples. Pressure will change the nature and size of the interconnecting necks and hence change conductance of the sample. So far, it has been assumed that the interstices are perfect insulators. At high temperatures and if the materials have low work function the pores may also become conducting due to electron gas present in the pores as a result of thermionic emission as has been observed in Barium oxide and Barium Strontium oxide by Loosjes and Vink (1949).

We propose to explain the results of our investigations on the basis of the foregoing discussion. We assume that for our material, on account of investigations at room temperature and low pressures neither pore conductance nor variation of forbidden energy gap with pressure apply (Bridgmann 1951, 1953, Bardeen 1949, Taylor 1950; Paul and Brooks 1954; Bretanno and Goldberg 1954).

For powder samples, when a force F is applied on the electrode of cross sectional area A_m , the pressure p on the particle contact area a is not the same as the pressure p_m on the electrode. This is obviously on account of the interstices present in the bulk of the powder. The particle contact area a is the sum of the contact areas for any cross section of the powder and represents the average pressure over the particle cross sectional area a . Neither p nor a is measurable but they are related to the macroscopic measurable quantities p_m and A_m by eqn (4)

$$F = p_m A_m = pa \quad \dots (4)$$

Following Holm (1958), the actual contact area increases with pressure up to a limit. The increase is large at low pressures and very small at high pressures. We assume that in the low pressure range, da/dp_m is constant in the first order.

For the semiconductor specimen under consideration, we represent conductance G by the following classical expression.

$$G = G' \exp \left(- \frac{E}{KT} \right) \quad \dots (5)$$

This expression is valid for $E \ll KT$ where E is the conductivity activation energy. This is true for cassiterite since its conductivity activation energy is greater than 0.5 e.v. (Kohnke 1962, Mitra 1967). G depends on the physical parameters of the sample including the geometry of the interconnecting necks. From (5)

$$L_n G = L_n G' - \frac{E}{2KT} \quad \dots (6)$$

We assume that G' and E are dependent on pressure only since the temperature is constant and can be represented by (7)

$$\left. \begin{aligned} G' &= G_0 + \frac{\partial G'}{\partial p_m} \cdot p_m \\ E &= E_0 + \frac{\partial E}{\partial p_m} \cdot p_m \end{aligned} \right\} \quad \dots (7)$$

From (6) and (7)

$$L_n G = \text{const} + \left(\frac{1}{G_0} \frac{\partial G'}{\partial p_m} - \frac{1}{2KT} \frac{\partial E}{\partial p_m} \right) p_m \quad \dots (8)$$

Analysis of our data shows that Holm's theory of constriction resistance for metal powder alone is inadequate to satisfy the experimental findings, which is understandable. Equation (8) agrees with eqn (3) if we assume that the expression within the bracket is a positive constant equal to K of eqn (3) where K is seen from the graph to vary slightly from specimen to specimen. Brentanno and Goldberg's results are in the high compression range and at pressures above conductance maxima, and hence beyond scope of comparison with our findings. In their range of pressure, logarithm of conductance decreases directly with pressure and the constant of proportionality is proportional to p_m and inversely proportional to the critical pressure P_m at which bruising or cracking of particles occurs. This

can be obtained from eqn (8) since at high pressure G' is constant and hence the first term within the bracket in eqn (8) vanishes.

It has not been possible with our present knowledge of surface and bulk effects to untangle the contributions of the respective components of eqn (8). A good deal of expertise will however, be needed before that is possible. Work is in progress along the line and will be reported in due course.

ACKNOWLEDGMENTS

The authors are grateful to Professor A. V. Brancker, Head, Department of Physics, University of Nigeria for facilities provided. Thanks are due to the Director, Geological Survey of Nigeria, Kaduna, for supplying the mineral and to Mr. A. K. Datta, Reader and Mr. R. Bhattacharya, Research Officer, Indian Association for the Cultivation of Science for helpful discussions.

REFERENCES

- Bardeen, J., 1949, *Phys. Rev.*, **71**, 717.
Brentanno, J. C. M. and Davis, D. H., 1950, *Phys. Rev.*, **79**, 216.
Brentanno, J. C. M. and Goldberg, C., 1954, *Phys. Rev.*, **94** 56.
Bridgmann, P. W., 1951, *Proc. Amm. Acad. Arts. Sci.*, **79**, 125.
Hannay, N. B., 1960, *Semiconductors*, Reinhold.
Holm, R. *Electric Contacts Handbook* 1958, ed. Springer, Berlin.
Kantorowicz, O., 1931, *Metallwirtschaft*, **10**, 45.
Kantorowicz, O., 1933, *Ann. Physk.*, **12**, 1.
Kohnke, E. E., 1962, *J. Phys. Chem. Solids*, **23**, 1557.
Loosjes, R. and Vink, V. J., 1949, *Philips Research Reports*, **4**, 449.
Mitra, S. C., 1967, *Ind. J. Phys*, 1967, **41**, 448.
Paul W, Brookes, H., 1954, *Phys. Rev.*, **94**, 1128.
Taylor, J. H., 1950, *Phys. Rev.*, **80**, 919.

A NOTE ON MECHANICAL RESPONSE IN A PIEZOELECTRIC CERAMIC TRANSDUCER UNDER THE INFLUENCE OF A BODY-FORCE

D. K. SINHA

MATHEMATICS DEPARTMENT, JADAVPUR UNIVERSITY, JADAVPUR, CALCUTTA-32, INDIA.

(Received July 19, 1967; Resubmitted January 6, 1968).

ABSTRACT. The present note seeks to investigate the mechanical responses in a piezoelectric transducer made up of a ceramic, when acted upon by a step electrical voltage.

INTRODUCTION

In recent years, there has been a considerable amount of studies on the responses in piezoelectric transducers from the standpoint of mechanics of continuous media, contrary to what has hitherto been followed by means of circuit-theory as in Mason (1948). The recent studies, which are of importance in ultrasonics and acoustics, seem to have been initiated by Redwood (1962), Fillipcyznaski (1956) and followed up by several authors, Sinha (1962, 1963, 1965, 1968), Giri (1966), Roy (1968), Das (1967) and others. In all these discussions, in which responses—both electrical and mechanical—have been studied in a piezoelectric transducer, when voltage or mechanical transients are applied only at one of its ends, the effect of a body-force on its responses has been kept out of consideration. Thus, what is attempted here is to accomodate a suitable body-force, dependent on time as well as dimension, in ascertaining the responses of a piezoelectric transducer. The mechanical response of such a transducer, subjected to a voltage step at one of its ends and rigidly backed at the other end, has been obtained by applying the method of Laplace transforms.

DERIVATION OF THE FUNDAMENTAL EQUATIONS, BOUNDARY CONDITIONS

We consider a transducer vibrating in the thickness mode of vibration. We take this thickness-direction to be the direction of the x -axis so that $x = 0$ and $x = X$ may be taken as the extremities of the transducer. To the end $x = 0$, is applied a voltage transient V given by

$$\begin{aligned} V &= V_0 \text{ when } t > 0 \\ &= 0 \text{ when } t < 0. \end{aligned}$$

The end $x = X$ is rigidly fixed so that the mechanical displacement ξ at $x = X$ is zero. As we seek the mechanical displacement ξ owing to the electrical voltage

given by (1), we must necessarily establish a relation between ξ and V . For this purpose, we take the usual constitutive relations for a piezoelectric ceramic as our starting point. These are given by

$$T = c \frac{\partial \xi}{\partial x} - hD \quad \dots (2)$$

$$E = -h \frac{\partial \xi}{\partial x} + \frac{D}{\epsilon} \quad \dots (3)$$

where T is the stress, E is the electric intensity and D is the electric displacement in the x -direction. The constants c, h, ϵ represent the elastic compliance, the piezoelectric constant and the dielectric permittivity, respectively.

The equation of motion in the x -direction is given by

$$\rho \frac{\partial^2 \xi}{\partial t^2} = \frac{\partial T}{\partial x} + \rho X_1 \quad \dots (4)$$

where ρ is the density of the material and X_1 is the body-force. Taking X_1 to be given by

$$X_1 = H(t)e^{-kx} \quad \dots (5)$$

where $H(t)$ is the Heaviside's unit function and k is a constant, we have from (4),

$$\rho \frac{\partial^2 \xi}{\partial t^2} = \frac{\partial T}{\partial x} + \rho H(t)e^{-kx} \quad \dots (6)$$

Because of (2), (6) becomes

$$\rho \frac{\partial^2 \xi}{\partial t^2} = c \frac{\partial^2 \xi}{\partial x^2} + \rho H(t)e^{-kx} - h \frac{\partial D}{\partial x} \quad \dots (7)$$

Next, in keeping with one simplifying assumption of Redwood (1961) namely, the wave propagation is plane in nature, we get

$$\frac{\partial D_y}{\partial y} = \frac{\partial D_z}{\partial z} = 0$$

which means from

$$\text{div } \vec{D} = 0$$

$$\frac{\partial D}{\partial x} = 0. \quad \dots (8)$$

Hence (7) becomes

$$\rho \frac{\partial^2 \xi}{\partial t^2} = c \frac{\partial^2 \xi}{\partial x^2} + \rho H(t) e^{-kx}. \quad \dots (9)$$

Let $\bar{f}(p)$ be the Laplace transform of $f(t)$ so that

$$\bar{f}(p) = \int_0^{\infty} e^{-pt} f(t) dt, \quad (p > 0).$$

Taking the Laplace transform of (9), we get

$$\frac{\partial^2 \bar{\xi}}{\partial x^2} - \frac{p^2}{v^2} \bar{\xi} = - \frac{e^{-kx}}{pv^2} \quad \dots (10)$$

where

$$v^2 = \frac{c}{\rho}.$$

Solving for $\bar{\xi}$, we have

$$\bar{\xi} = A e^{-\frac{px}{v}} + B e^{\frac{px}{v}} + \frac{1}{p(p^2 - v^2 k^2)} e^{-kx} \quad \dots (11)$$

where A and B are constants.

Setting, $F = TYZ$ and $Q = DYZ$

so that F is the force acting on an area of magnitude YZ normal to the x -axis and Q is the electrical charge, we get from (2), using (11),

$$\bar{F} + h\bar{Q} = pZ_c \left\{ -A e^{-\frac{px}{v}} + B e^{\frac{px}{v}} - \frac{vk}{p^2(p^2 - v^2 k^2)} e^{-kx} \right\} \quad \dots (12)$$

when

$$Z_c = \rho v YZ$$

Integrating the equation (3) between $x = 0$ and $x = X$, we have the voltage V across the transducer in the form given by

$$\bar{V} = -h\{(\bar{\xi})_x - (\bar{\xi})_0\} + \frac{\bar{Q}}{c_0} \quad \dots (13)$$

where

$$c_0 = \frac{\epsilon YZ}{X}$$

The equations (11), (12), (13) are the fundamental equations. The boundary conditions are nothing but the conditions of continuity of the force and displacement at the extremities $x = 0$ and $x = X$.

SOLUTION OF THE PROBLEM

At $x = 0$, the boundary conditions yield

$$B_1 = A + B + \frac{1}{p(p^2 - v^2 k^2)} \quad \dots (14)$$

$$pZ_1 B_1 = pZ_c \left\{ -A + B - \frac{vk}{p^2(p^2 - v^2 k^2)} \right\} - h\bar{Q} \quad \dots (15)$$

where B_1, Z_1 are the constants corresponding to B and Z_c in the material attached to the transducer at $x = 0$ and where $Z_c = \rho v Y Z$.

At $x = X$, since the plate is rigidly fixed, we get

$$(\xi)_X = 0$$

which gives from (11),

$$Ae^{-\frac{pX}{v}} + Be^{\frac{pX}{v}} + \frac{1}{p(p^2 - v^2 k^2)} e^{-kX} = 0 \quad \dots (16)$$

Since the voltage V given by (1) is applied at $x = 0$, we have from (13),

$$h \left\{ A + B + \frac{1}{p(p^2 - v^2 k^2)} \right\} + \frac{\bar{Q}}{c_0} = \frac{V_0}{p} \quad \dots (17)$$

The equations (14), (15), (16), (17) can be solved determinantly to evaluate the four unknowns, viz., A, B, B_1, \bar{Q} . For this purpose, we may write the above four equations as follows :

$$\begin{aligned} A + B - B_1 + O.\bar{Q} &= -\frac{1}{p(p^2 - v^2 k^2)} \\ Z_c.A - Z_c.B + Z_1 B_1 + h.\frac{\bar{Q}}{p} &= -\frac{z.vk}{p^2(p^2 - v^2 k^2)} \\ e^{-\frac{pX}{v}}.A + e^{\frac{pX}{v}}.B + O.B_1 + O.\bar{Q} &= -\frac{1}{p(p^2 - v^2 k^2)} e^{-kX} \\ h.A + h.B + O.B_1 + \frac{1}{c_0}.\bar{Q} &= \frac{V_0}{p} - \frac{h}{p(p^2 - v^2 k^2)} \end{aligned} \quad (18)$$

Solving for A and B , we get

$$A = \frac{1}{\Delta} \left[-Z_c \cdot \frac{1}{c_0 p(p^2 - v^2 k^2)} e^{-kX} - h \left\{ e^{\frac{pX}{v}} \cdot \frac{V_0}{p} - \frac{e^{\frac{pX}{v}}}{p(p^2 - v^2 k^2)} \right\} \right]$$

$$\begin{aligned}
 & + \frac{h}{p(p^2 - v^2 k^2)} e^{-kX} - \frac{Z_c v k}{p^2 c_0 (p^2 - v^2 k^2)} e^{\frac{2pX}{v}} \\
 & + \left[\frac{Z_1}{c_0 p (p^2 - v^2 k^2)} e^{-kX} - \frac{Z_1}{p(p^2 - v^2 k^2)} \cdot \frac{e^{\frac{2pX}{v}}}{c_0} \right] \quad \dots (19)
 \end{aligned}$$

$$\begin{aligned}
 B = \frac{1}{\Delta} & \left[\frac{Z_c}{p c_0 (p^2 - v^2 k^2)} e^{-kX} - h \left\{ \frac{e^{-\frac{2pX}{v}} V_0}{p} - \frac{e^{-\frac{2pX}{v}}}{p(p^2 - v^2 k^2)} \right\} \right. \\
 & + \frac{h e}{p(p^2 - v^2 k^2)} + \frac{Z_c v k}{p^2 (p^2 - v^2 k^2)} \cdot \frac{e^{-\frac{2pX}{v}}}{c_0} \\
 & \left. + \frac{Z_1}{p c_0 (p^2 - v^2 k^2)} e^{-kX} - \frac{Z_1}{p(p^2 - v^2 k^2)} \cdot \frac{e^{-\frac{2pX}{v}}}{c_0} \right] \quad \dots (20)
 \end{aligned}$$

where $\Delta = -e^{-\frac{2pX}{v}} \left[\frac{2Z_c}{c_0} \left(1 - \frac{h}{c_0} e^{-\frac{2pX}{v}} \right) - \frac{(Z_1 - Z_v)}{c_0} \left(1 - e^{-\frac{2pX}{v}} \right) \right]$

Substituting these values of A and B in (11) and taking its inverse transform, we get the mechanical displacement. In particular, the displacement of the end $x = 0$, may be obtained. For, from (11)

$$(\xi)_0 = A + B + \frac{1}{p(p^2 - v^2 k^2)}$$

Therefore, from (19) and (20),

$$\begin{aligned}
 (\xi)_0 = \frac{1}{\left(\frac{3Z_c - Z_1}{c_0} - \frac{Z_0}{Z_0} \right)} & \left[\left\{ \frac{h V_0}{p} - \frac{h}{p(p^2 - v^2 k^2)} + \frac{Z_1}{p(p^2 - v^2 k^2)} \cdot \frac{1}{c_0} \right\} \left(1 + e^{-\frac{2pX}{v}} \right) \right. \\
 & + \left\{ \frac{2h^2}{p(p^2 - v^2 k^2)} e^{-kX} - \frac{2Z_1 e^{-kX}}{p c_0 (p^2 - v^2 k^2)} \right\} e^{-\frac{2pX}{v}} \\
 & \left. + \left\{ \frac{Z_c v k}{p^2 c_0 (p^2 - v^2 k^2)} \left(1 - e^{-\frac{2pX}{v}} \right) \right\} \right] \\
 & \times \left[1 - r_0 e^{-\frac{pX}{v}} - r_1 e^{-\frac{2pX}{v}} \right]^{-1} + \frac{1}{p(p^2 - v^2 k^2)}
 \end{aligned}$$

where

$$r_0 = \frac{h}{3Z_c - Z_1}; \quad r_1 = \frac{Z_1 - Z_c}{3Z_c - Z_1}$$

We now expand $\left[1 - r_0 e^{-\frac{pX}{v}} - r_1 e^{-\frac{2pX}{v}}\right]^{-1}$ binomially, as in Redwood (1961) and substitute first few of its terms in (21) and consequently we get on the right of (21) an expression arranged in increasing powers of $e^{-\frac{pX}{v}}$. Considering only the first term of the expansion, we get

$$(\xi)_0 = \frac{1}{\left(\frac{3Z_c - Z_1}{Z_0} - \frac{Z_1}{Z_0}\right)} \left[\left\{ \frac{hV_0}{p} - \frac{h}{p(p^2 - v^2k^2)} + \frac{Z_1}{p(p^2 - v^2k^2)} \cdot \frac{1}{c_0} \right\} \left(1 + r_0 e^{-\frac{pX}{v}}\right) \right. \\ \left. + \frac{Z_c vk}{p^2 c_0 (p^2 - v^2k^2)} \left(1 + r_0 e^{-\frac{pX}{v}}\right) \right] + \frac{1}{p(p^2 - v^2k^2)}$$

where

$$r_0 = \frac{h}{3Z_c - Z_1}, \quad r_1 = \frac{Z_1 - Z_c}{3Z_c - Z_1}$$

Therefore,

$$(\xi)_0 = \frac{1}{\left(\frac{3Z_c - Z_1}{Z_0} - \frac{Z_1}{Z_0}\right)} \left[\left\{ \frac{hV_0}{p} - \frac{h}{p(p^2 - v^2k^2)} + \frac{(pZ_1 + Z_c vk)}{p^2 c_0 (p^2 - v^2k^2)} \right\} \right. \\ \left. \times \left(1 + r_0 e^{-\frac{pX}{v}}\right) \right] + \frac{1}{p(p^2 - v^2k^2)} \\ = \left[\frac{1}{\left(\frac{3Z_c - Z_1}{Z_0} - \frac{Z_1}{Z_0}\right)} \left\{ -h + \frac{Z_1}{c_0} \right\} + 1 \right] \frac{1}{p(p^2 - v^2k^2)} \\ + \frac{1}{\left(\frac{3Z_c - Z_1}{Z_0} - \frac{Z_1}{Z_0}\right)} \cdot \frac{hV_0}{p} + \frac{Z_c vk}{\left(\frac{3Z_c - Z_1}{Z_0} - \frac{Z_1}{Z_0}\right) c_0} \cdot \frac{1}{p^2(p^2 - v^2k^2)} \\ + \frac{hV_0 r_0}{\left(\frac{3Z_c - Z_1}{Z_0} - \frac{Z_1}{Z_0}\right)} \cdot \frac{e^{-\frac{pX}{v}}}{p} + \frac{(Z_1 r_0 - h)}{\left(\frac{3Z_c - Z_1}{Z_0} - \frac{Z_1}{Z_0}\right)} \cdot \frac{1}{(p^2 - v^2k^2)} \cdot \frac{e^{-\frac{pX}{v}}}{p} \\ + \frac{Z_c vk}{\left(\frac{3Z_c - Z_1}{Z_0} - \frac{Z_1}{Z_0}\right) c_0} \cdot \frac{1}{p(p^2 - v^2k^2)} \cdot \frac{e^{-\frac{pX}{v}}}{p}$$

Inverting we get

$$\begin{aligned}
 (\xi)_0 &= \left[\frac{(Z_1 - c_0 h_0)}{\left(\frac{3Z_c - Z_1}{Z_0} \right) c_0} + 1 \right] \frac{1}{2v^2 k^2} (e^{vkt} + e^{-vkt} - 2) \\
 &+ \frac{hV_0}{\left(\frac{3Z_c - Z_1}{Z_0} \right)} + \frac{Z_c}{\left(\frac{3Z_c - Z_1}{Z_0} \right) c_0} \cdot \frac{1}{v^2 k^2} (vkt - \sin vkt), \quad 0 < t < \frac{2X}{v} \\
 &= \left[\frac{(Z_1 - c_0 h_0)}{\left(\frac{3Z_c - Z_1}{Z_0} \right) c_0} + 1 \right] \cdot \frac{1}{2v^2 k^2} (e^{vkt} + e^{-vkt} - 2) \\
 &+ \frac{hV_0}{\left(\frac{3Z_c - Z_1}{Z_0} \right)} + \frac{Z_c}{\left(\frac{3Z_c - Z_1}{Z_0} \right) c_0} \cdot \frac{1}{v^2 k^2} (vkt - \sin vkt) \\
 &+ \frac{hV_0 r_0}{\left(\frac{3Z_c - Z_1}{Z_0} \right)} + \frac{(Z_1 r_0 - h)}{2 \left(\frac{3Z_c - Z_1}{Z_0} \right)} \cdot \frac{1}{v^2 k^2} (e^{vkt} + e^{-vkt} - 2) \\
 &+ \frac{Z_c \cdot r_0}{2 \left(\frac{3Z_c - Z_1}{Z_0} \right) c_0 v k} (e^{vkt} - e^{-vkt} - 2vkt), \quad t > \frac{2X}{v}
 \end{aligned}$$

The foregoing results bring out the effect that the body-force, (which is zero when $k \rightarrow \infty$), has on the mechanical response of the transducer. The above results are in accordance with those of Redwood (1961) in the absence of the body-force.

REFERENCES

- Das, N. C., 1967, *Indian J. Phys.* (in press).
 Fillipczynaski, N., 1956, *Proceedings of the Conference on Ultrasonics*. Polish Academy of Sciences, Warsaw.
 Mason, W. P., 1948, *Electromechanical Transducers and Wave Filters*. D. Van Nostrand Co. Inc., Princeton, New Jersey, 2nd Edition.
 Redwood, M., 1961, *Jour. Acoust. Soc. Amer.*, **33**, p. 527.
 Roy, P., *Ind. Jour. Pure & Appl. Phys.* (in press.).
 Sinha, D. K., 1962, *Appl. Phys. Qlly.*, **8**, p. 9.
 1963, *Ind. Jour. Theor. Phys.*, **11**, 9.3.
 1965, *Proc. Nat. Inst. Sc. India*, **31A**, 395.
 1968, *Ind. Jour. Pure & Appl. Phys.* (in press).
 Giri, R. R., 1968, *Rev. Rou. Tech. Sci.*, **11**, 253.

Letters to the Editor

The Board of Editors does not hold itself responsible for opinions expressed in the letter published in this section. The notes containing short reports of original investigations communicated to this section should not contain many figures and should not exceed 500 words in length. The contributions reaching the Secretary by the 15th of any month may be expected to appear in the issue for the next month. No proof will be sent to the author.

34

LOW-ANGLE X-RAY MEASUREMENTS ON AIR-DRIED AND ALKALI-TREATED MACROMOLECULAR SYSTEMS-WOOL

T. RATHO AND B. C. PANDA

REGIONAL ENGINEERING COLLEGE, ROURKELA, ORISSA, INDIA.

(Received January 1, 1968).

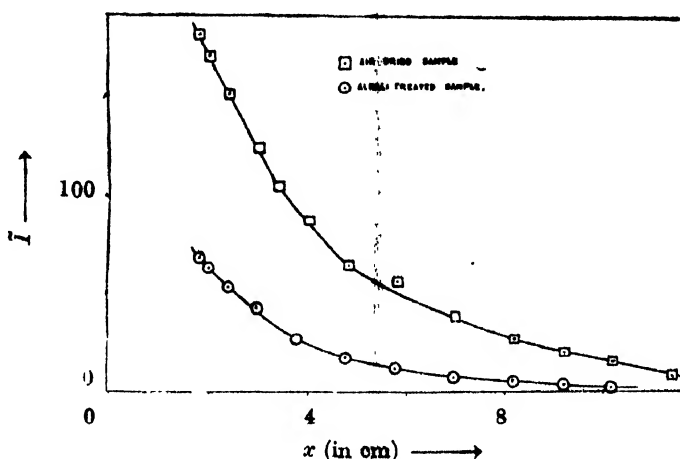
Precision measurements on alkali-treated Merino wool belonging to the macromolecular system have been made using the Low-angle Kratky (1958) camera of the latest design fitted with a crystal monochromator after Johansson (1933)-Guinier (1946). The wave length used was 1.54 \AA , CuK_α radiation. The determination of parameters like the radius of gyration of cross section and the radius of gyration of thickness are made by the Guinier (1937) procedure. Such parameters on cellulose fibres have been reported much earlier by Heyn (1949) and others.

Merino wool was treated with a Sodium hydroxide solution of pH-10 for 40 days. The scattering curve of this sample is shown with that of the air-dried one in the figure, where \bar{I} is the smeared-out intensity and x is a function of the scattering angle θ :

$$x = 2ap\theta$$

a being the sample-film distance, p the transformation factor related to the microphotometer curve i.e. the ratio of the distance in the microphotometer record to the actual distance in the photographic film, and x is the distance measured along the microphotometer record. The method of obtaining the intensity curves is the same as that reported by one of us (Ratho, 1964), except that a monochromator is used here. We have here adopted the same method for evaluation of parameters as reported earlier by us (Ratho *et al*, 1965).

From the study of the two scattering curves it appears that there is a considerable fall of intensity in the innermost region in the alkali-treated sample which is probably due to the splitting up of large sized particles into smaller ones after long treatment with alkali.



One can easily obtain the radius of gyration of cross section (R_q) and the radius of gyration of thickness (R_d) for the particles from the $\log \tilde{I}x$ vs x^2 and $\log \tilde{I}x^2$ vs x^2 curves according to Guinier approximation. The R_q , R_d , air-fraction as well as the specific surface (O/V) of the particles have been calculated and the results tabulated below :

Samples	R_q (\AA)	R_d (\AA)		O/V (\AA^{-1})	Air-fraction
		R_{d1}	R_{d2}		
Merino Air-dried	96.99	85.53	43.37	2.082×10^{-4}	0.7018%
Merino treated with pH-10 NaOH solution for 40 days	83.07	76.49	38.24	4.467×10^{-5}	0.1654%

Although there is considerable fall of intensity in the low-angle regions for the alkali-treated sample due to fragmentation of larger particles to smaller ones as evidenced from R_q values, the shape of the scattering curves remain unchanged as they should have been (Kratky *et al*, 1942; Janeschitz-Kriegl *et al*, 1953.)

REFERENCES

- Guinier, A. 1946, *C. R. [Doklady] Acad. Sci. URSS*, **223**, 31.
 1937, *C. R. Hebd. Seances Acad. Sci.*, **204**, 1115.
 Heyn, A. N. J., 1949, *Textile Research J.*, **19**, 163.

- Janeschitz-Kriegl, H., and Kratky, O., 1953, *Z. Elektrochem.*, **57**, 42.
 Johansson, T., 1933, *Z. Physik.*, **82**, 587.
 Kratky, O. and Scala, Z., 1958, *Z. Elektrochemie*, **62** (1), 66.
 Kratky, O., Sekora, A. and Treer, R., 1942, *Z. Elektrochem.*, **48**, 587.
 Ratho, T. and Panda, B. C., 1965, *Indian J. Phys.*, **39**, 207.
 Ratho, T., 1964, *Indian J. Phys.*, **38**, 475.

35

MATRIX ELEMENTS INCORPORATING MOMENTUM TRANSFER

G. CHATTERJEE, D. M. BHATTACHARYA and N. C. SIL

DEPARTMENT OF THEORETICAL PHYSICS, INDIAN ASSOCIATION FOR THE
CULTIVATION OF SCIENCE, CALCUTTA-32 INDIA

(Received January 30, 1968)

The theoretical calculations on electron capture phenomena in ion-atom collision at high energies, should include the translatory motion (momentum transfer) of the electron attached either with the target or the projectile ion. Different authors viz. McCarroll, (1961) and Willets *et al*, (1966) took recourse to approximate numerical analysis to evaluate the matrix elements $\langle \psi_A^n | V | \psi_B^m \rangle$ and $\langle \psi_A^n | \dot{\psi}_B^m \rangle$ occurring as coefficients in the set of differential equations to be solved cf. Basu *et al* (1967). But the difficulty is to call for the subroutine of the integrals at every step in the process of the solution of the differential equation (see Runge—Kutta Method). Cheshire (1967) has formulated a method in which the time derivatives of the said matrix elements can be found out analytically. He has pointed out how to calculate the matrix elements for 2s and 2p states. We had also pursued the problem with a straight forward alternative derivation and obtained results identical with those of Cheshire. Further the results have been utilised in calculating some of the matrix elements in alpha-hydrogen atom collision and proton-hydrogen atom collisions.

We write the hydrogenic wave functions (unnormalised) around two moving nuclei *A* and *B* as

$$\phi_{A,B} = \exp \left[-\lambda_{A,B} r + i V_{A,B} \cdot r - \frac{i}{2} V_{A,B}^2 t + \lambda_{A,B}^2 t \right].$$

where r_A , r_B , r refer to the position vectors of the electron from nuclei *A*, *B* or any arbitrary origin 0, and V_A , V_B the velocities of *A* and *B*. We note that

$$r_{A,B} = r - V_{A,B} t - S_{A,B}$$

$$r = V_A - V_B$$

$$r = V t + S_A - S_B.$$

We start with basic integral $I = \int \frac{\phi_A^* \phi_B}{r_A r_B} dv$

By using Fourier transform integral of $e^{\lambda R}/R$ and writing in terms of r , we get

$$I = \frac{1}{4\pi^4} \exp \left[\frac{i}{2} t (V_A^2 - V_B^2 - \lambda_A^2 + \lambda_B^2) \right] \times \\ \int \exp [i(\mathbf{p} + \mathbf{q} - \mathbf{V}) \cdot \mathbf{r} - i\mathbf{p} \cdot (\mathbf{V}_A t + \mathbf{S}_B) - i\mathbf{q} \cdot (\mathbf{V}_B t + \mathbf{S}_B)] \times \\ \frac{1}{q^2 + \lambda_B^2 - p^2 - \lambda_A^2} \left[\frac{1}{p^2 + \lambda_A^2} - \frac{1}{q^2 + \lambda_B^2} \right] d^3 r d^3 p d^3 q.$$

Now by using the Dirac δ -function, we have

$$I = \frac{2}{\pi} \exp \left[\frac{i}{2} t (V_A^2 - V_B^2 - \lambda_A^2 + \lambda_B^2) \right] \times \\ \int \exp [i\mathbf{q} \cdot (\mathbf{V}t + \mathbf{S}_A - \mathbf{S}_B)] \exp [-i\mathbf{V} \cdot (\mathbf{V}_A t + \mathbf{S}_B)] \times \\ \frac{1}{2\mathbf{q} \cdot \mathbf{V} - V^2 - \lambda_A^2 + \lambda_B^2} \left[\frac{1}{|\mathbf{q} - \mathbf{V}|^2 + \lambda_A^2} - \frac{1}{q^2 + \lambda_B^2} \right] d^3 \mathbf{q}.$$

Taking time-derivative of I , the factor $(2\mathbf{q} \cdot \mathbf{V} - V^2 - \lambda_A^2 + \lambda_B^2)$ cancels and using the relation $\frac{1}{2\pi^2} \int \frac{e^{i\mathbf{p} \cdot \mathbf{r}}}{p^2 + \lambda^2} d^3 p = \frac{e^{-\lambda r}}{r}$, we get finally $i \frac{\partial I}{\partial t} = K(F - G)$,

where

$$K = \frac{2\pi}{R} \exp [i(\epsilon_B - \epsilon_A)t] \\ F = \exp \left[-\frac{i}{2} V^2 t - \lambda_B R - i\mathbf{V} \cdot \mathbf{S}_A \right] \\ G = \exp \left[\frac{i}{2} V^2 t - \lambda_A R - i\mathbf{V} \cdot \mathbf{S}_B \right].$$

Thus $I = -i \int K(F - G)dt$.

Differentiating I with respect to λ_A and λ_B several times-we can evaluate the general integrals of the type

$$\int r_A^m r_B^n \phi_A^* \phi_B dv = \left(-it\lambda_A - \frac{\partial}{\partial \lambda_A} \right)^{m+1} \left(it\lambda_B - \frac{\partial}{\partial \lambda_B} \right)^{n+1} I$$

If the general integrals involve θ and ϕ dependent wave functions in other than s -states, then we need to differentiate with respect to x , y or z component of S_A and S_B as necessary, in addition to the differentiations with respect to λ_A and λ_B .

Let us apply this technique in the calculation of the capture probabilities in the excited states of He^+ ion in α -particle-hydrogen atom collision. The matrix elements to be calculated by this method are

$$g_{mn} = \int \psi_m^* \psi'_n dv, \quad G_{mn} = \int \psi_m^* \frac{1}{2} \left(\frac{2}{r_B} + \frac{1}{r_A} \right) \psi'_n dv$$

where ψ_m is the wave function of H atom and ψ'_n that of He^+ ion.

Considering only the ground state of hydrogen atom the expressions for g_{1n} and G_{1n} are as following :

$$\text{Taking } X = \frac{2\pi}{R} \exp \left[-2R + \frac{i}{2} (3 - V^2)t \right]$$

$$\text{and } Y = \frac{2\pi}{R} \exp \left[-R + \frac{i}{2} (3 + V^2)t \right],$$

$$g_{11} = \frac{2\sqrt{2}}{\pi} \left[-2it^2 \int (X - Y)dt + 4it \int t(X - Y)dt - 2i \int t^2(X - Y)dt - 2t \int RYdt \right. \\ \left. + 2 \int tRYdt - t \int RXdt + \int tRXdt \right]$$

$$G_{11} = \frac{\sqrt{2}}{\pi} i \left[2 \int RYdt - \int RXdt \right]$$

$$\text{Taking } M = \frac{2\pi}{R} \exp \left[-R - \frac{i}{2} V^2 t \right] \text{ and } N = \frac{2\pi}{R} \exp \left[-R + \frac{i}{2} V^2 t \right],$$

$$g_{12} = \frac{1}{\pi} \left[-t^3 \int (M - N)dt + 3t^2 \int t(M - N)dt - 3t \int t^2(M - N)dt + \int t^3(M - N)dt \right. \\ \left. - 2t \int RNdt + 2 \int tRNdt - t \int RMdt + \int tRMdt - \int tR^2Mdt + t \int R^2Mdt \right] \\ + \frac{i}{\pi} \left[-2t^2 \int (M - N)dt + 4t \int t(M - N)dt - 2 \int t^2(M - N)dt + t^2 \int RNdt \right. \\ \left. - 2t \int tRNdt + \int t^2RNdt + 2t^2 \int RMdt - 4t \int tRMdt + 2 \int t^2RMdt \right]$$

$$G_{12} = \frac{1}{\pi} \left[t \int RNdt - \int tRNdt \right] + \frac{i}{\pi} \left[\int RNdt - \frac{1}{2}t^2 \int Ndt + t \int tNdt - \frac{1}{2} \int t^2Ndt \right. \\ \left. - \frac{1}{2} \int RMdt + \frac{1}{2}t^2 \int Mdt - t \int tMdt + \frac{1}{2}t^2Mdt + \frac{1}{2} \int R^2Mdt \right]$$

$$\begin{aligned}
 g_{13} = & \frac{V}{\pi} \left[t^3 \int \left(\frac{1}{R} + \frac{1}{R^2} \right) t(M-N)dt - 3t^2 \int \left(\frac{1}{R} + \frac{1}{R^2} \right) t^2(M-N)dt \right. \\
 & + 3t \int \left(\frac{1}{R} + \frac{1}{R^2} \right) t^3(M-N)dt - \int \left(\frac{1}{R} + \frac{1}{R^2} \right) t^4(M-N)dt - 2it^2 \int tMdt \\
 & - 4it^2 \int tNdt + 4it \int t^2Mdt + 5it \int t^2Ndt - 2i \int t^3Mdt - 2i \int t^3Ndt \\
 & \left. + it^3 \int Ndt - t^2 \int RNdt + 2t \int tRNdt - t \int tRMdt + \int t^2RMdt - \int t^2RNdt \right] \\
 G_{13} = & \frac{V}{\pi} \left[-\frac{1}{2} it^2 \int \left(\frac{1}{R} + \frac{1}{R^2} \right) t(M-N)dt + i \int \left(\frac{1}{R} + \frac{1}{R^2} \right) t^2(M-N)dt \right. \\
 & - \frac{1}{2} i \int \left(\frac{1}{R} + \frac{1}{R^2} \right) t^3(M-N)dt - 2t \int tNdt + \frac{1}{2} \int t^2Ndt + \frac{1}{2} t^2 \int Ndt \\
 & \left. - i \int tRNdt - \frac{1}{2} \int tRMdt + it \int RNdt \right] \\
 g_{14} = & \frac{P}{\pi} \left[t^3 \int \left(\frac{1}{R} + \frac{1}{R^2} \right) (M-N)dt - 3t^2 \int \left(\frac{1}{R} + \frac{1}{R^2} \right) t(M-N)dt \right. \\
 & + 3t \int \left(\frac{1}{R} + \frac{1}{R^2} \right) t^2(M-N)dt - \int \left(\frac{1}{R} + \frac{1}{R^2} \right) t^3(M-N)dt - 2it^2 \int Mdt - it^2 \int Ndt \\
 & + 4it \int tMdt + 2it \int tNdt - 2i \int t^2Mdt - i \int t^2Ndt - t \int RMdt + \int tRMdt \left. \right] \\
 G_{14} = & \frac{P}{\pi} \left[-\frac{1}{2} it^2 \int \left(\frac{1}{R} + \frac{1}{R^2} \right) (M-N)dt + it \int \left(\frac{1}{R} + \frac{1}{R^2} \right) t(M-N)dt \right. \\
 & \left. - \frac{1}{2} i \int \left(\frac{1}{R} + \frac{1}{R^2} \right) t^2(M-N)dt - t \int Ndt + \int tNdt - \frac{1}{2} i \int RMdt \right] \\
 g_{15} = G_{15} = & 0.
 \end{aligned}$$

The authors are thankful to Prof. D. Basu for his kind interest in this problem. One of the authors (N.C.S) gratefully acknowledges the helpful discussion with Dr. Cheshire, during the Fifth International Conference of Electronic and Atomic Collisions, Leningrad (1967).

REFERENCES

- D. Basu, D. M. Bhattacharya, and G. Chatterjee. 1967, *Phys. Rev.* **163**, 8.
 I. M. Cheshire—*Private communication*.
 R. Mc Carroll 1961, *Proc. Roy. Soc. A*, **264**, 547.
 L. Wilets and D. F. Gallaher, 1966, *Phys. Rev.*, **147**, 1, 13,

A NOTE ON 222 KeV GAMMA-RAY TRANSITION IN THE DECAY OF Ba ¹³³*

P. C. MANGAL AND P. N. TREHAN

DEPARTMENT OF PHYSICS, PANJAB UNIVERSITY,
CHANDIGARH-14.

(Received August 1, 1967).

The electron capture decay of Ba¹³³ has been investigated by a number of workers, Crasemann (1957) Fagg (1958) Gupta (1958) Stewart (1960) Ramaswamy (1960) Mann (1963) and Thun (1966). Most of these authors are in accord concerning the existence of all the gamma-ray transitions, shown in fig. 1, except the one of energy 222 KeV. This gamma-ray transition was originally observed by Stewart and Lu (1960) but could not latter on be detected by Ramaswamy (1960)

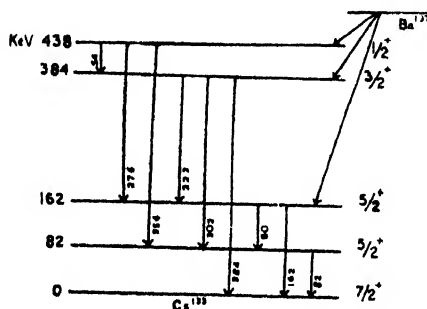


Fig. 1. Decay Scheme of Ba¹³³

and Mann (1963). The relative intensity of this gamma-ray has been estimated by Stewart and Lu (1960) to be 0.3% as compared to 356 KeV gamma-ray. Because of the weak intensity of this gamma-ray it could not be possible to confirm the existence of this gamma-ray and make any measurement on it by ordinary single or coincidence scintillation spectrometer or even with solid state detectors. In this present study a high efficiency sum-peak coincidence spectrometer of Kantele (1962) has been employed and it has been possible to confirm the existence of 222 KeV gamma-ray transition and to measure its relative intensity.

* This work has been supported by National Bureau of Standard Washington, D.C., U.S.A.

Measurement and Results

The high efficiency sum-peak coincidence spectrometer has been described in detail elsewhere by Kantele (1962). Two $3'' \times 3''$ NaI(Tl) detectors were placed at 90° to each other and a Compton shield was put in between them at 45° to avoid crystal-to-crystal scattering. The data was recorded on a 256 channel RCL analyser. The effective resolving time of the fast coincidence circuit was 100 n -secs. The integral biases were set at about 140 KeV on each side to completely bias out 80 and 82 KeV gamma-rays. The sum-peak coincidence spectrum was thus run for 10 hours. The random coincidences were also run for the same period by introducing a delay of 500 n -secs in one of the fast channels. After subtracting the random coincidence contribution the sum-peak coincidence spectrum is shown in fig. 2. This final spectrum predominantly shows two peaks one at 445 KeV which arises because of the summing of 162 and 276 KeV gamma-rays and the

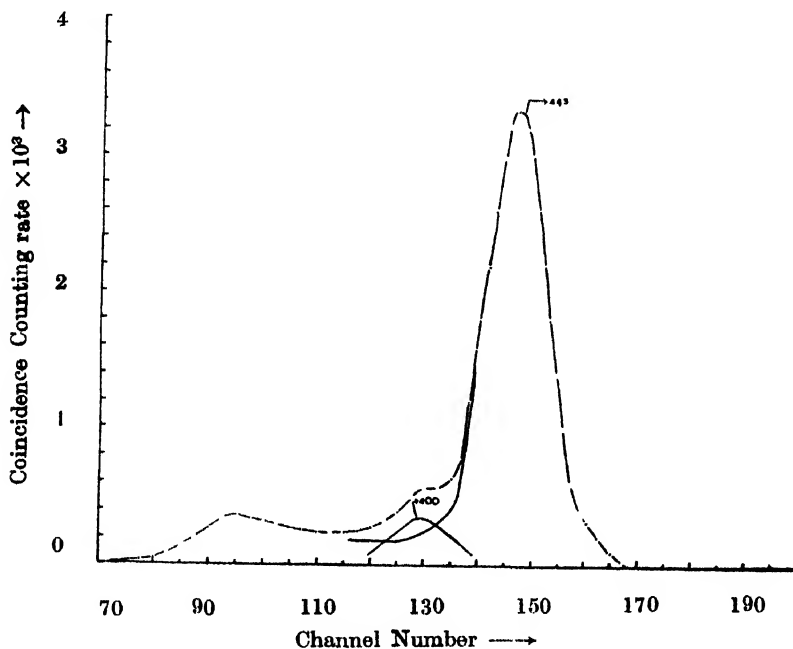


Fig. 2. Sum Peak coincidence spectrum of Ba^{133} taken with integral bias settings of 140 KeV.

second peak at 400 KeV is interpreted as the sum of 222 and 162 KeV gamma-rays cascade present in the decay of Ba^{133} . In both cases the sum peak energies are higher than the actual sum by the expected amount (Kantele *et al*, 1961). It is, therefore, concluded that there is 222 KeV gamma-ray present in the decay of Ba^{133} and since this gamma-ray is in coincidence with 162 KeV gamma-ray, therefore it originates from 384 KeV level and leads to 162 KeV level.

The relative intensity of this gamma-ray comes out to be 10.3% as compared to 162 KeV gamma-ray. The relative intensity of 162 KeV gamma-ray has been

measured by Mangal *et al.*, to be 2.8% as compared to 356 KeV gamma-ray. Therefore, the relative intensity of 222 KeV gamma-ray relative to 356 gamma-ray comes out to be 0.28 ± 0.03 . The error includes the summing effect of the K-x ray which is in coincidence with all the gamma-ray transmissions because of the electron capture decay of Ba^{133} .

REFERENCES

- Crasemann, B., Pengra, J. G. and Lindstorm, I. E., 1957, *Phys. Rev.*, **108**, 1500.
 Fagg, L. W., 1958, *Phys. Rev.*, **109**, 100.
 Gupta, R. K., Jha, S., Joshi, M. C. and Madan, B. K., 1958, *Nuovo Cimento*, **8**, 48.
 Ramaswamy, M. K., Skool, W. L. and Jastram, P. S., 1960, *Nucl. Phys.*, **16**, 619.
 Kantale, J. and Fink, R. W., 1961, *Nucl. Inst. and Methods*, **13**, 141.
 Kantale, 1962, *Nucl. Instr. and Methods*, **17**, 33.
 Mann, K. C. and Chaturvedi, R. P., 1963, *Can. J. Phys.*, **41**, 932.
 Mangal, P. C., Sud, S. P. and Trehan, P. N., *Indian J. Pure Appl. Phys.*, (Sen for publication).
 Stewart, M. G. and Lu, D. C., 1960, *Phys. Rev.*, **117**, 1044.
 Thun, J. E., *et al.*, 1966, *Nucl. Phys.*, **88**, 289.

37

THERMOELECTRIC POWER OF TUNGSTENITE (WS_2)
SINGLE CRYSTALS

S. R. GUHA THAKURTA

DEPARTMENT OF MAGNETISM, INDIAN ASSOCIATION FOR THE CULTIVATION OF SCIENCE,
CALCUTTA-32, INDIA

(Received January 25, 1968)

Thermoelectric power of naturally occurring single crystals (hexagonal) of tungstenite (WS_2) have been measured against copper along both the crystallographic directions and over the temperature range 300°K to 820°K . The results of preliminary measurements are shown in table 1 and in figures 1 and 2.

It is observed from the table I, that at the vicinity of room temperature the thermoelectric powers of crystals 1 and 3 are positive in both the crystallographic directions while that of crystal 2 is negative in these directions. The magnitude of thermoelectric power at room temperature which varies from sample to sample (evidently due to differences in the impurity contents which however has not been analysed) has been found to be slightly different in different crystallographic direc-

Table I

Thermoelectric power in WS_2 crystals along both the crystallographic directions at an ambient temperature 312°K (temperature gradient within 2°C to 3°C)

Crystal	t.e.p. along the c-axis in $\mu\text{V}/^\circ\text{C}$	Activation energy along the C-axis		t.e.p. \perp to c-axis in $\mu\text{V}/^\circ\text{C}$	Activation energy \perp to C-axis	
		within the range $300^\circ\text{--}400^\circ\text{K.}$	within the range $400^\circ\text{--}820^\circ\text{K.}$		within the range $300^\circ\text{--}400^\circ\text{K.}$	within the range $400^\circ\text{--}820^\circ\text{K.}$
1.	+ 4.0	0.5 ev	0.5 ev	+16.0	0.5 ev	0.47 ev
2.	-35.6	0.19 ev	0.33 ev	-33.5	0.28 ev	0.32 ev
3.	+ 4.7	0.34 ev	0.47 ev	+ 5.0	0.37 ev	0.45 ev
4.	+ 3.4	0.39 ev	0.44 ev	—	—	—

tions. At higher temperatures (fig. 1 and fig. 2) the t.e.p. of crystals having positive sign at room temperature remains always positive throughout the range of temperature studied. But in case of crystals with negative thermoelectric

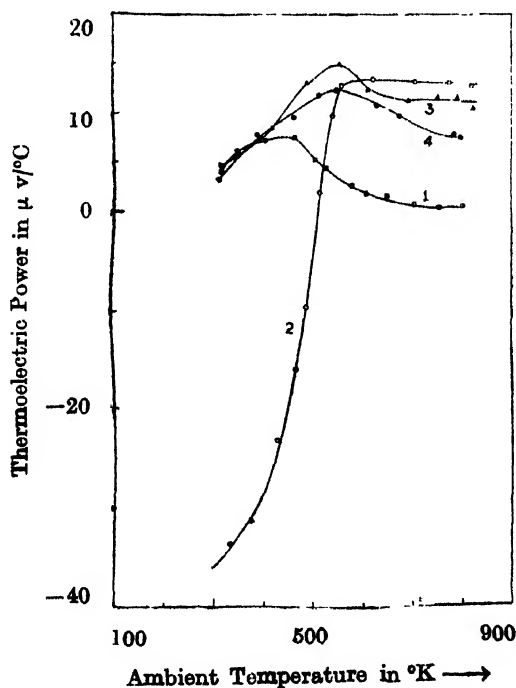


Fig. 1. Variation of thermoelectric power (along c-axis) with temperature. The number on the curve indicates the serial number of the crystal.

power at room temperature, the sign changes from negative to positive with the rise of temperature, and retains this positive sign at higher temperatures. Preliminary measurements of Hall effect with single crystals of WS_2 also appear to corroborate the above findings.

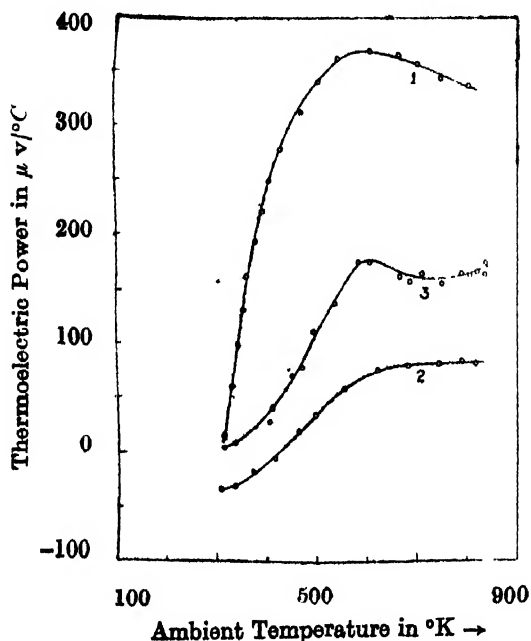


Fig. 2. Variation of thermoelectric power (\perp to σ -axis) with temperature. The number on the curve indicates the serial number of the crystal.

It may be mentioned here that Lagrenaudie (1954) from Hall effect measurements (within the temperature range 77°K – 293°K) with powered (artificial) WS_2 (activation energy 0.04 eV, 0.11 eV, 0.18 eV), observed that it was a p -type semiconductor, while Jean Decrue (1956) from electrical conductivity measurements in different atmospheres showed that powered (artificial) WS_2 (activation energy 0.17 eV) was a n -type semiconductor, within the temperature range 297°K – 373°K .

The Author conveys his best thanks to Shri A. K. Dutta for suggestion and guidance and to Prof. A. Bose for his kind interest in the work.

REFERENCES

- Decrue, J., 1956. *Helv. Chim. Acta.*, **39**, 619, 812.
Lagrenaudie, J., 1954. *J. Phys. Rad.*, **15**, 299.

TEMPERATURE VARIATION OF MAGNETIC SUSCEPTIBILITY OF MOLYBDENITE SINGLE CRYSTAL

D. PAUL (nee DAS)

DEPARTMENT OF MAGNETISM
INDIAN ASSOCIATION FOR THE CULTIVATION OF SCIENCE
CALCUTTA-32, INDIA

(Received February, 21, 1965)

The magnetic properties (anisotropy and absolute susceptibility) of molybdenite crystals at different temperatures were studied in this laboratory by Dutta (1945). But the measurements of susceptibility at high temperatures being done in air with quartz fibre torsion balance (Bose, 1947) utilising vertical gradient of the magnetic field were very much disturbed by convection currents. The results were therefore not very reliable. In consequence the susceptibility, χ_{\perp} (for directions in the basal plane) at different temperatures has been measured afresh in vacuum utilising very sensitive and accurate method of measurement (Das 1963).

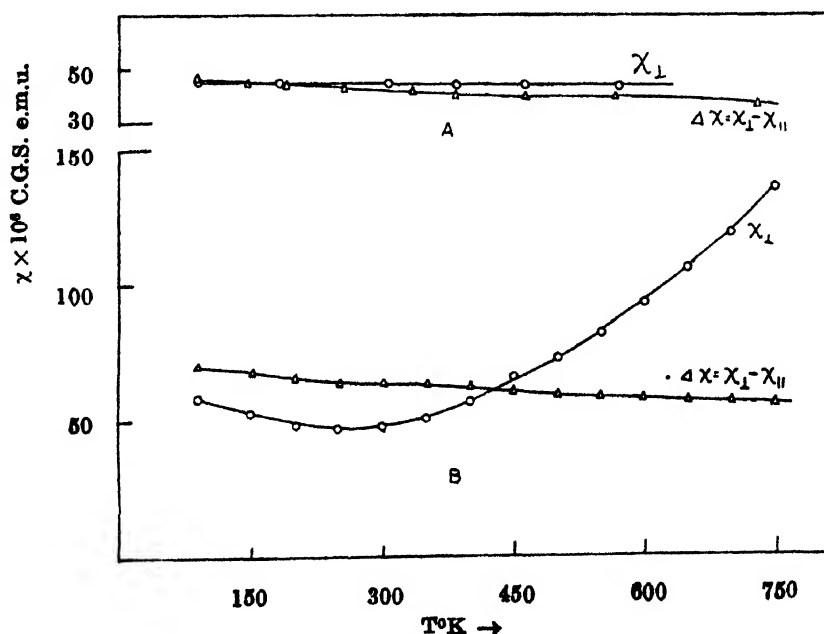


Figure 1. Temperature variation of anisotropy ($\Delta\chi = \chi_{\perp} - \chi_{\parallel}$) and susceptibility (χ_{\perp}) of molybdenite.

A \longrightarrow Earlier measurement
B \longrightarrow Present measurement

Results of these measurements as well as those of fresh measurements of anisotropy are shown in the adjoining figure wherein the results of earlier measurements by Dutta (1945) are also represented for the sake of comparison. It is seen from the figure that though the temperature variation of anisotropy has remained practically of the same nature in both the measurements yet that of susceptibility has undergone much change. In earlier measurements χ_1 continuously decreased with the rise of temperature whereas in the present measurements it first decreased with the rise of temperature (within the range $90^\circ K-250^\circ K$) then increased with further rise of temperature. This high temperature behaviour of χ_1 in case of molybdenite, a semiconductor, is evidently to be attributed to the increase of carrier concentration with the rise of temperature. Earlier interpretation of the results are therefore no longer tenable and the new results are to be interpreted in a different way. Investigation in this line are in progress and the results will be published in due course.

The author wishes to express her sincere thanks to Shri A. K. Dutta for suggestion and guidance and to Prof. A. Bose for his kind interest in the work.

REFERENCES

- Bose, A., 1947, *Indian J. Phys.*, **21**, 276
Das, D., 1963, *Indian J. Phys.*, **37**, 582
Dutta, A. K., 1945, *Indian J. Phys.*, **19**, 225

ERRATA

SPACE GROUP OF O-BENZOYL BENZOIC ACID

M. L. Kundu and S. C. Chakravorty

Department of Physics, Burdwan University, Burdwan, West Bengal, India

Vol. 41, No. 7, P. 548, Last two lines

The authors now reports that the experimental intensity distribution curves are actually centric, not hypercentric. A wrong scale factor was introduced in the calculation in averttently while putting the intensities of X-ray reflections to the same scale by the multiple film technique. The recalculated values of Wilson's ratio both for *okl* and *hol* reflections is 0.59.

COSMIC RAY STARS IN PHOTOGRAPHIC EMULSION AT HIGH ALTITUDE

S. R. Ganguly, S. K. Mondal and S. D. Chatterjee

Department of Physics, Jadavpur University, Calcutta-32

Vol. 41, No 7, P. 475. Last line of the figure caption :

Read (b) for (a)

and (a) for (b)

AN IMPROVEMENT IN THE TECHNIQUE OF TIME MEASUREMENT

B. N. Biswas and G. Dutta

Physics Department, Burdwan University, Burdwan, West Bengal

Vol. 41, No 7, Page 545-6.

The diagrams have interchanged their locations with the figure numbers remaining in their correct positions.